Tore A. Larheim
Per-Lennart A. Westesson

Maxillofacial Imaging

Second Edition

Springer

Maxillofacial Imaging

Tore A. Larheim • Per-Lennart A. Westesson

Maxillofacial Imaging

Second Edition

Springer

Tore A. Larheim
Department of Maxillofacial Radiology
Institute of Clinical Dentistry
University of Oslo Faculty of Dentistry
Oslo
Norway

Institute of Clinical Dentistry
UiT The Arctic University of Norway
Tromsø
Norway

Per-Lennart A. Westesson
Division of Diagnostic and Interventional Neuroradiology
University of Rochester School of Medicine and Dentistry
Rochester, NY
USA

ISBN 978-3-319-53317-9 ISBN 978-3-319-53319-3 (eBook)
https://doi.org/10.1007/978-3-319-53319-3

Library of Congress Control Number: 2017941286

Printed on acid-free paper

This Springer imprint is published by Springer Nature
The registered company is Springer International Publishing AG
The registered company address is: Gewerbestrasse 11, 6330 Cham, Switzerland

Foreword I

Anyone who is concerned with the management of pathologic conditions involving the oral and maxillofacial region is aware of the frequent need for diagnostic imaging. They are also aware of the need for a reliable resource text when faced with a condition with which they are unfamiliar. *Maxillofacial Imag*ing, written by Professors Tore A. Larheim and Per-Lennart A. Westesson, is highly recommended for that purpose. By joining together the expertise of a dentally and medically based radiologist, this book brings a new and unique perspective to diagnostic imaging, with the focus not only on conventional radiologic techniques, standard and computed tomography, and magnetic resonance imaging but also on the diagnostic use of positron emission tomography (PET) and ultrasonography. Other unique features of this book generally not found in other maxillofacial radiology textbooks include the grouping of the various conditions into a succinct, easily searchable order; a list of accompanying imaging and clinical features and often clinical photographs of each condition; and information on interventional radiology. All of these attributes make this book a valuable resource for oral and maxillofacial and medical radiologists; oral and maxillofacial, ENT, and plastic surgeons; and general dentists and dental specialists. Professors Larheim and Westesson are to be complimented on producing a text that will make the diagnosis of oral and maxillofacial pathology easier for all concerned.

Daniel M. Laskin
Department of Oral and Maxillofacial Surgery
Virginia Commonwealth University School of Dentistry
Richmond, VA, USA

Foreword II

At a recent case conference, one of our residents presented a patient with osteomyelitis of the mandible. She first described a panoramic view followed by CBCT images, which revealed more detail of the osseous changes. Her discussion of the case included the diagnostic contributions of CBCT and panoramic imaging in revealing the osseous changes and disease process. Although we did not have any MR imaging of this patient, we were fortunate to have a copy of the first edition of *Maxillofacial Imaging* by Larheim and Westesson. In the chapter on infections, we reviewed several MR images of osteomyelitis. With the benefit of the cases provided in this textbook, we were able to have a more informed discussion of the comparative diagnostic contributions of various advanced imaging modalities.

As with the first edition, this is an atlas-style book—using bullet text throughout—with a focus on diagnostic and anatomic imaging. In this second edition, the number of illustrations, primarily CT and MR, is increased from 1500 in the first edition to about 2500 in this edition. The page count is increased about 50%, and there is a new chapter on CBCT imaging.

The success of a textbook such as this depends primarily on two factors: the quality of the images and the quality of the accompanying text. In the first instance, it is often difficult to find good cases consisting of clinical photographs, routine and advanced imaging, and photomicrographs of biopsy specimens. It is also important to have access to many cases in order to be able to select those which are most representative of various stages or manifestations of a condition and which best illustrate the disease process. Only authors with extensive experience at busy clinics are able to accumulate such collections. Secondly, the text must clearly and succinctly identify the imaging features that are characteristic of the condition and help to reveal the underlying disease process. As with the illustrations, high-quality text requires authors with extensive experience and insight. Fortunately for readers of this book, it was prepared by two individuals who meet these standards. Professor Larheim is head of the Department of Maxillofacial Radiology at the Institute of Clinical Dentistry, Faculty of Dentistry, University of Oslo. He has an extensive record of research articles and lecturing in the field of maxillofacial imaging around the world with a particular focus on the temporomandibular joint. Professor Westesson is trained in both oral and maxillofacial radiology and in neuroradiology and was for many years the chief of Diagnostic and Interventional Neuroradiology at the University of Rochester. He has also an extensive record of publication and lecturing around the world, often on topics related to the temporomandibular joint. Both this writer and our residents are delighted that Professors Larheim and Westesson have decided to update and expand their valuable contribution.

Stuart C. White
UCLA School of Dentistry
Los Angeles, CA, USA

Preface from 1st Edition

Dr. Westesson (left) and Dr. Larheim (right)

There are substantial textbooks on head and neck imaging as well as on dental imaging, but since the early 1990s, there has been no book focusing on the gap between imaging in dentistry and in medicine, namely, maxillofacial imaging. Emanating from dentistry, maxillofacial radiology uses principles and techniques from medical radiology. There has been a significant advance in imaging technology during the last 15 years, and this maxillofacial imaging book demonstrates how advanced medical imaging technology can be successfully applied to dental and maxillofacial conditions.

Dental radiology is mainly based on intraoral and panoramic examinations with an ongoing replacement of plain films with their digital counterparts. Medical radiology, on the other hand, is moving away from projectional radiography and is using more and more cross-sectional imaging modalities such as computed tomography (CT), magnetic resonance (MR) imaging, ultrasound, and positron emission tomography (PET). These contemporary and advanced techniques have not been widely applied to maxillofacial imaging, and the purpose of this extensively illustrated book is to show how advanced imaging modalities, primarily CT and MRI, can be applied to maxillofacial imaging.

We have built this book around the images rather than an extensive text since we think others are like us—we like to see the images and read the text only if necessary. Thus, the book is atlas-like with a condensed and bulleted text. With all images of the patient on one or two pages, the reader will very quickly obtain an image overview of the specific condition. Demonstrating the use of advanced imaging techniques in dentistry is particularly important since maxillofacial radiology has been accepted as a specialty of dentistry in several countries and the international trend is a closer cooperation between professionals in dentistry and medicine to provide the best patient care. During the writing of this book, it has evolved into a rather comprehensive description of maxillofacial imaging and could easily be used as the foundation for building a formal curriculum in maxillofacial radiology.

The book is divided into 14 chapters starting with a quite comprehensive chapter on normal imaging anatomy of the maxillofacial structures followed by four chapters on advanced imaging of conditions of dental or non-dental etiology, affecting the mandible and maxilla. When dentists get more and more involved in the imaging of maxillofacial soft tissues, knowledge of

both hard and soft tissues becomes mandatory. Although the majority of patients with jaw problems are diagnosed with intraoral and panoramic (film or digital) examinations, advanced imaging has become necessary for a reliable diagnostic assessment of a number of conditions. The sixth chapter is on the temporomandibular joint. This is valuable for professionals in both medicine and dentistry since many patients with facial pain seek any doctor who gives hope of being able to help them irrespective of training background and subspecialty. The four following chapters focus on dental implants, maxillofacial trauma and fractures, face and skull deformities, and paranasal sinuses. These regions are closely related to the jaw, and many conditions involve both the dental structures and the adjacent regions.

The following two chapters cover soft-tissue imaging of the oral cavity and salivary glands. These are important topics, since traditional dental and maxillofacial imaging has been limited to evaluation of the hard tissue. In Chap. 13, we have focused on imaging abnormalities of structures adjacent to the maxillofacial region, namely, the cervical spine, neck, skull base, and orbit. It is not our intention to incorporate these areas into maxillofacial radiology, but we think it is important that the maxillofacial radiologist has a working understanding of what there is in the areas neighboring the maxillofacial region. At the end, we have included a chapter on interventional maxillofacial radiology. Interventional radiology is the fastest growing area of general medical radiology, but has not been extensively applied to maxillofacial imaging. Our intention in this chapter is to show how minimally invasive interventional radiologic techniques can be successfully used for maxillofacial conditions.

This book is an attribute to the early work of Dr. Karl-Åke Omnell, who was the pioneer of maxillofacial radiology. Already in the late 1960s, Dr. Omnell had the vision of centralized advanced maxillofacial imaging as a specialty of dentistry working closely with medical radiology. Dr. Omnell initiated the first hospital-based clinic for maxillofacial radiology in Sweden, and he promoted the recognition of oral and maxillofacial radiology as a specialty of dentistry. His pioneer work has later been followed by many. We are proud to present this contemporary book on maxillofacial imaging as an attribute to his pioneer work.

This book has evolved from a friendship of more than 25 years and professional cooperation between Drs. Larheim and Westesson. It started around 1980 when Dr. Larheim from the dental school in Oslo, Norway, crossed the border to the neighboring country, Sweden, and visited Dr. Westesson at the dental school in Malmö to observe the performance of double-contrast arthrotomography of the temporomandibular joint. Both have been working as maxillofacial radiologists ever since. Dr. Larheim is currently the head of the first maxillofacial radiology department outside Japan that installed its own CT scanner, recently replaced with a multislice scanner. Dr. Westesson took another step and went through medical training, radiology residency, and a neuroradiology fellowship and eventually became chief of diagnostic and interventional neuroradiology at the University of Rochester. Their combined experience is reflected in this book on maxillofacial imaging.

Dr. Larheim completed this work during a sabbatical stay at the University of Rochester Medical Center, Division of Diagnostic and Interventional Neuroradiology, and is highly grateful for the support he got from the Faculty of Dentistry, University of Oslo, Norway, and the Research Council of Norway. Without this support, the book would never have been accomplished.

We would like to express our sincere gratitude to our collaborators (in alphabetical order) Drs. Susan I. Blaser, Naoya Kakimoto, Alf Kolbenstvedt, Masaki Oka, Ravinder Sidhu, Hans-Jørgen Smith, Hanna Strømme-Koppang, and Geir Støre, for the fruitful discussion of the text and contribution of good-quality images. Special thanks goes to Dr. Kakimoto for his hard work in obtaining the best possible image quality throughout the book.

We thank Dr. Sven Ekholm at the University of Rochester Medical Center and Drs. Linda Arvidsson and Bjørn Mork Knutsen and medical radiographer Magne Borge at the Institute of Clinical Dentistry, University of Oslo, for supplying us with images when we were in need, as well as all others from whom we borrowed their images; they are acknowledged in the legends.

The secretarial work of Bjørg Jacobsen, Institute of Clinical Dentistry, University of Oslo, Norway, and Regina Cullen and Belinda De Libero, University of Rochester Medical Center, Rochester, NY, is highly appreciated with special thanks to Bjørg reviewing the reference lists.

We are grateful to graphic designer Margaret Kowaluk, University of Rochester Medical Center, Rochester, NY, and photographer Håkon Størmer, Faculty of Dentistry, University of Oslo, for professional work with the scanning of many images and obtaining some of the photos.

Editor Ute Heilman and desk editor Dörthe Mennecke-Bühler at Springer, as well as production editor Michael Reinfarth and copy editor John Nicholson, with their professional skill made this work to our satisfaction.

We are proud to present this maxillofacial imaging book, and we hope that our work will serve you well.

Rochester, NY, USA
August 2005

Tore A. Larheim
Per-Lennart A. Westesson

Preface from 2nd Edition

We are proud to present the 2nd edition of *Maxillofacial Imaging* 12 years after the first edition was released. This book is the result of many years of clinical and academic work with maxillofacial imaging at two academic institutions, namely University of Oslo, Norway, and University of Rochester, NY, USA. Both institutions are leading in their field and supplement each other for the collection of cases for this book. Many of the dental and maxillofacial cases emanate from the University of Oslo and the larger cases often come from hospital-based University of Rochester. Also a third institution is involved in this book, namely Oslo University Hospital, Rikshospitalet. Many advanced cases are collected from this hospital due to a close collaboration between the principal author of the book and the Head of Division of Radiology and Nuclear Medicine for many years.

The cases in the book range from those commonly seen in clinical practice of maxillofacial imaging to many exceedingly rare conditions. The book format has allowed us to generously illustrate the cases with imaging using multiple complimentary techniques. However, it must be emphasized that in routine clinical practice not all the imaging modalities, as applied in this book, are necessary for a satisfactory imaging evaluation of the case. Our idea has been to investigate and illustrate how precise a "pre-histopathologic" diagnosis can be when narrowing the differential diagnostic field by applying combinations of imaging modalities.

Imaging is a rapidly progressing specialty of medicine and dentistry. Over the last several years there has been enormous progress with refined technology, widened applications, and better understanding of pathophysiology. The 2nd edition of *Maxillofacial Imaging* has been updated to reflect the current status of maxillofacial imaging with the use of the most contemporary techniques; CT, cone beam CT, MRI, nuclear medicine including PET and PET/CT, as well as ultrasonography. The book has been expanded with an additional chapter on cone beam CT. In total more than 1000 new individual images have been added.

The new chapter on cone beam CT is dedicated to just this technique that has become the standard for advanced maxillofacial imaging. Ultrasonography is also making its way into maxillofacial imaging and has been incorporated into the chapters throughout the book where appropriate for imaging of soft tissue structures. This presentation of maxillofacial imaging

should be the most comprehensive clinical textbook on this subject to date. Presenting all images of one case on one page or, if necessary, on left and right page and with a short, bullet text, the book should be very friendly to read. Very quickly the reader will get an overview of a specific condition. Particular attention has of course been paid to the quality of images throughout the book because we radiologists strongly believe that a good image often tells the story.

We would like to express our sincere gratitude to Professor Hans-Jørgen Smith, Oslo University Hospital, for supplying us with so many nice cases and for reading the text in many chapters so carefully. We would also like to thank Drs. Anna-Karin Abrahamsson, Linda Z Arvidsson, Caroline Hol, Margaret Kristensen Ottersen, Bjørn Bamse Mork-Knutsen, Maria Redfors, and Ulf Riis, Department of Maxillofacial Radiology, University of Oslo, for their contribution and reviewing the images and the text in Chap. 15.

Special thanks go to Higher Executive Officer Bjørg M. Jacobsen for excellent secretarial work throughout the new edition and photographer/senior engineer Håkon Størmer for excellent photographic work. The principal author and the photographer have been spending an unknown number of hours to ensure that the quality of each of the individual images has been as good as possible to illustrate the specific condition. We are also very thankful to the technical staff at the Department of Maxillofacial Radiology, University of Oslo, the Division of Diagnostic and Interventional Radiology, University of Rochester, and the Department of Radiology and Nuclear Medicine, Oslo University Hospital, for good-quality daily clinical work. This is a prerequisite to obtain high-quality illustrations in a book like this.

We would also like to thank those involved at Springer for their professional skill so that the final work has been made to our satisfaction.

We are really proud to present this atlas-like maxillofacial imaging book and we hope that our work will serve you well.

Oslo, Norway
Rochester, NY, USA

Tore A. Larheim
Per-Lennart A. Westesson

Contents

1 Maxillofacial Imaging Anatomy 1
1.1 Introduction 1
1.2 3D CT. 2
1.3 Cone Beam 3D CT. 4
1.4 CT Sections: Bone Structures 6
1.5 Cone Beam CT Sections 10
1.6 Schematic Drawing: Floor of the Mouth 11
1.7 CT Sections: Soft-Tissue Structures 12
1.8 MR Sections. 14
1.9 Temporomandibular Joint 17
Suggested Reading 21

2 Jaw Cysts and Cyst-Like Conditions 23
2.1 Introduction 23
2.2 Cysts. 23
2.3 Periapical Cyst 24
2.4 Residual Cyst 29
2.5 Paradental (Mandibular Infected Buccal) Cyst 30
2.6 Lateral Periodontal Cyst 35
2.7 Incisive Canal Cyst 36
2.8 Follicular Cyst 37
2.9 Glandular Odontogenic Cyst 44
2.10 Odontogenic Keratocyst. 45
2.11 Cyst-Like Conditions. 45
2.12 Simple Bone Cyst 45
2.13 Stafne Bone Cyst 52
2.14 Retention Cyst 54
Suggested Reading 55

3 Benign Jaw Tumors and Tumorlike Conditions. 57
3.1 Introduction 57
3.2 Benign Tumors. 57
3.3 Keratocystic Odontogenic Tumor 57
3.4 Ameloblastomas. 71
3.5 Ameloblastoma, Solid/Multicystic Type 71
3.6 Ameloblastoma, Unicystic Type 71
3.7 Ameloblastoma, Desmoplastic Type 71
3.8 Lipoma 87
3.9 Odontogenic Fibroma (Central). 87
3.10 Odontogenic Myxoma/Myxofibroma 88
3.11 Osteoblastoma 90
3.12 Ossifying Fibroma 92
3.13 Juvenile Ossifying Fibroma 98

3.14 Benign Tumorlike Conditions 99
3.15 Aneurysmal Bone Cyst 99
3.16 Giant Cell Granuloma (Central) 103
3.17 Langerhans Cell Histiocytosis 106
3.18 Cherubism 108
3.19 Fibrous Dysplasia 111
3.20 Osseous Dysplasias 115
3.21 Osteoma 118
3.22 Exostoses 121
3.23 Idiopathic Osteosclerosis 124
3.24 Odontoma 126
Suggested Reading 127

4 Malignant Tumors in Jaws 129
4.1 Introduction 129
4.2 Bone-Destructive Tumors 129
4.3 Squamous Cell Carcinoma 129
4.4 Mucoepidermoid Carcinoma 137
4.5 Adenoid Cystic Carcinoma 141
4.6 Non-Hodgkin's Lymphoma 145
4.7 Multiple Myeloma 152
4.8 Leukemia 155
4.9 Bone-Destructive and Bone-Productive Tumors 157
4.10 Osteosarcoma 157
4.11 Chondrosarcoma 164
4.12 Ewing Sarcoma 166
4.13 Soft-Tissue Sarcomas 168
4.14 Rhabdomyosarcoma 168
4.15 Leiomyosarcoma 170
4.16 Jaw Metastases 171
Suggested Reading 177

5 Jaw Infections 179
5.1 Introduction 179
5.2 Osteomyelitis 179
5.3 Osteomyelitis with Periostitis 186
5.4 Osteoradionecrosis 193
5.5 Medication-Related Osteonecrosis 198
5.6 Abscess 209
Suggested Reading 212

6 Temporomandibular Joints 215
6.1 Introduction 215
6.2 Internal Derangements (with Normal Cortical Bone) 215
6.3 Osteoarthritis 224
6.4 Bone Marrow Abnormalities 234
6.5 Arthritides 237
6.6 Juvenile Idiopathic Arthritis 241
6.7 Ankyloses 247
6.8 Condylar Growth Disturbances (Anomalies) 251
6.9 Inflammatory or Tumorlike Conditions 255
6.10 Calcium Pyrophosphate Dehydrate Crystal Deposition Disease (Pseudogout) 255
6.11 Pigmented Villonodular Synovitis 256
6.12 Simple (Traumatic) Bone Cyst 256

6.13 Synovial Cyst . . . 257
6.14 Synovial Chondromatosis . . . 258
6.15 Benign Tumors . . . 261
6.16 Osteochondroma . . . 261
6.17 Osteoma . . . 262
6.18 Sphenoid Meningioma . . . 262
6.19 Malignant Tumors . . . 263
6.20 Osteoradionecrosis . . . 264
6.21 Coronoid Hyperplasia . . . 265
Suggested Reading . . . 266

7 Teeth and Dental Implants . . . 271
7.1 Introduction . . . 271
7.2 Tooth Anatomy, Tooth Pathology, and Adjacent Structures . . . 271
7.3 Preoperative and Postoperative Implant Imaging . . . 279
7.4 Imaging of Implant Complications . . . 285
Suggested Reading . . . 286

8 Facial Traumas and Fractures . . . 287
8.1 Introduction . . . 287
8.2 Non-fracture Traumas . . . 287
8.3 Fractures . . . 290
8.4 Mandibular Fractures . . . 291
8.5 Mandibular Fractures Combined with Other Fractures . . . 297
8.6 Complications of Mandibular Fractures . . . 301
8.7 Nasal Fractures . . . 303
8.8 Midfacial Fractures . . . 303
8.9 Isolated Maxillary Sinus Wall Fracture . . . 304
8.10 LeFort Fractures . . . 305
8.11 Tripod Fracture . . . 308
8.12 Blowout Fracture . . . 310
Suggested Reading . . . 312

9 Facial Growth Disturbances . . . 313
9.1 Introduction . . . 313
9.2 Isolated Disturbances . . . 313
9.3 Common Cleft Palate and/or Cleft Lip . . . 313
9.4 Choanal Atresia . . . 316
9.5 Torus Maxillaris, Palatinus, and Mandibularis . . . 317
9.6 Condylar Hyperplasia . . . 317
9.7 Cherubism . . . 318
9.8 Fibrous Dysplasia . . . 319
9.9 Mandibular Neck/TMJ Fracture or TMJ Infection Complication . . . 321
9.10 TMJ Internal Derangement Complication . . . 325
9.11 Juvenile Idiopathic Arthritis . . . 325
9.12 Syndromes . . . 327
9.13 Down Syndrome . . . 327
9.14 Premature Cranial Synostoses . . . 328
9.15 Non-synostotic Occipital Plagiocephaly . . . 329
9.16 Turner Syndrome . . . 330
9.17 Goldenhar Oculoauriculovertebral (OAV) Spectrum . . . 331
9.18 Goldenhar Syndrome . . . 331
9.19 Hemifacial Microsomia . . . 332
9.20 Treacher Collins Syndrome (Mandibulofacial Dysostosis) . . . 334
9.21 Syndromic Craniosynostoses (Craniofacial Dysostoses) . . . 336

9.22 Crouzon Syndrome . . . 336
9.23 Apert Syndrome . . . 338
9.24 Achondroplasia . . . 339
9.25 Pyknodysostosis . . . 342
9.26 Ectodermal Dysplasia . . . 343
9.27 Miscellaneous Conditions . . . 344
Suggested Reading . . . 347

10 Paranasal Sinuses . . . 349
10.1 Introduction . . . 349
10.2 Inflammatory Diseases . . . 349
10.3 Acute Rhinosinusitis . . . 349
10.4 Chronic Sinusitis . . . 352
10.5 Mucosal Imaging Findings in Asymptomatic Individuals . . . 355
10.6 Retention Cysts, Mucous and Serous . . . 355
10.7 Polyps . . . 356
10.8 Mucoceles . . . 359
10.9 Granulomatosis With Polyangiitis (Previously Known as Wegener's Granulomatosis) . . . 363
10.10 Inflammatory Dental Conditions . . . 364
10.11 Benign Tumors and Tumorlike Conditions . . . 365
10.12 Papilloma . . . 366
10.13 Osteoma . . . 366
10.14 Fibrous Dysplasia . . . 368
10.15 Nasolabial (Nasoalveolar) Cyst . . . 370
10.16 Malignant Tumors . . . 371
10.17 Adenocarcinoma . . . 371
10.18 Squamous Cell Carcinoma . . . 371
10.19 Lymphoma . . . 373
10.20 Ewing Sarcoma . . . 374
10.21 Osteosarcoma . . . 376
10.22 Expansile Odontogenic Conditions . . . 377
10.23 Miscellaneous Conditions . . . 380
Suggested Reading . . . 384

11 Maxillofacial Soft Tissues . . . 385
11.1 Introduction . . . 385
11.2 Infection (Abscess) . . . 385
11.3 Muscular Hypertrophy, Atrophy, and Dehiscence . . . 387
11.4 Calcifications . . . 387
11.5 Vascular Malformations . . . 393
11.6 Cysts . . . 399
11.7 Lingual Thyroid . . . 402
11.8 Benign Oropharyngeal Tumors . . . 404
11.9 Lipoma . . . 404
11.10 Schwannoma . . . 405
11.11 Malignant Oropharyngeal Tumors . . . 406
11.12 Squamous Cell (and Clear Cell) Carcinomas . . . 406
11.13 Adenoid Cystic Carcinoma . . . 409
11.14 Lymphoma . . . 409
Suggested Reading . . . 410

12 Salivary Glands 413
12.1 Introduction 413
12.2 Nonneoplastic Conditions 413
12.3 Infection/Inflammation 413
12.4 Sialolithiasis 417
12.5 Sjögren's Syndrome 424
12.6 Benign Lymphoepithelial Cysts Associated with HIV–AIDS 428
12.7 Ranula 429
12.8 Tumors 430
12.9 Benign Tumors 430
12.10 Pleomorphic Adenoma (Benign Mixed Tumor) 430
12.11 Warthin's Tumor (Papillary Cystadenoma Lymphomatosum) 434
12.12 Hemangioma 435
12.13 Malignant Tumors 438
12.14 Lymphoma 438
12.15 Carcinomas 439
12.16 Mucoepidermoid Carcinoma 439
12.17 Acinic Cell Carcinoma 440
12.18 Adenocarcinoma 441
12.19 Adenoid Cystic Carcinoma 442
12.20 Carcinoma ex Pleomorphic Adenoma 444
Suggested Reading 445

13 Adjacent Structures: Cervical Spine, Neck, Skull Base, and Orbit 447
13.1 Introduction 447
13.2 Cervical Spine 447
13.3 Calcific Tendinitis Longus Colli 448
13.4 Ossification of Posterior Longitudinal Ligament 448
13.5 Rheumatoid Pannus at Craniocervical Junction 451
13.6 Tuberculosis at Craniocervical Junction 452
13.7 Chiari Malformation Type I 453
13.8 Chordoma at Craniocervical Junction 454
13.9 Cervical Spine Teratoma 456
13.10 Cervical Spine Cord Astrocytoma 457
13.11 Extramedullary Cervical Lipoma with Cord Compression 458
13.12 Cervical Spine Meningioma 459
13.13 Cervical Spine Neurofibromatosis Type 1 (NF-1) 460
13.14 Cervical Spine Fracture 461
13.15 Neck 462
13.16 Hypopharynx Abscess 462
13.17 Thyroid Abscess 462
13.18 Tornwaldt's Cyst 463
13.19 Dermoid Cyst in the Floor of the Mouth 464
13.20 Goiter 465
13.21 Vocal Cord Paralysis 466
13.22 Neck Hemangioma 466
13.23 Neck Lipoma 468
13.24 Neck Plexiform Neurofibroma 468
13.25 Pharynx Rhabdomyosarcoma 469
13.26 Tongue Base Carcinoma 470
13.27 Hypopharynx Carcinoma 471

13.28 Burkitt's Lymphoma 472
13.29 Castleman's Disease. 473
13.30 Lymphadenopathy 474
13.31 Skull Base 476
13.32 Mastoiditis with Intracranial Abscess 476
13.33 Mastoiditis with Sigmoid Thrombosis. 478
13.34 Osteoradionecrosis Involving Skull Base 479
13.35 Langerhans Cell Histiocytosis 480
13.36 Fibrous Dysplasia. 481
13.37 Giant Aneurysm of Skull Base 482
13.38 Glomus Vagale Paraganglioma 482
13.39 Craniopharyngioma 483
13.40 Pituitary Macroadenoma Invading the Skull Base. 484
13.41 Trigeminal Schwannoma 485
13.42 Metastatic Disease to Hypoglossal Canal and Clivus 486
13.43 Orbit. 487
13.44 Orbital Infectious Disease 488
13.45 Dacryocystocele, Nasolacrimal Duct. 488
13.46 Dermoid 488
13.47 Fibrous Dysplasia. 491
13.48 Langerhans Cell Histiocytosis 492
13.49 Neurofibromatosis 493
13.50 Hemangioma 493
13.51 Meningioma 495
13.52 Rhabdomyosarcoma. 495
13.53 Lymphoblastic Leukemia. 495
Suggested Reading 498

14 Interventional Maxillofacial Radiology 499
14.1 Introduction 499
14.2 TMJ Arthrography 501
14.3 TMJ Arthroscopy 502
14.4 Sialography 506
14.5 Biopsy 509
14.6 Facial Hemangioma Embolization. 509
14.7 Nosebleed Embolization 509
14.8 Juvenile Angiofibroma Embolization 509
Suggested Reading 513

15 Cone Beam Computed Tomography 515
15.1 Introduction 515
15.2 Maxillofacial Imaging Anatomy 515
15.3 Jaw Cysts and Cyst-Like Conditions 516
15.4 Benign Jaw Tumors and Tumorlike Conditions. 522
15.5 Malignant Tumors in Jaws 528
15.6 Jaw Infections 531
15.7 Temporomandibular Joints. 535
15.8 Teeth and Dental Implants 541
15.9 Facial Traumas and Fractures 555
15.10 Facial Growth Disturbances. 557
15.11 Paranasal Sinuses 558
15.12 Maxillofacial Soft Tissues 560
15.13 Salivary Glands 561
Suggested Reading 561

Index 563

Collaborators

A. -K. Abrahamsson, DDS Department of Maxillofacial Radiology, Faculty of Dentistry, Institute of Clinical Dentistry, University of Oslo, Oslo, Norway

Linda Z. Arvidsson, DDS, PhD Department of Maxillofacial Radiology, Faculty of Dentistry, Institute of Clinical Dentistry, University of Oslo, Oslo, Norway

Susan I. Blaser, MD, PhD Department of Diagnostic Imaging, The Hospital for Sick Children, 555 University Avenue, Toronto, ON, Canada, M5G 1X8

Caroline Hol, DDS Department of Maxillofacial Radiology, Faculty of Dentistry, Institute of Clinical Dentistry, University of Oslo, Oslo, Norway

Naoya Kakimoto, DDS, PhD Department of Oral and Maxillofacial Radiology, Applied Life Sciences, Institute of Biomedical & Health Sciences, Hiroshima University, 1-2-3 Kasumi, Minami-ku, Hiroshima, 734-8553, Japan

Alf Kolbenstvedt, MD, PhD Department of Radiology and Nuclear Medicine, Oslo University Hospital, Rikshospitalet, Oslo, Norway

Faculty of Medicine, University of Oslo, Oslo, Norway

Bjørn Bamse Mork-Knutsen, DDS Department of Maxillofacial Radiology, Faculty of Dentistry, Institute of Clinical Dentistry, University of Oslo, Oslo, Norway

Margareth Kristensen Ottersen, DDS Department of Maxillofacial Radiology, Faculty of Dentistry, Institute of Clinical Dentistry, University of Oslo, Oslo, Norway

Maria Redfors, DDS Department of Maxillofacial Radiology, Faculty of Dentistry, Institute of Clinical Dentistry, University of Oslo, Oslo, Norway

Ulf Riis, DDS Department of Maxillofacial Radiology, Faculty of Dentistry, Institute of Clinical Dentistry, University of Oslo, Oslo, Norway

Ravinder Sidhu, MD Department of Imaging Sciences, University of Rochester Medical Centre, Rochester, NY, USA

Hans-Jørgen Smith, MD, PhD Division of Radiology and Nuclear Medicine, Oslo University Hospital, Oslo, Norway

Faculty of Medicine, University of Oslo, Oslo, Norway

Geir Støre, MD, DDS, PhD Section for MaxilloFacial Surgery ENT Department, Oslo University Hospital, Oslo, Norway

Institute of Clinical Dentistry, UiT The Arctic University of Norway, Tromsø, Norway

Hanna Strømme-Koppang, DDS, PhD Section of Pathology and Forensic Odontology, Institute of Oral Biology, Faculty of Dentistry, University of Oslo, Oslo, Norway

Maxillofacial Imaging Anatomy

1

Abstract

This chapter illustrates 3D images of the cranium and facial skeleton, CT sections (axial, coronal) of the face: bone structures, cone beam CT sections (panoramic, cross-sectional) of the jaws, schematic drawing of the floor of mouth, CT sections (axial, coronal) of the face: soft-tissue structures, MR sections (axial, coronal) of the face, and sections (CT, MR, autopsy, histology) of the temporomandibular joint.

1.1 Introduction

This chapter presents a series of high-quality images on maxillofacial imaging anatomy. The first intention is to familiarize those working in dental imaging with advanced maxillofacial imaging anatomy. In addition to 3D CT and cone beam 3D CT images of bone structures, we have included CT and cone beam CT sections with bone details, CT and MR sections with soft-tissue details, and a schematic drawing of the floor of the mouth. General radiologists and other specialists will benefit from the detailed description of the anatomic structures of the jaws and oral cavity. The description of anatomic details of the jaws and teeth is primarily directed toward the medical profession since these areas are well known to dentists and dental specialists. The temporomandibular joint section should be valuable for both professions, showing normal (asymptomatic volunteer) features in CT images, MR images, open-mouth MR images, autopsy specimen sections, bone marrow biopsies, and fluid- and contrast-enhanced images.

The anatomic structures in Fig. 1.1:

1. Anterior fontanelle
2. Anterior nasal spine
3. Anterolateral fontanelle
4. Choanae
5. Coronal suture
6. Coronoid process
7. External auditory canal
8. Foramen magnum
9. Frontal bone
10. Frontozygomatic suture
11. Glenoid fossa
12. Hard palate
13. Incisive foramen
14. Infraorbital foramen
15. Lambdoid suture
16. Lateral pterygoid plate
17. Mandible
18. Mandibular condyle
19. Maxilla
20. Medial pterygoid plate
21. Mental foramen
22. Metopic suture
23. Nasal bone
24. Nasofrontal suture
25. Nasomaxillary suture
26. Occipital bone
27. Parietal bone
28. Posterolateral fontanelle
29. Sagittal suture
30. Squamosal suture
31. Temporal squama
32. Zygoma
33. Zygomatic arch

In collaboration with N. Kakimoto · H.-J. Smith.

T.A. Larheim, P.-L.A. Westesson, *Maxillofacial Imaging*, https://doi.org/10.1007/978-3-319-53319-3_1

1.2 3D CT

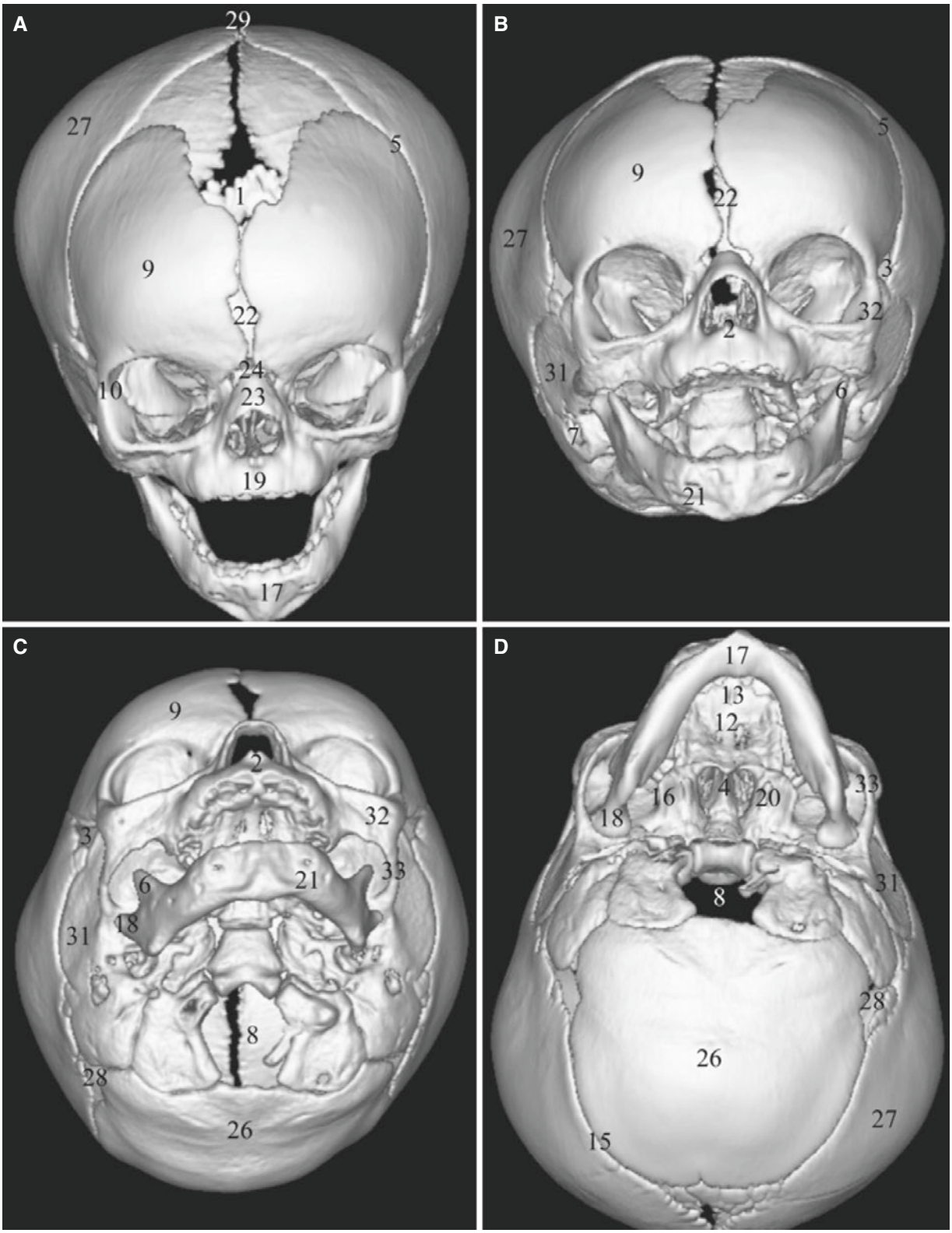

Fig. 1.1 Normal bone anatomy of the face and skull; 3D CT images. (**A**–**E**) 7-month-old, (**F**–**H**) 8-year-old

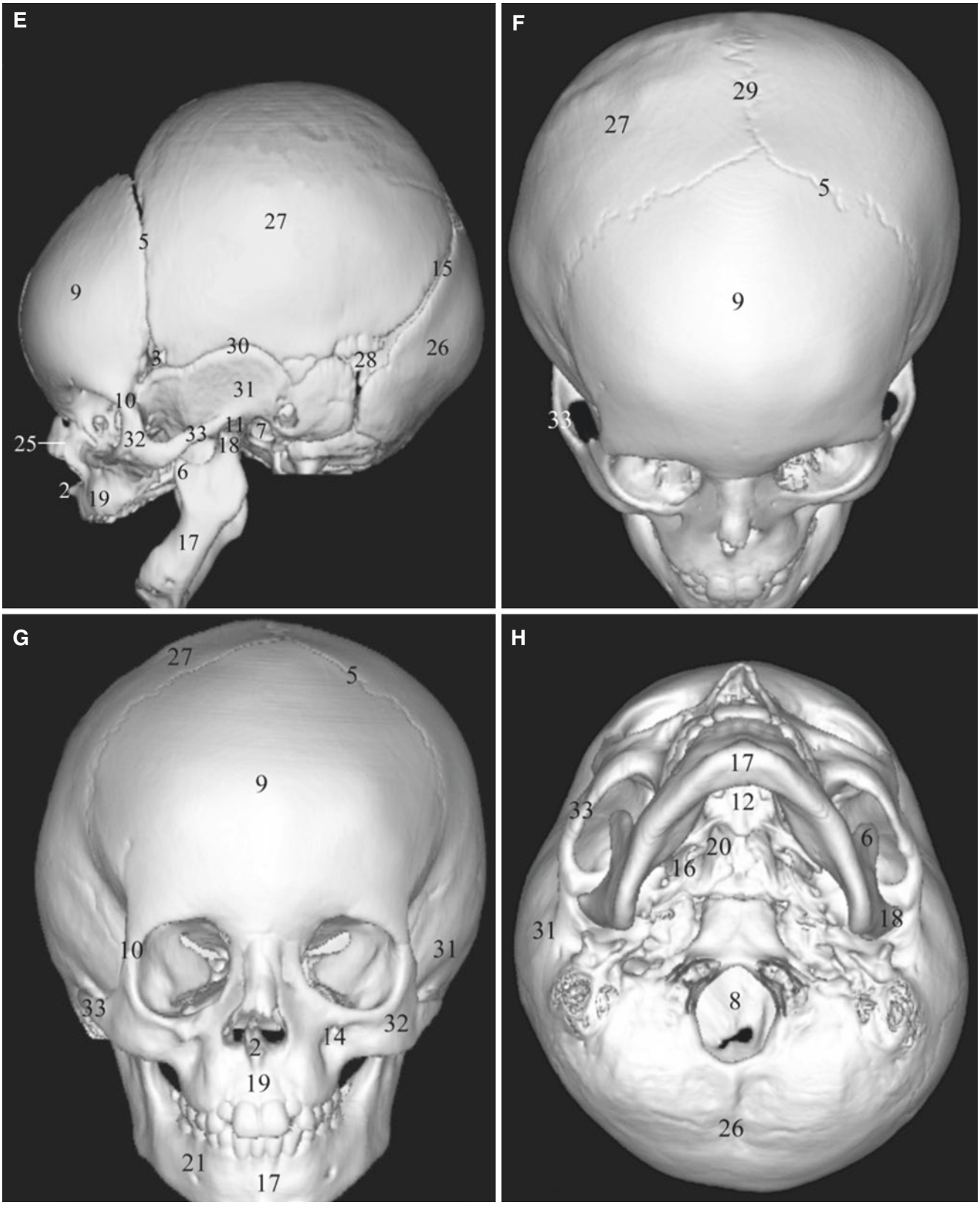

Fig. 1.1 (continued)

1.3 Cone Beam 3D CT

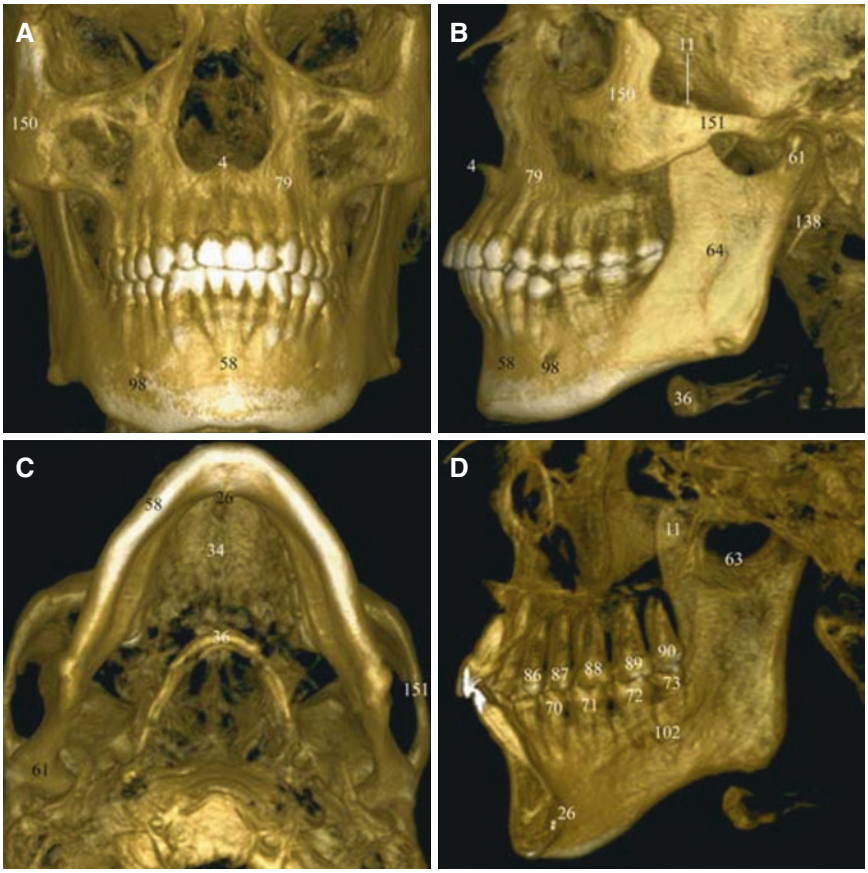

Fig. 1.2 Normal anatomy of facial skeleton; 3D cone beam CT images (**A**–**D**) (courtesy of Drs. A. G. Farman and W. C. Scharfe, University of Louisville School of Dentistry)

The anatomic structures in Figs. 1.2, 1.3, 1.4, 1.5, 1.6, 1.7, 1.8, 1.9, and 1.10:

1. Adenoidal tissue (nasopharyngeal tonsil)
2. Alveolar recess of maxillary sinus
3. Anterior belly of digastric muscle
4. Anterior nasal spine

4A. Posterior nasal spine

5. Base of tongue
6. Buccal space fat
7. Buccinator muscle
8. Carotid canal
9. Clivus
10. Concha bullosa
11. Coronoid process
12. Crista galli
13. Dens axis
14. Epiglottis
15. Ethmoid sinus

15A. Eustachian tube

16. External auditory canal
17. External carotid artery
18. External jugular vein
19. Facial vein
20. Foramen ovale
21. Foramen rotundum
22. Fossa of Rosenmüller (lateral pharyngeal fold)
23. Frontal bone
24. Frontal process of maxilla
25. Frontal sinus
26. Genial process of mandible
27. Genioglossus muscle
28. Geniohyoid muscle
29. Glenoid fossa
30. Greater palatine canal
31. Greater palatine foramen
32. Greater wing of sphenoid bone
33. Hamulus of medial pterygoid plate
34. Hard palate
35. Hyoglossus muscle
36. Hyoid bone
37. Incisive artery canal
38. Incisive canal
39. Incisive foramen
40. Inferior meatus
41. Inferior orbital fissure
42. Inferior turbinate
43. Infraorbital canal
44. Infratemporal fossa

45. Internal carotid artery
46. Internal jugular vein
47. Lacrimal bone
48. Lacrimal sac fossa
49. Lamina papyracea of ethmoid
50. Lateral pterygoid muscle
51. Lateral pterygoid plate
52. Lateral recess of sphenoid sinus
53. Lesser palatine canal
54. Levator labii superioris muscle
55. Lingual septum
56. Longus colli muscle
57. Major zygomatic muscle
58. Mandible
59. Mandibular alveolar bone
60. Mandibular canal
61. Mandibular condyle
62. Mandibular foramen
63. Mandibular notch
64. Mandibular ramus
65. Mandibular tooth
66. Mandibular tooth 1, central incisor
67. Mandibular tooth 2, lateral incisor
68. Mandibular tooth 3, canine
69. Mandibular tooth 4, first premolar
70. Mandibular tooth 5, second premolar
71. Mandibular tooth 6, first molar
72. Mandibular tooth 7, second molar
73. Mandibular tooth 8, third molar
74. Mandibular tooth crown pulp
75. Mandibular tooth root
76. Mandibular tooth root canal
77. Masseter muscle
78. Mastoid process
79. Maxilla
80. Maxillary alveolar bone
81. Maxillary sinus

81A. Hiatus semilunaris

81B. Uncinate process

82. Maxillary tooth
83. Maxillary tooth 1, central incisor
84. Maxillary tooth 2, lateral incisor
85. Maxillary tooth 3, canine
86. Maxillary tooth 4, first premolar
87. Maxillary tooth 5, second premolar
88. Maxillary tooth 6, first molar
89. Maxillary tooth 7, second molar
90. Maxillary tooth 8, third molar
91. Maxillary tooth crown pulp
92. Maxillary tooth root
93. Maxillary tooth root canal
94. Maxillary tuberosity
95. Medial pterygoid muscle
96. Medial pterygoid plate
97. Medial wall of maxillary sinus
98. Mental foramen
99. Middle meatus
100. Middle turbinate
101. Middle suture of hard palate
102. Mylohyoid line (ridge)
103. Mylohyoid muscle
104. Nasal ala

104A Nasal bone

105. Nasal cavity airway
106. Nasal septum
107. Nasal vestibule
108. Nasofrontal suture
109. Nasolacrimal canal
110. Nasopharynx
111. Olfactory recess
112. Orbicularis oris muscle
113. Orbit
114. Oropharynx
115. Palatal recess of maxillary sinus
116. Palatine tonsil
117. Parapharyngeal space
118. Parotid gland
119. Parotid gland, accessory
120. Parotid gland, deep lobe
121. Parotid gland, superficial lobe
122. Perpendicular plate of ethmoid bone
123. Platysma muscle
124. Posterior belly of digastric muscle
125. Pterygoid fossa
126. Pterygoid process of sphenoid
127. Pterygomandibular space
128. Pterygopalatine fossa
129. Retromandibular vein
130. Retromolar trigone
131. Soft palate
132. Sphenoid bone
133. Sphenoid sinus
134. Sphenoid sinus septum
135. Sphenozygomatic suture
136. Stensen's duct
137. Sternocleidomastoid muscle
138. Styloid process
139. Sublingual gland
140. Sublingual space
141. Submandibular gland
142. Submandibular space
143. Submental space
144. Superior turbinate
145. Temporalis muscle
146. Tongue, oral
147. Torus tubarius
148. Uvula
149. Vomer
150. Zygoma
151. Zygomatic arch

1.4 CT Sections: Bone Structures

Axial

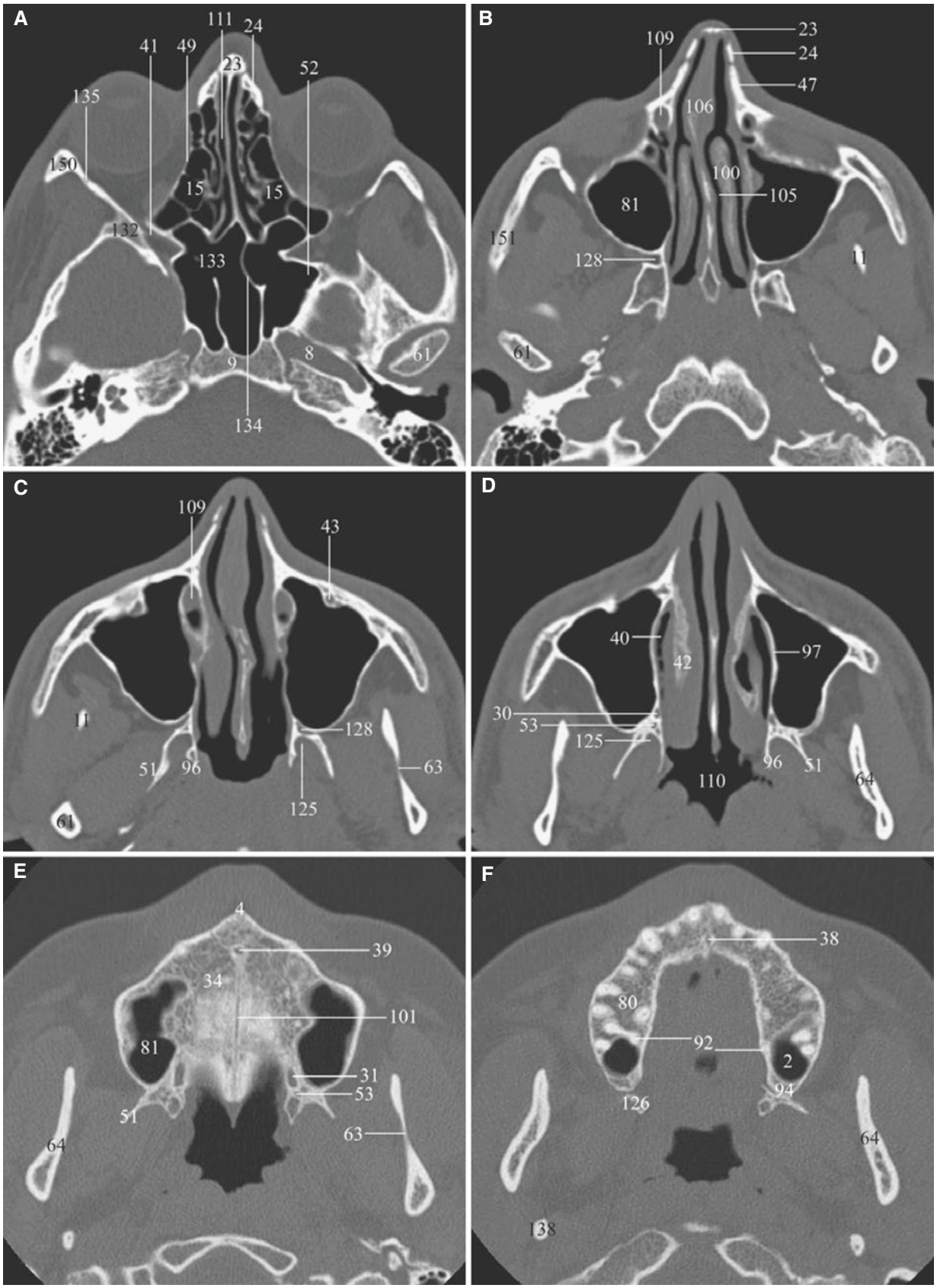

Fig. 1.3 Normal bone anatomy of face; axial CT images from superior (**A**) to inferior (**J**)

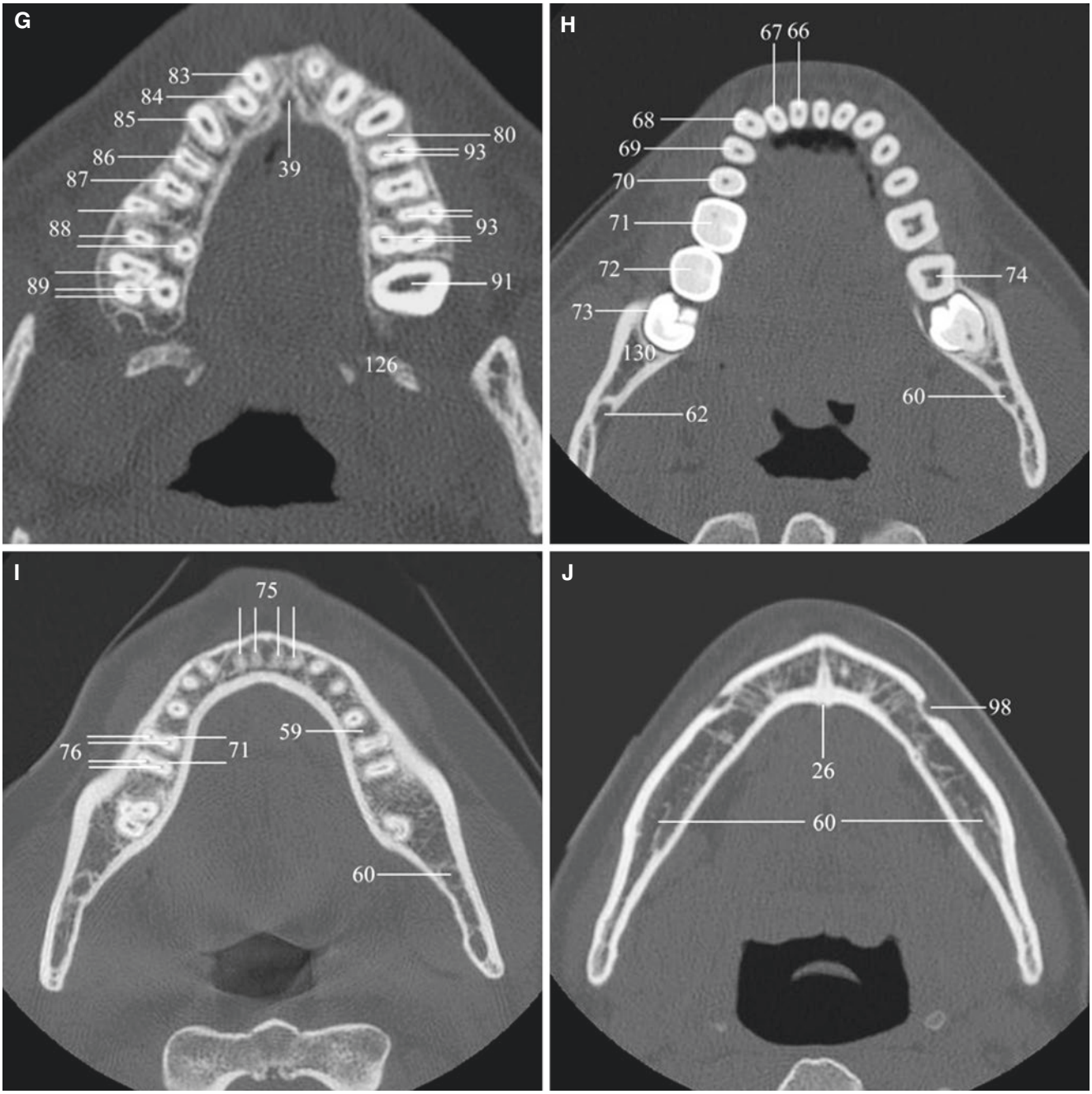

Fig. 1.3 (continued)

Coronal

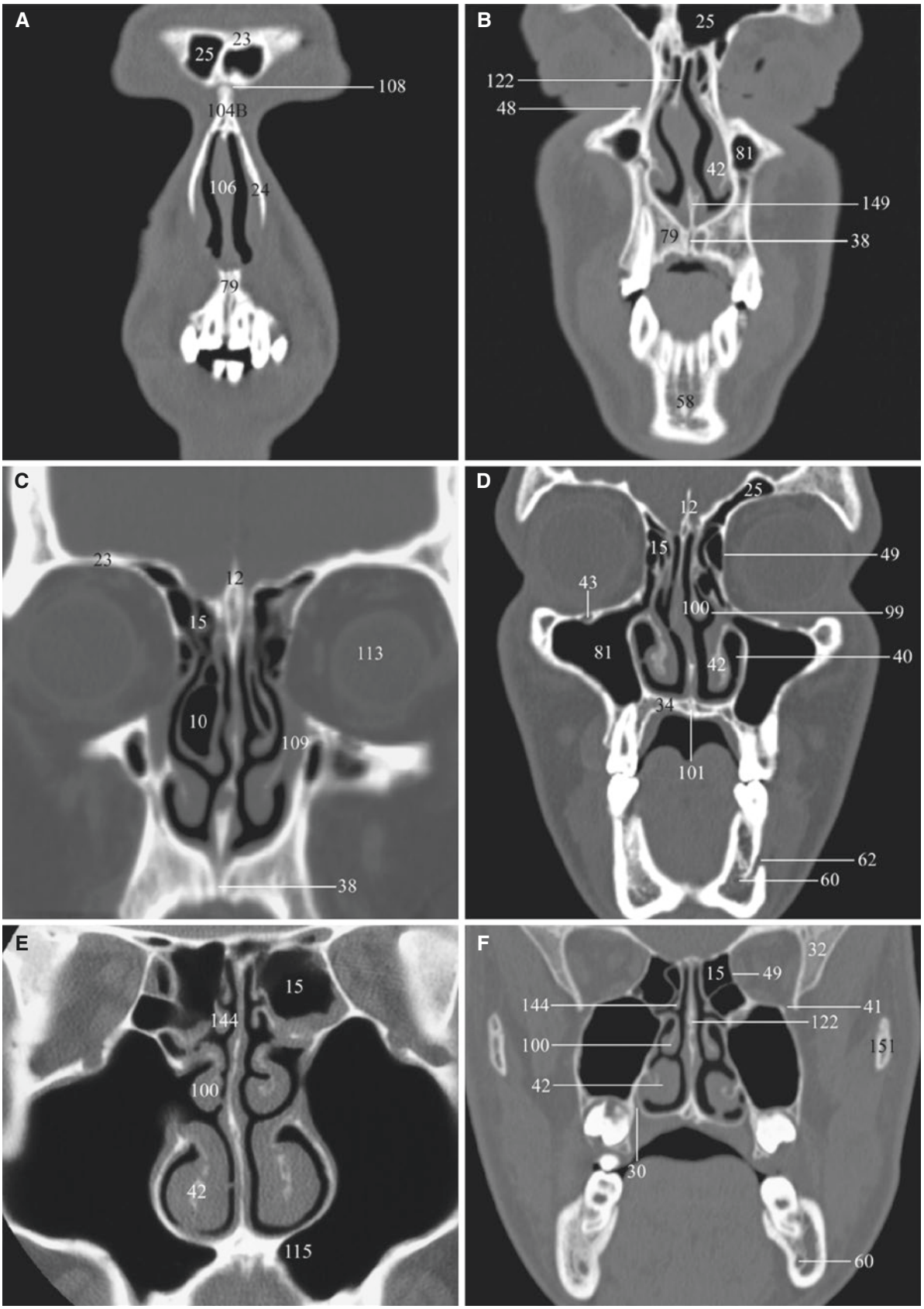

Fig. 1.4 Normal bone anatomy of face; coronal CT images from anterior (**A**) to posterior (**J**)

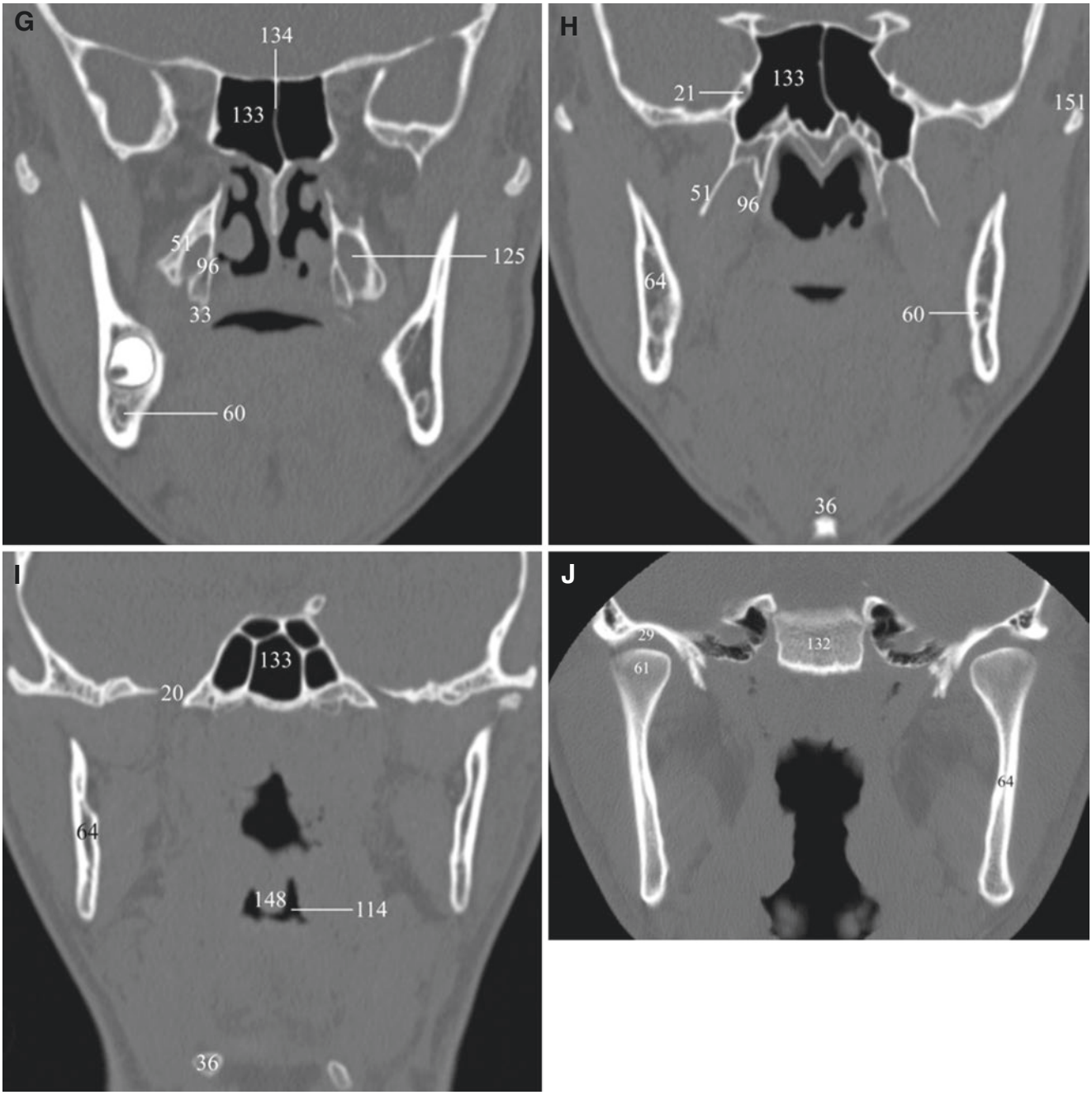

Fig. 1.4 (continued)

1.5 Cone Beam CT Sections

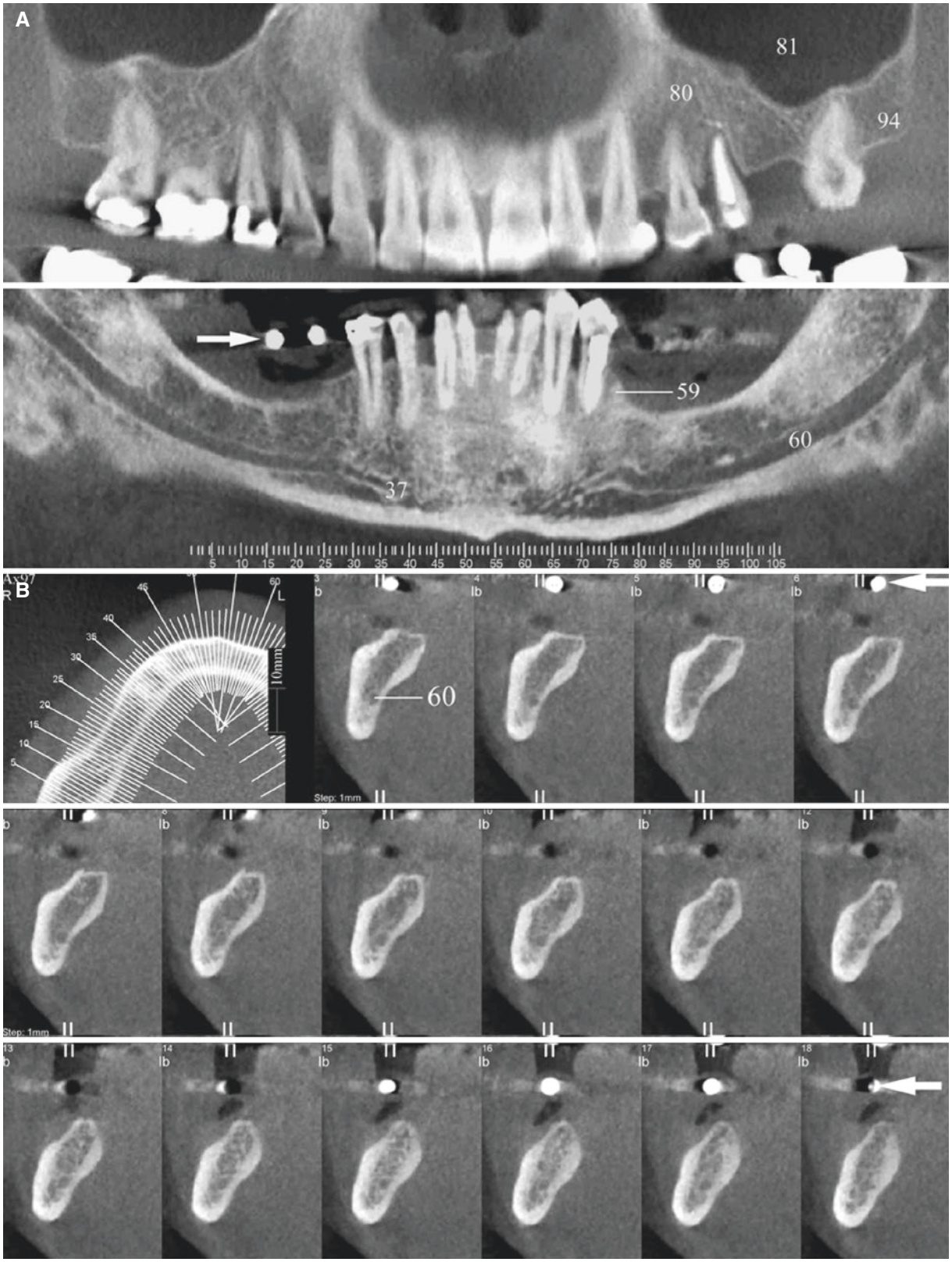

Fig. 1.5 Normal bone anatomy of the maxilla and mandible; cone beam CT images. (**A**) Panoramic view of the maxilla (*upper*) and mandible (*lower*); *arrow* metallic reference ball. (**B**) Scout view with cross-sectional images of posterior part of right mandible. (**C**) Cross-sectional images of anterior part of right mandible (courtesy of Drs. S. C. White and S. Tetradis, UCLA School of Dentistry)

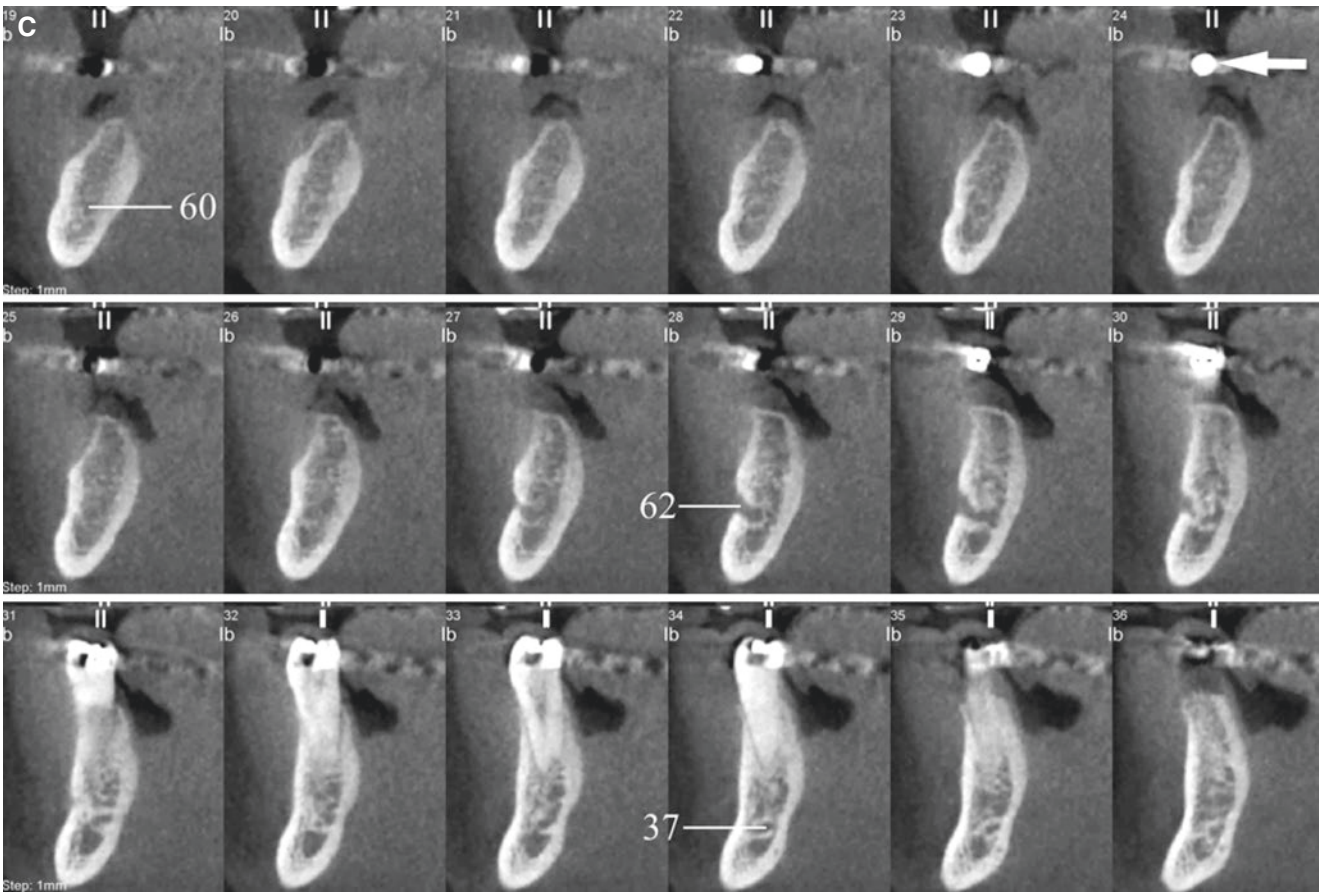

Fig. 1.5 (continued)

1.6 Schematic Drawing: Floor of the Mouth

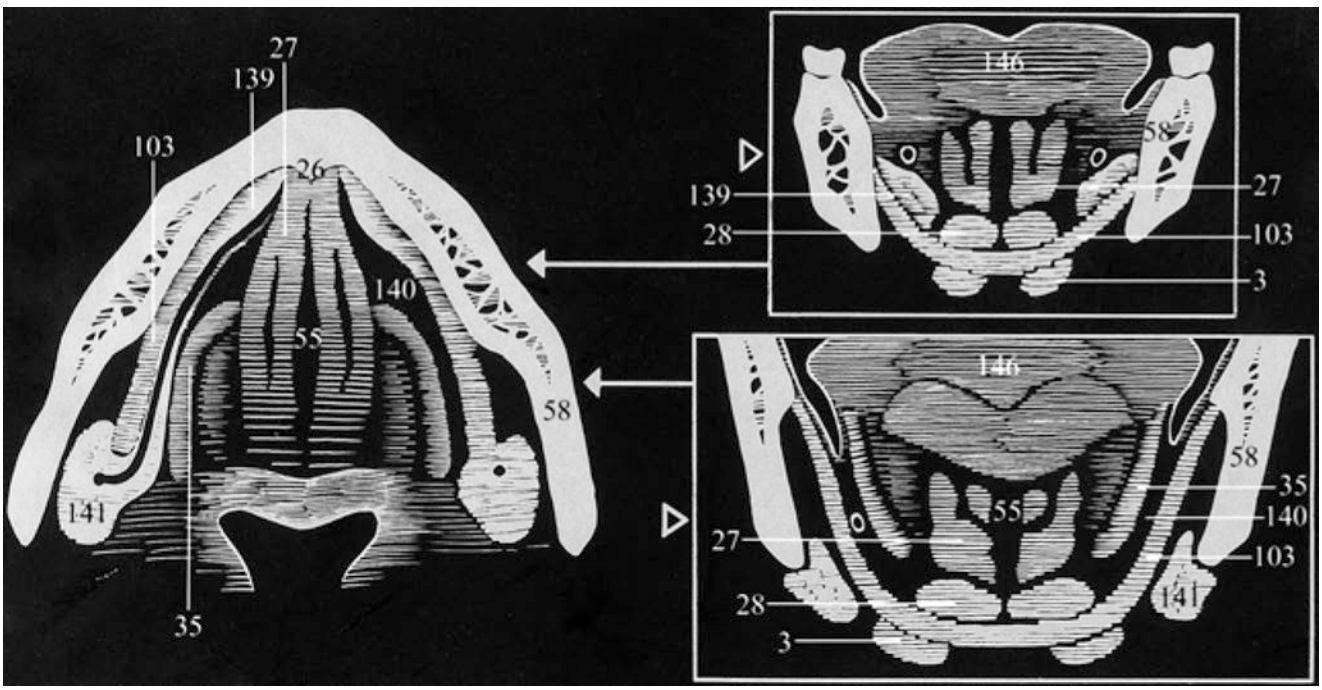

Fig. 1.6 Normal floor of the mouth anatomy; schematic drawing of one axial and two coronal sections (reproduced with permission from Aasen and Kolbenstvedt 1992)

1.7 CT Sections: Soft-Tissue Structures

Axial

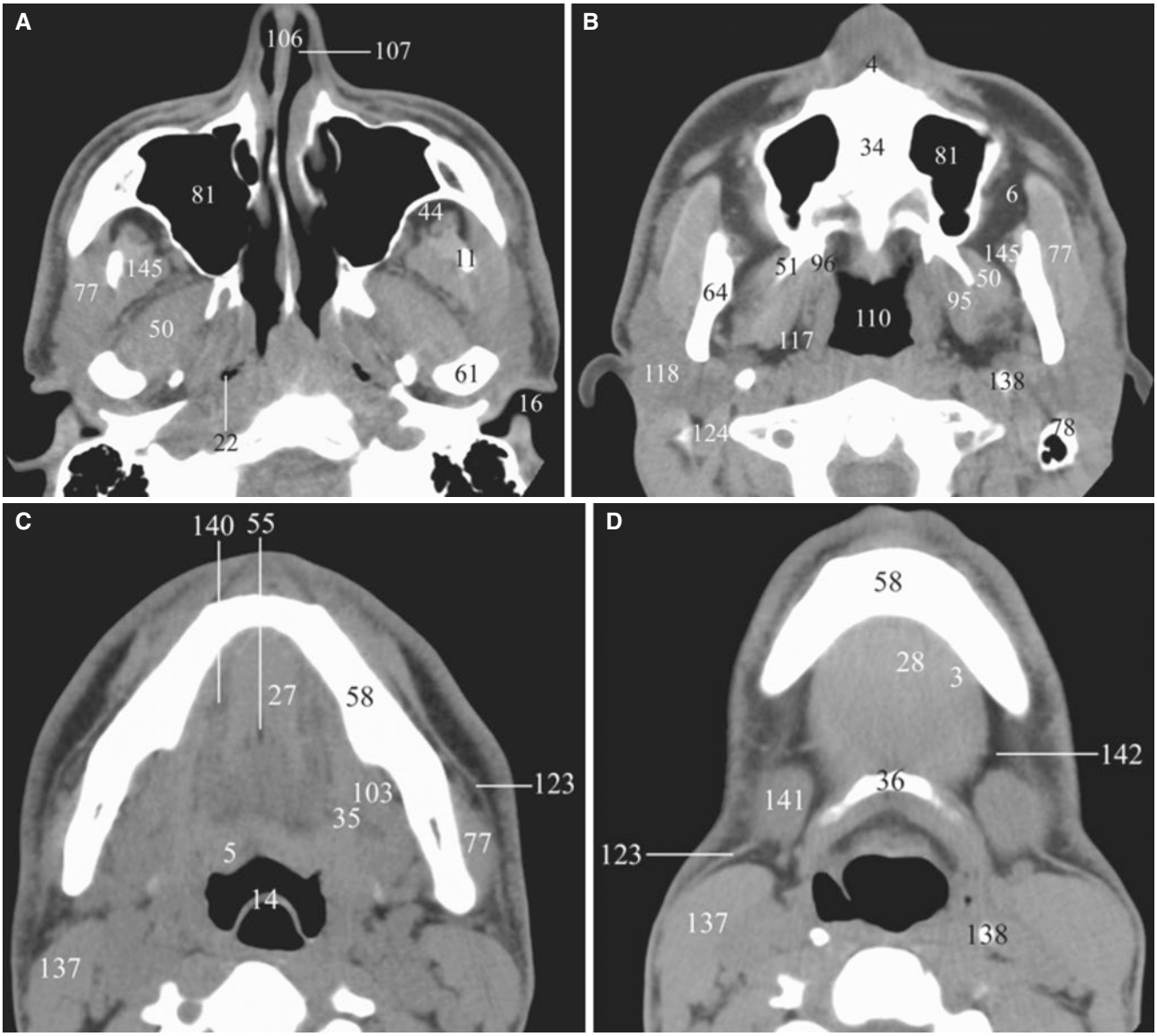

Fig. 1.7 Normal soft-tissue anatomy of the face; axial CT images from superior (**A**) to inferior (**D**)

Coronal

Fig. 1.8 Normal soft-tissue anatomy of the face; coronal CT images from anterior (**A**) to posterior (**D**)

1.8 MR Sections

Axial

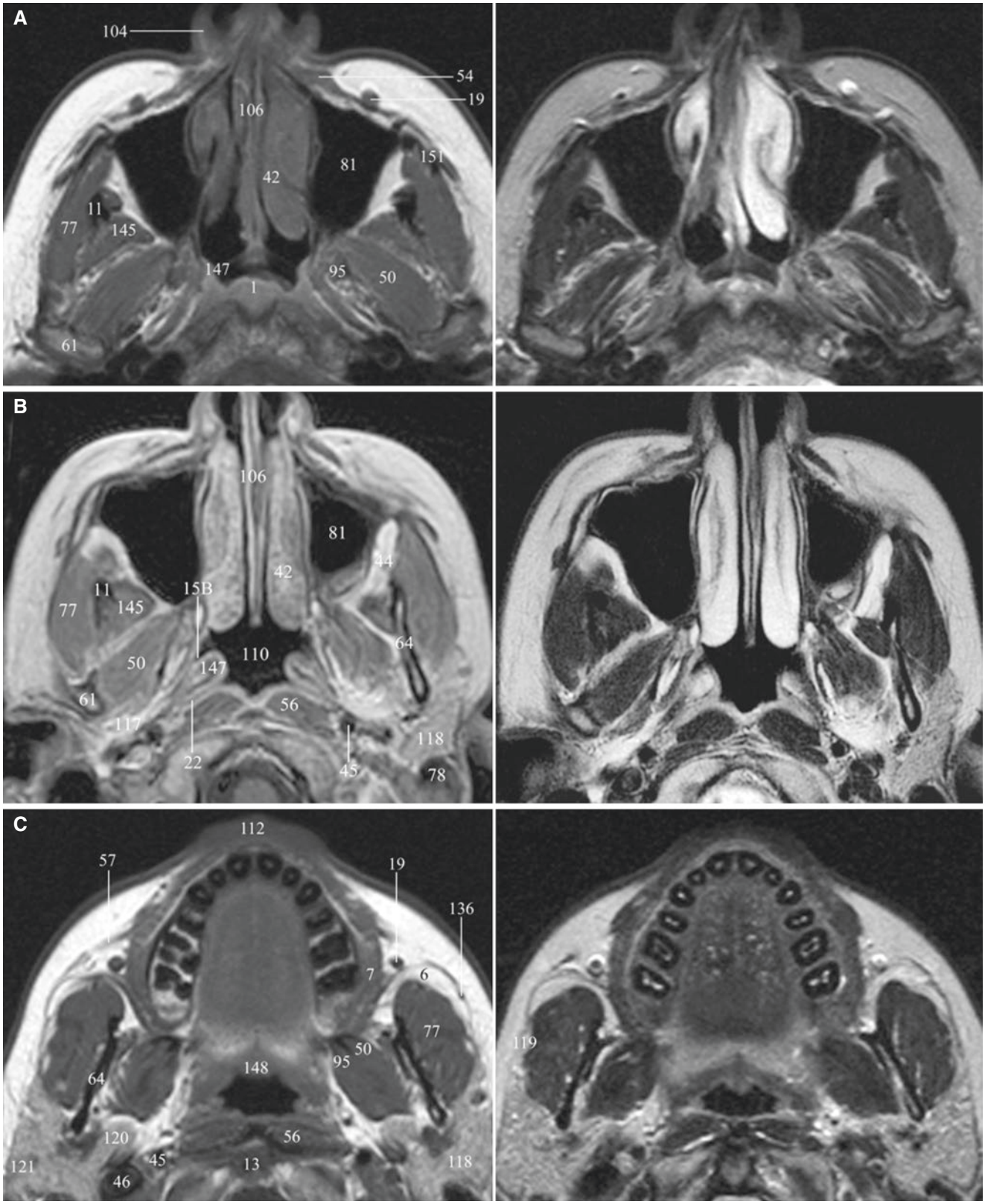

Fig. 1.9 Normal anatomy of the face; axial T1- and T2-weighted MR images from superior (**A**) to inferior (**G**)

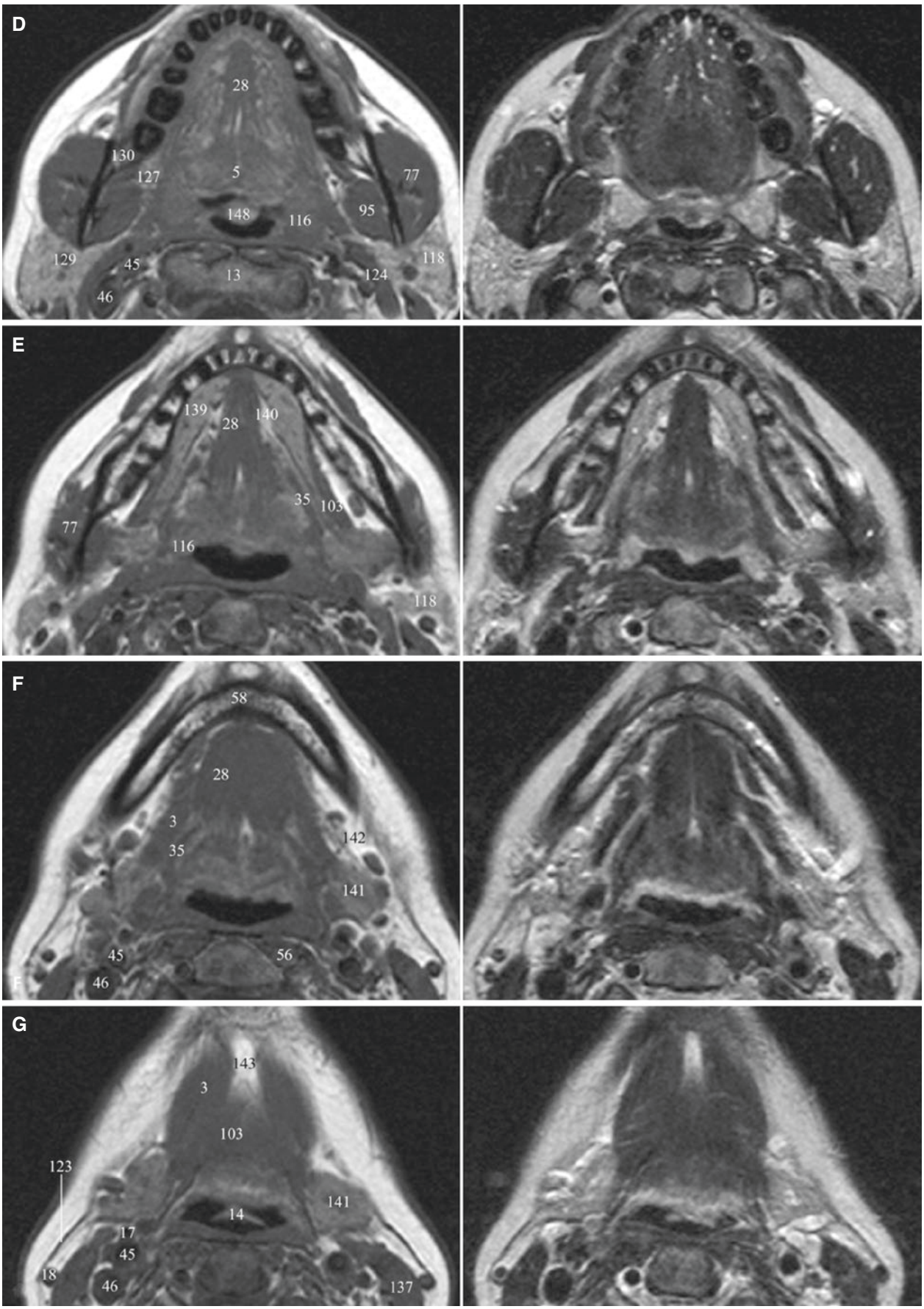

Fig. 1.9 (continued)

Coronal

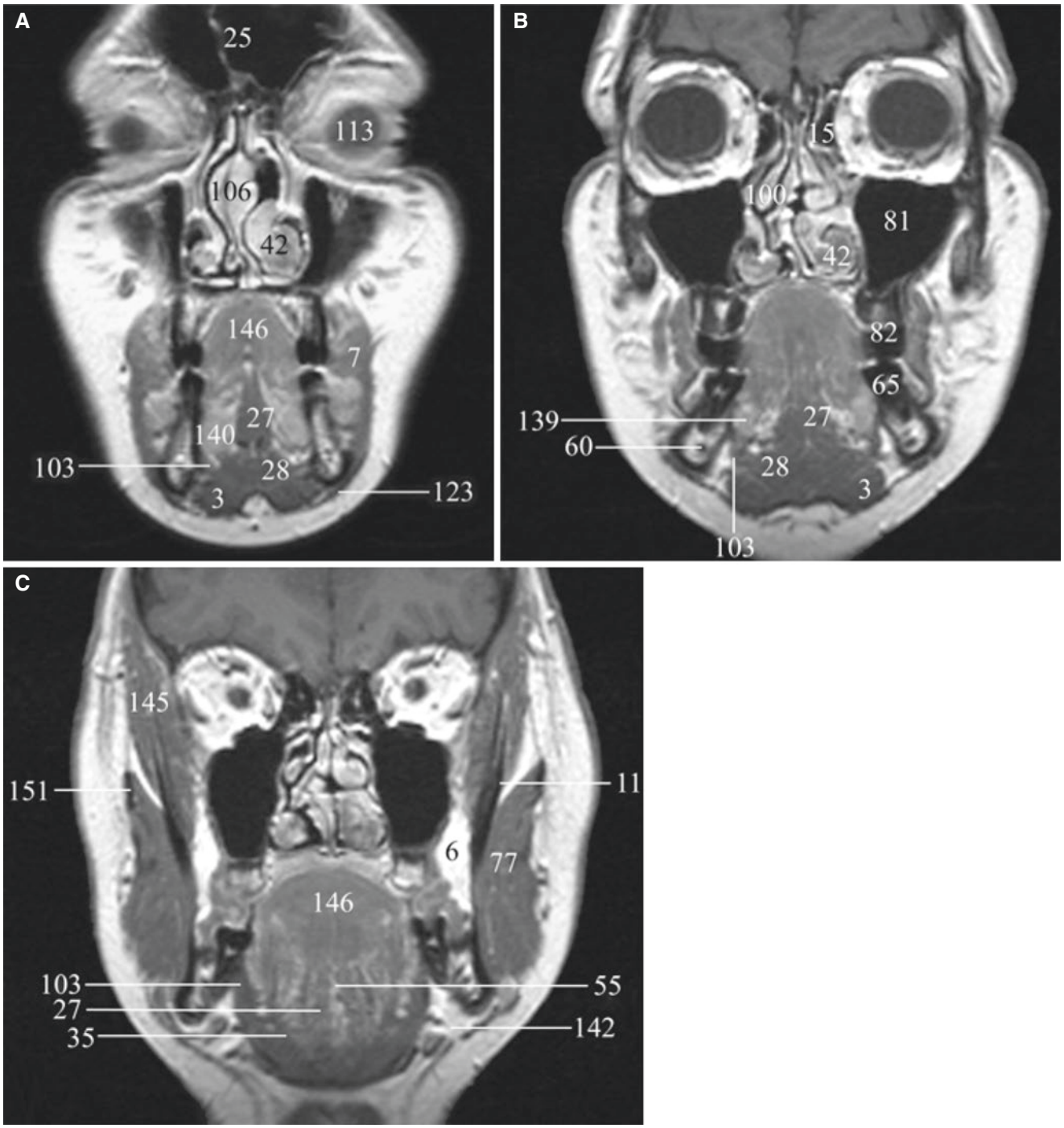

Fig. 1.10 Normal anatomy of the face; coronal T1-weighted post-Gd MR images from anterior (**A**) to posterior (**C**)

The anatomic structures in Figs. 1.11, 1.12, 1.13, 1.14, 1.15, 1.16, 1.17, and 1.18:

1. Anterior band of articular disc
2. Articular disc
3. Articular tubercle (eminence)
4. Glenoid fossa
5. Inferior joint space
6. Intermediate (central) thin zone
7. Lateral pterygoid muscle raphe
8. Interior head of lateral pterygoid muscle
9. Mandibular condyle (head)
10. Mandibular condyle articulating surface
11. Mandibular condyle marrow
12. Posterior band of articular disc
13. Posterior disc attachment
14. Superior joint space
15. Superior head of lateral pterygoid muscle

1.9 Temporomandibular Joint

Proton density (PD)-weighted or T1-weighted sequences are applied to obtain oblique sagittal and oblique coronal MR images, if sequences are not mentioned in legends.

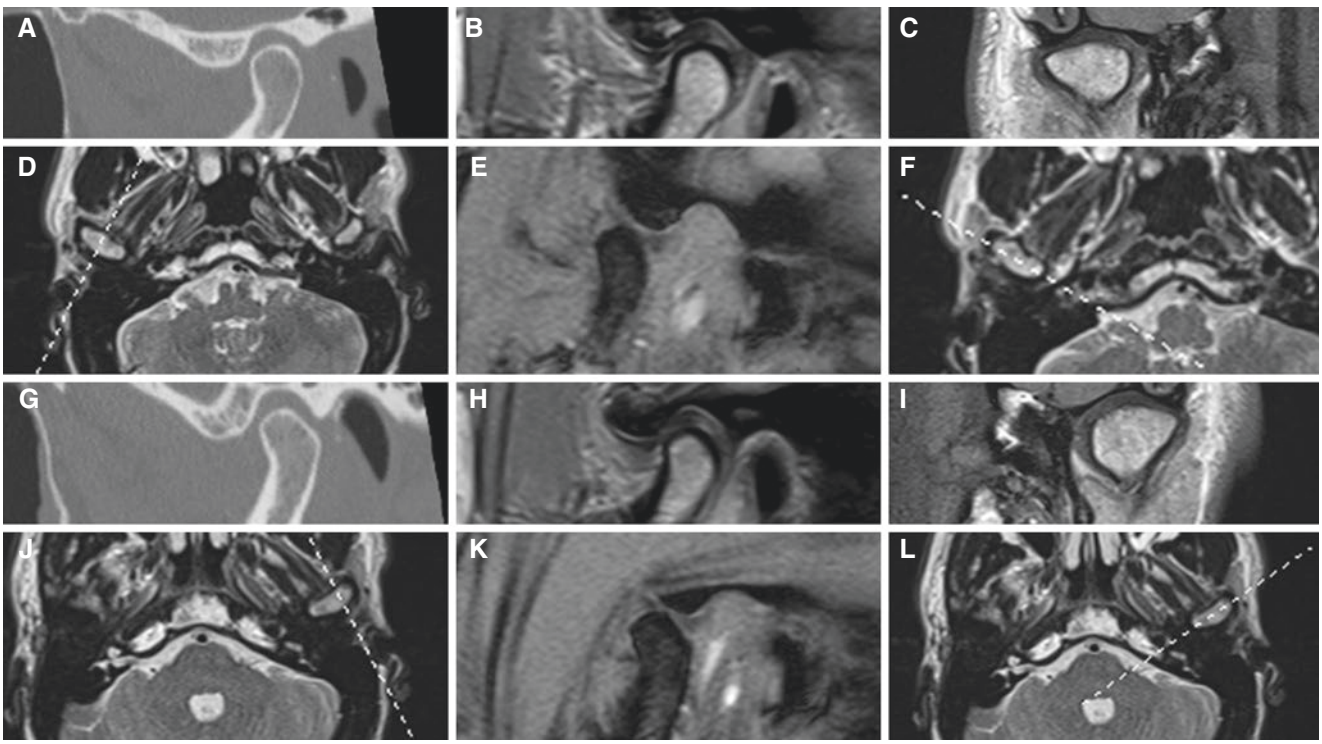

Fig. 1.11 Normal temporomandibular joint bone, disc, and function; 47-year-old male with myalgia. (**A**–**F**) Right joint. (**G**–**L**) Left joint. (**A**, **G**) Oblique sagittal CT at closed mouth. (**B**, **H**) Oblique sagittal MRI at closed mouth. (**C**, **I**) Oblique coronal MRI at closed mouth. (**D**, **J**) Axial MRI (cursor lines for oblique sagittal images). (**E**, **K**) Oblique sagittal open-mouth gradient-echo MRI. (**F**, **L**) Axial MRI (cursor lines for oblique coronal images)

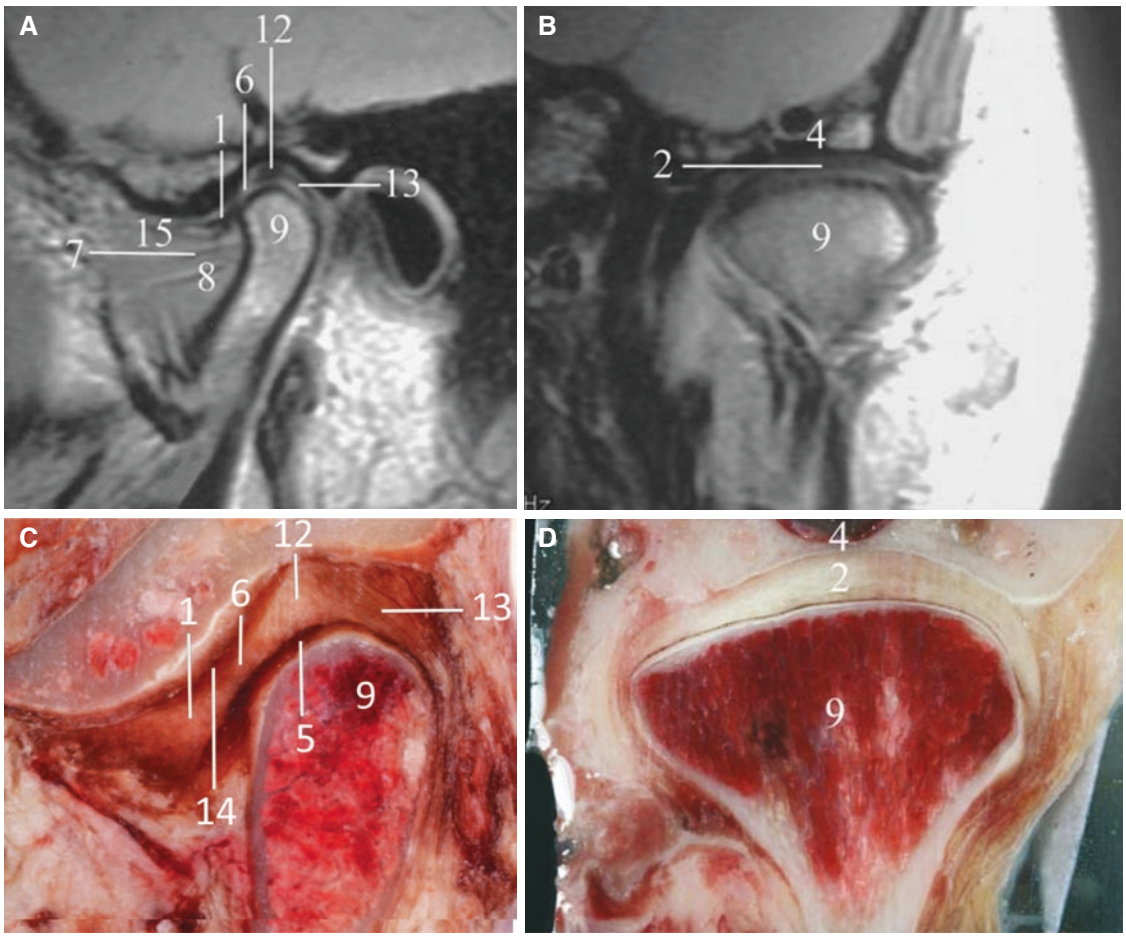

Fig. 1.12 Normal bone and disc (mid-condyle) anatomy; MRI (**A**, **B**) and autopsy specimen (**C**, **D**). (**A**) Oblique sagittal MRI. (**B**) Oblique coronal MRI. (**C**) Oblique sagittal autopsy section. (**D**) Oblique coronal autopsy section

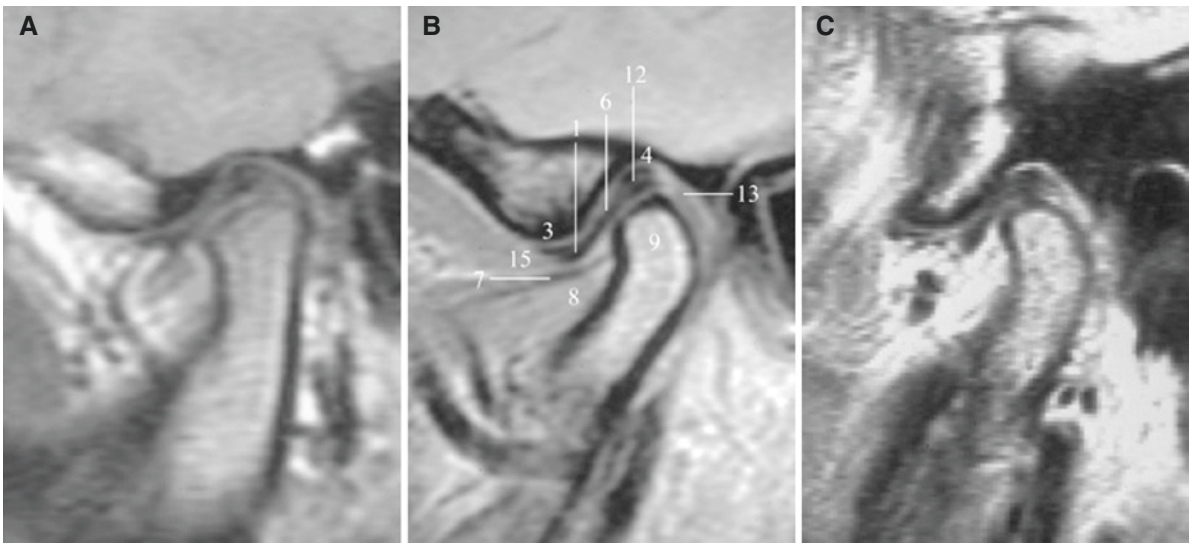

Fig. 1.13 Normal bone and disc anatomy, asymptomatic volunteers; oblique sagittal MRI. (**A**) 9-year-old, (**B**) 40-year-old, (**C**) 56-year-old (**C** reproduced with permission from Larheim et al. 2001a)

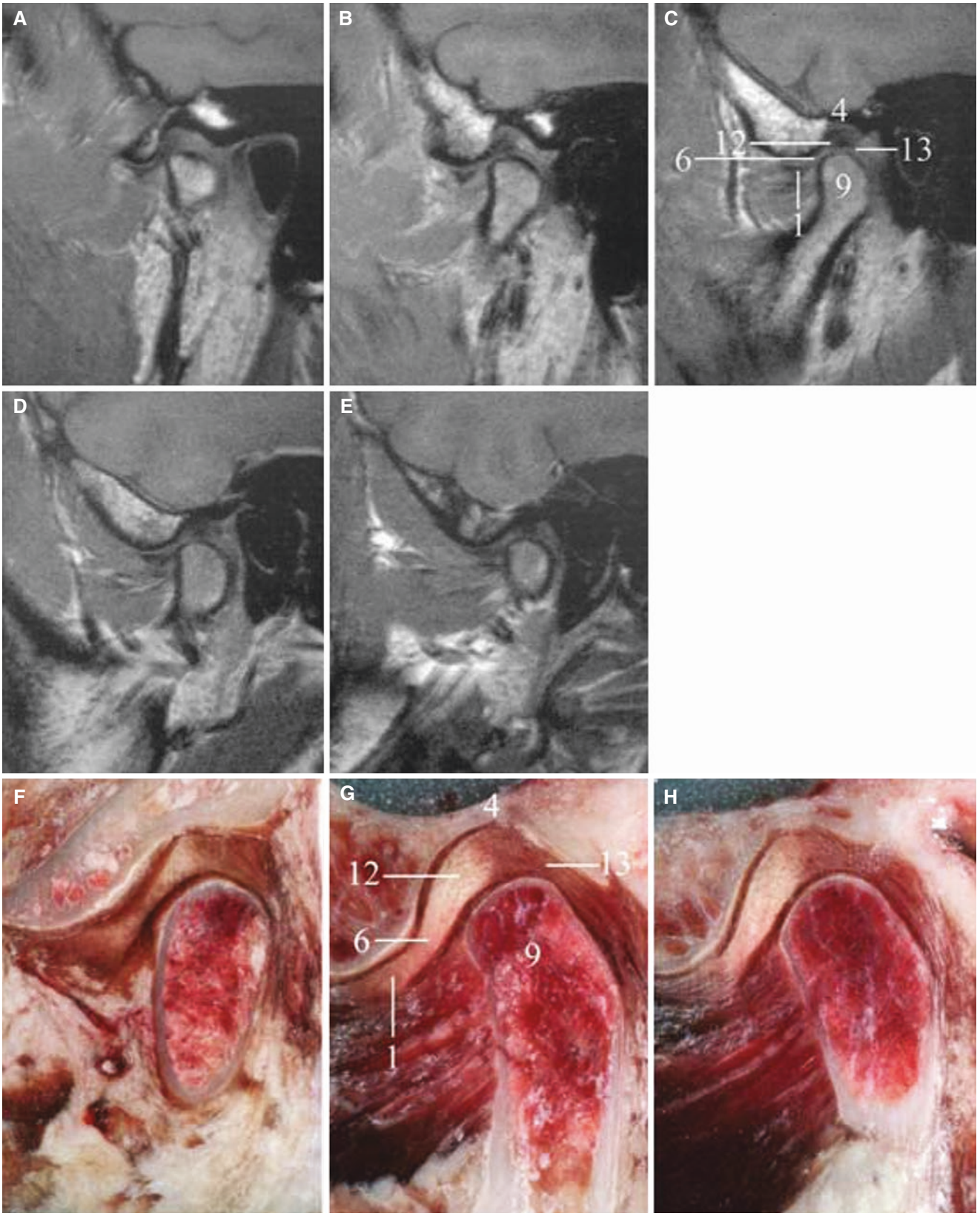

Fig. 1.14 Normal bone and disc anatomy throughout joint, asymptomatic volunteer; oblique sagittal MRI from lateral (**A**) to medial (**E**). Oblique sagittal autopsy sections from lateral (**F**) to medial (**H**)

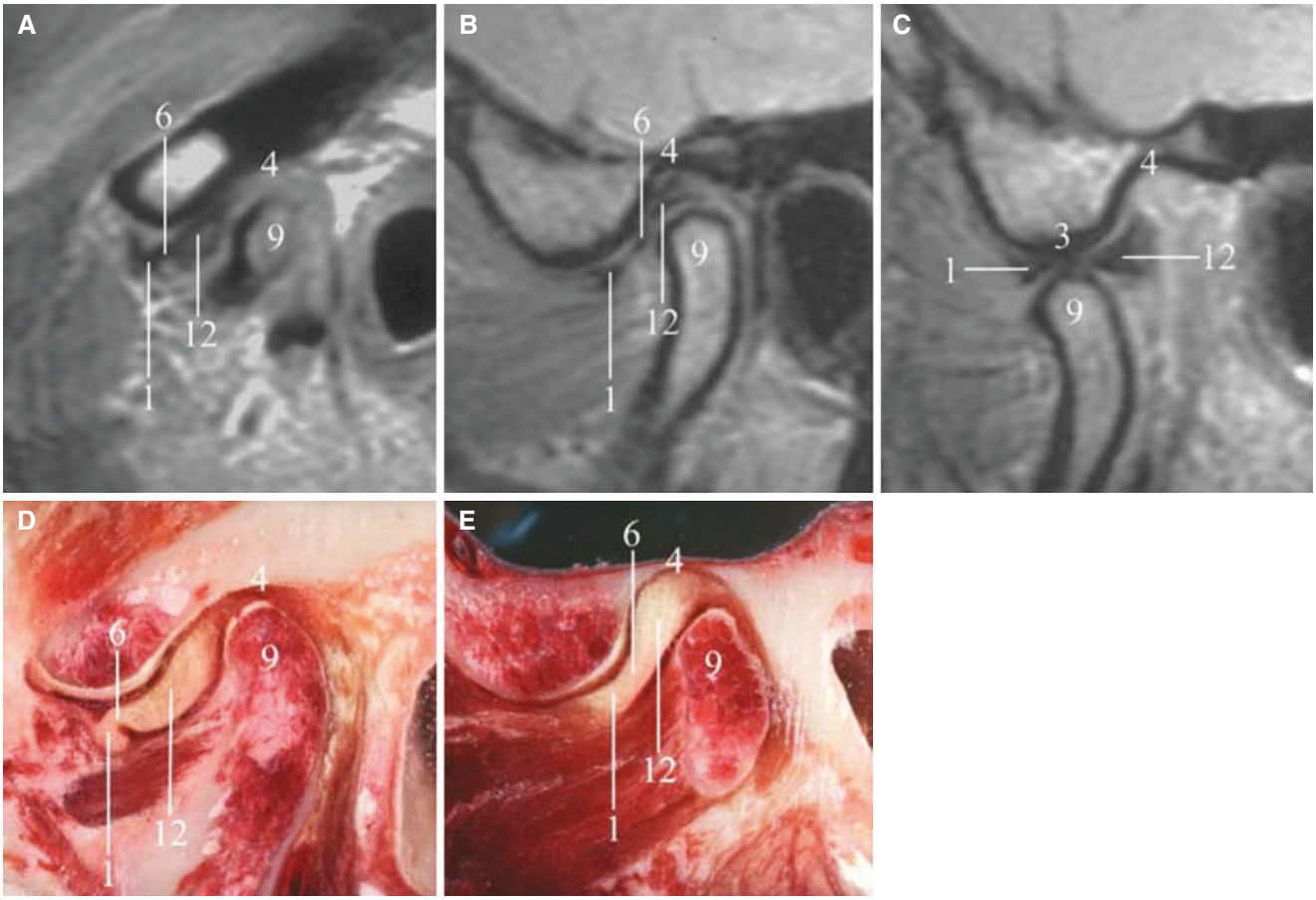

Fig. 1.15 Partial disc displacement (disc displaced only in one part of the joint) with reduction, asymptomatic volunteer; oblique sagittal MRI (**A**–**C**) and oblique sagittal sections of autopsy specimen (**D**, **E**). (**A**, **D**) Lateral sections show anteriorly displaced disc. (**B**, **E**) Centromedial sections show normally located disc. (**C**) Open-mouth MRI shows normally located disc (**A**–**C** reproduced with permission from Larheim et al. 2001a)

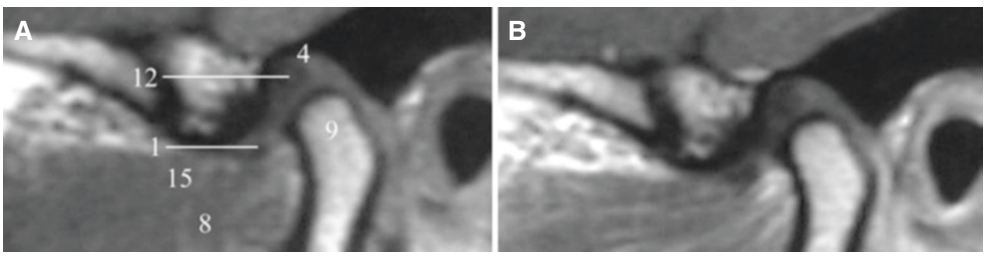

Fig. 1.16 Normal bone and disc anatomy, asymptomatic volunteer; i.v. injection of contrast medium. (**A**) Oblique sagittal T1-weighted pre-Gd and (**B**) oblique sagittal T1-weighted post-Gd MRI show no or minimal contrast enhancement

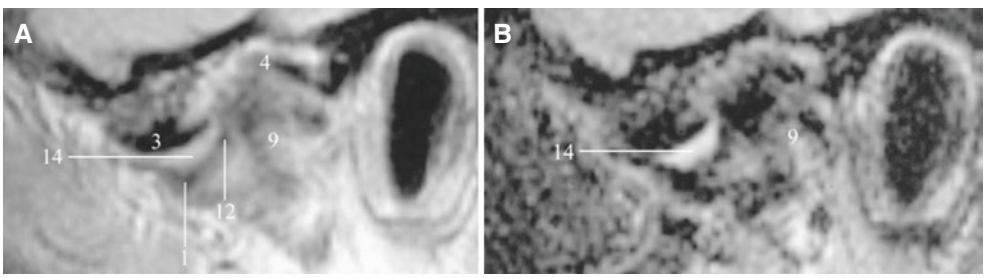

Fig. 1.17 Joint fluid, asymptomatic volunteer. (**A**) Oblique sagittal T1-weighted and (**B**) oblique sagittal T2-weighted MRI show increased signal intensity from upper joint space of anterior recess on T2-weighted image (reproduced with permission from Larheim et al. 2001b)

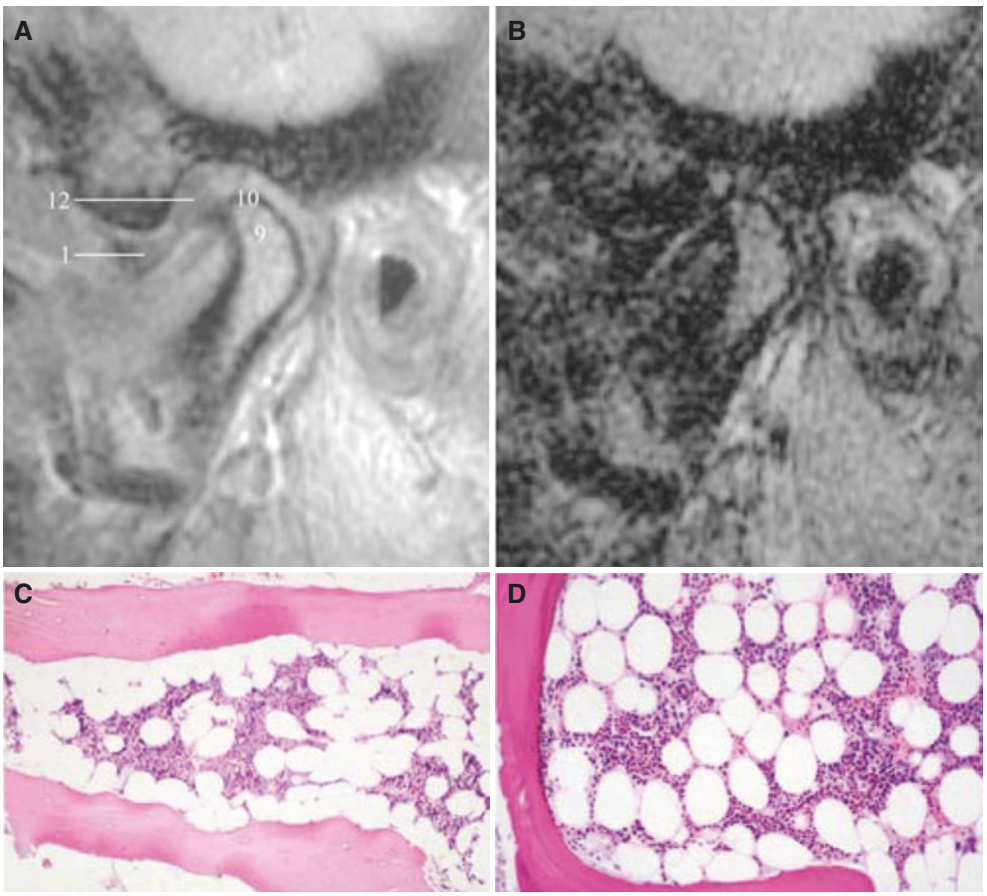

Fig. 1.18 Normal mandibular condyle bone marrow histology, patient surgically treated for painful disc displacement and osteoarthritis; MRI (**A**, **B**) and core biopsy (**C**). (**A**) Oblique sagittal T1-weighted and (**B**) oblique sagittal T2-weighted MRI show normal homogeneous signal intensity from condyle bone marrow. (**C**) Bone marrow biopsy shows normal hematopoietic elements interspersed with marrow fat. (**D**) Normal bone marrow histology of the hip for comparison (**A**, **B**, **C** reproduced with permission from Larheim et al. 1999)

Suggested Reading

Aasen S, Kolbenstvedt A (1992) CT appearances of normal and obstructed submandibular duct. Acta Radiol 33:414–419

Abrahams JJ, Rock R, Hayt MW (2003) Embryology and anatomy of the jaw and dentition. In: Som PM, Curtin HD (eds) Head and neck imaging, 4th edn. Mosby, St. Louis, pp 889–906

Brooks SL, Westesson P-L, Eriksson L, Hansson LG, Barsotti JB (1992) Prevalence of osseous changes in the temporomandibular joint of asymptomatic persons without internal derangement. Oral Surg Oral Med Oral Pathol 73:118–122

Katzberg RW, Westesson P-L, Tallents RH, Drake CM (1996) Anatomic disorders of the temporomandibular joint disc in asymptomatic subjects. J Oral Maxillofac Surg 54:147–153

Larheim TA, Westesson P-L, Hicks DG, Eriksson L, Brown DA (1999) Osteonecrosis of the temporomandibular joint: correlation of magnetic resonance imaging and histology. J Oral Maxillofac Surg 57:888–898

Larheim TA, Westesson P-L, Sano T (2001a) Temporomandibular joint disk displacement: comparison in asymptomatic volunteers and patients. Radiology 218:428–432

Larheim TA, Katzberg RW, Westesson P-L, Tallents RH, Moss ME (2001b) MR evidence of temporomandibular joint fluid and condyle marrow alterations: occurrence in asymptomatic volunteers and symptomatic patients. Int J Oral Maxillofac Surg 30:113–117

Mallaya SM, Tetradis S (2014) Cone-beam computed tomography: anatomy. In: White SC, Pharoah MJ (eds) Oral radiology. Principles and interpretation, 7th edn. Mosby, St. Louis, pp 214–228

Smith H-J, Larheim TA, Aspestrand F (1992) Rheumatic and non-rheumatic disease in the temporomandibular joint: Gadolinium-enhanced MR imaging. Radiology 185:229-234

Smoker WRK (2003) The oral cavity. In: Som PM, Curtin HD (eds) Head and neck imaging, 4th edn. Mosby, St. Louis, pp 1377–1464

Som PM, Shugar JMA, Brandwein MS (2003a) Sinonasal cavities: anatomy and physiology. In: Som PM, Curtin HD (eds) Head and neck imaging, 4th edn. Mosby, St. Louis, pp 87–147

Som PM, Smoker WRK, Balboni A, Reidenberg JS, Hudgins PA, Weissman JL, Laitman J (2003b) Embryology and anatomy of the neck. In: Som PM, Curtin HD (eds) Head and neck imaging, 4th edn. Mosby, St. Louis, pp 1757–1827

Jaw Cysts and Cyst-Like Conditions

2

Abstract

This chapter illustrates cysts; periapical and residual cyst, paradental cyst, lateral periodontal cyst, incisive canal cyst, follicular (dentigerous) cyst, glandular odontogenic cyst, and cyst-like conditions; simple bone cyst, Stafne bone cyst, and retention cyst.

2.1 Introduction

Cysts in the jaws are common and mostly diagnosed and managed by general dental practitioners and dental specialists using intraoral or panoramic radiography. However, advanced imaging modalities are increasingly used to assess more precisely those that are larger and cannot be adequately diagnosed, i.e., distinguished from other types of lesions, with conventional radiography. Advanced imaging is particularly valuable for lesions in the maxilla to assess their impact on neighboring structures. We present a number of cases richly illustrated, including CT and MR images, to give specialists both in the dental and in the medical field an opportunity to become familiar with the spectrum of appearances they represent.

2.2 Cysts

2.2.1 Definition

Epithelial-lined cavity containing fluid or semifluid material, surrounded by fibrous tissue.

Most jaw cysts originate from odontogenic epithelial residues after tooth development.

A jaw cyst may also be defined as a pathological cavity having fluid, semifluid, or gaseous contents and which is not created by accumulation of pus.

Although cysts in general are epithelial-lined, there are non-epithelial-lined cysts, which most pathologists prefer to describe as pseudocysts. Those included in this chapter are described under the heading Cyst-Like Conditions. Aneurysmal bone cyst, also named aneurysmal bone cavity, is described in Chap. 3 under the heading Tumorlike Conditions.

2.2.2 Clinical Features (General)

- Usually an incidental imaging finding
- Occasional swelling and jaw asymmetry
- No pain if not infected

2.2.3 Imaging Features (General)

- Radiolucency in bone (density in the maxillary sinus)
- Unilocular round, oval or scalloped, or influenced by surrounding structures
- Border well-defined thin, uniform, intact, and sclerotic
- May expand bone
- May displace or resorb teeth
- May displace walls of the maxillary sinus, nasal cavity, and mandibular canal
- When secondarily infected, border may become destroyed or more sclerotic
- Rarely, border may show defect also without infection
- Rarely, calcified tissue may be produced
- T1-weighted MRI: homogeneous intermediate signal (fluid content) or occasionally homogeneous high signal (cholesterol content)
- T2-weighted and STIR MRI: homogeneous high or occasionally homogeneous low signal or occasionally heterogeneous signal (high to intermediate to low), consistent with fluid or semifluid (large molecules, granulation tissue) content

In collaboration with H.-J. Smith · H. Strømme Koppang.

T.A. Larheim, P.-L.A. Westesson, *Maxillofacial Imaging*, https://doi.org/10.1007/978-3-319-53319-3_2

– T1-weighted post-Gd MRI: no enhancement, or enhancement of peripheral thin rim (partial or complete), consistent with cyst capsule
– T1-weighted and T2-weighted MRI: homogeneous high signal reported to be specific for nasopalatine duct cyst

For the pseudocysts; simple bone cyst, Stafne bone cyst, and retention cyst, see specific features under each entity.

2.3 Periapical Cyst

Figs. 2.1, 2.2, 2.3, 2.4, 2.5, 2.6, 2.7, 2.8, 2.9, and 2.10

Synonyms: Radicular cyst (WHO), apical periodontal cyst, dental cyst

2.3.1 Definition

Cyst arising from epithelial residues (rests of Malassez) in periodontal ligament as a consequence of inflammation, usually following death of dental pulp (WHO).

By histologic sectioning of periapical lesions, two types of periapical cysts have been demonstrated: one type with a close connection to tooth root ("pocket" cyst) and another type without such a connection ("true" cyst).

2.3.2 Clinical Features

– Odontogenic
– Inflammatory
– At or around a tooth root or lateral to root
– Nonvital tooth
– Most common type of jaw cyst
– Maxilla and mandible
– Anterior region of the maxilla in particular
– Males more frequent than females
– All ages, particularly third and fourth decades, but seldom in deciduous dentition

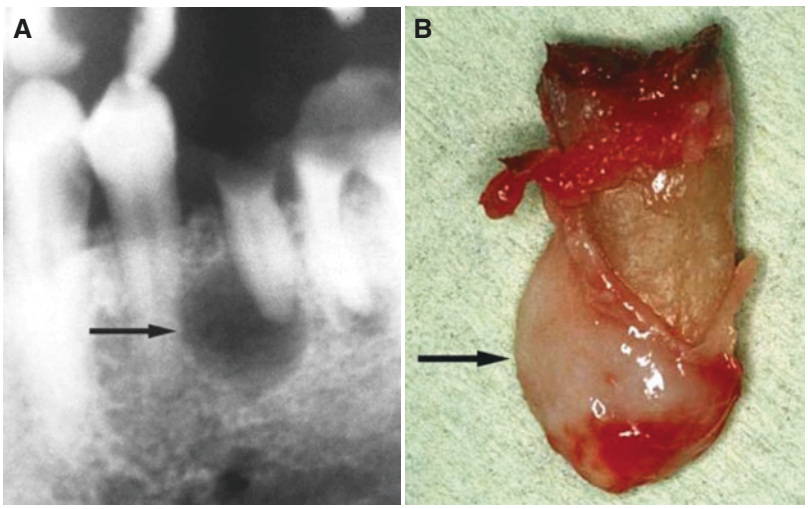

Fig. 2.1 Periapical cyst, mandible; asymptomatic, nonvital tooth root. (**A**) Panoramic view shows round radiolucency with sclerotic border (*arrow*). (**B**) Surgically removed tooth with cyst (*arrow*)

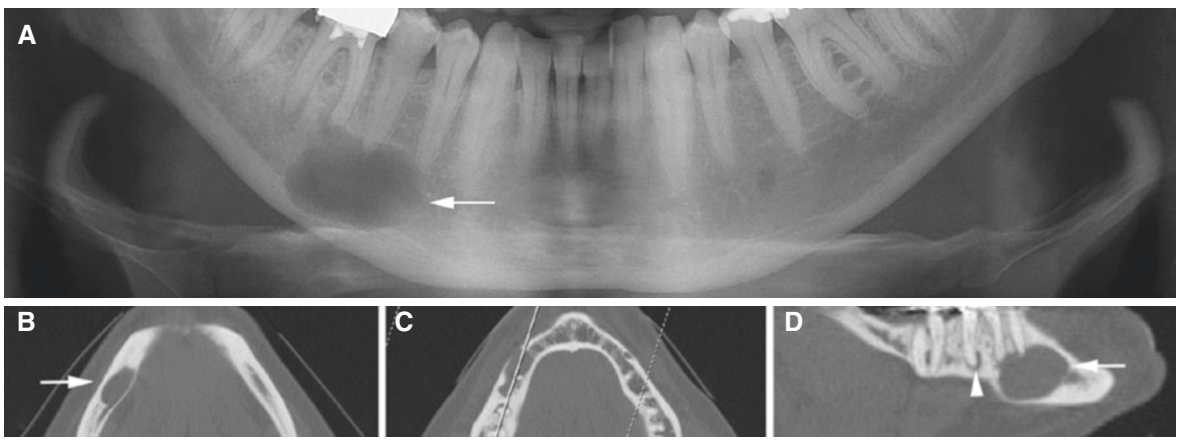

Fig. 2.2 Periapical cyst, mandible; 44-year-old male with incidental finding at routine dental radiography. (**A**) Panoramic view shows oval radiolucency (*arrow*) with connection to first molar (nonvital). (**B**) Axial and (**C**) axial (with cursor line) CT images show minimal buccolingual expansion (*arrow*). (**D**) Oblique sagittal CT image confirms connection between radiolucency and mesial root of first molar. Note small periapical radiolucency at distal root of first molar (*arrowhead*)

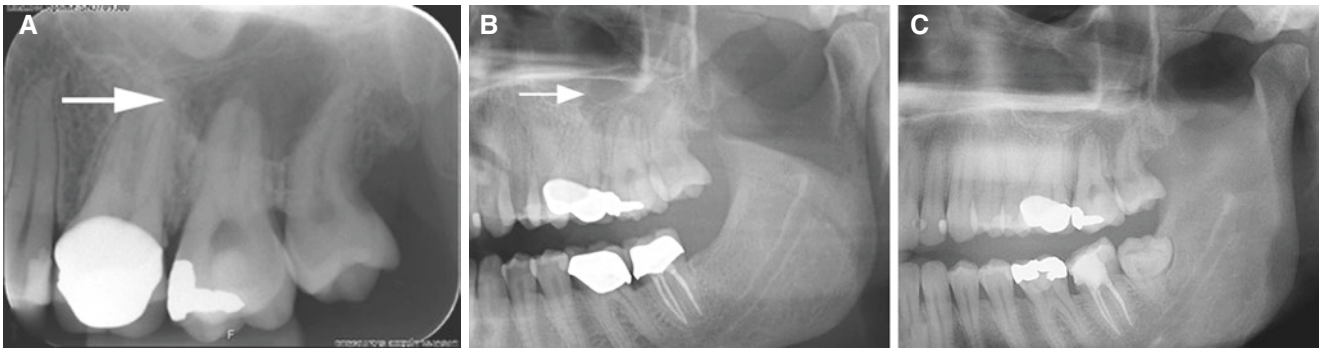

Fig. 2.3 Periapical cyst development, maxilla; 32-year-old female with some discomfort and palatal swelling in left molar region. (**A**) Intraoral view shows periapical radiolucency at second molar (*arrow*). (**B**) Panoramic view confirms radiolucency (*arrow*). (**C**) Panoramic view 2 years previously shows normal bone (*arrow*)

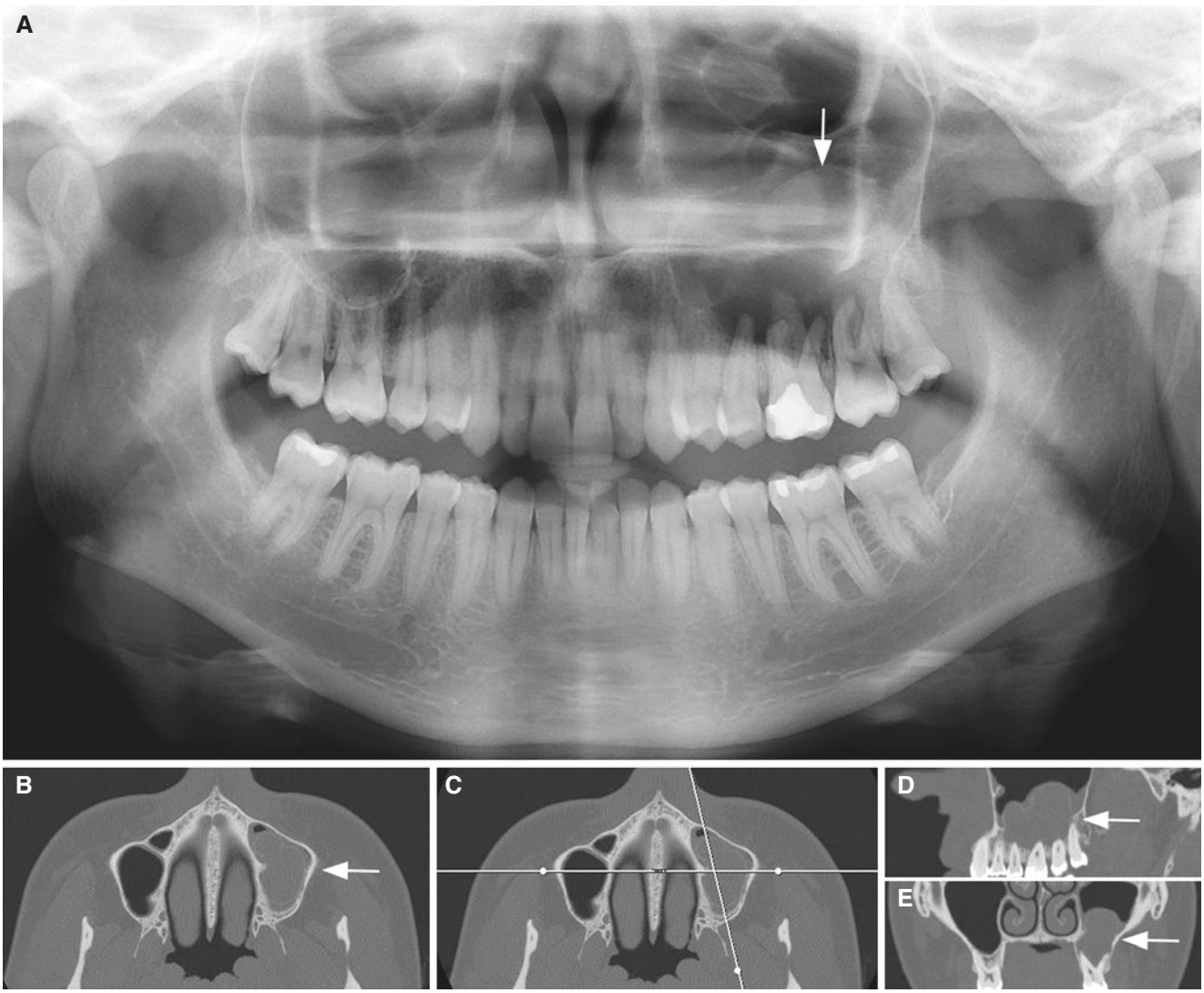

Fig. 2.4 Periapical cyst, maxilla; 23-year-old female with some discomfort and pressure in the left maxilla. (**A**) Panoramic view shows periapical radiolucency in the left maxilla/maxillary sinus (*arrow*) with lack of sinus delineation (compared with right side). (**B**, **C** Axial, **D**) oblique sagittal, and (**E**) coronal CT images show radiopacity with thin corticated outline in the left maxillary sinus (*arrow*)

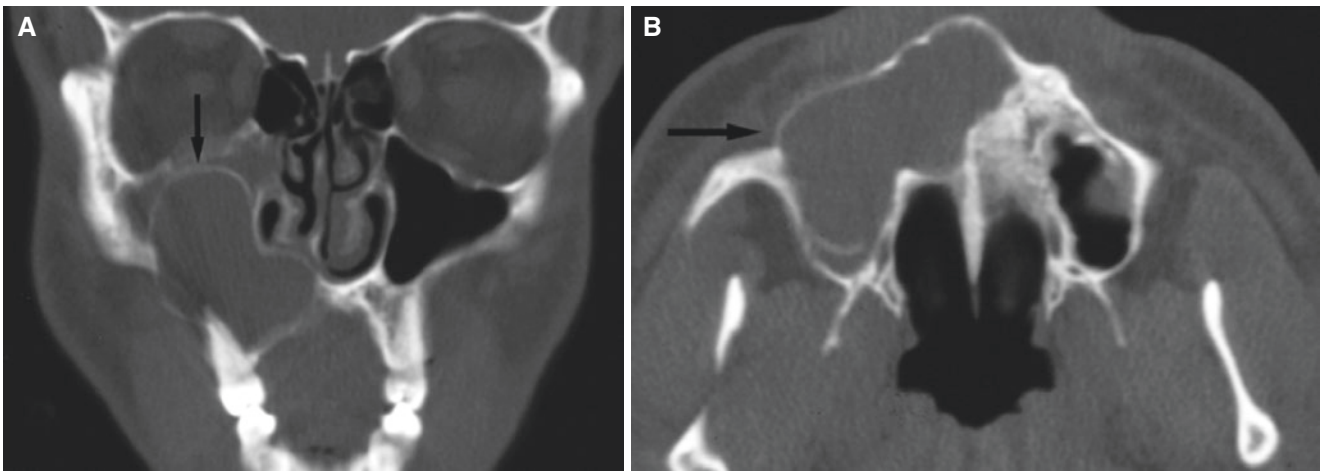

Fig. 2.5 Periapical cyst, maxilla; 38-year-old male with some discomfort and swelling of mucobuccal fold; nonvital right lateral incisor. (**A**) Coronal CT image shows expansive process displacing part of nasal cavity, with intact and sclerotic border, occupying most of the right maxillary sinus (*arrow*). (**B**) Axial CT image shows scalloped process destroying alveolar bone and hard palate (*arrow*)

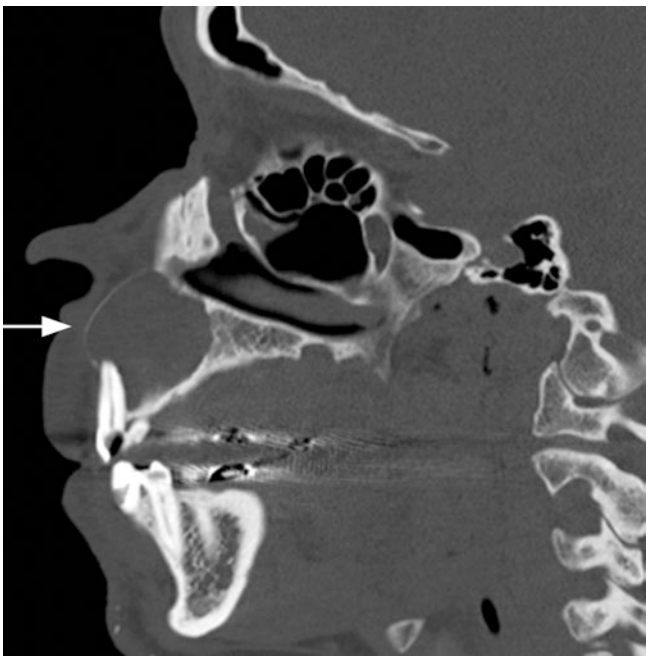

Fig. 2.6 Periapical cyst, maxilla; 26-year-old male with buccal swelling in front area. Sagittal CT image shows radiolucency with expansion and thin corticated outline (*arrow*) and caries destruction to pulp on nonvital incisor

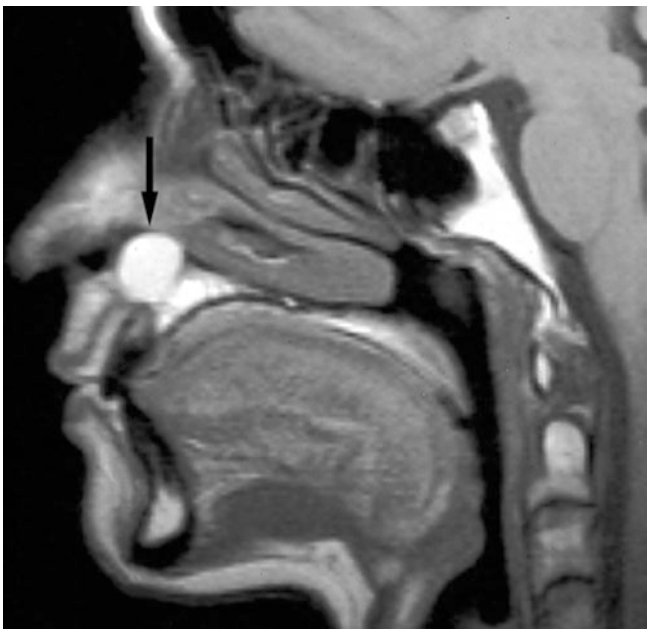

Fig. 2.7 Periapical cyst, maxilla; 58-year-old female with incidental finding at routine dental radiography, nonvital central incisor. Sagittal T1-weighted MRI shows oval expansive process with homogeneous high signal (*arrow*)

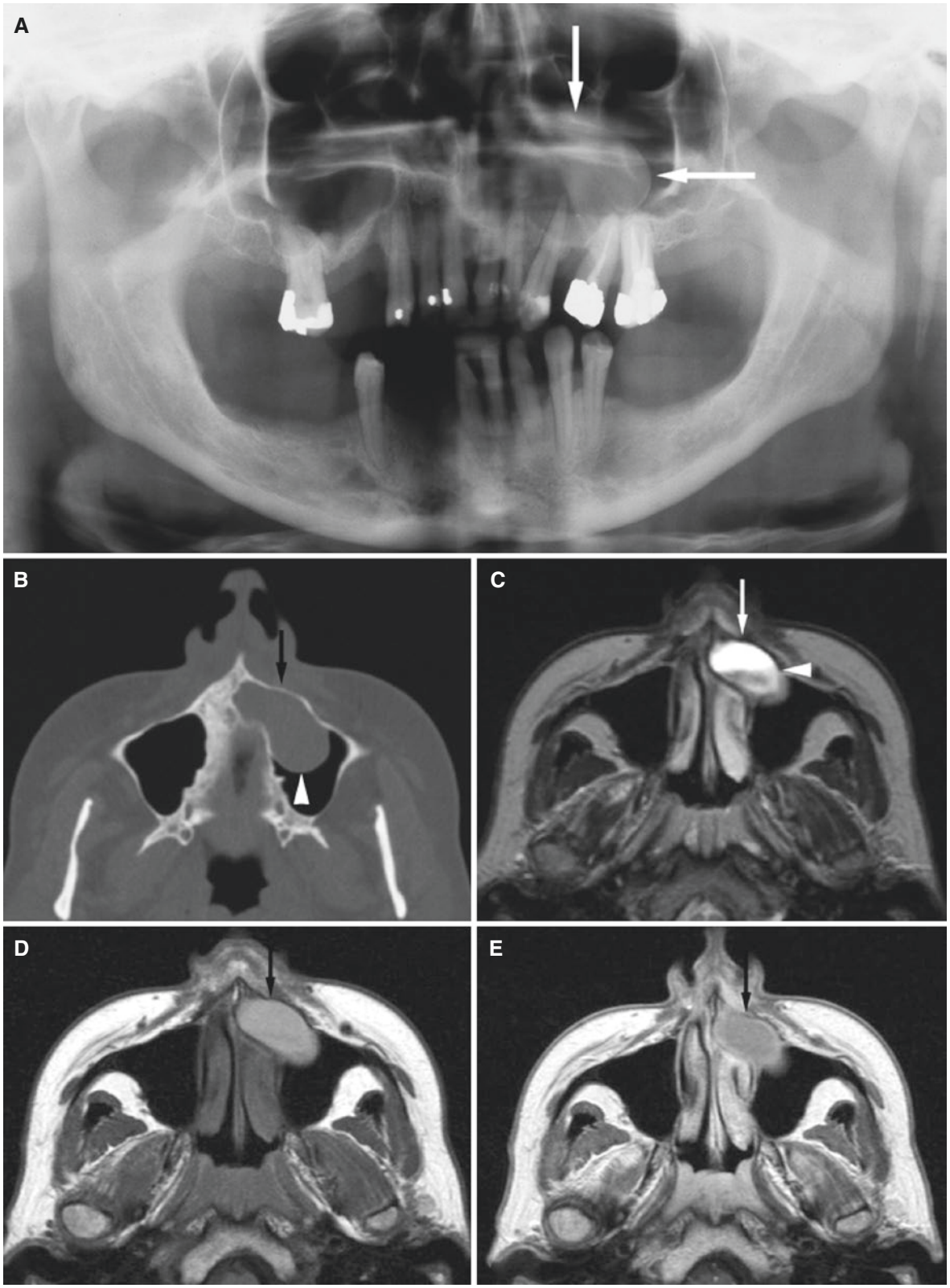

Fig. 2.8 Periapical cyst, maxilla; 45-year-old female with incidental finding at routine dental radiography, nonvital left lateral incisor. (**A**) Panoramic view shows round process (more dense than air) with sclerotic border (*arrows*). (**B**) Axial CT image shows expansive process (*arrow*) with intact sclerotic border in the maxillary sinus (*arrowhead*). (**C**) Axial T2-weighted MRI shows high-signal content (*arrow*) above intermediate-signal content in dependent part; *arrowhead* fluid level. (**D**) Axial T1-weighted pre-Gd MRI shows homogeneous intermediate signal (*arrow*). (**E**) Axial T1-weighted post-Gd MRI shows no enhancement except a thin peripheral rim (*arrow*)

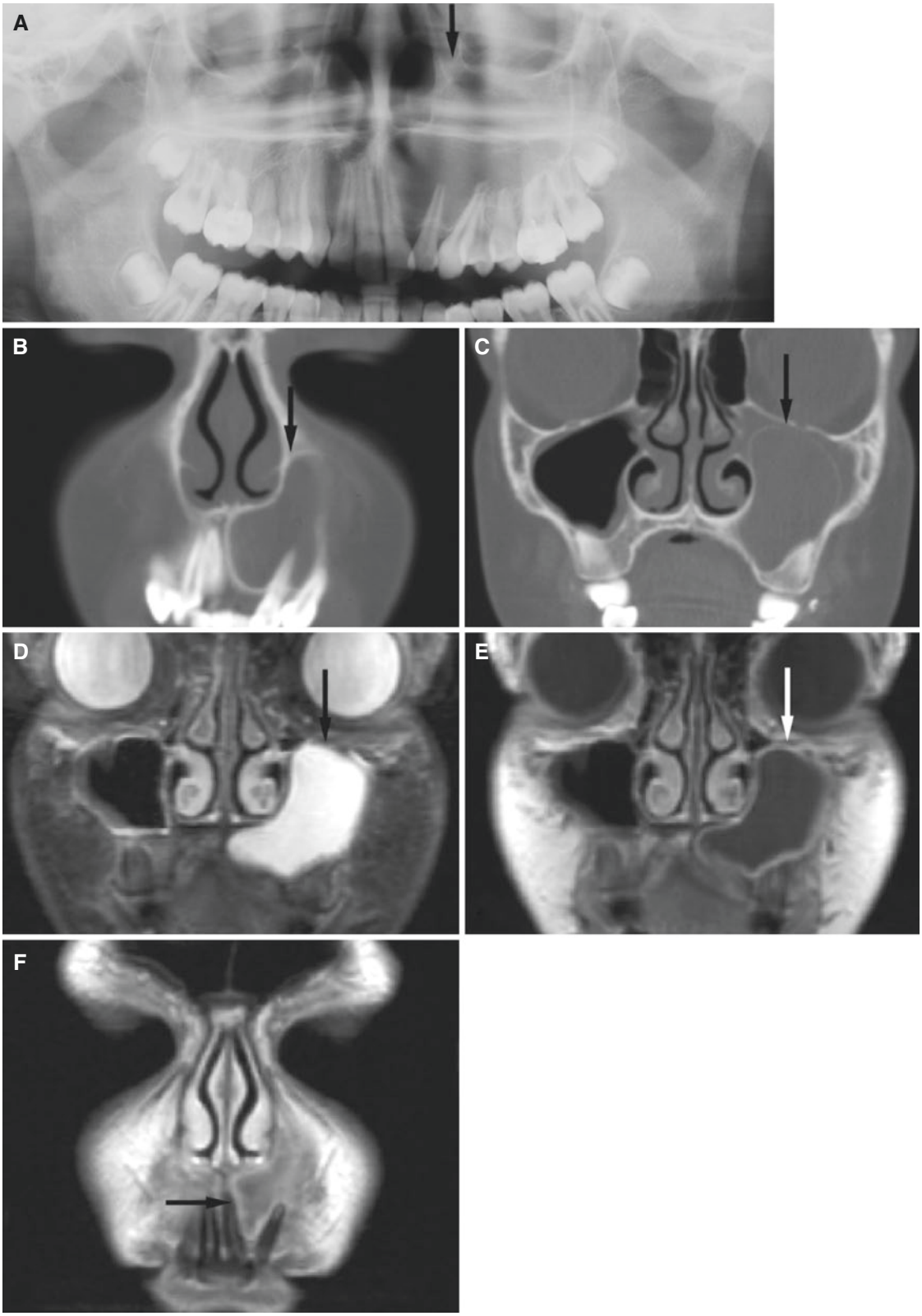

Fig. 2.9 Periapical cyst, maxilla; 13-year-old female with painless swelling of mucobuccal fold and nonvital left lateral incisor, with previous pain from incisor. (**A**) Panoramic view shows radiolucency with partially sclerotic border in alveolar process around left lateral incisor and lack of sinus demarcation (*arrow*) and deviation of central incisor and canine. (**B**) Coronal CT image shows expansive process with sclerotic border around incisor (*arrow*). (**C**) Coronal CT image shows process occupying most of the maxillary sinus with a very thin sclerotic border (*arrow*). (**D**) Coronal STIR MRI shows homogeneous high-signal content (*arrow*). (**E**) Coronal T1-weighted post-Gd MRI shows no enhancement except peripheral rim (*arrow*). (**F**) Coronal T1-weighted post-Gd MRI shows rim of enhancement and displacement of teeth (*arrow*)

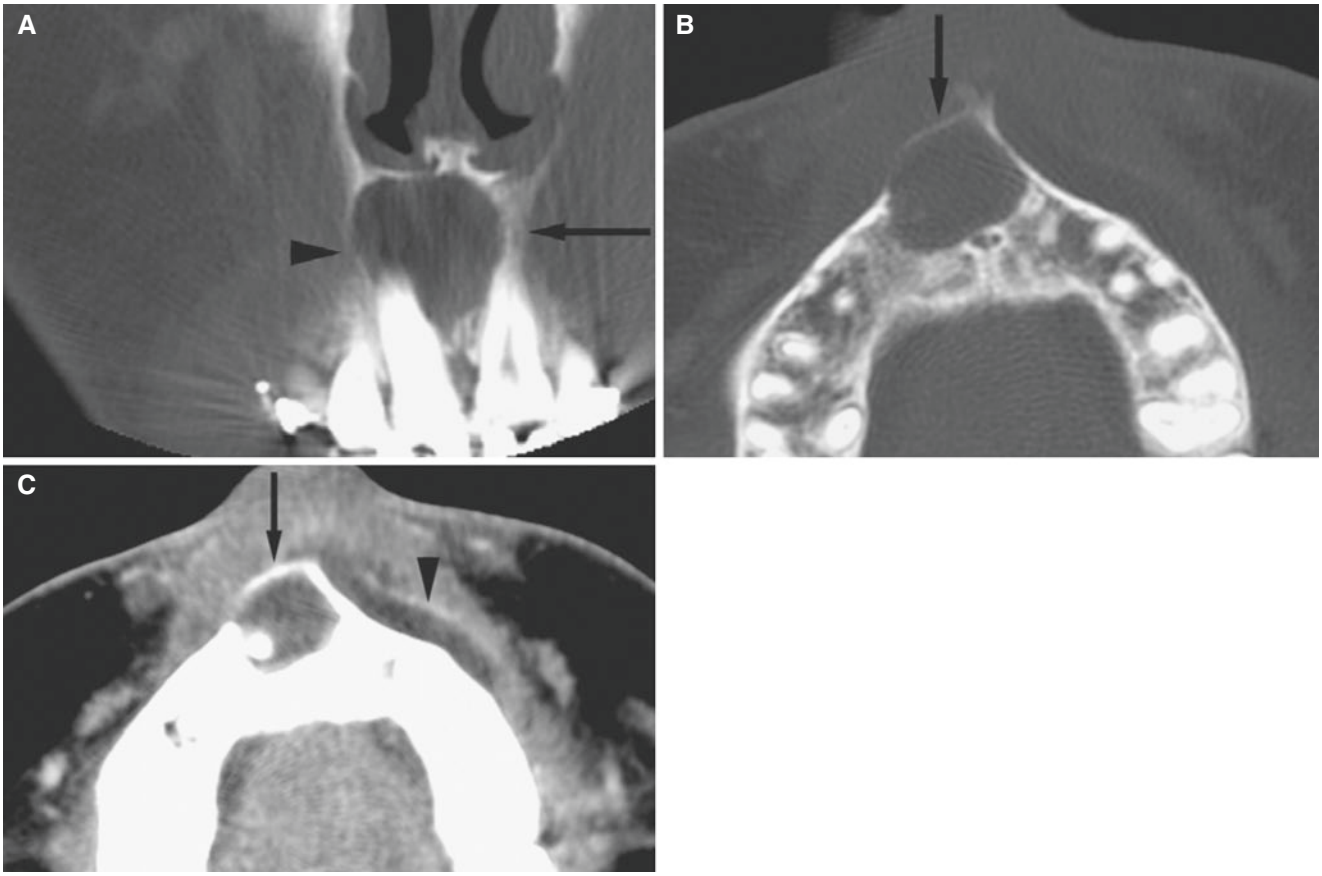

Fig. 2.10 Periapical cyst, maxilla, with abscess development; 14-year-old male with swelling of mucobuccal fold, pain, foul odor, and nonvital right central incisor. (**A**) Coronal CT image shows expansive process with well-defined border (*arrow*), thin and perforated on right side (*arrowhead*). (**B**) Axial CT image shows process (*arrow*) with no sclerotic border in alveolar bone on right side. (**C**) Axial CT image, soft-tissue window, shows cyst in alveolar process (*arrow*) with inflammatory exudate (*hypodense area*) along buccal surface and elevation of the periosteum (*arrowhead*)

2.4 Residual Cyst

Fig. 2.11

2.4.1 Definition

Periapical cyst which is retained in the jaw after removal of the associated tooth (WHO).

2.4.2 Clinical Features

- Odontogenic, but without a close connection to a neighboring tooth root
- See Periapical Cyst

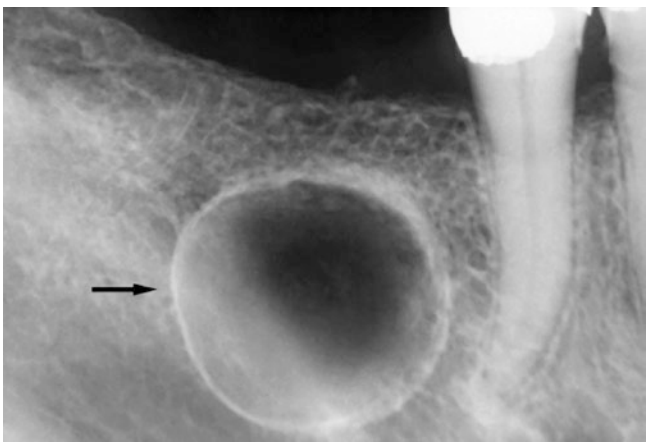

Fig. 2.11 Residual cyst, mandible; asymptomatic, teeth were extracted many years previously. Intraoral view shows round radiolucency with sclerotic border (*arrow*)

2.5 Paradental (Mandibular Infected Buccal) Cyst

Figs. 2.12, 2.13, 2.14, 2.15, 2.16, and 2.17

Synonyms: Mandibular buccal bifurcation cyst, inflammatory paradental cyst, inflammatory collateral cyst (WHO)

2.5.1 Definition

Cyst occurring near to cervical margin of lateral aspect of root as a consequence of inflammatory process in periodontal pocket (WHO).

2.5.2 Clinical Features

- Odontogenic
- Inflammatory
- Mandible, usually first molars
- Unilateral or bilateral
- Vital teeth
- 6–8 years of age
- Distinctive form may occur at mandibular molars, most commonly third molars associated with a history of pericoronitis

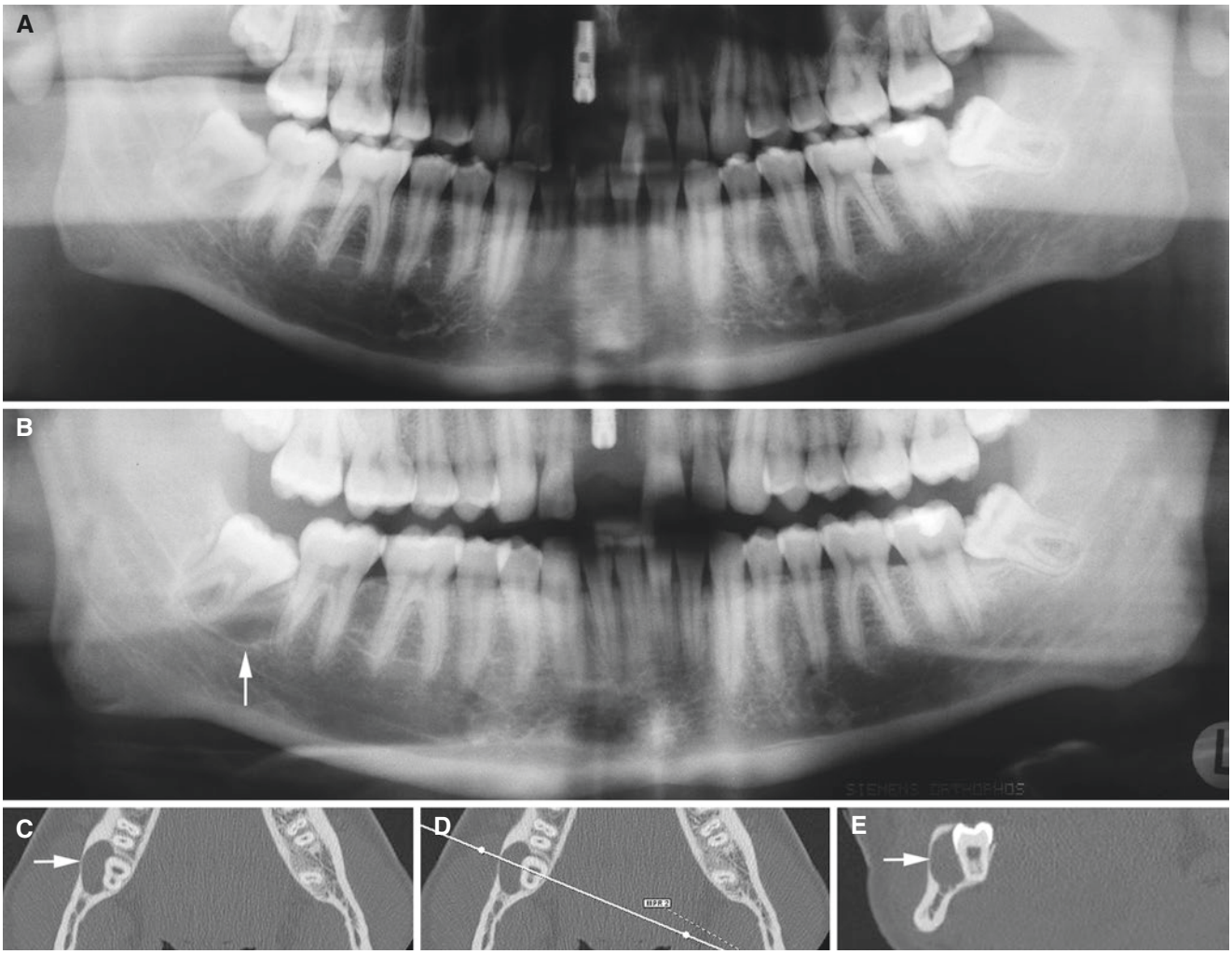

Fig. 2.12 Paradental cyst, mandible; 18-year-old female with routine dental radiography of implant in the maxilla. (**A**) Panoramic view shows normal bone at right mandibular wisdom tooth. (**B**) Panoramic view 4 months later shows radiolucency (*arrow*). (**C**) Axial, (**D**) axial (with cursor line), and (**E**) oblique coronal CT images show radiolucency buccally located (*arrow*)

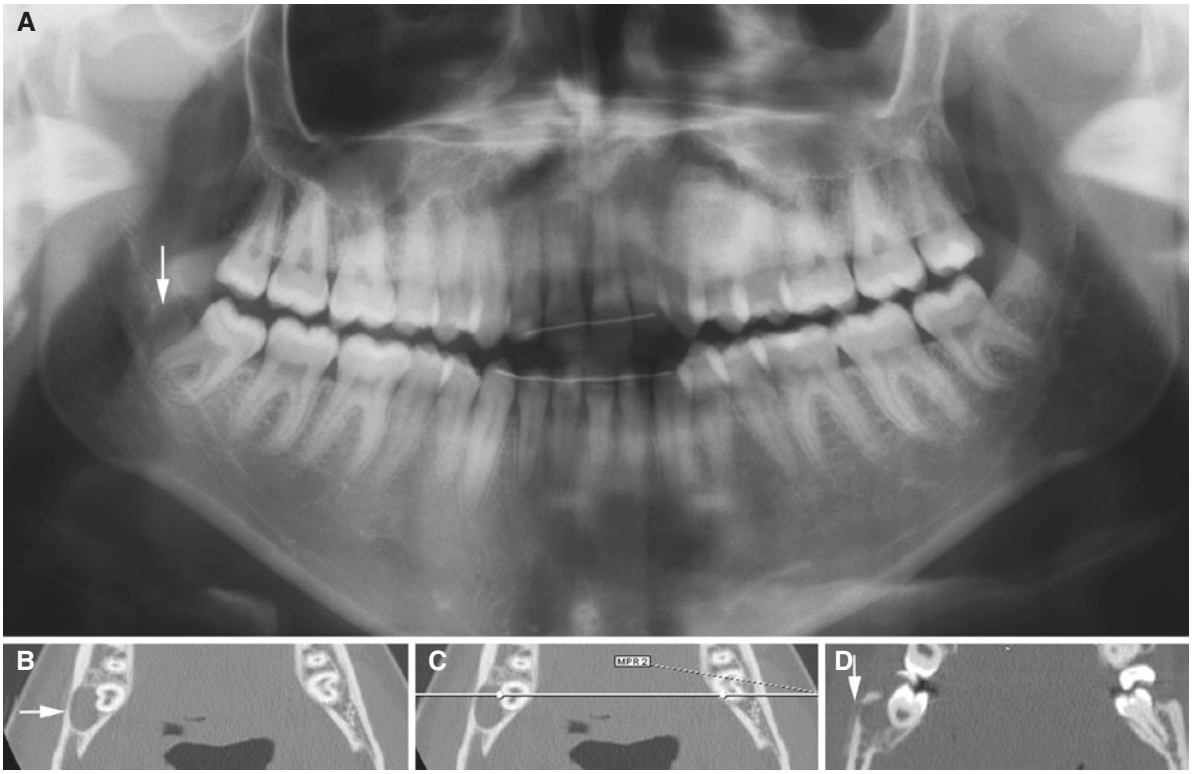

Fig. 2.13 Paradental cyst, mandible, periosteal reaction; 19-year-old female with variable discomfort in right wisdom tooth region. (**A**) Panoramic view shows radiolucency posterior to wisdom tooth (*arrow*). (**B**) Axial, (**C**) axial (with cursor line), and (**D**) coronal CT images show buccal radiolucency (*arrow* in **B**) with periosteal bone formation (*arrow* in **D**)

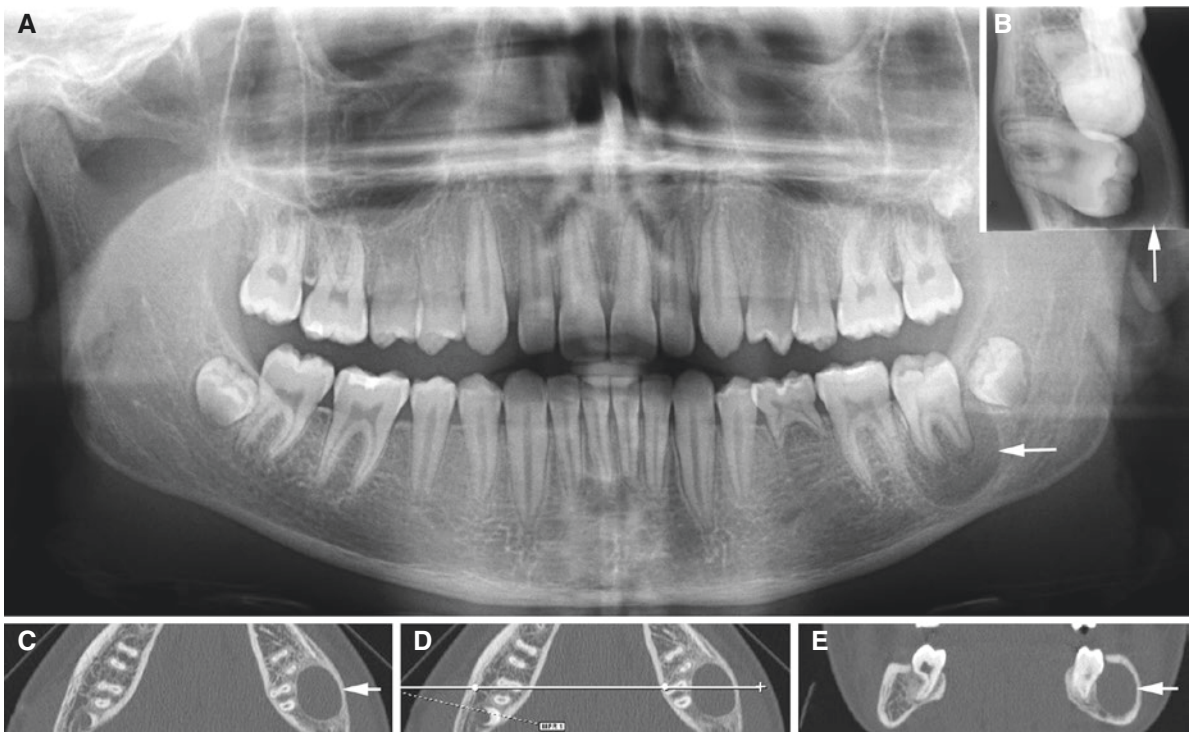

Fig. 2.14 Paradental cyst, bilateral, mandible; 13-year-old male without symptoms (routine control at orthodontist). (**A**) Panoramic view shows periapical radiolucency in the left mandible at second molar (*arrow*). (**B**) Occlusal (axial) view shows tilted second molar and radiolucency located buccally (*arrow*). (**C**) Axial, (**D**) axial (with cursor line), and (**E**) coronal CT images confirm radiolucency buccal to second molar (*arrow*). Note also periosteal bone apposition

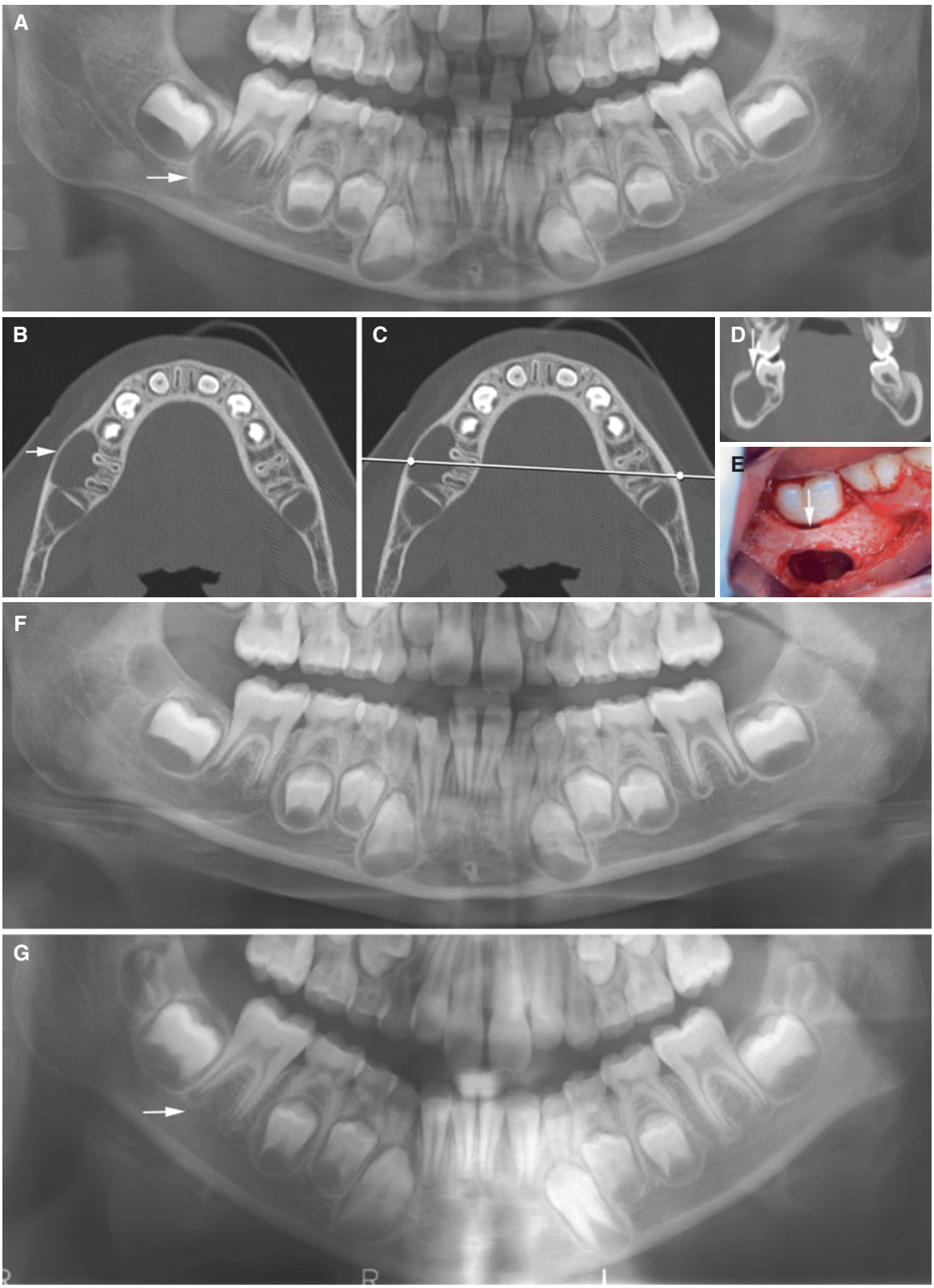

Fig. 2.15 Paradental cyst, mandible; 7-year-old male with variable right-sided perimandibular swelling and pain. (**A**) Panoramic view shows radiolucency in root area of first molar (*arrow*). (**B**) Axial and (**C**) axial (with cursor line) CT images show buccally located radiolucency with expansion at first molar (*arrow*). (**D**) Oblique coronal CT image shows marginal communication to expansion (*arrow*). (**E**) Peroperative photograph confirms marginal communication (*arrow*) (**E**: courtesy of Dr. B. B. Herlofson, University of Oslo, Norway). (**F**) One-year and (**G**) 2-year postoperative panoramic views show good healing at first molar in the right mandible (*arrow*)

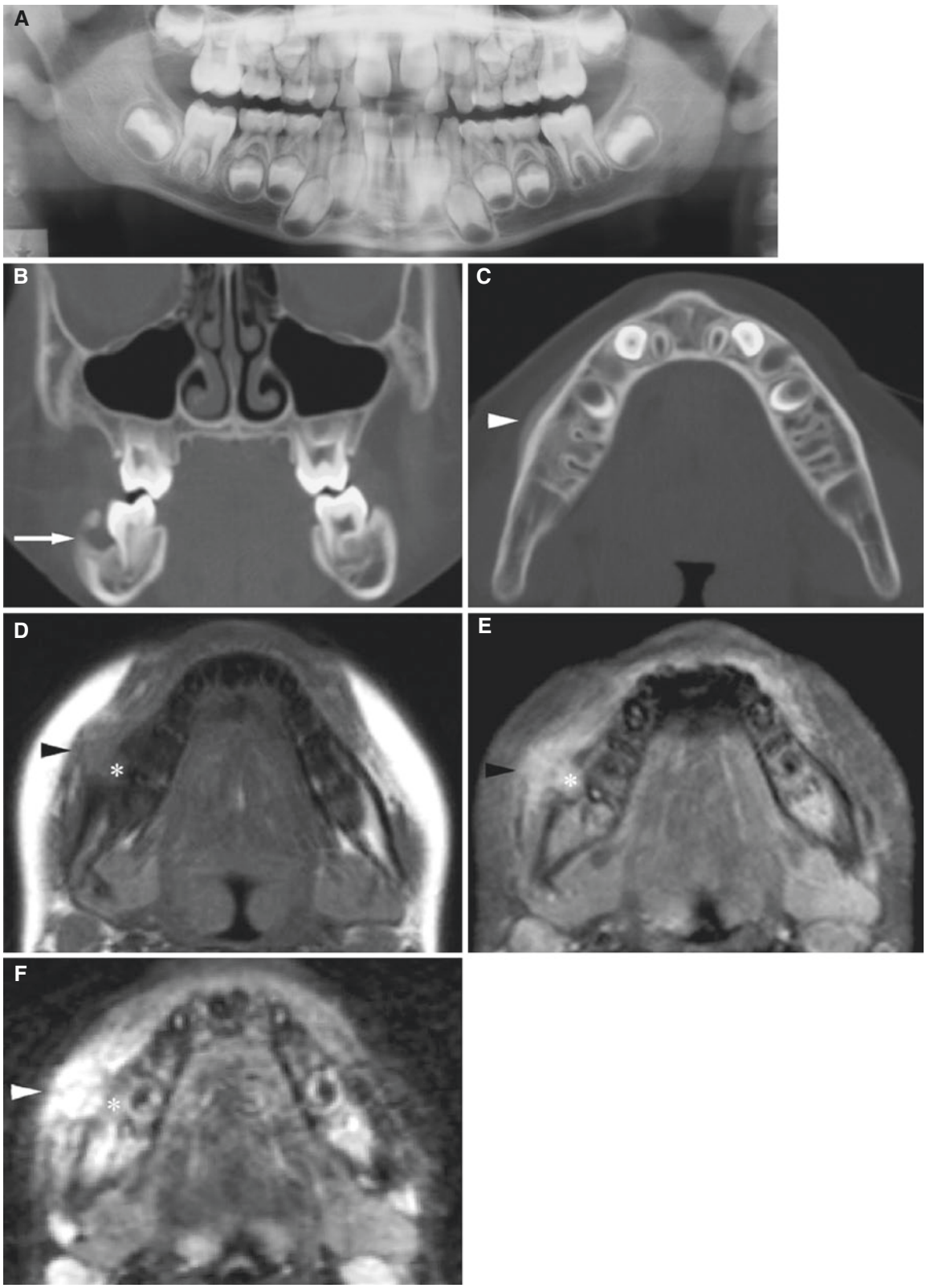

Fig. 2.16 Paradental cyst, mandible; 7-year-old male with right perimandibular swelling and pain. (**A**) Panoramic view shows no abnormalities. (**B**) Coronal CT image shows buccal cystic radiolucency in molar area (*arrow*). (**C**) Axial CT image shows periosteal reaction (*arrowhead*). (**D**) Axial T1-weighted pre-Gd MRI shows intermediate (to low) signal (*arrowhead*); *asterisk* area of bone destruction. (**E**) Axial T1-weighted fat sat post-Gd MRI shows contrast enhancement in bone destruction (*asterisk*) and in buccal soft tissue (*arrowhead*). (**F**) Axial STIR MRI shows diffuse but intense signal in buccal soft tissue, indicating inflammatory response (*arrowhead*); *asterisk* area of bone destruction

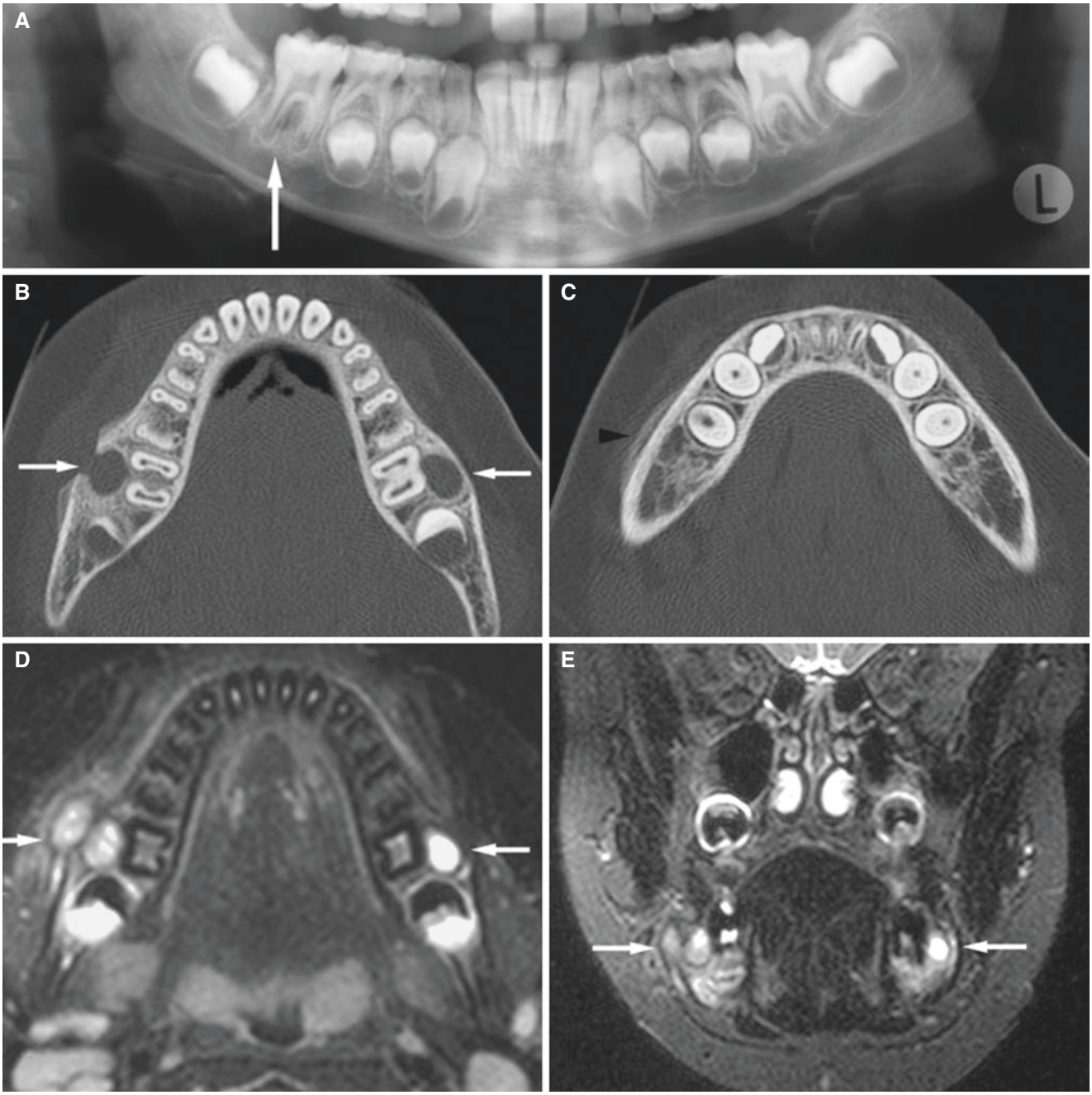

Fig. 2.17 Paradental cyst, bilateral, mandible; 8-year-old male with right perimandibular swelling and pain. (**A**) Panoramic view suggests small radiolucency in root area of first molar (*arrow*). (**B**) Axial CT image shows buccal oval bone cavities bilaterally at first molars (*arrows*), with sclerotic outline on left side and with cortical defect on more severely inflamed right side. (**C**) Axial CT image shows periosteal bone reaction (*arrowhead*). (**D**) Axial STIR MRI shows bilateral high signal at first molars (*arrows*); homogeneous signal on left side and double contour with heterogeneous signal on right side. (**E**) Coronal STIR MRI shows bilateral cysts with different shapes and signals (*arrows*)

2.6 Lateral Periodontal Cyst

Figs. 2.18 and 2.19

2.6.1 Definition

Cyst occurring on lateral aspect or between roots of vital teeth and arising from odontogenic epithelial remnants, but not as a result of inflammatory stimuli (WHO).

2.6.2 Clinical Features

- Odontogenic
- Developmental
- Vital teeth with normal periodontal ligament
- Mandibular premolar and maxillary anterior regions in particular
- Wide age distribution

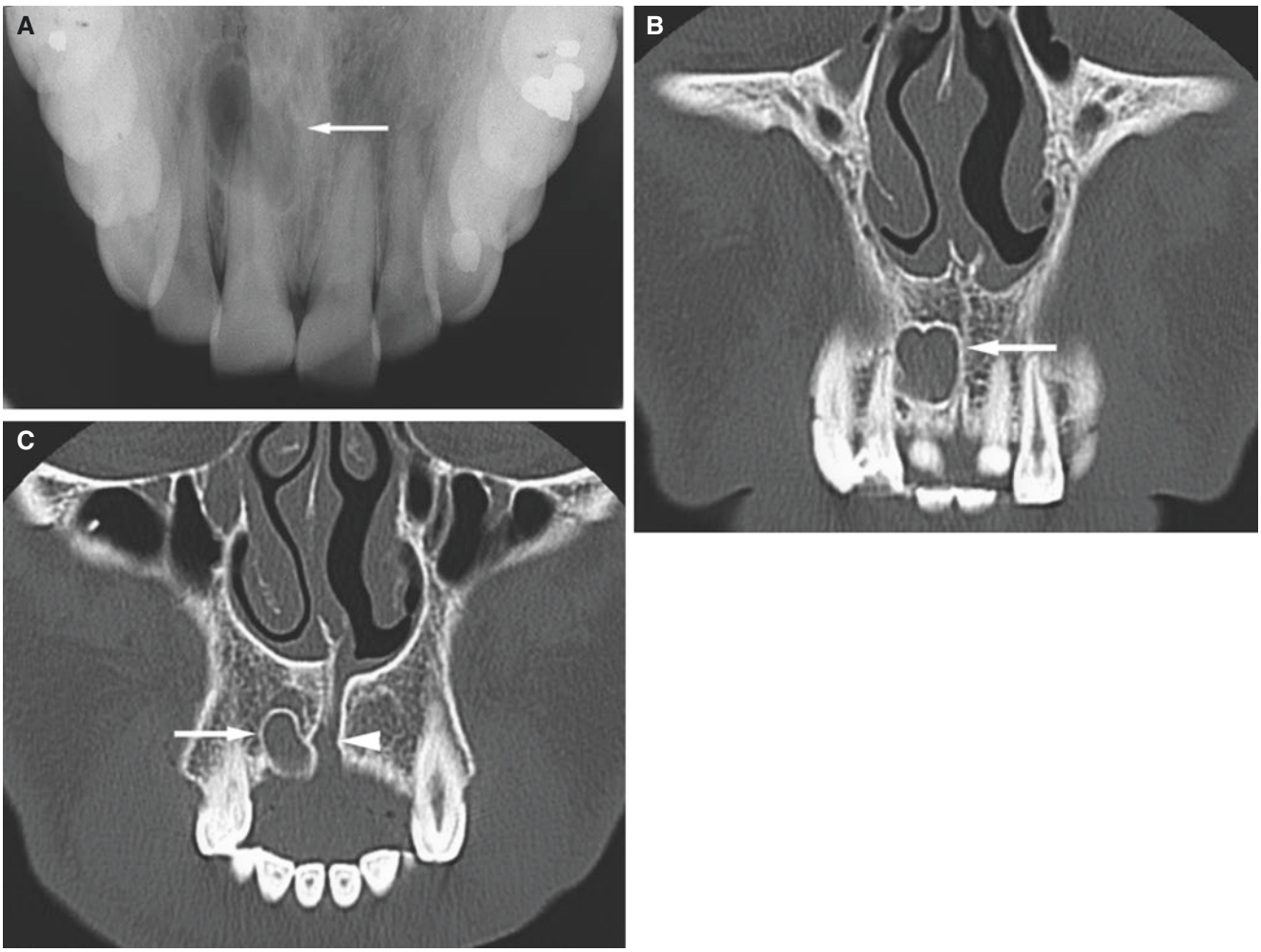

Fig. 2.18 Lateral periodontal cyst, maxilla; 35-year-old male with incidental finding at routine dental radiography; vital teeth. (**A**) Intraoral view shows oval periapical radiolucency with sclerotic border (*arrow*) and normal apical periodontal ligament of teeth. (**B**) Coronal CT image shows oval radiolucency with sclerotic border in alveolar process medial to incisor (*arrow*). (**C**) Coronal CT image shows radiolucency (*arrow*) separate from incisive canal (*arrowhead*)

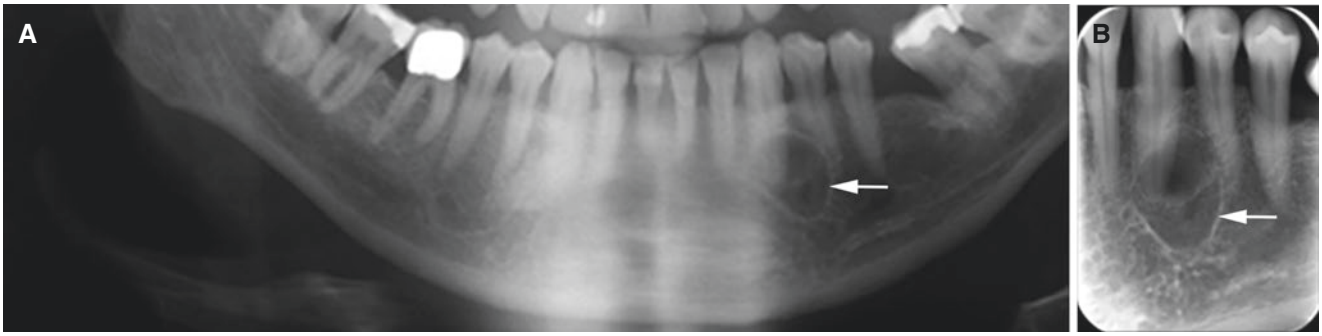

Fig. 2.19 Lateral periodontal cyst, mandible; pain-free swelling in left mandibular canine area. (**A**) Panoramic and (**B**) intraoral views show periapical radiolucency with sclerotic border at canine and first premolar (*arrow*) and apparently normal periodontal ligament space at apex of intact canine and first premolar

2.7 Incisive Canal Cyst

Figs. 2.20, 2.21, and 2.22

Synonym: Nasopalatine duct cyst (WHO)

2.7.1 Definition

Cyst arising from epithelial residues in nasopalatine (incisive) canal (WHO).

2.7.2 Clinical Features

- Non-odontogenic
- Developmental
- Located in nasopalatine canal
- Vital teeth
- Males more frequent than females
- Fourth decade and older

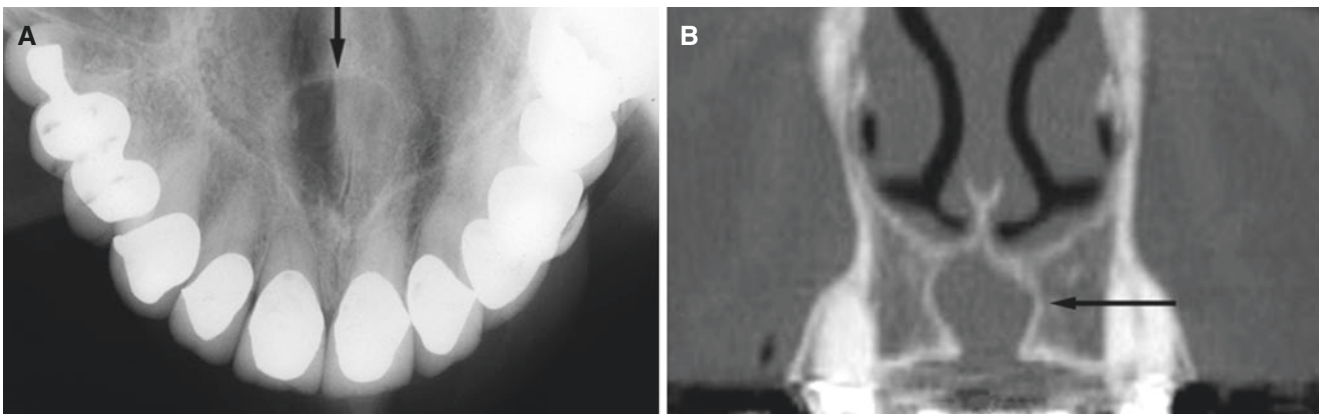

Fig. 2.20 Incisive canal cyst, maxilla; 60-year-old male with incidental finding at routine dental radiography. (**A**) Intraoral occlusal view shows round radiolucency in midline with sclerotic border (*arrow*) and normal apical periodontal ligament. (**B**) Coronal CT image shows radiolucency with sclerotic border (*arrow*)

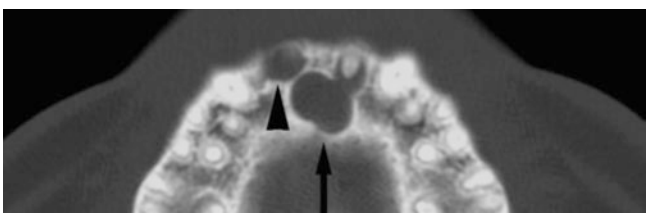

Fig. 2.21 Incisive canal cyst, maxilla; 27-year-old male with incidental finding at routine dental radiography. Axial CT image shows radiolucency in midline with sclerotic border (*arrow*) and communication to bone destruction at incisor. Also bone destruction at other incisor (*arrowhead*)

Fig. 2.22 Incisive canal cyst; painless swelling of palate, vital teeth. Panoramic and intraoral views show large cyst (*arrows*) resorbing tooth roots

2.8 Follicular Cyst

Figs. 2.23, 2.24, 2.25, 2.26, 2.27, 2.28, and 2.29

Synonym: Dentigerous cyst

2.8.1 Definition

Cyst which encloses crown and is attached to the neck of unerupted tooth. It develops by accumulation of fluid between reduced enamel epithelium and crown or between layers of reduced enamel epithelium (WHO).

2.8.2 Clinical Features

- Odontogenic
- Developmental
- Around tooth crown
- Mandibular third molar and second premolar, maxillary canine and third molar
- Males more frequent than females
- All ages, particularly second to fourth decades

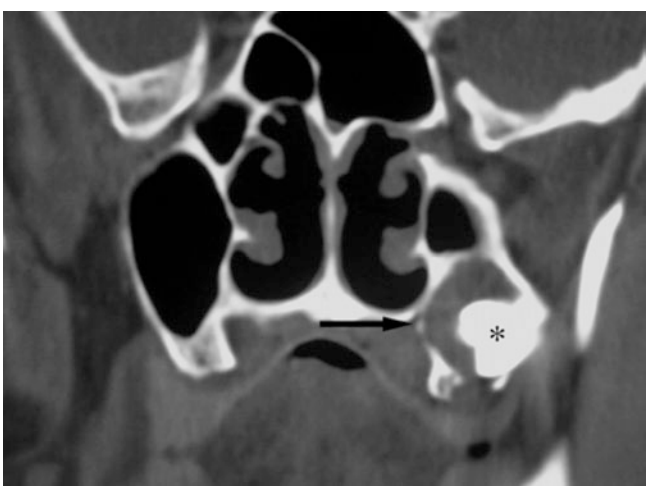

Fig. 2.23 Follicular cyst, maxilla; 54-year-old male with incidental finding at paranasal sinus examination. Coronal CT image shows expansive process (*arrow*) around crown of impacted third molar (*asterisk*)

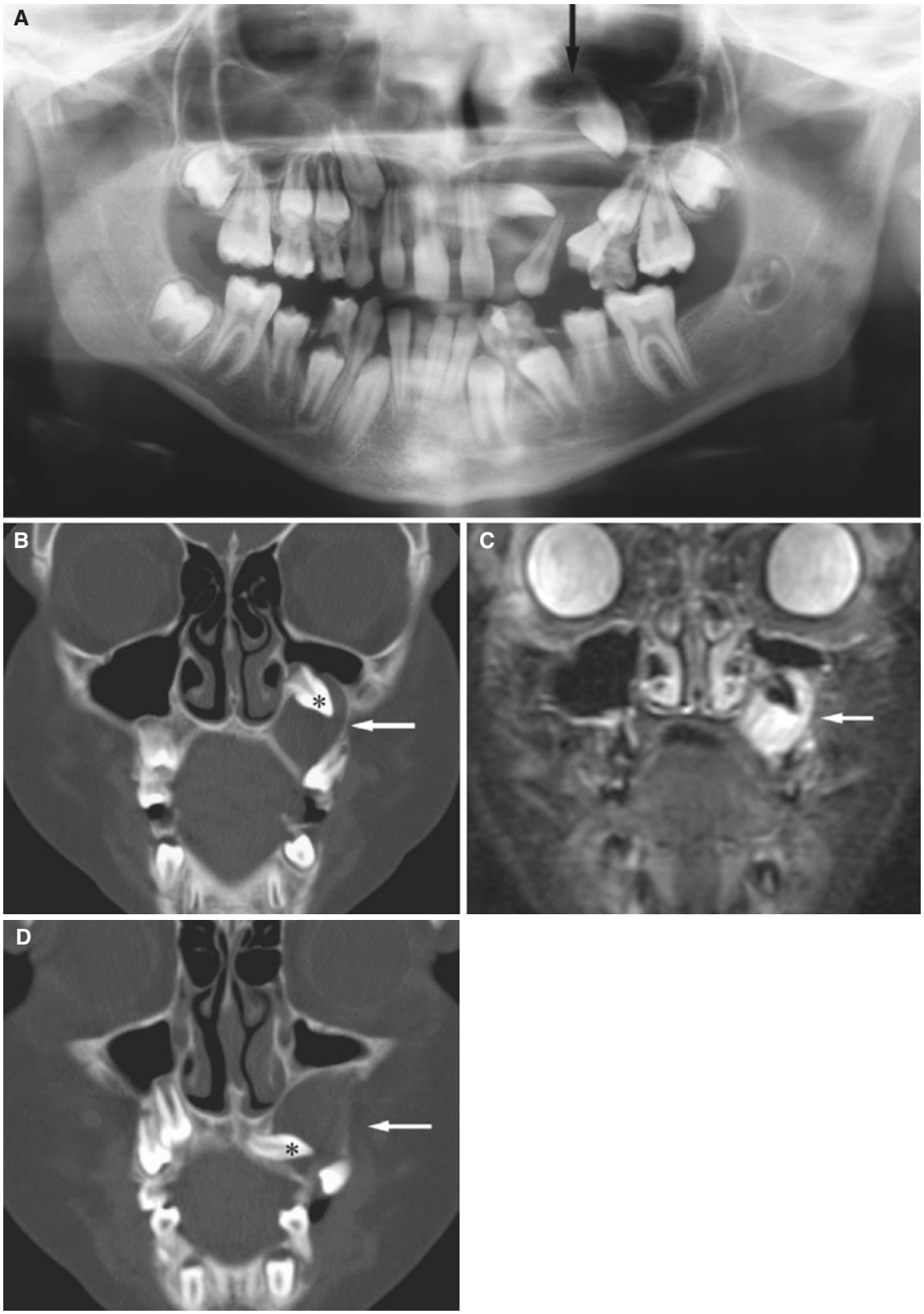

Fig. 2.24 Follicular cyst, maxilla; 8-year-old male with incidental finding when examined for an unerupted lateral incisor. (**A**) Panoramic view shows radiolucency and two unerupted teeth (*arrow*). (**B**) Coronal CT image shows process with sclerotic border (*arrow*) around crown of canine (*asterisk*). (**C**) Coronal STIR MRI shows homogeneous high-signal content (*arrow*). (**D**) Coronal CT image shows cyst (*arrow*) around crown of lateral incisor (*asterisk*)

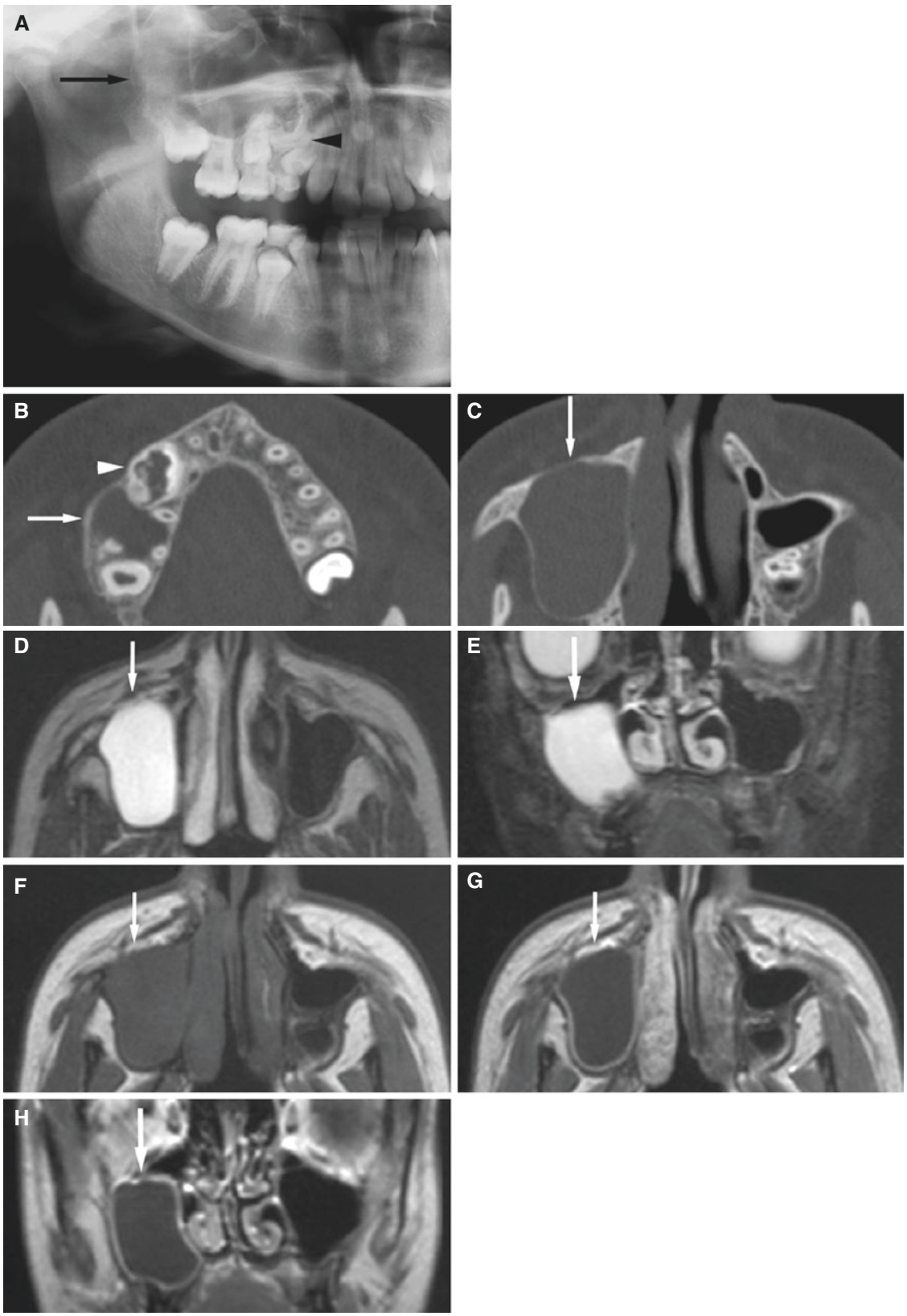

Fig. 2.25 Follicular cyst, maxilla; 13-year-old female examined for unerupted maxillary right first premolar. (**A**) Panoramic view shows expansive process, partially with sclerotic outline (*arrow*) in the right maxillary sinus, and an odontoma (*arrowhead*). (**B**) Axial CT image shows expansive radiolucency and root resorption (*arrow*) and complex odontoma (*arrowhead*) in alveolar process. (**C**) Axial CT image shows process occupying the entire maxillary sinus with expanded walls (*arrow*). (**D**) Axial T2-weighted MRI shows homogeneous high signal (*arrow*). (**E**) Coronal STIR MRI shows homogeneous high signal (*arrow*). (**F**) Axial T1-weighted pre-Gd MRI shows homogeneous intermediate signal (*arrow*). (**G**) Axial T1-weighted post-Gd MRI shows no enhancement except peripheral rim (*arrow*). (**H**) Coronal T1-weighted post-Gd MRI shows no enhancement except peripheral rim (*arrow*)

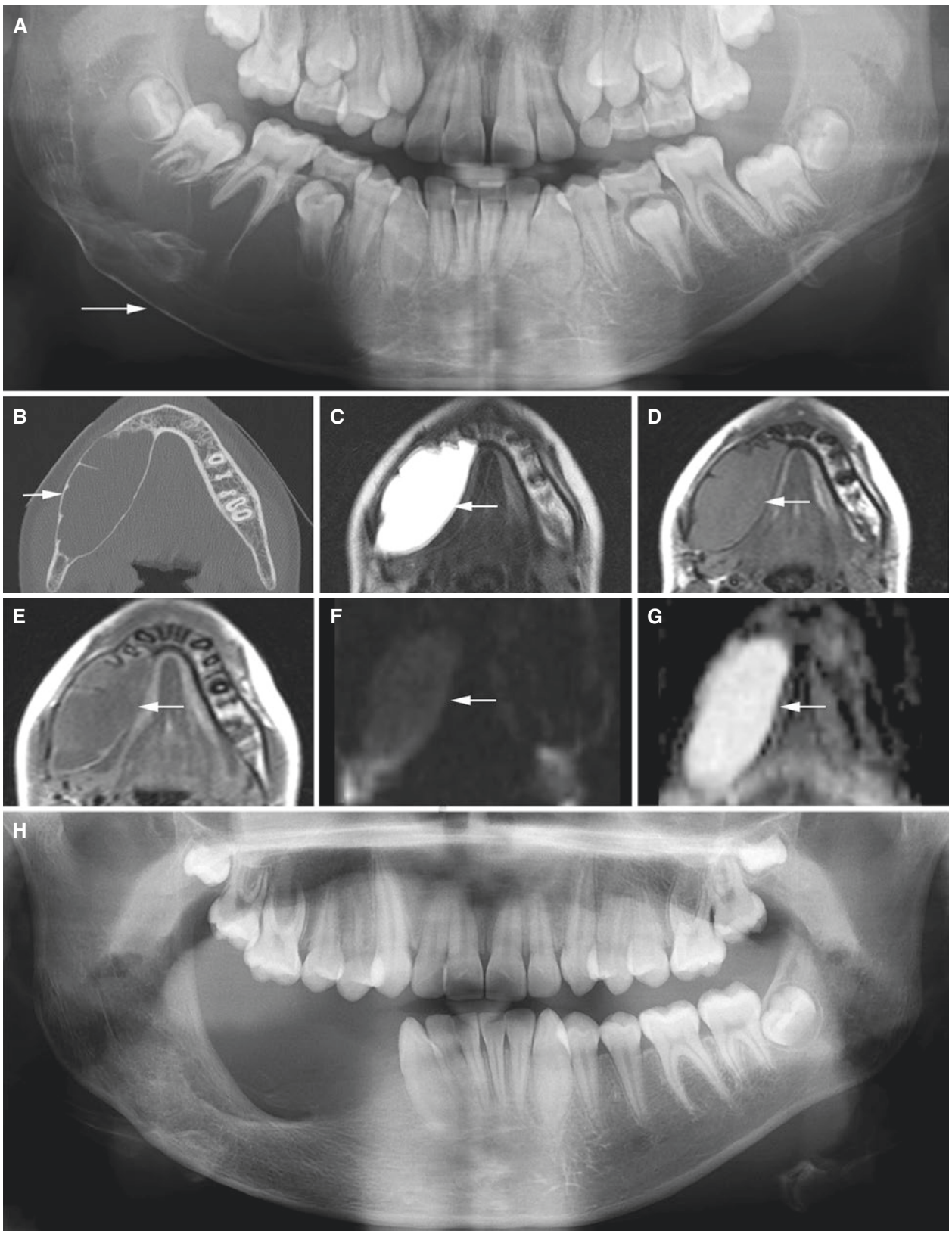

Fig. 2.26 Follicular cyst, mandible; 10-year-old male with minimal symptoms. (**A**) Panoramic view shows radiolucency in the right mandible (*arrow*). (**B**) Axial CT image shows expansive lesion with thin corticated outline (*arrow*). (**C**) Axial T2-weighted MRI shows homogeneous high signal intensity (*arrow*). (**D**) Axial T1-weighted pre-Gd and (**E**) axial T1-weighted post-Gd MRI show no contrast enhancement except in thin peripheral rim (*arrow*). (**F**) Axial diffusion-weighted MRI and (**G**) ADC map indicate high degree of diffusion within cyst (*arrow*). (**H**) 2-year postoperative panoramic view shows good bone healing

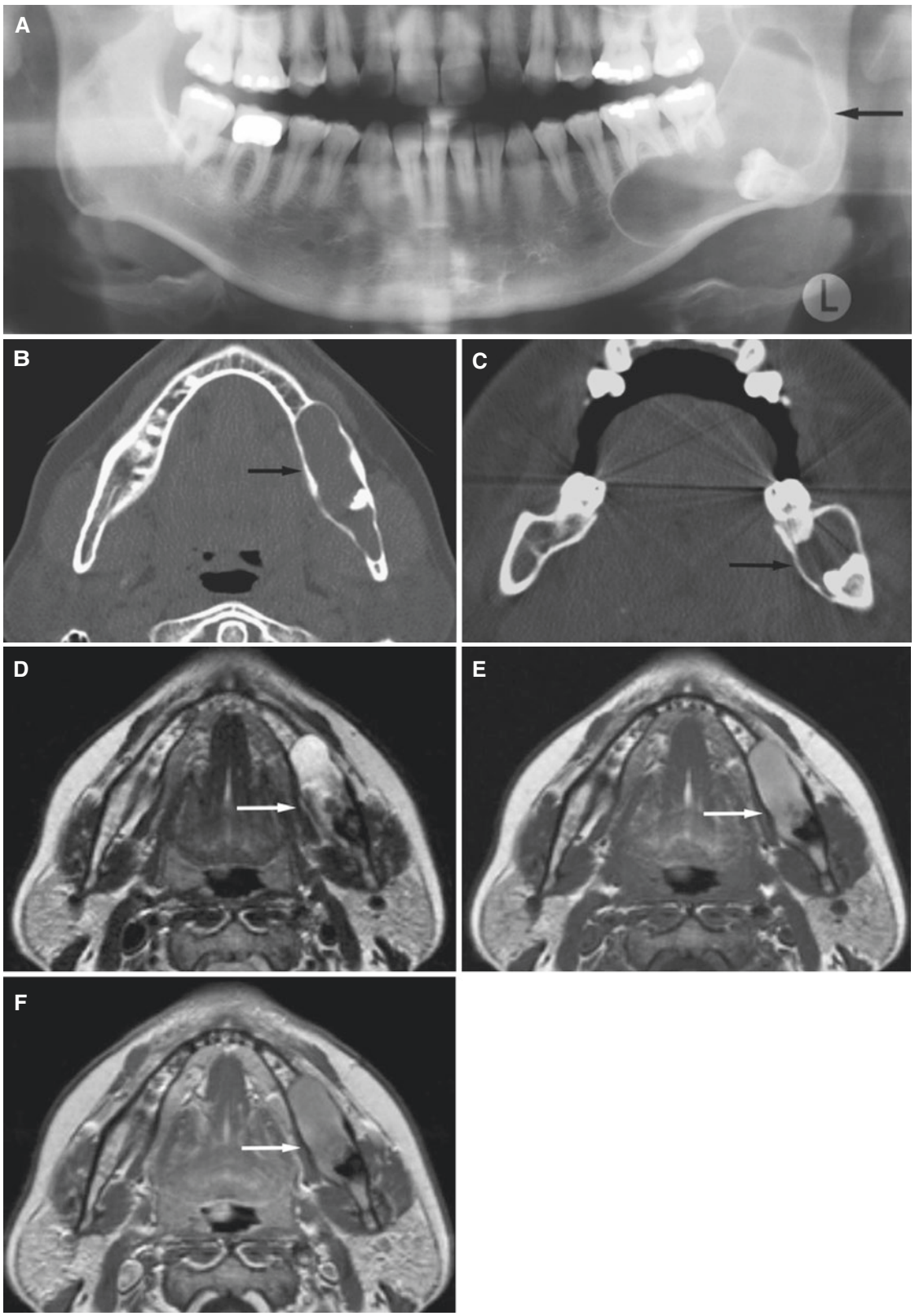

Fig. 2.27 Follicular cyst, mandible; 38-year-old female with incidental finding at routine dental radiography. (**A**) Panoramic view shows radiolucency with sclerotic border around crown of impacted third molar and root resorption of molars (*arrow*). (**B**) Axial CT image shows process with intact cortical bone (*arrow*) and part of impacted third molar. (**C**) Oblique coronal CT image shows process around crown of third molar with intact cortical bone expanding lingually (*arrow*) and buccally. (**D**) Axial T2-weighted MRI shows heterogeneous signal content: homogeneous high signal in one part and heterogeneous low to intermediate signal close to impacted tooth (*arrow*). (**E**) Axial T1-weighted pre-Gd MRI shows homogeneous intermediate-signal content (except small area close to impacted tooth) (*arrow*). (**F**) Axial T1-weighted post-Gd MRI shows no contrast enhancement (*arrow*)

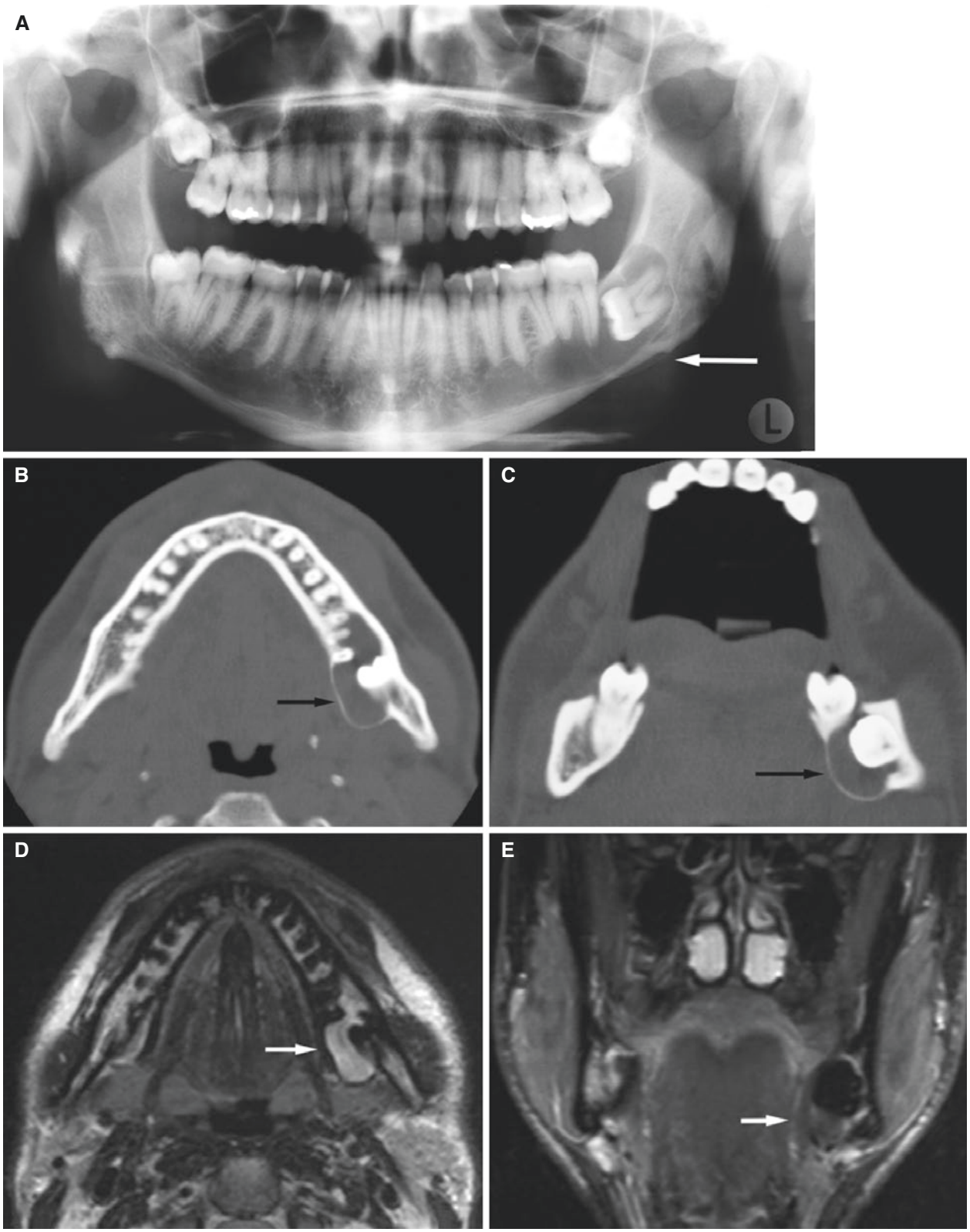

Fig. 2.28 Follicular cyst, mandible; 40-year-old male with incidental finding at routine dental radiography. (**A**) Panoramic view shows radiolucency with sclerotic border (*arrow*) and impacted third molar. (**B**) Axial CT image shows expansive process with thinned, intact cortical bone, partially around crown of impacted third molar (*arrow*). (**C**) Oblique coronal CT image shows process with intact cortical outline expanding lingually (*arrow*). (**D**) Axial T2-weighted MRI shows homogeneous intermediate- to high-signal content (*arrow*). (**E**) Coronal STIR MRI shows homogeneous low-signal content (*arrow*). (**F**) Axial T1-weighted pre-Gd MRI shows homogeneous intermediate to high signal (*arrow*). (**G**) Axial T1-weighted fat sat pre-Gd MRI shows homogeneous high signal (*arrow*). (**H**) Axial T1-weighted fat sat post-Gd MRI shows no contrast enhancement when compared to (**G**) (*arrow*)

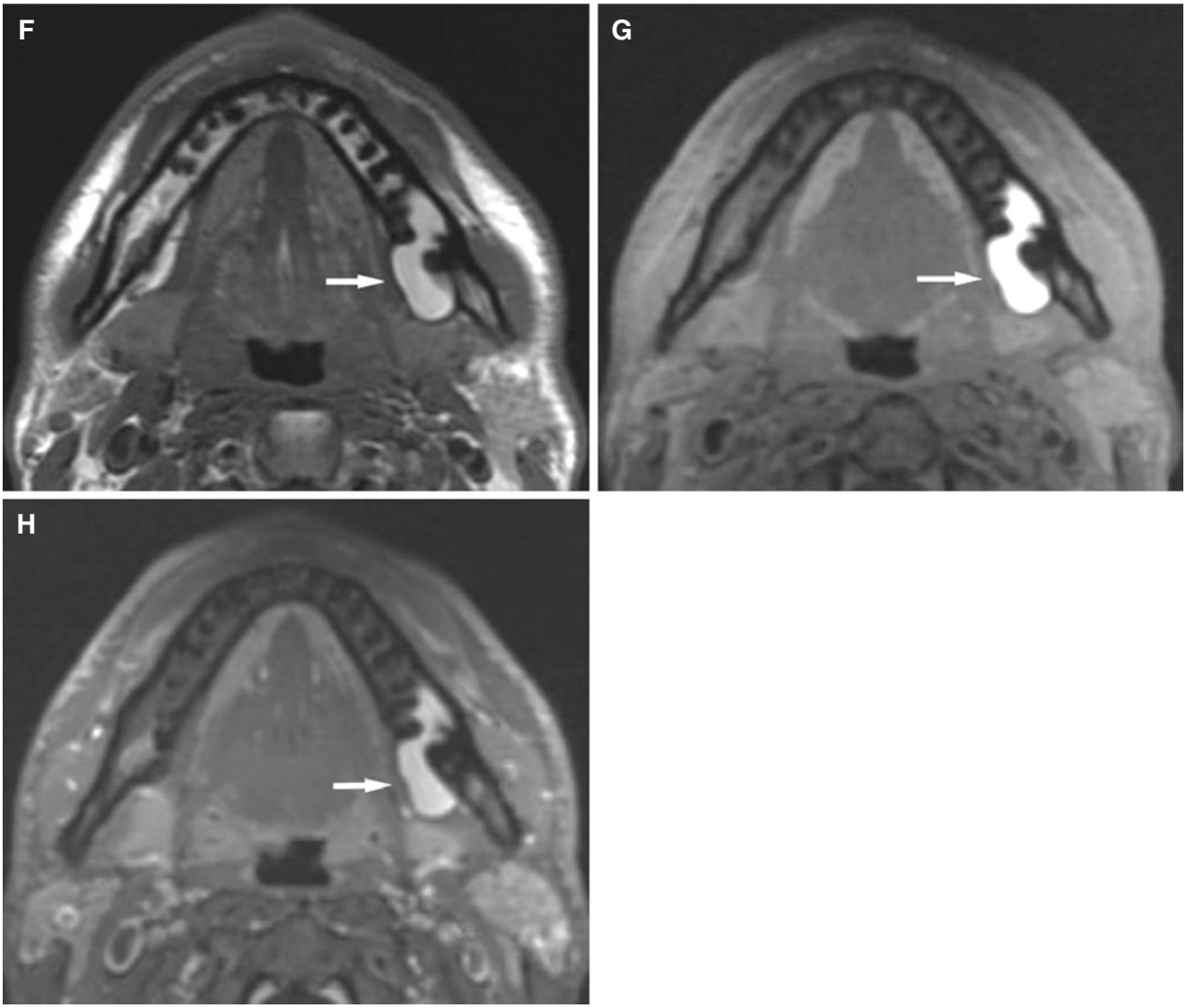

Fig. 2.28 (continued)

Fig. 2.29 Follicular cyst, mandible; 56-year-old male with incidental finding at routine dental radiovgraphy. 3D CT image shows large cortical defect on lingual side (*arrow*) and within cavity an impacted third molar (*lower arrowhead*) and roots of second molar (*arrowhead*)

2.9 Glandular Odontogenic Cyst

Fig. 2.30

Synonym: Sialo-odontogenic cyst

2.9.1 Definition

Cyst arising in tooth-bearing areas and characterized by epithelial lining with cuboidal or columnar cells both at surface and lining crypts or cyst-like spaces within thickness of epithelium, simulating salivary gland or glandular differentiation (WHO).

2.9.2 Clinical Features

- Odontogenic
- Developmental
- Mandible more often than maxilla, anterior region in particular
- Vital teeth
- Unilocular or multilocular (also bilocular reported)
- Border may be destroyed and penetrated, indicating some aggressivity
- High recurrence reported (about 20% in one study)

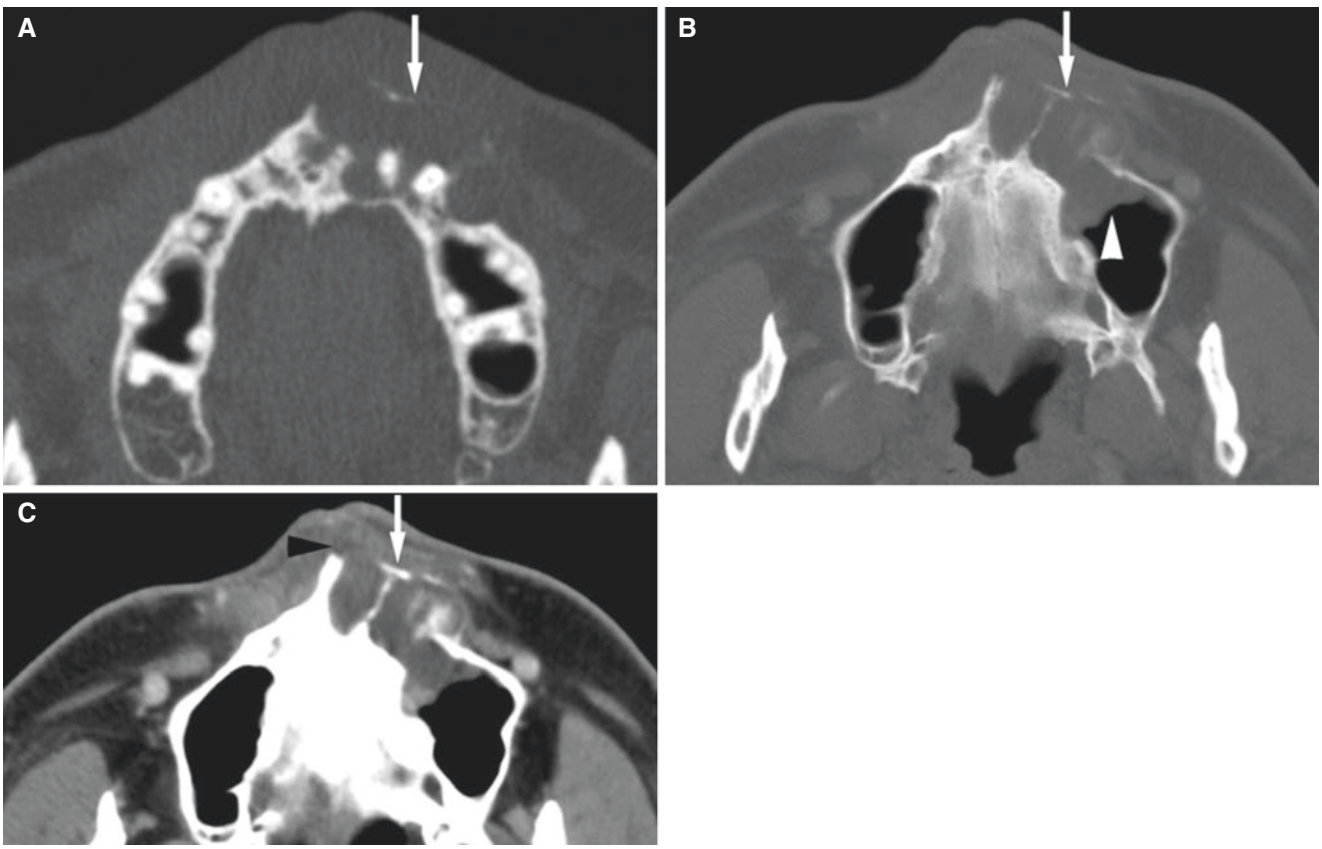

Fig. 2.30 Glandular odontogenic cyst, maxilla; 47-year-old male with painless swelling of mucobuccal fold. (**A**) Axial CT image shows radiolucency between teeth with expanded, destroyed cortical outline (*arrow*). (**B**) Axial CT image shows process (*arrow*) with no cortical outline in the maxillary sinus (*arrowhead*). (**C**) Axial post-contrast CT image with soft-tissue window shows process (*arrow*) with no demarcation from surrounding soft tissue (*arrowhead*) and no contrast enhancement

2.10 Odontogenic Keratocyst

Odontogenic keratocyst was classified as keratocystic odontogenic tumor by WHO in 2005, but reclassified by WHO just when the draft of this book was completed in 2017. The entity is therefore described in Chap. 3.

2.11 Cyst-Like Conditions

Figs. 2.31, 2.32, 2.33, 2.34, and 2.35

2.12 Simple Bone Cyst

Synonyms: Solitary bone cyst, traumatic bone cyst, hemorrhagic bone cyst, hemorrhagic cyst, idiopathic bone cavity, unicameral bone cyst

2.12.1 Definition

Intraosseous pseudocyst devoid of an epithelial lining, either empty or filled with serous or sanguinous fluid (WHO).

2.12.2 Clinical Features

- Incidental radiographic finding
- Second decade
- Mandible, usually body or anterior areas, but may occur anywhere
- Vital teeth
- No sex predilection in jaws (in contrast to long bones; males more frequent)

2.12.3 Imaging Features

- Radiolucency
- May be unilocular or bilateral
- Usually rounded in anterior region, often scalloped between teeth and roots in molar region, but shape may vary substantially
- Multilocular appearance may occur but rare
- Border usually well defined and corticated, but may be less well defined and non-corticated
- Usually no expansion of bone
- If expanding bone, only slightly with cortical thinning
- Usually no displacement or resorption of teeth
- Occasionally, may persist or even expand following surgical fenestration
- T1-weighted MRI: homogeneous intermediate signal
- T2-weighted and STIR MRI: homogeneous high signal
- T1-weighted post-Gd MRI: no contrast enhancement or enhancement in peripheral thin rim

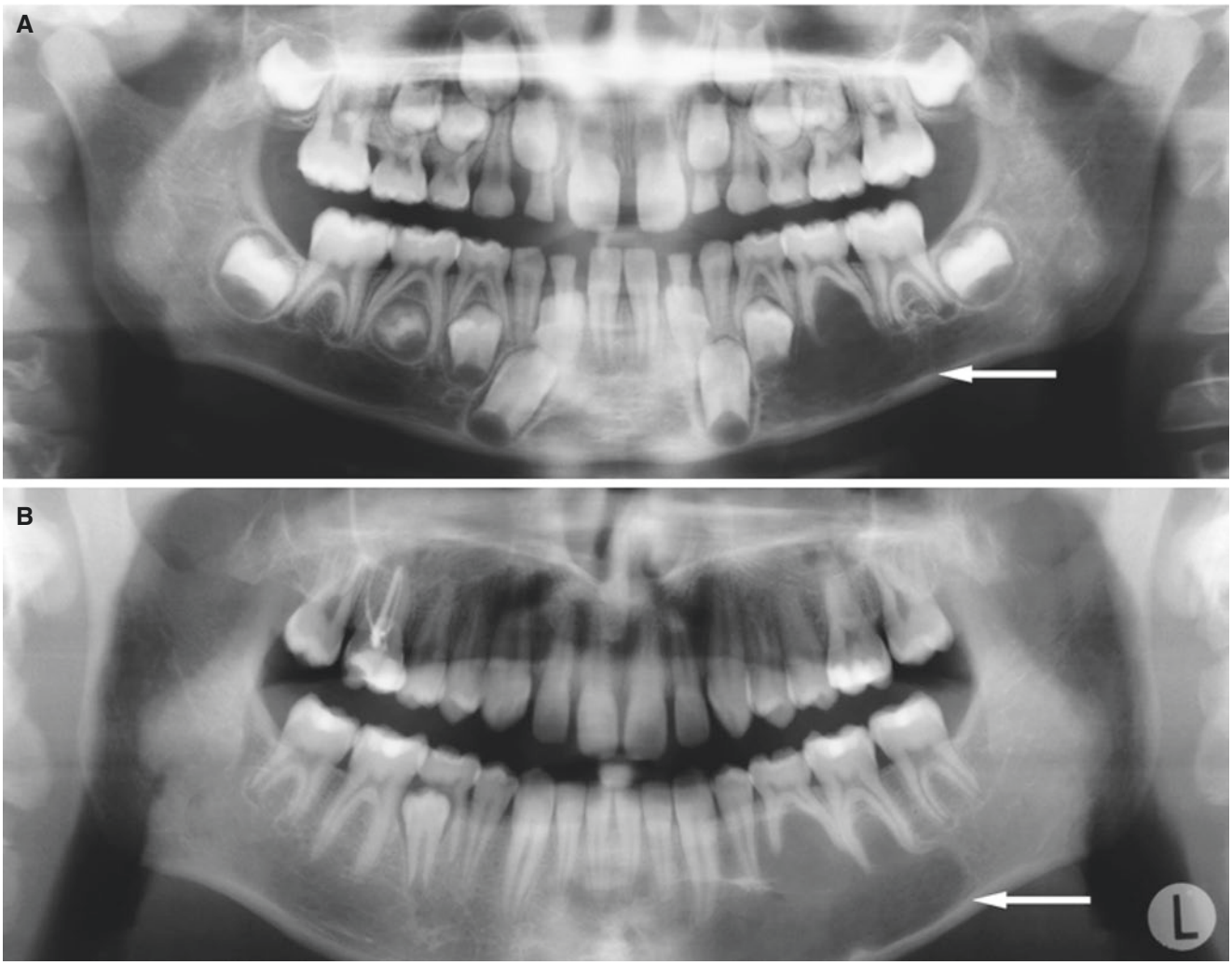

Fig. 2.31 Simple bone cyst, mandible; 8-year-old male at baseline with incidental finding at routine dental radiography and followed for 8 years. (**A**) Panoramic view shows poorly defined radiolucency with no sclerotic border (*arrow*). At 6-year follow-up, after two surgical interventions, (**B**) panoramic view shows enlarged radiolucency (*arrow*). (**C**) Axial CT image shows expanded, thinned, and intact cortical bone (*arrow*). (**D**) Axial T2-weighted MRI shows homogeneous high signal (*arrow*). (**E**) Axial STIR MRI shows homogeneous high signal (*arrow*). (**F**) Axial T1-weighted pre-Gd MRI shows homogeneous intermediate signal (*arrow*). (**G**) Axial T1-weighted post-Gd MRI shows no enhancement except thin peripheral rim buccally (*arrow*). At 8-year follow-up (2 years after third surgery), (**H**) panoramic view shows complete regeneration

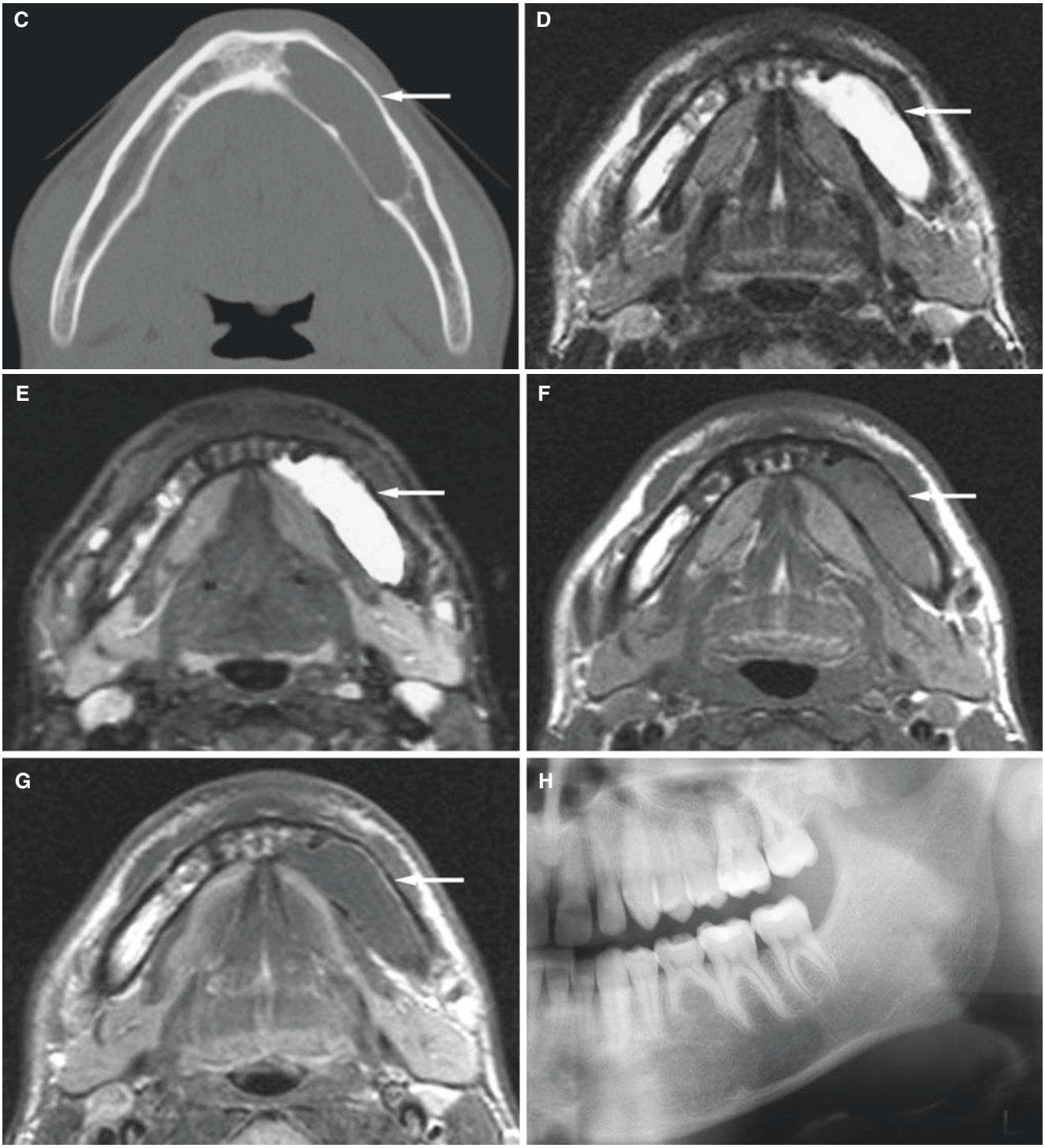

Fig. 2.31 (continued)

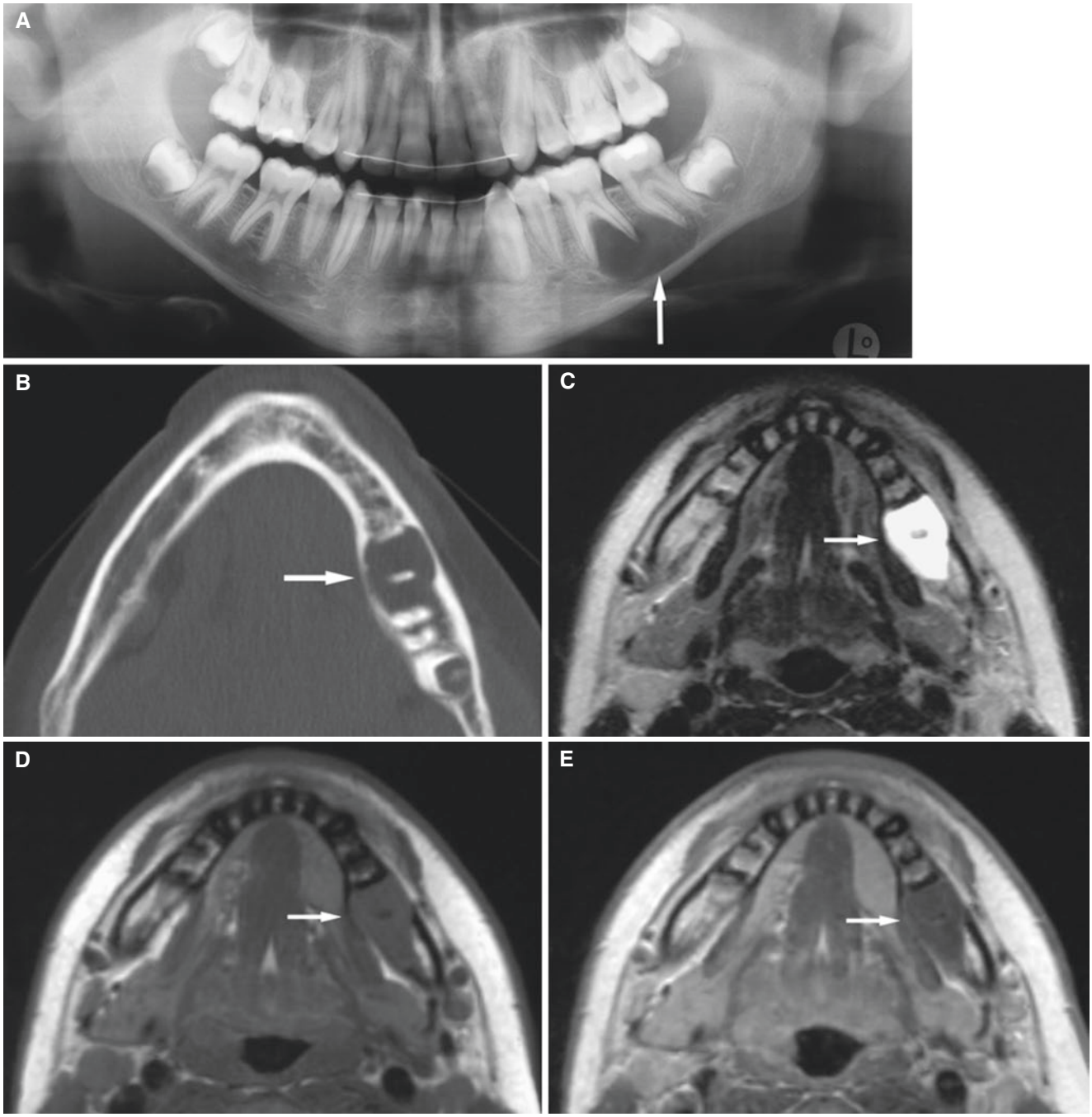

Fig. 2.32 Simple bone cyst, mandible; 15-year-old male with incidental finding at routine dental radiography. (**A**) Panoramic view shows well-defined radiolucency with no sclerotic border (*arrow*). (**B**) Axial CT image shows expanded, thinned, and intact cortical bone (*arrow*). (**C**) Axial T2-weighted MRI shows homogeneous high signal (*arrow*). (**D**) Axial T1-weighted pre-Gd MRI shows homogeneous intermediate signal (*arrow*). (**E**) Axial T1-weighted post-Gd MRI shows no contrast enhancement, or possibly in a very peripheral rim (*arrow*)

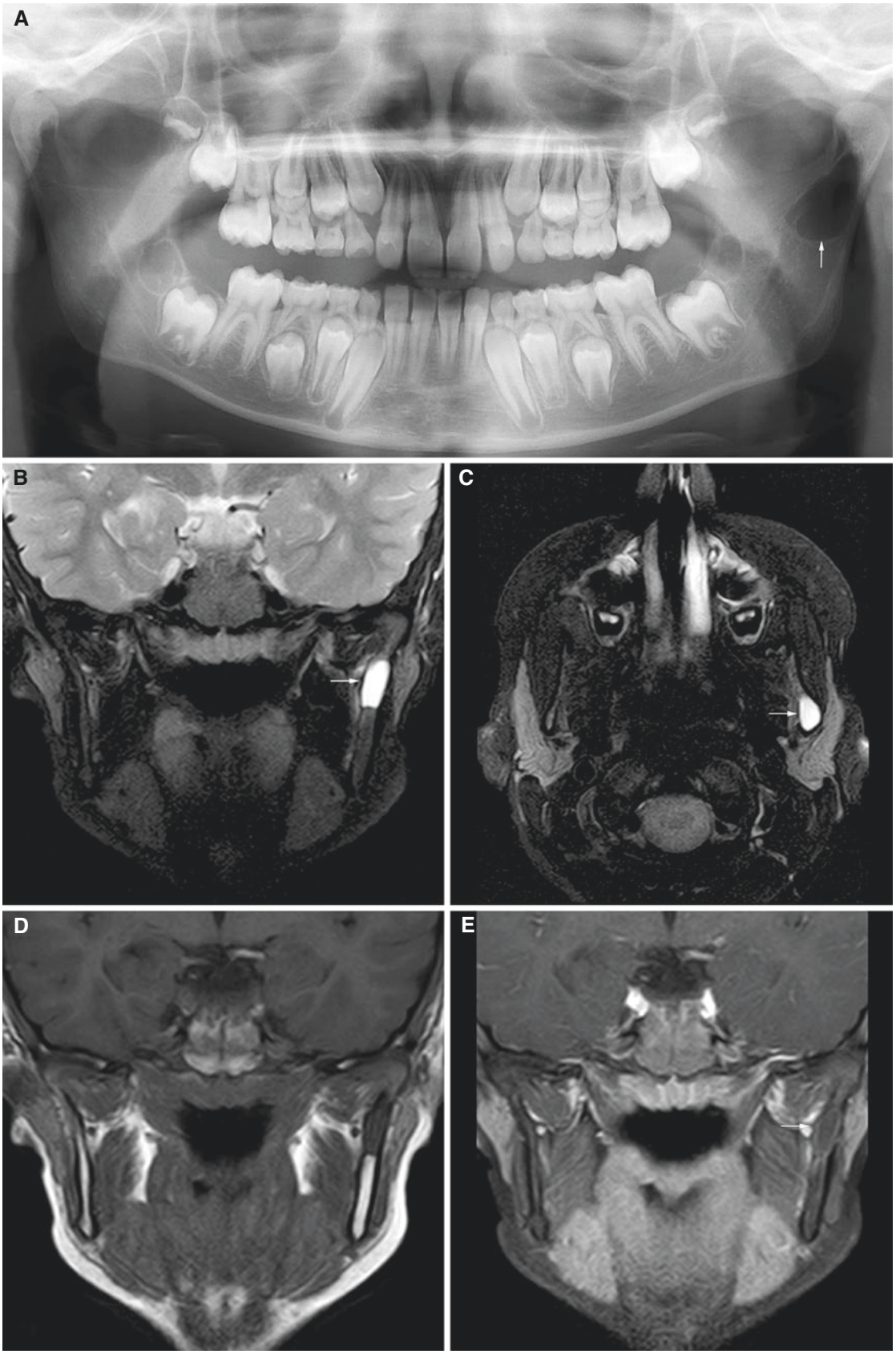

Fig. 2.33 Simple bone cyst, mandible; 10-year-old male without symptoms. (**A**) Panoramic view shows radiolucency in the left mandibular ramus/neck (*arrow*). (**B**) Coronal and (**C**) axial STIR MRI show homogeneous high signal intensity (*arrow*). (**D**) Coronal T1-weighted pre-Gd and (**E**) coronal T1-weighted fat sat post-Gd MRI show no contrast enhancement except in thin peripheral rim (*arrow*)

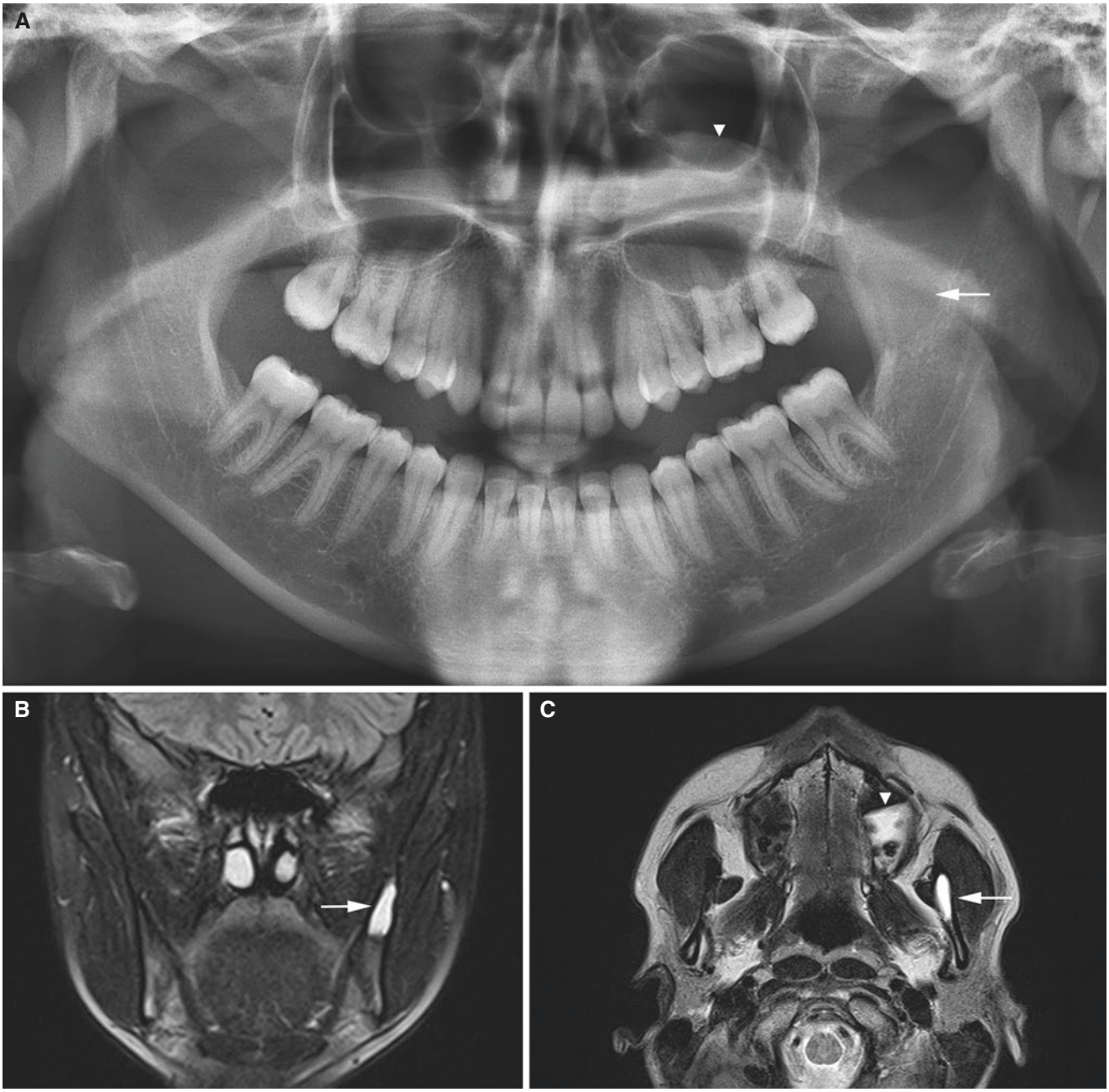

Fig. 2.34 Simple bone cyst, mandible; 18-year-old female, incidental finding. (**A**) Panoramic view suggests radiolucency in left coronoid process (*arrow*). This examination was made after incidental finding in the mandible on cerebral MRI. Retention cyst in the left maxillary sinus (*arrowhead*). (**B**) Coronal STIR and (**C**) axial T2-weighted MRI show homogeneous high signal intensity in the left mandibular ramus consistent with simple bone cyst (*arrow*) and high signal in the left maxillary sinus consistent with retention cyst (*arrowhead*)

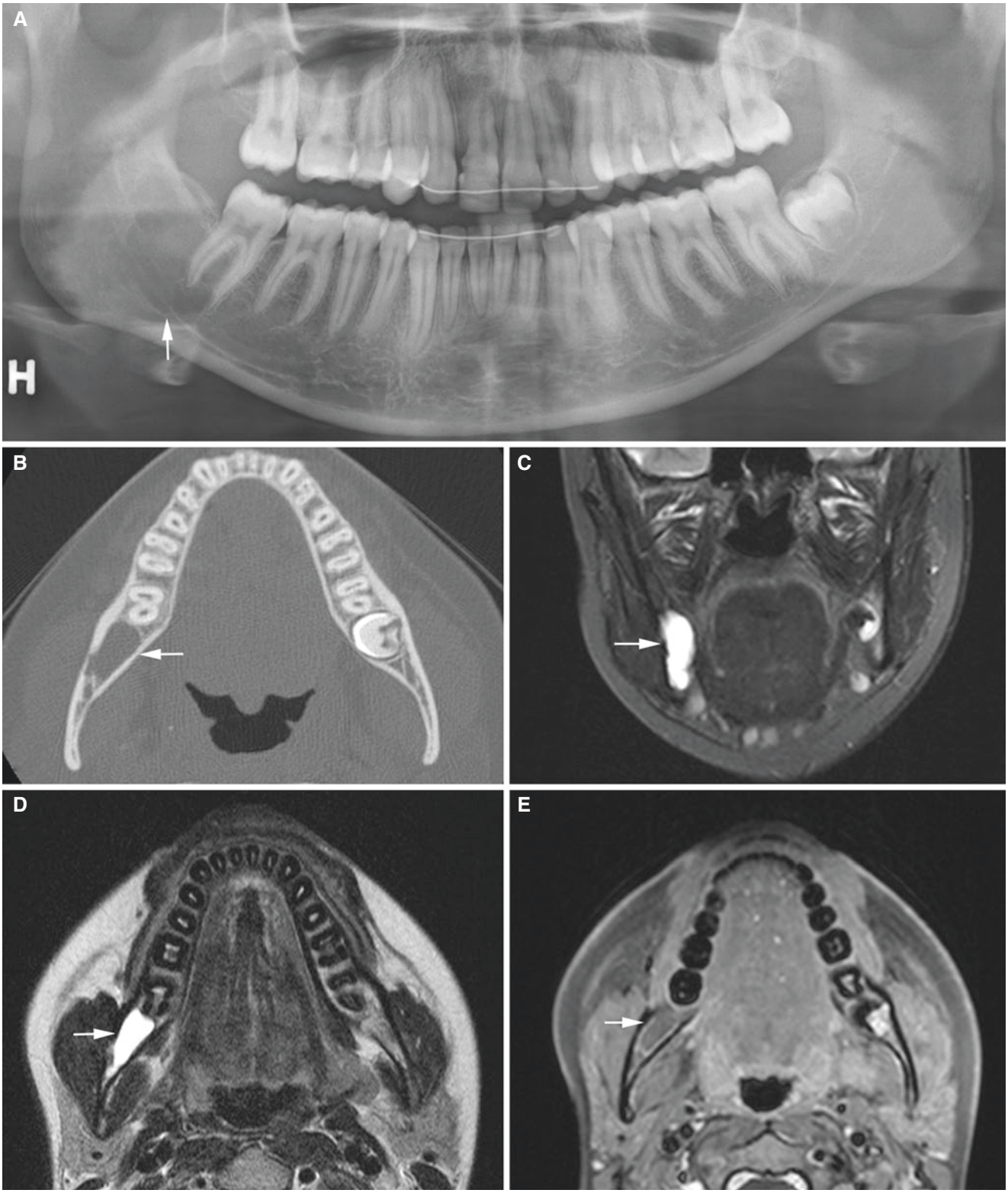

Fig. 2.35 Simple bone cyst, mandible; 15-year-old female, incidental finding. (**A**) Panoramic view shows radiolucency in retromolar area of the right mandible (*arrow*). (**B**) Axial CT image shows radiolucency without buccal or lingual expansion (*arrow*). (**C**) Coronal STIR and (**D**) axial T2-weighted MRI show homogeneous high signal intensity in retromolar area (*arrow*). (**E**) Axial T1-weighted post-Gd MRI shows no contrast enhancement except in thin peripheral rim (*arrow*)

2.13 Stafne Bone Cyst

Figs. 2.36, 2.37, and 2.38

Synonyms: Stafne defect, static bone cavity, developmental salivary gland defect, lingual salivary gland depression, lingual mandibular bone depression

2.13.1 Definition

Concavity in lingual surface of mandible. Also referred to as pseudocyst because of similarity to a cyst on conventional radiographs and no epithelial lining.

Stafne defect is usually considered to be associated with salivary gland content. However, some of these defects may occur without any gland tissue.

2.13.2 Clinical Features

- Incidental finding
- Usually developing in the second decade, but may develop in an older age
- Men more frequent than women
- Peak incidence in the fifth and sixth decades

2.13.3 Imaging Features

- Usually located at mandibular angle caudally to the mandibular canal
- Seldom seen in the anterior part of the mandible
- Well-defined round or oval defect, corticated or not

Fig. 2.36 Stafne bone cyst; 30-year-old male, incidental finding. Panoramic view shows oval radiolucency at left mandibular angle between the mandibular canal and lower mandibular border (*arrow*)

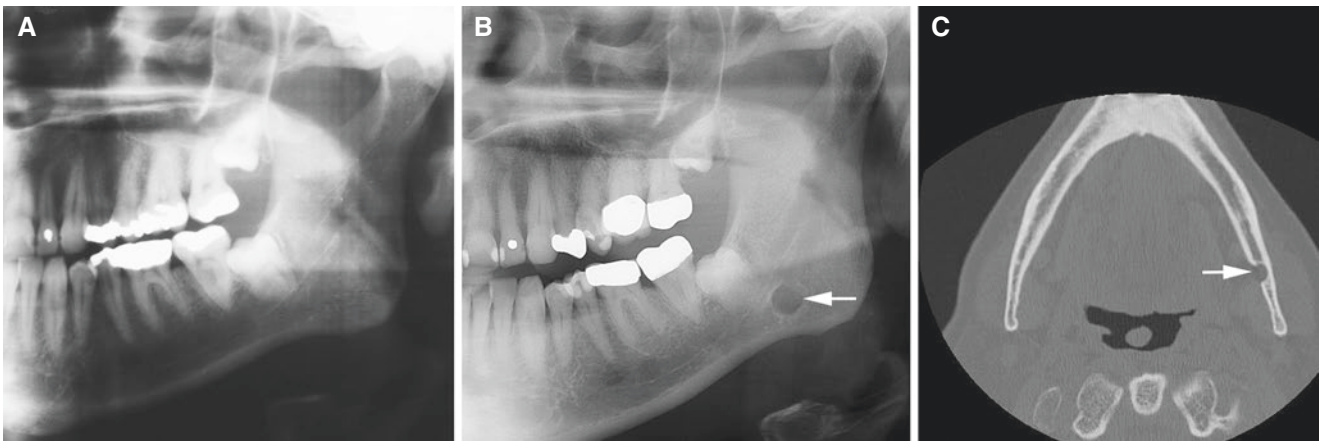

Fig. 2.37 Stafne bone cyst, developed in adult age, incidental finding. (**A**) Panoramic view (28-year-old male) with normal bone in the left mandibular angular region. (**B**) Panoramic view and (**C**) axial CT image (patient now 65 years old) show cyst/defect (*arrow*)

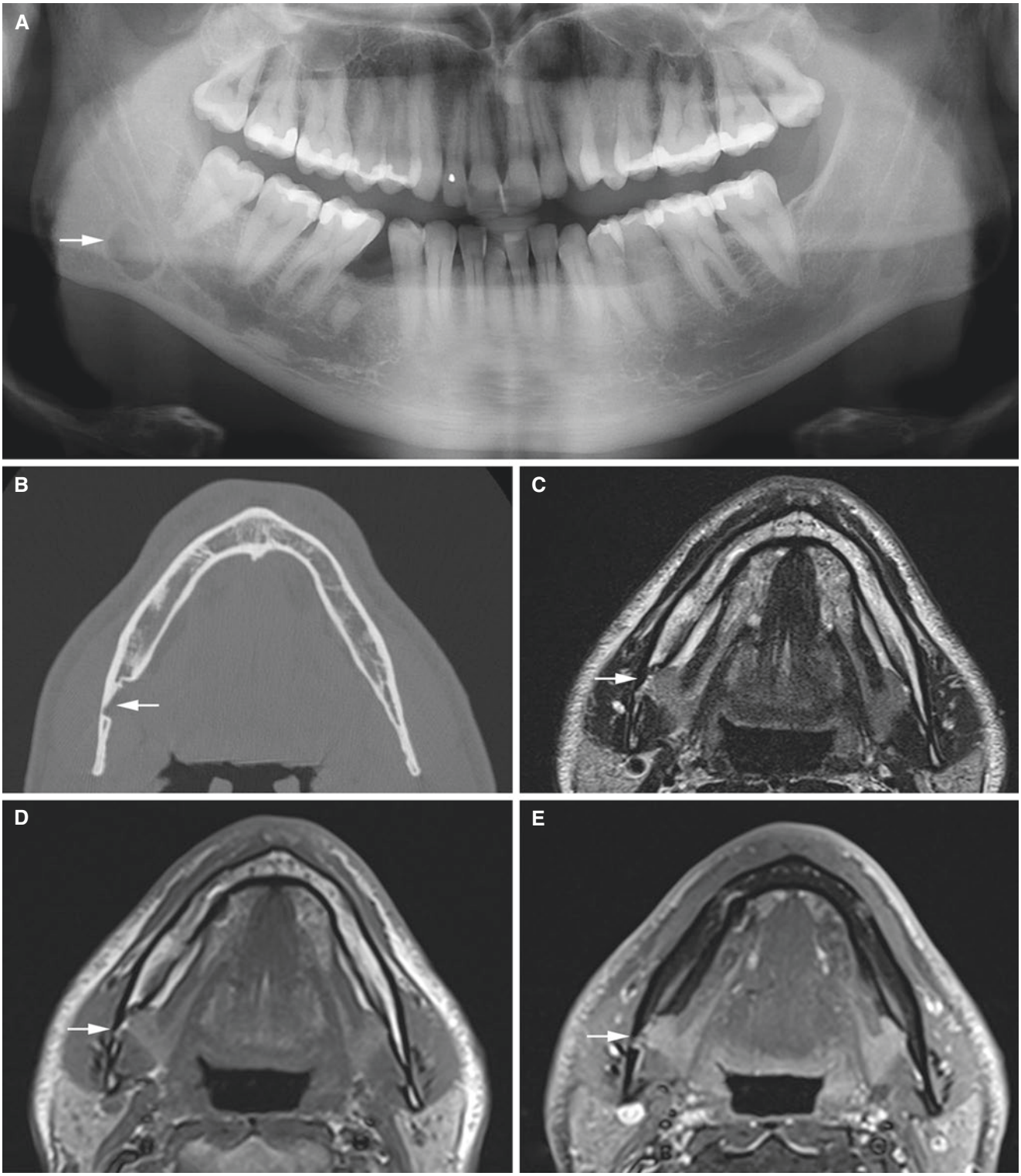

Fig. 2.38 Stafne bone cyst; 45-year-old male, incidental finding. (**A**) Panoramic view shows radiolucency in the right mandibular angular region (*arrow*). (**B**) Axial CT image shows lingual defect (*arrow*). (**C**) Axial T2-weighted MRI shows lingual defect with salivary gland content (*arrow*). (**D**) Axial T1-weighted pre-Gd and (**E**) axial T1-weighted fat sat post-Gd MRI show enhancing salivary gland in lingual defect (*arrow*)

2.14 Retention Cyst

Fig. 2.39

Synonyms: Retention pseudocyst, antral pseudocyst, benign mucus cyst, retention cyst of the maxillary sinus, benign mucosal cyst of sinus, mucosal antral cyst, serous nonsecretory retention pseudocyst

2.14.1 Definition

Swelling of paranasal sinus mucosa. Pathogenesis is controversial but one explanation is submucosal accumulation of secretions.

2.14.2 Clinical Features

- Incidental finding
- More common in males
- May occur more often in spring or fall but can be found all year round

2.14.3 Imaging Features

- Usually located in the maxillary sinus
- Unilateral or bilateral
- Size may vary substantially
- Usually seen on floor of sinus
- Well-defined smooth, dome-shaped form
- Homogeneous internal structure
- No corticated border
- No effect on surrounding structures (no bone destruction)
- T2-weighted and STIR MRI: homogeneous high signal
- T1-weighted post-Gd MRI: no enhancement except in thin peripheral rim

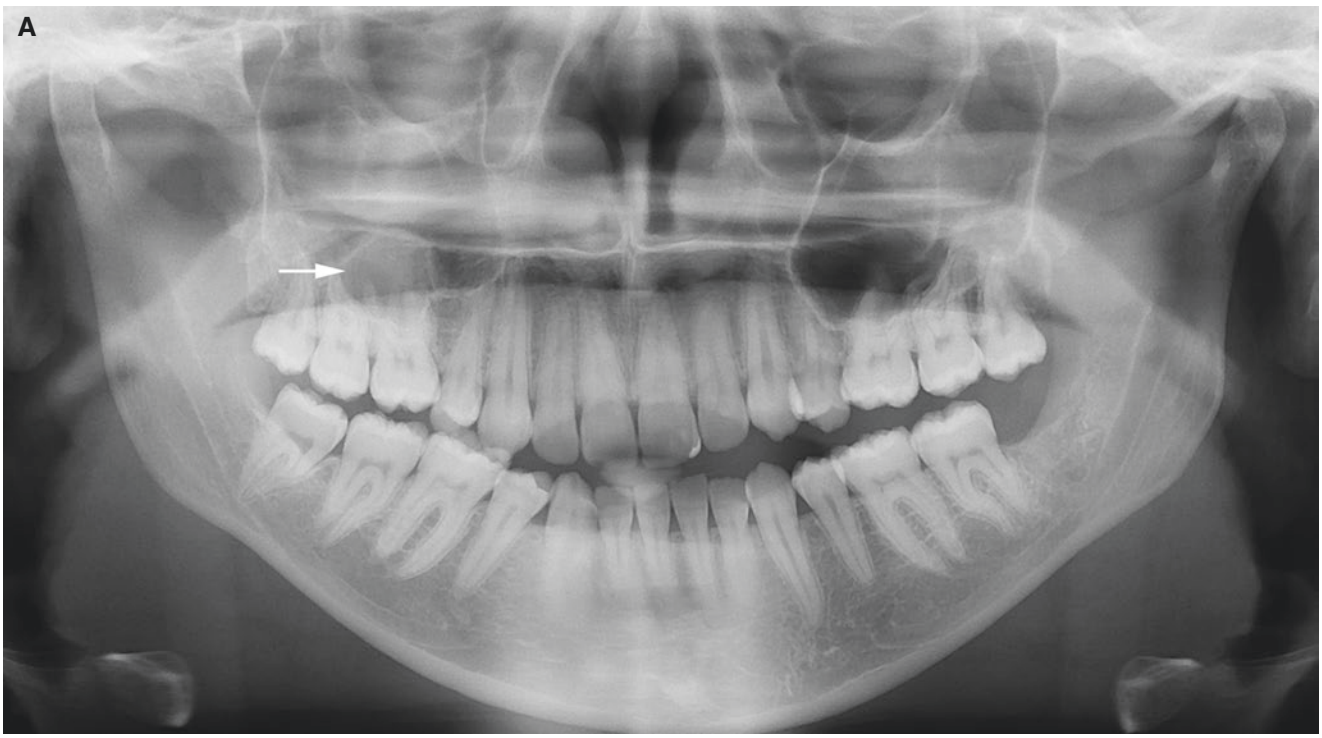

Fig. 2.39 Retention cyst, maxillary sinus; 23-year-old female, incidental finding. (**A**) Panoramic view shows radiopacity (*arrow*) in the right maxillary sinus, clinically suspected to be a keratocystic odontogenic tumor due to apparently corticated outline. (**B**) Axial (with cursor lines for **C** and **D**), (**C**) coronal, (**D**, **E**) sagittal, and (**F**) axial (with cursor line for **E**) CT images show radiopacity in the right maxillary sinus without cortical outline (*arrow*) and without bone destruction but with bone septa (*arrowheads*) in buccal part of retention cyst (**D**), simulating corticated outline on panoramic view (**A**). (**G**) Axial STIR, (**H**) coronal STIR, and (**I**) coronal T2-weighted MRI shows homogeneous high signal intensity (*arrow*). (**J**) Axial T1-weighted pre-Gd, (**K**) axial T1-weighted post-Gd, and (**L**) coronal T1-weighted fat sat post-Gd MRI show no contrast enhancement except in thin peripheral rim (*arrow*)

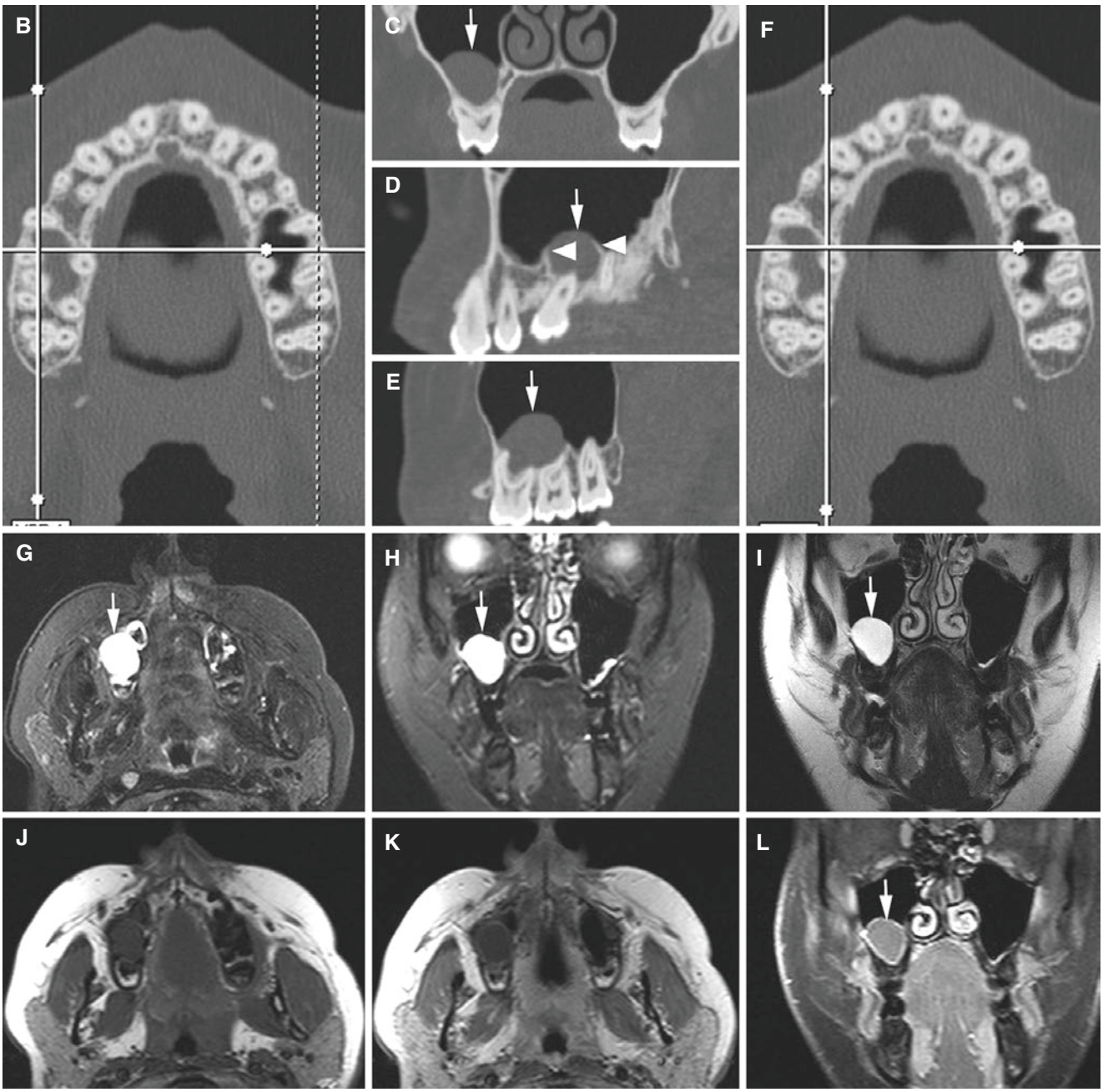

Fig. 2.39 (continued)

Suggested Reading

Abdolali F, Zoroofi RA, Otake Y, Sato Y (2016) Automatic segmentation of maxillofacial cysts in cone beam CT images. Comput Biol Med 72:108–119

Akinyamoju AO, Gbadebo SO, Adeyemi BF (2014) Periapical lesions of the jaws: a review of 104 cases in Ibadan. Ann Ib Postgrad Med 12:115–119

Akkas I, Toptas O, Ôzan F, Yilmaz F (2015) Bilateral glandular odontogenic cyst of mandible: a rare occurrence. J Maxillofac Oral Surg 14(Suppl 1):443–447

Anchlia S, Bahl S, Shah V, Vyas S (2015) Glandular odontogenic cyst: a rare entity revealed and a review of the literature. BMJ Case Rep. doi:10.1136/bcr-2015-211502

Arce K, Streff CS, Ettinger KS (2016) Pediatric odontogenic cysts of the jaws. Oral Maxillofac Surg Clin North Am 28:21–30

Chell M, Idle M, Green J (2015) Case report: an unusual finding of a solitary bone cyst in a patient with a fractured mandible. Dent Update 42:977–978

Chiapasco M, Palombo D (2015) Sinus grafting and simultaneous removal of large antral pseudocysts of the maxillary sinus with a micro-invasive intraoral access. Int J Oral Maxillofac Surg 44:1499–1505

Deepthi PV, Beena VT, Padmakumar SK, Rajeev R, Sivakumar R (2016) A study of 1177 odontogenic lesions in a South Kerala population. J Oral Maxillofac Pathol 20:202–207
El-Naggar AK, JKC C, Grandis JR, Takata T, Slootweg PJ (eds) (2017) WHO classification of head and neck tumours. IARC Press, Lyon
Farman AG, Nortje CJ, Wood RE (eds) (1993) Cysts of the jaws. In: Oral and maxillofacial diagnostic imaging. Mosby, St. Louis, pp 210–238
Gadipelly S, Reddy VB, Sudheer M, Kumar NV, Harsha G (2015) Bilateral calcifying odontogenic cyst: a rare entity. J Maxillofac Oral Surg 14:826–831
Hisatomi M, Asaumi J-I, Konouchi H, Shigehara H, Yanagi Y, Kishi K (2003) MR imaging of epithelial cysts of the oral and maxillofacial region. Eur J Radiol 48:178–182
Jones RS, Dillon J (2016) Nonodontogenic cysts of the jaws and treatment in the pediatric population. Oral Maxillofac Surg Clin North Am 28:31–44
Koppang HS, Johannessen S, Haugen LK, Haanaes HR, Solheim T, Donath K (1998) Glandular odontogenic cyst (sialo-odontogenic cyst): report of two cases and literature review of 45 previously reported cases. J Oral Pathol Med 27:455–462
Kramer IRH (1974) Changing views on oral disease. Proc R Soc Med 67:271–276
Kramer IRH, Pindborg JJ, Shear M (1992) World Health Organisation international histological classification of tumours. Histological typing of odontogenic tumours, 2nd edn. Springer, Berlin, pp 34–42
Kün-Dabois JD, Pare A, Goga D, Laure B (2015) In situ squamous cell carcinoma arising in a mandibular radicular cyst. Eur Ann Otorhinolaryngol Head Neck Dis 132:305–306
Lovas JGL (1991) Cysts. In: Miles DA, Van Dis M, Kaugars GE, Lovas JGL (eds) Oral and maxillofacial radiology. Radiologic/pathologic correlations. Saunders, Philadelphia, pp 21–50
MacDonald D (2016) Lesions of the jaws presenting as radiolucencies on a cone-beam CT. Clin Radiol 71:972–985
Malek M, Cortes LM, Sigurdsson A, Rosenberg PA (2015) Differential diagnosis of a periapical radiolucent lesion. A case report and review of the literature. NY State Dent J 81:52–56
Manjunatha BS, Harsch A, Purohit S, Naga MV (2015) Adenomatoid odontogenic tumor associated with a dentigerous cyst. J Cancer Res Ther 11:649
Maruyama S, Yamazaki M, Abé T, Babkair H, Cheng J, Saku T (2015) Paradental cyst is an inclusion cyst of the junctional/sulcular epithelium of the gingiva: histopathologic and immunohistochemical confirmation for its pathogenesis. Oral Surg Oral Med Oral Pathol Oral Radiol 120:227–237
Miloglu Ô, Sekerci AE, Yasa Y, Dagistan S (2015) Unilateral bone cavities situated near the angle of the mandible. J Craniofac Surg. doi:10.1097/SCS.0000000000001262
Minami M, Kaneda T, Ozawa K, Yamamoto H, Itai Y, Ozawa M, Yoshikawa K, Sasaki Y (1996) Cystic lesions of the maxillomandibular region: MR imaging distinction of odontogenic keratocysts and ameloblastomas from other cysts. AJR Am J Roentgenol 166:943–949
Mittal A, Narang V, Kaur G, Sood N (2015) Glandular odontogenic cyst of mandible: a rare entity. J Clin Diagn Res. doi:10.7860/JCDR/2015/15005.6901
Mortazavi H, Baharvand M (2016) Jaw lesions associated with impacted tooth: a radiographic diagnostic guide. Imaging Sci Dent 46:147–157
Nair PN (1998) Review. New perspectives on radicular cysts: do they heal? Int Endod J 31:155–160
Nayyer NV, Macluskey M, Keys W (2015) Odontogenic cysts – an overview. Dent Update 42(548-551):553–555
Okada K, Rysavy S, Flores A, Linguraru MG (2015) Noninvasive differential diagnosis of dental periapical lesions in cone-beam CT scans. Med Phys 42(4):1653–1665
Omoregie FO, Sede MA, Ojo AM (2015) Ameloblastomatous change in radicular cyst of the jaw in a Nigerian population. Ghana Med J 49:107–111
Owosho AA, Potluri A, Bauer Iii RE, Bilodeau EA (2015) Ameloblastic carcinoma of the mandible manifesting as an infected odontogenic cyst. Gen Dent 63:e1–e4
Pakchoian AJ, Mahdian M, Durschlag ME (2015) Orthokeratinized odontogenic cyst: case of a rare peripheral counterpart. J Calif Dent Assoc 43:251–254
Peker E, Ôgütlü F, Karaca IR, Gültekin ES, Cakir M (2016) A 5 year retrospective study of biopsied jaw lesions with the assessment of concordance between clinical and histopathological diagnoses. J Oral Maxillofac Pathol 20:78–85
Pindborg JJ, Kramer IRH, Torloni H (1971) Histological typing of odontogenic tumours, jaw cysts, and allied lesions, 1st edn. World Health Organization, Geneva
Probst FA, Probst M, Pautke CH, Kaltsi E, Otto S, Schiel S et al (2015) Magnetic resonance imaging: a useful tool to distinguish between keratocystic odontogenic tumours and odontogenic cysts. Br J Oral Maxillofac Surg 53:217–222
Reichart PA, Philipsen HP (2004) Aneurysmal bone cavity (aneurysmal bone cyst). In: Odontogenic tumors and allied lesions, 1st edn. Quintessence, London, pp 335–341
Resnick CM, Dentino KM, Garza R, Padwa BL (2016) a management strategy for idiopathic bone cavities of the jaws. J Oral Maxillofac Surg 74:1153–1158
Sethukumar P, Taghi A, Kuchai R (2015) A rare case of bilateral nasolabial cysts. BMJ Case Rep. doi:10.1136/bcr-2014-203543
Shah AA, Sangle A, Bussari S, Koshy AV (2016) Glandular odontogenic cyst: a diagnostic dilemma. Indian J Dent 7:38–43
Shear M, Speight PM (eds) (2007) Cysts of the oral and maxillofacial regions, 4th edn. Oxford, Blackwell Munksgaard
Sokhn S, Noujeim M, Bacho R, Nasseh HN (2015) Inflammatory paradental cyst in the mandibular region: a report of two cases. Tex Dent J 132:310–314
Spinelli HM, Isenberg JS, O'Brien M (1994) Nasopalatine duct cysts and the role of magnetic resonance imaging. J Craniofac Surg 5:57–60
Sridevi K, Kaushik A, Ramaswamy P, Manjula M, Vinod VC, Aravinda K (2015) Dentigerous cysts of maxillofacial region – clinical, radiographic and biochemical analysis. Kathmandu Univ Med (KUMJ) 13:8–11
Tkaczuk AT, Bhatti M, Caccamese JF Jr, Ord RA, Pereira KD (2015) Cystic lesions of the jaw in children: a 15-year experience. JAMA Otolaryngol Head Neck Surg 141:834–839
Trosman SJ, Krakovitz PR (2015) Pediatric maxillary and mandibular tumors. Otolaryngol Clin North Am 48:101–119
Walkolbinger R, Beck-Mannagetta J (2016) Long-term results after treatment of extensive odontogenic cysts of the jaws: a review. Clin Oral Investig 20:15–22
Weber AL, Kaneda T, Scrivani SJ, Aziz S (2003) Jaw: cysts, tumors, and nontumorous lesions. In: Som PM, Curtin HD (eds) Head and neck imaging, 4th edn. Mosby, St. Louis, pp 930–994
White SC, Pharoah MJ (eds) (2014) Cysts. In: Oral radiology. Principles and interpretation, 7th edn. Mosby, St. Louis, pp 334–358
Yao L, Xu X, Ren M, Liu D, Ni Z, Lin F (2015) Inflammatory dentigerous cyst of mandibular first premolar associated with endodontically treated primary first molar: a rare case report. Eur J Paediatr Dent 16:201–204

Benign Jaw Tumors and Tumorlike Conditions

3

Abstract

This chapter illustrates benign tumors; keratocystic odontogenic tumor, ameloblastoma, lipoma, odontogenic fibroma, odontogenic myxoma/myxofibroma, osteoblastoma, ossifying fibroma, juvenile ossifying fibroma, and benign tumorlike conditions; aneurysmal bone cyst, giant cell granuloma, Langerhans cell histiocytosis, cherubism, fibrous dysplasia, osseous dysplasia, osteoma, exostosis, idiopathic osteosclerosis, and odontoma.

3.1 Introduction

Benign processes in the jaws represent a wide spectrum of conditions, many of which are small sized and therefore adequately diagnosed with intraoral and panoramic radiography. However, larger processes may expand jaw bone extensively and grow into neighboring structures. Since some types of benign processes may be locally aggressive and may even be difficult to distinguish from malignant neoplasms, advanced imaging should be applied to precisely assess their structure, extent, and demarcation to surrounding tissues. We present a large number of different conditions so that specialists both in the dental and the medical fields can become familiar with their wide range of imaging appearances. Many cases are illustrated with advanced imaging modalities, in particular CT, but also MRI. In selected cases also 3D CT images and clinical photographs are shown.

3.2 Benign Tumors

The first condition in this section was reclassified to odontogenic keratocyst by WHO in 2017.

3.3 Keratocystic Odontogenic Tumor

Figs. 3.1, 3.2, 3.3, 3.4, 3.5, 3.6, 3.7, 3.8, 3.9, 3.10, 3.11, 3.12, and 3.13

In collaboration with H.-J. Smith · H. Strømme Koppang.

Synonyms: Odontogenic keratocyst (WHO 2017), primordial cyst

3.3.1 Definition

Benign uni- or multicystic, intraosseous tumor of odontogenic origin, with a characteristic, thin lining of parakeratinized stratified squamous epithelium and potentially aggressive, infiltrative behavior. It may be solitary or multiple. The latter is usually one of the stigmata of the inherited nevoid basal cell carcinoma syndrome (WHO 2005). Defined as an odontogenic cyst in 2017 (WHO).

Usually contains thick yellow, cheesy material (keratin).

3.3.2 Clinical Features

- Frequently asymptomatic
- May be very large before detected since swelling not prominent
- Frequently with an impacted tooth
- Two-thirds to more than 80% occur in mandible
- About one-half at angle of mandible, extending anteriorly and superiorly
- Second and third decades
- Males more frequent than females
- Recurrence rate up to 60% reported
- Gorlin–Goltz (basal cell nevus) syndrome and multiple tumors

T.A. Larheim, P.-L.A. Westesson, *Maxillofacial Imaging*, https://doi.org/10.1007/978-3-319-53319-3_3

3.3.3 Imaging Features

- Radiolucency
- Unilocular round, oval, scalloped (with or without bone septa), or occasionally multilocular
- Border usually sclerotic, may be thinned, intact, or perforated, even diffuse in parts
- Bone expansion or not; frequently not prominent
- Soft-tissue extension through cortical perforation
- May displace teeth, mandibular canal
- Tooth resorption rare
- Frequently located with, but unrelated to, impacted third molar
- T1-weighted MRI: homogeneous or heterogeneous intermediate signal
- T2-weighted and STIR MRI: heterogeneous high signal
- T1-weighted post-Gd MRI: no enhancement or enhancement of thin peripheral rim; more evident if secondarily inflamed

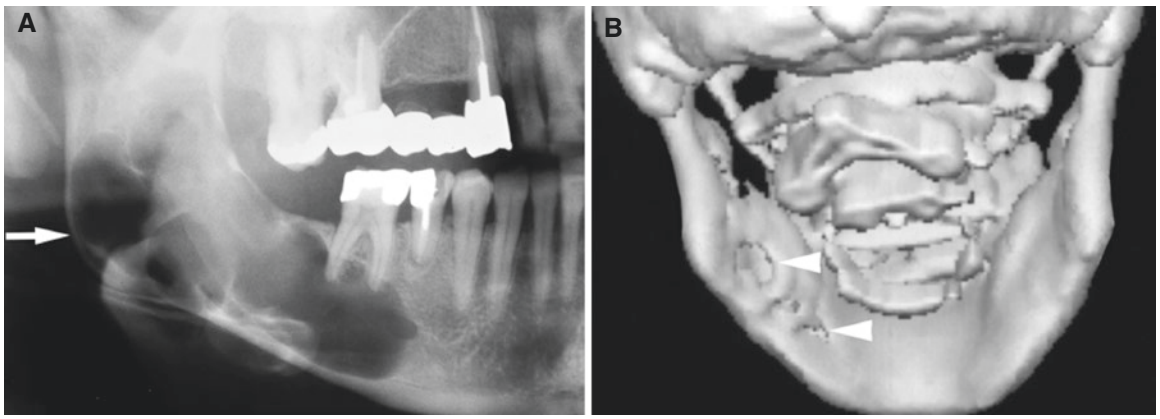

Fig. 3.1 Keratocystic odontogenic tumor, mandible; 52-year-old female with incidental finding at routine dental radiography. (**A**) Panoramic view shows scalloped radiolucency with bone septa and sclerotic border (*arrow*). (**B**) 3D CT image shows cortical defects on lingual side of mandible (*arrowheads*)

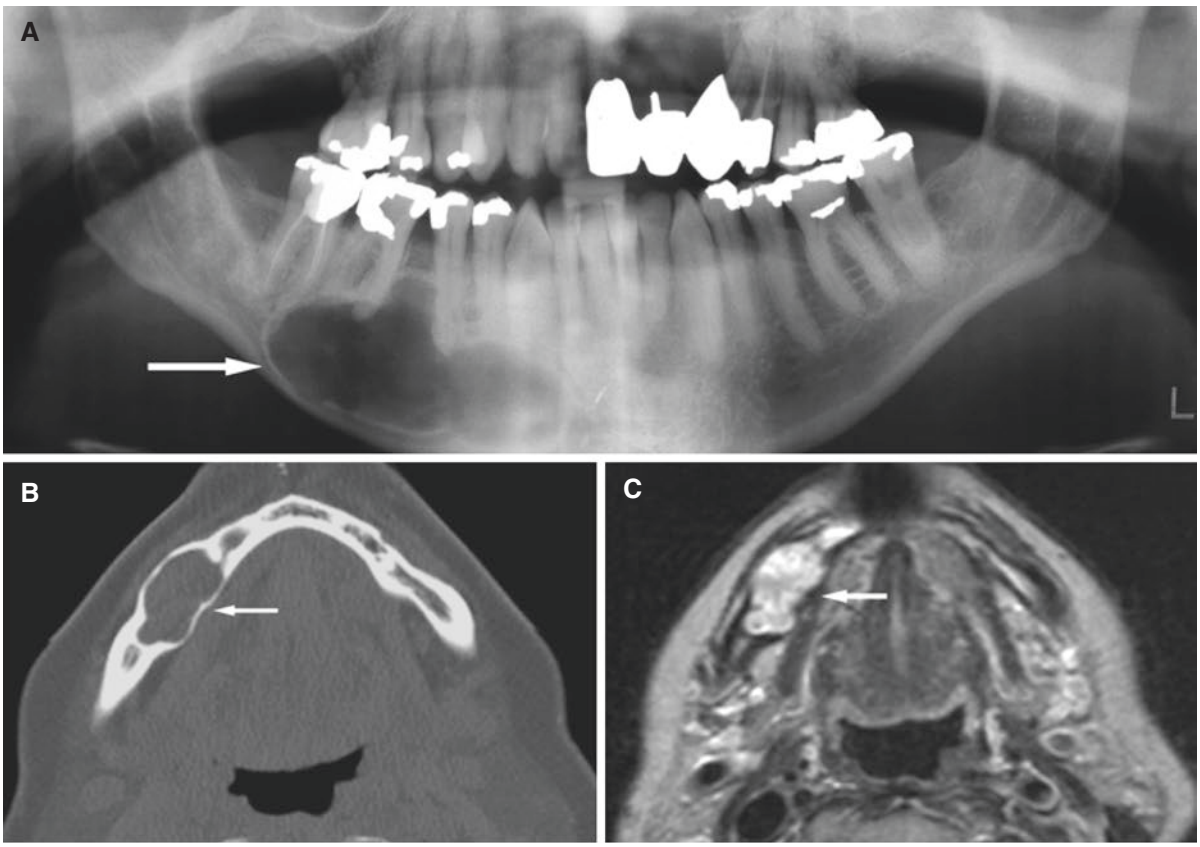

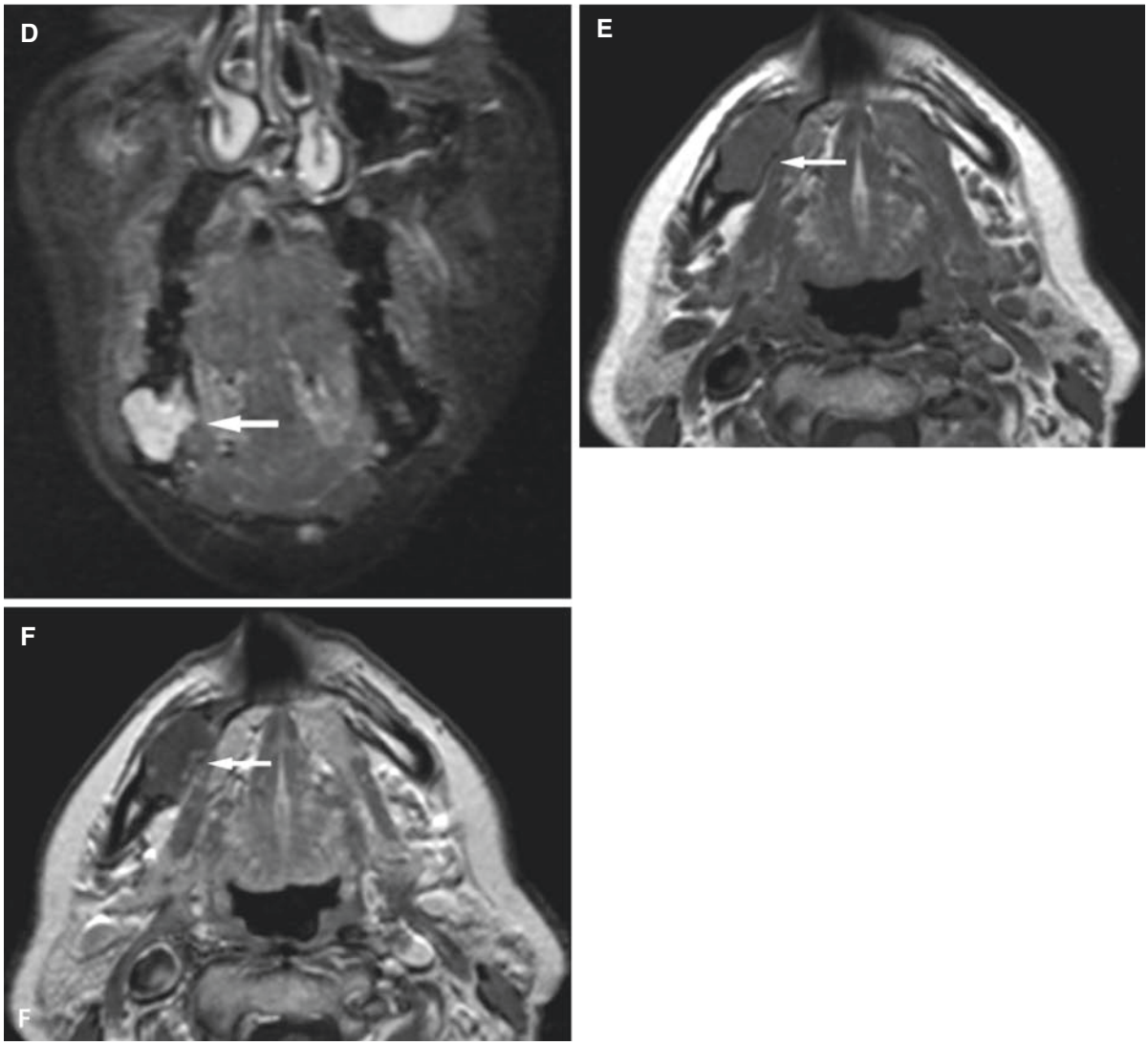

Fig. 3.2 (continued)

Fig. 3.2 Keratocystic odontogenic tumor, mandible; 61-year-old female with incidental finding at routine dental radiography. (**A**) Panoramic view shows unilocular radiolucency with sclerotic border (*arrow*). (**B**) Axial CT image shows oval expansive process with intact cortical outline (*arrow*). (**C**) Axial T2-weighted MRI shows slightly heterogeneous high signal (*arrow*). (**D**) Coronal STIR MRI shows slightly heterogeneous high signal (*arrow*). (**E**) Axial T1-weighted pre-Gd MRI shows homogeneous intermediate signal (*arrow*). (**F**) Axial T1-weighted post-Gd MRI shows no enhancement except partial enhancement of thin, peripheral rim (*arrow*)

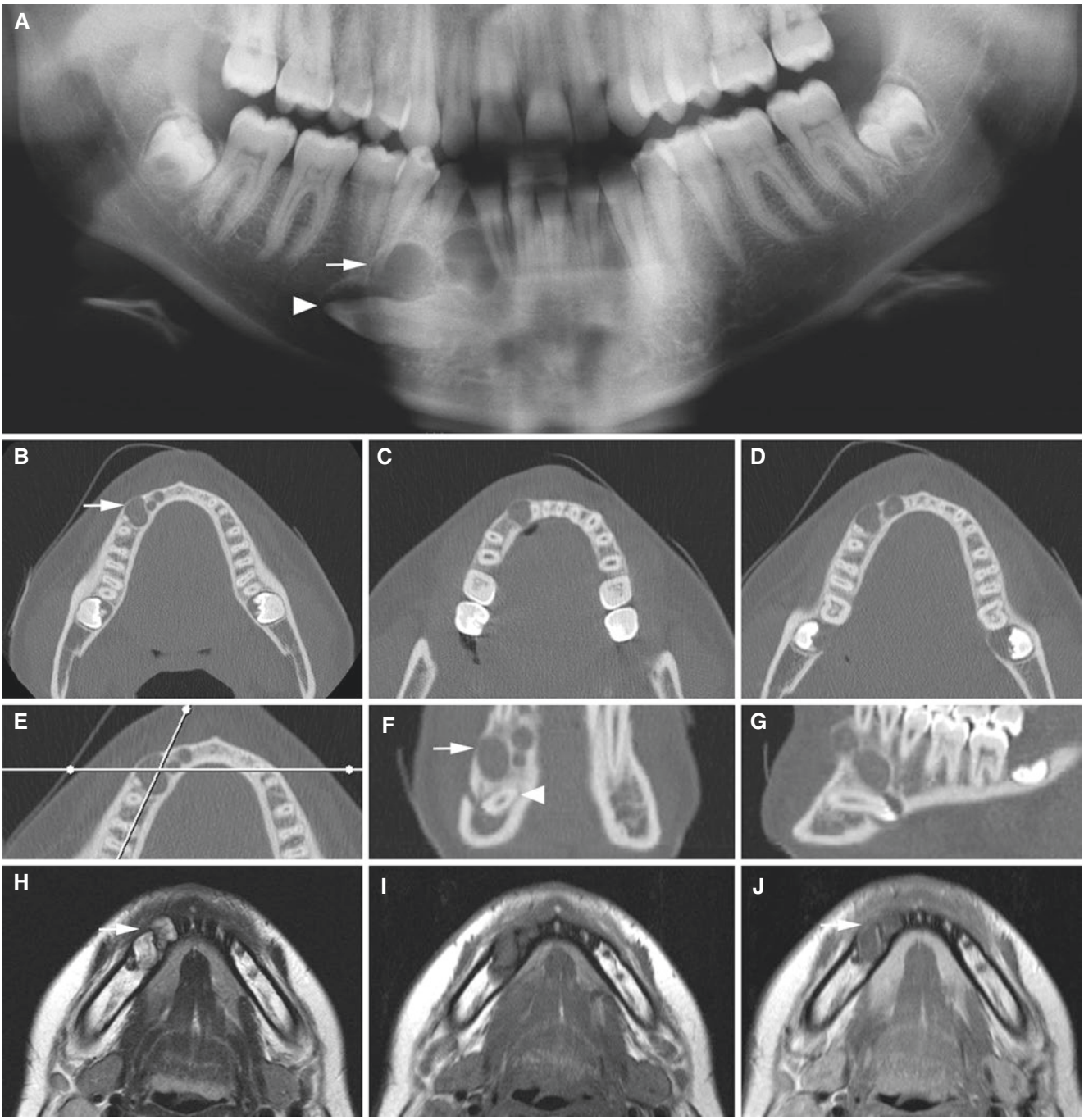

Fig. 3.3 Keratocystic odontogenic tumor, mandible; 15-year-old female with impacted right canine without symptoms. (**A**) Panoramic view shows multilocular radiolucency (*arrow*) and impacted canine (*arrowhead*). (**B**, **C,** and **D**) Axial CT images confirm multilocular radiolucency and additionally show only slight buccal expansion (*arrow*). (**E**) Axial (with cursor lines). (**F**) Coronal and (**G**) oblique sagittal CT images confirm multilocular radiolucency with slight buccal expansion (*arrow*) and impacted canine (*arrowhead*). (**H**) Axial T2-weighted MRI shows heterogeneous high signal (*arrow*). (**I**) Axial T1-weighted pre-Gd and (**J**) axial T1-weighted post-Gd MRI shows no contrast enhancement except in thin peripheral rim (*arrow*)

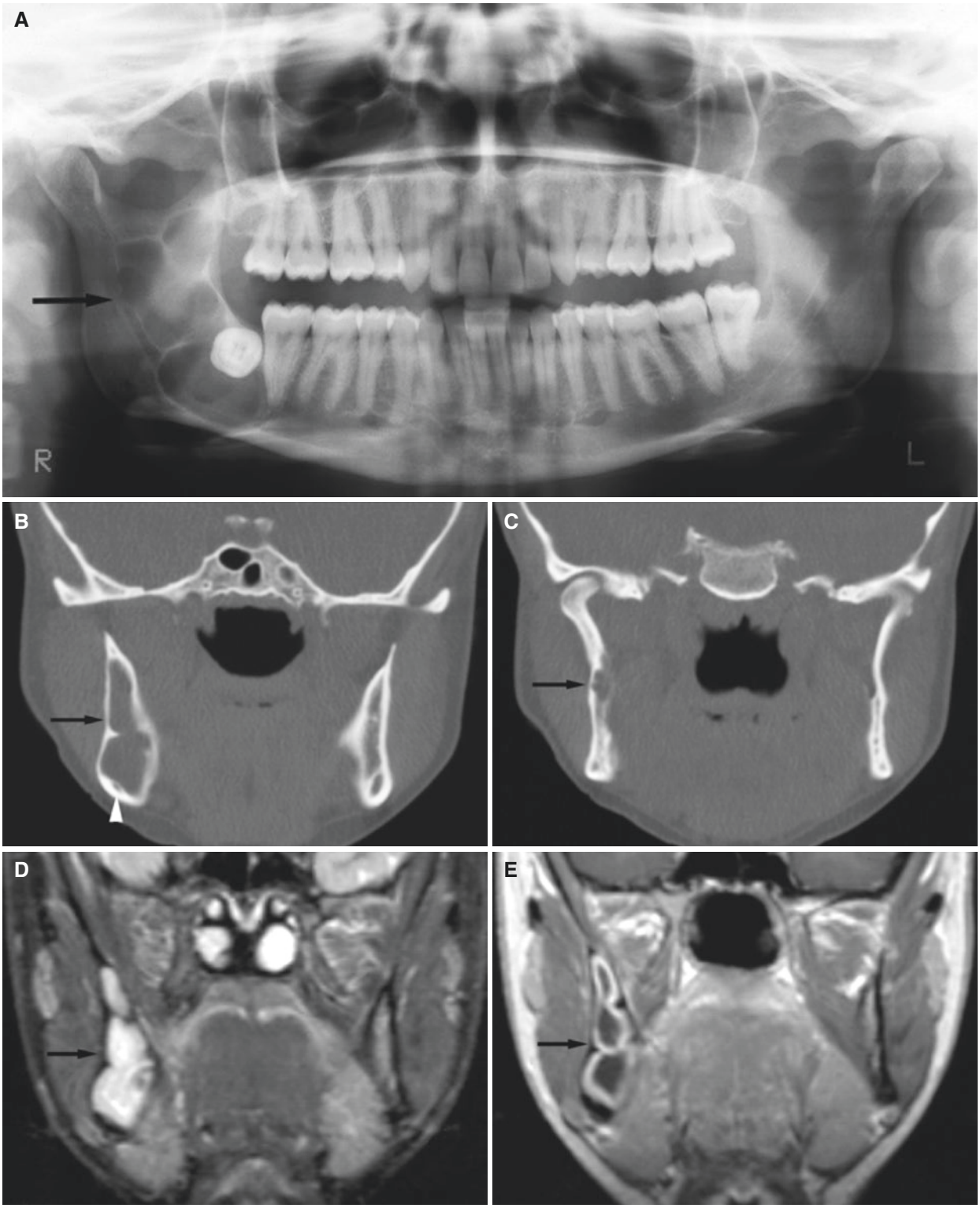

Fig. 3.4 Keratocystic odontogenic tumor, mandible; 42-year-old female with incidental finding at routine dental radiography. (**A**) Panoramic view shows scalloped radiolucency with bone septa and impacted third molar (*arrow*). (**B**) Coronal CT image shows expansive radiolucency with intact cortical bone (*arrow*), and mandibular canal displaced peripherally (*arrowhead*). (**C**) Coronal CT image shows scalloped border in ramus (*arrow*). (**D**) Coronal STIR MRI shows high signal (*arrow*) and possibly two compartments. (**E**) Coronal T1-weighted post-Gd MRI shows no enhancement except peripheral rim (*arrow*) and possibly three compartments. MRI was performed a few days after a biopsy was taken, probably with subsequent inflammatory reaction; evident soft-tissue membrane

Fig. 3.5 Keratocystic odontogenic tumor, infected, mandible; 66-year-old female with pus from fistula in retromolar area of the right mandible. (**A**) Panoramic view suggests radiolucency in retromolar area (*arrow*). (**B**, **C**) Axial CT images show radiolucency in retromolar area without buccolingual expansion and with some central air, lingual cortical defect (*arrow*), and thick cortical outline. (**D**) Axial T2-weighted MRI shows heterogeneous high signal (*arrow*). (**E**) Axial T1-weighted pre-Gd and (**F**) axial T1-weighted fat sat post-Gd MRI show almost solid contrast enhancement; thick soft-tissue membrane due to infection (*arrow*)

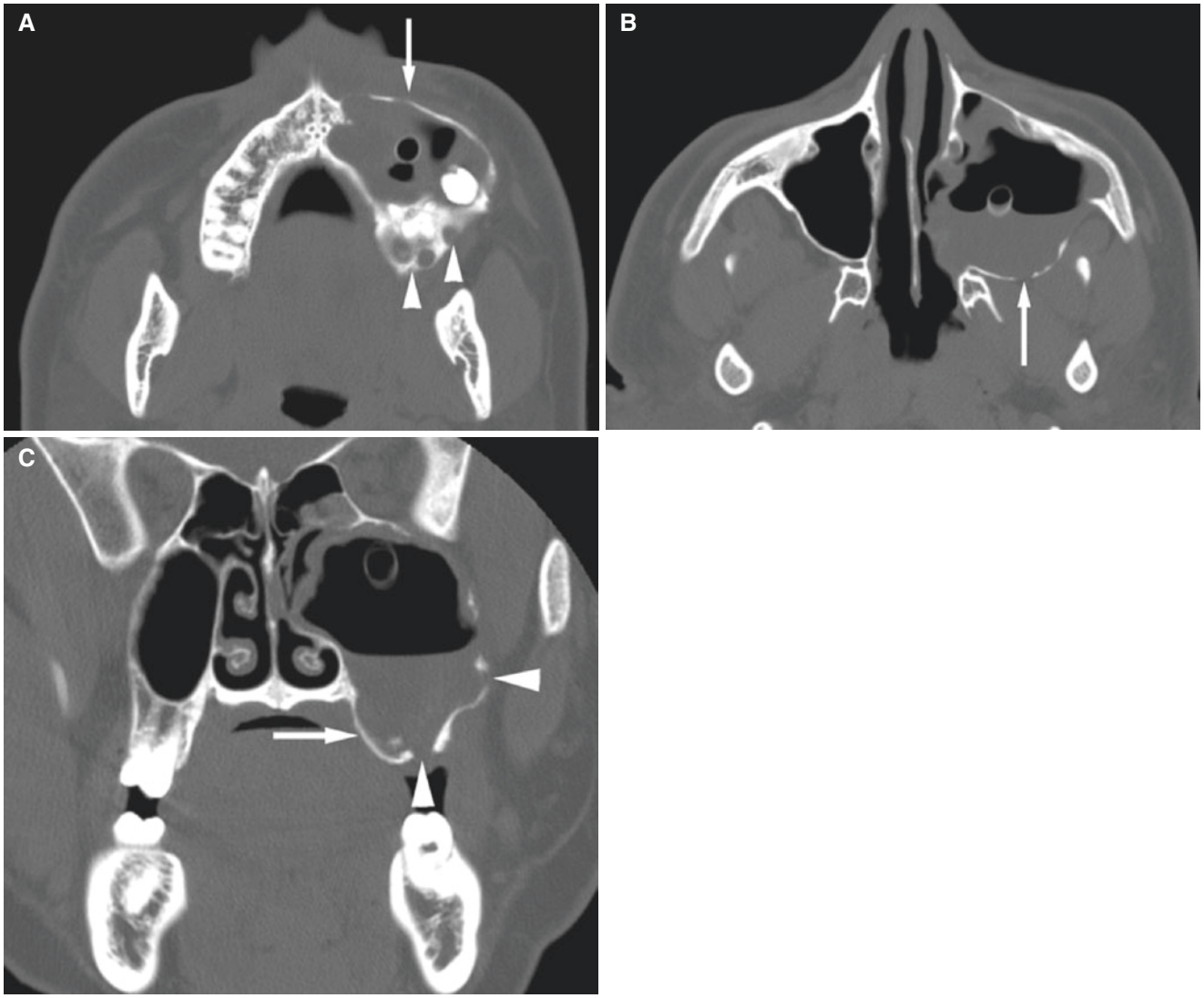

Fig. 3.6 Keratocystic odontogenic tumor, maxilla; 16-year-old male with painless expansion of maxilla, complicated by sinusitis. (**A**) Axial CT image (after biopsy with a drain in place) shows expansive process in the left maxillary sinus (*arrow*), multilocular in posterior part (*arrowheads*). (**B**) Axial CT image shows expansion of posterior thinned sinus wall with cortical defects (*arrow*) and fluid. (**C**) Coronal CT image shows expansion of palatal sinus wall (*arrow*), and cortical defects both in lateral and alveolar sinus walls (*arrowheads*), and fluid

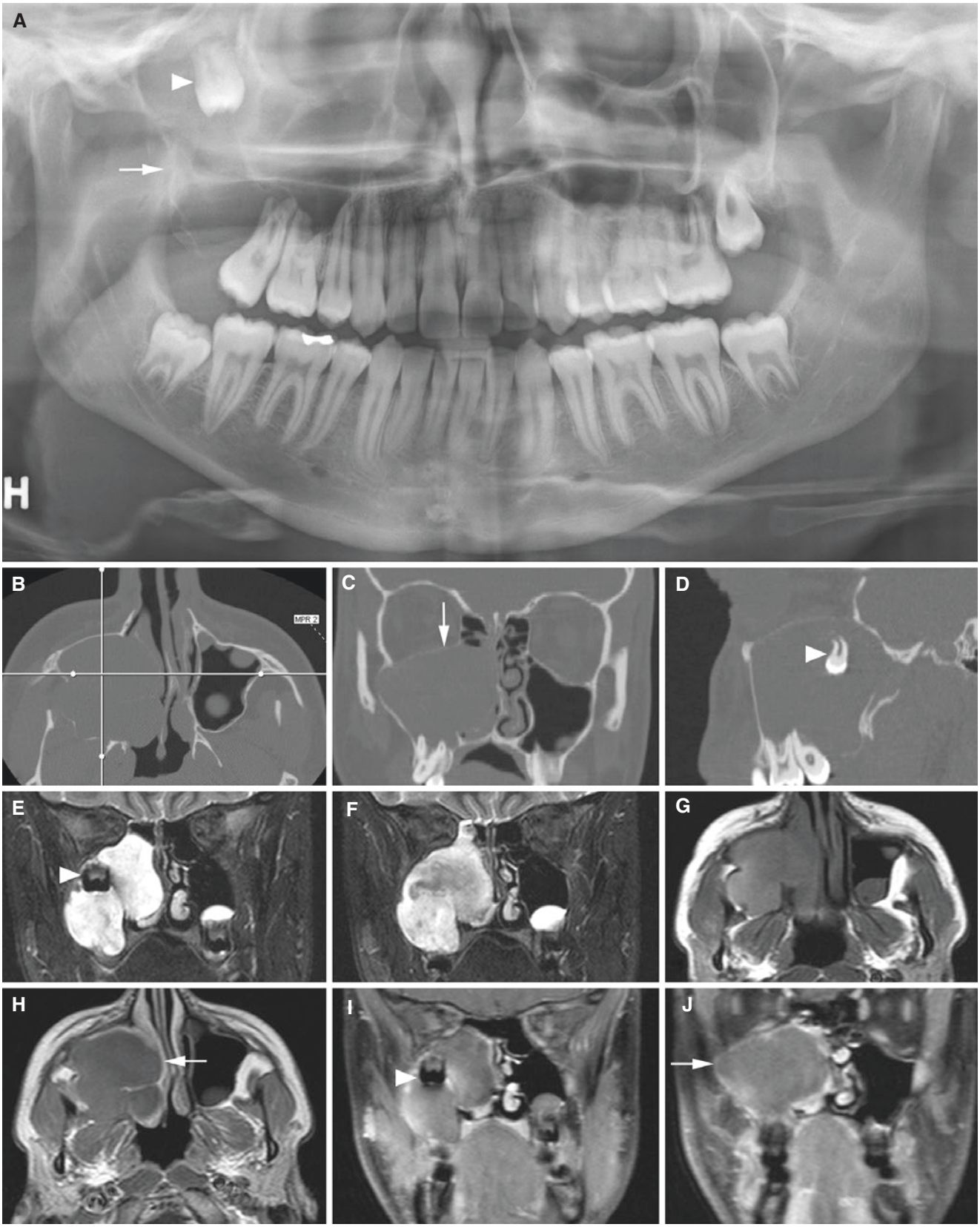

Fig. 3.7 Keratocystic odontogenic tumor, maxillary sinus/maxilla; 16-year-old male with variable sinus symptoms. (**A**) Panoramic view shows radiolucency in right maxilla (*arrow*) and displaced tooth (*arrowhead*). (**B**) Axial (with cursor lines), (**C**) coronal, and (**D**) sagittal CT images show expanding maxillary sinus with partially corticated outline (*arrow*) and impacted wisdom tooth (*arrowhead*). (**E**, **F**) Coronal STIR MRI shows well-defined expansion with heterogeneous high signal and impacted tooth (*arrowhead*). (**G**) Axial T1-weighted pre-Gd, (**H**) axial T1-weighted post-Gd, and (**I**, **J**) coronal T1-weighted fat sat post-Gd MRI show no contrast enhancement except in thin peripheral rim (*arrow*)

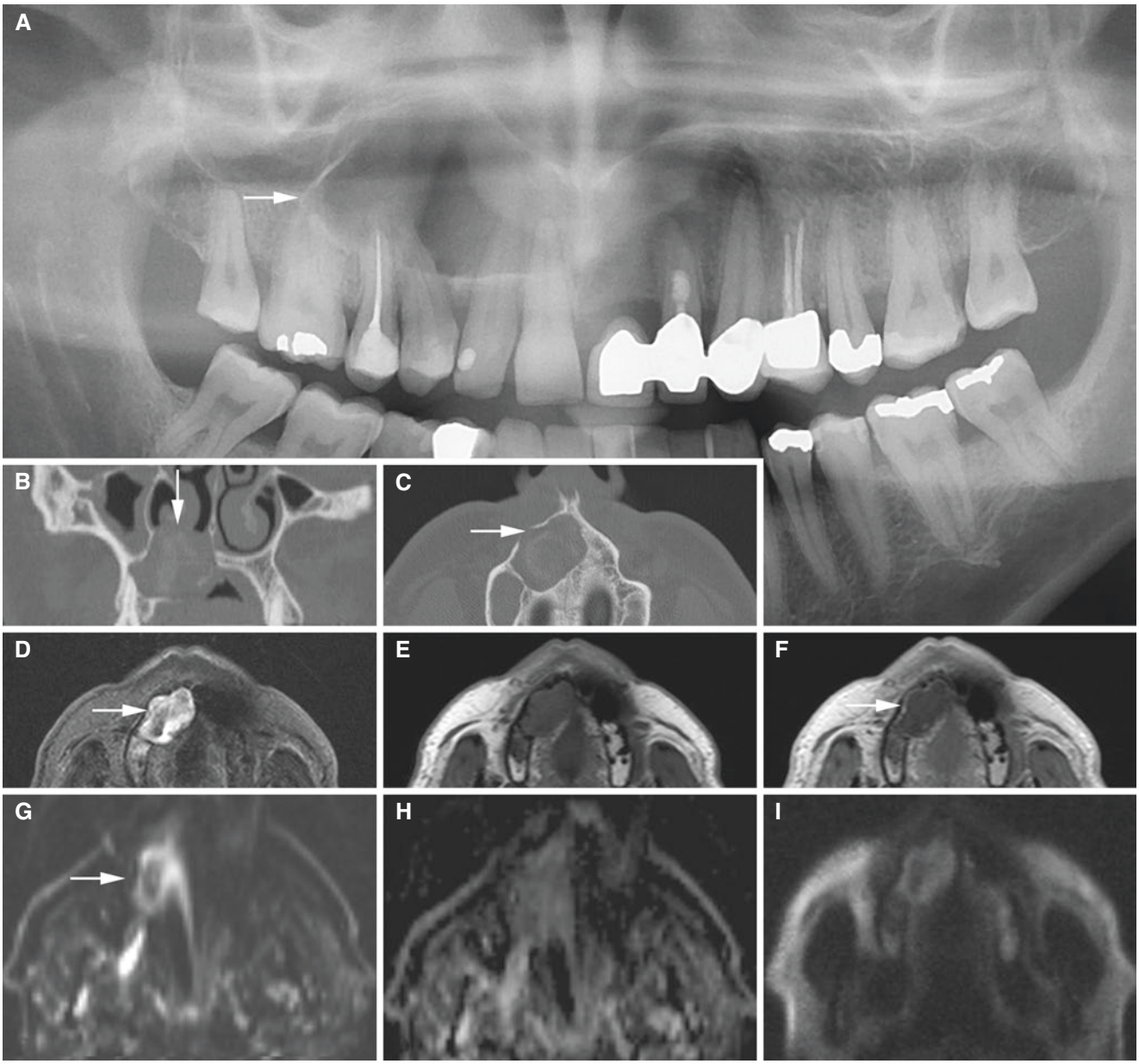

Fig. 3.8 Keratocystic odontogenic tumor, maxilla; 48-year-old male with swelling in anterior part of the right hard palate. (**A**) Panoramic view shows radiolucency with corticated outline (*arrow*). (**B**) Coronal and (**C**) axial CT images show well-defined, expanding radiolucency with cortical defects (*arrow*). (**D**) Axial T2-weighted MRI shows heterogeneous high signal (*arrow*). (**E**) Axial T1-weighted pre-Gd and (**F**) axial T1-weighted post-Gd MRI show no contrast enhancement except in thin peripheral rim (*arrow*). (**G**) Axial diffusion-weighted MRI, (**H**) axial ADC map, and (**I**) axial diffusion-weighted HASTE MRI all show restricted diffusion within lesion (compare with Fig. 2.26)

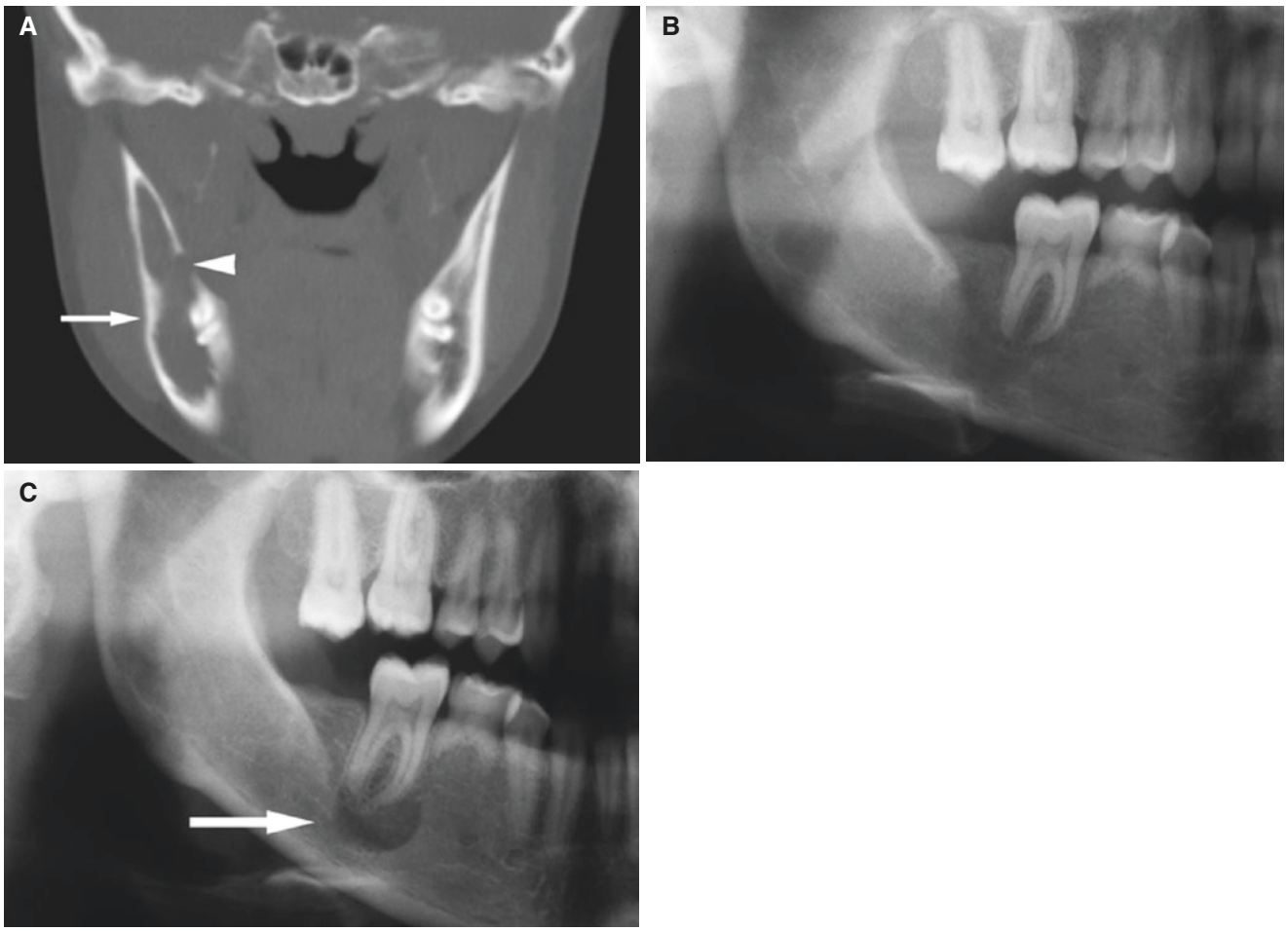

Fig. 3.9 Keratocystic odontogenic tumor, mandible; 19-year-old female with incidental finding at routine dental radiography, followed for 6 years, never symptomatic. (**A**) Coronal CT image shows radiolucency (*arrow*) with cortical defect (*arrowhead*). (**B**) Panoramic view, 4 years postoperatively, shows bone regeneration. (**C**) Panoramic view, 6 years postoperatively, shows recurrence of tumor (*arrow*)

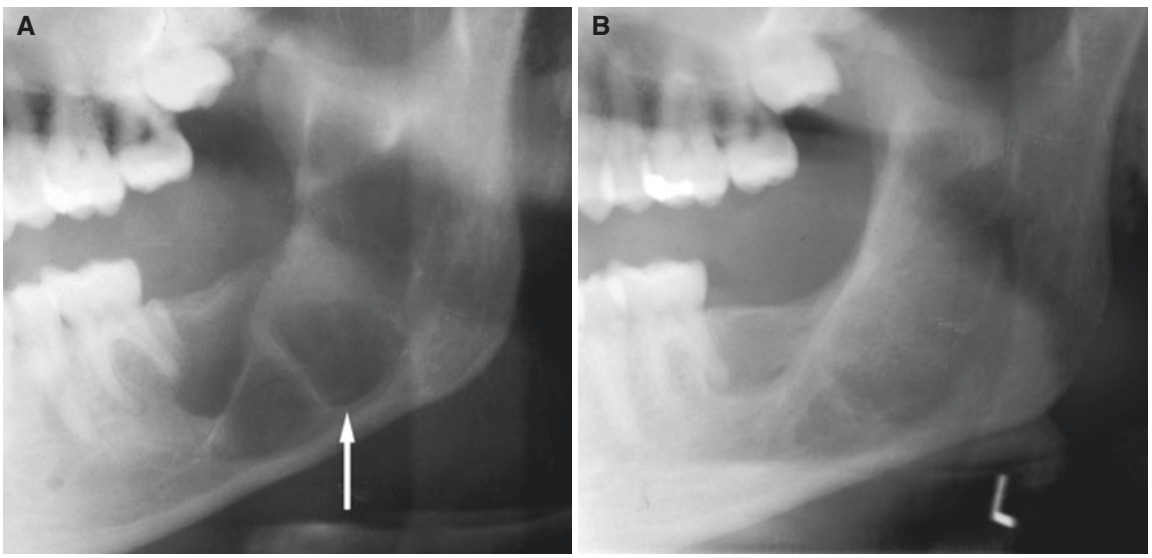

Fig. 3.10 Keratocystic odontogenic tumor, mandible; 33-year-old male, painless perimandibular swelling 12 years after the first surgery. (**A**) Panoramic view shows multilocular radiolucency (*arrow*). (**B**) Panoramic view 9 months postoperatively shows nearly complete regeneration. (**C**) Panoramic view 12 years after surgery shows recurrence of tumor, now crossing midline, being more extensive than initially (*arrow*). (**D**) Axial CT image shows expansive radiolucency with intact cortical bone (*arrow*). (**E**) Axial T2-weighted MRI shows heterogeneous high to intermediate signal (*arrow*). (**F**) Axial T1-weighted pre-Gd MRI shows heterogeneous intermediate to low signal (*arrow*). (**G**) Axial T-weighted post-Gd MRI shows no contrast enhancement (*arrow*)

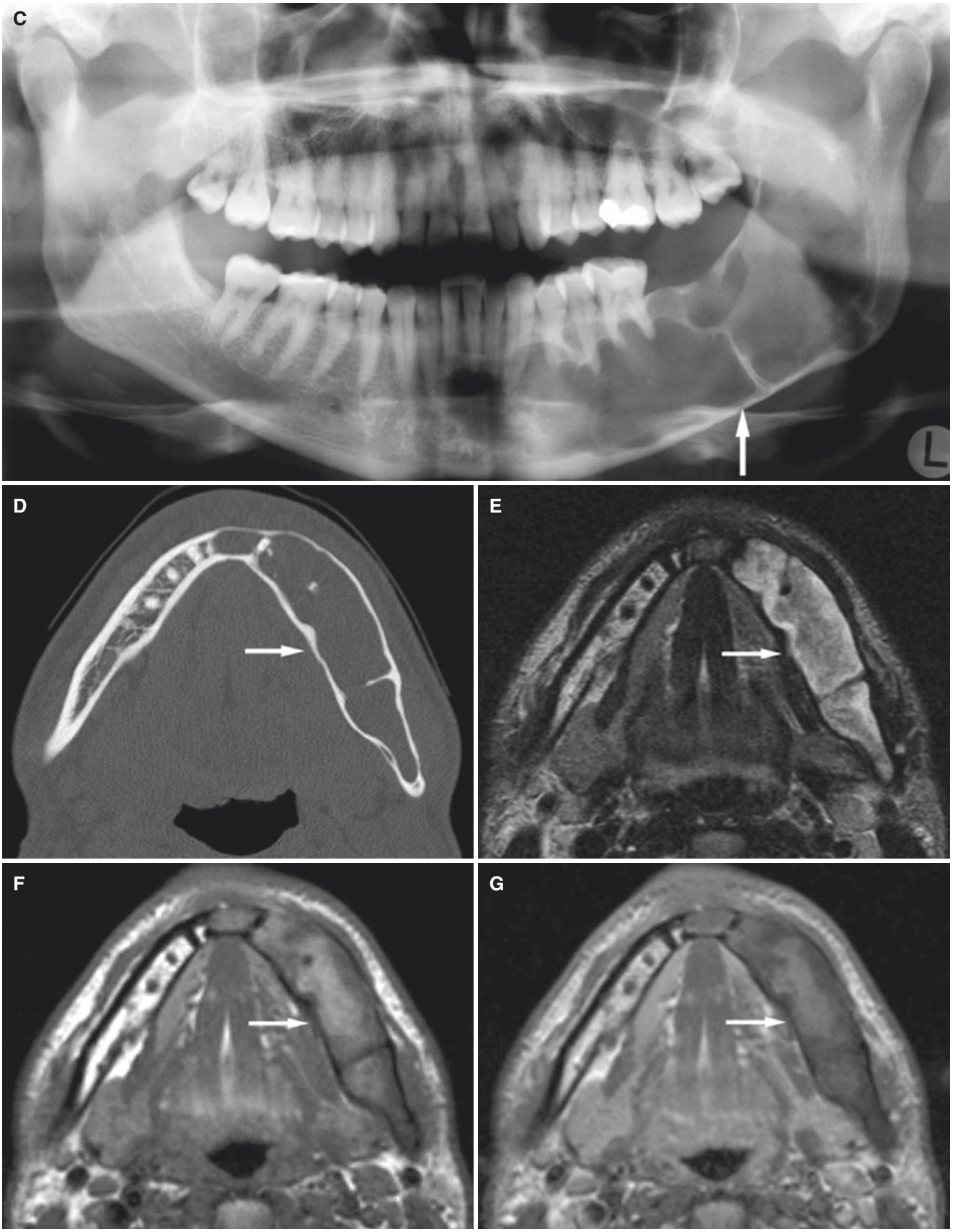

Fig. 3.10 (continued)

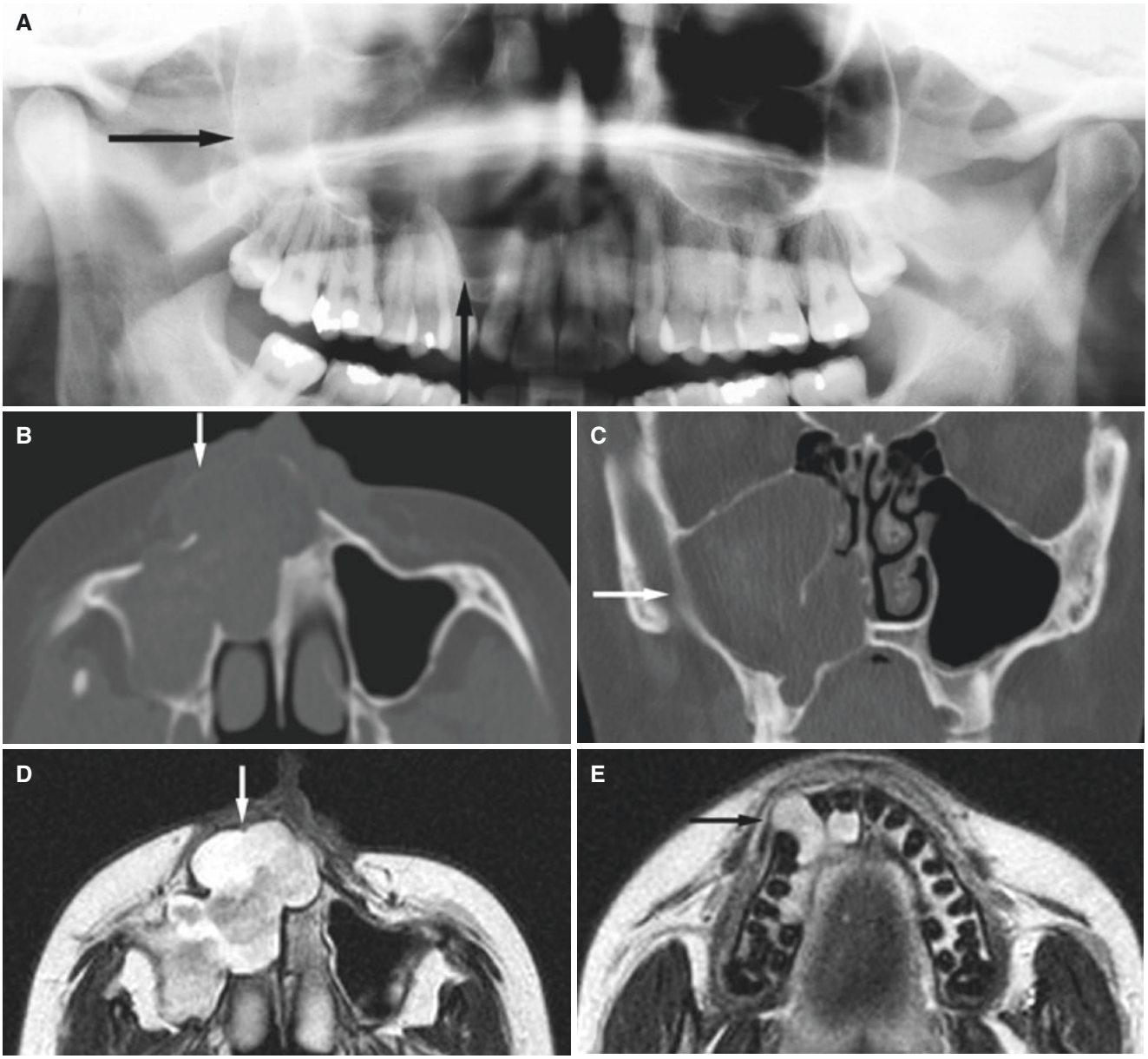

Fig. 3.11 Keratocystic odontogenic tumor, maxilla; 27-year-old female, Gorlin–Goltz (basal cell nevus) syndrome, painless swelling of alveolar process. (**A**) Panoramic view shows radiopacity in the maxillary sinus (*arrow*) and radiolucency in the right alveolar bone and absent alveolar sinus wall (*arrow*). (**B**) Axial CT image shows scalloped radiolucency in the hard palate and alveolar bone with destroyed cortical outline (*arrow*). (**C**) Coronal CT image shows mass occupying the right maxillary sinus and nasal cavity (*arrow*), expanding orbital floor. (**D**) Axial T2-weighted MRI shows heterogeneous high signal (*arrow*). (**E**) Axial T2-weighted MRI shows multilocular mass in alveolar bone (*arrow*). (**F**) Axial T1-weighted pre-Gd MRI shows homogeneous intermediate signal (*arrow*). (**G**) Axial T1-weighted post-Gd MRI shows no enhancement except partial enhancement of a peripheral thin rim (*arrow*). (**H**) Coronal T1-weighted post-GD MRI shows mass with partially enhancing peripheral rim occupying expanded maxillary sinus (*arrow*)

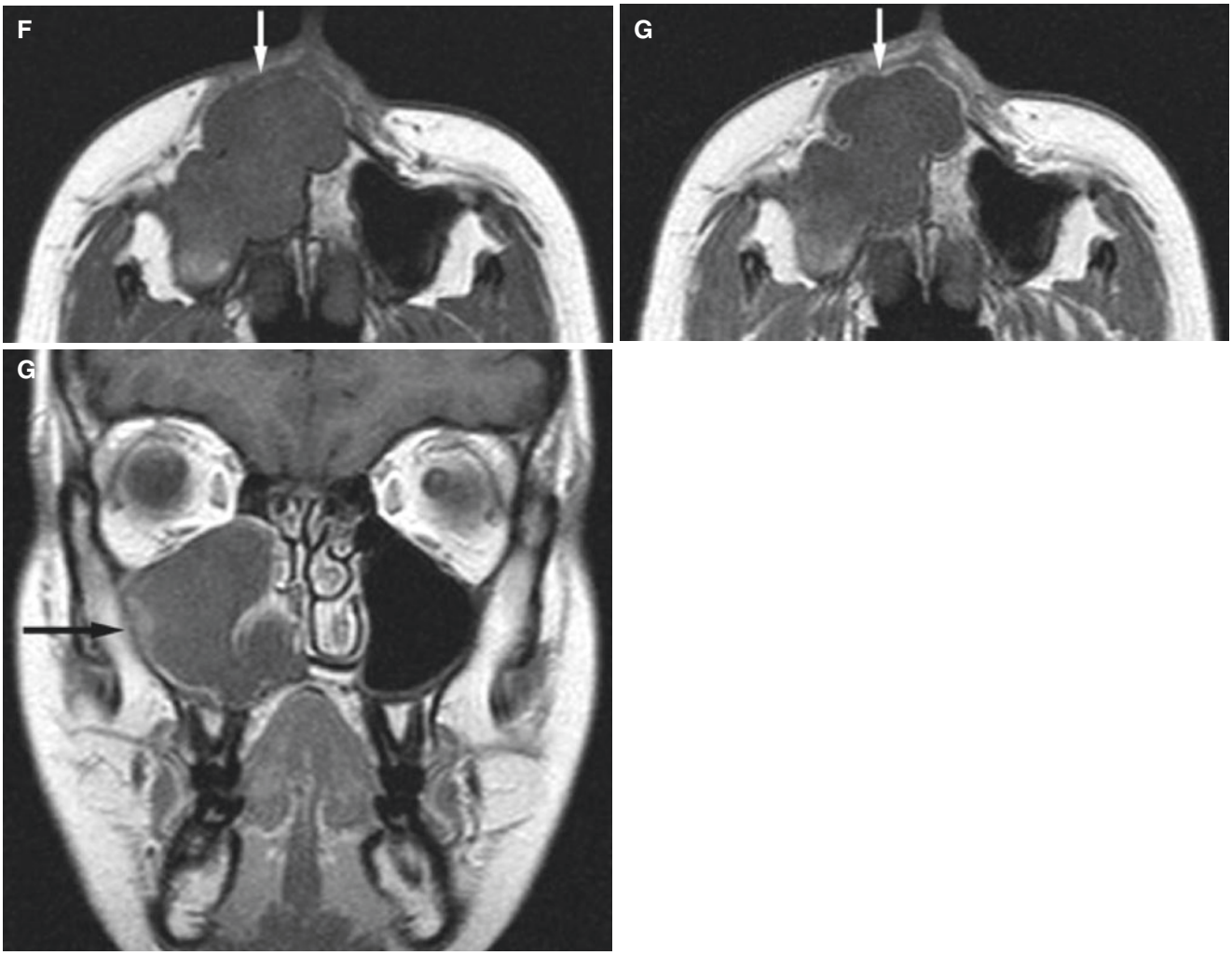

Fig. 3.11 (continued)

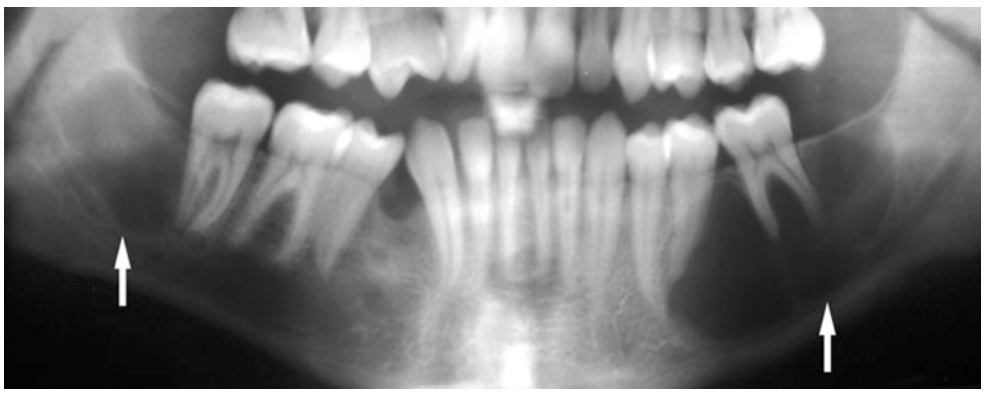

Fig. 3.12 Keratocystic odontogenic tumor, mandible; Gorlin–Goltz (basal cell nevus) syndrome, previously treated for maxillary cystic tumors. Panoramic view shows cystic tumors bilaterally (*arrows*)

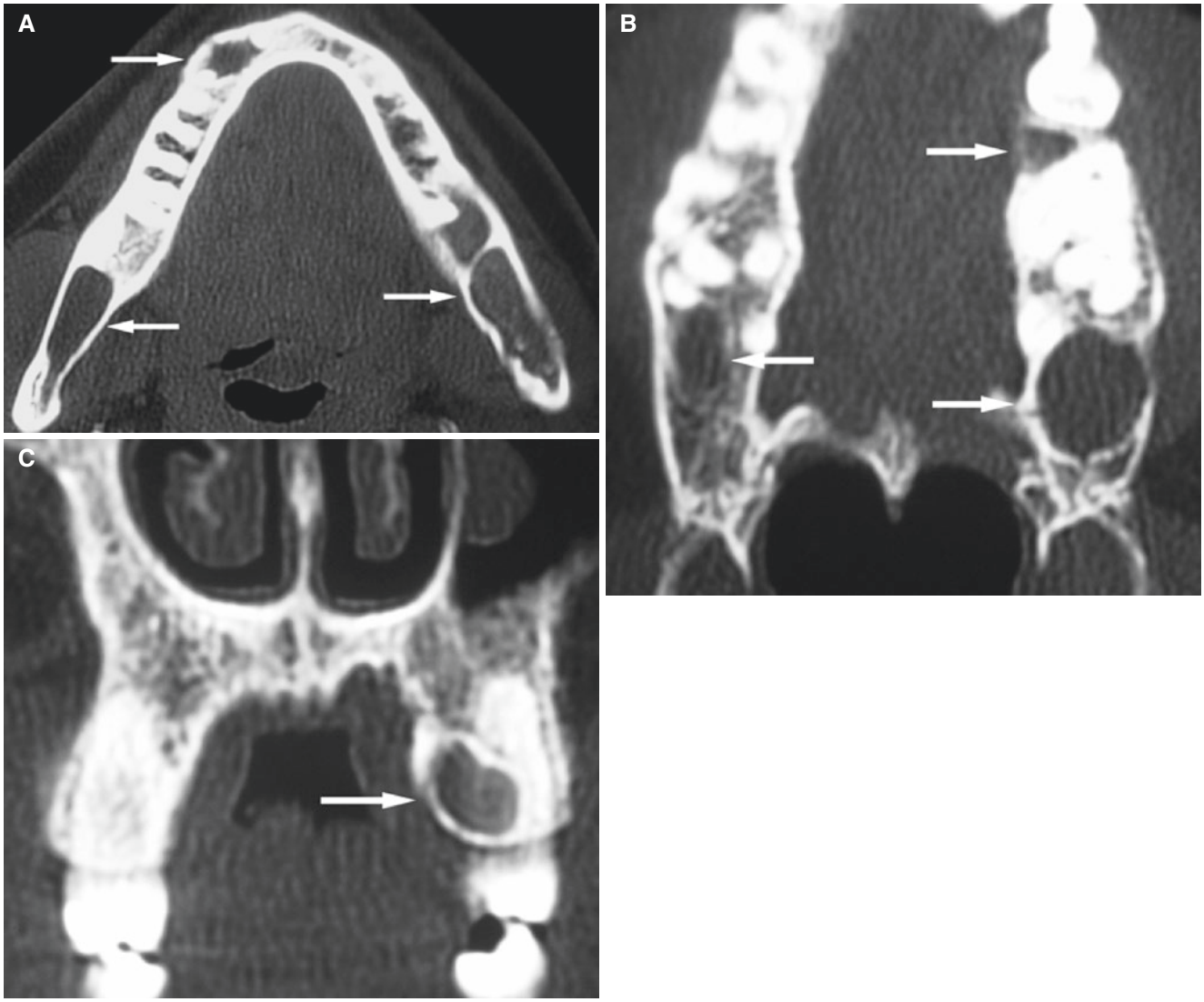

Fig. 3.13 Keratocystic odontogenic tumor, maxilla and mandible; Gorlin–Goltz (basal cell nevus) syndrome. (**A**) Axial CT image shows three cystic tumors in mandible (*arrows*). (**B**) Axial CT image shows three cystic tumors in maxilla (*arrows*). (**C**) Coronal CT image shows better cystic tumor in anterior part of maxilla (*arrow*)

3.4 Ameloblastomas

Figs. 3.14, 3.15, 3.16, 3.17, 3.18, 3.19, 3.20, 3.21, 3.22, 3.23, 3.24, 3.25, 3.26, 3.27, 3.28, and 3.29

3.5 Ameloblastoma, Solid/Multicystic Type

Synonyms: Conventional or classic intraosseous ameloblastoma

3.5.1 Definition

Slowly growing, locally invasive epithelial odontogenic tumor of the jaws with a high rate of recurrence, but with virtually no tendency to metastasize (WHO). Benign intraosseous progressively growing neoplasm characterized by expansion (WHO 2017).

3.5.2 Clinical Features

- Usually painless swelling (80%)
- Pain if secondarily inflamed
- Small; incidental radiographic finding
- No sex predilection
- Fourth to sixth decades, but wide range of age
- Malignancy very rare

3.5.3 Imaging Features

- Radiolucency
- Unilocular round, oval, scalloped, or multilocular
- Border sclerotic or not, thinned, expanded
- Defect border, soft-tissue extension
- Tooth root resorption common
- Mandible clearly more frequent than maxilla, at least 80%, mostly in molar region and ramus
- T1-weighted MRI: intermediate signal
- T2-weighted and STIR MRI: intermediate to high signal
- T1-weighted post-Gd MRI: contrast enhancement of solid components

3.6 Ameloblastoma, Unicystic Type

3.6.1 Definition

Variant of ameloblastoma, presenting as a cyst (WHO).

3.6.2 Imaging Features

- Represents 5–15% of all ameloblastomas; mean age significantly lower than solid/multicystic type
- More than 90% in mandible, mostly posterior region
- Frequently, unilocular corticated radiolucency
- Up to 80% associated with an unerupted mandibular third molar
- May have similar appearance to a follicular cyst

3.7 Ameloblastoma, Desmoplastic Type

3.7.1 Definition

Variant of ameloblastoma, characterized by specific clinical, radiologic and histologic features (WHO).

3.7.2 Imaging Features

- Mandible and maxilla ratio 1:1
- Less than 10% in mandibular molar region as opposed to nearly 40% of solid/multicystic type
- About 50% with mixture of radiolucency/radiopacity due to bone formation
- May show diffuse border

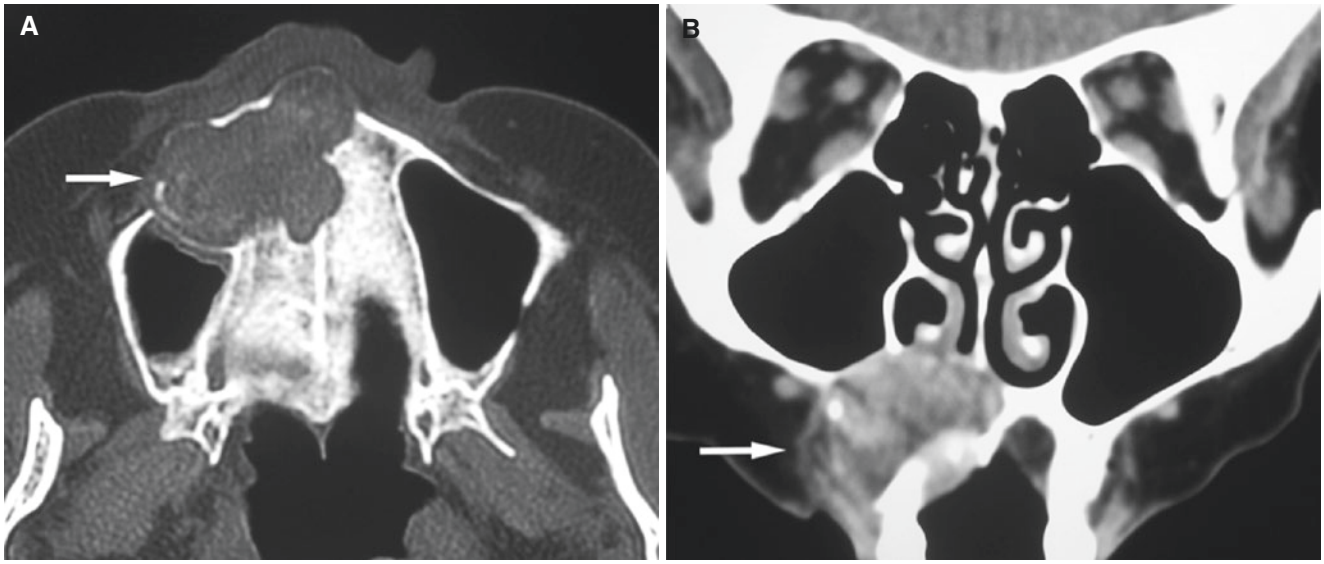

Fig. 3.14 Ameloblastoma, solid/multicystic, maxilla; 80-year-old female with painless swelling in the vestibulum and palate. (**A**) Axial CT image shows scalloped expansive process with destruction of palate and cortical bone defects (*arrow*). (**B**) Coronal CT image, soft-tissue window, shows well-defined soft-tissue mass without cortical outline palatally or buccally (*arrow*)

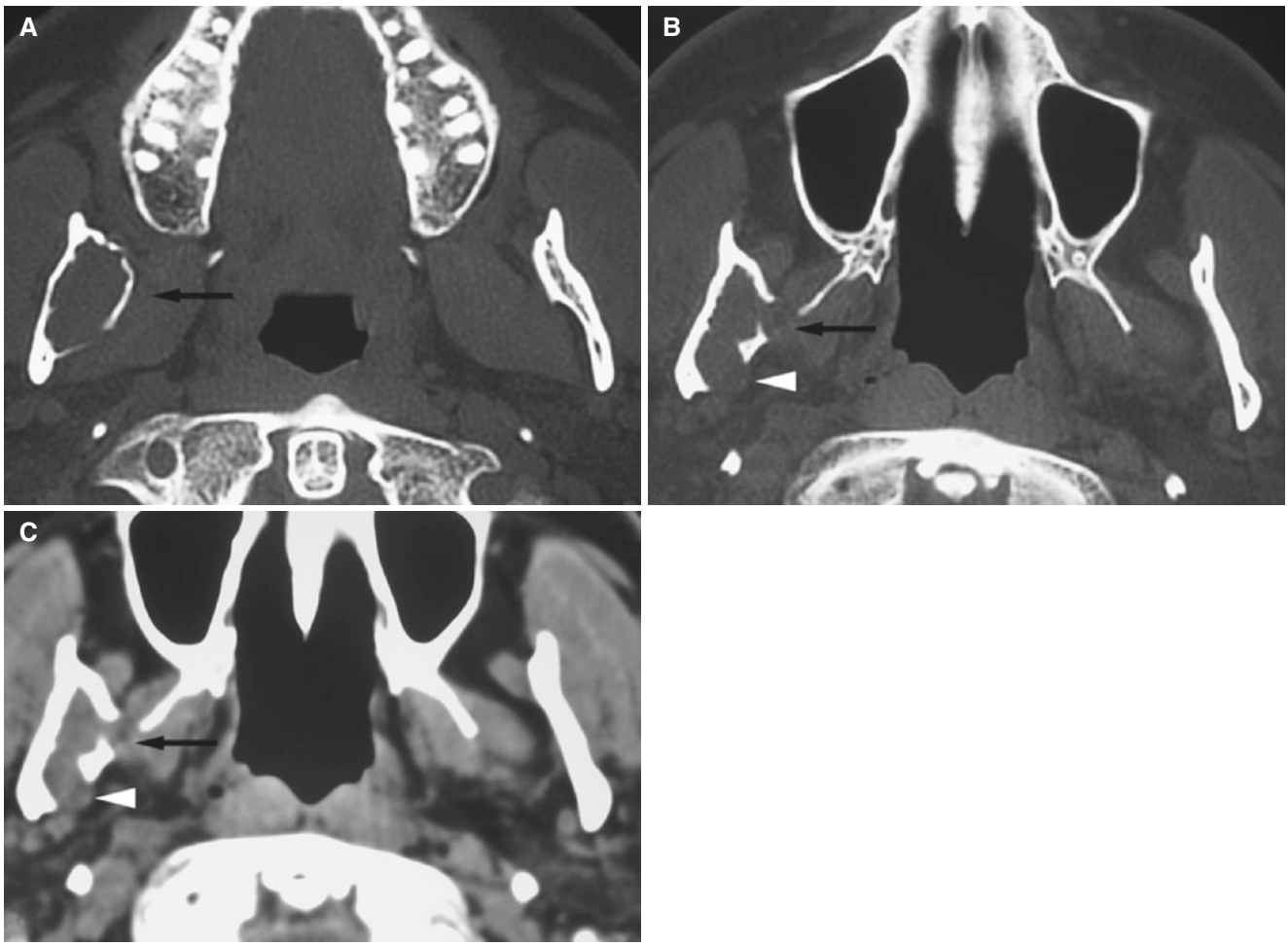

Fig. 3.15 Ameloblastoma, solid/multicystic, mandible; 45-year-old male with incidental finding at routine dental radiography. (**A**) Axial CT image shows unilocular expansive process with nearly intact cortical bone (*arrow*). (**B**) Axial CT image, another section, shows cortical defects (*arrow* and *arrowhead*). (**C**) Axial CT image, soft-tissue window, shows soft-tissue mass at cortical defects well demarcated from surrounding soft tissue (*arrow* and *arrowhead*)

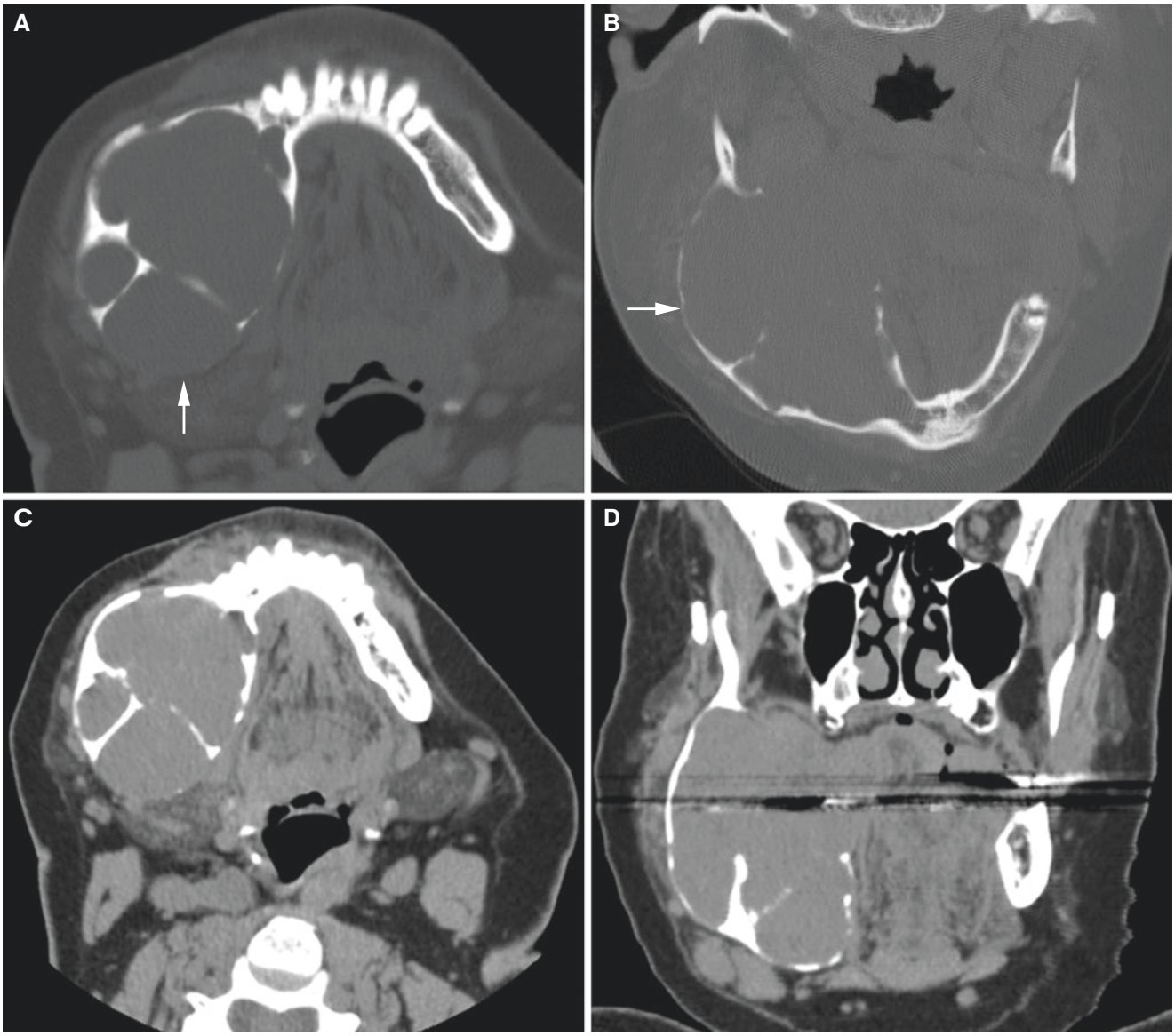

Fig. 3.16 Ameloblastoma, solid/multicystic, mandible; 32-year-old female with pain-free swelling of the right mandible. (**A**) Axial and (**B**) coronal (bone window) CT images and (**C**) axial and (**D**) coronal (soft-tissue window) CT images show expanding multilocular radiolucency with cortical defects (*arrow*)

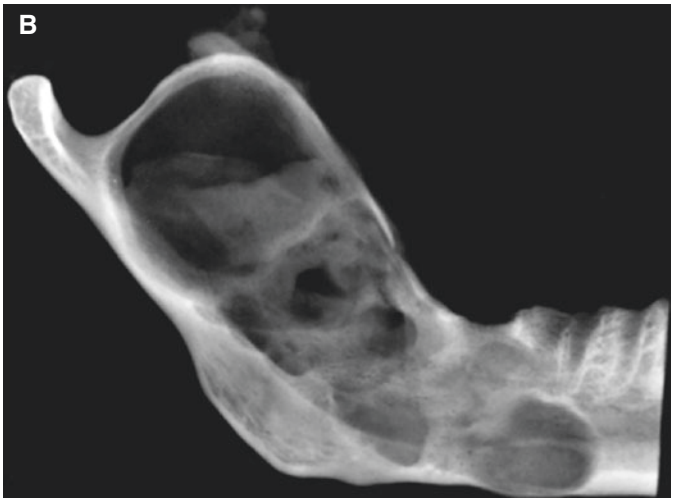

Fig. 3.17 Ameloblastoma, solid/multicystic, mandible; 57-year-old male, painless swelling of mandibular ramus. (**A**) 3D CT image shows expansive tumor in the entire mandibular ramus and part of body (*arrow*) with cortical defects. (**B**) Conventional radiograph of surgical specimen after hemimandible resection, with multilocular appearance

Fig. 3.18 Ameloblastoma, solid/multicystic, mandible; 21-year-old female with painless swelling of the right ramus. (**A**) Panoramic view shows expansive radiolucency and impacted third molar (*arrow*). (**B**) Axial CT image shows expanded cortical bone and partially scalloped border (*arrow*). (**C**) Coronal CT image shows expanded and thinned, intact cortical bone and root resorption (*arrow*). (**D**) Axial T1-weighted pre-Gd MRI shows homogeneous intermediate signal (*arrow*). (**E**) Axial T1-weighted post-Gd MRI shows homogeneous contrast enhancement (*arrow*)

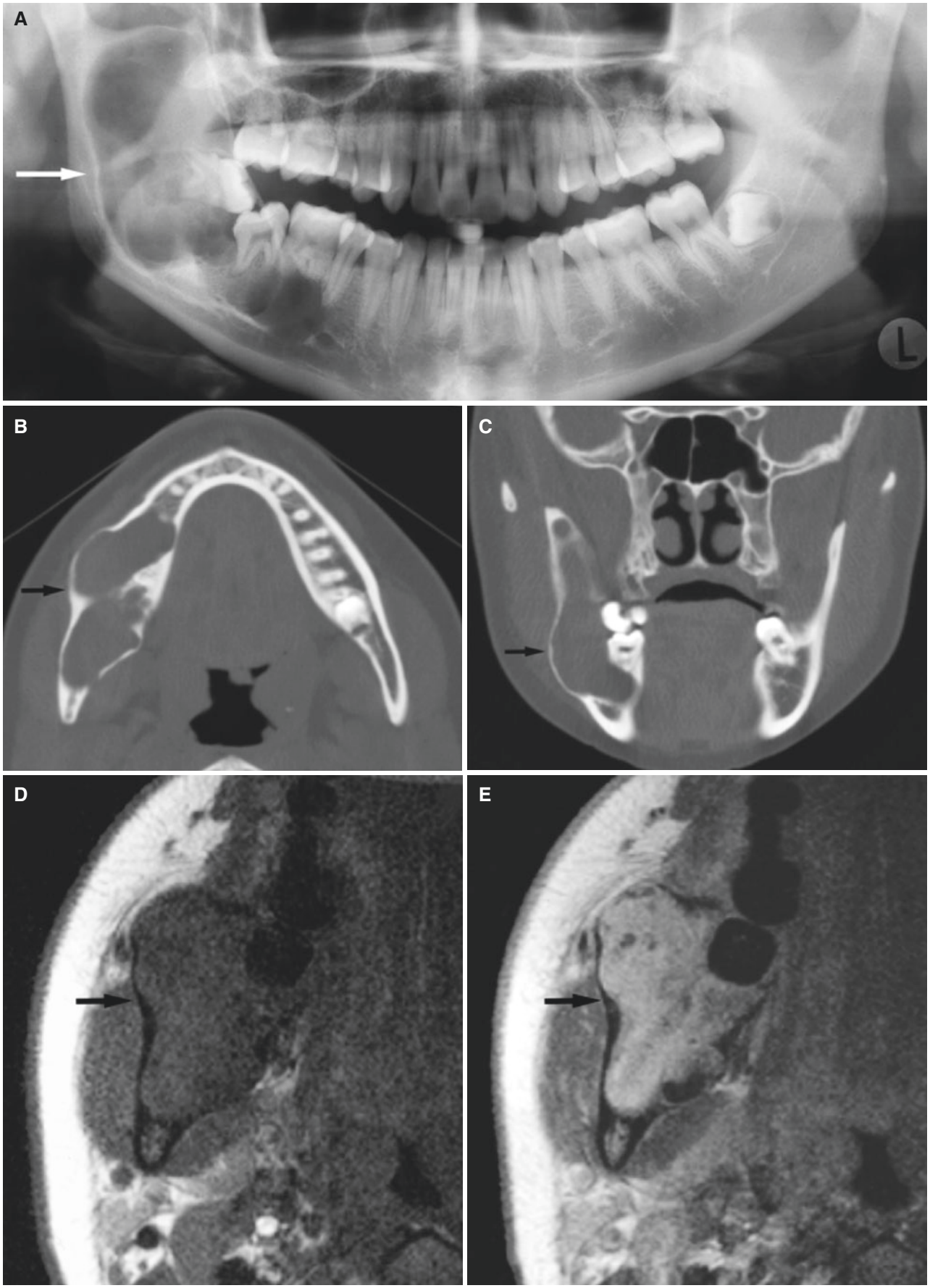
A
L
B
C
D
E

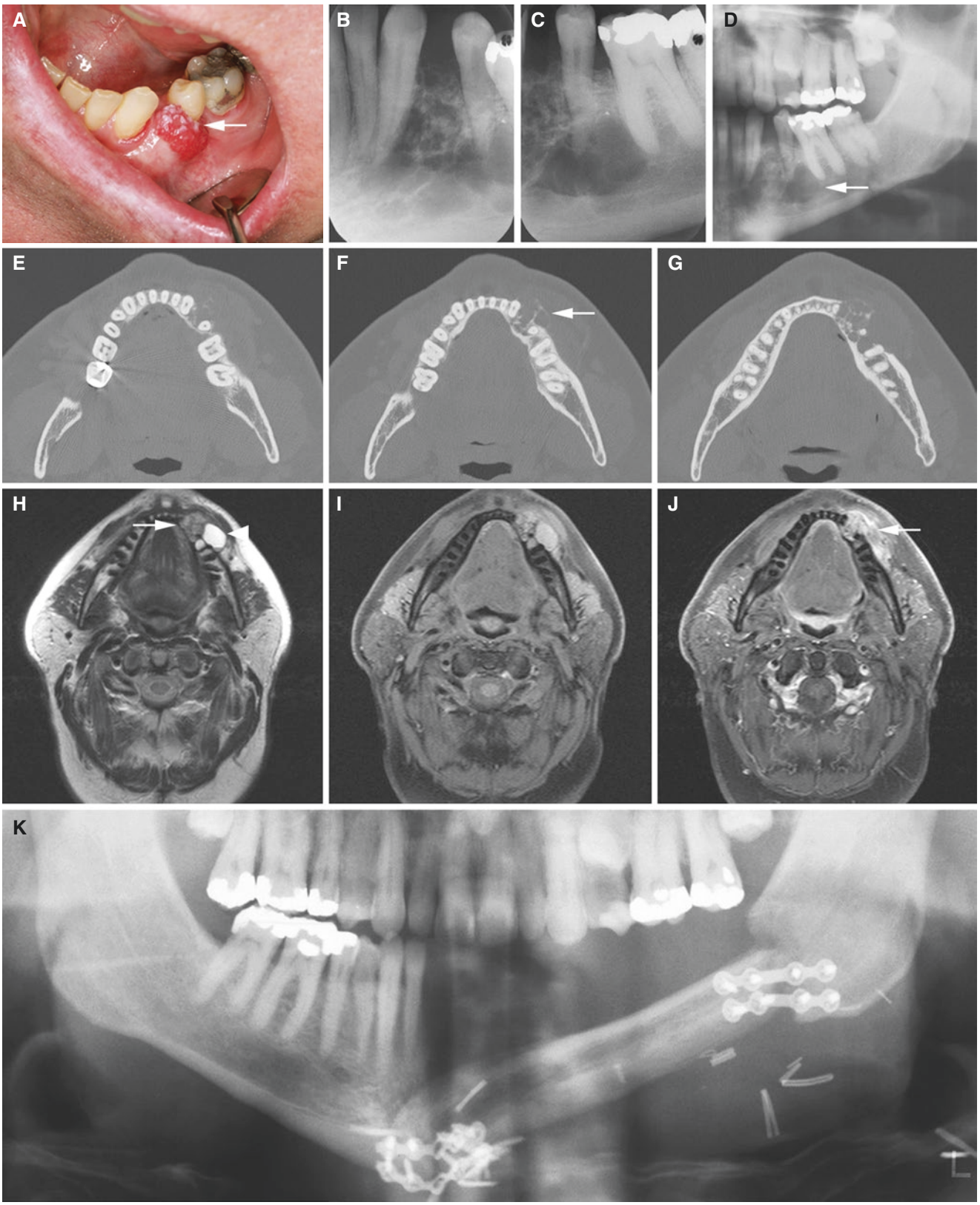

Fig. 3.19 Ameloblastoma, solid/multicystic, mandible; 59-year-old male with gingival mass but no pain or discomfort. (**A**) Clinical photograph shows exophytic gingival mass with granular red and white appearance (*arrow*). (**B**, **C**) Intraoral and (**D**) panoramic views show multilocular radiolucency (*arrow*). (**E**, **F**, **G**) Axial CT images show radiolucency with destroyed buccal cortex (*arrow*). (**H**) Axial T2-weighted MRI shows heterogeneous (high to intermediate) signal intensity with solid part (*arrow*) and cystic part (*arrowhead*). (**I**) Axial T1-weighted fat sat pre-Gd and (**I**) post-Gd MRI show heterogeneous contrast enhancement (*arrow*). (**K**) Panoramic view shows postoperative status with fibula graft after hemimandible ectomy

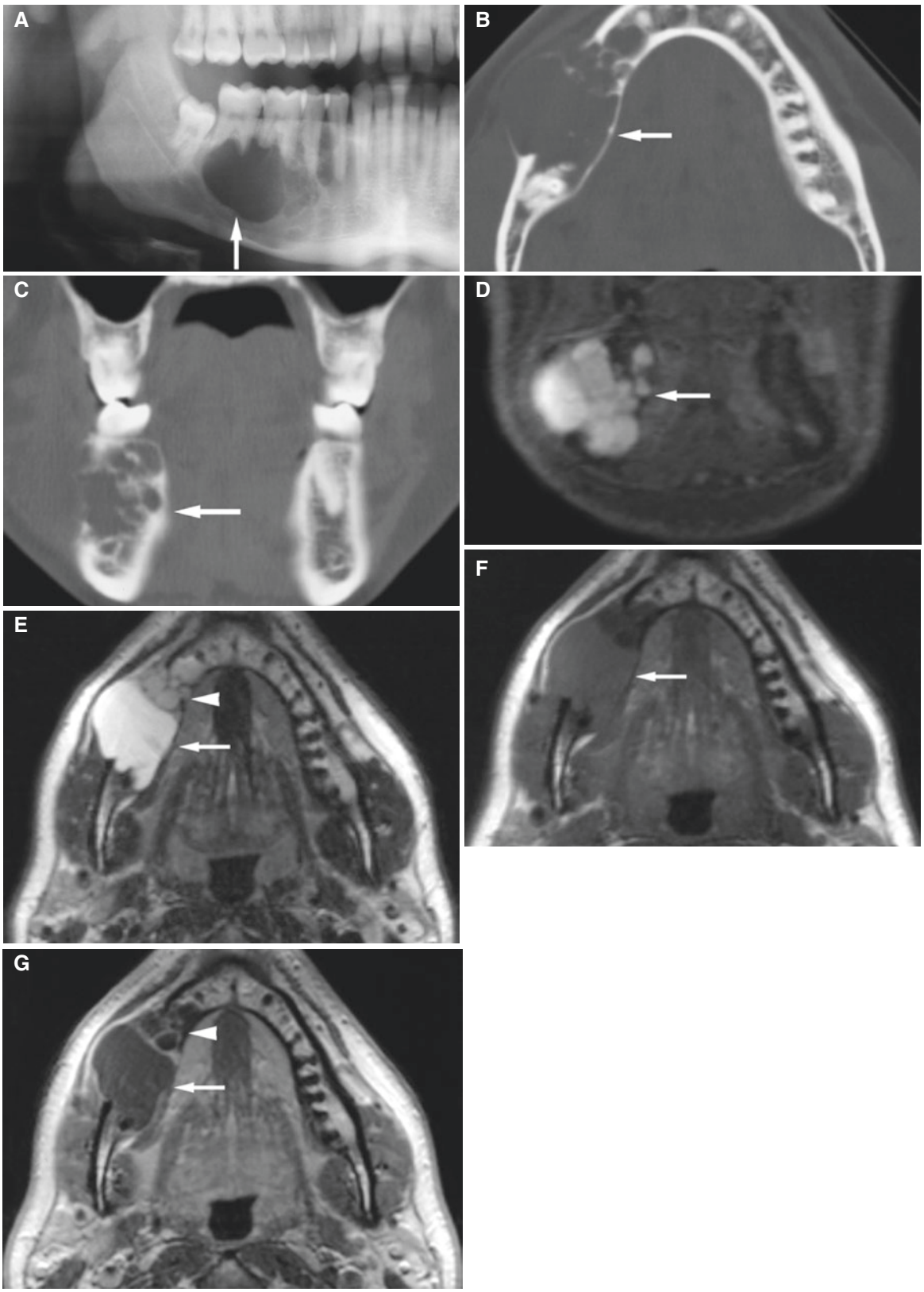

Fig. 3.20 Ameloblastoma, unicystic, mandible; 22-year-old male with painless perimandibular swelling. (**A**) Panoramic view shows radiolucency and root resorption (*arrow*). (**B**) Axial CT image shows destroyed bone with expansion of buccal cortical bone, which is very thin and partially absent (*arrow*). (**C**) Coronal CT image shows multilocular appearance in anterior part without cortical outline buccally (*arrow*). (**D**) Coronal STIR MRI shows multilocular appearance and heterogeneous intermediate to high signal (*arrow*). (**E**) Axial T2-weighted MRI shows high signal in posterior part (*arrow*) and intermediate signal in anterior part (*arrowhead*). (**F**) Axial T1-weighted pre-Gd MRI shows intermediate signal in posterior part (*arrow*) and intermediate to low signal in anterior part. (**G**) Axial T1-weighted post-Gd MRI shows no contrast enhancement in posterior part (*arrow*) except partially in periphery and septal enhancement in anterior part (*arrowhead*)

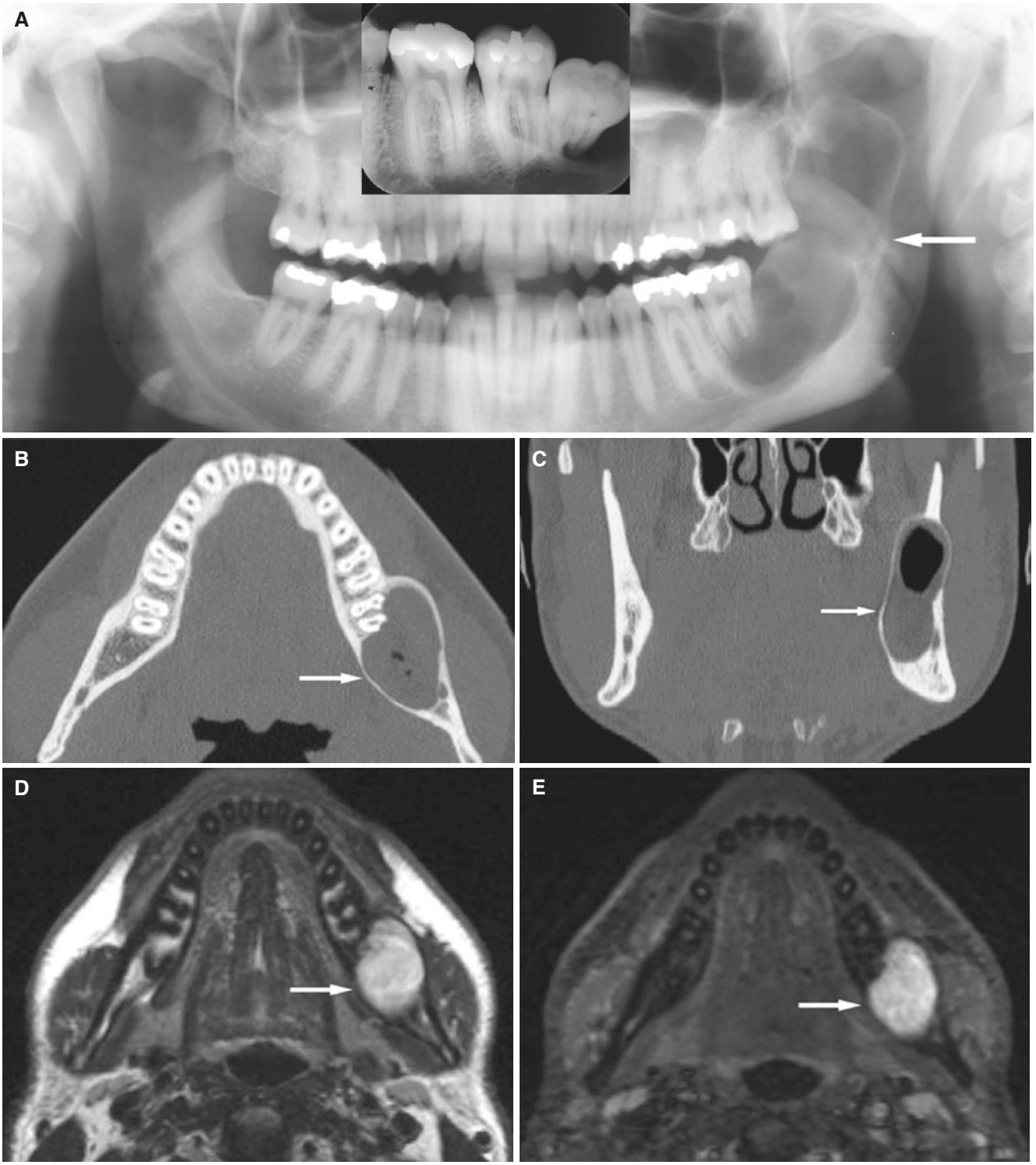

Fig. 3.21 Ameloblastoma, unicystic, mandible; 33-year-old male with drainage into oral cavity as the only symptom several months after the third molar surgery. (**A**) Panoramic view shows unilocular radiolucency with sclerotic border (*arrow*). Note intraoral view before surgical removal of the third molar, suggesting the lesion (which was not detected by the dentist). (**B**) Axial CT image shows expansive process with intact, sclerotic cortical outline and with mandibular canal in periphery (*arrow*). Note root resorption. (**C**) Coronal CT image shows expansion of thin intact, cortical outline (*arrow*), and some air. (**D**) Axial T2-weighted MRI shows homogeneous intermediate to high signal (*arrow*). (**E**) Axial STIR MRI shows homogeneous high signal (*arrow*). (**F**) Axial T2-weighted MRI shows soft-tissue capsule and fluid level (*arrow*). (**G**) Coronal STIR MRI shows high-signal soft-tissue capsule (*arrow*) with intraluminal tumor noduli (*arrowheads*). (**H**) Panoramic view 3 months postoperatively shows that only one molar was extracted; tumor was enucleated with intact mandibular canal (no paresthesia)

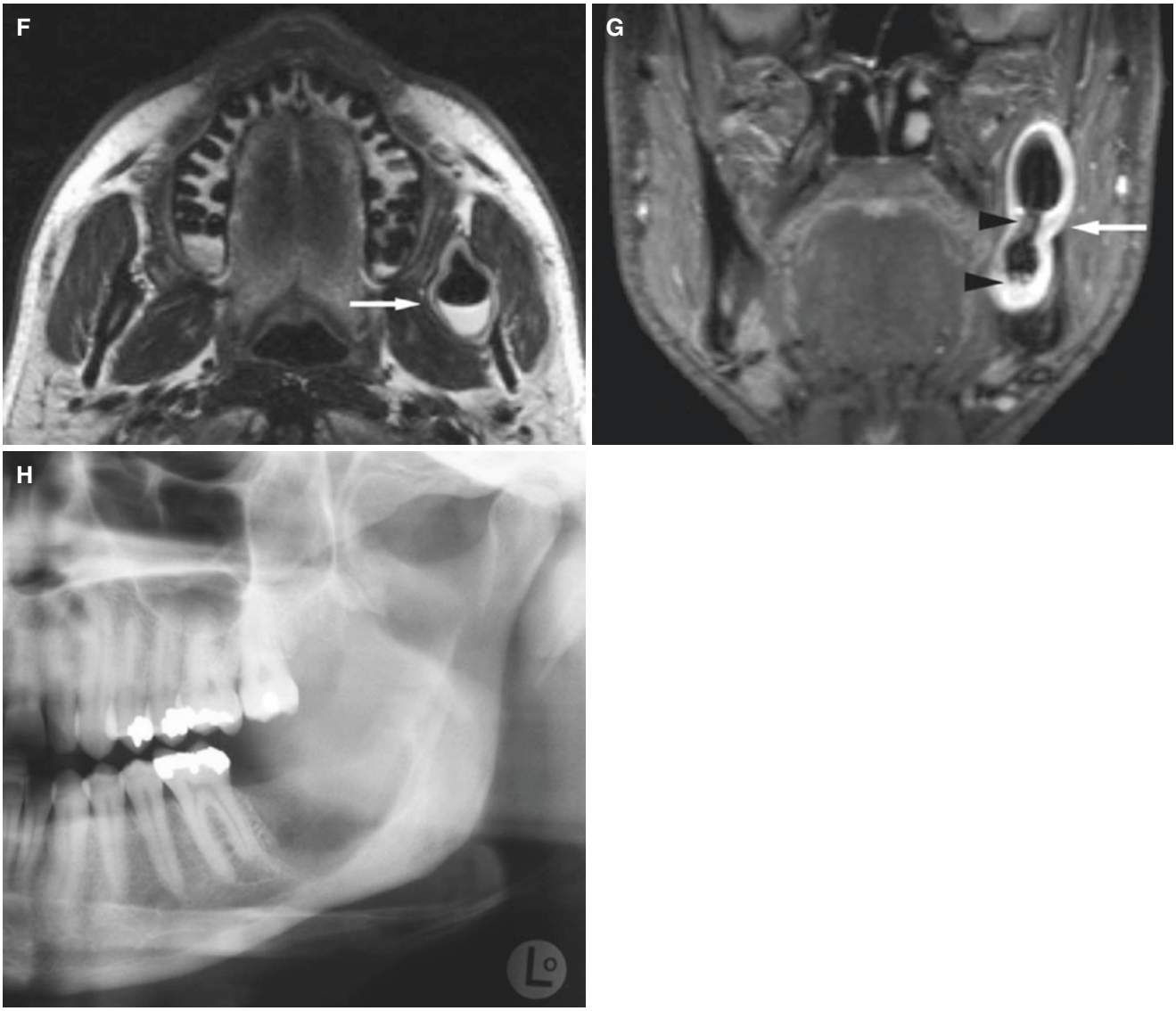

Fig. 3.21 (continued)

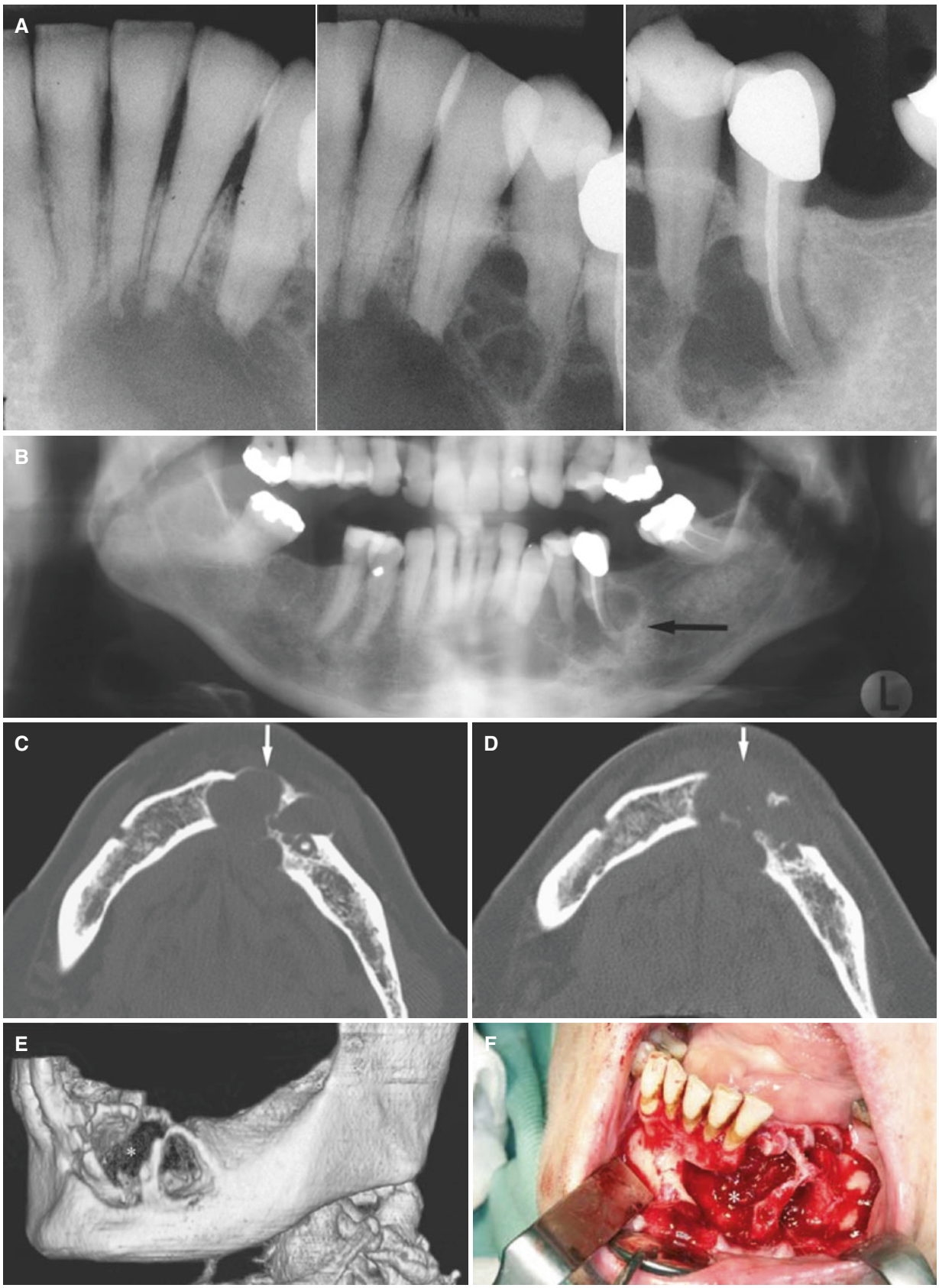

Fig. 3.22 Ameloblastoma, mandible; 64-year-old female with painless swelling, then abscess development with swelling and pain. (**A**) Intraoral views show multilocular radiolucency and root resorptions. (**B**) Panoramic view indicates size of radiolucency (*arrow*). (**C**) Axial CT image shows expanded, intact cortical bone buccally (*arrow*) and destroyed bone lingually. (**D**) Axial CT image, 6 weeks later with abscess development, and destruction of buccal cortical bone (*arrow*). (**E**) 3D CT image shows severe buccolingual destruction (*asterisk*). (**F**) Photograph at surgery confirms severe buccolingual bone destruction (F: courtesy of Dr. B. B. Herlofson, University of Oslo, Norway)

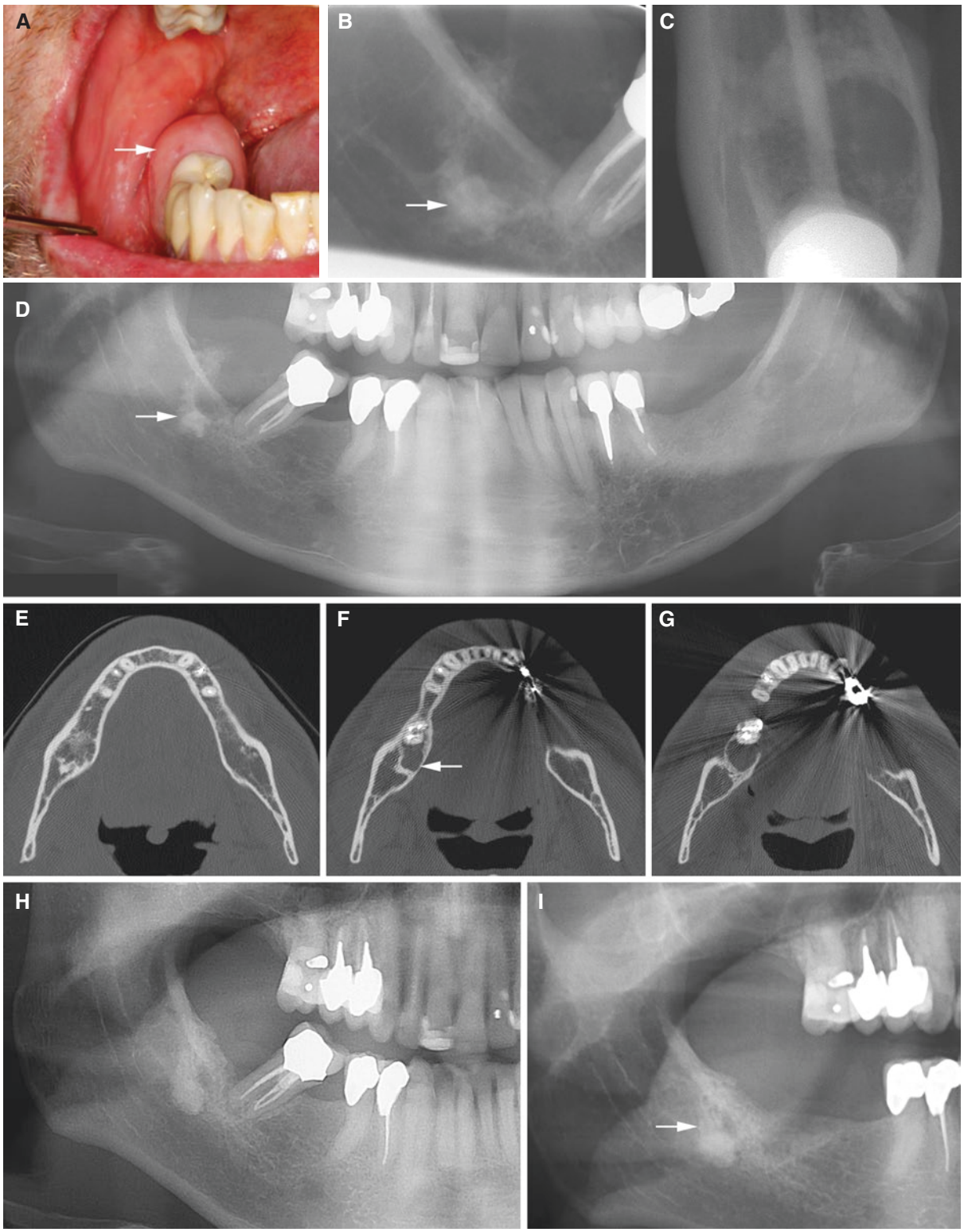

Fig. 3.23 Ameloblastoma, desmoplastic, mandible; 40-year-old male with pain-free swelling of the gingiva in the right mandible posterior to the remaining molar. (**A**) Clinical photograph shows gingival mass with normal mucosa (*arrow*). (**B**) Intraoral (periapical), (**C**) occlusal (axial), and (**D**) panoramic views show radiolucency with sclerotic margins (*arrow*). (**E**, **F**, **G**) Axial CT images show radiolucency with sclerotic bone and no or minimal expansion of cortical bone (*arrow*). (**H**) 1-year and (**I**) 2 1/3-year postoperative panoramic views show bone healing with sclerosis (molar tooth is extracted in **I**) (*arrow*)

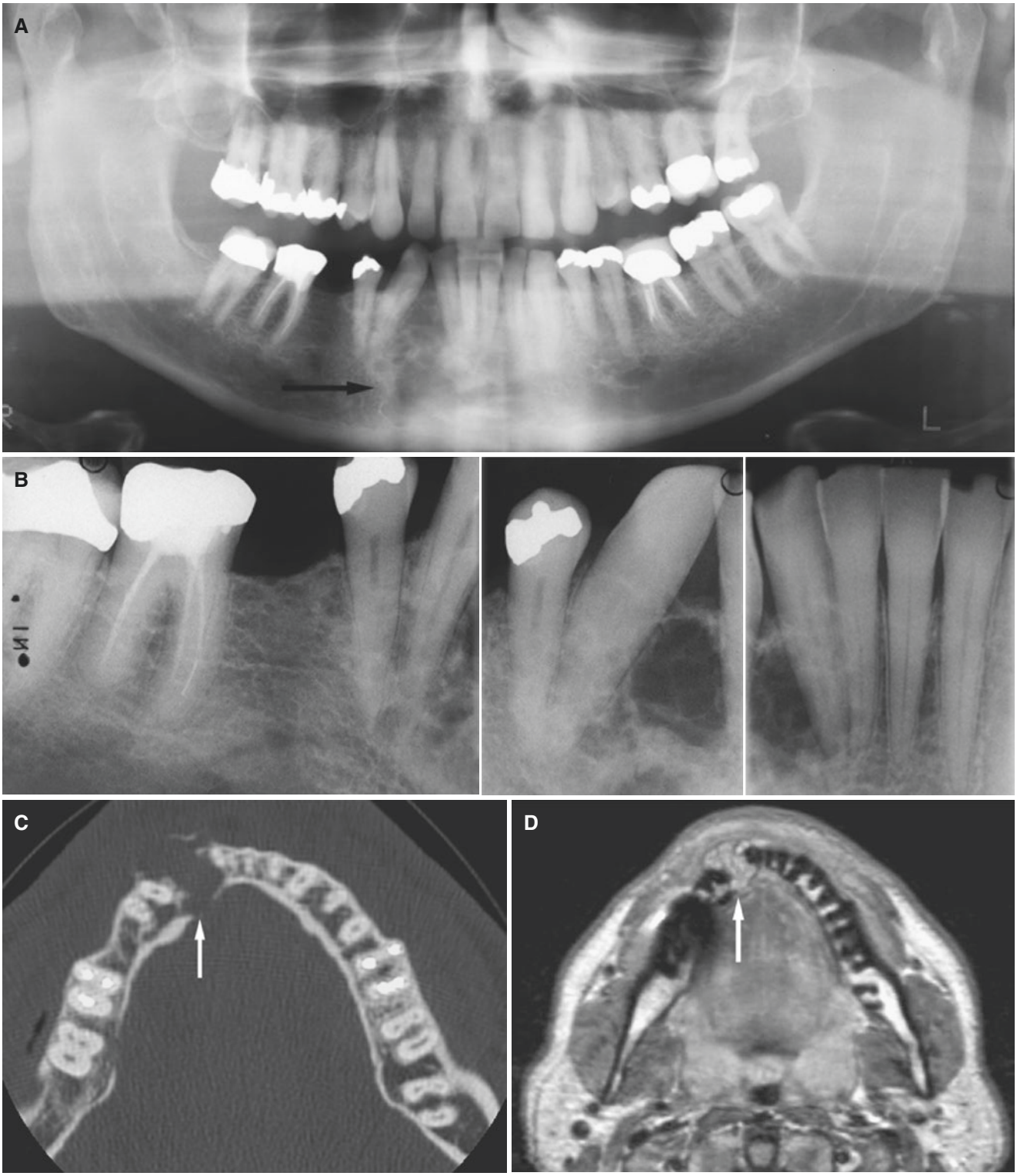

Fig. 3.24 Ameloblastoma, desmoplastic, mandible; 52-year-old male with painless swelling in the anterior part. (**A**) Panoramic view shows radiolucency (*arrow*) and displacement of canine and incisor. (**B**) Intraoral views show apparently multilocular radiolucency and displaced teeth. (**C**) Axial CT image shows cortical expansion and destruction buccally and lingually (*arrow*). (**D**) Axial PD MRI shows intermediate signal and septal appearance (*arrow*). (**E**) Axial T2-weighted MRI shows high-signal content and septal appearance (*arrow*). (**F**) Axial STIR MRI shows intermediate to high signal and septal appearance (*arrow*). (**G**) Coronal STIR MRI of anterior region shows intermediate to high signal of bilocular septate tumor (*arrow*); most caudal part reaches mandibular border (*arrowhead*), surgically confirmed at tumor resection

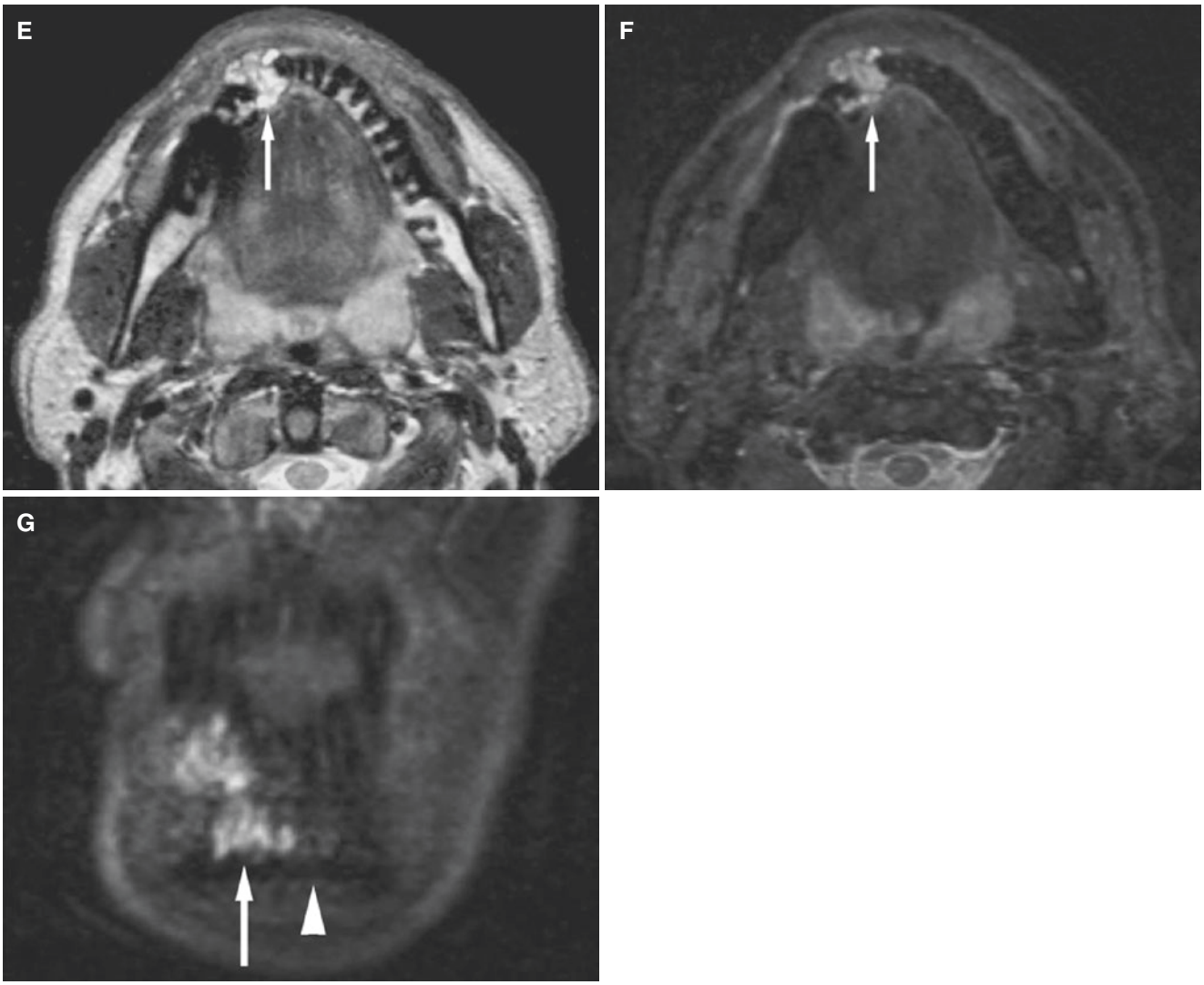

Fig. 3.24 (continued)

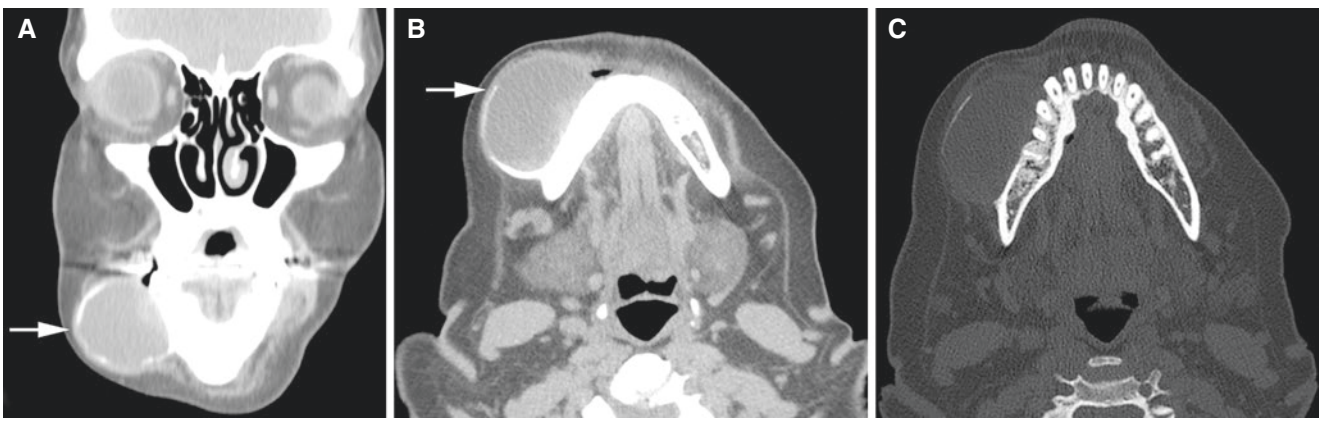

Fig. 3.25 Ameloblastoma, extraosseous, mandible; 51-year-old female with right mandibular fluctuant swelling. (**A**) Coronal and (**B**) axial (soft-tissue window) CT images show buccally expanding lesion delineated by thin, partially intact cortical bone and with homogeneous content (*arrow*). (**C**) Axial (bone window) CT image shows minimal (if any) bone depression

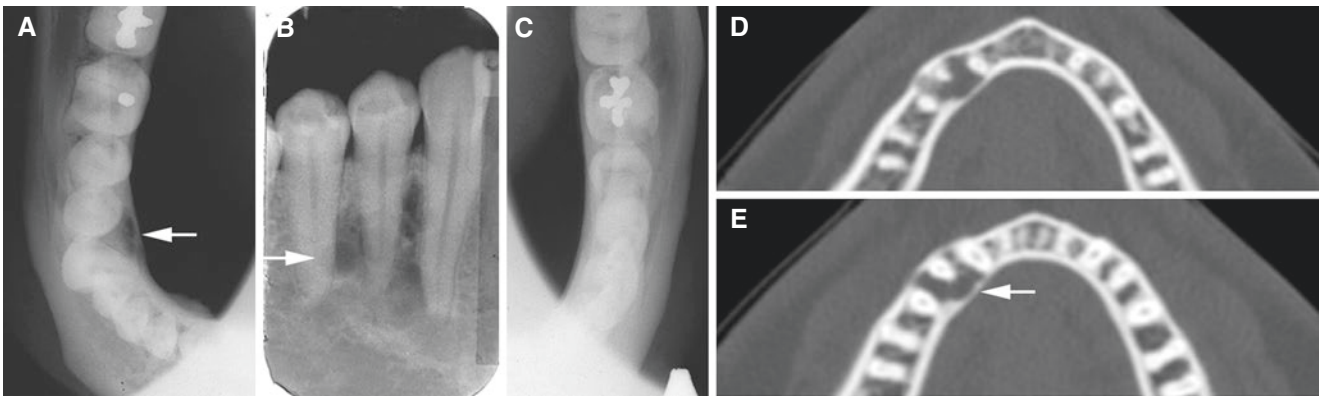

Fig. 3.26 Ameloblastoma, solid/multicystic, mandible, with follow-up; 31-year-old male with some swelling (pain-free) in the right anterior mandible. (**A**) Occlusal (axial) and (**B**) intraoral (periapical) views show multilocular, slightly expanding radiolucency (*arrow*). (**C**) Occlusal (axial) view of normal contralateral side for comparison. (**D**, **E**) Axial CT images confirm radiolucency with some lingual expansion and thinned but intact cortical bone (*arrow*). The first surgical intervention was then performed

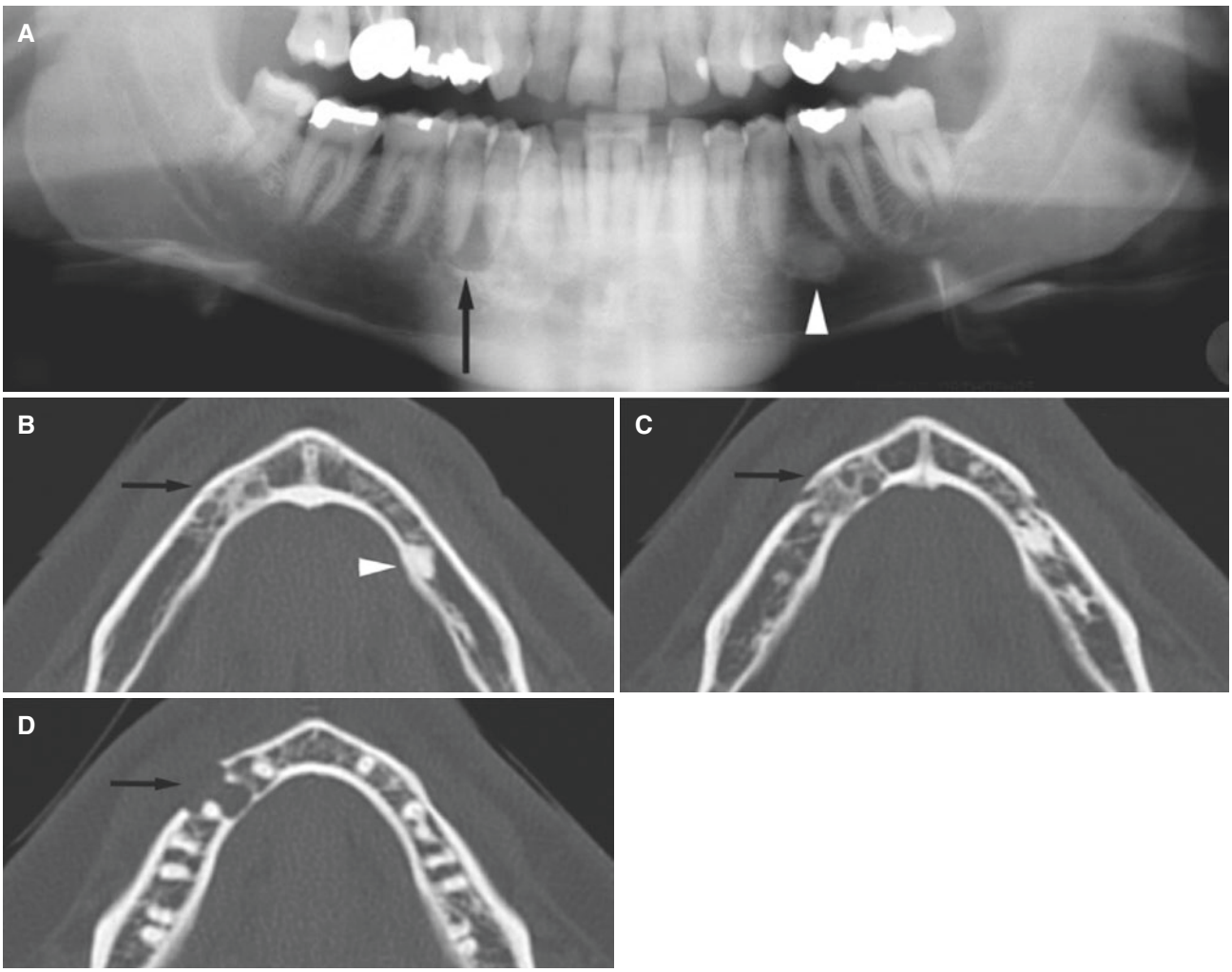

Fig. 3.27 Ameloblastoma, recurrence, mandible; same patient as in Fig. 3.26, 2 years after surgery. (**A**) Panoramic view shows small unilocular radiolucency (*arrow*) and small radiopacity as an incidental finding (*arrowhead*). (**B**) Axial CT image shows multilocular radiolucency caudal to mental foramina with diffuse osteosclerosis (*arrow*) and well-defined osteosclerosis, probably idiopathic (*arrowhead*). (**C**) Axial CT image shows two radiolucencies with some sclerosis at the level of mental foramina (*arrow*). (**D**) Axial CT image shows destroyed cortical bone buccally in tooth-bearing area (*arrow*)

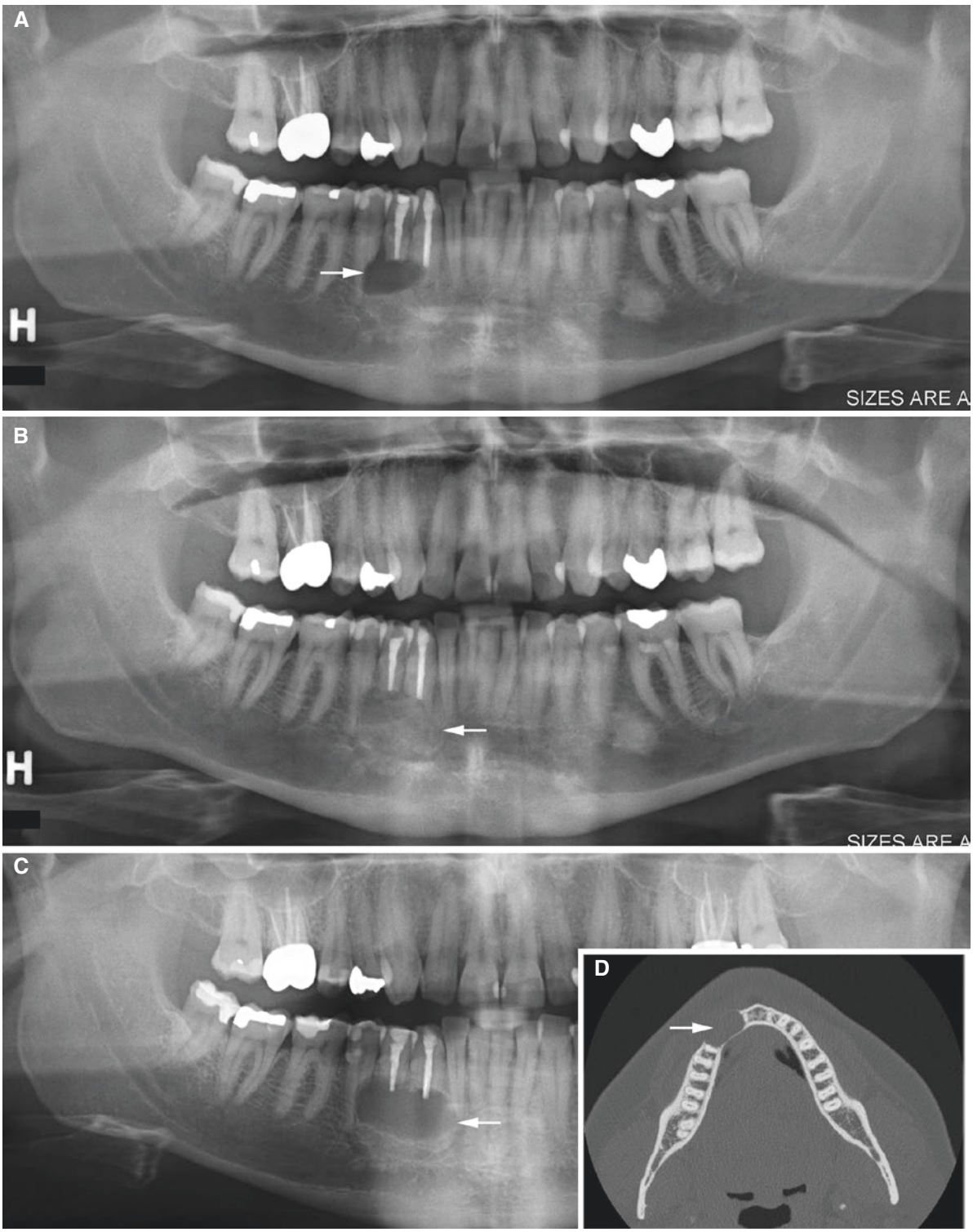

Fig. 3.28 Ameloblastoma, recurrence, mandible; the same patient as in Fig. 3.26 and 3.27, 8 years after the second operation. (**A**) Panoramic view shows well-defined radiolucency and root resorption of the second premolar (*arrow*). The third surgical intervention was then performed. (**B**) Panoramic view 1 year after the third operation shows bone healing (*arrow*). (**C**) Panoramic view and (**D**) axial CT image 3 years after the third operation show enlarged radiolucency and destruction throughout the entire alveolar ridge (*arrow*). Mandibular resection was then performed

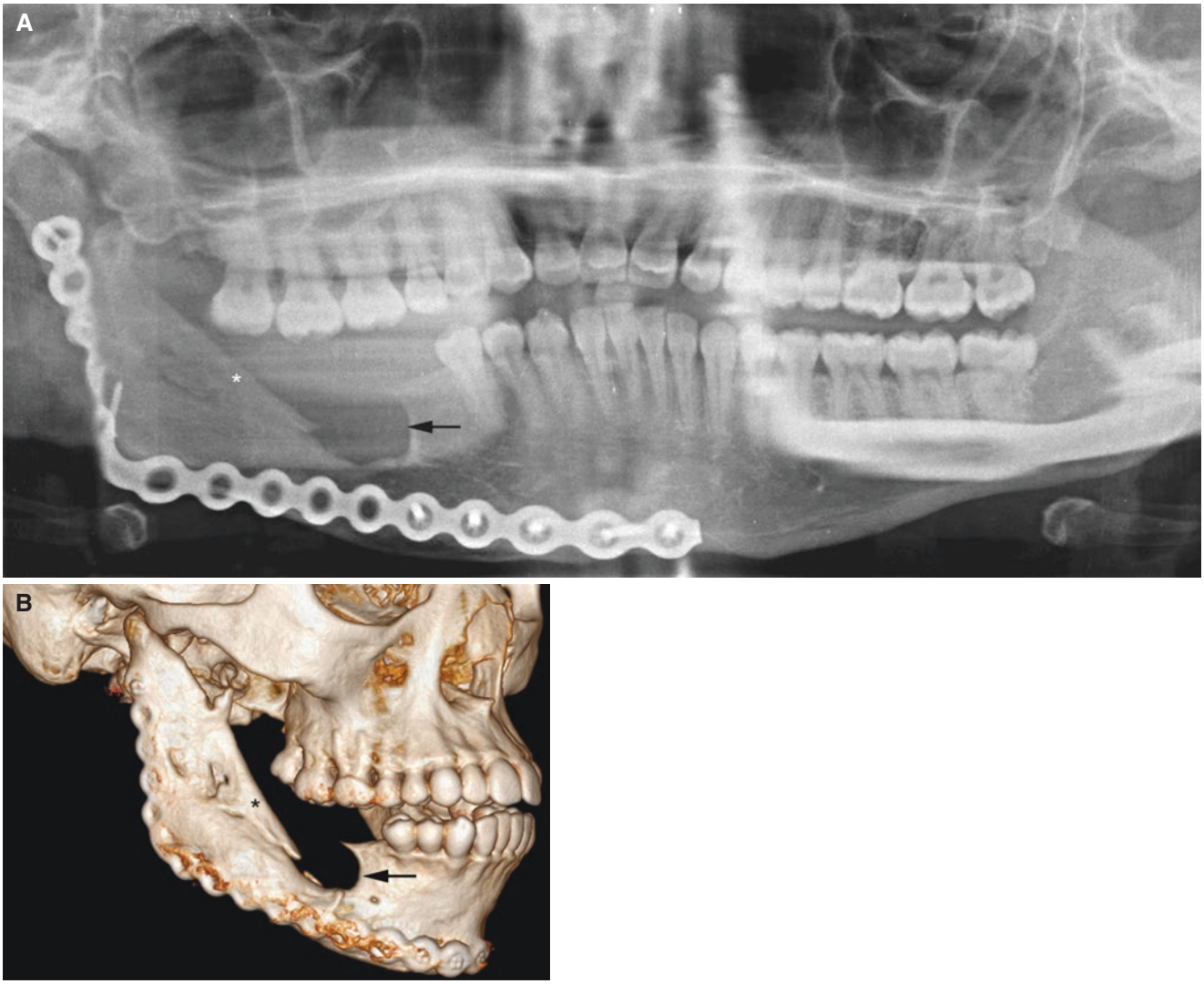

Fig. 3.29 Ameloblastoma, recurrence involving graft, mandible; 24-year-old female. (**A**) Panoramic view and (**B**) 3D CT image show fixation plates and fibula graft (*asterisk*) with tumor recurrence between graft and remaining mandible (*arrow*)

3.8 Lipoma

Fig. 3.30

Synonym: Adipose tumor

3.8.1 Definition

Abnormal (benign) growth of fat cells, neoplastic lipomatous growth. Sialolipoma also contains epithelial components, whereas ordinary lipoma does not (WHO).

3.8.2 Clinical Features

- Most often found just below the skin (between the skin and underlying muscle layer) on the torso, neck, upper thighs, upper arms, and armpits, but they can occur almost anywhere
- Soft to touch, usually movable, and generally painless
- Treatment generally not necessary
- Can be surgically removed if painful or if growing

3.8.3 Imaging Features

- Typically homogeneous.
- Low attenuation (dark) on CT and bright on T1 MRI.
- When extensive, internal structures, liposarcoma should be considered

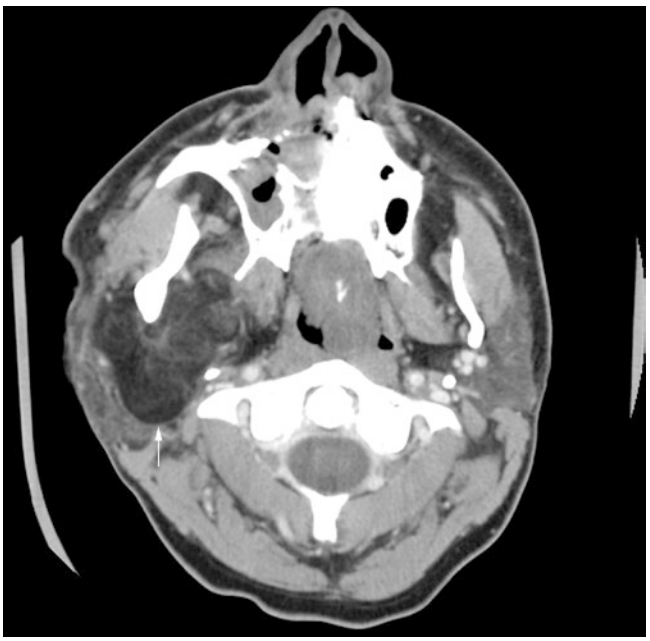

Fig. 3.30 Lipoma, right neck; 29-year-old male with pain-free neck mass. Axial contrast-enhanced (soft-tissue window) CT image shows mass in parotid space with signal intensity as subcutaneous fat (*arrow*)

3.9 Odontogenic Fibroma (Central)

Fig. 3.31

Synonyms: Central odontogenic fibroma, simple odontogenic fibroma

3.9.1 Definition

Rare neoplasm characterized by varying amounts of inactive-looking odontogenic epithelium embedded in a mature, fibrous stroma (WHO).

Two histologic types: epithelium-poor type (formerly termed simple WHO type) and epithelium-rich type (formerly termed complex WHO type).

3.9.2 Clinical Features

- Second to fourth decade
- Females more frequent than males
- Mandible more frequent than maxilla
- Painless swelling

3.9.3 Imaging Features

- Usually well-defined outline, often sclerotic
- Small lesions show unilocular radiolucency
- Larger lesions show scalloped margins or multilocular appearance
- Rarely, occurrence of calcified material may give mixed radiolucent/radiopaque appearance
- Tooth displacement more common than root resorption

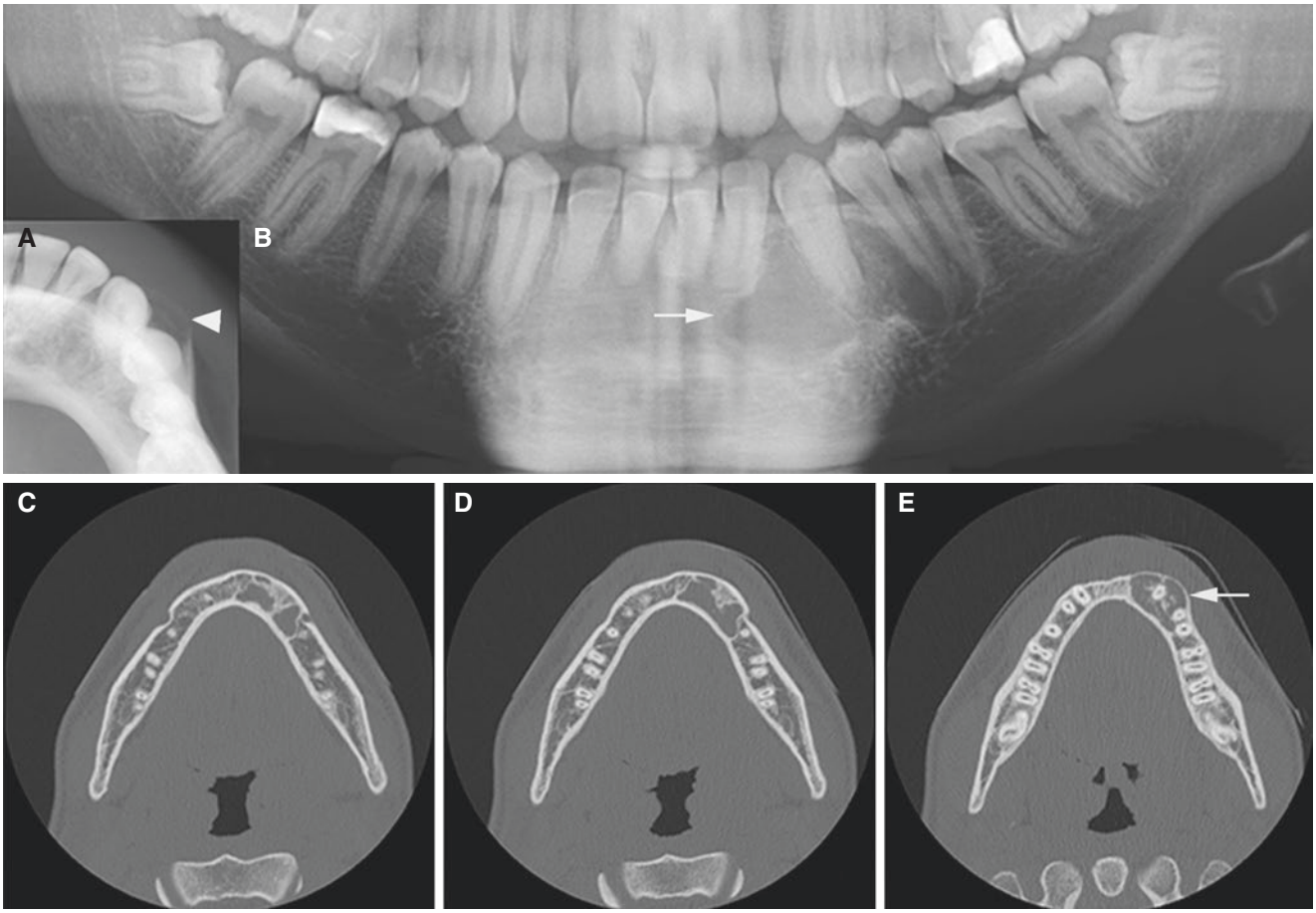

Fig. 3.31 Odontogenic fibroma, mandible; 25-year-old male with pain-free, hard swelling in the anterior part of the left mandible. (**A**) Occlusal (axial) and (**B**) panoramic views show radiolucency (*arrow*) with some buccal expansion (*arrowhead*). (**C**, **D**, **E**) Axial CT images show radiolucency with some expansion of thin, intact cortical bone and some calcification (*arrow*)

3.10 Odontogenic Myxoma/Myxofibroma

Fig. 3.32

Synonym: Odontogenic fibromyxoma

3.10.1 Definition

Odontogenic myxoma is an intraosseous benign neoplasm characterized by stellate and spindle-shaped cells embedded in an abundant myxoid or mucoid extracellular matrix. When a relatively greater amount of collagen is evident, the term Odontogenic myxofibroma may be used (WHO).

3.10.2 Clinical Features

- Painless swelling or incidental finding (small)
- About two-thirds in mandible
- Second to fourth decades, but wide range of age
- Recurrence rate about 25% after curettage, but good prognosis
- Third most frequent odontogenic tumor (3–20%) after odontoma and ameloblastoma
- Slightly more common in females

3.10.3 Imaging Features

- Radiolucency
- Unilocular, scalloped, or multilocular
- Border can be well defined and corticated or not so well defined and sclerotic
- May expand bone, but usually not prominent
- Tooth displacement or root resorption may occur
- T1-weighted MRI: homogeneous intermediate (to low) signal
- T2-weighted and STIR MRI: homogeneous high signal
- T1-weighted post-Gd MRI: homogeneous contrast enhancement

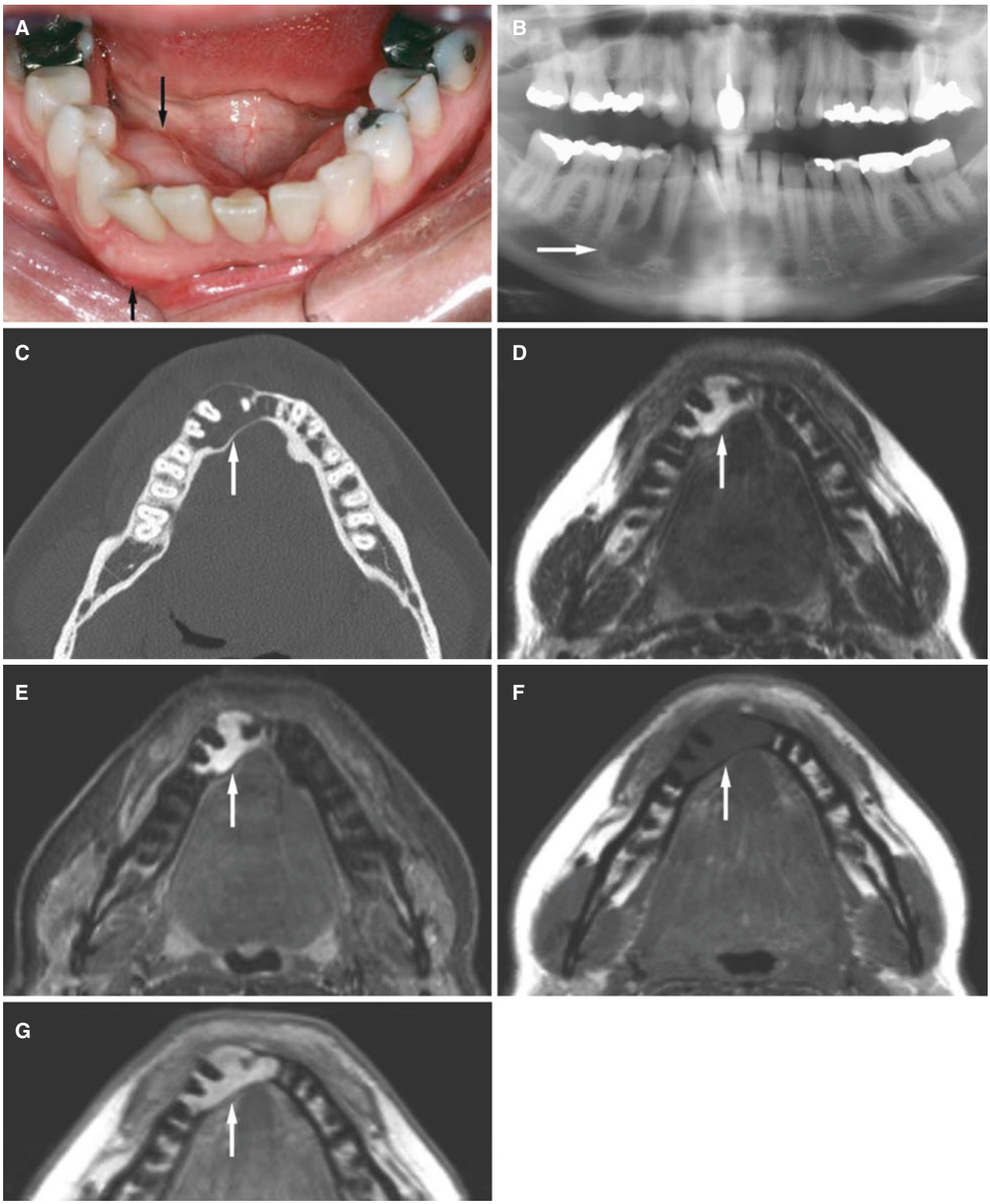

Fig. 3.32 Odontogenic myxoma, mandible; 45-year-old female with painless swelling which the patient did not notice because tumor was "filling out" mandibular torus on the right side. (**A**) Clinical photograph shows buccal and lingual jaw expansion (*arrows*). (**B**) Panoramic view shows scalloped radiolucency without sclerotic outline (*arrow*). (**C**) Axial CT image shows expanded but intact buccal and lingual cortical bone. Note tumor occupies mandibular torus on the right side (*arrow*). (**D**) Axial T2-weighted MRI shows homogeneous high signal (*arrow*). (**E**) Axial STIR MRI shows homogeneous high signal (*arrow*). (**F**) Axial T1-weighted pre-Gd MRI shows intermediate (to low) signal (*arrow*). (**G**) Axial T1-weighted post-Gd MRI shows homogeneous contrast enhancement (*arrow*)

3.11 Osteoblastoma

Figs. 3.33 and 3.34

Synonym: Osteoid osteoma is a similar tumor, but smaller (a nidus usually less than 1 cm), and being associated with nocturnal pain.

3.11.1 Definition

Mesenchymal benign tumor characterized by well-vascularized connective tissue stroma in which active production of osteoid or primitive woven bone occurs, bone occurs, forming a mass 20 mm in size (WHO).

3.11.2 Clinical Features

- Swelling, usually painful, but also without pain
- Mandible more frequent than maxilla
- Males more frequent than females
- Peak incidence in the second decade
- The most common site of occurrence is the vertebrae, flat bones, femur, and tibia, but generally considered a rare tumor
- Only 15% in the skull, maxilla, and mandible
- Nearly 15% recurrence rate has been reported for conventional mandibular osteoblastomas, without histologic atypia
- Juvenile aggressive osteoblastoma has high recurrence (close to 50%) after surgery, depending on histologic atypia

3.11.3 Imaging Features

- Highly variable; osteolytic to osteoblastic (ground-glass appearance)
- Coarse trabecular pattern
- Expansive growth, may resemble aneurysmal bone cyst
- Distinction between aggressive osteoblastoma and low-grade osteosarcoma may be difficult, but low-grade osteoblastoma has more well-defined border
- If close to teeth, it may cause displacement but not fuse with cementum (in contrast to benign cementoblastoma)

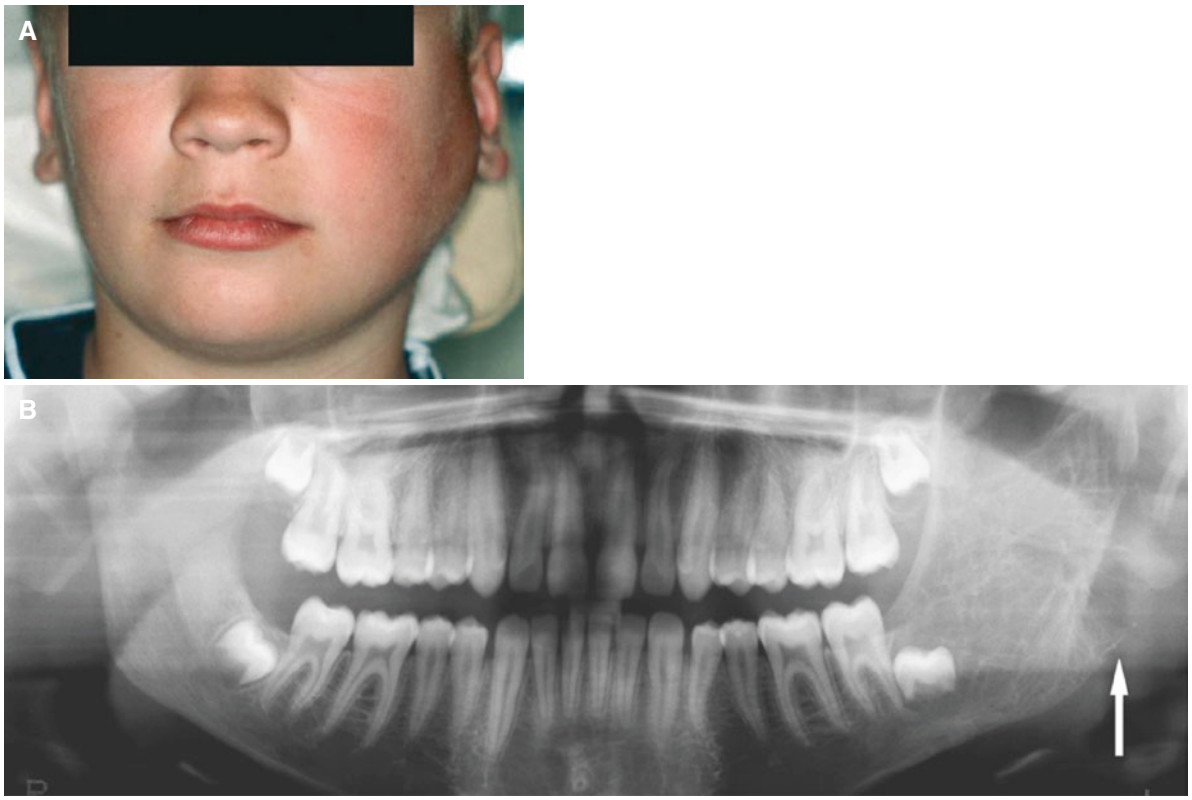

Fig. 3.33 Osteoblastoma, mandible; 10-year-old male with painless swelling of the left cheek, parotid region. (**A**) Clinical photograph shows swelling of the left parotid area. (**B**) Panoramic view shows expansive process in the ramus with coarse trabecular pattern (*arrow*). (**C**) Axial CT image shows expansive, osteolytic process with gracile structure (*arrow*). (**D**) Coronal CT image shows expansive process with thin but rather well-defined border (*arrow*). (**E**) Coronal CT image shows tumor including mandibular condyle (*arrow*). (**F**) Axial T2-weighted MRI shows intermediate (to high) signal (*arrow*). (**G**) Axial T1-weighted pre-Gd MRI shows intermediate signal (*arrow*). (**H**) Axial T1-weighted post-Gd MRI shows contrast enhancement (*arrow*). (**I**) Coronal T1-weighted post-Gd MRI shows contrast enhancement (*arrow*) (A: courtesy of Dr. T. Bjørnland, Rikshospitalet University Hospital, Oslo, Norway)

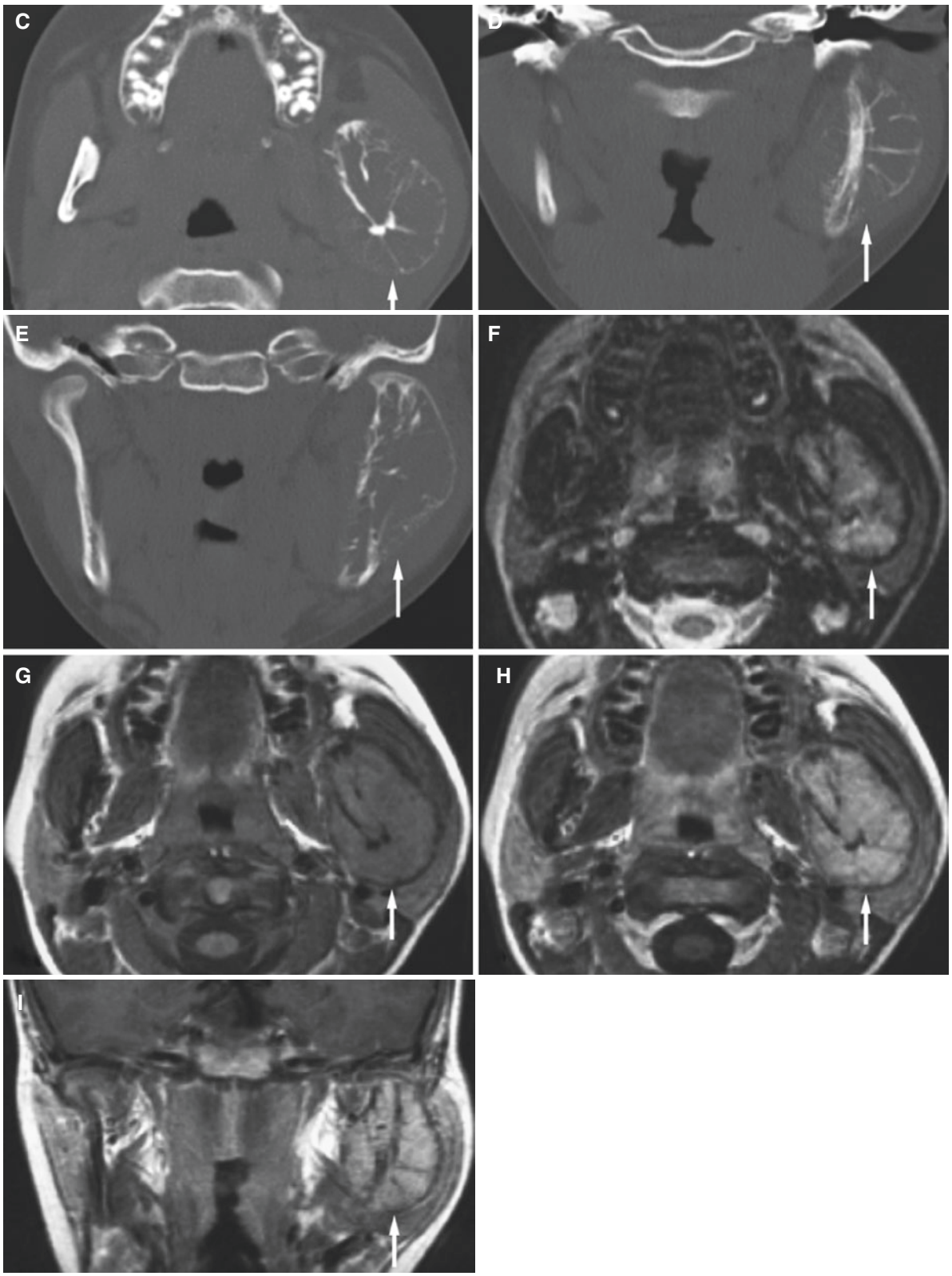

Fig. 3.33 (continued)

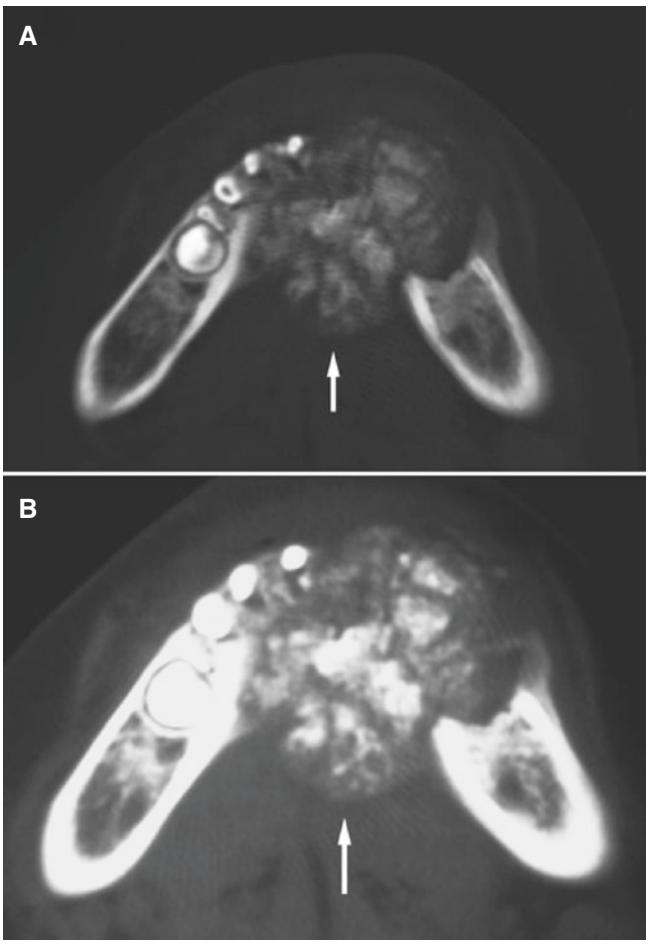

Fig. 3.34 Osteoblastoma, mandible; 3-year-old male, painless swelling of the anterior part of the mandible. (**A**) Axial CT image shows extensive bone production (*arrow*). (**B**) Axial CT image, soft-tissue window, shows rather well-defined mass (*arrow*)

3.12 Ossifying Fibroma

Figs. 3.35, 3.36, 3.37, 3.38, and 3.39

Synonyms: Cemento-ossifying fibroma, cementifying fibroma, juvenile (active/aggressive) ossifying fibroma

3.12.1 Definition

Well-demarcated benign fibro-osseous neoplasm composed of fibrocellular tissue and mineralized material of varying appearances. Juvenile trabecular ossifying fibroma and juvenile psammomatoid ossifying fibroma are two histologic variants of ossifying fibroma. Thus, three clinicopathological variants have been identified (WHO).

3.12.2 Clinical Features

- Painless swelling
- Mostly in the mandible, posterior region
- Juvenile variants mostly in the maxilla
- Second to fourth decades; mean age about 35 years
- Mean age of juvenile variants about 10 and 20 years
- Females more frequent than males
- Tumor more active/aggressive in young patients

3.12.3 Imaging Features

- Radiolucency, radiopacity, or mixed appearance; about half of the cases have been reported to be radiolucent
- Border usually well defined, may be multilocular
- Bone expansion may be evident in more than half of the cases
- May displace the maxillary sinus, nasal cavity, and mandibular canal
- Majority shows no relationship to tooth apices
- Only occasionally root displacement or resorption
- May be impossible to distinguish from fibrous dysplasia (ground-glass appearance)
- Discrete zones of variable amounts of either osseous or fibrous tissue give variable signal pattern on MRI
- T1-weighted MRI: low to intermediate to high signal
- T2-weighted and STIR MRI: low to intermediate to high signal
- T1-weighted post-Gd MRI: rather homogeneous contrast enhancement or contrast-enhanced areas interspersed with nonenhanced areas

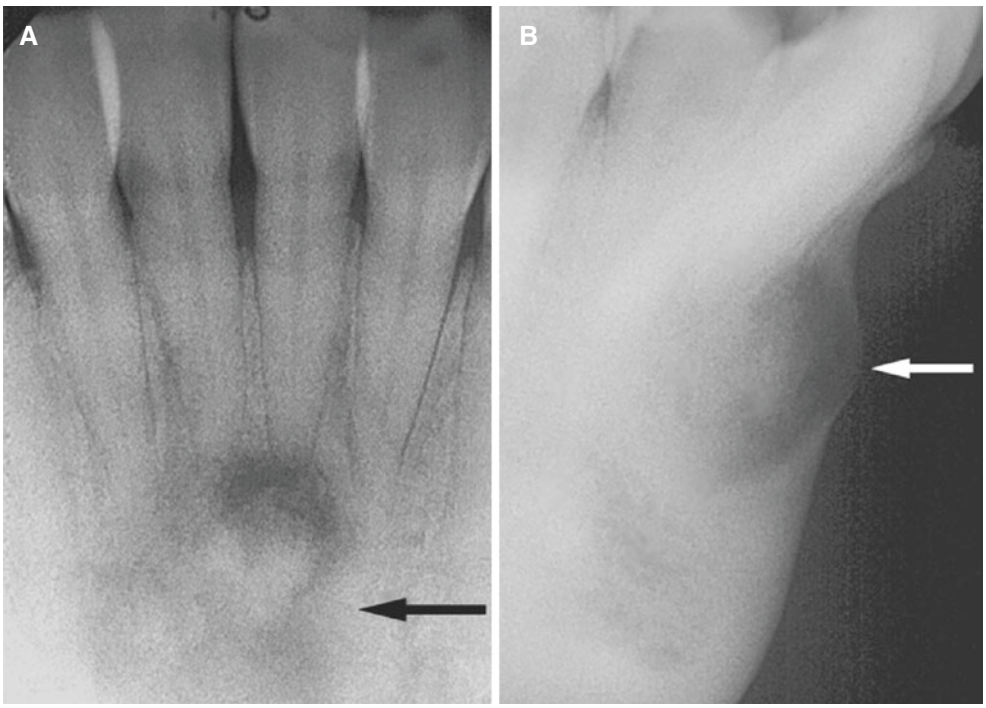

Fig. 3.35 Ossifying fibroma, mandible; painless swelling in the anterior part of the mandible. (**A**) Intraoral view shows radiolucency with diffuse, somewhat sclerotic border and central mineralization (*arrow*). (**B**) Side view shows expanded and intact buccal cortical bone (*arrow*)

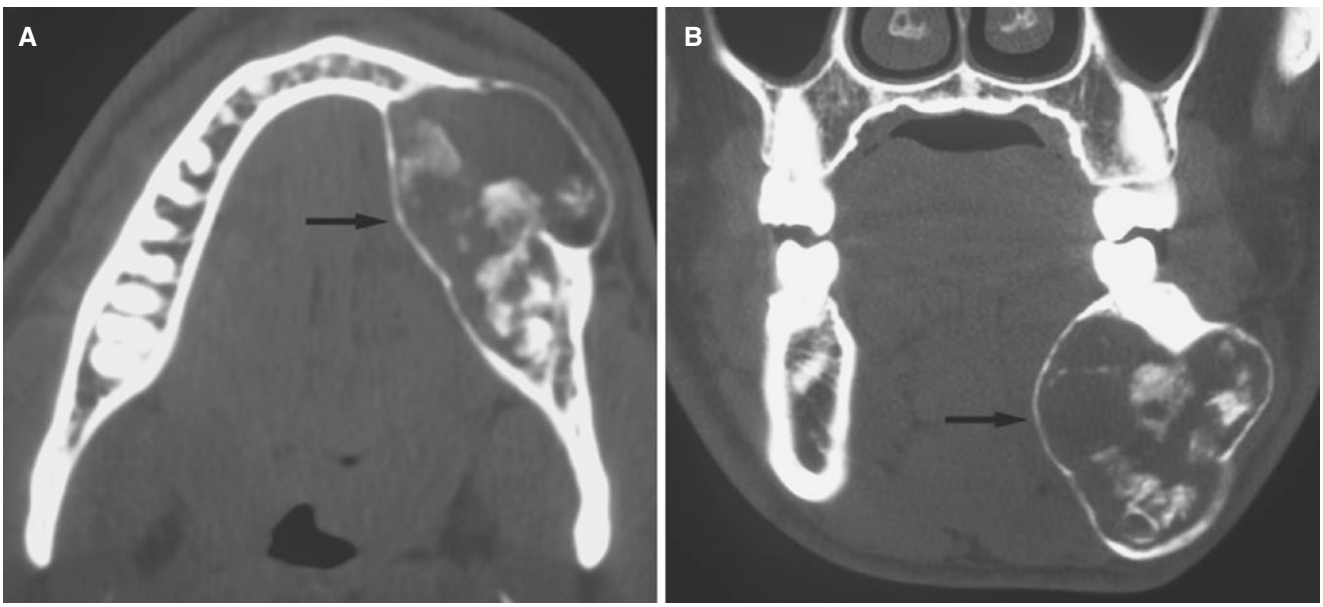

Fig. 3.36 Ossifying fibroma, mandible; 22-year-old male with painless swelling of the left mandible. (**A**) Axial CT image shows expansion with intact cortical border and central mineralization (*arrow*). (**B**) Coronal CT image shows expanded, intact cortical bone and central mineralization (*arrow*)

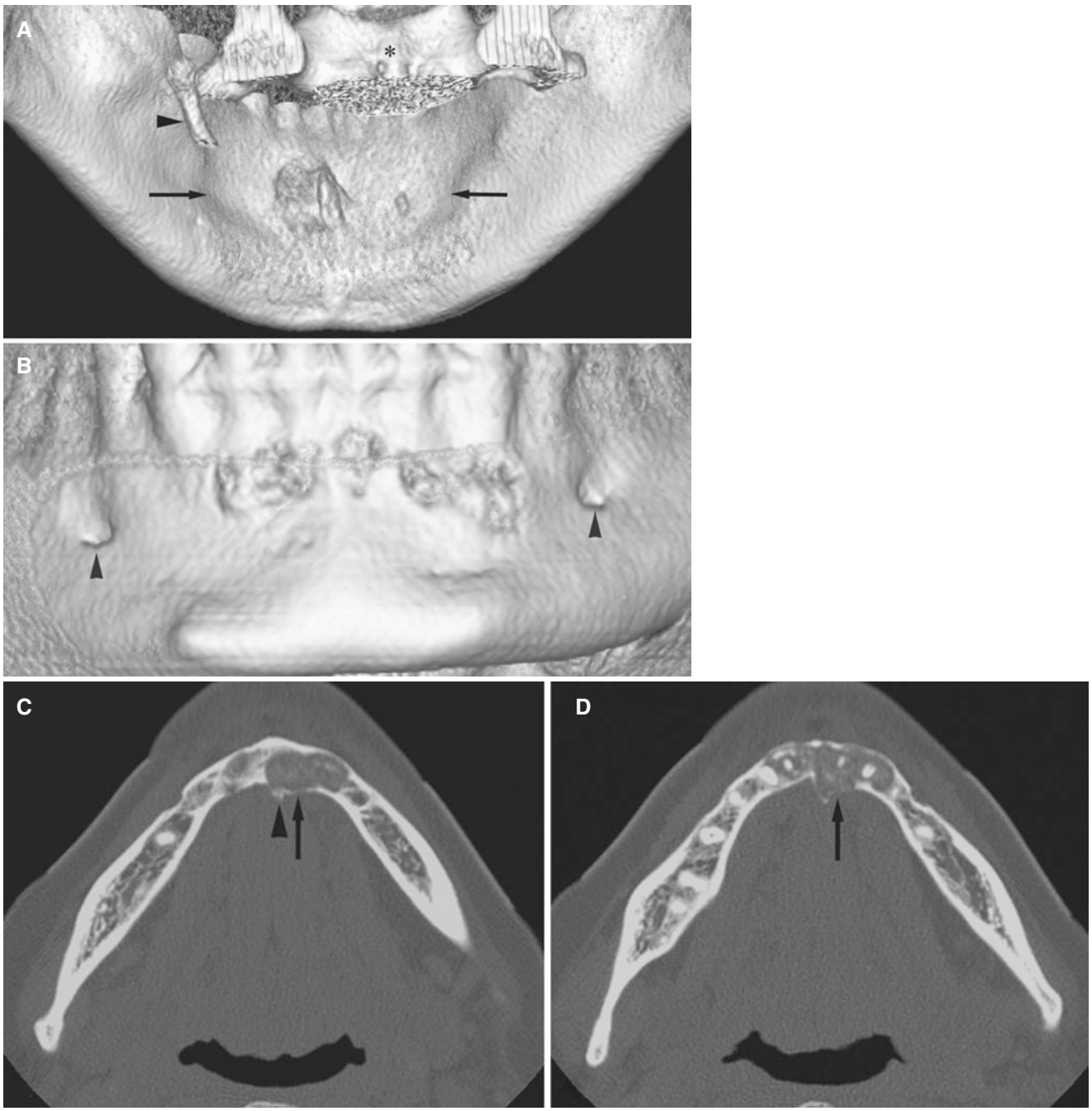

Fig. 3.37 Ossifying fibroma, mandible; 41-year-old female with painless swelling of lingual aspect of anterior mandible. (**A**) 3D CT image shows swelling on lingual side with cortical defects (*arrows*). Note the styloid process (*arrowhead*) and cervical spine (*asterisk*). (**B**) 3D CT image shows cortical defects on buccal side between mental foramina (*arrowheads*). (**C**) Axial CT image shows well-defined radiolucency with some expansion and intact cortical bone lingually (*arrow*). Note lingual crista (*arrowhead*) and small mineralizations. (**D**) Axial CT image shows tumor with small mineralizations and more expansion lingually (*arrow*). (**E**) Axial T2-weighted MRI shows intermediate, slightly heterogeneous signal (*arrow*). (**F**) Coronal STIR MRI shows intermediate signal (*arrow*). (**G**) Axial T1-weighted pre-Gd MRI shows intermediate signal (*arrow*). (**H**) Axial T1-weighted post-Gd MRI shows moderate contrast enhancement (*arrow*). (**I**) Coronal T1-weighted post-Gd MRI shows moderate contrast enhancement (*arrow*)

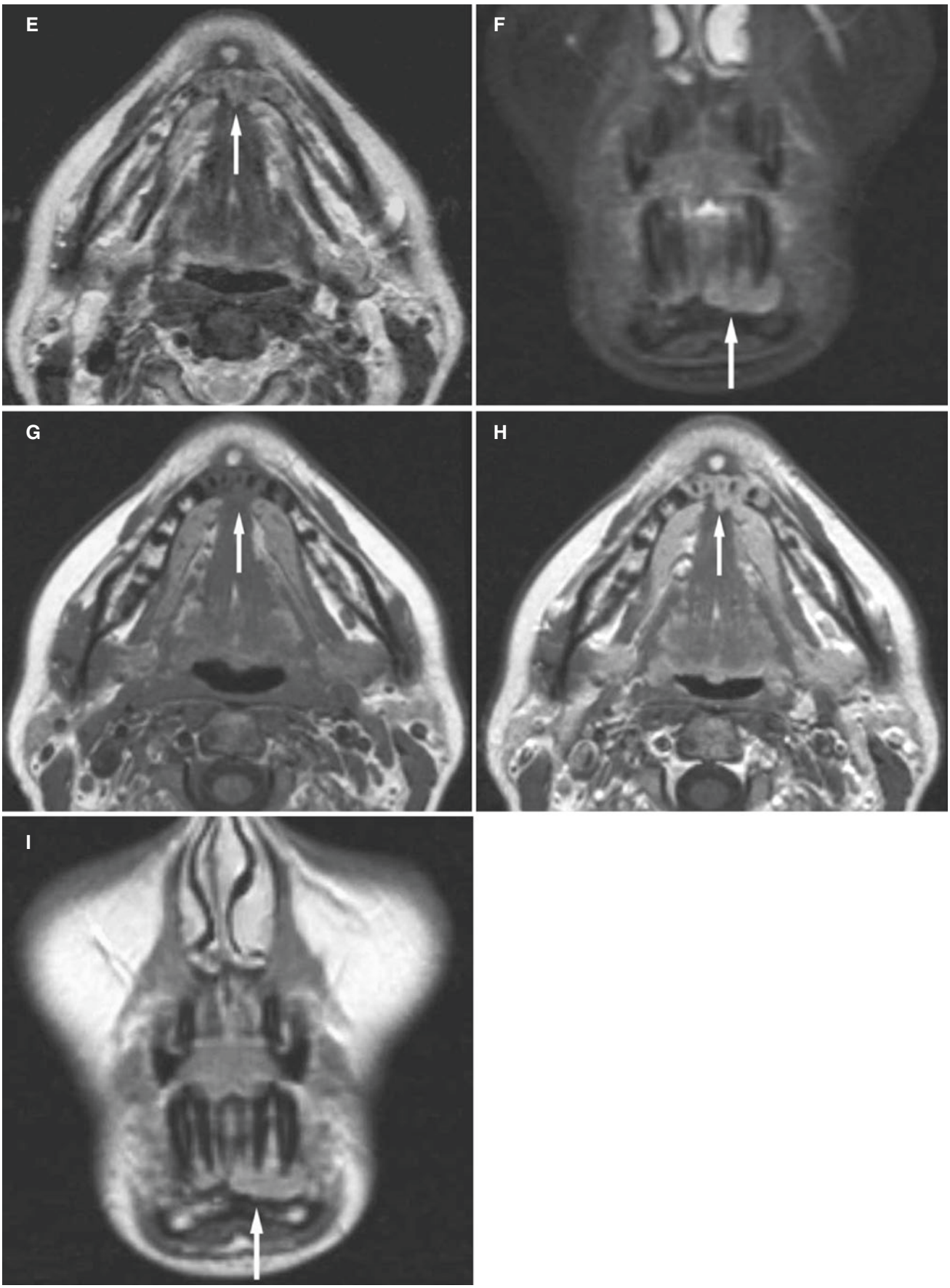

Fig. 3.37 (continued)

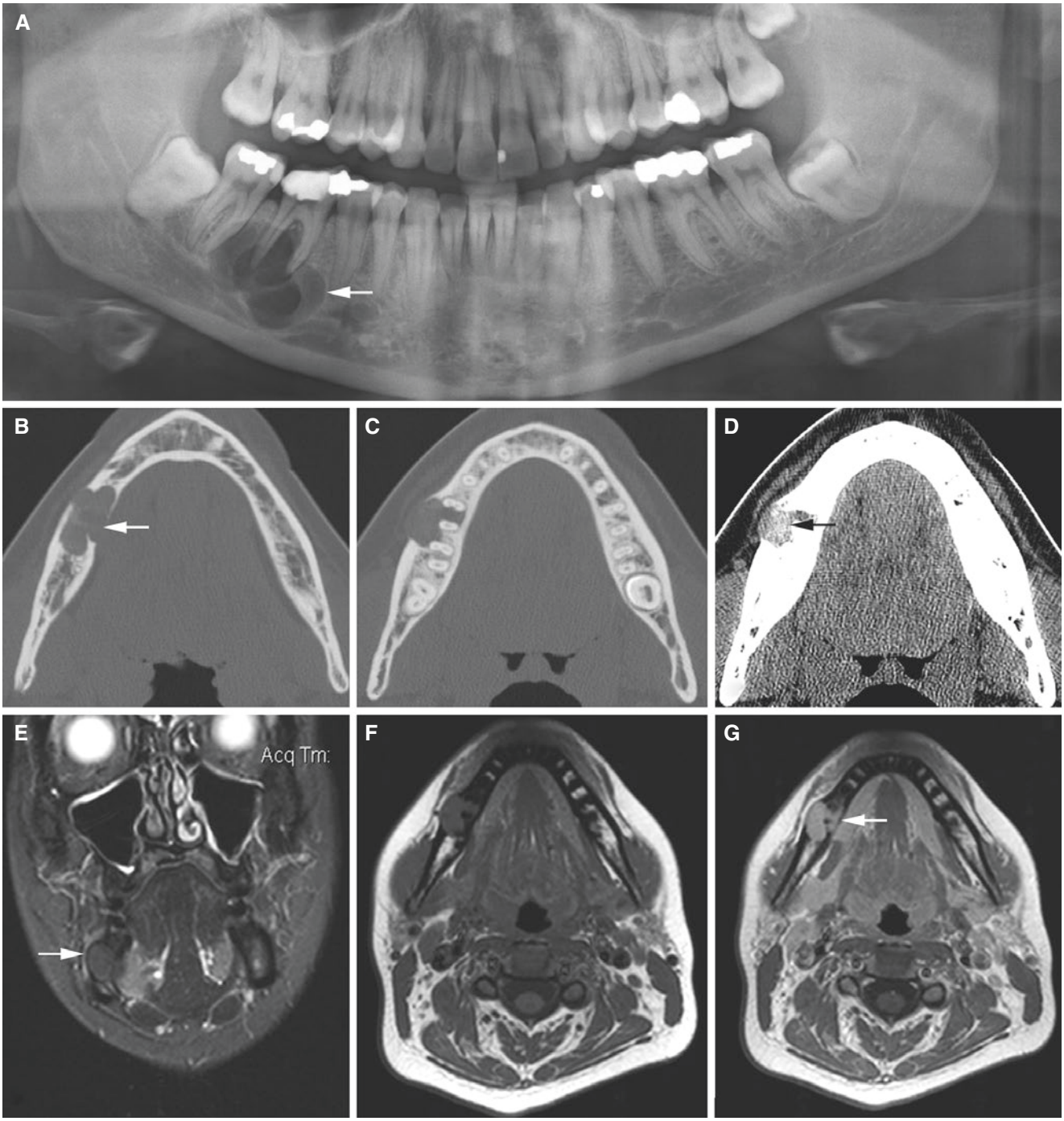

Fig. 3.38 Ossifying fibroma, mandible; 31-year-old female with hard, buccal swelling in the right mandible and variable pain from the first molar (deep filling, vital tooth). (**A**) Panoramic view shows well-defined multilocular radiolucency in periapical area of the first molar (*arrow*). (**B**, **C**) Axial CT images show radiolucency with defects in buccal and lingual cortical plate (*arrow*). (**D**) Axial (soft-tissue window) CT image shows slight buccal expansion of well-defined soft-tissue mass and normal subcutaneous fat (*arrow*). (**E**) Coronal STIR MRI shows low signal intensity (*arrow*). (**F**) Axial T1-weighted pre-Gd and (**G**) Axial T1-weighted post-Gd MRI show solid contrast enhancement (*arrow*). (**H**) Three-year postoperative panoramic view shows good healing in the right mandible (*arrow*). Ossifying fibroma also developed in the left mandible, now with good healing 2 years after surgery in this area (*arrowhead*)

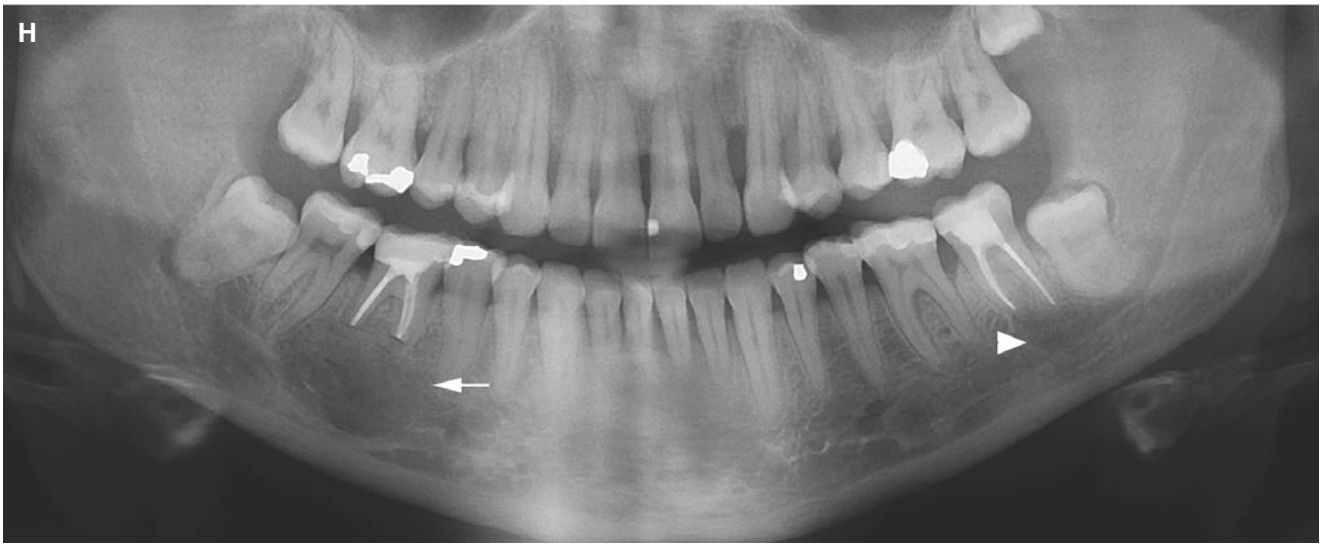

Fig. 3.38 (continued)

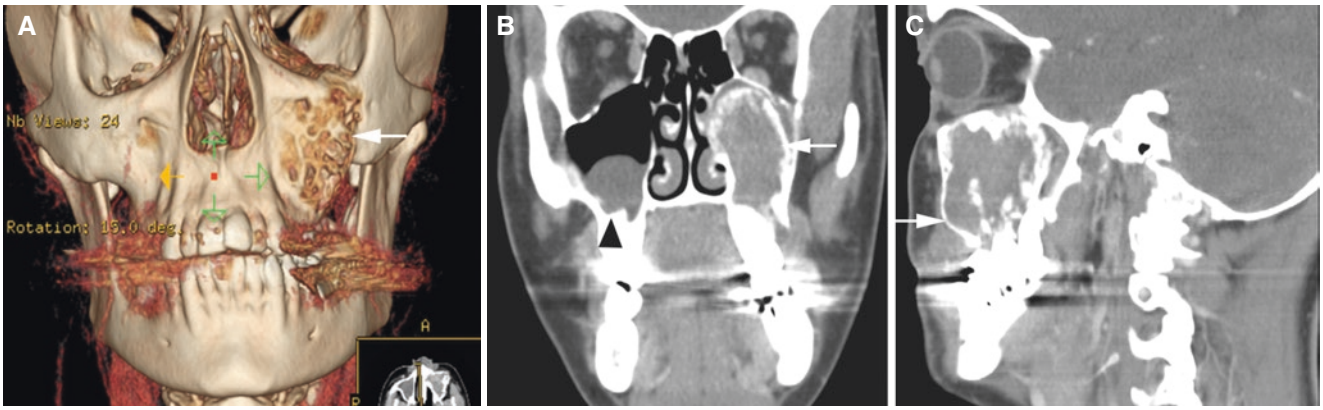

Fig. 3.39 Ossifying fibroma, maxillary sinus; 26-year-old female with pain-free facial swelling. (**A**) 3D CT shows expanding left maxillary sinus with irregularities of the sinus wall (*arrow*). (**B**) Coronal CT and (**C**) sagittal CT images show radiopaque lesion with irregular bone formation in the left maxillary sinus (*arrow*). Retention cyst in the right maxillary sinus, incidental finding (*arrowhead*)

3.13 Juvenile Ossifying Fibroma

Figs. 3.40 and 3.41

Synonyms: See **Ossifying Fibroma**

3.13.1 Definition

See **Ossifying Fibroma**

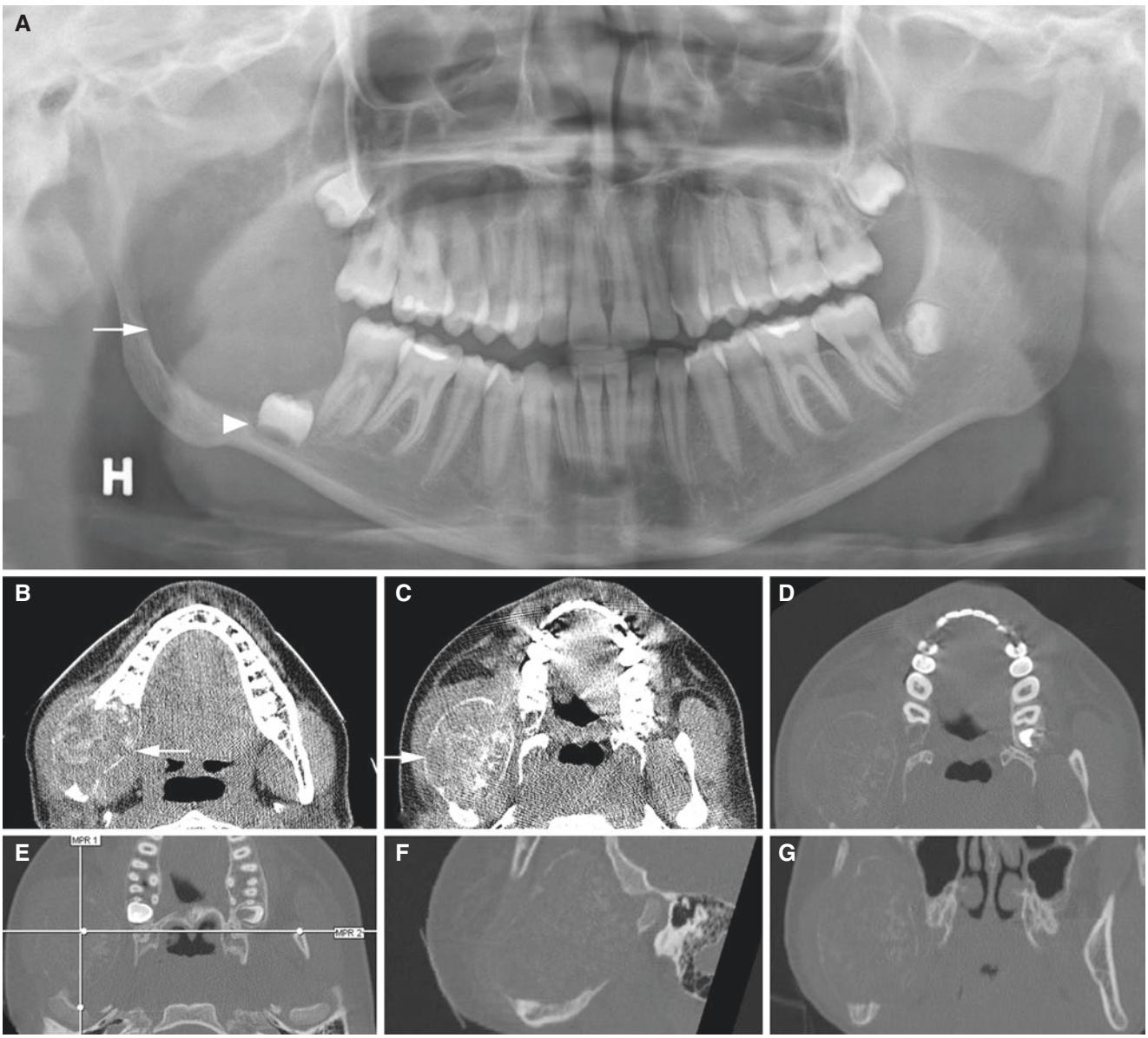

Fig. 3.40 Juvenile ossifying fibroma, mandible; 13-year-old female with pain-free swelling of the right mandible. (**A**) Panoramic view shows radiolucency in the right mandibular ramus (*arrow*) and displaced tooth germ (*arrowhead*). (**B**, **C**) Axial (soft-tissue window) CT images show expansive mass with rather well-defined and thinned cortical outline (*arrow*) and calcifications within mass. (**D**) Axial, (**E**) axial (with cursor lines), (**F**) sagittal, and (**G**) coronal (bone window) CT images show almost completely destroyed right mandibular ramus with rather well-defined cortical outline

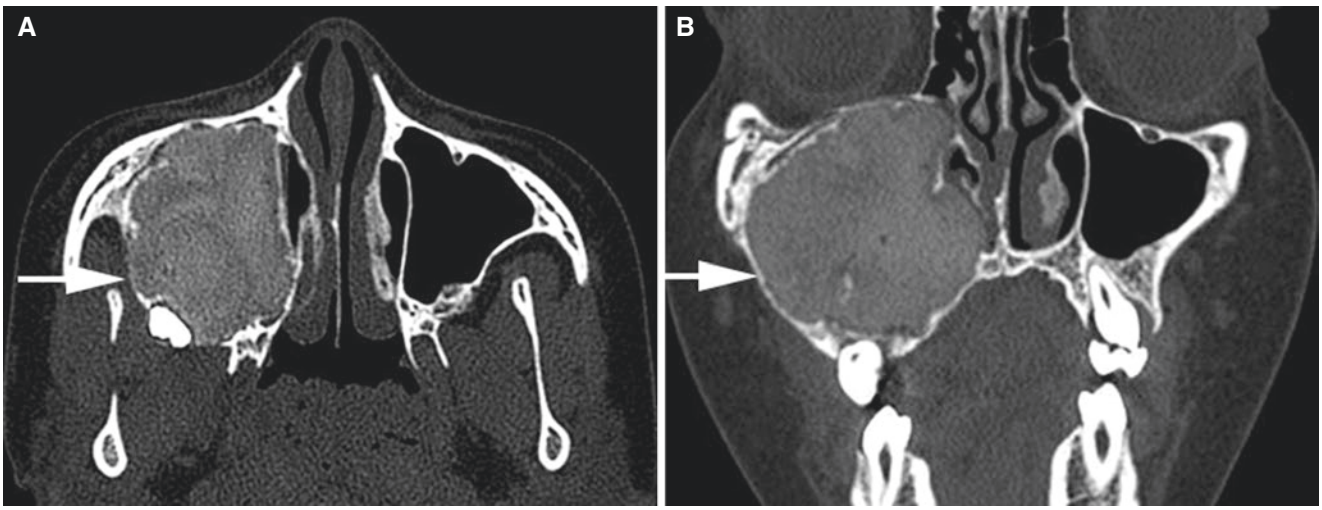

Fig. 3.41 Juvenile ossifying fibroma, maxilla/maxillary sinus; 10-year-old female with pain-free swelling of the right maxilla/maxillary sinus. (**A**) Axial and (**B**) coronal CT images show expanding radiopaque mass (ground-glass appearance) in the right maxillary sinus (*arrow*) with punctate calcifications within mass

3.14 Benign Tumorlike Conditions

A number of conditions are described including one tumor (osteoma).

3.15 Aneurysmal Bone Cyst

Figs. 3.42 and 3.43

Synonym: Aneurysmal bone cavity

3.15.1 Definition

Expansile osteolytic lesion often multilocular, containing blood-filled spaces separated by fibrous septa containing osteoclast-type giant cells and reactive bone (WHO).

Aneurysmal bone cyst may occur as hybrid lesions with ossifying fibroma, nonneoplastic fibrous dysplasia or nonneoplastic giant cell granuloma, or even other conditions.

3.15.2 Clinical Features

- Painless swelling, usually few symptoms
- Mandible more often than maxilla, mostly in posterior regions including ramus
- Usually below 30 years of age, but may present at any age in jaws
- No sex predominance or slight female
- Can occur anywhere in the skeleton; most frequently in long bones, followed by the spine
- In a large series of children (1.5–17 years), more than 60% occurred in long bones

3.15.3 Imaging Features

- Highly variable radiologic appearance in jaws
- Mostly radiolucent (close to 90%), but also mixed or rarely radiopaque
- Unilocular (less than half) or multilocular
- Usually expansile, ballooning (about 50% in jaws)
- Border well-defined and corticated in about one-third, thus majority without sclerosis or even diffuse in jaws
- Cortical perforation may occur
- Tooth displacement and root resorption may occur
- T1-weighted MRI: intermediate–low signal surrounded by low-signal well-defined rim and fluid–fluid level
- T2-weighted and STIR MRI: high signal, fluid–fluid level
- T1-weighted post-Gd MRI: enhancement of internal septations

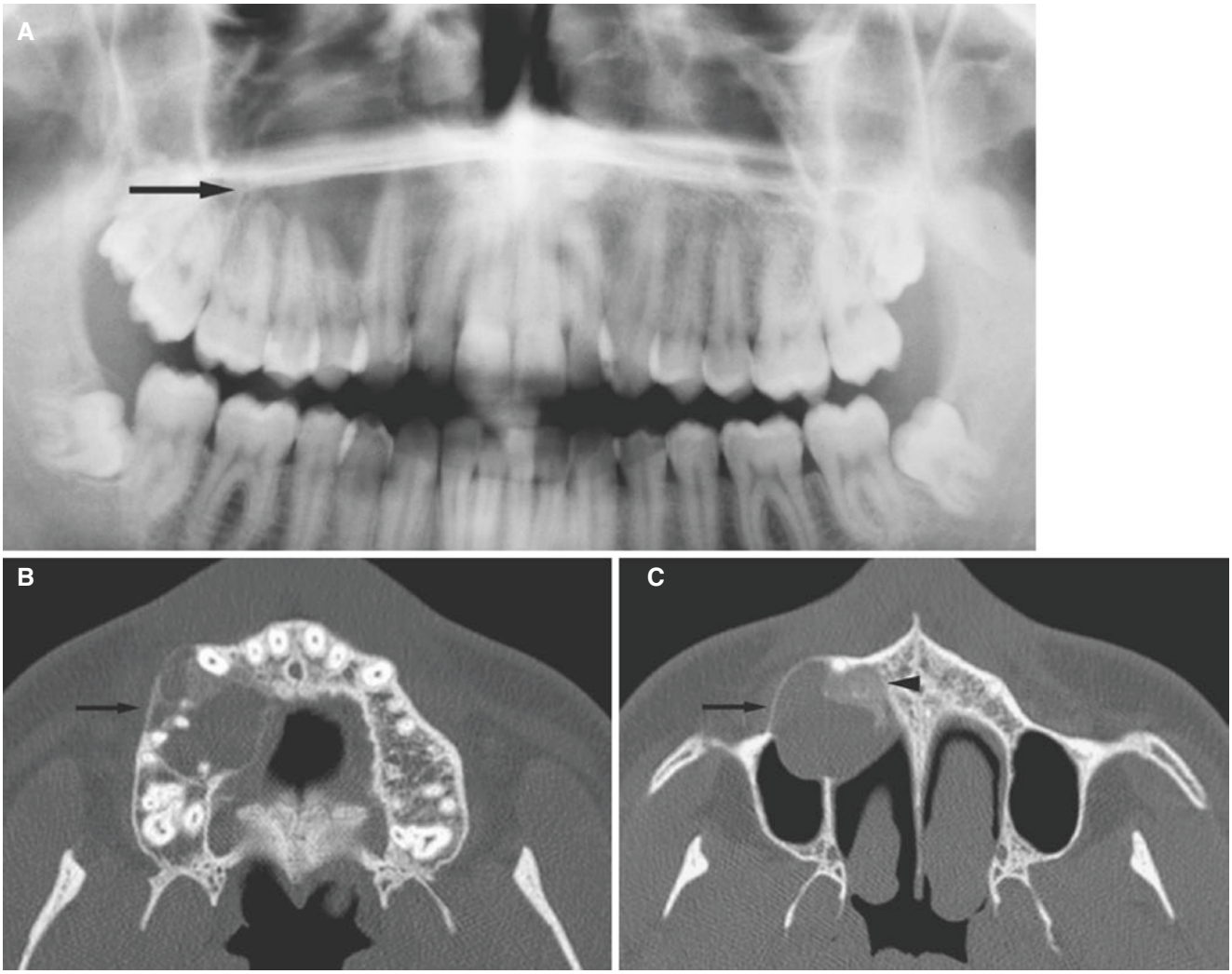

Fig. 3.42 Hybrid lesion of ossifying fibroma and aneurysmal bone cyst, maxilla; 22-year-old male with painless swelling of mucobuccal fold. (**A**) Panoramic view shows radiolucency with sclerotic border in the maxilla (*arrow*). (**B**) Axial CT image shows well-defined tumor with expanded, intact cortical delineation (*arrow*) with some mineralization in the anterior part. (**C**) Axial CT image shows well-defined expanded tumor with intact cortical plate (*arrow*) and more mineralization than in B (*arrowhead*). (**D**) Axial PD MRI shows high signal in a large portion and intermediate signal in a small portion of tumor (*arrow*). (**E**) Axial T2-weighted MRI shows high signal in a large portion (*arrow*) and low signal in a small portion. (**F**) Axial T1-weighted pre-Gd MRI shows intermediate signal (*arrow*). (**G**) Axial T1-weighted post-Gd MRI shows septal contrast enhancement (*arrow*). (**H**) Coronal T1-weighted post-Gd MRI shows septal contrast enhancement (*arrow*)

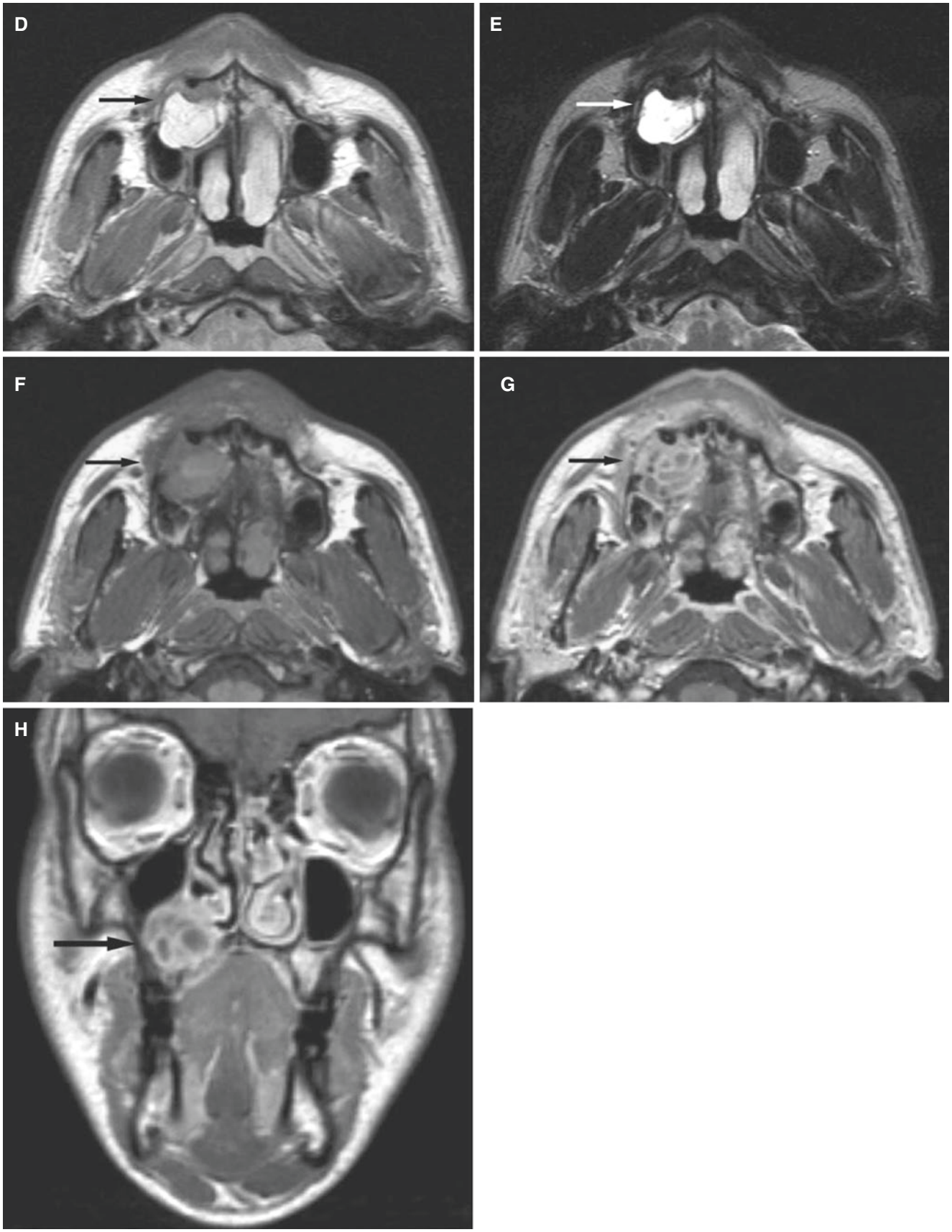

Fig. 3.42 (continued)

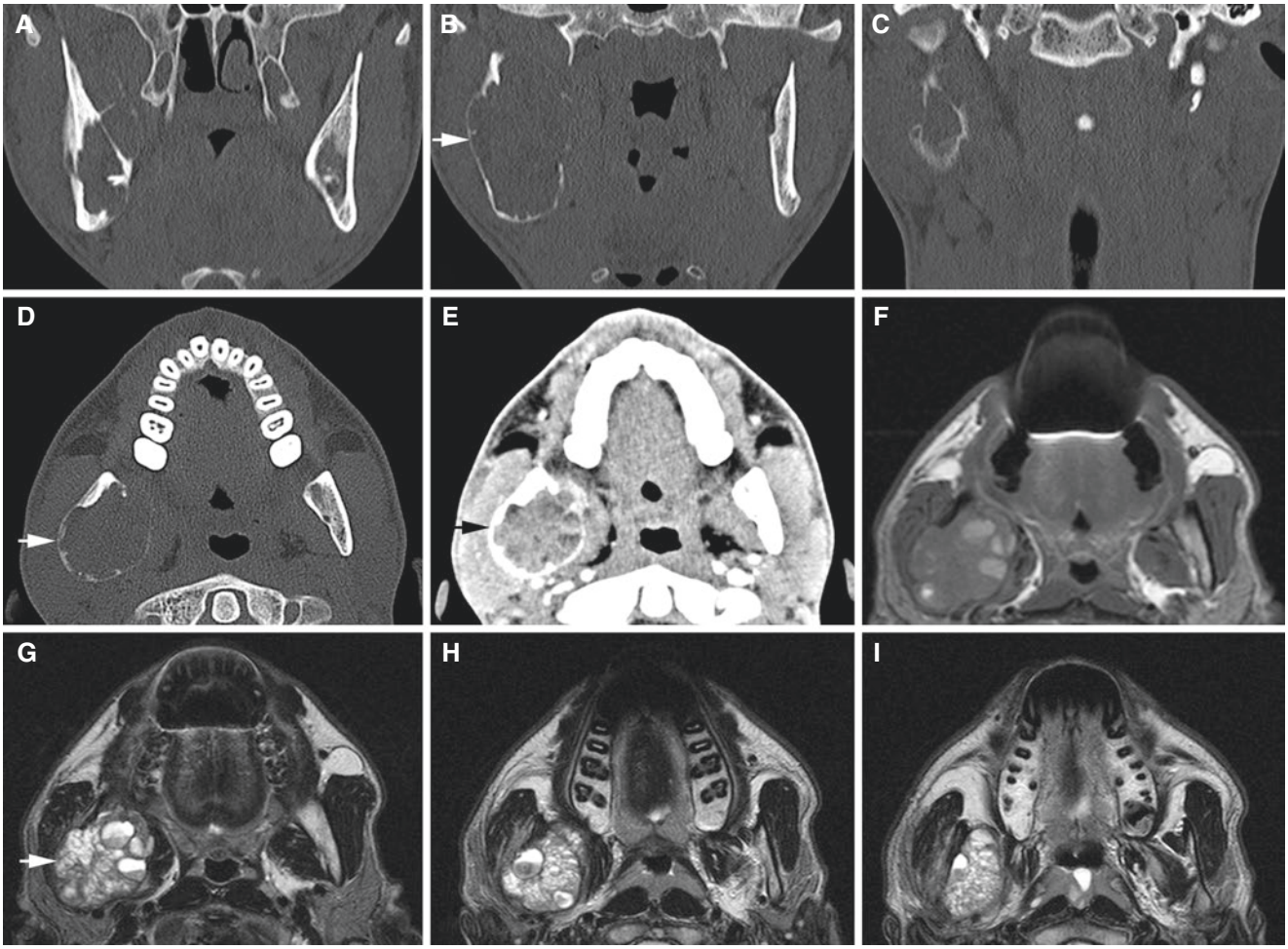

Fig. 3.43 Hybrid lesion of aneurysmal bone cyst, giant cell granuloma, and ossifying fibroma, mandible; 16- year-old male with pain-free swelling of the right mandible. (**A**, **B**, **C**) Coronal and (**D**) axial CT images show expansion with thinned, partially destroyed cortical outline (*arrow*). (**E**) Axial contrast-enhanced (soft-tissue window) CT image shows well-defined mass with heterogeneous content (*arrow*). (**F**) Axial T1-weighted and (**G**, **H**, **I**) axial T2-weighted MRI show well-defined mass with heterogeneity in signal intensity, also indicating fluid level (*arrow*)

3.16 Giant Cell Granuloma (Central)

Figs. 3.44, 3.45, and 3.46

Synonym: Giant cell lesion, giant cell tumor, giant cell reparative granuloma (obsolete)

3.16.1 Definition

Localized benign but sometimes aggressive osteolytic proliferation consisting of fibrous tissue with hemorrhage and hemosiderin deposits and presence of osteoclast-like giant cells in a vascular stroma (WHO).

3.16.2 Clinical Features

- Incidental finding or painless swelling
- First to third decades, but wide age range
- Females more frequent than males
- Mandible two-thirds, maxilla one-third
- Most often in the posterior region, less frequently in the anterior region (but also crossing the midline)
- May behave aggressively in younger patients, with recurrence after surgical treatment
- Noonan syndrome and bilateral abnormalities

3.16.3 Imaging Features

- Radiolucency
- Unilocular or more often multilocular; may be scalloped
- Border well defined or poorly defined, may be sclerotic but usually not
- May expand bone
- May displace or, less frequently, resorb teeth
- T1-weighted MRI: homogeneous or slightly heterogeneous intermediate signal
- T2-weighted and STIR MRI: homogeneous or slightly heterogeneous intermediate signal
- T1-weighted post-Gd MRI: contrast enhancement

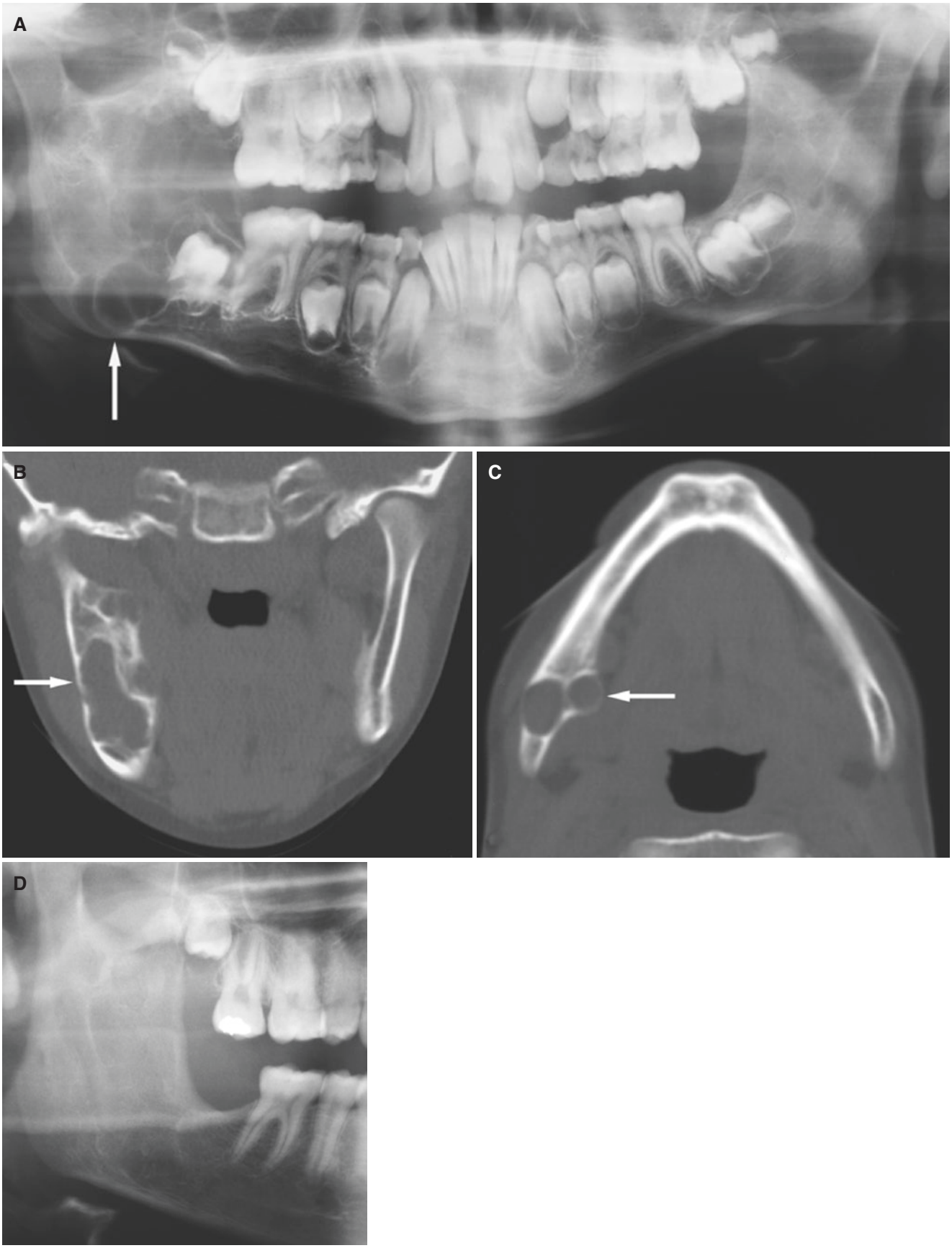

Fig. 3.44 Giant cell granuloma, mandible; 10-year-old male at presentation with painless jaw swelling. (**A**) Panoramic view shows multilocular radiolucency with sclerotic border (*arrow*). (**B**) Coronal CT image shows expansive, multilocular process (*arrow*). (**C**) Axial CT image shows two "compartments" at the lower mandibular border (*arrow*). (**D**) Panoramic view at 6-year follow-up shows complete regeneration after two surgical interventions

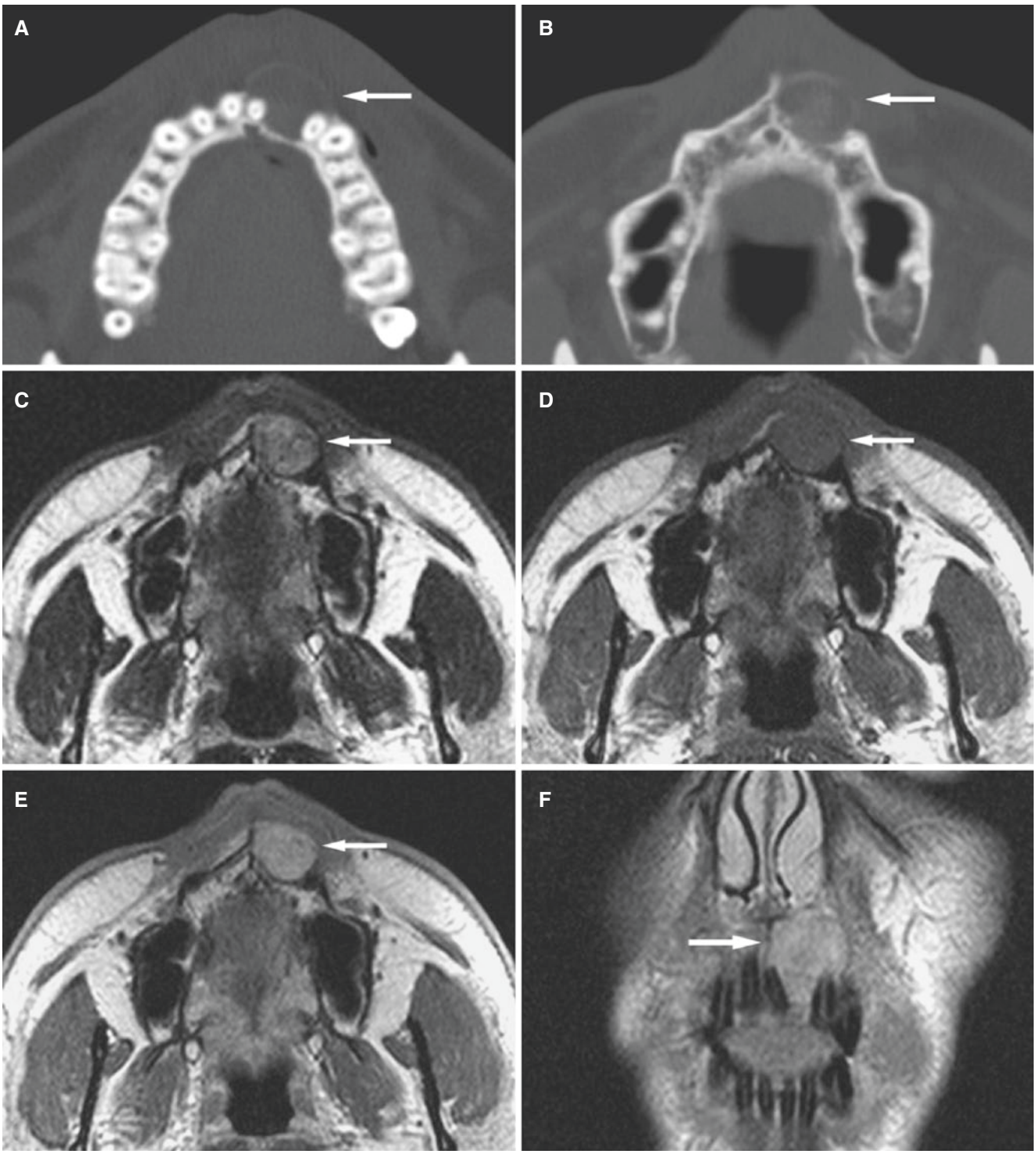

Fig. 3.45 Giant cell granuloma, maxilla; 22-year-old male with recurrence (painless swelling) after previous surgery. (**A**) Axial CT image shows well-defined expansive process (*arrow*). (**B**) Axial CT image shows corticated outline (*arrow*). (**C**) Axial T2-weighted MRI shows slightly heterogeneous intermediate signal (*arrow*). (**D**) Axial T1-weighted pre-Gd MRI shows homogeneous intermediate signal (*arrow*). (**E**) Axial T1-weighted post-Gd MRI shows homogeneous contrast enhancement (*arrow*). (**F**) Coronal T1-weighted post-Gd MRI shows contrast-enhanced and well-defined mass (*arrow*) displacing teeth

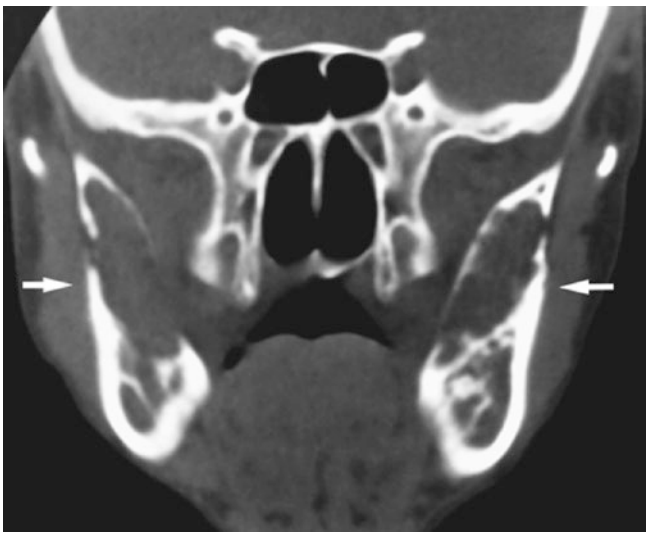

Fig. 3.46 Giant cell granuloma, bilateral, mandible; patient with Noonan syndrome. Coronal CT image shows bilateral, expansive radiolucencies with cortical defects (*arrows*)

3.17 Langerhans Cell Histiocytosis

Fig. 3.47

Synonyms: Langerhans cell disease, histiocytosis X, idiopathic histiocytosis, eosinophilic granuloma (uni- or multifocal)

3.17.1 Definition

Localized clonal proliferation of immature Langerhans cells (histiocytes) consisting of reticulum cells, multinucleated giant cells, eosinophils, lymphocytes, and plasma cells (inflammatory or reparative nonneoplastic nature). It is generally considered not to be a form of cancer.

Langerhans cell histiocytosis is a meoplastic proliferation of Langerhans cells (WHO).

3.17.2 Clinical Features

- Swelling, pain, tenderness
- Fever, general malaise
- Most common sites: skull, mandible, spine, ribs, and long bones
- Mandible more often than maxilla, posterior regions in particular
- Male predilection, 1–10 years of age
- Also generalized forms (considered malignant disorders, at least debatable)

3.17.3 Imaging Features

- Punched-out bone destruction, sharply demarcated, not corticated
- No reactive sclerosis, but periosteal reaction
- Associated soft-tissue mass
- Usually no tooth resorption, may give a "floating teeth" appearance

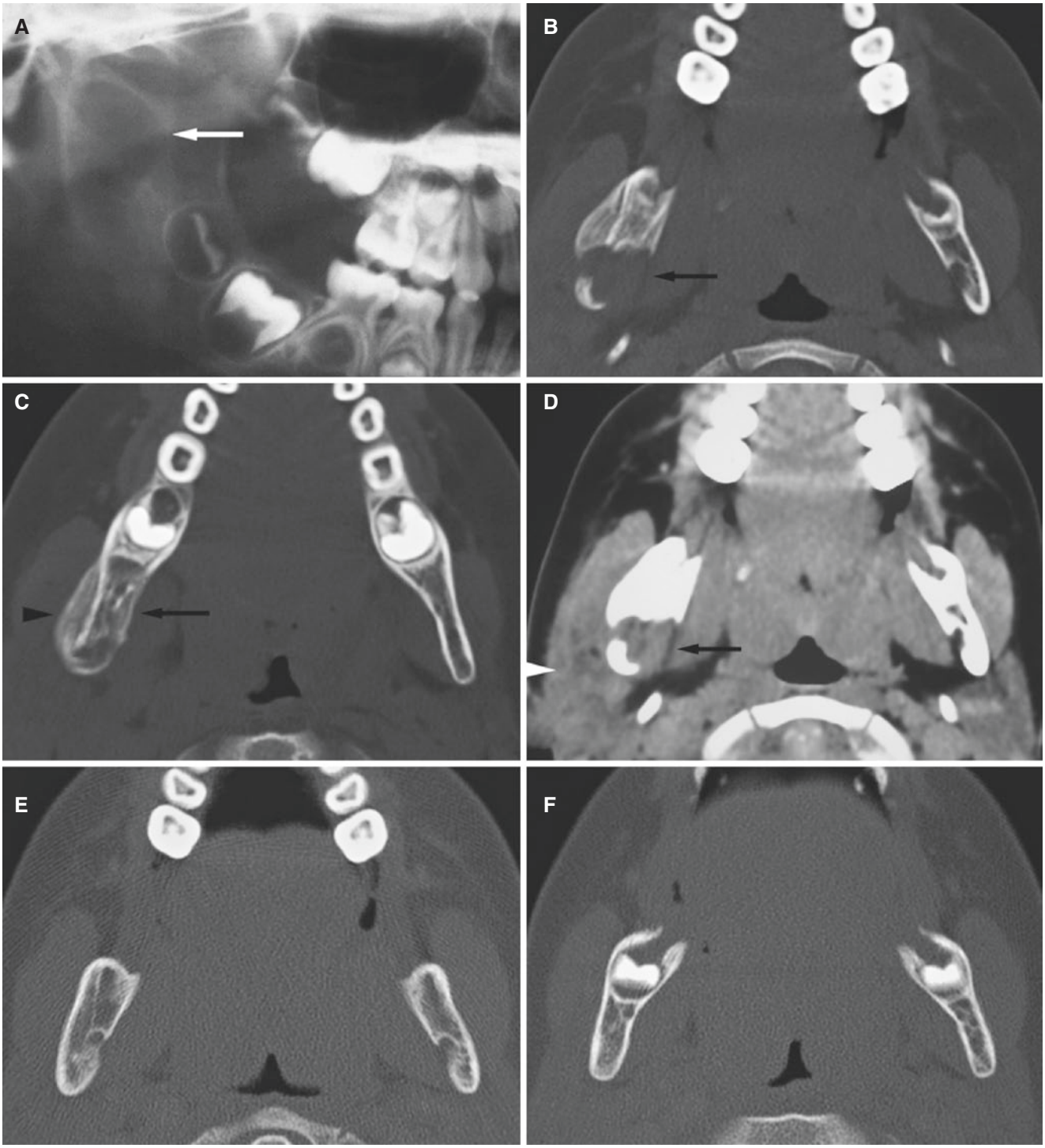

Fig. 3.47 Langerhans cell histiocytosis, mandible; 4-year-old male with pain and swelling in the right cheek and jaw (ramus). (**A**) Panoramic view shows rather well-defined radiolucency (*arrow*). (**B**) Axial CT image shows punched-out bone destruction at the level of mandibular foramina (*arrow*). (**C**) Axial CT image shows onion skin periosteal reaction lingually (*arrow*) and buccally (*arrowhead*). (**D**) Axial CT image, soft-tissue window, shows well-defined soft-tissue mass lingually (*arrow*) and inflammatory infiltrate in connective tissue space laterally (*arrowhead*). (**E**) Axial CT image 1 year after treatment (surgery, cortisone medication) shows somewhat thickened right ramus and remnant of original buccal cortex at the level of mandibular foramina, but otherwise normalized bone. (**F**) Axial CT image shows normalized bone also at another level

3.18 Cherubism

Figs. 3.48, 3.49, and 3.50

Synonym: Familiar fibrous dysplasia

3.18.1 Definition

Autosomal dominant inherited disease characterized by a symmetrical distension of the mandible and the maxilla as bone is replaced by cyst-like and giant cell lesions often leading to a typical facial expression. The histology is indistinguishable from giant cell granuloma (WHO).

3.18.2 Clinical Features

- Familial disease affecting 100% of males and up to 70% of females
- Diagnosis often made in early childhood or preadolescence, depending on severity
- Lesions regress with age
- More seldom lesions may show progression in adults
- Usually mandible, posterior regions, but all four jaw quadrants may be affected
- Symmetric painless swellings
- Tooth displacement and loosening
- Delayed tooth eruption

3.18.3 Imaging Features

- Well-delineated, bilateral multilocular radiolucencies; soap-bubble appearance
- Thin corticated outline, may be perforated
- More sclerotic abnormalities with increasing age

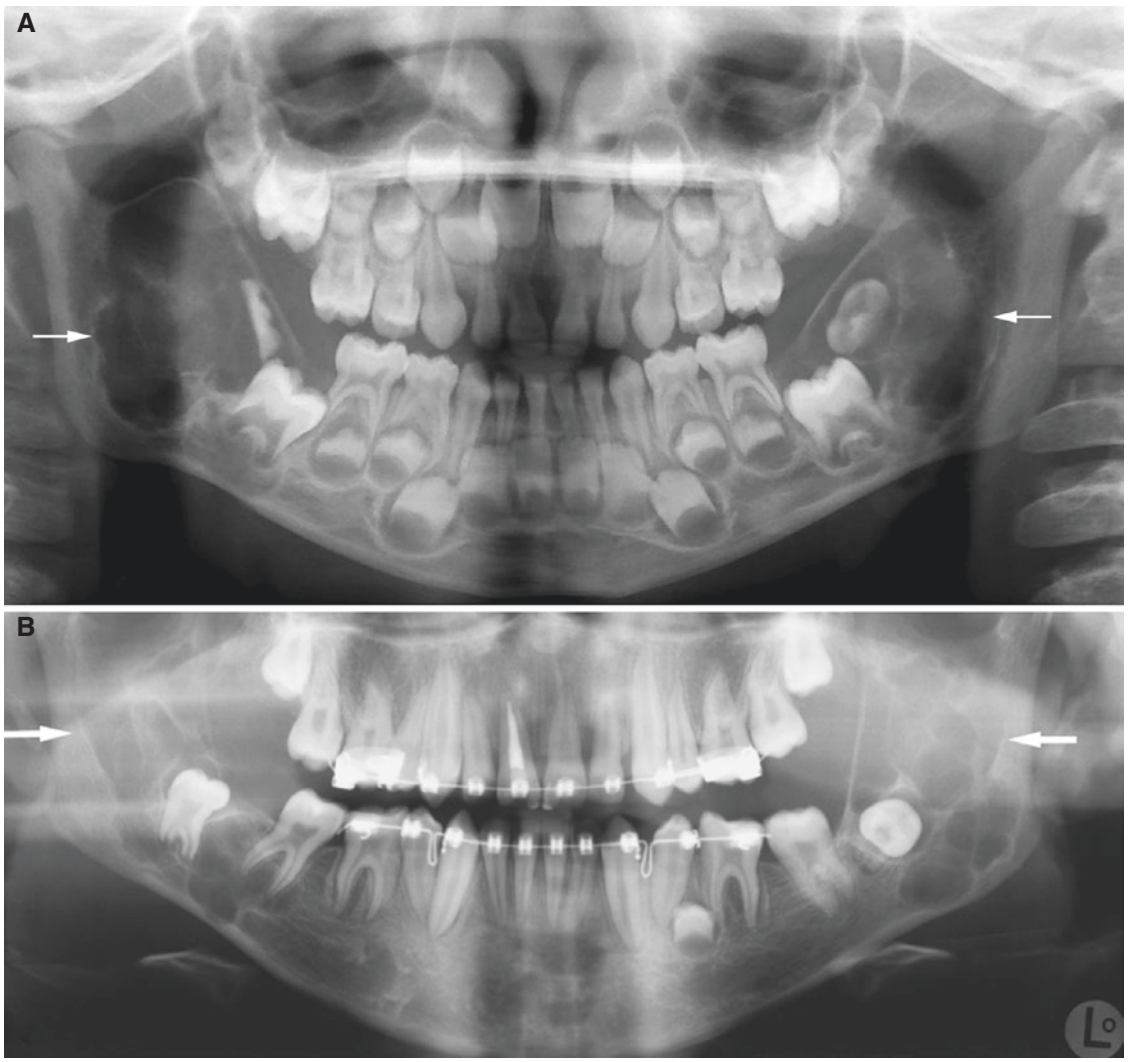

Fig. 3.48 Cherubism; 5-year-old male (**A**) and 13-year-old male (**B**). Both panoramic views show typical bilateral multilocular radiolucencies in mandibular ramus (*arrows*)

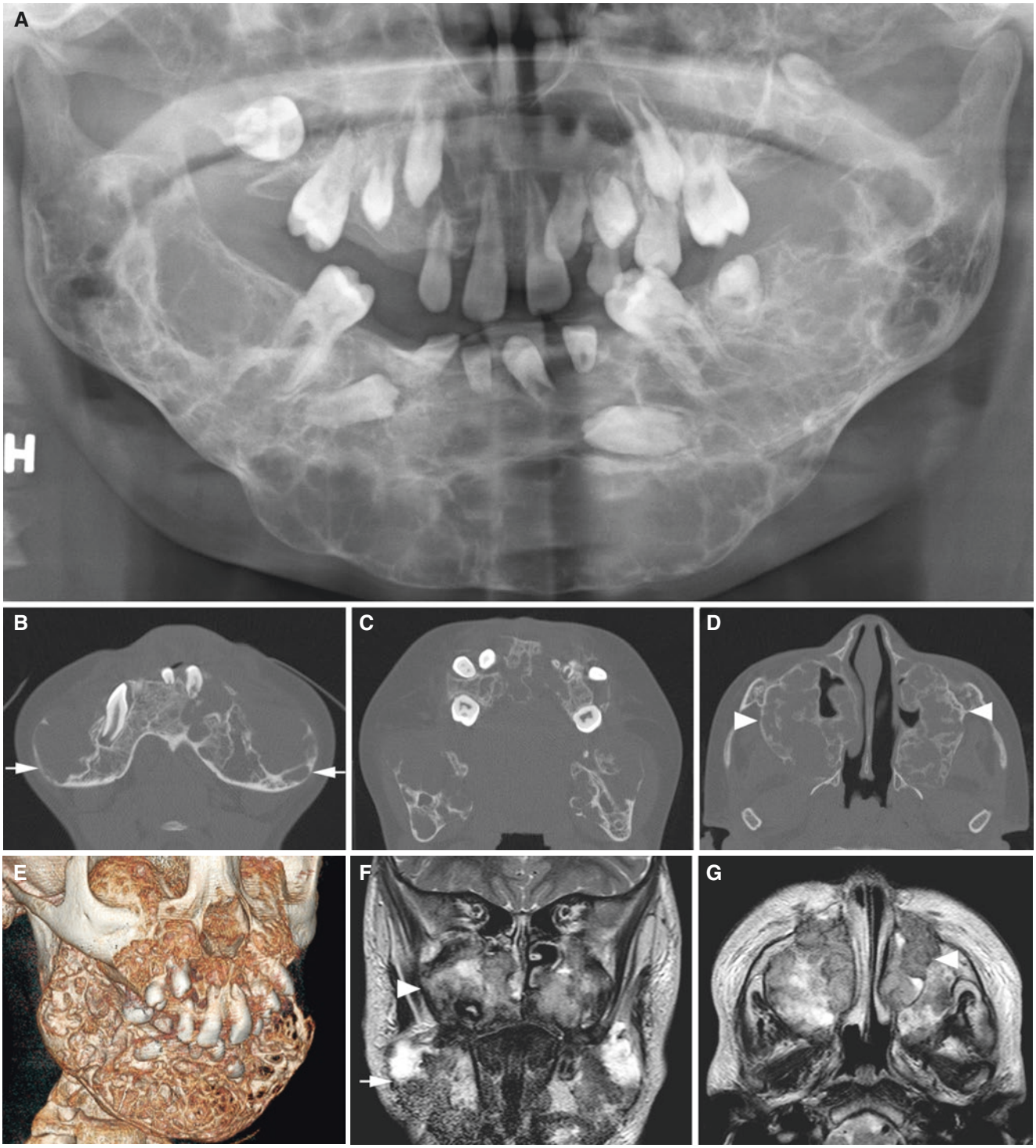

Fig. 3.49 Cherubism; 10-year-old male with facial deformity. (**A**) Panoramic view shows multilocular radiolucencies in the entire mandible (and unerupted teeth). (**B**, **C**, **D**) Axial and (**E**) 3D CT images show multilocular lesions in the mandible (*arrows*) and maxilla (*arrowheads*). (**F**) Coronal and (**G**) axial T2-weighted MRI show heterogeneous (high to low) signal intensity lesions in the mandible (*arrow*) and maxilla (*arrowhead*)

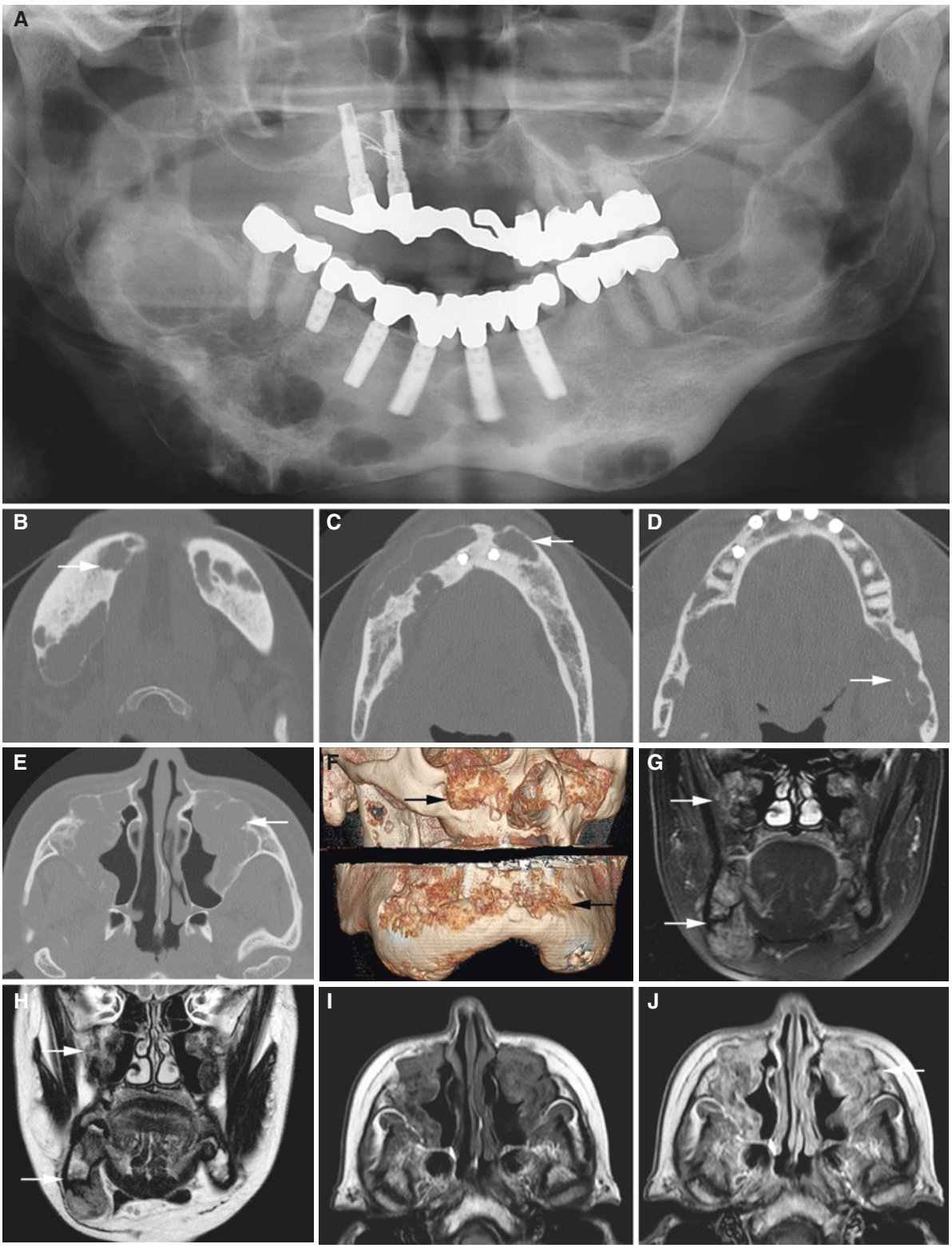

Fig. 3.50 Cherubism; 49-year-old female. (**A**) Panoramic view shows multilocular and monolocular radiolucencies in the mandible. (**B**, **C**, **D**) Axial CT images confirm radiolucencies in the mandible (*arrow*). (**E**) Axial CT image shows radiolucencies also in the maxilla (*arrow*). (**F**) 3D CT images of the maxilla and mandible show deformities in both jaws (*arrows*). (**G**) Coronal STIR and (**H**) coronal T2-weighted MRI show heterogeneous (low to intermediate) signal intensity in mandible and maxilla (*arrows*). (**I**) Axial T1-weighted pre-Gd and (**J**) axial T1-weighted post-Gd MRI show heterogeneous but solid contrast enhancement (*arrow*)

3.19 Fibrous Dysplasia

Figs. 3.51, 3.52, 3.53, and 3.54

3.19.1 Definition

Genetically based sporadic disease of bone that may affect single or multiple bones (monostotic or polyostotic). Fibrous dysplasia occurring in multiple adjacent craniofacial bones is regarded as monostotic (craniofacial fibrous dysplasia). May be part of the McCune–Albright syndrome (WHO).

Nonneoplastic, self-limiting but non-capsulated lesion occurring mainly in young subjects, showing replacement of normal bone by cellular tissue containing islands or trabeculae of metaplastic bone.

3.19.2 Clinical Features

- Monostotic most common (70–80%, femur, ribs)
- Craniofacial bones up to 25% of monostotic forms
- Maxilla, lateral region in particular, more frequent than mandible
- Painless swelling, jaw asymmetry
- Second and third decades
- No sex predilection
- McCune–Albright syndrome; polyostotic, café au lait spots

3.19.3 Imaging Features

- Radiolucency
- Mixture of radiolucency and radiopacity
- Radiopacity; ground-glass appearance
- Unilocular or multilocular
- Border poorly defined; blend into normal bone, but may be more well defined (and thus difficult to distinguish from ossifying fibroma; same histopathology)
- Usually expanded bone
- May displace teeth, walls of nasal cavity, paranasal sinuses, and orbits
- Mandibular canal may be displaced cranially
- Tooth resorption rare
- T1-weighted MRI: intermediate signal
- T2-weighted MRI and STIR: heterogeneous low signal
- T1-weighted MRI: contrast enhancement

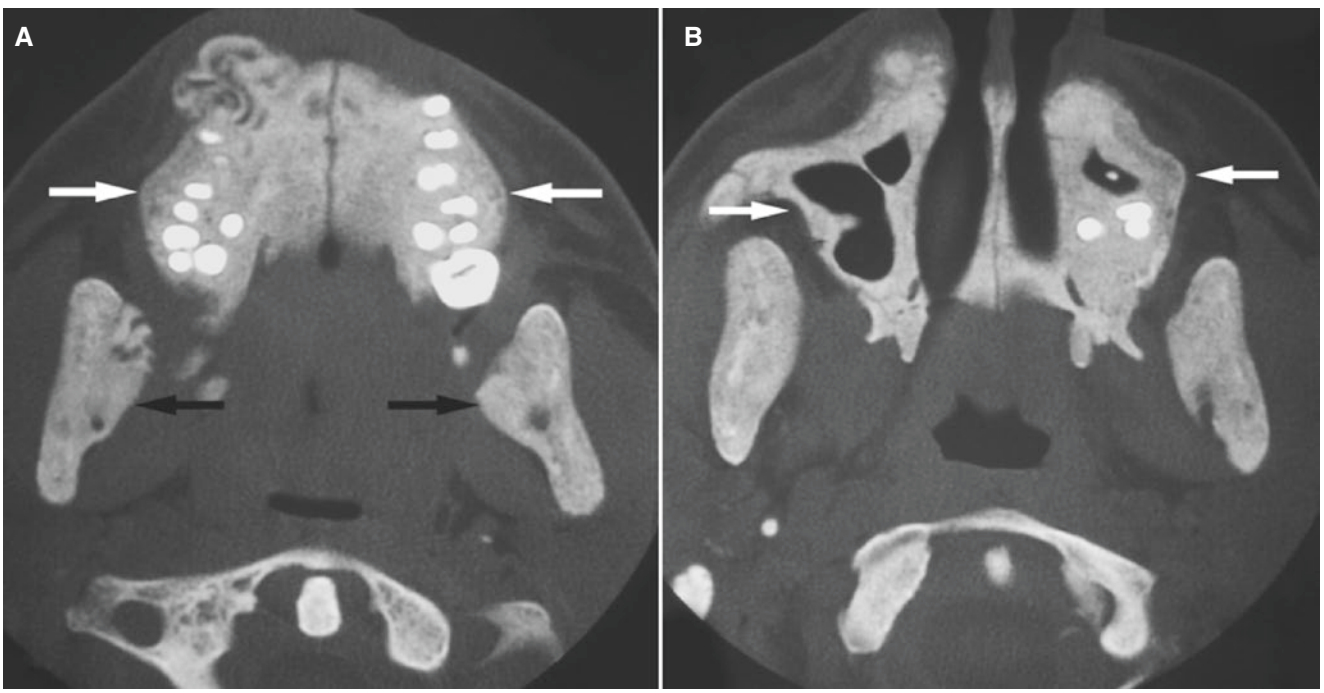

Fig. 3.51 Fibrous dysplasia, maxilla and mandible; 21-year-old male with chronic renal failure, end stage, and several months of history of slowly enlarging maxillary mass. (**A**) Axial CT image shows the maxilla and mandible with bilateral ground-glass appearance (*arrows*). (**B**) Axial CT image shows maxillary sinus involvement bilaterally (*arrows*)

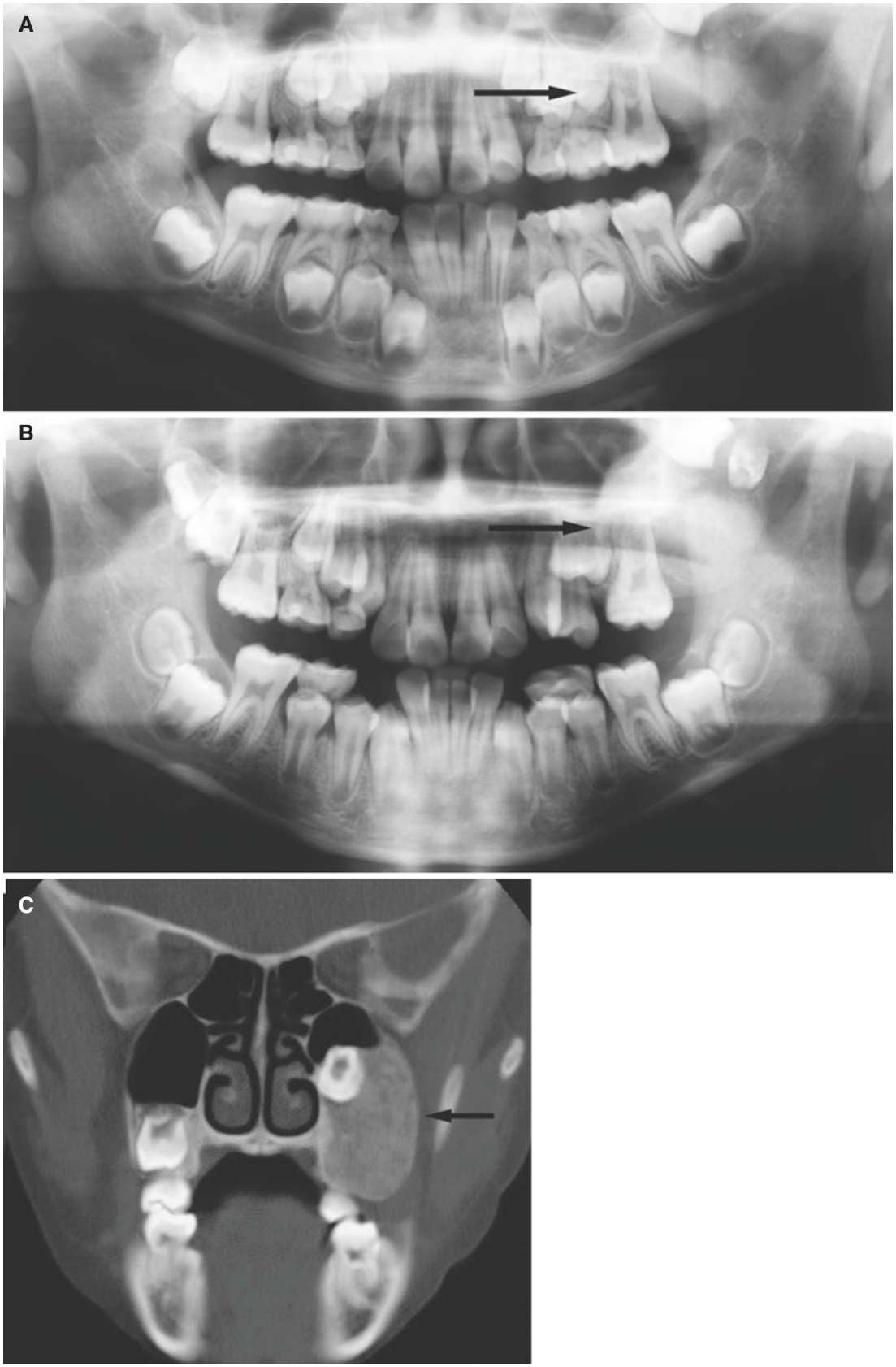

Fig. 3.52 Fibrous dysplasia, maxilla; 10-year-old male with unilateral painless swelling of the maxilla. (**A**) Panoramic view shows radiopaque expansive process (*arrow*) with displaced second molar. (**B**) Panoramic view at 2.5-year follow-up shows progression of process (*arrow*). (**C**) Coronal CT image shows well-defined process with typical ground-glass appearance (*arrow*); this could have been diagnosed as an ossifying fibroma

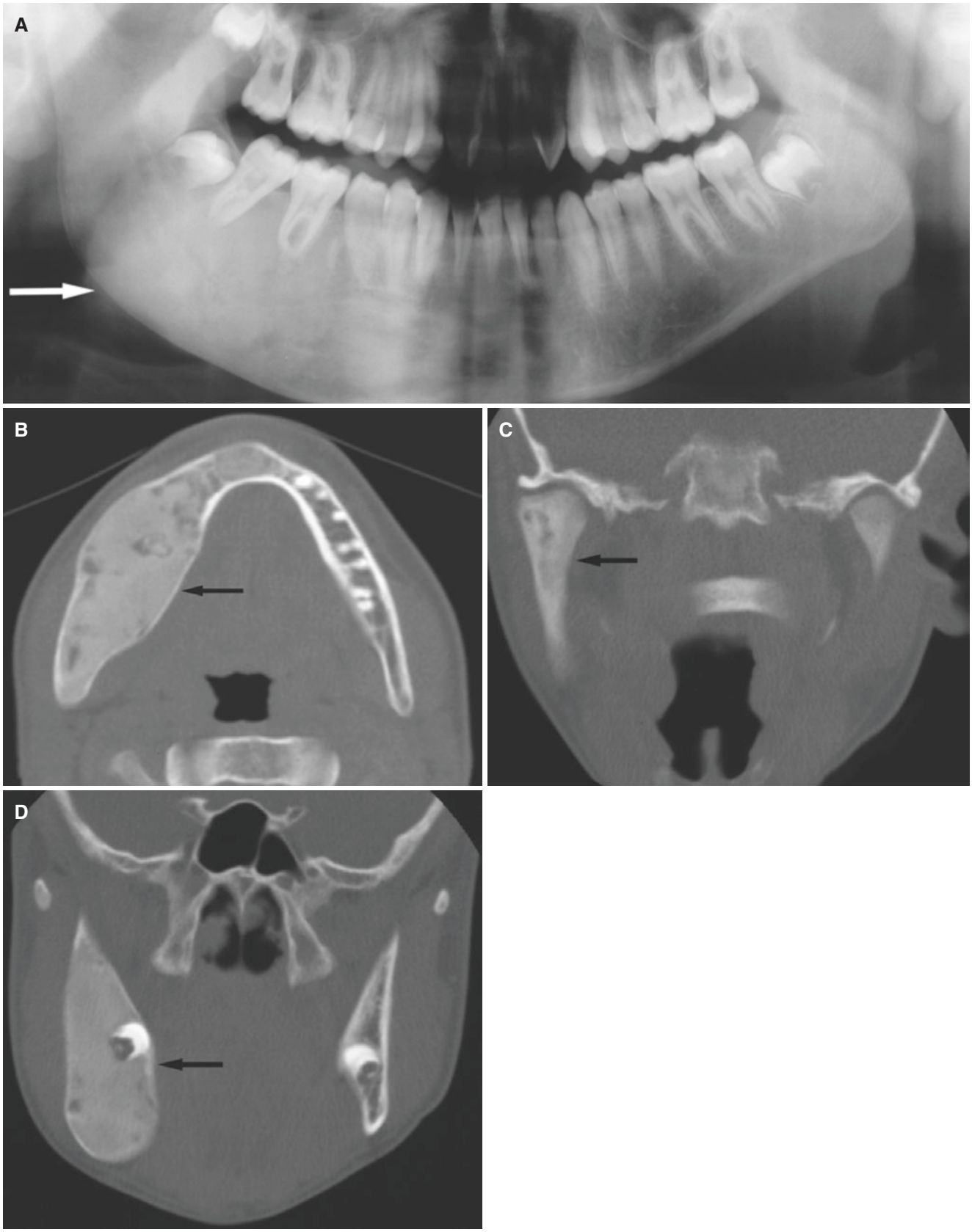

Fig. 3.53 Fibrous dysplasia, mandible; 14-year-old male with painless facial asymmetry. (**A**) Panoramic view shows enlarged mandible with ground-glass appearance (*arrow*). (**B**) Axial CT image shows expanded mandible with ground-glass appearance (*arrow*). (**C**) Coronal CT image shows process involving mandibular collum and condyle (*arrow*). (**D**) Coronal CT image shows process involving coronoid process (*arrow*)

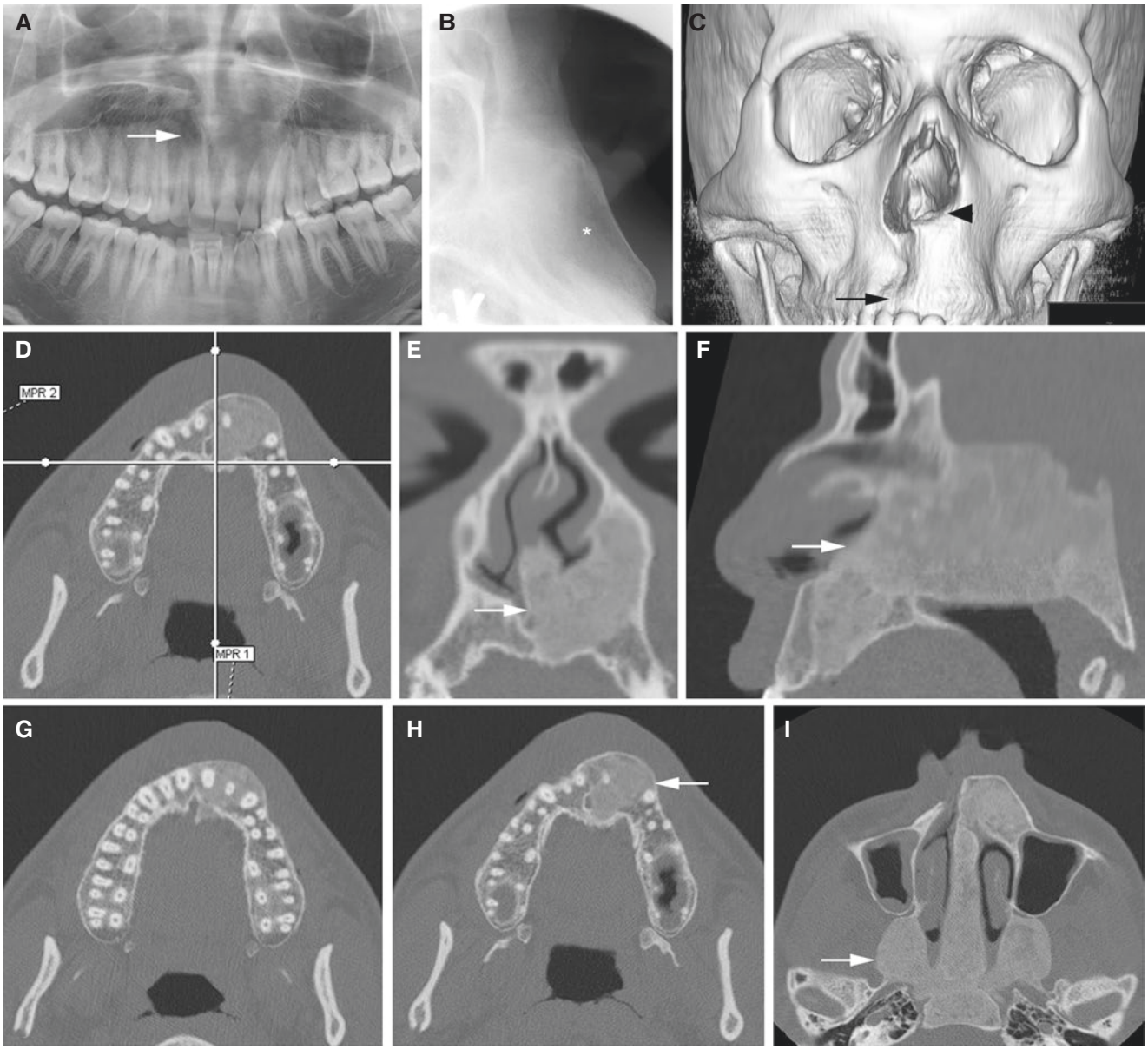

Fig. 3.54 Fibrous dysplasia, maxilla; 18-year-old male with painless and firm swelling in the anterior part of the maxilla. (**A**) Panoramic view shows diffuse area in maxillary front (*arrow*). (**B**) Occlusal (tangential) view shows ground-glass appearance of bone (*asterisk*). (**C**) 3D CT image shows nasal cavity deformity (*arrowhead*) and buccal expansion of the anterior maxilla (*arrow*). (**D**) Axial (with cursor lines), (**E**) coronal, (**F**) sagittal, and (**G**, **H,**) and (**I**) axial CT images show expanding bone with ground-glass appearance in the maxilla and skull base (*arrow*)

3.20 Osseous Dysplasias

Figs. 3.55, 3.56, 3.57, 3.58, and 3.59

Synonyms: Periapical cemental dysplasia, periapical osseous dysplasia, cemento-osseous dysplasia (WHO 2017), periapical cementoma

3.20.1 Definition

Idiopathic non-neoplastic fibro-osseous lesions located in periapical region of tooth-bearing jaw areas, characterized by replacement of normal bone by fibrous tissue and metaplastic bone (WHO).

3.20.2 Clinical Features

- Most common benign fibro-osseous lesion of the jaws
- Three types (variants): periapical, focal, and florid osseous dysplasia
- Incidental findings (periapical or focal types)
- May expand bone but usually (if not infected) no pain (florid type)
- Gigantiform cementoma (GC) considered, by WHO, a type of osseous dysplasia in 2005, but not in 2017
- GC; familiar, but may occur as a solitary lesion
- GC is a rare form of fibro-osseous lesion
- GC may show evident clinical swelling/expansion but no pain

3.20.3 Imaging Features

- Periapical osseous dysplasia is located in the anterior mandible
- Focal osseous dysplasia is located in the posterior mandible
- Florid osseous dysplasia is located in all four quadrants and may contain simple bone cyst-like areas
- Periapical and focal types usually will not expand bone
- Florid type may expand bone
- Osseous dysplasias may be predominantly radiolucent and predominantly radiopaque or have a mixed appearance
- Radiopacity tends to increase with time
- GC may expand bone and show highly mineralized mass

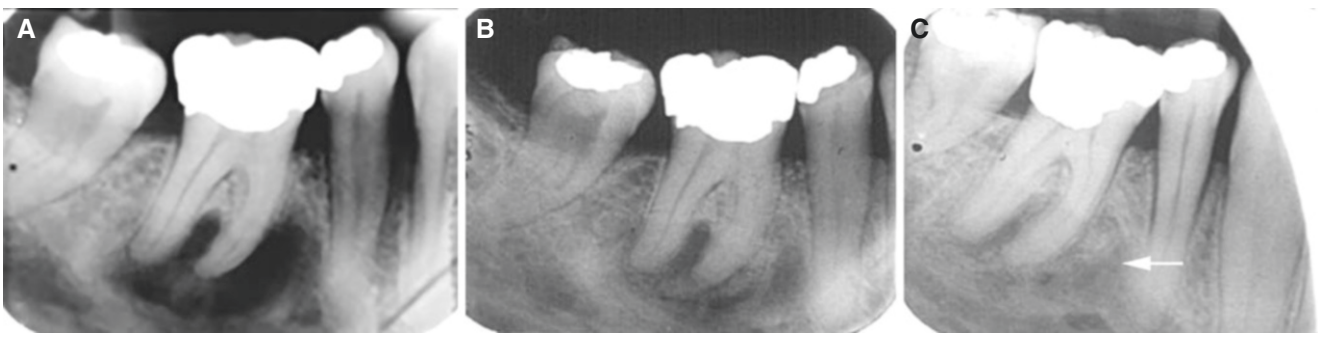

Fig. 3.55 Focal osseous dysplasia, mandible; asymptomatic, vital tooth, with follow-up. Intraoral (periapical) views of molar, (**A**) baseline, (**B**) about 2 years later, and (**C**) about 4 years after baseline, show periapical radiolucency gradually becoming more mineralized (*arrow*)

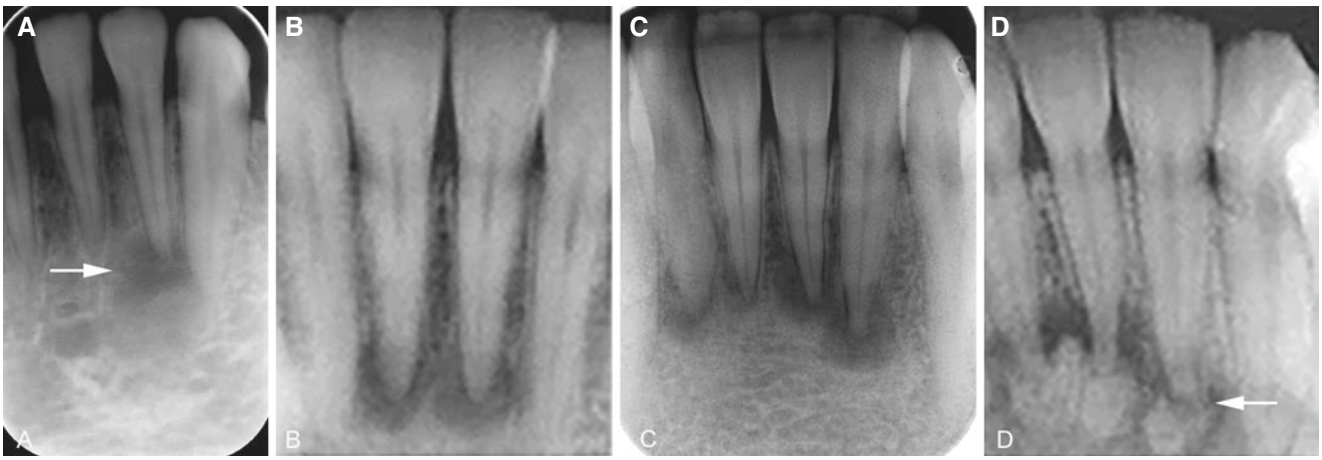

Fig. 3.56 Periapical osseous dysplasias, mandible, incidental finding, vital teeth. Intraoral (periapical) views of incisors: (**A**) one periapical radiolucency (*arrow*), (**B**) two periapical radiolucencies, (**C**) four periapical radiolucencies, and (**D**) periapical radiolucencies with radiopaque (mineralized) content (*arrow*)

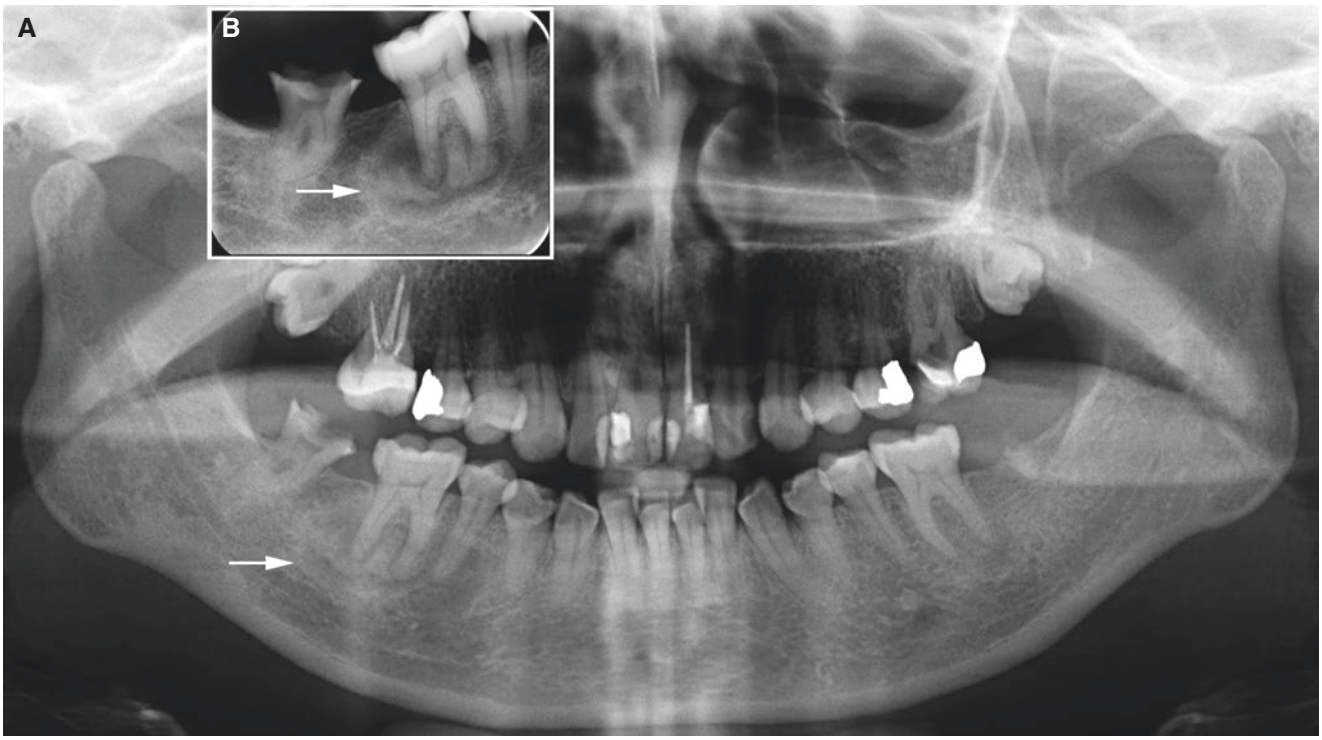

Fig. 3.57 Focal osseous dysplasia, mandible; 43-year-old female, incidental finding at the first mandibular molar (patient examined for variable pain from the posterior molar). (**A**) Panoramic and (**B**) intraoral views show mixed radiolucent and radiopaque area at the first molar roots (*arrow*)

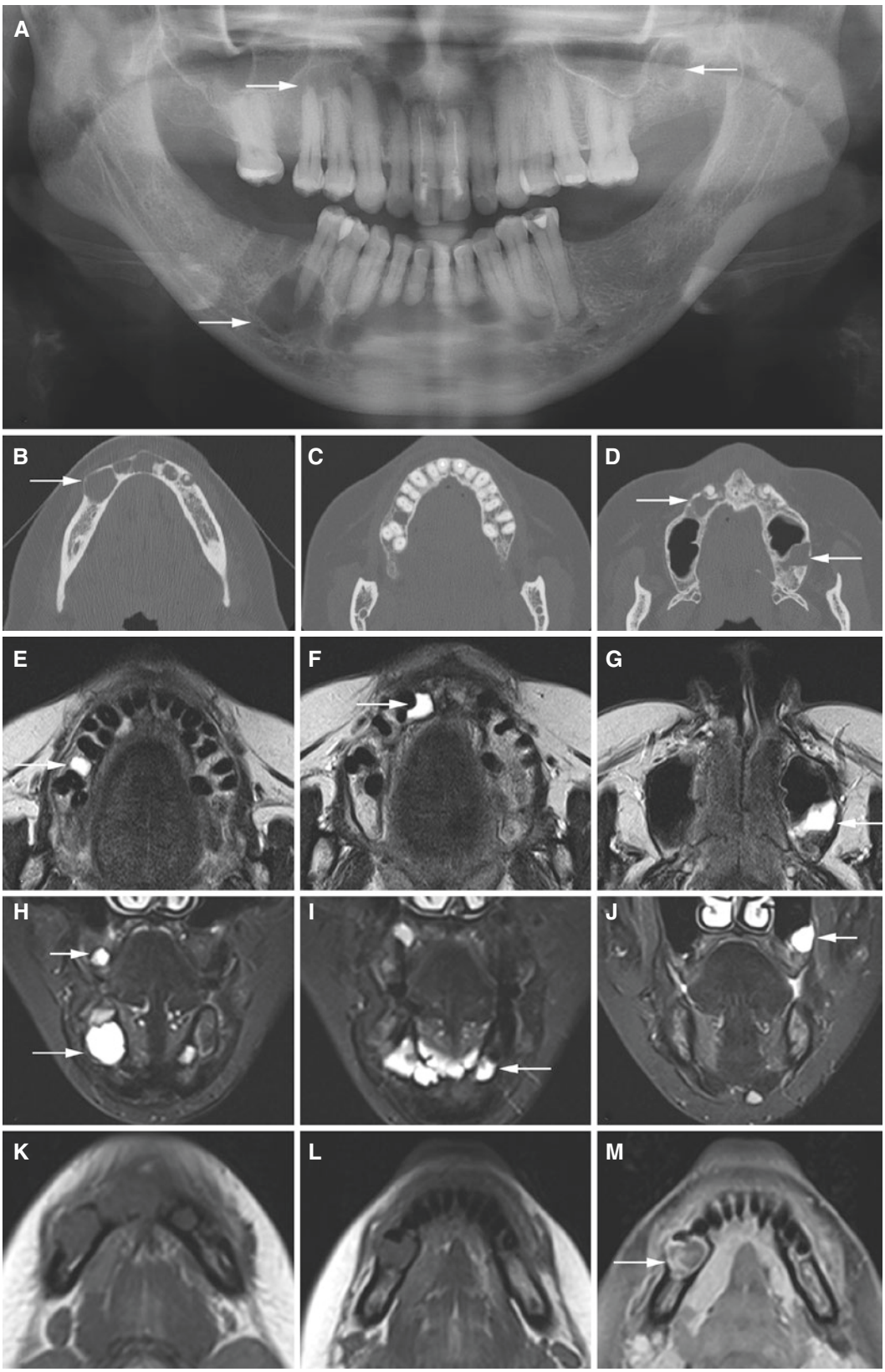

Fig. 3.58 Florid osseous dysplasia, mandible and maxilla; 45-year-old female with some pain from the second premolar in the left mandible. (**A**) Panoramic view shows radiolucent areas both in the mandible and in the maxilla (*arrows*). (**B**, **C**, **D**) Axial CT images confirm radiolucent areas in the mandible and maxilla (*arrows*). (**E**, **F**, **G**) Axial T2-weighted MRI and (**H**, **I**, **J**) coronal T2-weighted fat sat MRI show high-signal areas in the mandible and maxilla (*arrows*). (**K**, **L**) Axial T1-weighted pre-Gd and (**M**) axial T1-weighted fat sat post-Gd MRI show contrast enhancement, predominantly in periphery (*arrow*)

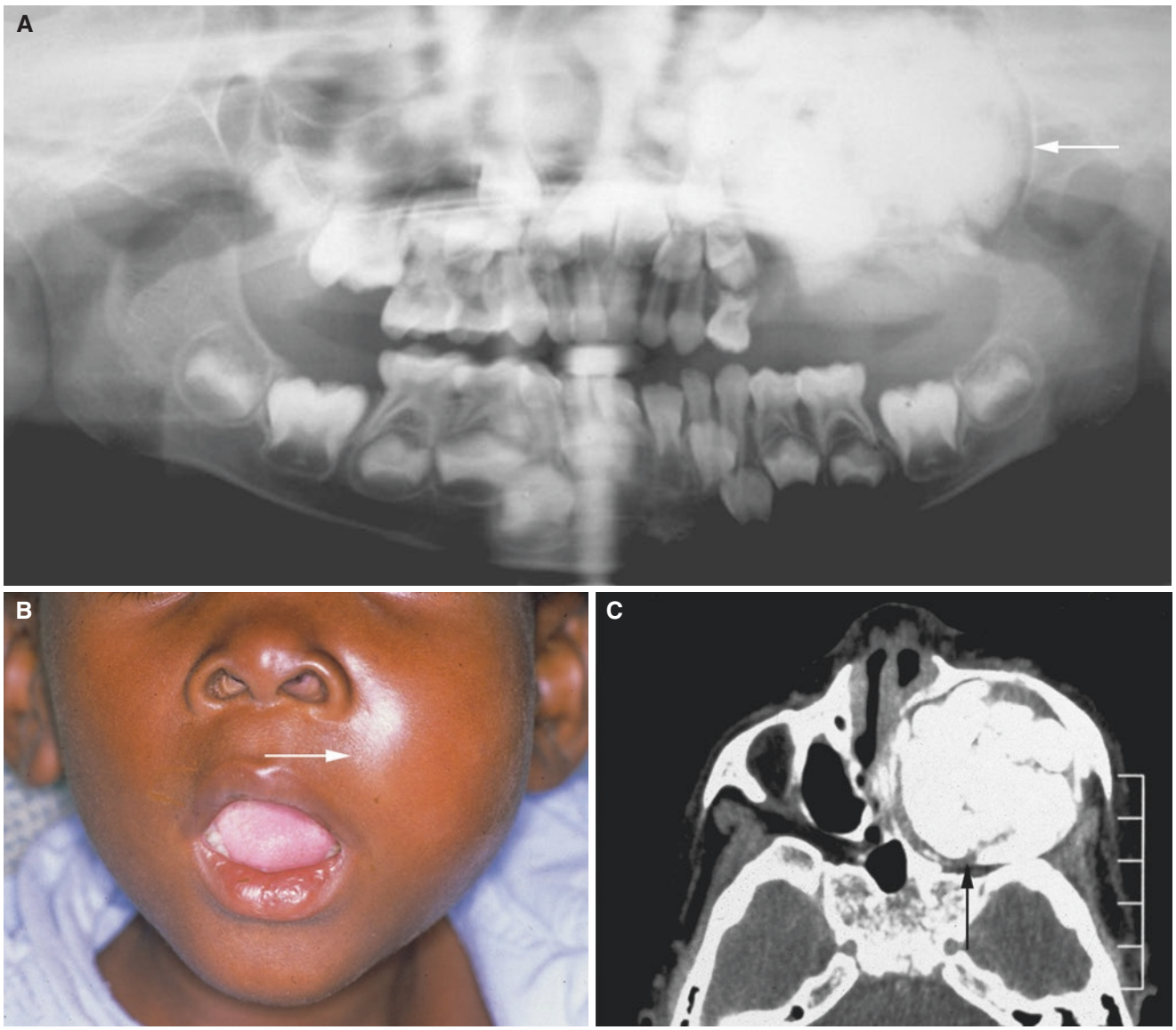

Fig. 3.59 Gigantiform cementoma, maxilla/maxillary sinus; 6-year-old female with painless swelling of the left cheek. (**A**) Panoramic view shows highly mineralized mass in the left maxilla/maxillary sinus with radiolucent margin around most of mass (*arrow*). (**B**) Clinical photograph shows expansion of the left cheek (*arrow*). (**C**) Axial CT image confirms highly mineralized, expanding mass in the maxilla/maxillary sinus surrounded by radiolucent zone (*arrow*). There was no family history (reproduced with permission from Noffke et al 2012)

3.21 Osteoma

Figs. 3.60, 3.61, 3.62, 3.63, and 3.64

3.21.1 Definition

Benign, slowly growing lesion consisting of well-differentiated mature bone, with a predominantly lamellar structure (WHO).

3.21.2 Clinical Features

- Incidental finding or painless hard swelling
- Mandible and maxilla
- All facial bones and paranasal sinuses
- Most frequent (more than one-third) in a large series of jaw lesions with hard-tissue formation

3.21.3 Imaging Features

- Variable amount of compact bone
- Variable amount of cancellous bone

Fig. 3.60 Osteoma, mandible; painless swelling lingually at mandibular angle. Intraoral views show exostotic tumor of cortical and cancellous bone (*arrows*)

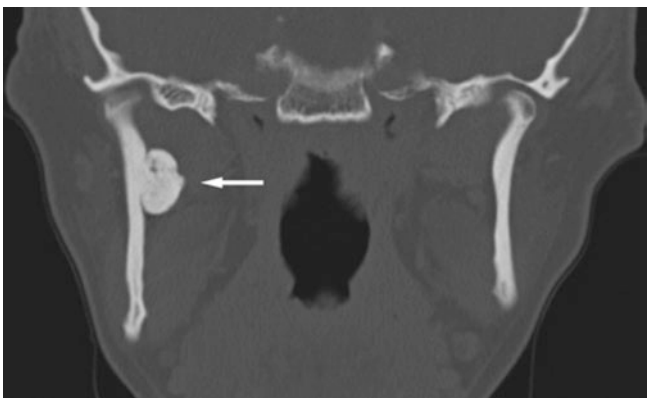

Fig. 3.61 Osteoma, mandible; 23-year-old male with incidental finding at routine dental radiography. Coronal CT image shows exostotic tumor predominantly of cortical bone (*arrow*) at lingual aspect of mandibular ramus

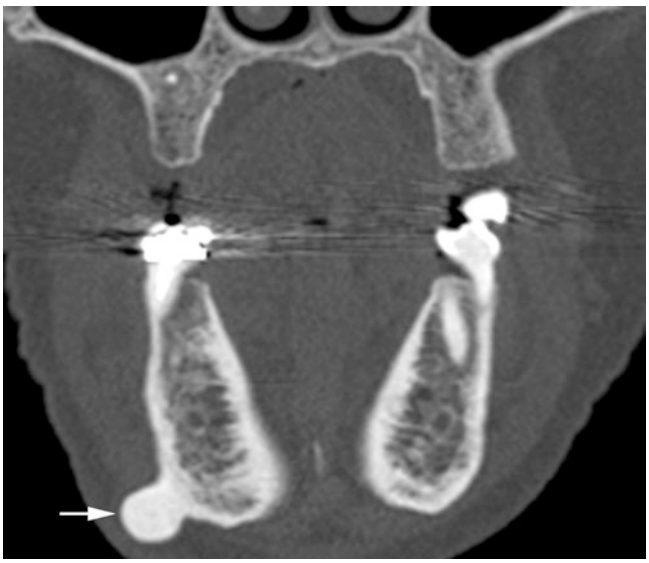

Fig. 3.62 Osteoma, mandible; 93-year-old female, incidental finding. Coronal CT shows bony outgrowth (exostosis) at lower mandibular border (*arrow*)

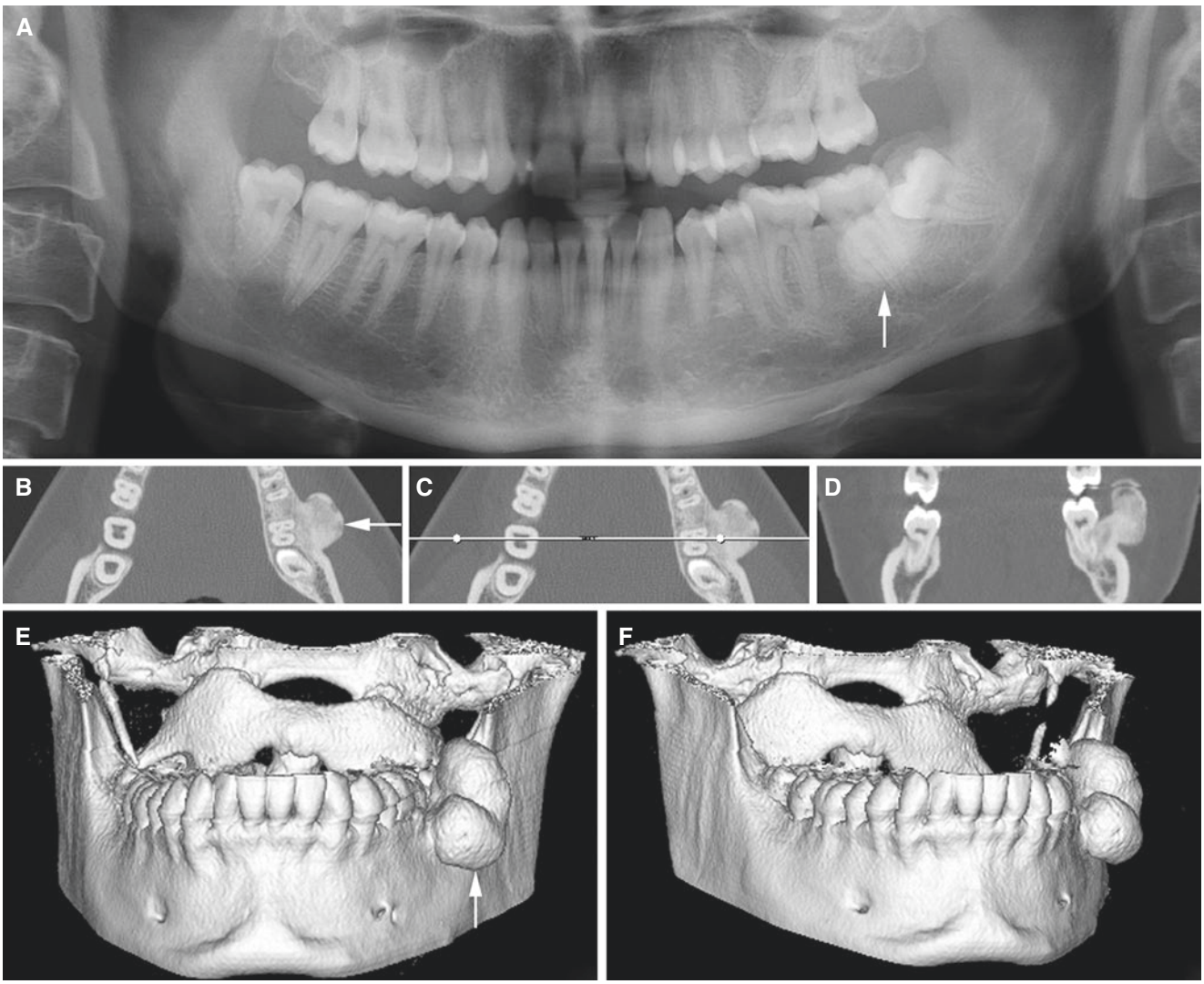

Fig. 3.63 Osteoma, mandible; 26-year-old female with hard swelling in molar region of the left mandible. (**A**) Panoramic view shows radiopacities in the left mandible (*arrow*). (**B**) Axial CT, (**C**) axial (with cursor line), and (**D**) coronal CT images show bony outgrowth in the left mandible (*arrow*). (**E**, **F**) 3D CT images better show morphology of bony outgrowths (*arrow*)

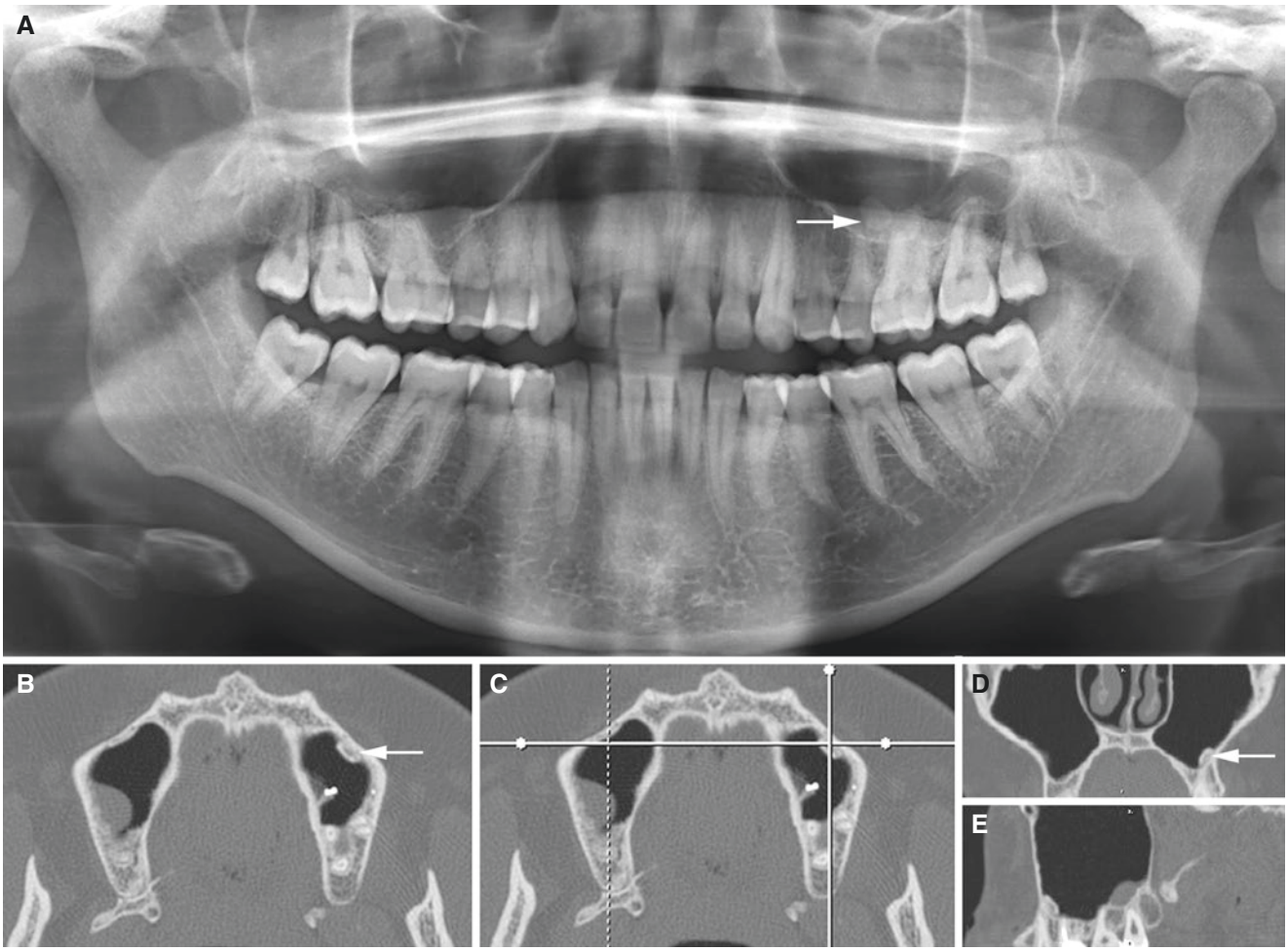

Fig. 3.64 Osteoma, maxillary sinus; 29-year-old female, incidental finding. (**A**) Panoramic view shows radiopacity in the left premolar–molar region (*arrow*). (**B**) Axial, (**C**) axial (with cursor lines), (**D**) coronal, and (**E**) sagittal CT images show bony outgrowth (exostosis) from the maxillary sinus wall (*arrow*)

3.22 Exostoses

Figs. 3.65, 3.66, 3.67, 3.68, and 3.69

3.22.1 Definition

Outgrowth of normal cancellous and compact bone in certain areas.

3.22.2 Clinical Features

- Mandible; torus mandibularis in premolar regions lingually and bilaterally
- Maxilla; torus palatinus in midline
- Maxilla; multiple exostoses in premolar region bilaterally; more common buccally than palatally

3.22.3 Imaging Features

- See Osteoma.

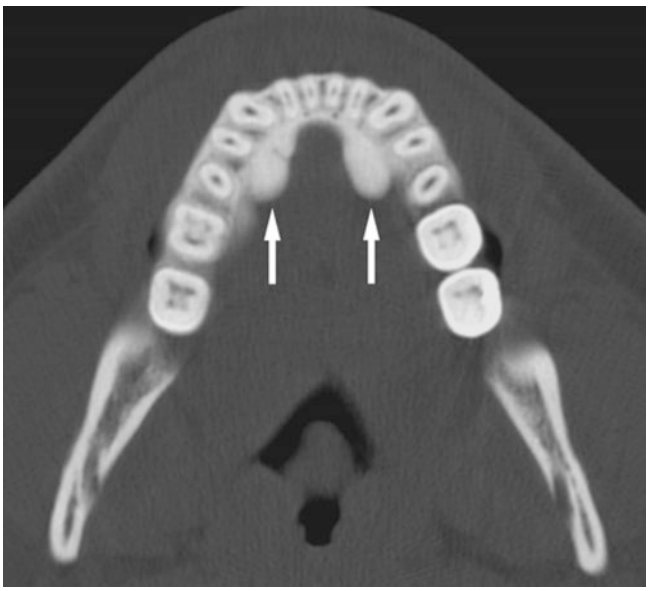

Fig. 3.65 Torus mandibularis; painless hard lingual swellings. Axial CT image shows bilateral exostoses (*arrows*)

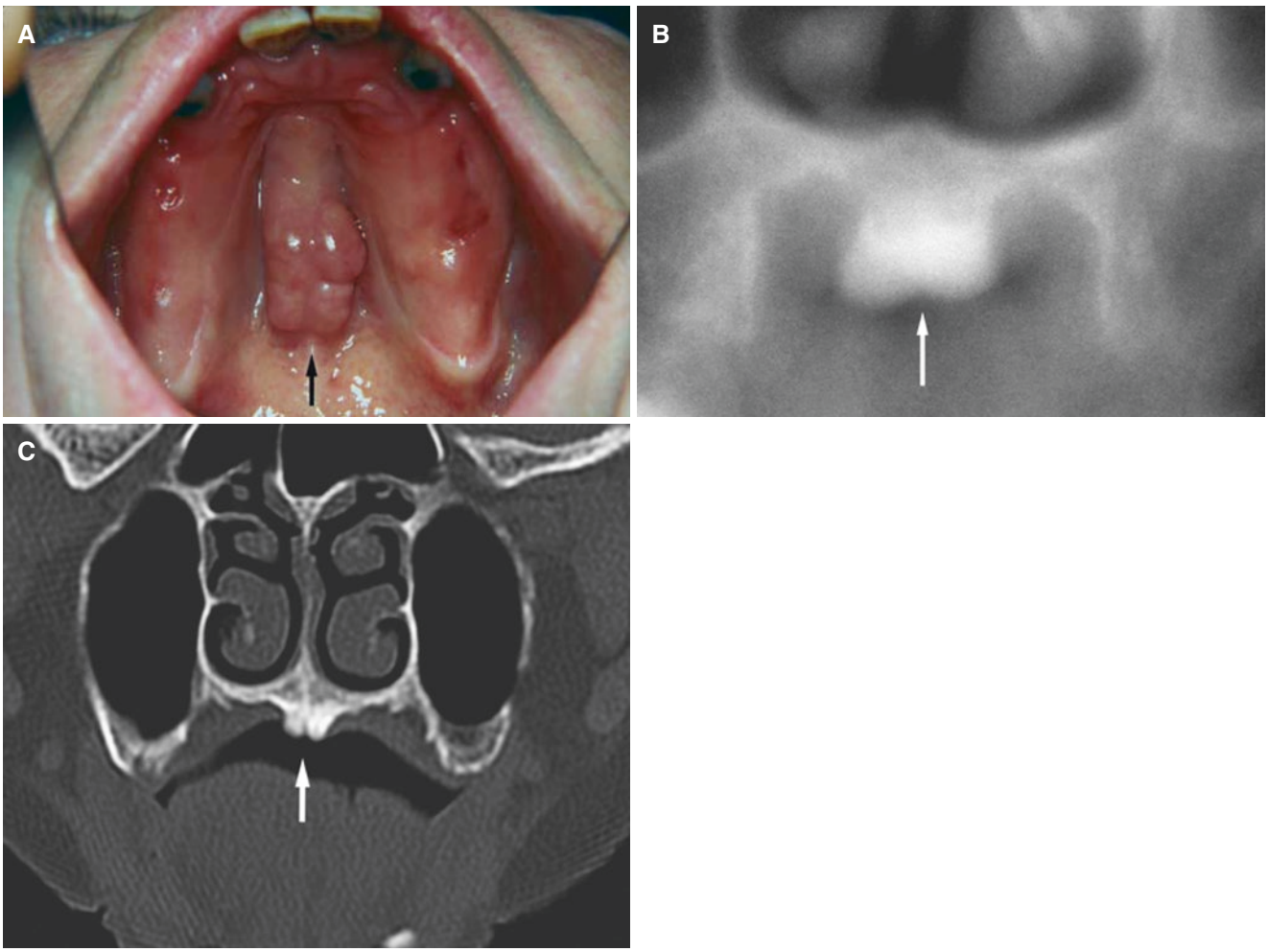

Fig. 3.66 Torus palatinus; painless hard swelling. (**A**) Clinical photograph shows large torus with normal mucosa in the midline of the palate (*arrow*). (**B**) Coronal conventional tomography of the same patient shows exostosis with thick layer of compact bone (*arrow*). (**C**) Coronal CT of smaller torus in another patient (*arrow*)

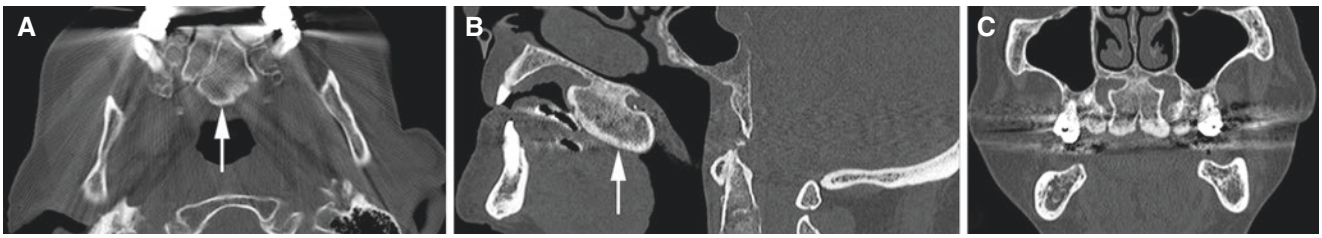

Fig. 3.67 Torus palatinus; 84-year-old male, incidental finding. (**A**) Axial, (**B**) sagittal, and (**C**) coronal CT images show bony outgrowth in the midline of the hard palate (*arrow*)

Fig. 3.68 Exostoses (palatal) in the maxilla and torus palatinus; 47-year-old female, incidental finding. Coronal CT image shows palatal exostoses bilaterally (*arrows*) in addition to torus palatinus

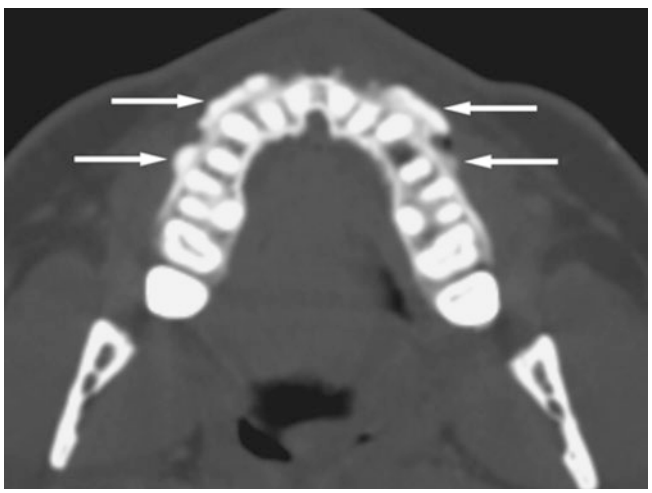

Fig. 3.69 Multiple exostoses in the maxilla; painless hard swellings buccally in premolar region. Axial CT image shows multiple buccal exostoses bilaterally (*arrows*)

3.23 Idiopathic Osteosclerosis

Figs. 3.70, 3.71, and 3.72

Synonyms: Dense bone island, enostosis, periapical idiopathic osteosclerosis

3.23.1 Definition

Localized growth of compact bone within cancellous bone.

3.23.2 Clinical Features

– Incidental finding

3.23.3 Imaging Features

– Well-defined outline without peripheral radiolucency (capsule, periodontal membrane)
– No expanding bone
– Usually homogeneous radiopacity but may be heterogeneous
– More common in mandible than in maxilla
– Most often in premolar–molar region
– Location independent of teeth
– Rarely related to root resorption
– If multiple, Gardner's syndrome should be considered

Fig. 3.70 Idiopathic osteosclerosis, incidental finding at the first molar in the left mandible. (**A**) Panoramic and (**B**) intraoral views show well-defined (sharply delineated) radiopacity without radiolucent peripheral zone (*arrow*)

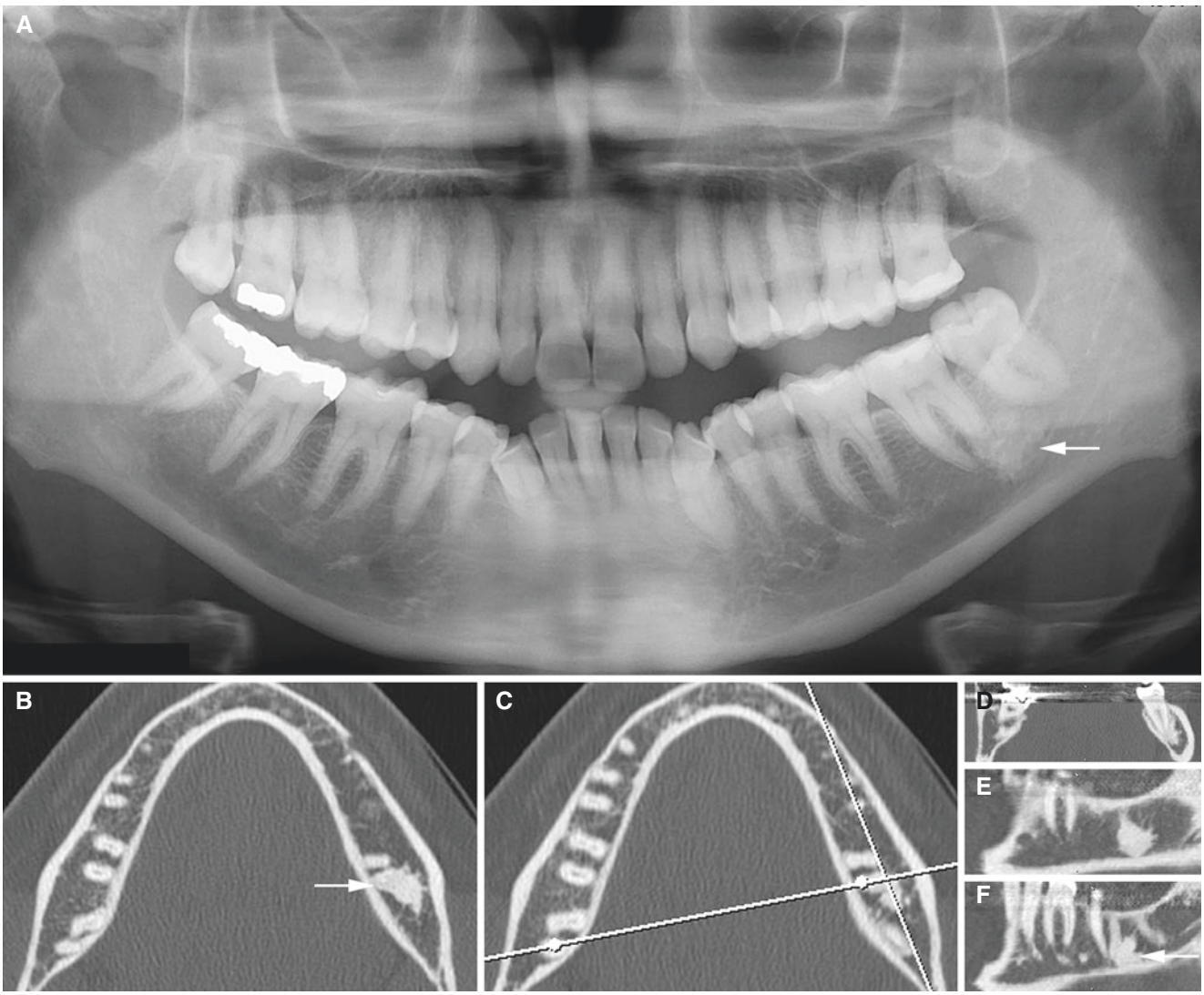

Fig. 3.71 Idiopathic osteosclerosis; 37-year-old female, incidental finding at the second molar in the left mandible. (**A**) Panoramic, (**B**) axial, (**C**) axial (with cursor lines), (**D**) oblique coronal, and (**E**, **F**) oblique sagittal CT images show well-defined (sharply delineated) radiopacity closely located to intact distal root of the second molar (*arrow*)

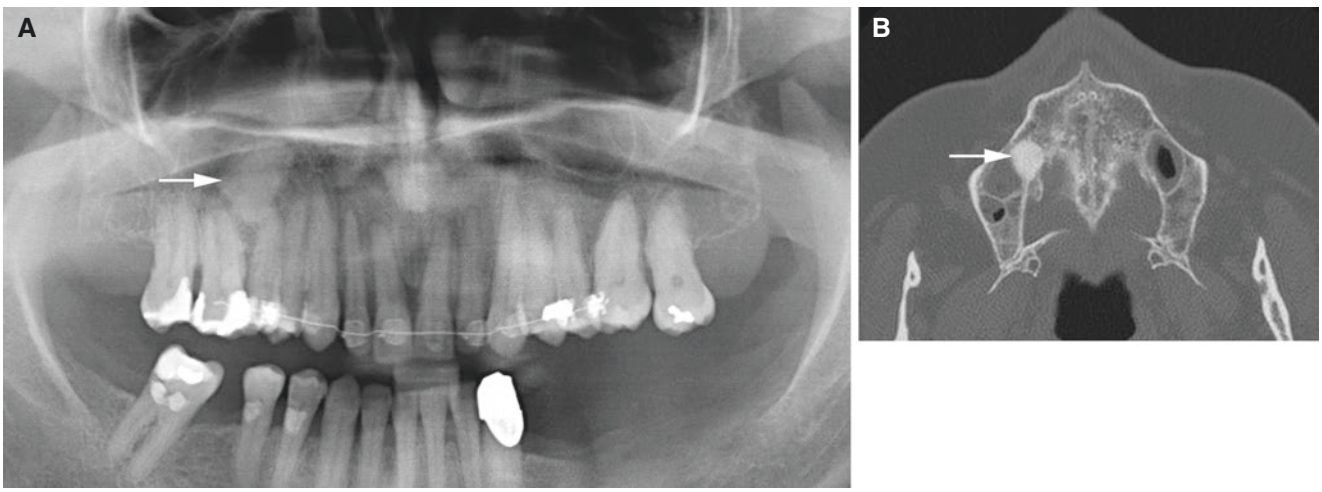

Fig. 3.72 Idiopathic osteosclerosis; 59-year-old male, incidental finding in the right maxilla. (**A**) Panoramic view and (**B**) axial CT image show well-defined (sharply delineated) radiopacity without radiolucent peripheral zone (*arrow*)

3.24 Odontoma

Fig. 3.73

3.24.1 Definition

Tumorlike malformation (hamartoma) in which enamel and dentin, and sometimes cementum, are present (WHO).

Characteristically surrounded by a fibrous capsule and subdivided into compound and complex odontoma.

3.24.2 Clinical Features

- Incidental finding
- Tooth-bearing regions of the maxilla or mandible, mostly in the posterior part of the mandible
- Usually found during the second decade
- No sex predilection

3.24.3 Imaging Features

- Predominantly an amorphous radiopacity, including enamel, but also soft tissue (complex type)
- Surrounded by a radiolucent zone; fibrous capsule
- Compound type, more similar to teeth, consisting of several individual odontoids

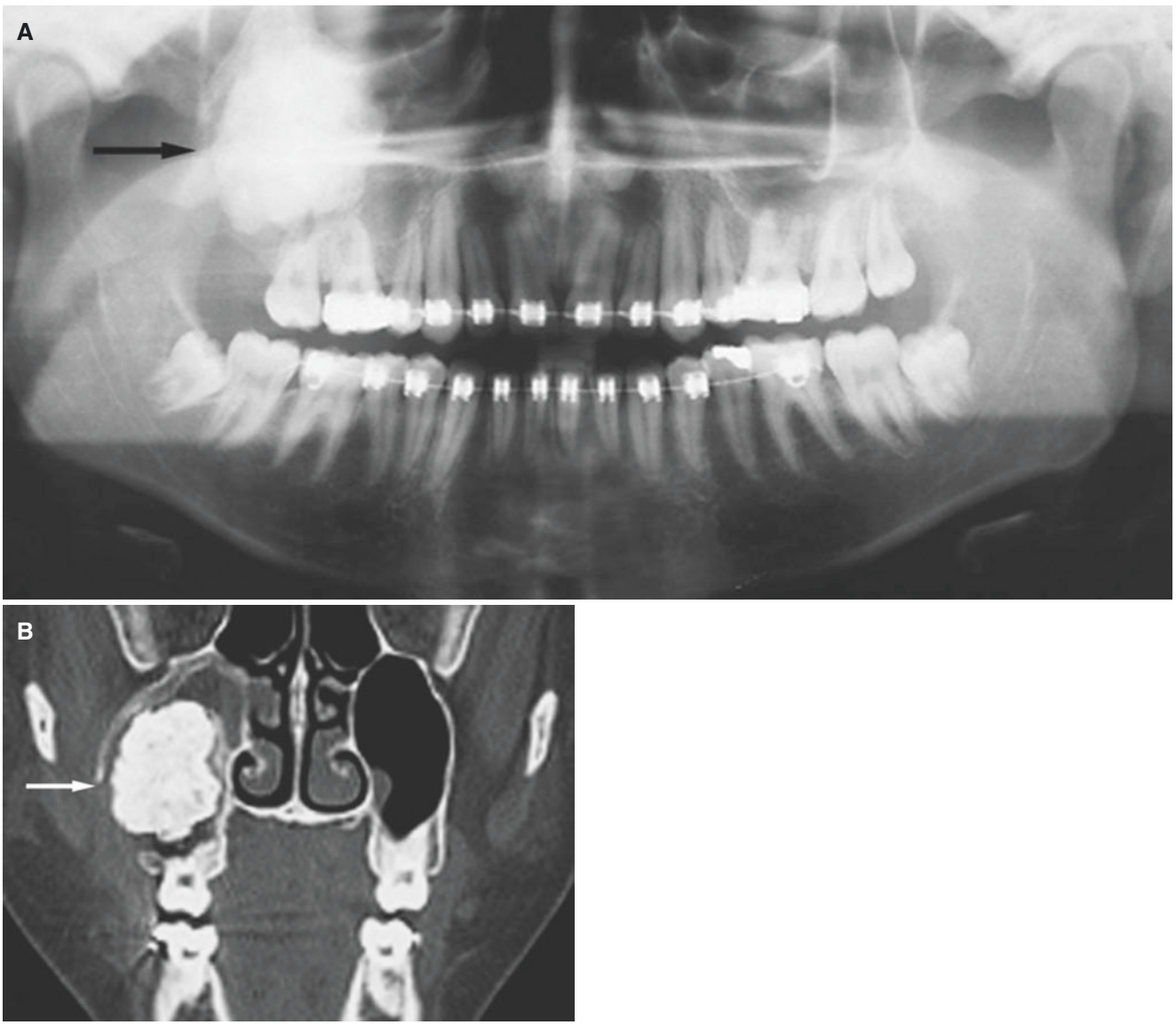

Fig. 3.73 Odontoma (complex type), maxilla; 15-year-old female with incidental finding at orthodontic consultation. (**A**) Panoramic view shows large radiopaque mass in the right maxillary sinus (*arrow*). (**B**) Coronal CT image shows large mass of cortex or enamel density in the right maxillary sinus (*arrow*), surrounded by fibrous capsule, with destroyed lateral sinus wall and root resorption

Suggested Reading

Arora SS, Paul S, Arora S, Kapoor V (2014) Secondary jaw aneurysmal bone cyst (JABC) – a possible misnomer? A review of literature on secondary JABCs, their pathogenesis and oncogenesis. J Oral Pathol Med 43:647–651

Asaumi J-I, Matsuzaki H, Hisatomi M, Konouchi H, Shigehara H, Kishi K (2002) Application of dynamic MRI to differentiating odontogenic myxomas from ameloblastomas. Eur J Radiol 43:37–41

Auclair PL, Cuenin P, Kratochvil FJ, Slater LJ, Ellis GL (1988) A clinical and histomorphologic comparison of the central giant cell granuloma and the giant cell tumor. Oral Surg Oral Med Oral Pathol 66:197–208

Aydil U, Kizil Y, Bakkal FK, Köybaşioğlu A, Uslu S (2014) Neoplasms of the hard palate. J Oral Maxillofac Surg 72:619–626

Barnes L, Eveson JW, Reichart P, Sidransky D (eds) (2005) World Health Organization classification of tumours. Pathology and genetics of head and neck tumours. IARC Press, Lyon

Beltran J, Simon DC, Levy M, Herman L, Weis L, Mueller CF (1986) Aneurysmal bone cysts: MR imaging at 1.5 T. Radiology 158:689–690

Benoit MM, Vargas SO, Bhattacharyya N, McGill TA, Robson CD, Ferraro N et al (2013) The presentation and management of mandibular tumors in the pediatric population. Laryngoscope 123:2035–2042

Bokhari K, Hameed MS, Ajmal M, Togoo RA (2012) Benign osteoblastoma involving maxilla: a case report and review of the literature. Case Rep Dent. doi:10.1155/2012/351241

Cottalorda J, Kohler R, Sales de Gauzy J, Chotel F, Mazda K, Lefort G, Louahem D, Bourelle S, Dimeglio A (2004) Epidemiology of aneurysmal bone cyst in children: a multicenter study and literature review. J Pediatr Orthop B 13:389–394

DelBalso AM, Werning JT (1986) The role of computed tomography in the evaluation of cemento-osseous lesions. Oral Surg Oral Med Oral Pathol 62:354–357

El-Naggar AK, JKC C, Grandis JR, Takata T, Slootweg PJ (eds) (2017) WHO classification of head and neck tumours. IARC Press, Lyon

Eriksson L, Hansson LG, Akesson L, Stahlberg F (2001) Simple bone cyst: a discrepancy between magnetic resonance and surgical observations. Oral Surg Oral Med Oral Pathol Oral Radiol Endod 92:694–698

Eversole LR, Merrell PM, Strub D (1985) Radiographic characteristics of central ossifying fibroma. Oral Surg Oral Med Oral Pathol 59:522–527

Farman AG, Nortje C, Wood RE (1993a) Benign tumors of the jaws. In: Oral and maxillofacial diagnostic imaging. Mosby, St. Louis, pp 239–279

Farman AG, Nortje C, Wood RE (1993b) Fibro-osseous lesions. In: Oral and maxillofacial diagnostic imaging. Mosby, St. Louis, pp 316–330

Gardner DG, Heikinheimo K, Shear M, Philipsen HP, Coleman H (2005a) Ameloblastomas. In: Barnes L, Eveson JW, Reichart P, Sidransky D (eds) World Health Organization classification of tumours. Pathology and genetics of head and neck tumours. 6. Odontogenic tumours. IARC Press, Lyon, p 296

Gardner DG, Heikinheimo K, Shear M, Philipsen HP, Coleman H (2005b) Ameloblastomas. In: Barnes L, Eveson JW, Reichart P, Sidransky D (eds) World Health Organization classification of tumours. Pathology and genetics of head and neck tumours. 6. Odontogenic tumours. IARC Press, Lyon, p 296

Gohel A, Villa A, Sakai O (2016) Benign jaw lesions. Dent Clin N Am 60:125–141

Gordon SC, MacIntosh RB, Wesley RKA (2001) A review of osteoblastoma and case report of metachronous osteoblastoma and unicystic ameloblastoma. Oral Surg Oral Pathol Oral Med Oral Radiol Endod 91:570–575

Goteti SH (2016) Odontogenic tumors: a review of 675 cases in Eastern Libya. Niger J Surg 22:37–40

Harmon M, Arrigan M, Toner M, O'Keeffe SA (2015) A radiological approach to benign and malignant lesions of the mandible. Clin Radiol 70:335–350

Hisatomi M, Asaumi J-I, Konouchi H, Shigehara H, Yanagi Y, Kishi K (2003) MR imaging of epithelial cysts of the oral and maxillofacial region. Eur J Radiol 48:178–182

Jones RE, Dillon J (2016) Nonodontogenic cysts of the jaws and treatment in the pediatric population. Oral Maxillofac Surg Clin North Am 28:31–44

Jundt G (2005) Fibrous dysplasia. Central giant cell lesion/granuloma. Cherubism. Aneurysmal bone cyst. Simple bone cyst. In: Barnes L, Eveson JW, Reichart P, Sidransky D (eds) World Health Organization classification of tumours. Pathology and genetics of head and neck tumours. 6. Odontogenic tumours. IARC Press, Lyon, pp 321, 324, 325, 326, 327

Kaffe I, Naor H, Calderon S, Buchner A (1999) Radiological and clinical features of aneurysmal bone cysts of the jaws. Dentomaxillofac Radiol 28:167–172

Kaugars G (1991a) Odontogenic tumors. In: Miles DA, Van Dis M, Kaugars GE, Lovas JGL (eds) Oral and maxillofacial radiology. Radiologic/pathologic correlations. Saunders, Philadelphia, pp 51–95

Kaugars G (1991b) Benign fibro-osseous lesions. In: Miles DA, Van Dis M, Kaugars GE, Lovas JGL (eds) Oral and maxillofacial radiology. Radiologic/pathologic correlations. Saunders, Philadelphia, pp 125–154

Knutsen BM, Larheim TA, Johannessen S, Hillestad J, Solheim T, Koppang HS (2002) Recurrent conventional cement-ossifying fibroma of the mandible. Dentomaxillofac Radiol 31:65–68

Kolomvos N, Theologie-Lygidakis N, Christopoulos P, Iatrou I (2013) Benign fibro-osseous lesions of the jaws in children. A 12-year retrospective study. J Craniomaxillofac Surg 41:574–580

Kramer IRH, Pindborg JJ, Shear M (1992) World Health Organisation International Histological Classification of Tumours. Histological typing of odontogenic tumours, 2nd edn. Springer, Berlin, pp 11–33

MacDonald D (2016) Lesions of the jaws presenting as radiolucencies on a cone-beam CT. Clin Radiol 71:972–985

MacDonald-Jankowski DS (2004) Fibro-osseous lesions of the face and jaws (review). Clin Radiol 59:11–25

Malek M, Cortes LM, Sigurdsson A, Rosenberg PA (2015) Differential diagnosis of a periapical radiolucent lesion. A case report and review of the literature. N Y State Dent J 81:52–56

Manjima S, Naik Z, Keluskar V, Bagewadi A (2015) Multiple jaw cysts-unveiling the Gorlin-Goltz syndrome. Contemp Clin Dent 6(Suppl 1):S102–S105

Matsumura S, Murakami S, Kakimoto N, Furukawa S, Kishino M, Ishida T, Fuchihata H (1998) Histopathologic and radiographic findings of the simple bone cyst. Oral Surg Oral Med Oral Pathol Oral Radiol Endod 85:619–625

Matsuura S, Tahara T, Ro T, Masumi T, Kasuya H, Yokota T (1999) Aneurysmal cyst of the coronoid process of the mandible. Dentomaxillofac Radiol 28:324–326

Matsuzaka K, Shimono M, Uchiyama T, Noma H, Inoue T (2002) Lesions related to the formation of bone, cartilage or cementum arising in the oral area: a statistical study and review of the literature. Bull Tokyo Dent Coll 43:173–180

McLeod RA, Dahlin DC, Beabout JW (1976) The spectrum of osteoblastoma. AJR Am J Roentgenol 126:321–325

Meyer KA, Bancroft LW, Dietrich TJ, Kransdorf MJ, Peterson JJ (2011) Imaging characteristics of benign, malignant, and infectious jaw lesions: a pictorial review. AJR Am J Roentgenol 197:W412–W421

Miles D (1991) Vascular and reactive lesions. In: Miles DA, Van Dis M, Kaugars GE, Lovas JGL (eds) Oral and maxillofacial radiology. Radiologic/pathologic correlations. Saunders, Philadelphia, pp 155–186

Minami M, Kaneda T, Yamamoto H, Ozawa K, Itai Y, Ozawa M, Yoshikawa K, Sasaki Y (1992) Ameloblastoma in the maxillomandibular region: MR imaging. Radiology 184:389–393

Minami M, Kaneda T, Ozawa K, Yamamoto H, Itai Y, Ozawa M, Yoshikawa K, Sasaki Y (1996) Cystic lesions of the maxillomandibular region: MR imaging distinction odontogenic keratocysts and ameloblastomas from other cysts. AJR Am J Roentgenol 166:943–949

Mortazavi H, Baharvand M (2016) Jaw lesions associated with impacted tooth: a radiographic diagnostic guide. Imaging Sci Dent 46:147–157

Mosier KM (2015a) Magnetic resonance imaging of the maxilla and mandible: signal characteristics and features in the differential diagnosis of common lesions. Top Magn Reson Imaging 24:23–37

Mosier KM (2015b) Lesions of the jaw. Semin Ultrasound CT MR 36:444–450

Mosqueda-Taylor A, Martinez-Mata G, Carlos-Bregni R, Vargas PA, Toral-Rizo V, Cano-Valdéz AM et al (2011) Central odontogenic fibroma: new findings and report of a multicentric collaborative study. Oral Surg Oral Med Oral Pathol Oral Radiol Endod 112:349–358

Noffke CE, Ngwenya SP, Nzima N, Raubenheimer EJ, Rakgwale NB (2012) Gigantiform cementoma in a child. Dentomaxillofac Radiol 41:264–266

Ogle OE, Santosh AB (2016) Medication management of jaw lesions for dental patients. Dent Clin N Am 60:483–495

Peacock ME, Krishna R, Gustin JW, Stevens MR, Arce RM, Abdelsayed RA (2015) Retrospective study on idiopathic bone cavity and its association with cementoosseous dysplasia. Oral Surg Oral Med Oral Pathol Oral Radiol 119:e246–e251

Peker E, Ôgütlü F, Karaca IR, Gültekin ES, Cakir M (2016) A 5 year retrospective study of biosied jaw lesions with the assessment of concordance between clinical and histopathological diagnoses. J Oral Maxillofac Pathol 20:78–85

Perdigao PF, Silva EC, Sakurai E, Soares de Araujo N, Gomez RS (2003) Idiopathic bone cavity: a clinical, radiographic, and histological study. Br J Oral Maxillofac Surg 41:407–409

Perry KS, Tkaczuk AT, Caccamese JF Jr, Ord RA, Pereira KD (2015) Tumors of the pediatric maxillofacial skeleton. A 20-year clinical study. JAMA Otolaryngol Head Neck Surg 141:40–44

Phattarataratip E, Pholjaroen C, Tiranon P (2014) A clinicopathologic analysis of 207 cases of benign fibro-osseous lesions of the jaws. Int J Surg Pathol 22:326–333

Philipsen HP, Reichart PA, Sciubba JJ, van der Waal I, Buchner A, Odell EW (2005) Odontogenic fibroma/myxoma. In: Barnes L, Eveson JW, Reichart P, Sidransky D (eds) World Health Organization classification of tumours. Pathology and genetics of head and neck tumours. 6. Odontogenic tumours. IARC Press, Lyon, p 316

Pogrel MA (2015) The kertocystic odontogenic tumour (KOOT) – an odyssey. Int J Oral Maxillofac Surg 44:1565–1568

Praetorius F, Piattelli A (2005) Odontoma, compound type. In: Barnes L, Eveson JW, Reichart P, Sidransky D (eds) World Health Organization classification of tumours. Pathology and genetics of head and neck tumours. 6. Odontogenic tumours. IARC Press, Lyon, p 311

Probst FA, Probst M, Pautke CH, Kaltsi E, Otto S, Schiel S et al (2015) Magnetic resonance imaging: a useful tool to distinguish between keratocystic odontogenic tumours and odontogenic cysts. Br J Oral Maxillofac Surg 53:217–222

Progrel MA (2015) The keratocystic odontogenic tumour (KCOT) – an odyssey. Int J Oral Macillofac Surg 44:1565–1568

Raubenheimer EJ, Noffke CE, Boy SC (2016) Osseous dysplasia with gross jaw expansion: a review of 18 lesions. Head Neck Pathol 10:437–443

Redfors EMC, Jensen JL, Storhaug K, Prescon T, Larheim TA (2013) Cherubism: panoramic and CT features in adults. Dentomaxillofac Radiol 42:20130034

Resnick D (1996) Bone and joint imaging, 2nd edn. Saunders, Philadelphia, pp 615, 616, 998

Rubio-Correa I, Manzano-Solo de Zaldivar D, González-Garcia R, Ruiz-Laza L, Villanueva-Alcojol L, Conzález-Ballester D et al (2012) Giant cell granuloma of the maxilla. Global management, review of literature and case report. J Clin Exp Dent 4:e129–e131

Saxena C, Aggarwal P, Wadhwan V, Bansal V (2015) Primary intraosseous squamous cell carcinoma in odontogenic keratocyst: a rare entity. J Oral Maxillofac Pathol. doi:10.4103/0973-029X.174615

Schajowicz F (1993) World Health Organisation. Histological typing of bone tumors, 2nd edn. Springer, Berlin, p 7

Shear M, Philipsen HP (2005) Keratocystic odontogenic tumour. In: Barnes L, Eveson JW, Reichart P, Sidransky D (eds) World Health Organization classification of tumours. Pathology and genetics of head and neck tumours. 6. Odontogenic tumours. IARC Press, Lyon, p 306

Slootweg PJ, El Mofty S (2005) Ossifying fibroma. In: Barnes L, Eveson JW, Reichart P, Sidransky D (eds) World Health Organization classification of tumours. Pathology and genetics of head and neck tumours. 6. Odontogenic tumours. IARC Press, Lyon, p 319

Slootweg PJ, Takeda Y, Tomich CE, Praetorius F, Piattelli A (2005) Odontoma, complex type. In: Barnes L, Eveson JW, Reichart P, Sidransky D (eds) World Health Organization classification of tumours. Pathology and genetics of head and neck tumours. 6. Odontogenic tumours. IARC Press, Lyon, p 310

Su L, Weathers DR, Waldron CA (1997) Distinguishing features of focal cemento-osseous dysplasia and cemento-ossifying fibroma. II: A clinical and radiologic spectrum of 316 cases. Oral Surg Oral Med Oral Pathol Oral Radiol Endod 84:540–549

Sullivan RJ, Meyer JS, Dormans JP, Davidson RS (1999) Diagnosing aneurysmal and unicameral bone cysts with magnetic resonance imaging. Clin Orthop 366:186–190

Sun ZJ, Zhao YF, Yang RL, Zwahlen RA (2010) Aneurysmal bone cysts of the jaws: analysis of 17 cases. J Oral Maxillofac Surg 68:2122–2128

Tkaczuk AT, Bhatti M, Caccamese JF Jr, Ord RA, Pereira KD (2015) Cystic lesions of the jaw in children. A 15-year experience. JAMA Otolaryngol Head Neck Surg 141:834–839

Trosman SJ, Krakovitz PR (2015) Pediatric maxillary and mandibular tumors. Otolaryngol Clin North Am 48:101–119

Veervarmal V, Madhavan RN, Nassar MM, Amsaveni R (2013) Central odontogenic fibroma of the maxilla. J Oral Maxillofac Pathol 17(2):319. doi:10.4103/0973-029X.119767

Vlcek D, Kuttenberger JJ (2013) Traumatic cyst of the mandible. From development to therapy – a case report. Schweiz Monatsschr Zahnmed 123:319–330

Weber AL, Kaneda T, Scrivani SJ, Aziz S (2003) Jaw: cysts, tumors, and non-tumorous lesions. In: Som PM, Curtin HD (eds) Head and neck imaging, 4th edn. Mosby, St. Louis, pp 930–994

White SC, Pharoah MJ (eds) (2014a) Benign tumors. In: Oral radiology. Principles and interpretation, 7. Mosby, St. Louis, pp 359–401

White SC, Pharoah MJ (eds) (2014b) Other bone diseases. In: Oral Radiology. Principles and interpretation, 7. Mosby, St. Louis, pp 402–426

Wright JM, Odell EW, Speight PM, Takata T (2014) Odontogenic tumors, WHO 2005: where do we go from here? Head Neck Pathol 8:373–382

Yoshiura K, Higuchi Y, Ariji Y, Shinohara M, Yuasa K, Nakayama E, Ban S, Kanda S (1994) Increased attenuation in odontogenic keratocysts with computed tomography: a new finding. Dentomaxillofac Radiol 23:138–142

Yuan Y, Tang W, Jiang M, Tao X (2016) Palatal lesions: discriminative value of conventional MRI and diffusion weighted imaging. Br J Radiol. doi:10.1259/bjr.20150911

Malignant Tumors in Jaws

4

Abstract

This chapter illustrates bone-destructive tumors; squamous cell carcinoma, mucoepidermoid carcinoma, adenoid cystic carcinoma, non-Hodgin's lymphoma, multiple myeloma, plasmacytoma, leukemia, bone-destructive and bone-productive tumors; osteosarcoma, chondrosarcoma, Ewing sarcoma, soft-tissue sarcomas; rhabdomyosarcoma, leiomyosarcoma, and jaw metastases.

4.1 Introduction

A simple, general definition of malignancy is "A term for diseases in which abnormal cells divide without control and can invade nearby tissues. Malignant cells can also spread to other parts of the body through the blood and lymph systems" (National Cancer Institute, USA, 2016).

Malignant tumors of the jaws are relatively uncommon in most parts of the world. When they occur, they should be examined with advanced imaging modalities to achieve the most precise diagnosis and hence the best possible treatment. This chapter is divided into tumors which are bone destructive and in those which are bone destructive and bone productive to emphasize their principal difference in imaging appearance. Soft-tissue sarcomas are also illustrated. The listing of malignant tumors is rather representative but far from complete.

Many cases in this chapter include a panoramic view and a few cases even intraoral views because specialists and practitioners in the dental field are familiar with conventional jaw radiography. However, in most cases, CT is applied, and several cases are supplemented with MRI and occasionally with PET, PET-CT, and other nuclear medicine scanning (I-131, technetium-99). In selected patients, follow-up images, clinical photos, and surgical specimens are shown.

4.2 Bone-Destructive Tumors

Squamous cell carcinoma, mucoepidermoid carcinoma, adenoid cystic carcinoma, non-Hodgin's lymphoma, multiple myeloma, plasmacytoma, and leukemia are illustrated.

4.3 Squamous Cell Carcinoma

Figs. 4.1, 4.2, 4.3, 4.4, 4.5, 4.6, 4.7, 4.8, and 4.9

Synonyms: Epidermoid carcinoma.

4.3.1 Definition

Malignant epithelial neoplasm exhibiting squamous differentiation as characterized by the formation of keratin and/or presence of intercellular bridges (WHO).

4.3.2 Clinical Features

- Most common malignancy of oral cavity
- Most common malignancy of jaw bone (due to frequent invasion)
- 2–4% of all malignancies in the USA and Europe

In collaboration with H.-J. Smith, G. Støre.

T.A. Larheim, P.-L.A. Westesson, *Maxillofacial Imaging*, https://doi.org/10.1007/978-3-319-53319-3_4

- Much higher prevalence in certain countries (due to habits such as inverse smoking)
- Males more frequent than females
- Older age groups (50 years and older), but also younger than 30 years
- Most frequent in tongue, floor of mouth, and mandibular gingiva; retromolar trigone, anterior tonsillar pillar, and soft palate
- Erythroplakia developing in leukoplakia
- Ulceration surrounded by indurated or sharply defined border
- Predominantly white and warty growth
- Advanced stage: pain, paresthesia, pathologic fracture

4.3.3 Imaging Features

- Soft-tissue mass
- Bone radiolucency, secondary invasion of bone
- Border of bone destruction ill defined
- Bone invasion frequent in gingival mandibular cancers, generally considered to be about 50%, but up to 85% reported in the upper jaw; maxillary sinus frequently involved
- Floating teeth; tooth resorption uncommon
- Advanced stage: pathologic fracture
- T1-weighted MRI: intermediate–low signal
- T2-weighted and STIR MRI: high signal
- T1-weighted MRI: contrast enhancement

Most carcinomas found in jaws have invaded from lesions of the oral cavity. However, primary intraosseous carcinoma may arise within the jaw "having no initial connection with oral mucosa, and presumably developing from residues of odontogenic epithelium" (WHO).

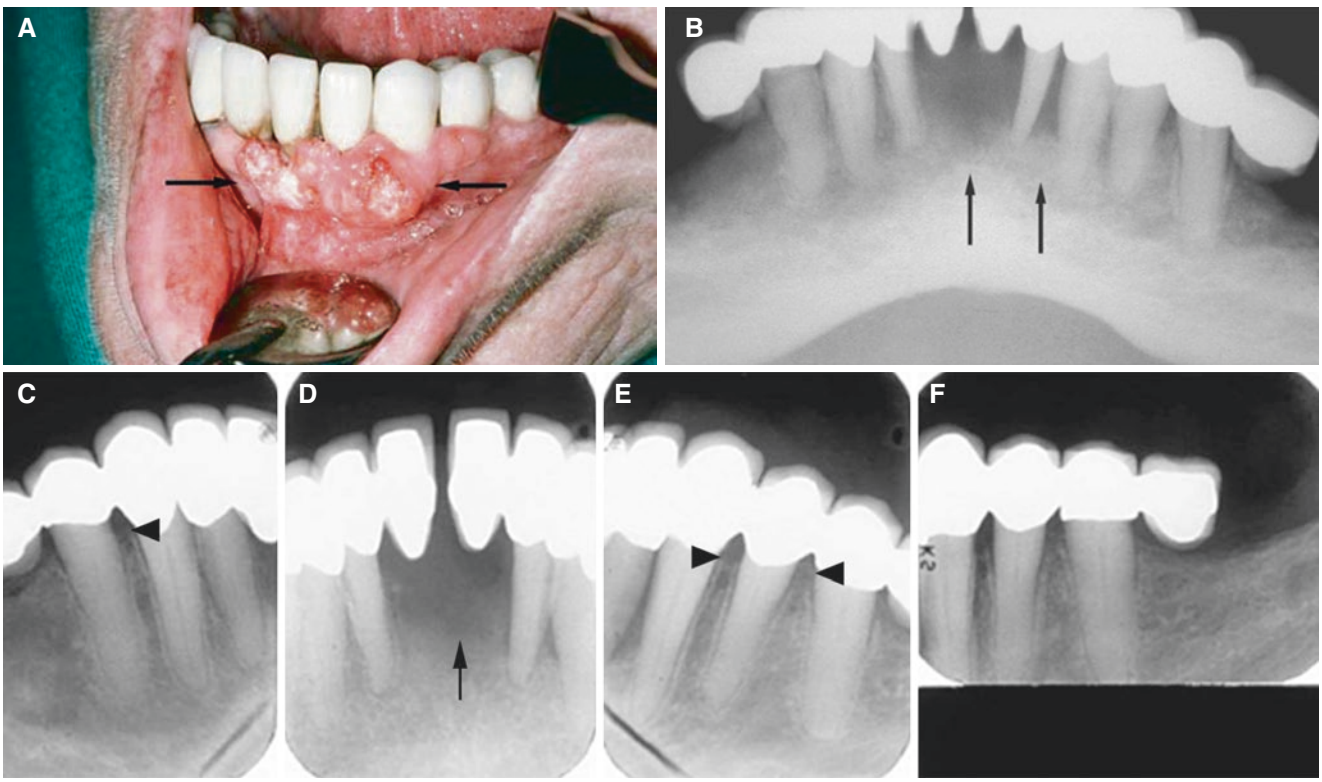

Fig. 4.1 Squamous cell carcinoma, mandible; 70-year-old female with previous oral leukoplakia that developed erythroplakia and soreness. (**A**) Clinical photograph shows leukoplakia that transformed to gingival cancer (*arrows*). (**B**) Intraoral panoramic view shows diffuse bone destruction (*arrows*) due to tumor infiltration. (**C**) Intraoral views confirm diffuse alveolar bone destruction in front area (*arrow*) but otherwise show normal periodontal bone support (*arrowheads*)

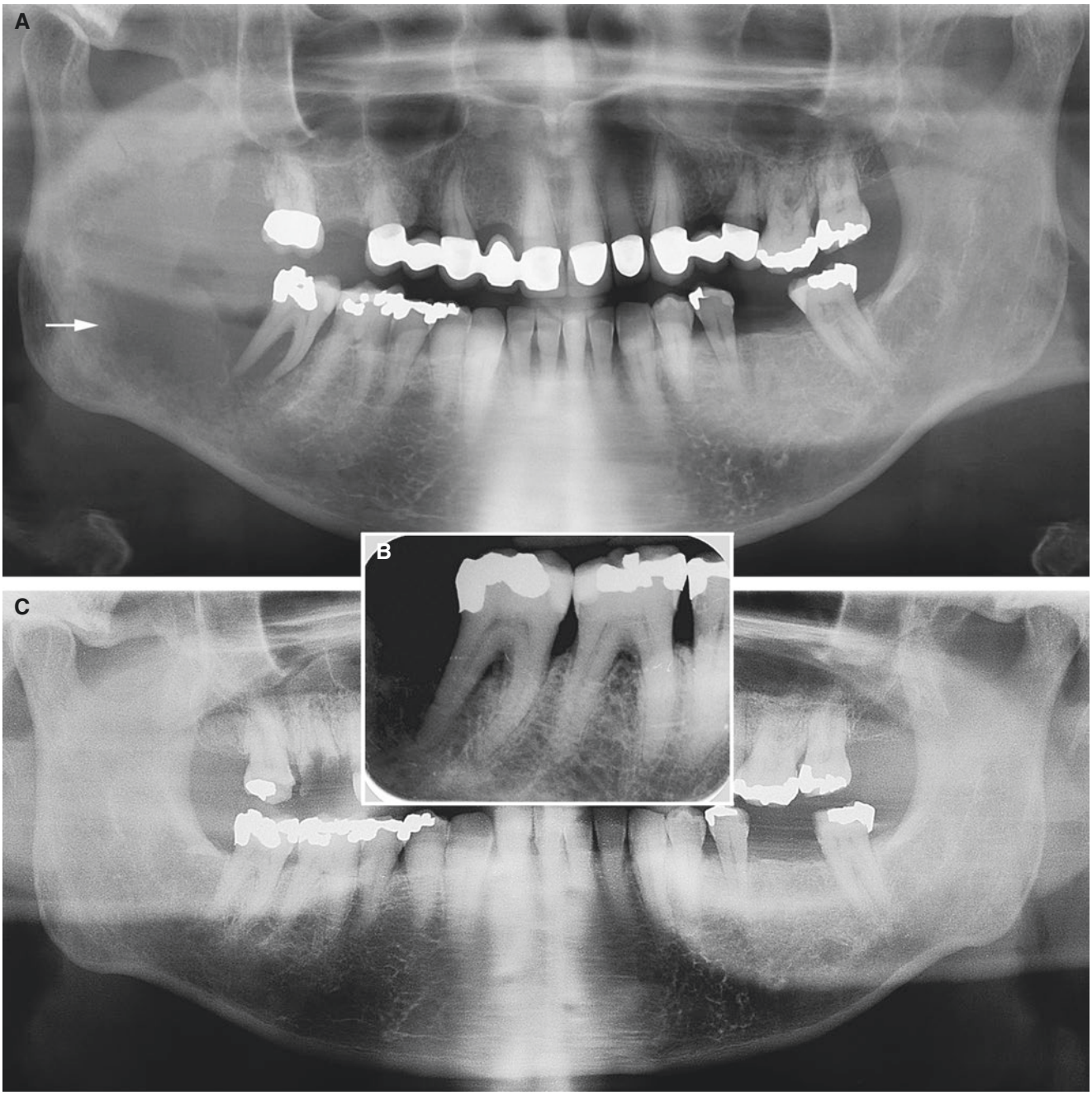

Fig. 4.2 Squamous cell carcinoma, mandible; 58-year-old male with mass in the right mandible, trismus, and some paresthesia. (**A**) Panoramic view shows severe destruction of almost the entire right mandibular ramus (*arrow*) and floating tooth (second molar). (**B**) Intraoral view about 1 month earlier shows bony destruction around second molar. (**C**) Panoramic view 3 years earlier shows normal mandibular bony structures

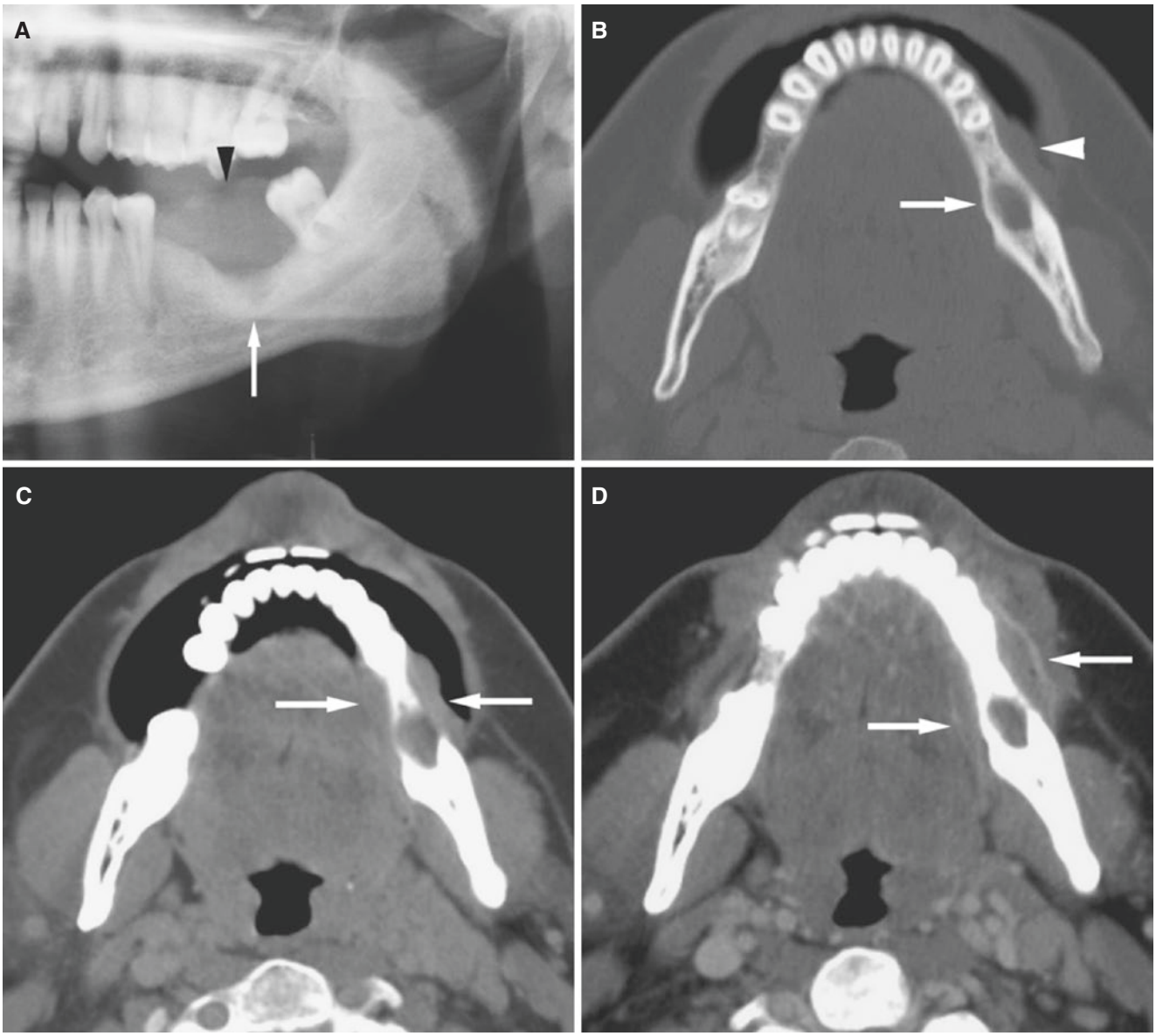

Fig. 4.3 Squamous cell carcinoma, mandible; 37-year-old male with painless gingival soft-tissue swelling. (**A**) Panoramic view shows diffuse bone destruction (*arrow*) and soft-tissue mass (*arrowhead*). (**B**) Axial CT image with cheek blowing shows bone destruction (*arrow*) and soft-tissue mass (*arrowhead*) adherent to the mandible. (**C**) Axial CT image, soft-tissue window, with cheek blowing shows soft-tissue mass (*arrows*) adherent to the mandible. (**D**) Axial contrast-enhanced CT image, soft-tissue window, shows contrast-enhanced soft-tissue mass (*arrows*)

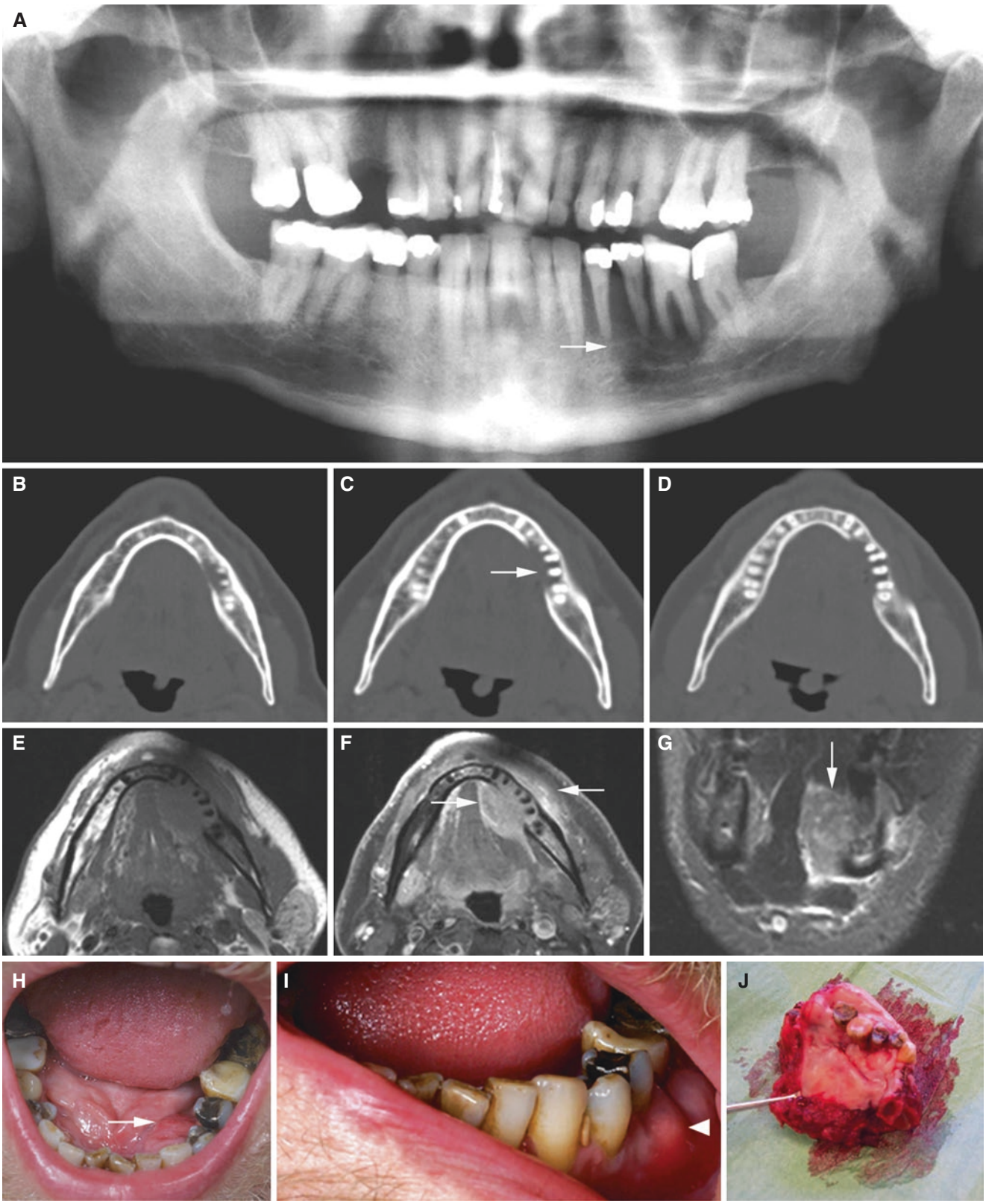

Fig. 4.4 Squamous cell carcinoma, mandible; 60-year-old male with pain-free mass and two loose teeth in left mandible. (**A**) Panoramic view shows destruction in alveolar ridge in left mandible (*arrow*). There is normal periodontal bone level in other parts of dentition. (**B**, **C**, **D**) Axial CT images show destruction of lingual cortical bone (*arrow*). (**E**) Axial T1-weighted pre-Gd and (**F**) axial T1-weighted fat sat post-Gd MRI shows contrast enhancement both lingually and buccally relative to mandible (*arrows*). (**G**) Coronal STIR MRI shows tumor in left sublingual and submandibular spaces infiltrating and destroying mylohyoid muscle on the left. Lesion is also invading intrinsic muscles of tongue (*arrow*). (**H**, **I**) Clinical photographs show mass lingually (*arrow*) and buccally (*arrowhead*). (**J**) Surgical specimen

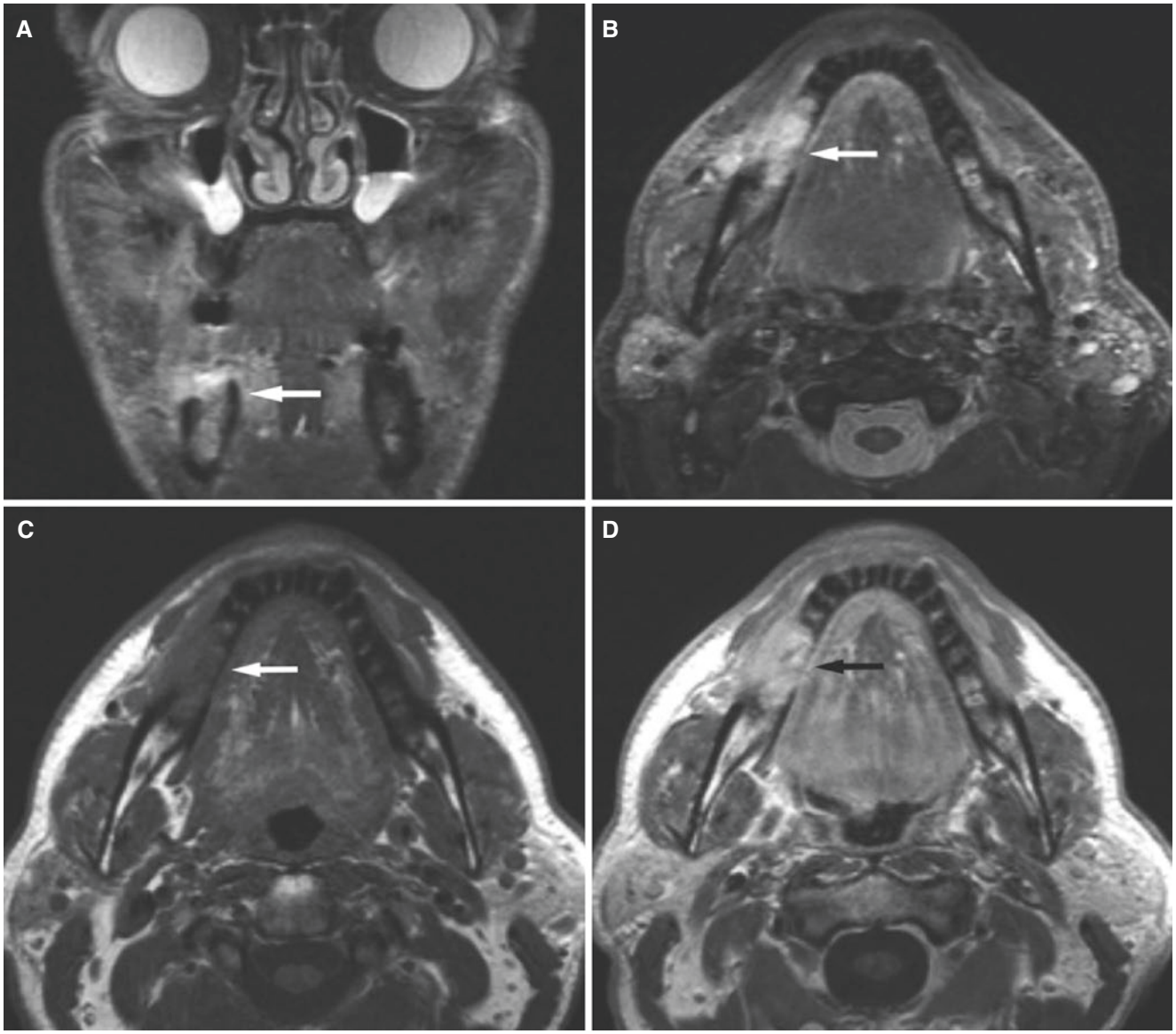

Fig. 4.5 Squamous cell carcinoma, mandible; 55-year-old male with oral leukoplakia several locations in oral cavity for many years, then developed pain and soreness, and cancer in tooth socket after molar extraction (panoramic view and CT were negative). (**A**) Coronal STIR MRI shows small area of high signal in cranial part of the alveolar bone and gingival tissue (*arrow*). (**B**) Axial STIR MRI shows high signal in the alveolar bone and buccally (*arrow*). (**C**) Axial T1-weighted pre-Gd MRI shows reduced signal in bone marrow (*arrow*). (**D**) Axial T1-weighted post-Gd MRI shows contrast enhancement in bone marrow and buccal mass (*arrow*)

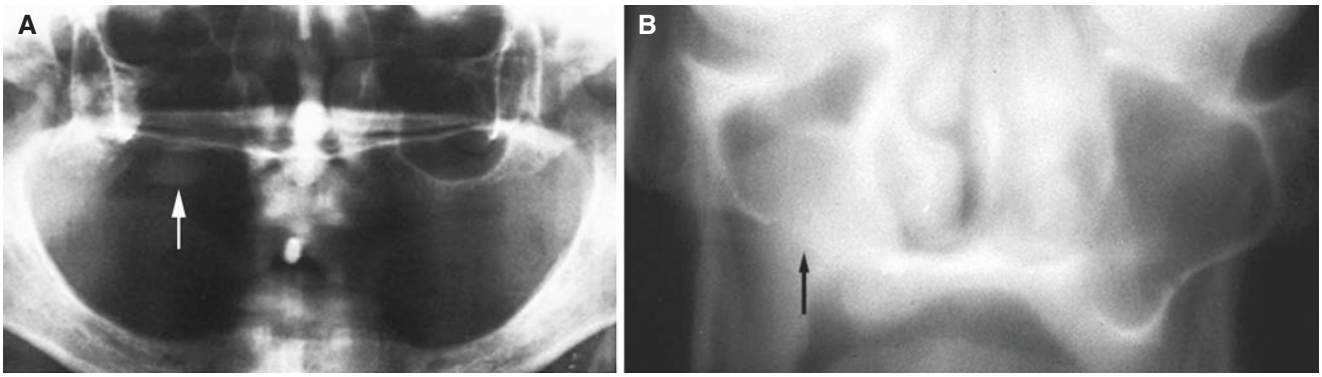

Fig. 4.6 Squamous cell carcinoma, maxilla; 65-year-old female with ulcer beneath the upper denture. (**A**) Panoramic view shows loss of bony wall of right maxillary sinus (*arrow*). (**B**) Coronal conventional tomogram shows destruction of the alveolar bone with tumor growth into the maxillary sinus (*arrow*)

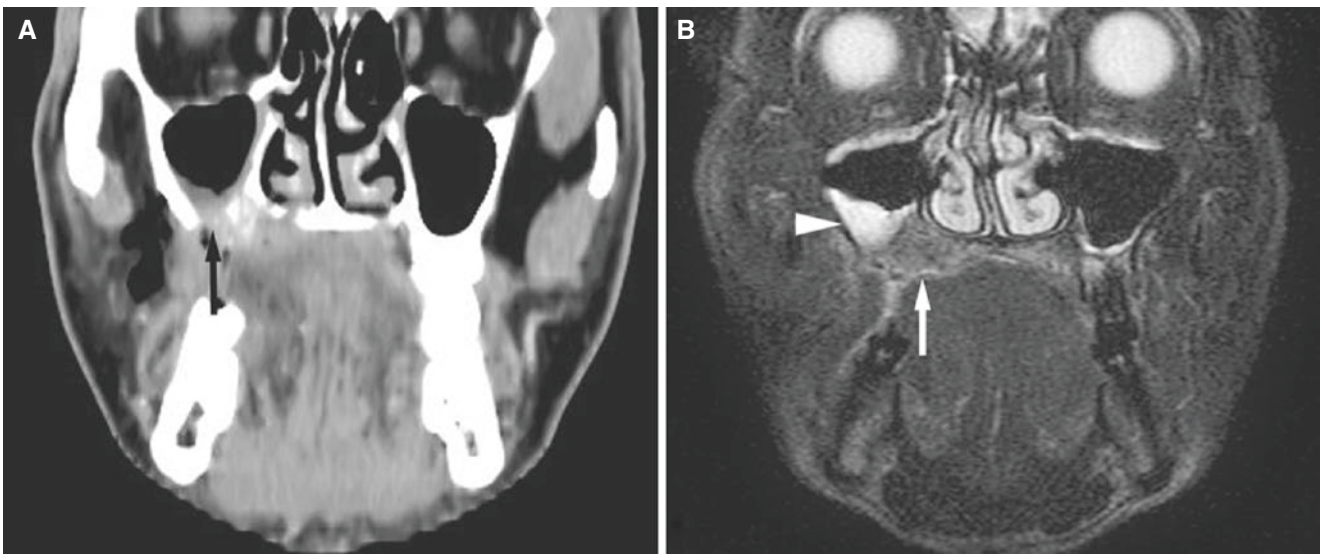

Fig. 4.7 Squamous cell carcinoma, maxilla; 70-year-old female with some bleeding from tender soft-tissue mass of right gingival mucosa. (**A**) Coronal CT image shows destruction of maxillary sinus delineation (*arrow*) and soft-tissue mass. (**B**) Coronal T2-weighted fat-suppressed MRI shows soft-tissue tumor invading maxillary sinus (*arrow*) and high-signal mucosal thickening (*arrow head*) (courtesy of Dr N Kakimoto, Osaka University Graduate School of Dentistry)

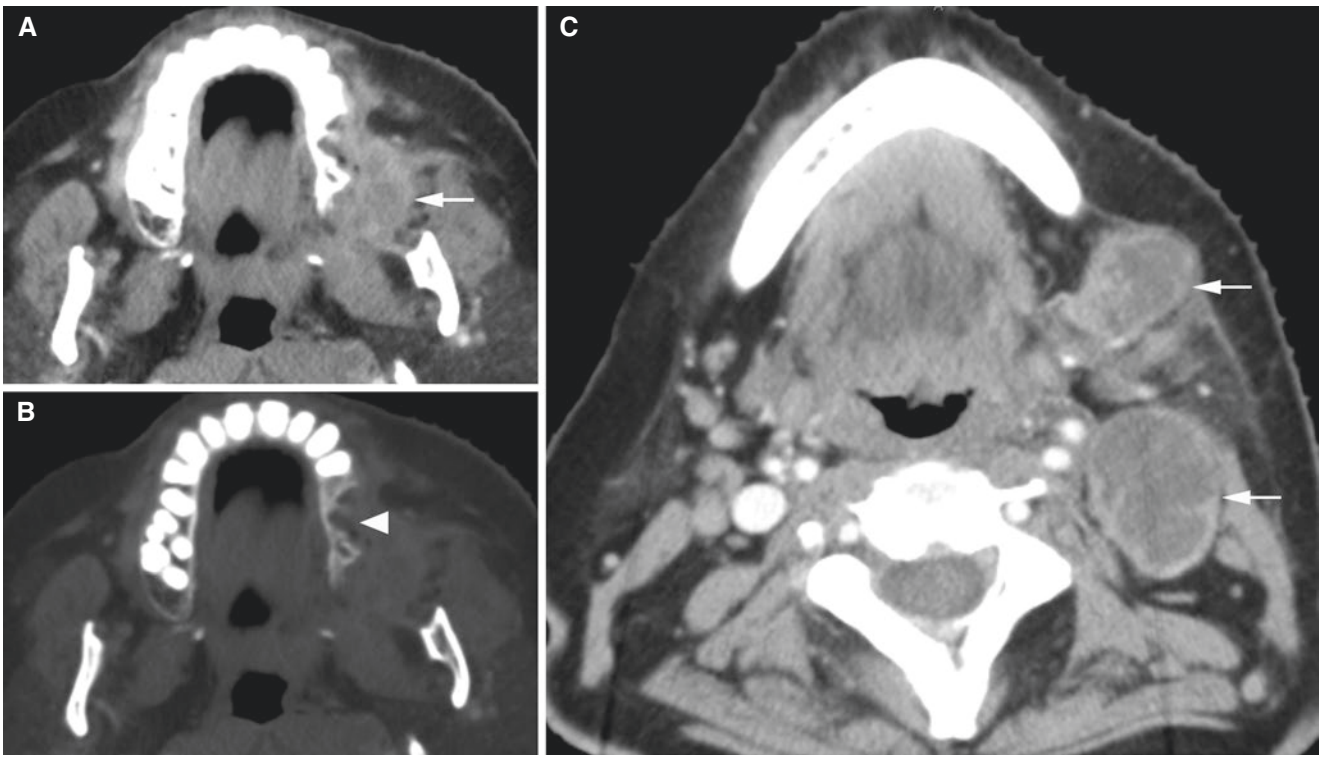

Fig. 4.8 Squamous cell carcinoma, maxilla; 64-year-old female with left maxillary mass. (**A**) Axial (soft-tissue) and (**B**) axial (bone window) CT images show large soft-tissue tumor (*arrow*) and destruction of maxillary alveolar process (*arrowhead*). (**C**) Axial contrast-enhanced CT image of submandibular region shows two enlarged and necrotic lymph nodes: levels Ib and IIa (*arrows*)

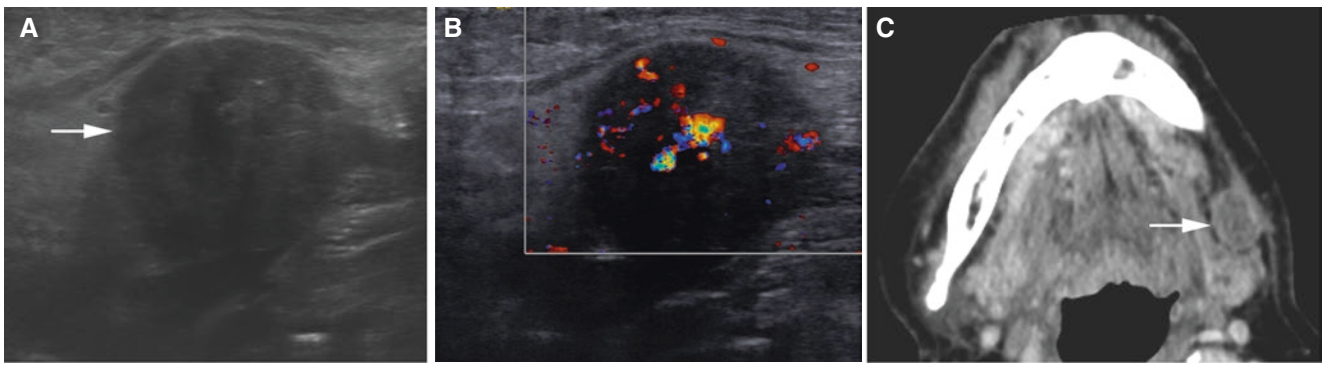

Fig. 4.9 Squamous cell carcinoma, mandible; 58-year-old male with known (and treated) cancer in anterior floor of the mouth with invasion of the anterior mandible. (**A**) US and (**B**) (US Doppler) images show lymph node features suspect for metastasis: enlargement (*arrow*), rounded shape, loss of fat hilus, and vascularization. (**C**) Axial post-contrast CT image of submandibular region shows corresponding enlarged and necrotic lymph node (*arrow*), level Ib. Viable metastatic node verified by cytology (courtesy of Dr. Lennart Flygare, Umeå University Hospital, Umeå, Sweden)

4.4 Mucoepidermoid Carcinoma

Figs. 4.10 and 4.11

4.4.1 Definition

Tumor characterized by the presence of squamous cells, mucus-producing cells, and cells of intermediate type (WHO).

Malignant epithelial neoplasm arising in bone likely originating from odontogenic epithelium residues or from cyst lining.

4.4.2 Clinical Features

- Swelling with or without pain, or incidental finding at routine dental radiography
- Mandible, posterior regions, more frequent than maxilla
- Females more frequent than males (unlike most oral carcinomas)
- Fourth and fifth decades, but may occur in any age group
- Spread to regional lymph nodes in less than 10% and only occasionally, metastasis

4.4.3 Imaging Features

- Unilocular or multilocular radiolucency
- Border well defined and sclerotic
- Cortical plates as well as lower mandibular border may be intact
- May be expansive and resembles ameloblastoma or odontogenic cyst; thus predominantly benign appearance
- Frequently associated with cyst and/or impacted tooth (30–50%)
- T1-weighted MRI: intermediate–low signal
- T2-weighted and STIR MRI: high signal
- T1-weighted post-Gd MRI: predominantly no contrast enhancement; only contrast enhancement in thin peripheral rim of cyst and areas of solid tumor

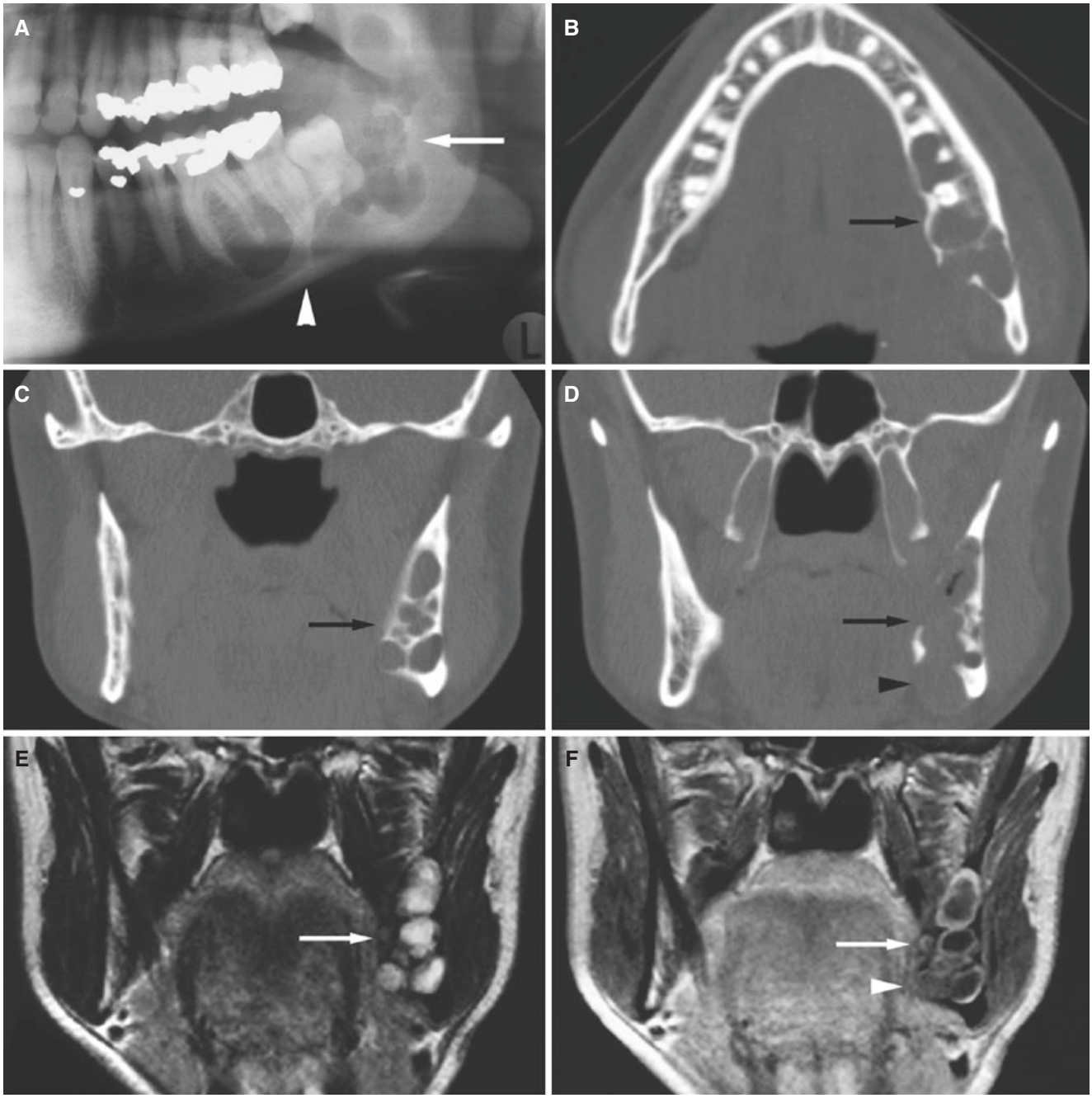

Fig. 4.10 Mucoepidermoid carcinoma, mandible; 46-year-old male with incidental finding at routine dental radiography of impacted wisdom teeth. (**A**) Panoramic view shows multilocular radiolucency (*arrows*) with intact mandibular border (*arrowhead*) and impacted third molar. (**B**) Axial CT image shows multilocular radiolucency (*arrow*) with defect in lingual cortical bone. (**C**) Coronal CT image shows multilocular radiolucency (*arrow*). (**D**) Coronal CT image shows bone destruction lingually (*arrow*); note in particular at the lower mandibular border (*arrowhead*). (**E**) Coronal T2-weighted MRI shows high signal in multilocular process (*arrow*). (**F**) Coronal T1-weighted post-Gd MRI shows contrast enhancement only in thin peripheral rim (*arrow*) except in a more solid component lingually at lower mandibular border (*arrowhead*). (**G**) Surgical specimen shows tumor lingually (*arrow*). (**H**) Vascular fibula graft. (**I**) Fibula graft in situ with titanium plate (**G**, **H**, **I**: courtesy of Dr. T. Bjornland, Oslo University Hospital, Rikshospitalet, Oslo, Norway). (**J**) 3D CT image 5 years postoperatively shows excellent healing of graft and no tumor recurrence. (**K**, **L**, and **M**) Clinical photographs en face, right and left (operated) side, respectively, 5 years after surgery show completely rehabilitated patient with normal mandibular function (mouth-opening capacity more than 40 mm)

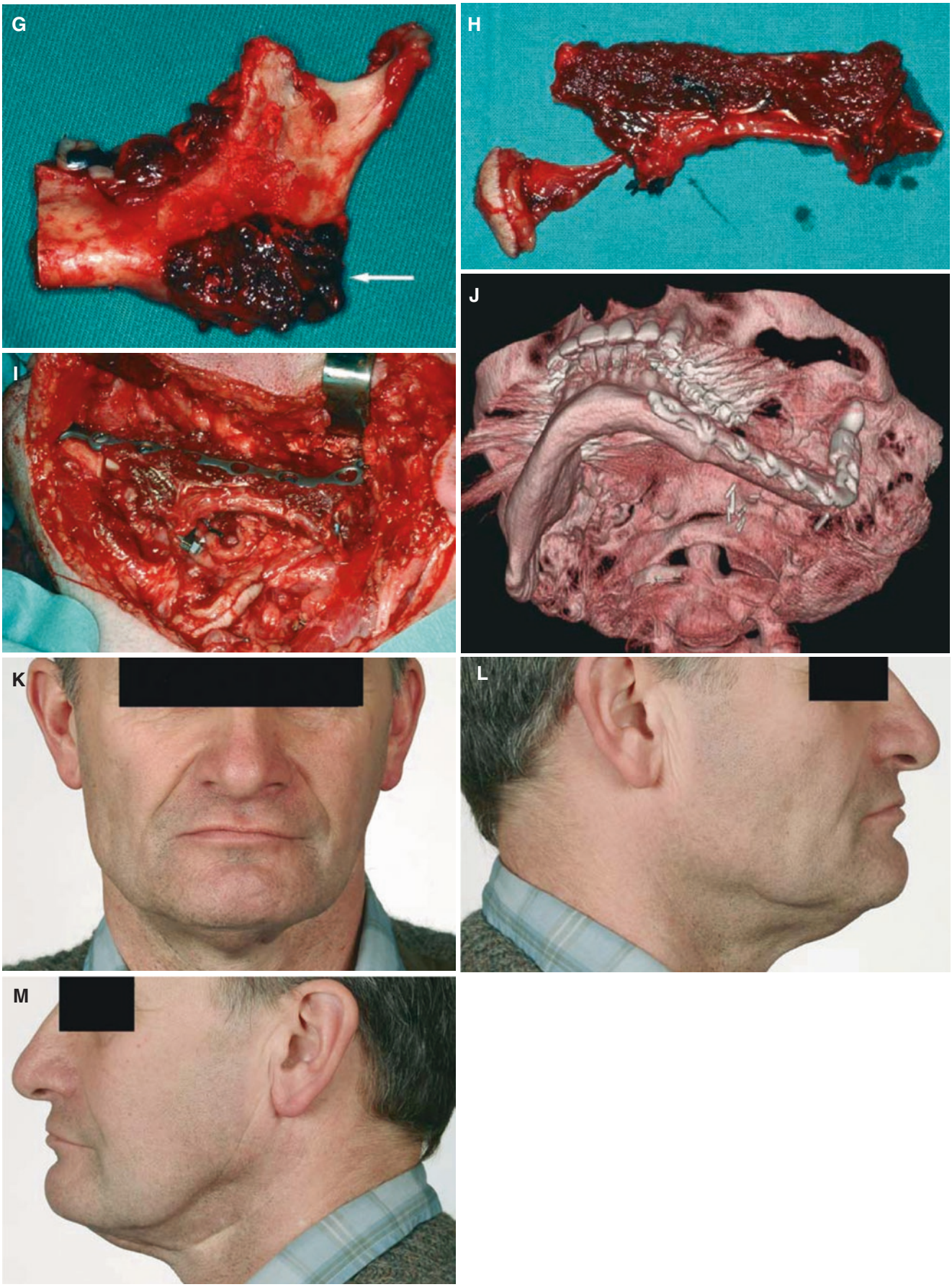

Fig. 4.10 (continued)

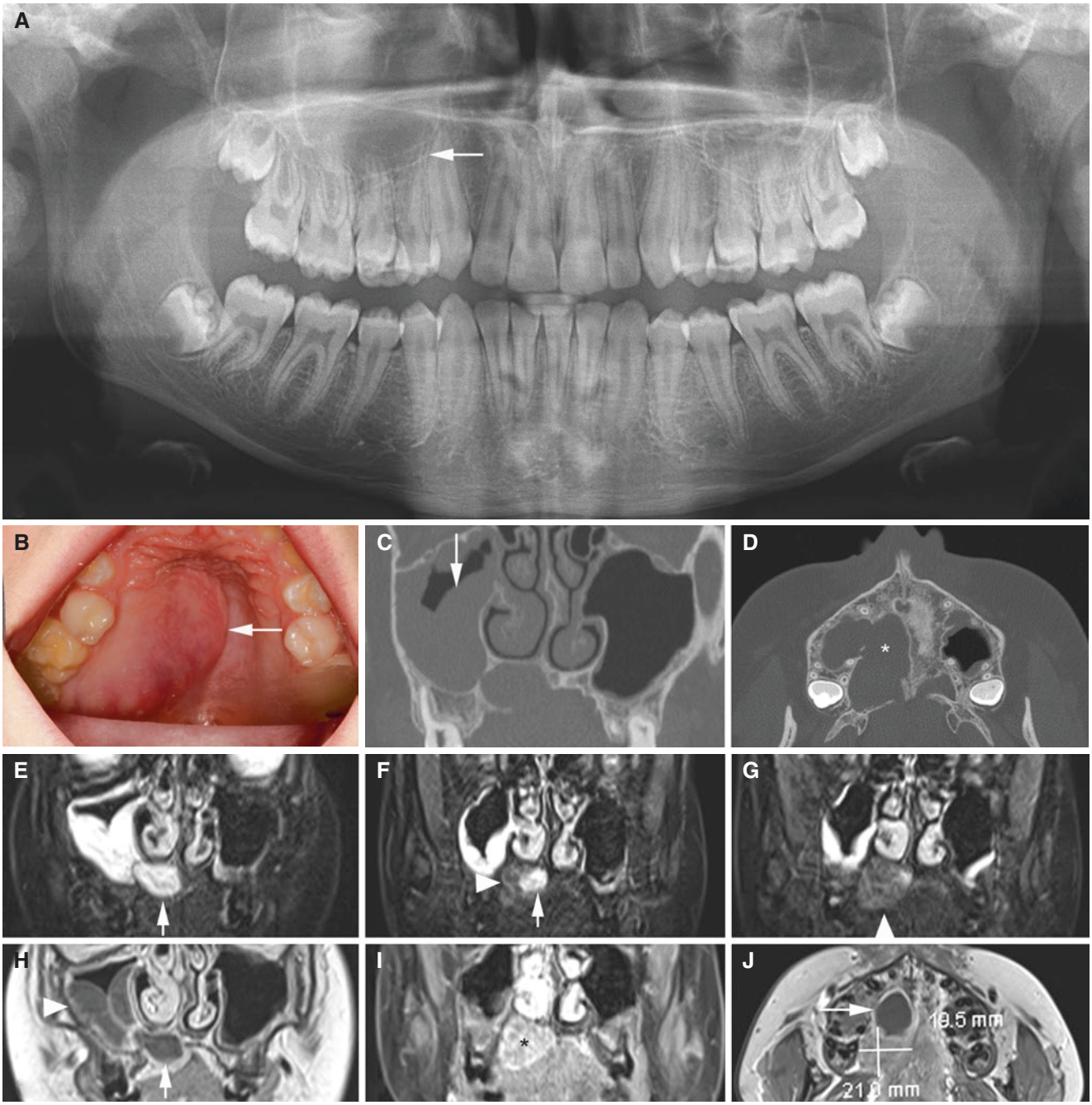

Fig. 4.11 Mucoepidermoid carcinoma, maxilla; 12-year-old male with pain-free mass in the hard palate. (**A**) Panoramic view shows apparently normal interior border of right maxillary sinus (*arrow*). (**B**) Clinical photograph of tumor (*arrow*). (**C**) Coronal and (**D**) axial CT images show destruction in the hard palate (*asterisk*) and soft-tissue mass (*arrow*) in right maxillary sinus, probably representing both tumor and mucosal thickening. (**E**, **F**, **G**) Coronal STIR MRI shows mucosal thickening in the right maxillary sinus and tumor in the hard palate with cystic (*arrow*) and solid (*arrowhead*) components. (**H**) Coronal T1-weighted post-Gd MRI and (**I**) coronal T1-weighted fat sat post-Gd MRI show contrast enhancement in periphery of maxillary sinus (mucosal thickening) (*arrowhead*) and in periphery of cystic/necrotic tumor (*arrow*) and in solid (enhancing) part of tumor (*asterisk*). (**J**) Axial T1-weighted post-Gd MRI shows cystic/necrotic (*arrow*) and solid (*annotated*) components of tumor.

4.5 Adenoid Cystic Carcinoma

Figs. 4.12 and 4.13

4.5.1 Definition

Infiltrative malignant tumor having various histologic features with three growth patterns: glandular (cribriform), tubular, or solid. Tumor cells are of two types: duct-lining cells and myoepithelial cells. Perineural or perivascular spread without stromal reaction is very characteristic. All structural types of adenoid cystic carcinoma can be associated in the same tumor (WHO).

4.5.2 Clinical Features

- Most commonly seen (although rare) in minor salivary glands of the head and neck, usually palate
- Mostly as a painless mass, slowly growing
- Unlike most carcinomas, seldom metastasizes to regional lymph nodes
- Lung most common site of metastasis
- Perineural spread in more than 50%; frequent distant metastasis
- High survival rate after 5 years, low after 15 years
- Slight female predominance
- Fourth to sixth decades

4.5.3 Imaging Features

- Soft-tissue mass
- Radiolucency
- Border of bone destruction ill defined
- Widened foramina such as major palatine foramen
- Perineural invasion of major nerves characteristically found; skip lesions

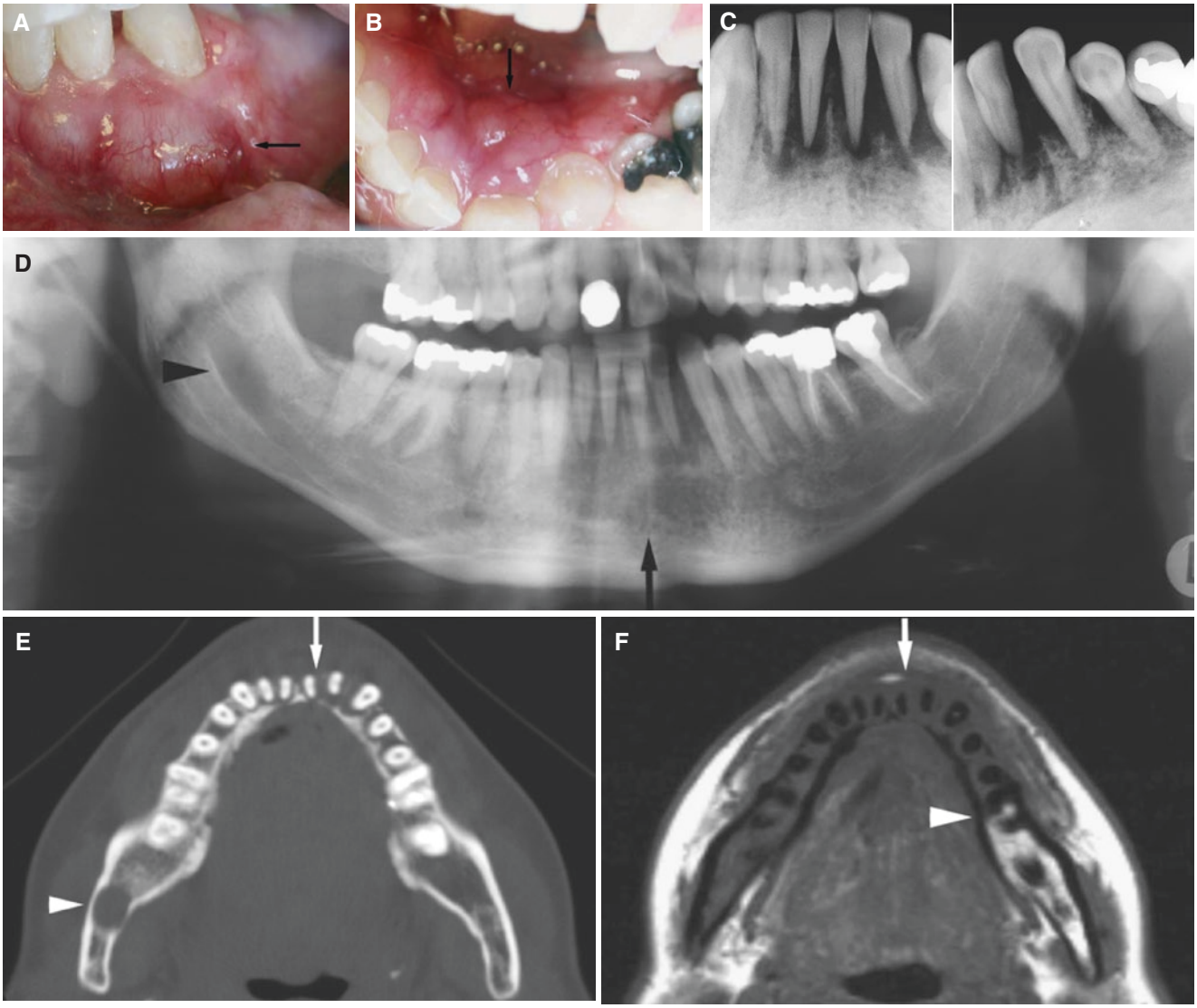

Fig. 4.12 Adenoid cystic carcinoma, mandible; 43-year-old female with loose anterior teeth and hard gingival swelling. (**A**) Clinical photograph shows buccal swelling with normal mucosa (*arrow*). (**B**) Clinical photograph shows lingual swelling with normal mucosa (*arrow*). (**C**) Intraoral views show ill-defined bone destruction around several teeth. (**D**) Panoramic view shows destruction around anterior teeth (*arrow*) and widened mandibular canal (*arrowhead*). (**E**) Axial CT image shows bone destruction around anterior teeth (*arrow*) and widened mandibular canal (*arrowhead*). (**F**) Axial T1-weighted pre-Gd MRI shows cortical bone destruction (*arrow*) and reduced signal from marrow in the entire mandible to molar region on the left side (*arrowhead*). (**G**) Axial T-weighted post-Gd MRI shows tumor expansion in anterior region (*arrow*) and enhancement of the entire mandibular marrow to molar region on the left side (*arrowhead*). (**H**) Coronal STIR MRI shows enhancement of neurovascular tumor spread from mandibular foramen, approaching oval foramen (*arrowhead*). (**I**) Sagittal STIR MRI shows high-signal neurovascular tumor spread from mandibular foramen (*arrowhead*). (**J**) Surgical specimen. (**K**) Surgical specimen, cut in two to show tumor invasion in mandibular canal (*arrow*). (**L**) Surgical specimen from neurovascular tumor spread from mandibular foramen (see **I**). (**M**) Panoramic view shows reconstructed lower jaw (fibula graft) with dental implants

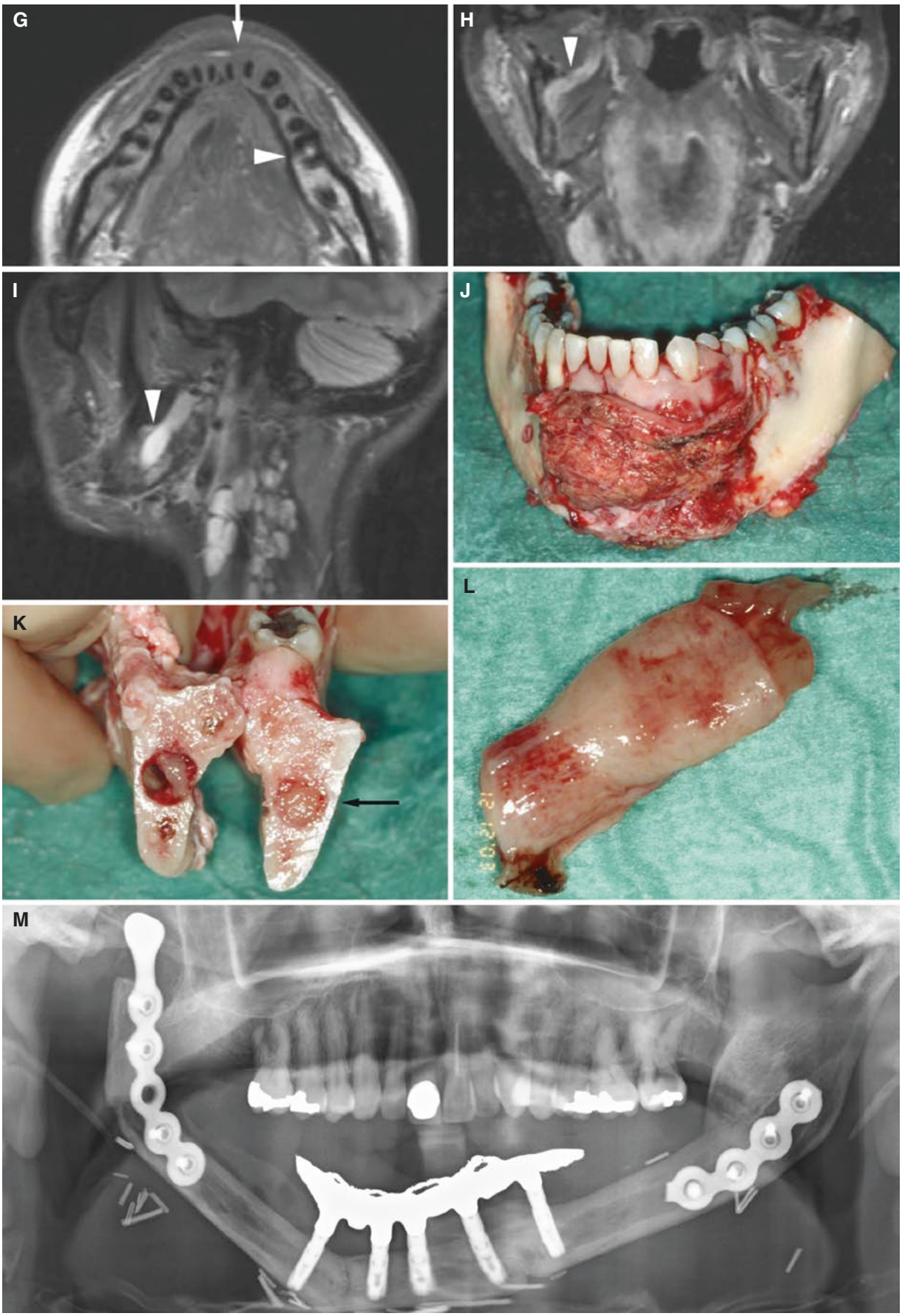

Fig. 4.12 (continued)

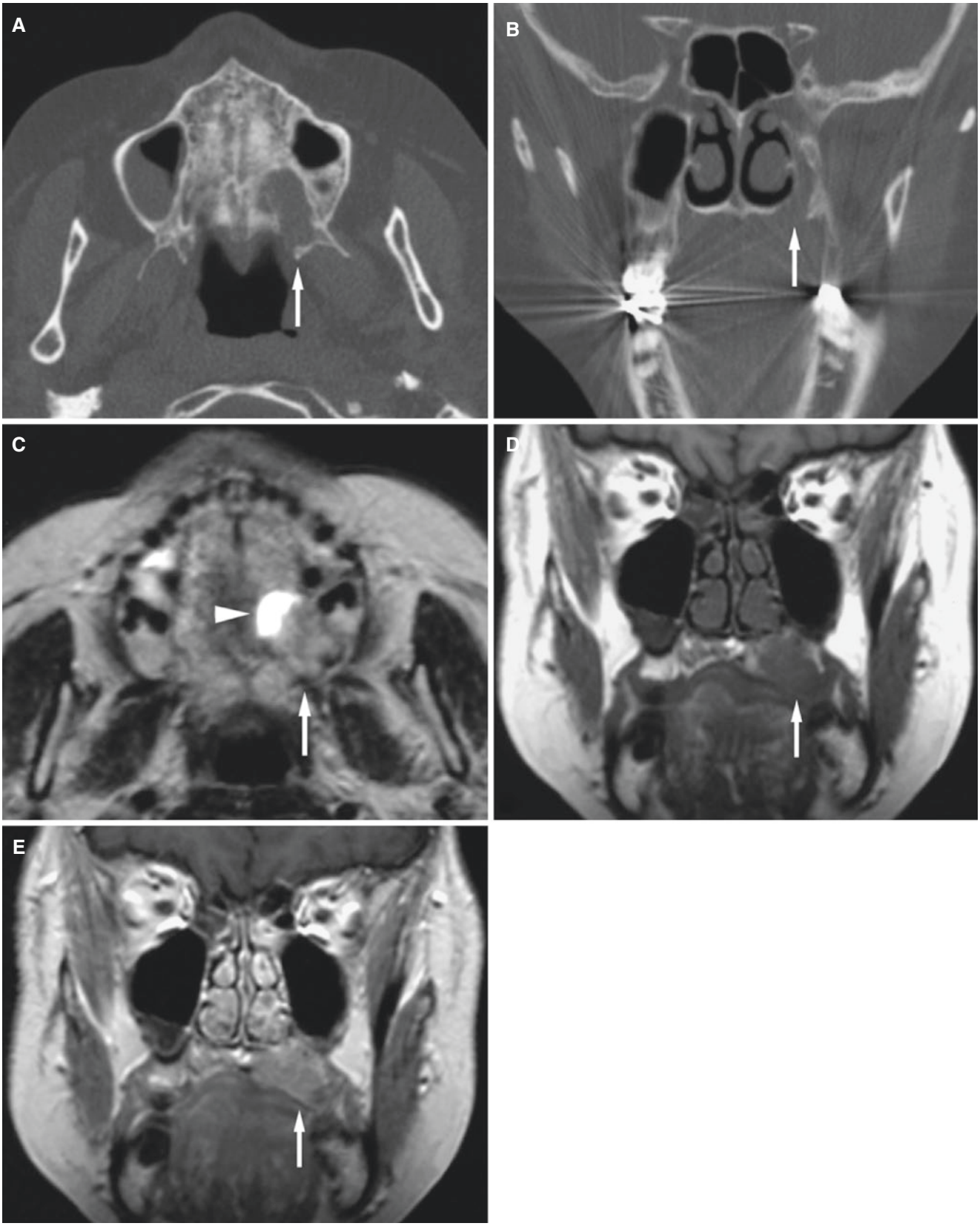

Fig. 4.13 Adenoid cystic carcinoma, maxilla; 70-year-old female with painless swelling in the hard palate; aspiration from soft part showed "fluid." (**A**) Axial CT image shows destruction in the hard palate (*arrow*). (**B**) Coronal CT image shows widened major palatine foramen and pterygopalatine fissure (*arrow*). (**C**) Axial T2-weighted MRI shows high signal consistent with fluid (*arrowhead*) and tumor (*arrow*). (**D**) Coronal T1-weighted pre-Gd MRI shows reduced signal in bone marrow; intermediate–low signal of tumor (*arrow*). (**E**) Coronal T1-weighted post-Gd MRI shows contrast enhancement of tumor (*arrow*)

4.6 Non-Hodgkin's Lymphoma

Figs. 4.14, 4.15, 4.16, 4.17, and 4.18

4.6.1 Definition

Malignancy of the lymphatic system without Reed–Sternberg cells (as opposed to Hodgkin's lymphoma presenting with Reed–Sternberg cells).

4.6.2 Clinical Features

- May involve all types of lymphocytes, most commonly B-cells.
- Most commonly seen in lymph nodes but may involve extranodal sites.
- Such sites include maxillary sinus and maxilla or, less frequently, mandible.
- Hodgkin's lymphoma is predominantly a nodal disease.
- All age groups, adults in particular (except Burkitt's lymphoma).
- Burkitt's (non-Hodgkin's) lymphoma was initially described as African jaw lymphoma, affects children, shows rapid growth, and may involve one or both jaws.

4.6.3 Imaging Features

- Soft-tissue mass
- Radiolucency
- Border of bone destruction ill defined
- Non-Hodgkin's lymphoma, and rarely Hodgkin's lymphoma, may present with necrotic lymph nodes
- However, it is not possible to definitely distinguish between non-Hodgkin's, Hodgkin's, and metastatic lymph nodes based on CT and MRI
- T1-weighted MRI: intermediate–low signal
- T2-weighted and STIR MRI: intermediate signal
- T1-weighted post-Gd MRI: contrast enhancement

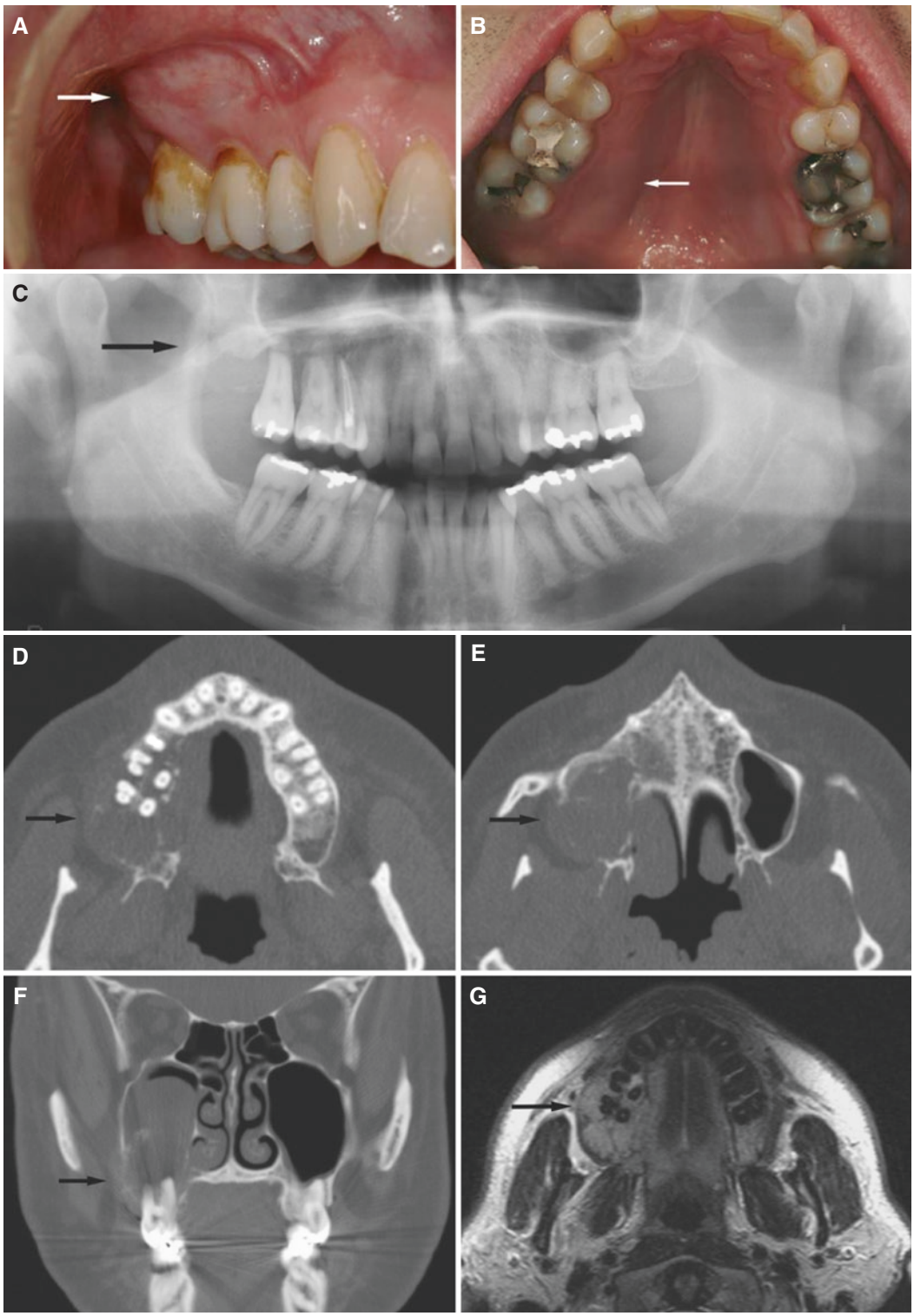

Fig. 4.14 B-cell lymphoma, maxilla; 49-year-old male with slight swelling, painless, but treated for apical periodontitis in the right maxilla. (**A**) Clinical photograph shows buccal swelling with normal mucosa (*arrow*). (**B**) Clinical photograph shows palatal swelling with normal mucosa (*arrow*). (**C**) Panoramic view shows diffuse alveolar bone destruction (*arrow*). (**D**) Axial CT image shows ill-defined alveolar bone destruction (*arrow*). (**E**) Axial CT image shows ill-defined bone destruction of sinus walls (*arrow*). (**F**) Coronal CT image shows bone destruction and tumor in maxillary sinus (*arrow*). (**G**) Axial T2-weighted MRI shows expanded alveolar bone with intermediate–low signal (*arrow*). (**H**) Coronal STIR MRI shows intermediate signal of tumor (*arrow*) and high signal from mucosal thickening in maxillary sinus. (**I**) Axial T1-weighted pre-Gd MRI shows intermediate–low-signal tumor in bone marrow of maxilla (*arrow*). (**J**) Axial T1-weighted post-Gd MRI shows contrast enhancement of tumor (*arrow*). (**K**) Coronal T1-weighted post-Gd MRI shows contrast enhancement of tumor (*arrow*)

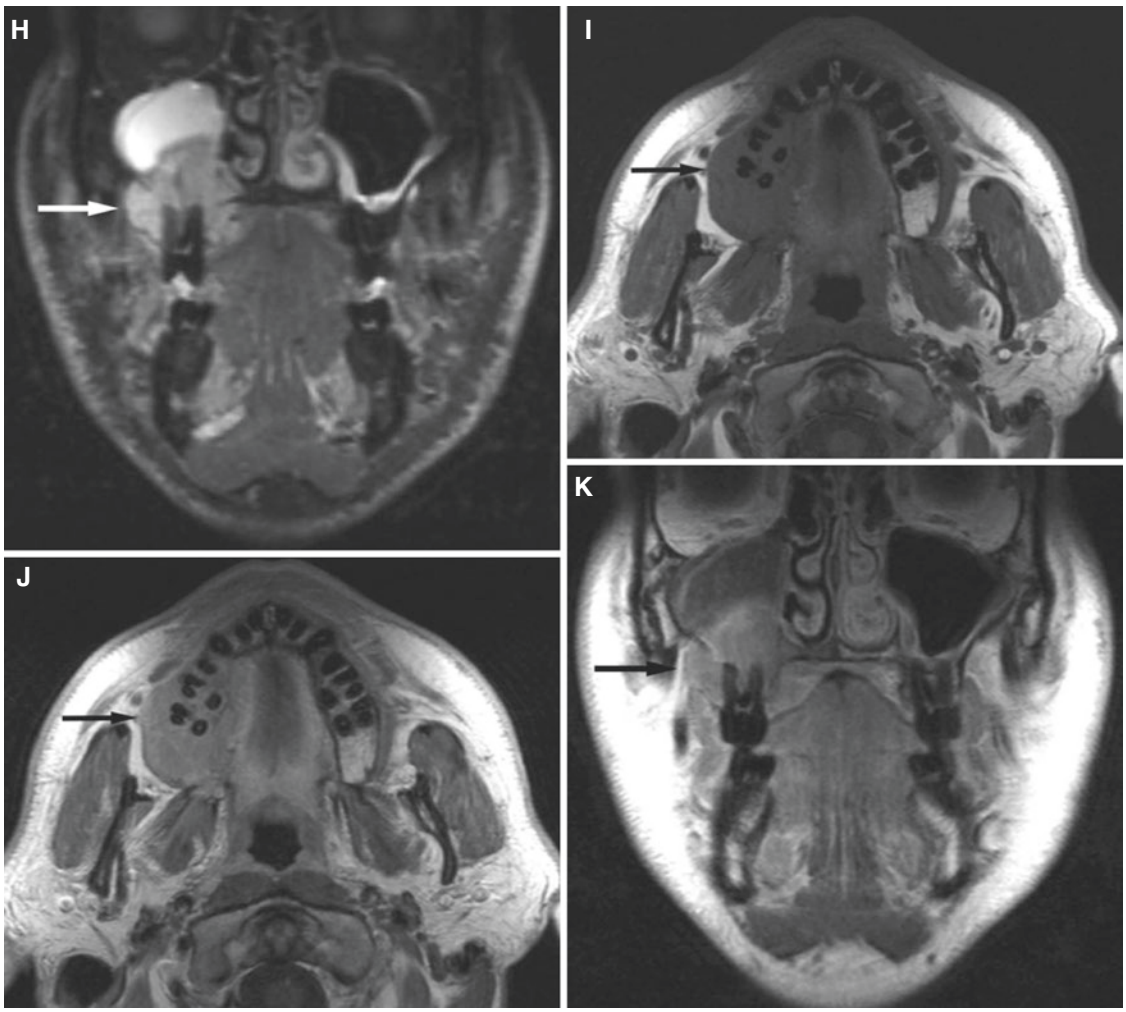

Fig. 4.14 (continued)

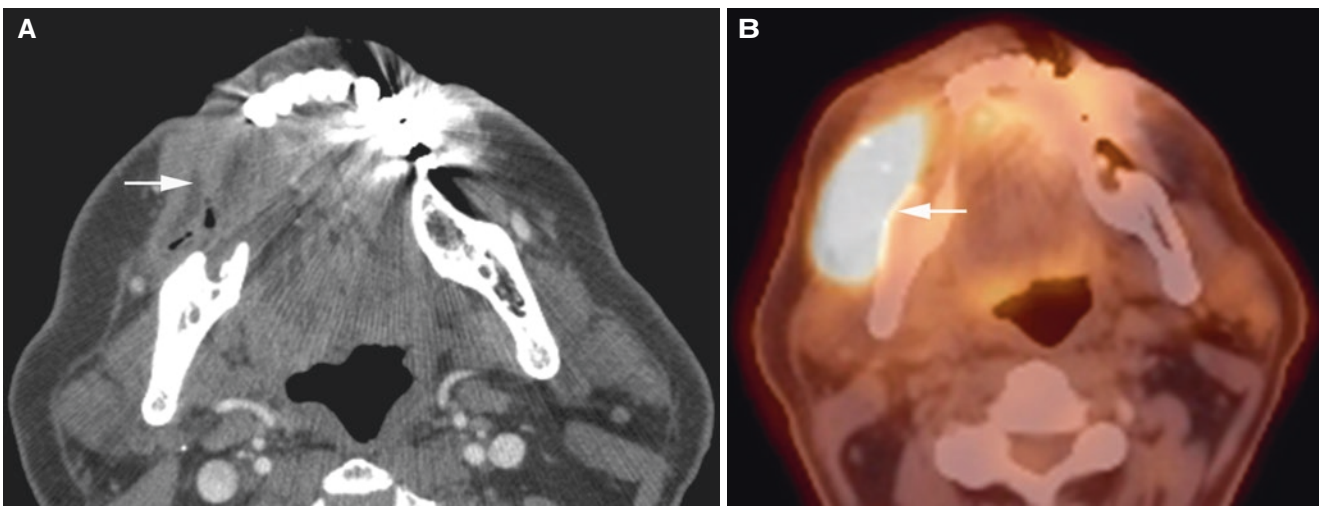

Fig. 4.15 B-cell lymphoma, mandible; 53-year-old male with right-sided neck mass. (**A**) Contrast-enhanced axial CT image shows destruction in the mandible (*arrow*). (**B**) Axial PET-CT image shows intense hypermetabolic activity in tumor (*arrow*)

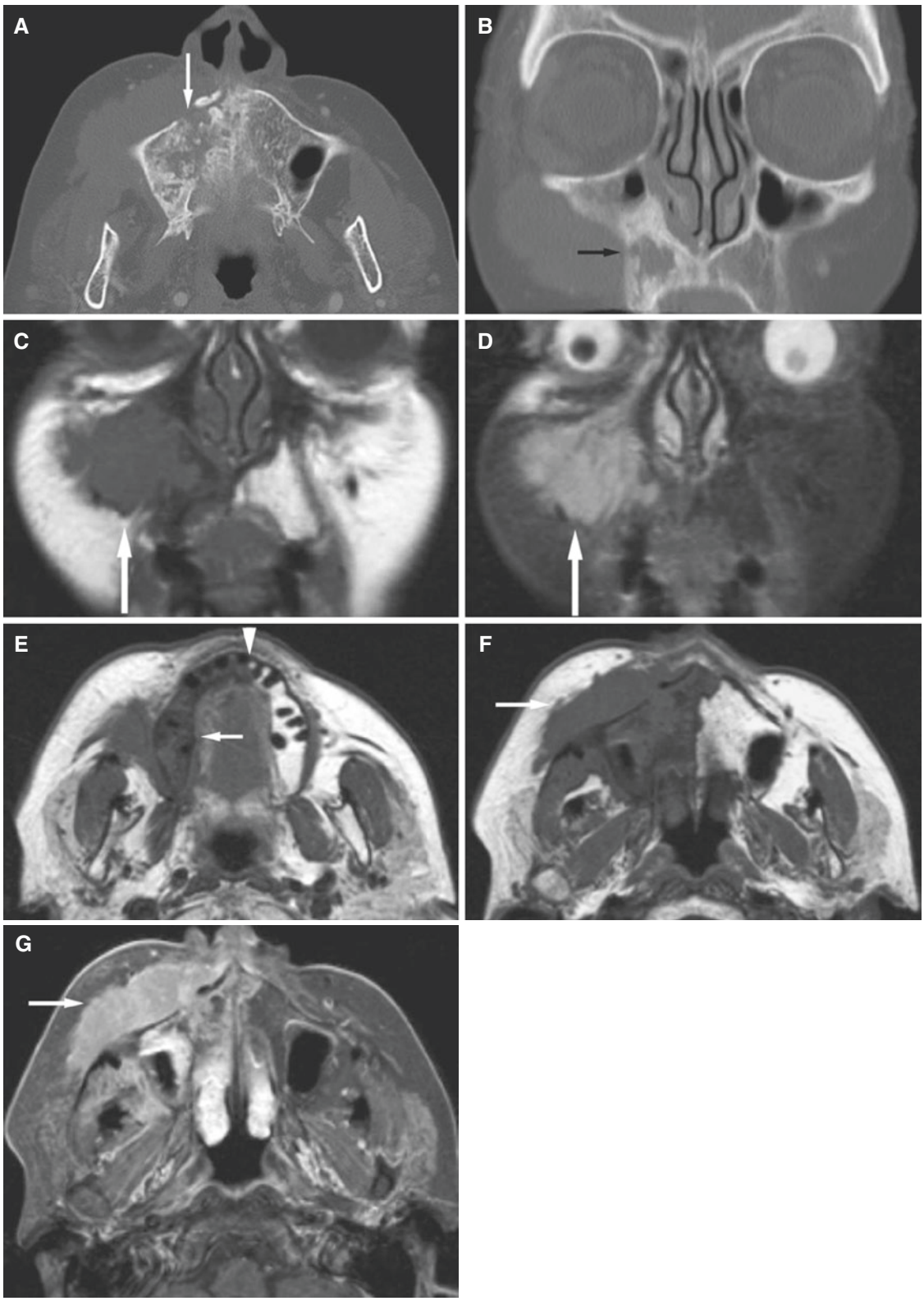

Fig. 4.16 B-cell lymphoma, maxilla; 74-year-old female with painless swelling of the cheek. (**A**) Axial CT image shows ill-defined bone destruction of the palate (*arrow*). (**B**) Coronal CT image shows ill-defined bone destruction of the alveolar bone (*arrow*). (**C**) Coronal T1-weighted pre-Gd MRI shows intermediate–low-signal tumor in bone marrow (*arrow*). (**D**) Coronal STIR MRI shows intermediate–high-signal tumor (*arrow*). (**E**) Axial T1-weighted pre-Gd MRI shows intermediate–low-signal tumor in buccal soft tissue and marrow of the alveolar bone (*arrow*), crossing the midline (*arrowhead*). (**F**) Axial T1-weighted pre-Gd MRI shows intermediate–low-signal tumor in more than half of maxilla and in buccal soft tissue (*arrow*). (**G**) Axial T1-weighted fat sat post-Gd MRI shows contrast enhancement in bone and soft tissue (*arrow*)

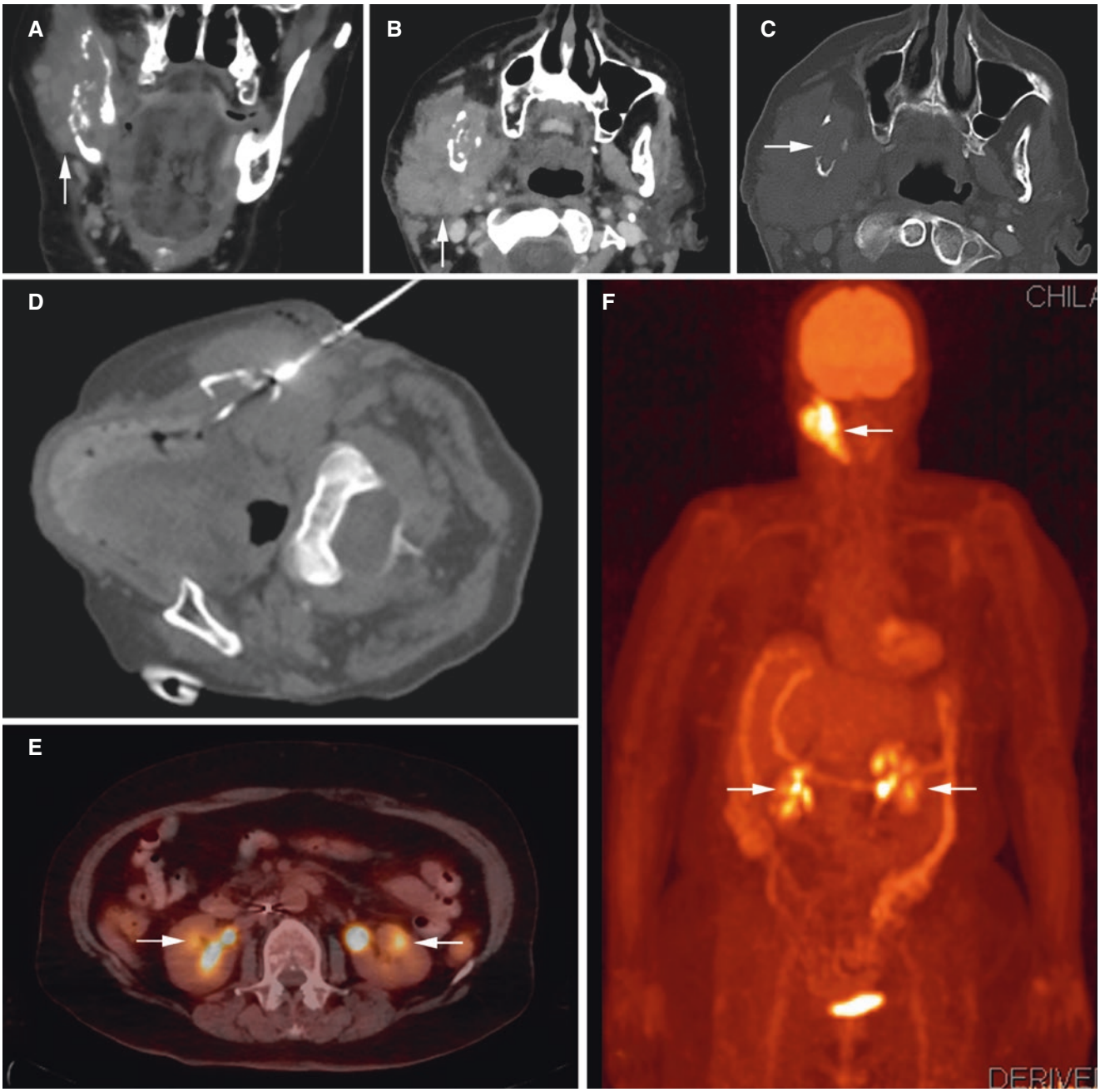

Fig. 4.17 B-cell lymphoma, mandible; 80-year-old female with mass in the right cheek. (**A**) Coronal (soft-tissue window) and (**B**) axial (soft-tissue window) CT images show destruction of mandibular ramus and soft-tissue mass (*arrow*). (**C**) Axial (bone window) CT image shows severe destruction of mandibular ramus (*arrow*). (**D**) Percutaneous core biopsy of tumor using a 16-gauge core biopsy needle. (**E**) Axial PET-CT image shows intense hypermetabolic activity consistent with lymphoma involvement of both kidneys (*arrows*). (**F**) Whole-body PET scanning shows intense hypermetabolic activity in the mandible and in both kidneys (*arrows*)

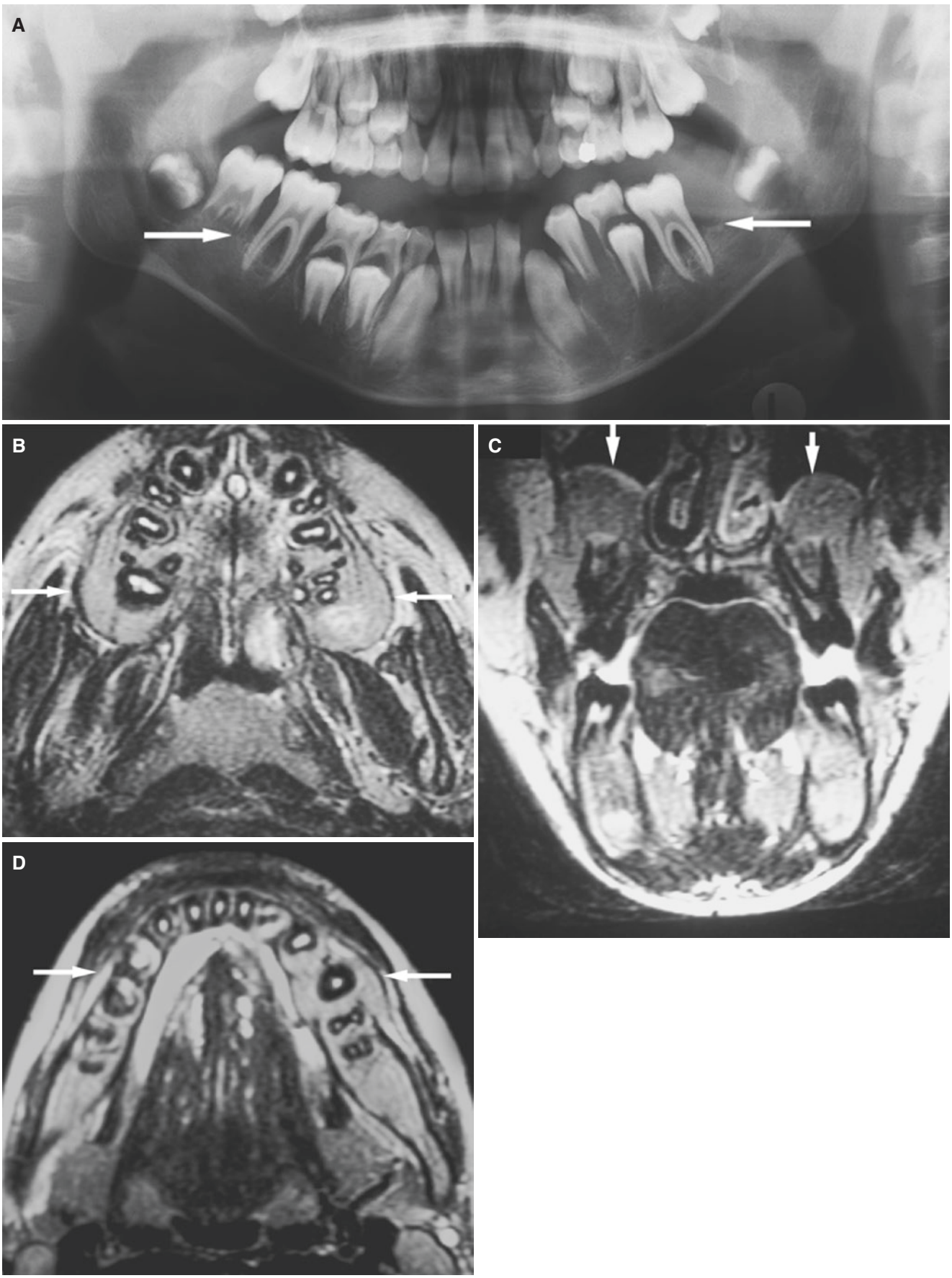
A
B
C
D

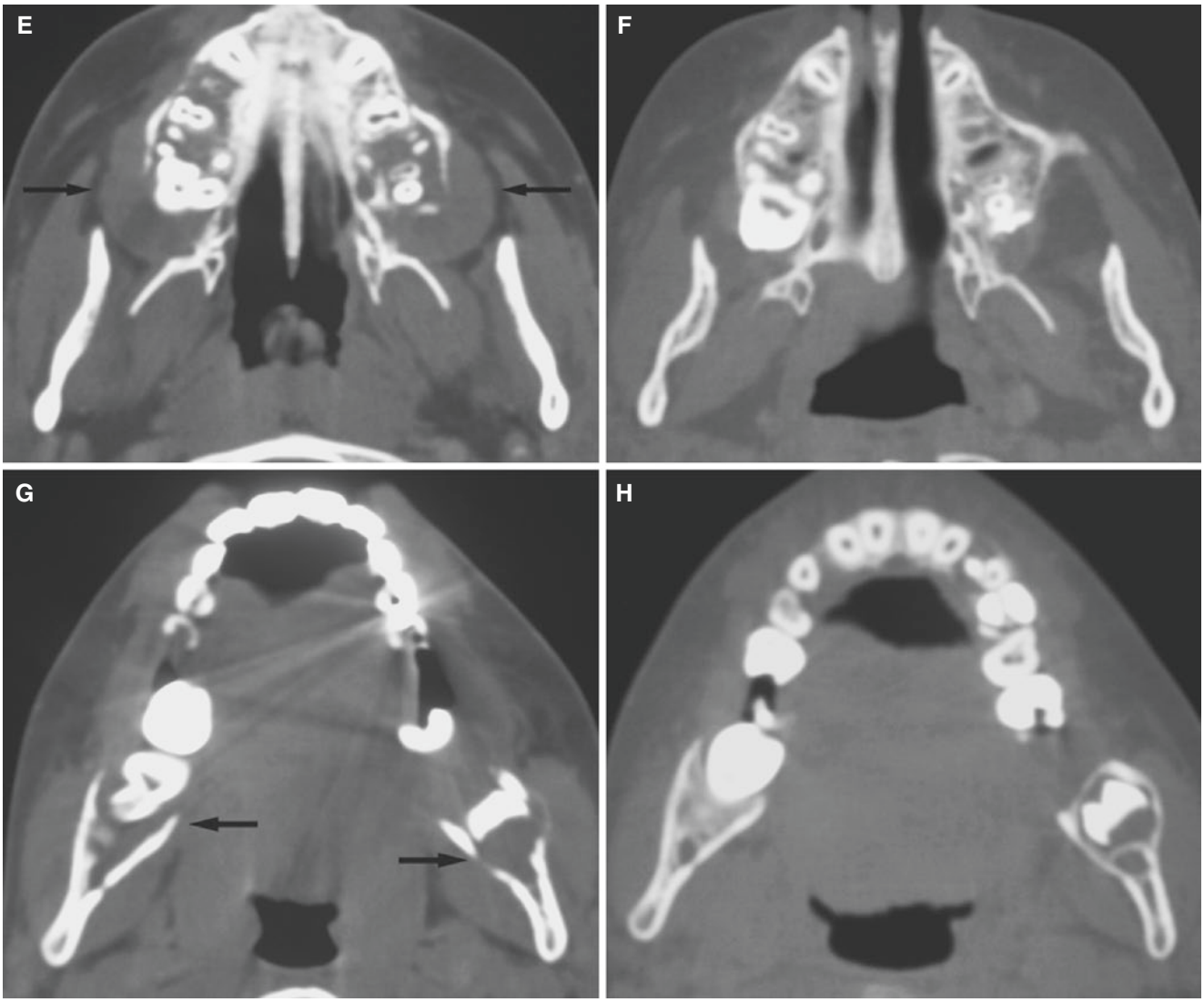

Fig. 4.18 (continued)

Fig. 4.18 Burkitt's lymphoma, mandible and maxilla; 11-year-old male with swelling of the upper and lower jaw. (**A**) Panoramic view shows destruction of the alveolar bone bilaterally in molar area (*arrows*). (**B**) Axial T2-weighted MRI shows expansion of alveolar processes bilaterally in the maxilla (*arrows*). (**C**) Coronal T2-weighted MRI shows tumor in maxillary sinus bilaterally (*arrows*). (**D**) Axial T2-weighted MRI shows tumor expansion bilaterally in the mandible (*arrows*). (**E**) Axial CT image shows expansion of maxilla with bone destruction bilaterally (*arrows*). (**F**) Axial CT image, 2 months posttreatment, shows near normalization of the maxilla. (**G**) Axial CT image shows bone destruction of mandible bilaterally (*arrows*). (**H**) Axial CT image, 2 months posttreatment, shows near normalization of the mandible

4.7 Multiple Myeloma

Figs. 4.19, 4.20, and 4.21

Synonyms: Myeloma, myelomatosis.

4.7.1 Definition

Malignant tumor, usually with multiple or diffuse bone involvement by neoplastic plasma cells showing varying degrees of immaturity, including atypical forms. Lesions are often associated with the presence of abnormal proteins in blood and urine and occasionally with the presence of amyloid or para-amyloid in tumor tissue or other organs (WHO).

Plasmacytoma is a solitary form of multiple myeloma.

4.7.2 Clinical Features

- Most common primary bone malignancy in adults
- Males more frequent than females
- Older age groups (50 years and older)
- Bone pain, malaise
- No curative treatment
- Jaw involvement seldom and usually asymptomatic

4.7.3 Imaging Features

- Multiple radiolucencies, skull more often than jaws
- Mandible more often than maxilla
- Punched-out bone destruction

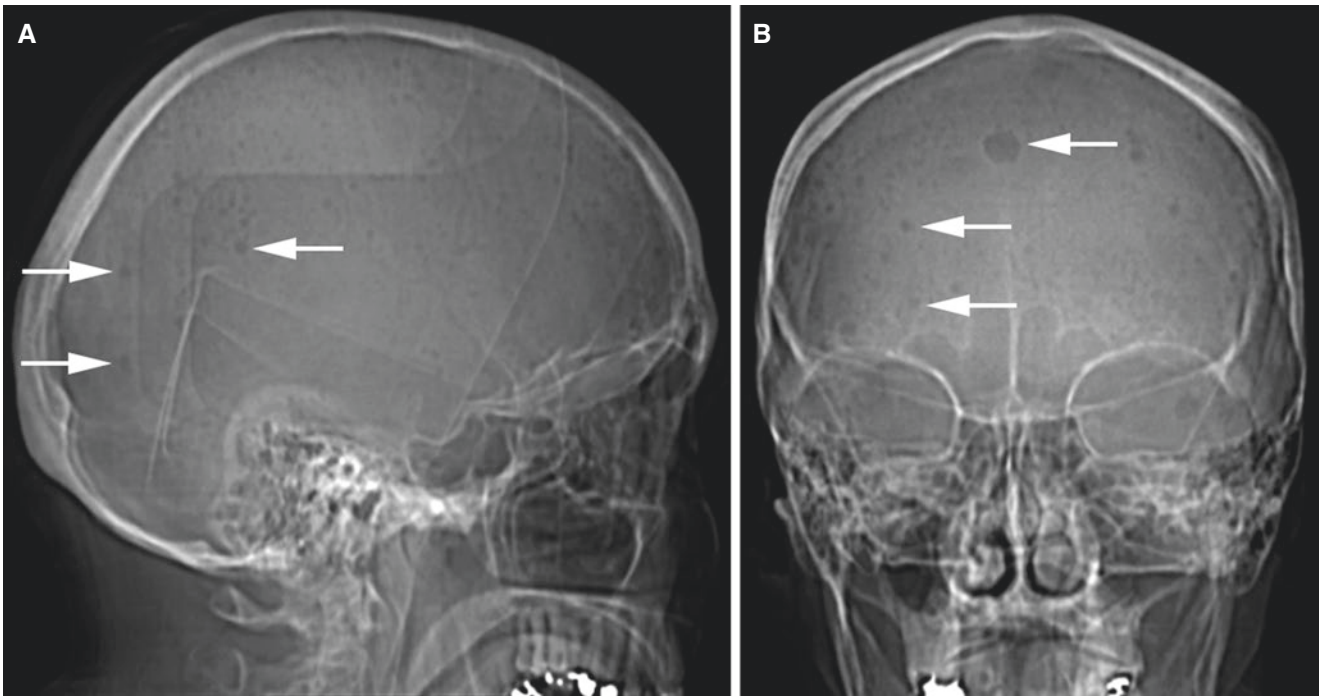

Fig. 4.19 Multiple myeloma, skull; 63-year-old female with incidental findings (discovered during paranasal sinus examination). (**A**) Lateral and (**B**) frontal CT scout view images show multiple punched-out radiolucencies in the skull without sclerotic margins (some radiolucencies indicated by *arrows*)

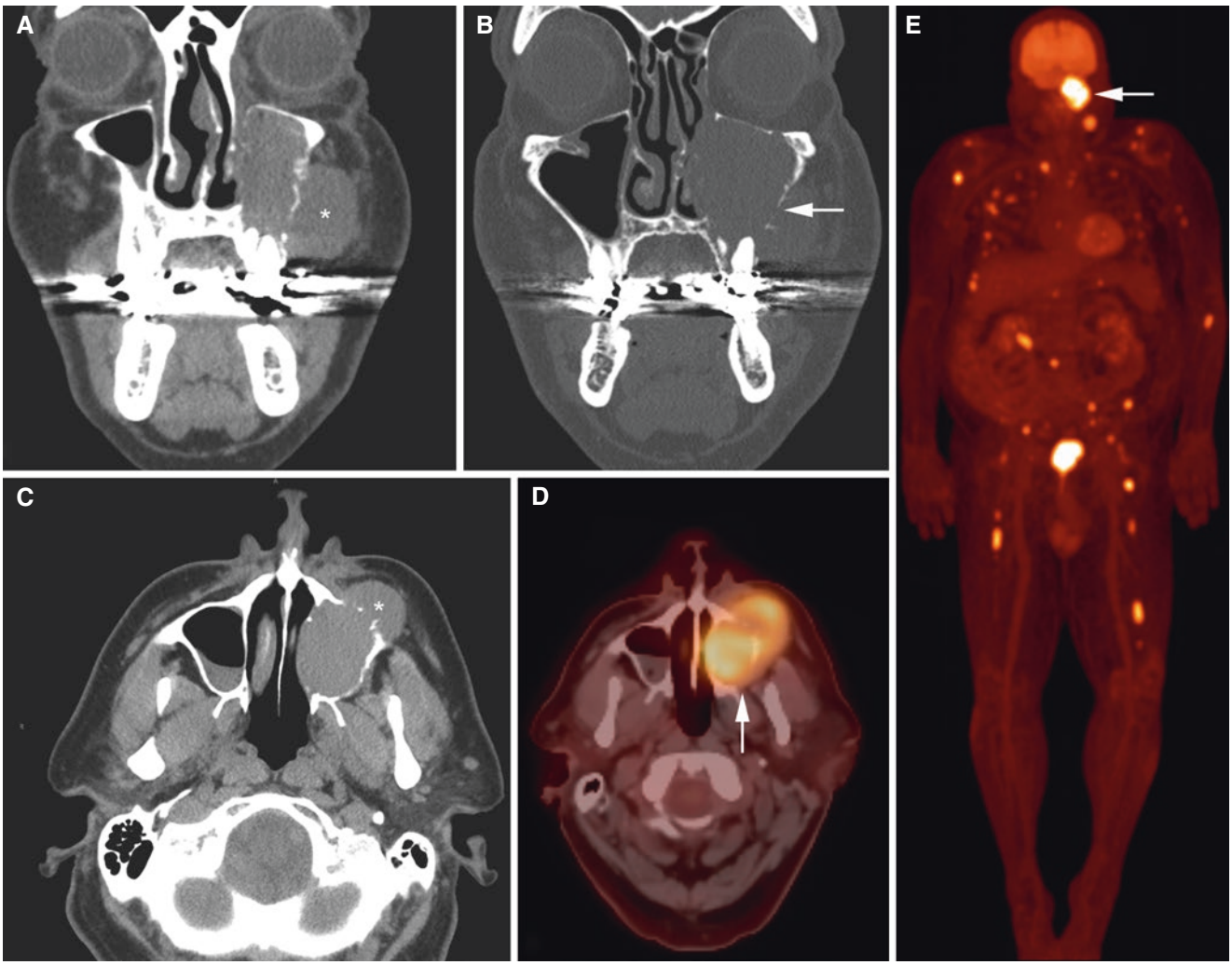

Fig. 4.20 Multiple myeloma, maxilla; 61-year-old male with mass in the left face. (**A**) Coronal (soft-tissue window) and (**B**) coronal (bone window) CT images show destruction of maxillary sinus anterior lateral wall (*arrow*) and a soft-tissue mass extending into facial soft tissues (*asterisk*). (**C**) Axial (soft-tissue window) CT image confirms soft-tissue mass in maxillary sinus and external to sinus in buccal soft tissues (*asterisk*). (**D**) Axial PET-CT image shows intense hypermetabolic activity in tumor (*arrow*). (**E**) Whole-body PET scanning shows hypermetabolic activity in facial skeleton (*arrow*) and diffusely in the rest of the skeleton

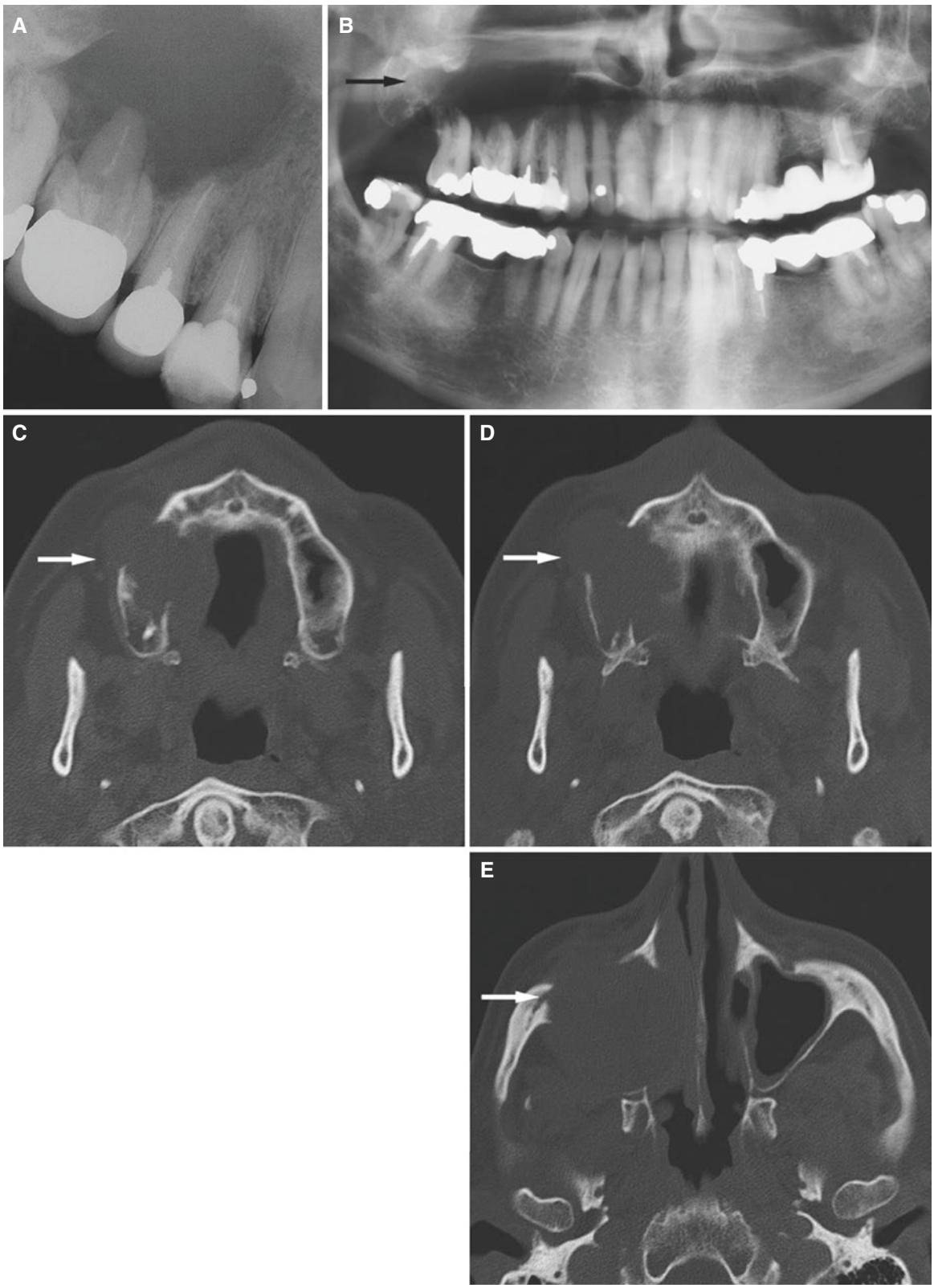

Fig. 4.21 Plasmacytoma, maxilla; 76-year-old male with diffuse pain in the right cheek, first treated for sinusitis and then endodontic treatment. (**A**) Intraoral view shows ill-defined bone destruction. (**B**) Panoramic view shows ill-defined demarcation of maxillary sinus (*arrow*). (**C**) Axial CT image shows destruction of alveolar process and soft-tissue mass (*arrow*). (**D**) Axial CT image shows destruction of the hard palate (*arrow*). (**E**) Axial CT image shows destruction of all walls of maxillary sinus (*arrow*) (courtesy of Drs. Sahlstrom, Eriksson, Lindh, and Warfvinge, University Hospital, Malmo, Sweden)

4.8 Leukemia

Fig. 4.22

4.8.1 Definition

Progressive malignancy of hematopoietic tissues, marked by diffuse replacement of bone marrow or lymph nodes and development of leukocytes and their precursors in blood and bone marrow.

Acute leukemias are accompanied by accumulation of immature or blast cells owing to the defect in the production of mature hemic cells; chronic leukemias are characterized by massive overgrowth of mature cells.

4.8.2 Clinical Features

- Acute and chronic forms
- Acute: younger age groups, usually with severe general symptoms (such as bone pain, fever, lymphadenopathy, general fatigue, and loss of appetite)
- Chronic: adults, usually with few or no symptoms
- Oral symptoms may include gingival inflammation and hyperplasia, ulceration, bleeding, petechiae, and loose teeth

4.8.3 Imaging Features

- Radiolucency
- Border of bone destruction ill defined
- Loss of lamina dura and floating teeth
- No bone expansion
- Jaw abnormalities reported in half of the patients or more
- One jaw, unilateral or bilateral, or both jaws
- MRI abnormalities with normal CT findings
- T1-weighted fat-suppressed post-Gd MRI: high signal from bone marrow and diffuse enhancement in surrounding soft tissue

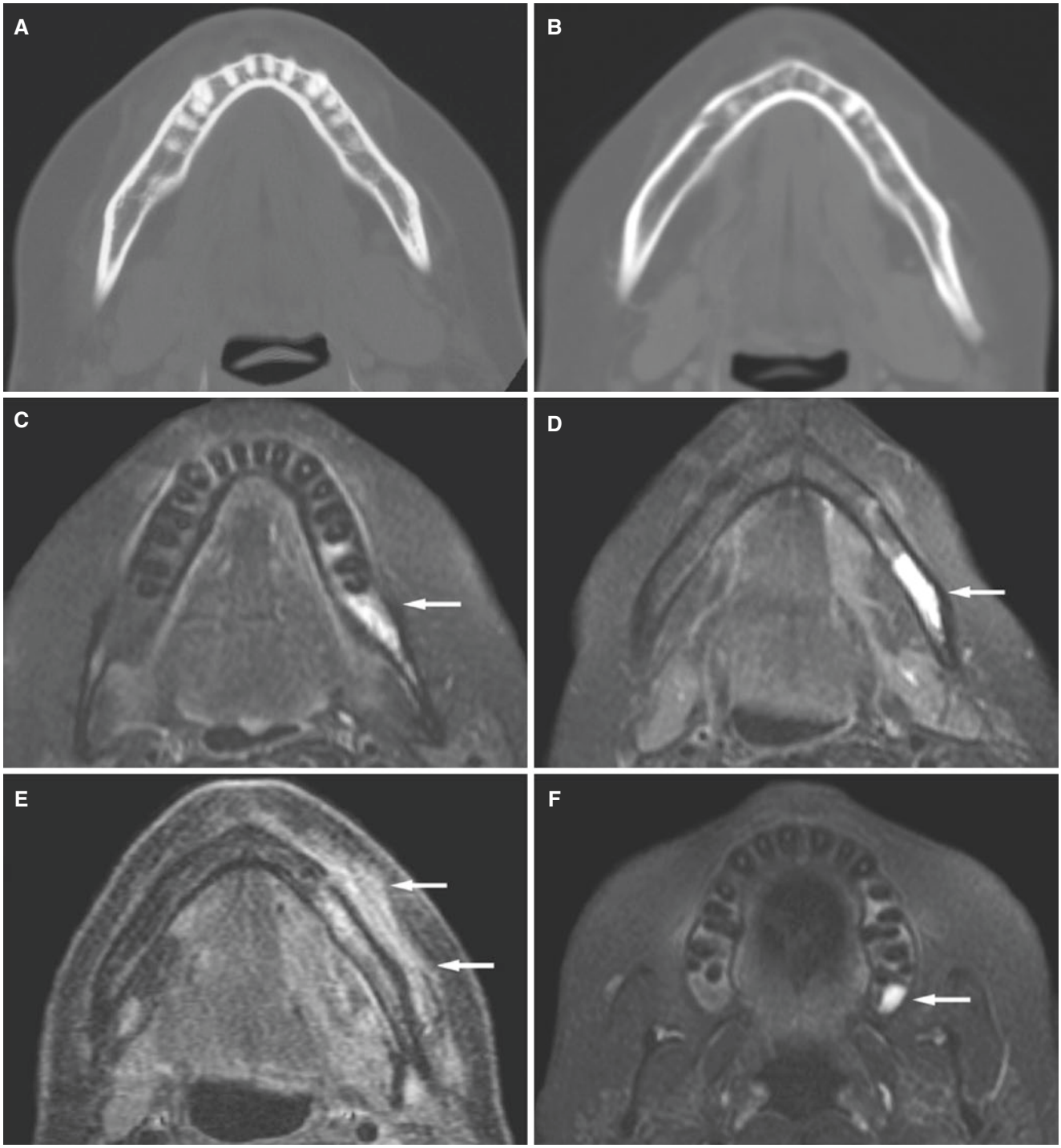

Fig. 4.22 Leukemia, mandible and maxilla; 42-year-old female with numbness and weakness of the left jaw. (**A**) Axial CT image shows normal bone of tooth-bearing areas. (**B**) Axial CT image shows normal bone caudad to teeth. (**C**) Axial T1-weighted fat sat post-Gd MRI shows high signal in bone marrow of tooth-bearing area (*arrow*). (**D**) Axial T1-weighted fat sat post-Gd MRI shows high signal from bone marrow caudad to teeth (*arrow*). (**E**) Axial T1-weighted fat sat post-Gd MRI shows diffuse enhancement also in surrounding soft tissue, buccally in particular (*arrows*), but also lingually. (**F**) Axial T1-weighted fat sat post-Gd MRI shows high signal in marrow of the maxilla (*arrow*)

4.9 Bone-Destructive and Bone-Productive Tumors

Osteosarcoma, chondrosarcoma, and Ewing sarcoma are illustrated.

4.10 Osteosarcoma

Figs. 4.23, 4.24, 4.25, 4.26, and 4.27

Synonym: Osteogenic sarcoma.

4.10.1 Definition

Malignant tumor characterized by direct formation of bone or osteoid by tumor cells (WHO).

4.10.2 Clinical Features

- Most common primary malignancy in the skeleton (apart from myeloma), usually in bones around the knee and primarily in children and adolescents; pain common
- Only 5–10% in the head and neck; mostly in jaws
- Usually painless swelling in jaws, but also pain and mental nerve paresthesia
- Mandible slight predominance
- Males slight predominance
- May occur in any age group; peak in the fourth decade
- Jaw osteosarcomas have tendency to occur in older patients than osteosarcomas in other bones and less likely to metastasize
- However, prognosis of jaw sarcoma is poor and does not seem to have improved with chemotherapy in a similar way to sarcomas in other bones
- Main cause of death is local recurrence

4.10.3 Imaging Features

- Soft-tissue mass, may grow aggressively and rapidly
- Radiolucent or, most frequently, a combination of radiolucent and radiopaque appearance; bone production may be extensive
- Border of bone destruction ill defined
- Bone production may typically have "sunburst" appearance, best seen on CT images
- T1-weighted MRI: heterogeneous (intermediate–low) signal
- T2-weighted and STIR MRI: heterogeneous signal (variable high to intermediate–low) depending on bone production and cellular content
- T1-weighted post-Gd MRI: heterogeneous (intense to low) contrast enhancement

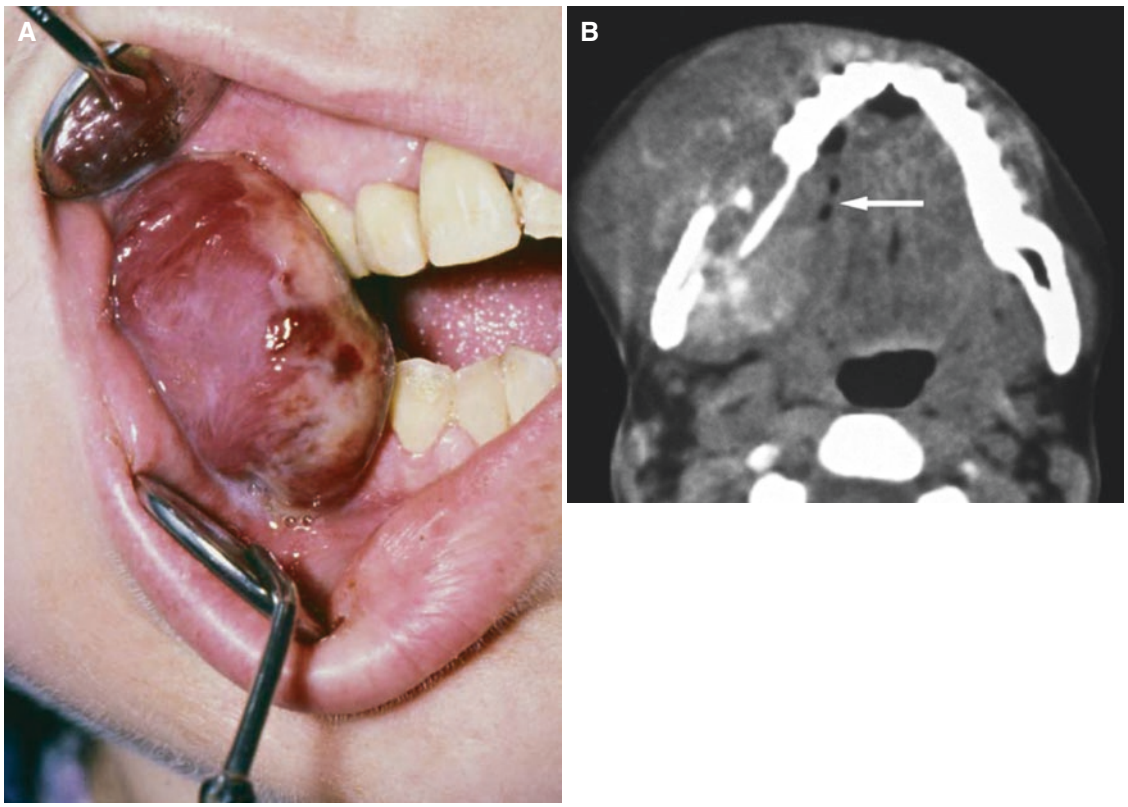

Fig. 4.23 Osteosarcoma, mandible; 37-year-old female with aggressive tumor growth, which "exploded" after extraction of the molar tooth in the right mandible. (**A**) Clinical photograph shows rapidly growing tumor mass. (**B**) Axial CT image shows bone destruction and aggressive tumor both buccally and lingually (*arrow*)

Fig. 4.24 Osteosarcoma, maxilla; 43-year-old male after about 6 months of chemotherapy now presenting for presurgical evaluation. Coronal CT image shows expansive process with intense radiating bone production (*lateral arrow*) around intensively sclerotic alveolar bone (*arrow*)

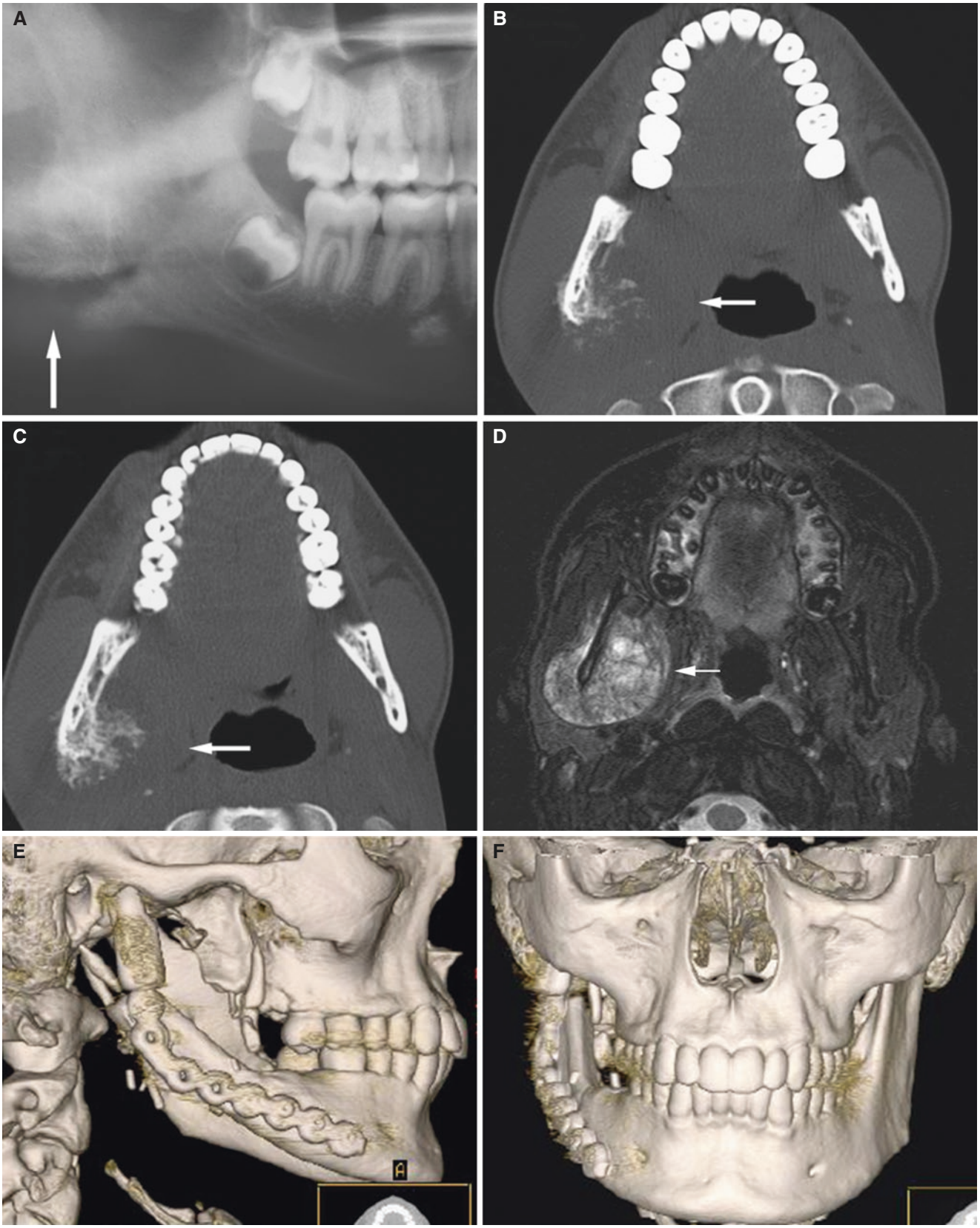

Fig. 4.25 Osteosarcoma, mandible; 16-year-old male with painless buccal swelling at the right mandibular angle. (**A**) Panoramic view shows diffuse bone mass (*arrow*). (**B**) Axial CT image shows bone production radiating from ramus, predominantly on lingual side (*arrow*). (**C**) Axial CT image shows more extensive bone production with evident sunburst appearance (*arrow*). (**D**) Axial T2-weighted MRI shows tumor with high to intermediate signal intensity, surrounding mandibular ramus (*arrow*). (**E**, **F**) Postoperative 3D CT images show right mandible reconstructed with fibula graft

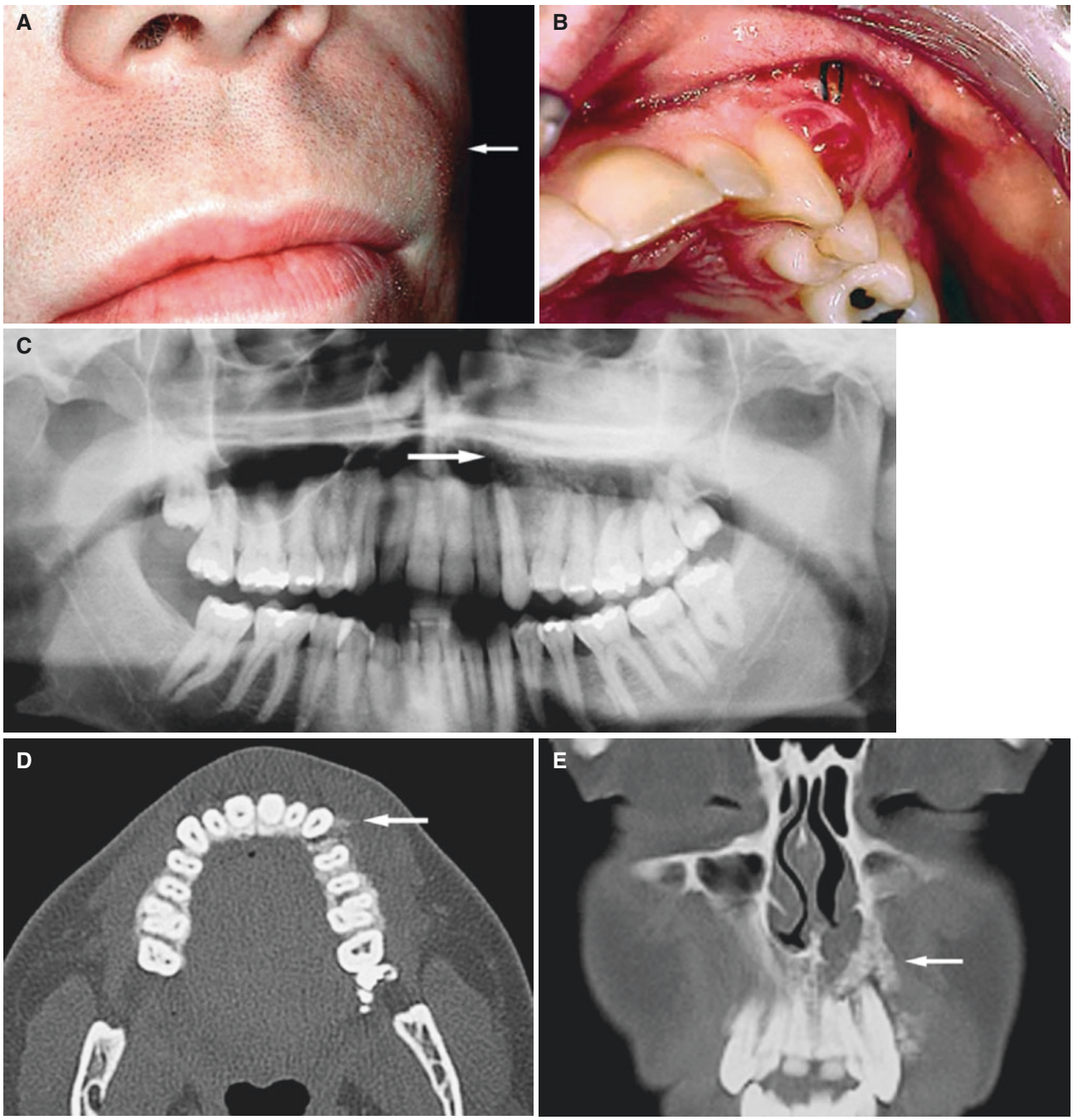

Fig. 4.26 Osteosarcoma, maxilla; 28-year-old male with painless swelling of the vestibulum. (**A**) Clinical photograph shows swelling of the lip (*arrow*). (**B**) Clinical photograph shows swelling of the gingiva (after biopsy). (**C**) Panoramic view shows opaque left maxillary sinus with absent alveolar sinus demarcation (*arrow*) and possible periapical bone destruction at the first molar. (**D**) Axial CT image shows bone production with sunburst appearance (*arrow*). (**E**) Coronal CT image shows destruction of piriform aperture (*arrow*) and bone production at canine. (**F**) Coronal CT image shows left maxillary sinus opacity with expanded floor of orbit and bone production in sinus walls (*arrow*). (**G**) Coronal T1-weighted fat sat post-Gd MRI shows intense contrast enhancement of tumor in maxillary sinus (*arrow*) with low-signal bone production in alveolar part (*arrowhead*). (**H**) Axial T1-weighted pre-Gd (left) and post-Gd (right) MRI shows contrast-enhanced maxillary sinus tumor penetrating the sinus wall and alveolar ridge (*arrows*). (**I**) Clinical photo of orbit with titanium implants (*arrow*) to fixate eye prosthesis. (**J**) Eye prosthesis. (**K**) Denture. (**L**) Clinical photo 10 years after surgical treatment; patient has no recurrence or metastases (**I**, **J**, **K**, **L**: courtesy of W. Widnes, C. D. T. anaplastologist, Oslo University Hospital, Rikshospitalet, Oslo, Norway)

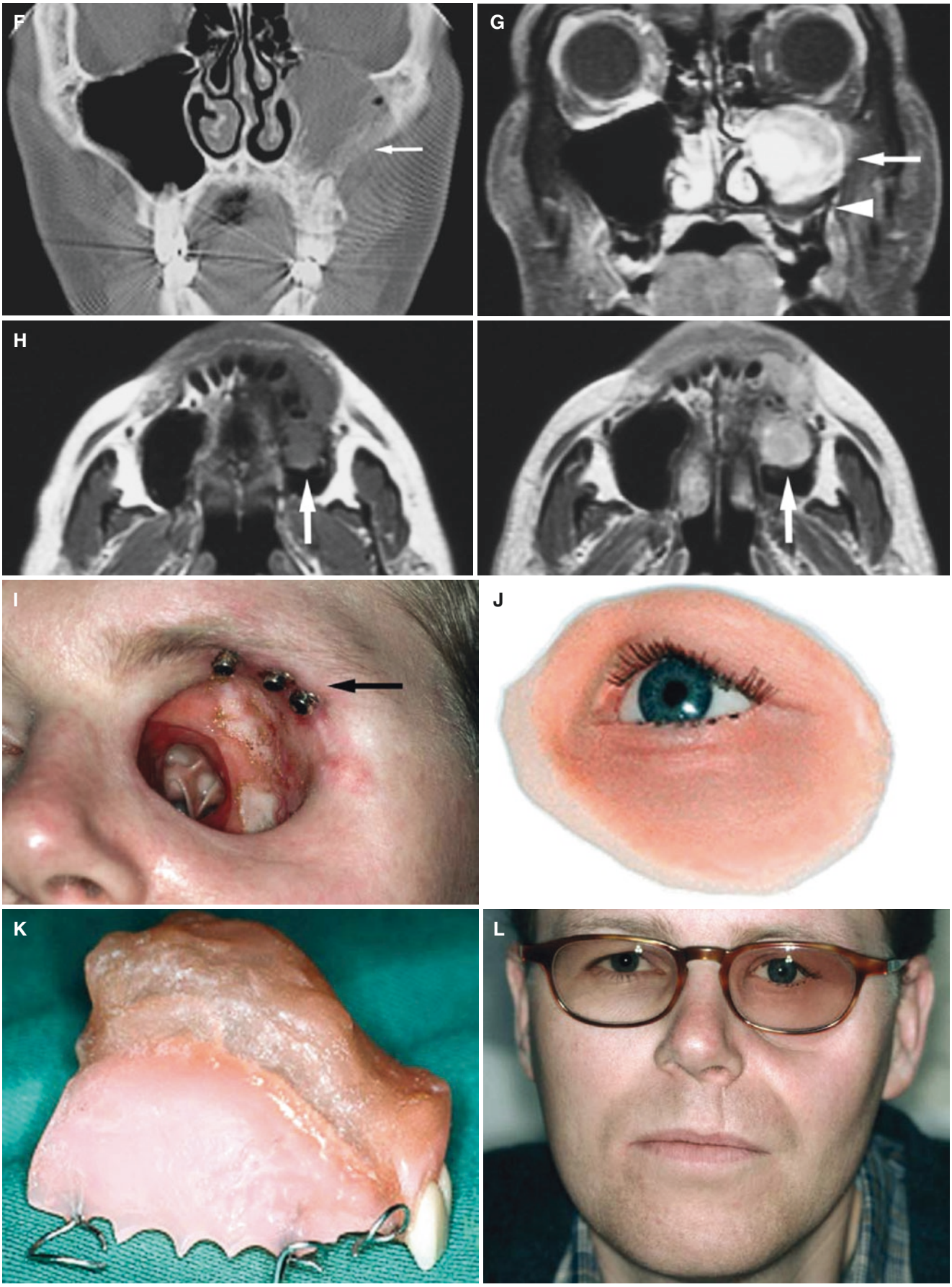

Fig. 4.26 (continued)

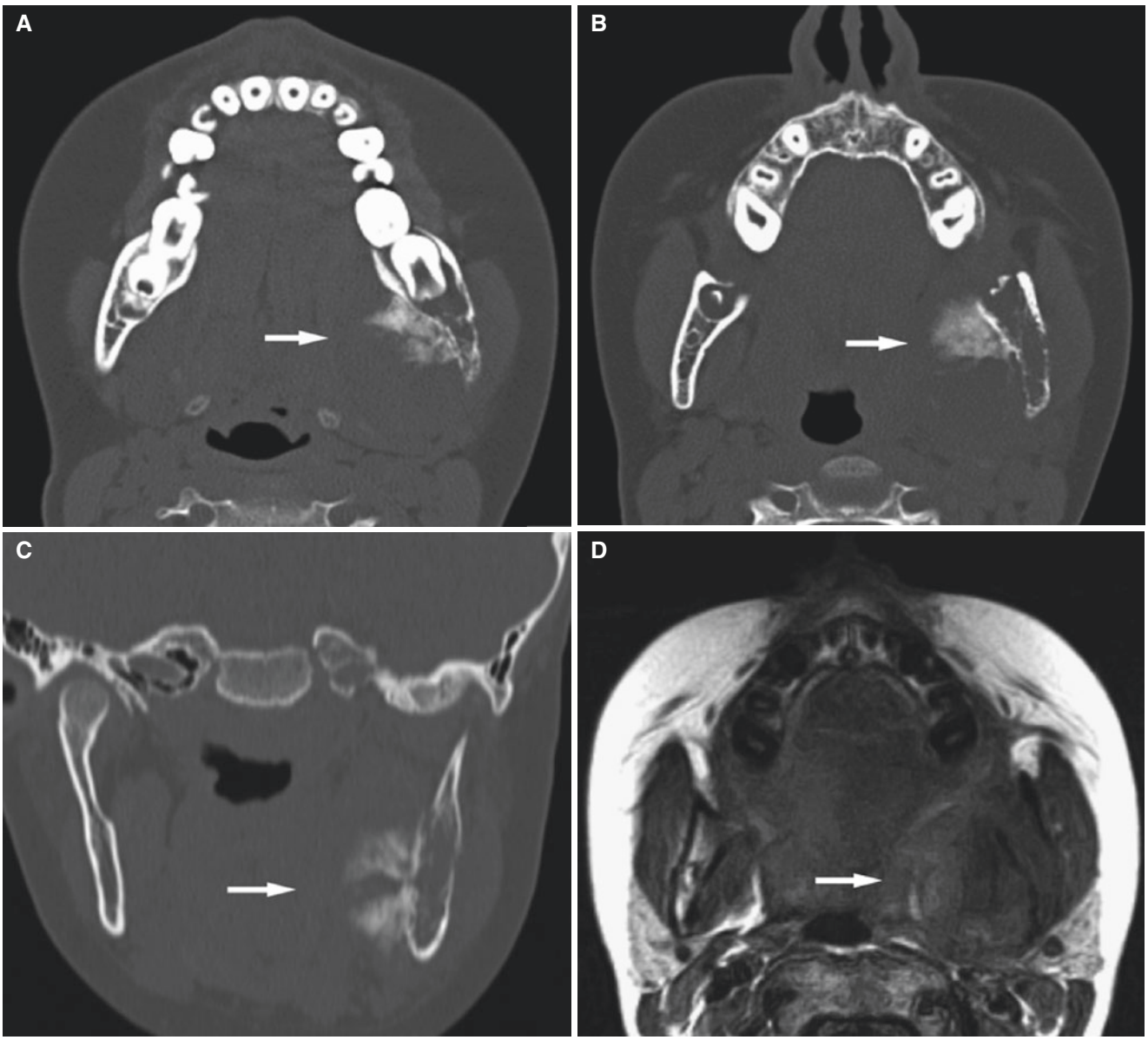

Fig. 4.27 Osteosarcoma, mandible; 10-year-old female with painful mass in the mandible and inability to open her mouth and 3-year history of femur osteosarcoma. (**A**) Axial CT image shows radiating bone production on lingual aspect of the mandible (*arrow*). (**B**) Axial CT image shows bone production and destruction of bone marrow and cortex (*arrow*). (**C**) Coronal CT image shows sunburst appearance (*arrow*). (**D**) Axial T1-weighted pre-Gd MRI shows intermediate–low-signal tumor lingually and in bone marrow (*arrow*). (**E**) Axial T1-weighted fat sat post-Gd MRI shows intense contrast enhancement in masseter muscle and heterogeneous (intense to low) enhancement of large lingual tumor (*arrow*) with displacement of the airway. (**F**) Axial T1-weighted fat sat post-Gd MRI shows another section of contrast enhancement (*arrow*), also in bone marrow. (**G**) Coronal T1-weighted fat sat post-Gd MRI shows tumor predominantly on lingual side (*arrow*)

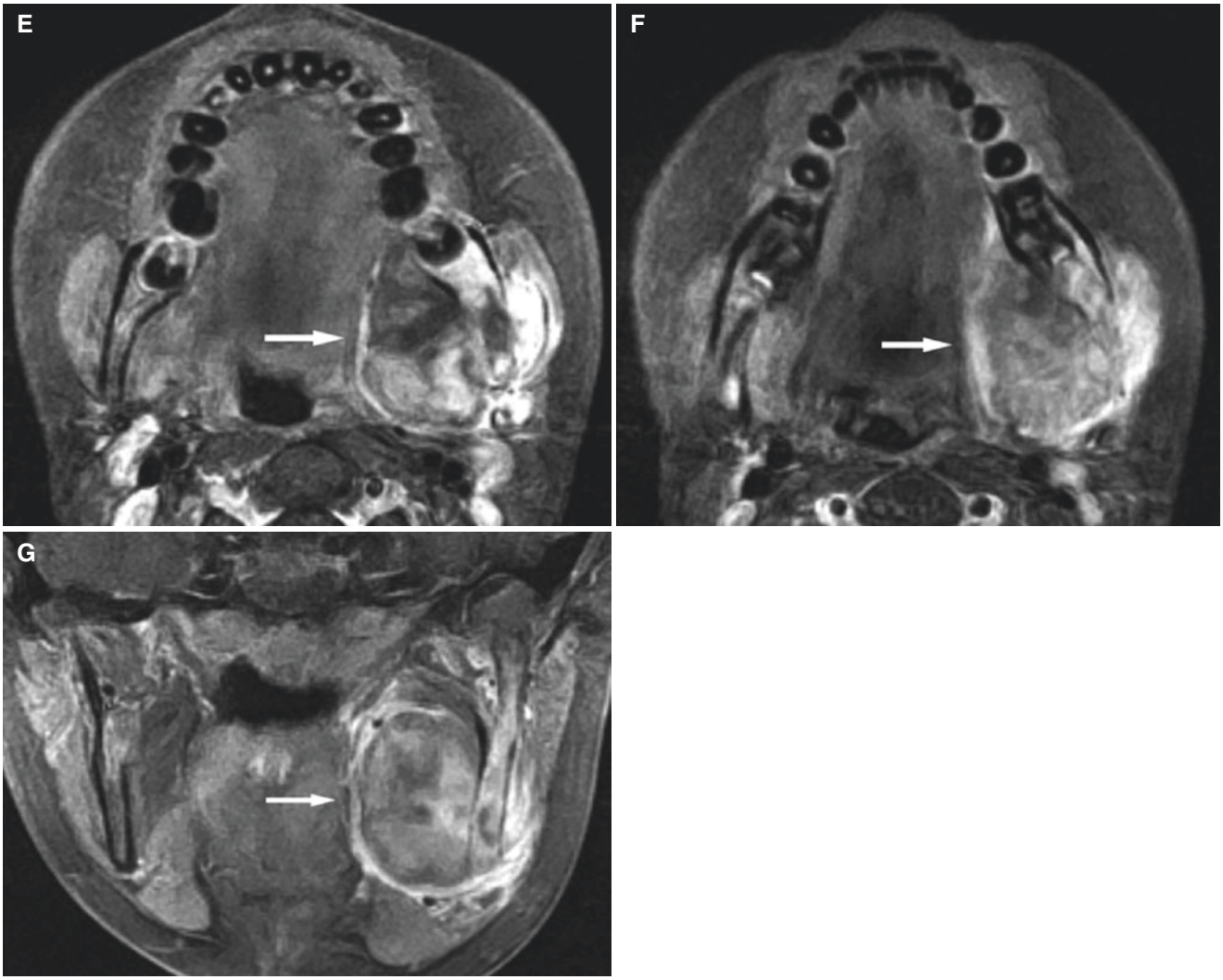

Fig. 4.27 (continued)

4.11 Chondrosarcoma

Fig. 4.28

4.11.1 Definition

Malignant tumor characterized by the formation of cartilage, but not of bone, by tumor cells. It is distinguished from chondroma by its higher cellularity, greater pleomorphism, and appreciable numbers of plump cells with large or double nuclei. Mitotic cells are infrequent (WHO).

May arise from a preexisting cartilaginous neoplasm.

4.11.2 Clinical Features

- Rather common
- Wide variation of clinical features
- Mostly in adults in fourth to sixth decades
- Less aggressive, more slowly growing than osteosarcoma
- Better prognosis; metastasizes more seldom than osteosarcoma
- Mandible and maxilla, but rare

4.11.3 Imaging Features

- Round soft-tissue mass with ring or crescent calcification characteristic, but may also show sunburst appearance
- MRI: heterogeneous (high to low) signal; see Osteosarcoma

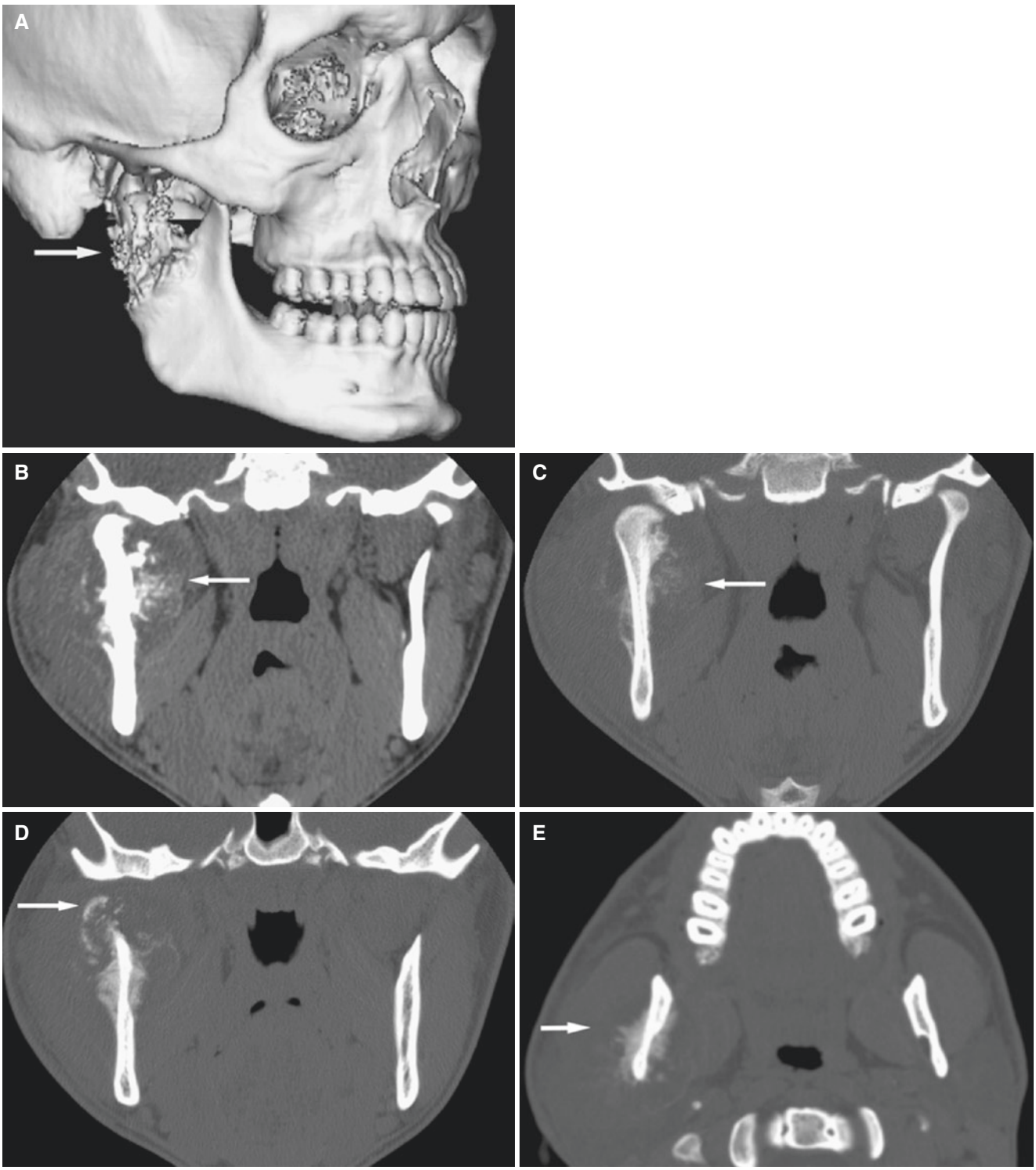

Fig. 4.28 Chondrosarcoma, mandible; 19-year-old male with facial swelling, no pain. (**A**) 3D CT image shows tumor in the right mandibular collum (*arrow*). (**B**) Coronal CT image, soft-tissue window, shows soft-tissue mass around ramus (*arrow*). (**C**) Coronal CT image shows radiating bone production (*arrow*). (**D**) Coronal CT image shows crescent calcification and dense sunburst appearance (*arrow*). (**E**) Axial CT image shows dense sunburst appearance (*arrow*)

4.12 Ewing Sarcoma

Figs. 4.29, 4.30, and 4.31

4.12.1 Definition

Malignant tumor with rather uniform histologic appearance composed of densely packed, glycogen-rich small cells with round nuclei but without prominent nucleoli or distinct cytoplasmic outlines. Tumor tissue is typically divided into irregular strands or lobules by fibrous septa, but intercellular network of reticulin fibers, which is a feature of malignant lymphoma, is not seen. Mitoses are generally infrequent. Hemorrhage and extensive areas of necrosis are common (WHO).

4.12.2 Clinical Features

- Only 1–4% in the head and neck area; most commonly the mandible
- Hard swelling, pain or pain-free
- Males more frequent than females
- Usually first and second decades, but may occur at any age

4.12.3 Imaging Features

- Soft-tissue mass
- "Moth-eaten" bone destruction
- Bone production characteristic; periosteal "onion skin" reaction (usually in long bones), but not so typical in jaws

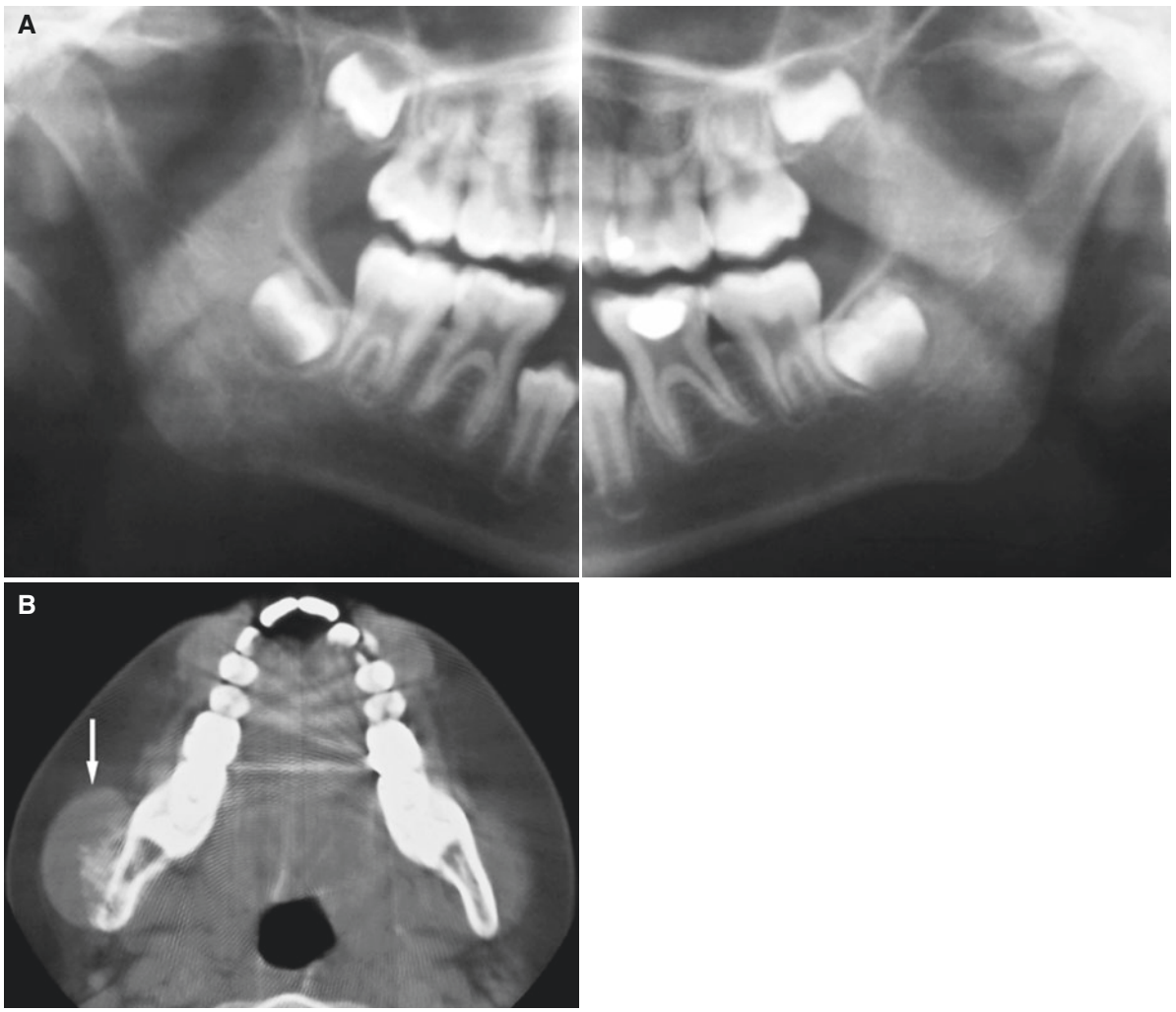

Fig. 4.29 Ewing sarcoma, mandible; 10-year-old male with painless swelling at the right mandibular angle. (**A**) Panoramic view shows no abnormality. (**B**) Axial CT image shows soft-tissue mass and radiating bone production on buccal aspect (*arrow*)

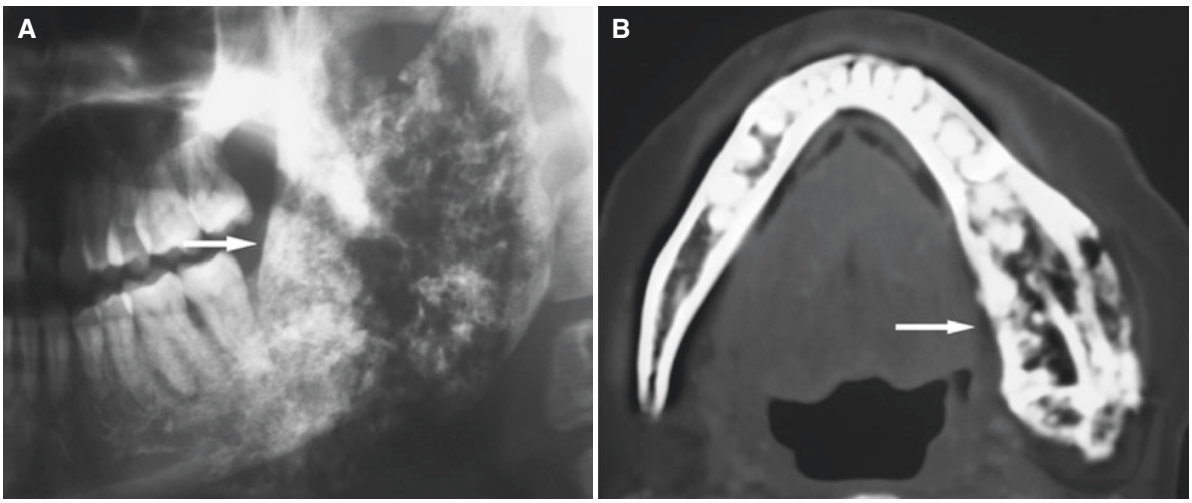

Fig. 4.30 Ewing sarcoma, mandible; 24-year-old female with 10-year history of Ewing sarcoma treated with radiotherapy and chemotherapy and a rather unchanged condition; now with pain and swelling and new soft-tissue mass, possibly due to infection. (**A**) Panoramic view shows bone production in the entire half of the mandible (*arrow*). (**B**) Axial CT image shows bone production both buccally and lingually (*arrow*)

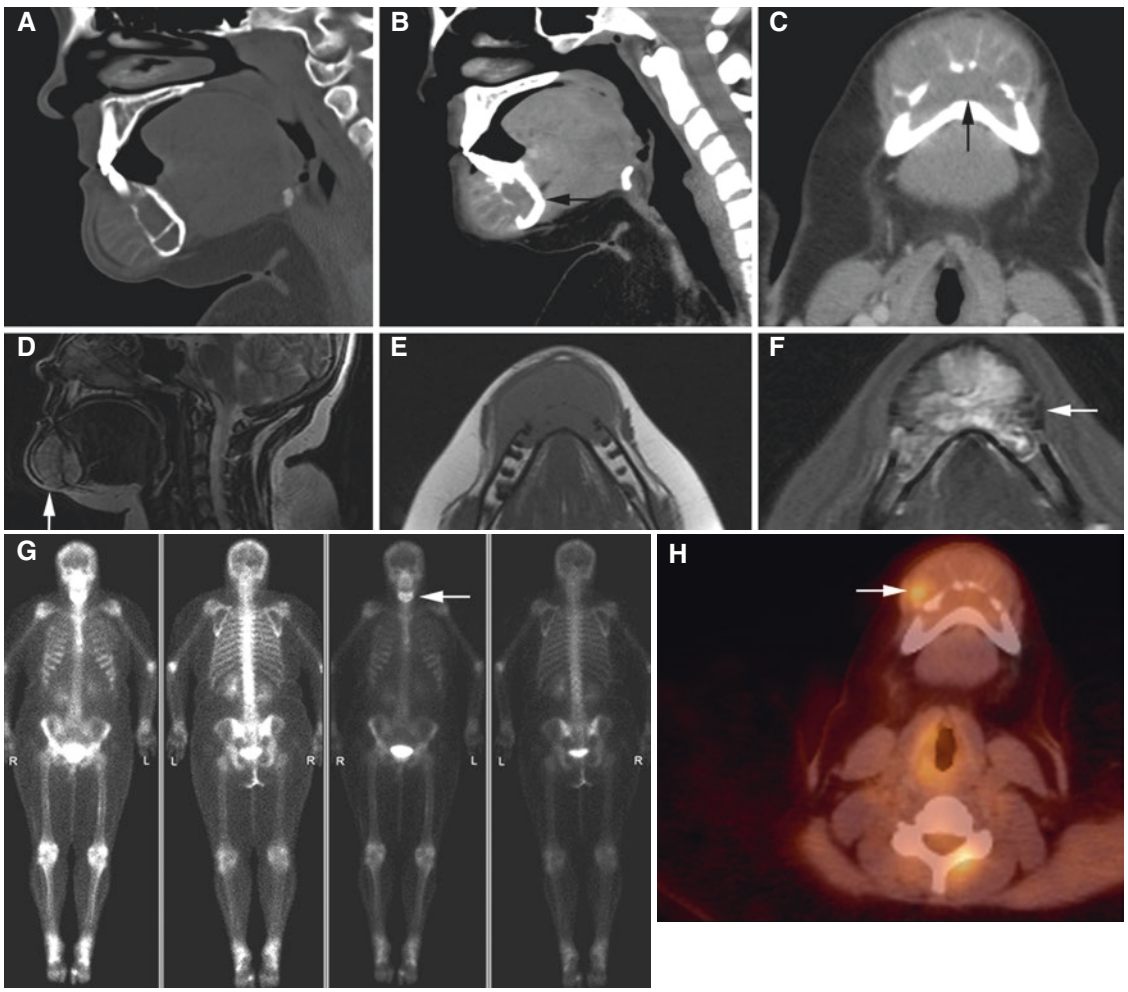

Fig. 4.31 Ewing sarcoma, mandible; 17-year-old female with mass in anterior part of the mandible. (**A**) Sagittal (bone window), (**B**) sagittal (soft-tissue window), and (**C**) axial (soft-tissue window) CT images show soft-tissue mass, bone destruction, and radiating bone septa (sunburst appearance) (*arrow*). (**D**) Sagittal STIR MRI confirms radiating bone septa in anterior portion of the mandible (*arrow*). (**E**) Axial T1-weighted pre-Gd and (**F**) axial T1-weighted fat sat post-Gd MRI show heterogeneous contrast enhancement in tumor (*arrow*). (**G**) Bone scans (technetium-99) show high activity in the mandible. (**H**) Axial PET-CT image shows hypermetabolic activity in tumor (*arrow*)

4.13 Soft-Tissue Sarcomas

Rhabdomyosarcoma and leiomyosarcoma are illustrated.

4.14 Rhabdomyosarcoma

Figs. 4.32 and 4.33

Synonym(s): Rhabdosarcoma, sarcoma.

4.14.1 Definition

Malignancy of embryonal (immature) skeletal (striated) muscle cells.

4.14.2 Clinical Features

- Most patients are under 18 years of age
- Rhabdomyosarcoma accounts for approximately 40% of soft-tissue sarcomas
- Can occur in any site on the body but is primarily found in the head and neck, orbit, genitourinary tract, genitals, and extremities
- Signs and symptoms vary according to tumor site, and prognosis is closely tied to location of primary tumor

4.14.3 Imaging Features

- Soft-tissue mass with infiltrative and irregular margins
- Enhancing mass lesion with variable T1 and T2 features

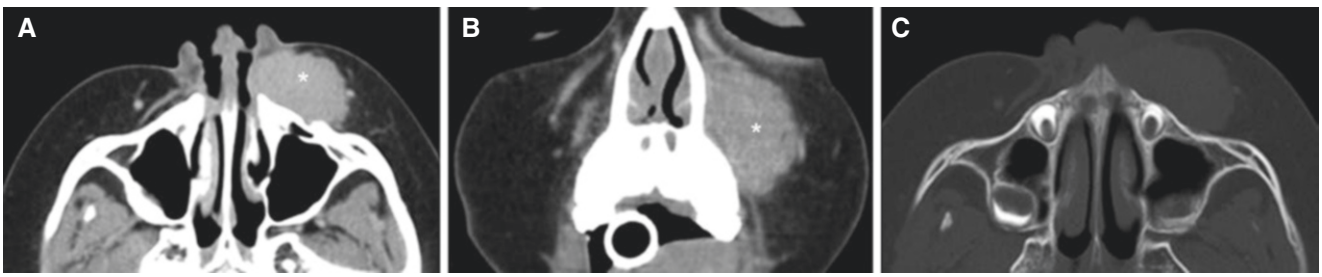

Fig. 4.32 Rhabdomyosarcoma, cheek; 4-year-old female with mass in the left cheek. (**A**) Axial (soft-tissue window), (**B**) coronal (soft-tissue window), and (**C**) axial (bone window) CT images show soft-tissue mass (*asterisk*) but no bone destruction

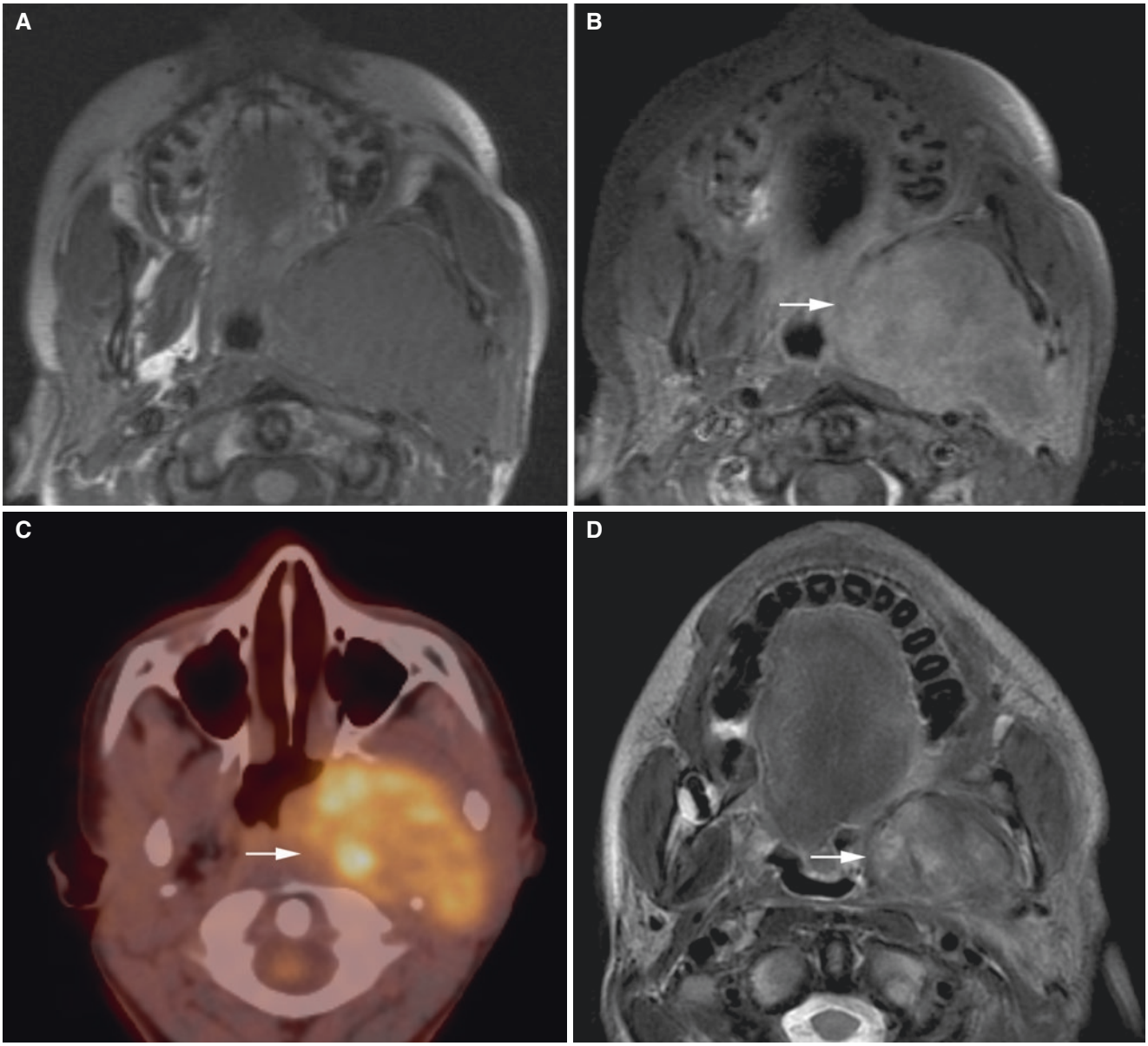

Fig. 4.33 Rhabdomyosarcoma, parapharyngeal; 12-year-old male with trismus and a left-sided neck mass. (**A**) Axial T1-weighted pre-Gd and (**B**) axial T1-weighted fat sat post-Gd MRI show homogeneous contrast enhancement in tumor (*arrow*). (**C**) Axial PET-CT image shows intense hypermetabolic activity in tumor (*arrow*). (**D**) Axial STIR MRI (3 months after baseline examination, under treatment) shows diminished tumor (*arrow*)

4.15 Leiomyosarcoma

Fig. 4.34

Synonym: Sarcoma.

4.15.1 Definition

Malignancy of smooth muscle cells.

4.15.2 Clinical Features

– Rare form of cancer; accounting for 5–10% of soft-tissue sarcomas, which are in themselves relatively rare
– Most commonly found in the uterus, stomach, small intestine, and retroperitoneum

4.15.3 Imaging Features

– Soft-tissue mass with infiltrative and irregular margins
– Enhancing mass lesion with variable T1 and T2 features

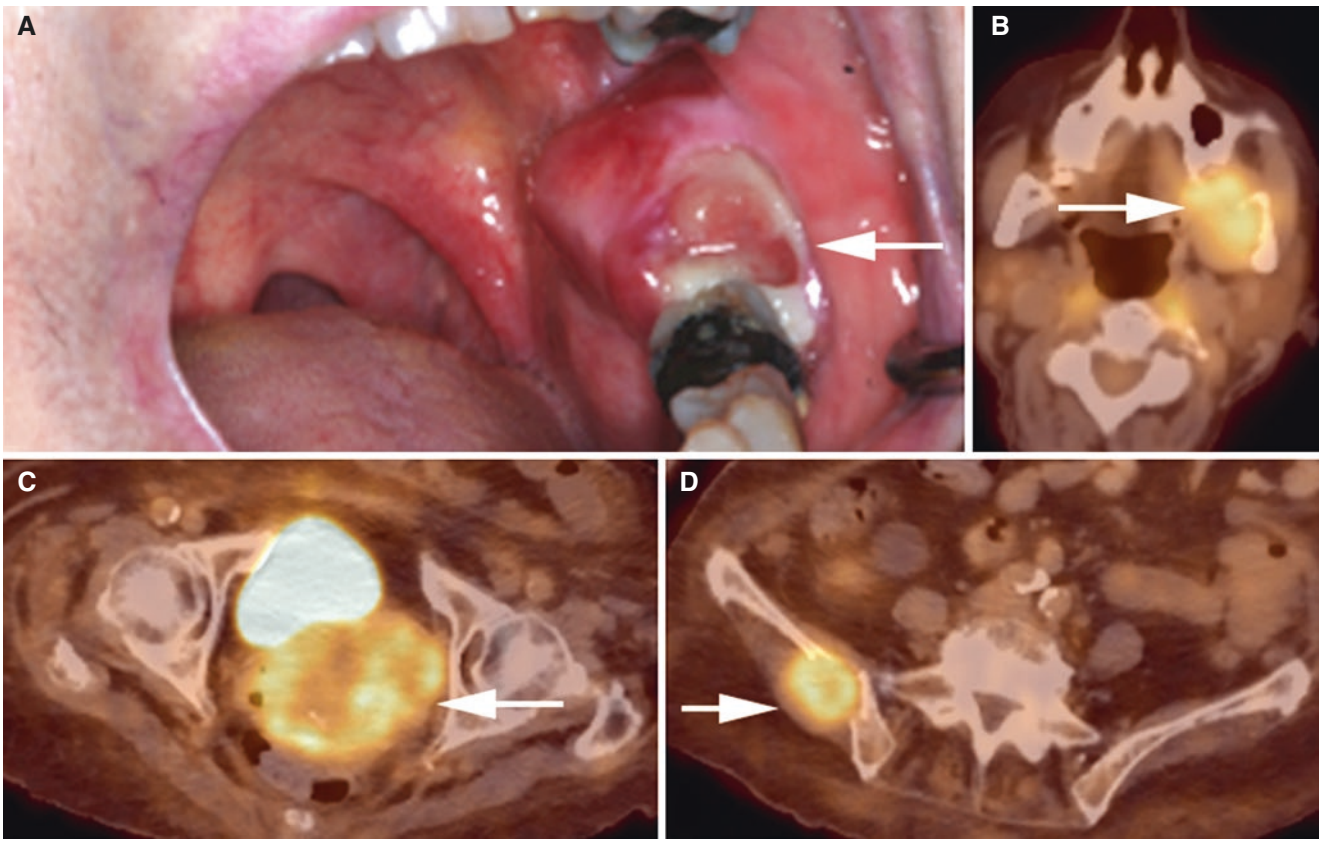

Fig. 4.34 Leiomyosarcoma, mandible; 85-year-old female with pain and swelling in posterior left mandible. (**A**) Clinical photograph shows ulcerated soft-tissue mass in retromolar area (*arrow*). (**B**, **C**, **D**) Axial PET-CT images show hypermetabolic destructive mass in the left mandible (*arrow*) (**B**), hypermetabolic tumor in the uterus (origin of leiomyosarcoma) (*arrow*) (**C**), and hypermetabolic destructive right ilium metastasis (*arrow*), with fracture (**D**). There were numerous skeletal metastases (not shown)

4.16 Jaw Metastases

Figs. 4.35, 4.36, 4.37, 4.38, 4.39, and 4.40

Synonym: Secondary malignancy.

4.16.1 Clinical Features

- Fifth to seventh decades
- Women far more frequent than men (breast cancer)
- Pain and/or swelling, paresthesia, hemorrhage
- May be incidental finding
- Less frequent than in the spine, pelvis, ribs, humerus, and skull
- Usually a carcinoma from a primary tumor in the breast, lung, prostate, colon, rectum, kidney, thyroid, stomach, melanoma, testicle, bladder, ovary, and uterine cervix

4.16.2 Imaging Features

- Soft-tissue mass
- Mandible more frequent than maxilla
- In maxilla: sinus most common site, followed by anterior hard palate
- Posterior parts of the jaw
- Ill-defined invasive margins
- May have rather well-defined margins
- Predominantly osteolytic/radiolucent
- New bone formation due to periosteal reaction (spiculated for prostate metastases)
- Sclerotic (patchy sclerosis) metastases may occur from prostatic and breast cancer
- Widened periodontal ligament
- Floating teeth

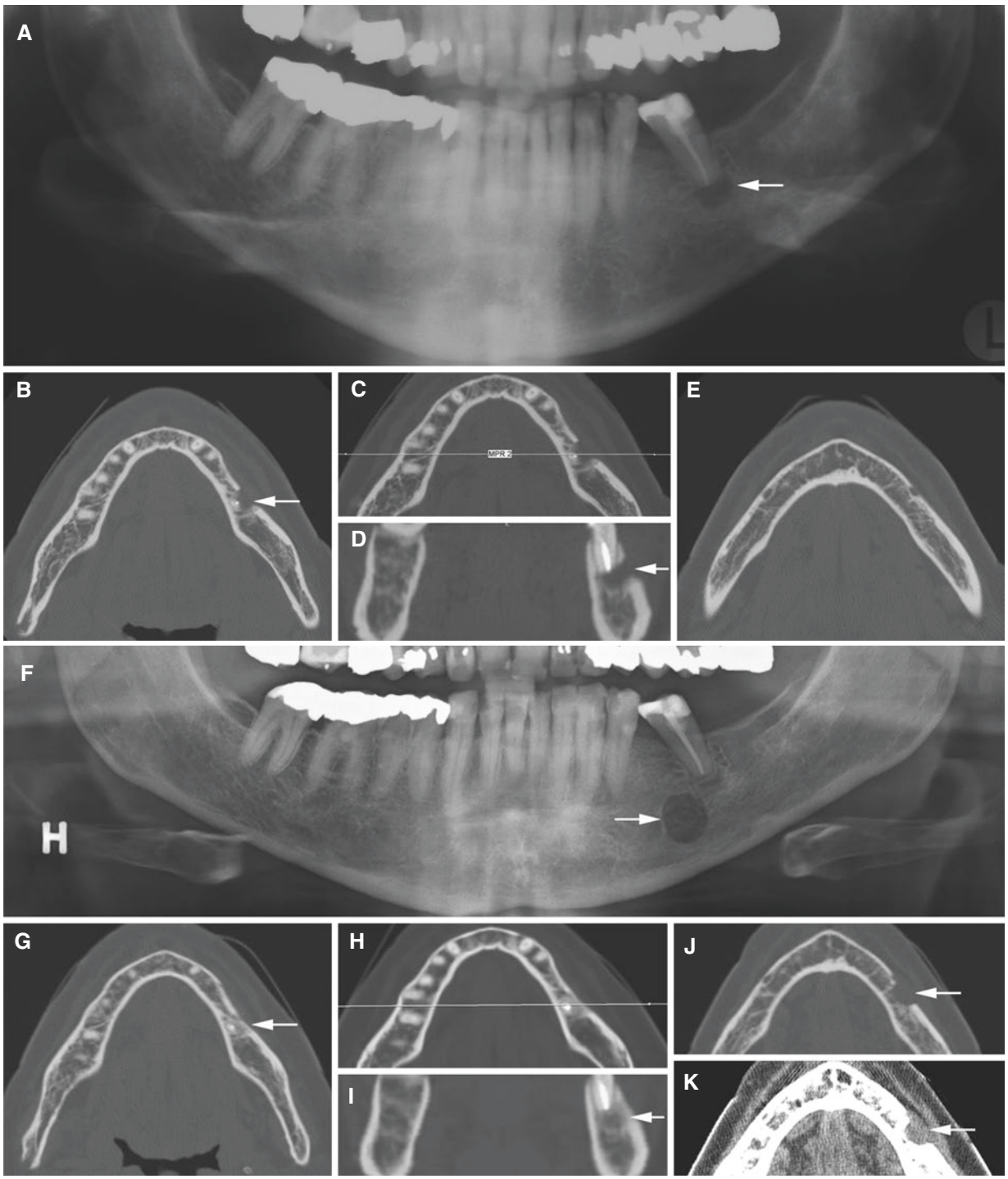

Fig. 4.35 Breast cancer metastasis, mandible; 58-year-old female with some pain in the left mandible after apicectomy. (**A**) Panoramic view and (**B**) axial, (**C**) axial (with cursor line), and (**D**) coronal CT images show postoperative status after apicectomy of the second premolar (*arrow*). (**E**) Axial CT image shows normal bone structures at mental foramen level. About 1 year later, (**F**) panoramic view shows bone destruction (*arrow*), and (**G**) axial, (**H**) axial (with cursor line), and (**I**) coronal CT images show healing after apicectomy (*arrow*). (**J**) Axial (bone window) and (**K**) axial (soft-tissue window) CT images show destruction and soft-tissue tumor at mental foramen level (*arrow*) (compare with **E**)

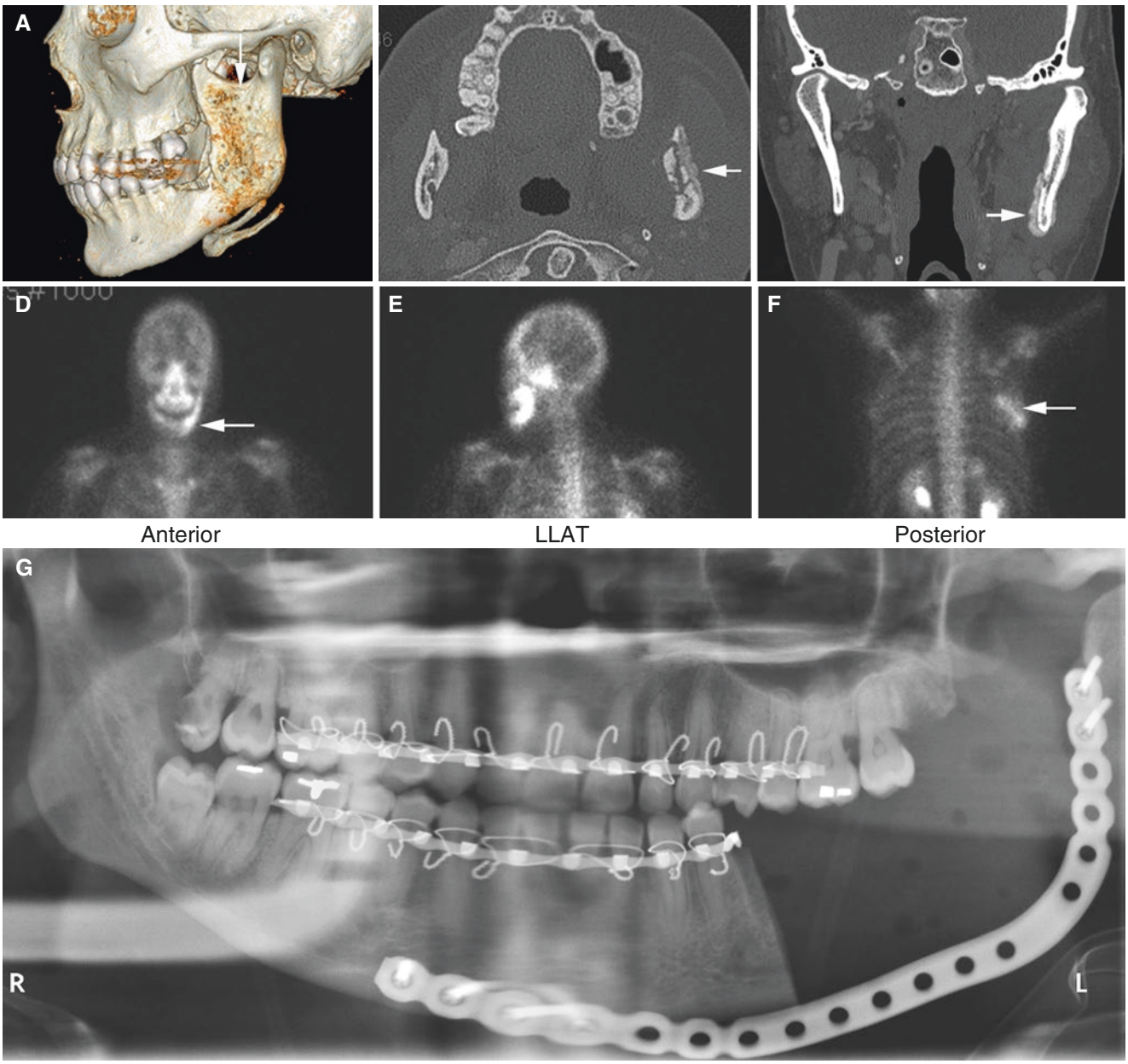

Fig. 4.36 Breast cancer metastasis, mandible; 46-year-old female with mass in the left mandibular ramus. (**A**) 3D, (**B**) axial, and (**C**) coronal CT images show irregular bone (destruction and apposition) in the left mandibular ramus (*arrow*). (**D**, **E**, **F**) Bone scans (technetium-99) show activity in the left mandible and right scapula (*arrow*). (**G**) Postoperative panoramic view shows status after hemimandibulectomy

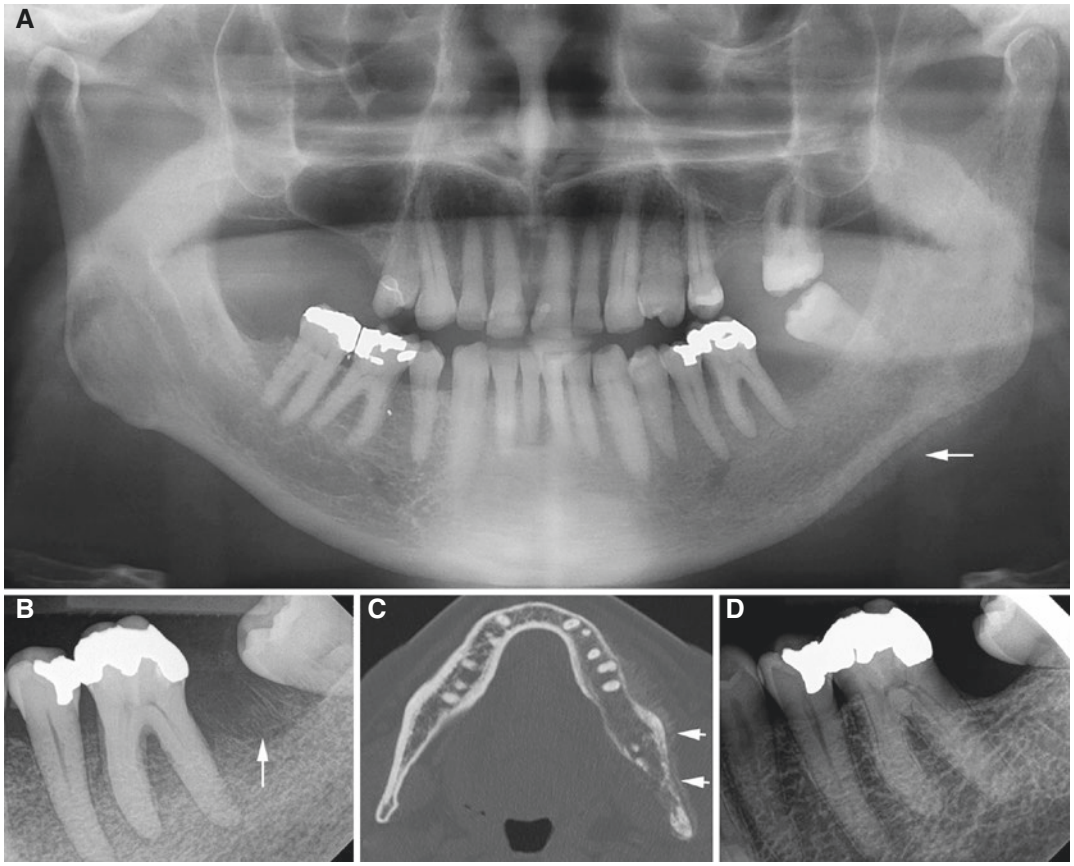

Fig. 4.37 Prostatic cancer metastasis, mandible; 60-year-old male with some pain and swelling in the left mandible. (**A**) Panoramic view shows diffuse destruction in the left mandible and bone apposition at lower mandibular border (*arrow*). (**B**) Intraoral view shows diffuse destruction with loss of lamina dura and bone apposition in the alveolar bone with sunburst appearance (*arrow*). (**C**) Axial CT image shows destruction in the left mandible with periosteal bone reaction (partially with sunburst appearance) buccally (*arrows*). (**D**) Intraoral view 2 years earlier shows normal bone and lamina dura (compare with **B**)

Fig. 4.38 Prostatic cancer metastasis, mandible; 79-year-old male with lower lip numbness. (**A**) Axial CT shows intense right-sided periosteal bone formation and sclerotic mandibular ramus (*arrow*). (**B**) Axial CT with biopsy needle

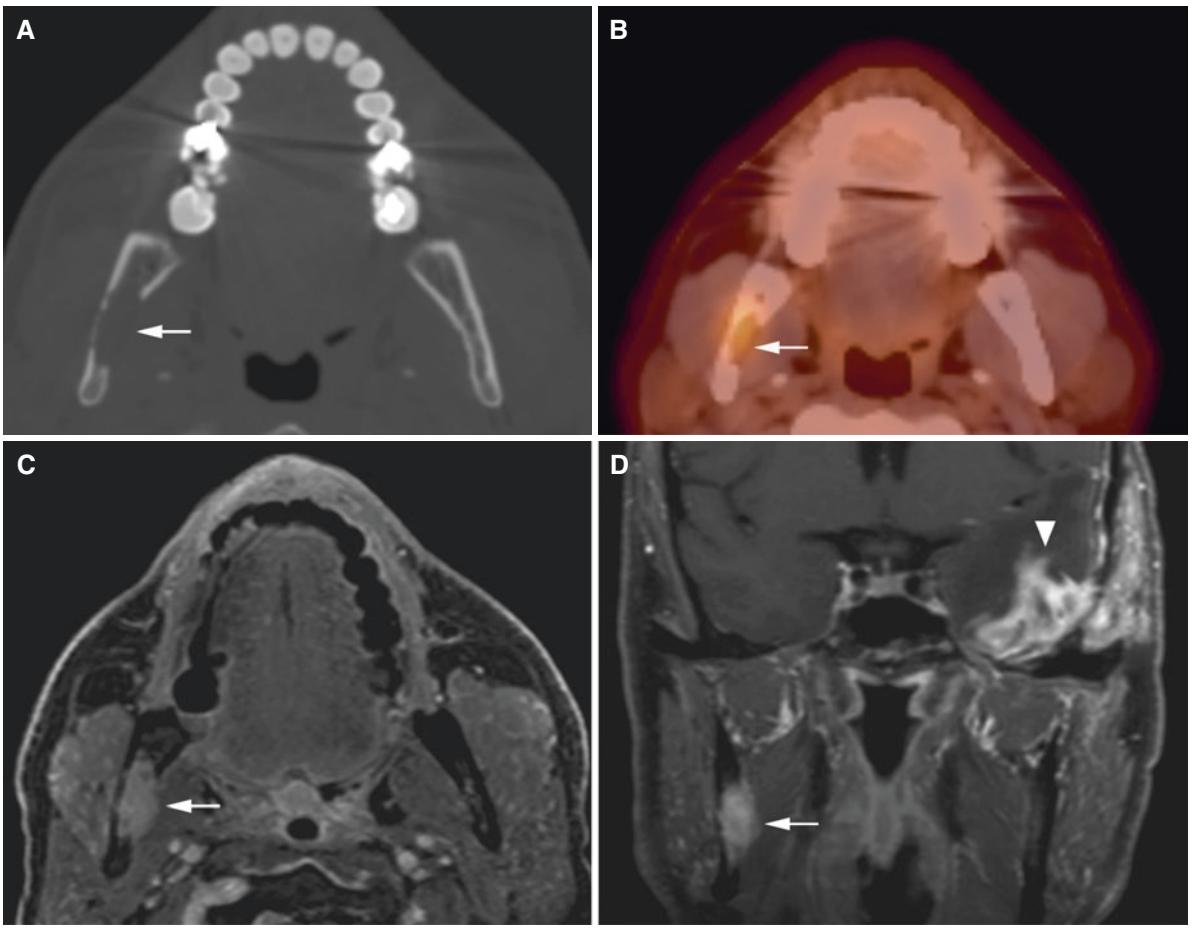

Fig. 4.39 Anaplastic malignant meningioma metastasis, mandible; 56-year-old male with pain (6 on a scale 1–10) under his lip and extending across the right lower cheek. (**A**) Axial CT image shows destruction of right lingual mandibular foramen (*arrow*). (**B**) Axial PET-CT image shows hypermetabolic activity in the same area (*arrow*). (**C**) Axial and (**D**) coronal T1-weighted fat sat post-Gd MRI show contrast-enhanced tumor at mandibular foramen (*arrow*) and contrast-enhanced meningioma (*arrowhead*)

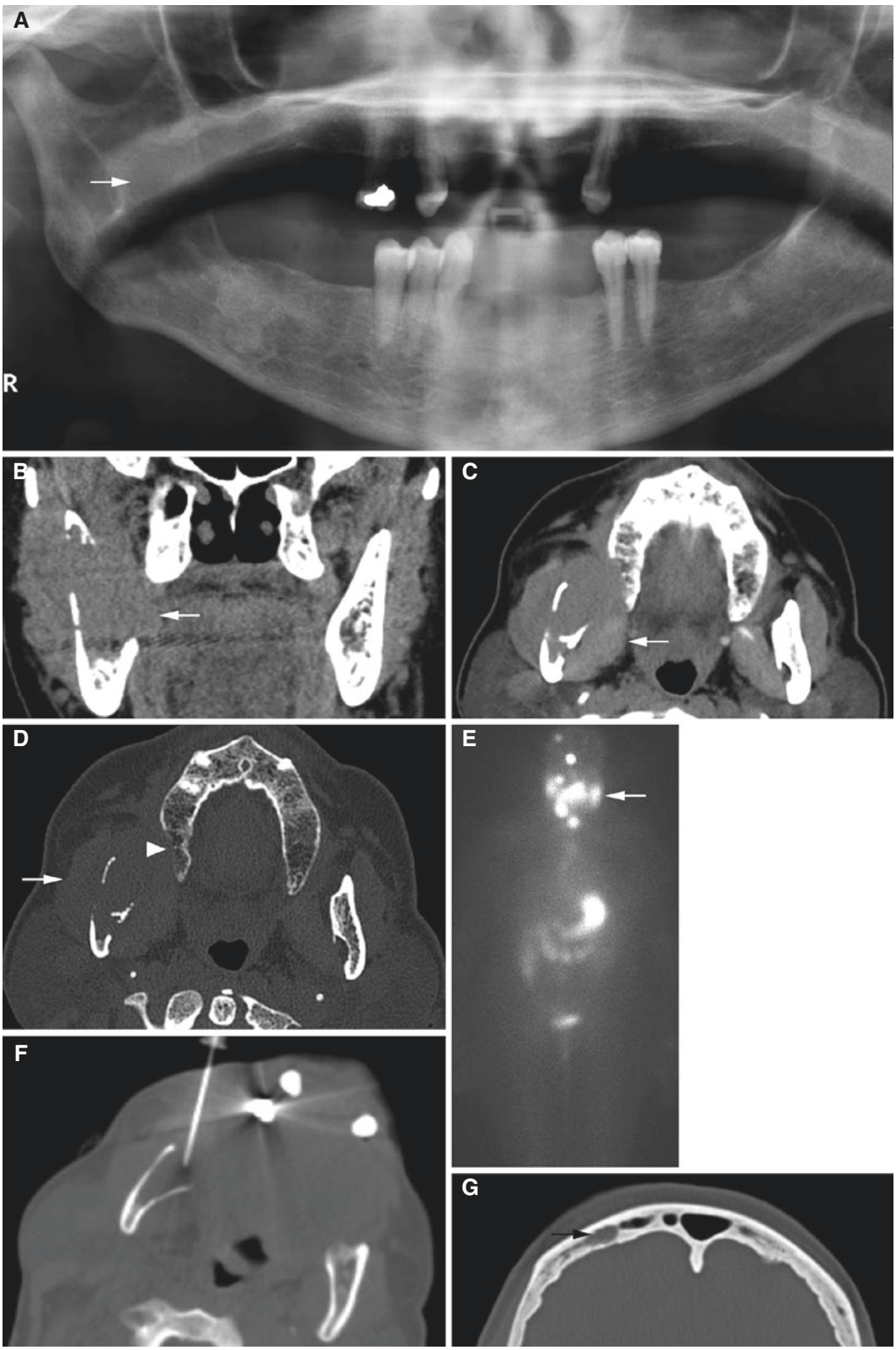

Fig. 4.40 Thyroid cancer metastasis, mandible; 62-year-old female with mass in the right mandible extending into the right maxilla. (**A**) Panoramic view shows destruction in the right mandible (*arrow*). (**B**) Coronal and (**C**) axial (soft-tissue window) CT images show soft-tissue mass and bone destruction (*arrow*). (**D**) Axial (bone window) CT image shows destruction in mandibular ramus (*arrow*) and maxilla (*arrowhead*). (**E**) CT-guided percutaneous core biopsy of tumor. (**F**) Whole-body nuclear medicine scanning (I-131) shows intense activity in the mandible (*arrow*) and two foci of uptake in the neck consistent with lymph node metastases. (**G**) Axial CT image shows lytic lesion in the right frontal bone (*arrow*) suspicious for metastasis

Suggested Reading

Alotaibi O, Al-Zaher N, Alotaibi F, Khoja H, Qannam A (2016) Solid-type primary intraosseous squamous-cell carcinoma in the mandible: report of a rare case. Hematol Oncol Stem Cell Ther 9:118–122

Ator GA, Abemayor E, Lufkin RB, Hanafee WN, Ward PH (1990) Evaluation of mandibular tumor invasion with magnetic resonance imaging. Arch Otolaryngol Head Neck Surg 116:454–459

Aydil U, Kizil Y, Bakkal FK, Köybaşioğlu A, Uslu S (2014) Neoplasms of the hard palate. J Oral Maxillofac Surg 72:619–626

Bassey GO, Osunde OD, Anynechi CE (2015) Analysis of 46 cases of malignant jaw tumours in Calabar, Nigeria. Niger Med J 56:240–243

Benoit MM, Vargas SO, Bhattacharyya N, McGill TA, Robson CD, Ferraro N et al (2013) The presentation and management of mandibular tumors in the pediatric population. Laryngoscope 123:2035–2042

Bianchi SD, Boccardi A (1999) Radiological aspects of osteosarcoma of the jaws. Dentomaxillofac Radiol 28:42–47

Boni P, Sozzi D, Novelli G, Pagni F, Valente G, Bozzetti A (2016) Primary intraosseous squamous cell carcinoma of the jaws: 6 new cases, experience, and literature comparison. J Oral Maxillofac Surg 74:541–546

Bredesen K, Aalokken TM, Kolbenstvedt A (2001) CT of the oral vestibule with distended cheeks. Acta Radiol 42:84–87

Browand BC, Waldron CA (1975) Central mucoepidermoid tumors of the jaws. Report of nine cases and review of the literature. Oral Surg Oral Med Oral Pathol 40:631–643

Brown JS, Griffith JF, Phelps PD, Browne RM (1994) A comparison of different imaging modalities and direct inspection after periosteal stripping in predicting the invasion of the mandible by oral squamous cell carcinoma. Br J Oral Maxillofac Surg 32:347–359

Brown JS, Barry C, Ho M, Shaw R (2016) A new classification for mandibular defects after oncological resection. Lancet Oncol 17(1):e23–e30. doi:10.1016/S1470-2045(15)00310-1

Danan D, Mukherjee S, Shonka DC Jr (2015) Submental neck mass in an adolescent female. JAMA Otolaryngol Head Neck Surg 141:851–852

Deepti S, Somanathan T, Ramdas K, Pandey M (2003) Central mucodermoid carcinoma of mandible. A case report and review of literature. World J Surg Oncol 1:1–5

DeSesa CR, Appugounder S, Haberland C, Johnson MP (2016) Osteonecrosis of the jaw in association with chemotherapy in the setting of cutaneous T-cell lymphoma. J Oral Maxillofac Surg 74:292–301

Eversole LR, Sabes WR, Rovin S (1975) Aggressive growth and neoplastic potential of odontogenic cysts: with special reference to central epidermoid and mucoepidermoid carcinomas. Cancer 35:270–282

Farman AG, Nortje C, Wood RE (1993) Malignancies affecting the jaws. In: Oral and maxillofacial diagnostic imaging. Mosby, St. Louis, pp 280–316

Favia G, Tempesta A, Limongelli L, Crincoli V, Piattelli A, Maiorano E (2015) Metastatic breast cancer in medication-related osteonecrosis around mandibular implants. Am J Case Rep 16:621–626

Fordice J, Kershaw C, El-Nagger A, Goepfert H (1999) Adenoid cystic carcinoma of the head and neck: predictors of morbidity and mortality. Arch Otolaryngol Head Neck Surg 125:149–152

Gangwar N, Balakrishnan R, Pujary P, Rao L, Kudva R (2016) Myofibrosarcoma-maxilla. Indian J Cancer 52:289–290

Geetha P, Avinash Tejasvi ML, Babu BB, Bhayya H, Pavani D (2015) Primary intraosseous carcinoma of the mandible. A clinicoradiographic view. J Cancer Res Ther 11:651

Gupta S, Tandon A, Ram H, Gupta OP (2015) Oral malignant melanoma: report of three cases with literature review. Natl J Maxillofac Surg 6:103–109

Harmon M, Arrigan M, Toner M, O'Keeffe SA (2015) A radiological approach to benign and malignant lesions of the mandible. Clin Radiol 70:335–350

Jain M, Mittal S, Gupta DK (2013) Primary intraosseous squamous cell carcinoma arising in odontogenic cysts: an insight in pathogenesis. J Oral Maxillofac Surg 71:e7–14

Kim RH, Yang P, Sung EC (2016) Managing intraoral lesions in oral cancer patients in general dental practice: an overview. J Calif Dent Assoc 44:85–92

Kimura Y, Sumi M, Sumi T, Ariji Y, Ariji E, Nakamura T (2002) Deep extension from carcinoma arising from the gingiva: CT and MR imaging features. AJNR Am J Roentgenol 23:468–472

Krishnamurthy A, Deen S, Ramshankar V, Majhi U (2016) Metastatic follicular carcinoma thyroid masquerading as a primary jaw tumor. J Maxillofac Oral Surg 15(Suppl 2):266–269

Kucukkurt S, Karan NB, Senguven B, Kahraman S (2016) Solitary plasmacytoma of the mandible: report of two cases. BMJ Case Rep. doi:10.1136/bcr-2015-214255

Kumar S, Hasan R, Paulraj SK, Mathew M (2015) Perivascular spread of adenoid cystic carcinoma: a novel imaging sign. BMJ Case Rep. doi:10.1136/bcr-2015-210969

Laine FJ, Braun IF, Jensen ME, Nadel L, Som PM (1990) Perineural tumor extension through the foramen ovale: evaluation with MR imaging. Radiology 174:65–71

Larheim TA, Kolbenstvedt A, Lien HH (1984a) Carcinoma of maxillary sinus, palate and maxillary gingiva: occurrence of jaw destruction. Scand J Dent Res 92:235–240

Larheim TA, Kolbenstvedt A, Lien HH (1984b) Bony destruction from intraoral carcinomas. Dentomaxillofac Radiol 13:33–37

Lovas JGL (1991) Malignant neoplasms. In: Miles DA, Van Dis M, Kaugers GE, Lovas JGL (eds) Oral and maxillofacial radiology. Radiologic/pathologic correlations. Saunders, Philadelphia, pp 97–124

Loyola AM, Cardoso SV, de Faria PR, Servato JP, Barbosa de Paulo LF, Eisenberg AL et al (2015) Clear cell odontogenic carcinoma: report of 7 new cases and systematic review of the current knowledge. Oral Surg Oral Med Oral Pathol Oral Radiol 120:483–496

Lukandu OM, Micha CS (2015) Primary intraosseous squamous cell carcinoma arising from keratocystic odontogenic tumor. Oral Surg Oral Med Oral Pathol Oral Radiol 120:e204–e209. doi:10.1016/j.oooo.2015.03.006

Mardinger O, Givol N, Talmi YP, Taicher S (2001) Osteosarcoma of the jaw. The Chaim Sheba Medical Center experience. Oral Surg Oral Med Oral Pathol Oral Radiol Endod 91:445–451

Meyer KA, Bancroft LW, Dietrich TJ, Kransdorf MJ, Peterson JJ (2011) Imaging characteristics of benign, malignant, and infectious jaw lesions: a pictorial review. AJR Am J Roentgenol 197:W412–W421

Mosier KM (2015a) Magnetic resonance imaging of the maxilla and mandible: signal characteristics and features in the differential diagnosis of common lesions. Top Magn Reson Imaging 24:23–37

Mosier KM (2015b) Lesions of the jaw. Semin Ultrasound CT MR 36:444–450

Moura LB, Gabrielli MF, Gabrielli MA, Filho VA (2016) Pathologic mandibular fracture as first sign of multiple myeloma. J Craniofac Surg 27(2):e138–e139. doi:10.1097/SCS.0000000000002386

Nakayama E, Yoshiura K, Ozeki S, Nakayama H, Yamaguchi T, Yoshikawa H, Kanda S, Ohishi M, Shirasuna K (2003) The correlation of histologic features with a panoramic radiography pattern and a computed tomography pattern of bone destruction in carcinoma of the mandibular gingiva. Oral Surg Oral Med Oral Pathol Oral Radiol Endod 96:774–782

Nawale KK, Vyas M, Kane S, Patil A (2016) Metastatic tumors in the jaw bones: a retrospective clinicopathological study of 12 cases at Tertiary Cancer Center. J Oral Maxillofac Pathol 20:252–255

Owosho AA, Potluri A, Bauer Iii RE, Bilodeau EA (2015) Ameloblastic carcinoma of the mandible manifesting as an infected odontogenic cyst. Gen Dent 63:e1–e4

Patankar S, Venkatraman P, Sridharan G, Kane S (2015) Burkitt's lymphoma of maxillary gingiva: a case report. World J Clin Cases 3:1011–1016

Perry KS, Tkaczuk AT, Caccamese JF Jr, Ord RA, Pereira KD (2015) Tumors of the pediatric maxillofacial skeleton. A 20-year clinical study. JAMA Otolaryngol Head Neck Surg 141:40–44

Pindborg JJ, Reichart PA, Smith CJ, van der Waal I (1997) World Health Organisation. Histological typing of cancer and precancer of the oral mucosa, 2nd edn. Springer, Berlin, p 11

Rajinikanth M, Prakash AR, Swathi TR, Reddy S (2015) Metastasis of lung adenocarcinoma to the jaw bone. J Oral Maxillofac Pathol 19:385–388

Resnick D (1996) Bone and joint imaging, 2nd edn. Saunders, Philadelphia, p 625

Saxena C, Aggarwal P, Wadhwan V, Bansal V (2015) Primary intraosseous squamous cell carcinoma in odontogenic keratocyst: a rare entity. J Oral Maxillofac Pathol. doi:10.4103/0973-029X.174615

Schajowicz F (1993) World Health Organisation. Histological typing of bone tumors, 2nd edn. Springer, Berlin, pp 10, 17, 22, 25

Scheer M, Koch AM, Drebber U, Kubler AC (2004) Primary intraosseous carcinoma of the jaws arising from an odontogenic cyst—a case report. J Craniomaxillofac Surg 32:166–169

Seifert G (1991) World Health Organisation. Histological typing of salivary gland tumors, 2nd edn. Springer, Berlin, pp 20, 21

Sengupta A, Brown J, Rudralingam M (2016) The use of intraoral ultrasound in the characterization of minor salivary gland malignancy: report of two cases. Dentomaxillofac Radiol. doi:10.1259/dmfr.20150354

Sigal R, Monnet O, de Baere T, Micheau C, Shapeero LG, Julieron M, Bosq J, Vanel D, Piekarski JD, Luboinski B (1992) Adenoid cystic carcinoma of the head and neck: evaluation with MR imaging and clinical-pathologic correlation in 27 patients. Radiology 184:95–101

Sivolella S, Rizzo G, Valente M, Lumachi F (2015) Sporadic Burkitt lymphoma mimicking osteomyelitis of the mandible revealing clinically unsuspected HIV infection. Anticancer Res 35:4837–4839

Sugiyama M, Yokoi T, Kawakami N, Kikkawa M, Tokunaga Y, Chayama K (2015) Chin numbness and pain in a patient with Burkitt acute lymphoblastic leukemia. J Pediatr 167:938–938.e1. doi:10.1016/j.jpeds.2015.06.070

Thomas G, Pandey M, Mathew A, Abraham EK, Francis A, Somanathan T, Iype M, Sebastian P, Nair MK (2001) Primary intraosseous carcinoma of the jaw: pooled analysis of the world literature and report of two new cases. Int J Oral Maxillofac Surg 30:349–355

Trosman SJ, Krakovitz PR (2015) Pediatric maxillary and mandibular tumors. Otolaryngol Clin North Am 48:101–119

Vrielinck LJ, Ostyn F, van Damme B, van den Bogaert W, Fossion E (1988) The significance of perineural spread in adenoid cystic carcinoma of the major and minor salivary glands. Int J Oral Maxillofac Surg 17:190–193

Waldron CA, Mustoe TA (1989) Primary intraosseous carcinoma of the mandible with probable origin in an odontogenic cyst. Oral Surg Oral Med Oral Pathol 67:716–724

Webber B, Webber M, Keinan D (2015) Extranodal large B cell lymphoma of the anterior maxilla. Case report and review of literature. N Y State Dent J 81:34–38

Weber AL, Kaneda T, Scrivani SJ, Aziz S (2003) Jaw: cysts, tumors, and nontumorous lesions. In: Som PM, Curtin HD (eds) Head and neck imaging, 4th edn. Mosby, St. Louis, pp 930–994

Wood RE (2014) Malignant diseases. In: White SW, Pharoah MJ (eds) Oral radiology. Principles and interpretation, 7th edn. Saunders, Philadelphia, pp 427–451

Wood RE, Nortje CJ, Hesseling P, Grotepass F (1990) Ewing's tumor of the jaw. Oral Surg Oral Med Oral Pathol 69:120–127

Wu Y, Huang W, Zhang Z, Zhang Z, Zou D (2016) Long-term success of dental implant-supported dentures in postirradiated patients treated for neoplasms of the maxillofacial skeleton: a retrospective study. Clin Oral Investig 20:2457–2465

Yuan Y, Tang W, Jiang M, Tao X (2016) Palatal lesions: discriminative value off conventional MRI and diffusion weighted imaging. Br J Radiol. doi:10.1259/bjr.20150911

Jaw Infections

5

Abstract

This chapter illustrates osteomyelitis, osteomyelitis with periostitis, osteoradionecrosis, medication-related osteonecrosis, and abscess.

5.1 Introduction

Dental caries, periodontal disease, and apical periodontitis (periapical granuloma, abscess, or cyst) are common pathologic conditions and usually restricted to the region of the teeth and adjacent bone. These conditions are most often adequately assessed by intraoral or panoramic radiography. Infection also appears as condensing or sclerosing osteitis frequently defined as a localized form of osteomyelitis but usually limited to the periapical region of the mandibular molars. However, other and larger areas of the jaw bone may become infected as a direct extension from a common odontogenic infection or as a result trauma, large doses of therapeutic radiation, medication (an increasing number of patients worldwide receive antiresorptive treatment), and hematogenous spread from a distant site. Most cases of jaw osteomyelitis are nonspecific infections (in contrast to osteomyelitis in other parts of skeleton), but specific types such as tuberculosis and actinomycosis may occur.

When infection develops in jaw bone marrow as an osteomyelitis or in surrounding soft tissues as an abscess, advanced imaging in particular CT but also MRI and even PET-CT may be of diagnostic value as a supplement to conventional radiography. Also in the assessment of medication-related osteonecrosis, advanced imaging modalities should be considered.

5.2 Osteomyelitis

Figs. 5.1, 5.2, 5.3, 5.4, 5.5, and 5.6

5.2.1 Definition

Inflammatory process accompanied by bone destruction and caused by infecting microorganisms.

The infection can be limited to a single portion of bone or can involve several regions including the marrow, cortex, periosteum, and surrounding soft tissue.

5.2.2 Clinical Features

- Mandible far more often than maxilla
- Acute form presents with severe symptoms, and chronic form with vague or no symptoms, but episodes of exacerbation
- Pain and swelling, may be variable
- Regional lymphadenopathy, fever, and malaise
- Mobile teeth sensitive to percussion
- Fistula draining of pus
- Paresthesia in lower lip (mental nerve)
- Trismus if masticatory muscles are infiltrated
- Enlargement of mandible; jaw asymmetry
- Usually odontogenic infectious etiology, but idiopathic, chronic, nonsuppurative forms may occur in adults, children, or adolescents

In collaboration with G. Støre, H.-J. Smith.

T.A. Larheim, P.-L.A. Westesson, *Maxillofacial Imaging*, https://doi.org/10.1007/978-3-319-53319-3_5

5.2.3 Imaging Features

- Initial blurring of bone trabeculae
- Ill-defined ("moth-eaten") osteolytic areas, apparently interspersed by normal bone
- Sequestrum; fragment of necrotic bone
- Involucrum; sequestrum surrounded by viable bone
- Periosteal bone formation; "onion skin" appearance
- Mixture of ill-defined osteolytic and ill-defined osteosclerotic areas
- Completely radiopaque areas
- T1-weighted MRI: reduced signal from bone marrow
- T2-weighted and STIR MRI: high signal from bone marrow
- T1-weighted post-Gd MRI: contrast enhancement of bone marrow and adjacent soft tissue
- T1-weighted, T2-weighted, and STIR MRI: low signal from sequestra

Comment

From a radiologic point of view, three types of osteomyelitis may be distinguished: rarefying or destructive (suppurative) osteomyelitis, diffuse sclerosing osteomyelitis, and osteomyelitis with periostitis. A mixture of these types is common.

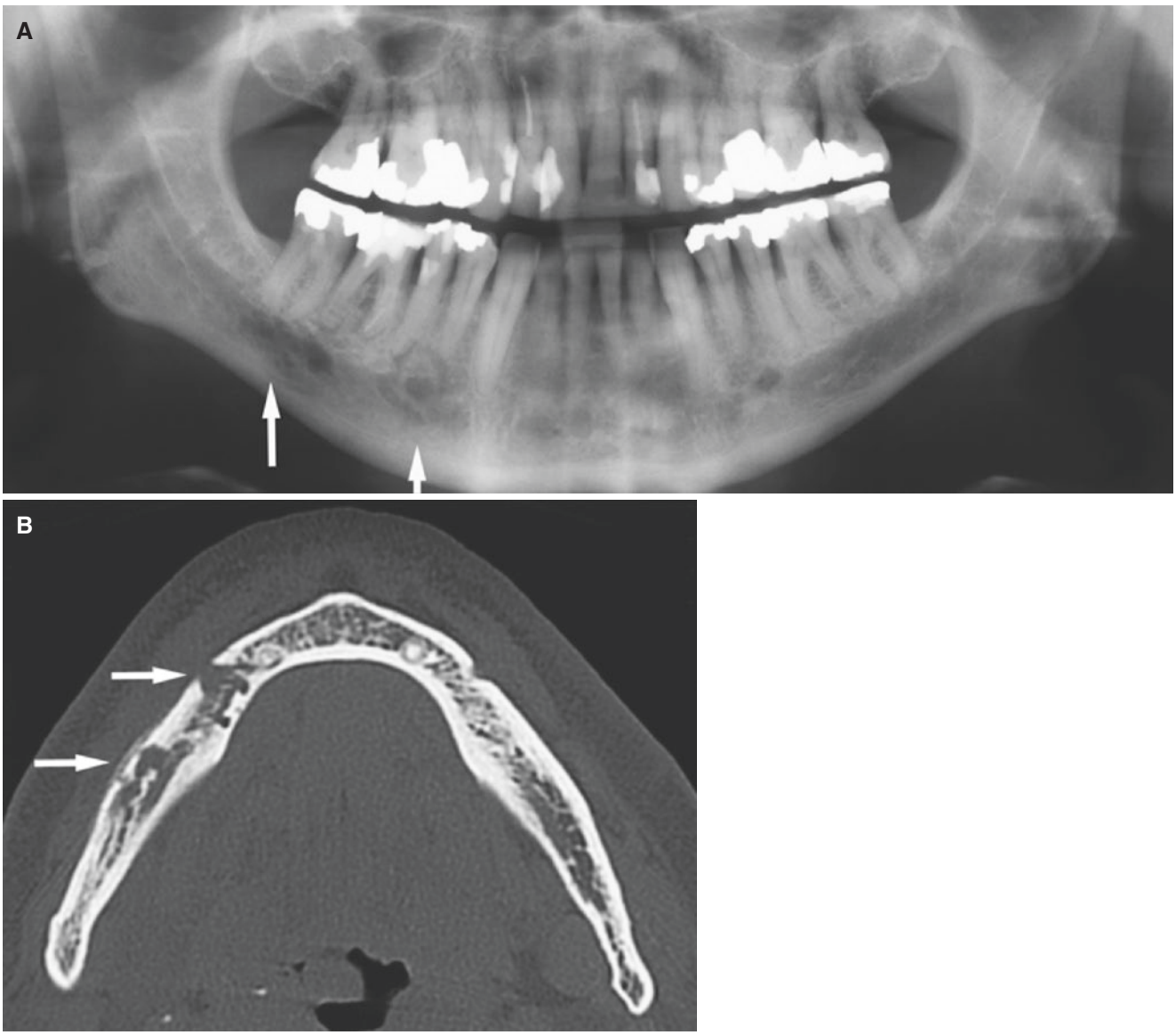

Fig. 5.1 Osteomyelitis, mandible; 58-year-old male with pain and perimandibular swelling. (**A**) Panoramic view shows diffuse bone destruction caudal to molars (*upper arrow*) and suspected sequestrum caudal to premolars (*arrow*). (**B**) Axial CT image shows destruction from widened mental foramen (*upper arrow*) to molar area and defects in lingual cortical bone at mental foramen level, but no sequestrum. Note small buccal periosteal reaction in molar region (*arrow*)

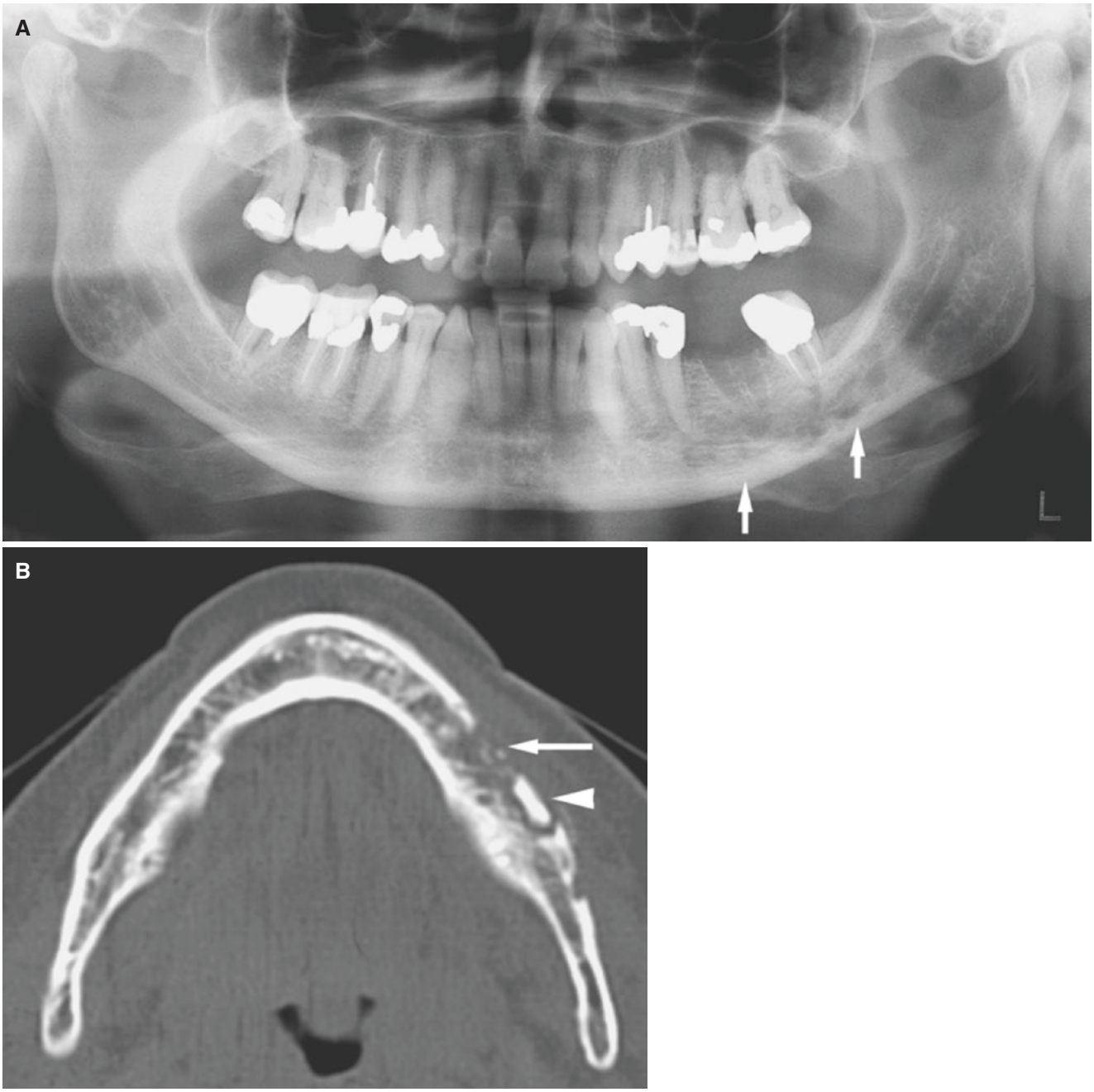

Fig. 5.2 Osteomyelitis, mandible; 46-year-old female with previous pain from molar that was extracted, but still some discomfort and, additionally, perimandibular swelling. (**A**) Panoramic view shows diffuse bone destruction (*arrows*). (**B**) Axial CT image shows diffuse destruction of buccal cortical bone (*arrow*) and sequestrum (*arrowhead*)

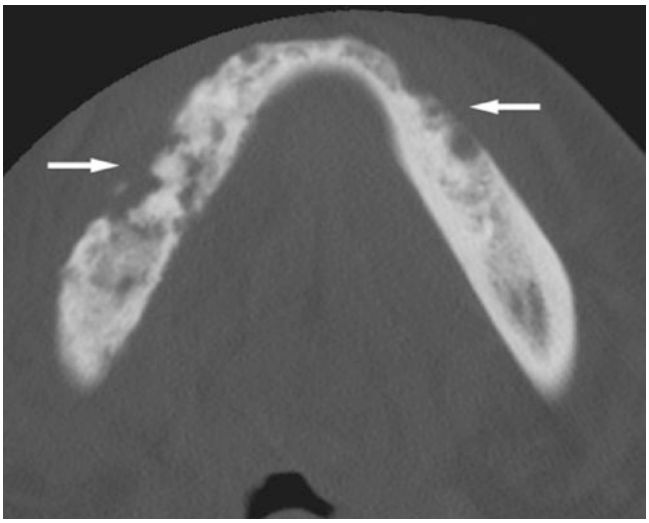

Fig. 5.3 Osteomyelitis, mandible; 68-year-old female with pain, cellulitis around the mandible, and diffuse swelling in the neck. Axial CT image shows "moth-eaten" and extensive destruction bilaterally (*arrows*)

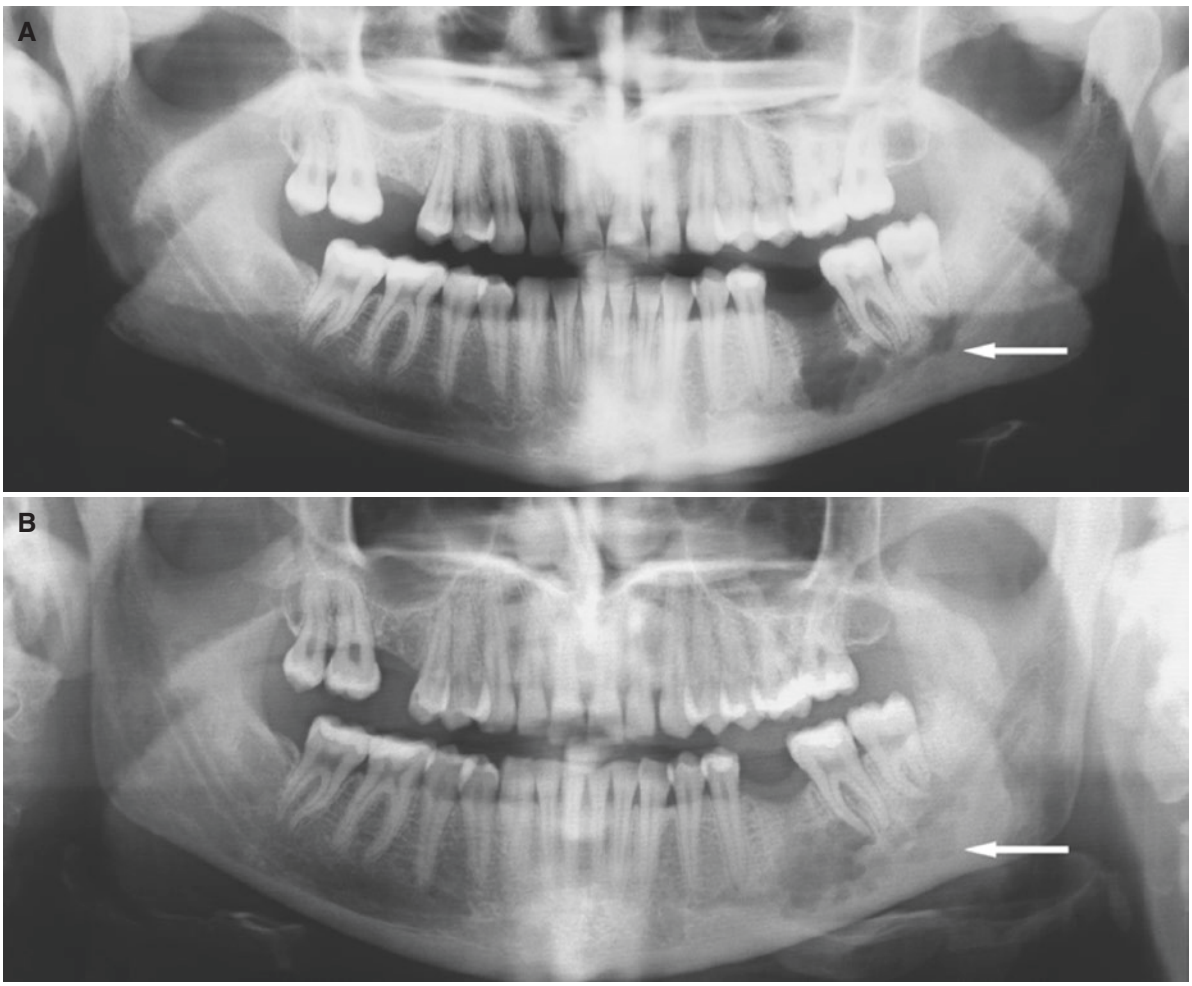

Fig. 5.4 Osteomyelitis, mandible; 25-year-old female with molar extracted after unsuccessful endodontic therapy, but progression of mandibular infection despite antibiotic therapy, little pain. (**A**) Panoramic view shows bone destruction in molar area with diffuse sclerotic bone (*arrow*). (**B**) Panoramic view about 1 year later shows healing in alveolar bone, but progression of bone destruction in caudal areas (*arrow*), with "honey-bubble" appearance that required a tumor diagnosis to be ruled out. (**C**) Axial CT image shows severe bone destruction, with cortical defect (*arrow*), but no periosteal reaction. (**D**) Axial CT image shows multilocular appearance in lower mandibular border and sclerosis (*arrow*). (**E**) Axial T1-weighted pre-Gd MRI shows reduced signal in bone marrow (*arrow*). (**F**) Axial T1-weighted post-Gd MRI shows contrast enhancement (*arrow*). (**G**) Coronal STIR MRI shows intense (high) signal in bone marrow (*arrow*). Surgical decortication confirmed osteomyelitis and no tumor

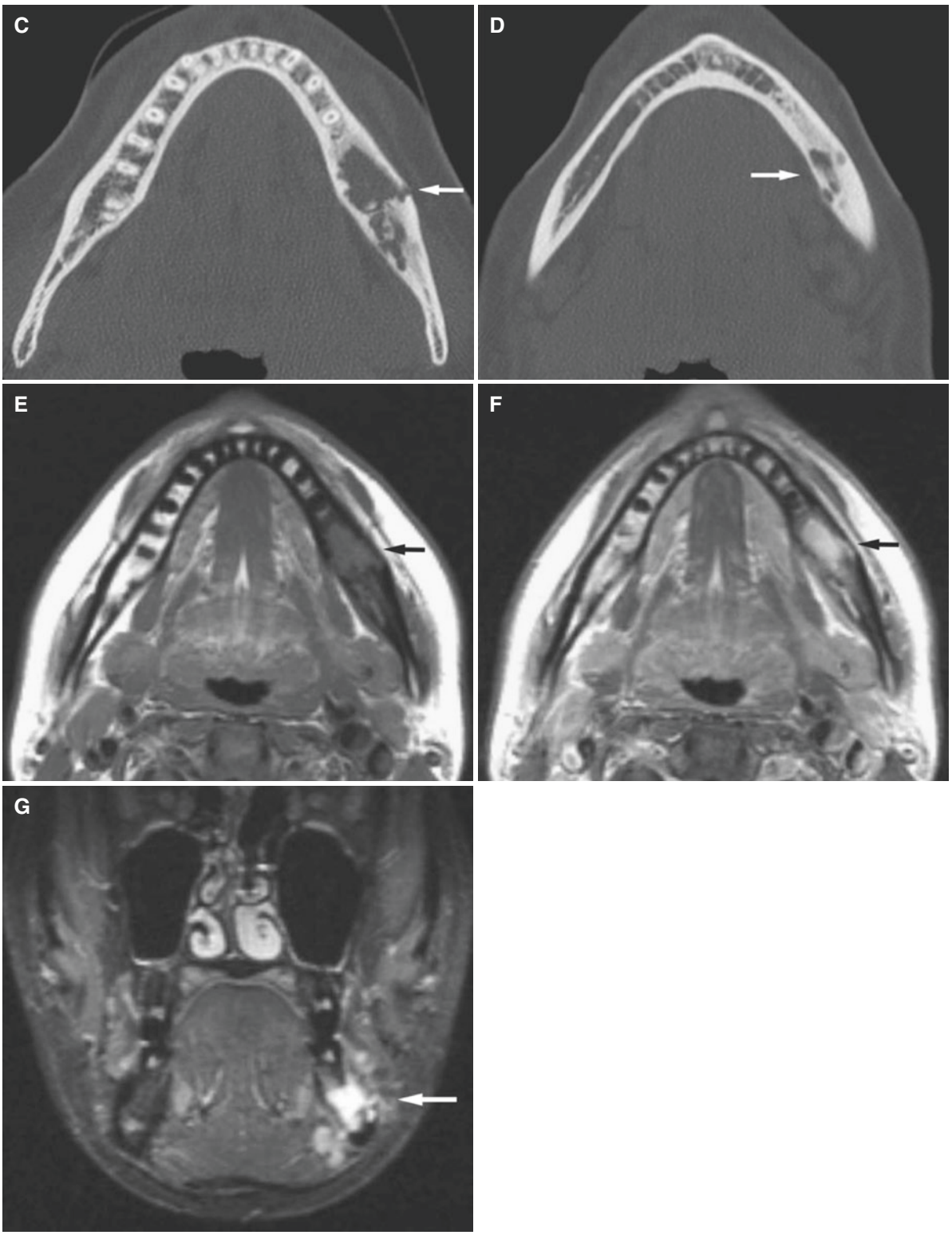

Fig. 5.4 (continued)

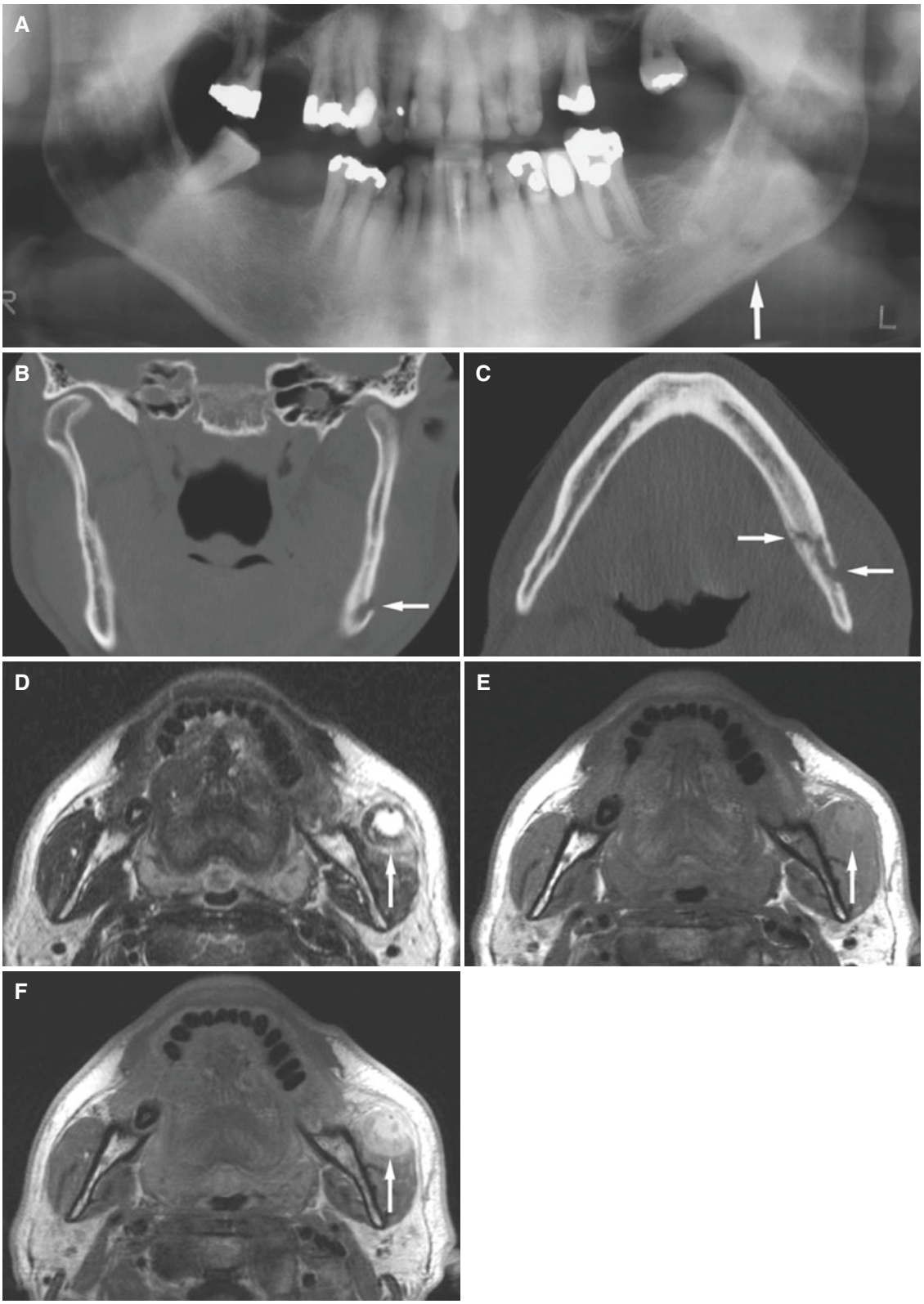

Fig. 5.5 Osteomyelitis with spread to masseter muscle; 55-year-old male with variable swelling in parotid and cheek area after tooth extraction many months previously, no pain. (**A**) Panoramic view shows sclerotic mandible with suggestion of small destruction (*arrow*). (**B**) Coronal CT image shows buccal cortical destruction (*arrow*). (**C**) Axial CT image shows buccolingual destruction (*arrow*) and slight periosteal reaction lingually (*arrow*). (**D**) Axial T2-weighted MRI shows focus of increased signal surrounded by low-signal rim in masseter muscle, consistent with encapsulated abscess (*arrow*). (**E**) Axial T1-weighted pre-Gd MRI shows intermediate signal (*arrow*). (**F**) Axial T1-weighted post-Gd MRI shows contrast enhancement (*arrow*)

Fig. 5.6 Osteomyelitis, mandible; 72-year-old female with variable but little pain and variable swelling 3 years after teeth extraction, now with mental nerve paresthesia. (**A**) Panoramic view shows diffuse sclerotic changes (*arrow*) and small focus of bone destruction (*arrowhead*). (**B**) Axial CT image shows diffuse, extensive sclerotic changes in right mandible, crossing the midline. (**C**) Coronal CT image through mental foramina shows severe bone destruction on the right side (*arrow*), explaining paresthesia. (**D**) Axial CT 7 years later still shows sclerotic osteomyelitis, now with exacerbation and sequestration (*arrowheads*)

5.3 Osteomyelitis with Periostitis

Figs. 5.7, 5.8, 5.9, 5.10, 5.11, 5.12, 5.13, and 5.14

Synonyms: Periostitis ossificans, proliferative periostitis.

5.3.1 Definition

Osteomyelitis with dominating periosteal new bone formation.

5.3.2 Clinical Features

- Mostly in children and young adults
- Unilateral hard swelling of jaw, asymmetry
- May be bilateral
- Symptoms usually vague
- Predominantly in mandible

5.3.3 Imaging Features

- Cortical expansion by periosteal bone formation; buccal, lingual, and inferior aspects
- Characteristic "onion skin" appearance
- Usually also bone destruction

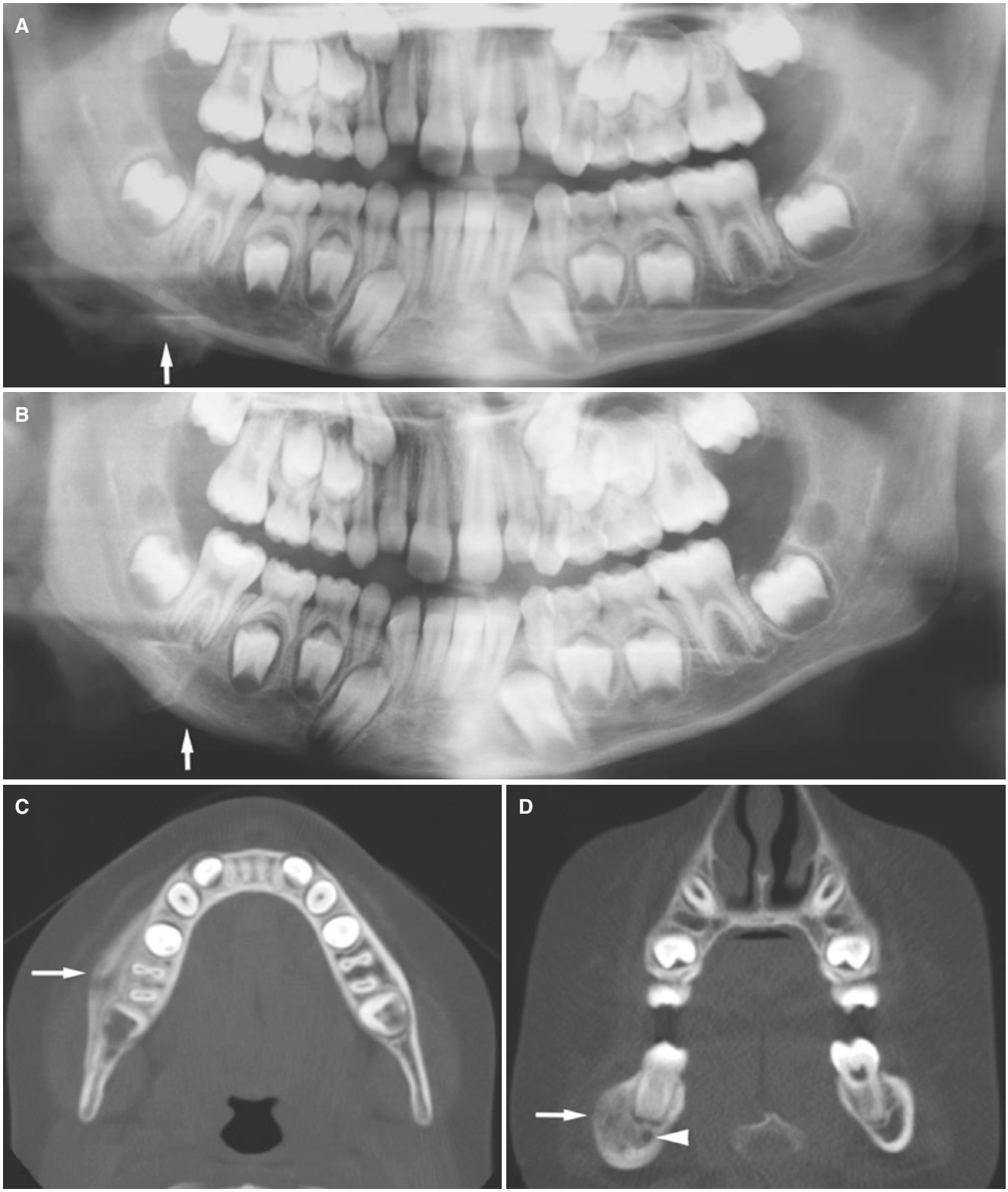

Fig. 5.7 Osteomyelitis with periostitis, mandible; 7-year-old female with variable perimandibular swelling, painless, probably caused by trauma against mandible 1 month before. (**A**) Panoramic view shows no abnormalities except slight periosteal reaction (*arrow*) (not noted until later examinations were performed). (**B**) Panoramic view 2 months after trauma shows more clearly periosteal reaction (*arrow*). (**C**) Axial CT image shows severe periosteal reaction buccally (*arrow*). (**D**) Coronal CT image shows sclerotic mandible with thickness almost twice normal (*arrow*), with radiolucent mandibular canal (*arrowhead*)

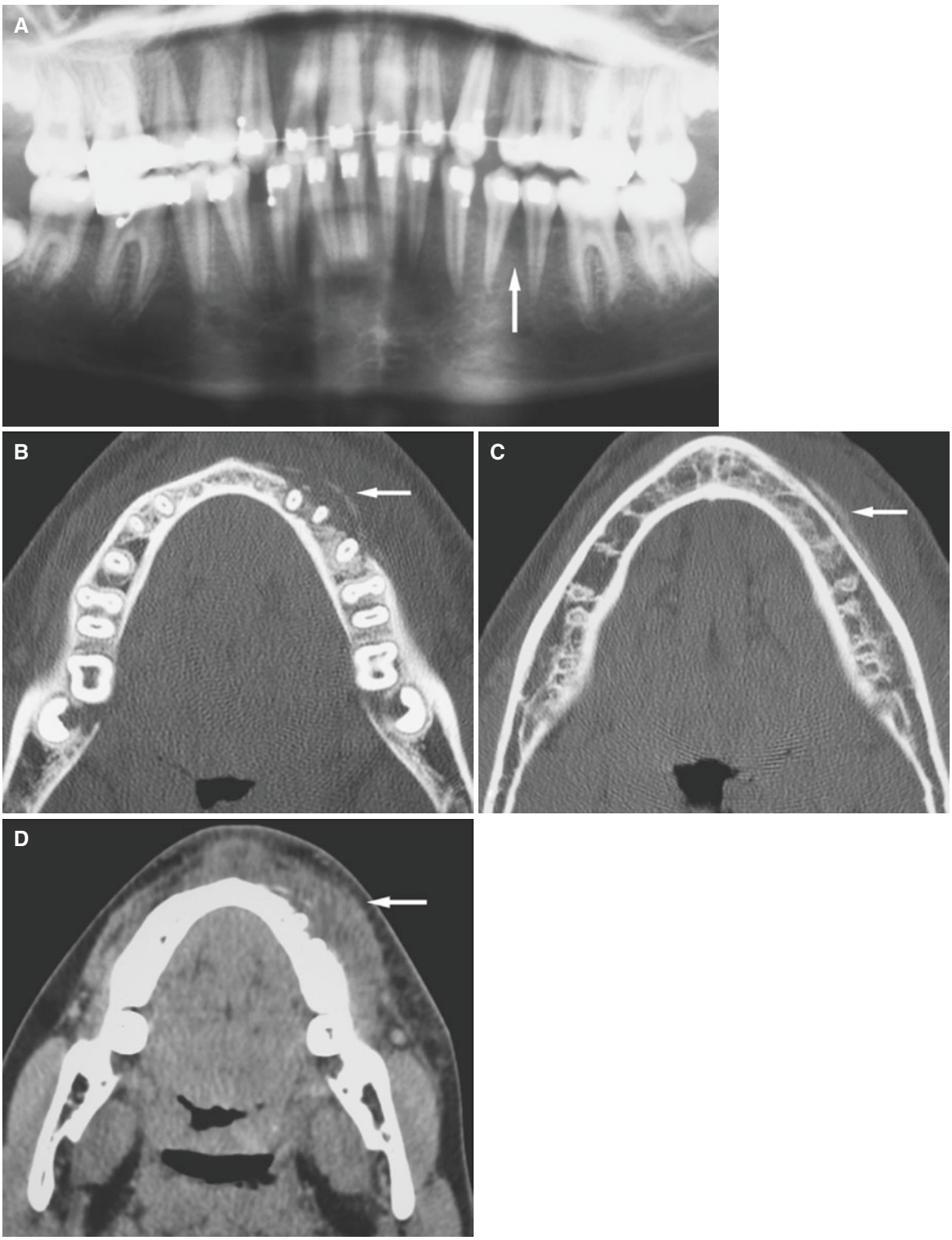

Fig. 5.8 Osteomyelitis with periostitis, mandible; 12-year-old female with 3-week history of gingival swelling that began less than a week after orthodontic adjustment of braces. (**A**) Panoramic view shows diffuse destruction in premolar area (*arrow*). (**B**) Axial CT image shows bone destruction and periosteal reaction in premolar area (*arrow*). (**C**) Axial CT image shows periosteal reaction caudad to teeth (*arrow*). (**D**) Axial CT image, soft-tissue window, shows diffuse soft-tissue swelling consistent with inflammatory infiltrate (*arrow*)

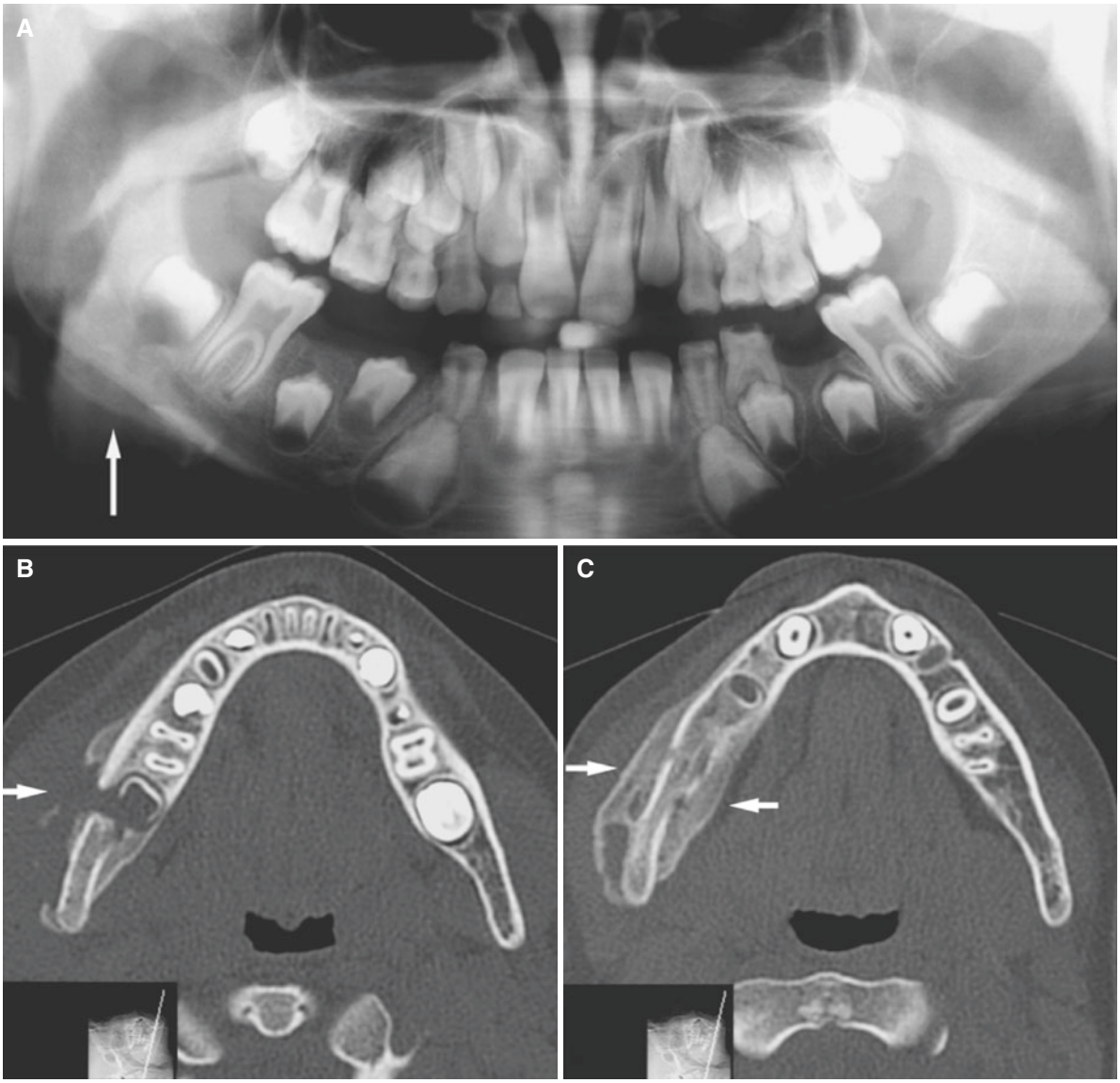

Fig. 5.9 Osteomyelitis with periostitis, mandible; 8-year-old male with variable right perimandibular swelling and pain for some months. (**A**) Panoramic view shows periosteal reaction (*arrow*). (**B**) Axial CT image shows destruction of buccal bone at the second molar germ (*arrow*). (**C**) Axial CT image shows extensive periosteal bone, buccally and lingually (*arrows*)

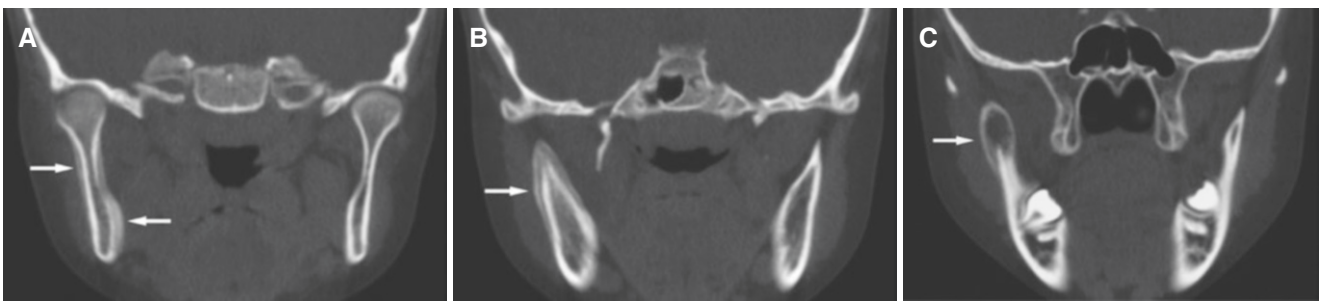

Fig. 5.10 Osteomyelitis with periostitis, mandible; 10-year-old female with variable facial swelling and restricted mouth-opening capacity. (**A**) Coronal CT image shows periosteal reaction buccally and lingually (*arrows*). (**B**) Coronal CT image shows periosteal reaction caudad for semilunar incisure (*arrow*). (**C**) Coronal CT image shows extensive reaction in coronoid process (*arrow*)

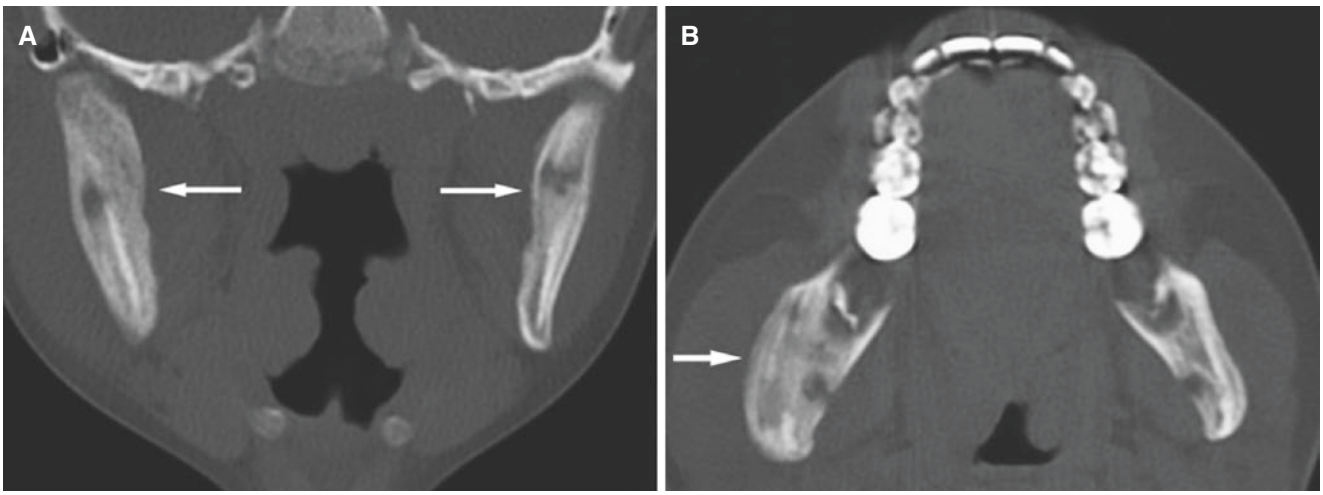

Fig. 5.11 Osteomyelitis with bilateral periostitis, mandible; 11-year-old female with variable pain and mouth-opening capacity for about 6 months, believed to be caused by juvenile arthritis. (**A**) Coronal CT image shows extensive periosteal bone bilaterally in ramus (*arrows*). (**B**) Axial CT image shows characteristic "onion skin" periosteal bone (*arrow*)

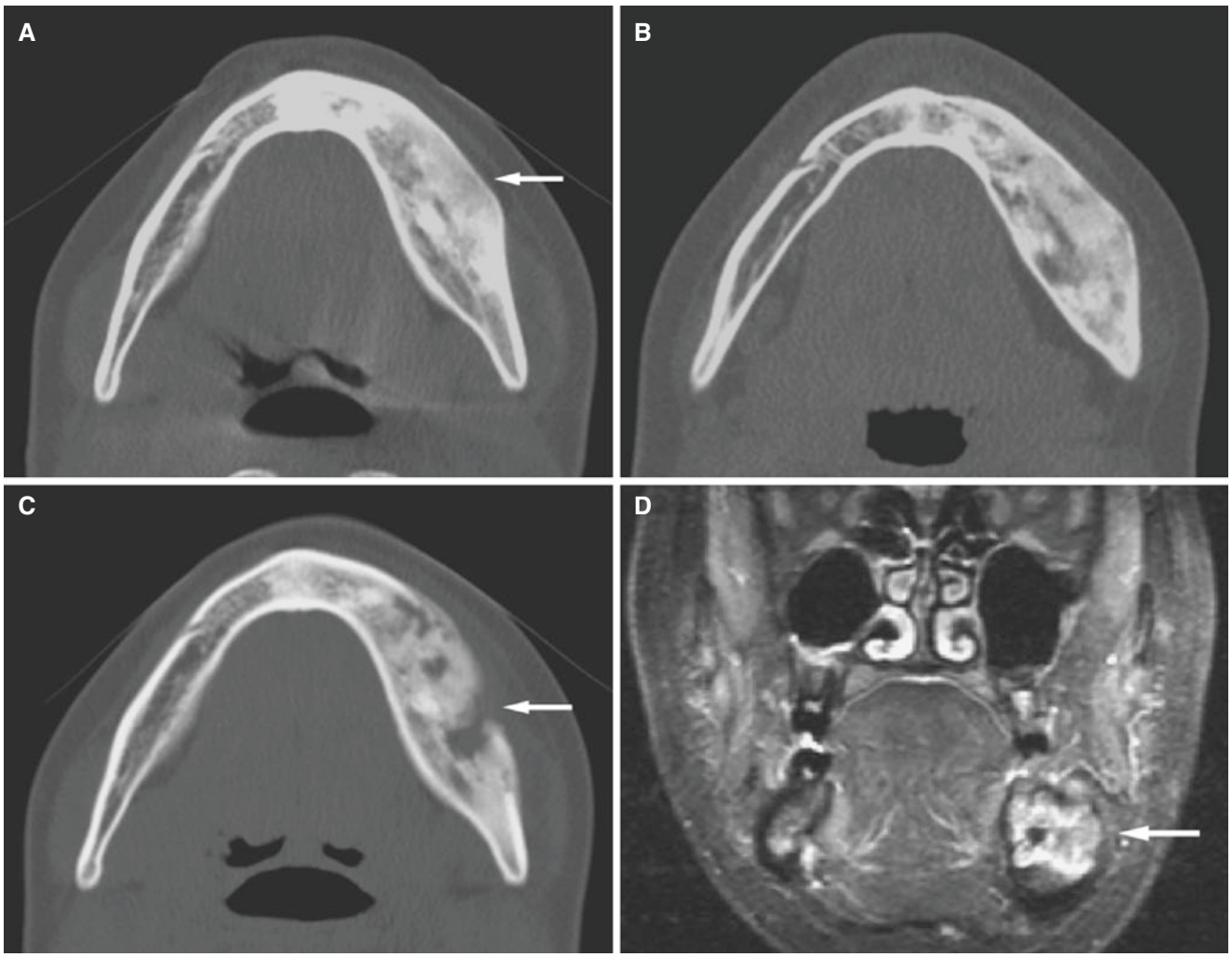

Fig. 5.12 Osteomyelitis with periostitis, mandible; 16-year-old female with a 2-year history of infection, with development of facial asymmetry after unsuccessful endodontic treatment of the first and second molars that eventually were extracted. (**A**) Axial CT image shows sclerotic and thickened mandibular bone (*arrow*). (**B**) Axial CT image, 1-year follow-up, shows small areas of bone destruction. (**C**) Axial CT image, 2-year follow-up, shows larger areas of bone destruction (*arrow*). (**D**) Coronal STIR MRI, 2-year follow-up, shows high signal consistent with active inflammation (*arrow*)

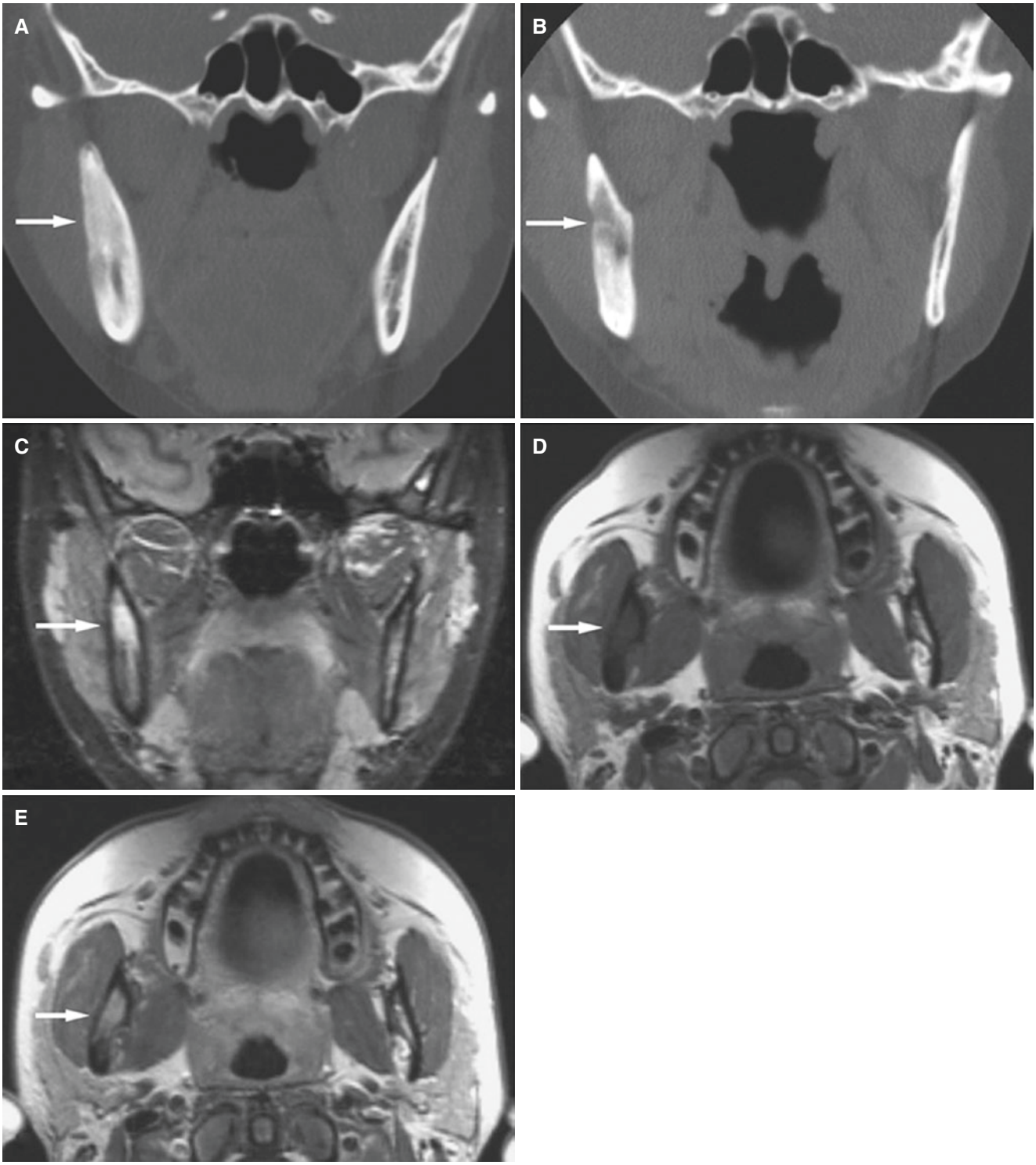

Fig. 5.13 Osteomyelitis with periostitis, mandible; 25-year-old female with a 4-year history of infection; after a 3-year period of silence because of antibiotic and hyperbaric oxygenic treatment, now with pain in the right cheek. (**A**) Coronal CT image shows sclerotic, thickened ramus (*arrow*). At 3-year follow-up, (**B**) coronal CT shows area of bone destruction (*arrow*). (**C**) Coronal STIR MRI shows high signal in ramus (*arrow*). (**D**) Axial T1-weighted pre-Gd MRI shows low signal in bone marrow (*arrow*). (**E**) Axial T1-weighted post-Gd MRI shows contrast enhancement consistent with inflammatory activity (*arrow*). Surgical intervention confirmed inflammatory activity (granulation tissue)

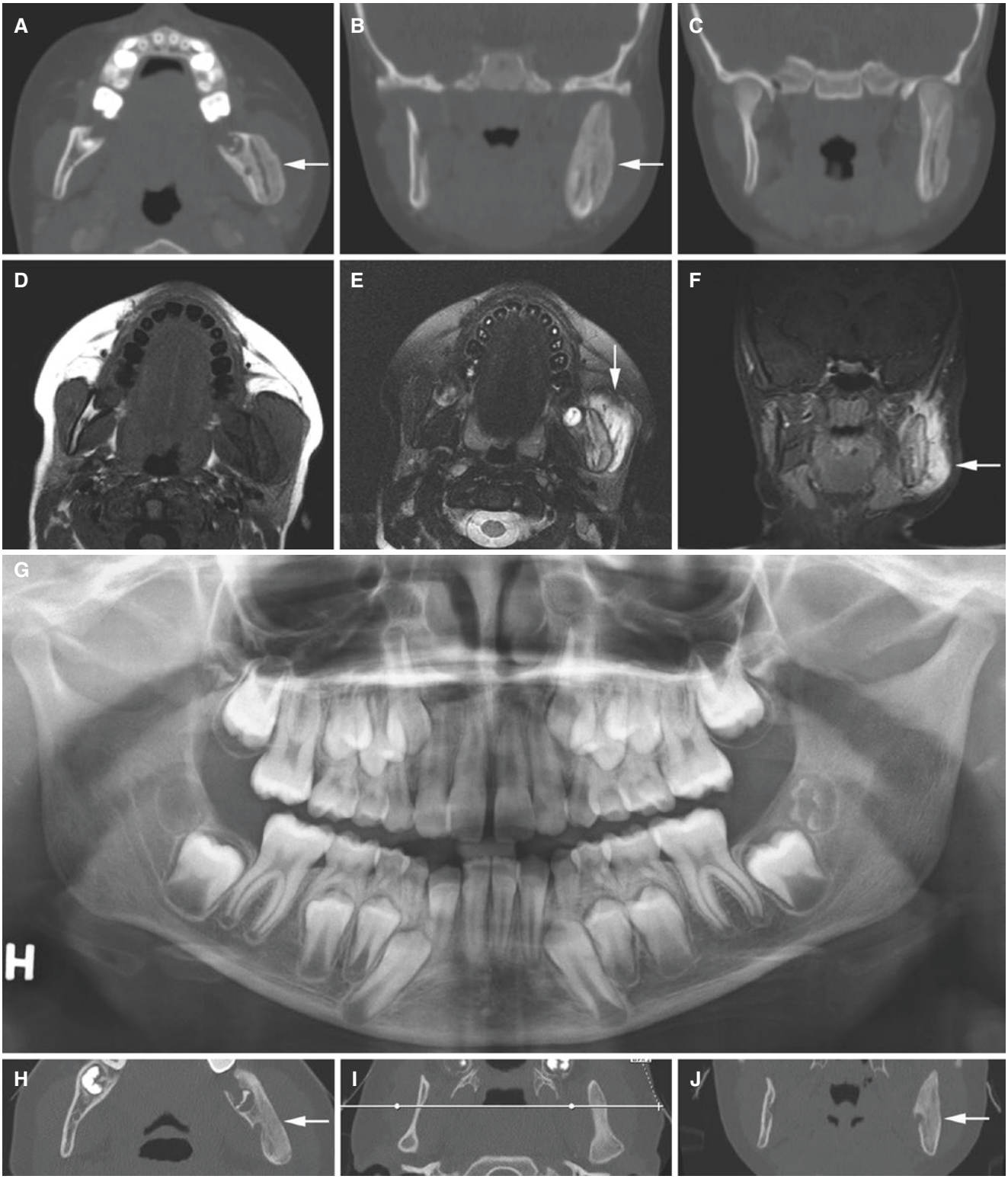

Fig. 5.14 Osteomyelitis with periostitis, mandible; 9-year-old female with left-sided facial swelling. (**A**) Axial and (**B**, **C**) coronal CT images show large buccal and small lingual periosteal bone apposition (*arrow*). (**D**) Axial T1-weighted, (**E**) axial T2-weighted, and (**F**) coronal T1-weighted fat sat post-Gd MRI show high signal intensity on T2 (*arrow*) and contrast enhancement in enlarged soft-tissue surrounding bone apposition buccally (*arrow*). Five months later, (**G**) panoramic view shows no evident bone pathology, but (**H**) axial, (**I**) axial (with cursor line), and (**J**) coronal CT images show new bone emerging into original bone (*arrow*)

5.4 Osteoradionecrosis

Figs. 5.15, 5.16, 5.17, 5.18, and 5.19

5.4.1 Definition

Several proposed. One frequently used is an "area of exposed bone (larger than 1 cm) in the field of irradiation that has failed to show any evidence of healing for at least 6 months."

An alternative is "radiologic evidence of bone necrosis within radiation field where tumor recurrence has been excluded," also including cases with intact oral mucosa.

With a history of antiresorptive therapy to the jaws, medication-related osteonecrosis should be considered.

5.4.2 Clinical Features

- Mandible far more often than maxilla
- Wide spectrum; acute/chronic, nonsuppurative/suppurative
- Pain or no pain
- Exposed bone frequent, but also soft-tissue cover
- In advanced stage: trismus, fistula, and pathologic fracture

5.4.3 Imaging Features

- Mainly destructive; cancellous and/or cortical bone
- Mixture of radiolucent and radiopaque appearance may occur
- Unilateral or bilateral
- Usually without periosteal bone reaction
- Advanced stage: sequestration and pathologic fracture
- T1-weighted MRI: reduced signal in bone marrow
- T2-weighted and STIR MRI: high signal in bone marrow
- T1-weighted post-Gd MRI: contrast enhancement in bone marrow
- T1-weighted, T2-weighted, and STIR MRI: low signal from sequestra

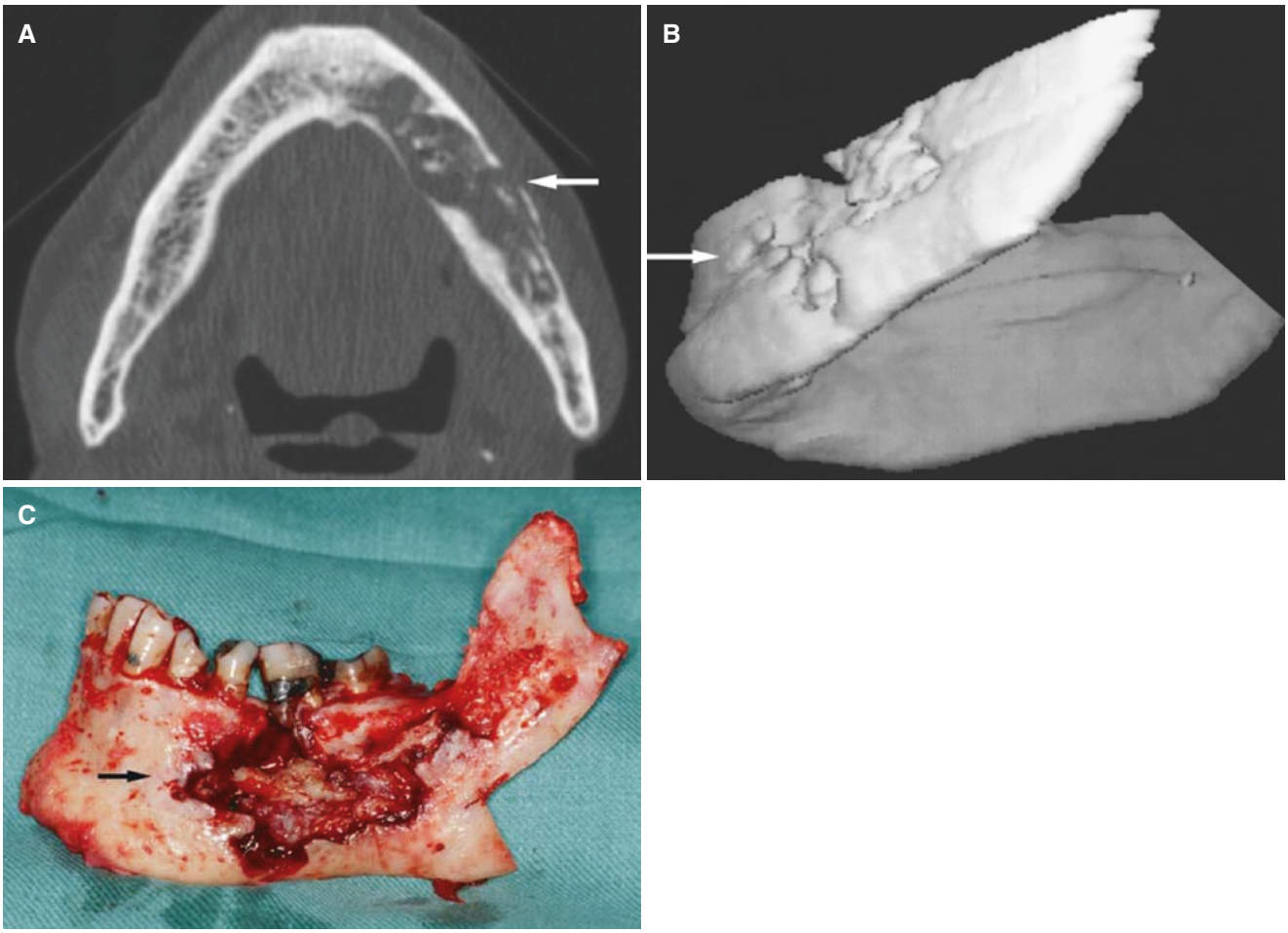

Fig. 5.15 Osteoradionecrosis, mandible; 79-year-old male with extensive bone destruction and severe symptoms. (**A**) Axial CT image shows severe destruction of left mandibular body (*arrow*). (**B**) 3D CT image shows severe destruction of buccal cortical bone (*arrow*). (**C**) Surgical hemimandible specimen with destruction (*arrow*) corresponding to 3D CT image presentation

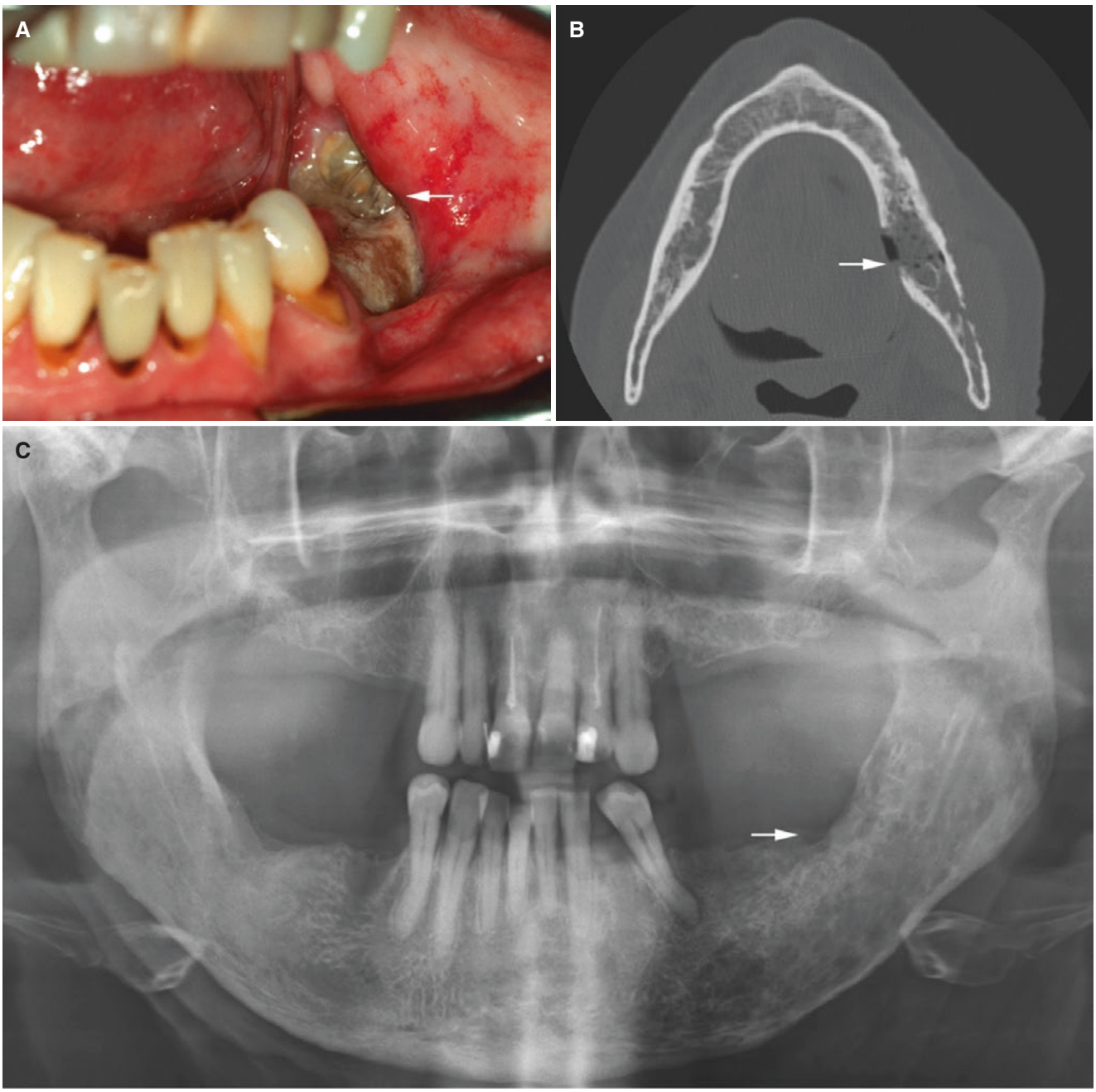

Fig. 5.16 Osteoradionecrosis, mandible; 63-year-old female with exposed bone in the left mandible after surgical treatment of tongue cancer and postoperative radiation therapy. (**A**) Clinical photograph shows exposed bone (*arrow*). (**B**) Axial CT image shows destructive changes of cortical and cancellous bone (*arrow*). (**C**) Panoramic view indicates bone destruction (*arrow*), also in mandibular body

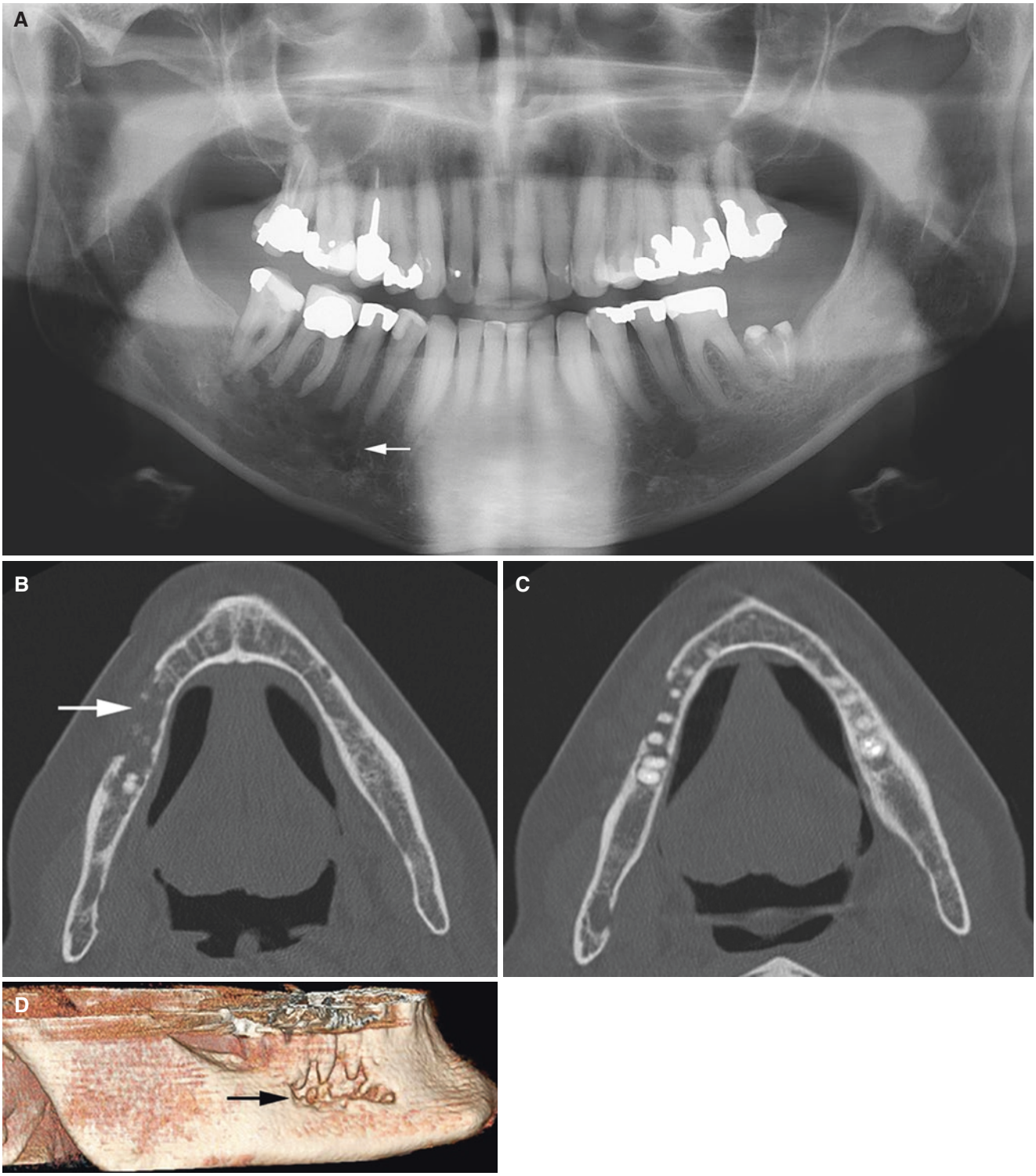

Fig. 5.17 Osteoradionecrosis, mandible; 67-year-old male with routine control of dentition after radiation therapy of B-cell lymphoma. (**A**) Panoramic view shows bone destruction in right mandibular body (*arrow*). (**B**, **C**) Axial and (**D**) 3D CT images show destruction of buccal cortical plate and cancellous bone (*arrow*)

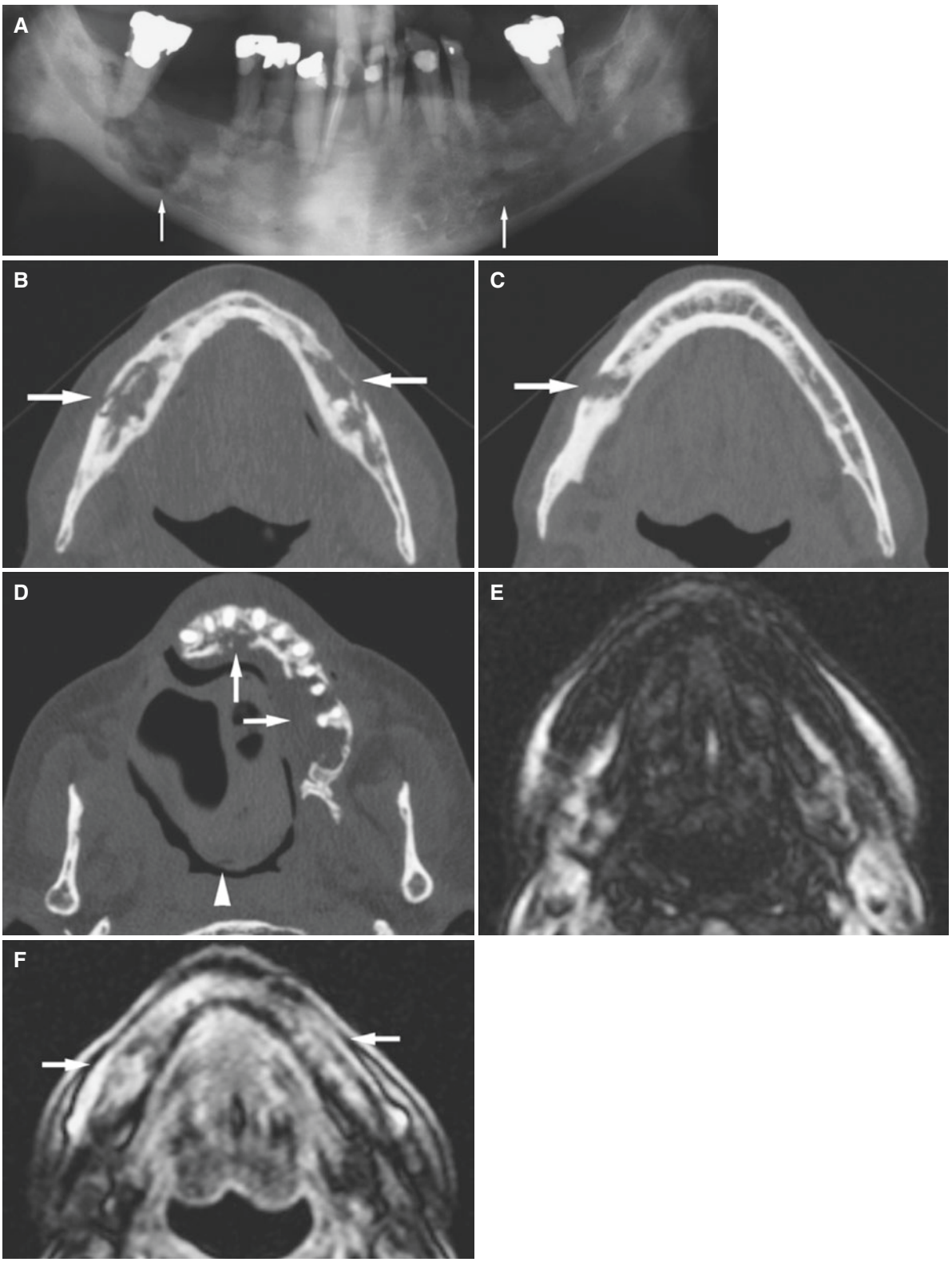

Fig. 5.18 Osteoradionecrosis, mandible and maxilla; 55-year-old male 2 years after hemimaxillectomy and radiation therapy of adenoid cystic carcinoma. Denture could not be removed (see *arrowhead* in **D**). (**A**) Panoramic view shows destructive changes bilaterally (*arrows*). (**B**) Axial CT image shows evident bilateral destruction with sequestra (*arrows*). (**C**) Axial CT image shows more severe buccal destruction on the right side (*arrow*). (**D**) Axial CT maxilla shows severe destruction of palatal alveolar bone (*arrows*). (**E**) Axial T1-weighted pre-Gd MRI shows low signal bilaterally in bone marrow. (**F**) Axial T1-weighted post-Gd MRI shows bilateral contrast enhancement in bone marrow (*arrows*)

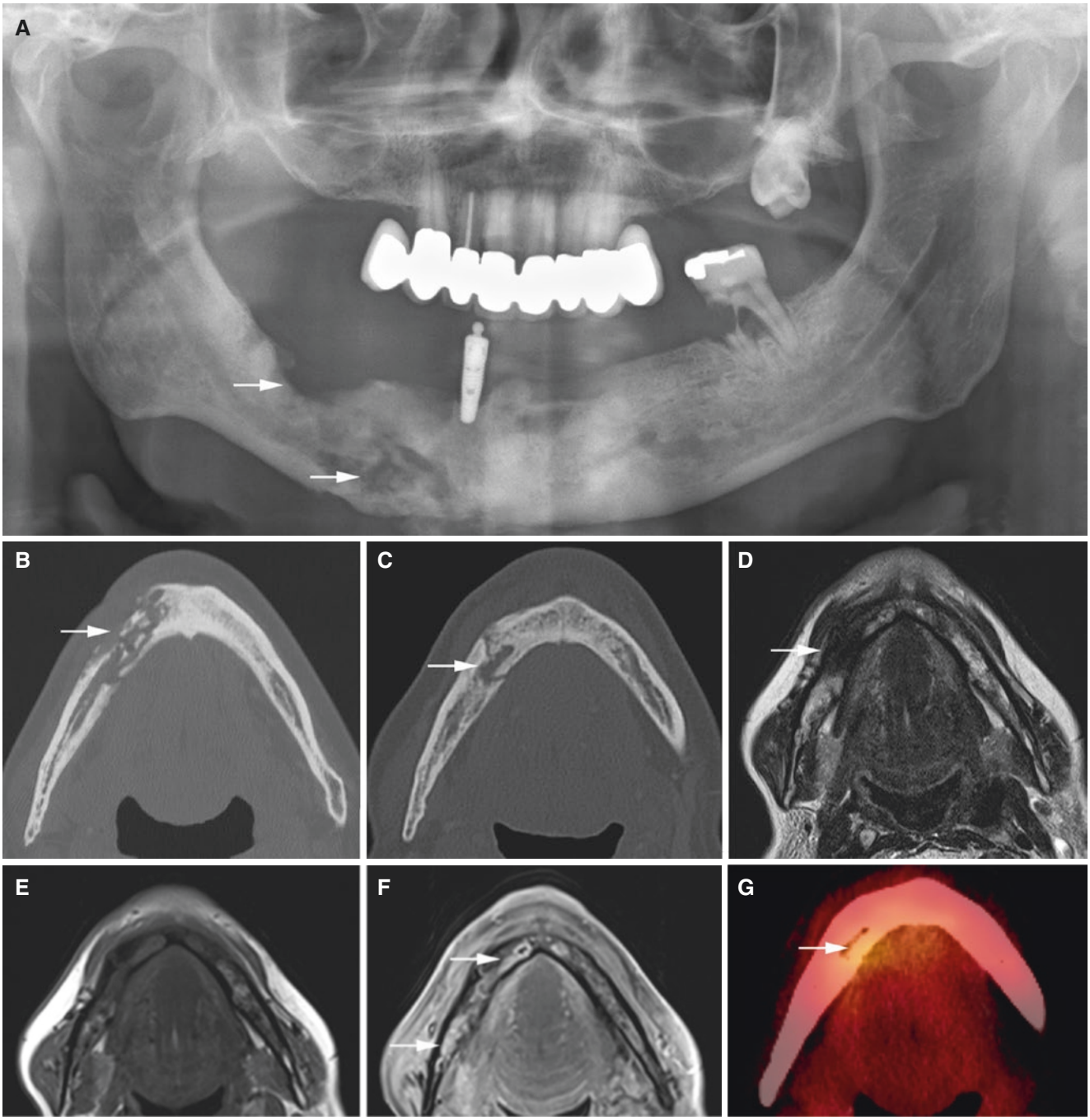

Fig. 5.19 Osteoradionecrosis, mandible; 47-year-old male with right-sided surgically treated sublingual cancer and postoperative radiation therapy. (**A**) Panoramic view shows bone destruction (*arrows*). (**B**) Axial CT image shows destruction with sequestration in right mandible (*arrow*). Nine months later, (**C**) axial CT image shows bone healing, but still fissure-like bone defect (*arrow*). (**D**) Axial T2-weighted MRI shows low signal in the same area (*arrow*). (**E**) Axial T1-weighted pre-Gd and (**F**) axial T1-weighted fat sat post-Gd MRI show moderate contrast enhancement in the right mandible (*arrows*) and probably also in the left mandible. (**G**) PET-CT image shows slightly increased FDG uptake in the right mandible (*arrow*)

5.5 Medication-Related Osteonecrosis

Figs. 5.20, 5.21, 5.22, 5.23, 5.24, 5.25, 5.26, 5.27, 5.28, and 5.29

Synonyms: Bisphosphonate-related necrosis, antiresorptive therapy-related osteonecrosis.

5.5.1 Definition

Patients may be considered to have medication-related osteonecrosis if all the following characteristics are present:

- Current or previous treatment with antiresorptive or anti-angiogenic agents
- Exposed bone or bone that can be probed through an intraoral or extraoral fistula in the maxillofacial region that has persisted for longer than 8 weeks
- No history of radiation therapy to the jaws or obvious metastatic disease to the jaws

(American Association of Oral and Maxillofacial Surgeons Position Paper on Medication-Related Osteonecrosis of the Jaw—2014 Update).

A number of bisphosphonates and other highly potent antiresorptive medicaments may lead to osteonecrosis, particularly when used intravenously and after invasive dental surgical procedures.

5.5.2 Clinical Features

See **Osteoradionecrosis**

5.5.3 Imaging Features

See **Osteoradionecrosis**:

- Bone sclerosis may be evident
- Periosteal bone formation may be evident

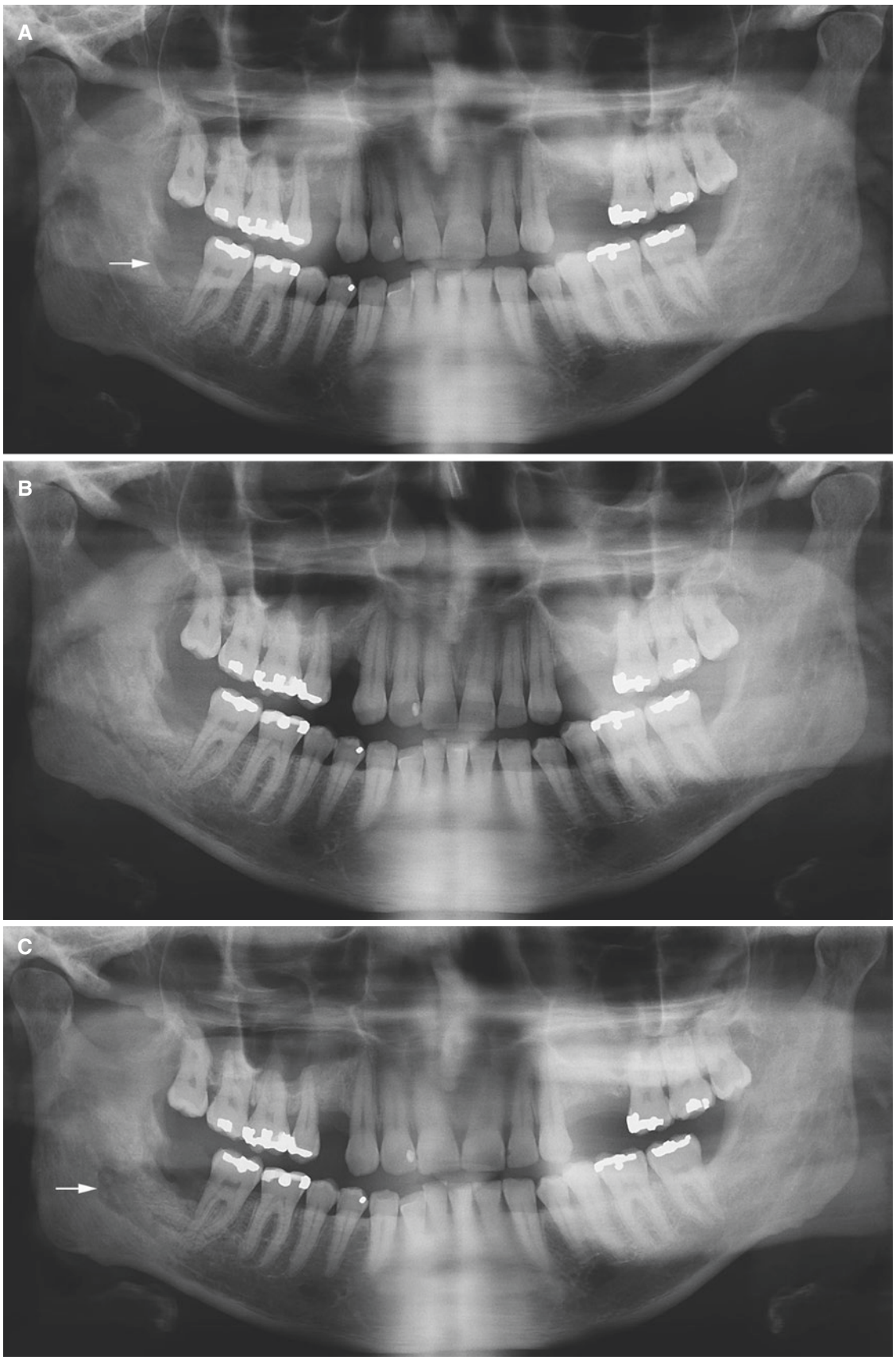

Fig. 5.20 Medication-related osteonecrosis, mandible, with progression at follow-up; 48-year-old male (prostatic cancer and skeletal metastases, under antiresorptive therapy) with unhealed tooth socket. (**A**) Panoramic view shows no healing after extraction of wisdom tooth in the right mandible 4 months earlier (*arrow*). (**B**) Panoramic view 6 months later (than **A**) and (**C**) panoramic view 5 months later (than **B**) show progressive destruction with sequestration (*arrow*)

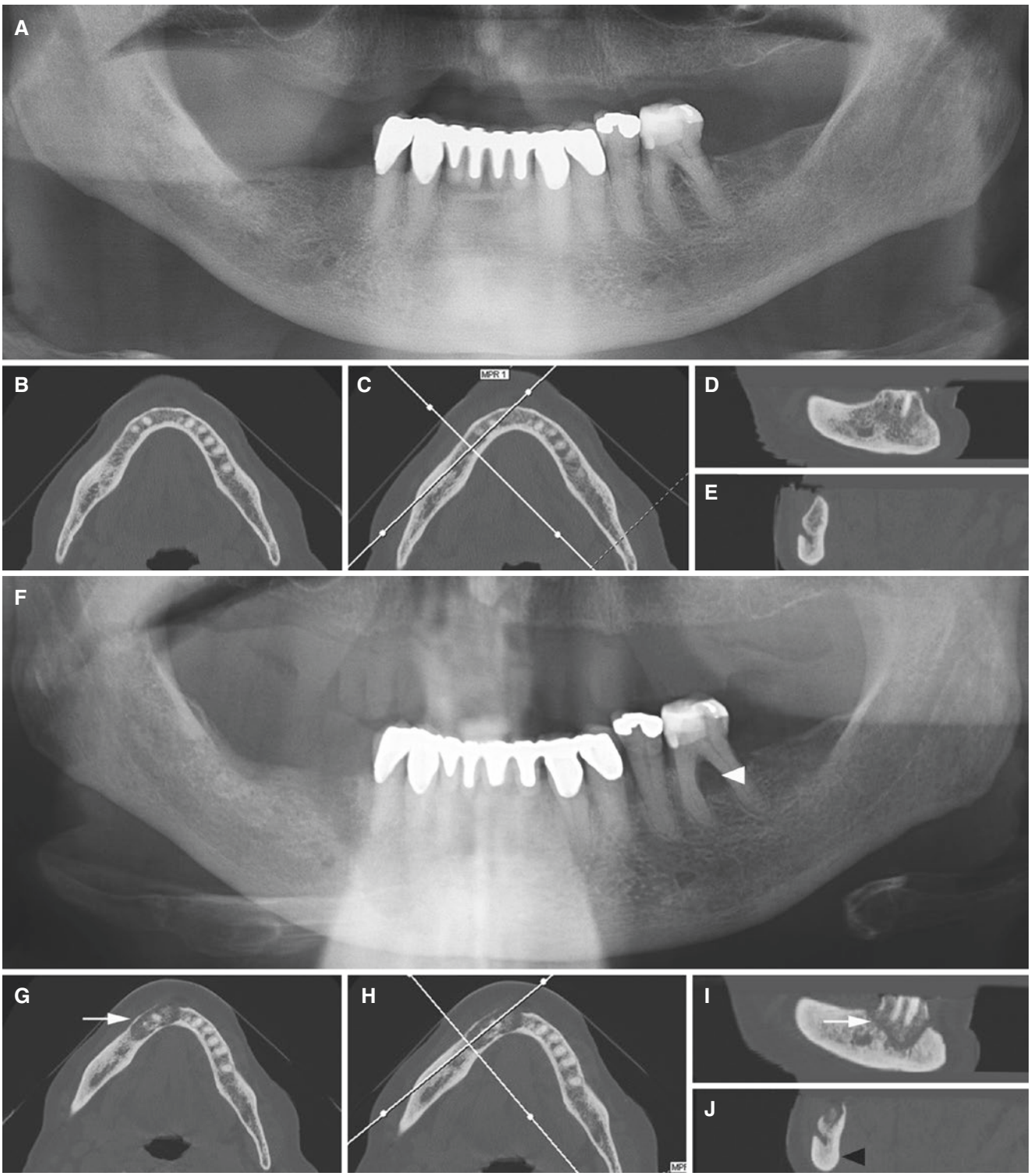

Fig. 5.21 Medication-related osteonecrosis, mandible, with progression at follow-up; 74-year-old female (breast cancer and metastases, under antiresorptive therapy) with exposed bone and fistula at canine and first premolar in the right mandible. (**A**) Panoramic view, (**B**) axial, (**C**) axial (with *cursor lines*), (**D**) oblique sagittal, and (**E**) oblique coronal CT images show apparently normal bone. Six months later, (**F**) panoramic view, (**G**) axial, (**H**) axial (with *cursor lines*), (**I**) oblique sagittal, and (**J**) oblique coronal CT images show bone destruction with sequestration (*arrow*) and sclerosis (*black arrowhead*). Bone destruction progression also in bifurcation of the first molar (*white arrowhead*)

Fig. 5.22 Medication-related osteonecrosis, mandible, stable at follow-up; 67-year-old male (prostatic cancer and metastases for more than 8 years, under antiresorptive therapy) with variable pain, chin fistulas, and sharp bony edges after exfoliation of mandibular incisors. (**A**) Panoramic view shows severely sclerotic mandible and periosteal bone reaction (*arrows*). Fourteen months later (under antibiotic treatment), (**B**) panoramic view shows more solid periosteal bone apposition (*arrows*) and more evident lamina dura in empty (unhealed) tooth sockets (*arrowheads*)

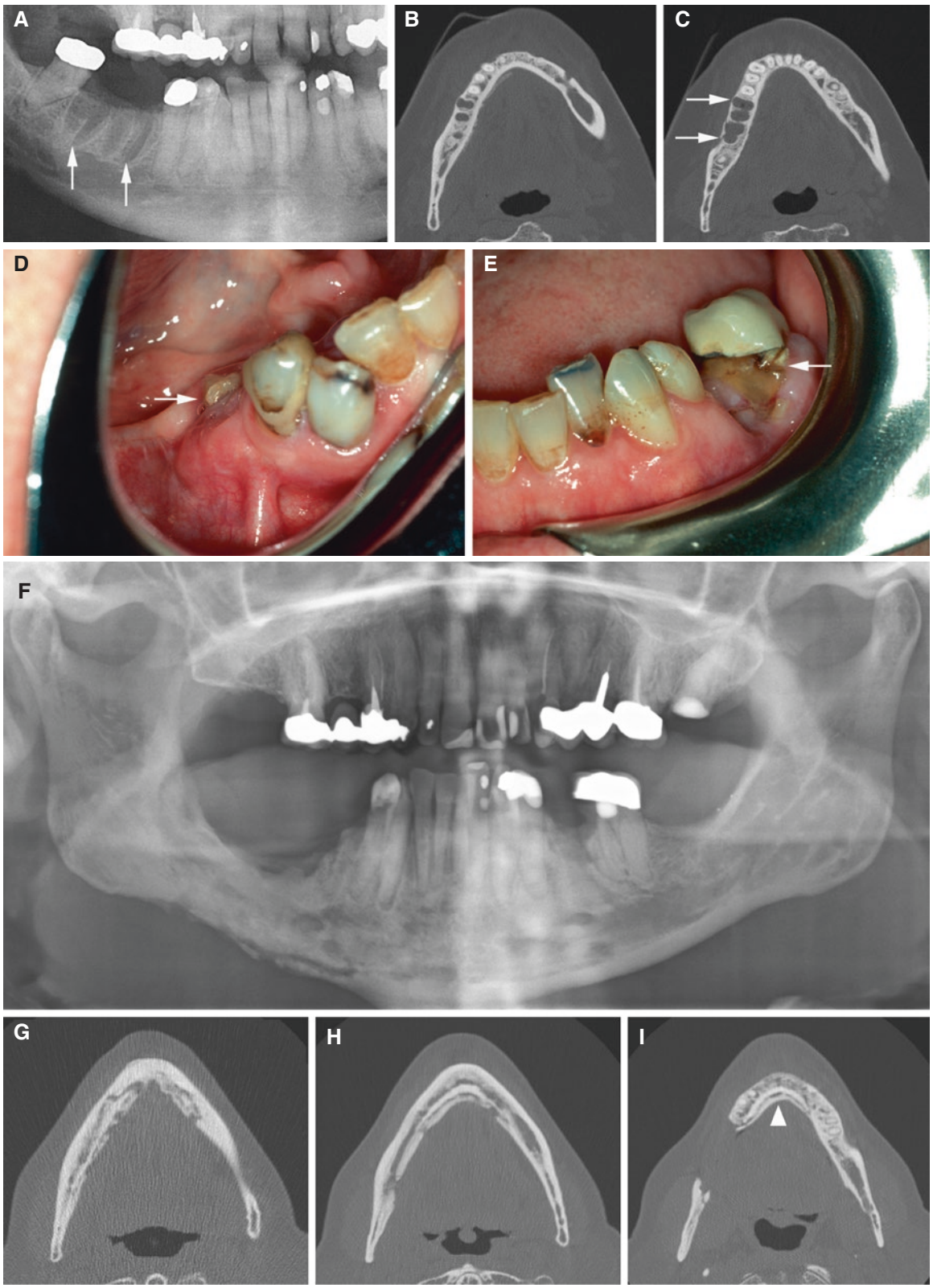

Fig. 5.23 Medication-related osteonecrosis, mandible, with progression at follow-up; 68-year-old female (multiple myeloma, under antiresorptive therapy) with exposed bone bilaterally. (**A**) Panoramic view and (**B**, **C**) axial CT images show no healing of tooth sockets (*arrows*) in the right mandible after extraction of the second molar 7 months earlier and first molar 3 months earlier. Remaining molar in the right mandible and second premolar in the left mandible were extracted shortly after. Three years and 2 months later, (**D**, **E**) clinical photographs show exposed bone in areas of extraction (*arrow*). (**F**) Panoramic view and (**G**, **H**, **I**) axial CT images now show severe destruction with sequestration and sclerosis in the right mandible and anterior part of the left mandible and lingual bone apposition (*arrowhead*), compare with (**B**, **C**)

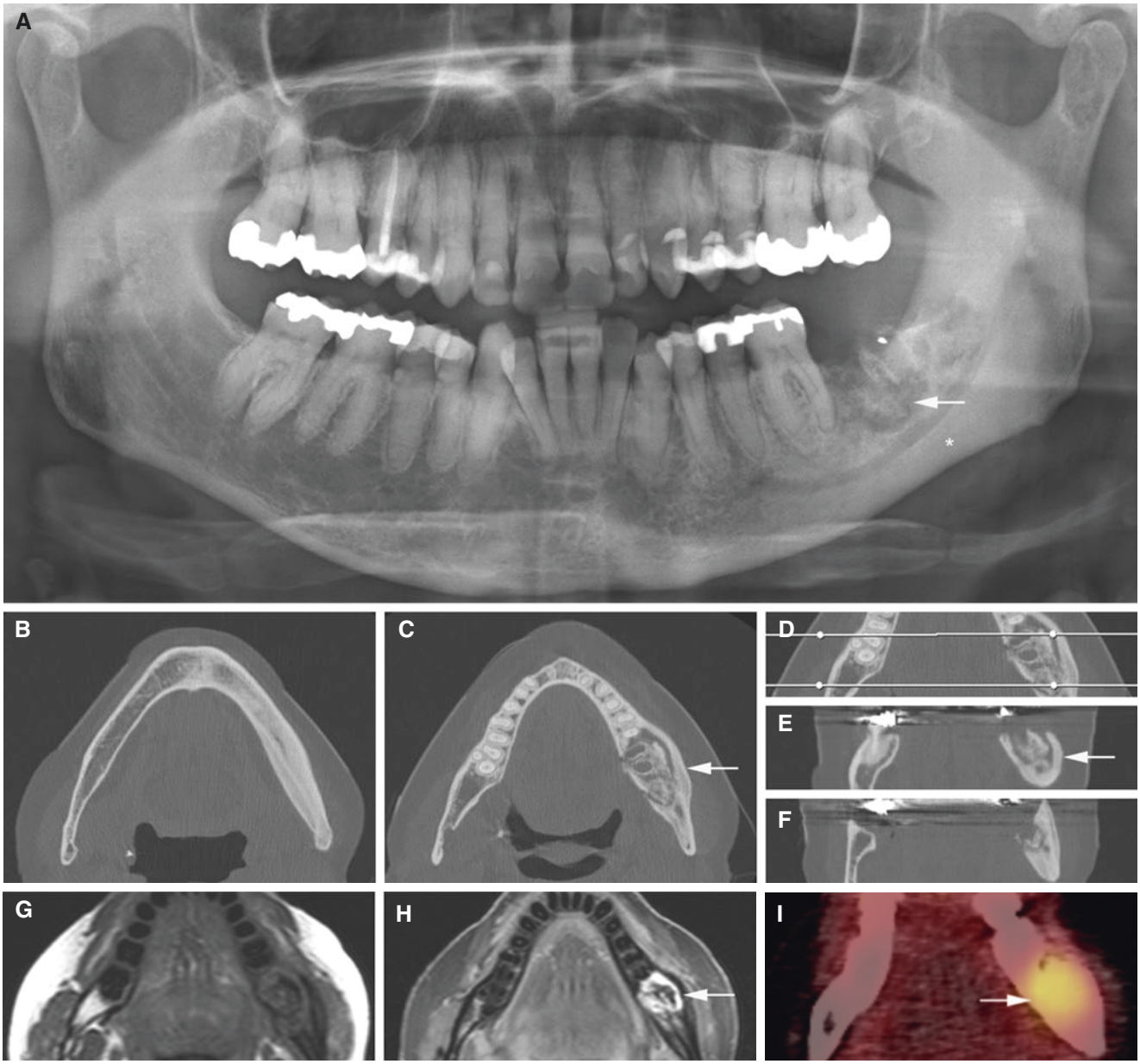

Fig. 5.24 Medication-related osteonecrosis, mandible; 64-year-old female (breast cancer and metastases, under antiresorptive therapy) with some pain, swelling, and exposed bone after tooth extraction (second molar) in the left mandible about 2 years earlier. (**A**) Panoramic view shows bone destruction with sequestration (*arrow*) and sclerosis (*asterisk*). (**B**, **C**) Axial, (**D**) axial (with *cursor lines*), and (**E**, **F**) coronal CT images confirm bone destruction, sequestration, and sclerosis (*arrow*). (**G**) Axial T1-weighted pre-Gd and (**H**) axial T1-weighted fat sat post-Gd MRI show contrast enhancement around sequester (*arrow*). (**I**) PET-CT image shows increased FDG uptake (*arrow*)

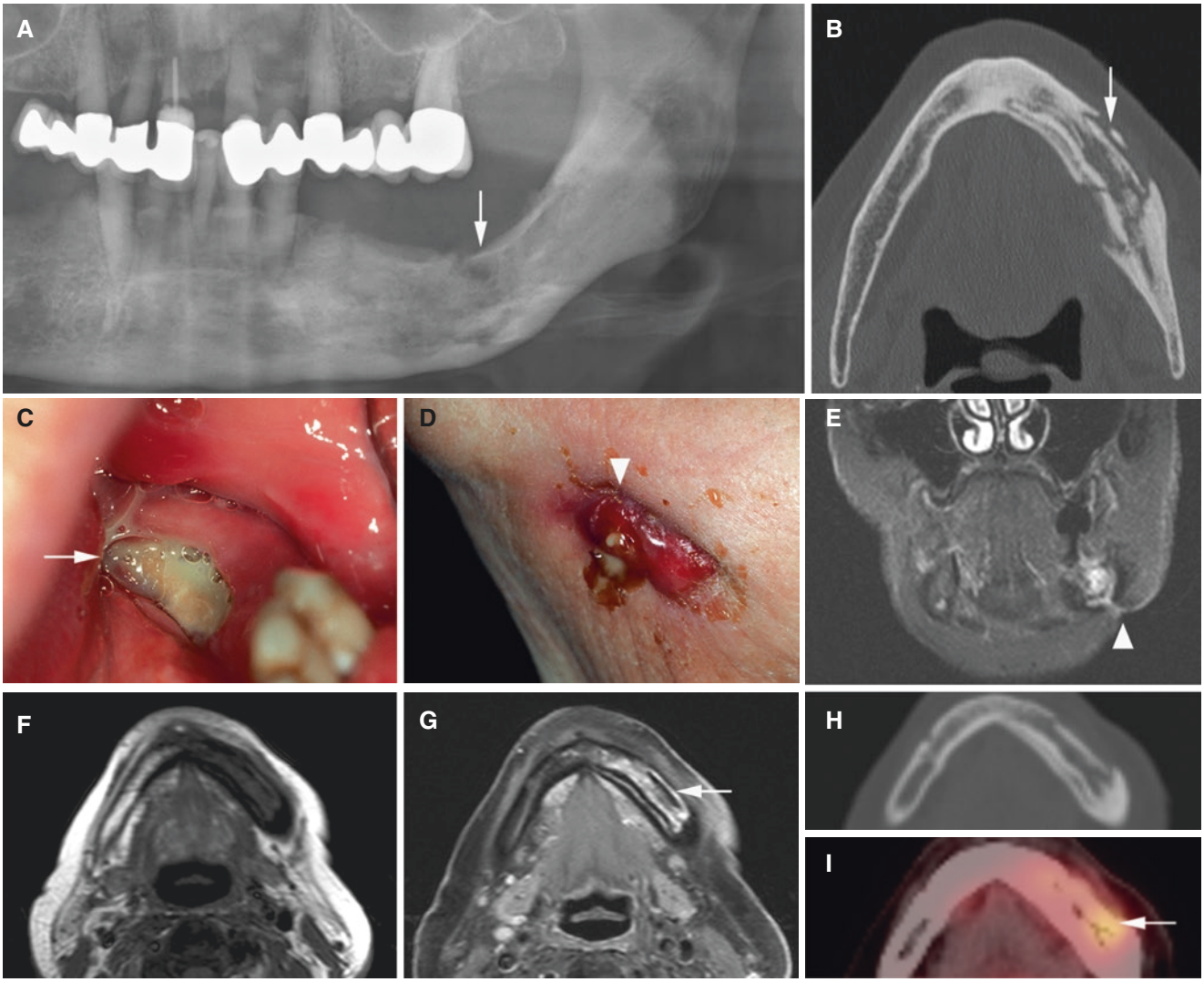

Fig. 5.25 Medication-related osteonecrosis, mandible, with pathological fracture and fistula; 64-year-old female (breast cancer and skeletal metastases, under antiresorptive therapy) with exposed bone and fistula to the skin in the left mandible. (**A**) Panoramic view shows irregular radiolucent area in left mandibular body, indicating pathologic fracture (*arrow*). (**B**) Axial CT image shows severe destruction with sequestration (*arrow*). (**C**, **D**) Clinical photographs show exposed bone (*arrow*) and fistula to the skin (*arrowhead*). Nine months later, (**E**) coronal STIR MRI shows high signal in the left mandible and in persistent fistula to the skin (*arrowhead*). (**F**) Axial T1-weighted pre-Gd and (**G**) axial T1-weighted fat sat post-Gd MRI show contrast enhancement (*arrow*). (**H**) Low-dose CT image shows bone healing in the left mandible, compared with (**B**). (**I**) PET-CT image (the day after MRI) shows slightly increased FDG uptake (*arrow*), compare with Fig. 5.24 (**I**)

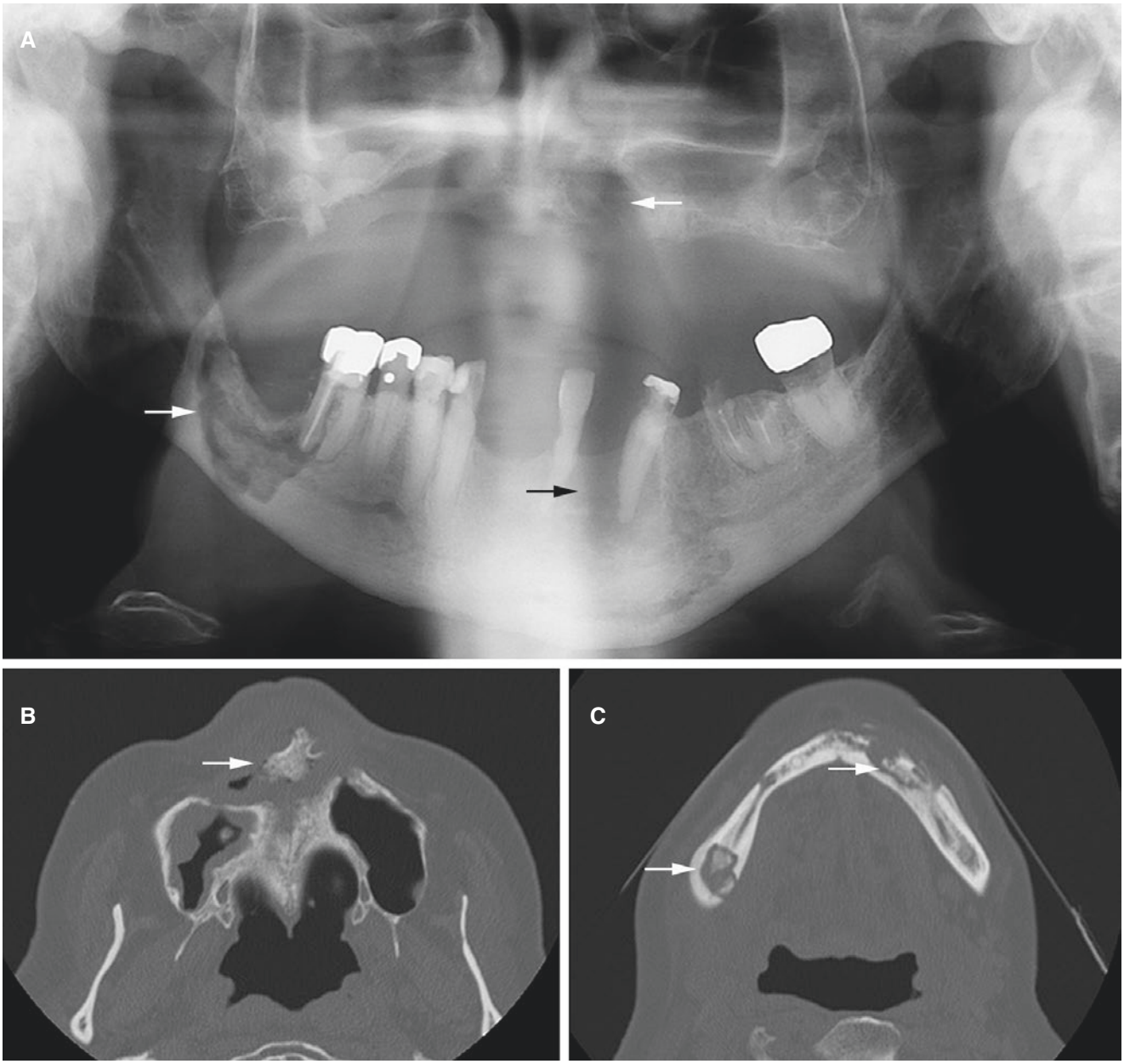

Fig. 5.26 Medication-related osteonecrosis, mandible and maxilla; 81-year-old male (prostatic cancer and metastases, 2.5 years with anti-resorptive therapy) with exposed bone both in the mandible and maxilla and with pain on chewing. (**A**) Panoramic view shows destruction and sequestration in the right mandible, in anterior part of left mandible, and in anterior maxilla (*arrows*). (**B**) Axial CT image of maxilla and (**C**) axial CT image of mandible confirm destruction and sequestration (*arrows*)

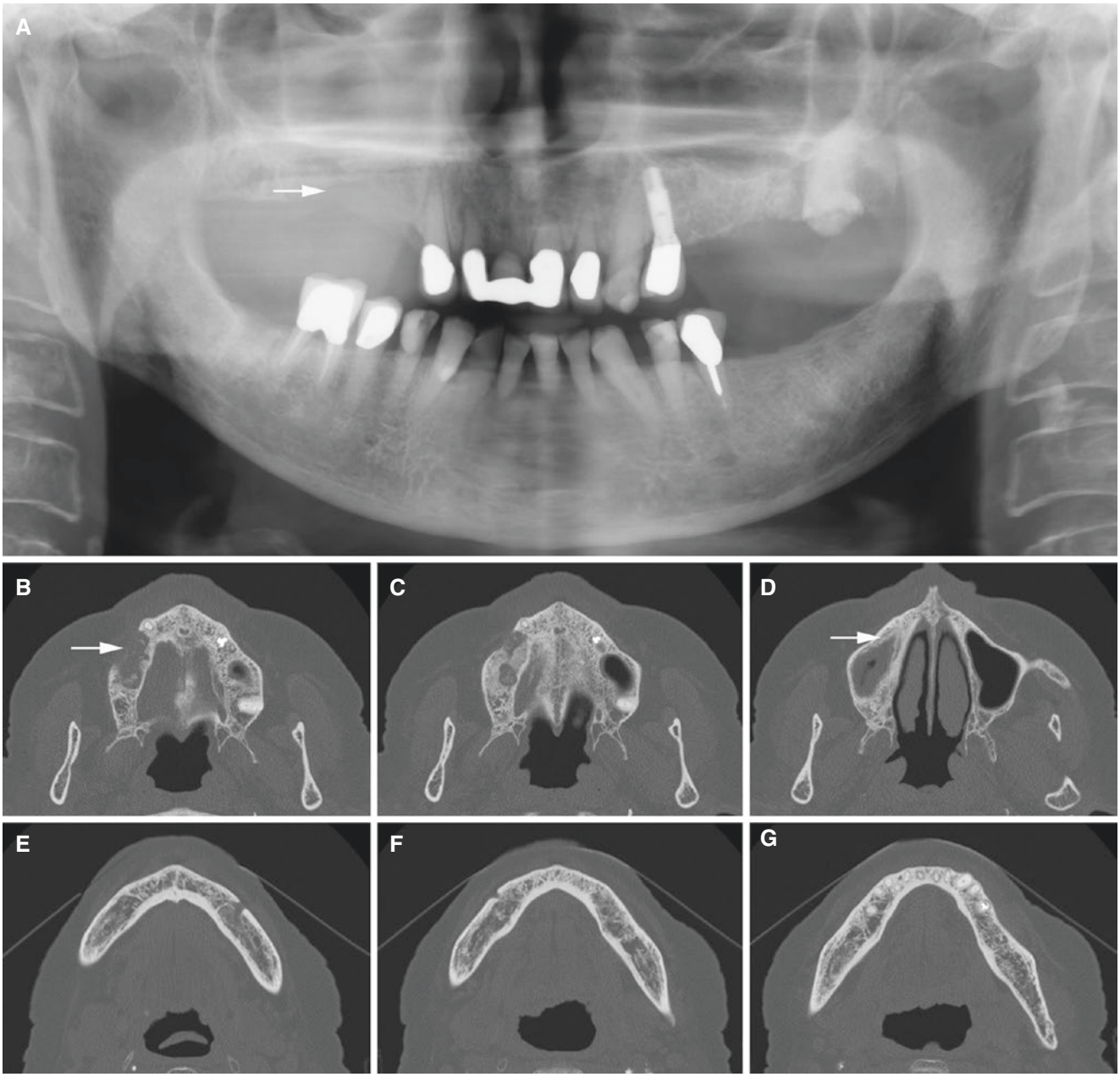

Fig. 5.27 Medication-related osteonecrosis, maxilla; 78-year-old female (osteoporosis, more than 10 years with antiresorptive therapy); loose teeth with pus recently removed from the right maxilla. (**A**) Panoramic view shows diffuse destruction (*arrow*). (**B**, **C**) Axial CT images confirm destruction in the right maxilla (*arrow*). (**D**) Axial CT image shows mucosal thickening in right maxillary sinus and bone apposition within sinus (*arrow*). (**E**, **F**, **G**) Axial CT images of mandible show normal bone

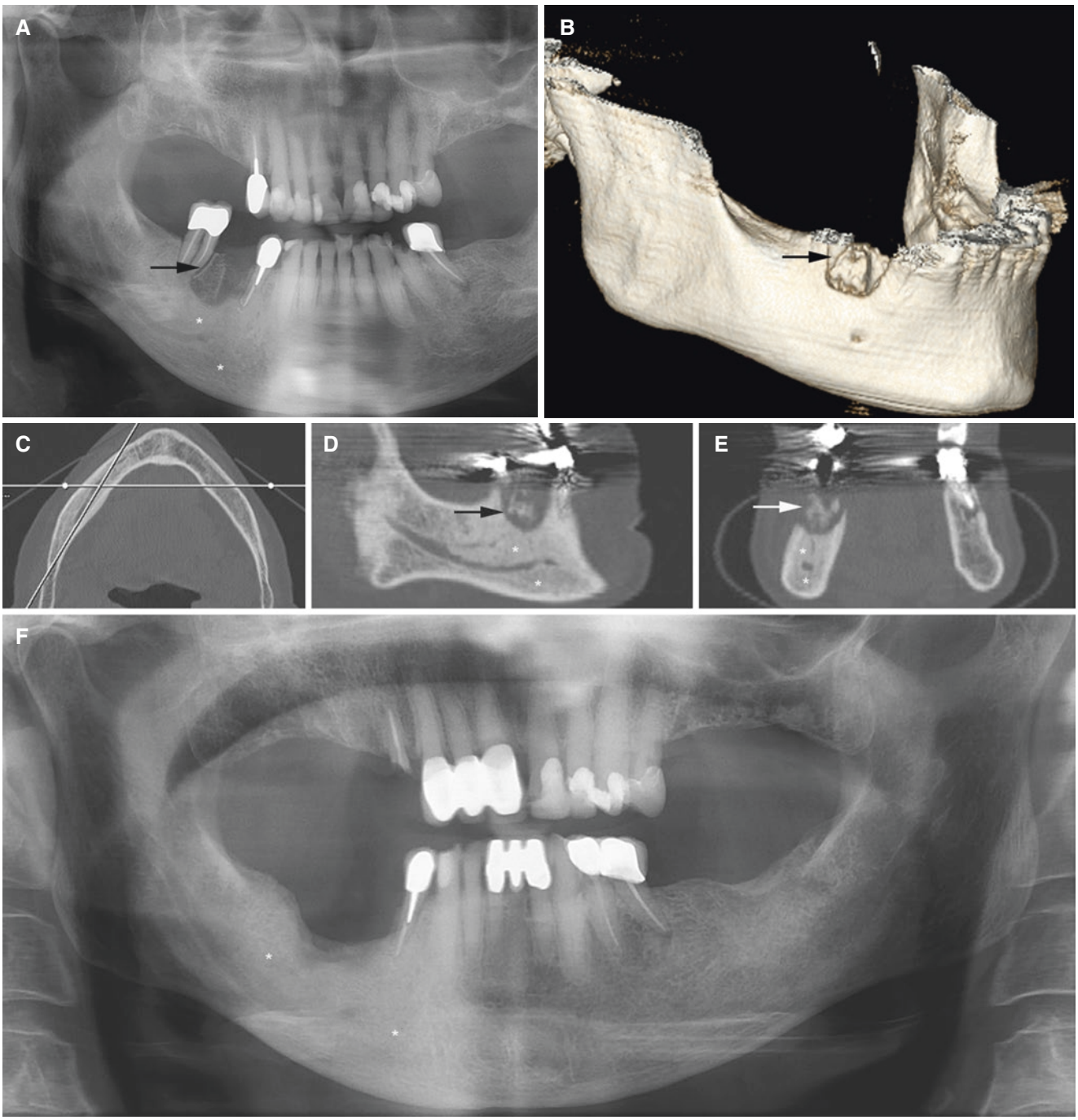

Fig. 5.28 Medication-related osteonecrosis, mandible with some healing/improvement at follow-up; 80-year-old female (osteoporosis, more than 10 years with antiresorptive therapy) with exposed bone and fistula and lack of healing 1 year after tooth extraction (first molar) in the right mandible. (**A**) Panoramic view shows bone destruction, with sequestration (*arrow*) and sclerosis (*asterisks*). (**B**) 3D CT image confirms sequestration (*arrow*). (**C**) Axial (with *cursor lines*), (**D**) oblique sagittal, and (**E**) coronal CT images confirm sequestration (*arrow*) and sclerosis (*asterisks*). One year and 11 months after discontinuation of antiresorptive therapy and 1 year and 3 months after sequestrectomy and extraction of the second molar, (**F**) panoramic view shows more normal but still sclerotic bone (*asterisks*)

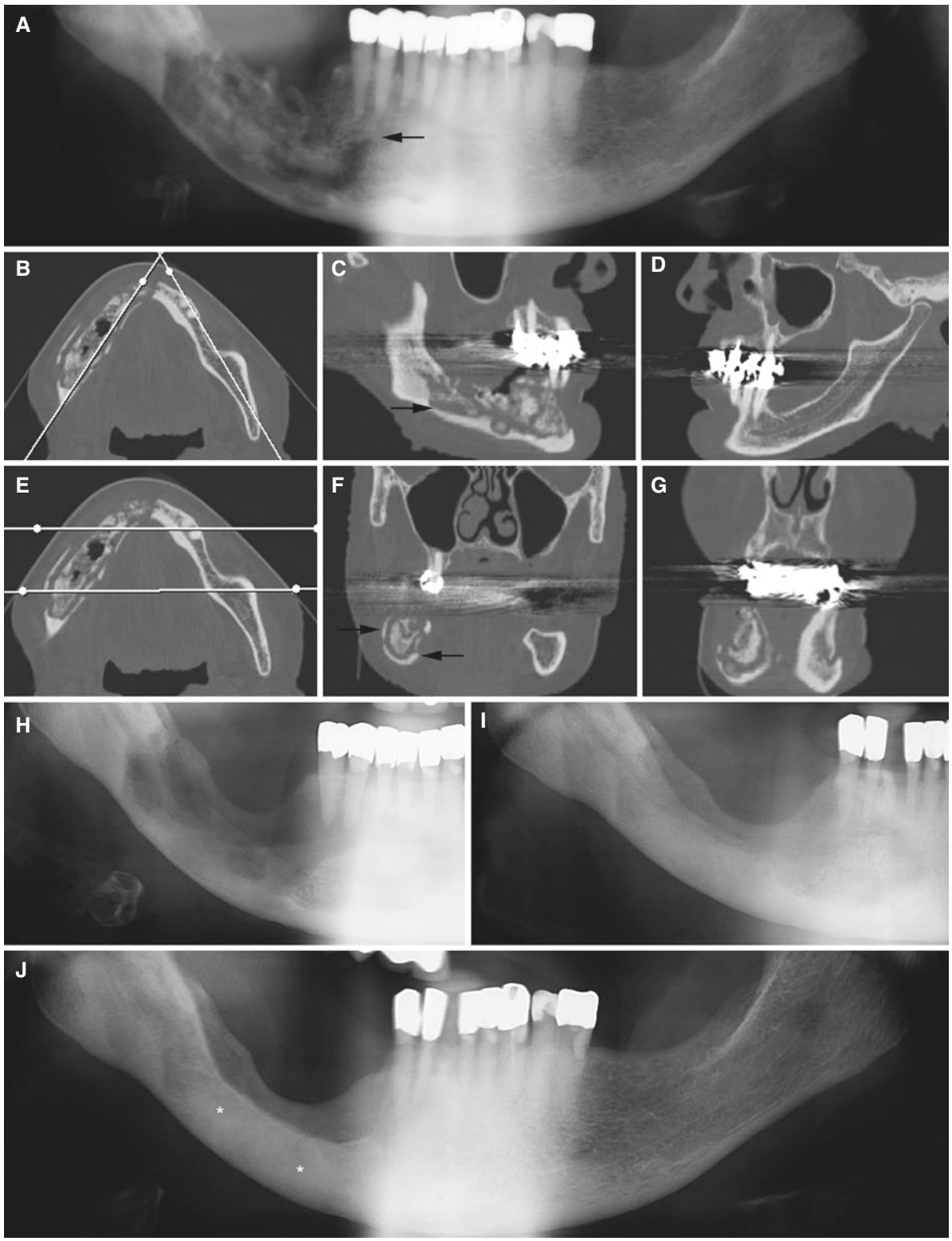

Fig. 5.29 Medication-related osteonecrosis, mandible, with some healing/improvement at follow-up; 90-year-old female (osteoporosis, more than 10 years with antiresorptive therapy) with variable pain/discomfort, some paresthesia, and exposed bone with suppuration; tooth extractions performed during the last 3-year period in the right mandible. (**A**) Panoramic view shows severe destruction and sequestration (*arrow*). (**B**) Axial (with *cursor lines*) and (**C**) oblique sagittal CT images confirm destruction and sequestration (*arrow*). (**D**) Oblique sagittal CT image of normal contralateral side for comparison. (**E**) Axial (with *cursor lines*) and (**F**, **G**) coronal CT images confirm sequestration and bone apposition in the right mandible (*arrows*). Panoramic views (**H**) 5 weeks (under antibiotic treatment) after initial examination and sequestrectomy, (**I**) 7 months later (than **H**), and (**J**) 18 months later (than **I**) show bone healing but still sclerotic bone (*asterisks*)

5.6 Abscess

Figs. 5.30, 5.31, 5.32, 5.33, and 5.34

5.6.1 Definition

Collection of pus in bone or soft tissue.

5.6.2 Clinical Features

- Swelling and pain
- Redness and warmth
- Trismus
- Fever and malaise
- Swallowing problems
- Breath problems

5.6.3 Imaging Features

- Bone destruction if infection is in bone
- Round or lobulated soft-tissue structure with enhancing peripheral rim and hypodense (necrotic) center
- T2-weighted MRI and STIR: high-signal center surrounded by low-signal periphery
- T1-weighted pre-Gd MRI: intermediate signal
- T1-weighted post-Gd MRI: no contrast enhancement except periphery
- A phlegmon or cellulitis will enhance diffusely and entirely

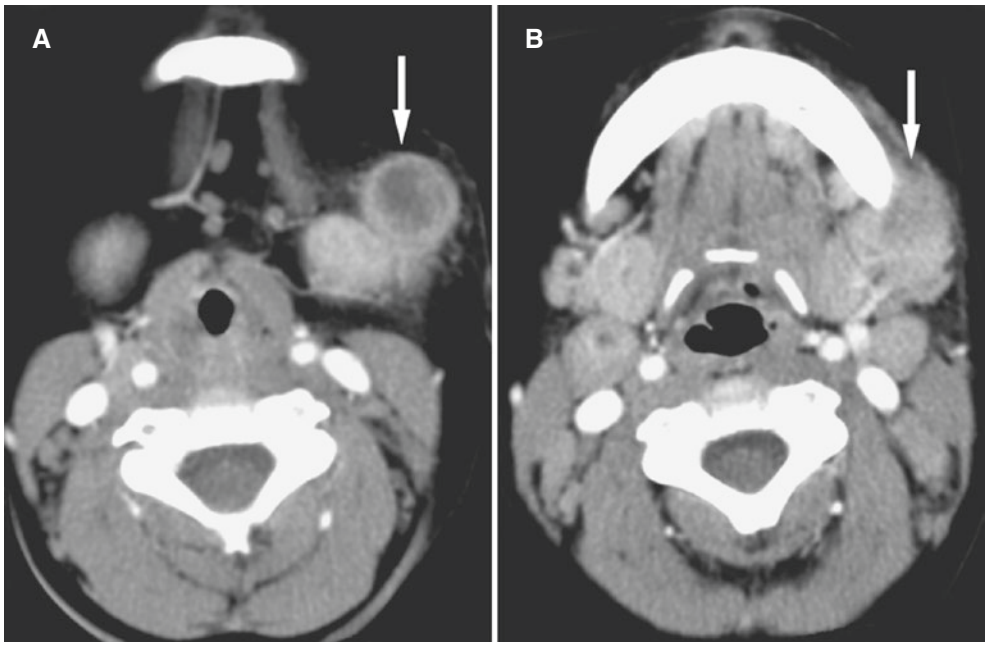

Fig. 5.30 Abscess, submandibular; 22-month-old male with history of left neck mass, strep throat, and fever. (**A**) Axial post-contrast CT image, soft-tissue window, shows anterior and lateral to left submandibular gland a hypodense nodular, circular structure surrounded by hyperintense rim (*arrow*). (**B**) Axial post-contrast CT image, soft-tissue window, shows abscess (*arrow*) surrounded by diffuse infiltration in fat planes and scattered cervical lymphadenopathy. Normal bone structures not shown

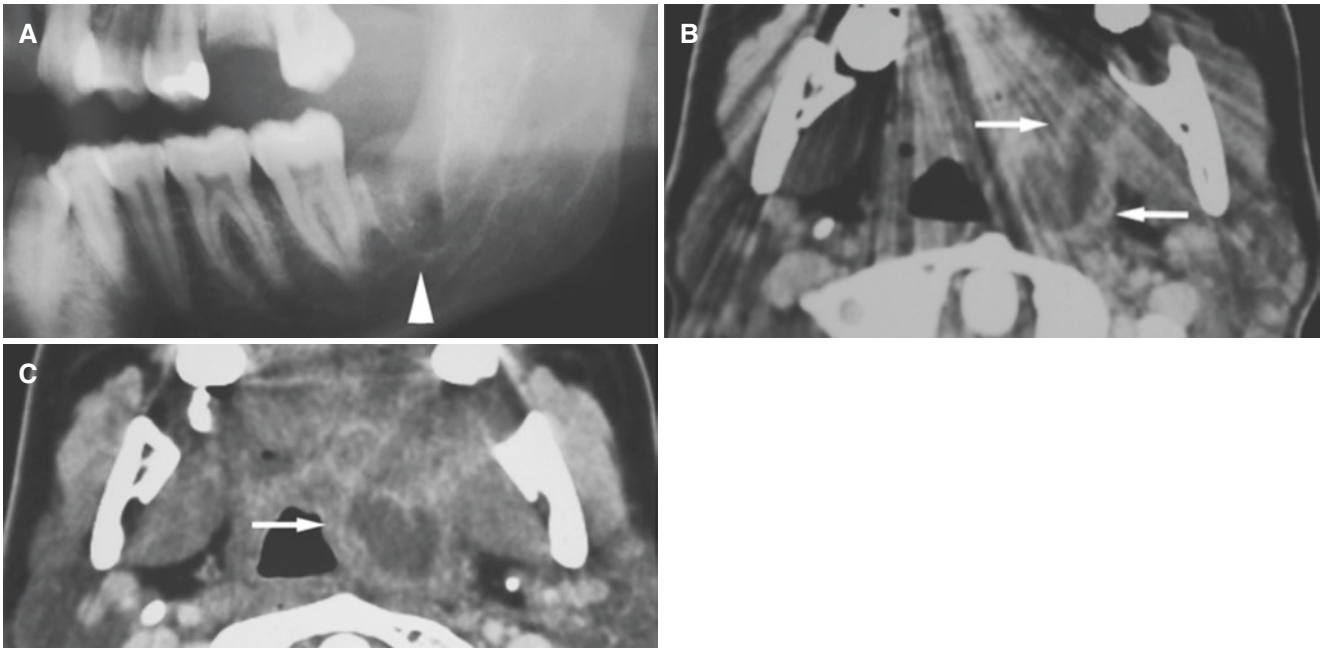

Fig. 5.31 Abscess, parapharyngeal; 24-year-old female with pharyngeal swelling after extraction of infected third molar. (**A**) Panoramic view shows tooth socket (*arrowhead*) and infectious first molar in the maxilla. (**B**) Axial post-contrast CT image, soft-tissue window, shows abscess from tooth socket, extending parapharyngeally (*arrows*). (**C**) Axial post-contrast CT image, soft-tissue window, shows parapharyngeal abscess and narrowing air space (*arrow*)

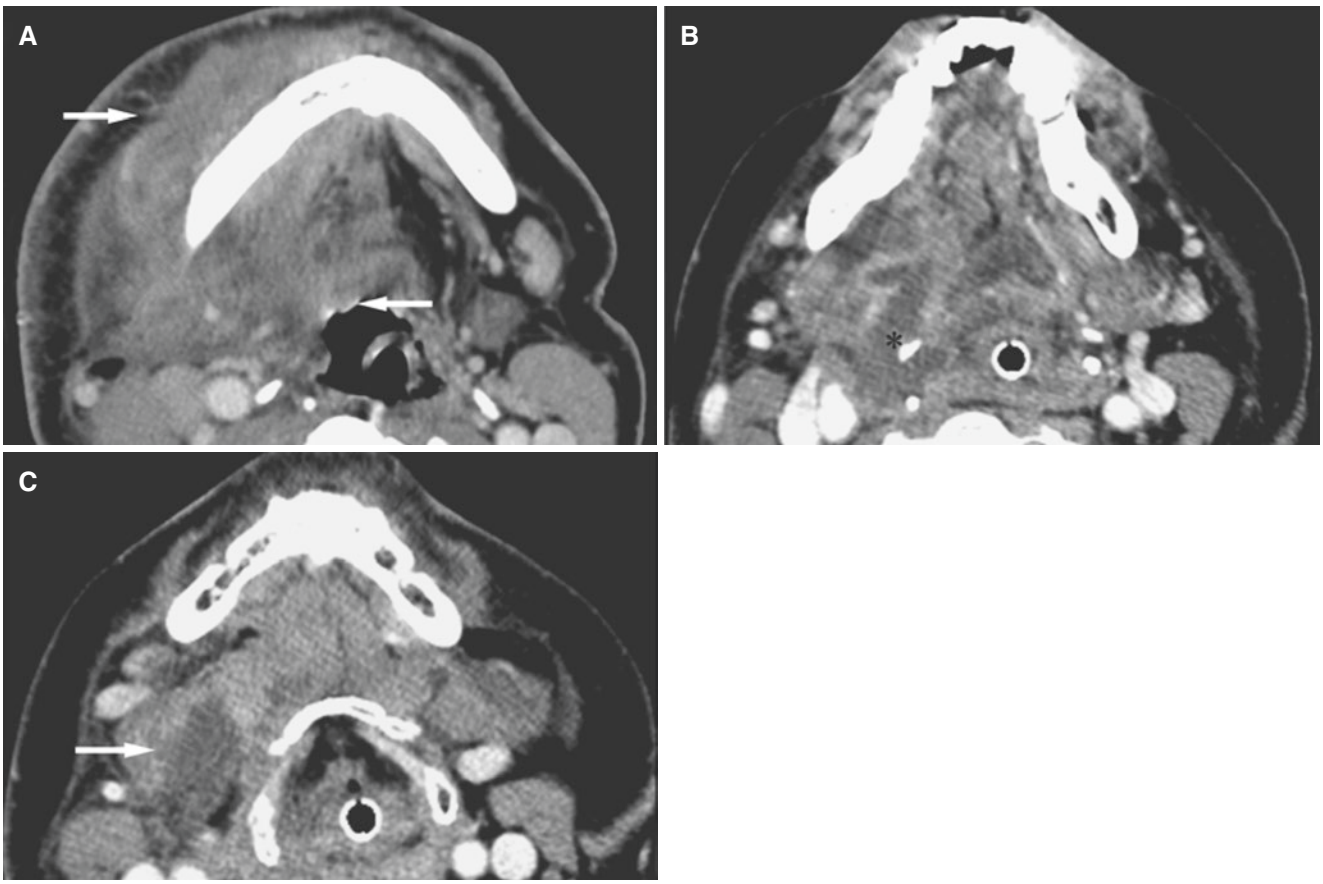

Fig. 5.32 Abscess, parapharyngeal; 36-year-old male with swelling of the face from the orbit to the neck from mandibular osteomyelitis. (**A**) Axial post-contrast CT image, soft-tissue window, shows soft-tissue swelling in masticator, submandibular, submental, and parapharyngeal spaces, as well as in tonsillar region (*arrows*). (**B**) Axial post-contrast CT image, soft-tissue window, shows parapharyngeal abscess (*asterisk*) and edema in the floor of the mouth and around the pharynx (note cannula in place), which is displaced. (**C**) Axial post-contrast CT image, soft-tissue window, shows abscess at level of hyoid bone (*arrow*)

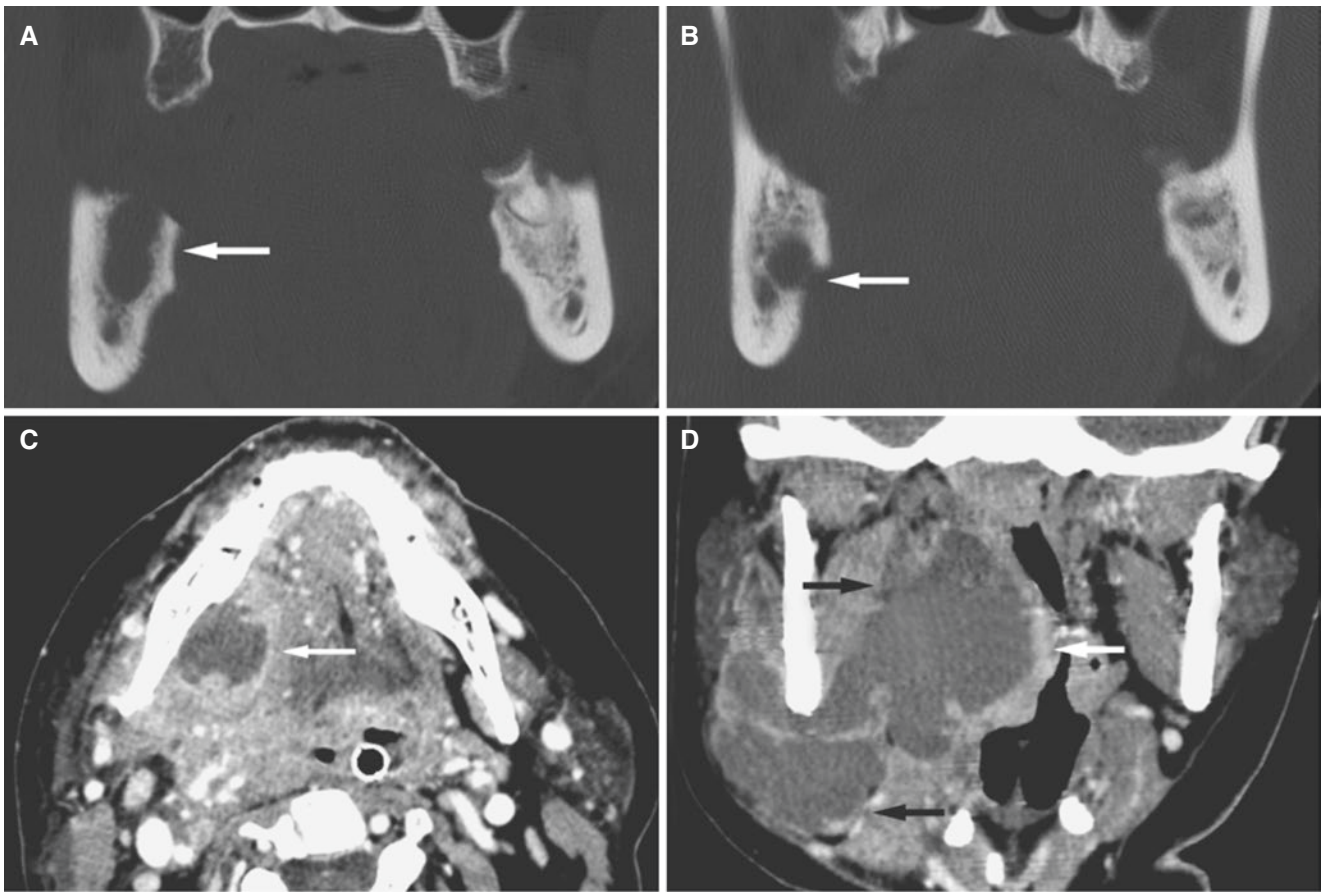

Fig. 5.33 Abscess, parapharyngeal; 29-year-old female with infected third mandibular molar extracted 1 week previously and history of lateral pharyngeal wall infection, large perimandibular swelling, swelling in the floor of the mouth, and air-breathing problems. (**A**) Coronal post-contrast CT image shows tooth socket (*arrow*) and infectious root also on contralateral side. (**B**) Coronal post-contrast CT image shows destruction of lingual cortical plate below the attachment of mylohyoid muscle (*arrow*). (**C**) Axial post-contrast CT, soft-tissue window, shows abscess lingual to tooth socket (*arrow*) and diffuse edema in the entire floor of the mouth, closure of airspace, and cannula in place. (**D**) Coronal post-contrast CT image, soft-tissue window, shows large abscess in masticator, submandibular, and parapharyngeal spaces with closure of airspace (*arrows*). Enlarged lymph nodes (more than 1 cm) were seen

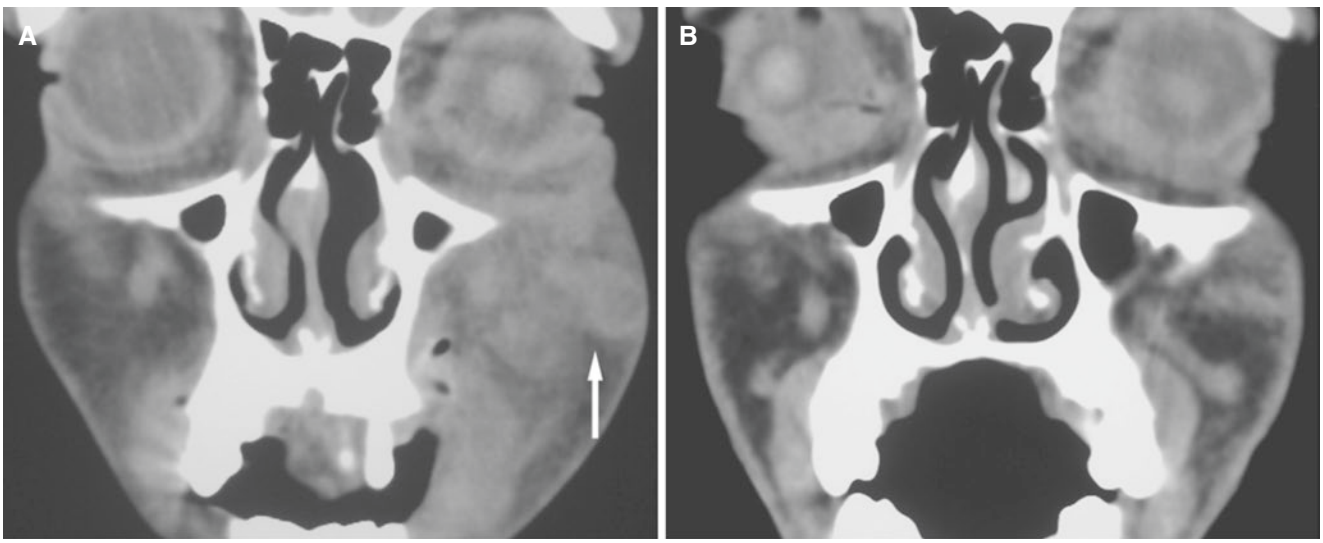

Fig. 5.34 Abscess in cheek; 31-year-old female with dental infection with pain and swelling in the palate and cheek (history of multiple dental abscesses). (**A**) Coronal post-contrast CT image, soft-tissue window, shows soft-tissue swelling in the palate, small gas collections close to alveolar process, and abscess in the cheek (*arrow*). (**B**) Coronal post-contrast CT image, soft-tissue window, 4 years later shows normal cheek (possibly some scar tissue)

Suggested Reading

Acquavella J, Ehrenstein V, Schiødt M, Heide-Jørgensen U, Kjellman A, Hansen S et al (2016) Design and methods for a Scandinavian pharmacovigilance study of osteonecrosis of the jaw and serious infections among cancer patients treated with antiresorptive agents for the prevention of skeletal-related events. Clin Epidemiol 8:267–272

Aghaloo TL, Tetradis S (2016) Osteonecrosis of the jaw in the absence of antiresorptive or antiangiogenic exposure: a series of 6 cases. J Oral Maxillofac Surg. doi:10.1016/j.joms.2016.07.019

Arce K, Assael LA, Weissman JL, Markiewicz MR (2009) Imaging findings in bisphosphonate-related osteonecrosis of jaws. J Oral Maxillofac Surg 67(Suppl 5):75–84

Bagan JV, Cibrian RM, Lopez J, Leopoldo-Rodado M, Carbonell E, Bagán L et al (2015) Sclerosis in bisphosphonate-related osteonecrosis of the jaws and its correlation with the clinical stages: study of 43 cases. Br J Oral Maxillofac Surg 53:257–262

Baltensperger M, Gratz K, Bruder E, Lebeda R, Makek M, Eyrich G (2004) Is primary chronic osteomyelitis a uniform disease? Proposal of a classification based on a retrospective analysis of patients treated in the past 30 years. J Craniomaxillofac Surg 32:43–50

Bianchi SD, Scoletta M, Cassione FB, Migliaretti G, Mozzati M (2007) Computerized tomographic findings in bisphosphonate-associated osteonecrosis of the jaw in patients with cancer. Oral Surg Oral Med Oral Pathol Oral Radiol Endod 104:249–258

Bisdas S, Chambron Pinho N, Smolarz A, Sader R, Vogt TJ, Mack MG (2008) Biphosphonate-induced osteonecrosis of the jaws. CT and MRI spectrum of findings in 32 patients. Clin Radiol 63:71–77

Carlson ER, Fleisher KE, Ruggiero SL (2013) Metastatic cancer identified in osteonecrosis specimens of the jaws in patients receiving intravenous bisphosphonate medications. J Oral Maxillofac Surg 71:2077–2086

Ceponis P, Keilman C, Guerry C, Freiberger JJ (2016) Hyperbaric oxygen therapy and osteonecrosis. Oral Dis. doi:10.1111/odi.12489

Christodoulou C, Pervena A, Klouvas G, Galani E, Falagas ME, Tsakalos G et al (2009) Combination of bisphosphonates and antiangiogenic factors induces osteonecrosis of the jaw more frequently than bisphosphonates alone. Oncology 76:209–211

Eyrich GK, Baltensperger MM, Bruder E, Graetz KW (2003) Primary chronic osteomyelitis in childhood and adolescence: a retrospective analysis of 11 cases and review of the literature. J Oral Maxillofac Surg 61:561–573

Farman AG, Nortje C, Wood RE (1993) Infections of the teeth and jaws. In: Oral and maxillofacial diagnostic imaging. Mosby, St. Louis, pp 181–209

Fedele S, Porter SR, D'Aiuto F, Aljohani S, Vescovi P, Manfredi M et al (2010) Nonexposed variant of bisphosphonate-associated osteonecrosis of the jaw: a case series. Am J Med 123:1060–1064

Fizazi K, Carducci M, Smith M, Damião R, Brown J, Karsh L et al (2011) Denosumab versus zoledronic acid for treatment of bone metastases in men with castration-resistant prostate cancer: a randomised, double-blind study. Lancet 377:813–822

Hermans R, Fossion E, Ioannides C, Van den Bogaert W, Ghekiere J, Baert AL (1996) CT findings in osteoradionecrosis of the mandible. Skelet Radiol 25:31–36

Kaneda T, Minami M, Ozawa Y, Akimoto T, Utsunomiya T, Yamamoto H, Suzuki H, Sasaki Y (1995) Magnetic resonance imaging of osteomyelitis. Comparative study with other radiologic modalities. Oral Surg Oral Med Oral Pathol Oral Radiol Endod 79:634–640

Kim HJ, Park TJ, Ahn KM (2016) Bisphosphonate-related osteonecrosis of the jaw in metastatic breast cancer patients: a review of 25 cases. Maxillofac Plast Reconstr Surg 38. doi:10.1186/s40902-016-0052-6

Klingelhöffer C, Klingelhöffer M, Müller S, Ettl T, Wahlmann U (2016) Can dental panoramic radiographic findings serve as indicators for the development of medication-related osteonecrosis of the jaw? Dentomaxillofac Radiol 45:20160065

Kucukyilmaz E, Sener Y, Tosun G, Savas S (2015) Periostitis ossificans managed with endodontic treatment. J Dent Child (Chic) 82:53–56

Kumar V, Sinha RK (2014) Bisphosphonate related osteonecrosis of the jaw: an update. J Maxillofac Oral Surg 13:386–393

Larheim TA, Aspestrand F, Trebo S (1993) Periostitis ossificans of the mandible. The value of computed tomography. Dentomaxillofac Radiol 22:93–96

Lee L (2004) Inflammatory lesions of the jaws. In: White SW, Pharoah MJ (eds) Oral radiology. Principles and interpretation, 5th edn. Saunders, Philadelphia, pp 373–383

Lee K, Kaneda T, Mori S, Minami M, Motohashi J, Yamashiro M (2003) Magnetic resonance imaging of normal and osteomyelitis in the mandible: assessment of short inversion time inversion recovery sequence. Oral Surg Oral Med Oral Pathol Oral Radiol Endod 96:499–507

Lee SC, Kim JH, Kim CH, Kim BJ (2015) Temporomandibular joint disorder from skull-base osteomyelitis: a case report. Maxillofac Plast Reconstr Surg 37. doi:10.1186/s40902-015-0041-1

Lew DP, Waldvogel FA (2004) Osteomyelitis. Lancet 364:369–379

Lovas JGL (1991) Infection/inflammation. In: Miles DA, Van Dis M, Kaugars GE, Lovas JGL (eds) Oral and maxillofacial radiology. Radiologic/pathologic correlations. Saunders, Philadelphia, pp 7–20

Marx RE (1983) Osteoradionecrosis: a new concept of its pathophysiology. J Oral Maxillofac Surg 41:283–288

Marx R (2011) Oral and intravenous bisphosphonate induced osteonecrosis of the jaws: history, etiology, prevention, and treatment, 2nd edn. Quintessence Publishing, Hanover Park

Mosier KM (2015) Magnetic resonance imaging of the maxilla and mandible: signal characteristics and features in the differential diagnosis of common lesions. Top Magn Reson Imaging 24:23–37

Mücke T, Krestan CR, Mitchell DA, Kirschke JS, Wutzl A (2016) Bisphosphonate and medication-related osteonecrosis of the jaw: a review. Semin Musculoskelet Radiol 20:305–314

Mufeed A, Mangalath U, George A, Hafiz A (2015) Infected florid osseous dysplasia: clinical and imaging follow-up. BMJ Case Rep 9. doi:10.1136/bcr-2014-209099

Nicolatou-Galitis O, Migkou M, Psyrri A, Barnias A, Pectasides D, Economopoulos T et al (2012) Gingival bleeding and jaw bone necrosis in patients with metastatic renal cell carcinoma receiving sunitinib: a report of 2 cases with clinical implications. Oral Surg Oral Med Oral Pathol Oral Radiol 113:234–238

Nortje CJ, Wood RE, Grotepass F (1988) Periostitis ossificans versus Garre's osteomyelitis. Part II: radiographic analysis of 93 cases in the jaws. Oral Surg Oral Med Oral Pathol 66:249–260

Notani K, Yamazaki Y, Kitada H, Sakakibara N, Fukuda H, Omori K, Nakamura M (2003) Management of mandibular osteoradionecrosis corresponding to the severity of osteoradionecrosis and the method of radiotherapy. Head Neck 25:181–186

O'Ryan FS, Khoury S, Liao W, Han MM, Hui RL, Baer D et al (2009) Intravenous bisphosphonate-related osteonecrosis of the jaw: bone scintigraphy as an early indicator. J Oral Maxillofac Surg 67:1363–1372

Padwa BL, Dentino K, Robson CD, Woo SB, Kurek K, Resnick CM (2016) Pediatric chronic nonbacterial osteomyelitis of the jaw: clinical, radiographic, and histopathologic features. J Oral Maxillofac Surg. doi:10.1016/j.joms.2016.05.021

Reiss S, Sultan D (2015) Risk factors in the development of oral bisphosphonate-induced osteonecrosis. N Y State Dent J 81:30–33

Ribeiro NR, Silva Lde F, Santana DM, Nogueira RL (2015) Bisphosphonate-related osteonecrosis of the jaw after tooth extraction. J Craniofac Surg 26. doi:10.1097/SCS.0000000000002051

Ruggiero SL, Mehrotra B, Rosenberg TJ, Engroff SL (2004) Osteonecrosis of the jaws associated with the use of bisphosphonates: a review of 63 cases. J Oral Maxillofac Surg 62:527–534

Ruggiero SL, Dodson TB, Fantasia J, Goodday R, Aghaloo T, Mehrotra B, O'Ryan F (2014) American association of oral and maxillofacial surgeons position paper on medication-related osteonecrosis of the jaw-2014 update. J Oral Maxillofac Surg 72:1938–1956

Schiodt M, Reibel J, Oturai P, Kofod T (2014) Comparison of nonexposed and exposed bisphosphonate-induced osteonecrosis of the jaws: a retrospective analysis from the Copenhagen cohort and a proposal for an updated classification system. Oral Surg Oral Med Oral Pathol Oral Radiol 117:204–213

Seabold JE, Simonson TM, Weber PC, Thompson BH, Harris KG, Rezai K, Madsen MT, Hoffman HT (1995) Cranial osteomyelitis: diagnosis and follow-up with In-111 white blood stem and Tc-99m methylene diphosphonate bone SPECT, CT, and MR imaging. Radiology 196:779–788

So H, Lee CY, Jung J, Kim DY, Walter C, Kwon YD (2016) A retrospective study of osteomyelitis and osteonecrosis of the jaws and its etiologic implication of bisphosphonate in Asians. Clin Oral Investig. doi:10.1007/s00784-016-1973-2

Stockmann P, Hinkmann FM, Lell MM, Fenner M, Vairaktaris E, Neukam FW et al (2010) Panoramic radiograph, computed tomography or magnetic resonance imaging. Which imaging technique should be preferred in bisphosphonate-associated osteonecrosis of the jaw? A prospective clinical study. Clin Oral Investig 14:311–317

Støre G, Boysen M (2000) Mandibular osteoradionecrosis: clinical behaviour and diagnostic aspects. Clin Otolaryngol 25:378–384

Støre G, Larheim TA (1999) Mandibular osteoradionecrosis: a comparison of computed tomography with panoramic radiography. Dentomaxillofac Radiol 28:295–300

Støre G, Smith H-J, Larheim TA (2000) Dynamic MR imaging of mandibular osteoradionecrosis. Acta Radiol 41:31–37

Støre G, Evensen J, Larheim TA (2001) Osteoradionecrosis of the mandible. Comparison of the effects of external beam irradiation and brachytherapy. Dentomaxillofac Radiol 30:114–119

Thorn JJ, Hansen HS, Specht L, Bastholt L (2000) Osteoradionecrosis of the jaws: clinical characteristics and relation to the field of irradiation. J Oral Maxillofac Surg 58:1088–1093

Vermeer JA, Renders GA, Everts V (2016) Osteonecrosis of the jaw—a bone site-specific effect of bisphosphonates. Curr Osteoporos Rep 14:219–225

Weber AL, Kaneda T, Scrivani SJ, Aziz S (2003) Jaw: cysts, tumors, and nontumorous lesions. In: Som PM, Curtin HD (eds) Head and neck imaging, 4th edn. Mosby, St. Louis, pp 930–994

Yamazaki T, Yamori M, Ishizaki T, Asai K, Goto K, Takahashi K et al (2012) Increased incidence of osteonecrosis of the jaw after tooth extraction in patients with bisphosphonate: a cohort study. Int J Oral Maxillofac Surg 41:1397–1403

Temporomandibular Joints

6

Abstract

This chapter illustrates internal derangements, osteoarthritis, bone marrow abnormalities, arthritides; rheumatoid artritis, psoriatic arthritis, ankylosing spondylitis, inflammatory arthritis without known generalized joint disease, and juvenile idiopathic arthritis, juvenile osteoarthritis, ankyloses, condylar growth disturbances (anomalies); condylar hyperplasia, condylar hypoplasia, and bifid condyle, inflammatory or tumorlike conditions; calcium pyrophosphate dehydrate crystal deposition disease, pigmented villonodular synovitis, simple bone cyst, synovial cyst, and synovial chondromatosis, benign tumors; osteochondroma, osteoma, and sphenoid meningioma, malignant tumors; metastatic osteosarcoma and metastatic tumor from lung cancer, osteoradionecrosis, and coronoid hyperplasia.

6.1 Introduction

Patients with temporomandibular disorders constitute a heterogeneous group. Many have symptoms that are not directly related to the joints proper. Although the clinical assessment of the temporomandibular joint (TMJ) provides limited information with respect to its anatomic-pathologic status, imaging should only be performed if a thorough physical examination indicates the need for more information and for patient management.

A number of imaging modalities have been used in the past and are still used to examine patients with TMJ problems. MRI has become the leading method, being the only one to assess disc integrity, disc position, condylar bone marrow, and inflammatory soft-tissue changes. For evaluation of the cortical bone, CT is superior to MRI. Since cone beam CT became available, this method is increasingly used to examine the TMJ. It does not seem to be any diagnostic difference between CT and cone beam CT for the evaluation of the bone components of the TMJ. Therefore, the chapter focuses on CT and MRI findings in a number of conditions that may affect this joint. Usually one method is sufficient, but occasionally, both CT and MRI may add valuable diagnostic information.

The imaging protocols consist of oblique sagittal and oblique coronal images that are obtained perpendicular or parallel to the long axis of the mandibular condyle, at closed mouth. Most patients examined with MRI will have supplementary open-mouth MRI, frequently using a rapid (gradient-echo) oblique sagittal sequence. If not specifically mentioned in the legends, the MR images in this chapter are PD (proton density)-weighted (intermediate-weighted) or T1-weighted images. Routinely, *arrow* indicates posterior band of the disc.

When appropriate, other imaging modalities are presented. In selected cases, clinical photos, histologic evidence, surgical specimens, and autopsy specimen sections are shown.

Normal (asymptomatic volunteer) features in CT and MR images, as well as normal features in autopsy specimen sections and normal condylar bone marrow histology, are shown in Chap. 1, "Maxillofacial Imaging Anatomy".

6.2 Internal Derangements (with Normal Cortical Bone)

Figs. 6.1, 6.2, 6.3, 6.4, 6.5, 6.6, 6.7, 6.8, 6.9, 6.10, 6.11, 6.12, 6.13, 6.14, and 6.15

In collaboration with H.-J. Smith.

T.A. Larheim, P.-L.A. Westesson, *Maxillofacial Imaging*, https://doi.org/10.1007/978-3-319-53319-3_6

6.2.1 Definition

General orthopedic term implying a mechanical fault that interferes with the smooth action of a joint; internal arrangement is a functional diagnosis, and for the TMJ the most common internal derangement is displacement of the articular disc.

6.2.2 Clinical Features

- Clicking sounds from joint(s)
- Clicking sounds that have disappeared
- Restricted or normal mouth-opening capacity
- Deviation or other irregular jaw motion on opening

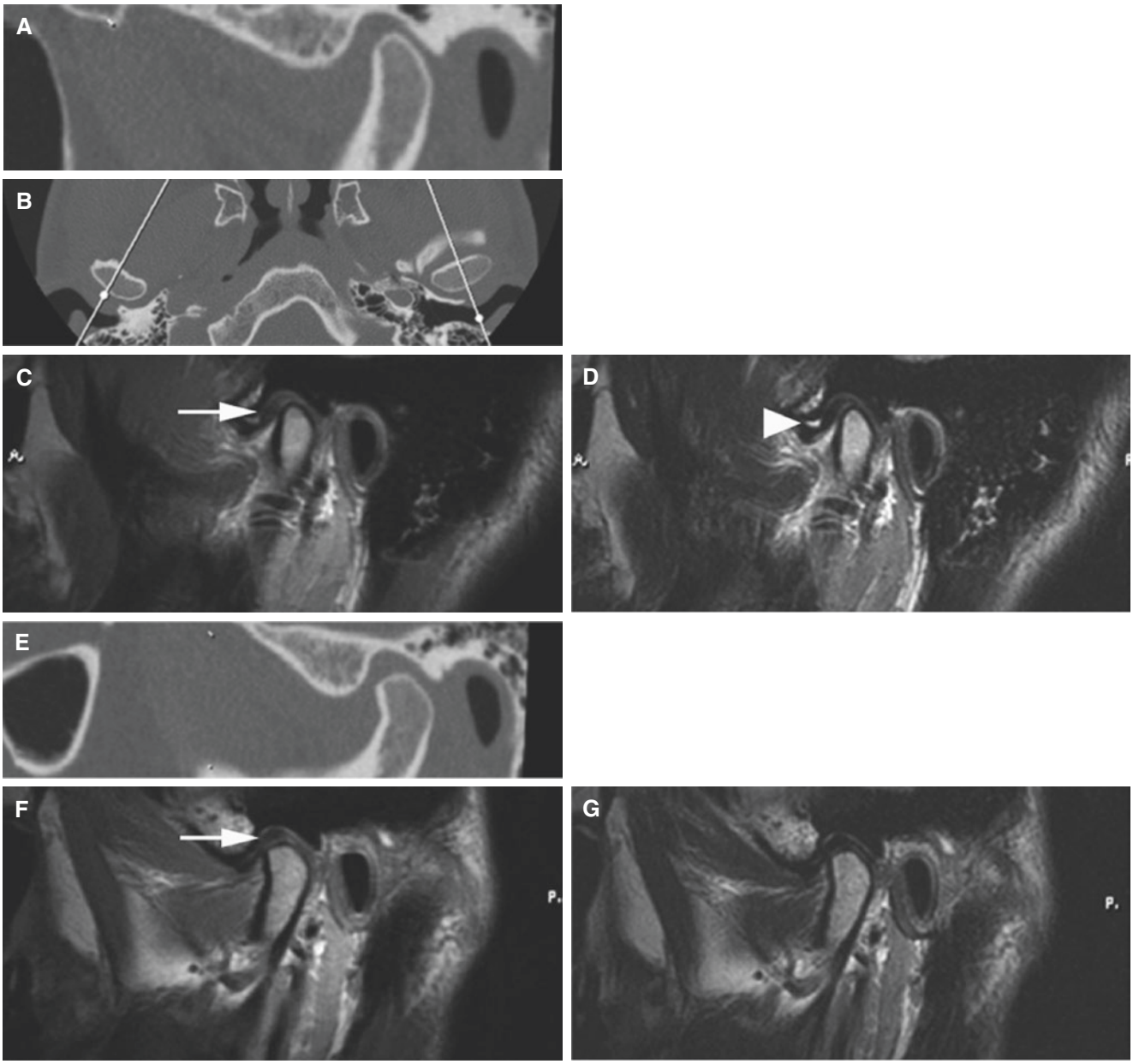

Fig. 6.1 Disc displacement, normal bone in the right joint (**A**, **B**, **C**, **D**), normal disc position, normal bone in the left joint (**B**, **E**, **F**, **G**); 29-year-old male. (**A**) Oblique sagittal CT image shows normal cortical bone and condyle posteriorly positioned in fossa. (**B**) Axial CT image (*cursor lines* for oblique sagittal images). (**C**) Oblique sagittal PD-weighted MRI shows disc displacement; posterior band (*arrow*) anterior to the condyle. (**D**) Oblique sagittal T2-weighted MRI shows minimal (normal) joint fluid (*arrowhead*). (**E**) Oblique sagittal CT image shows normal cortical bone. (**F**) Oblique sagittal PD-weighted MRI shows normal disc position; posterior band (*arrow*) superior to the condyle. (**G**) Oblique sagittal T2-weighted MRI shows no joint fluid

- Pain or no pain in joint areas and/or masticatory muscles
- Occasionally, joints may show inflammatory signs
- A variety of other symptoms such as headache
- Women more frequent than men
- Also younger age groups

6.2.3 Imaging Features

- Anterior disc displacement: posterior band of the disc located anterior to the superior portion of the condyle at closed mouth on oblique sagittal images
- The disc may have normal (biconcave) or deformed morphology
- In open-mouth image, the disc may be in a normal position ("with reduction") or continue to be displaced ("without reduction" or "non-reducing")
- Anterior disc displacement without or with lateral or medial disc displacement most common
- Lateral or medial disc displacement best seen on oblique coronal images
- Pure lateral or medial or posterior disc displacement uncommon
- Complete disc displacement; the disc is displaced throughout the joint, i.e., in all oblique sagittal sections
- Partial disc displacement; the disc is displaced in only one part of the joint
- Complete disc displacement may show non-reducing or reducing (normalizing) disc on mouth opening
- Discs that are non-reducing are usually displaced completely
- Partial disc displacement will frequently show reducing disc on mouth opening
- The disc may be in normal position at closed mouth, but not move on mouth opening; stuck disc or fixed disc
- Effusion, typically located in anterior recess of the upper compartment, may be seen
- Bone marrow edema in the condyle may be seen.
- Cortical bone is normal

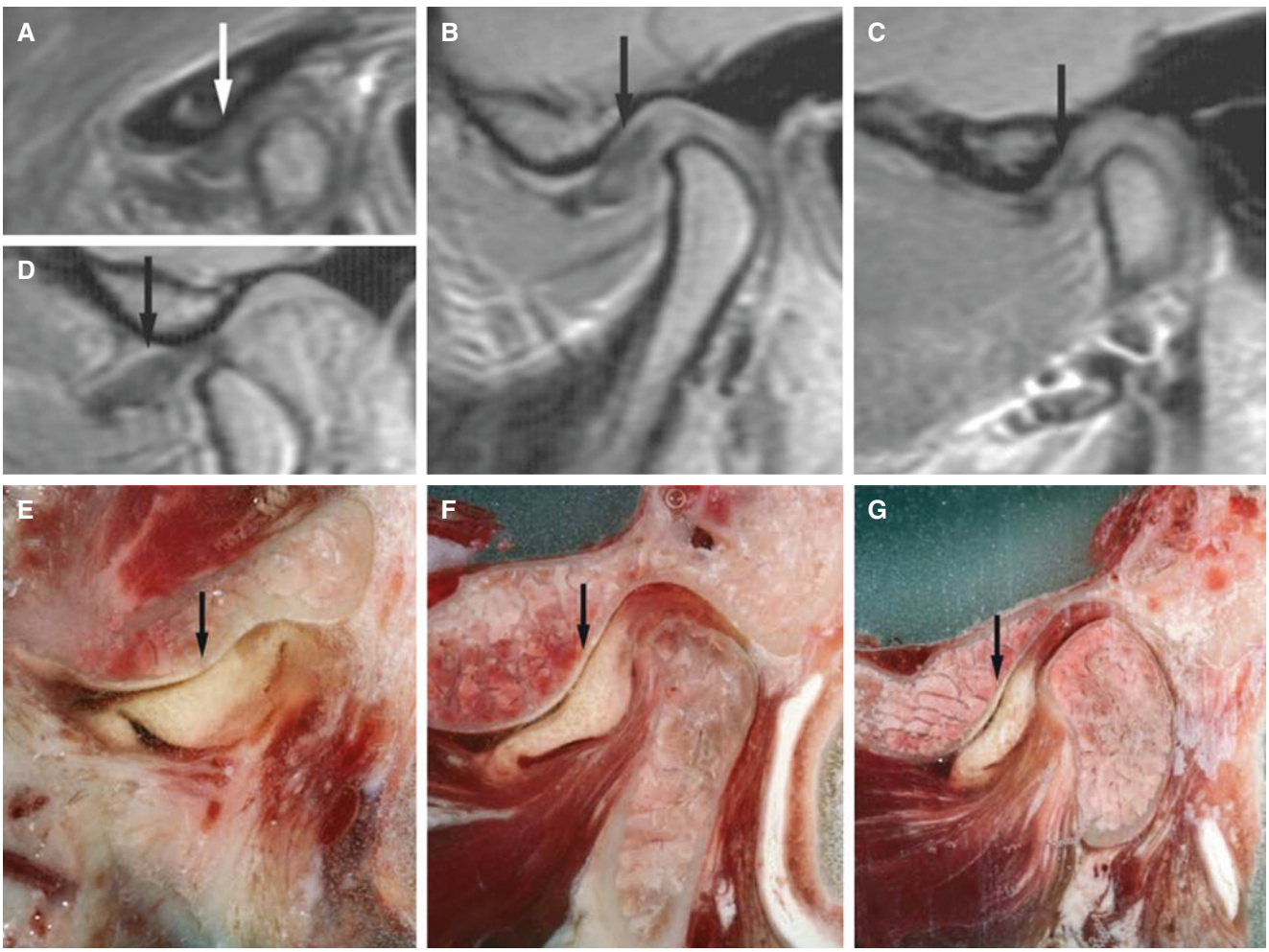

Fig. 6.2 Complete anterior disc displacement (disc displaced throughout the joint) without reduction, normal bone. (**A**, **B**, **C**) Oblique sagittal MRI shows displaced and deformed disc (*arrow*) in lateral (**A**), central (**B**), and medial (**C**) section. (**D**) Oblique sagittal open-mouth MRI shows anteriorly displaced disc (*arrow*). (**E**, **F**, **G**) Autopsy specimen shows anteriorly displaced disc (*arrow*) in lateral (**E**), central (**F**), and medial (**G**) sections. (**A**–**D**) reproduced with permission from Larheim et al. (2001a)

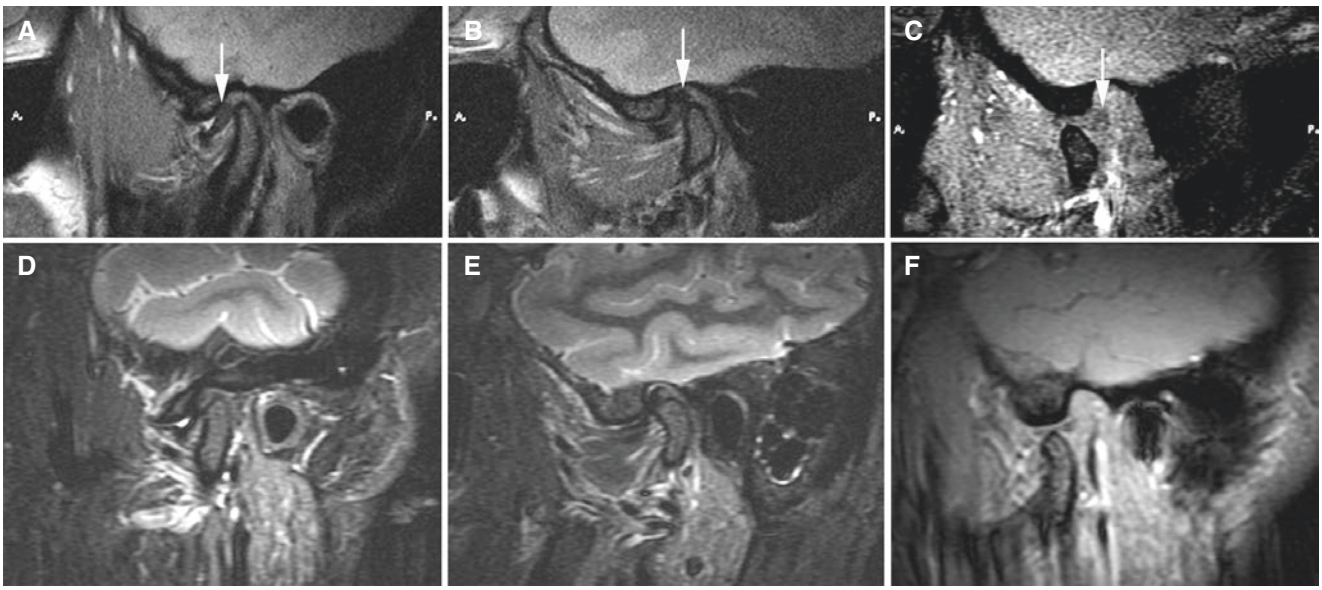

Fig. 6.3 Partial disc displacement (disc displaced only in one part of the joint) with reduction, normal bone; 39-year-old female (**A**, **B**, **C**). (**A**) Oblique sagittal T2-weighted MRI shows small amount of fluid and disc displacement; posterior band (*arrow*) located in anterior position to the condyle in one section. (**B**) Oblique sagittal T2-weighted MRI shows normal disc position with posterior band (*arrow*) superior to the condyle in a more medial section. (**C**) Oblique sagittal open-mouth MRI shows normal disc position (*arrow*) and normal condylar translation. (**D**, **E**, **F**) Partial disc displacement with reduction in another patient; oblique sagittal MR images correspond to (**A**, **B**, **C**)

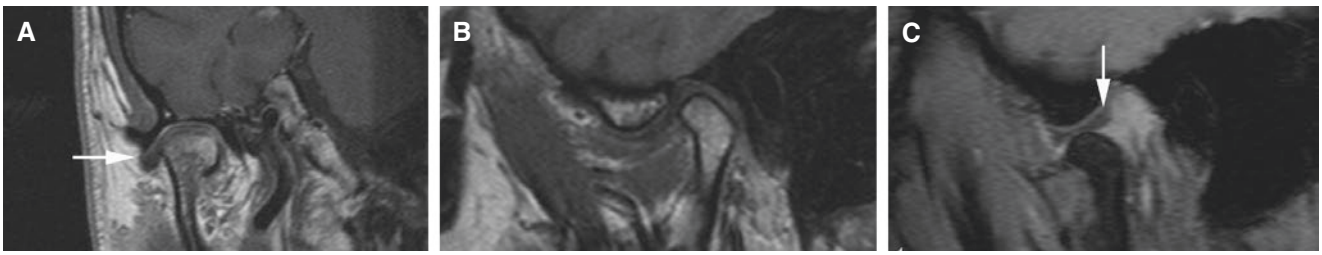

Fig. 6.4 Partial disc displacement, normal bone; 65-year-old male. (**A**) Oblique coronal T1-weighted post-Gd MRI shows laterally displaced disc (*arrow*). (**B**) Oblique sagittal T1-weighted MRI shows apparently normal disc position. (**C**) Oblique sagittal open-mouth MRI shows apparently normal disc position (*arrow*) and slightly reduced condylar translation

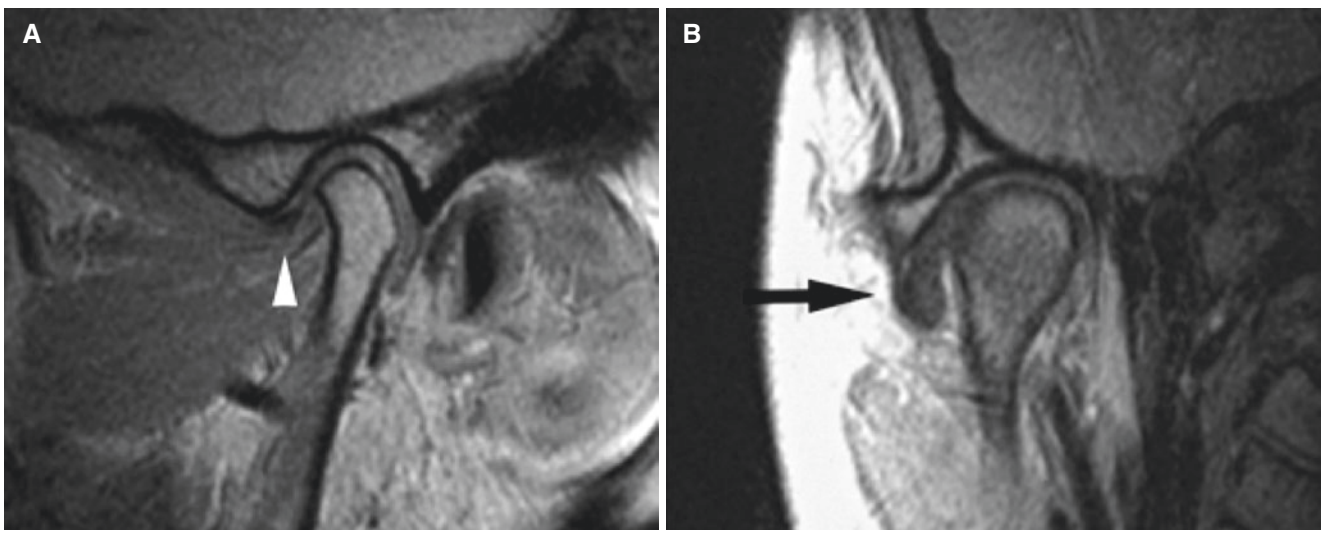

Fig. 6.5 Lateral disc displacement, normal bone. (**A**) Oblique sagittal MRI shows little disc tissue, but tendon to lateral pterygoid muscle (*arrowhead*). (**B**) Oblique coronal MRI shows the disc (*arrow*) displaced laterally

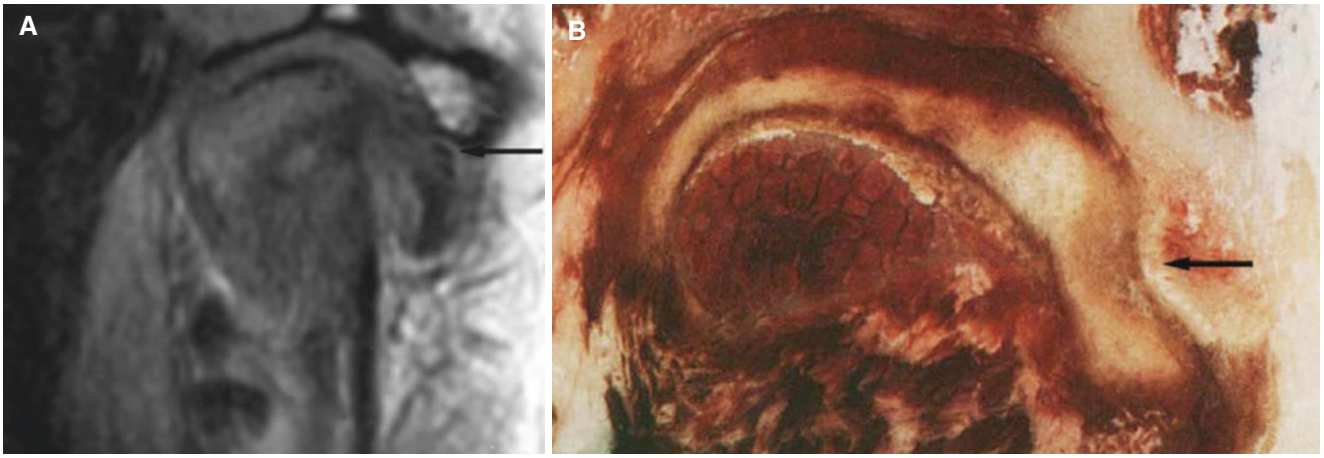

Fig. 6.6 Lateral disc displacement, normal bone. (**A**) Oblique coronal MRI shows laterally displaced disc (*arrow*). (**B**) Autopsy specimen shows laterally displaced disc (*arrow*). Reproduced with permission from Tasaki et al. (1996)

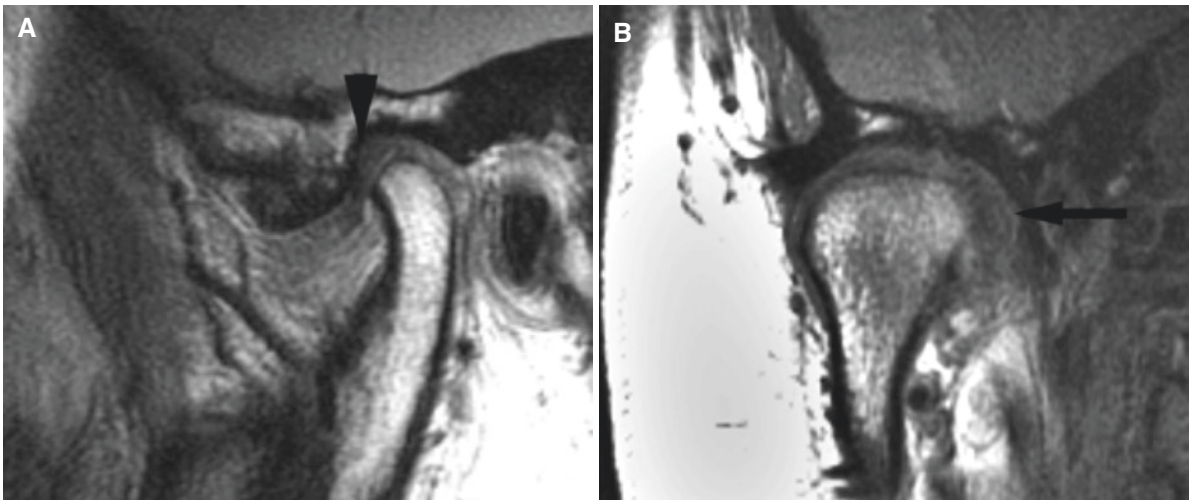

Fig. 6.7 Medial disc displacement, normal bone. (**A**) Oblique sagittal MRI shows normal position of the disc (*arrowhead*). (**B**) Oblique coronal MRI shows medially displaced disc (*arrow*)

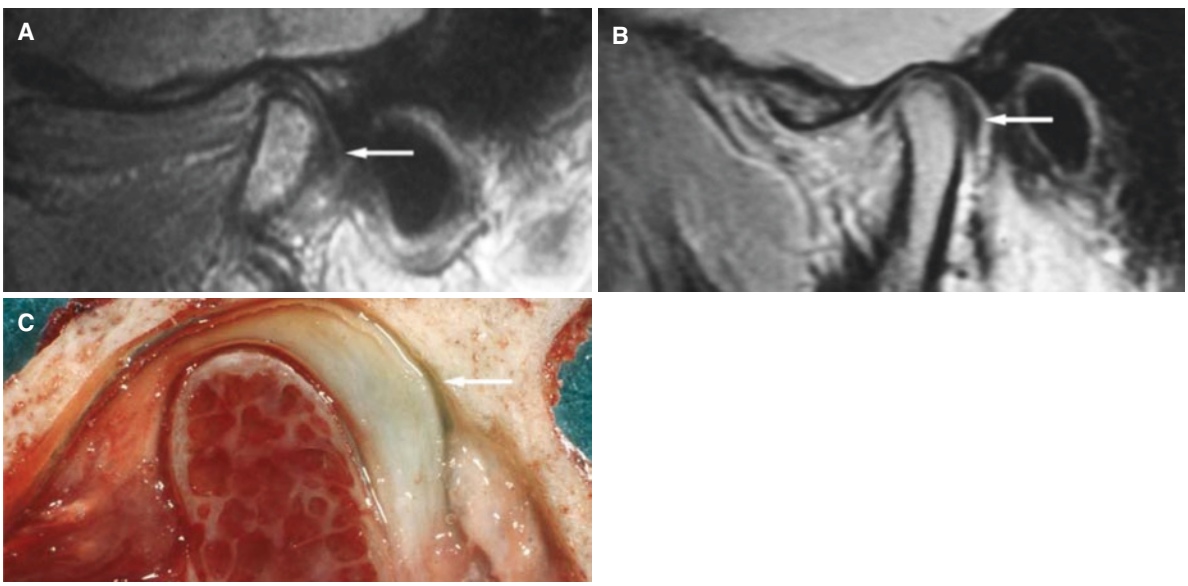

Fig. 6.8 Posterior disc displacement, normal bone. (**A**, **B**) Oblique sagittal MRI shows posteriorly displaced disc (*arrow*) in two patients. (**C**) Autopsy specimen shows posteriorly displaced disc (*arrow*). Reproduced with permission from Westesson et al. (1998)

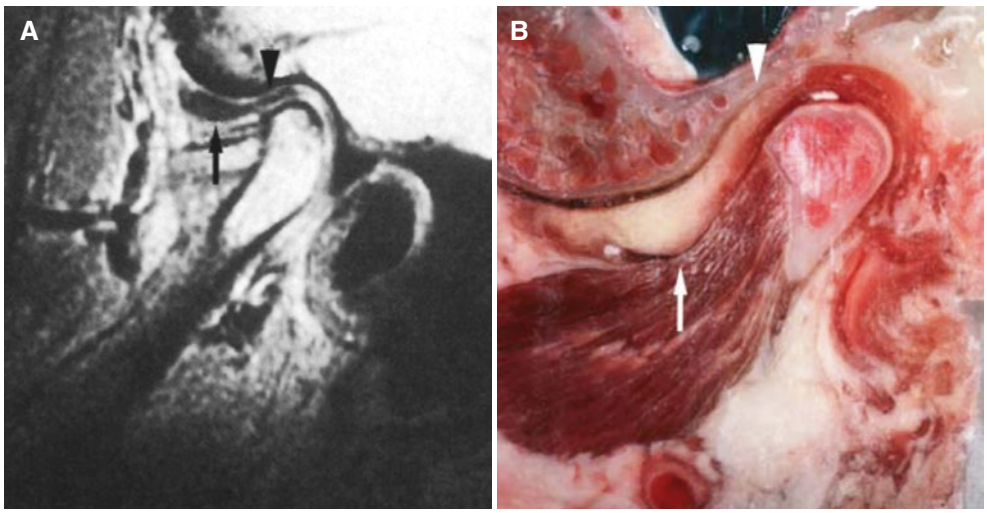

Fig. 6.9 Anterior disc displacement, fibrous posterior attachment (pseudodisc), normal bone. (**A**) Oblique sagittal MRI shows anteriorly displaced disc (*arrow*) and thin, low-signal posterior attachment (*arrowhead*). (**B**) Autopsy specimen shows anteriorly displaced disc (*arrow*) and elongated, thin, and fibrotic posterior attachment (*arrowhead*). Reproduced with permission from Westesson et al. (2003)

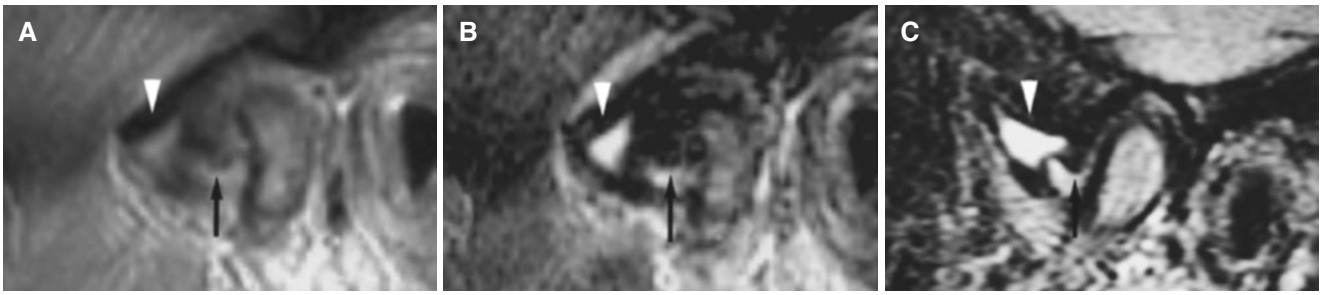

Fig. 6.10 Anterior disc displacement, joint effusion, normal cortical bone, one patient without (**A**, **B**) and one patient with (**C**) bone marrow edema in the condyle. (**A**) Oblique sagittal MRI shows anteriorly displaced and deformed disc (*arrow*) and intermediate signal from anterior recess of the upper compartment (*arrowhead*). (**B**) Oblique sagittal T2-weighted MRI shows increased signal from the upper (*arrowhead*) and lower compartment, consistent with evident fluid, but normal condyle marrow (*arrow* indicates disc) (**A** and **B** have been used as reference images for definition of joint effusion and are reproduced with permission from Larheim et al. 2001b). (**C**) Oblique sagittal T2-weighted MRI of another patient shows anteriorly displaced, deformed disc (*arrow*), more extensive fluid in the upper compartment (*arrowhead*), and increased signal in condyle marrow indicating marrow edema

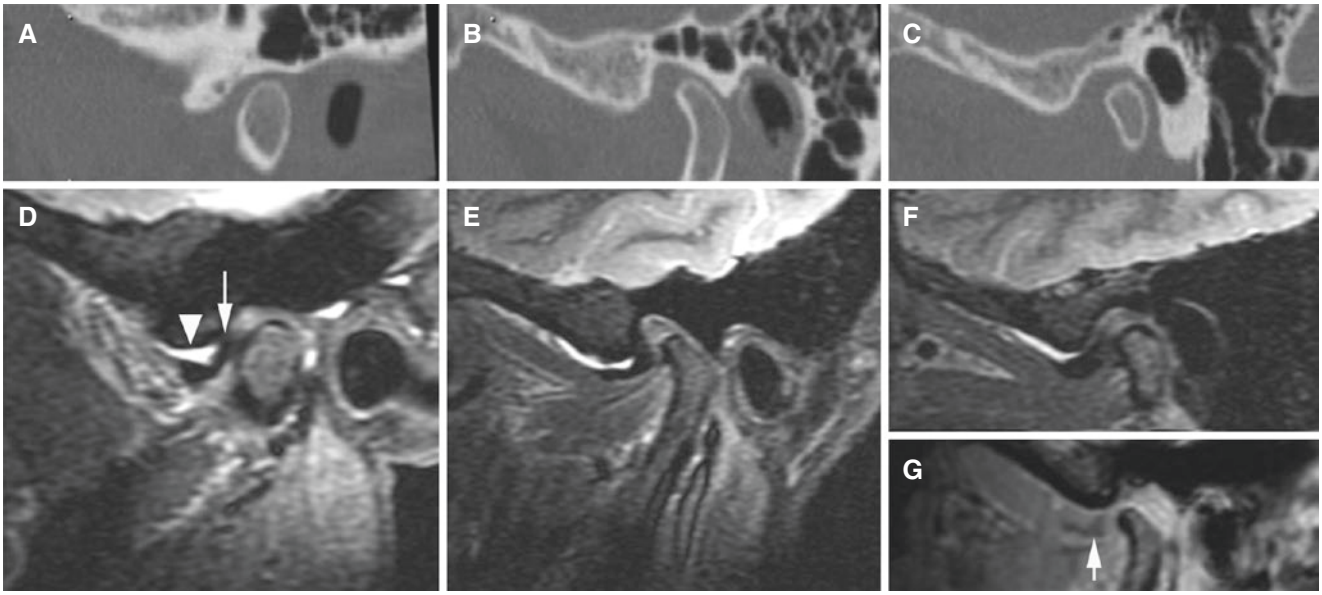

Fig. 6.11 Complete anterior disc displacement without reduction, normal bone; 61-year-old male. (**A**, **B**, **C**) Oblique sagittal CT images show normal bone in lateral, central, and medial sections and condyle posteriorly positioned in fossa in central and medial sections. (**D**, **E**, **F**) Oblique sagittal STIR MRI shows anteriorly displaced disc (*arrow*) in lateral, central, and medial sections and joint effusion (*arrowhead*) throughout the joint. (**G**) Oblique sagittal open-mouth MRI shows displaced disc (*arrow*) and reduced condylar translation

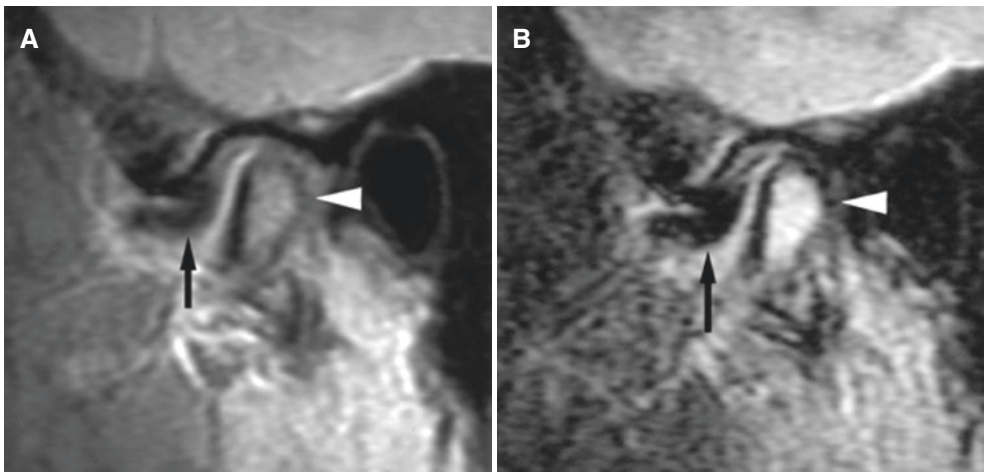

Fig. 6.12 Anterior disc displacement, bone marrow edema, normal cortical bone. (**A**) Oblique sagittal MRI shows anteriorly displaced disc (*arrow*) and intermediate signal in condyle marrow (*arrowhead*). (**B**) Oblique sagittal T2-weighted MRI shows increased signal in condyle marrow; *arrowhead* edema, *arrow* displaced disc. Reproduced with permission from Larheim et al. (2001c)

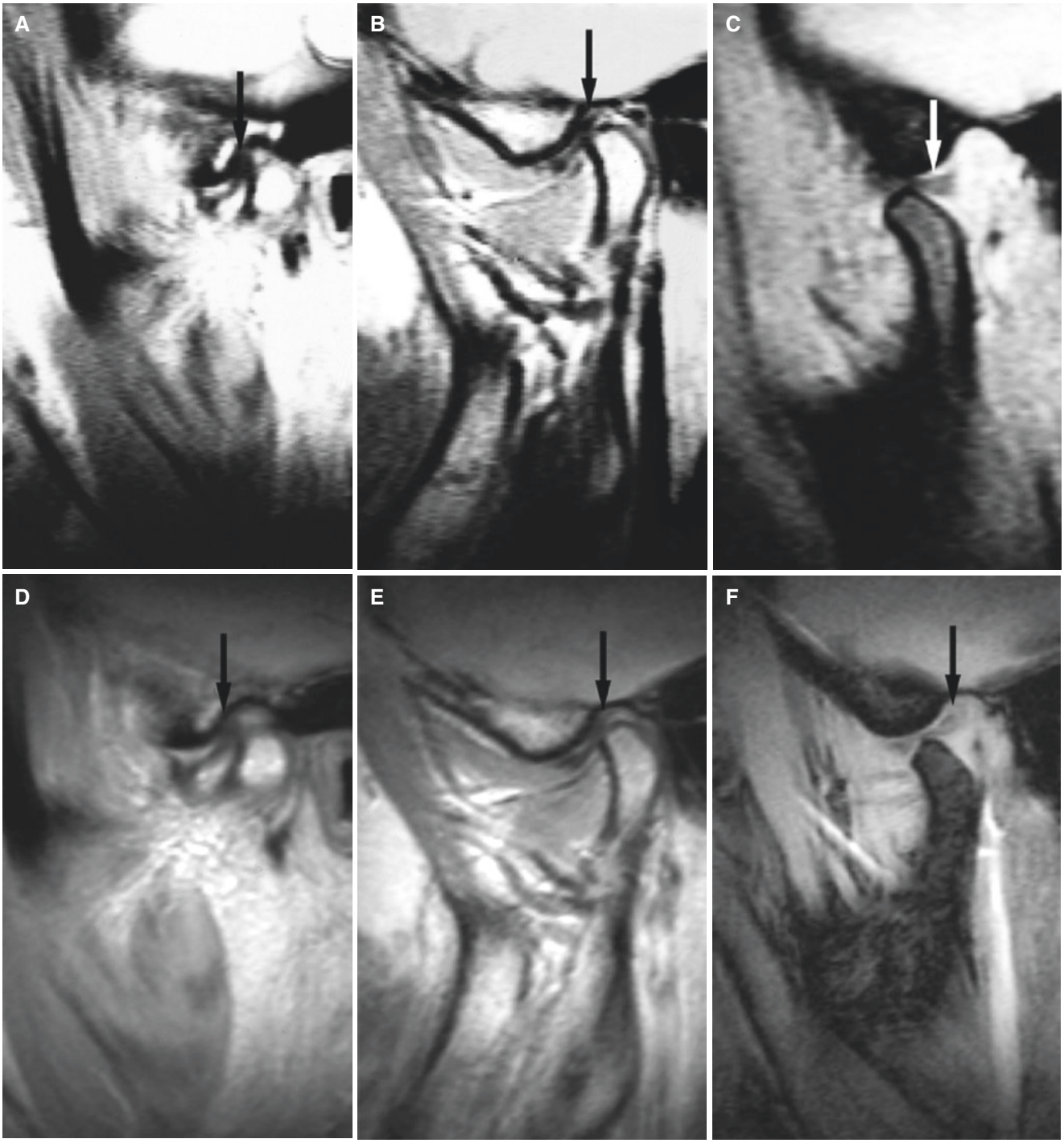

Fig. 6.13 Partial anterior disc displacement at baseline (**A**, **B**, **C**) and at 8-year follow-up (**D**, **E**, **F**), normal bone; identical joint status (except function) at both examinations. (**A**, **D**) Oblique sagittal MRI shows displaced disc (*arrow*) in lateral sections. (**B**, **E**) Oblique sagittal MRI shows normal position of the disc (*arrow*) in central sections. (**C**, **F**) Oblique sagittal MRI shows normal position of the disc (*arrow*) in open-mouth images; condylar translation somewhat reduced at follow-up compared to baseline

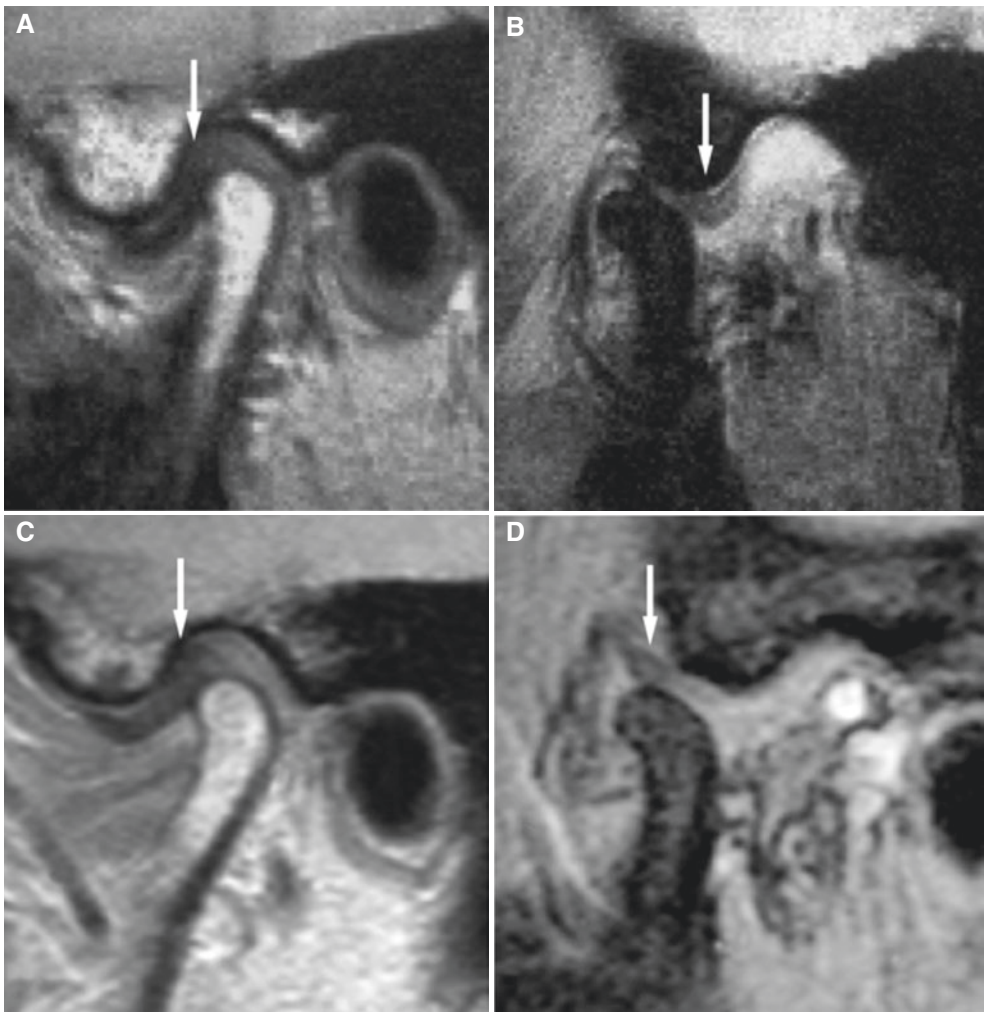

Fig. 6.14 Reducing disc displacement progressing to non-reducing disc displacement, normal bone, from baseline (**A**, **B**) to 10-year follow-up (**C**, **D**). (**A**) Oblique sagittal MRI shows anteriorly displaced disc (*arrow*). (**B**) Disc (*arrow*) reduced to normal in oblique sagittal open-mouth image. (**C**) Oblique sagittal MRI shows anteriorly displaced disc (*arrow*). (**D**) Disc (*arrow*) displaced also in oblique sagittal open-mouth image

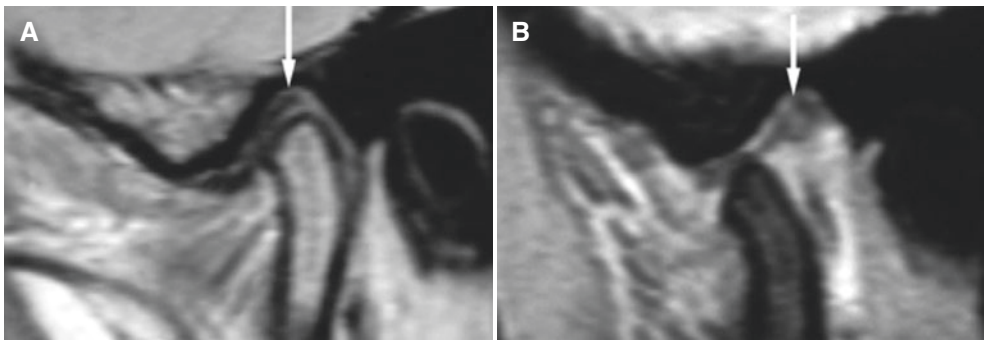

Fig. 6.15 Stuck (fixed) disc, normal bone. (**A**) Oblique sagittal MRI shows the disc (*arrow*) in normal position. (**B**) Oblique sagittal open-mouth MRI shows the disc (*arrow*) in the same position, no motion of the disc with the condyle, probably due to fibrous adhesions

6.3 Osteoarthritis

Figs. 6.16, 6.17, 6.18, 6.19, 6.20, 6.21, 6.22, 6.23, 6.24, 6.25, 6.26, 6.27, 6.28, 6.29, 6.30, and 6.31

Synonyms: osteoarthrosis, degenerative joint disease.

6.3.1 Definition

Previously, osteoarthritis (OA) was considered a non-inflammatory, degenerative disorder of synovial joints, primarily affecting articular cartilage and subchondral bone, initiated by deterioration of articular soft-tissue cover and exposure of the bone. OA is now accepted as an inflammatory condition (with variable activity) that involves all components of the joint.

6.3.2 Clinical Features

- Crepitation sounds from joint(s)
- Restricted or normal mouth-opening capacity
- Pain or no pain from joint areas and/or of mastication muscles
- Occasionally, joints may show inflammatory signs
- A variety of other symptoms such as headache
- Women more frequent than men
- Older age groups more frequent than younger age groups
- Arthrosis deformans juvenilis (juvenile osteoarthritis) in young patients

6.3.3 Imaging Features

- Disc displacement, degenerated or absent disc very frequent
- Abnormal cortical bone; both joint components; most evident in the condyle
- Early stage: cortical erosion
- Advanced stage: joint space reduction and bone production; osteophytosis, sclerosis
- Joint effusion may be seen, either in early or advanced stage
- Bone marrow edema or bone marrow sclerosis, or in combination, may be seen, either in early or advanced stage
- Usually intravenous contrast injection is not applied, but osteoarthritis may demonstrate contrast enhancement of thickened synovium
- Osteoarthritis secondary to trauma or inflammatory arthritis usually shows normal disc position
- Bone remodeling, particularly in young age (juvenile osteoarthritis)

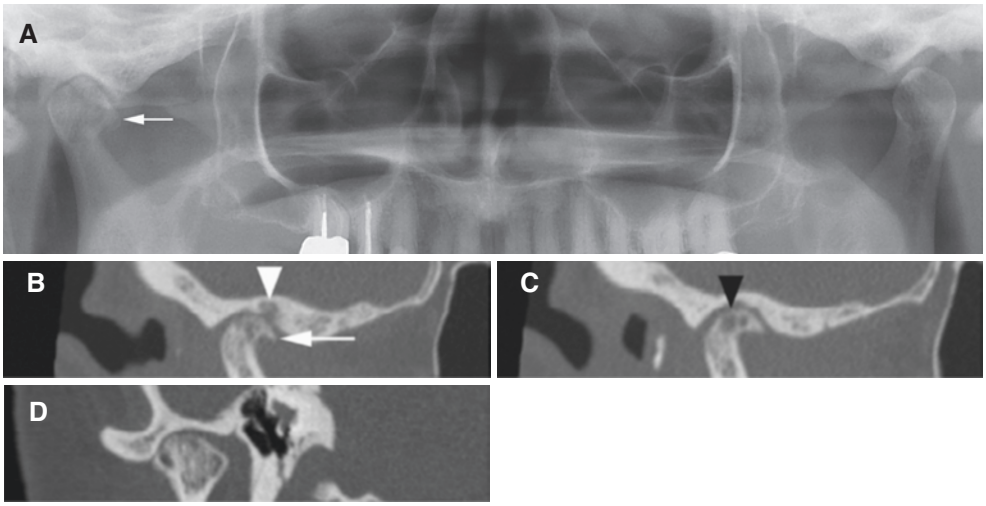

Fig. 6.16 Osteoarthritis; 50-year-old female. (**A**) Panoramic view suggests right-sided osteoarthritis (condylar osteophyte) (*arrow*). (**B**, **C**) Oblique sagittal and (**D**) oblique coronal CT images show large condylar osteophyte (*arrow*), severe erosion in temporal bone (*arrowhead*), and subcortical cysts in the condyle (*black arrowhead*)

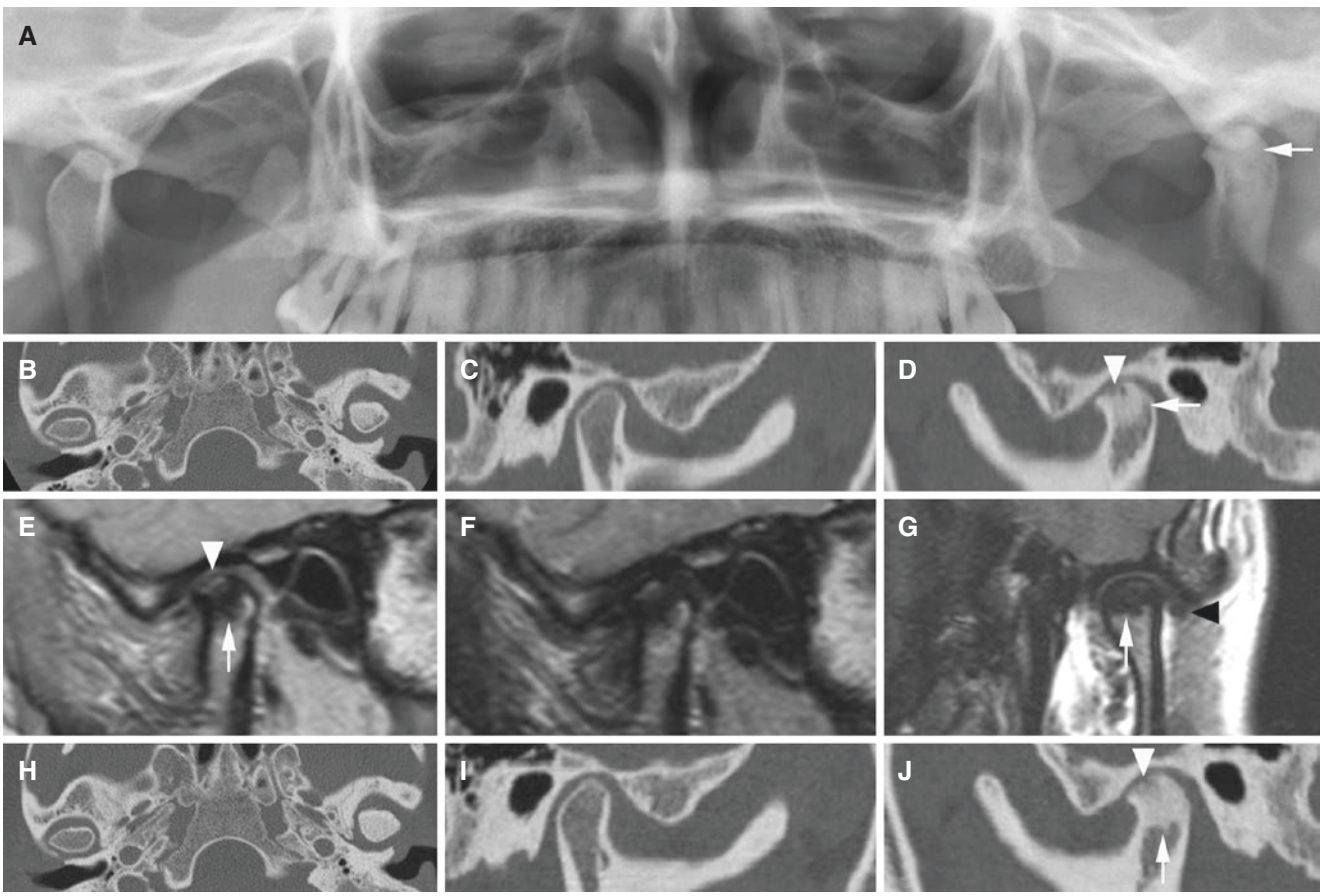

Fig. 6.17 Osteoarthritis, with 5-year follow-up; female 37-year-old at baseline (**A**, **B**, **C**, **D**, **E**, **F**, **G**). (**A**) Panoramic view shows sclerotic and flattened left mandibular condyle (*arrow*). (**B**) Axial and (**C**, **D**) oblique sagittal CT images show normal right joint (**B**, **C**) and osteoarthritic left joint (**B**, **D**); *arrowhead* condylar erosion, *arrow* condylar sclerosis. (**E**) Oblique sagittal PD-weighted, (**F**) oblique sagittal T2-weighted, and (**G**) oblique coronal T1-weighted MRI show sclerosis (reduced signal intensity) in the condyle (*arrow*), condylar erosion (*arrowhead*), and laterally displaced disc (*black arrowhead*) in the left joint. At 5-year follow-up, (**H**) axial and (**I**, **J**) sagittal CT images show normal right joint (**H**, **I**) and more pronounced sclerosis (*arrow*) and less pronounced cortical erosion (*arrowhead*) in the left joint (**H**, **J**), compared with (**B**, **C**, **D**)

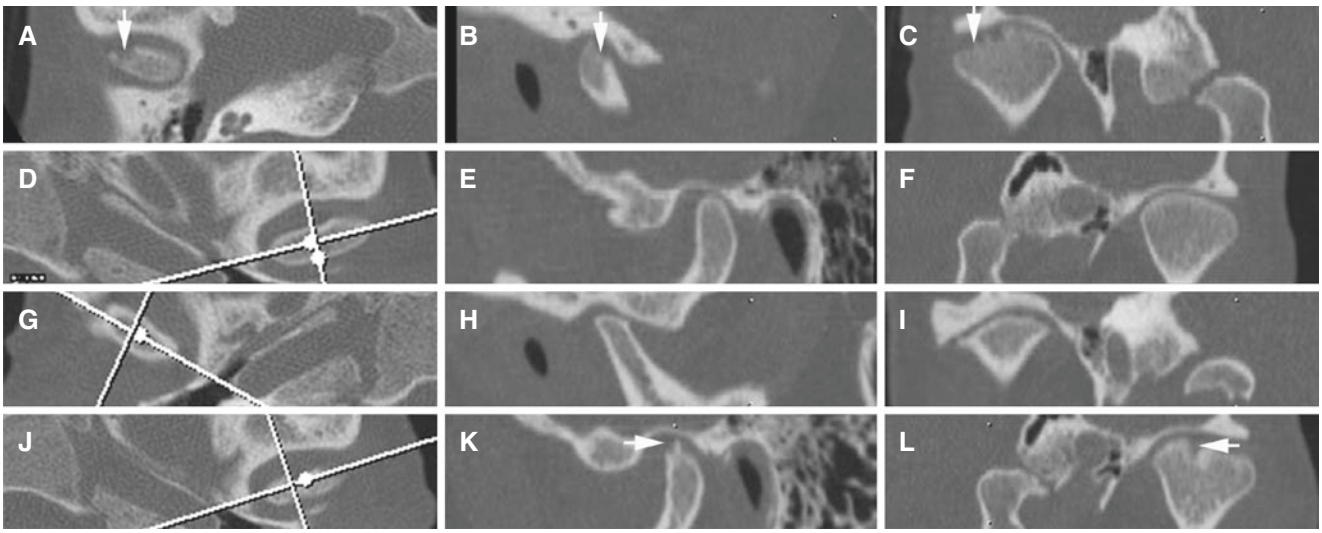

Fig. 6.18 Osteoarthritis, with 5-year follow-up: "improvement" in one joint, progression in contralateral joint; female 36-year-old at baseline (**A**–**F**). (**A**) Axial, (**B**) oblique sagittal, and (**C**) oblique coronal CT images of the right joint show cortical erosion in lateral part of the condyle (*arrow*). (**D**) Axial CT (with *cursor lines*), (**E**) oblique sagittal, and (**F**) oblique coronal CT images of the left joint show normal bone. At 5-year follow-up (**G**–**L**), (**G**) axial CT (with *cursor lines*), (**H**) oblique sagittal, and (**I**) oblique coronal CT images of the right joint show flattened (remodeled) condyle with "healed" cortical bone, compared with (**B**, **C**). Steroid injections had been performed twice. (**J**) Axial CT (with *cursor lines*), (**K**) oblique sagittal, and (**L**) oblique coronal CT images of the left joint show cortical erosion (*arrow*), compared with (**E**, **F**)

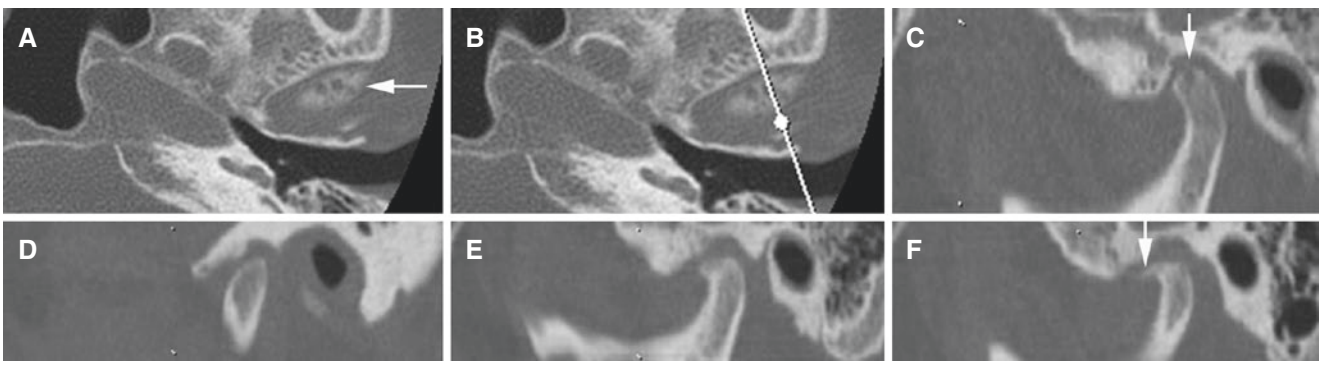

Fig. 6.19 Inflammatory arthritis/erosive osteoarthritis developing into (symptom-free) bone-productive osteoarthritis within a 2-year period; male 66-year-old at baseline, with inflammatory ENT symptoms for about 1 month and impaired jaw function. (**A**) Axial CT, (**B**) axial (with *cursor line*), and (**C**) oblique sagittal CT images show punched-out erosions in the condyle (*arrow*). At 2-year follow-up, (**D**, **E**, **F**) oblique sagittal CT images of lateral, central, and medial parts show flattened condyle with osteophyte formation (*arrow*)

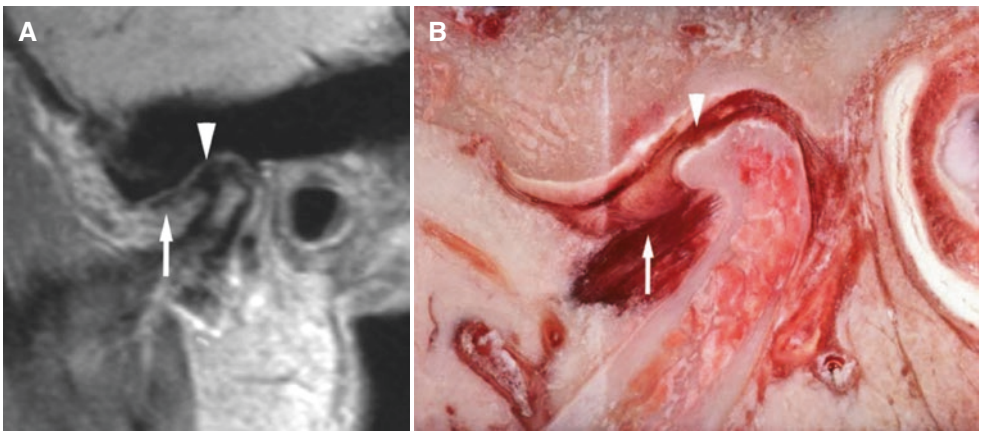

Fig. 6.20 Osteoarthritis, anterior disc displacement. (**A**) Oblique sagittal MRI shows anteriorly displaced disc remnant (*arrow*) and irregular cortical outline with condylar osteophyte/sclerosis (*arrowhead*). (**B**) Autopsy specimen shows anteriorly displaced, deformed disc (*arrow*) and osteophyte/sclerosis of the condyle (*arrowhead*)

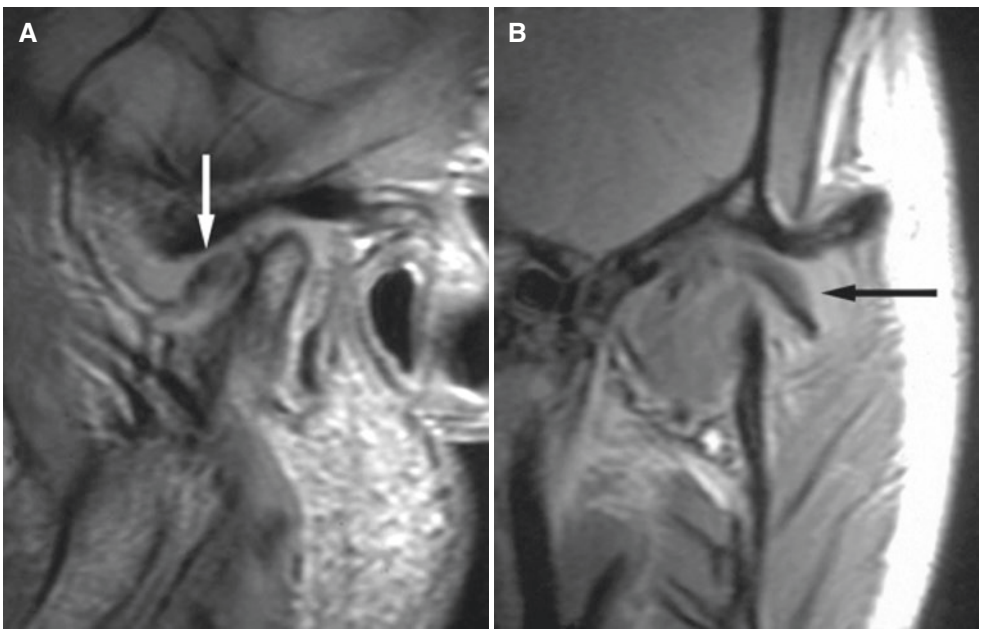

Fig. 6.21 Osteoarthritis, anterolateral disc displacement. (**A**) Oblique sagittal MRI shows anteriorly displaced, deformed disc (*arrow*) and cortical irregularities and flattening of the condyle. (**B**) Oblique coronal MRI shows laterally displaced disc (*arrow*)

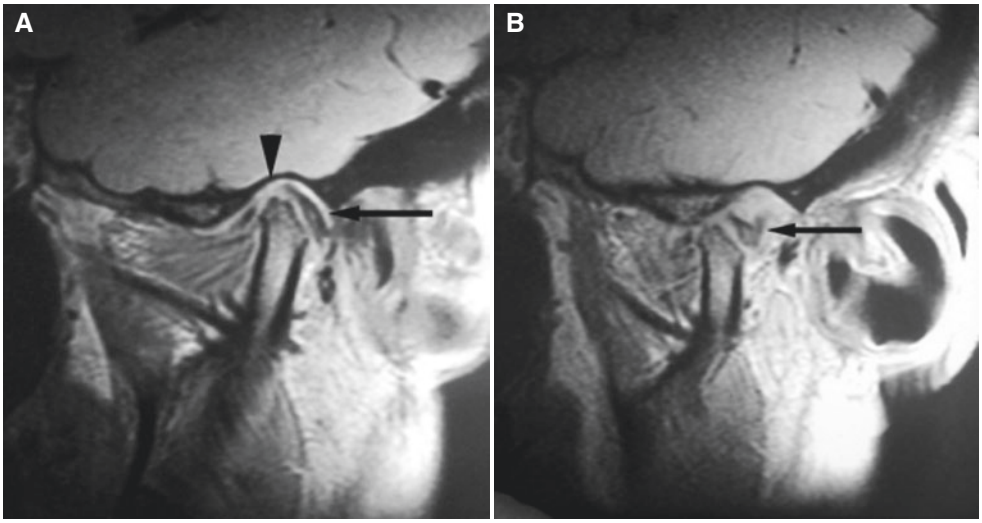

Fig. 6.22 Osteoarthritis, posterior disc displacement. (**A**) Oblique sagittal MRI shows disc perforation and cortical irregularities of the condyle (*arrowhead*) and posteriorly displaced disc (*arrow*). (**B**) Oblique sagittal open-mouth MRI shows the disc (*arrow*) adherent to the condyle. Reproduced with permission from Westesson et al. (1998)

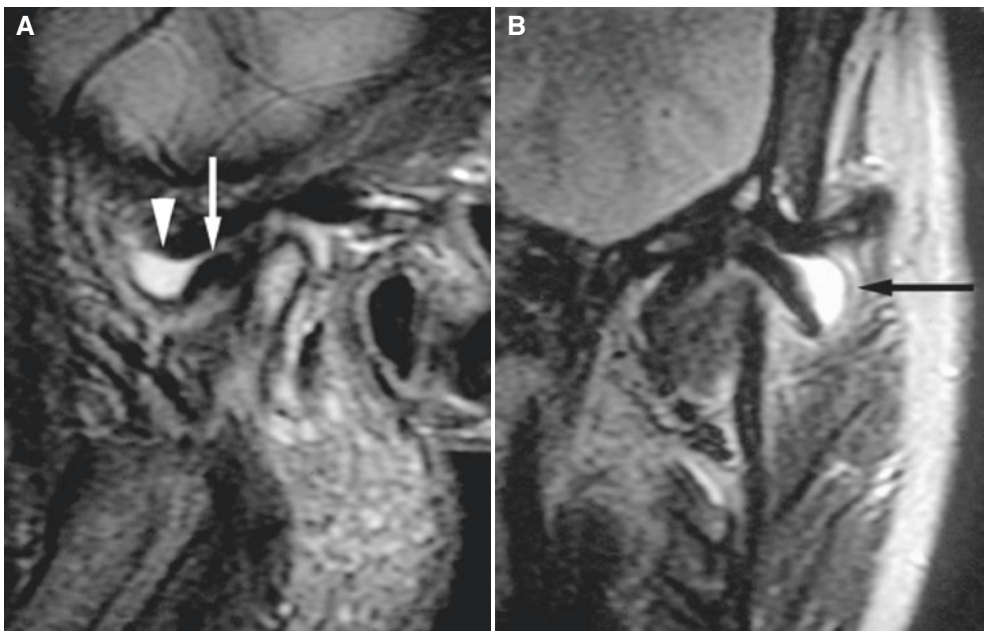

Fig. 6.23 Osteoarthritis and anterolateral disc displacement, with joint effusion. Same patient as in Fig. 6.21. (**A**) Oblique sagittal T2-weighted MRI shows anteriorly displaced disc (*arrow*), flattened condyle, and joint effusion (*arrowhead*) in anterior recess of the upper compartment. (**B**) Oblique coronal T2-weighted MRI shows joint effusion in lateral part of the joint above laterally displaced disc (*arrow*)

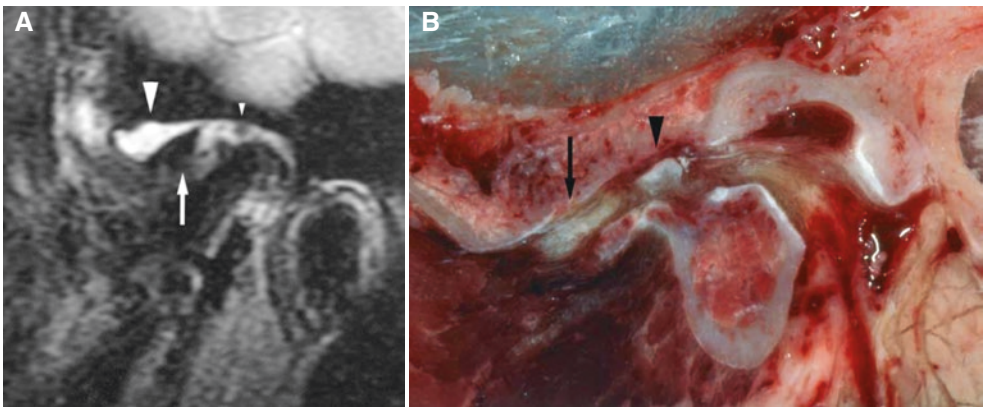

Fig. 6.24 Advanced osteoarthritis, anterior disc displacement, joint effusion. (**A**) Oblique sagittal T2-weighted MRI shows anteriorly displaced, deformed disc (*arrow*), large joint effusion (*large arrowhead*) in anterior recess of the upper compartment, and possible bone fragment (*small arrowhead*) superior to the condyle, which has cortical irregularities and is completely sclerotic ("black condyle"). Reproduced with permission from Larheim et al. (2001c). (**B**) Autopsy specimen shows anteriorly displaced, deformed disc (*arrow*), osteophyte and cortical irregularities of the condyle, and bone fragment in joint space (*arrowhead*) suggesting osteochondritis dissecans. Reproduced with permission from Westesson et al. (2003)

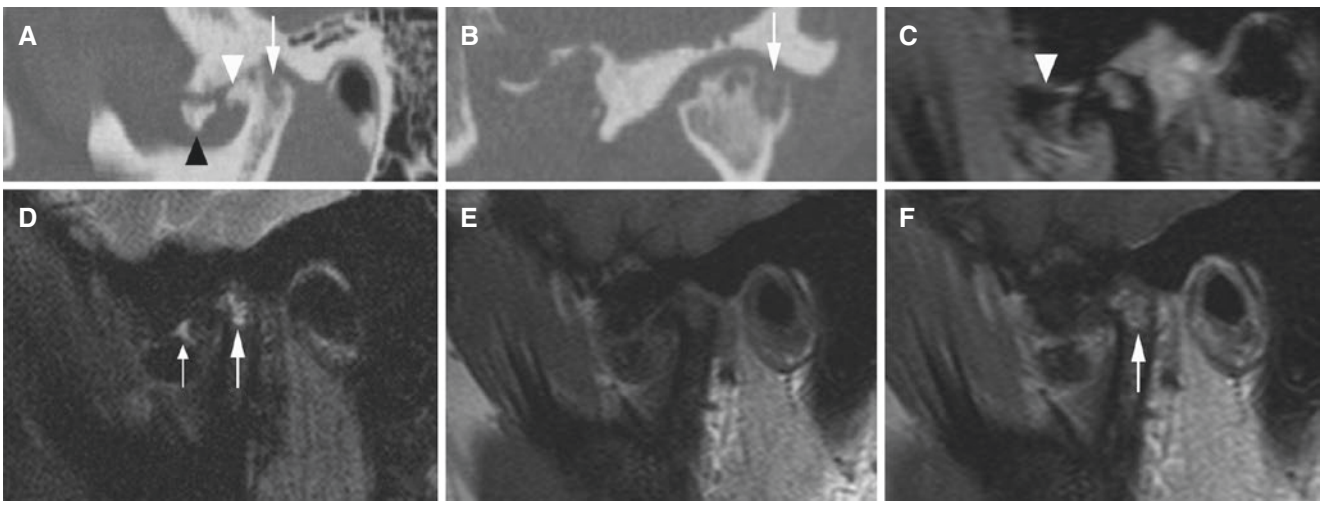

Fig. 6.25 Osteoarthritis, loose body, bone marrow edema, and/or extensive erosion in the condyle; 65-year-old male. (**A**) Oblique sagittal and (**B**) oblique coronal CT images show severe erosion (*arrow*), osteophyte (*arrowhead*), and loose body (*black arrowhead*). (**C**) Oblique sagittal open-mouth MRI shows loose body (*arrowhead*) moved anterior to eminence and reduced condylar translation. (**D**) Oblique sagittal T2-weighted MRI shows marrow edema and/or extensive erosion in the condyle (*arrow*) and some joint effusion (*thin arrow*). (**E**) Oblique sagittal T1-weighted pre-Gd and (**F**) oblique sagittal T1-weighted post-Gd MRI show contrast enhancement in the condyle (*arrow*)

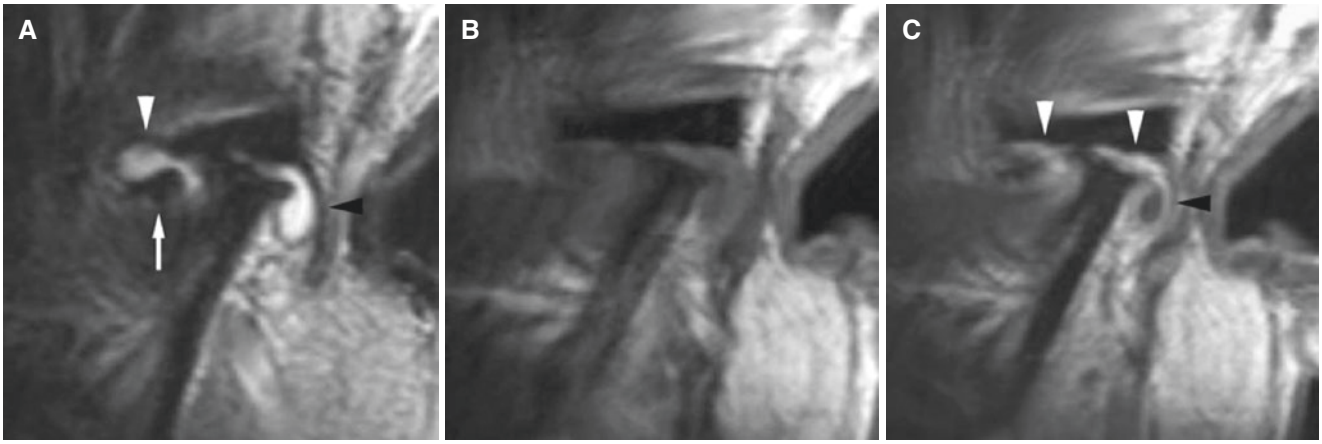

Fig. 6.26 Advanced osteoarthritis, anterior disc displacement, joint effusion, synovitis. (**A**) Oblique sagittal T2-weighted MRI shows anteriorly displaced, deformed disc (*arrow*), deformed condyle with osteophyte/sclerosis, and large effusion in anterior (*white arrowhead*) and posterior (*black arrowhead*) recesses of joint compartment. (**B**) Oblique sagittal T1-weighted pre-Gd and (**C**) oblique sagittal T1-weighted post-Gd MRI show contrast enhancement in periphery of joint effusion in anterior (*left arrowhead*) and posterior (*black arrowhead*) recesses of joint compartment. Contrast enhancement also in joint space above the condyle consistent with thickened (inflamed) synovium (*central arrowhead*)

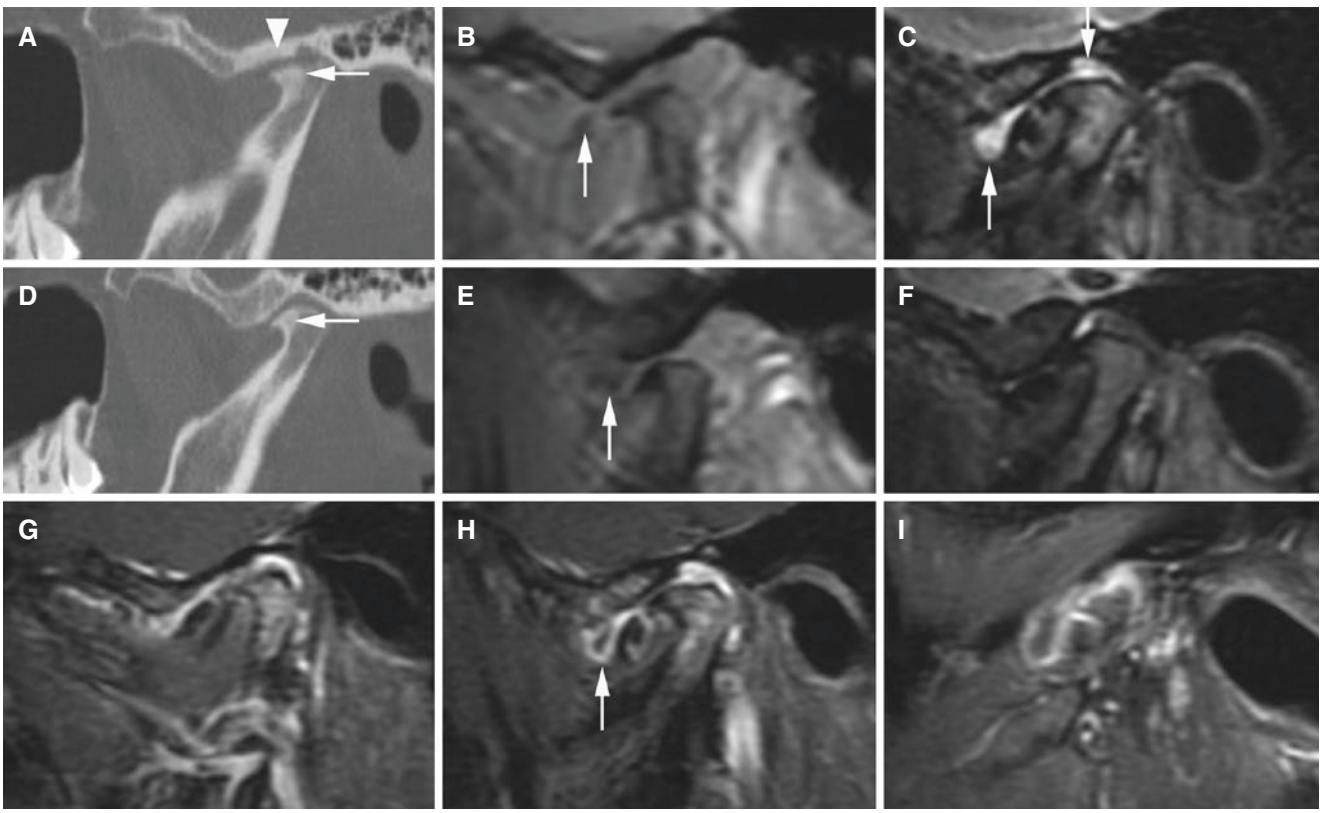

Fig. 6.27 Osteoarthritis with contrast enhancement (synovitis), surgically treated; 27-year-old female. (**A**, **B**, **C**, **G**, **H**, **I**) Right joint. (**D**, **E**, **F**) Left joint. (**A**) Oblique sagittal CT image shows flattened articular surfaces, condylar osteophyte/sclerosis (*arrow*), and sclerosis in fossa/eminence (*arrowhead*). (**B**) Oblique sagittal open-mouth MRI shows displaced disc (*arrow*) and reduced condylar translation. (**C**) Oblique sagittal T2-weighted MRI shows large joint effusion in the upper joint compartment, both anterior and posterior recess (*arrows*). (**D**) Oblique sagittal CT image shows flattened condylar surface and condylar osteophyte/sclerosis (*arrow*). (**E**) Oblique sagittal open-mouth MRI shows anteriorly displaced disc (*arrow*) and reduced condylar translation. (**F**) Oblique sagittal T2-weighted MRI shows minimal joint fluid. (**G**, **H**, **I**) Oblique sagittal T1-weighted fat sat post-Gd MRI shows evident contrast enhancement in the synovial membrane (synovitis) surrounding effusion in anterior recess (*arrow*). There was no/minimal contrast enhancement in the left joint (not shown)

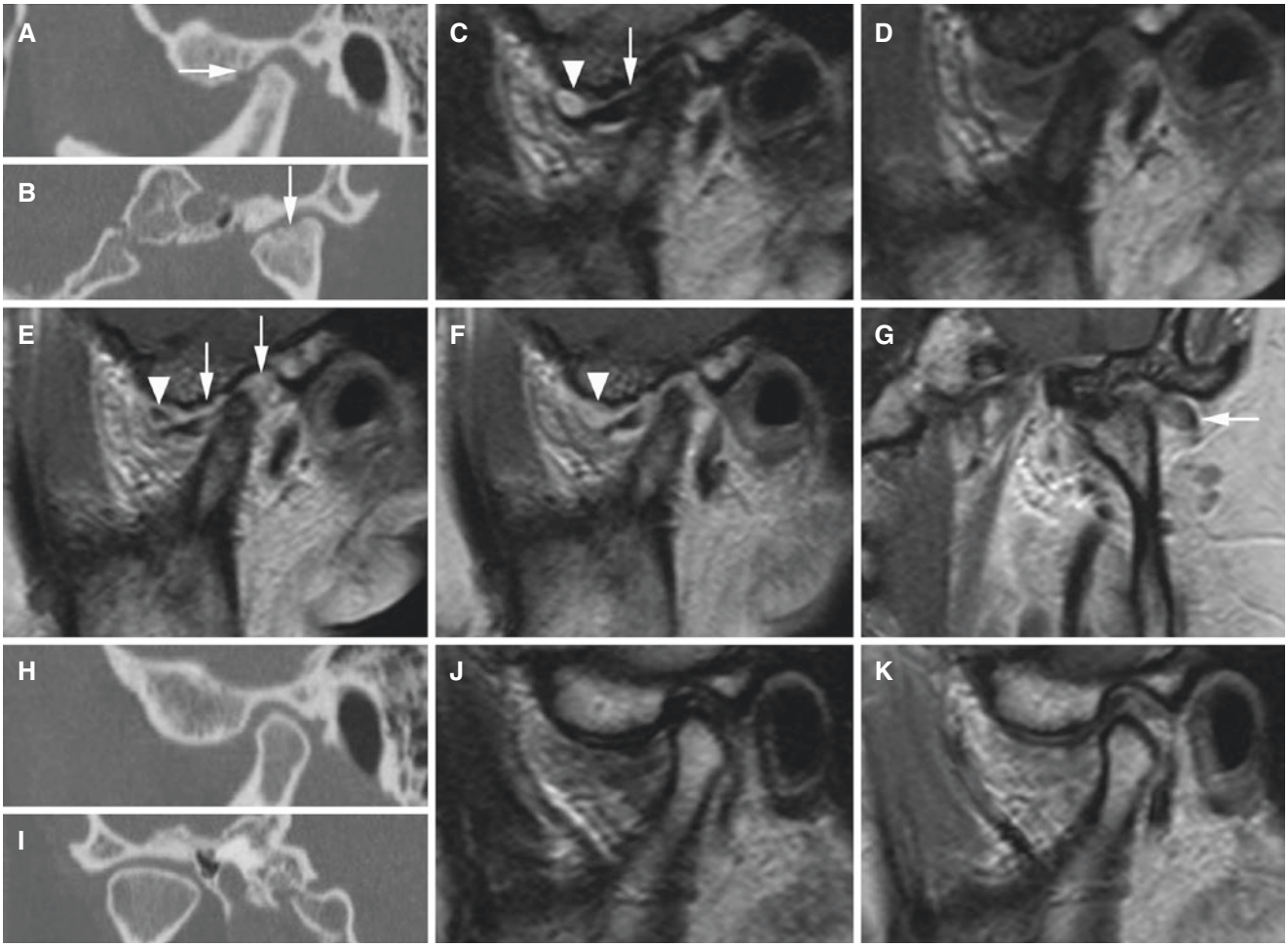

Fig. 6.28 Osteoarthritis with contrast enhancement (synovitis), surgically treated; 38-year-old female. (**A**) Oblique sagittal and (**B**) oblique coronal CT images show somewhat sclerotic condyle and surface irregularities of eminence and condyle (*arrow*). (**C**) Oblique sagittal T2-weighted MRI shows joint effusion particularly in anterior recess of the upper compartment (*arrowhead*) and anteriorly displaced disc (*arrow*). (**D**) Oblique sagittal T1-weighted pre-Gd and (**E**) oblique sagittal T1-weighted post-Gd MRI show contrast enhancement in joint compartment (*arrows*); note in particular around effusion (*arrowhead*) consistent with synovitis/pannus formation. (**F**) Oblique sagittal T1-weighted post-Gd MRI about 10 min later shows contrast enhancement in the entire joint effusion (*arrowhead*). (**G**) Oblique coronal T1-weighted post-Gd MRI shows laterally displaced disc (*arrow*). (**H**) Oblique sagittal, (**I**) oblique coronal CT images, (**J**) oblique sagittal T2-weighted, and (**K**) oblique sagittal T1-weighted post-Gd MRI show normal contralateral joint

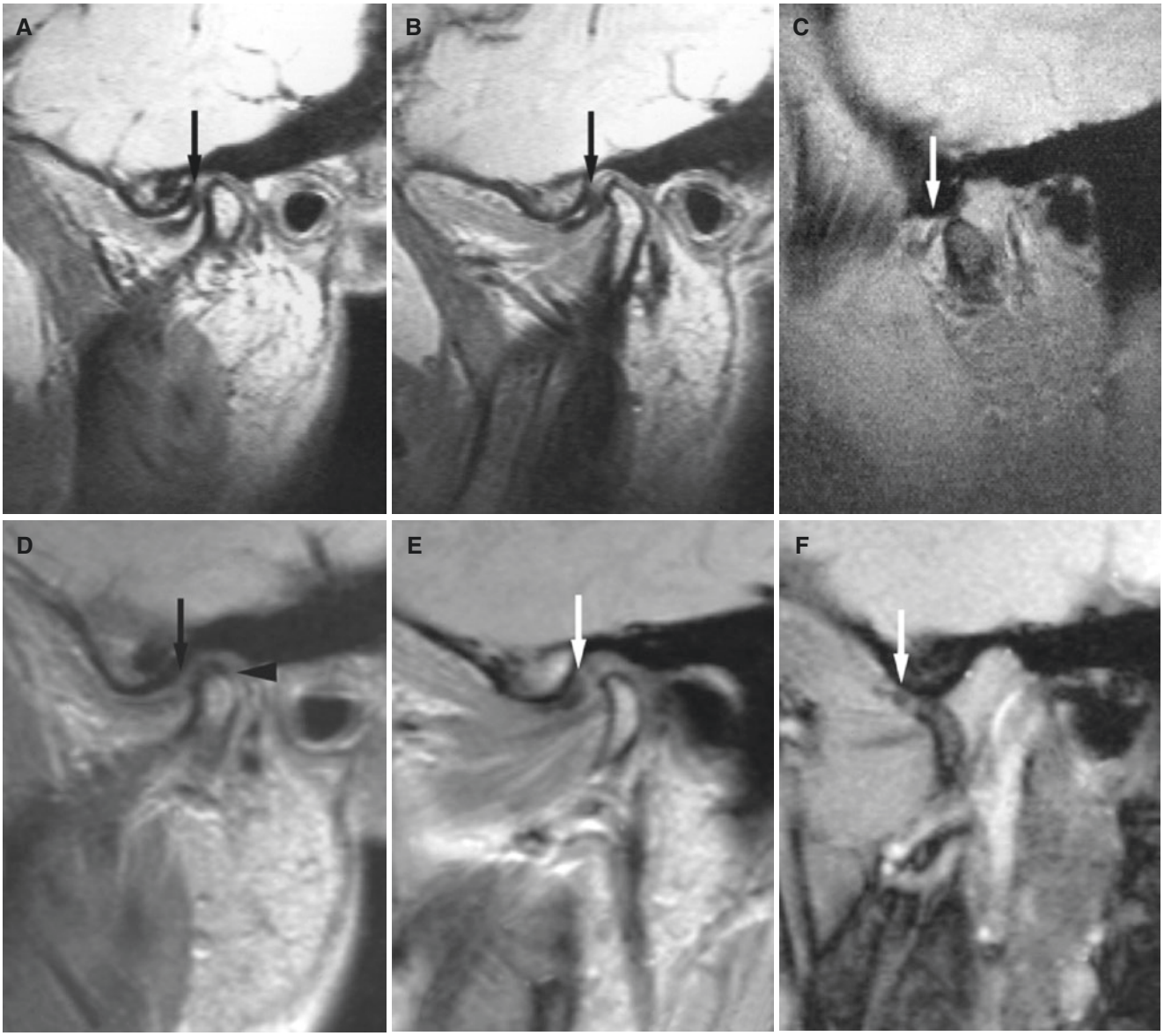

Fig. 6.29 Osteoarthritis developed during a 15-year period from non-reducing disc displacement and normal bone. At baseline, (**A**, **B**, **C**) oblique sagittal MRI shows anteriorly displaced disc (*arrow*) in lateral (**A**) and central (**B**) images and in open-mouth image (**C**) and normal cortical bone. At follow-up (**D**, **E**, **F**) oblique sagittal MRI shows anteriorly displaced disc (*arrow*) in lateral (**D**) and central–medial (**E**) images and in open-mouth image (**F**) and abnormal cortical bone; the condyle has now irregular, flattened, sclerotic surface laterally (*arrowhead*) (**D**). Note better condylar translation in osteoarthritic joint at follow-up (**F**), compared to non-osteoarthritic joint at baseline (**C**)

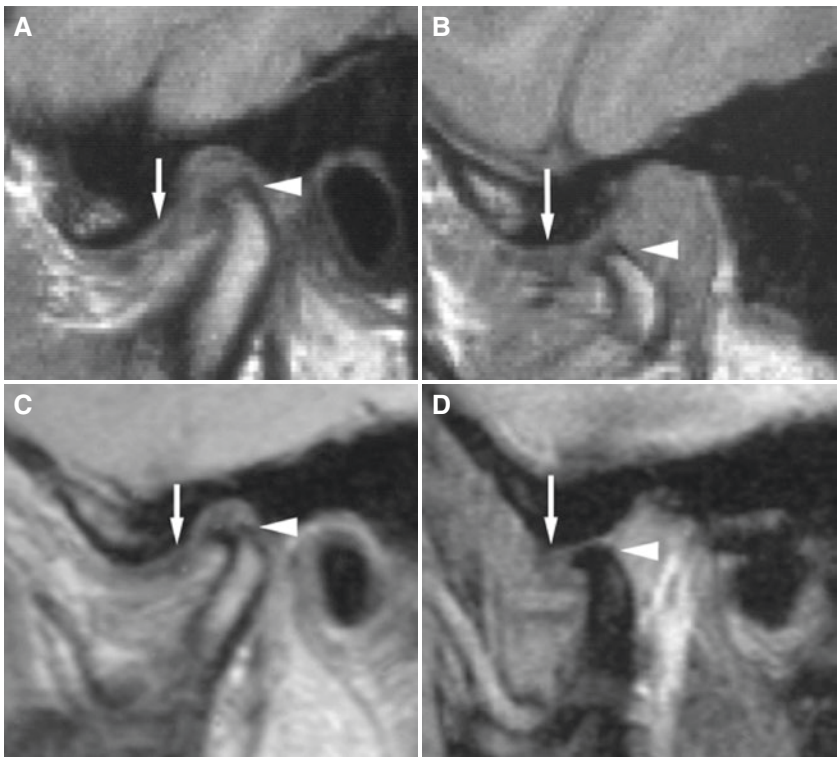

Fig. 6.30 Osteoarthritis progression, with non-reducing disc displacement at baseline (**A**, **B**) and at 15-year follow-up (**C**, **D**). Contralateral joint of patient in Fig. 6.29. (**A**, **B**) Oblique sagittal MRI shows anteriorly displaced disc (*arrow*), also in open-mouth image (**B**), and flattened condyle (*arrowhead*). (**C**, **D**) Oblique sagittal MRI shows anteriorly displaced disc (*arrow*), also in open-mouth image (**D**), and osteoarthritic condyle (*arrowhead*). Osteoarthritis is more evident in a more lateral section of the same joint (see **A** in Fig. 6.20)

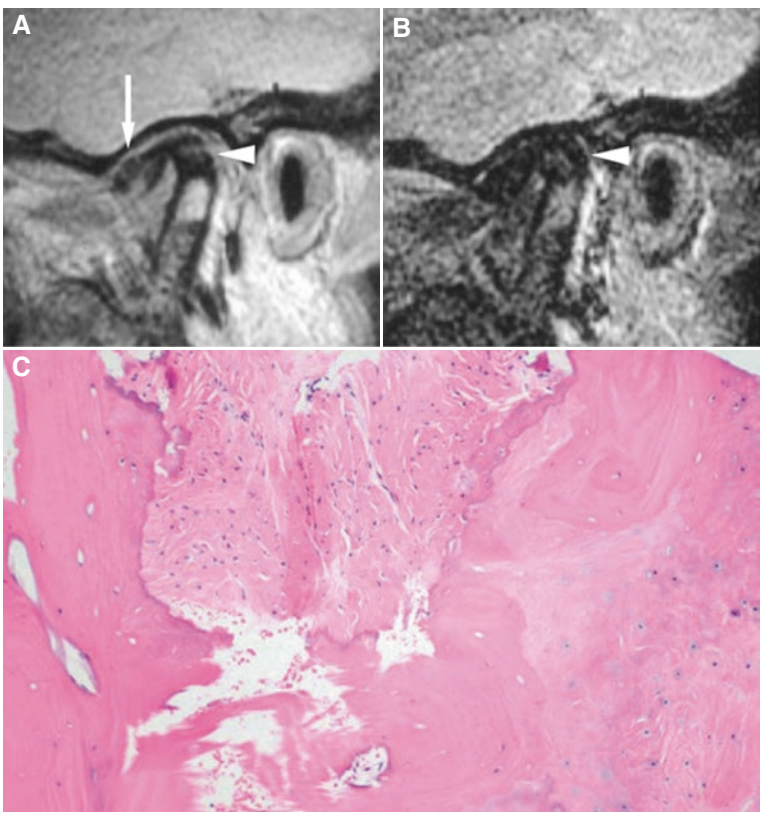

Fig. 6.31 Advanced osteoarthritis, anterior disc displacement. (**A**) Oblique sagittal MRI shows anteriorly displaced disc (*arrow*) and flattened condyle with osteophyte and extensive marrow sclerosis or fibrosis (*arrowhead*). (**B**) Oblique sagittal T2-weighted MRI shows reduced signal in condyle marrow confirming marrow sclerosis or fibrosis (*arrowhead*). (**C**) Histologic section from condyle marrow of the same patient shows replacement of marrow by dense, sclerotic bone and fibrous tissue, suggesting a reparative process (hematoxylin eosin; original magnification × 50). Reproduced with permission from Larheim et al. (1999)

6.4 Bone Marrow Abnormalities

Figs. 6.32, 6.33, 6.34, and 6.35

6.4.1 Definition

Bone marrow edema: serum proteins within marrow interstitium surrounded by normal hematopoietic marrow.

Osteonecrosis: complete loss of hematopoietic marrow.

6.4.2 Clinical Features

- More pain from joints with internal derangement and abnormal bone marrow than from joints with internal derangement and normal bone marrow is reported
- Otherwise, there are no specific features compared to internal derangement or osteoarthritis

6.4.3 Imaging Features

- Abnormal signal on T2-weighted image from condyle marrow: increased signal indicates marrow edema; reduced signal indicates marrow sclerosis or fibrosis
- Combination of marrow edema signal and marrow sclerosis (or fibrosis) signal in the condyle is the most reliable sign for histologic diagnosis of osteonecrosis
- Marrow sclerosis (or fibrosis) signal may indicate advanced osteoarthritis without osteonecrosis or osteonecrosis
- Abnormal bone marrow signal is frequently associated with joint effusion
- Marrow edema or osteonecrosis is occasionally seen in joints with normal cortical bone and disc displacement but more frequently in joints with osteoarthritis

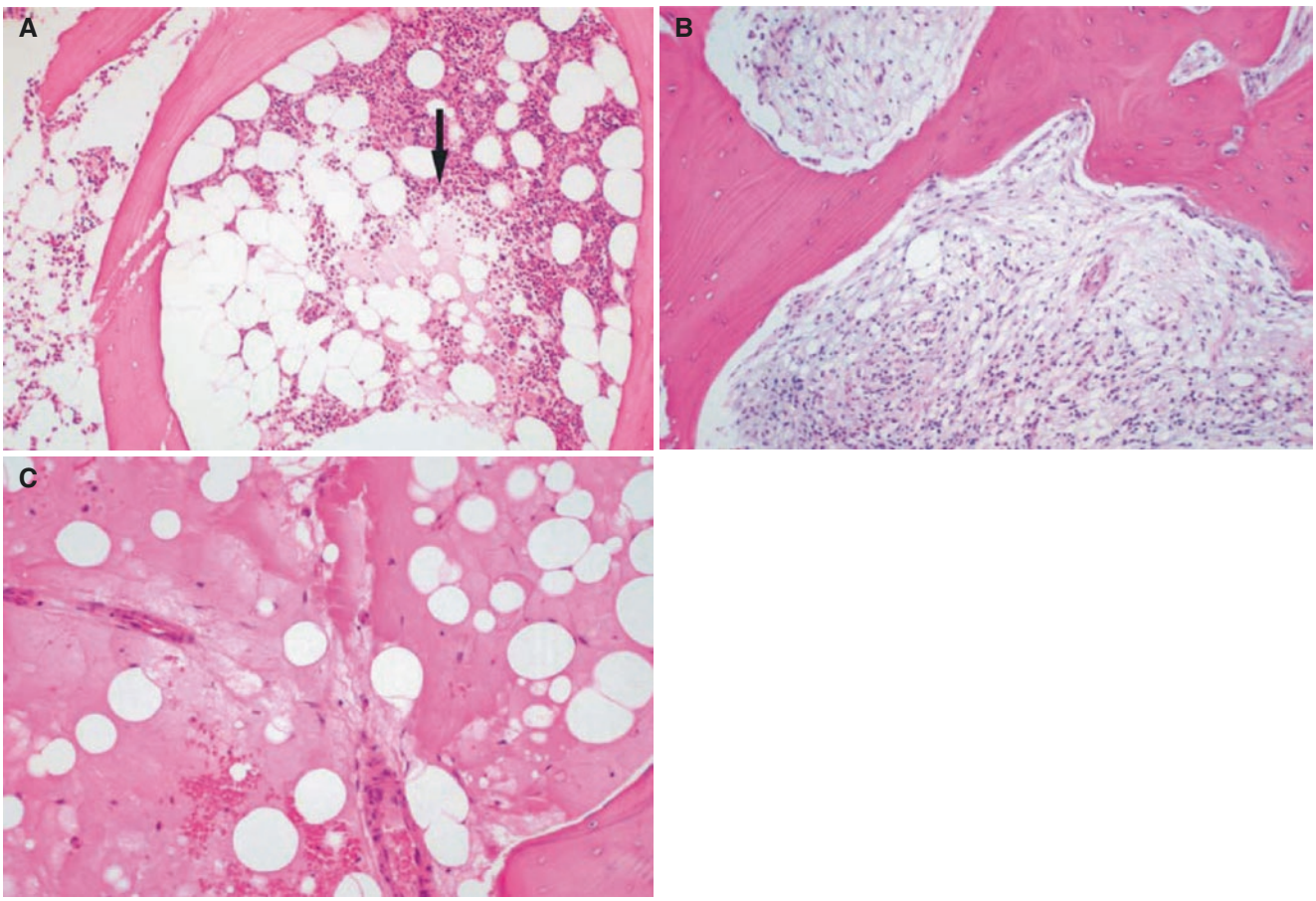

Fig. 6.32 Bone marrow edema, osteonecrosis. (**A**) Histologic section from mandibular condyle marrow shows early marrow edema (*arrow*); a patchy focus of serum proteins surrounded by normal marrow. (**B**) Histologic section from mandibular condyle marrow shows osteonecrosis; complete loss of hematopoietic marrow with evidence of inflammatory cell infiltrate. (**C**) Histologic section from femoral head marrow shows complete loss of hematopoietic marrow (avascular necrosis) (hematoxylin eosin; original magnification × 50). (**A**, **B**) reproduced with permission from Larheim et al. (1999)

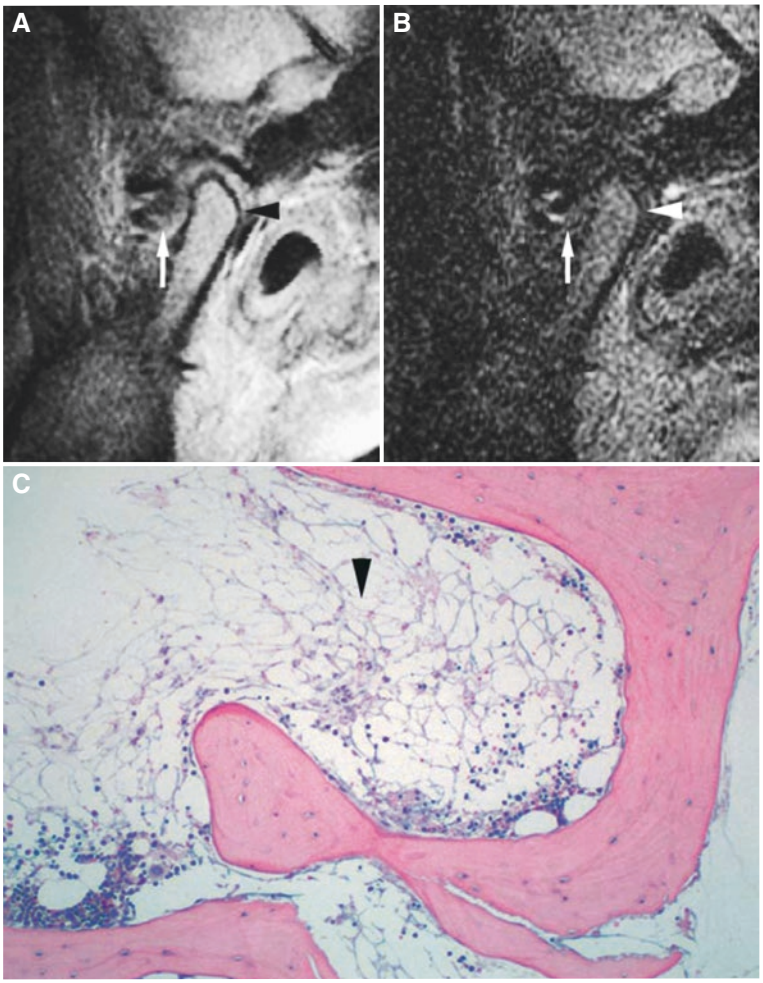

Fig. 6.33 Osteonecrosis, anterior disc displacement, apparently normal cortical bone. (**A**) Oblique sagittal MRI shows anteriorly displaced, deformed disc (*arrow*) and normal bone; cortex and marrow (*arrowhead*). (**B**) Oblique sagittal T2-weighted MRI shows displaced disc (*arrow*), minimal fluid in the upper and lower compartment, and normal, low signal from bone marrow (*arrowhead*). (**C**) Histologic section of the same patient shows focus of marrow necrosis; loss of hematopoietic elements (*arrowhead*) with breakdown of marrow fat (hematoxylin eosin, original magnification × 50). Reproduced with permission from Larheim et al. (1999)

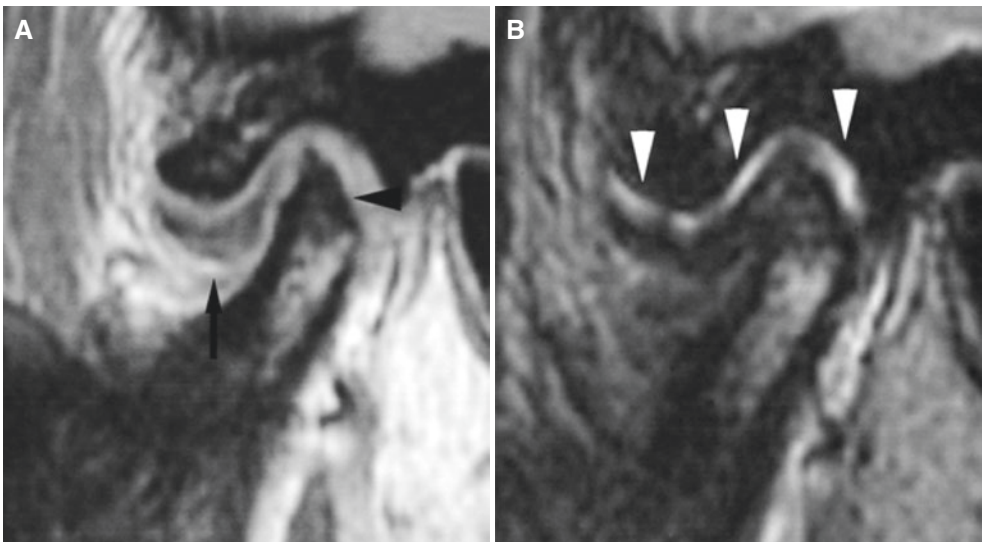

Fig. 6.34 Osteonecrosis, anterior disc displacement, osteoarthritis, joint effusion. (**A**) Oblique sagittal MRI shows anteriorly displaced, deformed disc (*arrow*) and cortical irregularities of the condyle with reduced signal from condyle marrow (*arrowhead*). (**B**) Oblique sagittal T2-weighted MRI shows effusion in the entire upper compartment (*arrowheads*) and marrow sclerosis or fibrosis in the condyle, but no marrow edema. Histologic section from condyle marrow (not shown) demonstrated osteonecrosis. Reproduced with permission from Larheim et al. (1999)

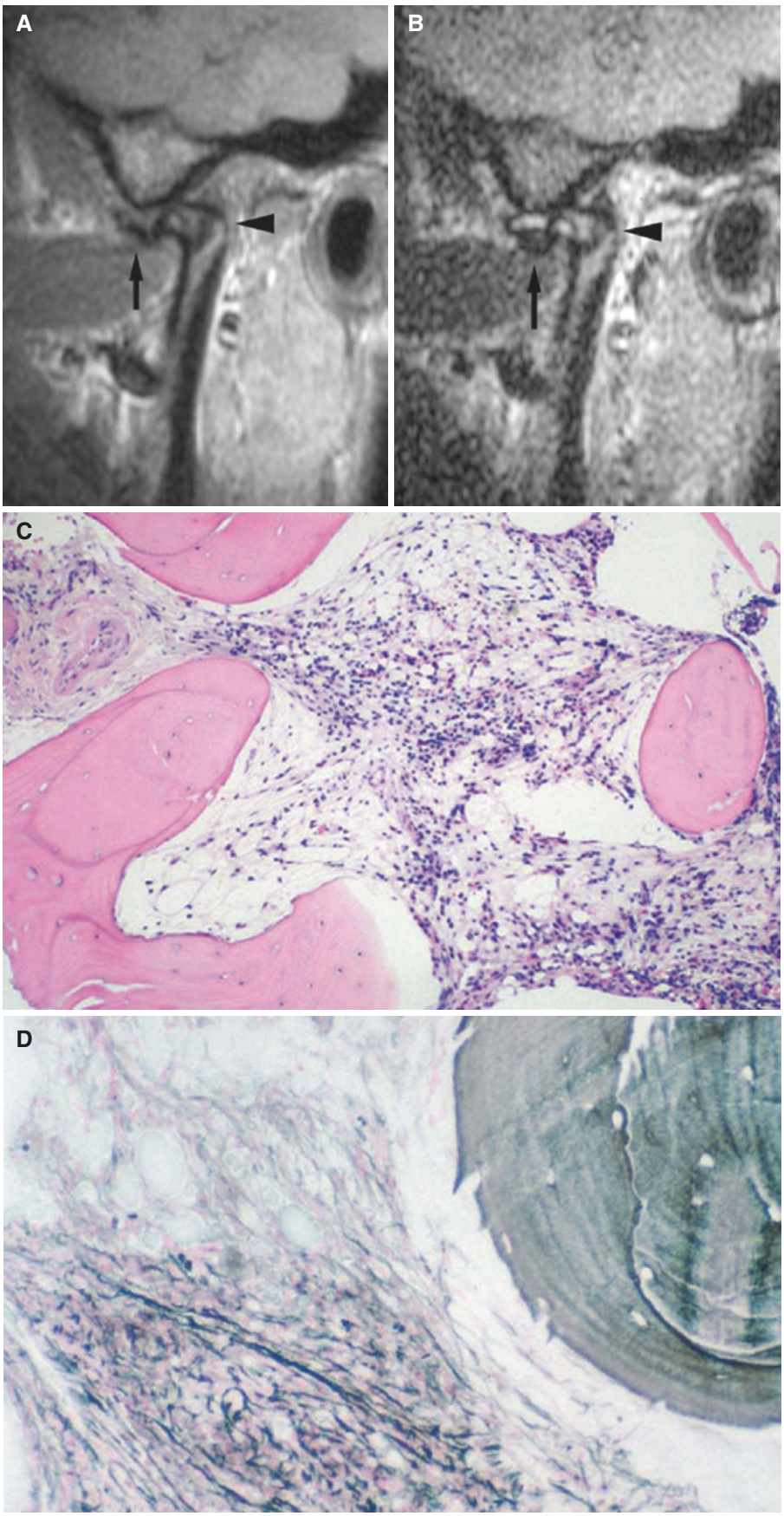

Fig. 6.35 Osteonecrosis (characteristic MRI findings), anterior disc displacement, osteoarthritis. (**A**) Oblique sagittal open-mouth MRI shows anteriorly displaced, deformed disc (*arrow*), condyle osteophyte, and reduced signal in condyle marrow (*arrowhead*), consistent with sclerosis or fibrosis. (**B**) Oblique sagittal open-mouth T2-weighted MRI shows fluid in anterior recess of the upper compartment above the disc (*arrow*) and characteristic MRI findings of osteonecrosis: both increased signal in condyle marrow; marrow edema and reduced signal in condyle marrow; marrow sclerosis or fibrosis (*arrowhead*). (**C**) Histologic section of condyle marrow shows complete loss of hematopoietic marrow, with evidence of inflammatory cell infiltrate (hematoxylin eosin; original magnification × 50). (**D**) Histologic section of condyle marrow shows irreversible changes: marked increase of reticulin fiber deposition (reticulin fiber stain; original magnification × 50). Reproduced with permission from Larheim et al. (1999)

6.5 Arthritides

Figs. 6.36, 6.37, 6.38, 6.39, 6.40, 6.41, 6.42, and 6.43

6.5.1 Definition

Inflammation of the synovial membrane characterized by edema, cellular accumulation, and synovial proliferation (villous formation).

6.5.2 Clinical Features

- A wide range of conditions of which rheumatoid arthritis, followed by ankylosing spondylitis and psoriatic arthropathy, is the most frequent
- Swelling of joint area, not frequently seen in TMJ
- Pain (in active disease) from joints
- Restricted mouth-opening capacity
- Morning stiffness, in particular stiff neck
- Dental occlusion problems; "my bite doesn't fit"
- Anterior bite opening, contact only on molars at closed mouth
- Crepitation due to secondary osteoarthritis
- Symptoms may be similar to those of common TMJ disorders
- Clicking sounds uncommon but may occur in a rheumatic joint

6.5.3 Imaging Features

- Cortical punched-out erosions
- Abnormal disc; flattened, elongated, and perforated
- Disc fragments or completely destroyed disc may be found
- Usually the (abnormal) disc is normally located but may be displaced
- Active disease: marrow edema and/or joint effusion
- Active disease: enhancement of the synovial membrane, pannus after intravenous contrast injection
- Secondary osteoarthritis, usually in long-standing disease
- Fibro-osseous ankylosis may be "end stage" of inflammatory disease
- No principal difference in TMJ imaging signs of rheumatoid arthritis, ankylosing spondylitis, or psoriatic arthropathy

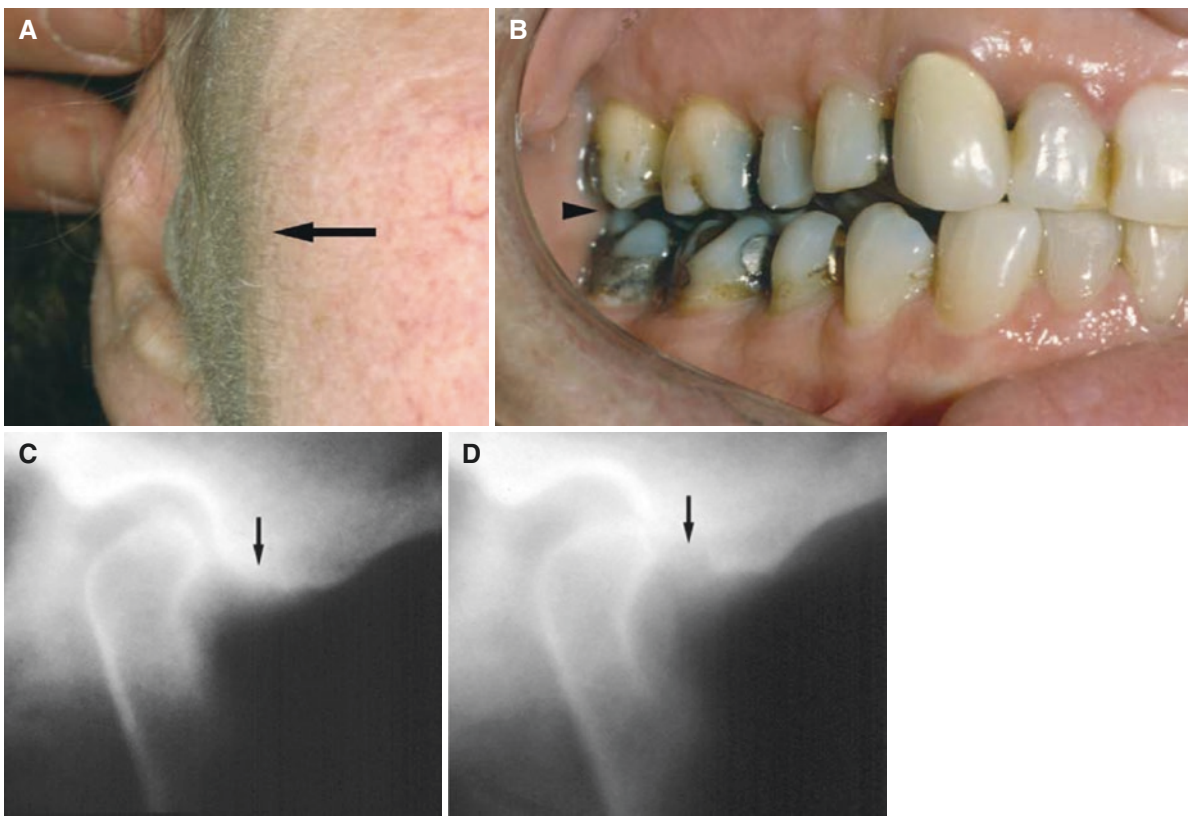

Fig. 6.36 Rheumatoid arthritis. (**A**) Clinical photograph shows swelling over joint area (*arrow*). (**B**) Dental occlusion does not fit properly (*arrowhead*). (**C**) Oblique sagittal conventional tomography 1 year previously showed normal position of the condyle in the fossa and normal bone; note in particular the eminence (*arrow*). (**D**) Corresponding tomography now shows the condyle displaced anteriorly (probably due to joint effusion) and erosion in articular eminence (*arrow*)

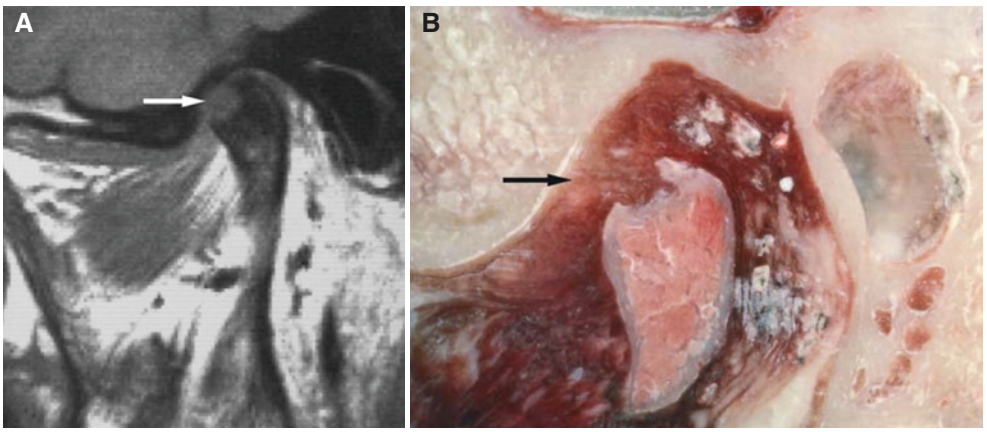

Fig. 6.37 Rheumatoid arthritis. (**A**) Oblique sagittal MRI shows completely destroyed disc (*arrow*) replaced by fibrous or vascular pannus and cortical punched-out erosion with (low-signal) sclerosis (shown by CT) in the condyle. (**B**) Autopsy specimen shows no disc structure but pannus and erosion in the condyle (*arrow*) from the patient with known long-standing rheumatoid arthritis (**B** reproduced with permission from Westesson et al. 2003)

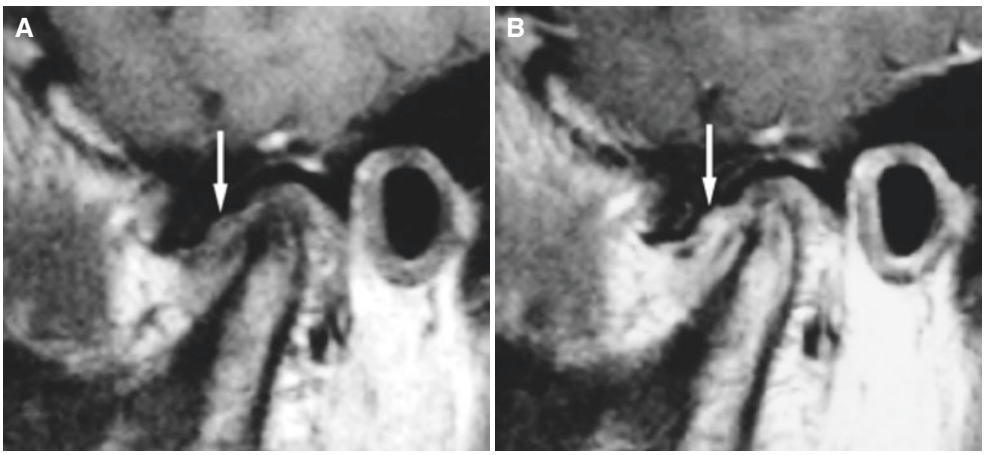

Fig. 6.38 Rheumatoid arthritis. (**A**) Oblique sagittal T1-weighted pre-Gd and (**B**) oblique sagittal T1-weighted post-Gd MRI show contrast enhancement of pannus that has replaced disc structure (*arrow*) and cortical erosions in the condyle and temporal bone. Note contrast enhancement also in the condyle

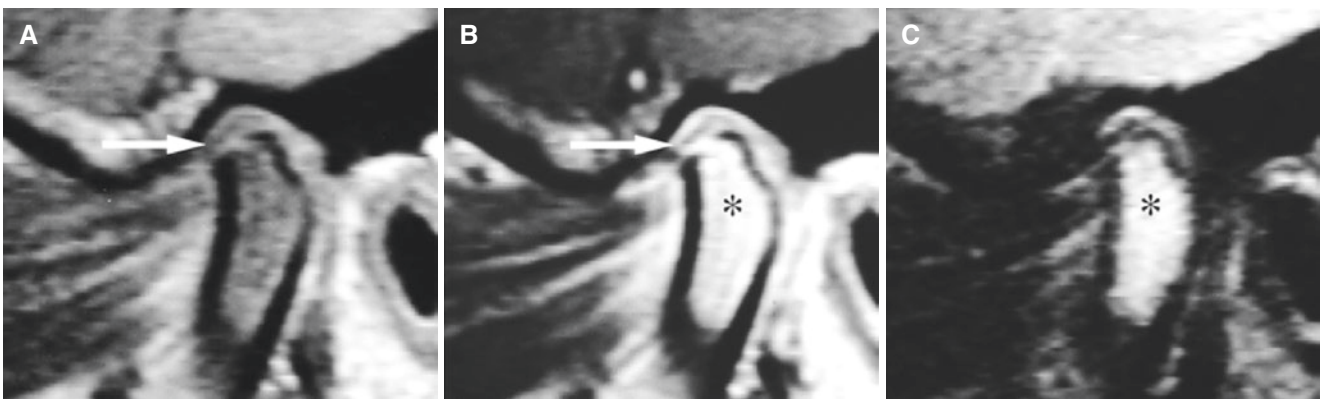

Fig. 6.39 Ankylosing spondylitis. (**A**) Oblique sagittal T1-weighted pre-Gd and (**B**) oblique sagittal T1-weighted post-Gd MRI show cortical erosion; deformed, thin disc in normal position (*arrow*); and contrast enhancement in the upper and lower compartment and in condyle marrow (*asterisk*). (**C**) Oblique sagittal T2-weighted MRI shows bone marrow edema in the entire condyle (*asterisk*)

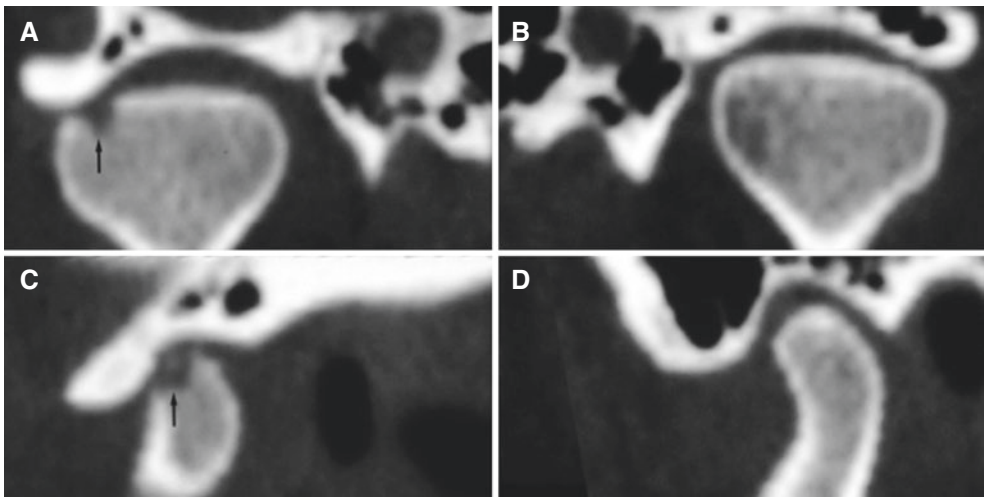

Fig. 6.40 Psoriatic arthropathy. (**A**) Oblique coronal and (**C**) oblique sagittal CT images show punched-out erosion in lateral part of the condyle (*arrow*). (**B**) Oblique coronal and (**D**) oblique sagittal CT images of contralateral joint show normal bone

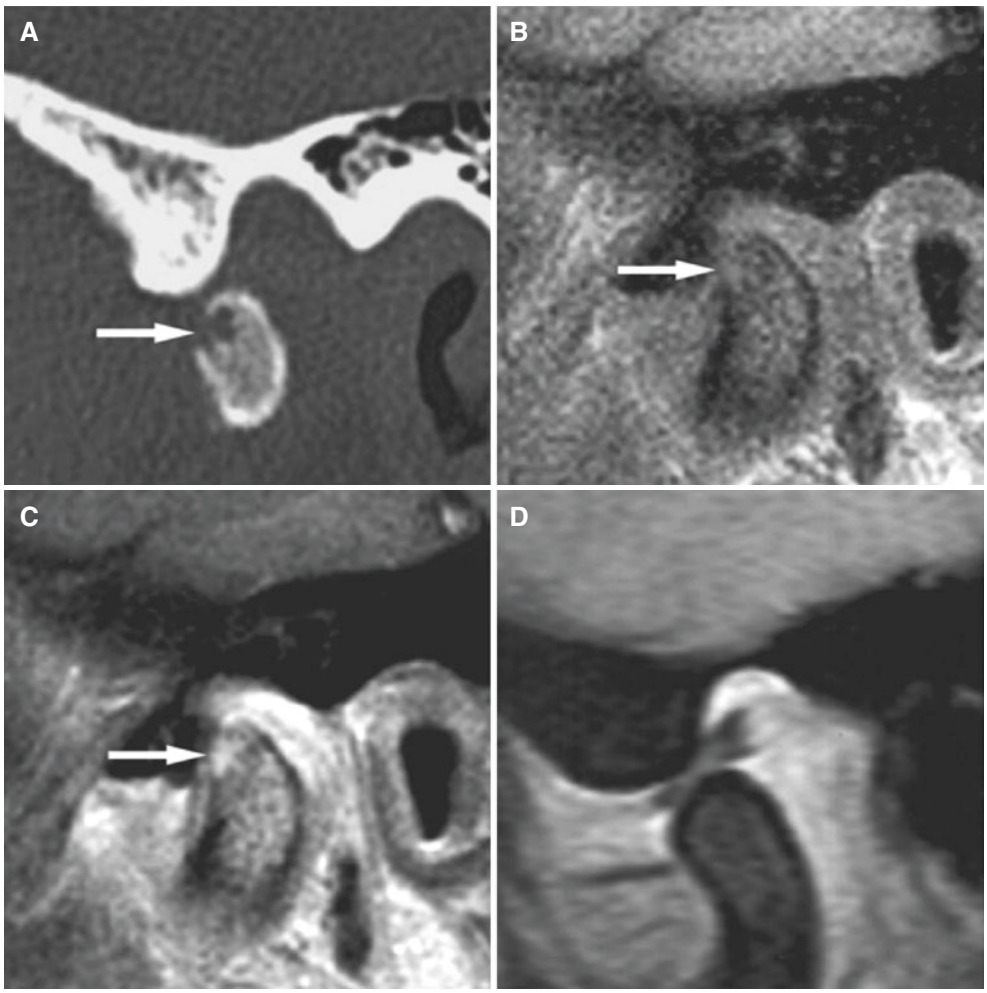

Fig. 6.41 Psoriatic arthropathy (same patient as in Fig. 6.40). (**A**) Direct sagittal CT image shows punched-out erosion (*arrow*). (**B**) Oblique sagittal T1-weighted pre-Gd and (**C**) oblique sagittal T1-weighted post-Gd MRI show contrast enhancement within bone erosion (*arrow*) and in joint space, consistent with thickened synovium/pannus formation. (**D**) Oblique sagittal open-mouth MRI shows reduced condylar translation and normally located disc (bone normal in this section)

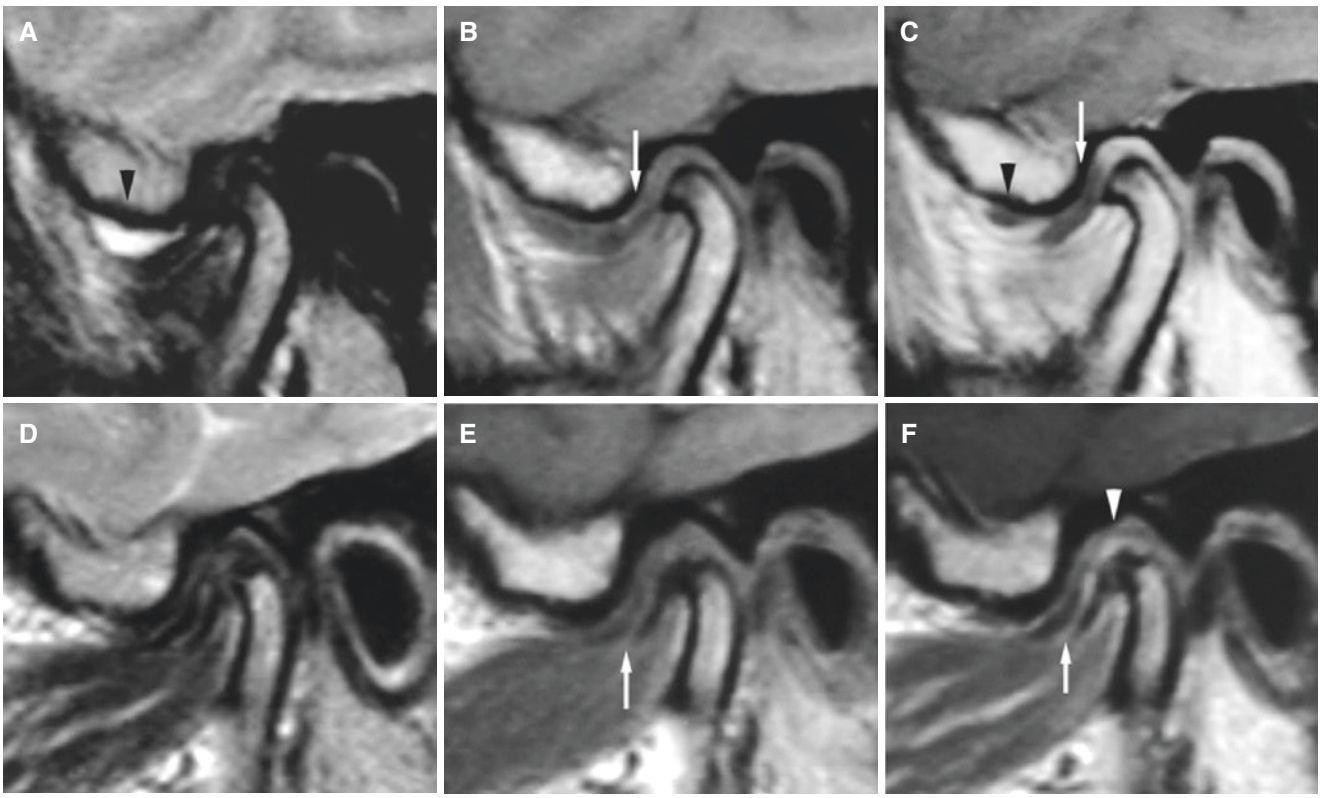

Fig. 6.42 Rheumatoid arthritis, disc displacement of the right (**A**, **B**, **C**) and left (**D**, **E**, **F**) joint. (**A**) Oblique sagittal T2-weighted MRI shows effusion in anterior recess of the upper compartment (*arrowhead*). (**B**) Oblique sagittal T1-weighted pre-Gd and (**C**) oblique sagittal T1-weighted post-Gd MRI show anteriorly displaced disc (*arrow*) and contrast enhancement in peripheral rim of effusion (*arrowhead*) and in posterior attachment, consistent with thickened synovium. Secondary osteoarthritis. (**D**) Oblique sagittal T2-weighted MRI shows no fluid. (**E**) Oblique sagittal T1-weighted pre-Gd and (**F**) oblique sagittal T1-weighted post-Gd MRI show anteriorly displaced disc (*arrow*) and slight contrast enhancement in joint space above the condyle (*arrowhead*), consistent with thickened synovium. Secondary osteoarthritis

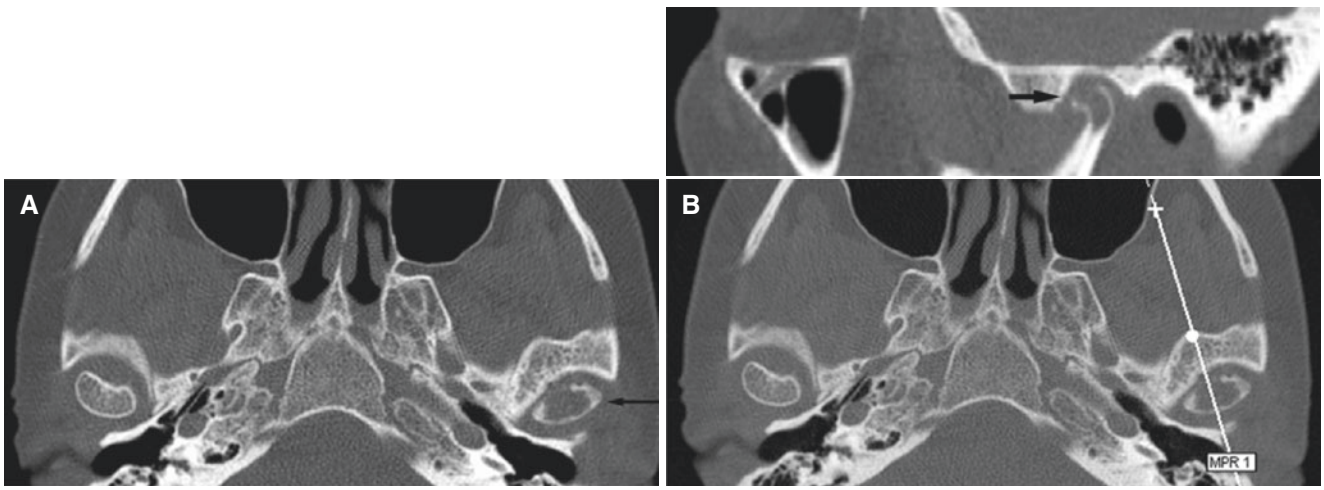

Fig. 6.43 Inflammatory arthritis; patient without known generalized joint disease. (**A**) Axial CT image shows severe destruction in mandibular condyle (*arrow*). (**B**) Oblique sagittal CT image and axial CT image (with *cursor line*) show destruction of the entire condyle (*arrow*). (**C**) Oblique sagittal T1-weighted pre-Gd and (**D**) oblique sagittal T1-weighted post-Gd MRI show contrast enhancement, particularly in the upper compartment and in the condyle (*arrow*), and thin, elongated disc, apparently in normal position. (**E**) Oblique sagittal (post-Gd) open-mouth MRI shows increased signal from condyle marrow (*arrow*) and increased signal from joint space (*small arrowhead*). The disc is anteriorly displaced and deformed (*large arrowhead*). (**F**) Coronal STIR image shows marrow edema or vascular pannus in the condyle and vascular pannus in joint space, particularly in lateral region (*arrow*). Surgery (by Dr. T. Bjørnland, Oslo University Hospital, Rikshospitalet, Oslo, Norway) confirmed severe condyle destruction and inflammatory pannus within and around the condyle, particularly in lateral part of joint (patient was referred for rheumatologic evaluation due to family history of rheumatic disease, but had no symptoms from other joints)

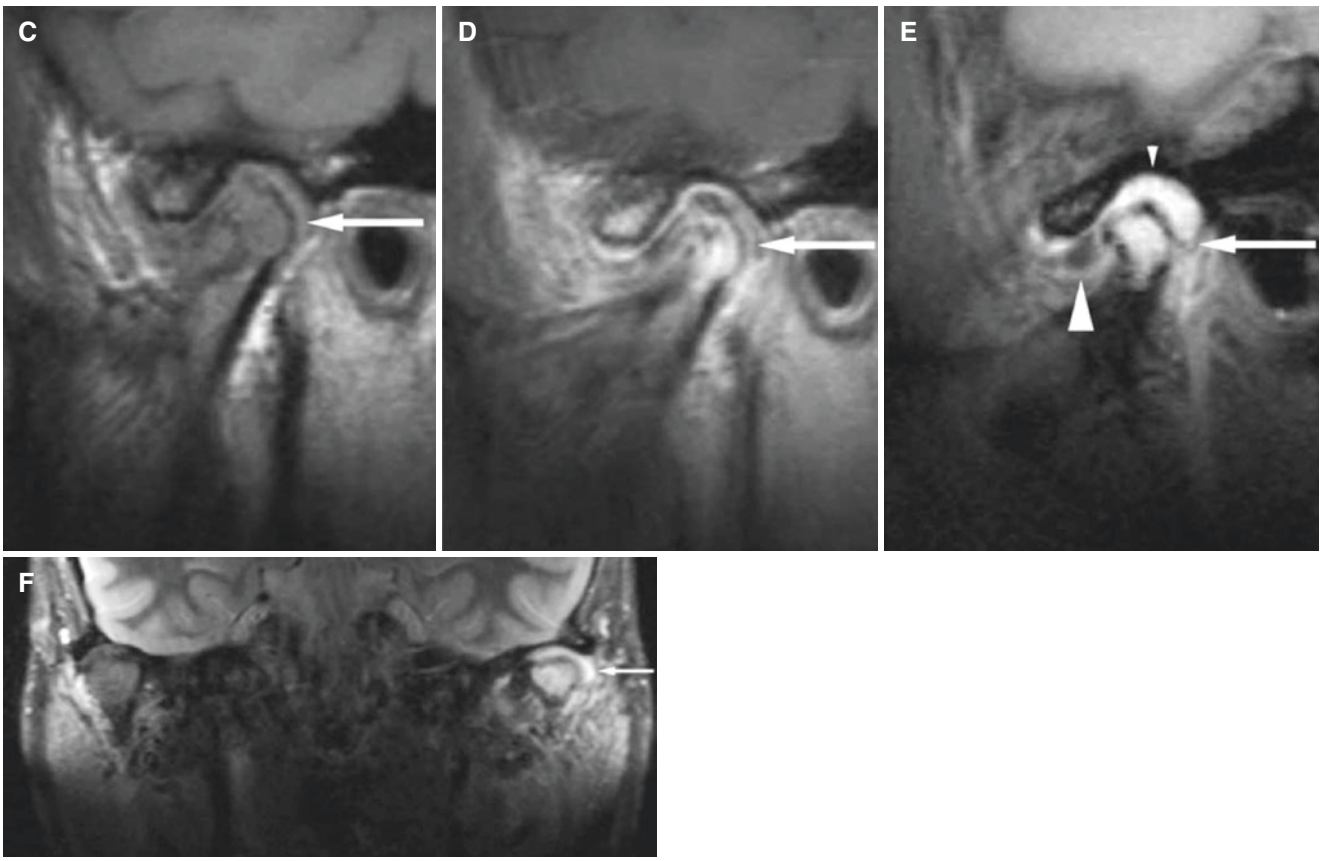

Fig. 6.43 (continued)

6.6 Juvenile Idiopathic Arthritis

Figs. 6.44, 6.45, 6.46, 6.47, 6.48 and 6.49. Figs. 6.50, and 6.51 illustrate juvenile osteoarthritis (arthrosis deformans juvenilis)

6.6.1 Definition

Swelling within a joint, or limitation in the range of joint movement with joint pain or tenderness, which persists for at least 6 weeks, is observed by a physician and is not due to primarily mechanical disorders or to other identifiable causes (Petty et al. 2004).

6.6.2 Clinical Features

- Juvenile arthritis differs in many respects from rheumatoid arthritis in adults
- Heterogeneous disease with different subgroup classifications
- Rheumatoid factor seropositivity not common
- Two peaks of onset, between 1 and 3 years of age and around 9 years of age
- More girls than boys
- Large joints (knees, wrists, and ankles) more prominently involved than small peripheral joints
- Bony ankylosis in cervical spine characteristic
- Underdeveloped mandible, micrognathia, characteristic
- Restricted mouth-opening capacity
- Pain from TMJs not so common

6.6.3 Imaging Features

- Bony joint components abnormal, frequently without cortical erosions
- Flat fossa, underdeveloped eminence
- Condyle deformed: short, thick, flat, bifid
- Condyle located anteriorly in fossa at closed mouth
- Restricted condylar translation at opened mouth
- Soft-tissue abnormalities: flat, thin, elongated, or destroyed disc
- Active disease: bone marrow edema and/or joint effusion
- Active disease: enhancement of the synovial membrane, pannus after intravenous contrast injection
- Secondary remodeling, osteoarthritis

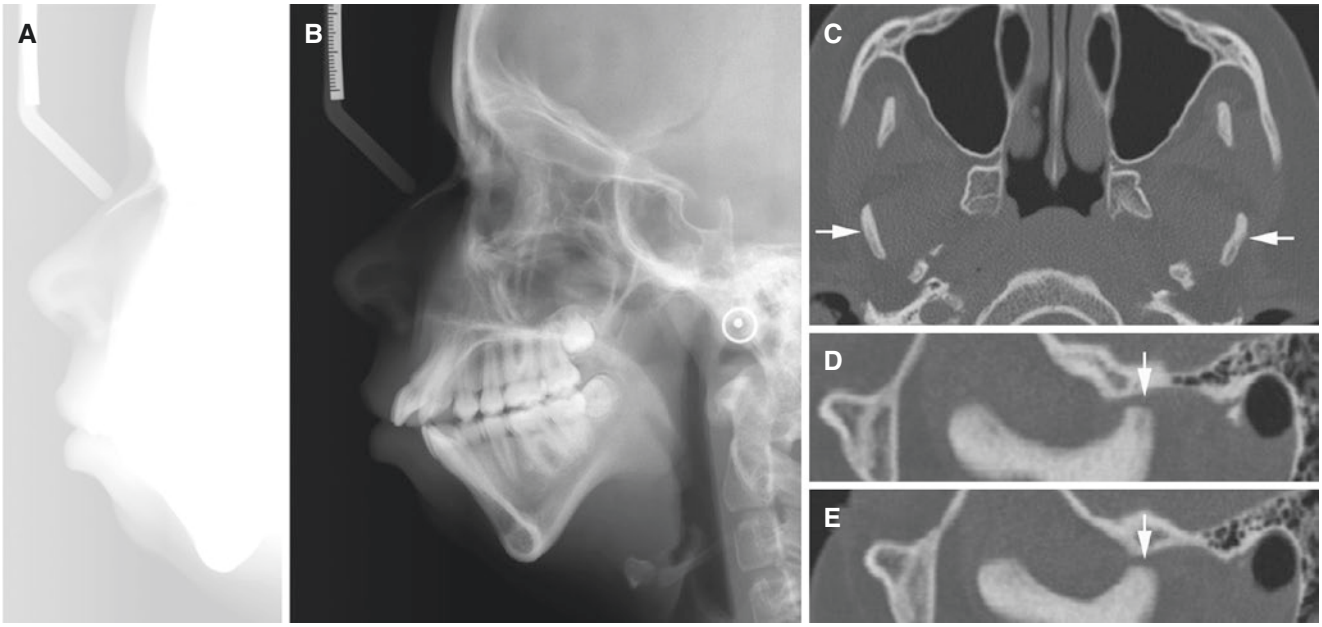

Fig. 6.44 Juvenile idiopathic arthritis, micrognathia; 13-year-old female. (**A**) Lateral view, soft-tissue profile, and (**B**) lateral view, bone profile, show micrognathia (retruded chin). (**C**) Axial CT image shows abnormal long axis angulation of both condyles (*arrows*) and very thin condyles. (**D**, **E**) Oblique sagittal CT images of right (**D**) and left (**E**) joints show almost flat eminence and rudimentary condyle (*arrow*) anteriorly located in fossa, almost at apex of eminence, in closed-mouth images (these could be mistaken for open-mouth images)

Fig. 6.45 Juvenile idiopathic arthritis, facial asymmetry; 17-year-old female. (**A**) Panoramic view shows jaw asymmetry; underdevelopment of the right side with antegonial notching (*arrowhead*) and small, flattened condyle (*arrow*). (**B**) Lateral view, soft-tissue profile, and (**C**) lateral view, bone profile, show rather normal profile despite evidently asymmetric mandible. (**D**) Axial CT image shows very thin right condyle with abnormal angulation of long axis (*arrow*) (similar to Fig. 6.44C) and normal left condyle. (**E**) Oblique sagittal CT image of the right joint shows almost flat fossa/eminence and hypoplastic condyle (*arrow*). (**F**) Oblique sagittal CT image of normal left joint

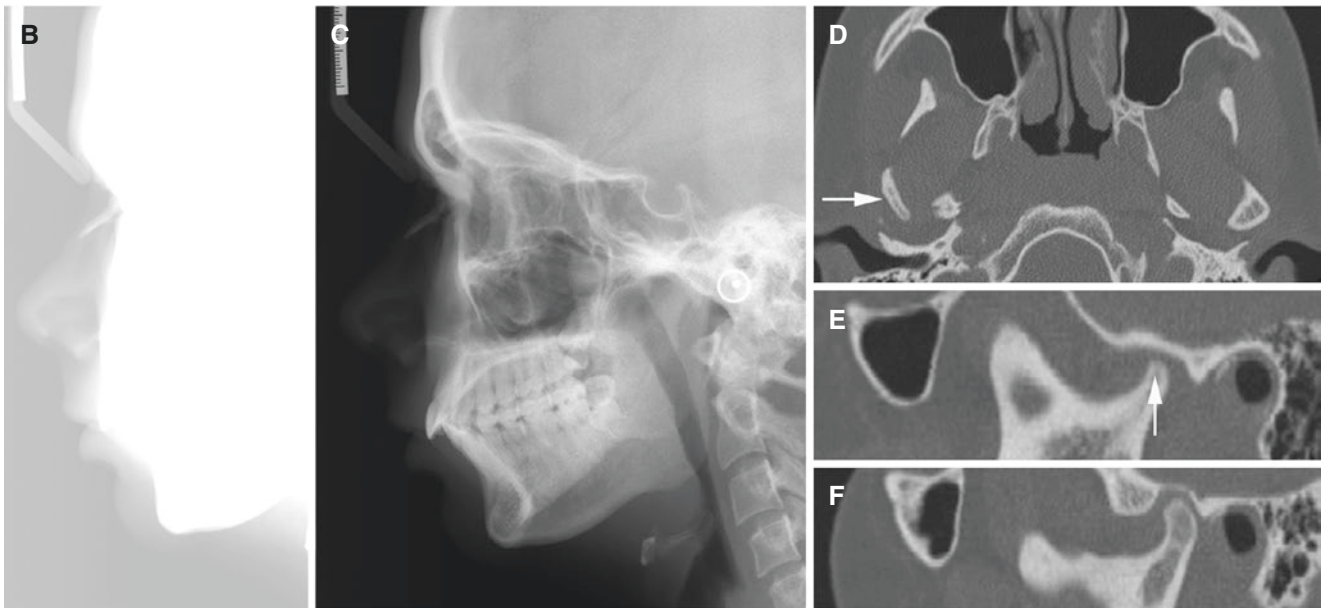

Fig. 6.45 (continued)

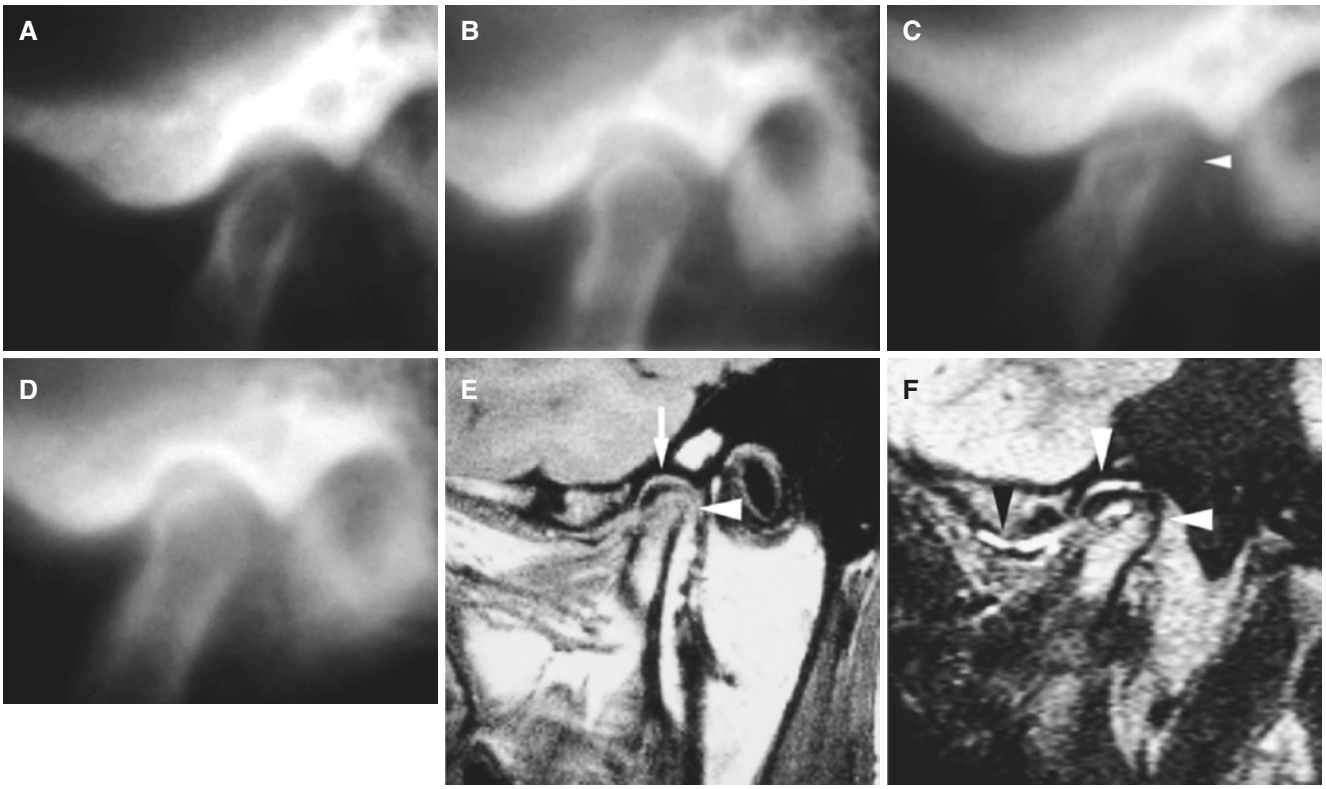

Fig. 6.46 Juvenile idiopathic arthritis; 14-year-old female. Conventional tomography at baseline (**A**, **B**) and at 4-month follow-up (**C**, **D**), with supplementary MRI at follow-up (**E**, **F**). (**A**, **C**) Oblique sagittal tomography shows flattening/resorption of the condyle (*arrowhead*) during the 4-month period (with high disease activity) compared to normal contralateral joint (**B**, **D**). (**E**) Oblique sagittal T1-weighted MRI shows normally positioned disc (*arrow*), elongated and with central perforation; flat, deformed condyle with lack of cortical outline; and reduced signal from condyle marrow (*arrowhead*). (**F**) Oblique sagittal T2-weighted MRI shows extensive effusion in the upper and lower compartments (*vertical arrowheads*) and bone marrow edema in the condyle (*horizontal arrowhead*)

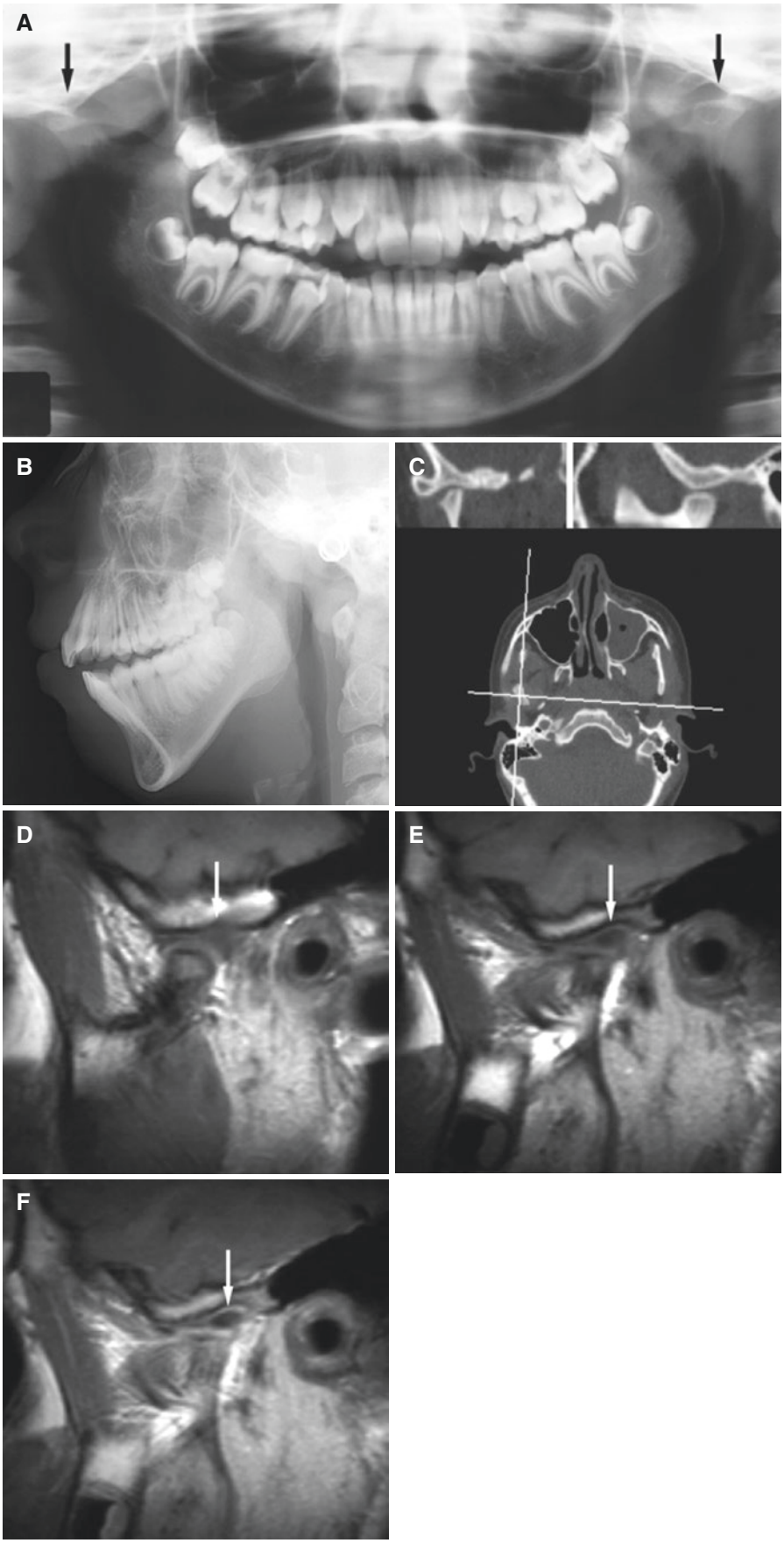

Fig. 6.47 Juvenile idiopathic arthritis; 12-year-old female with no history of generalized joint disease. (**A**) Panoramic view shows flattened condyles bilaterally (*arrows*). (**B**) Lateral view shows anterior bite opening at orthodontic consultation. (**C**) Oblique coronal and oblique sagittal CT images of the right joint (similar changes in the left joint) show deformed condyle (flat, short, and small in mediolateral direction) (*left image*) and condyle located at eminence at closed mouth, with abnormal flat fossa (*right image*). Axial CT image with *cursor lines* shows abnormal angulation of condylar long axis, which may partially explain the small condylar mediolateral dimension. (**D**, **E**) Oblique sagittal T1-weighted pre-Gd and (**F**) oblique sagittal T1-weighted post-Gd MRI of the left joint (similar changes in the right joint) show normally positioned disc (*arrow*) and contrast enhancement around the disc in the upper and lower joint compartment, consistent with thickened synovium. The patient was then referred for rheumatologic examination which confirmed diagnosis of generalized juvenile idiopathic arthritis

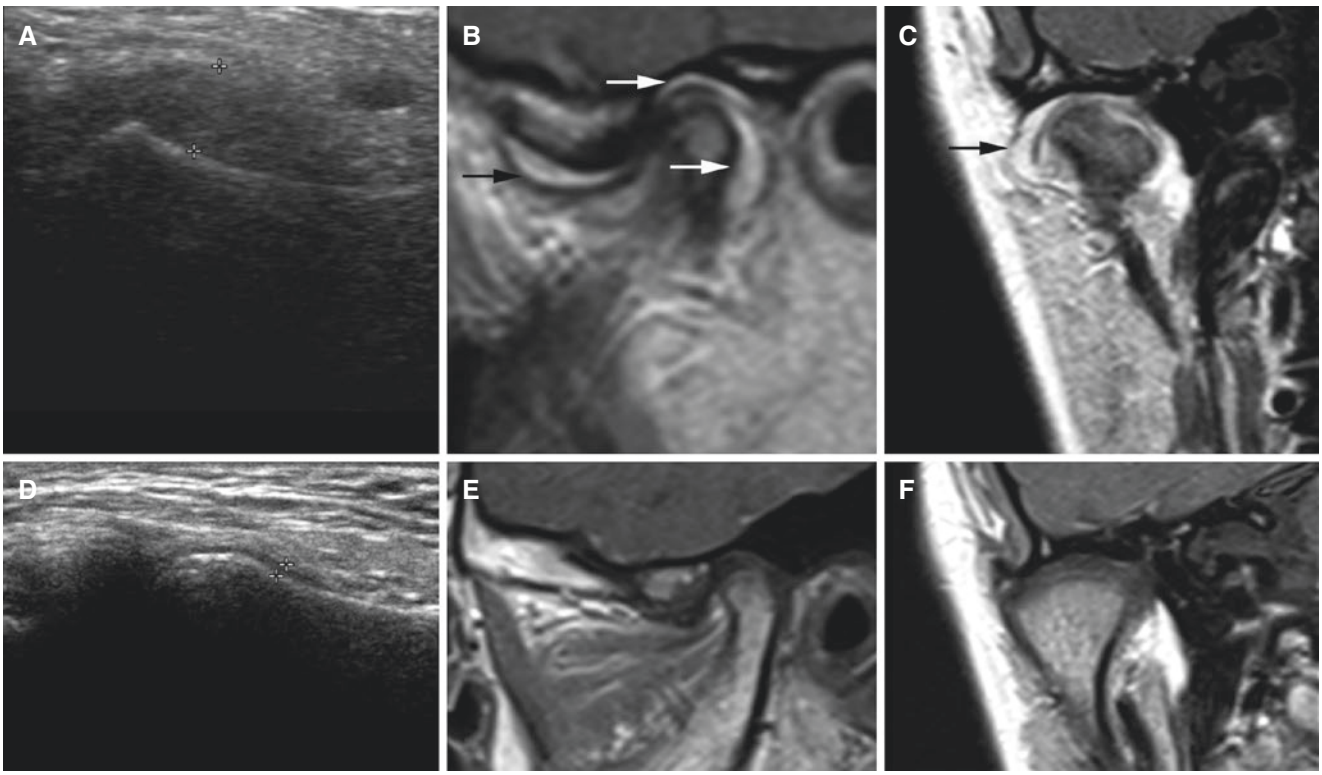

Fig. 6.48 Juvenile idiopathic arthritis; 17-year-old female with contrast enhancement (synovitis) (**A**–**C**) and 10-year-old female without contrast enhancement (**D**–**F**). (**A**) Ultrasonography shows increased capsule width (distance measured to 4.3 mm). (**B**) Oblique sagittal and (**C**) oblique coronal T1-weighted post-Gd MRI show extensive contrast enhancement (synovitis) (*arrows*) (**A**, **B**, **C** reproduced with permission from Kirkhus et al. 2016a). (**D**) Ultrasonography shows normal capsule width (distance measured to 0.6 mm). (**E**) Oblique sagittal and (**F**) oblique coronal T1-weighted post-Gd MRI show no contrast enhancement (no synovitis)

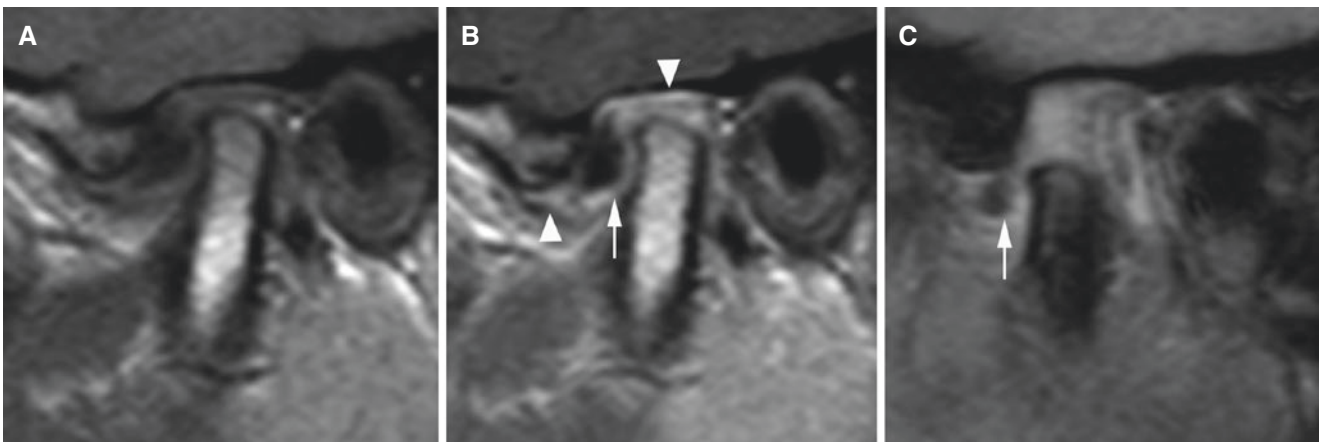

Fig. 6.49 Juvenile idiopathic arthritis and disc displacement; 15-year-old female with contrast enhancement (synovitis). (**A**) Oblique sagittal T1-weighted pre-Gd and (**B**) oblique sagittal T1-weighted post-Gd MRI show contrast enhancement in the upper and lower joint compartments (*arrowheads*) and anteriorly displaced disc (*arrow*). (**C**) Oblique sagittal open-mouth MRI shows anteriorly displaced disc (*arrow*) and reduced condylar translation (reproduced with permission from Kirkhus et al. 2016b)

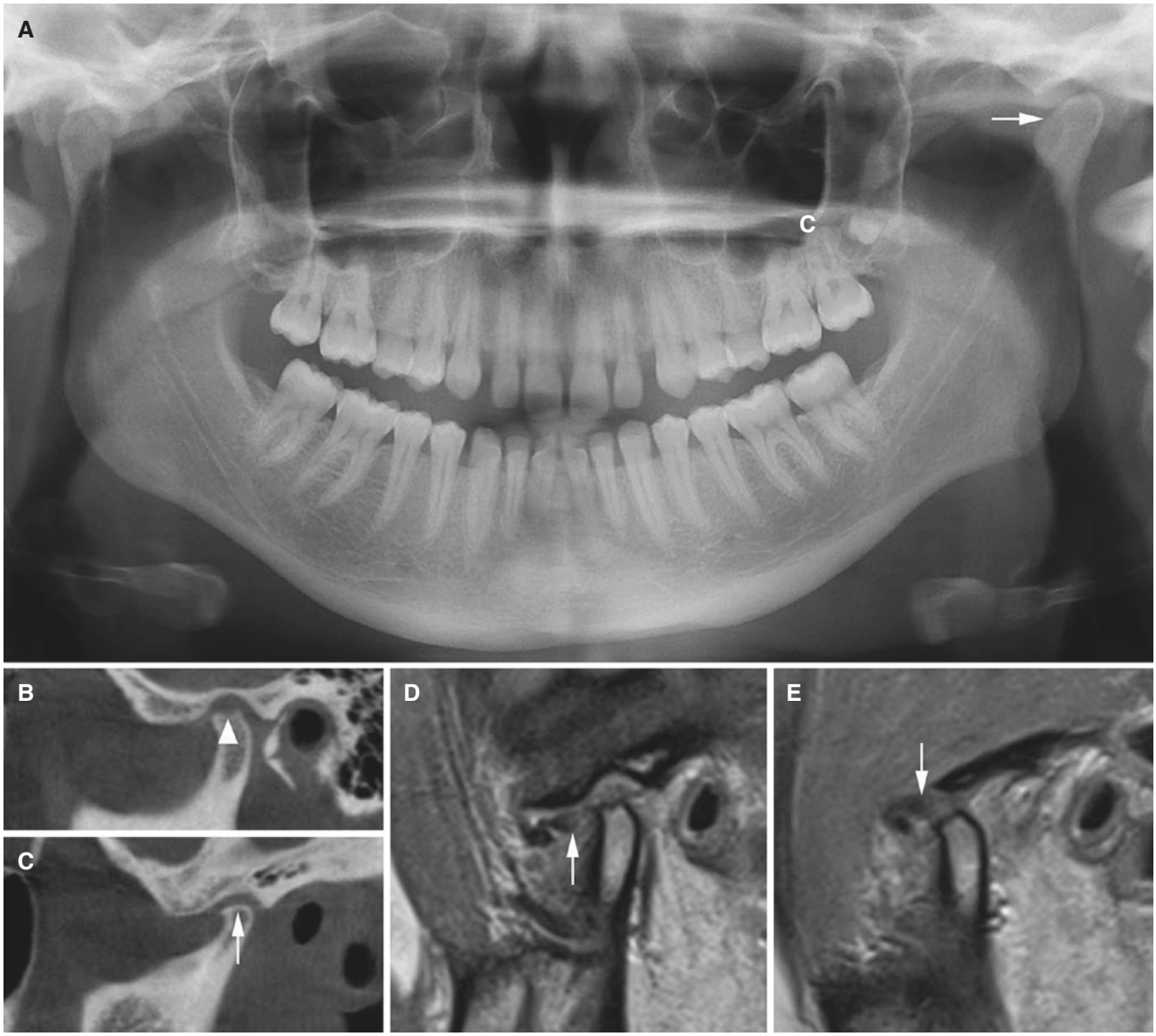

Fig. 6.50 Juvenile osteoarthritis; 18-year-old female. (**A**) Panoramic view shows jaw asymmetry with flattened left condyle (*arrow*). (**B**) Oblique sagittal CT image of the right joint shows condylar erosion (*arrowhead*). (**C**) Oblique sagittal CT image of the left joint shows hypoplastic and flattened condyle with osteophyte (*arrow*). (**D**) Closed-mouth and (**E**) open-mouth oblique sagittal PD-weighted MRI of the right joint show anteriorly displaced disc (*arrow*). Similar disc abnormalities seen in the left joint (not shown)

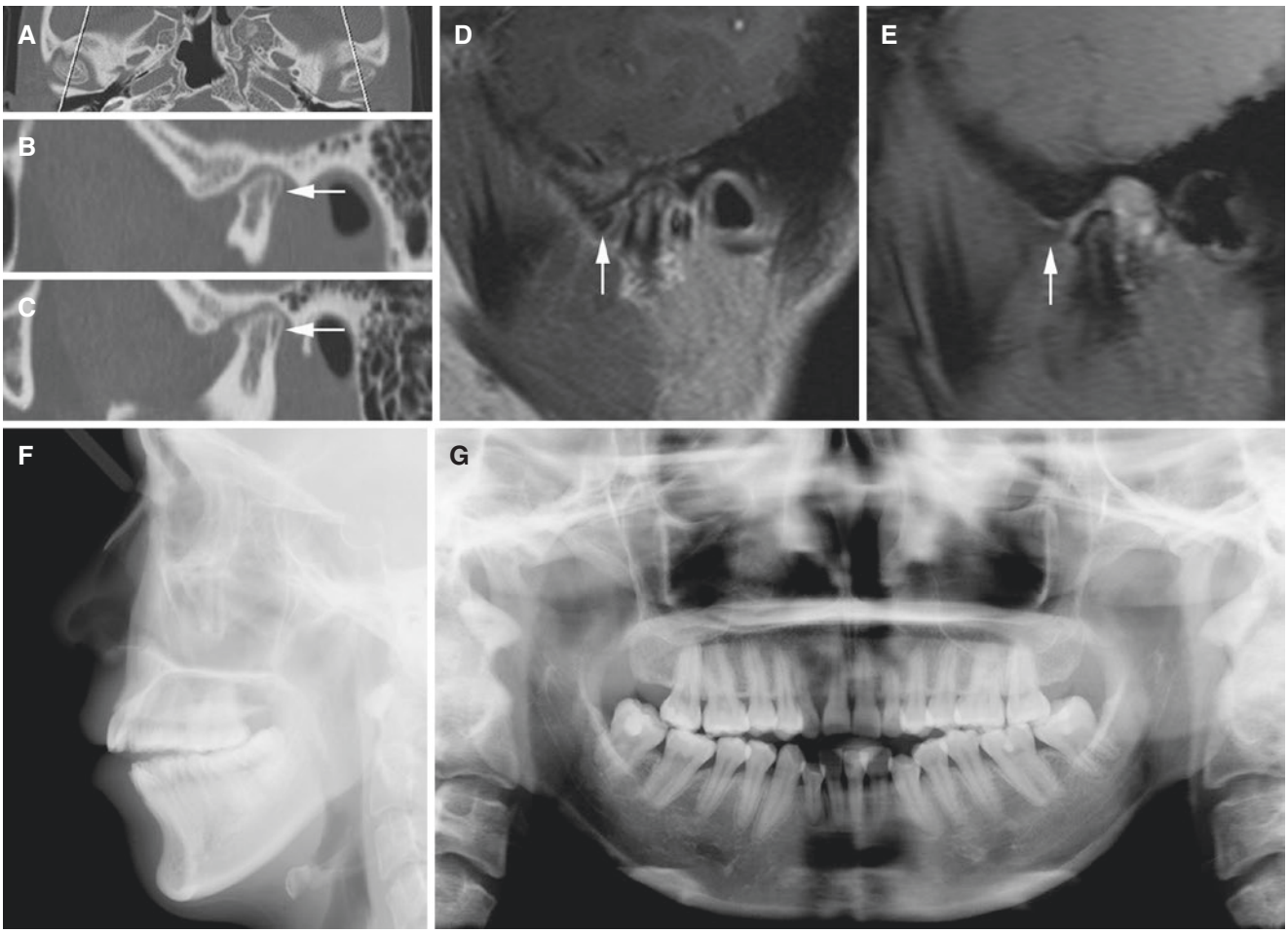

Fig. 6.51 Juvenile osteoarthritis; 21-year-old female with long history of discomfort with dental occlusion (open bite). (**A**) Axial CT (with *cursor lines*), (**B**) oblique sagittal CT of the left joint, and (**C**) oblique sagittal CT of the right joint show remodeled condyles (flattened with posterior bone apposition) (*arrow*). (**D**) Oblique sagittal closed-mouth T1-weigted post-Gd MRI and (**E**) oblique sagittal open-mouth MRI of the left joint show anteriorly displaced disc (*arrow*). Similar finding seen in the right joint (not shown). At 2-year follow-up, (**F**) lateral view shows open bite, and (**G**) panoramic view shows flattened condyles. Orthognathic surgery was then performed

6.7 Ankyloses

Figs. 6.52, 6.53, 6.54, 6.55, and 6.56

6.7.1 Definition

Fibrous or bony union between joint components.

6.7.2 Clinical Features

- Severely limited mouth-opening capacity, gradually
- Usually no pain
- No joint sounds
- Secondary to arthritides, in particularly ankylosis spondylitis
- Secondary to trauma, fracture
- Idiopathic

6.7.3 Imaging Features

- Fibrous ankylosis; joint space visible
- Bony ankylosis; no joint space (at least in parts of the joint) visible
- Joint space better seen on CT than on MRI
- No clear definition of any joint structures
- No joint effusion or contrast enhancement
- No or very limited condylar translation at (very) restricted mouth-opening capacity

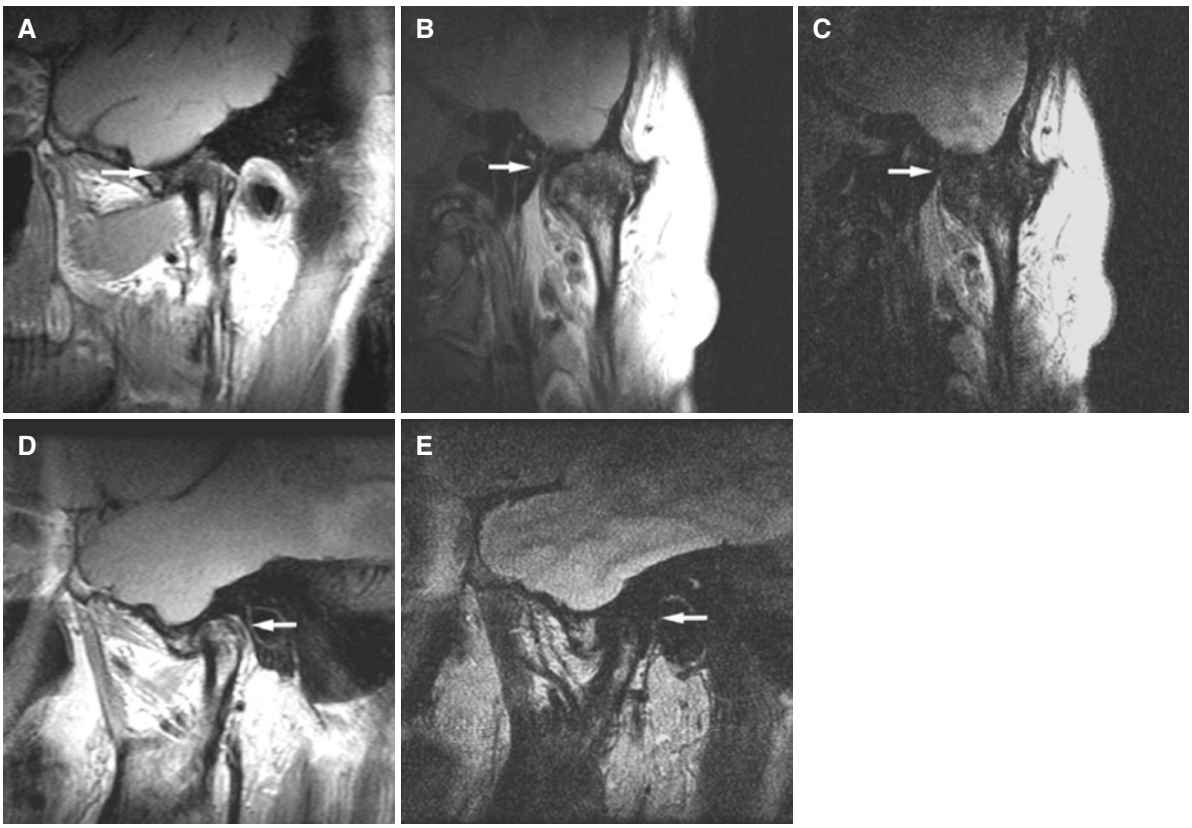

Fig. 6.52 Ankylosis of the right (**A**, **B**, **C**) and left (**D**, **E**) joints. (**A**) Oblique sagittal T1-weighted MRI shows no delineation of the disc, fossa, or condyle (*arrow*). (**B**) Oblique coronal T1-weighted MRI confirms loss of structures (*arrow*). (**C**) Oblique coronal T2-weighted MRI shows no structures or effusion (*arrow*). (**D**) Oblique sagittal T1-weighted MRI shows poor delineation of structures (*arrow*). (**E**) Oblique sagittal T2-weighted MRI shows no structures or effusion (*arrow*). Condylar translation is absent in open-mouth images (**A**, **D**). Fibrous or osseous union cannot be determined

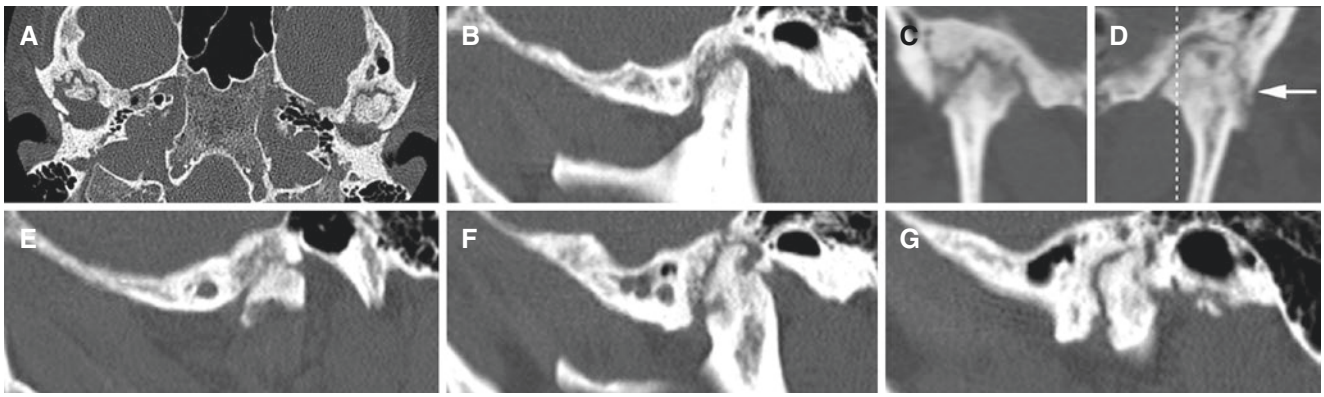

Fig. 6.53 Fibro-osseous ankylosis; 53-year-old male with psoriatic arthritis. (**A**) Axial CT image, (**B**) oblique sagittal CT image of the right joint, (**C**) oblique coronal CT image of the right joint, and (**D**) oblique coronal CT image of the left joint show irregularities of joint surfaces in both joints but somewhat more evident joint space in the right joint than in the left joint (*arrow*). (**E**, **F**, **G**) Oblique sagittal CT images of lateral, central, and medial parts of the left joint show irregular articular surfaces of the condyle and temporal bone with no evident joint space in some places

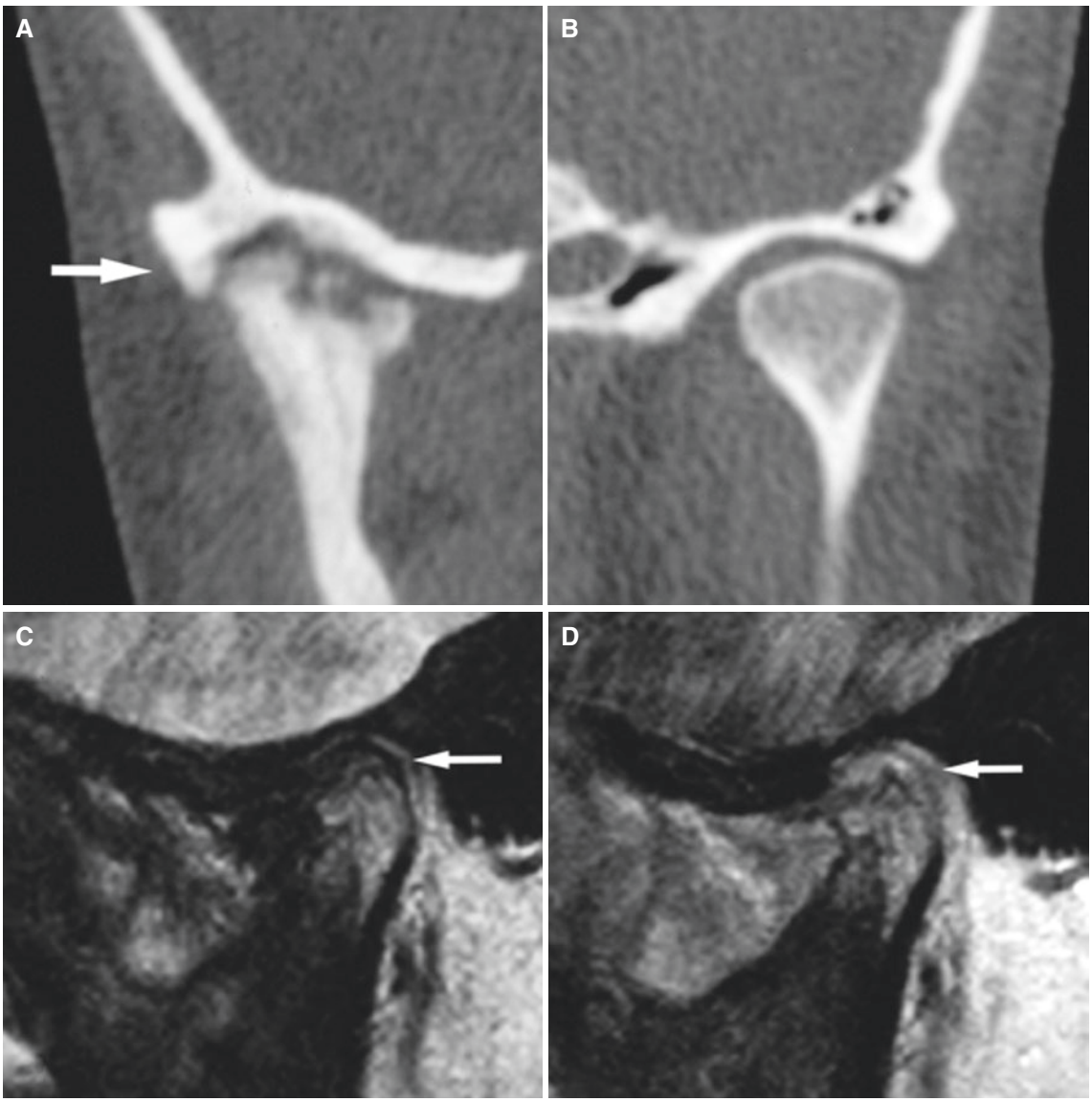

Fig. 6.54 Fibrous ankylosis. (**A**) Oblique coronal CT image shows severe cortical irregularities, particularly in mandibular condyle, but evident joint space through the entire joint (*arrow*). Oblique coronal CT of normal contralateral joint for comparison. (**B**) Oblique sagittal T2-weighted MRI shows no joint structures or effusion (*arrow*). (**C**) Oblique sagittal T1-weighted post-Gd MRI shows no contrast enhancement (*arrow*)

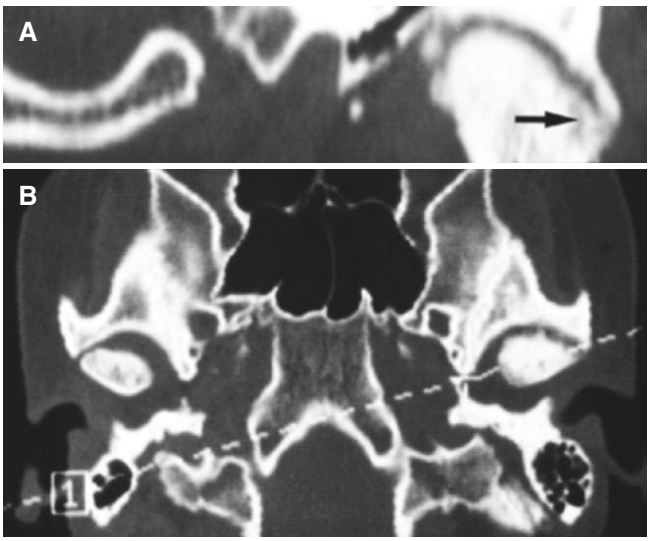

Fig. 6.55 Bony ankylosis; patient with ankylosing spondylitis. Oblique coronal CT image shows bony union in lateral part of the joint (*arrow*). Axial CT shows *cursor line* for coronal image

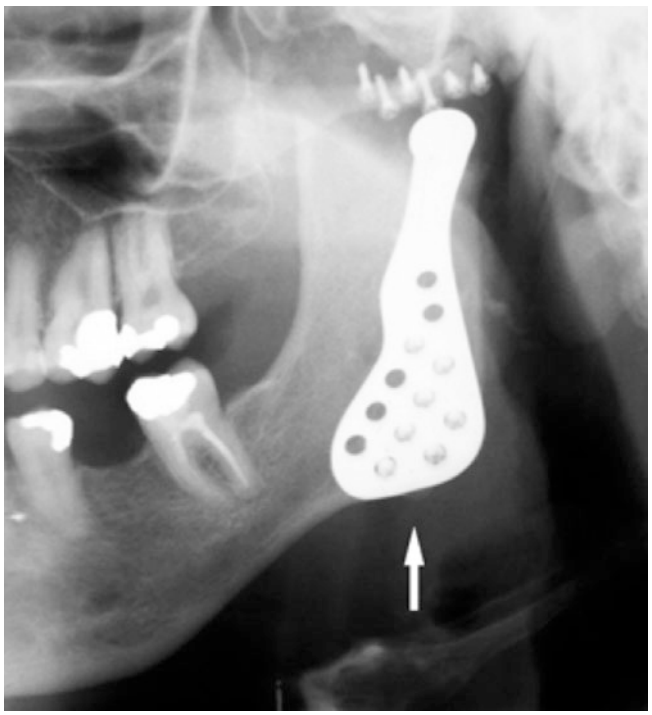

Fig. 6.56 Ankylosis treated with total joint prosthesis (Lorenz). Panoramic view shows prosthesis (*arrow*), consisting of artificial fossa (fixed with six titanium screws in temporal bone) and artificial condylar process (fixed with seven titanium screws to mandibular ramus) (courtesy of Dr. G. Støre, Oslo University Hospital, Rikshospitalet, Oslo, Norway)

6.8 Condylar Growth Disturbances (Anomalies)

Figs. 6.57, 6.58, 6.59, 6.60, 6.61, and 6.62

6.8.1 Definition

Abnormal growth of mandibular condyle; overgrowth, undergrowth, or bifid appearance.

6.8.2 Clinical Features

- Facial (mandibular) asymmetry
- Mandibular overgrowth
- Mandibular undergrowth

6.8.3 Imaging Features

- Unilateral hyperplastic condyle
- Usually not enlarged in mediolateral direction
- Normal bone structure
- Normal disc position
- Hypoplastic condyle, unilaterally or bilaterally
- Normal disc position or anterior disc displacement
- Condyle remodeling (flattened, deformed)
- Arthrosis deformans juvenilis (juvenile osteoarthritis), see figs. 6.50 and 6.51
- Bifid or split condyle

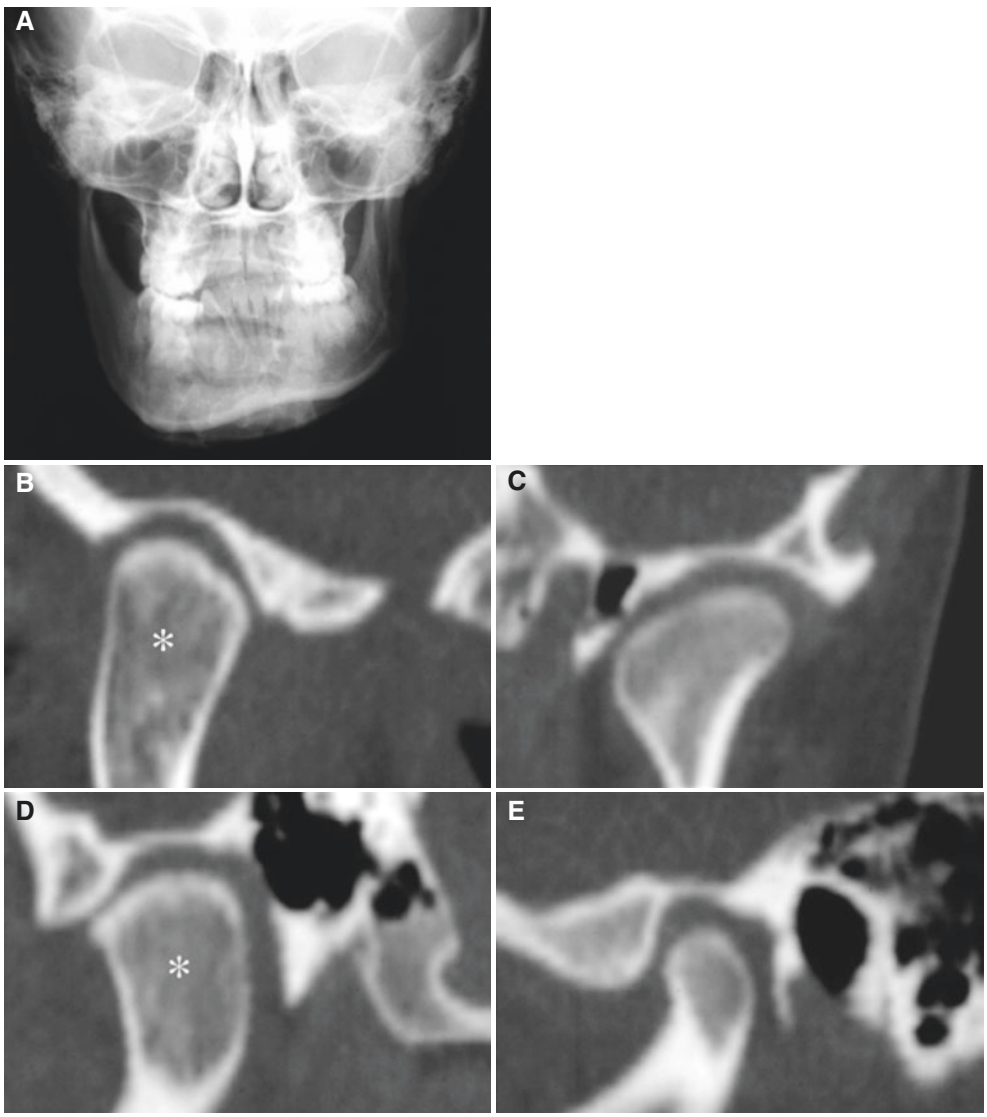

Fig. 6.57 Condylar hyperplasia and facial asymmetry; 23-year-old female. (**A**) Facial (*front*) view shows jaw asymmetry due to unilateral mandibular overgrowth (*right side*). (**B**) Oblique coronal and (**D**) oblique sagittal CT images show mandibular condyle (*asterisk*) with abnormal shape and size, enlarged but not in mediolateral dimension, and widened fossa in anteroposterior dimension. (**C**) Oblique coronal and (**E**) oblique sagittal CT images show normal contralateral joint. Panoramic view of this patient is shown in Fig. 9.6

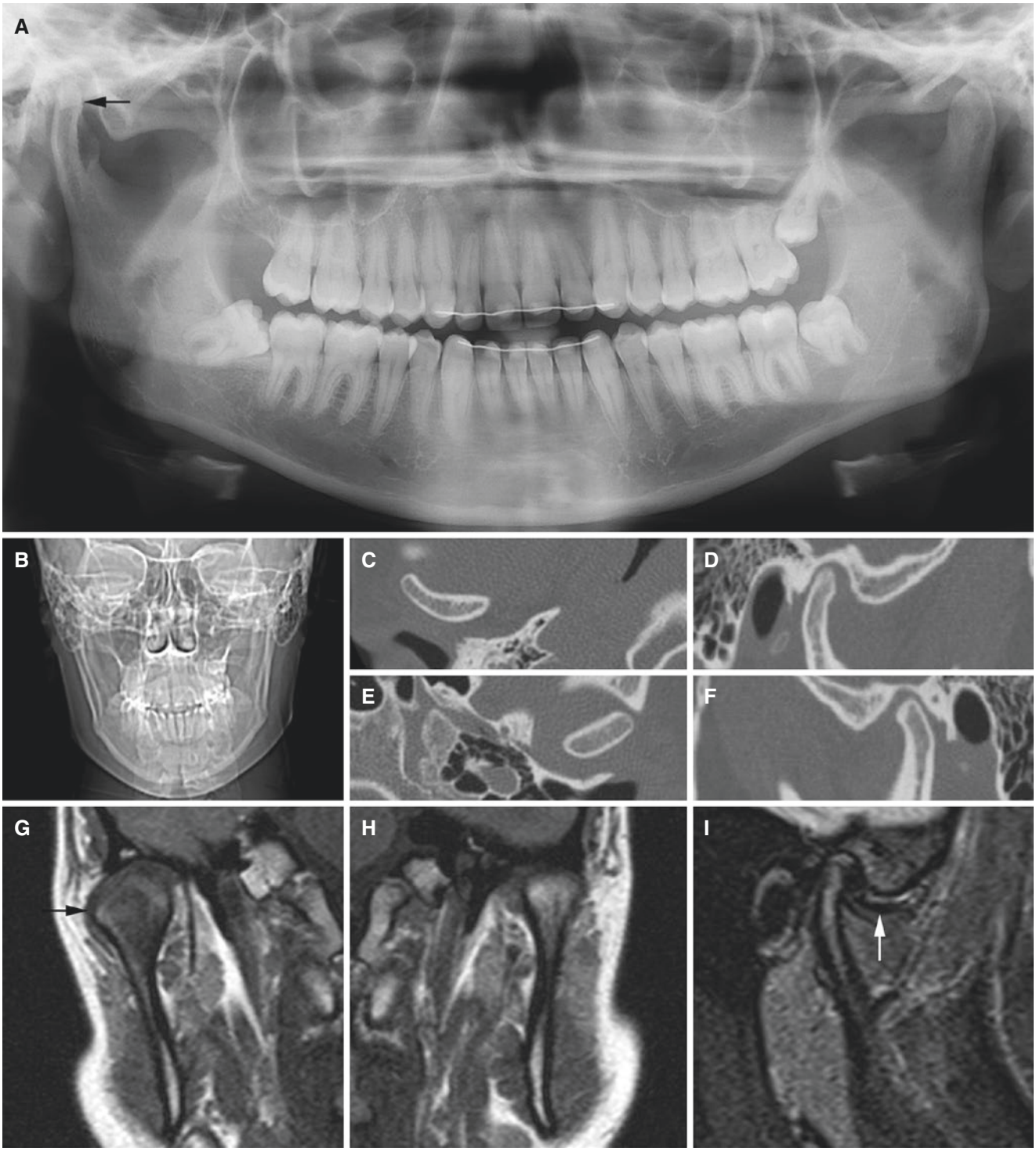

Fig. 6.58 Condylar hyperplasia; 22-year-old female. (**A**) Panoramic view shows hyperplastic right condyle (*arrow*). (**B**) Facial (*front*) view shows facial asymmetry with more growth on the right side. (**C**) Axial and (**D**) oblique sagittal CT images of the right joint and (**E**) axial and (**F**) oblique sagittal CT images of the left joint show right-sided condylar hyperplasia. (**G**) Oblique coronal T1-weighted MRI of the right joint and (**H**) oblique coronal T1-weighted MRI of the left joint confirm right-sided condylar hyperplasia (*arrow*). (**I**) Oblique sagittal MRI of the right joint shows anteriorly displaced disc (*arrow*)

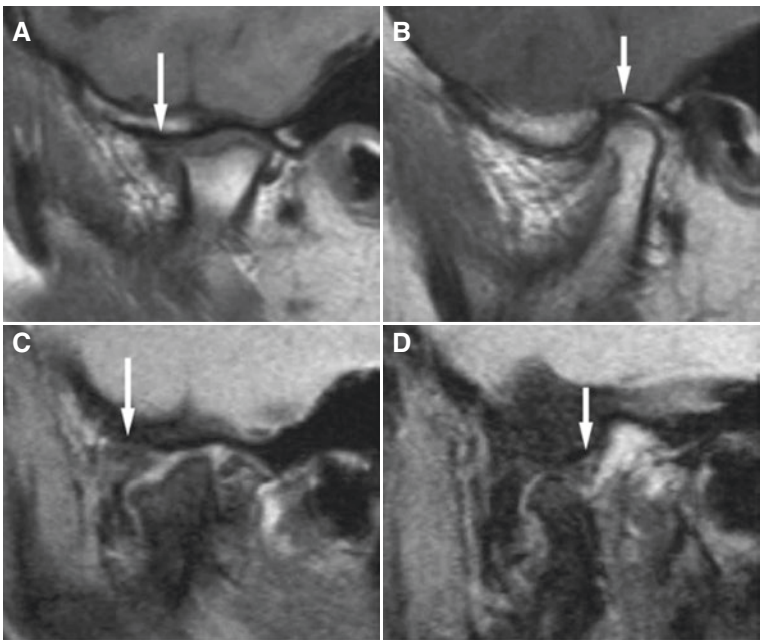

Fig. 6.59 Condylar hypoplasia and facial asymmetry (underdeveloped right side) of a 12-year-old female with 4-year history of trauma, but no confirmed fracture. (**A**, **C**) Oblique sagittal MRI shows abnormal right joint with displaced disc (*arrow*), also in open-mouth image (**C**). Condyle is deformed, flat, and enlarged in anteroposterior direction, and fossa is flattened. (**B**, **D**) Oblique sagittal MRI of the left joint shows normal bone and normal disc position (*arrow*), also in open-mouth image (**D**). Same patient is also shown in Fig. 8.22

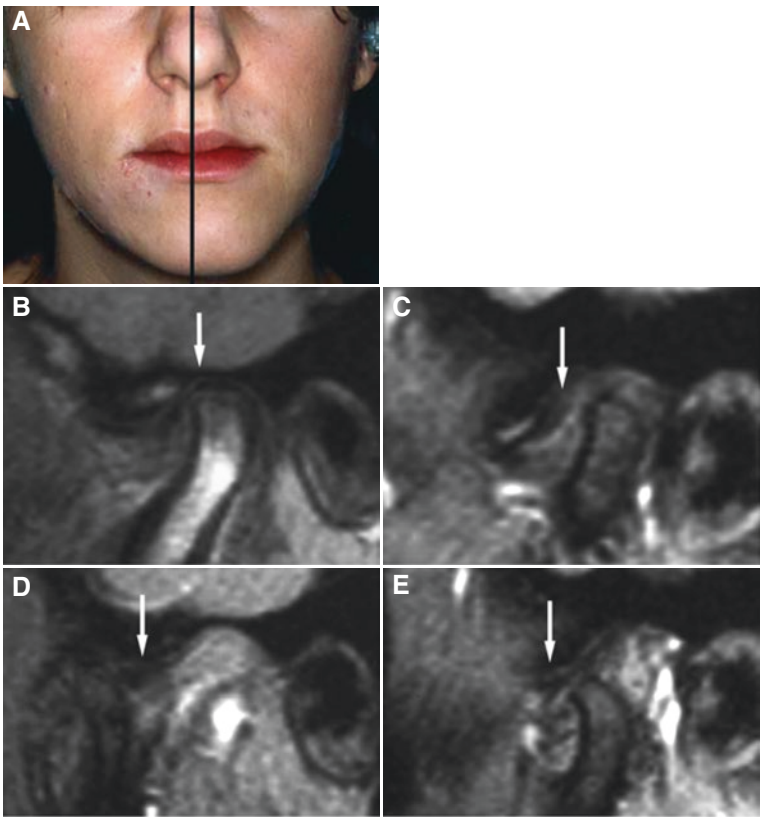

Fig. 6.60 Condylar hypoplasia and facial asymmetry without history of trauma. (**A**) Clinical photograph shows mandible deviating to the patient's left side. (**B**, **D**) Oblique sagittal MRI of the right joint shows normal disc (*arrow*) and normal bone, also in open-mouth image (**D**). (**C**, **E**) Oblique sagittal MRI of the left joint shows anteriorly displaced disc (*arrow*), also in open-mouth image (**E**). The left condyle is small but otherwise normal, and translation is restricted compared to the right joint (courtesy of Drs. A. Isberg and P. E. Legrell, Umea University, Sweden)

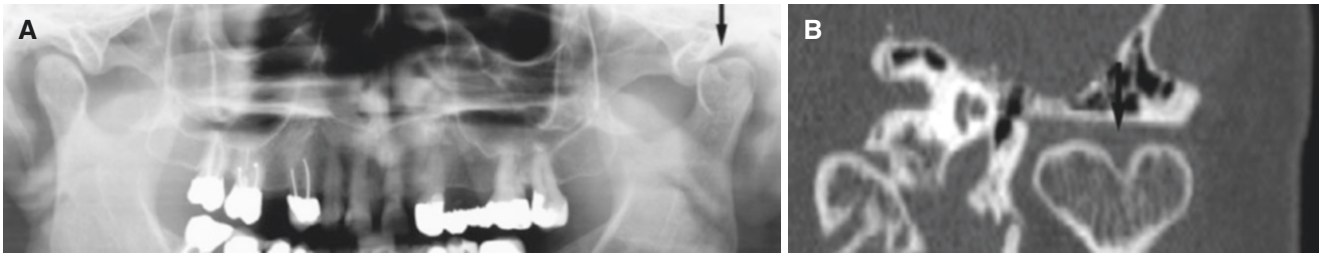

Fig. 6.61 Bifid condyle; unilateral. (**A**) Panoramic view shows abnormal left condyle (*arrow*) as an incidental finding. (**B**) Oblique coronal CT image shows split condyle (*arrow*) but otherwise normal bone structure

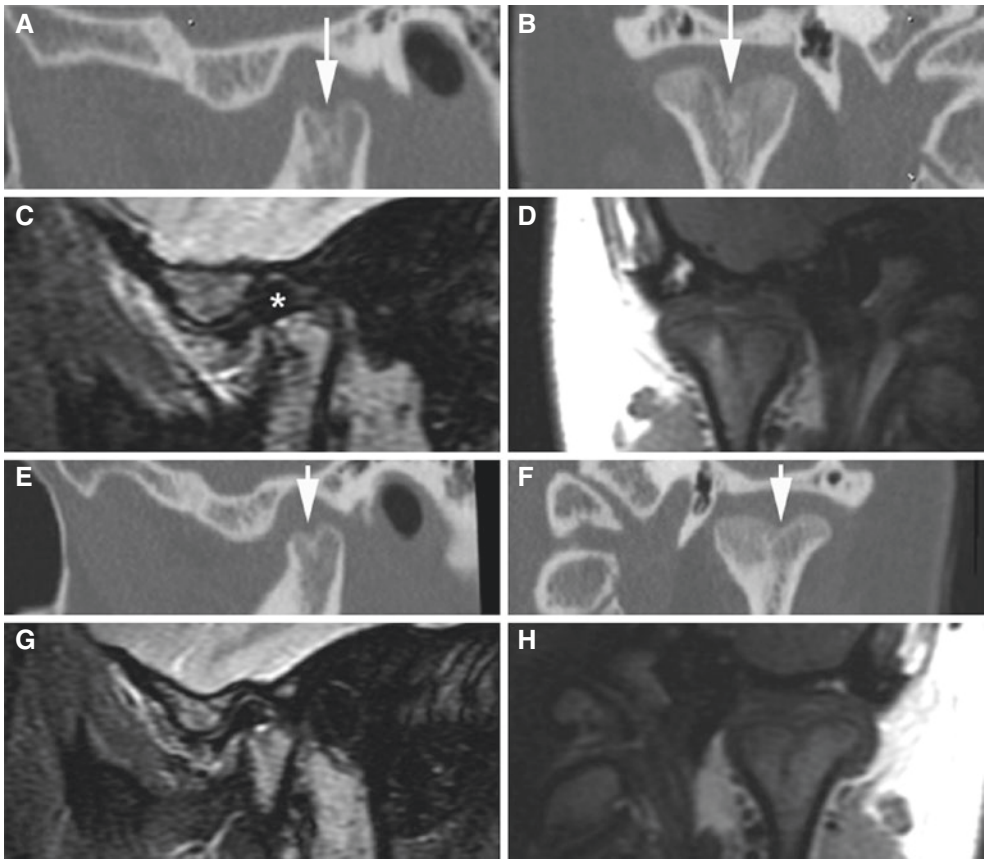

Fig. 6.62 Bifid condyle, bilateral; 18-year-old female. (**A**) Oblique sagittal and (**B**) oblique coronal CT images of the right joint show bifid condyle (*arrow*). (**C**) Oblique sagittal STIR MRI and (**D**) oblique coronal T1-weighted MRI confirm bifidity and additionally show normal disc with posterior band superior to the condyle (*asterisk*). (**E**) Oblique sagittal and (**F**) oblique coronal CT images of the left joint show bifid condyle (*arrow*). (**G**, **H**) MR images corresponding to those in (**C**) and (**D**) confirm bifidity and additionally show normal disc

6.9 Inflammatory or Tumorlike Conditions

Pseudogout, pigmented villonodular synovitis, simple bone cyst, synovial cyst, and synovial chondromatosis are illustrated

6.10 Calcium Pyrophosphate Dehydrate Crystal Deposition Disease (Pseudogout)

Figs. 6.63 and 6.64

6.10.1 Definition

Gout-like joint inflammation with subtle or severe calcium crystal deposits (chondrocalcinosis), not uric acid as in gout.

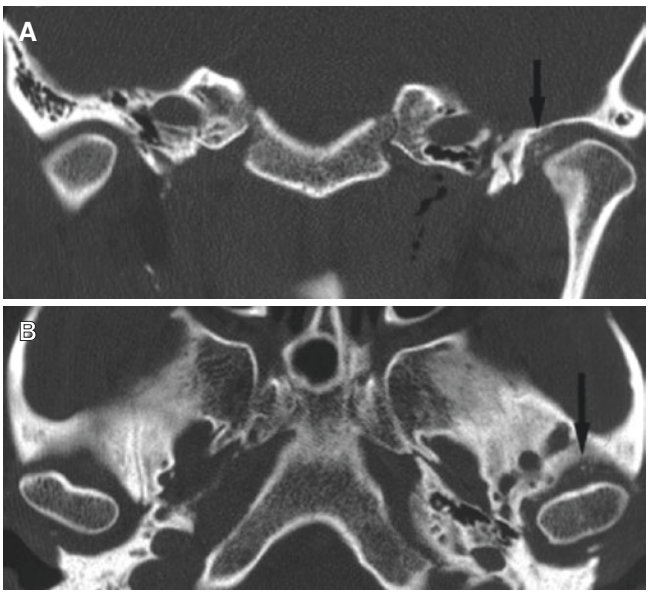

Fig. 6.63 Pseudogout. (**A**) Coronal and (**B**) axial CT images show subtle calcifications within joint space (*arrows*) consistent with early stage

6.10.2 Clinical Features

- Joint pain and swelling
- Symptoms may be similar to those of common TMJ disorders

6.10.3 Imaging Features

- Calcifications within joint space
- Subtle or massive calcifications
- Both the condyle and glenoid fossa may be eroded and actually simulate malignancy

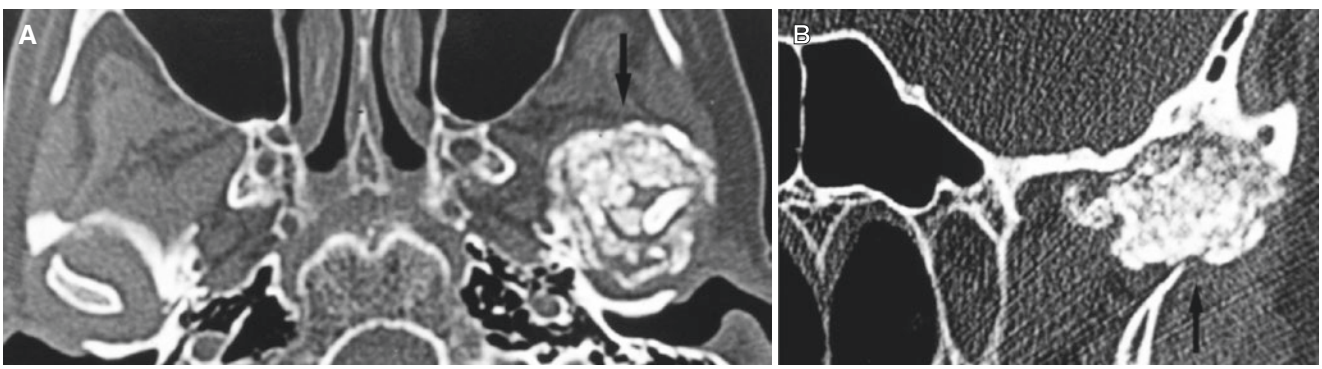

Fig. 6.64 Pseudogout. (**A**) Axial and (**B**) coronal CT images show extensive calcifications (*arrow*) consistent with advanced stage

6.11 Pigmented Villonodular Synovitis

Fig. 6.65

6.11.1 Definition

Joint inflammation, or benign neoplastic process, characterized by synovial proliferation, joint effusion, hemosiderin deposition, histiocytes, giant cells, and, occasionally, bone erosions.

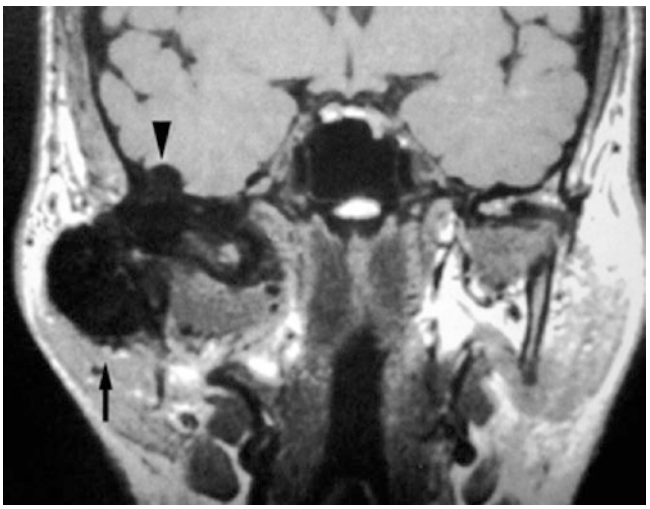

Fig. 6.65 Pigmented villonodular synovitis. Coronal T1-weighted MRI shows large mass of very low signal (*arrow*), penetrating skull base (*arrowhead*). Very low signal also characteristic on T2-weighted and post-Gd MRI (not shown) (courtesy of Dr. T. Larsson, Seattle, Washington)

6.11.2 Clinical Features

- Joint swelling and swelling, but symptoms may be vague.
- Symptoms may be similar to those of common TMJ disorders.

6.11.3 Imaging Features

- The condyle may show erosions
- Glenoid fossa may show erosions, with intracranial extension
- Periarticular soft-tissue density may be seen
- T1-weighted and T2-weighted MRI shows characteristic (almost pathognomonic) low signal because of hemorrhage by-products

6.12 Simple (Traumatic) Bone Cyst

Fig. 6.66
See Chap. 2.

6.12.1 Definition

Cavity within the bone, empty or partially filled with sanguineous fluid, without epithelial lining, with or without expansion of the bone.

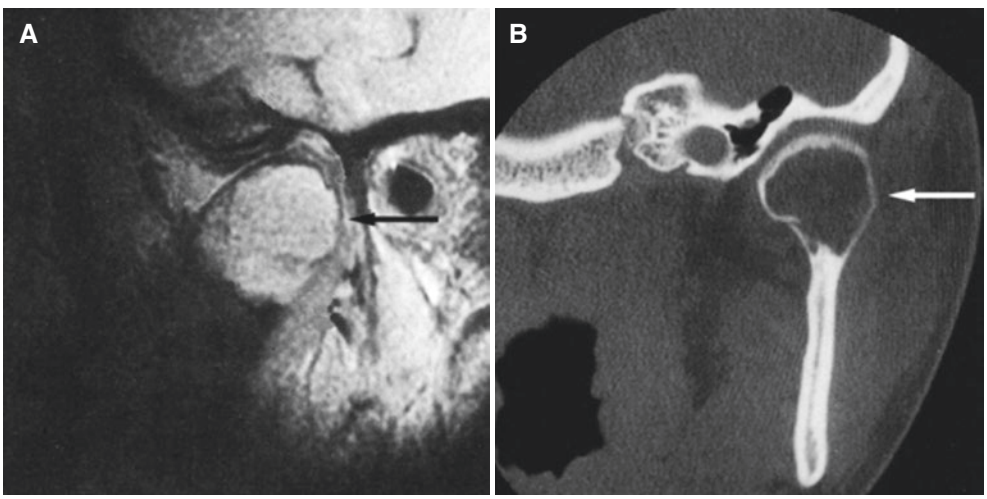

Fig. 6.66 Traumatic bone cyst. (**A**) MRI shows enlarged mandibular condyle (*arrow*), with normal disc and temporal bone. (**B**) Coronal CT image shows enlarged condyle with intact cortical bone (*arrow*)

6.13 Synovial Cyst

Fig. 6.67

6.13.1 Definition

Para-articular fluid-filled sacs or pouch-like structures containing fluid and lined by the synovial membrane.

6.13.2 Clinical Features

– Seldom in the TMJ, incidental finding or with pain, swelling
– Can occur around any joint in the body, also around tendon sheaths and bursae

6.13.3 Imaging Features

– Like a cyst anywhere

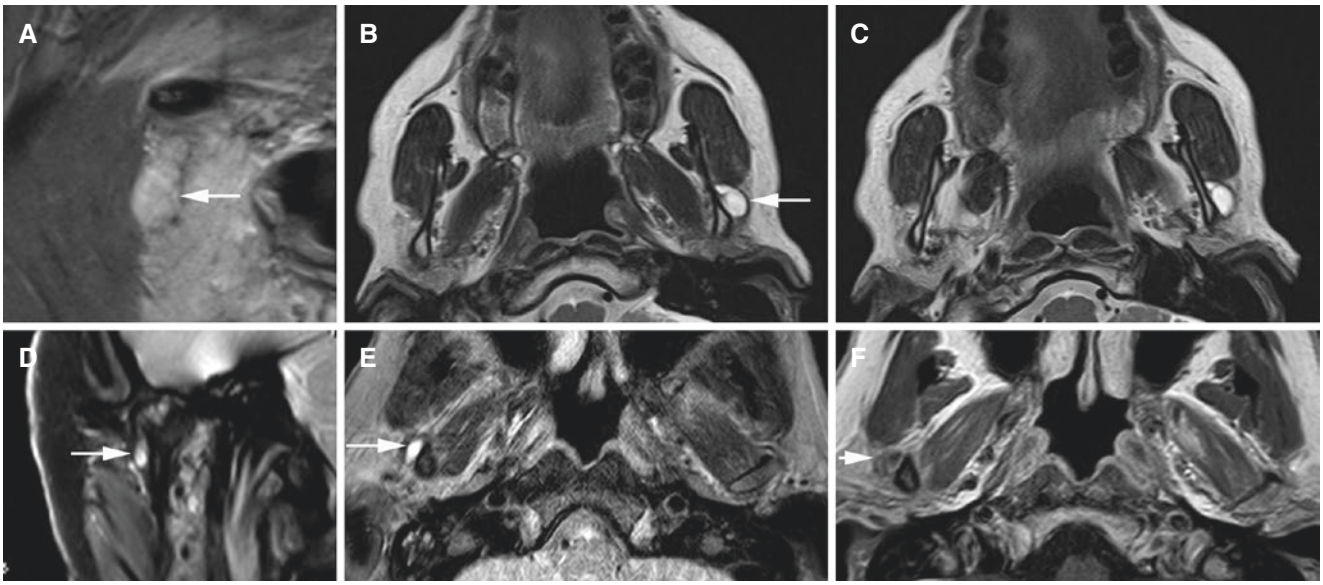

Fig. 6.67 Synovial cysts; 57-year-old female (**A**, **B**, **C**) and 50-year-old female (**D**, **E**, **F**). (**A**) Oblique sagittal PD-weighted MRI shows well-defined lesion with intermediate signal intensity (*arrow*). (**B**, **C**) Axial T2-weighted MRI shows well-defined lesion with high, homogeneous signal intensity (*arrow*). (**D**) Oblique coronal and (**E**) axial T2-weighted MRI show well-defined high, homogeneous signal intensity area (*arrow*). (**F**) Axial T1-weighted post-Gd MRI shows no contrast enhancement except in thin peripheral rim (*arrow*)

6.14 Synovial Chondromatosis

Figs. 6.68, 6.69, 6.70, and 6.71

Synonyms: Synovial osteochondromatosis, synovial chondrometaplasia.

6.14.1 Definition

Benign tumor characterized by cartilaginous metaplasia of the synovial membrane, usually in the knee, producing small nodules of cartilage, which essentially separate from the membrane to become loose bodies that may ossify.

6.14.2 Clinical Features

- Joint pain and swelling, but symptoms may be vague.
- Facial asymmetry
- Dental occlusion problems; "my bite doesn't fit"
- Symptoms may be similar to those of common TMJ disorders

6.14.3 Imaging Features

- Cartilage nodules and Calcifications within joint space
- Large or small calcifications, usually multiple
- Joint effusion, synovitis
- Condyle normal or osteoarthritis
- May be locally aggressive with destruction of fossa
- Intracranial extension has been reported

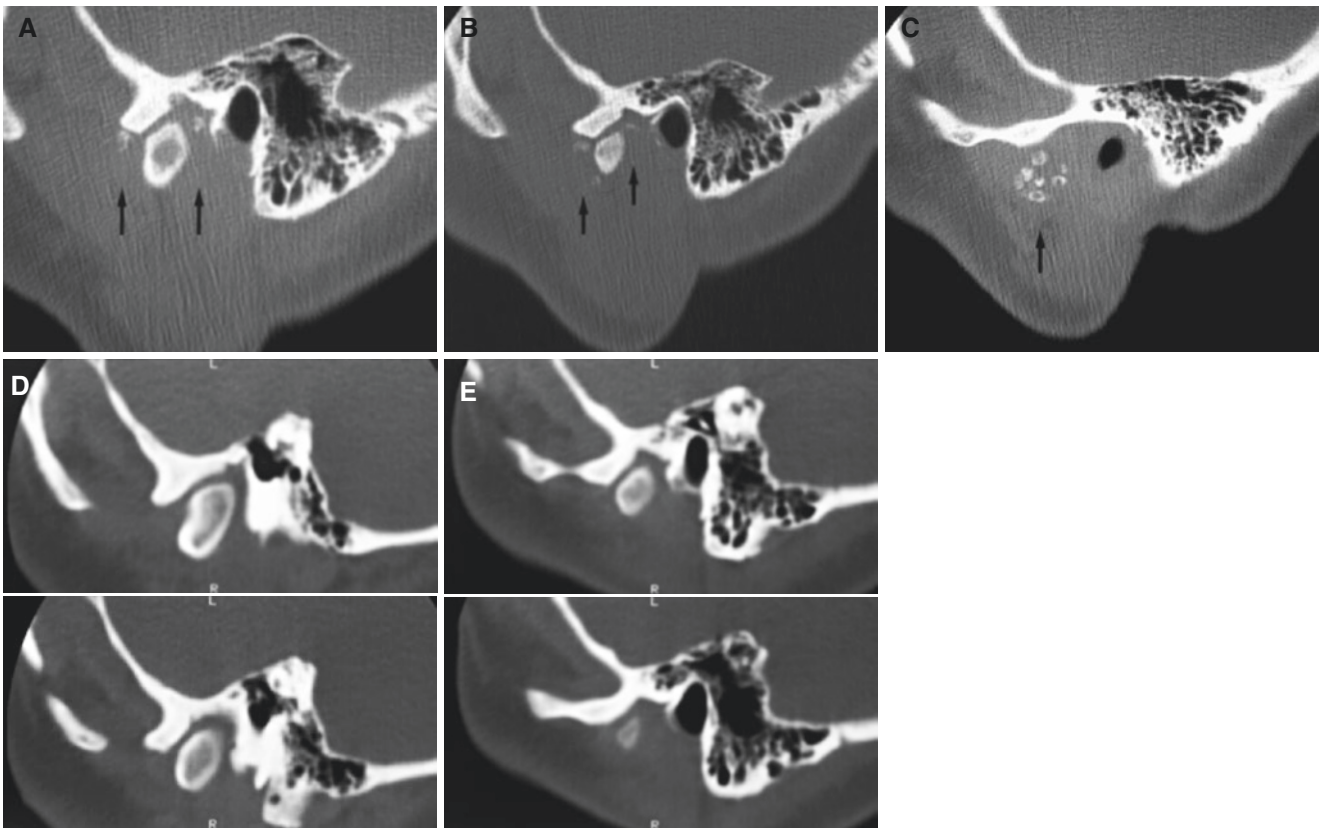

Fig. 6.68 Synovial chondromatosis. (**A**, **B**, **C**) Oblique sagittal CT images show multiple soft-tissue calcifications (*arrows*) anterior, posterior, and lateral to the condyle. (**D**, **E**) Four oblique sagittal CT images from an examination 4 years previously do not show calcifications when patient was referred for TMJ disorder

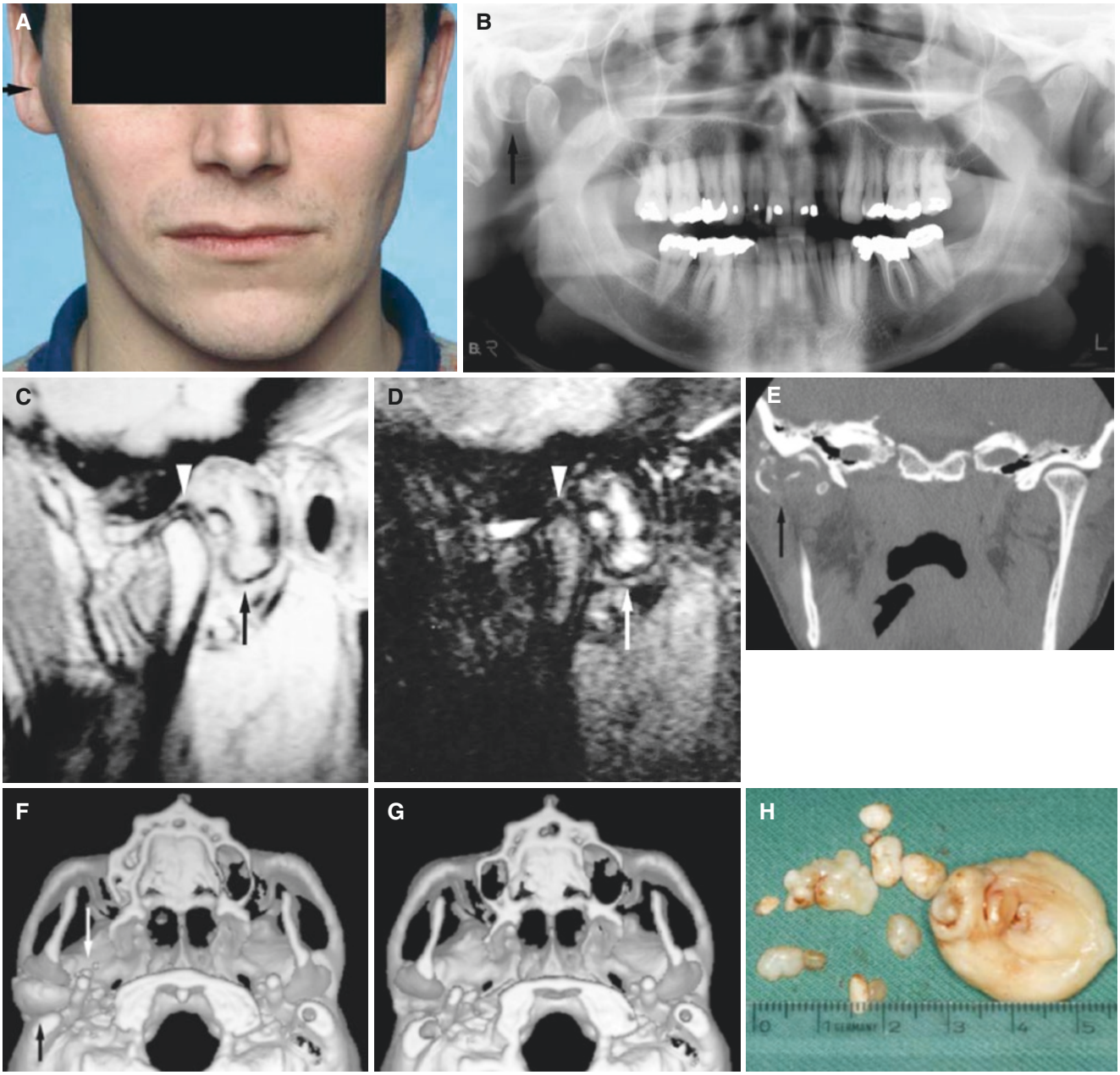

Fig. 6.69 Synovial chondromatosis. (**A**) Clinical photograph shows facial asymmetry and swelling over the right joint (*arrow*). (**B**) Panoramic view shows large calcification (*arrow*) posterior to the condyle. (**C**) Oblique sagittal T1-weighted MRI shows large structure (*arrow*) posterior to the condyle, which is normal but displaced anteriorly with normal disc (*arrowhead*) at closed mouth. (**D**) Oblique sagittal T2-weighted MRI shows increased signal from expansive process (*arrow*) and effusion in the upper joint space; *arrowhead* condyle. (**E**) Coronal CT image confirms calcifications posterior to the condyle (*arrow*). (**F**) Axial 3D CT image before surgery shows large calcification (*black arrow*) and smaller ones (*white arrow*). (**G**) Axial 3D CT image after surgery for comparison. (**H**) One large and a number of smaller calcifications were removed (**H** courtesy of Drs. G. Støre and T. Bjørnland, Oslo University Hospital, Rikshospitalet, Oslo, Norway)

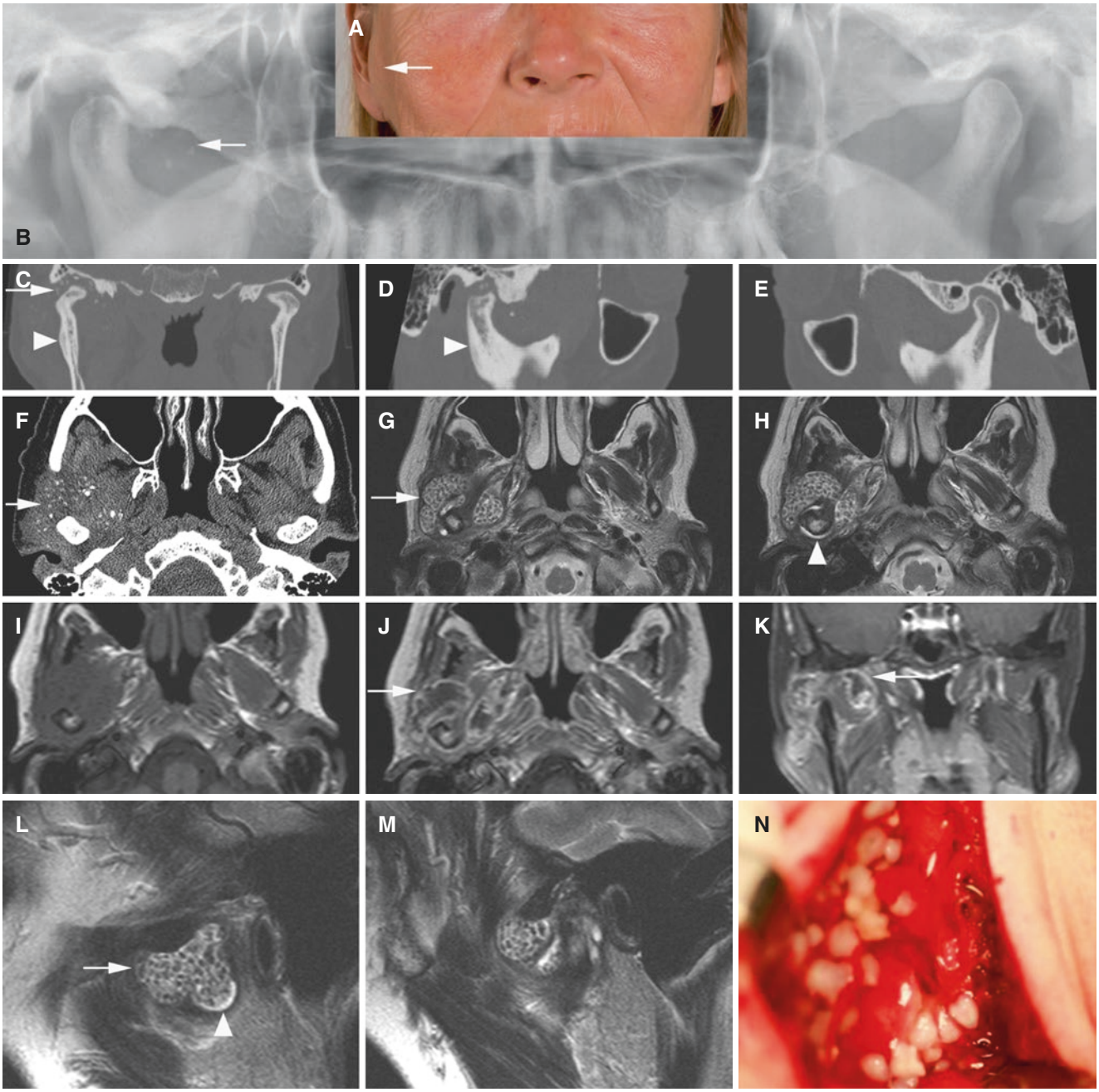

Fig. 6.70 Synovial chondromatosis; 53-year-old female. (**A**) Clinical photograph shows swelling of the right TMJ (*arrow*). (**B**) Panoramic view shows calcifications in the right TMJ area (*arrow*). (**C**) Coronal and (**D**, **E**) oblique sagittal CT images of the right (**D**) and normal left (**E**) joint show soft-tissue calcifications in the right joint (*arrow*) and periosteal reaction on the right ramus (*arrowhead*). (**F**) Axial CT image shows several small soft-tissue calcifications (*arrow*). (**G**, **H**) Axial T2-weighted MRI shows multiple small low-signal nodules (*arrow*) and joint effusion in the right joint (*arrowhead*). (**I**) Axial T1-weighted pre-Gd, (**J**) axial T1-weighted post-Gd, and (**K**) coronal T1-weighted fat sat post-Gd MRI show contrast enhancement in thin rim (synovial membrane) (*arrow*) throughout the right joint consistent with synovitis. (**L**, **M**) Oblique sagittal T2-weighted MRI of the right joint shows joint effusion (*arrowhead*) and multiple low signal intensity nodules (*arrow*). (**N**) Clinical photograph confirms multiple nodules (calcified or cartilaginous) peroperatively

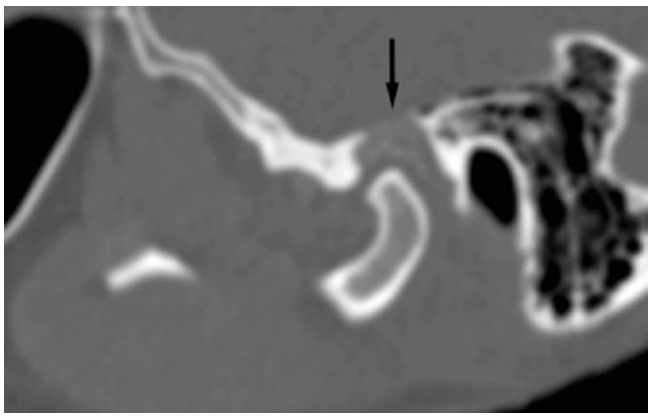

Fig. 6.71 Synovial chondromatosis. Oblique sagittal CT image shows destruction of fossa and slightly calcified tissue in joint space (*arrow*). Surgery confirmed destruction of fossa and calcified tissue, but no intracranial tumor growth

6.15 Benign Tumors

Osteochondroma, osteoma, and sphenoid meningioma are illustrated

6.16 Osteochondroma

Fig. 6.72

Synonym: Osteocartilaginous exostosis.

6.16.1 Definition

Benign tumor characterized by normal bone and cartilage, near growth zones.

6.16.2 Clinical Features

- Asymptomatic (no pain)
- Facial, mandibular asymmetry

6.16.3 Imaging Features

- Enlarged condyle
- Irregular in cortical outline and internal structure
- Cortical outline may be smooth

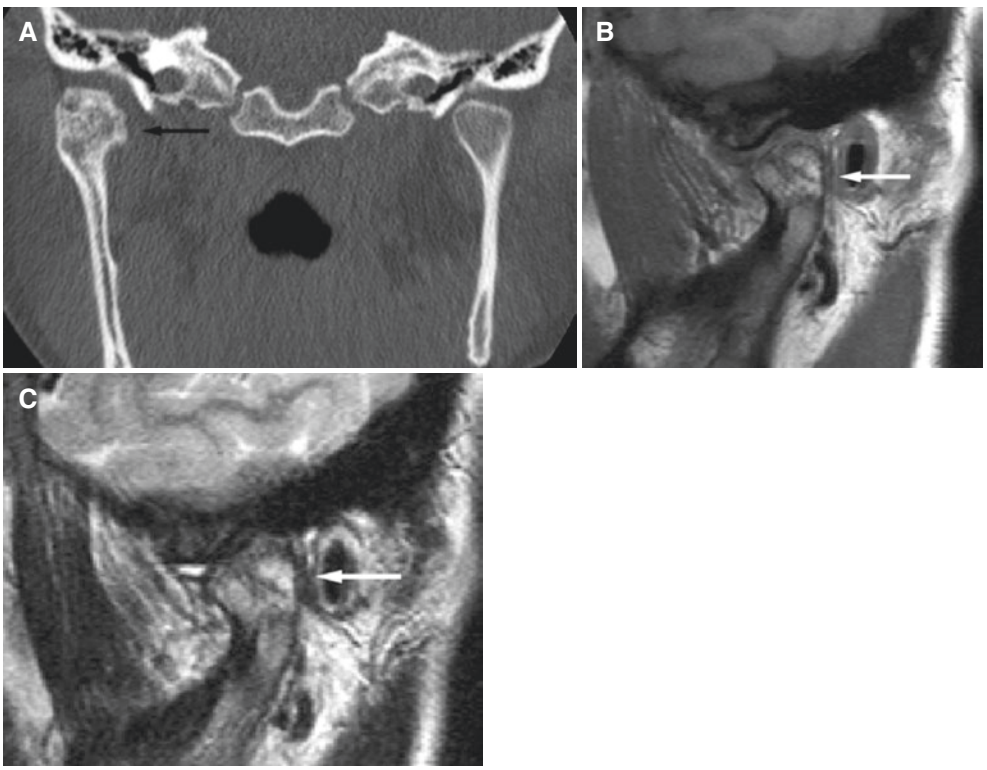

Fig. 6.72 Osteochondroma. (**A**) Coronal CT shows enlarged condyle with irregular outline and mineralization (*arrow*). (**B**) Oblique sagittal T1-weighted and (**C**) oblique sagittal T2-weighted MRI show heterogeneous signal from the condyle (*arrow*) and normal disc in normal position, with minimal fluid

6.17 Osteoma

Fig. 6.73
See Chap. 3

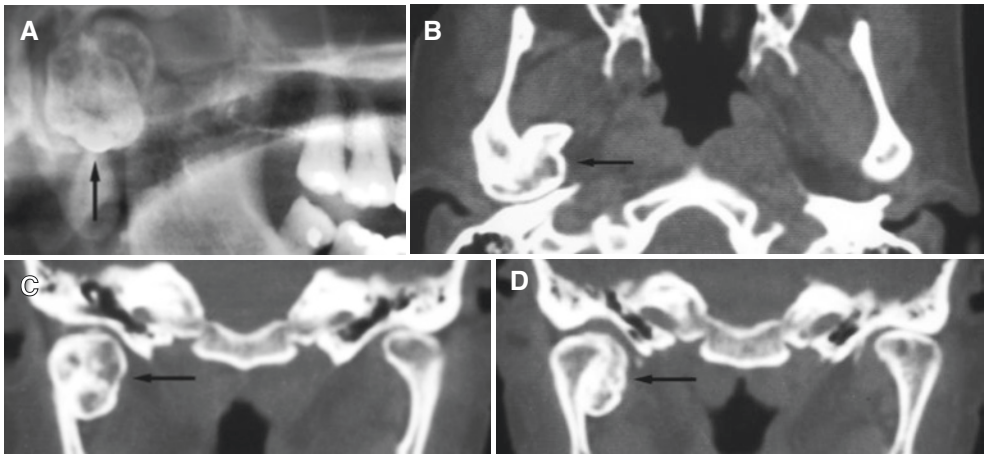

Fig. 6.73 Osteoma, incidental finding at routine panoramic radiography. (**A**) Panoramic view shows bone mass (*arrow*) partially superimposed on mandibular condyle. (**B**) Axial and (**C**, **D**) coronal CT images show bony outgrowth (*arrow*) of medial aspect of the condyle

6.18 Sphenoid Meningioma

Fig. 6.74

6.18.1 Definition

Benign brain tumor (meninges) from greater wing of sphenoid.

6.18.2 Clinical Features

- Restricted mouth-opening capacity
- No pain or other symptoms

6.18.3 Imaging Features

- Normal bone structures except destruction of fossa

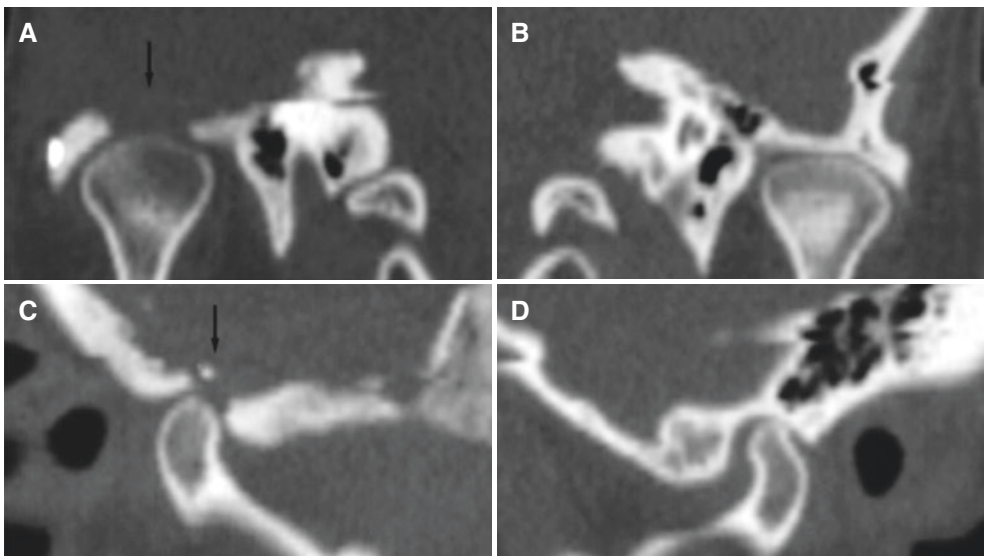

Fig. 6.74 Sphenoid meningioma; restricted mouth-opening capacity as only TMJ symptom. (**A**) Oblique coronal and (**C**) oblique sagittal CT images show destruction of fossa (*arrow*). (**B**) Oblique coronal and (**D**) oblique sagittal CT images of normal contralateral joint for comparison

6.19 Malignant Tumors

Figs. 6.75 and 6.76

Malignant tumors rarely affect the TMJ but should never be forgotten in the differential diagnostics; two cases of metastases are presented

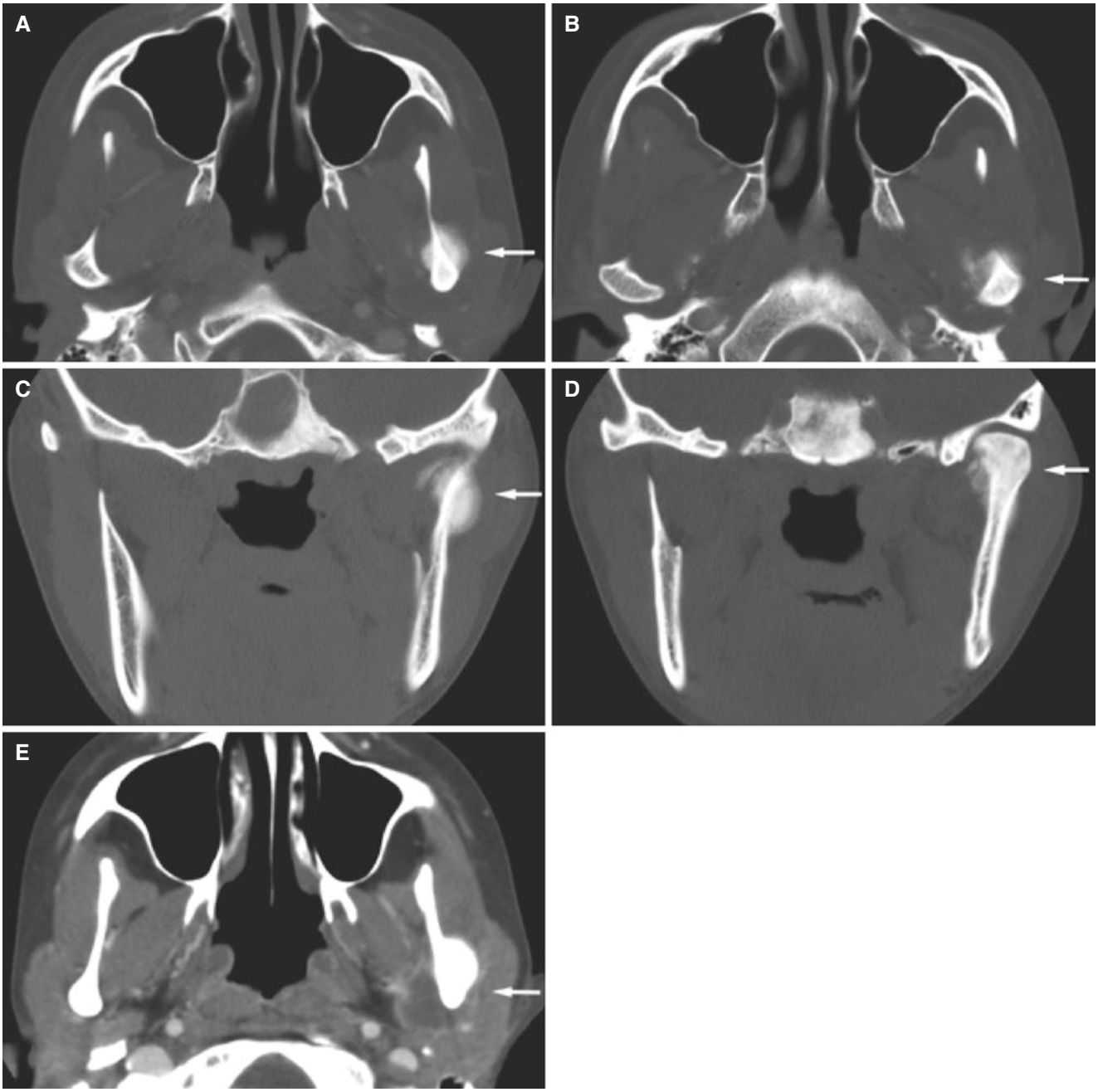

Fig. 6.75 Metastatic osteosarcoma, mandible; 18-year-old female with terminal widespread osteosarcoma (2.5-year history). (**A**, **B**) Axial CT images show intense periosteal bone production in the ramus (*arrow*) and in the condyle (*arrow*). (**C**, **D**) Coronal CT images show intense bone production (*arrow*), but no evident bone destruction in the ramus. (**E**) Axial CT image, soft-tissue window, shows contrast-enhancing tumor surrounding and encasing the condyle. Peripheral contrast enhancement suggests central necrosis

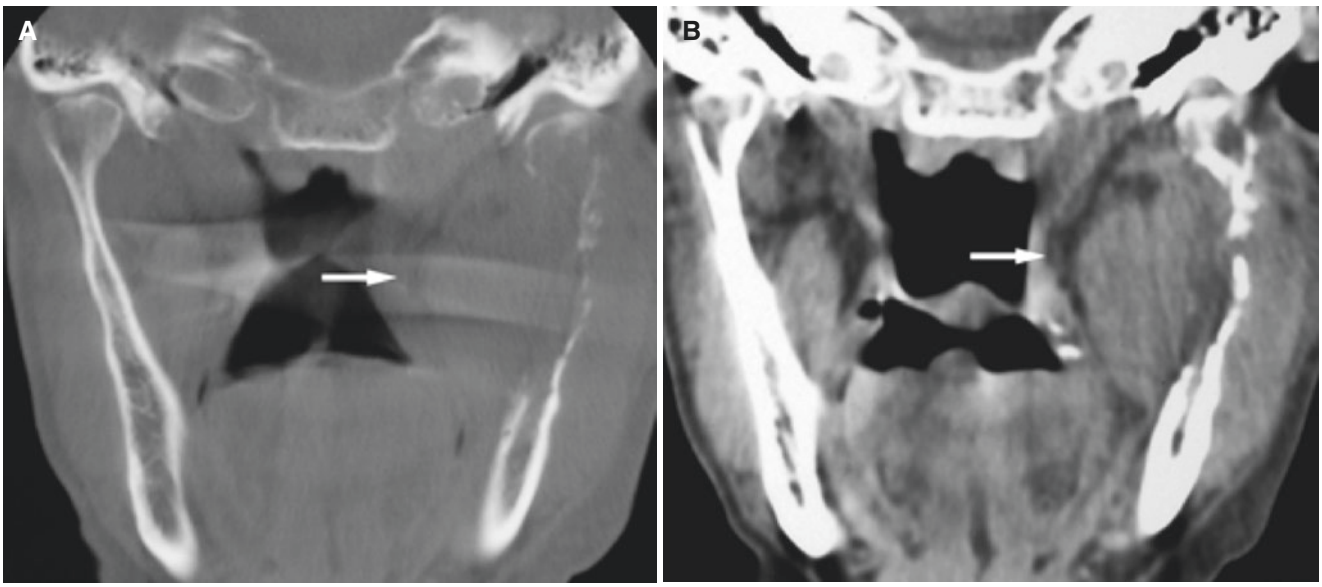

Fig. 6.76 Metastatic tumor, mandible; 70-year-old male with lung cancer spread and restricted mouth-opening capacity as only TMJ symptom. (**A**) Coronal CT image shows destruction of the ramus and condyle (*arrow*). (**B**) Coronal CT image, soft-tissue window, shows soft-tissue mass in masticator space infiltrating mandible (*arrow*)

6.20 Osteoradionecrosis

Fig. 6.77
See Chap. 5

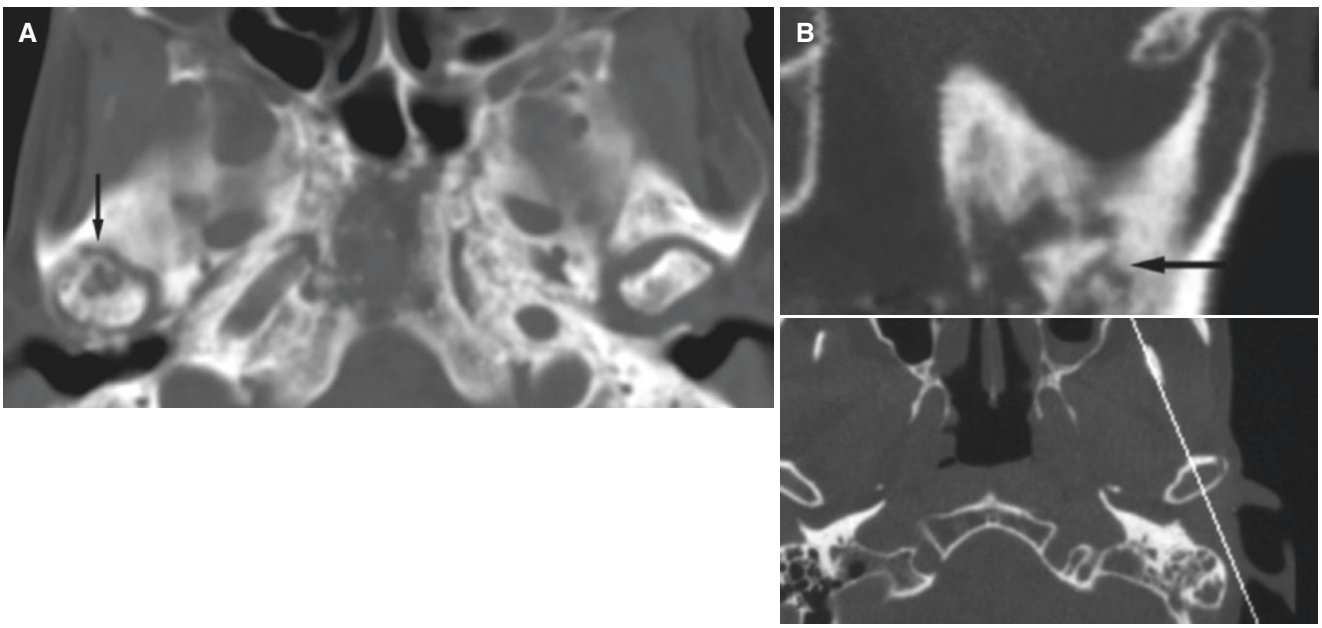

Fig. 6.77 Osteoradionecrosis, mandible. (**A**) Axial CT image shows destruction of the condyle (*arrow*) in one patient; also note destruction in the clivus. (**B**) Oblique sagittal CT image of mandibular ramus of another patient (with axial image showing *cursor line* for sagittal image) shows destruction of coronoid process (*arrow*)

6.21 Coronoid Hyperplasia

Fig. 6.78

6.21.1 Definition

Enlarged coronoid process, unilaterally or bilaterally (1 cm above zygomatic arch has been mentioned as a definition).

6.21.2 Clinical Features

- Restricted mouth-opening capacity over time
- No pain

6.21.3 Imaging Features

- Enlarged coronoid process, otherwise normal
- Interfering with mouth opening; coronoid process is not allowed to move freely

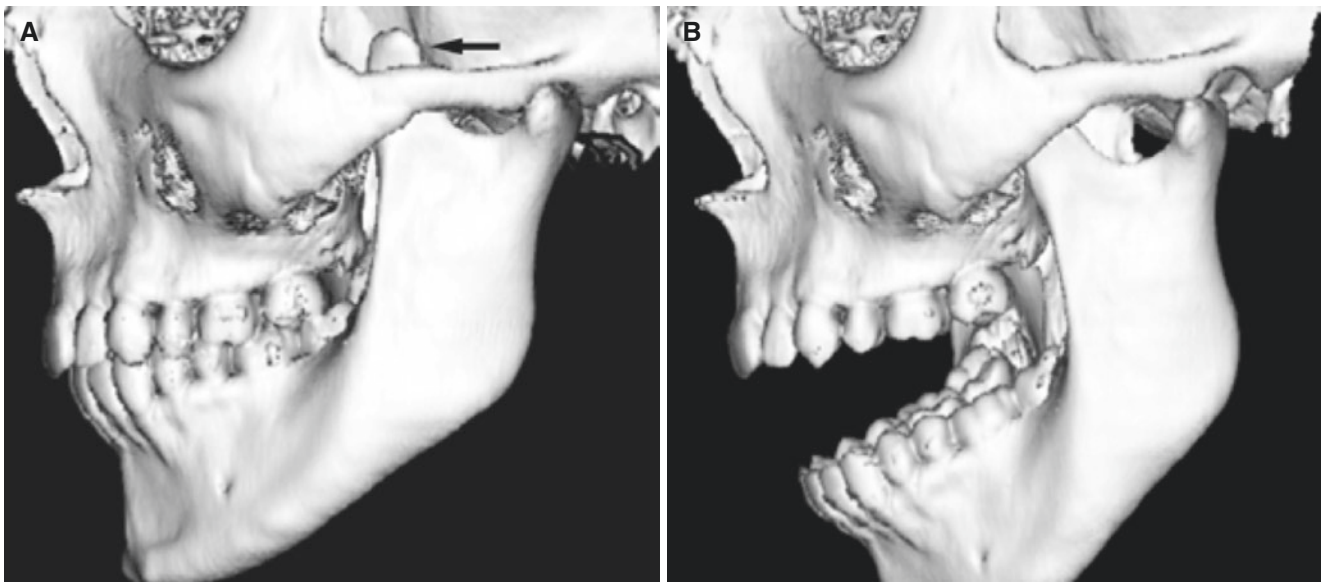

Fig. 6.78 Coronoid hyperplasia. (**A**) Closed-mouth and (**B**) open-mouth 3D CT images show enlarged coronoid process (*arrow*), not allowing normal motion of mandible. See also Fig. 9.33c

Suggested Reading

Abboud W, Yahalom R, Leiba M, Greenberg G, Yarom N (2016) Temporomandibular joint involvement in patients with multiple myeloma—a retrospective study. Int J Oral Maxillofac Surg 45:1545–1550

Adams JC, Hamblen DL (2001) Outline of orthopedics, 13th edn. Churchill Livingstone, London, p 135

Ahmad M, Schiffman EL (2016) Temporomandibular joint disorders and orofacial pain. Dent Clin N Am 60:105–124

Ahmad M, Hollender L, Anderson Q, Kartha K, Ohrbach R, Truelove EL et al (2009) Research diagnostic criteria for temporomandibular disorders (RDC/TMD): development of image analysis criteria and examiner reliability for image analysis. Oral Surg Oral Med Oral Pathol Oral Radiol Endod 107:844–860

Alexiou K, Stamatakis H, Tsiklakis K (2009) Evaluation of the severity of temporomandibular joint osteoarthritic changes related to age using cone beam computed tomography. Dentomaxillofac Radiol 38:141–147

Al-Khalisy HM, Nikiforov I, Mansoora Q, Goldman J, Cheriyath P (2015) Septic arthritis in the temporomandibular joint. N Am J Med Sci 7:480–482

Al-Saleh MA, Alsufyani NA, Lagravere M, Nebbe B, Lai H, Jaremko JL, Major PW (2016) MRI alone versus MRI-CBCT registered images to evaluate temporomandibular joint internal derangement. Oral Surg Oral Med Oral Pathol Oral Radiol 122:638–645

Ängelo DF, Sousa R, Pinto J, Sanz D, Gil FM, Salvado F (2015) Early magnetic resonance imaging control after temporomandibular joint arthrocentesis. Ann Maxillofac Surg 5:255–257

Arvidsson LZ, Flatø B, Larheim TA (2009) Radiographic TMJ abnormalities in patients with juvenile idiopathic arthritis followed for 27 years. Oral Surg Oral Med Oral Pathol Oral Radiol Endod 108:114–123

Arvidsson LZ, Fjeld M, Smith H-J, Flatø B, Øgaard B, Larheim TA (2010a) Craniofacial growth disturbance is related to temporomandibular joint abnormality in patients with juvenile idiopathic arthritis, but normal facial profile was also found at the 27-year follow-up. Scand J Rheumatol 39:373–379

Arvidsson LZ, Smith H-J, Flatø B, Larheim TA (2010b) Temporomandibular joint findings in adults with long-standing juvenile idiopathic arthritis: CT and MR imaging assessment. Radiology 256:191–200

Bae WC, Tafur M, Chang EY, Du J, Biswas R, Kwack KS et al (2016) High-resolution morphologic and ultrashort time-to-echo quantitative magnetic resonance imaging of the temporomandibular joint. Skelet Radiol 45:383–391

Basat SO, Surmeli M, Demirel O, Ceran F, Saydam FA, Basaran K (2016) Assessment of the relationship between clinicophysiologic and magnetic resonance imaging findings of the temporomandibular disorder patients. J Craniofac Surg. doi:10.1097/SCS.0000000000000317

Berenbaum F (2013) Osteoarthritis as an inflammatory disease (osteoarthritis is not osteoarthrosis!). Osteoarthr Cartil 21:16–21

Bristela M, Schmid-Schwap M, Eder J, Reichenberg G, Kundi M, Piehslinger E, Robinson S (2016) Magnetic resonance imaging of temporomandibular joint with anterior disk dislocation without reposition—long-term results. Clin Oral Investig. doi:10.1007/s00784-016-1800-9

De Boer EW, Dijkstra PU, Stegenda B, de Boat LG, Spijkervet FK (2013) Value of cone beam computed tomography in the process of diagnosis and management of disorders of the temporomandibular joint. Br J Oral Maxillofac Surg 52:241–246

De Bont LG, Dijkgaaf LC, Stegenga B (1997) Epidemiology and natural progression of articular temporomandibular disorders. Oral Surg Oral Med Oral Pathol Oral Radiol Endod 83:72–76

De Leeuw R, Boering G, Stegenga B, de Bont LG (1995) TMJ articular disc position and configuration 30 years after initial diagnosis of internal derangement. J Oral Maxillofac Surg 53:234–241

Dias IM, Cordeiro PC, Devito KL, Tavares ML, Leite IC, Tesch Rde S (2016) Evaluation of temporomandibular joint disc displacement as a risk factor for osteoarthrosis. Int J Oral Maxillofac Surg 45:313–317

Ekberg E, Hansson LG, List T, Eriksson L, Sahlström LE, Petersson A (2015) Can MRI observations predict treatment outcome of lavage in patients with painful TMJ disc displacement without reduction? J Oral Maxillofac Res 6(1):e5. doi:10.5037/jomr.2014.6105

Emshoff R, Brandlmaier I, Schmid C, Bertram S, Rudisch A (2003) Bone marrow edema of the mandibular condyle related to internal derangement, osteoarthrosis, and joint effusion. J Oral Maxillofac Surg 61:35–40

Eriksson L, Westesson P-L (1983) Clinical and radiological study of patients with anterior disk displacement of the temporomandibular joint. Swed Dent J 7:55–64

Felson DT (2014) Osteoarthritis: priorities for osteoarthritis research: much to be done. Nat Rev Rheumatol 10:447–448

Fjeld M, Arvidsson LA, Stabrun AE, Birkeland K, Larheim TA, Øgaard B (2009) Average craniofacial development from 6 to 35 years of age in a mixed group of patients with juvenile idiopathic arthritis. Acta Odontol Scand 67:153–160

Fjeld M, Arvidsson LA, Smith H-J, Flatø B, Øgaard B, Larheim TA (2010) Relationship between disease course in the temporomandibular joints and mandibular growth rotation in patients with juvenile idiopathic arthritis followed from childhood to adulthood. Pediatr Rheumatol Online J 8:13. doi:10.1186/1546-0096-8-13

Frid PHT, Nordal EB, Bovis F, Giancane G, Larheim TA, Rygg M et al (2016) Temporomandibular joint involvement is associated with quality of life, disability and high disease activity in juvenile idiopathic arthritis. Arthritis Care Res. doi:10.1002/acr.23003

Grossmann E, Remedi MP, Ferreira LA, Carvalho AC (2016) Magnetic resonance image evaluation of temporomandibular joint osteophytes: influence of clinical factors and artrogenics changes. J Craniofac Surg 27:334–338

Hirahara N, Kaneda T, Muraoka H, Fukuda T, Ito K, Kawashima Y (2017) Characteristic magnetic resonance imaging findings in rheumatoid arthritis of the temporomandibular joint: focus on abnormal bone marrow signal of the mandibular condyle, pannus, and lymph node swelling in the parotid glands. J Oral Maxillofacial Surg 75:735–741

Honda K, Larheim TA, Johannessen S, Arai Y, Shinoda K, Westesson P-L (2001) Ortho cubic super-high resolution computed tomography: a new radiographic technique with application to the temporomandibular joint. Oral Surg Oral Med Oral Pathol Oral Radiol Endod 91:239–243

Honda K, Larheim TA, Maruhashi K, Matsumoto K, Iwai K (2006) Osseous abnormalities of the mandibular condyle: diagnostic reliability of cone beam computed tomography compared with helical computed tomography based on an autopsy material. Dentomaxillofac Radiol 35:152–157

Hu YK, Yang C, Xie QY (2016a) Changes in disc status in the reducing and nonreducing anterior disc displacement of temporomandibular joint: a longitudinal retrospective study. Sci Rep 6:34253. doi:10.1038/srep34253

Hu YK, Yang C, Cai XY, Xie QY (2016b) Does condylar height decrease more in temporomandibular joint nonreducing disc displacement than reducing disc displacement?: a magnetic resonance imaging retrospective study. Medicine (Baltimore) 95:e4715. doi:10.1097/MD.0000000000004715

Ikeda R, Ikeda K (2016) Directional characteristics of incipient temporomandibular joint disc displacements: a magnetic resonance imaging study. Am J Orthod Dentofac Orthop 149:39–45

Isberg A, Isacsson G, Nah K-S (1987) Mandibular coronoid process locking: a prospective study of frequency and association with internal derangement of the temporomandibular joint. Oral Surg Oral Med Oral Pathol 63:275–279

Katzberg RW, Keith DA, Guralnick WC, Manzione JV Jr, Ten Eick WR (1983) Internal derangements and arthritis of the temporomandibular joint. Radiology 146:107–112

Katzberg RW, Tallents RH, Hayakawa K, Miller TL, Goske MJ, Wood BP (1985) Internal derangements of the temporomandibular joint: findings in the pediatric age group. Radiology 154:125–127

Katzberg RW, Westesson P-L, Tallents RH, Drake CM (1996) Anatomic disorders of the temporomandibular joint disc in asymptomatic subjects. J Oral Maxillofac Surg 54:147–153

Kellenberger CJ, Arvidsson LA, Larheim TA (2015) Magnetic resonance imaging of temporomandibular joints in juvenile idiopathic arthritis. Semin Orthod 21:111–120

Khawaja SN, Crow H, Mahmoud RF, Kartha K, Gonzalez Y (2016) Is there an association between temporomandibular joint effusion and arthralgia? J Oral Maxillofac Surg pii:S0278–2391(16)30761–3. doi:10.1016/j.joms.2016.08.027

Kim HK, Lim JH, Jeon KJ, Huh JK (2016) Bony window approach for a traumatic bone cyst on the mandibular condyle: a case report with long-term follow-up. J Korean Assoc Oral Maxillofac Surg 42:209–214

Kirkhus E, Gunderson RB, Smith H-J, Flatö B, Hetlevik SO, Larheim TA, Arvidsson LA (2016a) Temporomandibular joint involvement in childhood arthritis: comparison of ultrasonography-assessed capsular width and MRI-assessed synovitis. Dentomaxillofac Radiol 45:20160195

Kirkhus E, Arvidsson LZ, Smith H-J, Flatø B, Hetlevik SO, Larheim TA (2016b) Disk abnormality coexists with any degree of synovial and osseous abnormality in the temporomandibular joints of children with juvenile idiopathic arthritis. Pediatr Radiol 46:331–341

Kohinata K, Matsumoto K, Suzuki T, Tsunoda M, Hayashi Y, Araki M et al (2016) Retrospective magnetic resonance imaging study of risk factors associated with sideways disk displacement of the temporomandibular joint. J Oral Sci 58:29–34

Kothari SF, Baad-Hansen L, Hansen LB, Bang N, Sørensen LH, Eskildsen HW, Svensson P (2016) Pain profiling of patients with temporomandibular joint arthralgia and osteoarthritis diagnosed with different imaging techniques. J Headache Pain 17:61. doi:10.1186/s10194-016-0653-6

Krohn S, Gersdorff N, Wassmann T, Merboldt KD, Joseph AA, Buergers R, Frahm J (2016) Real-time MRI of the temporomandibular joint at 15 frames per second-a feasibility study. Eur J Radiol 85:2225–2230

Kuhn FP, Spinner G, Del Grande F, Wyss M, Piccirelli M, Erni S et al (2016) MR imaging of the temporomandibular joint: comparison between acquisitions at 7.0 tesla using dielectric pads and 3.0 tesla. Dentomaxillofac Radiol 5:20160280

Kuroda M, Otonari-Yamamoto M, Sano T, Fujikura M, Wakoh M (2015) Diagnosis of retrodiscal tissue in painful temporomandibular joint (TMJ) by fluid-attenuated inversion recovery (FLAIR) signal intensity. Cranio 33:271–275

Kuseler A, Pedersen TK, Herlin T, Gelineck J (1998) Contrast enhanced magnetic resonance imaging as a method to diagnose early inflammatory changes in the temporomandibular joint in children with juvenile chronic arthritis. J Rheumatol 25:1406–1412

Larheim TA (1981) Radiographic appearance of the normal temporomandibular joint in newborns and small children. Acta Radiol 22:593–599

Larheim TA (1991) Imaging of the temporomandibular joint in juvenile rheumatoid arthritis. In: Westesson P-L, Katzberg RW (eds) Imaging of the temporomandibular joint, vol 1. Cranio Clinics International, Williams and Wilkins, Baltimore, pp 155–172

Larheim TA (1993) Rheumatoid arthritis and related joint diseases. In: Katzberg RW, Westesson P-L (eds) Diagnosis of the temporomandibular joint. Saunders, Philadelphia, pp 303–326

Larheim TA (1995) Current trends in temporomandibular joint imaging. Oral Surg Oral Med Oral Pathol Oral Radiol Endod 80:555–576

Larheim TA (2005) Role of magnetic resonance imaging in the clinical diagnosis of the temporomandibular joint. Cells Tissues Organs 180:6–21

Larheim TA (2014) Diagnostic imaging of the TMJ. In: Busaidy KF (ed) Oral and maxillofacial surgery knowledge update 2014, vol V (OMSKU V). http://aaoms2.centrax.com/?page_id=821

Larheim TA, Kolbenstvedt A (1984) High-resolution computed tomography of the osseous temporomandibular joint. Some normal and abnormal appearances. Acta Radiol Diagn (Stock) 25:465–469

Larheim TA, Kolbenstvedt A (1990) Osseous temporomandibular joint abnormalities in rheumatic disease. Computed tomography versus hypocycloidal tomography. Acta Radiol 31:383–387

Larheim TA, Westesson P-L (2006) TMJ imaging. In: Laskin DM, Greene CS, Hylander WL (eds) Temporomandibular disorder: an evidence-based approach to diagnosis and treatment. Quintessence Publishing, Chicago

Larheim TA, Smith H-J, Aspestrand F (1990) Rheumatic disease of the temporomandibular joint: MR imaging and tomographic manifestations. Radiology 175:527–531

Larheim TA, Westesson P-L, Hicks DG, Eriksson L, Brown DA (1999) Osteonecrosis of the temporomandibular joint: correlation of magnetic resonance imaging and histology. J Oral Maxillofac Surg 57:888–898

Larheim TA, Westesson P-L, Sano T (2001a) Temporomandibular joint disk displacement: comparison in asymptomatic volunteers and patients. Radiology 218:428–432

Larheim TA, Katzberg RW, Westesson P-L, Tallents RH, Moss ME (2001b) MR evidence of temporomandibular joint fluid and condyle marrow alterations: occurrence in asymptomatic volunteers and symptomatic patients. Int J Oral Maxillofac Surg 30:113–117

Larheim TA, Westesson P-L, Sano T (2001c) MR grading of temporomandibular joint fluid: association with disk displacement categories, condyle marrow abnormalities and pain. Int J Oral Maxillofac Surg 30:104–112

Larheim TA, Sano T, Yotsui Y (2012) Clinical significance of changes in the bone marrow and intra-articular soft tissues of the temporomandibular joint. Semin Orthod 18:30–43

Larheim TA, Doria AS, Kirkhus E, Parra DA, Kellenberger CJ, Arvidsson LZ (2015a) TMJ imaging in JIA patients—an overview. Semin Orthod 21:102–110

Larheim TA, Abrahamsson A-K, Kristensen M, Arvidsson LZ (2015b) CBCT special issue: review article. Temporomandibular joint diagnostics using CBCT. Dentomaxillofac Radiol 44:20140235

Laskin DM, Greene CS, Hylander WL (eds) (2006) Temporomandibular disorders: an evidence-based approach to diagnosis and treatment. Quintessence Publishing, Chicago

Laviv A, Sadow PM, Keith DA (2015) Pseudogout in the temporomandibular joint with imaging, arthroscopic, operative, and pathologic findings. Report of an unusual case. J Oral Maxillofac Surg 73:1106–1112

Levarek LE, Nolan PJ (2016) Temporomandibular joint ganglion cyst: a unique case of complete resolution following subtotal excision. J Oral Maxillofac Surg 74:1783–1791

Lieberman JM, Gardner CL, Milgram JW (1990) Osteonecrosis due to traumatic and idiopathic causes in radiologic and histologic pathology of non-tumorous diseases of bone and joints. Northbrook Publishing, Northbrook, p 959

Lieberman JM, Gardner CL, Motta AO, Schwartz RD (1996) Prevalence of bone marrow signal abnormalities observed in the temporomandibular joint using magnetic resonance imaging. J Oral Maxillofac Surg 54:434–439

Liu X, Huang Z, Zhu W, Liang P, Tao Q (2016) Clinical and imaging findings of temporomandibular joint synovial chondromatosis: an analysis of 10 cases and literature review. J Oral Maxillofac Surg 74:2159–2168

Lohiya S, Dillon J (2016) Septic arthritis of the temporomandibular joint—unusual presentations. J Oral Maxillofac Surg 74:87–94

Ma GM, Amirabadi A, Inarejos E, Tolend M, Stimec J, Moineddin R et al (2015) MRI thresholds for discrimination between normal and mild temporomandibular joint involvement in juvenile idiopathic

arthritis. Pediatr Rheumatol Online J 13:53. doi:10.1186/s12969-015-0051-7
Manoliu A, Spinner G, Wyss M, Ettlin DA, Nanz D, Kuhn et al (2015) Magnetic resonance imaging of the temporomandibular joint at 7.0 T using high-permittivity dielectric pads: a feasibility study. Investig Radiol 50:843–849
Manoliu A, Spinner G, Wyss M, Filli L, Erni S, Ettlin DA et al (2016a) Comparison of a 32-channel head coil and a 2-channel surface coil for MR imaging of the temporomandibular joint at 3.0 T. Dentomaxillofac Radiol 45(4):20150420. doi:10.1259/dmfr.20150420
Manoliu A, Spinner G, Wyss M, Erni S, Ettlin DA, Nanz D, et al (2016b) Quantitative and qualitative comparison of MR imaging of the temporomandibular joint at 1.5 and 3.0 T using an optimized high-resolution protocol. Dentomaxillofac Radiol 45(1):20150240. doi:10.1259/dmfr.20150240
Massilla Mani F, Sivasubramanian SS (2016) A study of temporomandibular joint osteoarthritis using computed tomographic imaging. Biomed J 39:201–206
Meyers AB, Oberle EJ (2016) Sonographic evaluation of the temporomandibular joint: uses and limitations. J Ultrasound Med 35:452–453
Millon-Cruz A, Martin-Granizo R, Encinas A, Berguer A (2015) Relationship between intra-articular adhesions and disc position in temporomandibular joints: magnetic resonance and arthroscopic findings and clinical results. J Craniomaxillofac Surg 43:497–502
Mitchell DG, Steinberg ME, Dalinka MK, Rao VM, Fallon M, Kressel HY (1989) Magnetic resonance imaging of the ischemic hip: alterations within the osteonecrotic, viable, and reactive zones. Clin Orthop Relat Res 244:60–77
Moe JS, Desai NK, Aiken AH, Soares BP, Kang J, Abramowicz S (2016) Magnetic resonance imaging of temporomandibular joints of children. J Oral Maxillofac Surg 74:1723–1727
Morales H, Cornelius R (2016) Imaging approach to temporomandibular joint disorders. Clin Neuroradiol 26:5–22
Muraoka H, Kaneda T, Kawashima Y, Hirahara N, Fukuda T, Muramatsu T, Ito K (2016) Parotid lymphadenopathy is associated with joint effusion in non-neoplastic temporomandibular disorders. J Oral Maxillofac Surg. doi:10.1016/j.joms.2016.09.013
Mutlu A, Sari F, Öztürk M, Iseri M (2015) Giant cell granuloma of the temporomandibular joint: a report of the two cases. Kulak Burun Bogaz Ihtis Derg 25:189–192
Nebbe B, Major PW, Prasad NG (1999) Male adolescent facial pattern associated with TMJ disk displacement and reduction in disk length: part II. Am J Orthod Dentofac Orthop 116:301–307
Niibo P, Pruunsild C, Voog-Oras Û, Nikopensius T, Jagomägi T, Saag M (2016) Contemporary management of TMJ involvement in JIA patients and its orofacial consequences. EPMA J 7:12. doi:10.1186/s13167-016-0061-7
Oh KY, Yoon HJ, Lee JI, Hong SP, Hong SD (2015) Chondrosarcoma of the temporomandibular joint: a case report and review of the literature. Cranio 29:1–9
Omani G (2016) TMJ imaging: bridging the gap. J Oral Maxillofac Surg 74(9):1711. doi:10.1016/j.joms.2016.04.034
Paesani D, Salas E, Martinez A, Isberg A (1999) Prevalence of temporomandibular joint disk displacement in infants and young children. Oral Surg Oral Med Oral Pathol Oral Radiol Endod 87:15–19
Pahwa S, Bhalla AS, Roychaudhary A, Bhutia O (2015) Multidetector computed tomography of temporomandibular joint: a road less travelled. World J Clin Cases 3:442–449
Parks KS, Song HC, Cho SG, Kang SR, Kim J, Jun HM et al (2016) Open-mouth bone scintigraphy is better than closed-mouth bone scintigraphy in the diagnosis of temporomandibular osteoarthritis. Nucl Med Mol Imaging 50:213–218
Peacock ZS, Vakilian P, Caruso P, Resnick CM, Vangel M, Kaban LB (2016) Quantifying synovial enhancement of the pediatric temporomandibular joint. J Oral Maxillofac Surg 74:1937–1945
Peck CC, Goulet JP, Lobbezoo F, Schiffman EL, Alstergren P, Anderson GC et al (2014) Expanding the taxonomy of the diagnostic criteria for temporomandibular disorders. J Oral Rehabil 41:2–23
Petty R, Southwood T, Manners P, Baum J, Glass D, Goldenberg J et al (2004) International league of associations for rheumatology classification of juvenile idiopathic arthritis: second revision, Edmonton, 2001. J Rheumatol 31:390–392
Peyron JG, Altman RD (1992) The epidemiology of osteoarthritis. In: Moskowitz RW, Howell DS, Goldberg VM, Mankin HJ (eds) Osteoarthritis: diagnosis and medical/ surgical management, 2nd edn. Saunders, Philadelphia, pp 15–37
Pianosi K, Rigby M, Hart R, Trites J, Taylor SM (2016) Pigmented villonodular synovitis of the temporomandibular joint: a unique presentation. Plast Reconstr Surg Glob Open 4(4):e674. doi:10.1097/GOX.0000000000000658
Rao VM, Liem MD, Farole A, Razek AA (1993) Elusive "stuck" disk in the temporomandibular joint: diagnosis with MR imaging. Radiology 189:823–827
Resnick D (1988) Common disorders of synovium-lined joints: pathogenesis, imaging abnormalities, and complications. AJR Am J Roentgenol 151:1079–1093
Resnick CM, Vakilian PM, Breen M, Zurakowski D, Caruso P, Henderson L et al (2016) Quantifying temporomandibular joint synovitis in children with juvenile idiopathic arthritis. Arthritis Care Res (Hoboken). doi:10.1002/acr.22911
Sano T, Westesson P-L, Larheim TA, Takagi R (2000) The association of temporomandibular joint pain with abnormal bone marrow in the mandibular condyle. J Oral Maxillofac Surg 58:254–257
Saurenmann RK, Kellenberger CJ (2015) Assessing arthritis in the temporomandibular joint. J Rheumatol 42:2000–2002
Sawada K, Schulze D, Matsumoto K, Hirai S, Hashimoto K, Honda K (2015) Osteochondroma of the coronoid process of the mandible. J Oral Sci 57:389–392
Schellhas KP, Wilkes CH (1989) Temporomandibular joint inflammation: comparison of MR fast scanning with T1-and T2-weighted imaging techniques. AJR Am J Roentgenol 153:93–98
Schellhas KP, Wilkes CH, Fritts HM, Omlie MR, Lagrotteria LB (1989) MR of osteochondritis dissecans and avascular necrosis of the mandibular condyle. AJR Am J Roentgenol 152:551–560
Schiffman E, Orbach R (2016) Executive summary of the diagnostic criteria for temporomandibular disorders for clinical and research applications. J Am Dent Assoc 147:438–445
Schiffman E, Orbach R, Truelove E, Look J, Anderson G, Goulet JP et al (2014) International RDC/TMD consortium network, international association for dental research; orofacial pain special interest group, international association for the study of pain. Diagnostic criteria for temporomandibular disorders (DC/TMD) for clinical and research applications: recommendations of the international RDC/TMD consortium network and orofacial pain special interest group. J Oral Facial Pain Headache 28:6–27
Schiffman EL, Ahmad M, Hollender L, Kartha K, Ohrbach R, Truelove EL, et al (2016) Longitudinal stability of common TMJ structural disorders. J Dent Res pii:0022034516679396
Smith HJ, Larheim TA, Aspestrand F (1992) Rheumatic and nonrheumatic disease in the temporomandibular joint: gadolinium-enhanced MR imaging. Radiology 185:229–234
Sokoloff L (1980) The pathology of osteoarthrosis and the role of aging. In: Nuki G (ed) The etiopathogenesis of osteoarthrosis. Pitman Medical, London, pp 1–15
Steen MW, Hofstede DJ (2015) Ganglion and synovial cyst of the temporomandibular joint: a case report and literature review. Plast Reconstr Surg Glob Open 3(9):e524. doi:10.1097/GOX0000000000000494
Stegenga B, de Bont LG, Boering G, Van Willigen JD (1991) Tissue responses to degenerative changes in the temporomandibular joint: a review. J Oral Maxillofac Surg 49:1079–1088

Su N, Poon R, Friedman L, Darling M, Grushka M (2015) TMJ changes in adolescent TMD patients seen on MRI in clinical setting. N Y State Dent J 81:27–30

Sweet DE, Madewell JE (1988) Pathogenesis of osteonecrosis. In: Resnick D, Niwayama G (eds) Diagnosis of bone and joint disorders. Saunders, Philadelphia, p 3188

Tasaki MM, Westesson P-L (1993) Temporomandibular joint: diagnostic accuracy with sagittal and coronal MR imaging. Radiology 186:723–729

Tasaki MM, Westesson P-L, Isberg AM, Ren Y-F, Tallents RH (1996) Classification and prevalence of temporomandibular joint disk displacement in patients and symptom-free volunteers. Am J Orthod Dentofac Orthop 109:249–262

Tsiklakis K, Syriopoulos K, Stamatakis HC (2004) Radiographic examination of the temporomandibular joint using cone beam computed tomography. Dentomaxillofac Radiol 33:196–201

Vogl TJ, Lauer HC, Lehnert T, Naguib NN, Ottl P, Filmann N et al (2016) The value of MRI in patients with temporomandibular joint dysfunction: correlation of MRI and clinical findings. Eur J Radiol 85:714–719

Wahaj A, Hafeez K, Zafar MS (2016) Association of bone marrow edema with temporomandibular joint (TMJ) osteoarthritis and internal derangements. Cranio 8:1–6

Westesson P-L, Brooks SL (1992) Temporomandibular joint: relationship between MR evidence of effusion and the presence of pain and disk displacement. AJR Am J Roentgenol 159:559–563

Westesson P-L, Larheim TA, Tanaka H (1998) Posterior disc displacement in the temporomandibular joint. J Oral Maxillofac Surg 56:1266–1273

Westesson P-L, Yamamoto M, Sano T, Okano T (2003) Temporomandibular joint. In: Som PM, Curtin HD (eds) Head and neck imaging, 4th edn. Mosby, St. Louis, pp 995–1053

Wilkes CH (1989) Internal derangements of the temporomandibular joint. Pathological variations. Arch Otolaryngol Head Neck Surg 115:469–477

Woo MH, Yoon KH, Park KS, Park JA (2016) Post-traumatic bifid mandibular condyle: a case report and literature review. Imaging Sci Dent 46:217–222

Wu VW, Lam YN (2016) Radiation-induced temporomandibular joint disorder in post-radiotherapy nasopharyngeal carcinoma patients: assessment and treatment. J Med Radiat Sci 63:124–132

Xie Q, Yang C, He D, Cai X, Ma Z, Shen Y (2016) Will unilateral temporomandibular joint anterior disc displacement in teenagers lead to asymmetry of condyle and mandible? A longitudinal study. J Craniomaxillofac Surg 44:590–596

Yamamoto M, Sano T, Okano T (2003) Magnetic resonance evidence of joint fluid with temporomandibular joint disorders. J Comput Assist Tomogr 27:694–698

Yura S, Harada S, Kobayashi K (2015) Diagnostic accuracy on magnetic resonance imaging for the diagnosis of osteoarthritis of the temporomandibular joint. J Clin Diagn Res 9:95–97

Zheng ZW, Yang C, Wang MH, Zhu XH, Fang YM (2016) Non-joint effusion is associated with osteoarthritis in temporomandibular joints with disk displacement. J Craniomaxillofac Surg 44:1–5

Zhuo Z, Cai X, Xie Q (2015) Is anterior disc displacement without reduction associated with temporomandibular joint condylar height in juvenile patients younger than 20 years? J Oral Maxillofac Surg 73:843–849

Teeth and Dental Implants

7

Abstract

This chapter illustrates mandibular wisdom tooth anatomy/pathology and relationship to the mandibular canal, maxillary lateral incisor anatomy and relationship to neighboring teeth, apical periodontitis and periodontal disease, preoperative and postoperative implant imaging, and imaging of implant complications.

7.1 Introduction

Intraoral or panoramic radiography is the mainstay of imaging teeth and surrounding structures such as lamina dura and alveolar bone. However, advanced imaging in particular CT may be a supplementary diagnostic tool in selected cases. With multidetector CT scanners, virtually any desired high-quality section may be obtained.

In this short chapter, we present patients to illustrate the potential of CT for imaging dentoalveolar structures, with focus on the mandibular wisdom tooth and the maxillary canine, impaction, pathology, and relation to neighboring structures. Also the diagnostic value of CT for assessing periodontal and disease is illustrated.

CT has in particular proved valuable in the evaluation of the dental implant patient, to measure edentulous alveolar process dimensions preoperatively. Dental CT reformatting programs have been available since the late 1980s. Also complications to dental implant treatment may be visualized by CT. Patient dose can be significantly lowered when imaging dentoalveolar hard tissues by lowering mAs, compared to the standard maxillofacial CT.

In recent years cone beam computed tomography (CBCT) scanners have become increasingly more available. They have replaced conventional CT scanners for dentoalveolar diagnostics (see Chap. 15).

7.2 Tooth Anatomy, Tooth Pathology, and Adjacent Structures

Figs. 7.1, 7.2, 7.3, 7.4, 7.5, 7.6, 7.7, 7.8, 7.9, and 7.10.

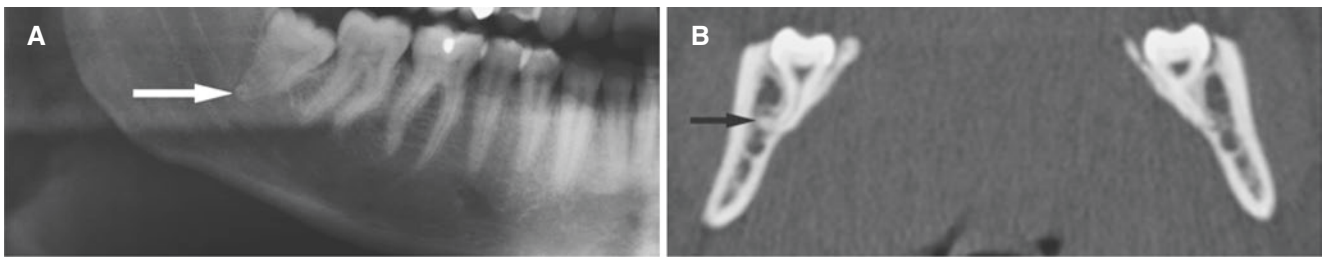

Fig. 7.1 Impacted wisdom tooth anatomy, mandible; 20-year-old patient with clinical symptoms of third molar pericoronitis. (**A**) Panoramic view shows apparently smooth (uncomplicated) root complex of impacted tooth, but note apex anatomy (*arrow*). (**B**) CT image parallel to long axis of wisdom tooth (similar as shown in Fig. 7.2C) demonstrates a 90° angulation of root in buccal direction (*arrow*)

In collaboration with N. Kakimoto.

T.A. Larheim, P.-L.A. Westesson, *Maxillofacial Imaging*, https://doi.org/10.1007/978-3-319-53319-3_7

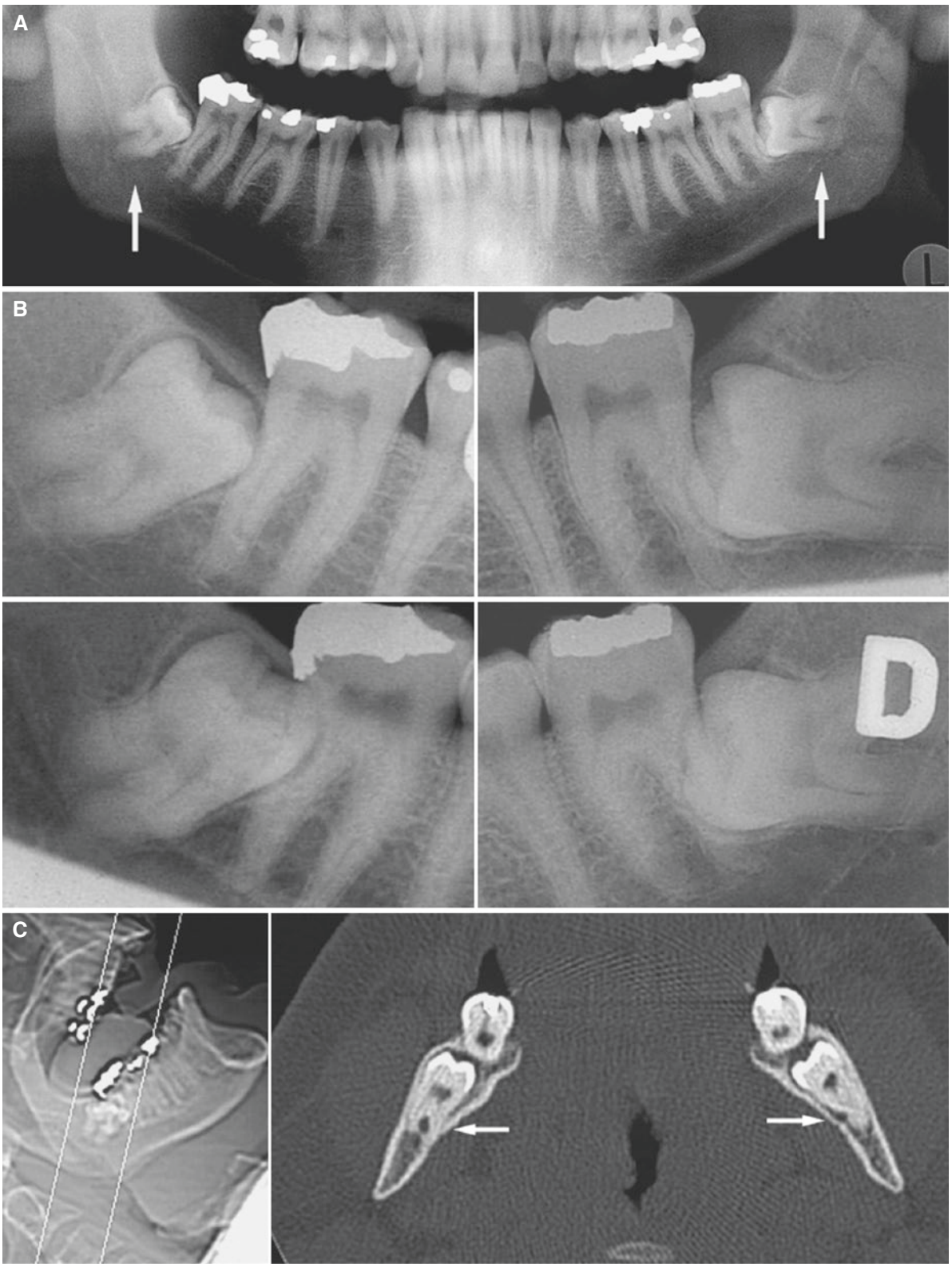

Fig. 7.2 Impacted wisdom tooth and mandibular canal relationship; 28-year-old patient with impacted, asymptomatic third molars. (**A**) Panoramic view suggests possible intimate relationship between impacted tooth and mandibular canal bilaterally (*arrows*) that needs to be assessed before surgery. (**B**) Intraoral views (tube-shift technique, buccal object rule) indicate intimate relationship between the tooth and canal bilaterally, but no conclusion with regard to exact canal location can be made. (**C**) Coronal CT image (radiation direction and field shown with *cursor lines* in scout view, open mouth) demonstrates that mandibular canal penetrates right wisdom tooth root and makes a lingual groove in left wisdom tooth root (*arrows*)

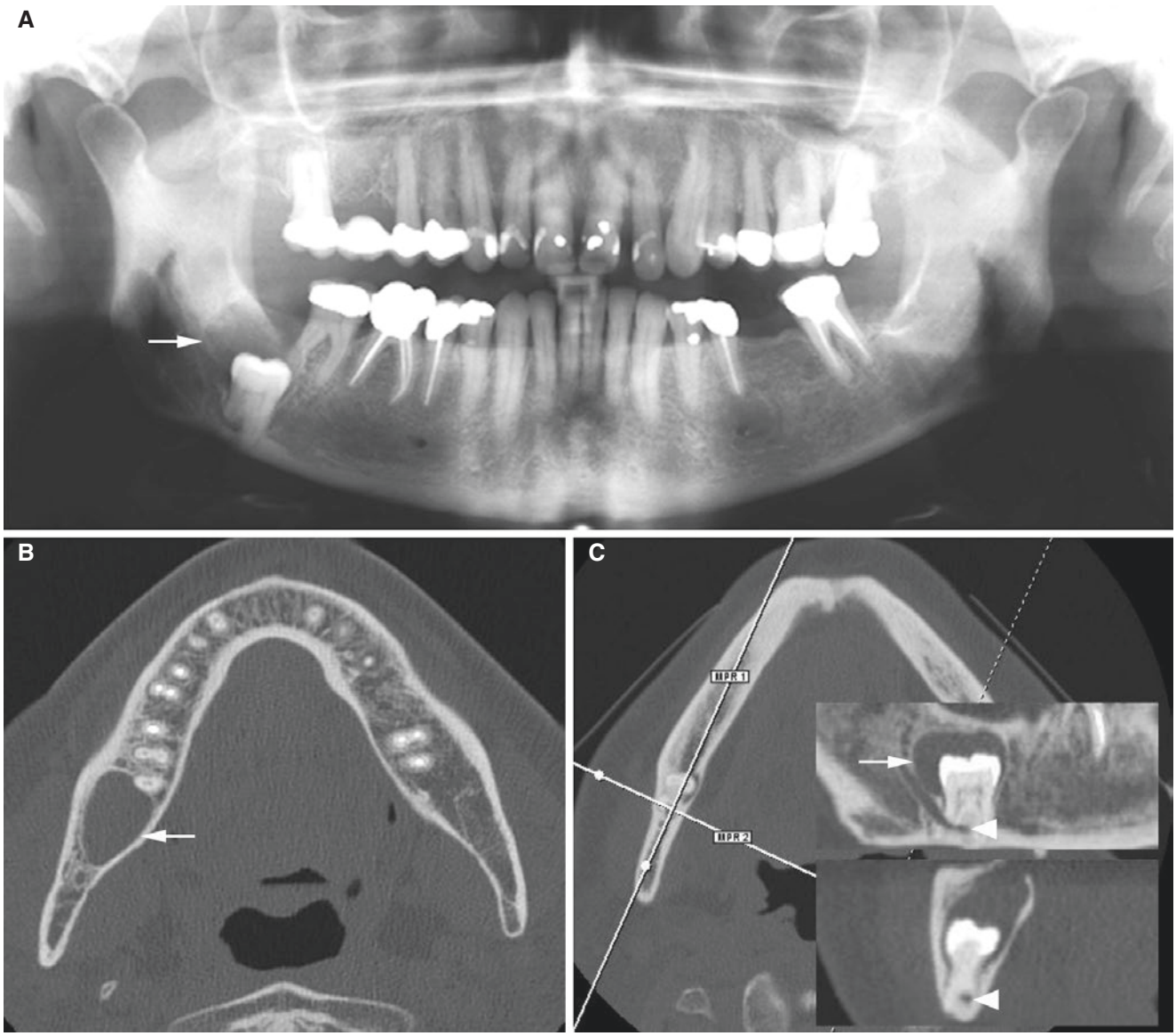

Fig. 7.3 Impacted wisdom tooth, follicular cyst, mandible; 58-year-old patient with incidental finding. (**A**) Panoramic view shows wisdom tooth in right mandible with pericoronal radiolucency (*arrow*). (**B**) Axial CT image shows radiolucency with no or minimal buccal or lingual expansion (*arrow*) and no root resorption. (**C**) Axial (with *cursor lines*), oblique sagittal (*upper*), and oblique coronal (*lower*) CT images confirm pericoronal radiolucency from enamel-cementum margin to enamel-cementum margin (*arrow*) consistent with follicular (dentigerous) cyst. Note mandibular canal penetrating wisdom tooth root (*arrowhead*)

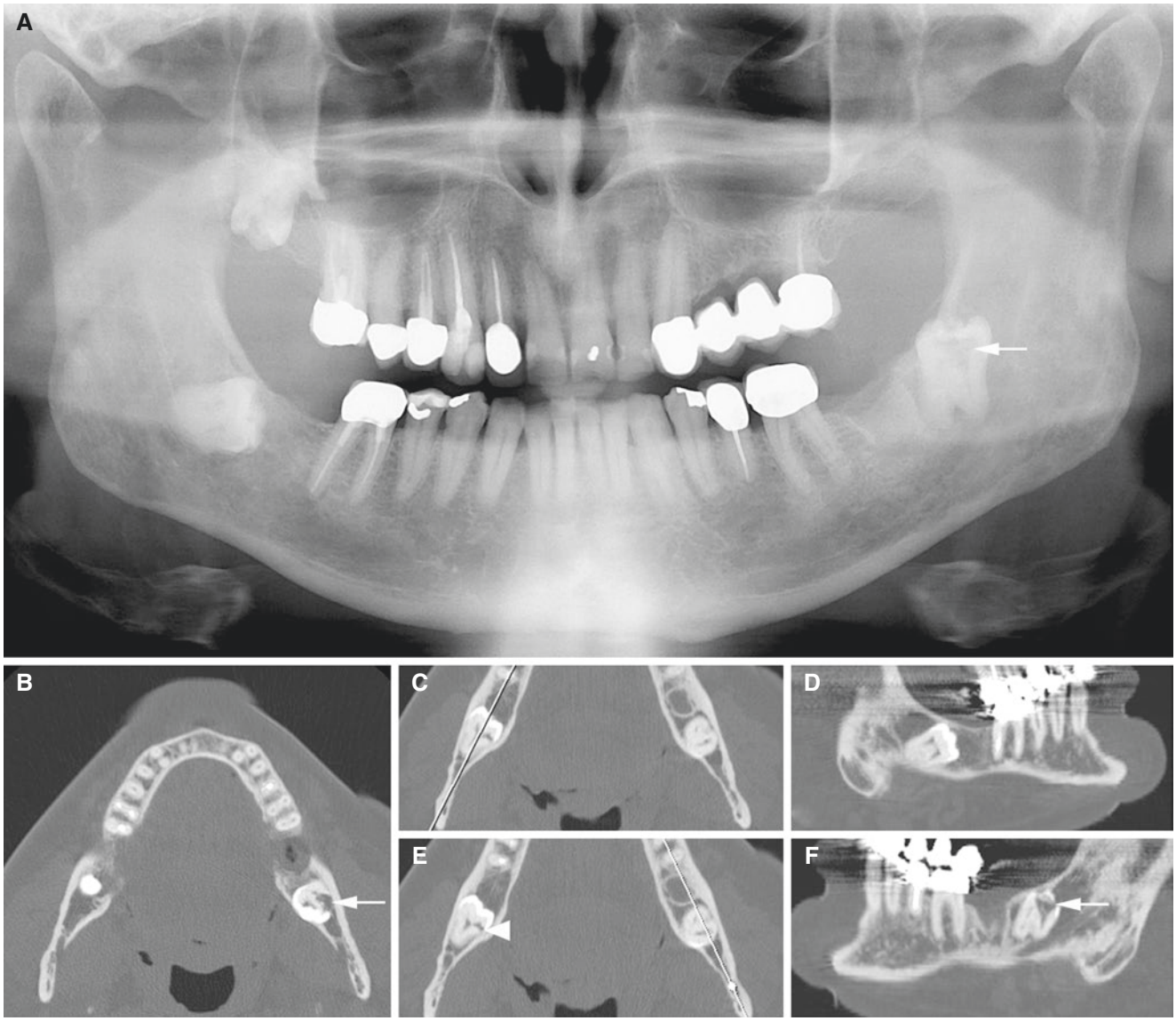

Fig. 7.4 Impacted wisdom teeth, crown resorption, mandible; 73-year-old male without symptoms. (**A**) Panoramic view shows impacted wisdom teeth in the mandible and maxilla and crown resorption (*arrow*). (**B**) Axial, (**C**, **E**) axial (with *cursor lines*), and (**D**, **F**) oblique sagittal CT images of the right (**D**) and left (**F**) mandible show crown resorption of the left (*arrow*) and right (*arrowhead*) wisdom tooth

Fig. 7.5 Impacted wisdom tooth, crown resorption, mandible; 70-year-old female without symptoms. Panoramic view shows resorption of almost the entire crown of wisdom tooth in the left mandible (*arrow*)

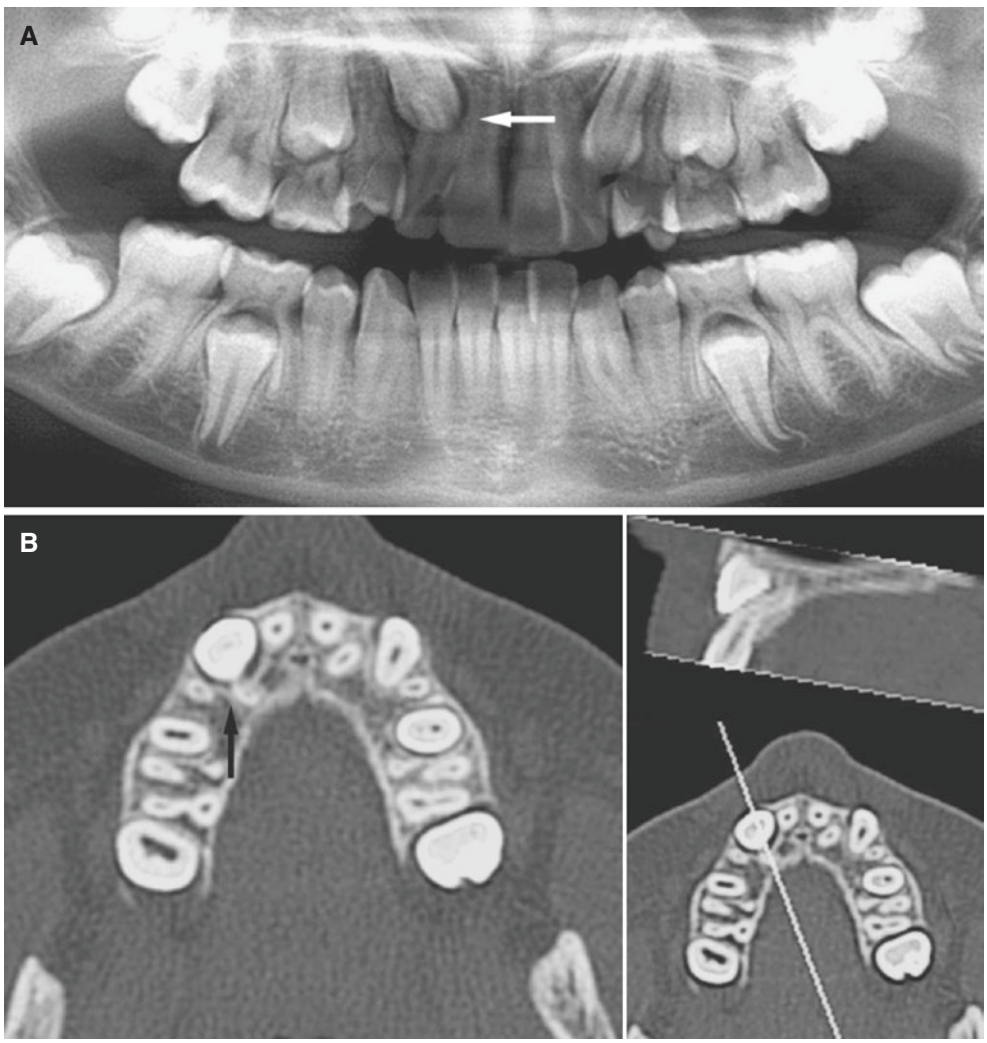

Fig. 7.6 Lateral incisor curved root anatomy and relation to erupting canine; 10-year-old patient. (**A**) Panoramic view suggests close relationship between lateral incisor root and erupting canine (*arrow*). (**B**) Axial CT image with oblique sagittal section (*upper right*) according to cursor line in reference image (*lower right*) demonstrates close relationship between lateral incisor and buccally erupting canine (*arrow*) but no injury to incisor root

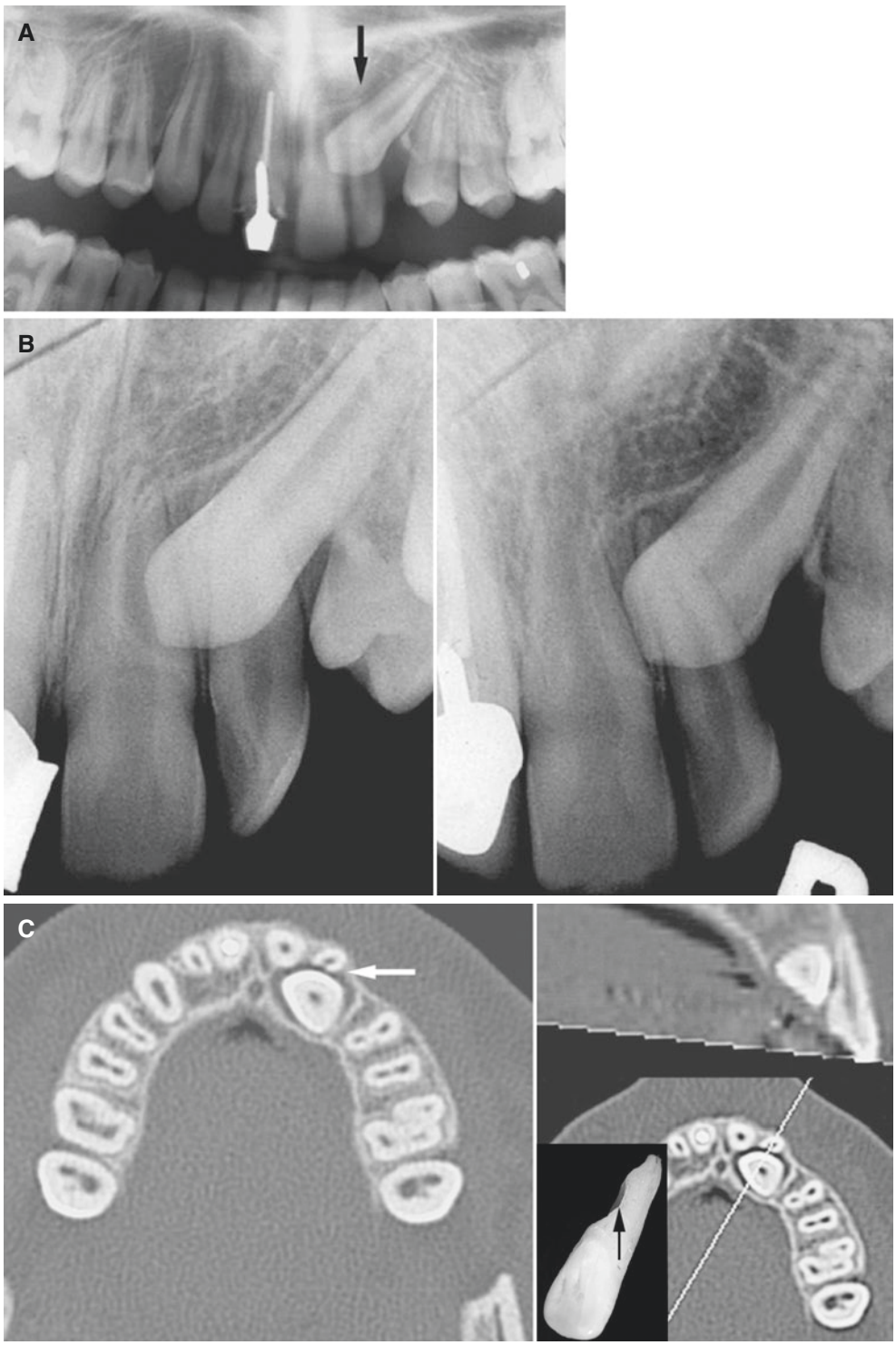

Fig. 7.7 Lateral incisor resorption due to impacted canine; 16-year-old patient with previous injury to central incisor, with subsequent endodontic therapy. (**A**) Panoramic view shows that relationship between canine and lateral incisor (*arrow*) needs to be assessed before treatment, leading to removal of either impacted canine or lateral incisor. (**B**) Intraoral views (tube-shift technique) indicate no injury to lateral incisor root. (**C**) Axial CT image with oblique sagittal section (*upper right*) according to cursor line in reference image (*lower right*) demonstrates intimate relationship between lateral incisor and palatally erupting canine with evident resorption of incisor root (*arrow*). Colored photograph of extracted lateral incisor confirms root resorption (*arrow*)

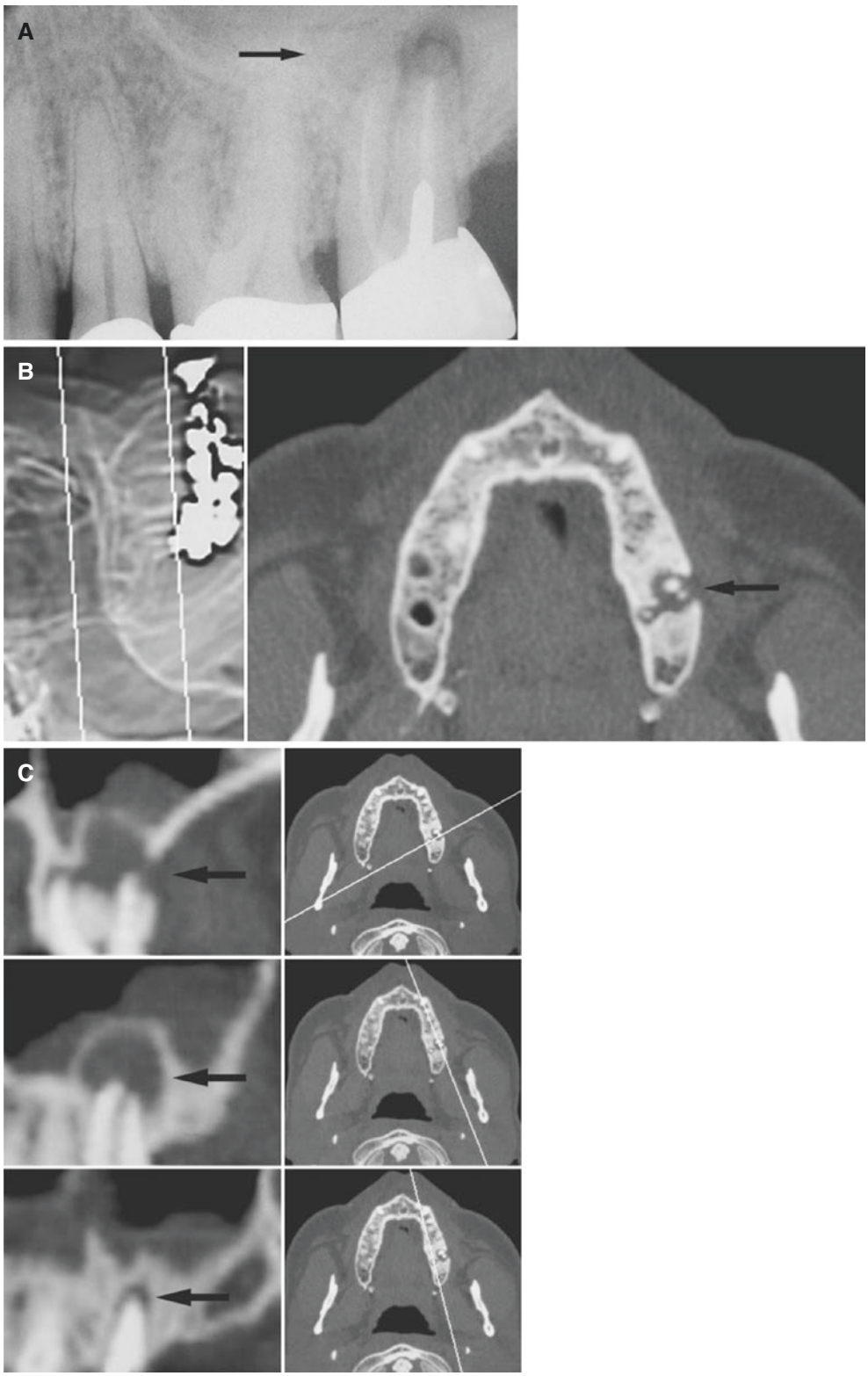

Fig. 7.8 Apical periodontitis; 50-year-old male with variable pain from the left maxilla. (**A**) Intraoral view shows apical radiolucency of the second molar, apparently only at palatal root (*arrow*). Involvement of different roots needs to be assessed to decide whether or not apicoectomy can be successfully performed. (**B**) Axial CT image (scout view with scanning direction and field to avoid amalgam artifacts from teeth) shows a larger radiolucency (*arrow*) at buccal roots than at palatal root of the second molar, with surrounding bone sclerosis. (**C**) Oblique coronal CT image (*upper row*) (according to cursor line in reference image) shows cystic process with destroyed buccal cortex (*arrow*). (**C**) Oblique sagittal CT image (*middle row*) (according to cursor line in reference image) shows cystic process with intact cortical outline (*arrow*). (**C**) Oblique sagittal CT image (*lower row*) (according to cursor line in reference image) shows small radiolucency (widened periodontal space) at palatal root (*arrow*), with surrounding sclerotic bone. Note some antral mucosal thickening

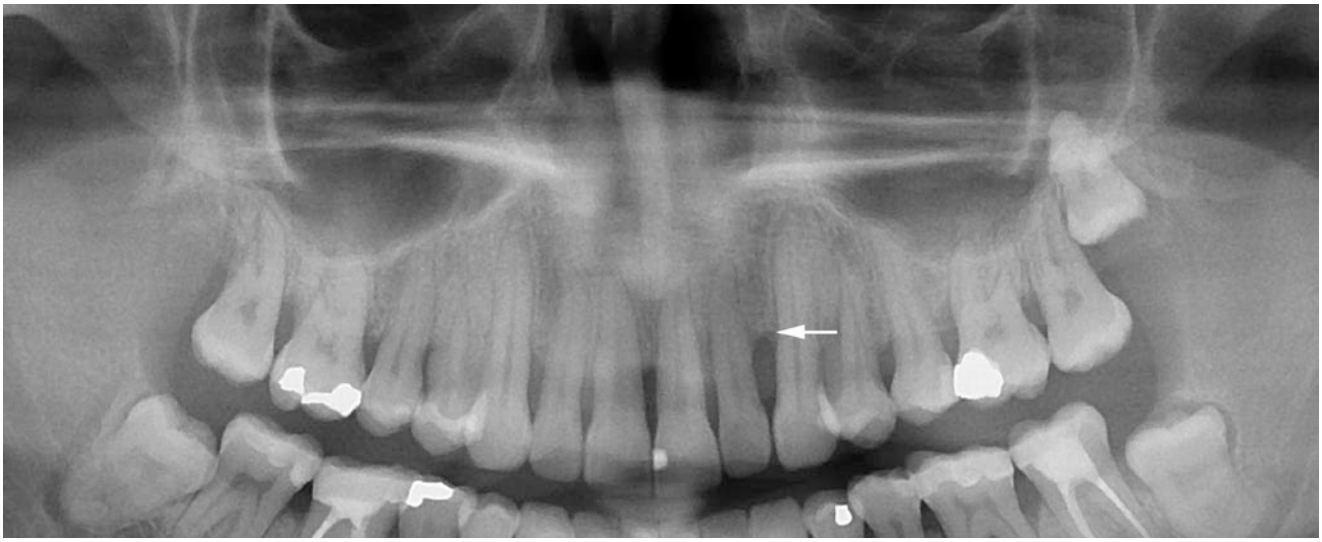

Fig. 7.9 Periodontal disease; 34-year-old female with bleeding gingiva. Panoramic view shows loss of periodontal bone support in the entire dentition, with more evident bone loss in some places such as between lateral incisor and canine in the left maxilla (*arrow*)

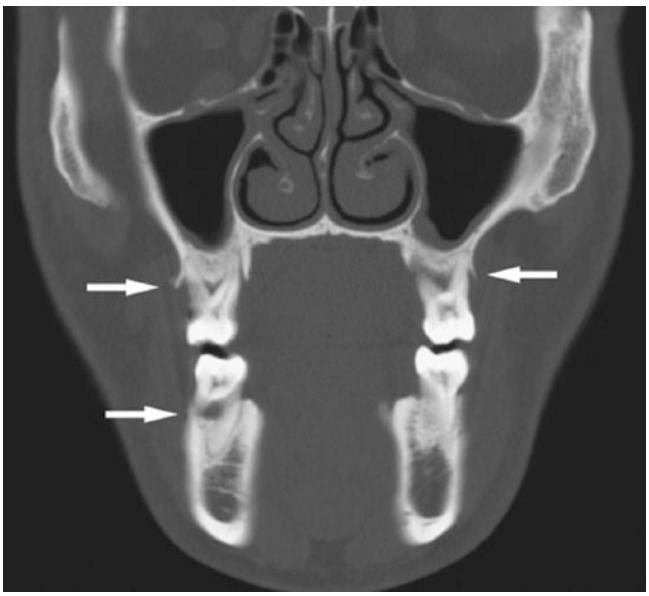

Fig. 7.10 Periodontal disease; 35-year-old male with incidental finding. Coronal CT image shows destruction of alveolar bone in the maxilla and mandible with loss of periodontal bone support in bifurcation of mandibular molar roots and trifurcation of maxillary molar roots (*arrows*); left maxillary molar has no remaining bone support of palatal "floating" root

7.3 Preoperative and Postoperative Implant Imaging

Figs. 7.11, 7.12, 7.13, 7.14, 7.15, and 7.16

– Single reformatted scans perpendicular to alveolar process

– Dental reformatting programs with multiple cross-sectional views perpendicular to the entire alveolar process and curved panoramic reconstructions "parallel" to alveolar process

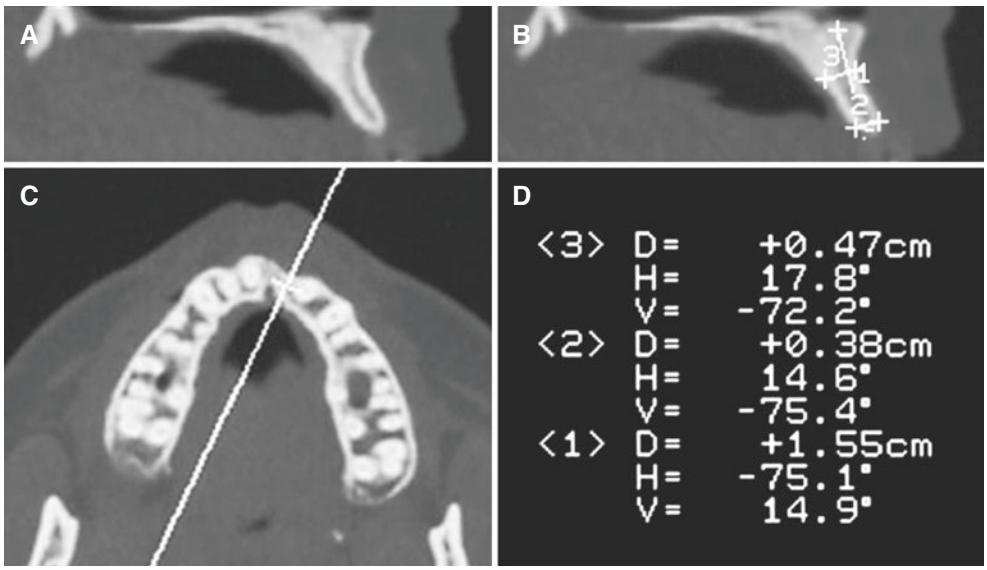

Fig. 7.11 Alveolar process examination before dental implant surgery; 20-year-old male with loss of incisor due to trauma many years previously. (**A**) Oblique sagittal CT image according to reference image (**C**). (**B**) Same image as in (**A**), with measures of distances. (**D**) Alveolar process dimensions (from **B**): height of alveolar process just above 15 mm, width of alveolar process from just below 4 to almost 5 mm

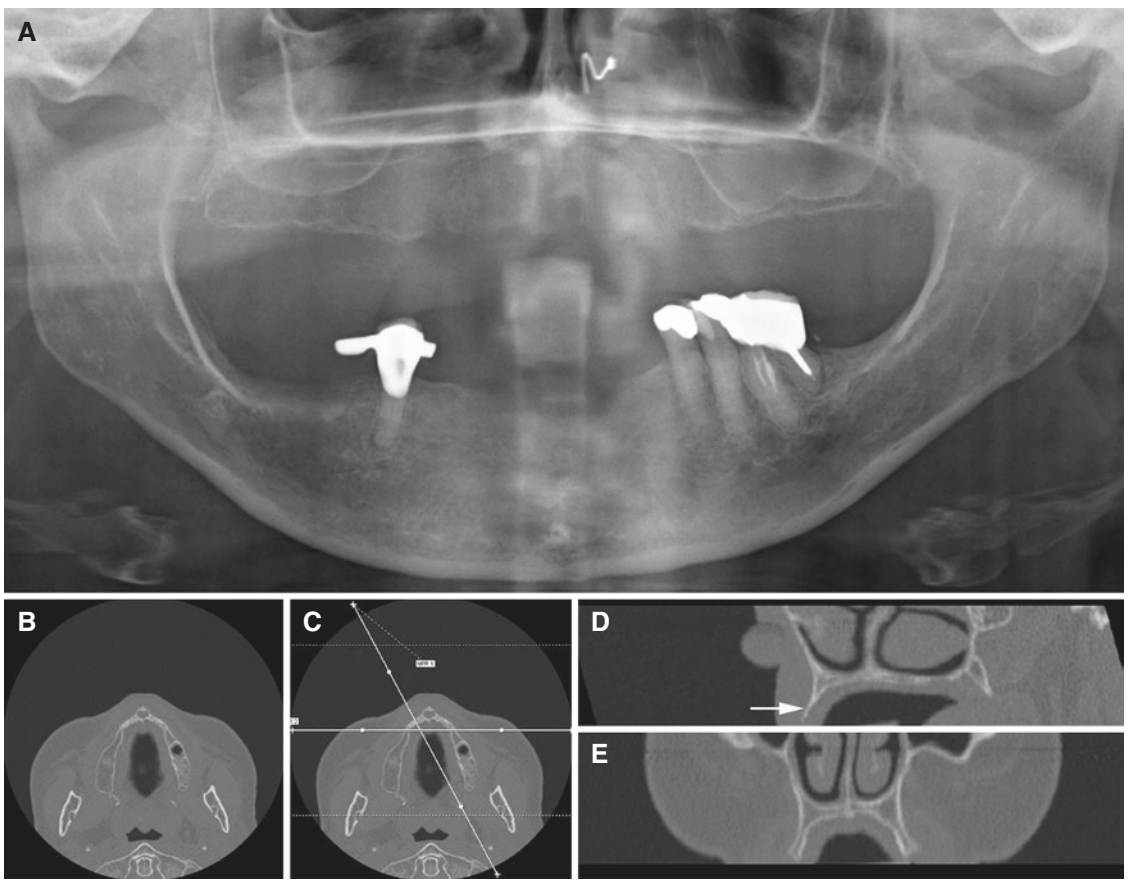

Fig. 7.12 Pre-implant evaluation of edentulous maxilla; 57-year-old female. (**A**) Panoramic view shows apparently good height of alveolar process in the maxilla for implant treatment. (**B**) Axial, (**C**) axial (with *cursor lines*), (**D**) oblique sagittal, and (**E**) coronal CT images show very thin alveolar process in bucco-palatal dimension (*arrow*). CT examination was made with only 20 mA exposure, giving a patient dose similar to a cone beam CT examination

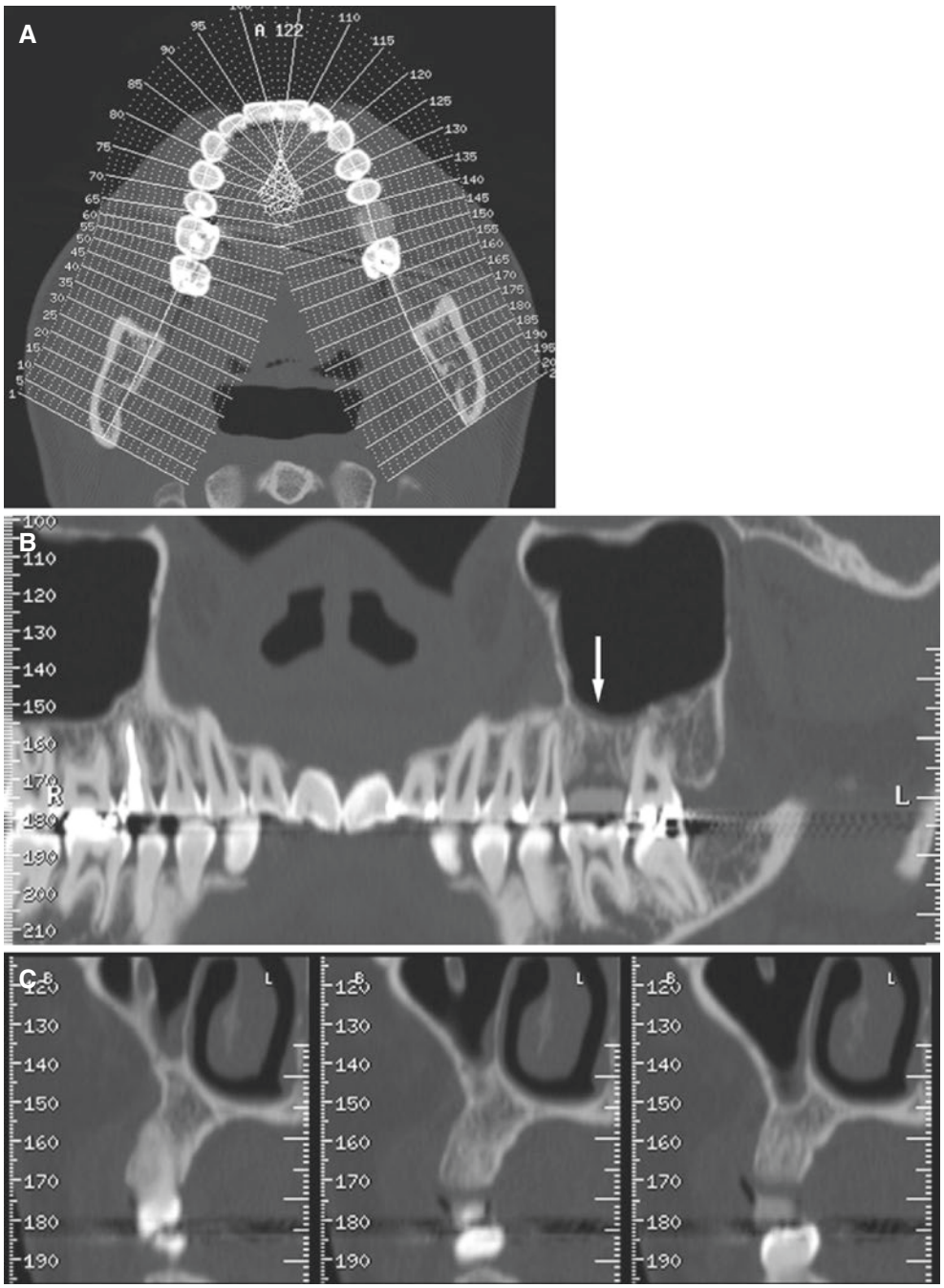

Fig. 7.13 Alveolar process examination before and after dental implant surgery; one-tooth implant. (**A**) Axial CT image with DentaScan program, preoperative. (**B**) Panoramic and (**C**) cross-sectional images show edentulous area of alveolar process (*arrow*) with acceptable height and width. (**D**) Axial CT image with DentaScan program, postoperative. (**E**) Panoramic and (**F**) cross-sectional images of alveolar process show implant (*arrow*) correctly placed

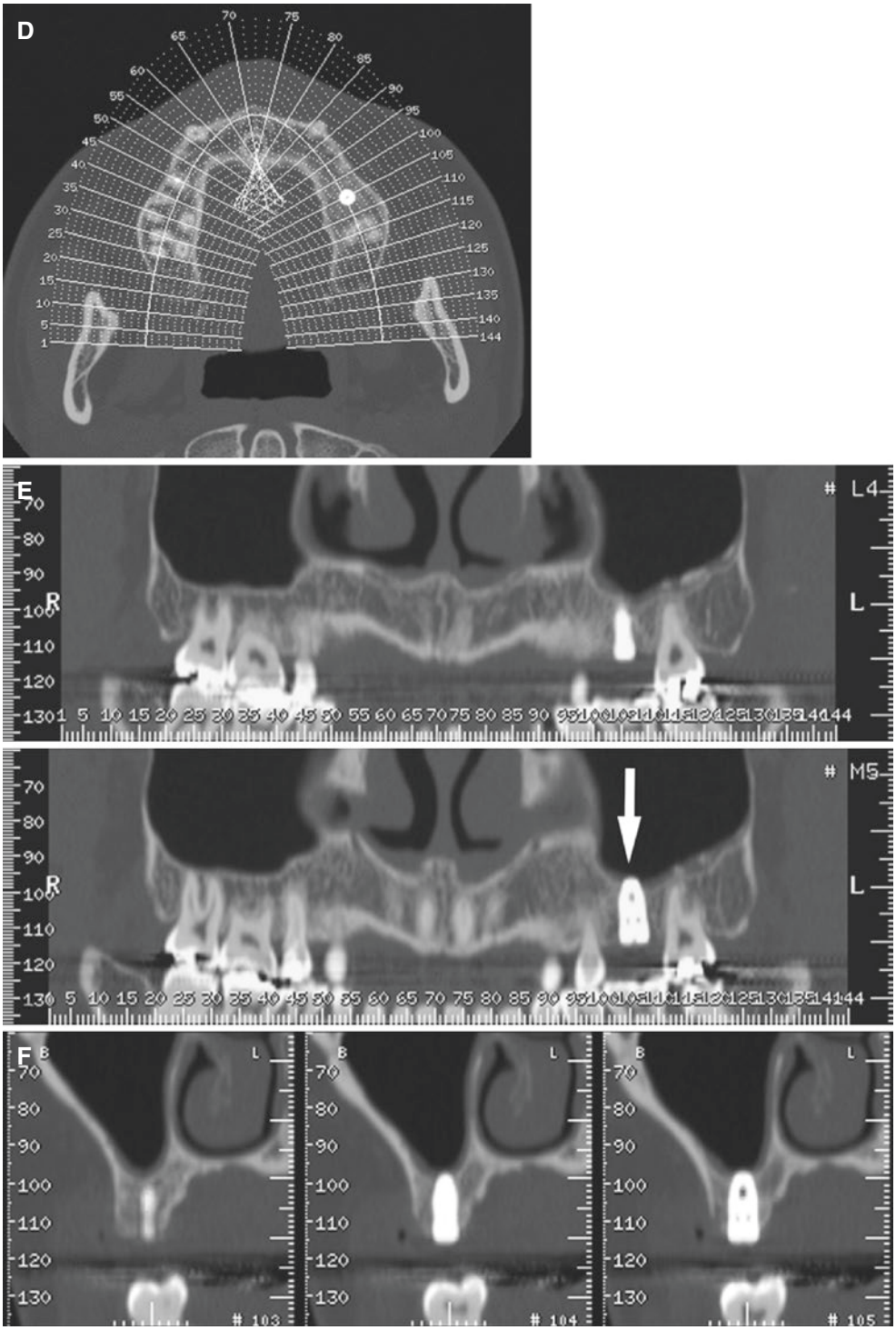

Fig. 7.13 (continued)

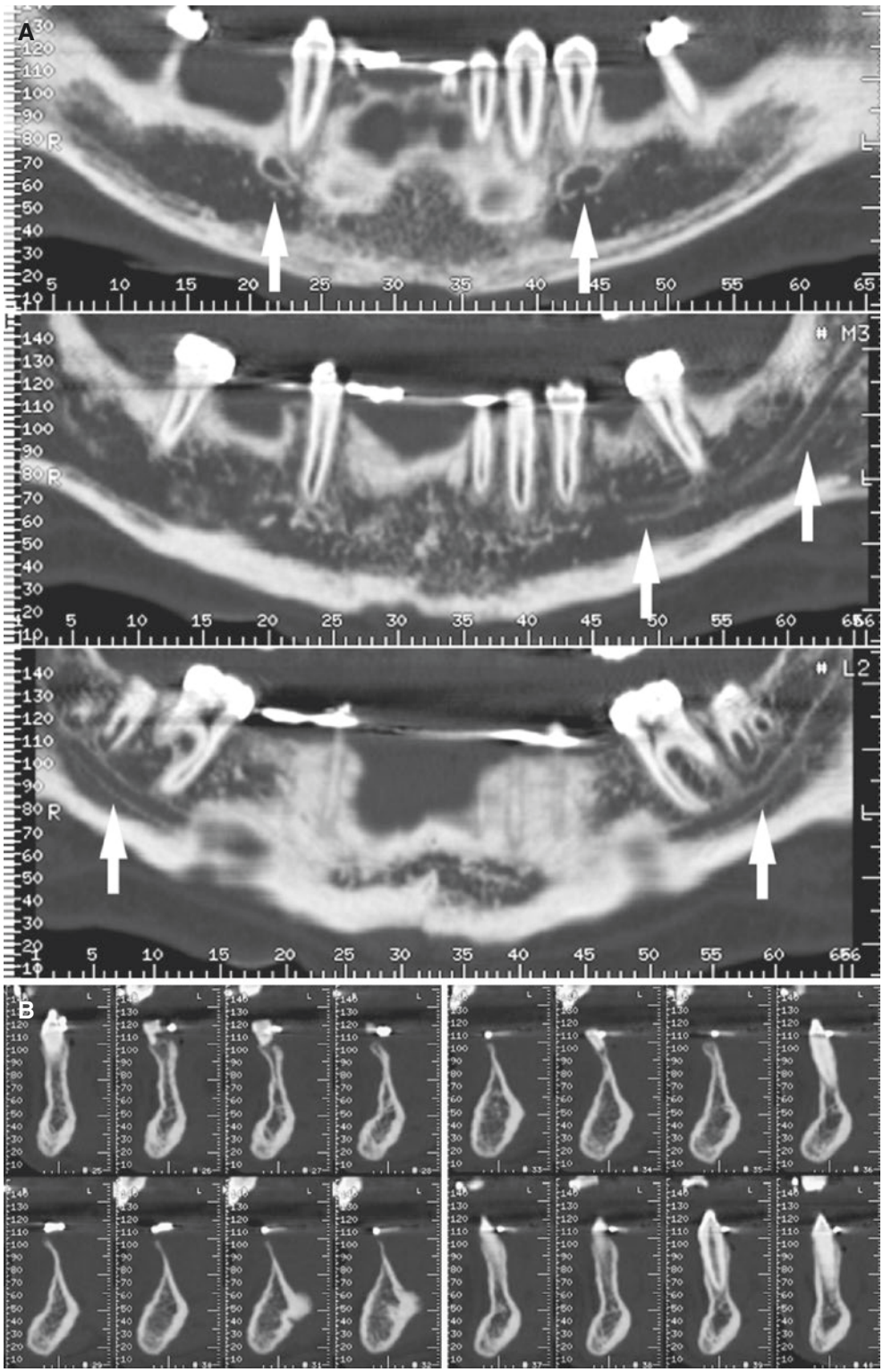

Fig. 7.14 Alveolar process examination before dental implant surgery; 15-year-old male with multiple agenesia. (**A**) Panoramic DentaScan reconstructions of the mandible show agenesia of three incisors and two premolars; note mandibular foramina (*arrows*) and mandibular canal (*arrows*). (**B**) Cross-sectional images perpendicular to alveolar process of the mandible (altogether 16 sections) show extremely thin edentulous alveolar process

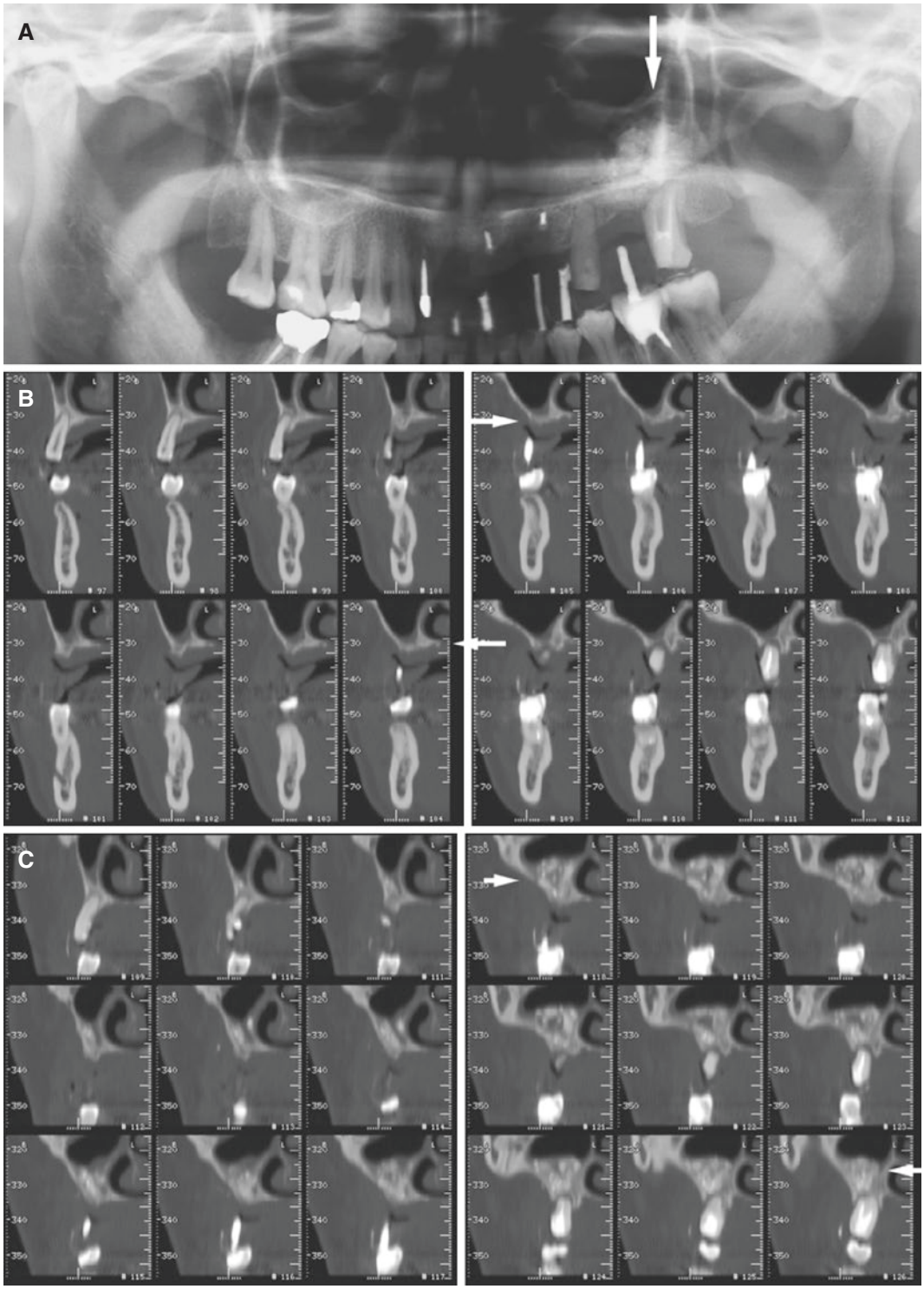

Fig. 7.15 Sinus lift, bone graft, artificial bone; 39-year-old female with one-tooth implant. (**A**) Panoramic view, postoperative, shows increased dimension of alveolar process in the maxilla with the bone from the patient's chin and artificial bone chips (*arrow*). (**B**) Preoperative cross-sectional DentaScan images of the left maxilla show that edentulous alveolar process is too small for implant placement (*arrows*). (**C**) Postoperative cross-sectional DentaScan images show that the new bone has increased alveolar process to an acceptable width (*arrows*)

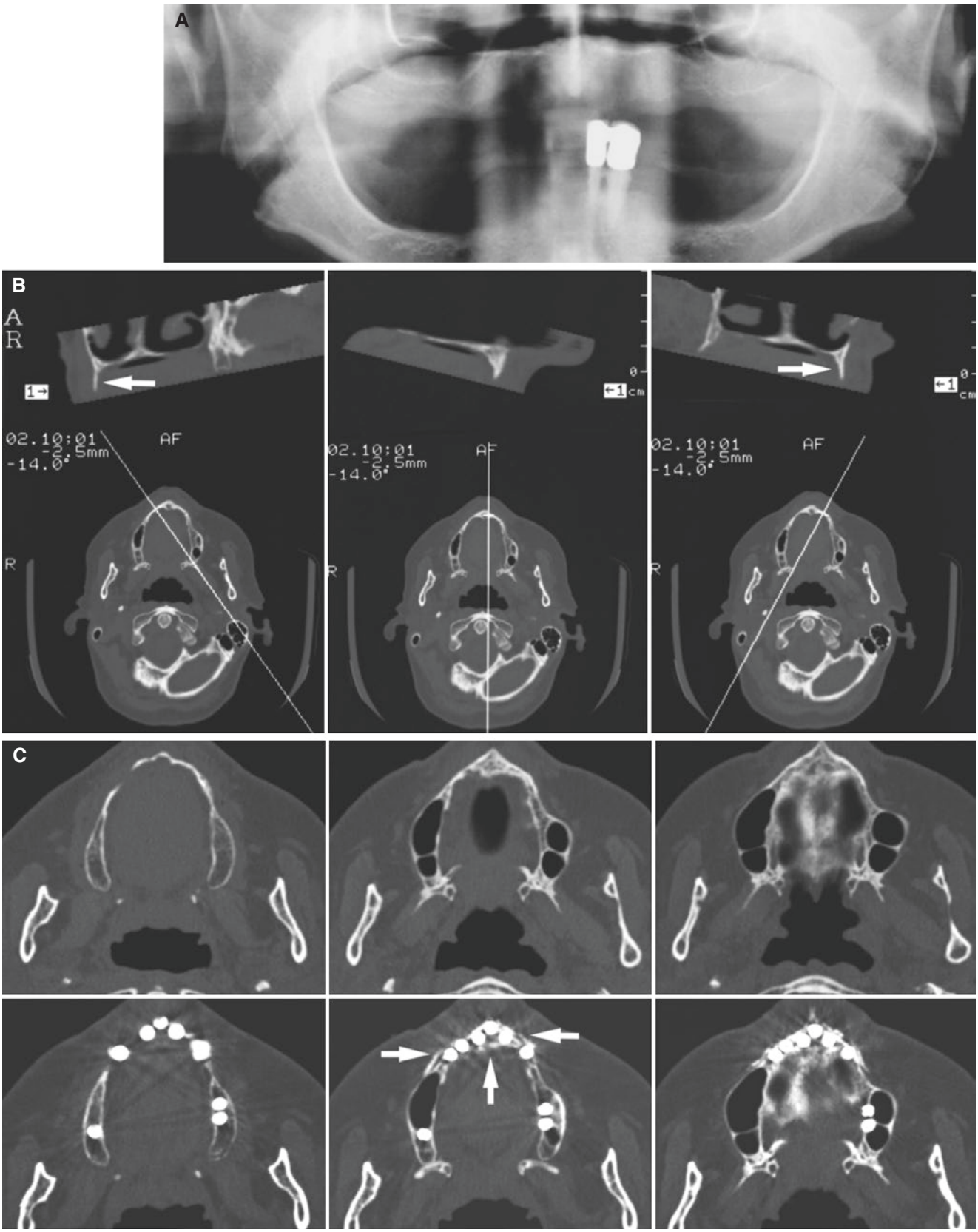

Fig. 7.16 Dental implant surgery with bone graft from the chin; 68-year-old female who could not accept her complete maxillary denture. (**A**) Panoramic view does not indicate that edentulous maxillary alveolar process is very thin. (**B**) Three CT sections perpendicular to maxillary alveolar process (according to *cursor lines* in reference images) show that alveolar process (*arrows*) is very thin (1–2 mm), but has acceptable height (about 10 mm). (**C**) Axial preoperative CT sections (*upper row*) and corresponding axial CT sections (*lower row*) after implant surgery with bone graft (*arrows*) taken from patient's chin

7.4 Imaging of Implant Complications

Figs. 7.17 and 7.18.

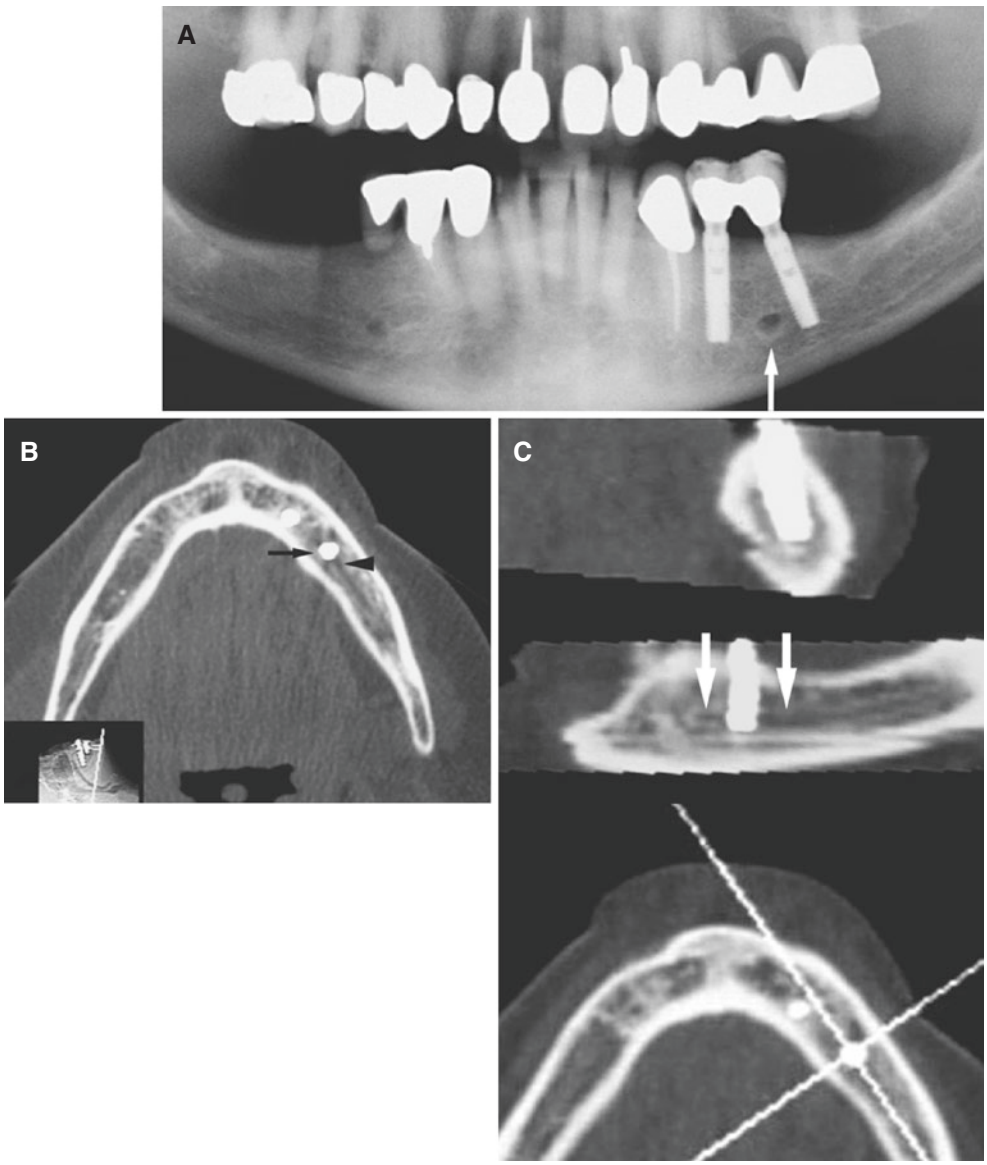

Fig. 7.17 Dental implant complication; 67-year-old female with mental nerve paresthesia after implant surgery. (**A**) Panoramic view indicates that the relationship between distal implant and mandibular canal needs to be further assessed (*arrow* mental foramen). (**B**) Axial CT image according to cursor line in reference image shows that implant (*arrow*) is located just in the area of mandibular canal (*arrowhead*). (**C**) Oblique coronal (*upper*) and oblique sagittal (*middle*) CT images according to *cursor lines* in reference image (*lower*) show that implant is located in mandibular canal (*arrows*)

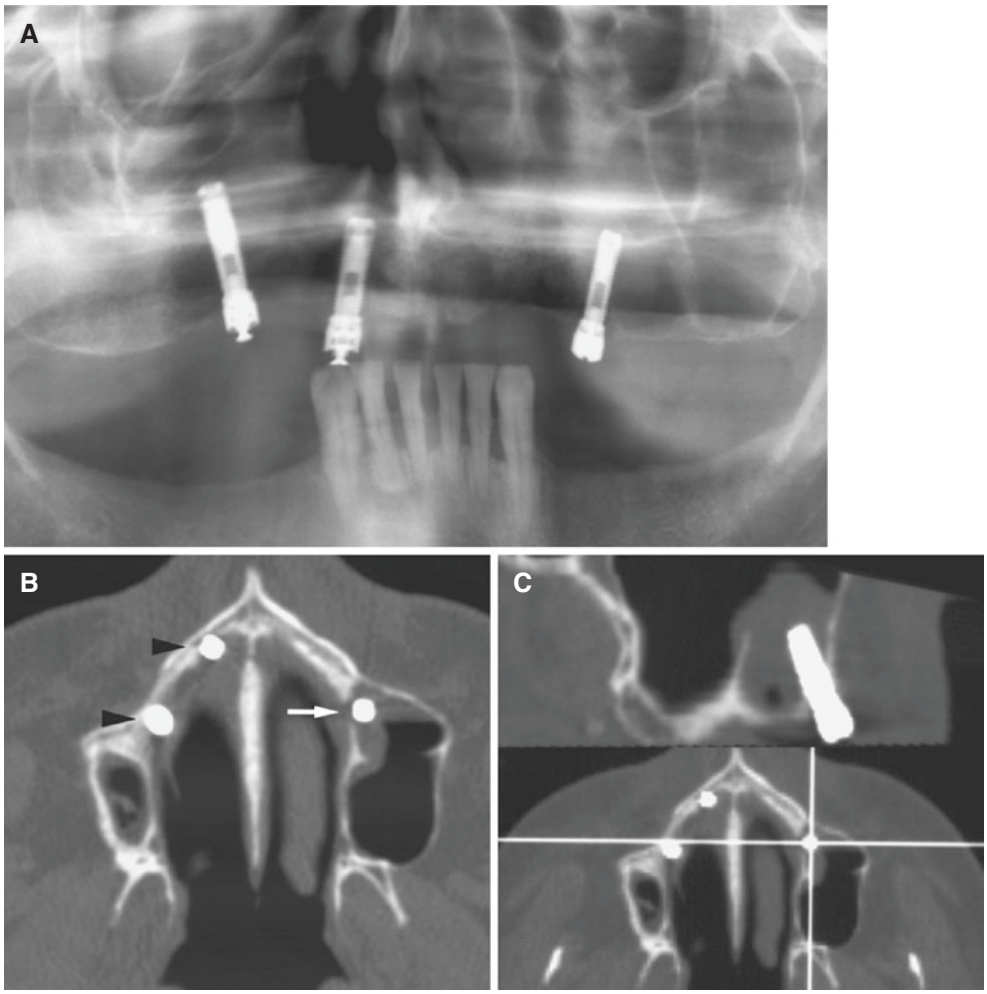

Fig. 7.18 Dental implant complication; 45-year-old male with pain and implants that would not heal adequately (three implants already lost). (**A**) Panoramic view shows apparently normal bone conditions around three remaining implants, but reliable evaluation is impossible. (**B**) Axial CT image shows two implants located in the nasal cavity (*arrowheads*) and one implant located in the maxillary sinus with resorption of medial sinus wall (*arrow*). Note very small maxillary sinus on the right side. (**C**) Sagittal CT image (*upper)*, according to cursor line in reference image (*lower*), shows implant in the maxillary sinus with no bone support other than the sinus wall and some mucosal thickening around the implant

Suggested Reading

Abrahams JJ, Hayt MW, Rock R (2003) Dental CT reformatting programs and dental imaging. In: Som PM, Curtin HD (eds) Head and neck imaging, 4th edn. Mosby, St. Louis, pp 907–918

Cohnen M, Kemper J, Mobes O, Pawelzik J, Modder U (2002) Radiation dose in dental radiology. Eur Radiol 12:634–637

Ericson S, Kurol J (2000a) Incisor root resorptions due to ectopic maxillary canines imaged by computerized tomography: a comparative study in extracted teeth. Angle Orthod 70:276–283

Ericson S, Kurol PJ (2000b) Resorption of incisors after ectopic eruption of maxillary canines: a CT study. Angle Orthod 70:415–423

Germain L (2015) Tooth resorption: the "black hole" of dentistry. Dent Today 34:78, 80, 82–83

Heiland M, Schulze D, Adam G, Schmelzle R (2003) 3D-imaging of the facial skeleton with an isocentric mobile C-arm system (Siremobil Iso-C3D). Dentomaxillofac Radiol 32:21–25

Linsenmaier U, Rock C, Euler E, Wirth S, Brandl R, Kotsianos D, Mutschler W, Pfeifer KJ (2002) Three-dimensional CT with a modified C-arm image intensifier: feasibility. Radiology 224:286–292

Ning R, Kruger RA (1988) Computer simulation of image intensifier-based computed tomography detector: vascular application. Med Phys 15:188–192

Ritman EL, Kinsey JH, Robb RA, Gilbert BK, Harris LD, Wood EH (1980) Three-dimensional imaging of heart, lungs, and circulation. Science 210:273–280

Rothman SL, Chaftez N, Rhodes ML, Schwarz MS (1988) CT in the preoperative assessment of the mandible and maxilla for endosseous implant surgery. Work in progress. Radiology 168: 171–175

Schulze D, Heiland M, Thurmann H, Adam G (2004) Radiation exposure during midfacial imaging using 4- and 16-slice computed tomography, cone beam computed tomography systems and conventional radiography. Dentomaxillofac Radiol 33:83–86

Vannier MW, Hildebolt CF, Conover G, Knapp RH, Yokoyama-Crothers N, Wang G (1997) Three-dimensional dental imaging by spiral CT. A progress report. Oral Surg Oral Med Oral Pathol Oral Radiol Endod 84:561–570

Zohrabian VM, Abrahams JJ (2015) Inflammatory diseases of the teeth and jaws. Semin Ultrasound CT MR 36:434–443

Facial Traumas and Fractures

8

Abstract

This chapter illustrates non-fracture trauma, mandibular fracture, mandibular fracture combined with other fractures, complications of mandibular fracture, nasal fracture, and midfacial fractures; isolated maxillary wall fracture, LeFort fractures, tripod fracture, and blowout fracture.

8.1 Introduction

The main objective of imaging patients with traumas to the face is to detect fractures. CT is the superior imaging modality to assess bone structures, and routinely the examination will include axial thin section CT with coronal and sagittal reformatted images. With multidetector CT, high-quality images can be obtained in any desired plane and 3D reconstruction can be very valuable in the evaluation of the complex facial skeleton. Although some detail is lost as part of the smoothing algorithm, the 3D images will visualize the fracture segments and their relationship to one another better than different series of 2D images. In the present chapter we have a main focus on mandibular traumas and fractures.

If clinical examination indicates that only the mandible is injured in a minor trauma, a panoramic view with a supplementary posteroanterior view of the mandible and/or intraoral/occlusal views may be sufficient. However, it has been reported that coronal CT alone is more accurate than panoramic radiography alone for diagnosing mandibular condyle fractures. Thus, CT is increasingly used to assess also mandibular fractures.

Tooth fractures are in most cases adequately evaluated with intraoral radiography, but cone beam CT is increasingly used for dento-alveolar traumas. However, dental traumatology is beyond the scope of this chapter. In general, radiographic examination of any suspected fracture should be in at least two planes, preferably perpendicular to each other.

The diagnosis of facial fractures usually is accomplished by a combination of clinical and imaging examinations.

8.2 Non-fracture Traumas

Figs. 8.1, 8.2, 8.3, 8.4, and 8.5

8.2.1 Definition

Minor and/or blunt and/or low-velocity traumas not leading to fracture.

8.2.2 Clinical Features

- Pain
- Dental occlusion does not fit
- Abnormal jaw mobility, usually restricted (trismus)
- Soft-tissue injury
- Hematoma, epistaxis, edema
- Mandibular luxation

T.A. Larheim, P.-L.A. Westesson, *Maxillofacial Imaging*, https://doi.org/10.1007/978-3-319-53319-3_8

8.2.3 Imaging Features

- Mandibular condyle displaced anteriorly in fossa at closed mouth (probably due to joint effusion; may be seen on MRI)
- Restricted condyle translation
- Articular disc displacement
- Paranasal sinus opacification or fluid-air level or dome-shaped blood clot
- Soft-tissue swelling (subcutaneous hematoma, edema)
- Foreign body

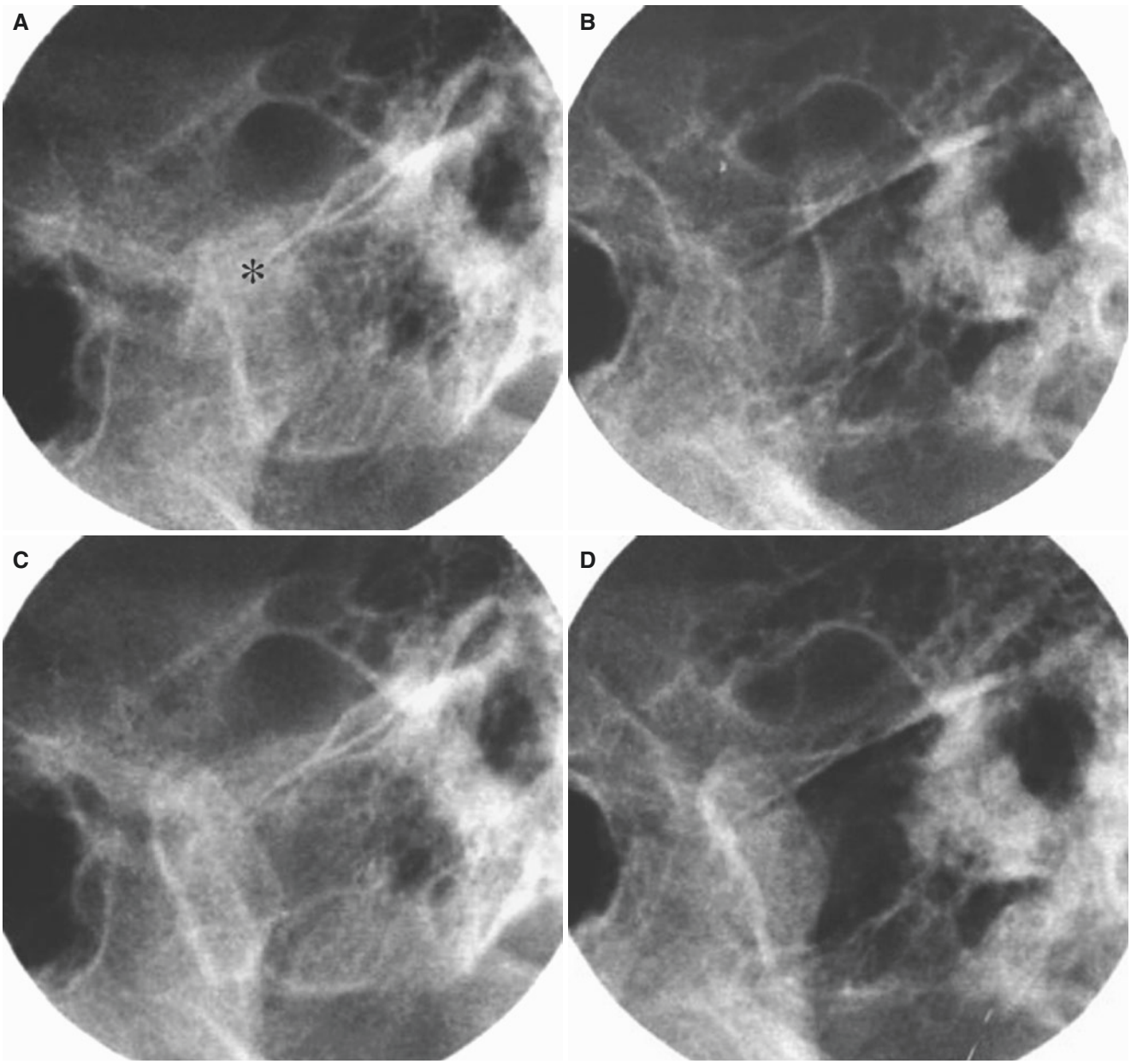

Fig. 8.1 Non-fracture trauma to the mandible; 14-year-old male with trauma to the chin due to bicycle accident and problems with mouth opening and dental occlusion. (**A**, **B**) Conventional (lateral transcranial) TMJ radiography at closed mouth shows abnormal position of condyle (*asterisk*) in fossa of the right joint (**A**) and wide joint space in the left joint (**B**). (**C**, **D**) Open-mouth images show restricted condylar translation of the right (**C**) and left (**D**) joint (at this age condyles usually move clearly in front of eminences)

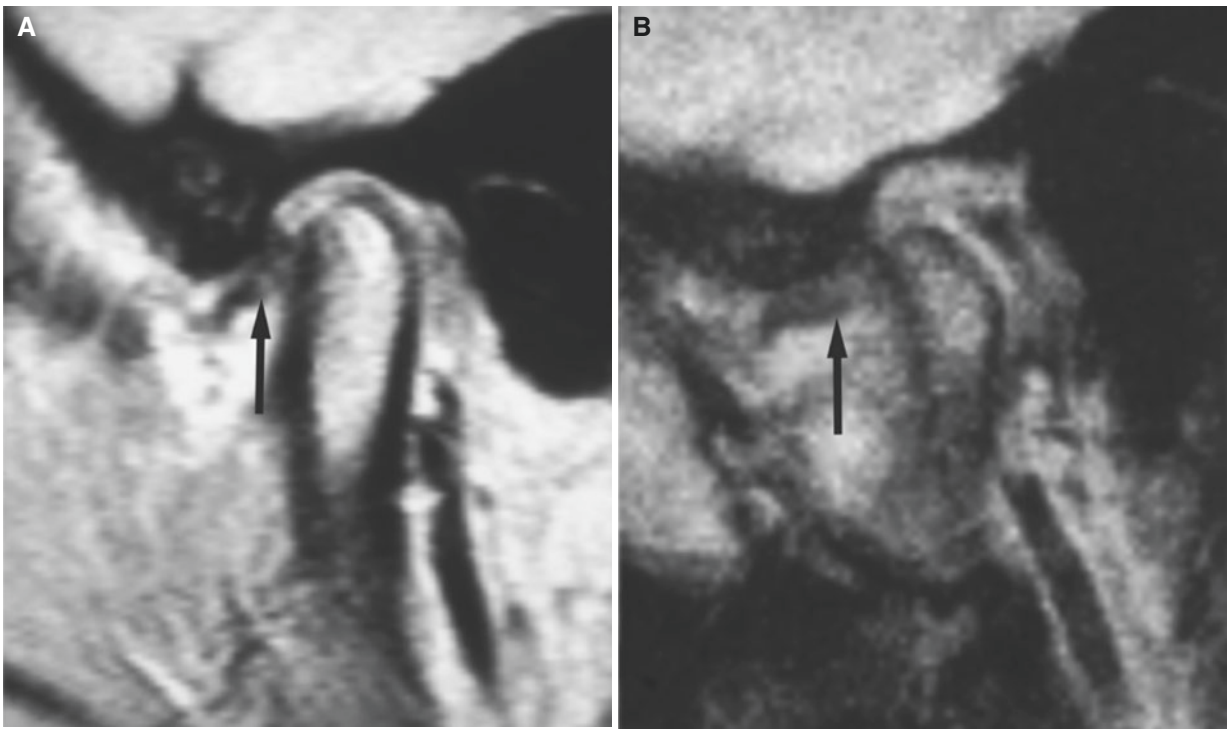

Fig. 8.2 Non-fracture trauma to the mandible; 20-year-old female with trauma to the chin 2 months previously, still with pain and limited mouth-opening capacity without joint sound; before trauma she had a clicking jaw but no pain or mouth-opening problem (no fractures were found after thorough examinations). (**A**, **B**) Oblique sagittal TMJ MRI shows anteriorly displaced disc (*arrow*) both at closed (**A**) and at open mouth (**B**) and restricted condyle translation

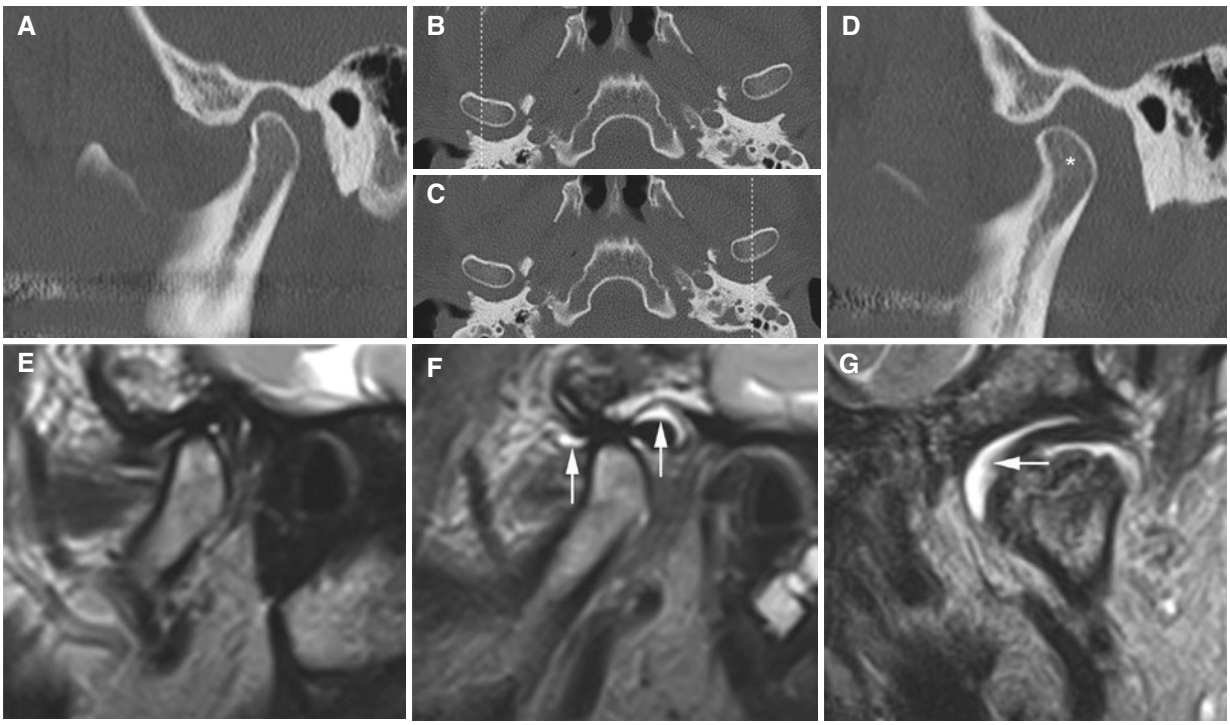

Fig. 8.3 Non-fracture trauma to the mandible; 63-year-old male with mouth-opening and dental occlusion problems. (**A**) Oblique sagittal, (**B**, **C**) axial (with *cursor line*), and (**D**) oblique sagittal CT images of the right (**A**, **B**) and left (**C**, **D**) joint show normal bone contours but the left condyle (*asterisk*) displaced in fossa. (**E**) Oblique sagittal (right), (**F**) oblique sagittal (left), and (**G**) oblique coronal (left) T2-weighted MRI show normal disc position in both joints and displaced condyle and joint effusion (*arrows*) in the left joint. Possibly marrow edema in both condyles. After a couple of weeks, dental occlusion, condyle position, and mouth-opening capacity normalized

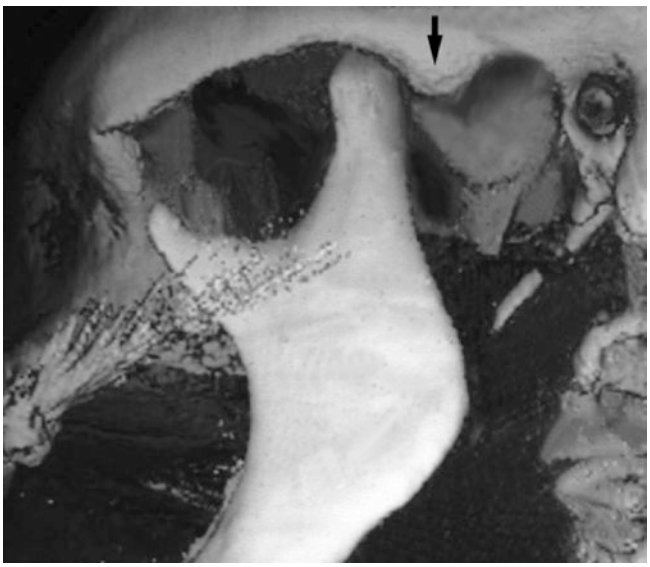

Fig. 8.4 Non-fracture trauma to the mandible; patient with jaw luxation. 3D CT image shows condyle in front of eminence (*arrow*), also on contralateral side (not shown) (courtesy of Dr. A. Kolbenstvedt, Oslo University Hospital, Rikshospitalet, Oslo, Norway)

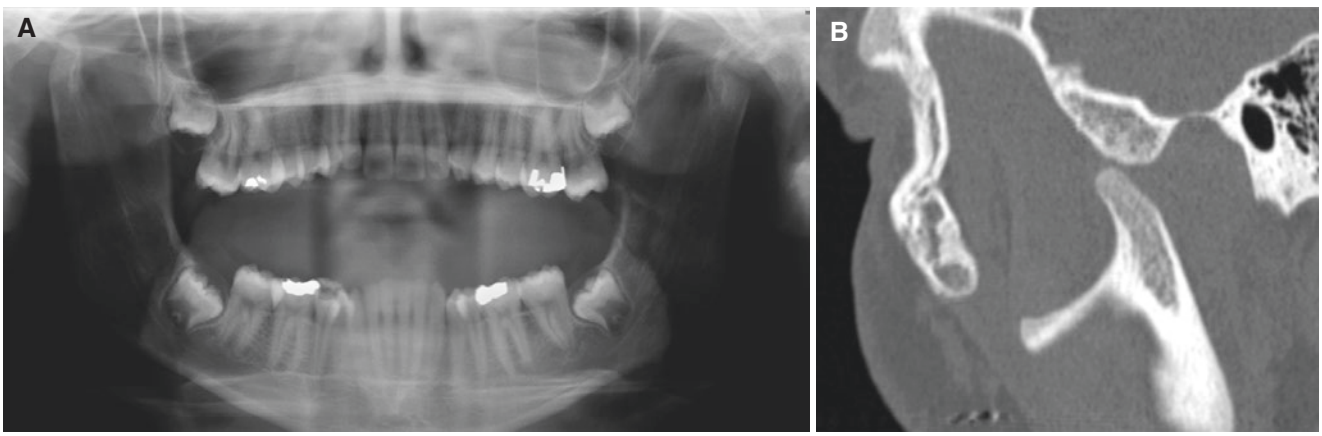

Fig. 8.5 Non-fracture trauma to the mandible; patient with jaw luxation. (**A**) Panoramic view and (**B**) oblique sagittal CT image show condyle in front of eminence

8.3 Fractures

8.3.1 Definition

Traumatic cortical discontinuity with or without dislocation.

8.3.2 Clinical Features

- See Non-fracture Traumas
- Abnormal morphology such as flattening
- Palpable step-off of the bone
- Crepitation due to emphysema
- Paresthesia, anesthesia
- Hemorrhage

8.3.3 Imaging Features

- See Non-fracture Traumas
- Cortical discontinuity, defect
- Abnormal angulation
- Absent or displaced bone
- Abnormal linear density
- Bone overlap ("double radiopacity")
- Greenstick in young patients
- "Empty fossa" sign on axial CT images
- Localized air collection

8.4 Mandibular Fractures

Figs. 8.6, 8.7, 8.8, 8.9, 8.10, 8.11, 8.12, 8.13, and 8.14

8.4.1 Clinical Features

- See Fractures
- Most common fractures in facial skeleton after nasal fractures
- Unilateral mandibular body fracture reported as most frequent mandibular fracture in oral and maxillofacial surgery practice
- The most common site of mandibular body fracture is junction of the body and ramus, followed by molar region
- Mandibular condyle fractures constitute up to about one-half of mandibular fractures and affect all age groups; reported as the most frequent mandibular fracture in children
- More than one fracture of mandible common; typically, mandibular body fracture on one side and mandibular neck/condyle fracture on contralateral side; almost half of patients with condyle fractures have mandibular body fractures
- In one study of condyle fractures, interpersonal violence was the most frequent cause
- Symphyseal and coronoid process area uncommon sites, but in one series with interpersonal violence as a frequent cause, symphyseal fractures were the second most common to mandibular angle fractures
- Assault reported to be a more frequent cause than motor vehicle accident, falls, and sports, but assault also reported equally frequent to motor vehicle accident
- Males clearly more frequent than females

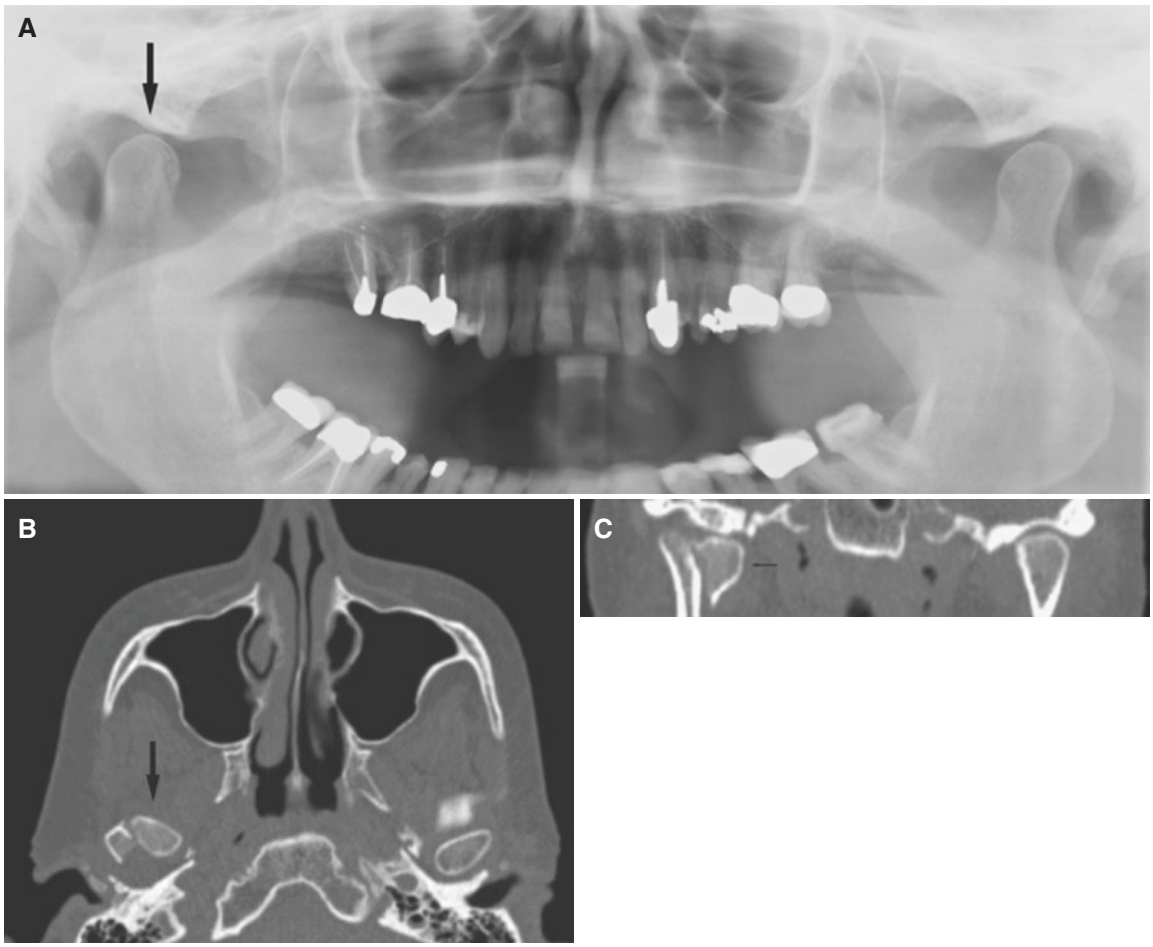

Fig. 8.6 Mandibular condyle fracture, unilateral; 48-year-old female 2 weeks after trauma to the mandible, now with dental occlusion problems and pain from the right TMJ on mouth opening. (**A**) Panoramic view (open mouth) shows intracapsular fracture of the right condyle, apparently without dislocation (*arrow*). (**B**) Axial CT image shows fragment of condyle slightly dislocated medially (*arrow*). (**C**) Coronal CT image shows intracapsular fracture with some dislocation of fragment (*arrow*)

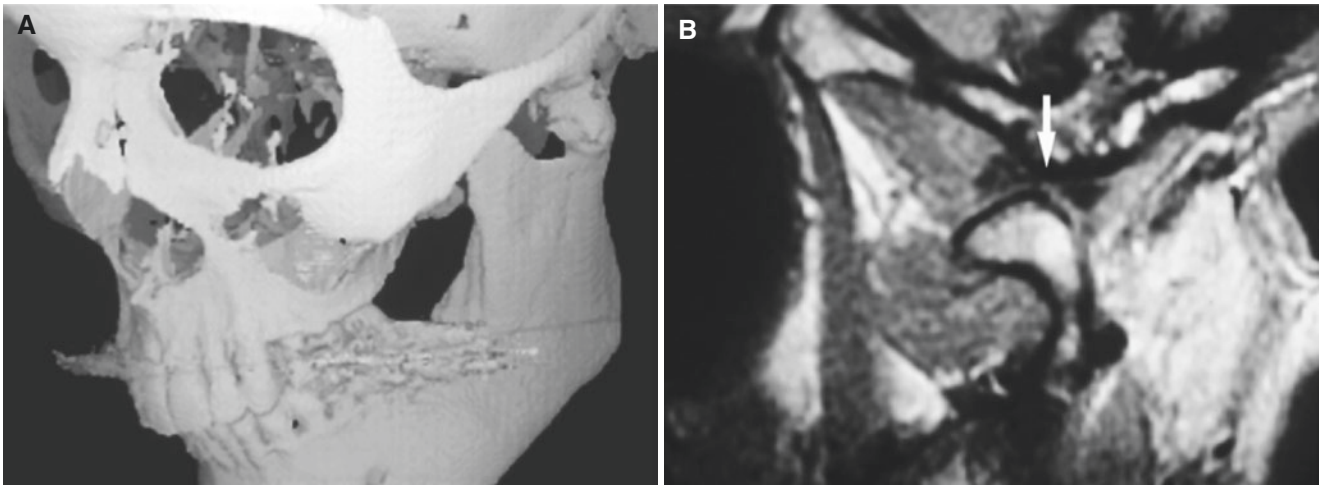

Fig. 8.7 Mandibular neck fracture, unilateral, several years old, and healed without symptoms or signs. (**A**) 3D CT image shows satisfactory dental occlusion. (**B**) MRI of TMJ shows mandibular condyle healed in open-mouth position at closed mouth, apparently with normal disc in normal position (*arrow*)

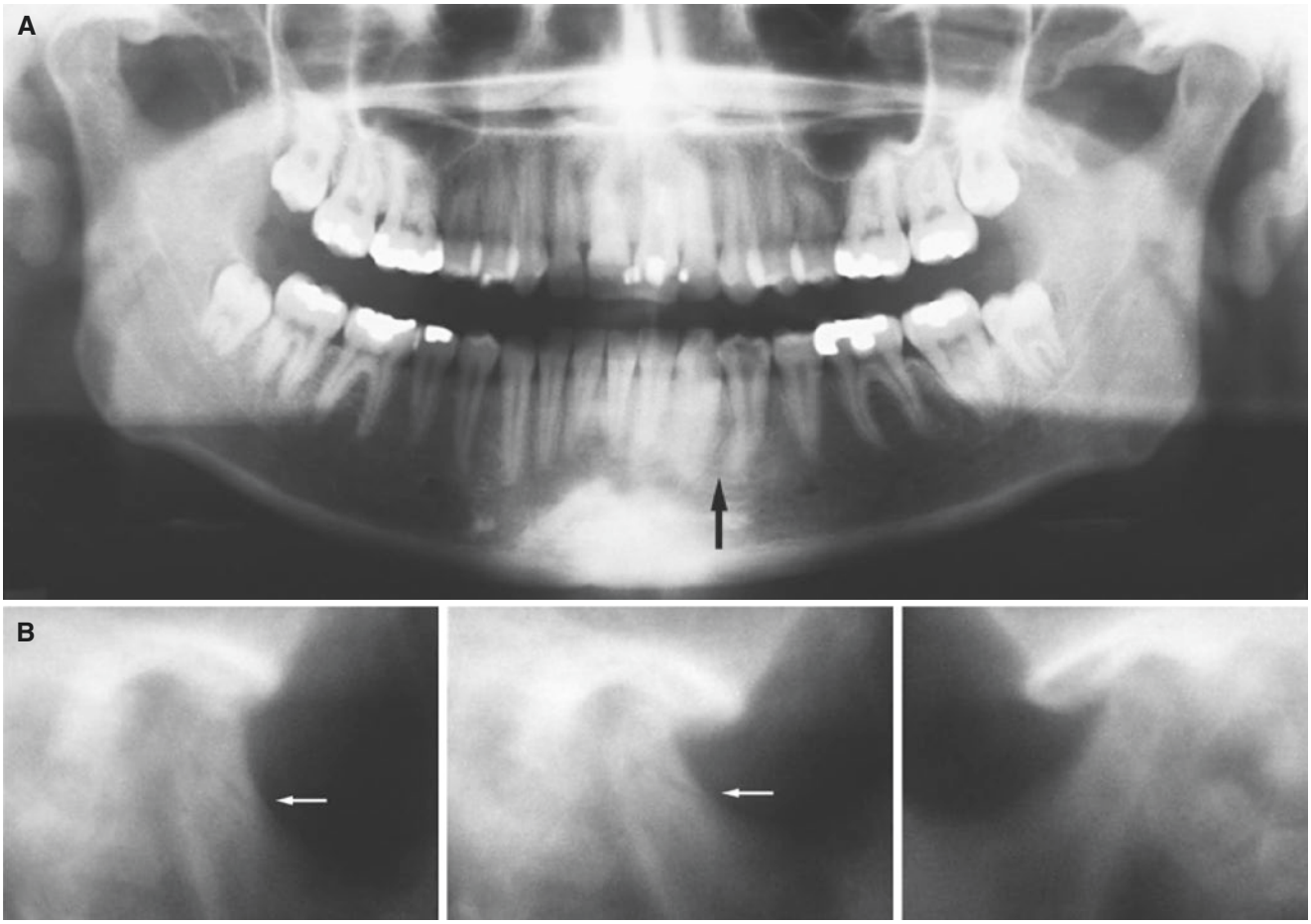

Fig. 8.8 Mandibular body and contralateral neck fractures, without dislocation; 19-year-old female with tooth fracture (first premolar in the left mandible) and pain with limited mouth opening due to bicycle accident. (**A**) Panoramic view shows fracture line in the left mandibular body (*arrow*) and suggests possible fracture of the right mandibular condyle/neck. (**B**) Conventional tomography of the right TMJ at open (*left*) and closed mouth (*middle*) and of the left TMJ at closed mouth (*right*) for comparison confirms fracture line in the right mandibular neck/condyle area (*arrow*), apparently without dislocation (cannot be definitely decided without coronal imaging)

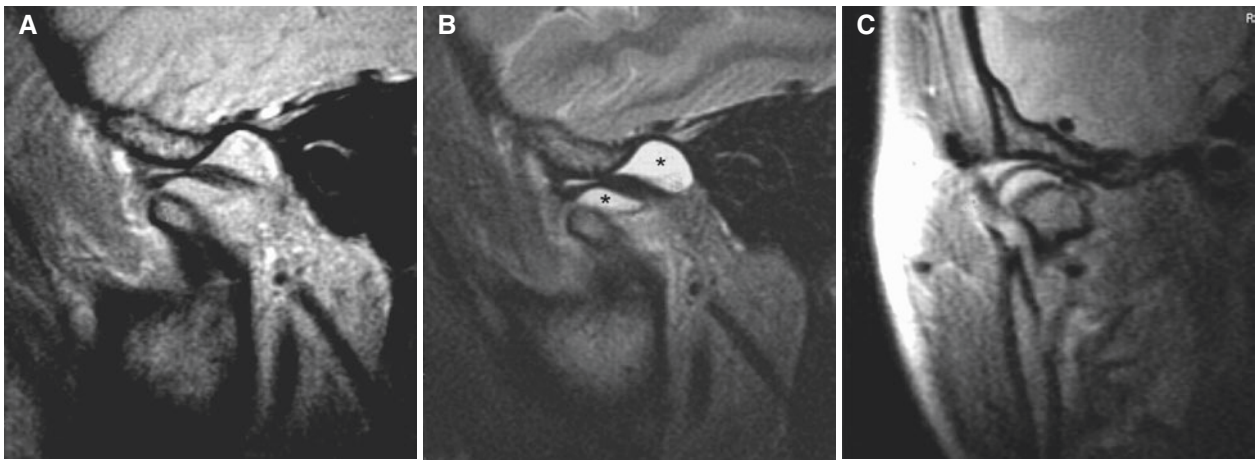

Fig. 8.9 Mandibular neck fracture, unilateral; patient with severe TMJ pain and severely impaired mouth-opening capacity immediately after trauma. (**A**) Oblique sagittal PD-weighted, (**B**) oblique sagittal T2-weighted, and (**C**) oblique coronal T2-weighted MRI show condyle and disc in abnormal position and large effusion in both upper and lower joint compartments (*asterisks*)

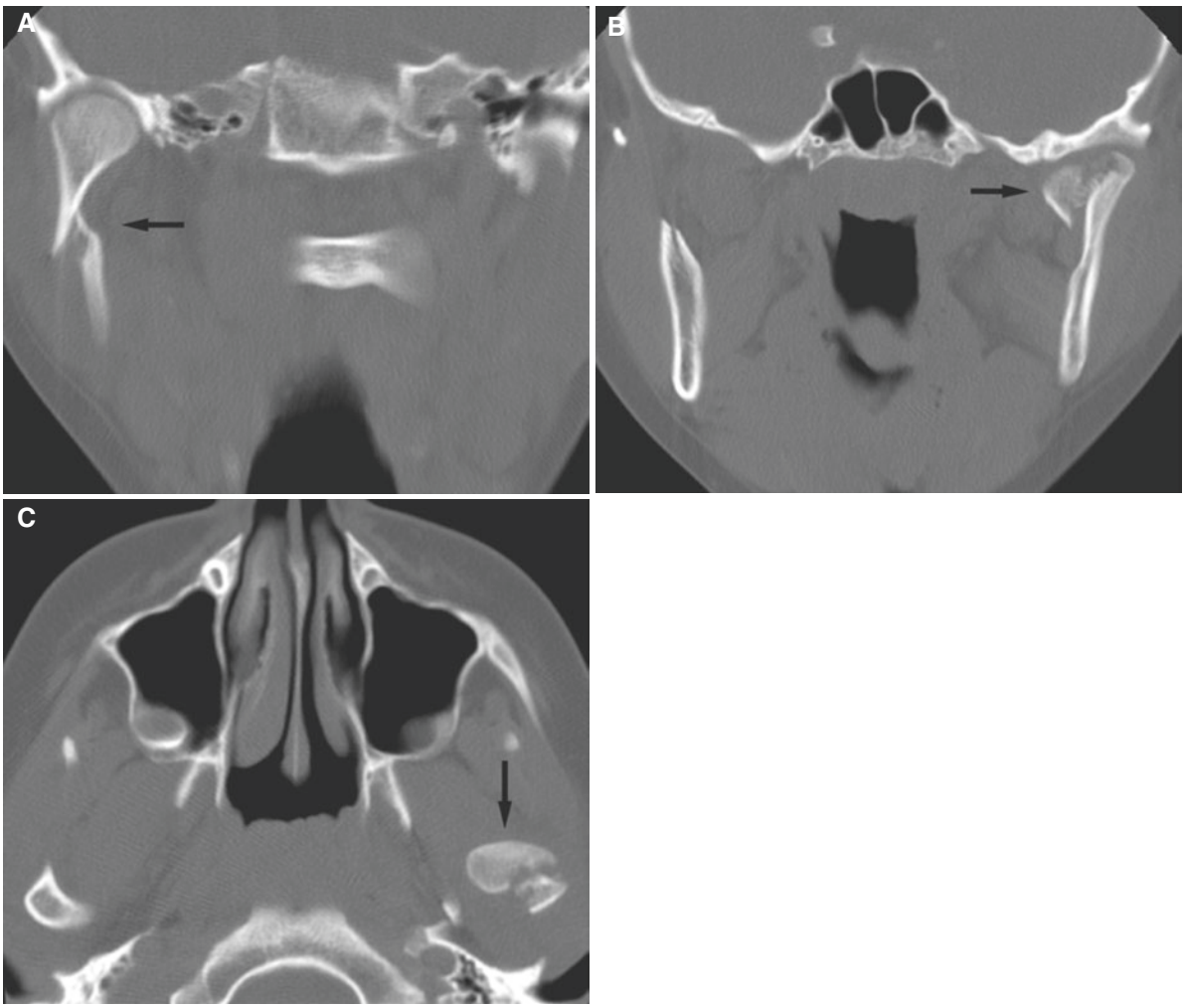

Fig. 8.10 Mandibular neck and contralateral mandibular condyle fractures; 10-year-old male who fell over handlebars of his bike, landing on his chin. (**A**) Coronal CT shows right mandibular neck fracture (*arrow*). (**B**) Coronal CT shows intracapsular fracture of contralateral mandibular condyle with some medial dislocation of medial fragment (*arrow*). (**C**) Axial CT confirms intracapsular condyle fracture with dislocation (*arrow*)

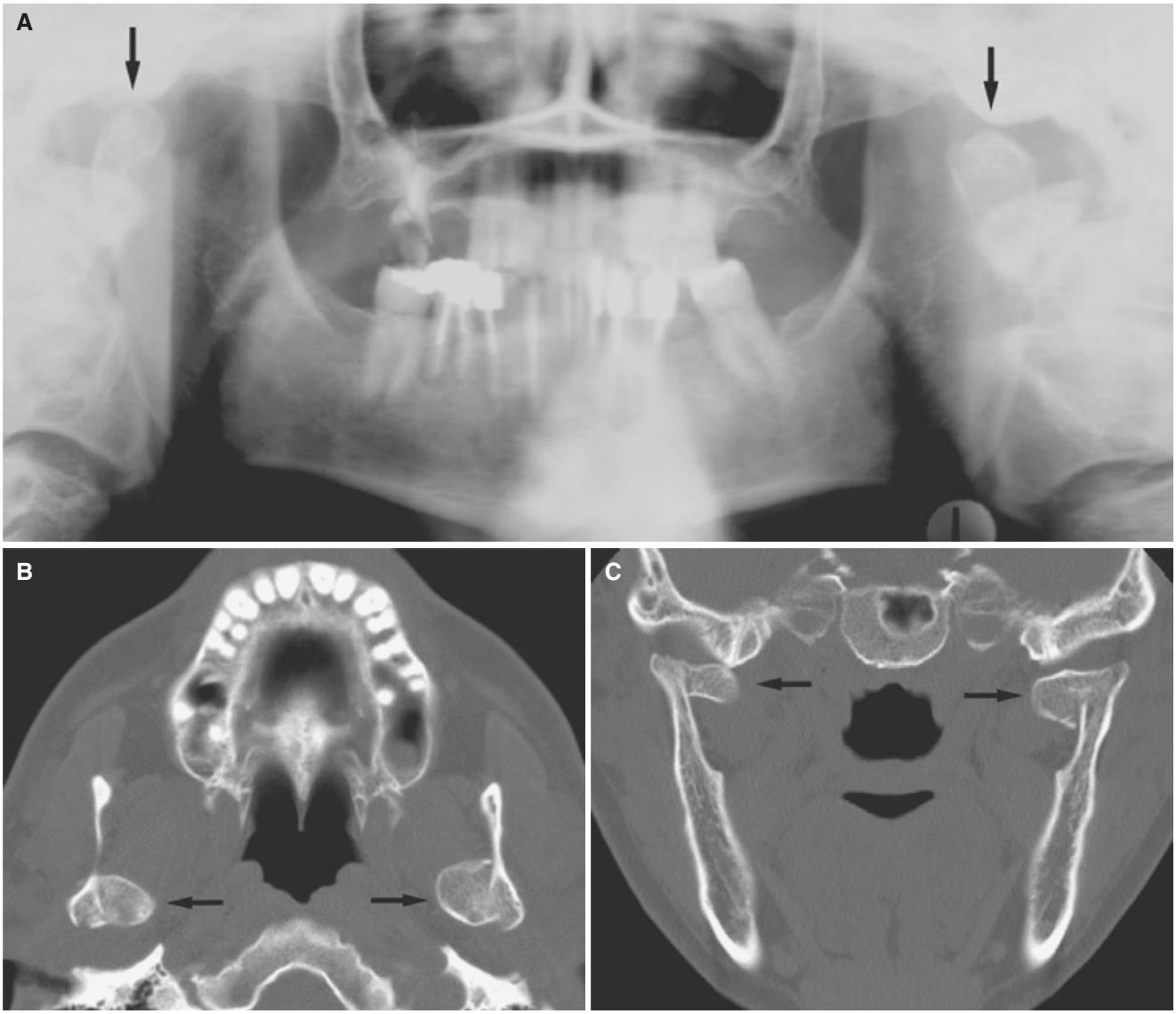

Fig. 8.11 Mandibular neck fractures, bilateral; 37-year-old male with 5-year-old healed mandibular fractures without symptoms or signs and with satisfactory dental occlusion, now with new trauma to face but no new fractures. (**A**) Panoramic view shows deformed mandibular condyles bilaterally (*arrows*). (**B**) Axial CT image shows bony union between fragments and remaining mandible bilaterally (*arrows*). (**C**) Coronal CT image shows medially displaced and healed fragments bilaterally (*arrows*)

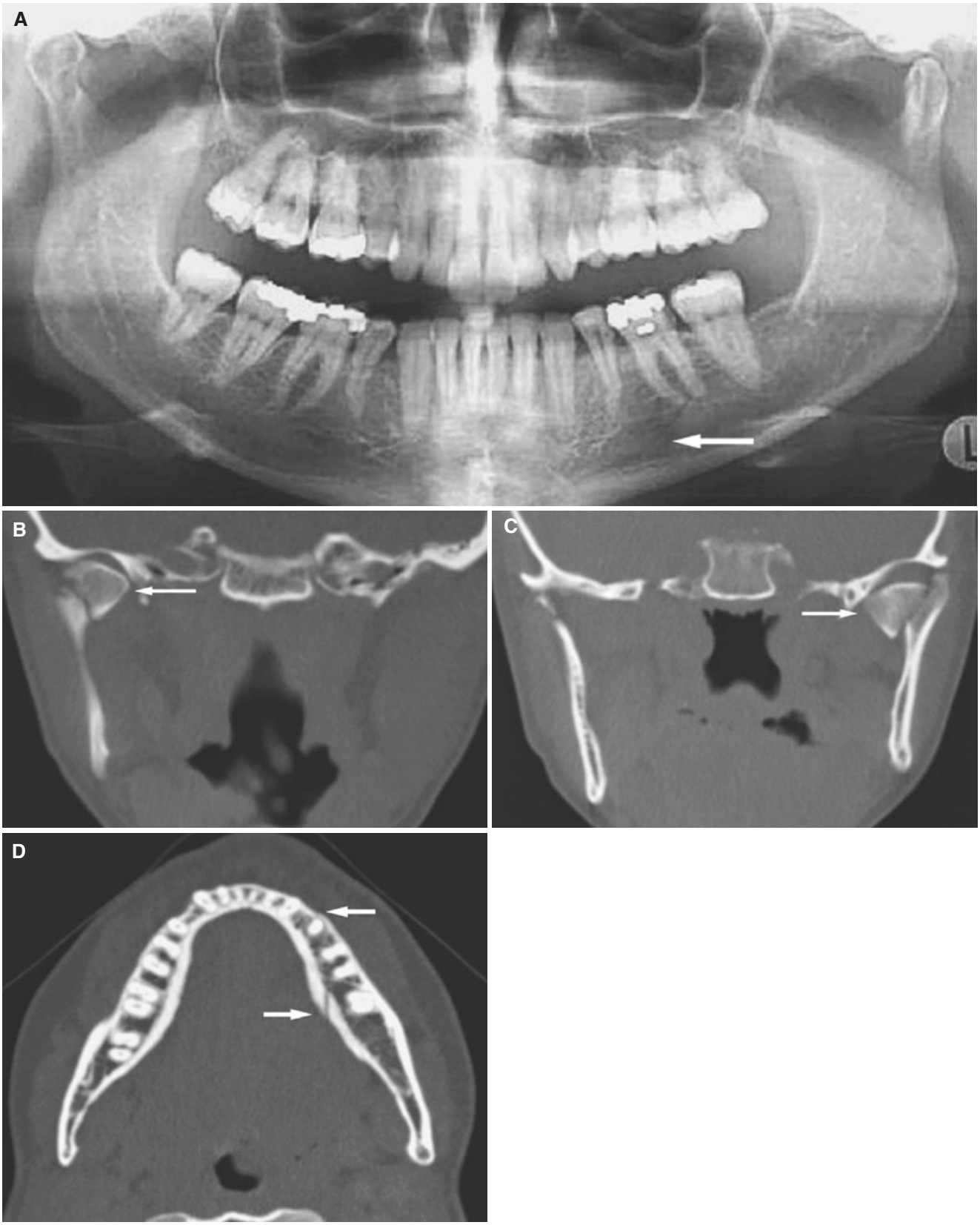

Fig. 8.12 Mandibular bilateral neck and mandibular body fractures; 44-year-old female with trauma to the chin 3 weeks previously, but still some problems with dental occlusion (only tooth fractures diagnosed by clinical and intraoral radiographic examinations). (**A**) Panoramic view shows fracture of mandibular body (*arrow*) and suggests possible fractures of condyles. (**B**) Coronal CT image shows intracapsular fracture of the right mandibular condyle with minimal dislocation (*arrow*). (**C**) Coronal CT image shows intracapsular fracture of the left mandibular condyle with small dislocation (*arrow*). (**D**) Axial CT image shows mandibular body fracture without dislocation (*arrows*)

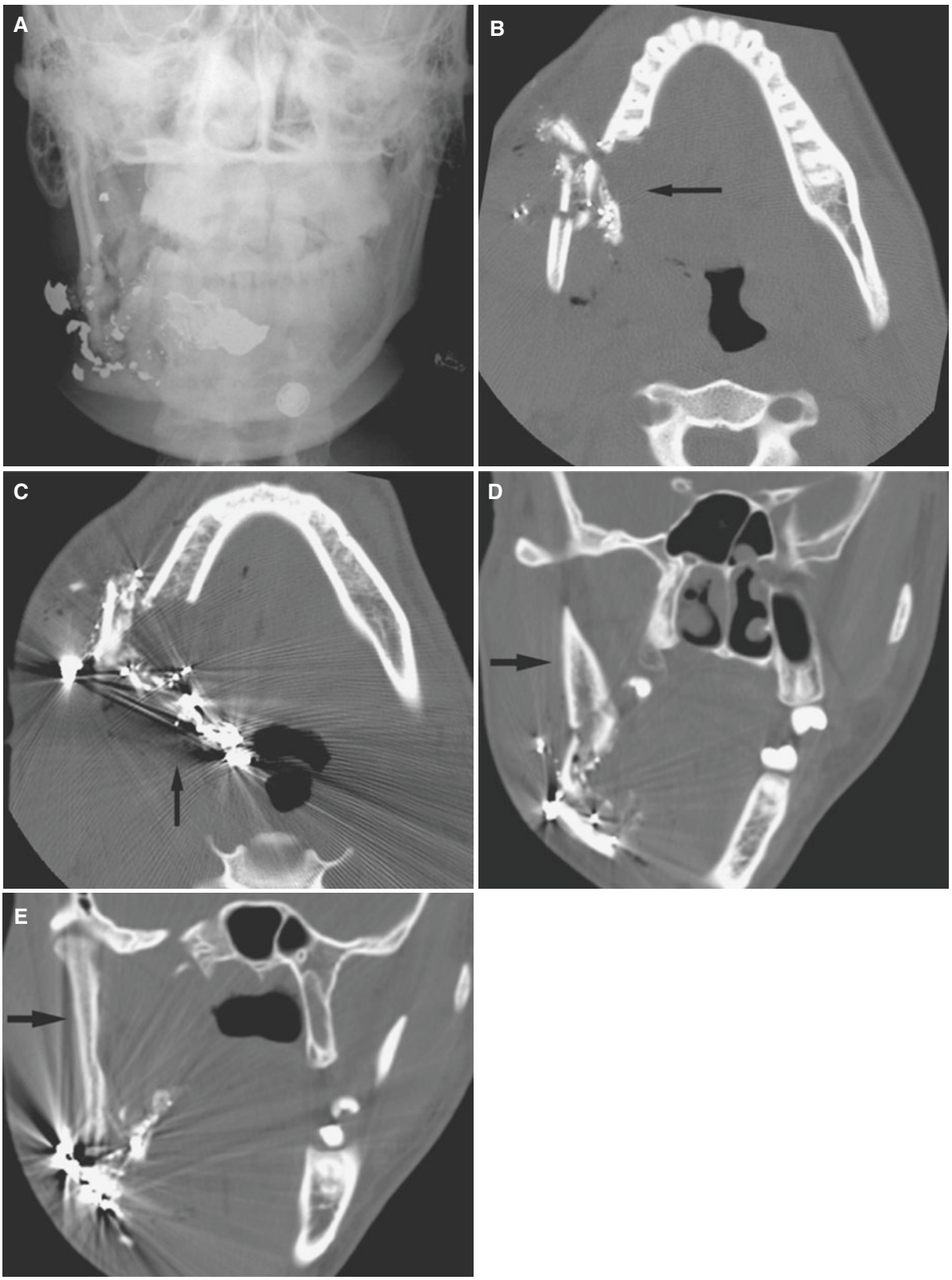

Fig. 8.13 Mandibular body fracture, comminuted; 17-year-old male with gunshot to the face. (**A**) En face view shows multiple bone and metallic fragments and an intratracheal tube. (**B**) Axial CT image of tooth-bearing area shows comminuted fracture with many bone and metallic fragments (*arrow*). (**C**) Axial CT image at a more caudal level shows multiple metallic bullet fragments, from the cheek area to air space with air bubbles along the bullet track (*arrow*), and soft-tissue swelling. (**D**) Coronal CT image shows intact coronoid process (*arrow*). (**E**) Coronal CT image shows intact mandibular neck and condyle (*arrow*)

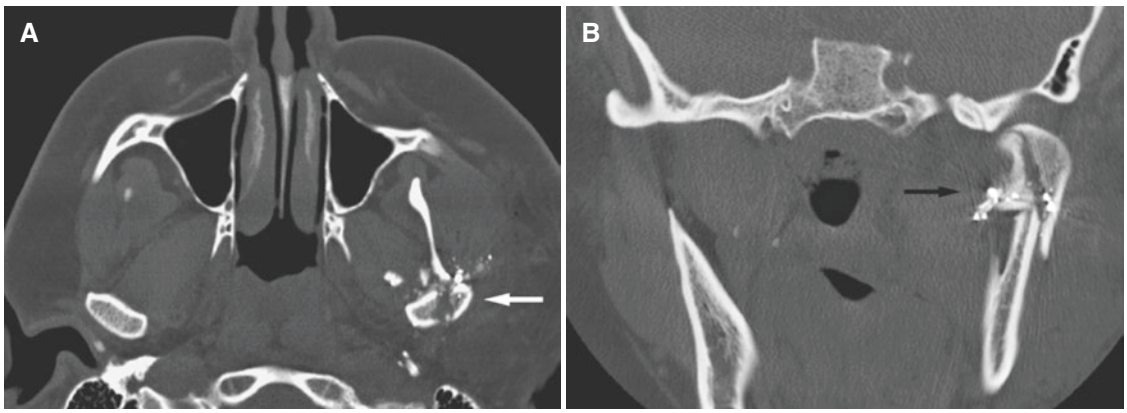

Fig. 8.14 Mandibular condyle fracture, comminuted; 23-year-old female with gunshot to the face. (**A**) Axial CT image shows multiple bone and metallic fragments and intracapsular condyle fracture (*arrow*). (**B**) Coronal CT image shows multiple bony and metallic fragments and condyle divided into two main pieces (*arrow*)

8.5 Mandibular Fractures Combined with Other Fractures

Figs. 8.15, 8.16, 8.17, 8.18, 8.19, and 8.20

8.5.1 Clinical Features

- 15% of patients with mandibular fractures have at least one other facial bone fracture
- In patients with severe facial traumas also mandible frequently injured; in about half of LeFort fractures
- Compound fractures communicate with soft-tissue wounds

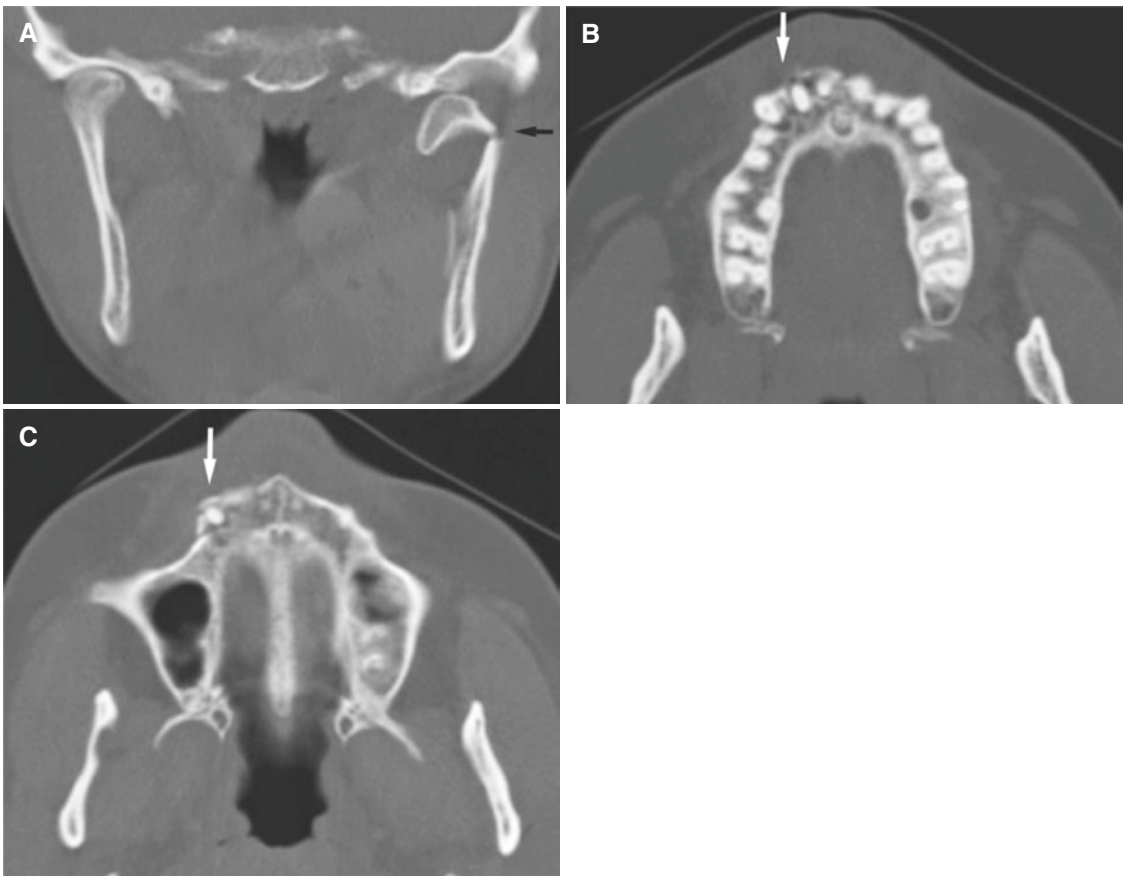

Fig. 8.15 Mandibular neck and maxillary alveolar process fractures; 33-year-old female with trauma to the chin and maxilla. (**A**) Coronal CT image shows fracture of the left mandibular neck (*arrow*). (**B**) Axial CT image shows right maxillary alveolar process fracture with dislocated tooth (*arrow*). (**C**) Axial CT image shows comminuted fracture of maxillary alveolar process (*arrow*)

Fig. 8.16 Mandibular bilateral neck (greenstick on one side) and maxillary alveolar process fractures; 14-year-old male with trauma to the chin and maxilla. (**A**) Coronal CT image shows right mandibular neck fracture with fragment dislocated medially (*arrow*) and greenstick fracture of the left mandibular neck with minimal displacement (*arrow*). (**B**) Axial CT image confirms displacement of the right mandibular condyle (*arrow*) and no evident displacement of the left side. (**C**) Axial CT image shows fracture of maxillary alveolar process in anterior region with loss of one incisor (*arrow*)

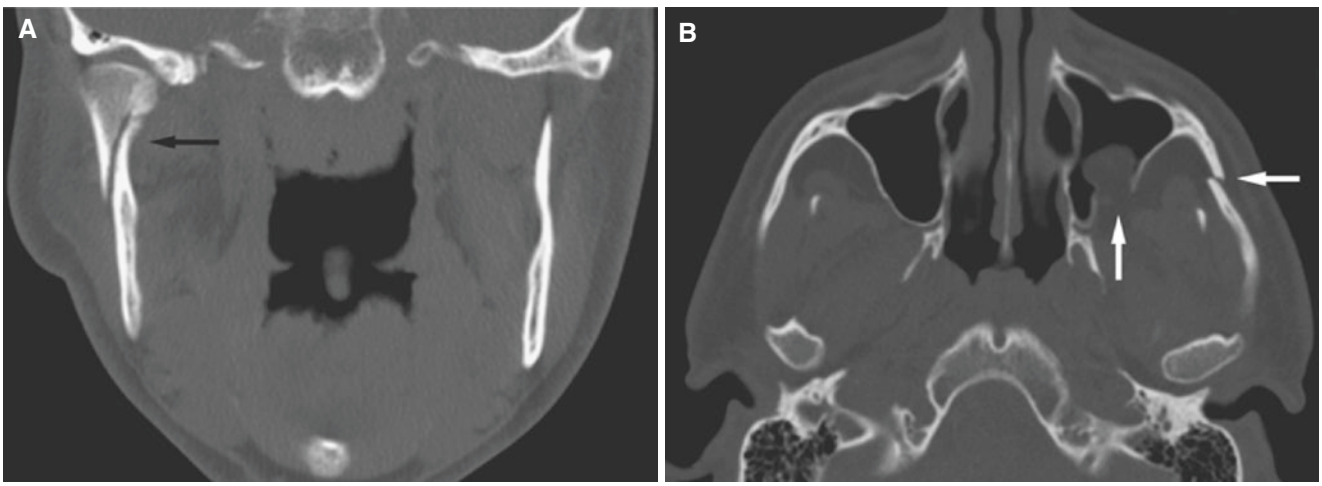

Fig. 8.17 Mandibular neck, maxillary sinus wall and zygomatic arch fractures; 38-year-old male who had been assaulted 1 month previously, now with limited mouth opening, dental occlusion problem, and tenderness to the left zygomatic arch (1 week after trauma, only sinus wall fracture was diagnosed at a hospital). (**A**) Coronal CT image shows mandibular neck fracture with minimal dislocation (*arrow*). (**B**) Axial CT image shows maxillary sinus wall fracture and zygomatic arch fracture (*arrows*)

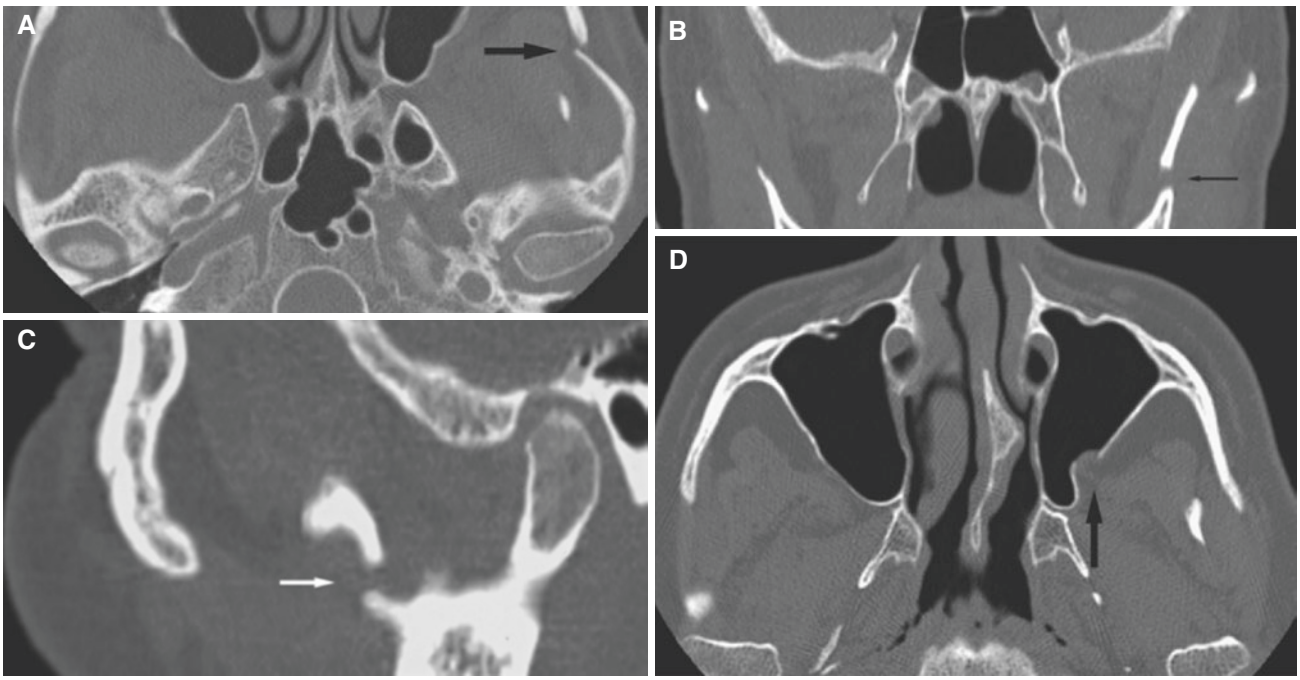

Fig. 8.18 Mandibular coronoid process, maxillary sinus wall and zygomatic arch fractures; 54-year-old female with bicycle accident 3 weeks previously, but still with mouth-opening problem. (**A**) Axial CT image shows fracture of zygomatic arch (*arrow*). (**B**) Coronal CT image shows fracture of mandibular coronoid process (*arrow*). (**C**) Sagittal CT image confirms coronoid process fracture (*arrow*), but mandibular condyle is located normally in fossa. (**D**) Axial CT image shows maxillary sinus wall fracture (*arrow*)

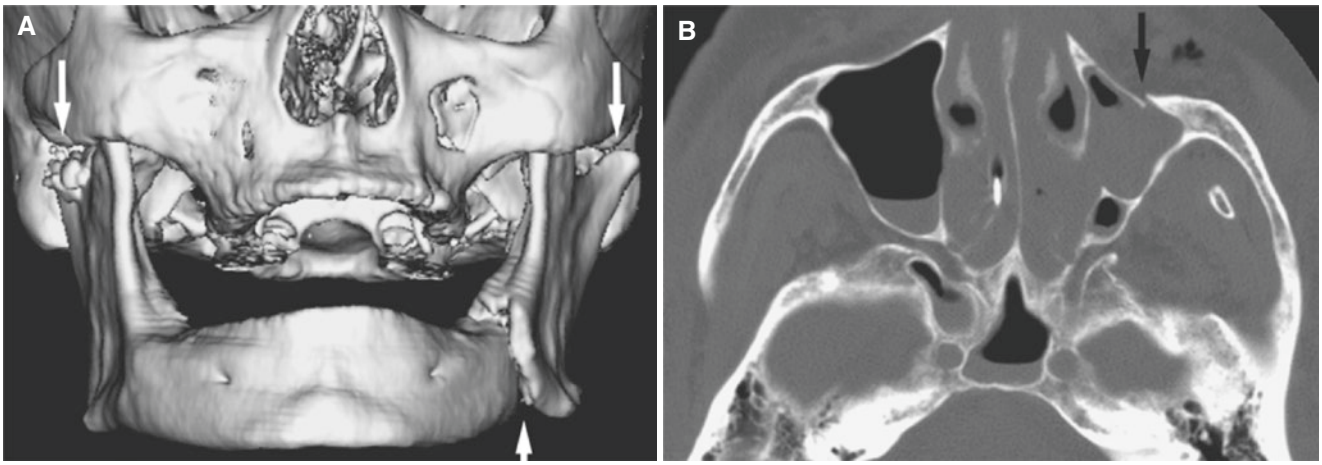

Fig. 8.19 Mandibular bilateral neck, mandibular body and maxillary sinus wall fractures; 58-year-old female who was struck by a car with loss of consciousness. (**A**) 3D CT image shows fracture of left mandibular body (*arrow*) and bilateral mandibular neck fractures (*arrows*). (**B**) Axial CT image shows maxillary sinus wall fracture (*arrow*), intrasinus hemorrhage, and subcutaneous air collection

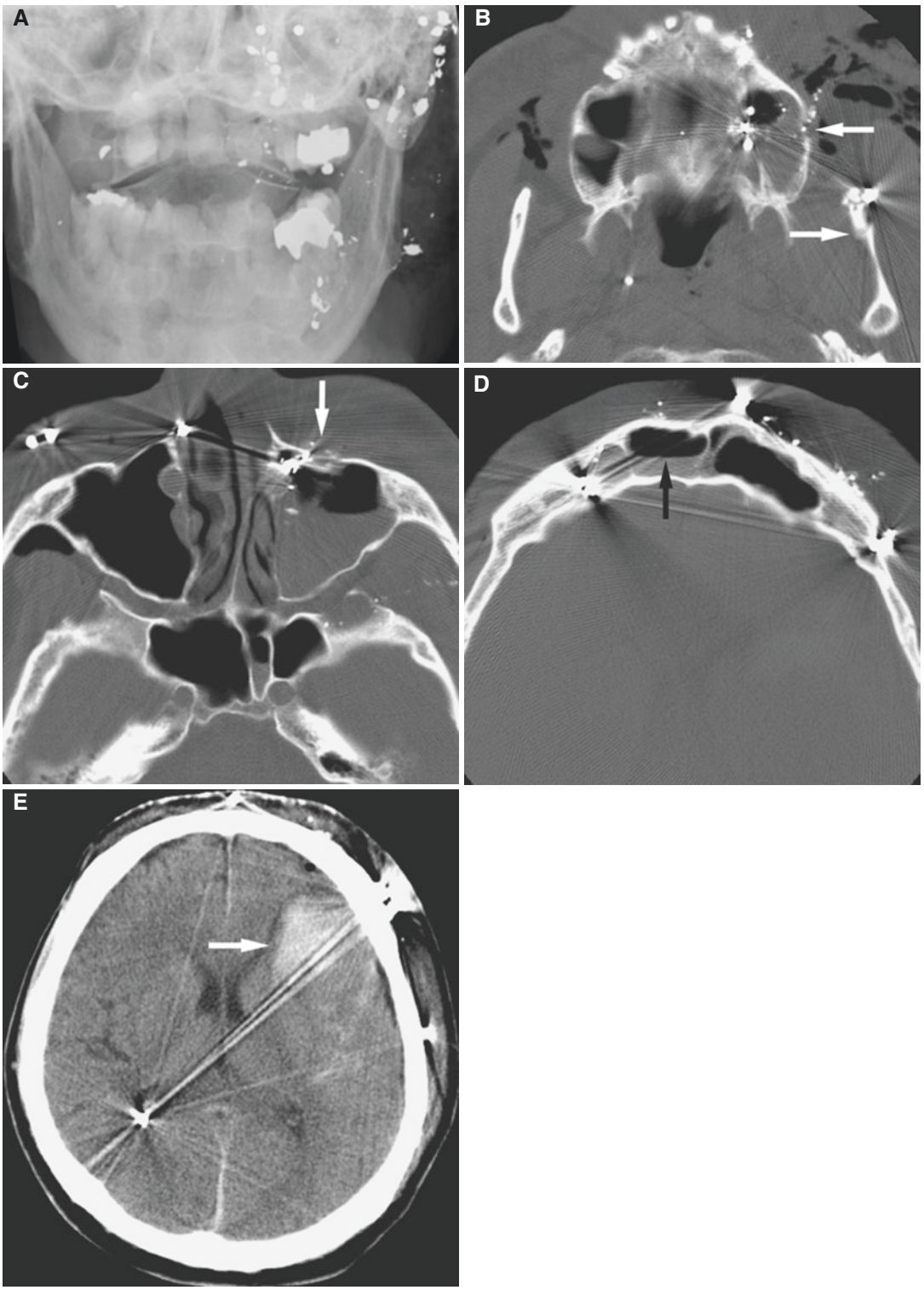

Fig. 8.20 Mandibular and maxillary fractures not pronounced and without dislocations, but severe hemorrhage intracranially and in most paranasal sinuses; 60-year-old male with gunshot to the face. (**A**) Posteroanterior view shows numerous bullet pellets and fragments, but no obvious fractures. (**B**) Axial CT image shows mandibular fracture (*arrow*), maxillary sinus wall fracture (*arrow*), left maxillary sinus opacification (hemorrhage), and a number of metallic fragments and air collections, in particular in the bullet track. (**C**) Axial CT image shows fracture of the anterior maxillary wall (*arrow*), left maxillary sinus fluid-air level (hemorrhage), and metallic fragments. (**D**) Axial CT image shows fluid-air level (hemorrhage) of the frontal sinus (*arrow*) and a number of metallic fragments. (**E**) Axial CT image shows large intraparenchymal hemorrhage in the left frontotemporal lobes (*arrow*) causing some mass effect onto frontal horn of the left lateral ventricle, some widening of extra-axial space over the left frontal area possibly due to subdural hematoma, pneumocephalus in the left frontal area, and bullet fragments, one in particular adjacent to occipital horn of the right lateral ventricle

8.6 Complications of Mandibular Fractures

Figs. 8.21, 8.22, and 8.23

8.6.1 Clinical Features

- Mandibular fractures are easily overlooked in the diagnostic workup of traumatized patients, particularly of those with severe head injuries
- Undetected mandibular fractures may lead to various complications, some of which could have been avoided
- Infections, osteomyelitis, and nonunion seem to be the most frequent complications after surgical treatment; mandibular angle fractures have the highest overall morbidity rate
- Dental occlusion problems and marked deviation of the mandible on mouth opening seem to be the most frequent complications after nonsurgical treatment of condyle fractures

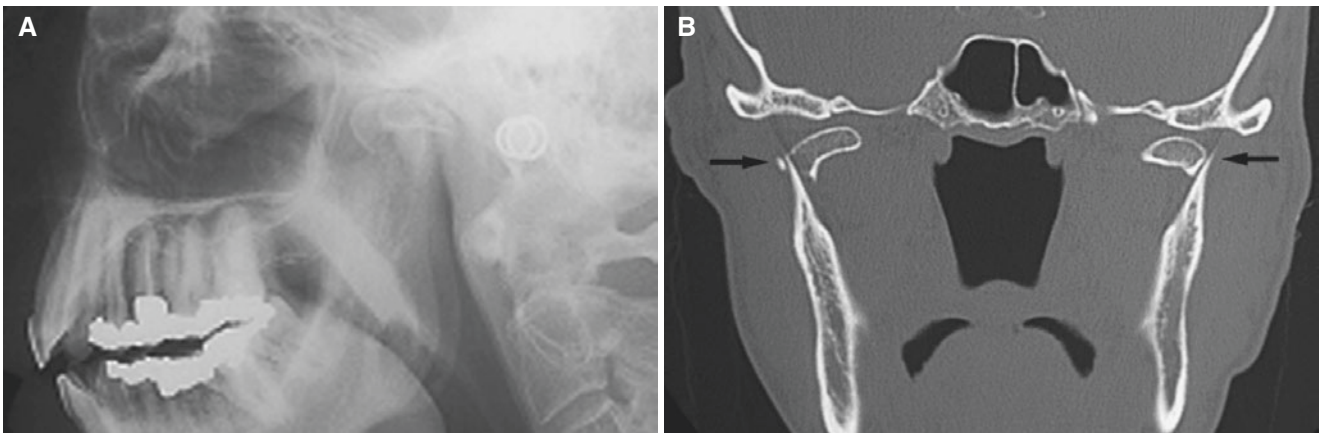

Fig. 8.21 Open bite; 61-year-old male with trauma to the face and head 3 weeks previously with loss of consciousness, no mandibular fractures diagnosed, now with contact only on molar teeth at closed mouth. (**A**) Lateral view shows anterior bite opening. (**B**) Coronal CT image shows bilateral mandibular neck fractures (*arrows*)

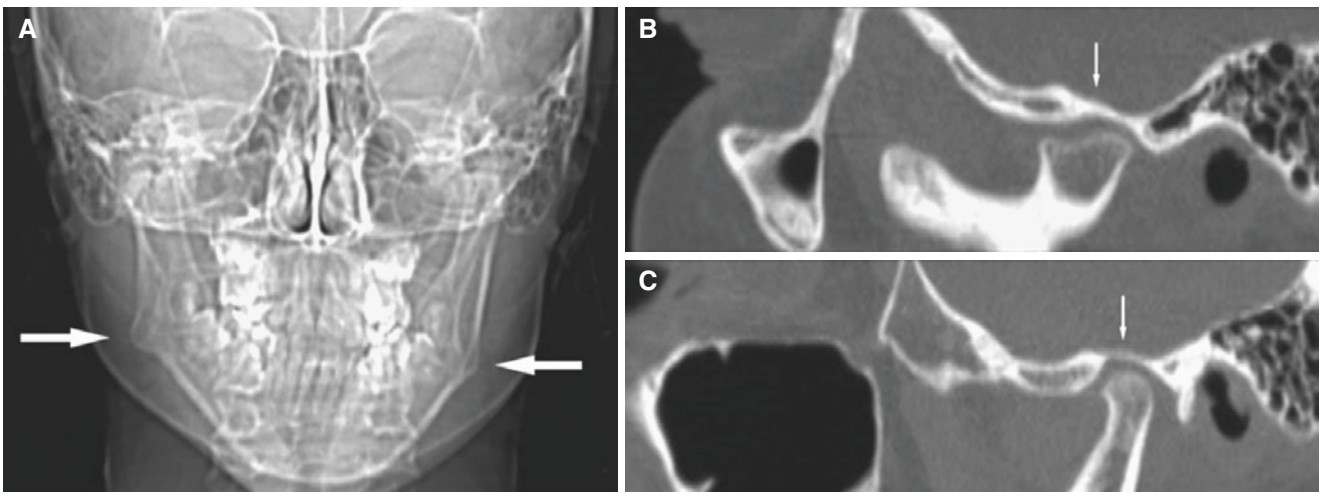

Fig. 8.22 Facial asymmetry; 12-year-old female with a 4-year history of trauma to the chin but no fractures diagnosed. (**A**) Scout view shows facial asymmetry with mandibular underdevelopment on the right side (*arrows*). (**B**) Oblique sagittal CT image of right TMJ shows deformed mandibular condyle and flattened fossa. (**C**) Oblique sagittal CT image of left TMJ shows normal mandibular condyle and fossa (other images of this patient in Fig. 6.59)

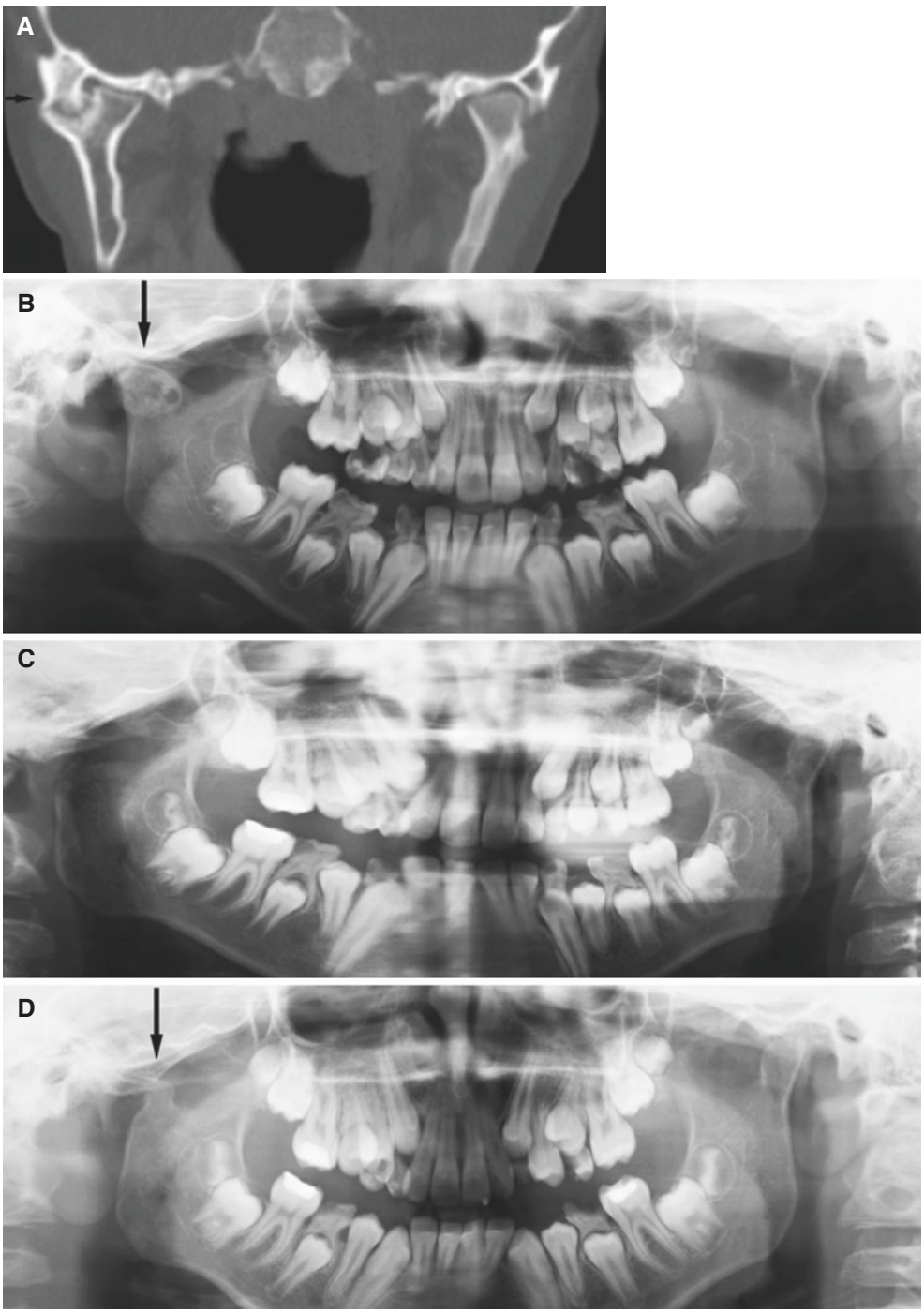

Fig. 8.23 TMJ ankylosis; 10-year-old male with a 4-year history of trauma to the head with loss of consciousness; no jaw fractures diagnosed, but mouth-opening capacity gradually reduced to less than 10 mm; postoperatively it increased to 33 mm. (**A**) Coronal CT image shows fibro-osseous ankylosis of the lateral part of right TMJ (*arrow*), probably also previous fracture of the left joint. (**B**) Panoramic view shows abnormal right mandibular condyle (*arrow*). (**C**) Panoramic, postoperative view shows most of the right mandibular condyle resected. (**D**) Panoramic view, 1 year postoperative, shows small, new mandibular condyle (*arrow*)

8.7 Nasal Fractures

Fig. 8.24

8.7.1 Clinical Features

- See Fractures
- Nasal bone or nasal pyramid fractures are most frequent and constitute 40–50% of all facial bone fractures
- 66% result from a lateral force, and only 13% from a frontal force
- The majority involve thinner distal third of nasal bones, with intact nasal–ethmoid margin
- More severe fractures may result in detachment of the entire nasal pyramid, saddle nose, hypertelorism, and telecanthus

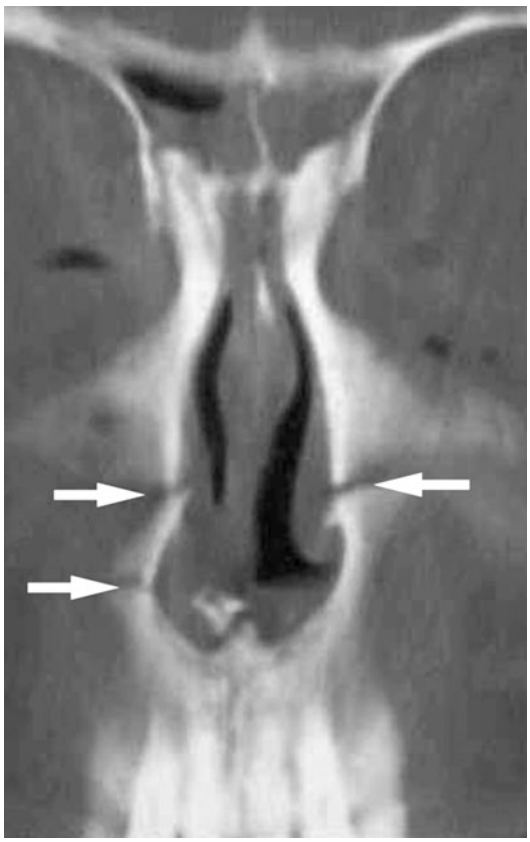

Fig. 8.24 Nasal aperture fractures. Coronal CT image shows three fractures of nasal aperture (*arrows*), as well as fractures of frontal sinus with fluid-air level and nasal septum (courtesy of Dr. A. Kolbenstvedt, Rikshospitalet University Hospital, Oslo, Norway)

8.8 Midfacial Fractures

8.8.1 Clinical Features

- See Fractures
- Central midfacial fractures; all forms of fractures that occur between the root of the nose and maxillary alveolar processes, without involvement of zygomas; isolated maxillary fractures, nasal–ethmoidal–orbital fractures, LeFort fractures 1 and 2
- Lateral midfacial fractures; isolated zygomatic arch fracture, tripod fracture, blowout fracture
- Fractures may be bilateral or unilateral
- About one-fourth as common as mandibular fractures
- Majority of severe midfacial fractures occur in road traffic accidents
- More than 80% of patients are males
- Peak age incidence third decade
- Rare in children
- Trismus is reported in about 33% of all zygomatic fractures and in about 45% of zygomatic arch fractures; a fractured arch may impinge on coronoid process or temporalis muscle
- 1% to near 15% of central–lateral midfacial fractures are reported to have accompanying fractures of anterior skull base
- Posttraumatic complications; meningitis, hypertelorism, olfactory dysfunction, mucocele

8.9 Isolated Maxillary Sinus Wall Fracture

Fig. 8.25

8.9.1 Clinical Features

– Uncommon, but usually comminuted
– Alveolar fractures most frequent

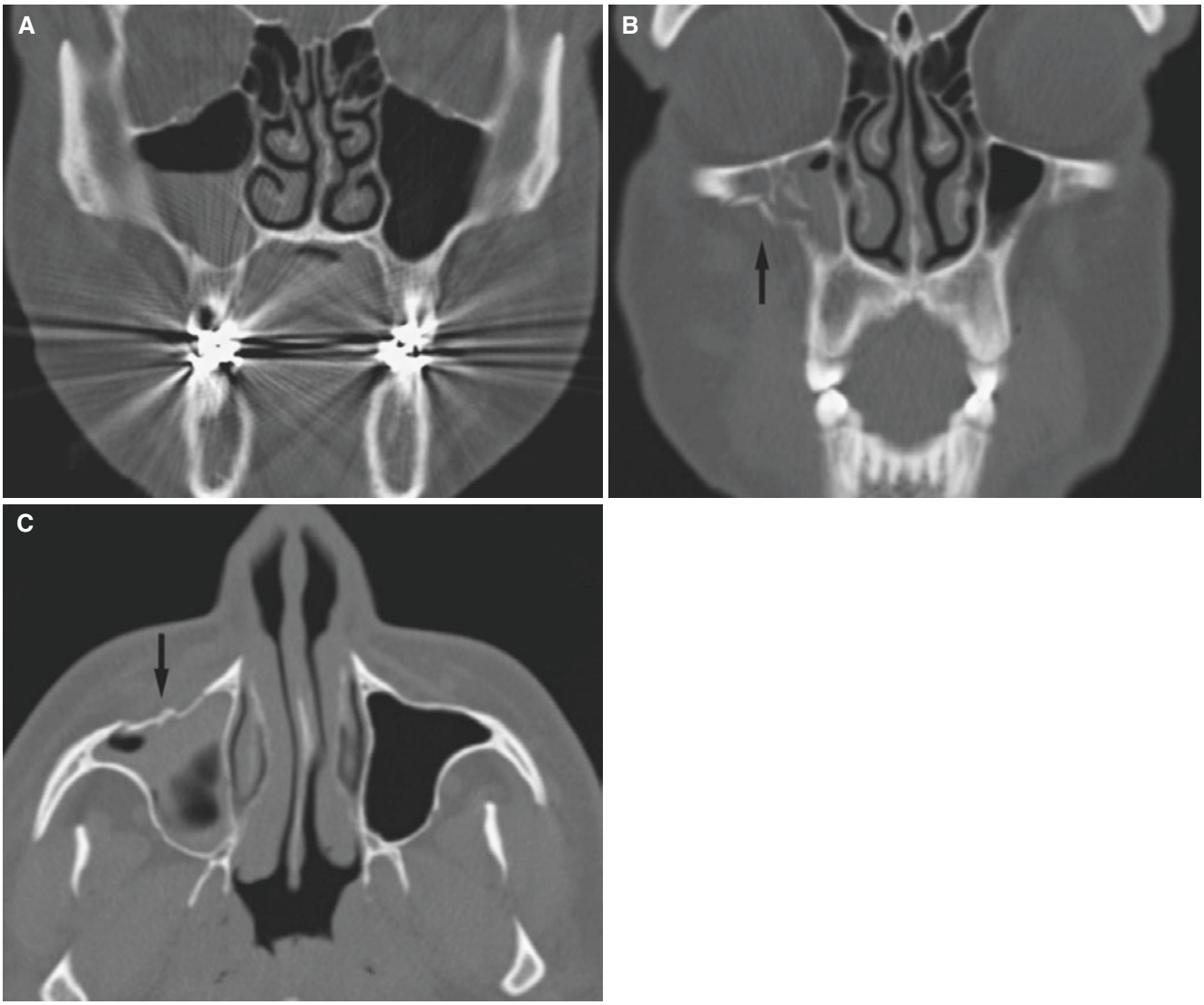

Fig. 8.25 Maxillary sinus wall fracture; 32-year-old male victim of violence 3 days previously, with infraorbital hematoma and pain. (**A**) Coronal CT image shows normal bony walls of maxillary sinuses but unilateral fluid-air level. (**B**) Coronal CT image shows comminuted fracture of lateral maxillary sinus wall (*arrow*). (**C**) Axial CT shows fracture of anterior maxillary sinus wall (*arrow*)

8.10 LeFort Fractures

Figs. 8.26, 8.27, 8.28, 8.29, and 8.30

8.10.1 Definition

LeFort fractures involve separation of all or a portion of the midface from the skull base and are classified as horizontal (1), pyramidal (2), or transverse (3) with hallmark of traumatic pterygomaxillary separation:

- **LeFort type 1**—floating palate
  - Horizontal maxillary fracture, separating the teeth from the upper face
  - Fracture line passes through the alveolar ridge, lateral nose, and inferior wall of maxillary sinus
- **LeFort type 2**—floating maxilla
  - Pyramidal fracture, with teeth at pyramid base and nasofrontal suture at its apex
  - Fracture arch passes through the posterior alveolar ridge, lateral walls of maxillary sinuses, inferior orbital rim, and nasal bones
- **LeFort type 3**—floating face
  - Craniofacial disjunction
  - Fracture line passes through the nasofrontal suture, maxillo-frontal suture, orbital wall, and zygomatic arch/zygomaticofrontal suture

8.10.2 Clinical Features

- Usually, different fracture types occur in combination
- Dental occlusion does not fit
- "Floating palate" (LeFort 1)
- "Dish face," hemorrhage, edema, emphysema, and in near 80% anesthesia of infraorbital nerve(s) (LeFort 2)
- "Dish face," CSF rhinorrhea, hemorrhage, edema, emphysema, damage to lacrimal apparatus, and in near 70% anesthesia of infraorbital nerve(s) (LeFort 3)

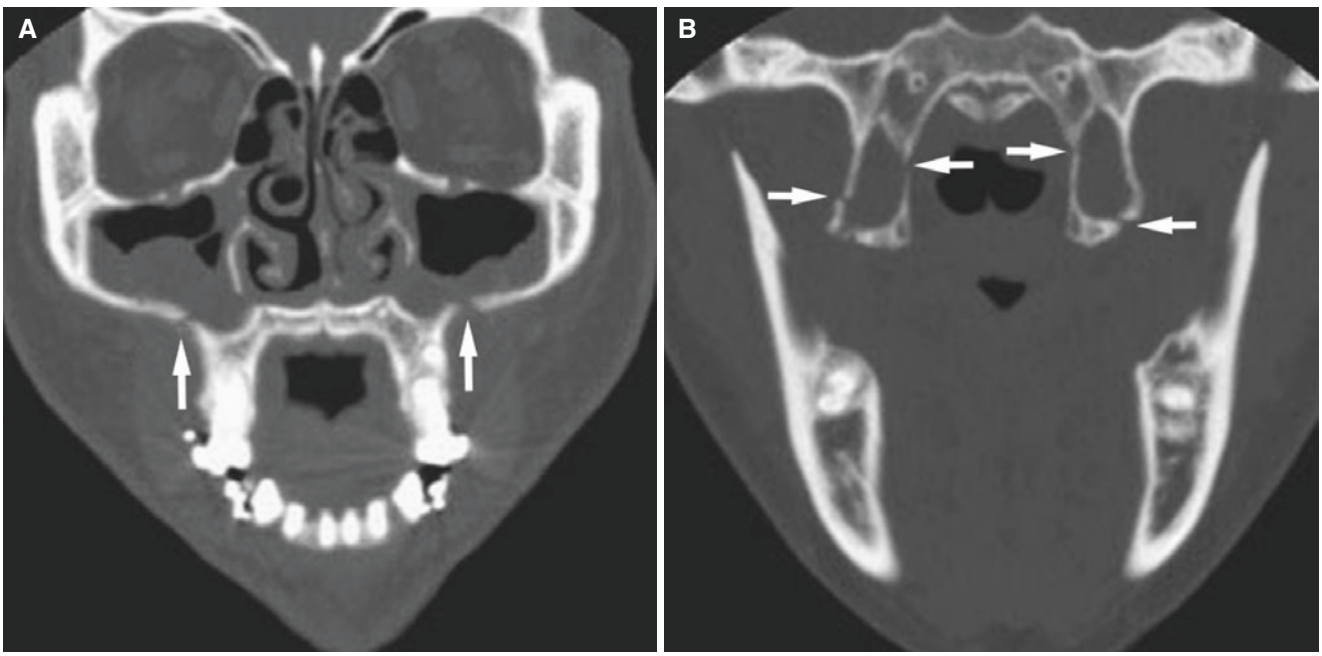

Fig. 8.26 LeFort 1 osteotomies; 48-year-old female with pain and facial swelling after maxillary surgery. (**A**) Coronal CT image shows osteotomy defects in anterolateral maxillary walls (*arrows*) and through inferior portion of the nasal cavity. Associated mucosal thickening in maxillary sinuses characteristically seen after surgery. (**B**) Coronal CT image shows osteotomy defects in pterygoid plates (*arrows*)

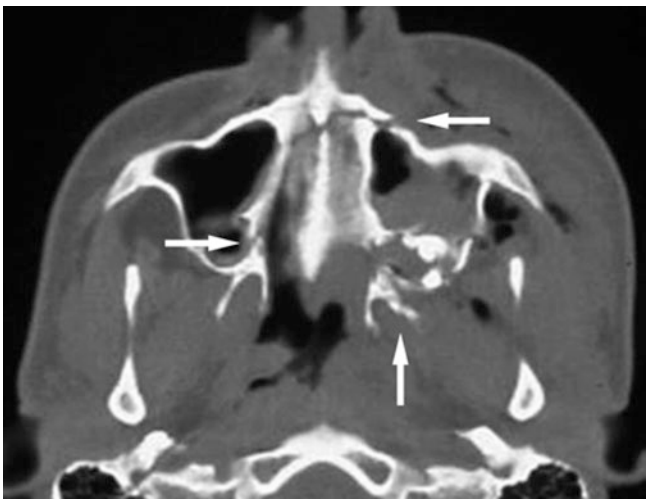

Fig. 8.27 LeFort 1 fracture. Axial CT image shows fracture line in anterior, inferior part of the nasal cavity (*arrow*); in posterior, inferior part of maxillary sinus, most prominent on the left side; and in the left pterygoid plate (*arrow*). Note also fracture in the right medial maxillary sinus wall (*arrow*) (courtesy of Dr. A. Kolbenstvedt, Rikshospitalet University Hospital, Oslo, Norway)

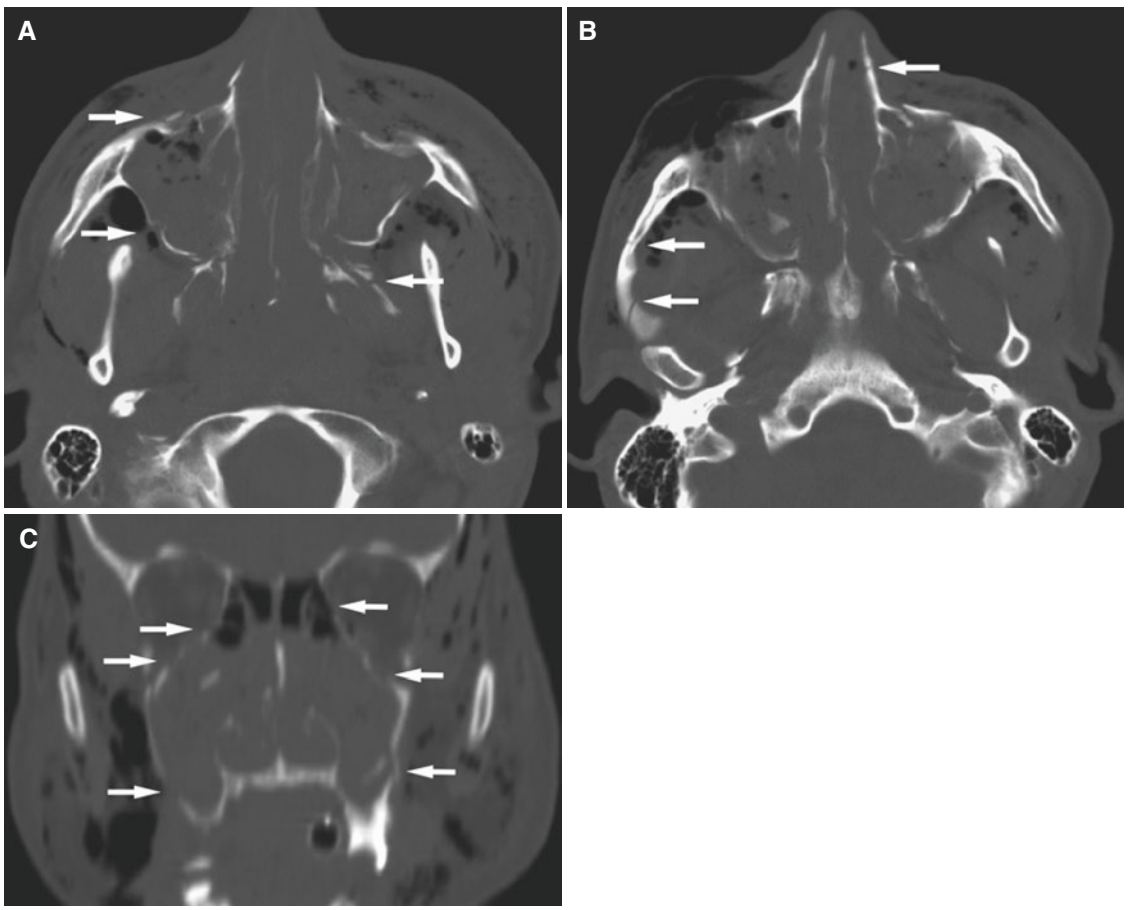

Fig. 8.28 LeFort 2 fracture with a zygomatic arch nondisplaced fracture; 37-year-old male who was assaulted. (**A**) Axial CT image shows bilateral fractures of the anterior part of the maxilla (*arrow*), lateral–posterior part of the maxilla (*arrow*), and pterygoid plates (*arrow*). Hemorrhage in maxillary sinuses and multiple air collections. (**B**) Axial CT image shows bilateral fracture of the nasal bone (*arrow*) and fractures of the right zygomatic arch (*arrows*). Note large emphysema in the cheek. (**C**) Coronal, reformatted CT image shows bilateral fractures of medial orbital walls (*arrows*), superior and inferior lateral maxillary sinus walls (*arrows*), and nasal aperture. Note intratracheal tube

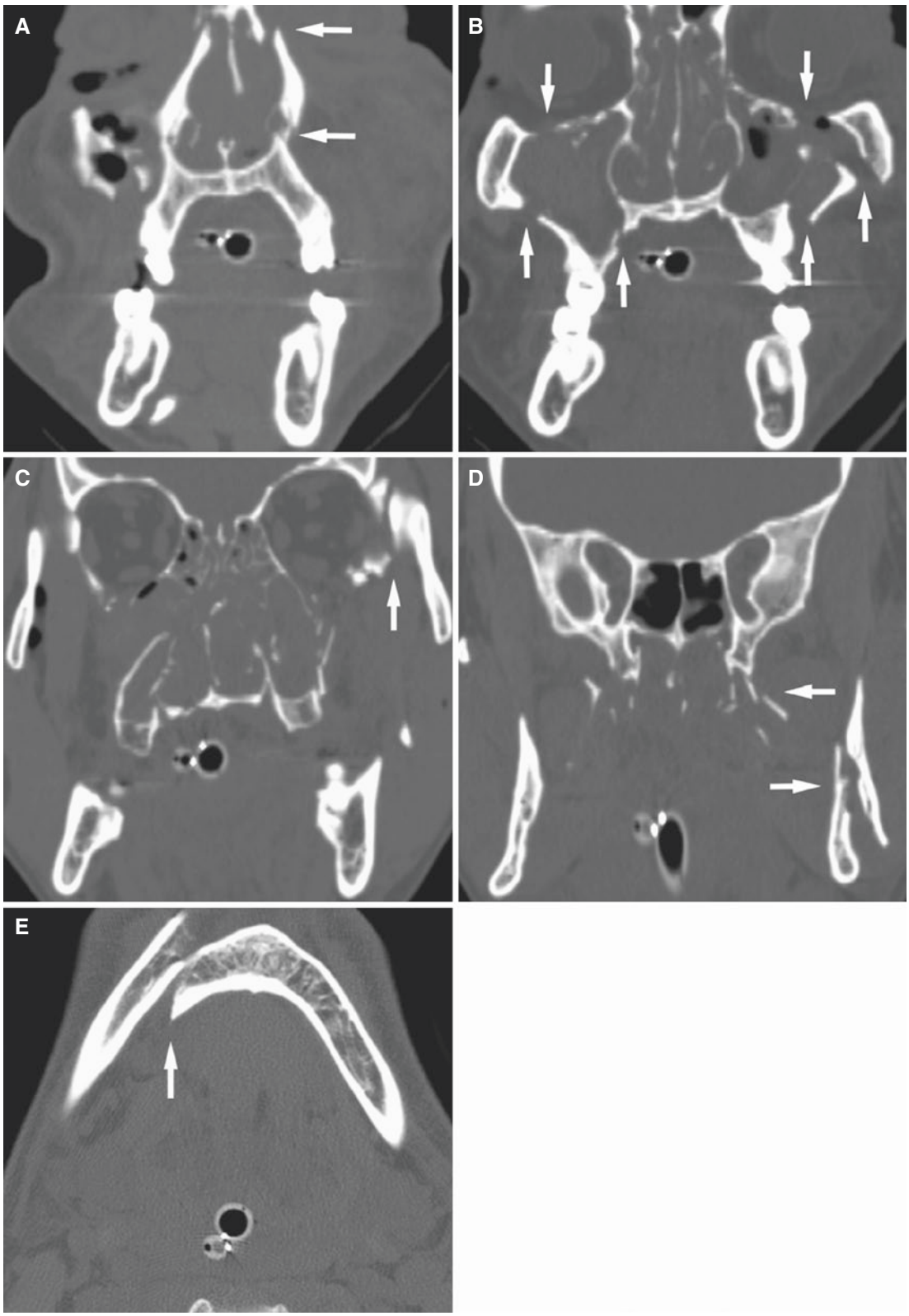

Fig. 8.29 LeFort 3 and mandibular body fractures; 45-year-old male after motor vehicle crash with trauma to the face and head and loss of consciousness. (**A**) Coronal CT image shows bilateral fractures of superior nasal aperture near the nasal bone and inferior nasal aperture above the palate (*arrows*), opacification due to hemorrhage of the nasal cavity, bone fragments and air collections in the right cheek, and intratracheal tube. (**B**) Coronal CT image shows bilateral fractures of orbital floor and maxillary sinus wall (*arrows*) and opacification of the nasal cavity and all sinuses except the left frontal, due to hemorrhage. (**C**) Coronal CT image shows fracture of the left lateral orbital wall (*arrow*), necessary for definition of a LeFort 3 fracture; zygomatic arch was also fractured. (**D**) Coronal CT image shows bilateral fractures of pterygoid plates (*arrow*) and left mandibular ramus (*arrow*). (**E**) Axial CT image shows fracture of right mandibular body (*arrow*)

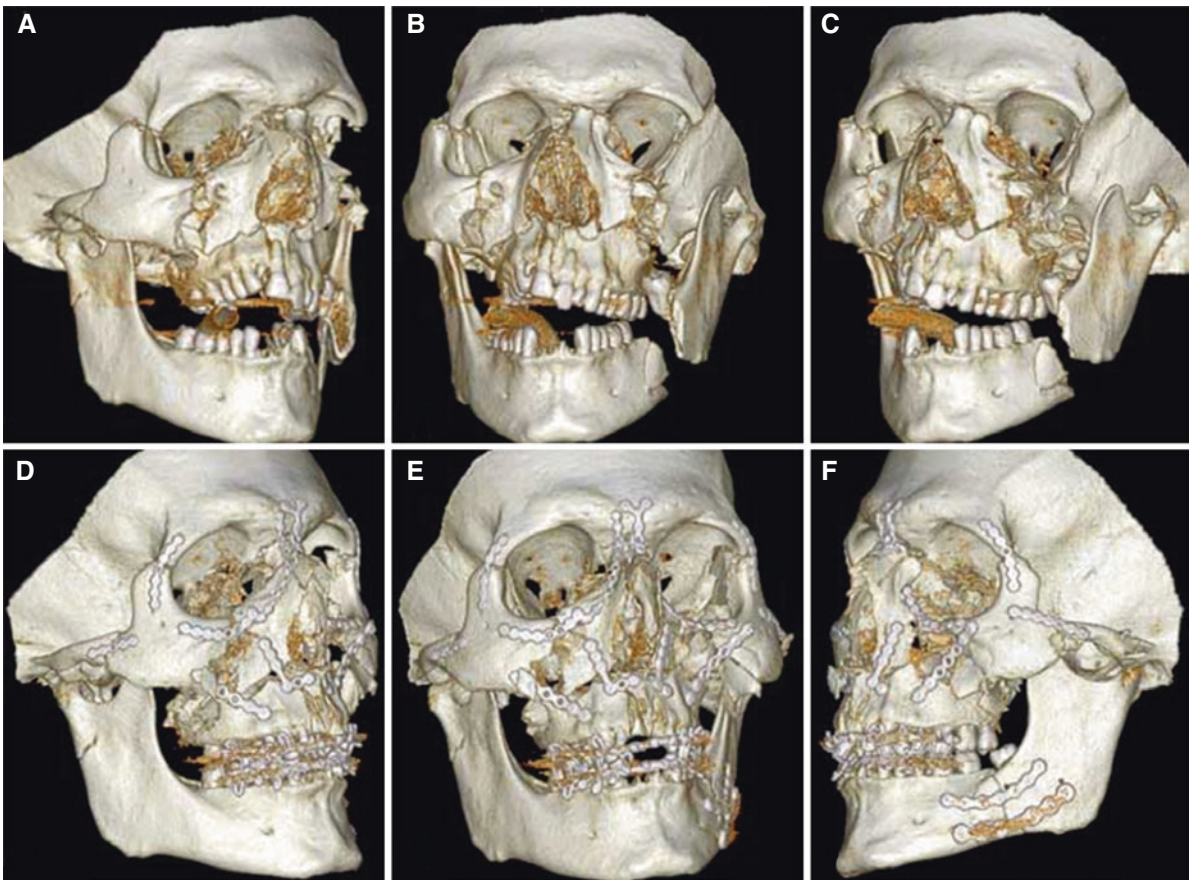

Fig. 8.30 LeFort 1, 2, 3 and mandibular fractures; 28-year-old male, motor vehicle crash. (**A**, **B**, **C**) Preoperative and (**D**, **E**, **F**) postoperative 3D CT images show a mixture of all LeFort fractures and, additionally, mandibular fractures

8.11 Tripod Fracture

Figs. 8.31 and 8.32

Synonyms: Trimalar or zygomatic fracture.

8.11.1 Definition

Fracture through (1) lateral orbital wall with fracture site at zygomaticofrontal suture, (2) zygoma and maxilla with fracture site at zygomaticomaxillary suture, and (3) zygomatic arch with fracture site at zygomaticotemporal suture.

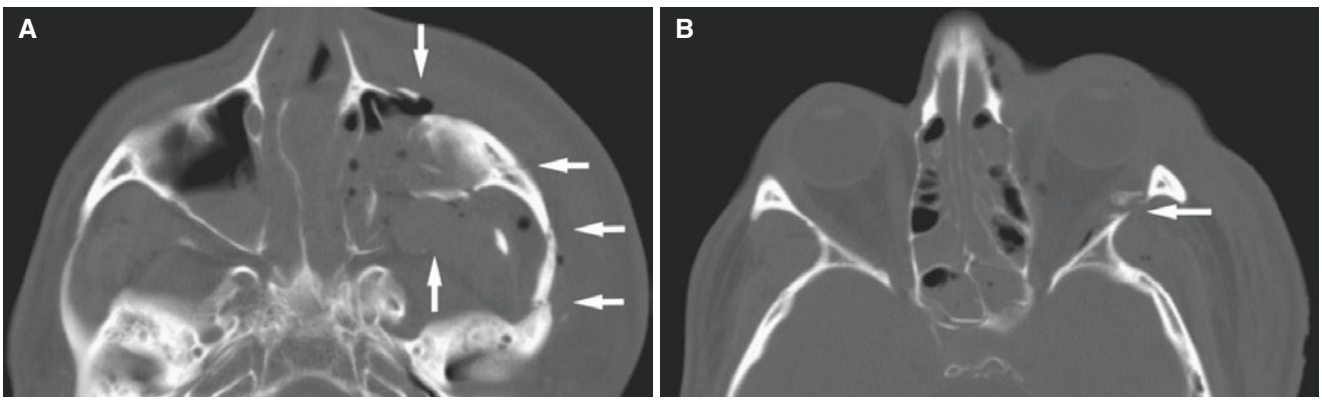

Fig. 8.31 Tripod fracture, classic; 45-year-old and with facial trauma. (**A**) Axial CT image shows fractures of anterior maxillary sinus wall, lateral–posterior maxillary sinus wall, and zygomatic arch (*arrows*) and intrasinus hemorrhage. (**B**) Axial CT image shows fracture of lateral orbital wall (*arrow*), hemorrhage in ethmoid cells, and swelling due to subcutaneous edema

8.11.2 Clinical Features

- Most common fracture of facial skeleton after nasal and mandibular fractures
- About half of all midfacial fractures (more than two-thirds in one study), either alone or in combination with other midfacial fractures
- Infraorbital nerve paresthesia or anesthesia in almost 95%

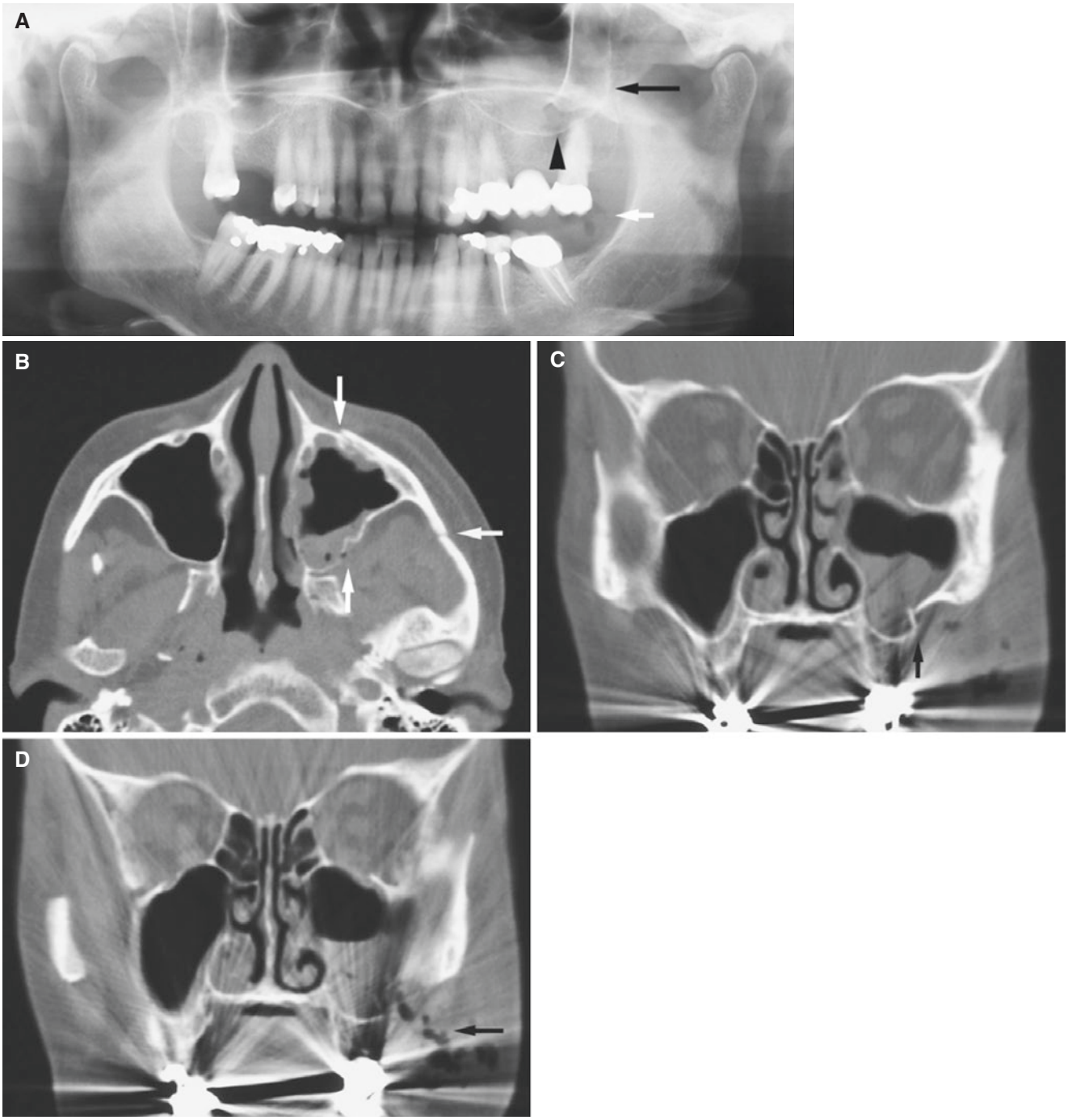

Fig. 8.32 Tripod fracture, but no evident lateral orbital wall fracture; 70-year-old female with trauma to face 3 days previously. (**A**) Panoramic view shows opacification of the left maxillary sinus (*arrow*) with abnormal structure (*arrow head*) and possibly some air collections (*white arrow*). (**B**) Axial CT image shows fractures of anterior maxillary sinus wall, lateral–posterior maxillary sinus wall, and zygomatic arch (*arrows*). (**C**) Coronal CT image confirms comminuted fracture of lateral maxillary sinus wall (*arrow*) with soft-tissue swelling in sinus, probably blood clot. (**D**) Coronal CT image shows fluid-air level and collections of subcutaneous air close to destroyed maxillary sinus wall (*arrow*)

8.12 Blowout Fracture

Figs. 8.33, 8.34, and 8.35

8.12.1 Definition

Fracture of inferior or medial orbital wall, usually not involving orbital rim (classic).

8.12.2 Clinical Features

- Only 3–5% of all midfacial fractures
- Diplopia
- Enophthalmos, exophthalmos

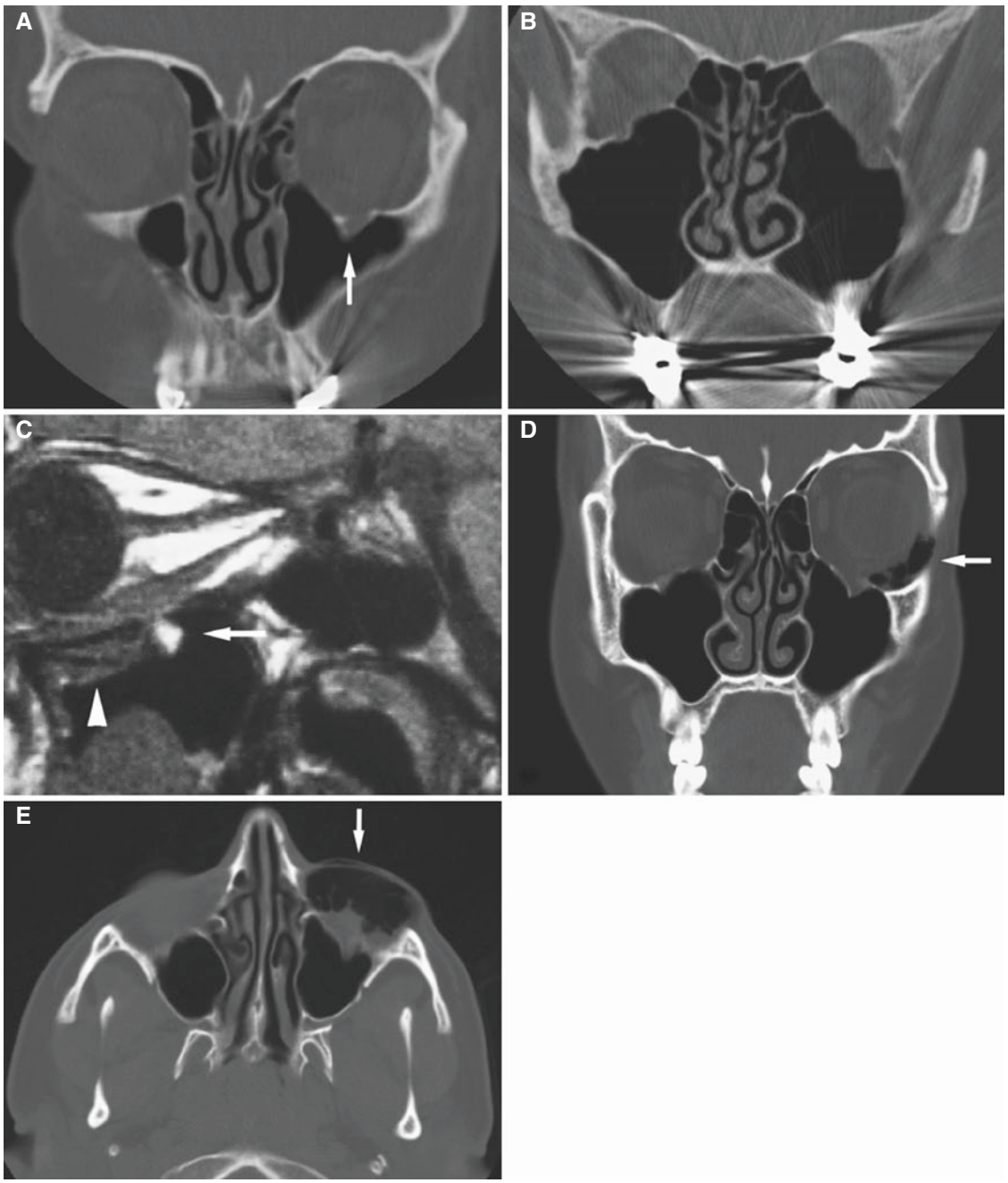

Fig. 8.33 Blowout fracture, classic; 60-year-old female with fall on the face 10 days previously, with infraorbital hematoma and some tenderness. (**A**) Coronal CT image shows fracture of orbital floor (*arrow*). (**B**) Coronal CT image, more posterior section, shows otherwise normal sinuses. (**C**) Sagittal MRI of another patient shows orbital fat (*arrow*) and bone fragment and mucosal swelling or muscle tissue (*arrowhead*) in maxillary sinus due to blowout fracture; note intact orbital rim (courtesy of Dr. A. Kolbenstvedt, Oslo University Hospital, Rikshospitalet, Oslo, Norway). (**D**) Coronal CT image of another patient shows orbital air collection (*arrow*). (**E**) Axial CT image of same patient as in (**D**) shows large subcutaneous emphysema (*arrow*)

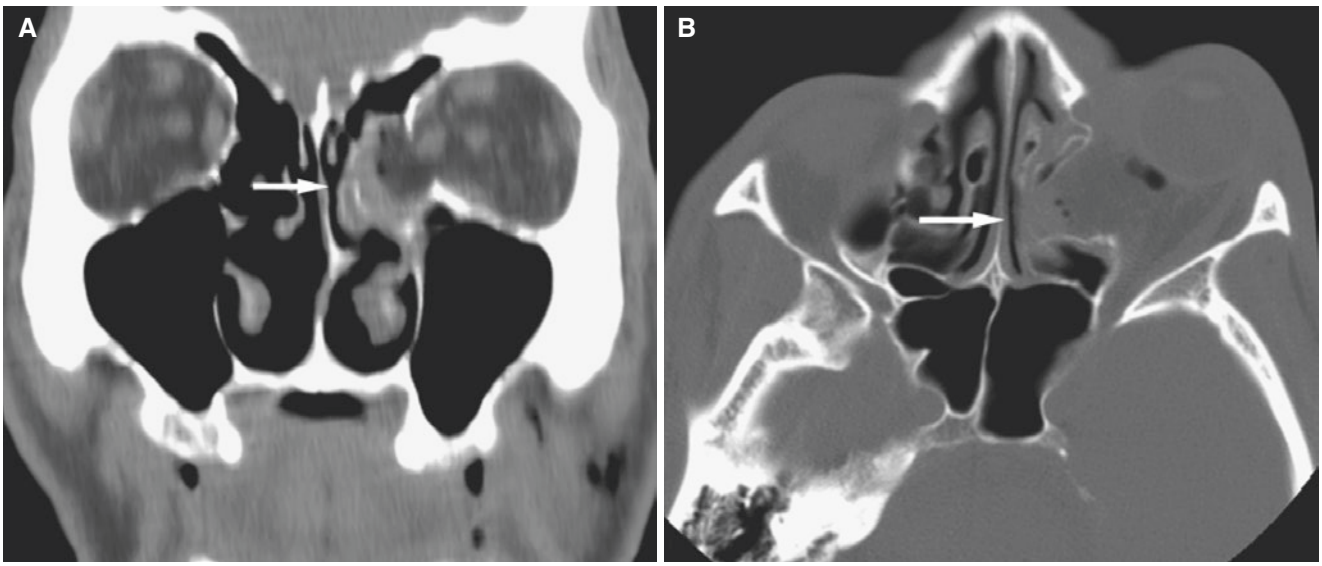

Fig. 8.34 Blowout fracture, medial; 54-year-old male who was struck by a car from behind. (**A**) Coronal CT image shows fracture of the left medial orbital wall and soft tissue with periorbital fat in ethmoid cells (*arrow*). (**B**) Axial CT image shows fracture of the lamina papyracea with opacification of the left ethmoid cells (*arrow*) and air collection in orbit. Soft-tissue swelling over the left periorbital area

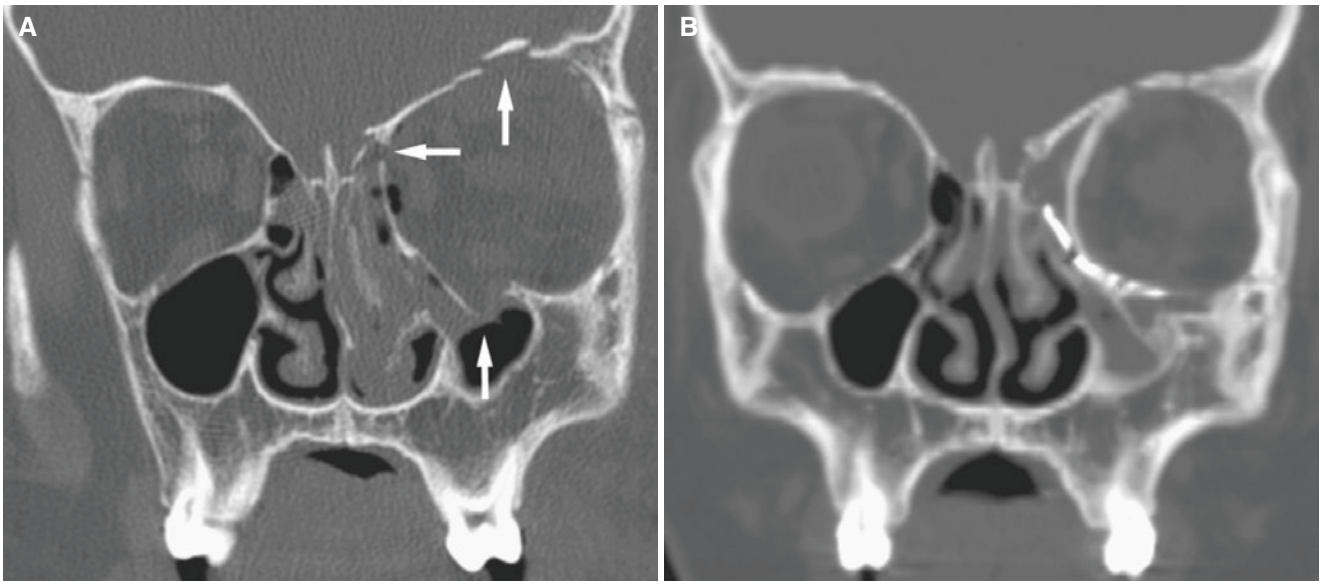

Fig. 8.35 Blowout fracture, extensive with fractures of the maxillary wall and nasal bone; 15-year-old male with trauma to the left face and eye; now to postoperative examination of bone graft from calvarial bone. (**A**) Coronal CT image shows fractures of the left orbital floor and medial and superior walls (*arrows*), some air collection in orbit, and soft-tissue swelling in ethmoid cells, nasal cavity, and maxillary sinus. (**B**) Coronal CT image, postoperative, shows normal configuration of the left orbit, with opacification of ethmoid cells and maxillary sinus

Suggested Reading

Adi M, Odgen GE, Chisholm DM (1990) An analysis of mandibular fractures in Dundee, Scotland. Br J Oral Maxillofac Surg 28:194–199

Arden RL, Crumley RL (1993) Cartilage grafts in open rhinoplasty. Facial Plast Surg 9:285–294

Boffano P, Roccia F, Gallesio C, Berrone S (2013) Pathological mandibular fractures : a review of the literature of the last two decades. Dent Traumatol 29:185–196

Chacon GE, Dawson KH, Myall RW, Beirne OR (2003) A comparative study of two imaging techniques for the diagnosis of condylar fractures in children. J Oral Maxillofac Surg 61:668–672

Cooke HE, Rowe M (1990) A retrospective study of 356 midfacial fractures occurring in 225 patients. J Oral Maxillofac Surg 48: 574–578

Dolan KD, Ruprecht A (1992) Imaging of midfacial fractures. In: Westesson P-L (ed) Contemporary maxillofacial imaging. Oral and maxillofacial surgery clinics of North America. Saunders, Philadelphia, pp 125–151

Durst A, Clibbon J, Davis B (2015) Distal tibial fractures are a poorly recognised complication with fibula free flaps. Ann R Coll Surg Engl 97:409–413

Farman AG, Nortje C, Wood RE (1993) Traumatic injuries. In: Oral and maxillofacial diagnostic imaging. Mosby, St. Louis, pp 158–180

Haug RH, Foss J (2000) Maxillofacial injuries in the pediatric patient—a review. Oral Surg Oral Med Oral Pathol Oral Radiol Endod 90:126–134

Heiland M, Schmelzle R, Hebecker A, Schulze D (2004) Intraoperative 3D imaging of the facial skeleton using the SIREMOBIL Iso-C3D. Dentomaxillofac Radiol 33:130–132

Henriksen LH, Trebo S (1988) Post-traumatic coronoid impingement on zygomatic arch: CT demonstration. J Comput Assist Tomogr 12:712–713

Honda K, Larheim TA, Johannessen S, Arai Y, Shinoda K, Westesson P-L (2001) Ortho cubic super-high resolution computed tomography: a new radiographic technique with application to the temporomandibular joint. Oral Surg Oral Med Oral Pathol Oral Radiol Endod 91:239–243

Kucik CJ, Clenney T, Phelan J (2004) Management of acute nasal fractures. Am Fam Physician 70:1315–1320

Lam EW (2014a) Trauma. In: White SW, Pharoah MJ (eds) Oral radiology. Principles and interpretation, 7th edn. Mosby, St. Louis, pp 562–581

Lam WNE (2014b) Traumata. In: White SW, Pharoah MJ (eds) Oral radiology. Principles and interpretation, 7th edn. Mosby, St. Louis, pp 562–581

Lamphier J, Ziccardi V, Ruvo A, Janel M (2003) Complications of mandibular fractures in an urban teaching center. J Oral Maxillofac Surg 61:745–750

Munate-Cardenas JL, Facchina Nunes PH, Passeri LA (2015) Etiology, treatment, and complications of mandibular fractures. J Craniofac Surg 26:611–615

Roman R, Hedeșiu M, Fildan F, Ileșan R, Mitea D, Dinu C, Băcuit M (2016) The use of reformatted cone beam CT images in assessing mid-face trauma, with a focus on the orbital floor fractures. Clujul Med 89:519–524

Rowe NL (1985) Maxillofacial injuries—current trends and techniques. Injury 16:513–525

Scheyerer MJ, Döring R, Fuchs N, Metzier P, Sprengel K, Werner CM et al (2015) Maxillofacial injuries in severely injured patients. J Trauma Manag Outcomes 9:4. doi:10.1186/s13032-015-0025-2

Schimming R, Eckelt U, Kittner T (1999) The value of coronal computer tomograms in fractures of the mandibular condyle process. Oral Surg Oral Med Oral Pathol Oral Radiol Endod 87:632–639

Schuknecht B, Graetz K (2005) Radiologic assessment of maxillofacial, mandibular, and skull base trauma. Eur J Radiol 15:560–568

Schwenzer N (1986) Corrective operations following primary surgical management of facial cleft patients (in German). Fortschr Kieferorthop 47:540–546

Silvennoinen U, Iizuka T, Lindqvist C, Oikarinen K (1992) Different patterns of condylar fractures: an analysis of 382 patients in a 3-year period. J Oral Maxillofac Surg 50:1032–1037

Silvennoinen U, Iizuka T, Oikarinen K, Lindqvist C (1994) Analysis of possible factors leading to problems after nonsurgical treatment of condylar fractures. J Oral Maxillofac Surg 52:793–799

Smith PH (1967) Blow out fracture of the floor of the orbit. Aust N Z J Surg 36:319–322

Som PM, Brandwein MS (2003) Facial fractures and postoperative findings. In: Som PM, Curtin HD (eds) Head and neck imaging, 4th edn. Mosby, St. Louis, pp 374–438

Sullivan SM, Banghart PR, Anderson Q (1995) Magnetic resonance imaging assessment of acute soft tissue injuries to the temporomandibular joint. J Oral Maxillofac Surg 53:763–766

Takahashi T, Ohtani M, Sano T, Ohnuki T, Kondoh T, Fukuda M (2004) Magnetic resonance evidence of joint effusion of the temporomandibular joint after fractures of the mandibular condyle: a preliminary report. Cranio 22:124–131

Tanaka H, Westesson PL, Larheim TA (1998) Juxta-articular ankylosis of the temporomandibular joint as an unusual cause of limitation of mouth opening: case report. J Oral Maxillofac Surg 56:243–246

Timashpolsky A, Dagum AB, Sayeed SM, Romeiser JL, Rosenfeld EA, Conkling N (2016) A prospective analysis of physical examination findings in the diagnosis of facial fractures: determining predictive value. Plast Surg (Oakv) 24:73–79

Yanagisawa E, Smith HW (1973) Normal radiographic anatomy of the paranasal sinuses. Otolaryngol Clin N Am 6:429–457

Ziegler CM, Woertche R, Brief J, Hassfeld S (2002) Clinical indications for digital volume tomography in oral and maxillofacial surgery. Dentomaxillofac Radiol 31:126–130

Facial Growth Disturbances

9

Abstract

This chapter illustrates isolated disturbances; cleft palate/lip, choanal atresia, torus maxillaris, condylar hyperplasia, cherubism, fibrous dysplasia, TMJ fracture/infection complication. TMJ internal derangement complication, and juvenile idiopatic arthritis, and syndromes; Down syndrome, premature cranial synostoses, non-synostotic occipital plagiocephaly, Turner syndrome, Hemifacial microsomia, Treacher Collins syndrome, Crouzon syndrome, Apert syndrome, Achondroplasia, Pyknodysostosis, and Ectodermal dysplasia, and miscellaneous conditions.

9.1 Introduction

A number of growth disturbances may occur of the facial bones, of which some are rather frequent and may have an obvious impact on facial appearance and vital functions. Jaws and dentitions may be involved. Thus, such anomalies are of great interest to dental professionals.

Advanced imaging evaluation is necessary, and in particular 3D CT imaging is increasingly used to assess growth disturbances of this complicated anatomic region. The visualization of bone (and skin) morphology is superior to different series of 2D images although some detail is lost as part of the smoothing algorithm used. This chapter illustrates a number of cases, frequently with 3D CT images. A combination of 3D for overview with 2D images for bony details represents up-to-date imaging of facial growth disturbances.

9.2 Isolated Disturbances

A number of isolated growth disturbances may occur in the facial skeleton.

9.3 Common Cleft Palate and/or Cleft Lip

Figs. 9.1, 9.2, and 9.3

In collaboration with S. I. Blaser, N. Kakimoto.

9.3.1 Definition

Congenital defect involving lip only, lip and palate, or palate only.

9.3.2 Clinical Features

- Most common facial birth defect; cleft lip with or without cleft palate in about 1 per 1000 live births (range 0.7–1.3)
- More common in American Indians and Japanese and less common in blacks
- Almost 99% of all facial clefts
- Isolated cleft palate less frequent
- Most often unilateral
- Males more frequent than females in severe cases
- 50–70% of patients are nonsyndromic
- Part of more than 300 recognized entities
- Obvious esthetic and functional problems such as insufficient suction for feeding

9.3.3 Imaging Features (Bone Structures)

- The maxillary alveolar process is split in lateral incisor region, either unilaterally or bilaterally
- The anterior hemimaxilla shows narrowed curvature and upward tilting of premaxillary segment on the cleft side

T.A. Larheim, P.-L.A. Westesson, *Maxillofacial Imaging*, https://doi.org/10.1007/978-3-319-53319-3_9

- Palatal end of the nasal septum on the cleft side, anterior nasal spine on contralateral side in unilateral clefts
- Partial or complete bony defect with corticated margins of the alveolar ridge and hard palate
- In newborns; premaxilla "loosened" from the remaining maxilla in bilateral cases
- Variable degrees of midfacial hypoplasia
- Teeth missing, deformed, displaced, or supernumerary

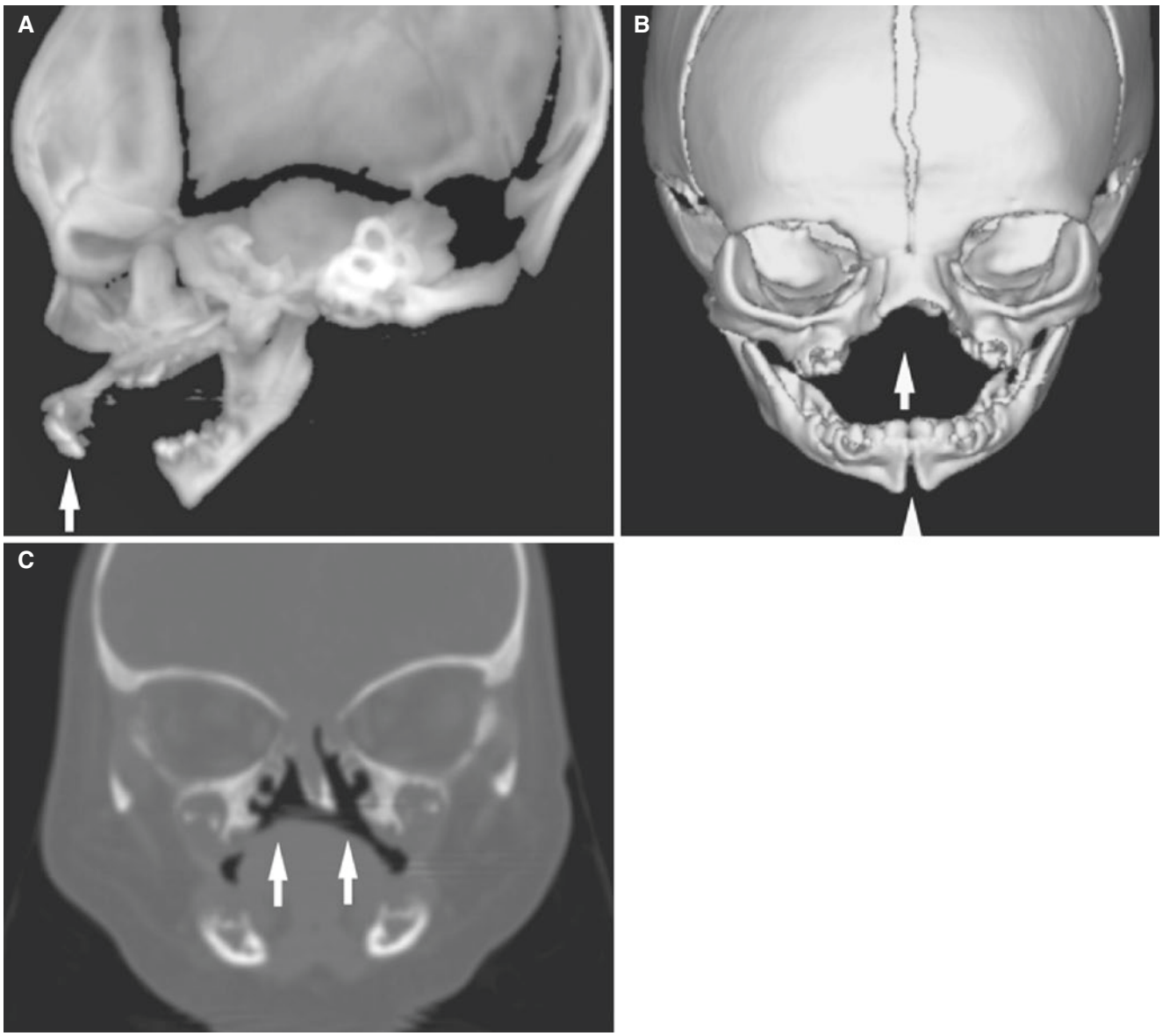

Fig. 9.1 Cleft lip and palate, bilateral; 1-day-old male with multiple congenital anomalies (syndromic features). (**A**) Lateral CT scout image shows dislocation of premaxilla (*arrow*). (**B**) 3D CT image shows bilateral maxillary cleft (*arrow*) and mandibular midline cleft as well (*arrowhead*). Single nasal bone (which usually indicates intracranial abnormalities in patients with midline anomalies). (**C**) Coronal CT image shows bilateral maxillary cleft (*arrows*)

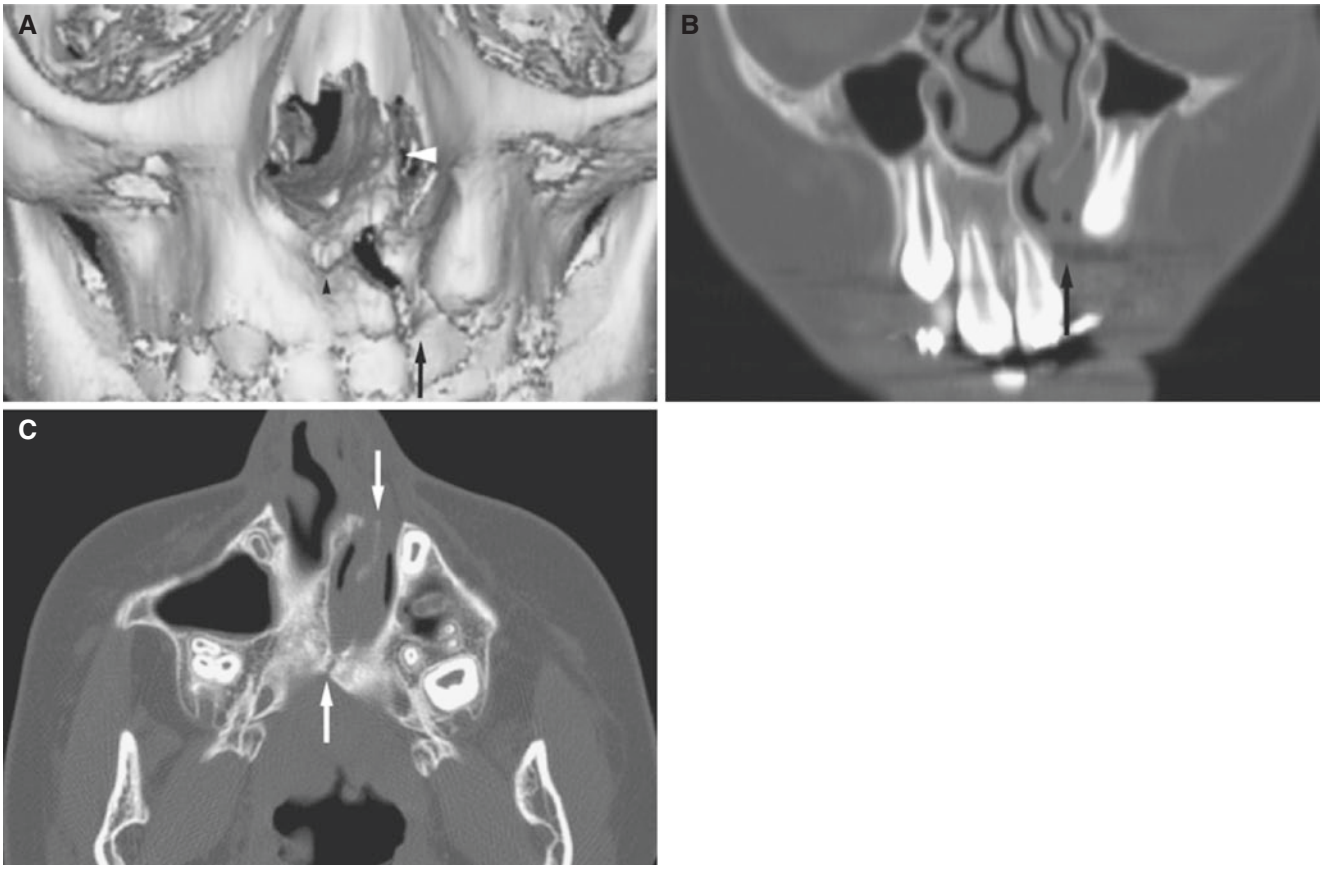

Fig. 9.2 Cleft palate, unilateral; 11-year-old male with untreated deformity. (**A**) 3D CT image shows cleft on left side (*arrow*). Note the nasal septum deviating to the cleft side (*arrowhead*) and the anterior nasal spina (*small arrowhead*) deviating to the non-cleft side. (**B**) Coronal CT image shows cleft through alveolar process and nasal cavity (*arrow*). (**C**) Axial CT image shows that cleft is corticated and completely through palate (*arrows*)

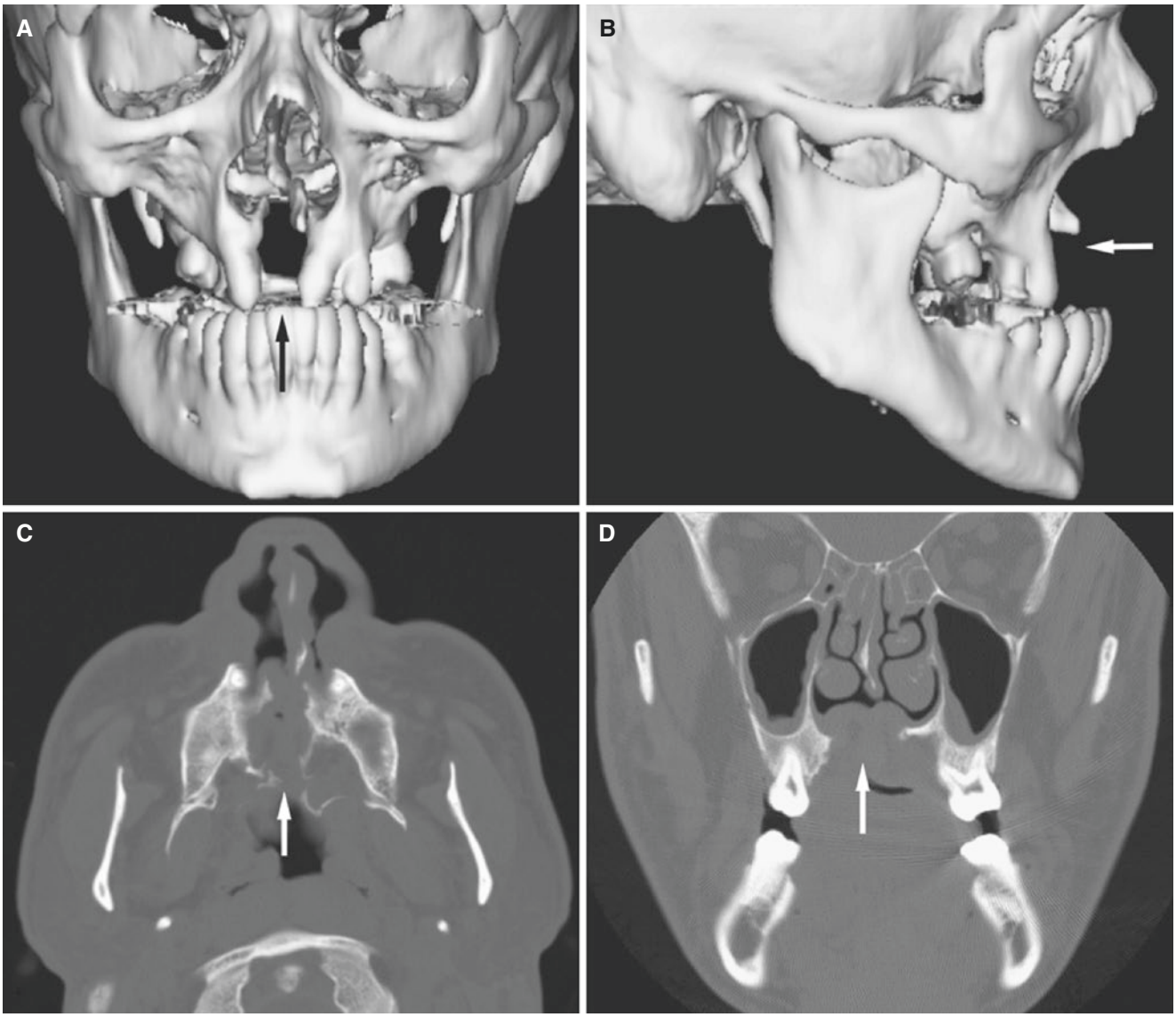

Fig. 9.3 Cleft palate, midline; 31-year-old male with untreated deformity. (**A**) 3D CT image, en face view, shows almost symmetric cleft (*arrow*) with premaxillary segment and incisors absent. Narrow nasal bone. (**B**) 3D CT image, lateral view, shows hypoplastic maxilla (*arrow*). (**C**) Axial CT shows large, complete defect (*arrow*). (**D**) Coronal CT image shows soft-tissue lining to nasal cavity (*arrow*), mucosal thickening in ethmoid sinuses, and minimal mucosal thinning in maxillary sinuses

9.4 Choanal Atresia

Fig. 9.4

9.4.1 Definition

Congenital anomaly of occluded posterior choana (either bony or membranous) with no communication between nasal cavity and nasopharynx on one or both sides.

9.4.2 Clinical Features

- Incidence about 1 per 5000–7000 births
- 20–50% of patients have other congenital anomalies such as cleft palate and a syndrome
- Males more frequent than females
- Present at birth with immediate respiratory distress, in particular if bilateral since neonates are obligate nose breathers and cannot feed because a patent nose is necessary to breathe during feeding
- Nasal stuffiness and mucoid discharge. Mucus in posterior nasal cavity can simulate a membrane

9.4.3 Imaging Features

- Bony plate (80–90%) or membranous web (10–20%) between the vomer and lateral nasal wall
- Bony thickening of the posterolateral nasal wall and posterior vomer, narrowing of posterior nasal cavity
- Two-thirds are unilateral

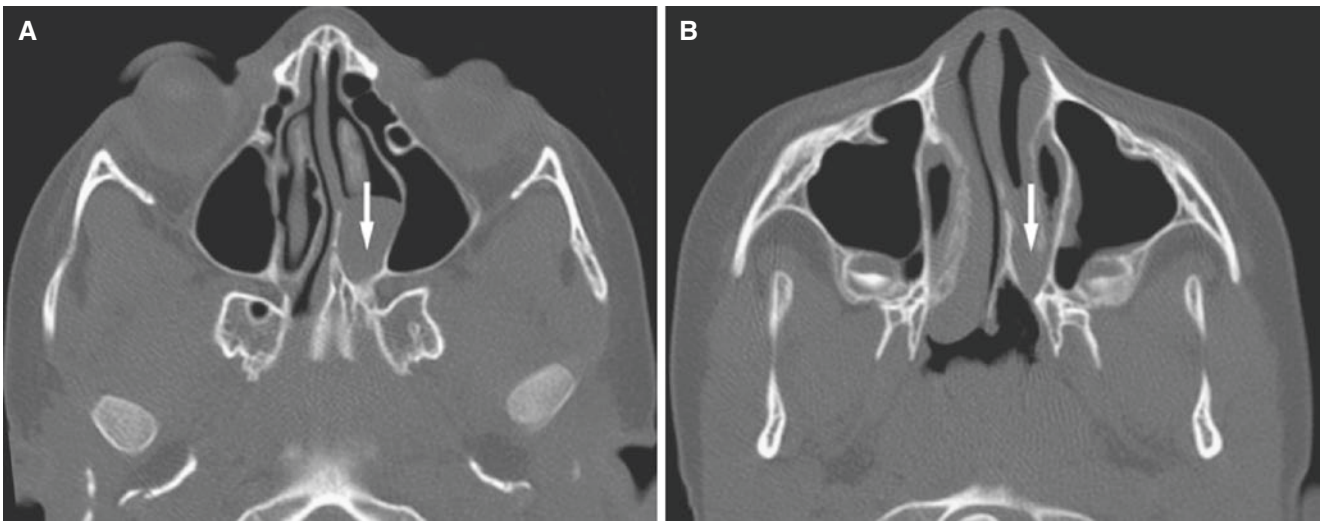

Fig. 9.4 Choanal atresia; 7-year-old female presented with chronic left nasal obstruction. (**A**) Axial CT image shows bony plate between the posterior vomer and posterior lateral nasal wall (*arrow*) and probable mucus plug in the nasal cavity. (**B**) Axial CT image, more caudal section, shows a very thin bony plate (*arrow*)

9.5 Torus Maxillaris, Palatinus, and Mandibularis

Fig. 9.5

9.5.1 Definition

Hyperostosis of normal cortical and medullary bone.

9.5.2 Clinical Features

- Torus palatinus: midline of hard palate along intermaxillary–interpalatine suture; nasal aspect of palate never affected
- Torus maxillaris: alveolar process either on buccal aspect (externus) or on palatal aspect (internus); frequently bilateral and usually in premolar area; single or multiple (most frequent)
- Torus mandibularis: alveolar process on lingual aspect in premolar area; frequently bilateral (80%); single or multiple

9.5.3 Torus Palatinus

- Found in at least 20% of a general US population
- Highly variable incidence in diverse ethnic populations; high in Amerindians and Alaskan Eskimos
- Inherited anomalies documented; 40–60% chance of occurrence with one or both affected parents compared with 5–8% chance with unaffected parents

Fig. 9.5 Torus maxillaris; 50-year-old male with incidental finding. Clinical photo shows multiple buccal exostoses of the right maxilla (*arrow*), similar on the left side (not shown)

- Only about 2% in newborns, increasing incidence with age
- Growth with individual up to 20–30 years; usually noticeable in adult age
- Females more frequent than males

See also Chap. 3

9.6 Condylar Hyperplasia

Fig. 9.6

9.6.1 Definition

Unilateral overgrowth of mandibular condyle.

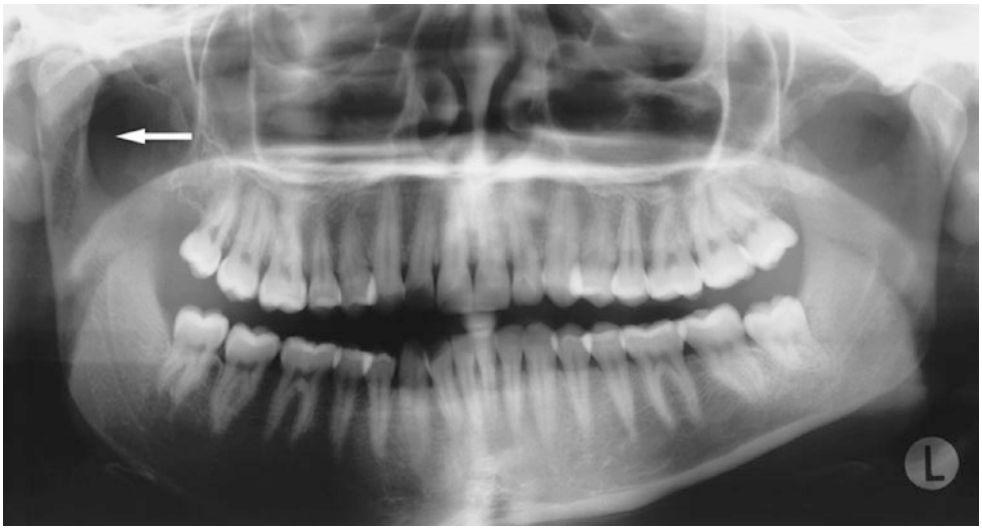

Fig. 9.6 Condylar hyperplasia; 23-year-old female with facial asymmetry and dental malocclusion. Panoramic view shows enlarged right mandibular condyle and neck (*arrow*) as well as enlarged mandibular body (other images of this patient in Fig. 6.57)

9.6.2 Clinical Features

- Facial asymmetry; right or left side equally often
- Frequently noticeable in the third decade
- Females more frequent than males
- Dental malocclusion

9.6.3 Imaging Features

- Unilaterally enlarged condyle in cranial direction
- Entire mandible on one side my also become enlarged; hemifacial hypertrophy (hyperplasia), which may be present at birth or later

See also Chap. 6

9.7 Cherubism

Fig. 9.7

9.7.1 Definition

Hereditary condition characterized by progressive bilateral swelling of the mandibular angles during childhood, histopathologically similar to giant cell granuloma.

9.7.2 Clinical Features

- Sporadic cases reported
- Usually detected during early childhood around 4 years of age
- Symmetric and painless, rarely unilateral
- Occasionally also maxilla; tuberosities
- No other parts of skeleton involved

9.7.3 Imaging Features

- Bilateral multilocular radiolucencies; jaw expansion may be extensive
- Displacement of mandibular canals
- Usually not condyle regions
- Displacement of the teeth mesially, problematic eruption
- Premature exfoliation of the primary teeth

See also Chap. 3

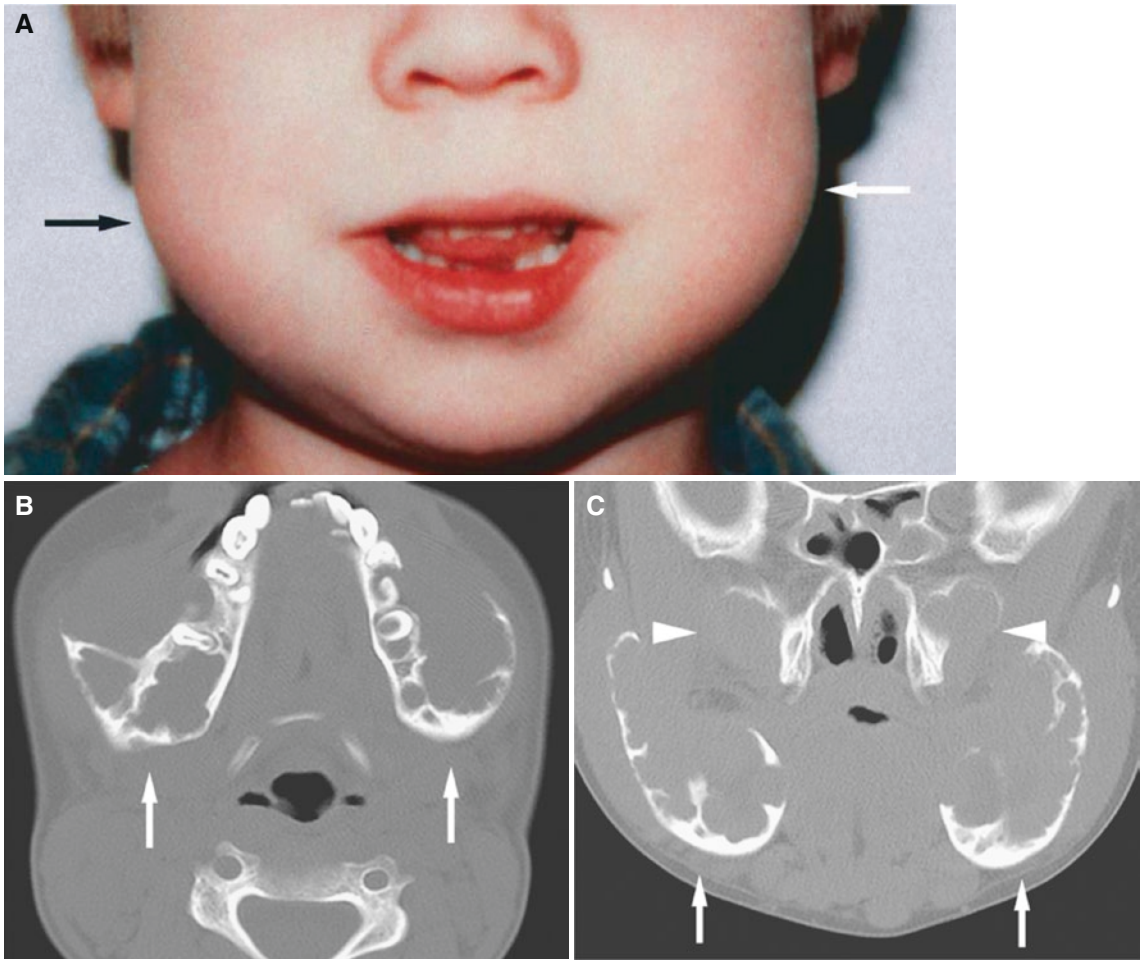

Fig. 9.7 Cherubism; 6-year-old male with gradually increasing swelling of the face and mandible bilaterally. (**A**) Clinical photograph shows bifacial swelling (*arrows*). (**B**) Axial CT image shows expanded jaw radiolucencies bilaterally (*arrows*). (**C**) Coronal CT image confirms bilateral jaw expansion (*arrows*). Note also bilateral expansion of the maxilla (*arrowheads*)

9.8 Fibrous Dysplasia

Fig. 9.8

9.8.1 Definition

Benign skeletal disorder; medullary bone replaced by metaplastic fibrous tissue.

9.8.2 Clinical Features

- Painless increasing bone deformity
- Most common benign skeletal disorder

9.8.3 Imaging Features

- Bone deformity may be extensive
- Radiolucent and/or radiopaque bone
- Ground-glass appearance characteristic; thick and sclerotic bone

See also Chap. 3

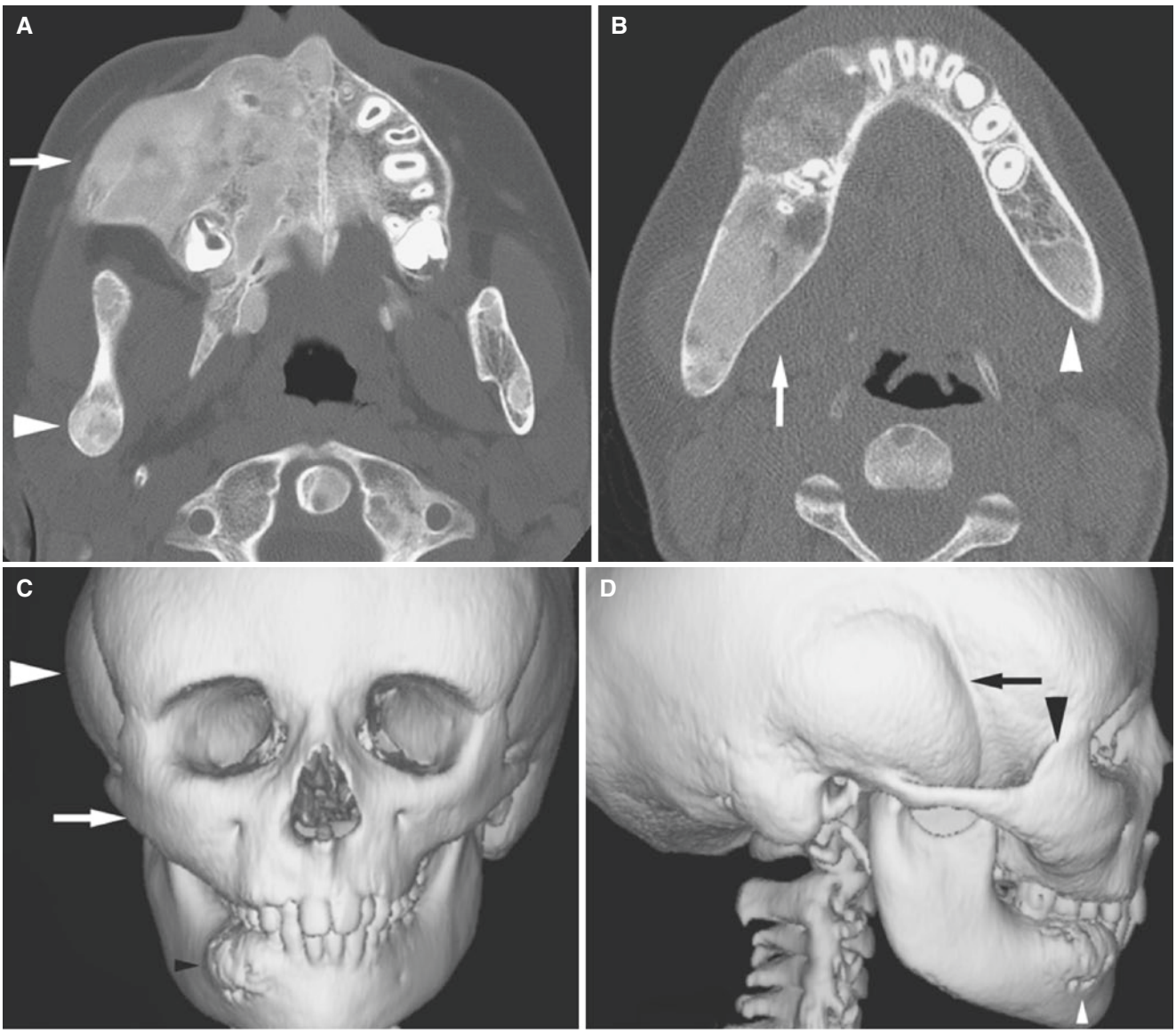

Fig. 9.8 Craniofacial fibrous dysplasia; 11-year-old female with painless gradually increasing swelling of the right face and mandible. (**A**) Axial CT image shows typical ground-glass appearance of evidently expanded right maxilla (*arrow*) and of the right mandible (*arrowhead*). (**B**) Axial CT image shows ground-glass appearance of the entire right mandibular body (*arrow*) and also in the minor part of the left mandible (*arrowhead*). (**C**) 3D CT image, en face view, shows evident growth deformity of the right maxilla and zygoma (*arrow*), right temporal bone (*arrowhead*), and right mandible (*small arrowhead*). (**D**) 3D CT image, right side, shows growth deformity of the temporal bone (*arrow*), zygoma (*arrowhead*), and mandible (*small arrowhead*). (**E**) 3D CT image, axial view, shows growth deformity of the left occiput (*arrow*)

Fig. 9.8 (continued)

9.9 Mandibular Neck/TMJ Fracture or TMJ Infection Complication

Figs. 9.9 and 9.10

Fractures or infections may lead to growth disturbances when they occur in younger patients and are not treated properly; in adults fractures may lead to dental occlusion problems such as open bite (see Fig. 8.19) or restricted mouth-opening capacity due to contact between the coronoid process and fractured zygomatic arch.

9.9.1 Clinical Features

- Micrognathic growth; bilateral complication
- Mandibular asymmetric growth; unilateral complication
- Dental malocclusion
- Variable restricted mouth-opening capacity
- Deviation of mandible on opening

9.9.2 Imaging Features

- TMJ deformity or fibro-osseous ankylosis (see Chap. 6)

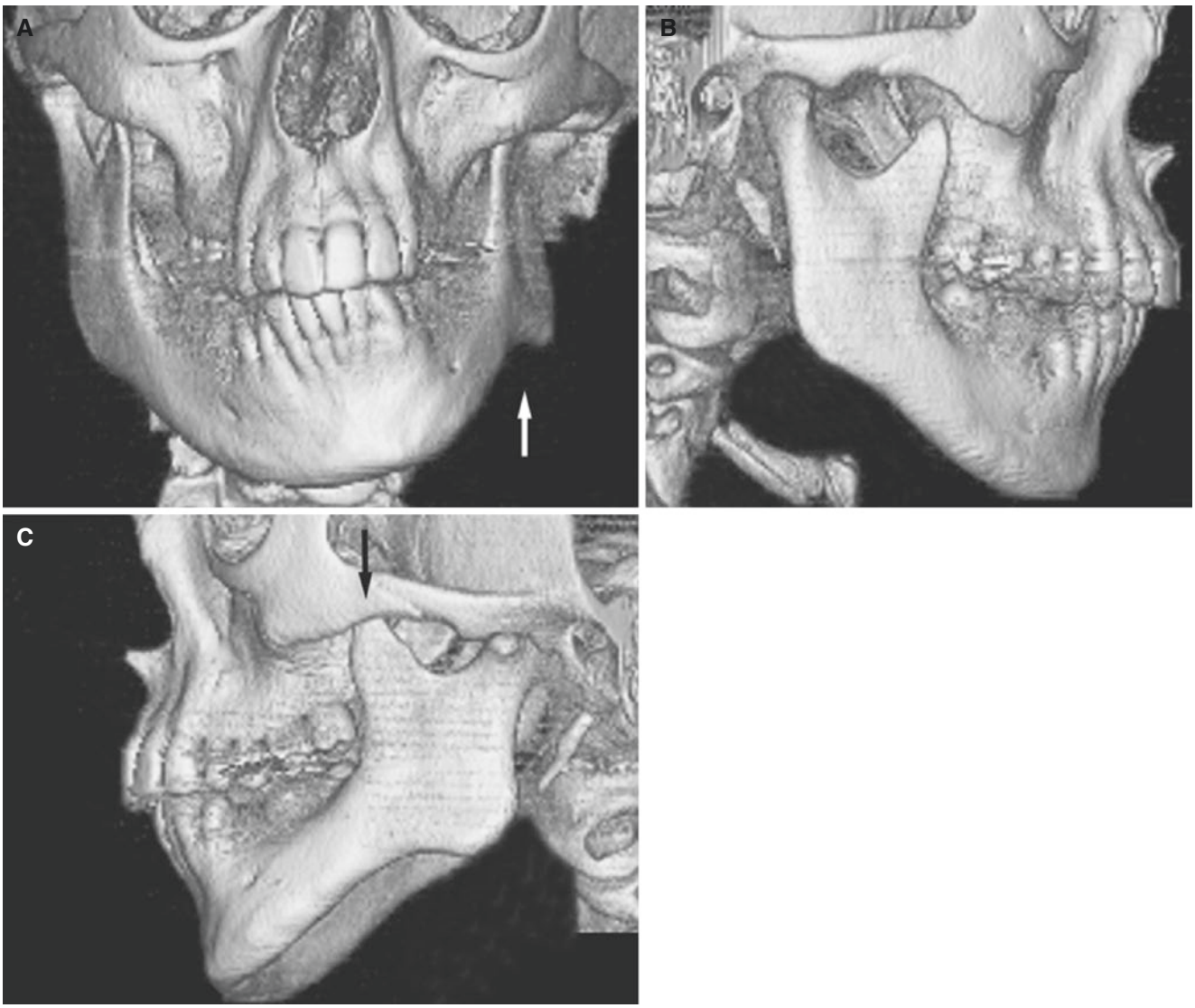

Fig. 9.9 Facial asymmetry; 15-year-old male with previous trauma to the mandible. (**A**) 3D CT image, en face view, shows evident mandibular asymmetry with antegonial notching (*arrow*) of abnormal side. (**B**) 3D CT image, lateral view, shows normally developed right mandible. (**C**) 3D CT image, lateral view, shows underdeveloped left mandible. Note the large coronoid process (*arrow*) compared to contralateral normal side. (**D**) Oblique coronal CT image, mid-condyle section (*left*); oblique sagittal CT image, mid-condyle section (*central*); and oblique sagittal CT image, lateral section (*right*), of the left TMJ show deformed condyle and fossa, flattened with cortical irregularities (*arrow*). (**E**) Oblique coronal CT image, mid-condyle section (*left*), and oblique sagittal CT image, mid-condyle section (*right*), of the right TMJ show normal bone and well-developed fossa (*arrow*)

Fig. 9.9 (continued)

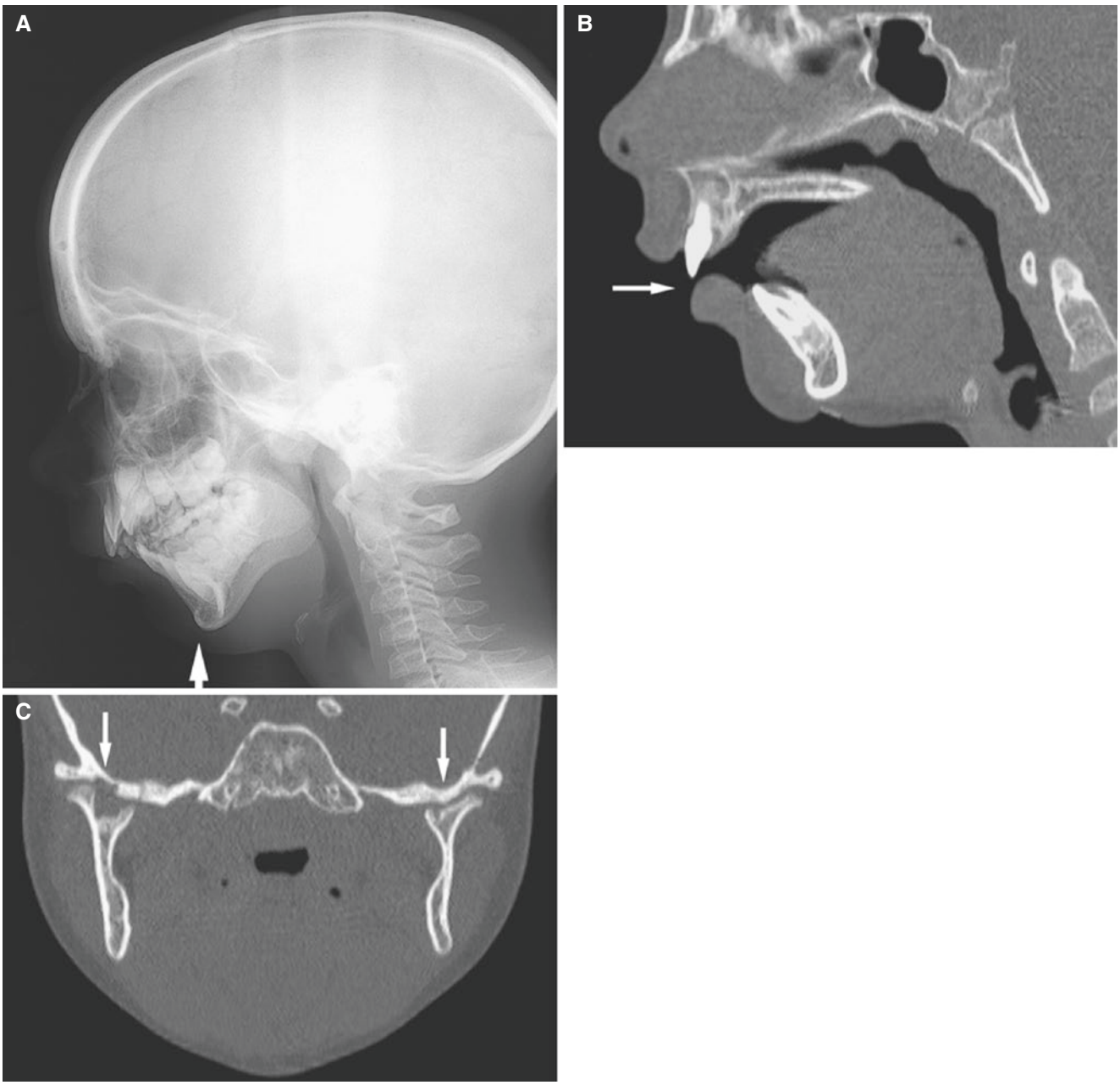

Fig. 9.10 Mandibular underdevelopment; 7-year-old male with history of septic arthritis at birth with subsequent osteomyelitis and surgery of hips, now with gradually inhibited mandibular growth and mouth-opening capacity (27 mm). (**A**) Lateral view shows mandibular retrognathia (*arrow*) with some asymmetry. (**B**) Sagittal CT image shows severe dental malocclusion (*arrow*). (**C**) Coronal CT image shows bilaterally deformed TMJs but no ankyloses (*arrows*)

9.10 TMJ Internal Derangement Complication

There is evidence that anterior disc displacement with accompanying joint abnormalities (but without fractures) in younger age groups may have an impact on mandibular growth.

See Chap. 6

9.11 Juvenile Idiopathic Arthritis

Figs. 9.11 and 9.12

9.11.1 Definition

Inflammatory synovial disease that attacks children before 16 years of age.

9.11.2 Clinical Features

- Micrognathia, but compensatory growth of the anterior part of mandible
- Facial asymmetry
- More frequent in those with early onset and polyarticular disease; in particular with a disease course from pauciarticular (four or fewer joints) to polyarticular (five or more joints)
- Females more frequent than males

9.11.3 Imaging Features

- TMJ abnormalities; bilateral in micrognathia cases
- Unilateral TMJ abnormalities, or more severe on one side, in mandibular asymmetry cases
- Abnormal condyle; hypoplastic, flat
- Abnormal fossa; flat

See also Chap. 6

Fig. 9.11 Micrognathia; 28-year-old female with juvenile idiopathic arthritis presenting before the age of 4 years and now with severe bilateral TMJ abnormalities. Lateral view shows severely underdeveloped mandible with bilateral notching (*arrow*). Note atlantoaxial dislocation and bony ankylosis of the cervical spine and surgical fixation of the spine to the skull

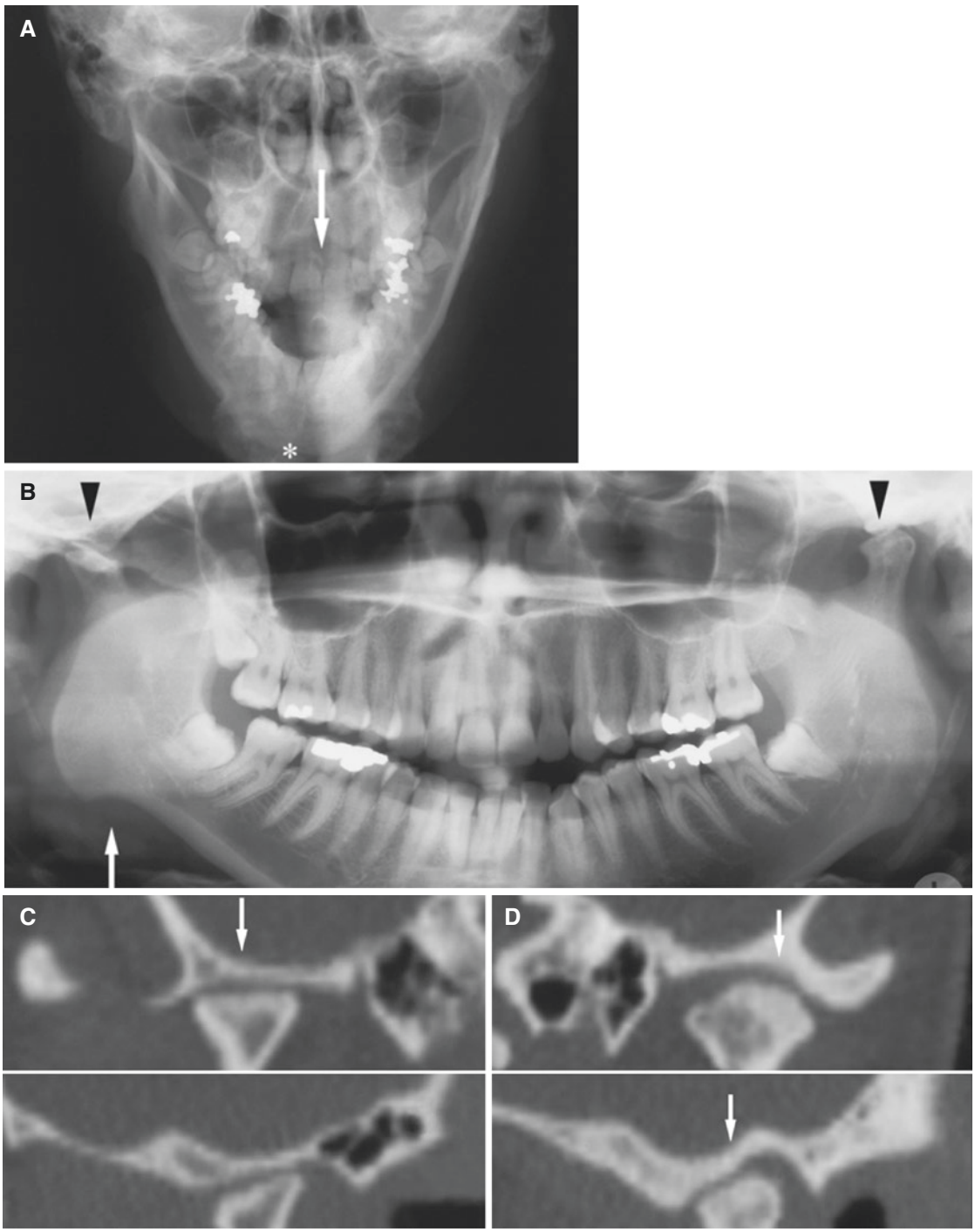

Fig. 9.12 Retrognathia, slight micrognathia, and facial asymmetry; 35-year-old female with juvenile idiopathic arthritis from early childhood. (**A**) Posteroanterior view shows asymmetric mandible (*asterisk* midpoint of the chin) with deviation to the right side on the mouth opening (*arrow* midline of the maxilla). (**B**) Panoramic view shows mandibular asymmetry with most underdevelopment and antegonial notching (*arrow*) on the right side and bilateral condyle abnormalities (*arrowheads*) with most severe abnormalities of the right joint. (**C**) CT images, oblique coronal (*upper*) and oblique sagittal (*lower*) views, of the right TMJ show deformed, flattened condyle and fossa with cortical (irregular) outline (*arrow*). (**D**) CT image, oblique coronal (*upper*) and oblique sagittal (*lower*) views, of the left TMJ show deformed condyle and fossa, but less pronounced than in the contralateral joint. Note also sclerosis both in the condyle and fossa (*arrows*), indicating secondary osteoarthritis

9.12 Syndromes

A number of syndromes may have facial growth disturbances as part of their anomalies.

9.13 Down Syndrome

Figs. 9.13 and 9.14

9.13.1 Clinical Features

- Most common genetic syndrome; incidence about 1 per 650 live births, but highly variable in different populations (1/600–1/2000)
- High association with increased maternal age
- Muscular hypotonia, large tongue
- Hyperextensibility of joints
- Short stature
- Cardiovascular anomalies
- Mental retardation
- Flattened facial profile and occiput
- Hypodontia
- Airway and hearing problems
- Average life expectancy less than half normal

9.13.2 Imaging Features

- Midfacial hypoplasia
- Flattened nose bridge
- Maxillary sinus hypoplasia; absent frontal and sphenoid sinuses
- Relative mandibular prognathism
- Ear abnormalities
- Atlantoaxial dislocation

Fig. 9.13 Down syndrome; 16-year-old. (**A**) Axial CT image shows hypoplastic, retruded left maxilla (*arrow*). (**B**) Coronal CT image shows hypoplastic left maxillary sinus (*arrow*)

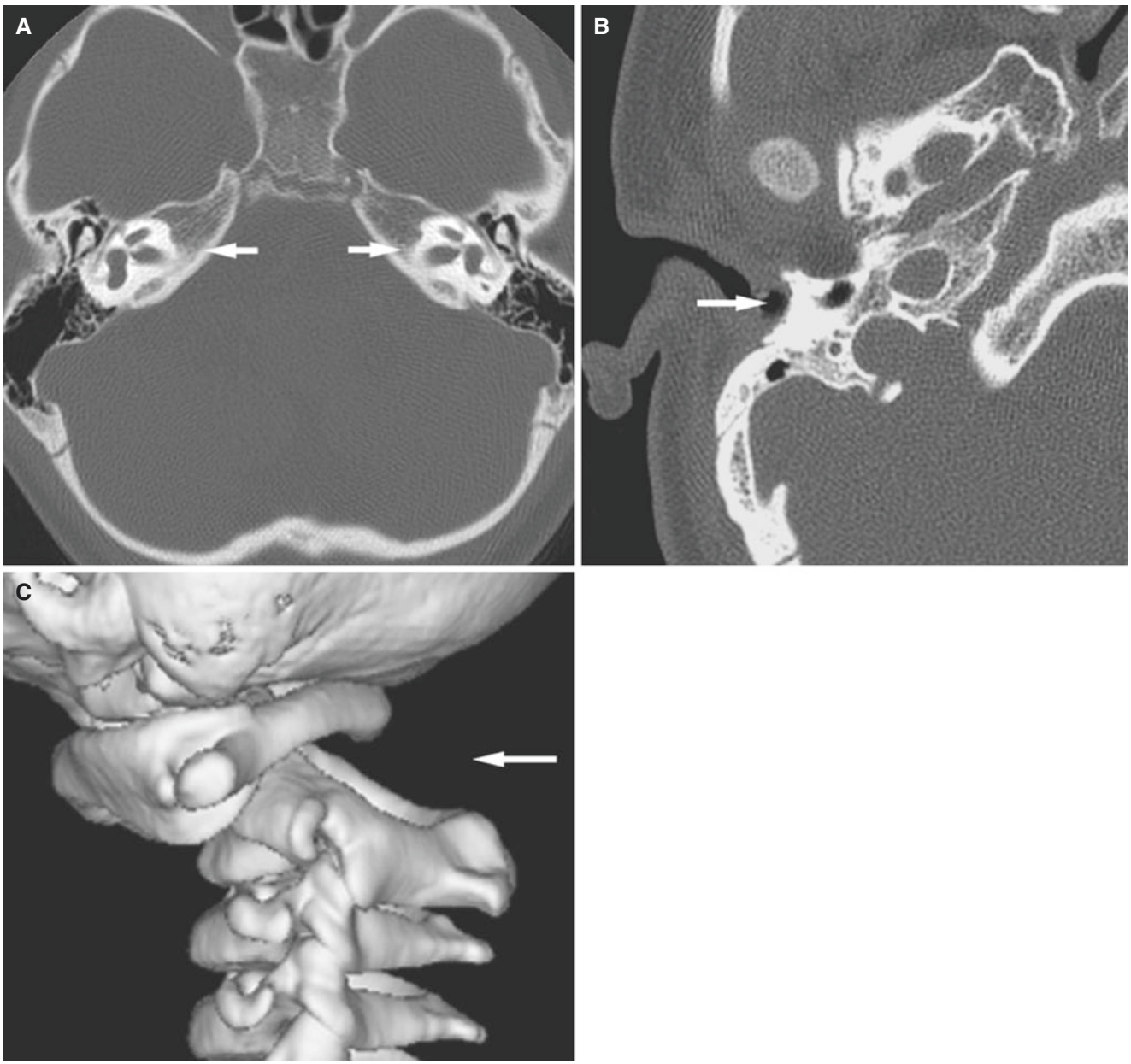

Fig. 9.14 Down syndrome; 4-year-old. (**A**) Axial CT image shows vestibular dysplasia (*arrows*). (**B**) Axial CT image shows stenosis of external auditory canal (*arrow*). (**C**) 3D CT image shows C1–C2 dislocation (*arrow*)

9.14 Premature Cranial Synostoses

Fig. 9.15

9.14.1 Definition

Premature fusion of one or more cranial sutures resulting in abnormal skull shape.

9.14.2 Clinical Features

- Estimated incidence up to 1 per 2000 live births
- Mostly isolated (85%)
- Classic types: scaphocephaly, plagiocephaly (anterior or posterior), brachycephaly, trigonocephaly, oxycephaly (turricephaly), cloverleaf skull
- Only 15% syndromic (see Syndromic Craniosynostoses)

9.14.3 Imaging Features

- Premature cranial suture closure; sagittal synostosis (scaphocephaly) and unilateral coronal synostosis (plagiocephaly) most frequent
- Cranial deformity of variable degree

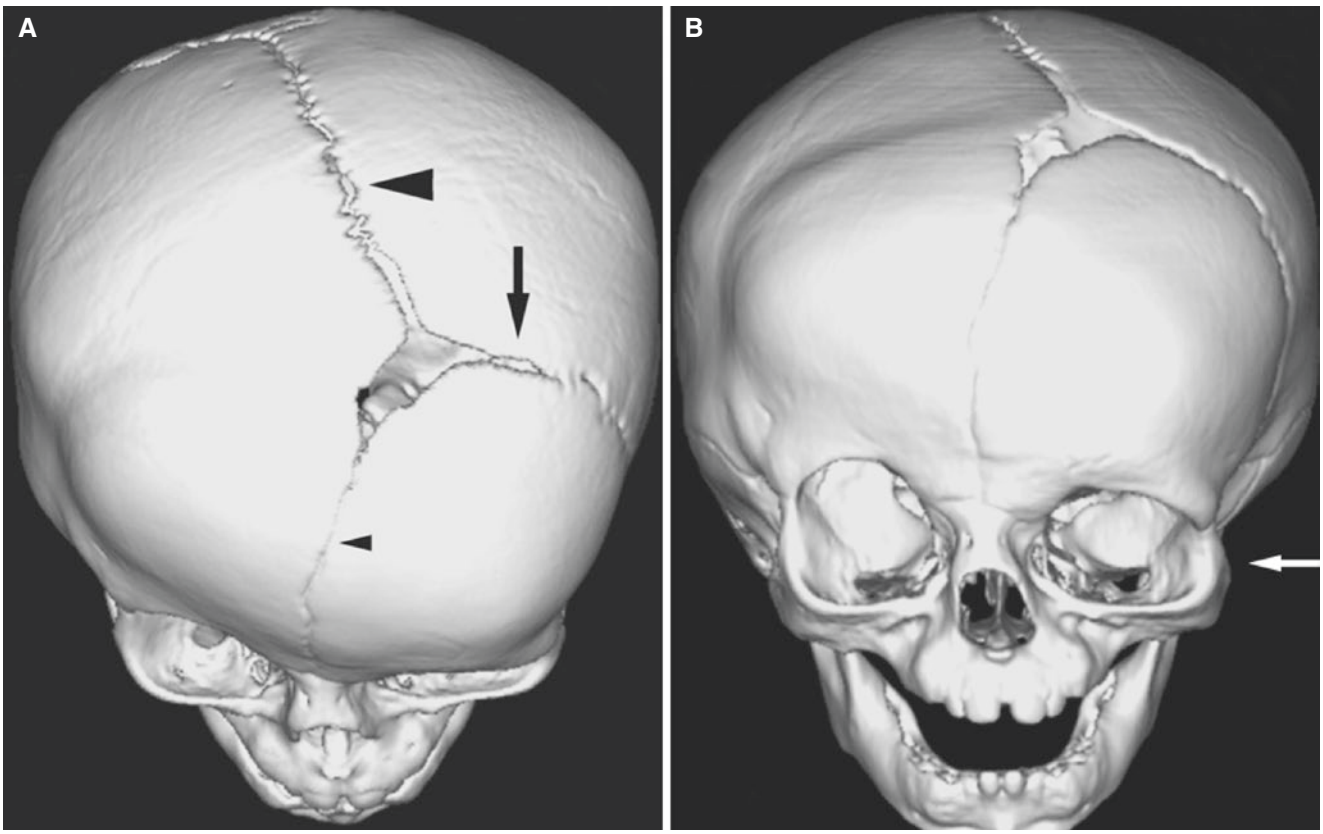

Fig. 9.15 Premature unilateral synostosis, 7-month-old male. (**A**) 3D CT image shows closure of the right side of the coronal suture but left side open (*arrow*), as is sagittal suture (*large arrowhead*). Anterior fontanelle open and metopic suture closed but can be seen (*small arrowhead*). Asymmetric deformity of the anterior part of the head. (**B**) 3D CT image shows evident asymmetry of the right and left orbita (*arrow*) due to the abnormal growth

9.15 Non-synostotic Occipital Plagiocephaly

Fig. 9.16

9.15.1 Definition

Traditionally occipital plagiocephaly has been associated with lambdoid craniosynostosis, but when the American Academy of Pediatricians in 1992 suggested supine sleeping position for neonates, the incidence of "occipital plagiocephaly" increased dramatically. The majority of these cases were, however, not associated with true craniosynostosis caused by premature closure of the lambdoid, but rather were secondary to unilateral head position during sleep.

9.15.2 Clinical Features

- Positional molding
- Deformational plagiocephaly; flat asymmetric head
- Patent lambdoid suture
- Treatment not surgical, rather molding of head with helmets and changing sleeping position

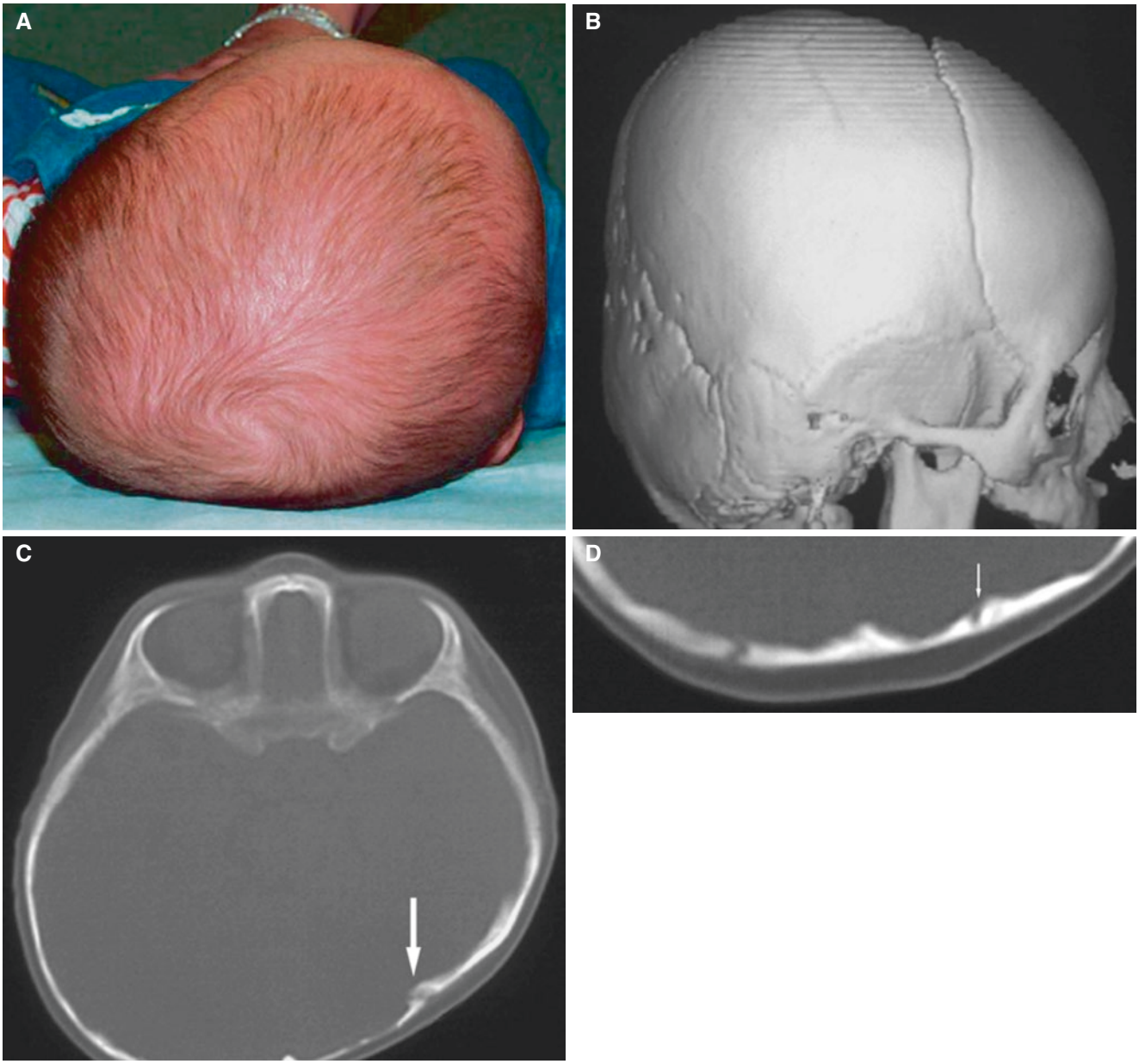

Fig. 9.16 Occipital plagiocephaly unrelated to craniosynostosis; patent lambdoid suture. (**A**) Baby sleeping supine on one side. (**B**) 3D CT image shows flat head. (**C**) Axial CT image shows patent suture (*arrow*) but left occipital plagiocephaly. (**D**) Axial CT image shows complete closure of lambdoid suture (*arrow*) representing true lambdoid craniosynostosis from different patients for comparison

9.16 Turner Syndrome

Fig. 9.17

9.16.1 Clinical Features

- Incidence about 1 per 2500 live female births
- Sex chromosome anomaly; only females
- Short stature
- Webbed neck
- Absent secondary sex characteristics
- Heart defects
- Mental deficiency; not consistently
- High palate
- Hypertelorism

9.16.2 Imaging Features

- Facial retrognathism
- Small mandible

- Delayed fusion of epiphyses
- Hypoplasia of odontoid process of C2
- Short metacarpals

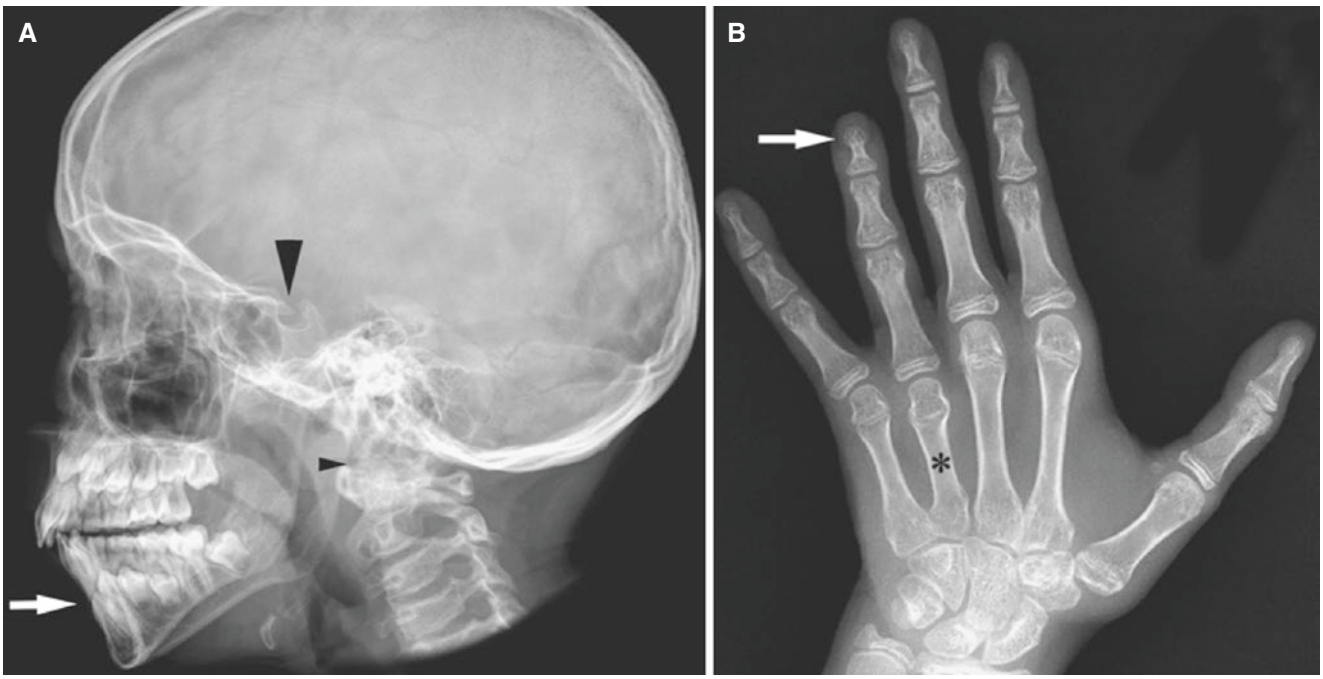

Fig. 9.17 Turner syndrome; 10-year-old. (**A**) Lateral view shows facial retrognathism (*arrow*), bridged sella (*large arrowhead*) and odontoid hypoplasia (*small arrowhead*). (**B**) Hand view shows shortening of the fourth finger due to the short fourth metacarpal bone (*asterisk*), drumstick distal phalanges, slender shaft and large distal heads (*arrow*), phalangeal predominance (proximal phalanges dominate over metacarpals in length)

9.17 Goldenhar Oculoauriculovertebral (OAV) Spectrum

9.17.1 Definition

Heterogeneous and complex group of overlapping conditions with ocular, auricular, vertebral, and facial anomalies from first and second branchial arches; Goldenhar first described the triad of ocular, auricular, and mandibulofacial dysostosis in 1952, today known as Goldenhar syndrome. Later, cases with vertebral anomalies, as well as unilateral facial hypoplasia, previously named hemifacial microsomia, have been included in the expanded OAV complex. Up to about 80% of OAV complex cases are sporadic. Extreme variability of expression is characteristic.

9.18 Goldenhar Syndrome

9.18.1 Clinical Features

- Unilateral facial hypoplasia
- Ear anomalies; external and middle ear frequent, inner ear at least 6%
- Seven nerve palsy frequent
- Eye anomalies; dermoid of eyeball, coloboma (vertical fissure of eyelid)
- Variable vertebral anomalies may occur

9.19 Hemifacial Microsomia

Figs. 9.18 and 9.19

9.19.1 Clinical Features

- Second most common facial birth defect after cleft palate/lip; about 1 per 5000 live births, but variable frequencies reported
- Males more frequent than females
- Most frequent syndrome from first and second branchial arches
- May not be appreciable in infancy; usually evident by the age of about 4 years
- Facial asymmetry and ear anomalies are characteristic
- Right side facial underdevelopment more frequent than the left side
- Skin tags between the ear and corner of the mouth
- Seven nerve palsy frequent
- Dental malocclusion, hypodontia
- Plagiocephaly in 10%
- Bifacial microsomia has been reported

9.19.2 Imaging Features

- Underdeveloped mandible without mandibular condyle
- Flat zygomatic arch without glenoid fossa; may be absent
- Auricular malformations

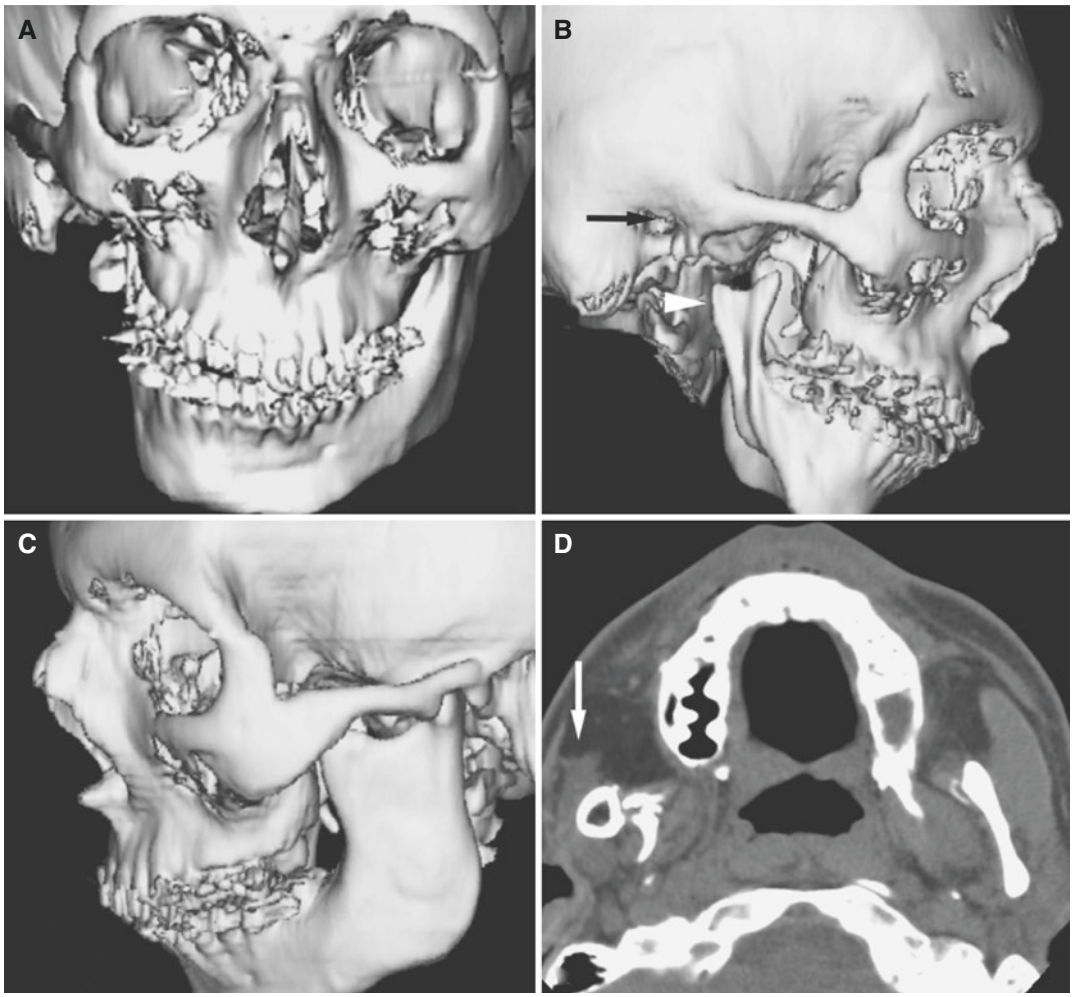

Fig. 9.18 Hemifacial microsomia; 17-year-old male; pre- and postoperatively. (**A**) 3D CT image, en face view, shows facial asymmetry due to right-sided mandibular hypoplasia. (**B**) 3D CT image, lateral view, shows right-sided zygomatic arch without glenoid fossa (*arrow*) and hypoplastic mandible without mandibular condyle (*arrowhead*). Note orthodontic braces on the teeth. (**C**) 3D CT image, lateral view, shows normal left side for comparison. (**D**) Axial CT image, soft tissue, shows severe atrophy of the right masseter muscle (*arrow*) compared to normal left side. (**E**) Coronal CT image, soft tissue, shows severe atrophy of the masseter muscle (*arrow*) and temporalis muscle (*arrowhead*) compared to normal left side. (**F**) 3D CT image, postoperative lateral view, shows right-sided fibula graft with miniplates and screws to reinforce the created mandibular angle of the graft (*arrow*). Note also miniplates and screws after LeFort 1 osteotomy (*arrowhead*). (**G**) 3D CT image, postoperative en face view, shows osteotomy of the left mandible with miniplate fixation (*arrow*) to obtain symmetric facial skeleton. (**H**) 3D CT image, postoperative lateral view, shows osteotomy correction of normal left side with miniplates (*arrow*). (**I**) Coronal CT image, postoperative view, shows fibula graft "articulating" against infratemporal fossa (*arrow*)

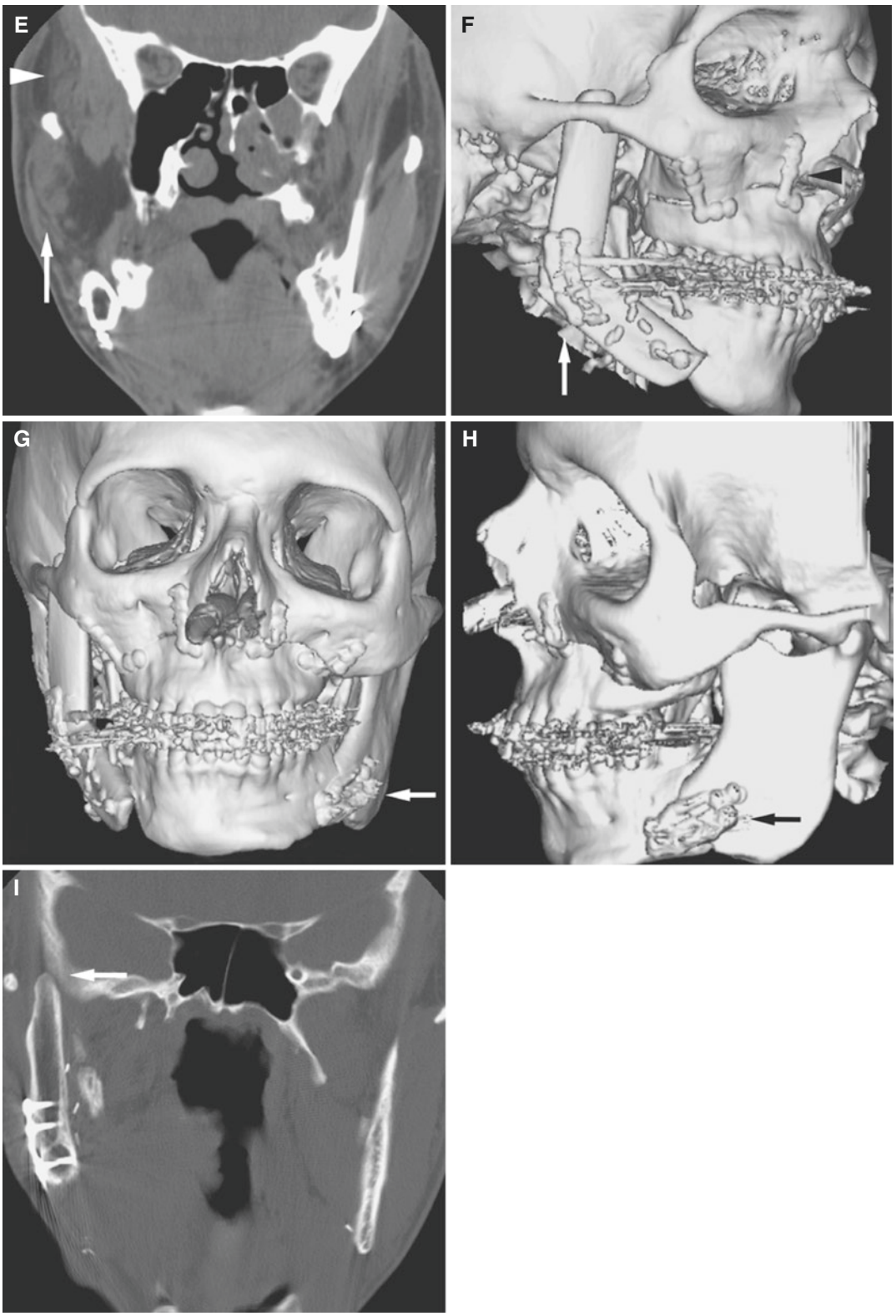

Fig. 9.18 (continued)

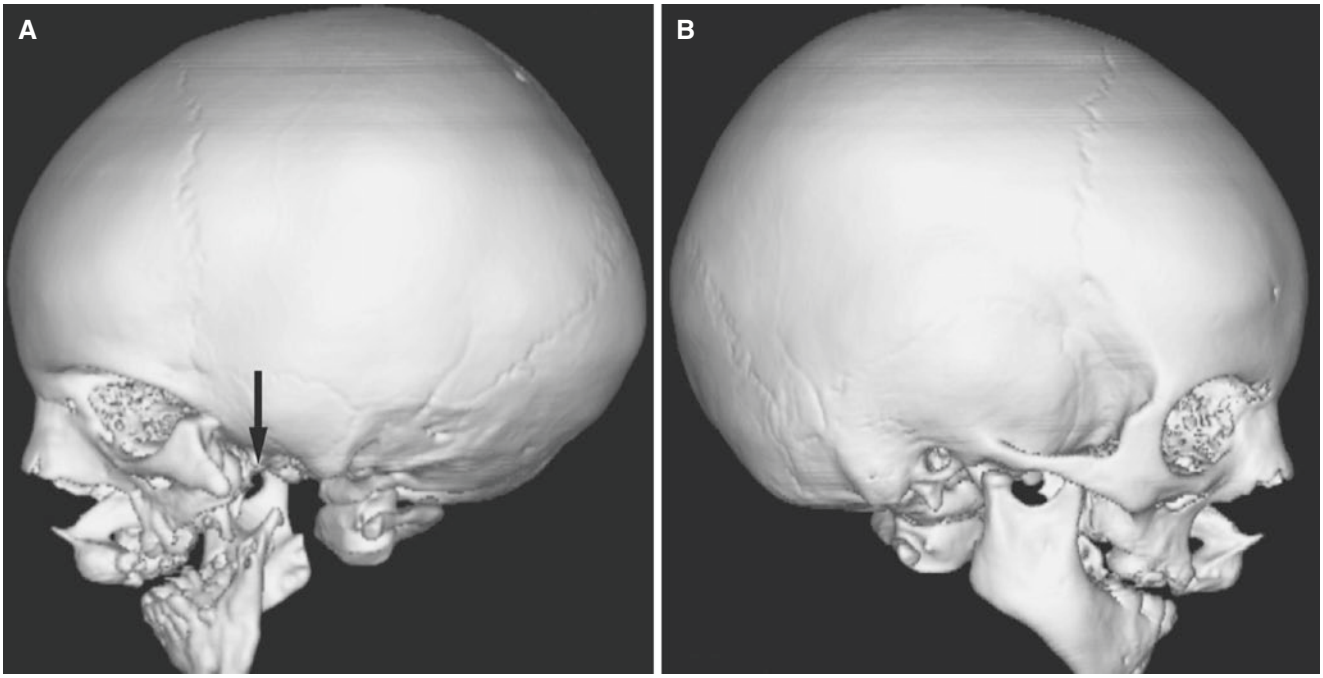

Fig. 9.19 Hemifacial microsomia; 4-year-old male with multiple anomalies including cleft palate and lip. (**A**) 3D CT image, lateral view, shows left-sided severely hypoplastic mandible and absent zygomatic arch (*arrow*). (**B**) 3D CT image, lateral view, shows normal right side for comparison

9.20 Treacher Collins Syndrome (Mandibulofacial Dysostosis)

Figs. 9.20 and 9.21

9.20.1 Clinical Features

- Syndrome from first and second branchial arches; about 1 per 50,000 live births
- Micrognathia ("bird face"); symmetric underdevelopment of the mandible
- Antimongoloid angulation of palpebral fissures with vertical notching or coloboma of outer parts
- Absence or deficiency of medial eyelashes
- Flattening of cheeks
- Ear tags between tragus and angle of mouth may occur

9.20.2 Imaging Features

- Mandibular hypoplasia; very short rami, bilateral antegonial notching, compensatory growth of anterior part
- Dental malocclusion
- Bilateral hypoplasia or agenesia of the malar bone
- Malformation of the external and middle ear
- Disproportionately small facial bones
- Paranasal sinuses often small, may be absent
- Lacrimal duct atresia
- Narrow palate
- Cleft palate in about one-third

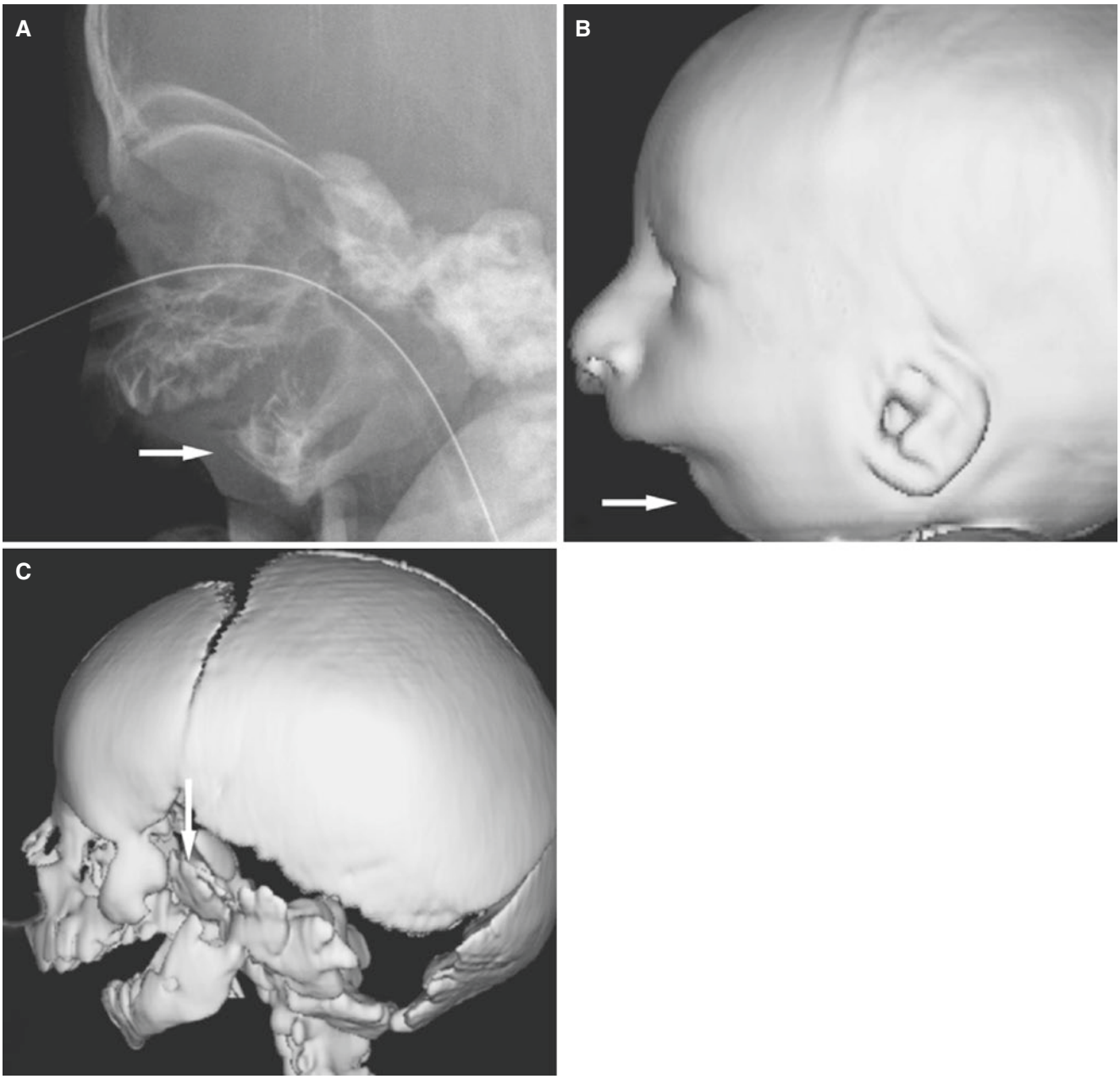

Fig. 9.20 Treacher Collins syndrome; newborn with respiratory distress. (**A**) Lateral view shows very small and retruded mandible (*arrow*) and airway tube. (**B**) 3D CT image of the skin, lateral view, shows severe micrognathia (*arrow*). (**C**) 3D CT image, lateral view, shows absent zygoma (*arrow*)

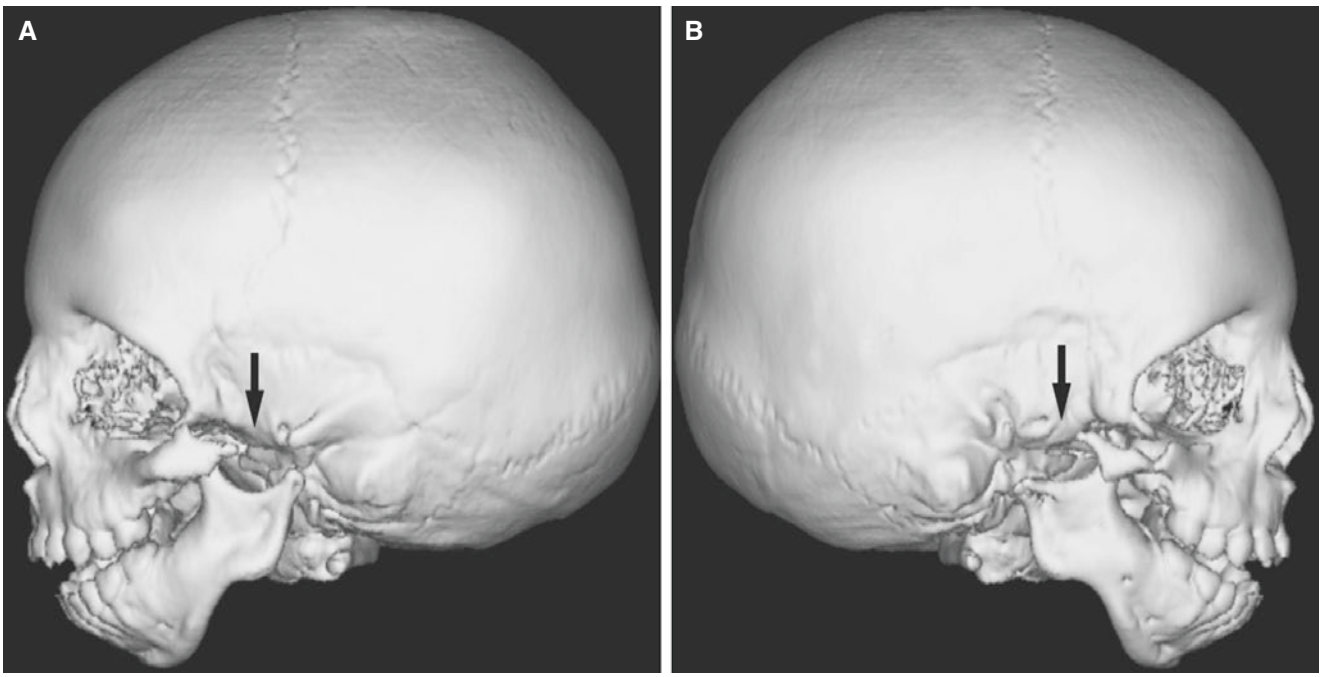

Fig. 9.21 Treacher Collins syndrome; 4-year-old male. (**A**) 3D CT image of the left side shows an underdeveloped mandible with antegonial notching and part of zygoma with zygomatic arch absent (*arrow*); micrognathia with open bite and small facial skeleton compared to the skull. (**B**) 3D CT image of right side; similar absence of zygoma (*arrow*) and appearance of the mandible as contralateral side, except less developed condylar process

9.21 Syndromic Craniosynostoses (Craniofacial Dysostoses)

9.21.1 Definition

Group of syndromes showing both premature synostoses as a prominent feature and facial growth disturbances; about 15% of all craniosynostoses.

More than 100 such syndromes are recognized, but Crouzon is probably best known because craniofacial dysostosis is frequently used synonymously with this syndrome.

9.22 Crouzon Syndrome

Figs. 9.22 and 9.23

9.22.1 Clinical Features

- Most frequent craniofacial dysostosis; about 1 per 25,000 births
- About one-half are familial and one-half are sporadic
- Absence of major limb abnormalities
- Oxycephaly
- Hypertelorism, exorbitism
- Shallow orbits
- Midfacial hypoplasia; relatively prominent mandible

9.22.2 Imaging Features

- Oxycephaly
- Bilateral coronal synostosis with brachycephaly but also sagittal synostosis with narrowing in transverse dimension
- Hypertelorism, exorbitism
- Shallow orbits
- Maxillary hypoplasia
- Partial obstruction of nasal passages, narrow palate
- Relative mandibular prognathism
- Cervical spine abnormalities; C2–C5 fusion 40%
- Calcification of stylohyoid ligament, 50%
- Intracranial anomalies common, including venous drainage and hydrocephalus

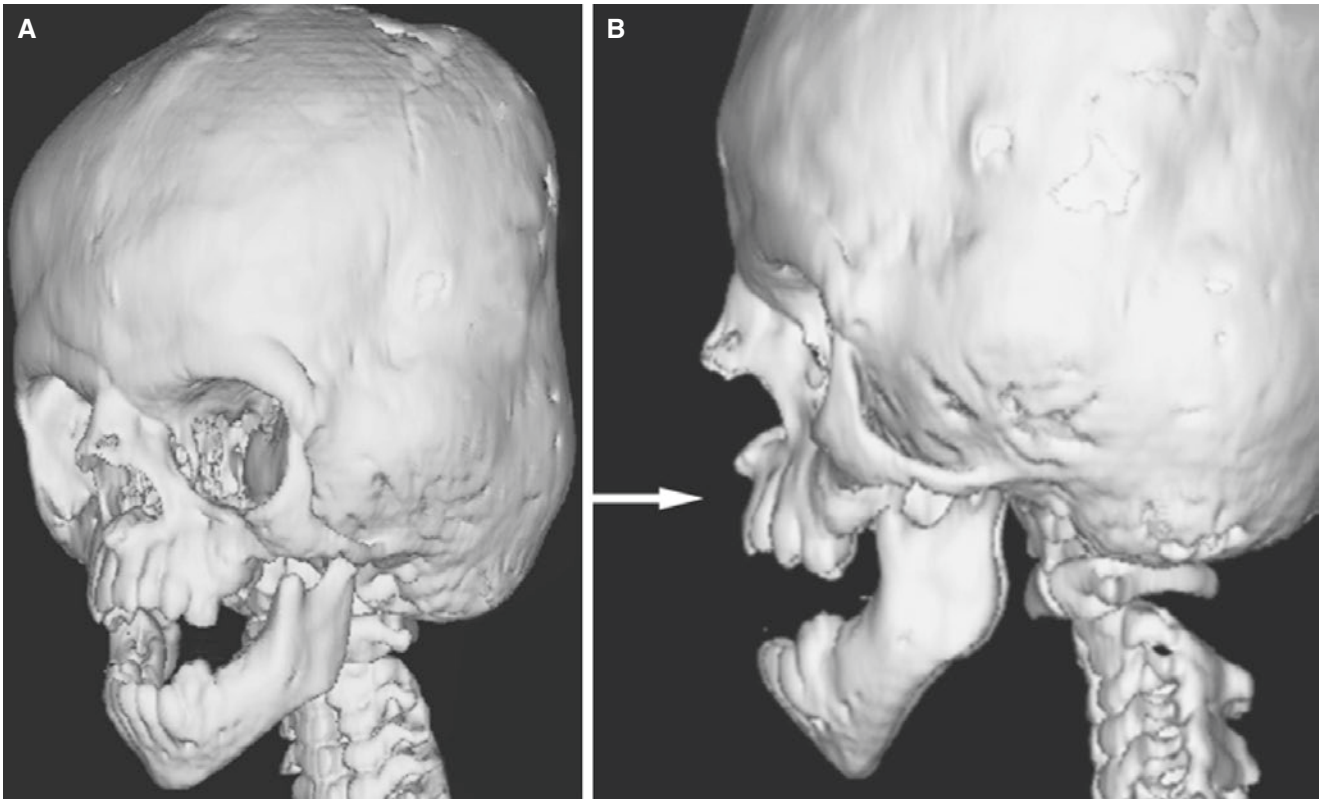

Fig. 9.22 Crouzon syndrome; 2-year-old. (**A**) 3D CT image, oblique view, shows superior elongation of the skull and typically "opened mouth." The maxilla and zygomas are hypoplastic. (**B**) 3D CT image, lateral view, shows maxillary hypoplasia (*arrow*)

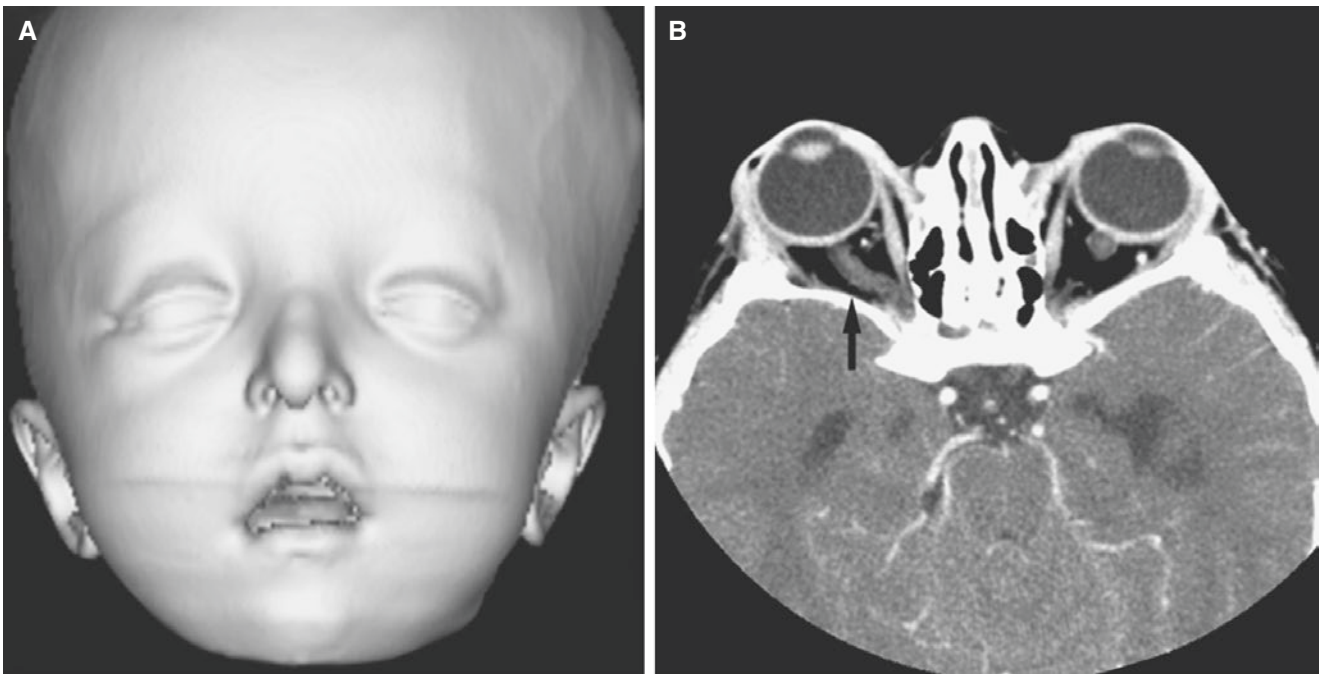

Fig. 9.23 Crouzon syndrome; 3-year-old. (**A**) 3D CT image of the skin, en face view, shows hypertelorism, exorbitism, and open downturned mouth. (**B**) Axial CT image, soft tissue, shows shallow orbits with exorbitism and apparently enlarged optic nerve (*arrow*); MRI would probably have shown prominent perineural subarachnoid spaces and normal nerves bilaterally

9.23 Apert Syndrome

Fig. 9.24

9.23.1 Clinical Features

- Craniofacial dysostosis; about 1 per 100,000 births
- Most cases are sporadic
- Many similar features to Crouzon syndrome, but generally more enhanced, except varying degrees of syndactyly or brachydactyly; various acrocephalosyndactyly types
- Hearing loss common
- Cleft palate in 30–42%

9.23.2 Imaging Features

- Similar skull type to Crouzon syndrome but more severe abnormalities; midfacial hypoplasia present at birth
- Choanal stenosis common
- Cervical spine abnormalities; fusion of C5–C6 70%
- Calcification of stylohyoid ligament 38–88%
- Intracranial anomalies

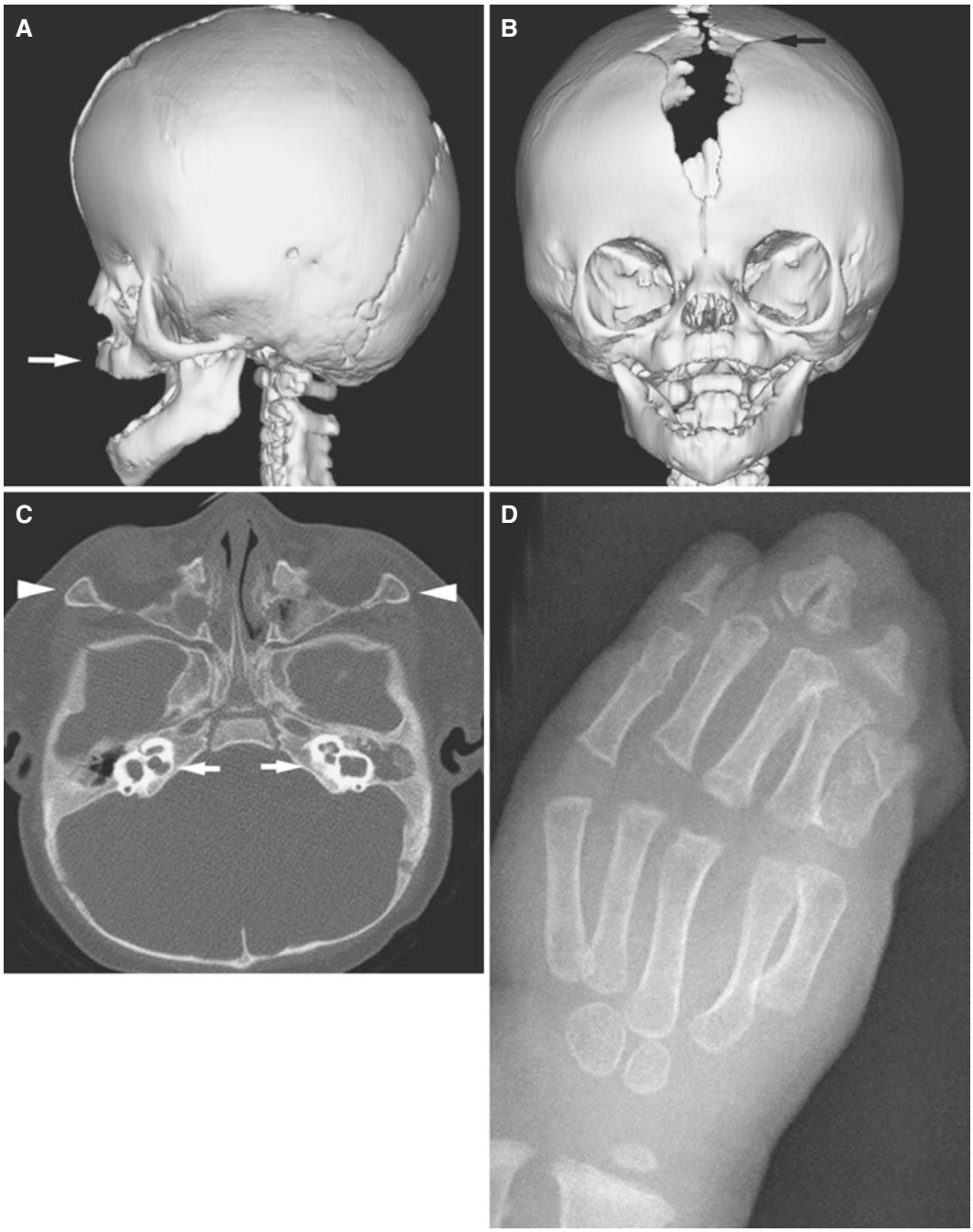

Fig. 9.24 Apert syndrome; 6-month-old. (**A**) 3D CT image, lateral view, shows oxycephaly and midfacial hypoplasia (*arrow*) and typically "opened mouth." (**B**) 3D CT image, en face view, shows large, open anterior fontanelle, brachycephaly with fused coronal sutures bilaterally. (**C**) Axial CT image shows vestibular dysplasia (*arrows*) and shallow orbits (*arrowheads*). (**D**) Hand view shows syndactyly (fusion of fingers)

9.24 Achondroplasia

Figs. 9.25, 9.26, 9.27, and 9.28

9.24.1 Clinical Features

- Familial or sporadic
- Most common form of dwarfism
- Defect of generalized endochondral osteogenesis
- Disproportionately short limbs
- Lumbar lordosis
- Large, brachycephalic head with a prominent forehead
- Midfacial underdevelopment
- Nasal bone deformed (saddle nose)
- Normal lower third of face; relative mandibular prognathism
- Occurs in several dominant disorders often associated with neurologic complications such as hydrocephalus, brain stem compression, and small foramina magnum, which can result in sleep apnea, sudden infant death, and spinal cord compression

9.24.2 Imaging Features

- Disproportionately enlarged calvaria
- Maxillary retrognathia
- Saddle nose
- Normal mandible due to periosteal chondrogenesis

Fig. 9.25 Achondroplasia; newborn. Lateral view shows midfacial hypoplasia, relative mandibular prognathism, and large tongue

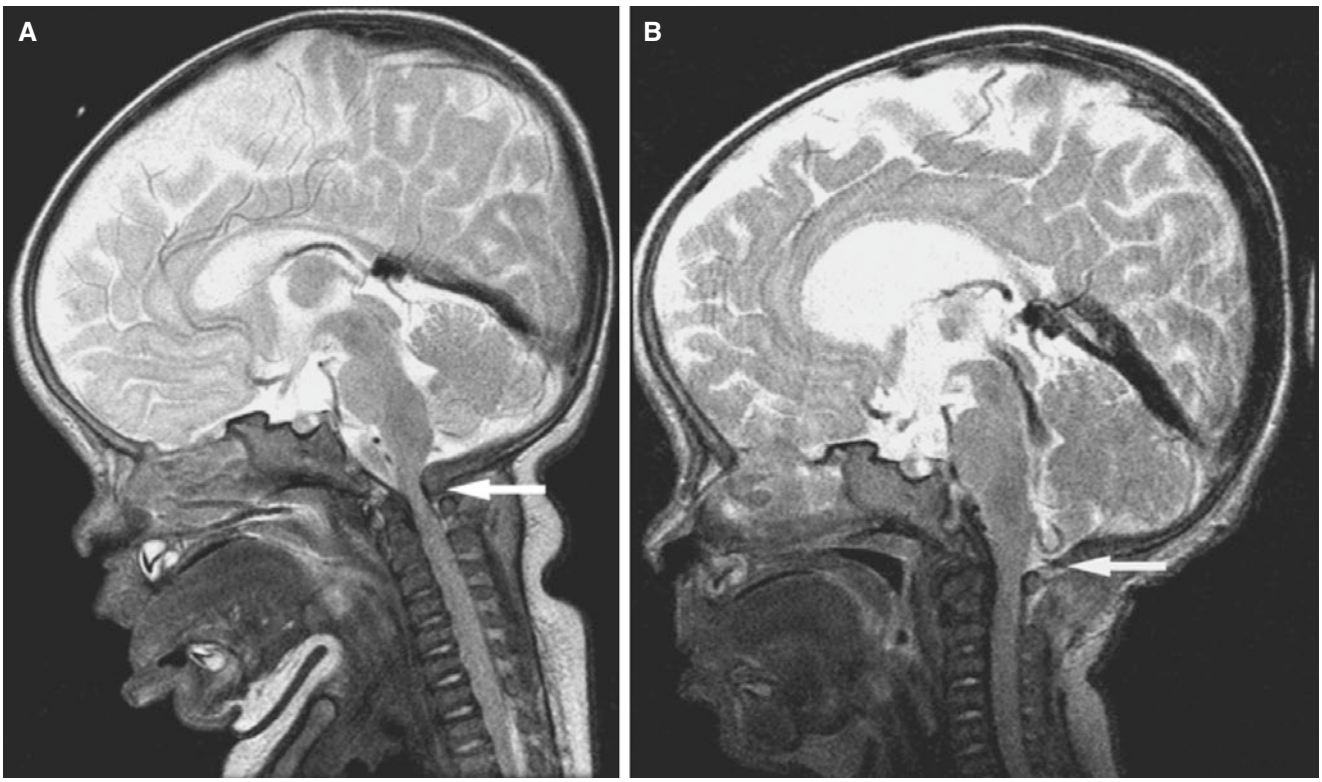

Fig. 9.26 Achondroplasia; 3-month-old female. (**A**) Sagittal T2-weighted MRI shows spinal cord narrowing; at foramen magnum (*arrow*). (**B**) Sagittal T2-weighted MRI after surgery shows removal of posterior margin of foramen magnum (*arrow*) with decreased compression of brain stem/medulla/upper cervical spinal cord

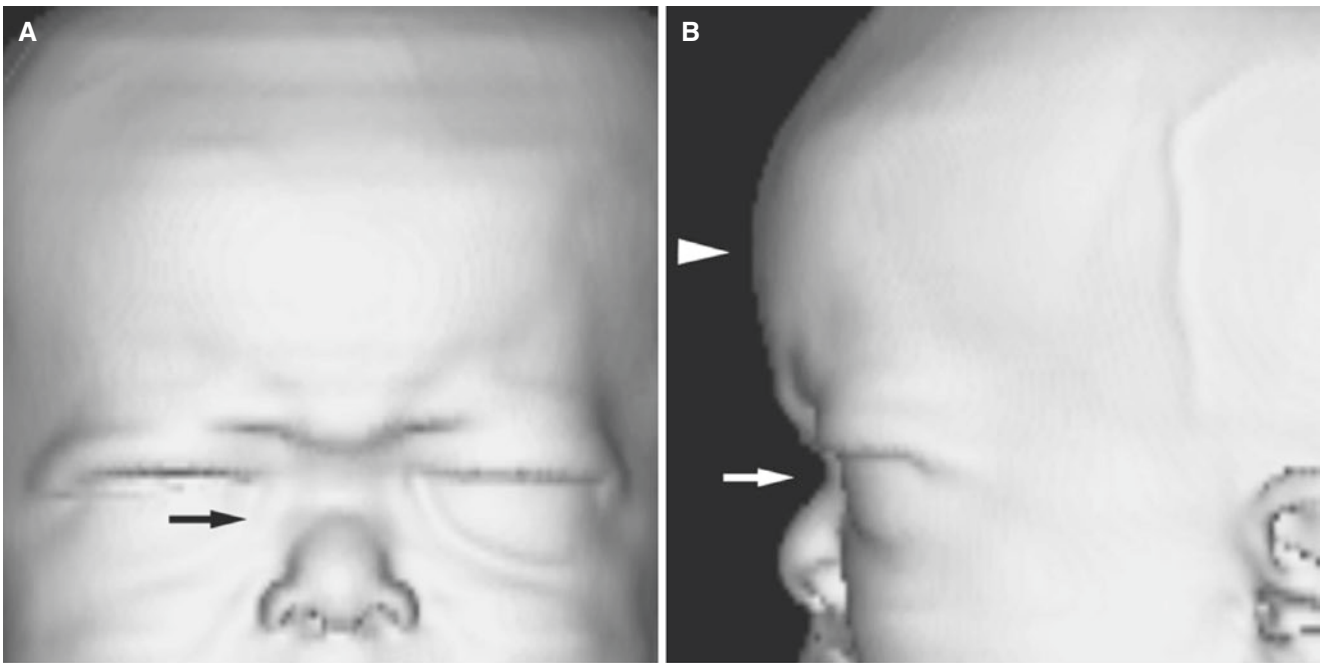

Fig. 9.27 Achondroplasia; 7-month-old. (**A**) 3D CT image, en face view of the skin, shows saddle nose (*arrow*). (**B**) 3D CT image, lateral view of the skin, shows saddle nose (*arrow*) and prominent forehead (*arrowhead*). (**C**) 3D CT image, en face view, shows macrocephaly with parietal prominence and open anterior fontanelle

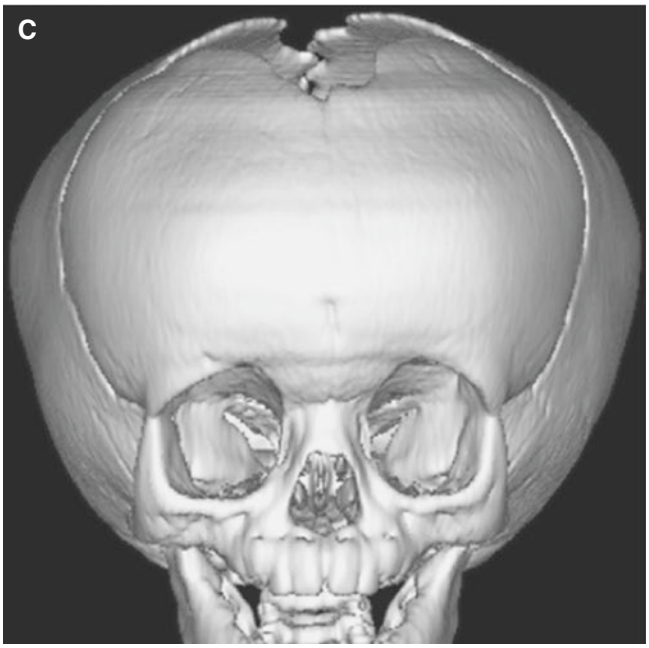

Fig. 9.27 (continued)

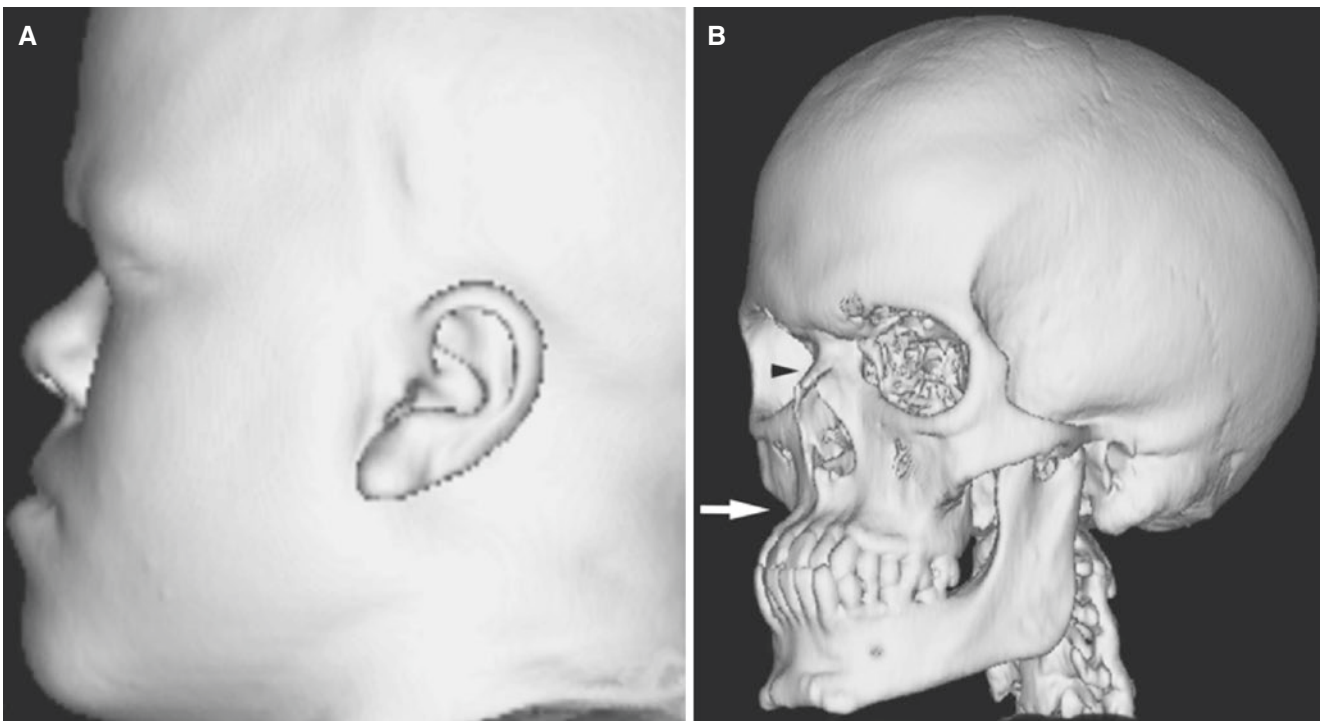

Fig. 9.28 Achondroplasia; teenage. (**A**) 3D CT lateral view of the skin shows midfacial hypoplasia and saddle nose. (**B**) 3D CT image, oblique view, shows maxillary hypoplasia (*arrow*) and short, deformed, depressed nasal bone (*arrowhead*)

9.25 Pyknodysostosis

Fig. 9.29

9.25.1 Clinical Features

- Rare, inherited form of dwarfism
- Short stature
- Dense, fragile bones
- Predisposed to osteomyelitis

9.25.2 Imaging Features

- Open fontanelles, cranial sutures
- Partial agenesia of terminal phalanges of hands and feet
- Hypoplasia of maxilla, mandible, paranasal sinuses
- Dense, fractured bones
- Abnormal dental eruption, crowding of teeth

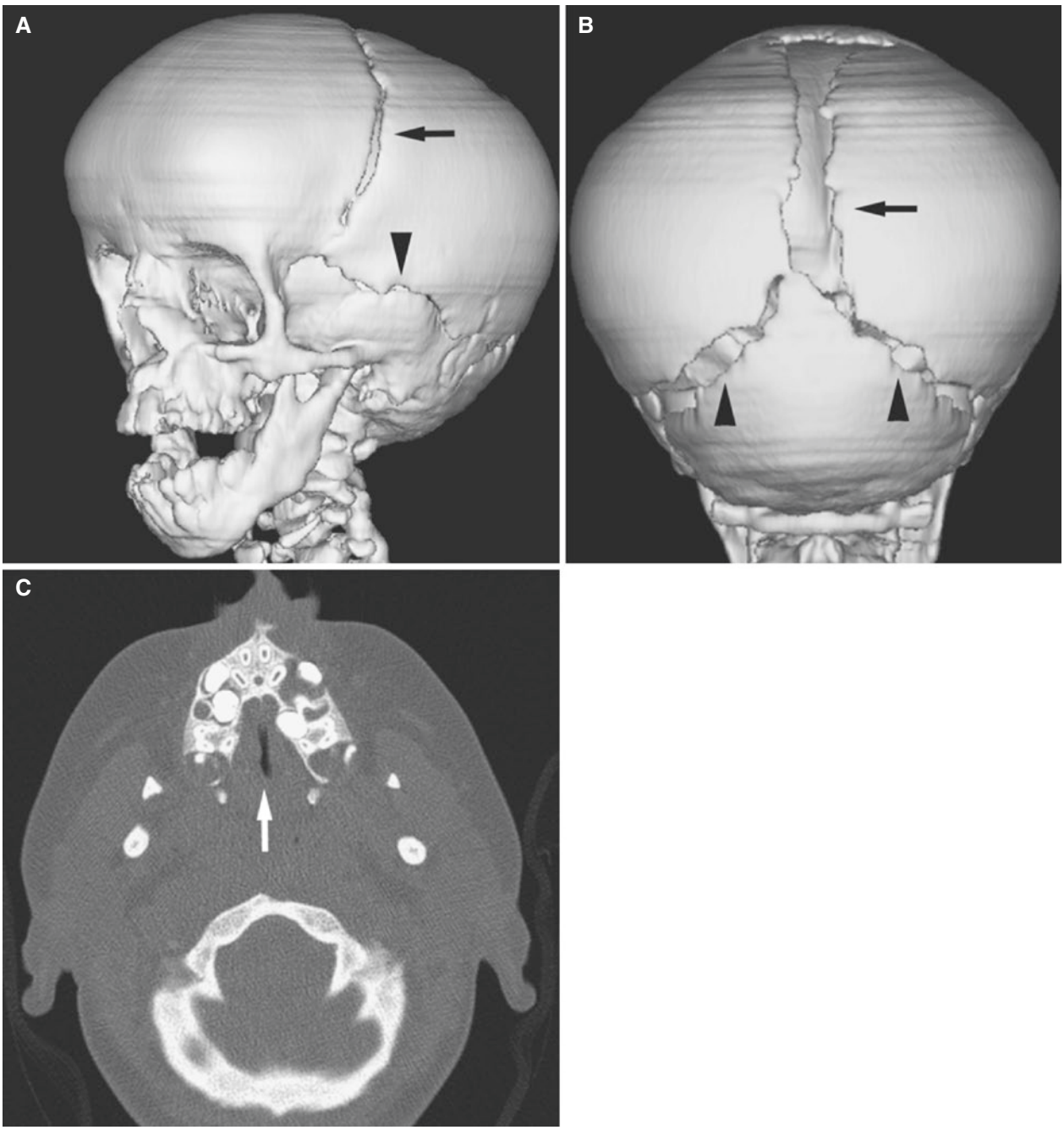

Fig. 9.29 Pyknodysostosis; 9-year-old. (**A**) 3D CT image, oblique view, shows hypoplasia of the maxilla and mandible and open coronal suture (*arrow*) and squamosal suture (*arrowhead*). (**B**) 3D CT image, axial view, shows wide open sagittal suture (*arrow*), open anterior fontanelle, and open lambdoid sutures (*arrowheads*). (**C**) Axial CT image shows narrow, dense maxilla and crowded teeth (some with widened follicles); incisors almost in sagittal line (*arrow*)

9.26 Ectodermal Dysplasia

Fig. 9.30

9.26.1 Clinical Features

- Developmental abnormalities of ectodermal tissues
- Many types with various inheritance patterns
- Abnormal hearing
- Abnormal or missing sweat glands
- Multiple agenesia of teeth
- Poorly developed alveolar processes
- Sebaceous glands, hair follicles, and salivary glands (xerostomia) may also be defective

9.26.2 Imaging Features

- Lack of tooth germs both in permanent and primary dentition
- Disproportionately small facial skeleton compared with calvaria
- Mandible anteriorly rotated

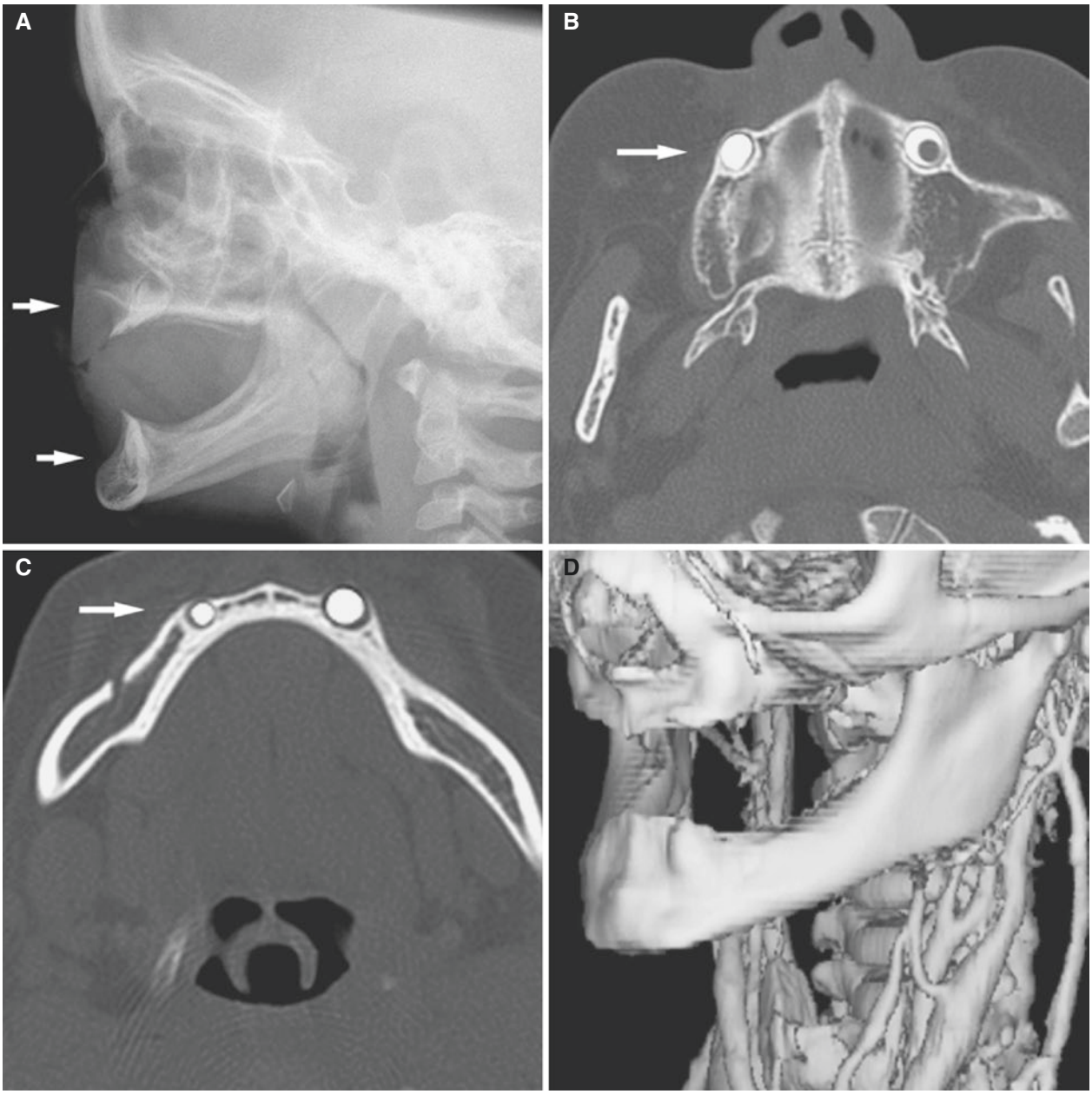

Fig. 9.30 Ectodermal dysplasia; 3-year-old female. (**A**) Lateral view shows only a couple of tooth germs (*arrows*) in the anterior maxilla and mandible and poorly developed alveolar processes (as if they were old and atrophic). (**B**) Axial CT image shows two teeth, possibly canines, in upper jaw (*arrow*). (**C**) Axial CT image shows two teeth, possibly canines, in lower jaw (*arrow*). (**D**) 3D CT image, oblique view, shows underdeveloped jaws without other teeth

9.27 Miscellaneous Conditions

Figs. 9.31, 9.32, and 9.33

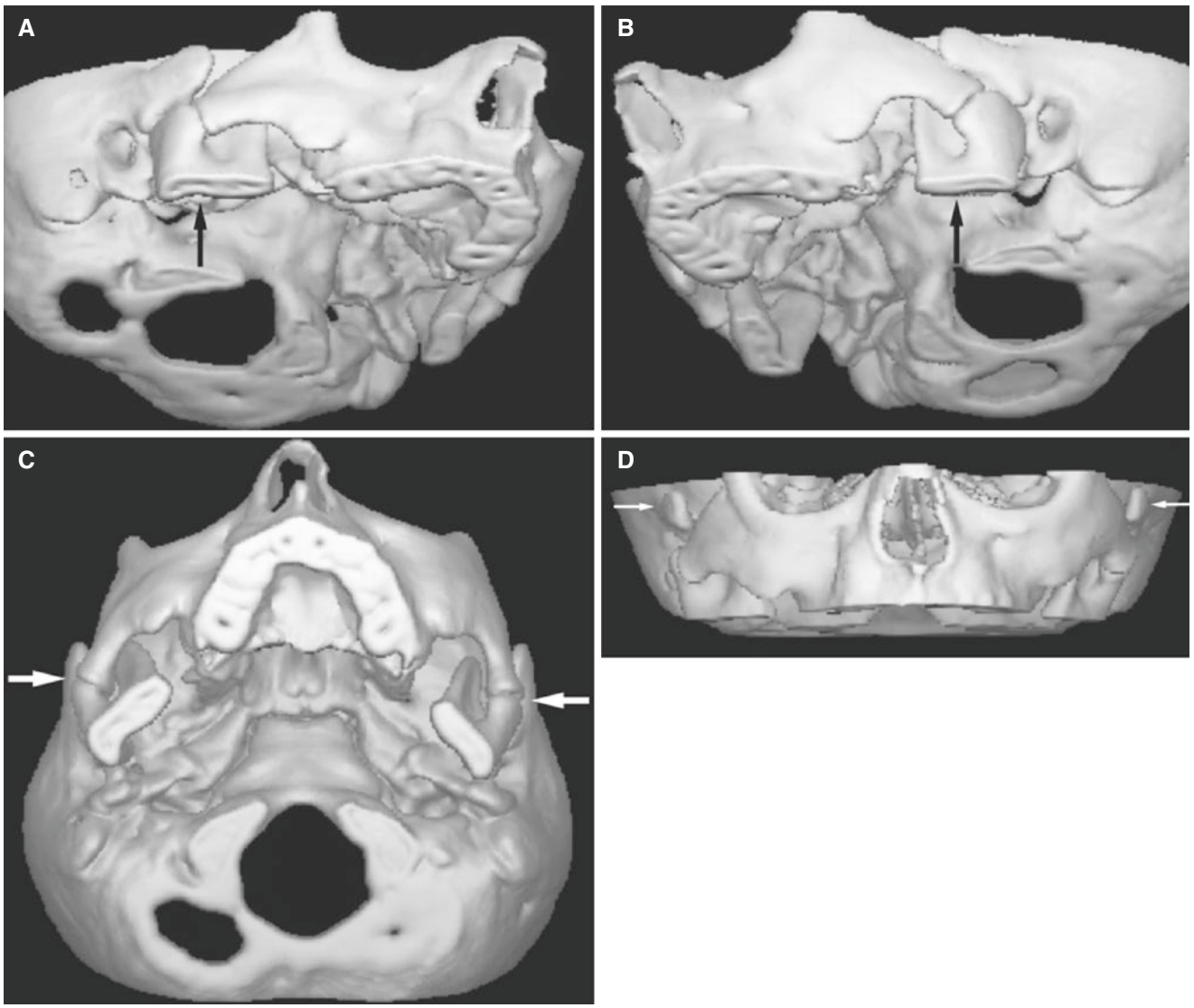

Fig. 9.31 Micrognathia, bilateral split zygomatic arch; 7-year-old female with retruded mandible and mouth-opening capacity of about 30 mm. (**A**) 3D CT image, oblique view of right side, shows that the zygomatic arch is split with the anterior part articulating with the mandible (*arrow*). (**B**) 3D CT image, oblique view of contralateral side, shows similar deformities (*arrow*). (**C**) 3D CT image, axial view, shows the symmetric deformity (*arrows*). (**D**) 3D CT image, en face view, shows the posterior "free" part of the split zygomatic arch bilaterally (*arrows*)

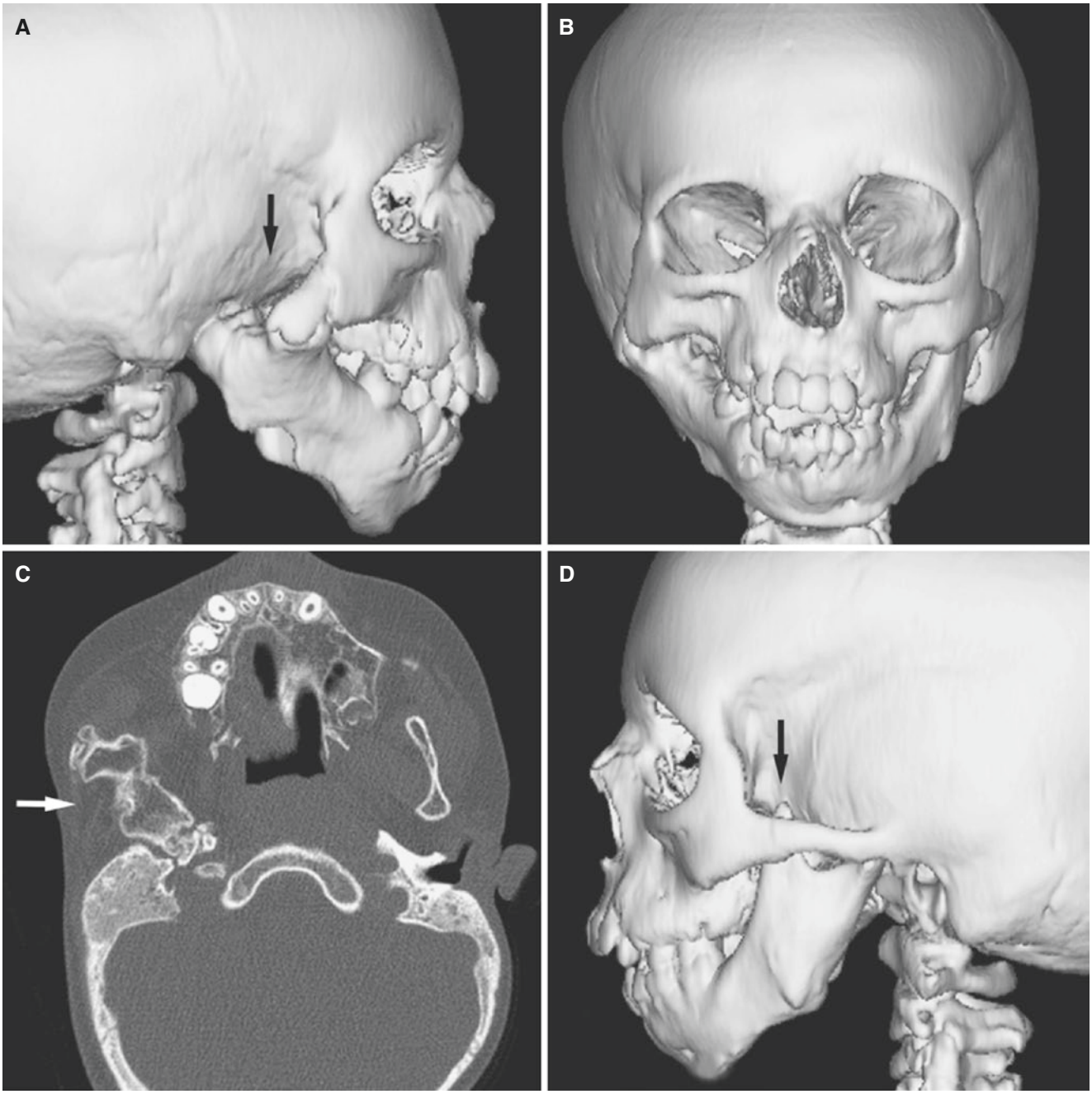

Fig. 9.32 Facial asymmetry, unilateral ankylosis, and absent zygomatic arch; 8-year-old. (**A**) 3D CT image, lateral view of right side, shows absent zygomatic arch (*arrow*) and thus no glenoid fossa; ankylosis between mandible and remaining abnormal zygomatic bone. (**B**) 3D CT image, en face view, shows mandibular asymmetry and open anterior bite and some maxillary asymmetry as well. (**C**) Axial CT image shows bony union between mandible and zygomatic bone (*arrow*). (**D**) 3D CT image, lateral view of left side, shows normal zygomatic arch but coronoid hyperplasia (*arrow*), probably of a compensatory nature

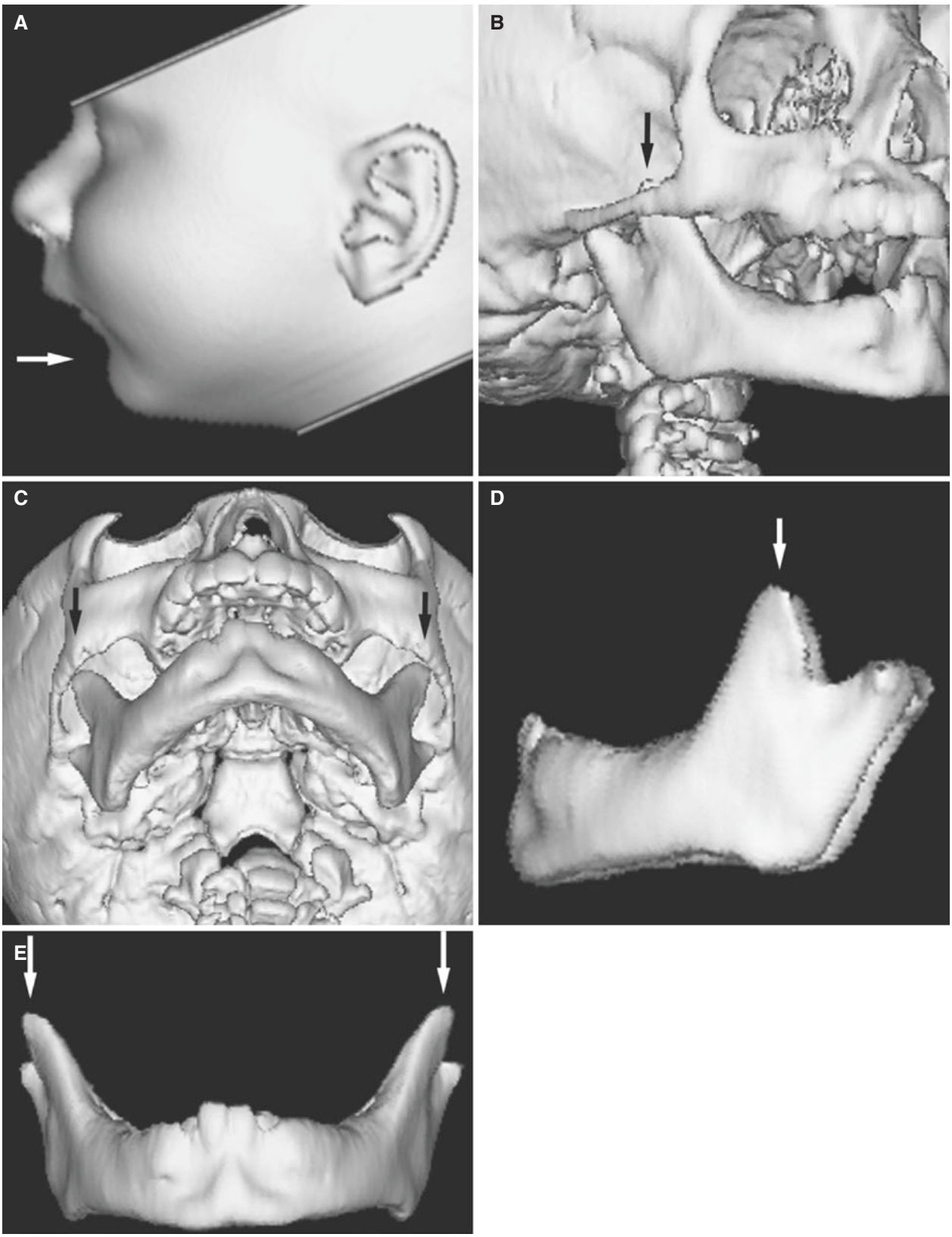

Fig. 9.33 Micrognathia, coronoid hyperplasia with blocking on mouth opening; 10-month-old. (**A**) 3D CT image of skin surface shows micrognathia ("bird face"). (**B**) 3D CT image shows coronoid hyperplasia (*arrow*). (**C**) 3D CT image, oblique axial view, shows that both coronoid processes are blocking against zygomatic arch (*arrows*). (**D**) Segmented 3D CT image, lateral view of mandible, shows bilateral coronoid hyperplasia (*arrow*). (**E**) Segmented 3D CT image, en face view of mandible, shows bilateral coronoid hyperplasia (*arrows*)

Suggested Reading

AlZarea BK (2016) Prevalence and pattern of torus palatinus and torus mandibularis among edentulous patients of Saudi Arabia. Clin Interv Aging 11:209–213

Arvidsson LZ, Flatø B, Larheim TA (2009) Radiographic TMJ abnormalities in patients with juvenile idiopathic arthritis followed for 27 years. Oral Surg Oral Med Oral Pathol Oral Radiol Endod 108:114–123

Arvidsson LZ, Fjeld MG, Smith HJ, Flatø B, Ôgaard B, Larheim TA (2010) Craniofacial growth disturbance is related to temporomandibular joint abnormality in patients with juvenile idiopathic arthritis, but normal facial profile was also found at the 27-year follow-up. Scand J Rheumatol 39:373–379

Carinci F, Pezzetti F, Scapoli L, Martinelli M, Carinci P, Tognom M (2000) Genetics of nonsyndromic cleft lip and palate: a review of international studies and data regarding the Italian population. Cleft Palate Craniofac J 37:33–40

David DJ, Mahatumarat C, Cooter RD (1987) Hemifacial microsomia: a multisystem classification. Plast Reconstr Surg 80:525–535

Farman AG, Nortje C, Wood RE (1993) Developmental anomalies of the skull and jaws. In: Oral and maxillofacial diagnostic imaging. Mosby, St. Louis, pp 105–157

Fjeld M, Arvidsson L, Stabrun AE, Birkeland K, Larheim TA, Ôgaard B (2009) Average craniofacial development from 6 to 35 years of age in a mixed group of patients with juvenile idiopathic arthritis. Acta Odontol Scand 67:153–160

Fjeld M, Arvidsson L, Smith HJ, Flatø B, Ôgaard B, Larheim TA (2010) Relationship between disease course in the temporomandibular joints and mandibular growth rotation in patients with juvenile idiopathic arthritis followed from childhood to adulthood. Pediatr Rheumatol Online J 8:13. doi:10.1186/1546-0096-8-13

Fogh-Andersen P (1965) Rare clefts of the face. Acta Chir Scand 129:275–281

Goldenhar M (1952) Associations malformatives de l'oeil et de l'oreille, en particulier le syndrome dermöide epibulbaire-appendices auriculaires-fistula auris congenita et ses relations avec la dysostose mandibulo-faciale. J Genet Hum 1:243–282

Gorlin RJ, Cohen MM Jr, Levin LS (1990) Syndromes of the head and neck, 3rd edn. Oxford University Press, New York, pp 33–35, 54, 521, 524, 641, 649, 695

Hsu CL, Hsu CW, Chang PC, Huang WH, Weng CH, Yang HY et al (2016) Oral tori in chronic peritoneal dialysis patients. PLoS One 11(6):e0156988. doi:10.1371/journal.pone.0156988

Lai WS, Wang HW (2016) Nodular torus palatinus. J Am Osteopath Assoc 116:491. doi:10.7556/jaoa.2016.100

Maduakor SN, Nwoga MC (2017) Prevalence of mandibular and palatine tori among the Ibos in Enugu, South-East Nigeria. Niger J Clin Pract 20:57–60

Murray JC (1995) Invited editorial. Face facts: genes, environment, and clefts. Am J Hum Genet 52:227–232

Naidich TP, Smith MS, Castillo M, Thompson JE, Sloan GM, Jayakar P, Mukherji SK (1996) Facies to remember. Number 7. Hemifacial microsomia. Goldenhar syndrome. OAV complex. Int J Neuroradiol 2:437–449

Naidich TP, Blaser SI, Bauer BS, Armstrong DK, McLone DG, Zimmerman RA (2003) Embryology and congenital lesions of the midface. In: Som PM, Curtin HD (eds) Head and neck imaging, 4th edn. Mosby, St. Louis, pp 3–86

Scrieciu M, Mercu½ V, Mercu½ R, Birjovanu C, Stan MC, Marinescu IR et al (2016) Morphological and clinical characteristics of the torus palatinus and torus mandibularis in a sample of young and adults' Romanian people. Romanian J Morphol Embryol 57:139–144

Stabrun AE, Larheim TA, Hoyeraal HM, Rosler M (1988) Reduced mandibular dimensions and asymmetry in juvenile rheumatoid arthritis. Pathogenetic factors. Arthritis Rheum 31:602–611

Van der Meulen J, Mazzola R, Stricker M, Raphael B (1990) Classification of craniofacial malformations. In: Stricker M, Van der Meulen J, Raphael B, Mazzola R (eds) Craniofacial malformations. Churchill Livingstone, Edinburgh, pp 149–309

Paranasal Sinuses

10

Abstract

This chapter illustrates inflammatory diseases; acute and chronic sinusitis, mucosal imaging finding in asymptomatic individuals (including retention cyst), polyps, mucoceles, granulomatosis with polyangiitis (previously known as Wegener's granulomatosis), inflammatory dental conditions, benign tumors and tumor-like conditions; papilloma, osteoma, fibrous dysplasia, nasolabial cyst, malignant tumors; squamous cell carcinoma, adenocarcinoma, lymphoma, Ewing sarcoma, and osteosarcoma, expansile odontogenic conditions, and miscellaneous conditions.

10.1 Introduction

Diseases of the paranasal sinuses are common and may cause symptoms simulating dental disease. Due to the close relationship between the dental structures and the sinuses, it may also be the opposite: dental disease causing sinusitis. Thus, diseases of the paranasal sinuses are important both in medicine and dentistry. Tumors of the paranasal sinuses are rare, but may present with oral mucosa or dental symptoms.

Advanced imaging modalities are routinely used for diagnostic assessment of paranasal sinus problems, and in general they have replaced conventional radiography. CT is the primary method to evaluate diseases of the paranasal sinuses. MRI is used as a supplement primarily to determine the extent of soft-tissue abnormalities extending outside the confinement of the sinus cavities. In this chapter we present a number of cases illustrated with these imaging modalities so professionals in the dental field may become more familiar with the different conditions and their imaging appearances.

10.2 Inflammatory Diseases

A number of inflammatory conditions may occur in the paranasal sinuses.

10.3 Acute Rhinosinusitis

Figs. 10.1, 10.2, and 10.3

10.3.1 Definition

Acute inflammation in nose and paranasal sinuses.

10.3.2 Clinical Features

- One of the most common medical afflictions
- Viral rhinosinusitis most common (common cold, influenza)
- Bacterial rhinosinusitis may develop secondarily (*Haemophilus influenzae*, *Streptococcus pneumoniae*)
- Pain over sinuses; cheek, frontal, between eyes, or suboccipital
- Toothache, teeth tenderness to percussion; more than one tooth of maxillary lateral segment(s)
- Headache seldom
- Dental etiology in 10–20%; larger frequencies have been reported depending on patient materials

In collaboration with H.-J. Smith

T.A. Larheim, P.-L.A. Westesson, *Maxillofacial Imaging*, https://doi.org/10.1007/978-3-319-53319-3_10

10.3.3 Imaging Features

- Nodular or smooth mucosal thickening or complete sinus opacification
- Contrast-enhanced inflamed mucosa lining; variable amounts of submucosal edema and surface secretions
- Air-fluid level, most frequent in maxillary sinus, due to bacterial sinusitis with obstruction of ostium, but only in 25–50% of patients with this disease
- T1-weighted MRI: low to intermediate signal
- T2-weighted MRI: high signal of inflamed mucosa and fluid
- T1-weighted post-Gd MRI: intense enhancement of inflamed mucosa; no enhancement of fluid

Fig. 10.1 Acute rhinosinusitis secondary to common cold. Coronal CT shows fluid level in the right maxillary sinus (*arrow*), probably also in the left sinus, and mucosal thickening of ethmoid cells bilaterally. Normal bone structures

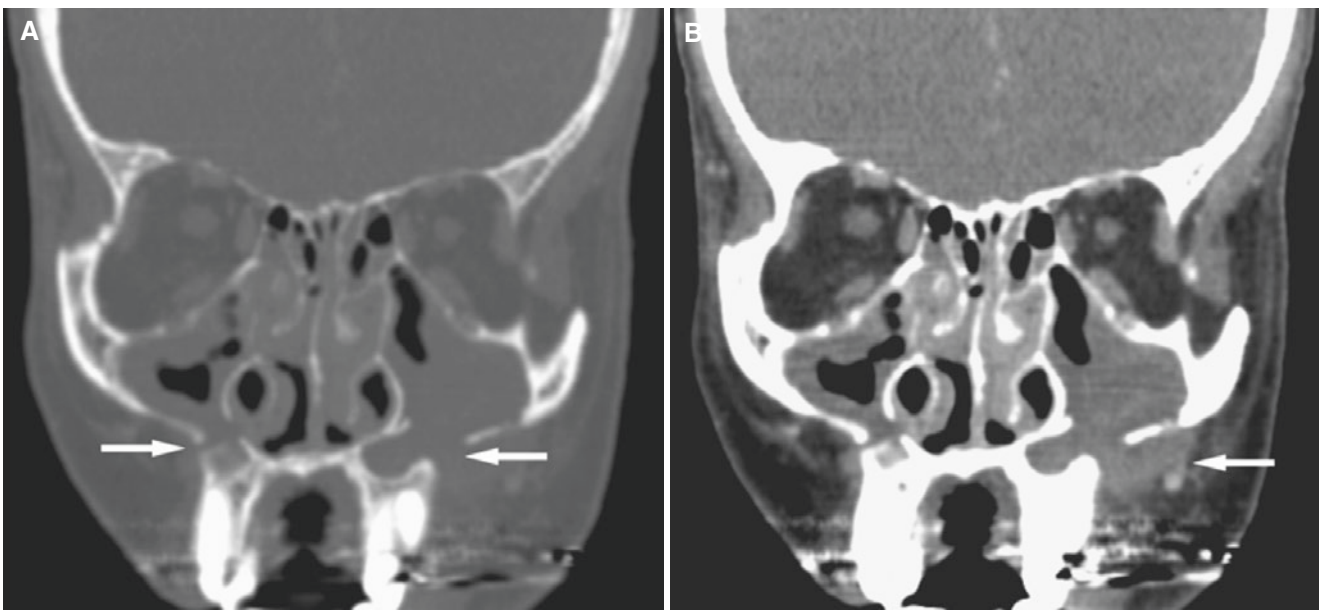

Fig. 10.2 Acute sinusitis; 37-year-old female with a history of LeFort I osteotomy now with facial pain and swelling. (**A**) Coronal CT image shows bilateral osteotomies through the maxilla and nasal cavity (*arrows*) and mucosal thickening of ethmoid and maxillary sinuses and nasal cavity. (**B**) Coronal CT image, soft-tissue window, shows inflammatory tissue penetrating left maxillary osteotomy being responsible for facial swelling (*arrow*). Sinusitis does not normally cause facial swelling, but since there was a passage from the maxillary sinus to the facial soft tissue via the osteotomy defect in this patient, facial swelling resulted

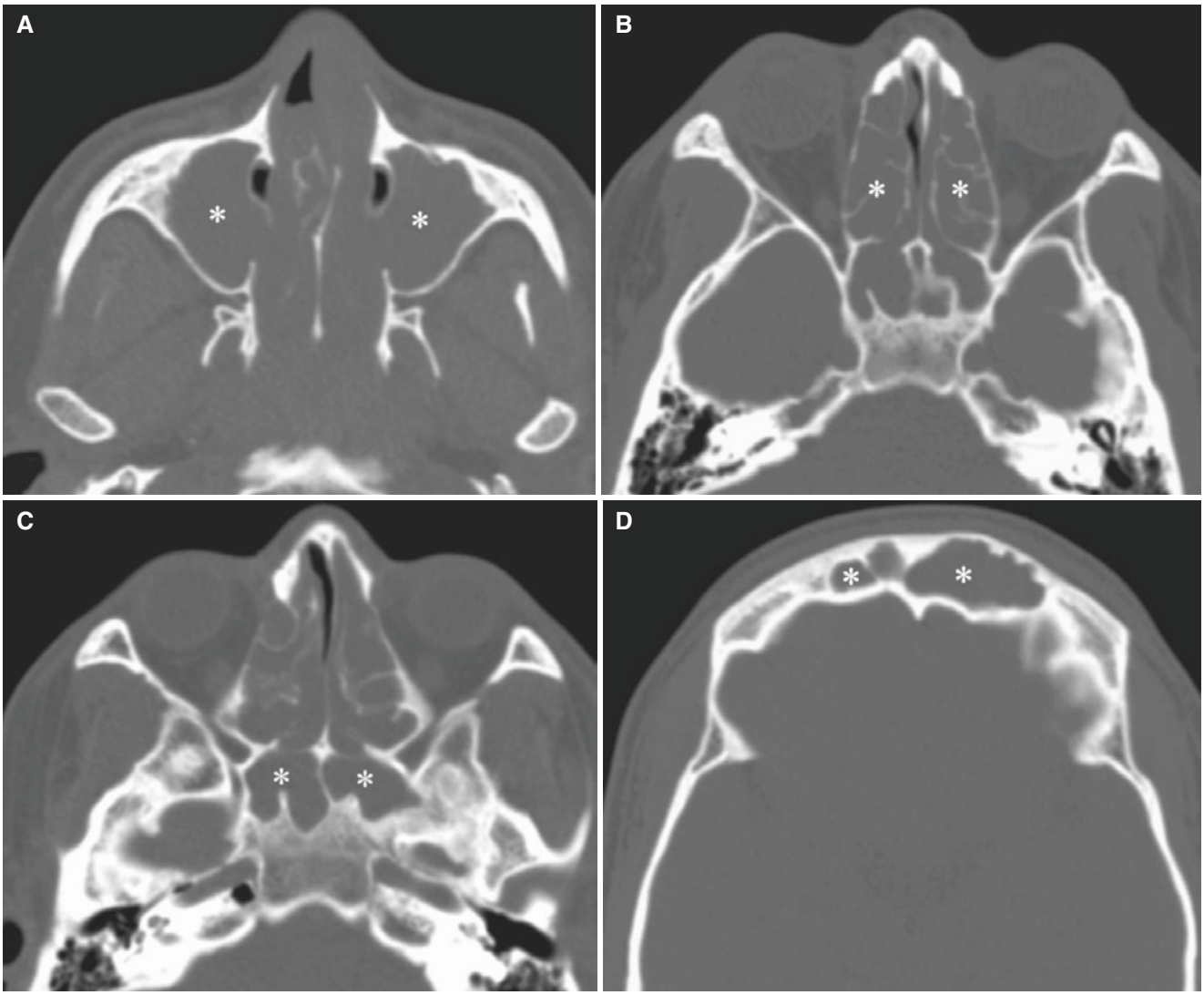

Fig. 10.3 Pansinusitis; 19-year-old male with history of sinusitis and cough, now with headache and eye and cheek pain. (**A**) Axial CT image shows complete opacification of the maxillary sinuses (*asterisks*). (**B**) Axial CT image shows complete opacification of ethmoid sinuses (*asterisks*). (**C**) Axial CT image shows complete opacification of sphenoid sinuses (*asterisks*). (**D**) Axial CT image shows complete opacification of frontal sinuses (*asterisks*)

10.4 Chronic Sinusitis

Figs. 10.4, 10.5, 10.6, and 10.7

10.4.1 Definition

Develops from either persistent acute inflammation or repeated episodes of acute or subacute sinusitis:

- Allergic sinusitis
- Vasomotor rhinitis
- Fungal sinusitis (90% *Aspergillus fumigatus*; may be fulminant and invasive in immunosuppressed patients)

10.4.2 Clinical Features

- Anaerobic microorganisms frequently isolated

10.4.3 Imaging Features

- Varying mucosal swelling, smooth or irregular swelling due to edema and secretion
- Thickened, sclerotic, fibrotic sinus walls, particularly of maxillary sinuses
- Dystrophic calcification
- T1-weighted MRI: low to intermediate signal
- T2-weighted MRI: usually high signal of inflamed mucosa, low signal of sclerosis and fibrosis. Inspissated mucus can be dark on all sequences resulting in false-negative MR diagnosis of chronic sinusitis

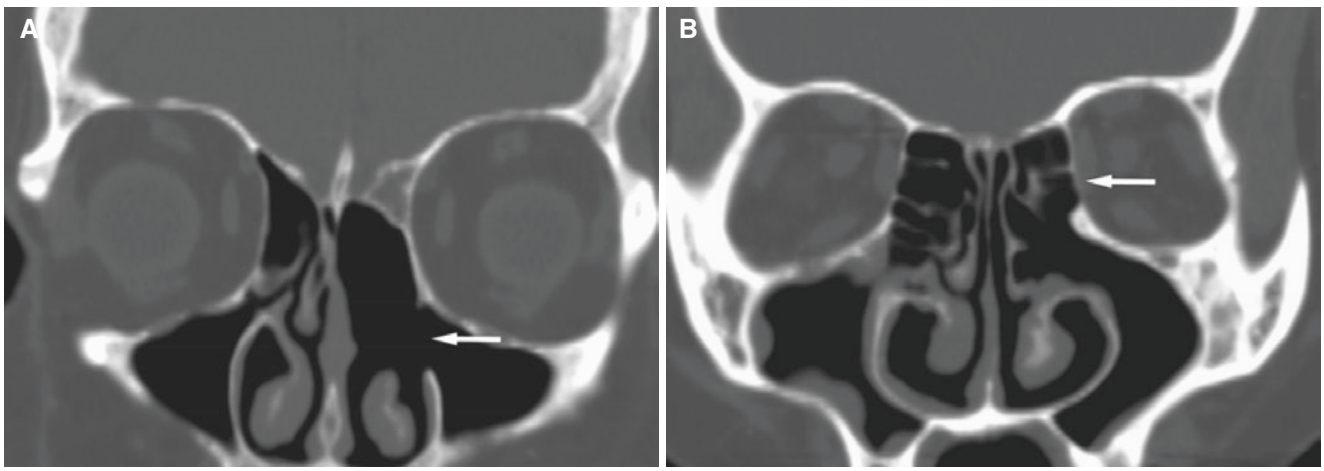

Fig. 10.4 Post endoscopic surgery; 41-year-old female 9 years after septoplasty with left concha bullosa and partial ethmoid sinus resection, now with "nose problem." (**A**) Coronal CT image shows that the left medial maxillary sinus wall is removed (*arrow*), together with the left middle turbinate and ethmoid cells; otherwise, normal bone and air. (**B**) Coronal CT image, more posterior section, shows that ethmoid cells are partially intact (*arrow*). Only minimal mucosal thickening of the right maxillary sinus

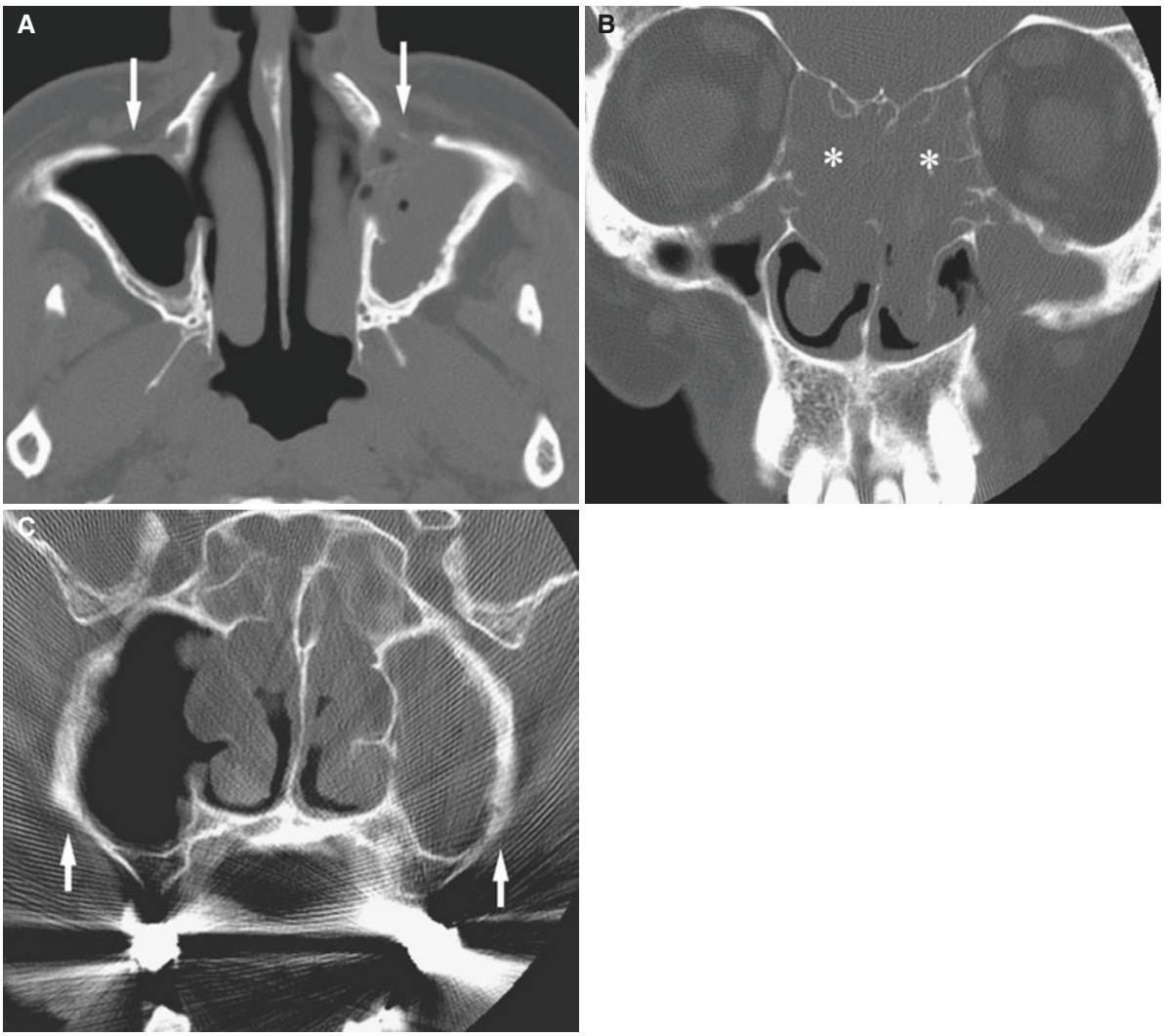

Fig. 10.5 Chronic sinusitis; 61-year-old female with history of previous surgery for sinusitis. (**A**) Axial CT image shows surgical maxillary defects bilaterally (*arrows*), opacification of left sinus, and thickening with sclerosis of sinus walls bilaterally. (**B**) Coronal CT image shows opacification of ethmoid sinuses bilaterally (*asterisks*). (**C**) Coronal CT image shows evenly thickened maxillary sinus wall in the entire sinus bilaterally (*arrows*)

Fig. 10.6 Chronic sinusitis; 69-year-old male with history of previous sinus surgery, now with history of motor vehicle accident and trauma to head. Axial CT image shows that medial maxillary sinus walls had been surgically removed (*arrows*), together with part of the right anterior maxillary sinus wall. Note some bilateral mucosal thickening and thickening/sclerosis of bony sinus walls

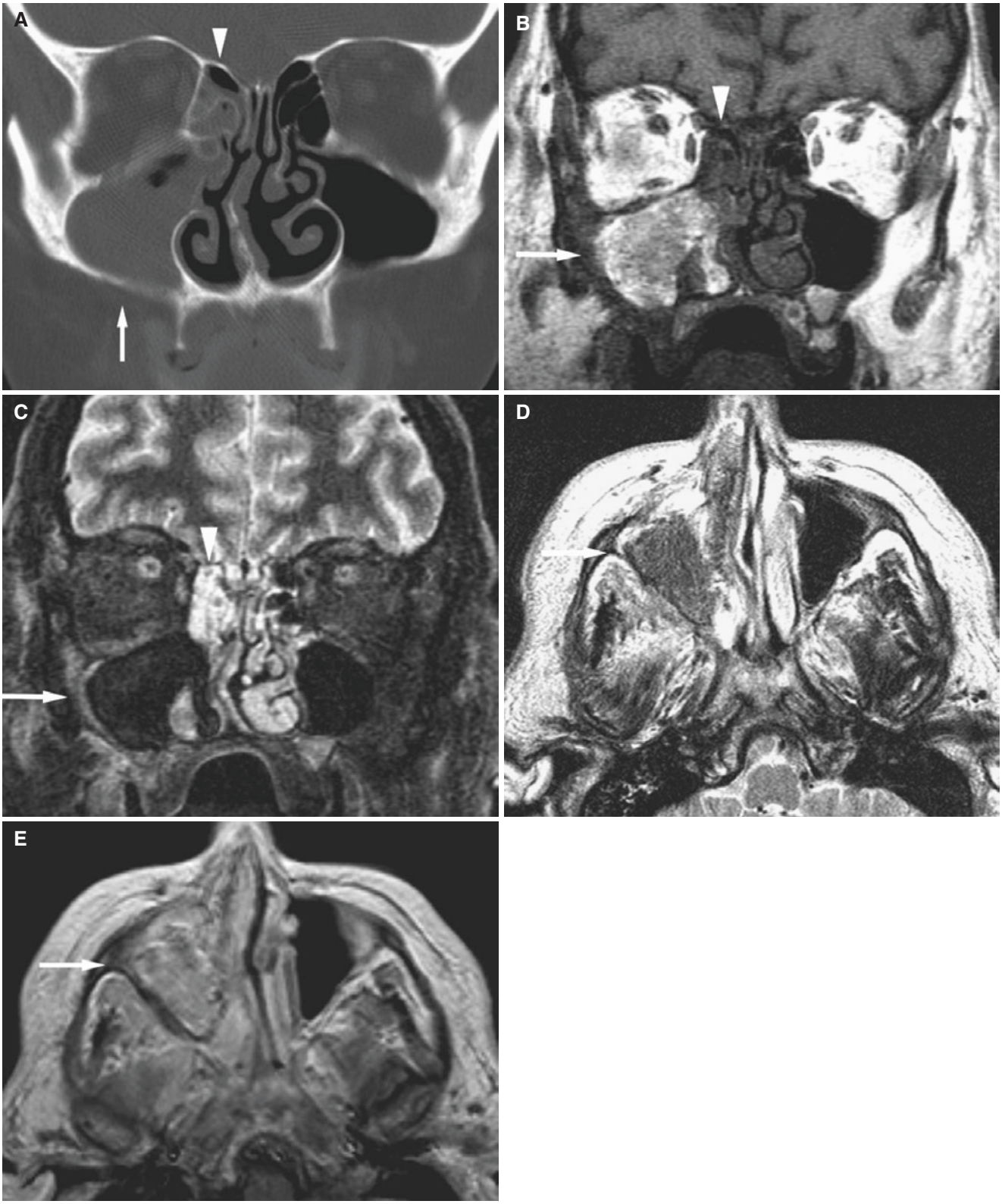

Fig. 10.7 Chronic *Aspergillus* sinusitis; 57-year-old female with history of acute lymphatic leukemia, neutropenic status post chemotherapy, now with eye and cheek pain. (**A**) Coronal CT image shows opacification of right maxillary sinus (*arrow*) and ethmoid sinus (*arrowhead*). (**B**) Coronal T1-weighted MRI shows intermediate to high signal in maxillary sinus (*arrow*) and low signal in ethmoid sinus (*arrowhead*). (**C**) Coronal STIR MRI shows low "normal" signal in the right maxillary sinus (*arrow*) and high signal in the ethmoid sinus (*arrowhead*). (**D**) Axial T2-weighted MRI shows intermediate to low signal in right maxillary sinus (*arrow*). (**E**) Axial T1-weighted post-Gd MRI shows heterogeneous contrast enhancement (*arrow*)

10.5 Mucosal Imaging Findings in Asymptomatic Individuals

MRI findings of paranasal sinuses in patients with brain imaging:

- Mucosal thickening up to 3 mm may be present in clinically normal individuals.
- Clinically silent focal areas of mucosal thickening occur from about one-fourth and up to two-thirds of asymptomatic individuals.

10.6 Retention Cysts, Mucous and Serous

Figs. 10.8 and 10.9

10.6.1 Definition

Mucous retention cyst: obstruction of submucosal mucinous gland, thus cyst wall of duct epithelium and gland capsule.

Serous retention cyst: accumulation of serous fluid in submucosal layer of sinus mucosa, thus cyst lining of elevated mucosa.

10.6.2 Clinical Features

- Incidental finding

10.6.3 Imaging Features

- Smooth, spherical soft-tissue mass
- Retention cysts found incidentally in 10–35% of patients, most commonly in maxillary sinus, but can occur in any sinus
- Frequently small, may become large but always some air
- Almost in every case normal bone
- T1-weighted MRI: usually low to intermediate signal, but may show high signal if cyst has high protein content
- T2-weighted MRI: high signal

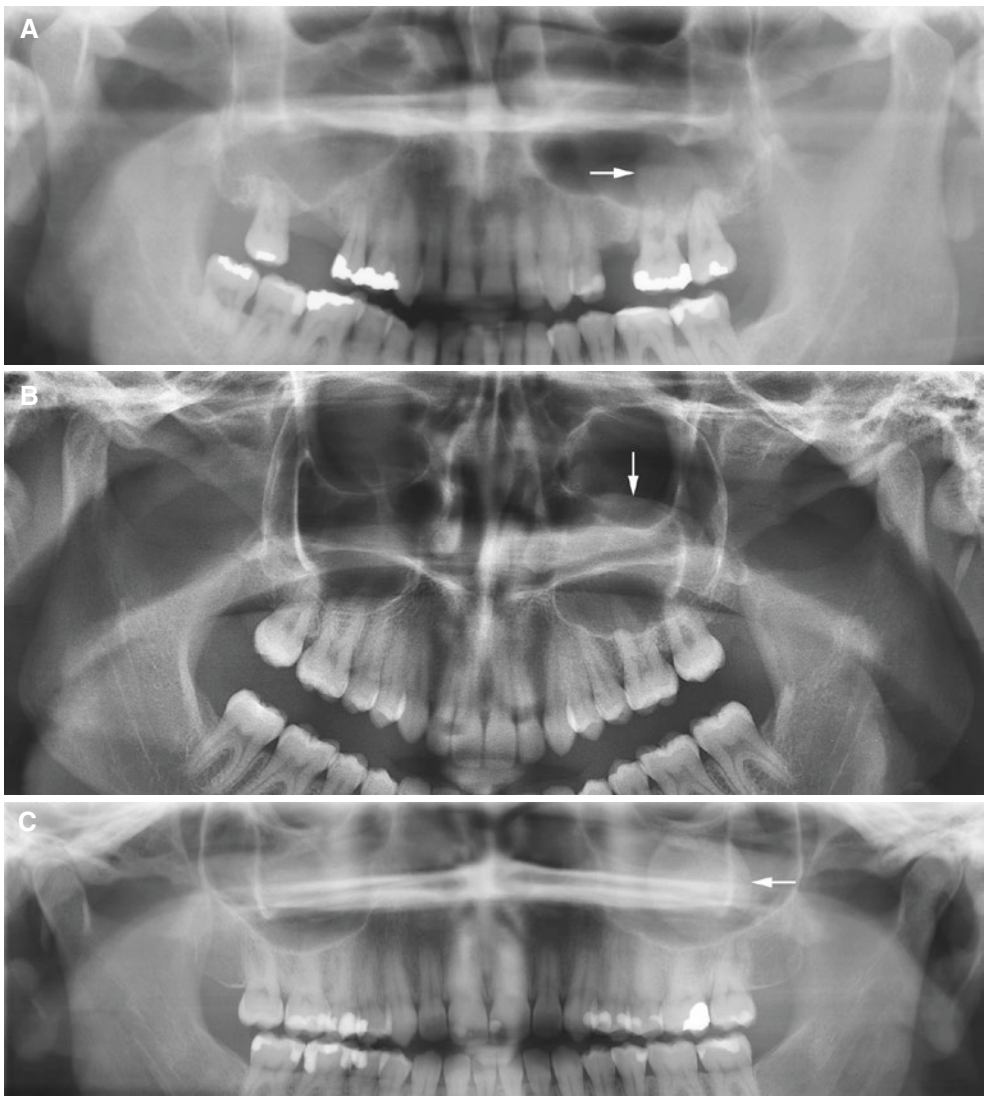

Fig. 10.8 Retention cyst in maxillary sinus; incidental finding. (**A**, **B**, **C**) Panoramic views of different patients show retention cysts (*arrow*) with various sizes and morphologies

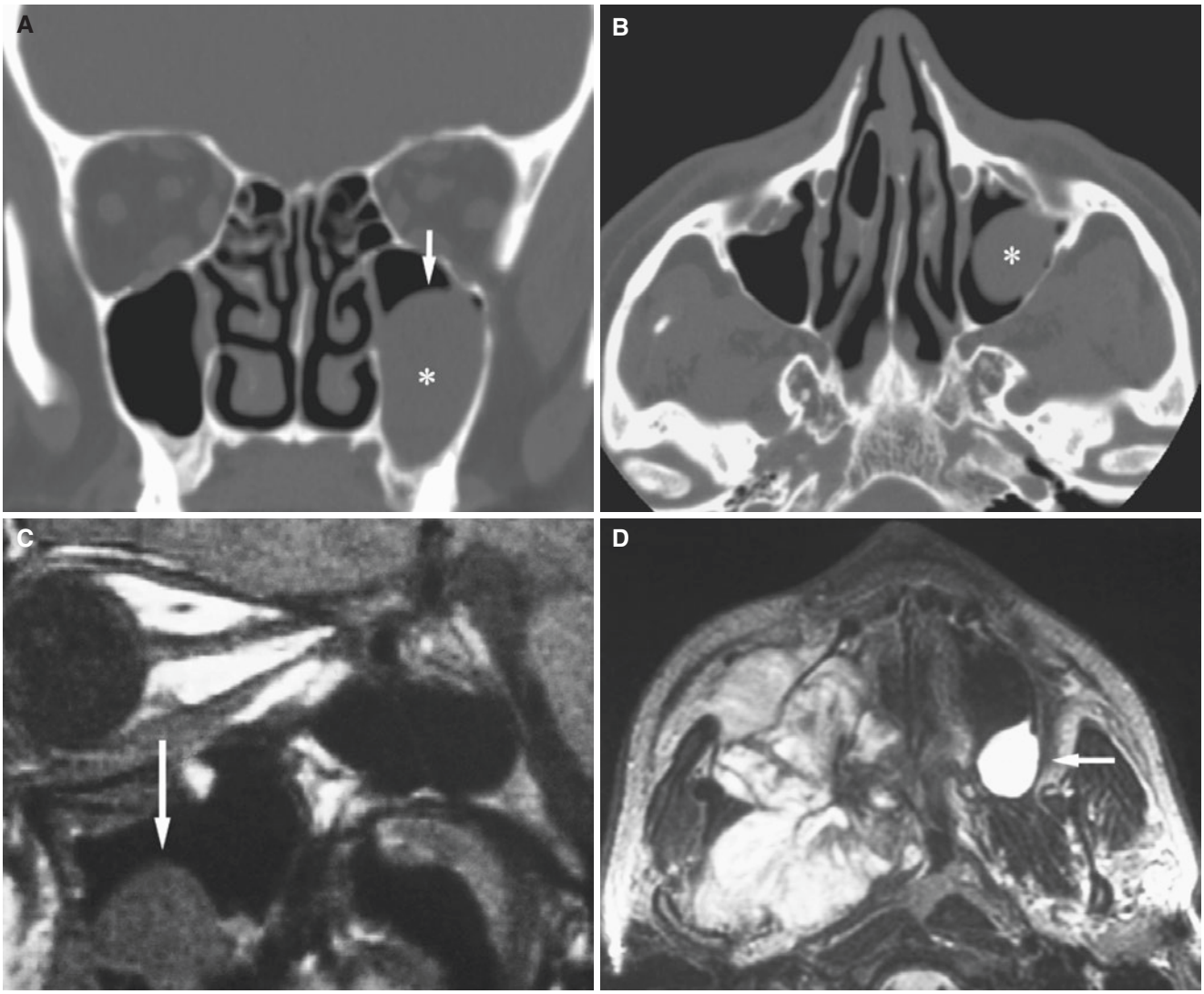

Fig. 10.9 Retention cyst in the maxillary sinus; incidental finding. (**A**) Coronal CT image shows retention cyst in maxillary sinus (*asterisk*) with soft-tissue lining (*arrow*), without expansion of sinus walls, but with remaining air. (**B**) Axial CT image of same patient shows soft-tissue lined retention cyst (*asterisk*). (**C**) Sagittal T1-weighted MRI shows retention cyst with intermediate signal (*arrow*); patient with blowout fracture. (**D**) Axial T2-weighted MRI shows retention cyst with high signal (*arrow*); patient with osteosarcoma of the right maxilla

10.7 Polyps

Figs. 10.10, 10.11, 10.12, and 10.13

10.7.1 Definition

Expansion of fluids in deeper lamina propria of Schneiderian mucosa in nasal fossa and paranasal sinuses.

10.7.2 Clinical Features

- Most common expansile condition in the nasal cavity; about 4% in general population
- Nasal polyps most often associated with allergy, and frequently multiple and symmetric, but may result from infectious rhinosinusitis, vasomotor rhinitis, cystic fibrosis, diabetes mellitus, aspirin intolerance, and nickel exposure
- In patients with polyps up to about 70% with asthma
- Nasal stuffiness
- When seen in children, cystic fibrosis should be ruled out

10.7.3 Imaging Features

- Smooth, spherical soft-tissue mass
- If multiple, complete opacification of nasal cavity and sinuses
- T1-weighted MRI: low to intermediate signal
- T2-weighted MRI: high signal
- Heterogeneous MR signal characteristic in chronic polyps; can also enhance

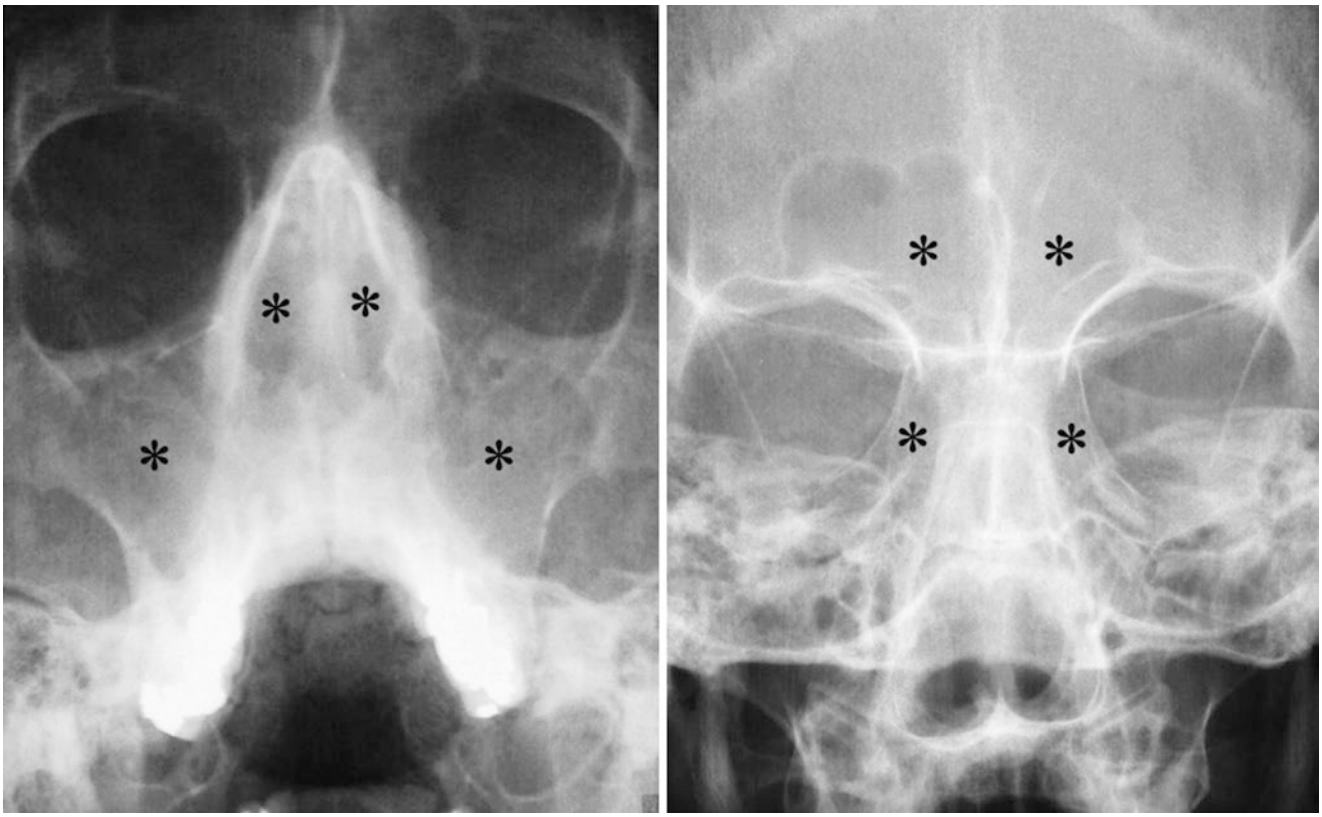

Fig. 10.10 Nasal polyposis; 38-year-old male with nasal obstruction. Conventional films show complete opacification of the nasal cavity and all paranasal sinuses (*asterisks*), except some air in the right frontal sinus (courtesy of Dr. A. Kolbenstvedt, Oslo University Hospital, Rikshospitalet, Oslo, Norway)

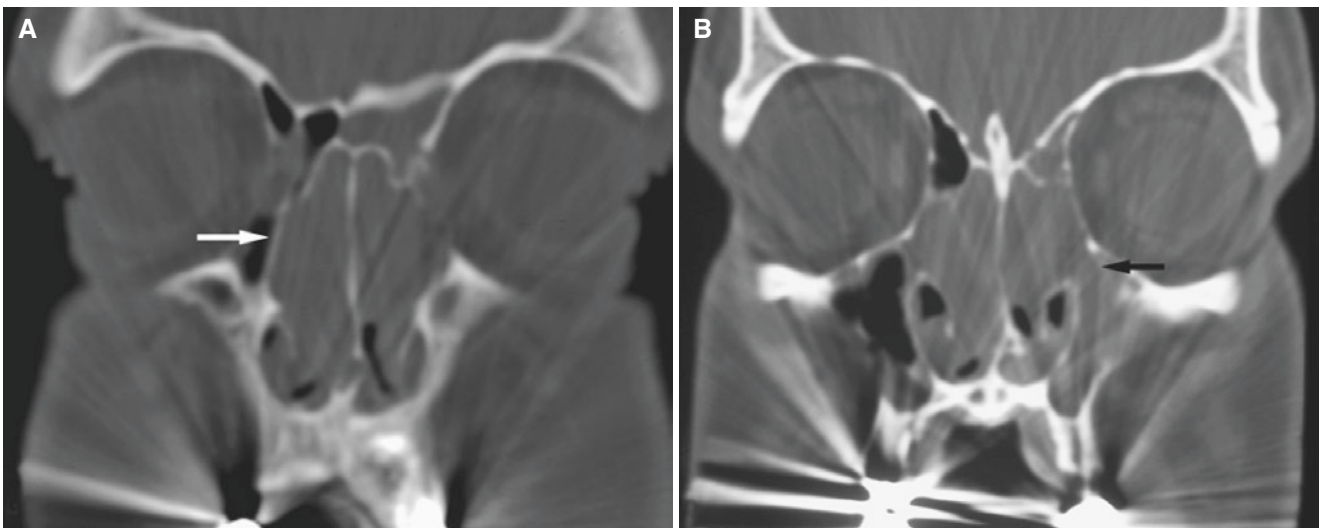

Fig. 10.11 Nasal polyposis; patient with history of chronic nasal obstruction and sinusitis. (**A**) Coronal CT image shows opacification of nasal cavity (*arrow*). (**B**) Coronal CT image shows opacification of the nasal cavity with soft-tissue bulging through widened ostiomeatal complex particularly on the left side (*arrow*) but to a lesser extent also on the right, with secondary sinusitis

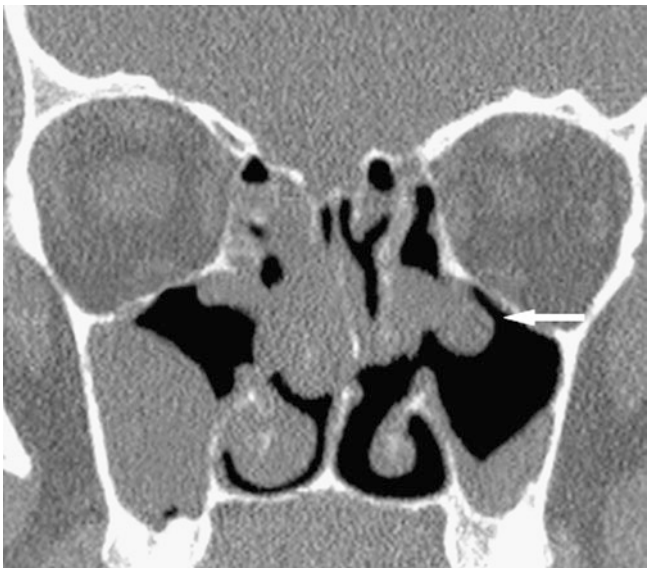

Fig. 10.12 Nasal polyposis; 43-year-old male with previous surgery for nasal polyposis, now with recurrence. Coronal CT image shows polyps in nose bulging through ostiomeatal complex (*arrow*) but also mucosal thickening in ethmoid and maxillary sinuses (courtesy of Dr. A. Kolbenstvedt, Oslo University Hospital, Rikshospitalet, Oslo, Norway)

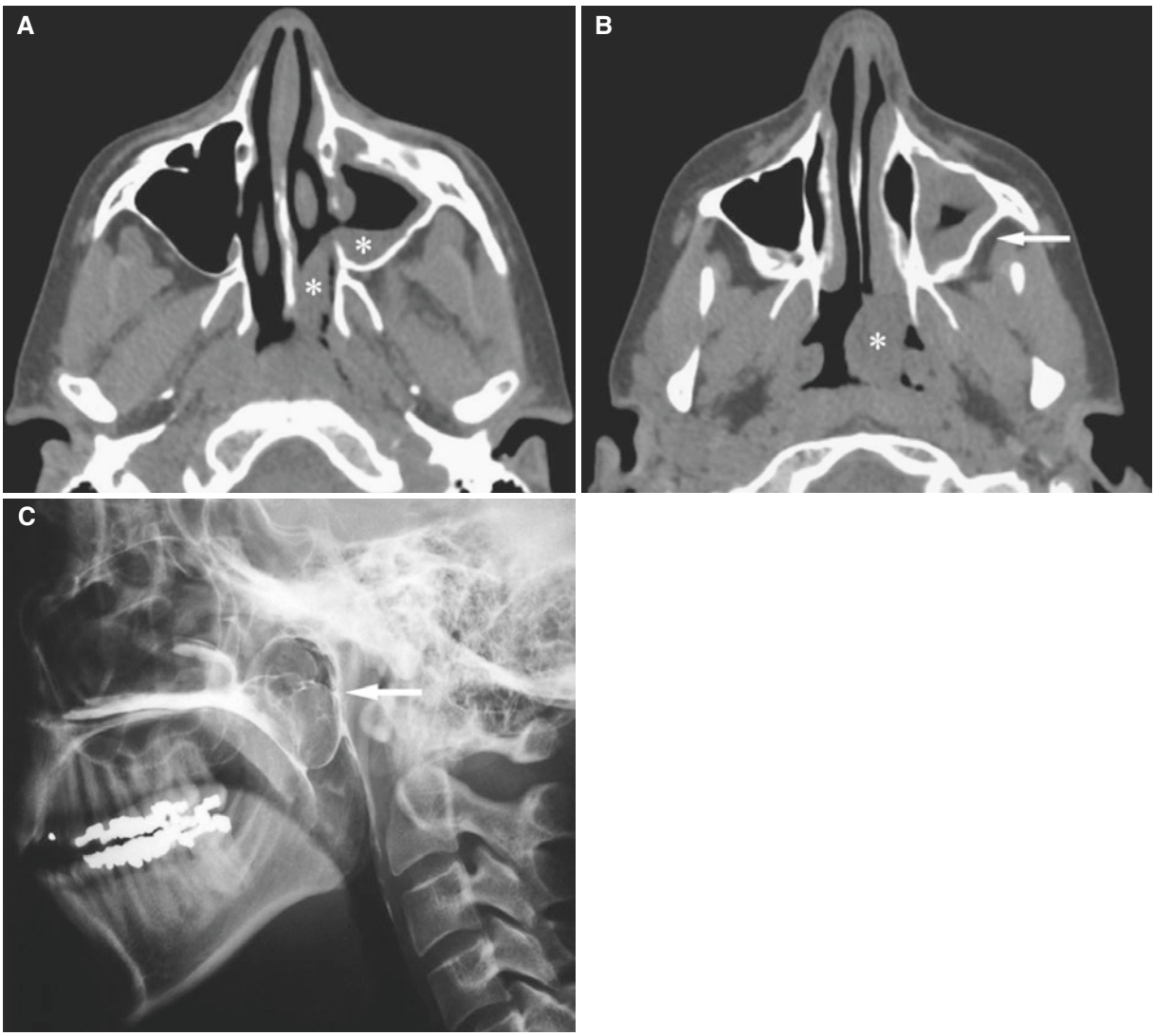

Fig. 10.13 Antrochoanal polyp; 12-year-old male with history of sinusitis and nasopharyngeal mass. (**A**) Axial CT image shows left maxillary sinus thickening (*asterisk*) with extension of soft-tissue mass into the posterior nasal cavity down to the nasopharynx (*asterisk*), via the ethmoidal infundibulum. No bone destruction. (**B**) Axial CT image shows polyp in the nasopharynx (*asterisk*) and soft-tissue thickening in the maxillary sinus (*arrow*). (**C**) Lateral view with contrast in the nose of another patient shows how polyp blocks the nasopharynx (*arrow*) (**C**: courtesy of Dr. A. Kolbenstvedt, Oslo University Hospital, Rikshospitalet, Oslo, Norway)

10.8 Mucoceles

Figs. 10.14, 10.15, 10.16, 10.17, 10.18, and 10.19

10.8.1 Definition

Collection of mucoid secretions surrounded by mucus-secreting respiratory epithelium.

Both retention and mucocele cysts consist of mucous secretions surrounded by epithelial lining, but are distinguished by their clinical and imaging features. Mucocele develops due to obstruction of sinus ostium or a compartment of a sinus with the sinus mucosa as the mucocele wall and always with expanded sinus walls.

10.8.2 Clinical Features

- Most common expansile condition in paranasal sinuses
- Most frequent in frontal sinuses (60–65%); only 5–10% in sphenoid as well as in maxillary sinuses
- Both sexes, wide range of age: 20–60 years
- Classic mucocele is sterile with signs and symptoms from mass effect
- Pain uncommon
- If infected, pain; mucopyocele or pyocele
- Ostial obstruction may be caused by inflammatory scar, trauma, or tumor

10.8.3 Imaging Features

- Initially, intact but remodeled, expanded surrounding bone
- With progressive growth, sinus wall will be destroyed
- Completely airless sinus
- T1-weighted and T2-weighted MRI: variable MR signals depending on protein content, state of dehydration, and viscosity of content; most frequently observed pattern is moderate-to-marked high signal on T2
- T1-weighted post-Gd MRI: no enhancement except of thin peripheral rim

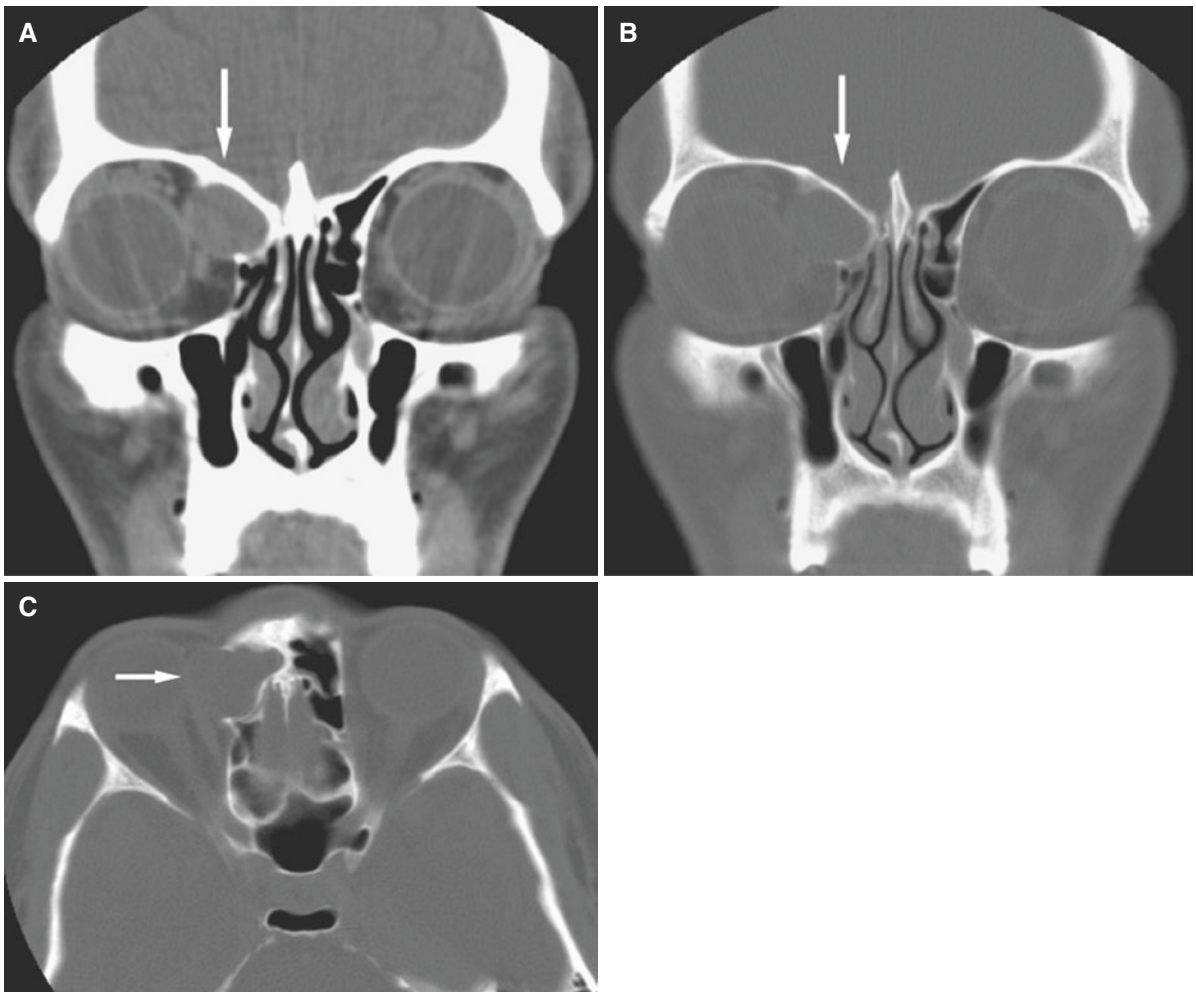

Fig. 10.14 Frontal sinus mucocele; 50-year-old male with diplopia and right eye down and laterally deviated. (**A**) Coronal CT image, soft-tissue window, shows ovoid well-defined soft-tissue mass in the right orbit (*arrow*) with displacement of globe laterally down. (**B**) Coronal CT image, bone window, shows bone expansion and absent frontal sinus wall against orbit (*arrow*), but otherwise normal bone structures. (**C**) Axial CT image shows well-defined delineation of bone expansion (*arrow*)

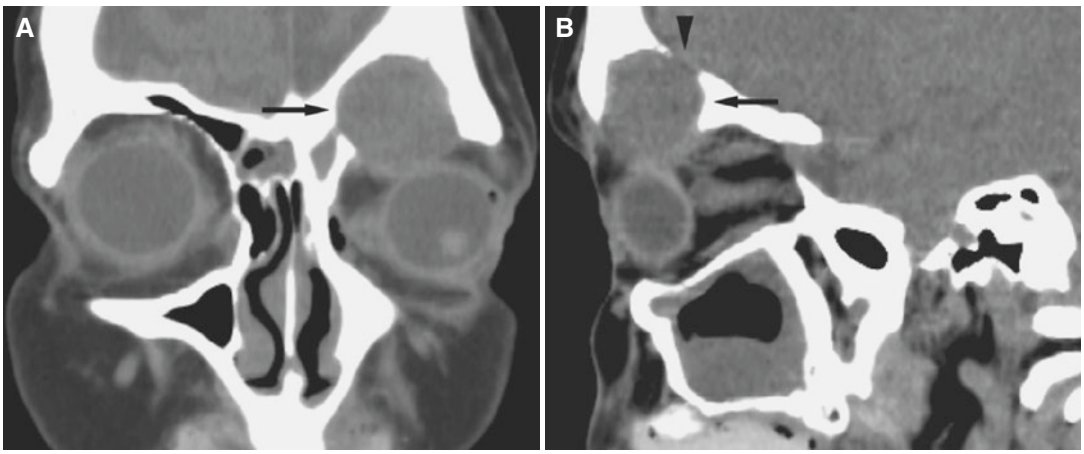

Fig. 10.15 Frontal sinus mucocele; 52-year-old female with headache and diplopia. (**A**) Coronal CT image shows well-defined soft-tissue mass with no air in the left frontal sinus with bone expansion (*arrow*), displacing globe down and laterally. (**B**) Sagittal CT image shows mucocele with bone expansion (*arrow*) and destroyed bone delineation to anterior cranial fossa (*arrowhead*). Note mucosal thickening in maxillary sinus

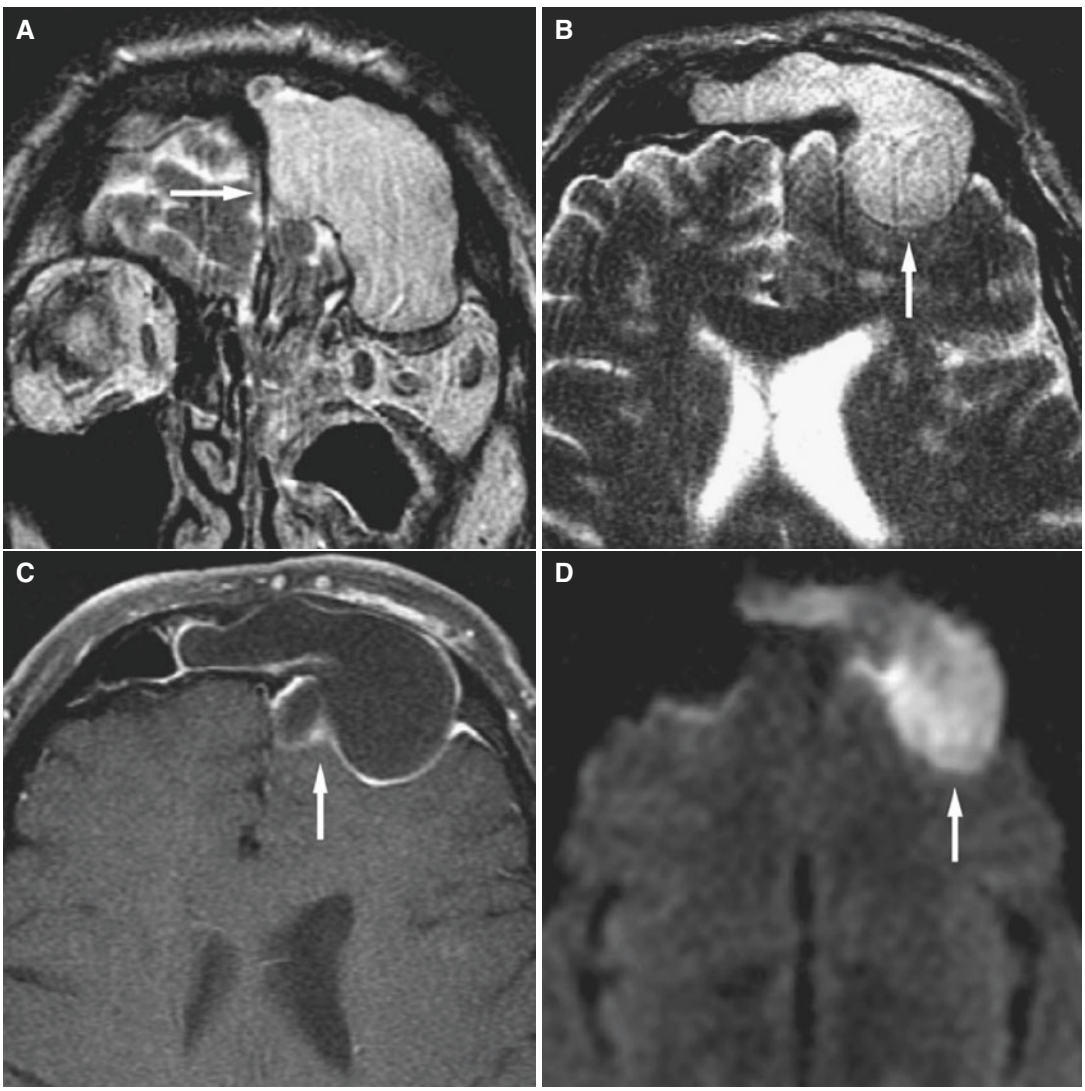

Fig. 10.16 Frontal sinus mucocele; 60-year-old male presented with headache and diplopia. (**A**) Coronal T2-weighted MRI shows intermediate-signal large expansive mucocele (*arrow*). (**B**) Axial T2-weighted MRI shows expansion into cranial fossa with displacement of the left frontal lobe (*arrow*). (**C**) Axial T1-weighted post-Gd MRI shows no enhancement except in the thin peripheral rim (*arrow*). (**D**) Axial diffusion-weighted MRI shows high signal (*arrow*) compatible with restricted diffusion in mucocele

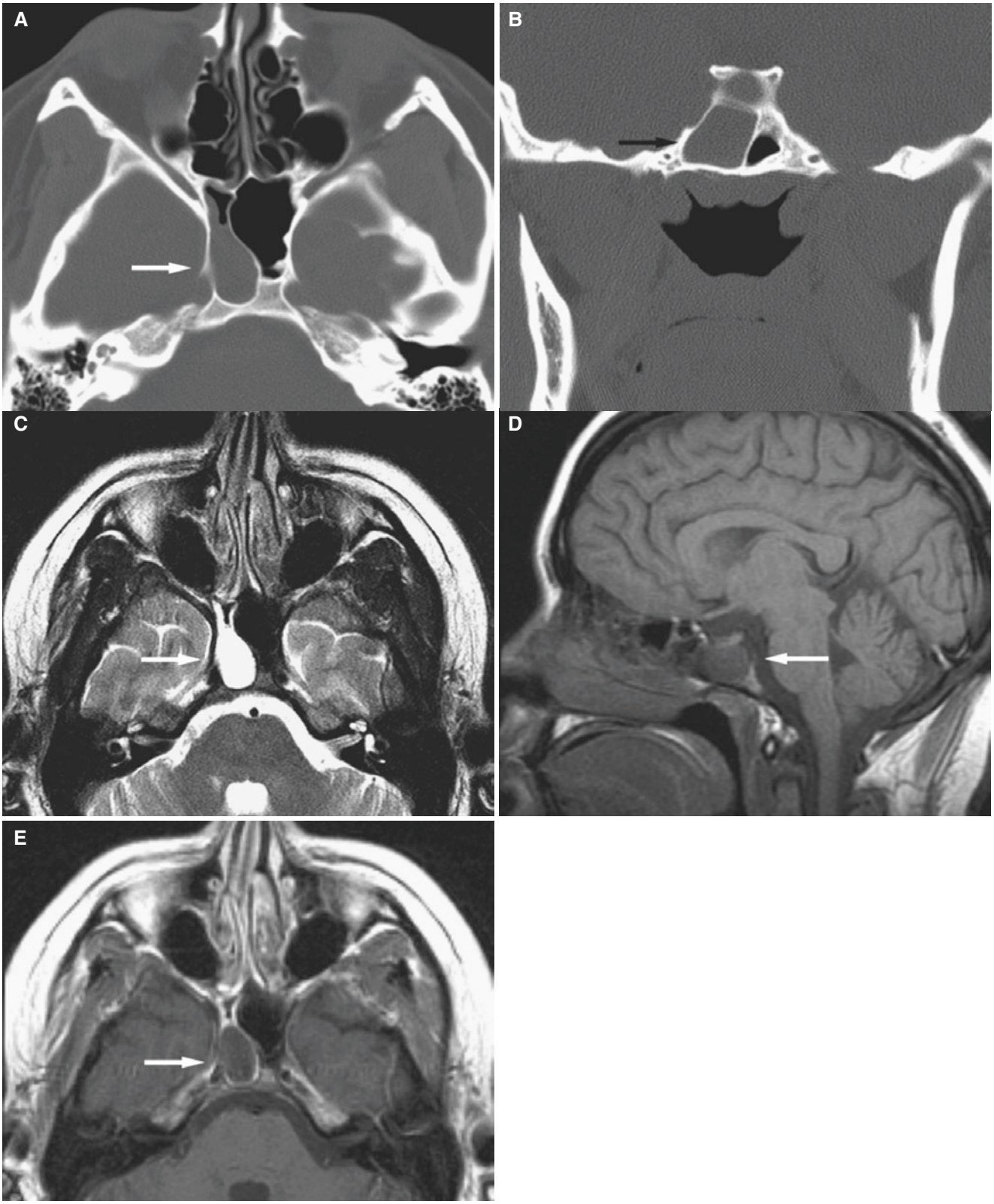

Fig. 10.17 Sphenoid sinus mucocele; 19-year-old female with past medical history significant for morbid obesity who presented with history of headache for 6 weeks, as well as occasional nausea and vomiting; initially evaluated for suspicion of brain tumor, pseudotumor cerebri, and venous thrombosis. (**A**) Axial CT image shows expansive mass in the right compartment of sphenoid sinus with intact cortical outline (*arrow*). (**B**) Coronal CT image shows mucocele in the right compartment of sphenoid sinus (*arrow*). (**C**) Axial T2-weighted MRI shows high signal of mucocele (*arrow*). (**D**) Sagittal T1-weighted MRI shows intermediate to low signal (*arrow*). (**E**) Axial T1-weighted post-Gd MRI shows no enhancement except in the thin peripheral rim (*arrow*)

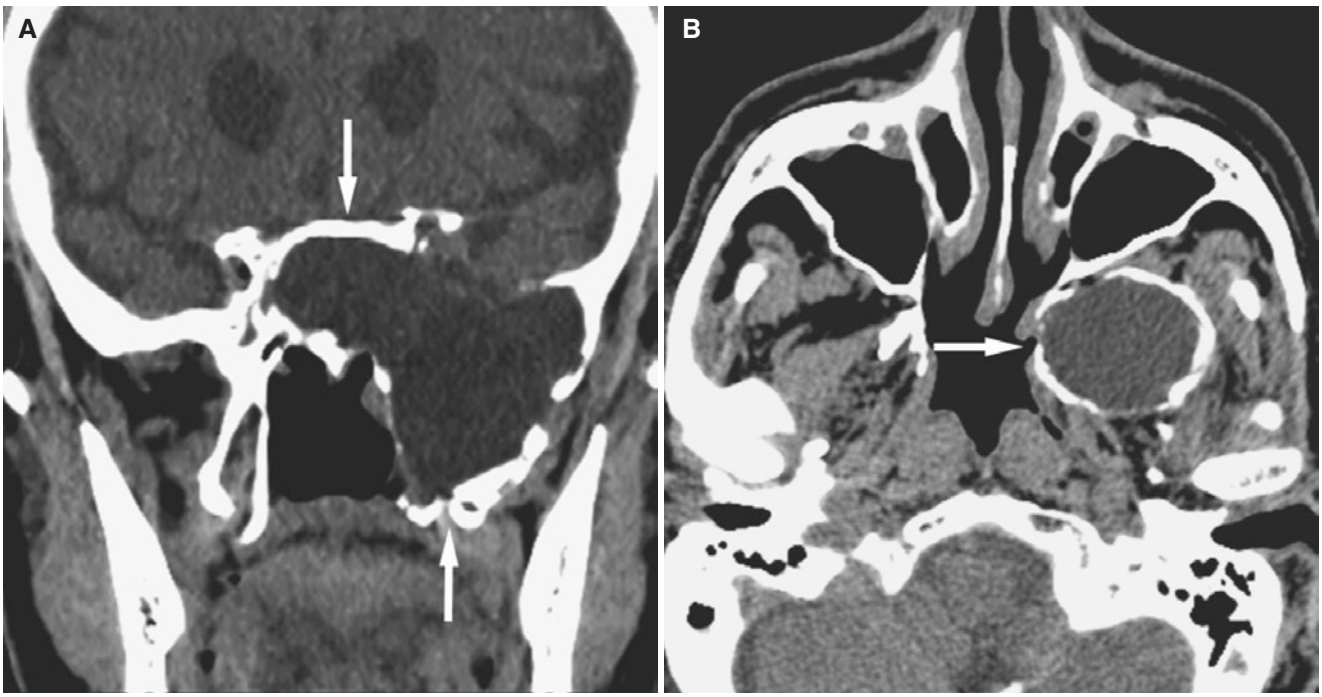

Fig. 10.18 Sphenoid sinus mucocele; 85-year-old male with known chronic sinusitis, now with headache. (**A**) Coronal CT image, soft-tissue window, shows large expansive mass (*arrows*) with homogeneous hypodense content extending into the clivus and pterygoid process of the sphenoid bone. (**B**) Axial CT image, soft-tissue window, shows mucocele extending into parapharyngeal space (*arrow*)

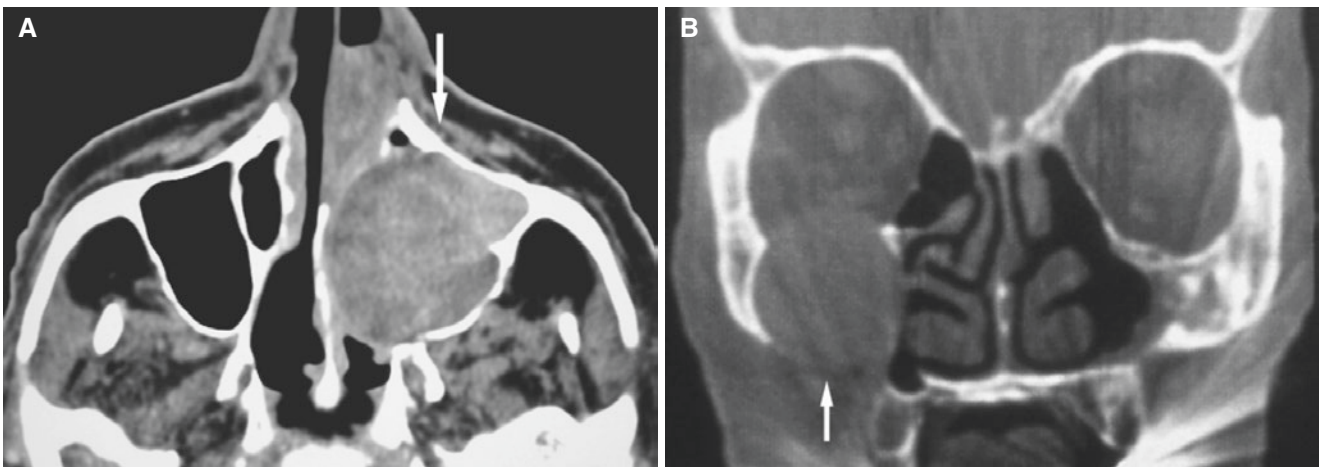

Fig. 10.19 Maxillary sinus mucocele; two patients with long history of chronic sinusitis and sinus surgery. (**A**) Axial CT image shows expansive process in the entire left maxillary sinus (*arrow*) extending to midline of the nasal cavity. (**B**) Coronal CT image shows expansive mass in the entire right maxillary sinus extending into orbit (*arrow*)

10.9 Granulomatosis With Polyangiitis (Previously Known as Wegener's Granulomatosis)

Fig. 10.20

10.9.1 Definition

Necrotizing granulomatous vasculitis that usually affects upper and lower respiratory tracts and causes renal glomerulonephritis, with a limited form only in sinonasal tract with a more benign course.

Two other forms are eosinophilic granulomatosis with polyangiitis and microscopic polyangiitis.

10.9.2 Clinical Features

- Rare noninfectious, destructive disease; diagnosis difficult to establish early in disease course
- Chronic, nonspecific (autoimmune) inflammatory process of nose and sinuses, and also trachea, lungs, and kidney
- Can affect any site in the body
- Nasal septum affected in more than 90%, with ulceration and perforation ("saddle nose" deformity)
- Rarely diagnosis may lead to full recovery
- Without treatment the disease can be fatal

10.9.3 Imaging Features

- Nasal involvement precedes sinus disease; secretions, soft-tissue mass of nasal septum, septal erosion
- Sinuses affected in more than 90%; nonspecific inflammation with mucosal thickening of maxillary and ethmoid sinuses in particular
- Bones of nasal vault and affected sinuses may be thickened and severely sclerotic due to chronic inflammation but also bone destruction reflecting either osteomyelitis or necrosis

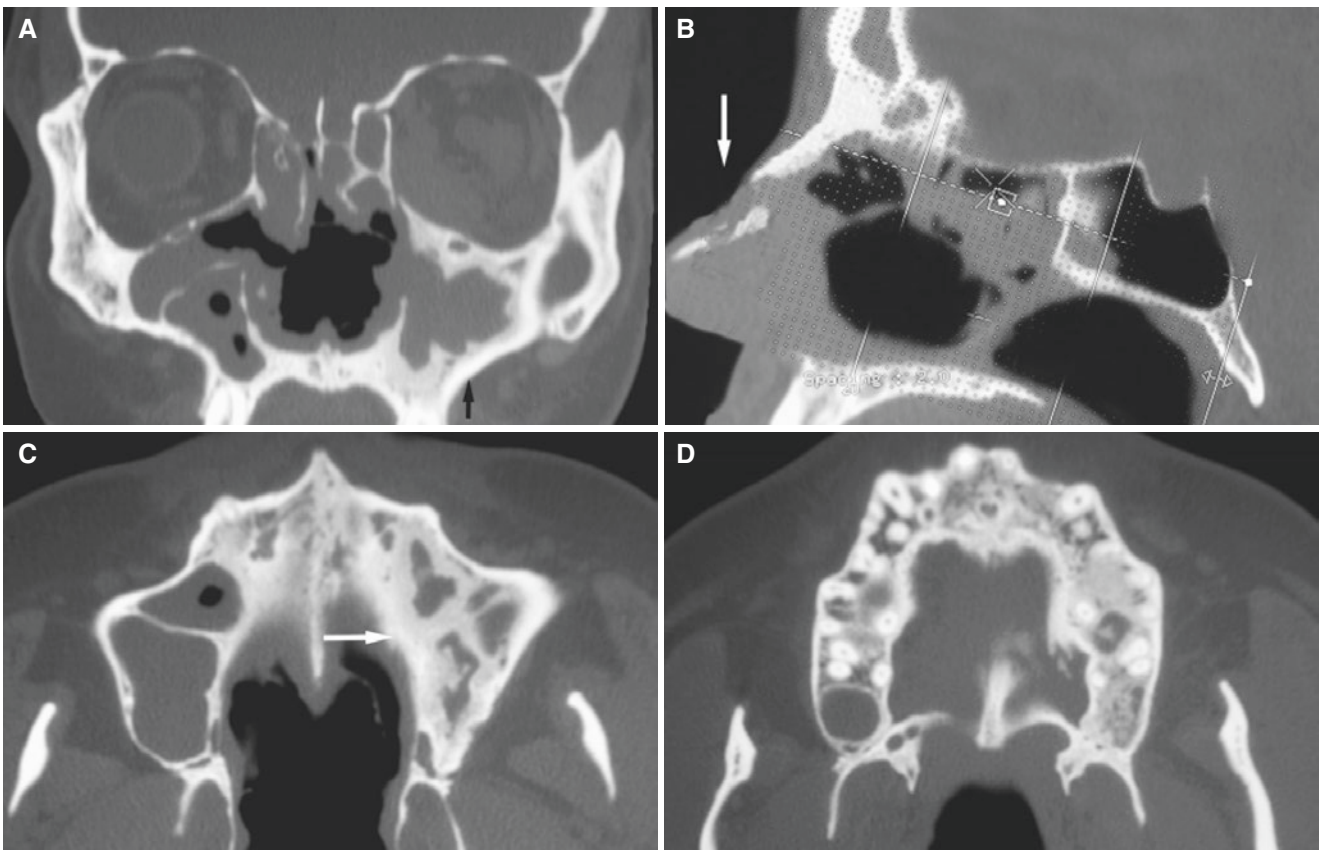

Fig. 10.20 Granulomatosis with polyangiitis; 46-year-old male with long history of nonspecific sinus problems. Mucosal biopsy consistent with Wegener's granulomatosis. (**A**) Coronal CT image shows destruction of nasal cavity structures and chronic sinusitis; opacification and mucosal thickening of ethmoid cells and maxillary sinuses, with severe sclerosis of maxillary sinus walls (*arrow*). (**B**) Sagittal CT image shows destruction of nasal bone, saddle nose (*arrow*). (**C**) Axial CT image shows severe sclerosis of sinus walls (*arrow*) and palate, crossing midline. (**D**) Axial CT image shows sclerotic bone in the maxillary alveolar process

10.10 Inflammatory Dental Conditions

Figs. 10.21, 10.22, and 10.23

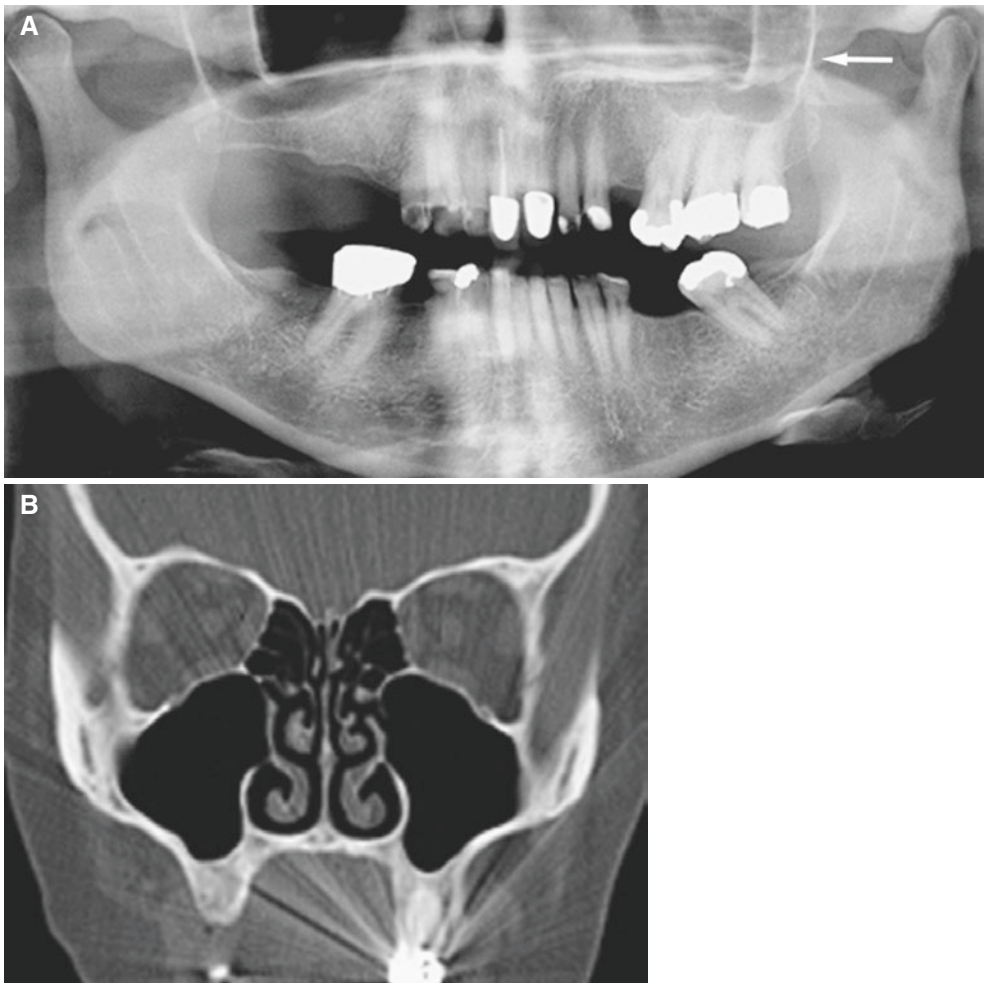

Fig. 10.21 Normal paranasal sinuses; false-positive panoramic view opacification of the maxillary sinus. (**A**) Panoramic view indicates opacification of the left maxillary sinus (*arrow*). (**B**) Coronal CT image shows normal air and bony walls of the maxillary and ethmoid sinuses

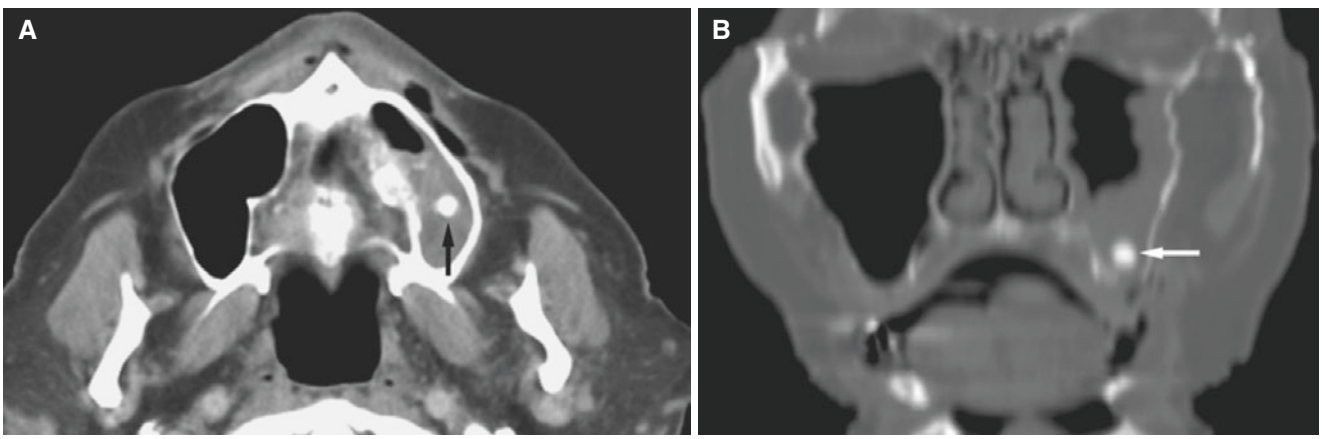

Fig. 10.22 Maxillary sinusitis due to displaced root; patient with history of problematic tooth extraction. (**A**) Axial CT image shows root in the maxillary sinus with mucosal thickening (*arrow*). (**B**) Coronally reformatted CT image shows root in the alveolar part of the sinus (*arrow*)

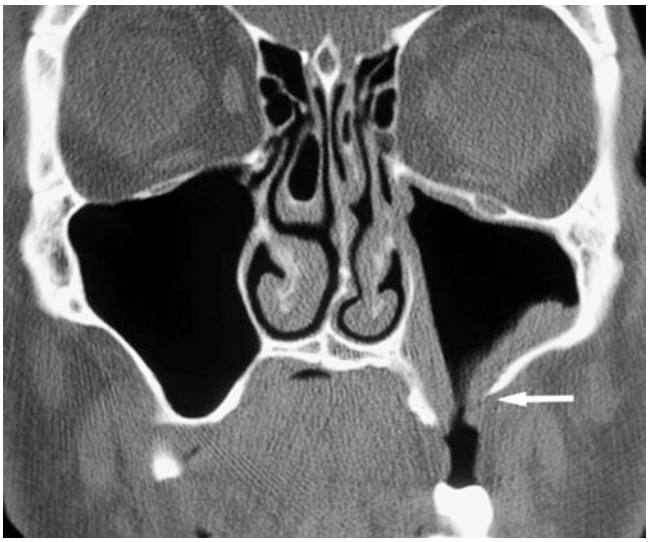

Fig. 10.23 Oroantral fistula; patient with history of previous problematic tooth extraction. Coronal CT shows opening between the oral cavity and maxillary sinus (*arrow*) and minimal mucosal thickening

10.11 Benign Tumors and Tumorlike Conditions

10.11.1 Clinical Features (in General)

- Tumors and tumorlike expansile masses are generally rare
- Benign more frequent than malignant
- Vague symptoms; masses frequently extensive when detected

10.11.2 Imaging Features (in General)

- Soft-tissue mass
- Benign: expansion, remodeling of bone, bone or dental hard-tissue production, may resorb teeth
- Malignant: destruction of bone, occasionally bone production, "floating teeth"
- T1-weighted MRI: intermediate signal
- T2-weighted MRI: intermediate to high signal
- T1-weighted post-Gd MRI: contrast enhancement
- May be difficult to decide whether mass originated in the sinus or not

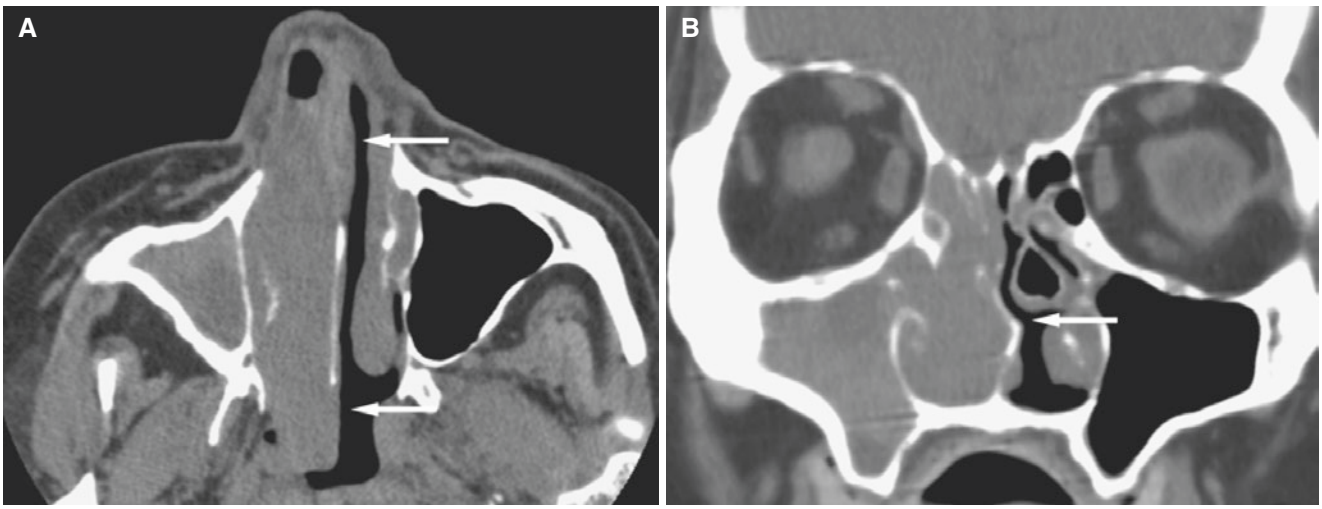

Fig. 10.24 Inverted papilloma; 71-year-old male with history of nasal papilloma that developed malignancy. (**A**) Axial CT image shows soft-tissue mass in the right nasal cavity with some deviation of the nasal septum extending into the nasopharynx (*arrows*). (**B**) Coronal CT image shows complete opacification of the right nasal cavity, maxillary sinus (*arrow*), and right ethmoid sinus and some widening of the ostiomeatal complex

10.12 Papilloma

Fig. 10.24

10.12.1 Definition

Benign tumor of nasal cavity composed of vascular connective tissue covered by well-differentiated stratified squamous epithelium that tends to grow under and elevate mucosa (inverted).

10.12.2 Clinical Features

- Less common than allergic polyps; less than 3% in general population
- Most common in males aged 40–70 years
- Unilateral from lateral nasal wall near ethmoids
- Nasal stuffiness or obstruction
- Secondary bacterial sinusitis
- Postoperative recurrence 35–40%
- May be associated with malignancy (about 10%)

10.12.3 Imaging Features

- Small to extensive mass
- Bone remodeling that may deviate, not cross nasal septum
- Mass may extend into ethmoid or maxillary sinuses
- T1-weighted MRI: low or intermediate signal
- T2-weighted MRI: intermediate to high signal, usually high
- T1-weighted post-Gd MRI: some contrast enhancement

10.13 Osteoma

Figs. 10.25 and 10.26

10.13.1 Definition

Benign tumor of normal mature bone.

10.13.2 Clinical Features

- Usually an incidental finding

10.13.3 Imaging Features

- Most common in frontal sinuses, followed by the ethmoid and maxillary sinuses
- May occlude sinus ostia causing sinusitis or mucocele formation

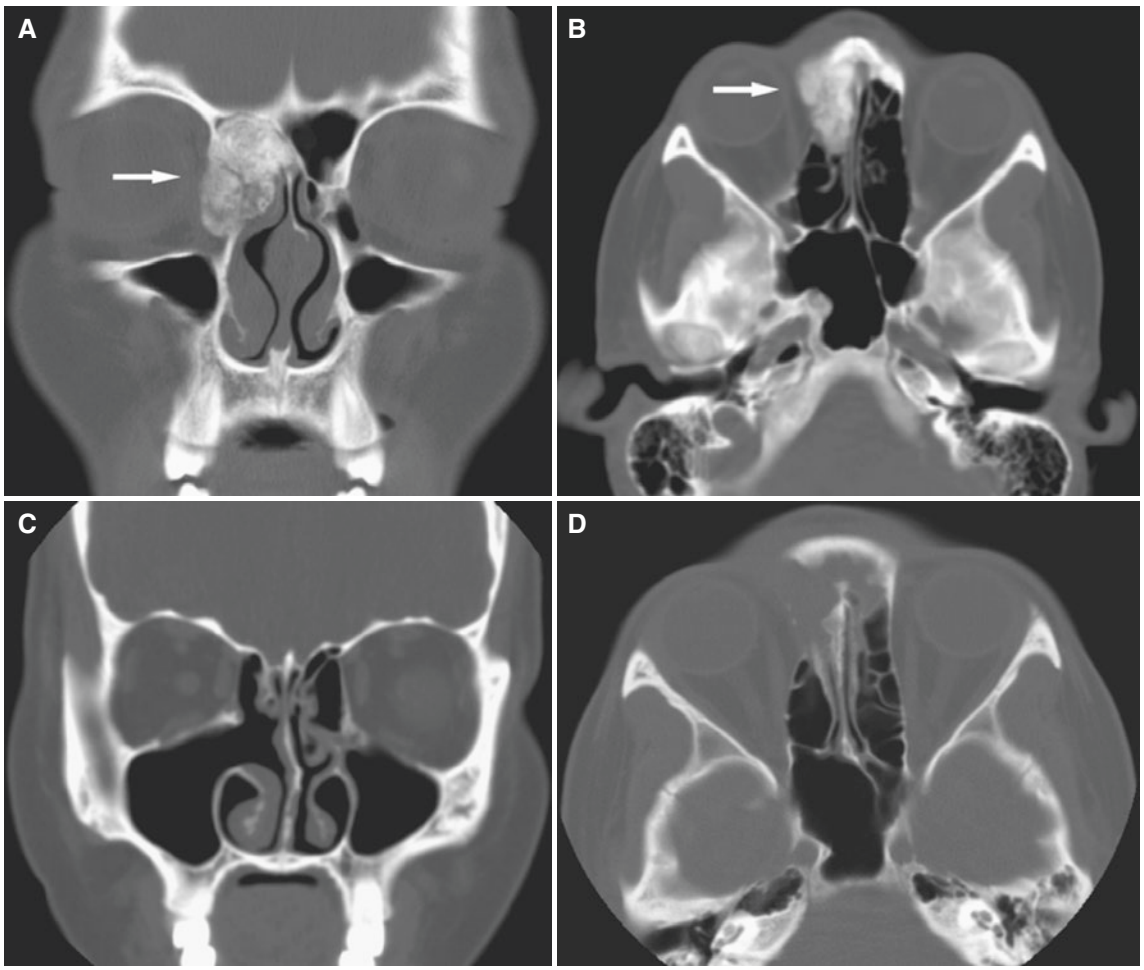

Fig. 10.25 Frontal/ethmoid osteoma; 19-year-old female. (**A**) Coronal CT image shows well-defined bone mass in the right frontal and ethmoid sinuses crossing midline (*arrow*), with left ethmoid and maxillary sinuses normal. (**B**) Axial CT image shows osteoma extending to frontal recess of the maxilla anteriorly (*arrow*), with otherwise normal ethmoid and sphenoid sinuses. (**C**) Coronal CT image, post-surgery, shows resection of the right middle turbinate and part of the ethmoid sinus but otherwise normal bone structures and sinus air. (**D**) Axial CT image, post-surgery, shows partial resection of the ethmoid sinus, but otherwise normal bone structures and sinus air

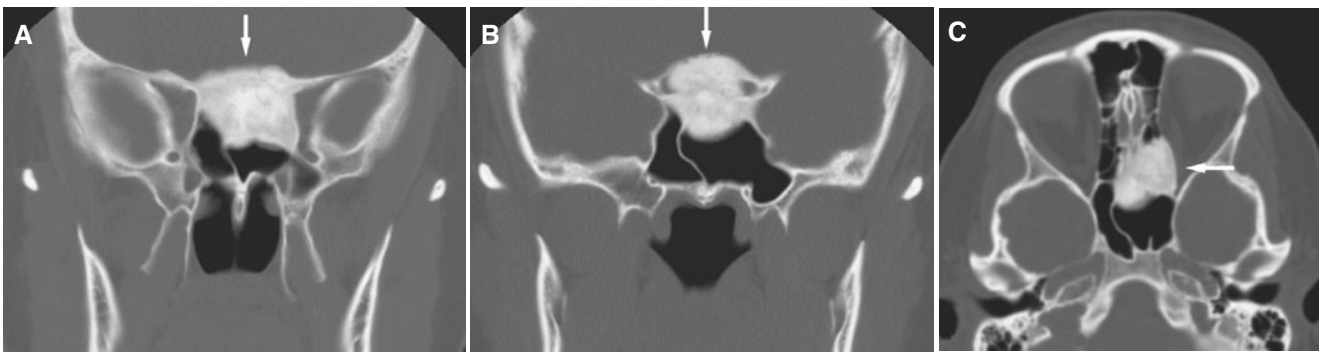

Fig. 10.26 Sphenoid/ethmoid osteoma surgically confirmed, 24-year-old female with headache. (**A**) Coronal CT image shows well-defined dense mass in the sphenoid bone extending into sinus (*arrow*). (**B**) Coronal CT image shows mass involving the sella turcica (*arrow*). (**C**) Axial CT image shows mass extending into the ethmoid and sphenoid sinuses (*arrow*)

10.14 Fibrous Dysplasia

Figs. 10.27 and 10.28

10.14.1 Definition

Benign bone disease; metaplastic fibrous tissue.

10.14.2 Clinical Features

– Painless swelling, deformity

10.14.3 Imaging Features

– Radiolucent and/or radiopaque areas, depending on amount of fibrous tissue
– Ground-glass appearance typical

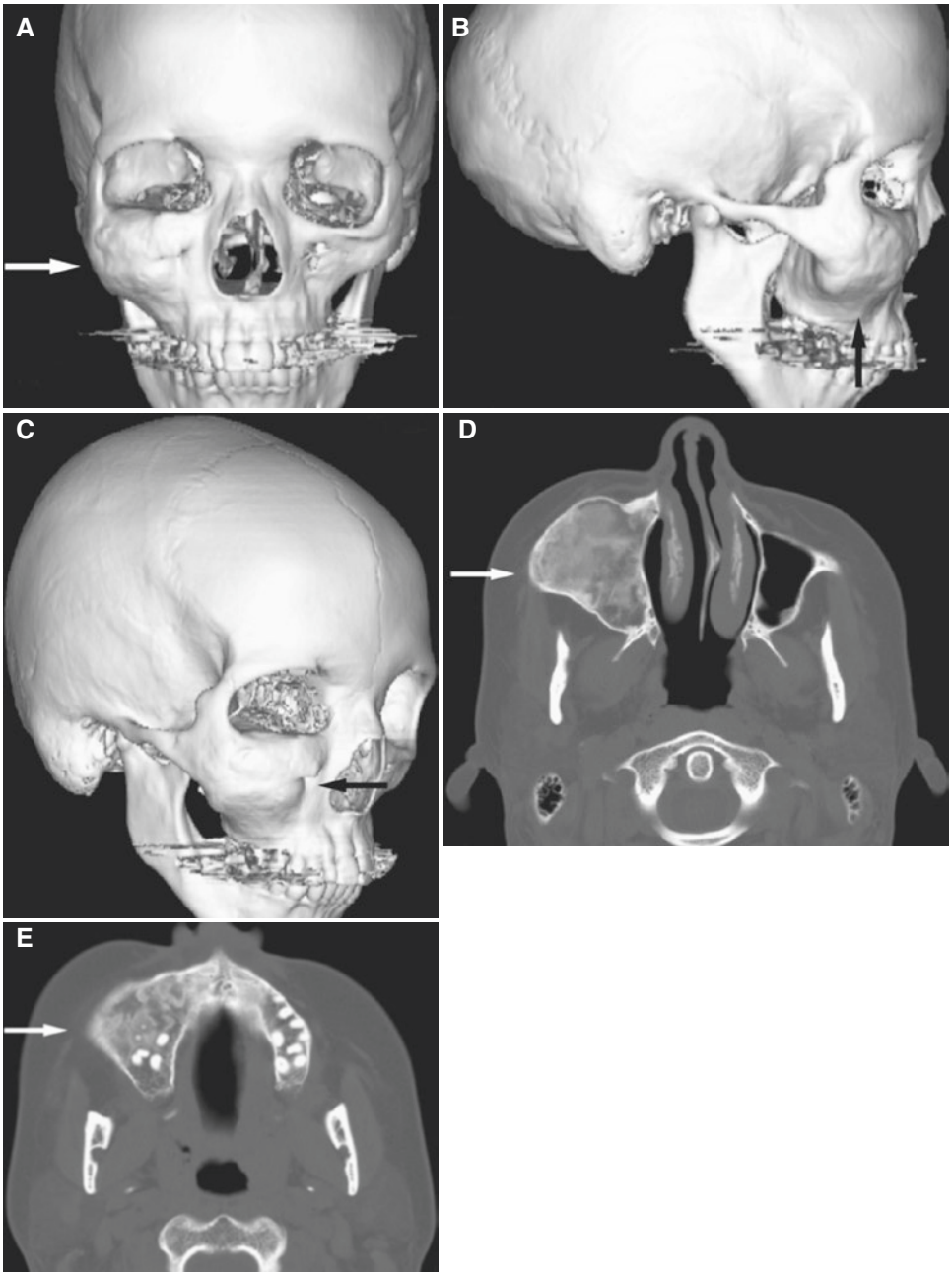

Fig. 10.27 Fibrous dysplasia; 23-year-old female with painless swelling of cheek. (**A**) 3D CT image, en face, shows the expanded right maxilla and zygoma (*arrow*) with elevated orbital floor. (**B**) 3D CT image, lateral, shows the expanded frontal process and anterior wall of the maxilla (*arrow*). (**C**) 3D CT image, oblique view, shows the elevated orbital floor and expansion around the infraorbital foramen (*arrow*). (**D**) Axial CT image shows ground-glass appearance (*arrow*). (**E**) Axial CT image of the alveolar process shows no evident displacement or resorption of teeth (*arrow*)

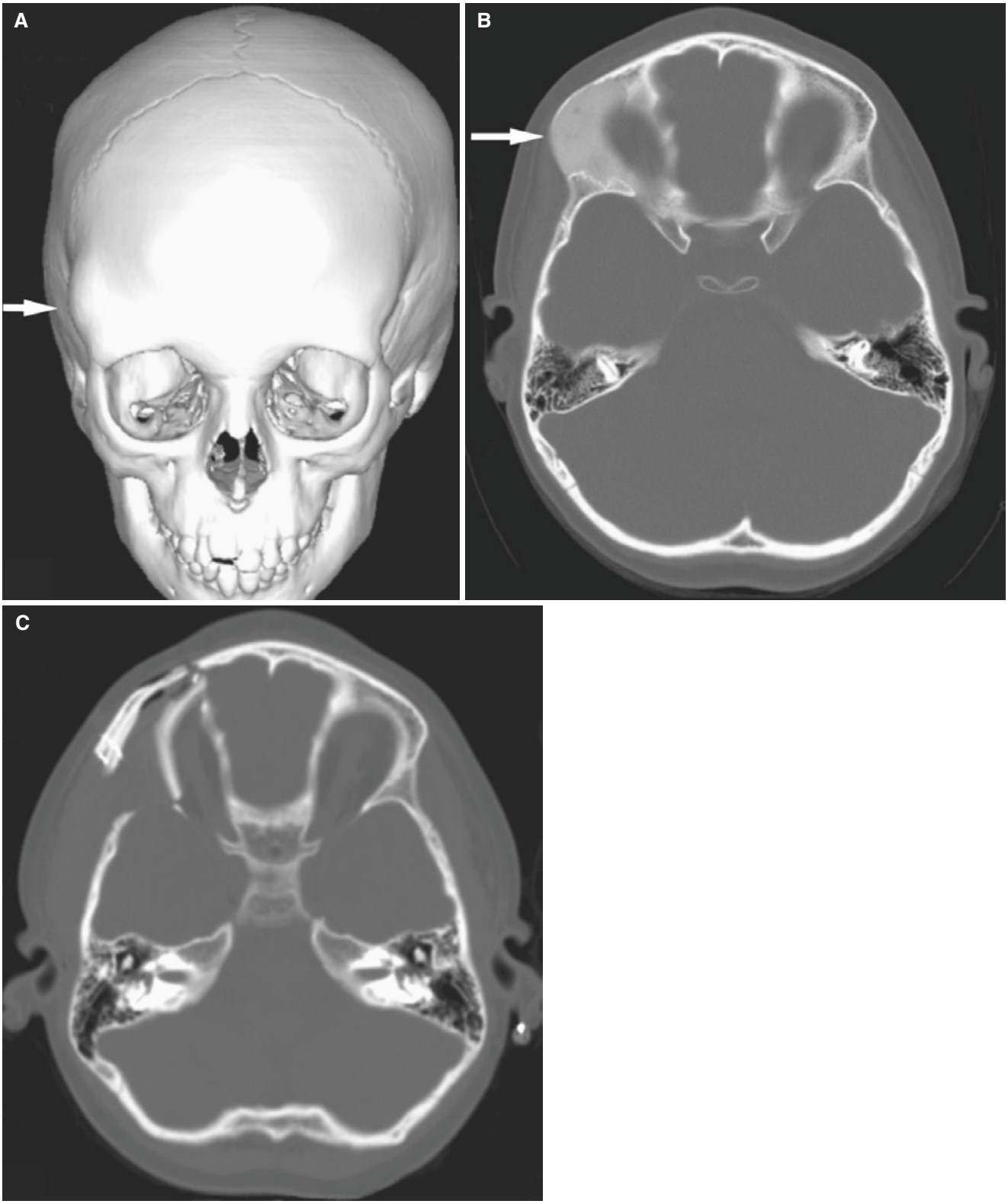

Fig. 10.28 Frontal fibrous dysplasia; 6-year-old female with painless swelling of the right frontal bone. (**A**) 3D CT image, en face, shows well-defined and smooth swelling (*arrow*). (**B**) Axial CT image shows ground-glass appearance (*arrow*). (**C**) Axial CT image, postoperative, shows normal morphology in the area

10.15 Nasolabial (Nasoalveolar) Cyst

Fig. 10.29

10.15.1 Definition

Developmental cyst from epithelial rests either in the fusion of globular, lateral nasal, and maxillary processes or in the embryonic nasolacrimal duct.

10.15.2 Clinical Features

- Usually unilateral, but may be bilateral
- Wide range of age
- More frequent in females
- Pain-free swelling or may give discomfort or pain, in particular if infected

10.15.3 Imaging Features

- Soft-tissue lesion
- Located above apices of maxillary incisors
- May not be shown on plain radiographs
- May cause erosion of underlying bone
- Homogeneous internal structure
- No contrast enhancement except in the periphery

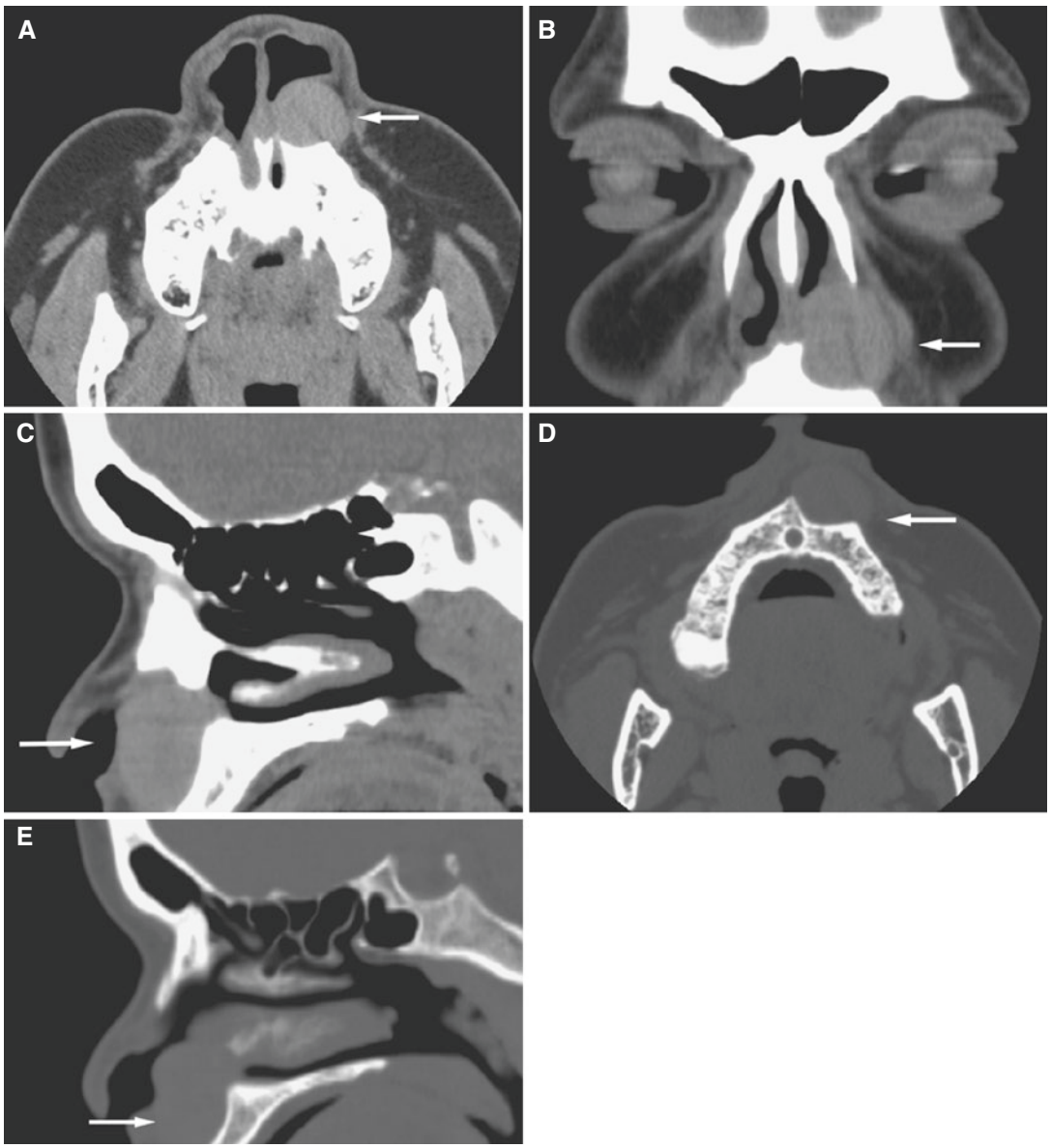

Fig. 10.29 Nasolabial cyst; 45-year-old female with left nostril and nasal cavity mass. (**A**) Axial CT image, soft-tissue window, shows well-defined soft-tissue mass (*arrow*). (**B**) Coronal CT image, soft-tissue window, confirms well-defined soft-tissue mass (*arrow*). (**C**) Sagittal CT image, soft-tissue window, confirms well-defined soft-tissue mass (*arrow*). (**D**) Axial CT image, bone window, shows well-delineated corticated bone erosion of maxilla (*arrow*). (**E**) Sagittal CT image, bone window, confirms well-delineated corticated bone erosion of the maxilla (*arrow*)

10.16 Malignant Tumors

A number of malignant conditions may occur in the paranasal sinuses.

10.17 Adenocarcinoma

Fig. 10.30

10.18 Squamous Cell Carcinoma

Fig. 10.31

10.18.1 Definition

Malignant epithelial tumor.

10.18.2 Clinical Features

- 50–80% of all malignant sinus masses
- More than 60% originate in the maxillary sinuses, followed by nasal cavity, and ethmoid sinuses
- Oral symptoms and signs may be initial; occasionally considered an intraoral cancer clinically

10.18.3 Imaging Features

- Usually advanced when detected; bone destruction in 80%
- Alveolar bone destruction reported in half of patients with maxillary sinus carcinoma

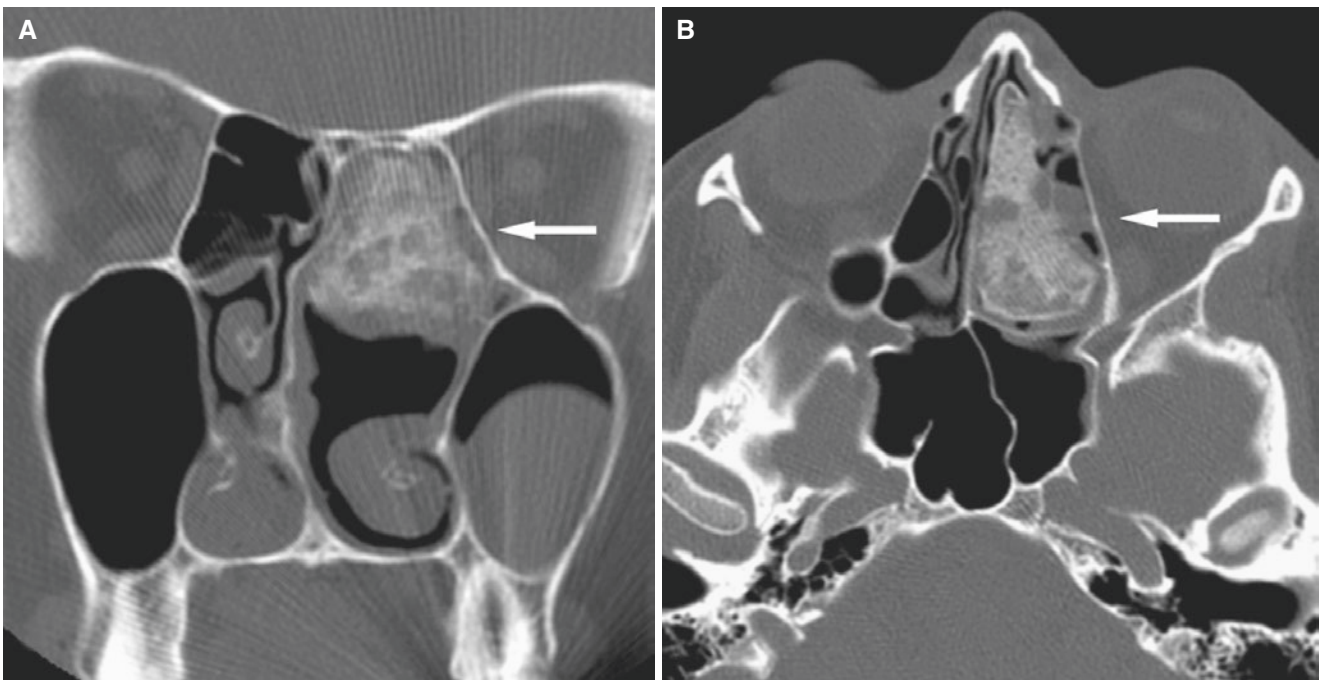

Fig. 10.30 Ethmoid adenocarcinoma (low grade); 18-year-old female, complaining of headache, following biopsy of ethmoid sinus mass. (**A**) Coronal CT image shows rather well-defined, dense mass in the left ethmoid sinus (*arrow*) with some displacement of the nasal septum to the right and expanding into the nasal cavity. Left middle turbinate not seen (removed during biopsy and/or incorporated in tumor). Incidental finding of a retention cyst in the left maxillary sinus. (**B**) Axial CT image shows tumor occupying the entire ethmoid sinus with some expansion of the medial orbit wall and nasal septum, without penetration (*arrow*)

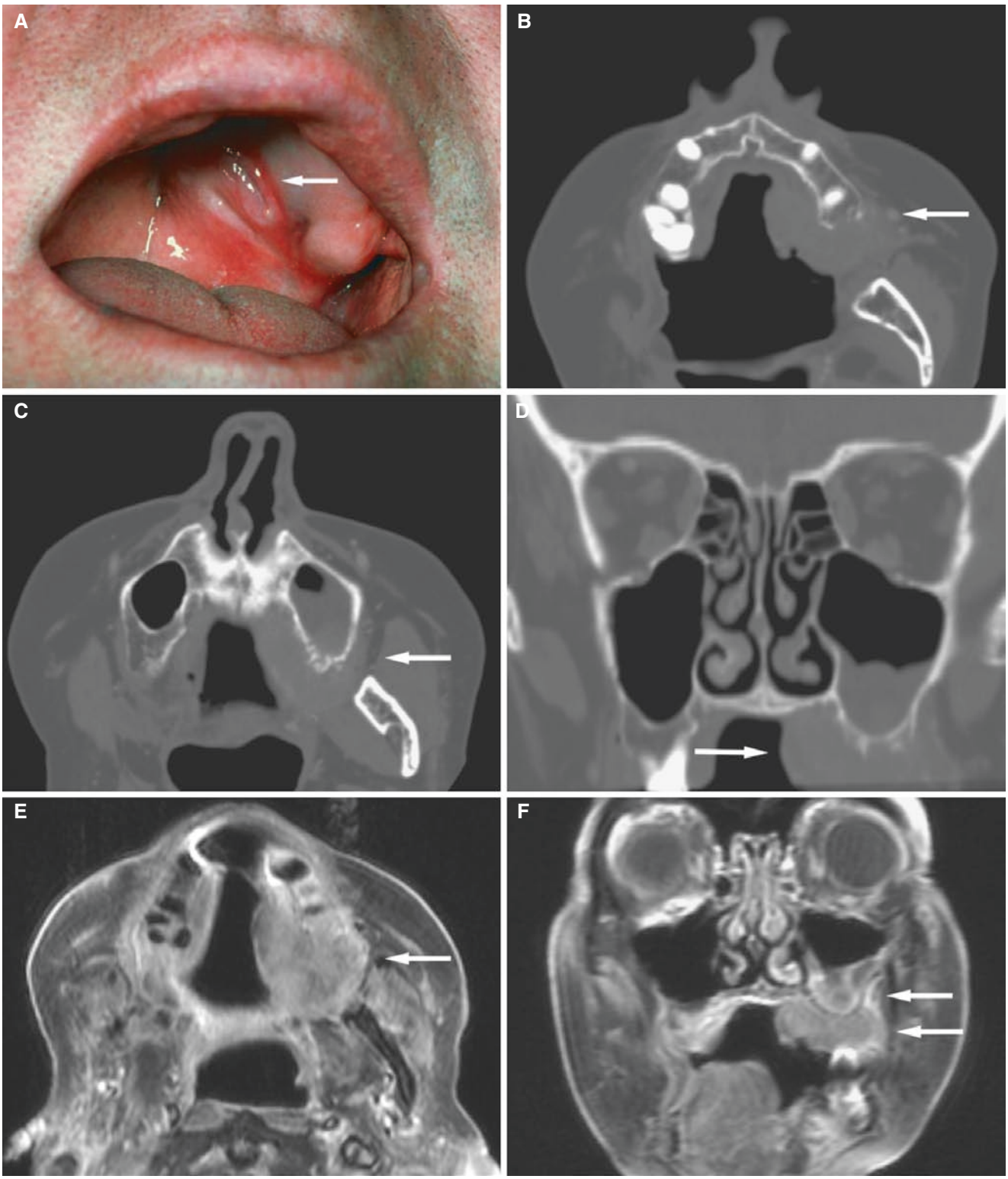

Fig. 10.31 Squamous cell carcinoma of the left maxillary sinus; 80-year-old female with a 13-year history of successfully treated tongue cancer, now with mass in oral cavity. (**A**) Clinical photograph of another patient with the same diagnosis shows similar clinical picture; palatal swelling (*arrow*) posterior to complete denture (removed) as initial tumor sign. (**B**) Axial CT image shows destruction of the left maxilla and soft-tissue swelling (*arrow*). (**C**) Axial CT image shows intrasinus mass and irregular destruction of the maxillary sinus wall (*arrow*). (**D**) Coronal CT image confirms intraoral and intrasinus mass with irregular destruction of the maxillary sinus wall, alveolar ridge (*arrow*). (**E**) Axial T1-weighted post-Gd MRI shows contrast enhancement of mass (*arrow*). (**F**) Coronal T1-weighted post-Gd MRI confirms contrast enhancement of intrasinus and intraoral mass (*arrows*)

10.19 Lymphoma

Fig. 10.32

Lymphoma is one of the most common malignancies in human immunodeficiency virus (HIV) patients and occurs much more commonly than in the general population. It may be highly aggressive, but paranasal sinus involvement is rare in HIV patients.

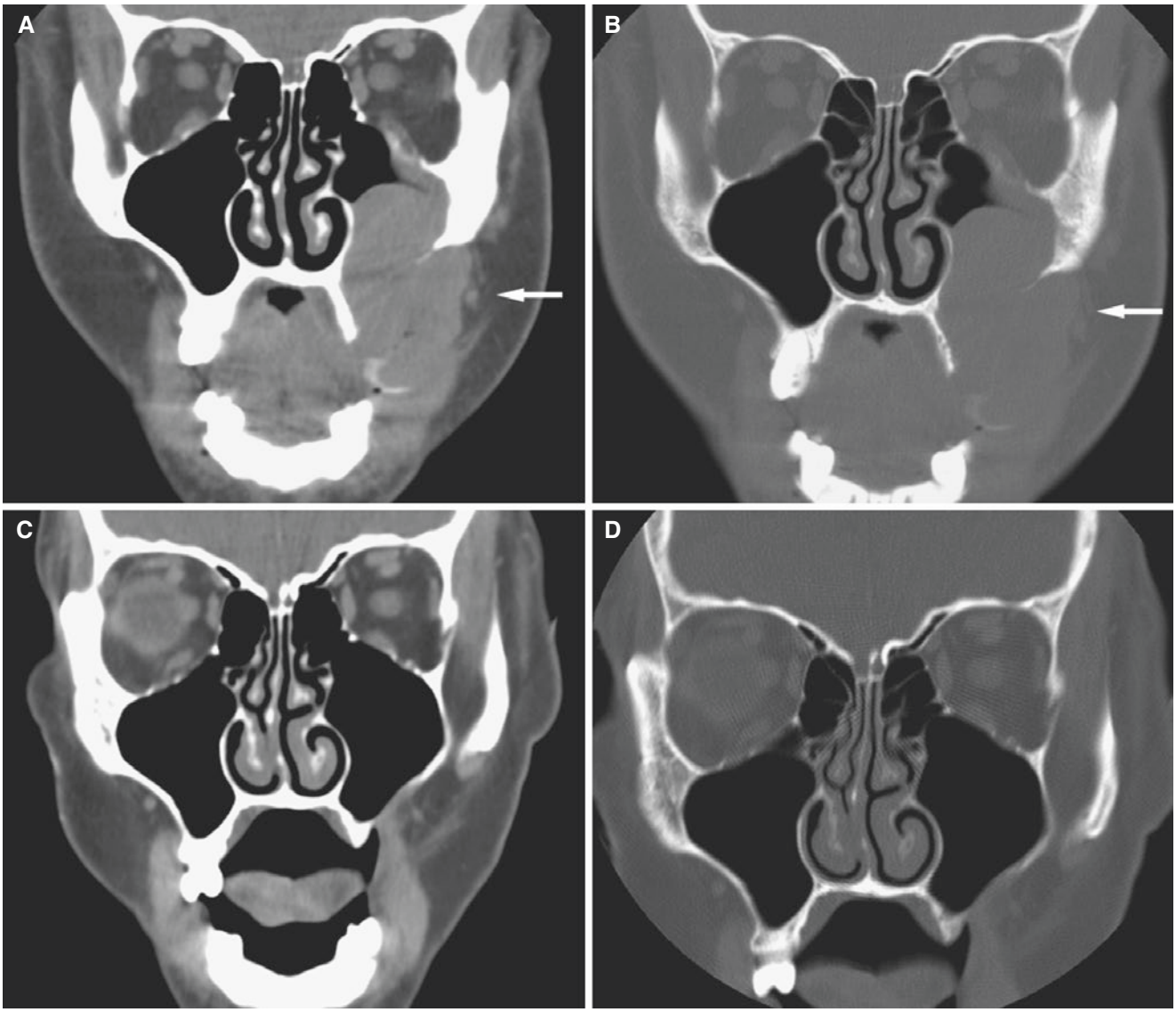

Fig. 10.32 Maxillary plasmablastic lymphoma; 39-year-old male, HIV-positive status, presented with left facial pain and swelling. (**A**) Coronal CT image, soft-tissue window, shows soft-tissue mass in infratemporal fossa that invades the left maxillary sinus with bone destruction (*arrow*). (**B**) Coronal CT image (bone window) shows severe destruction of the maxillary sinus wall, alveolar ridge (*arrow*). (**C**) Coronal CT image, soft-tissue window, posttreatment shows normal structures. (**D**) Coronal CT, posttreatment, shows almost normal maxillary sinus wall

10.20 Ewing Sarcoma

Fig. 10.33

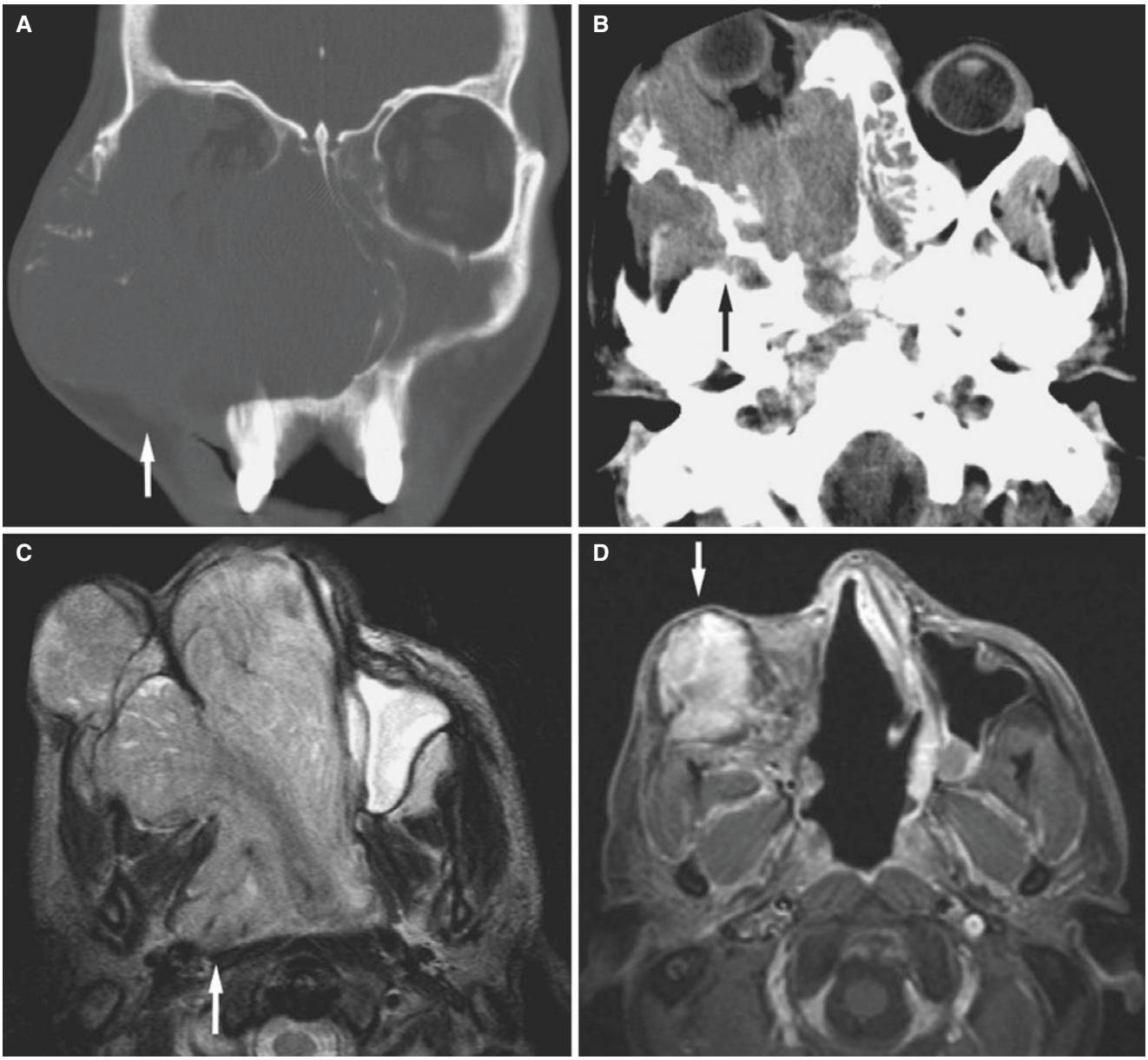

Fig. 10.33 Maxillary Ewing sarcoma; 30-year-old male with huge facial mass, proptosis, shortness of breath, and dysphasia. (**A**) Coronal CT image shows enormous tumor (*arrow*) with destruction of the maxilla, zygoma, orbital floor, and nasal cavity, crossing the midline with expanding medial wall of the left maxillary sinus. (**B**) Axial CT image shows the huge destruction and displacement of the right globe (*arrow*). (**C**) Axial T2-weighted fat-suppressed MRI shows the huge exophytic tumor (*arrow*) sparing only the left maxillary sinus. (**D**) Axial T1-weighted post-Gd MRI after first surgery, showing contrast enhancement of tumor recurrence (*arrow*). (**E**) Coronal CT image, after second surgery with facial flap (*arrowhead*). (**F**) Axial CT image shows facial flap (*arrowhead*). (**G**) Axial T1-weighted MRI shows facial flap (*arrowhead*). (**H**) Axial T1-weighted fat-suppressed post-Gd MRI shows facial flap (*arrowhead*)

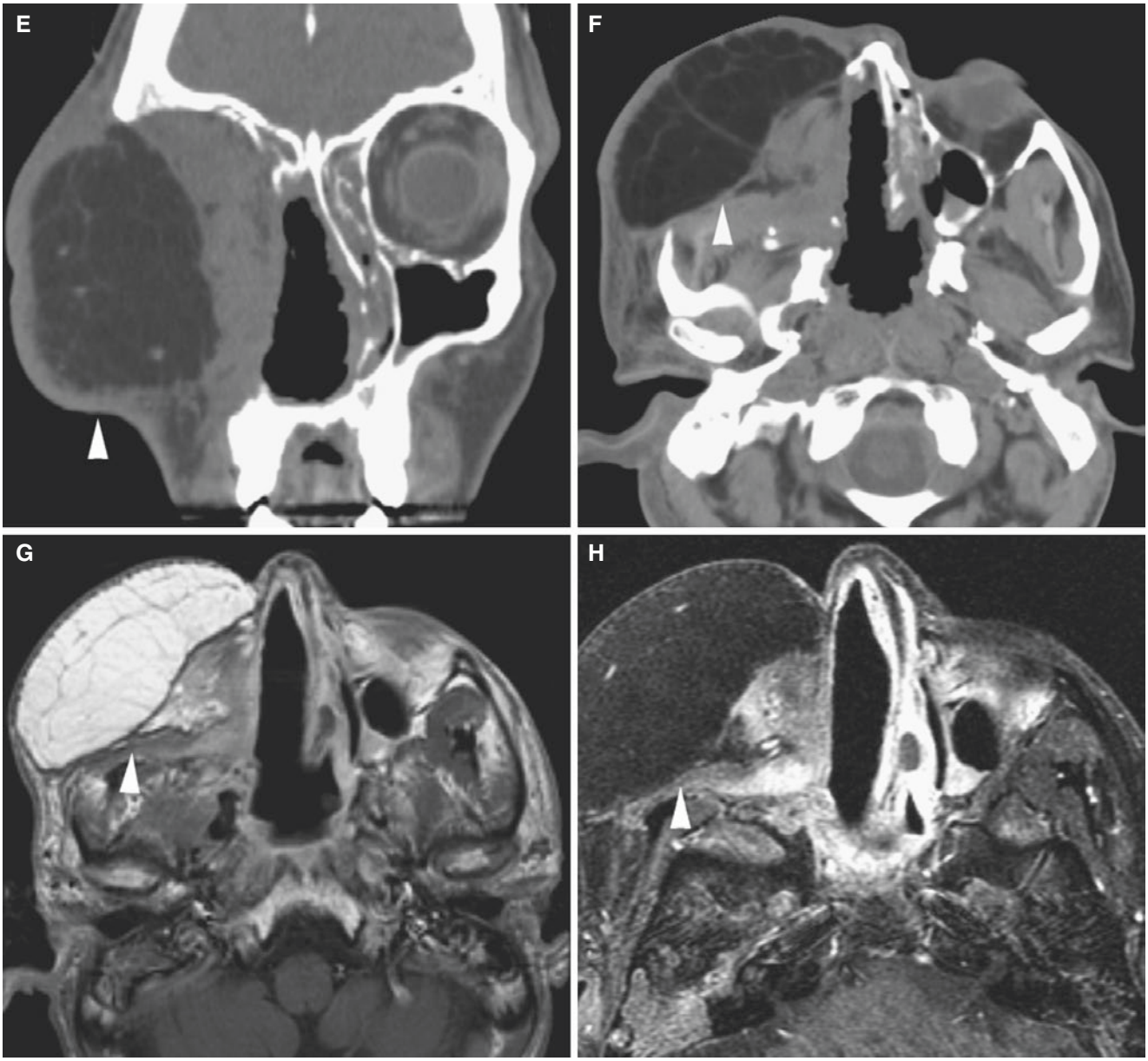

Fig. 10.33 (continued)

10.21 Osteosarcoma

Fig. 10.34

Fig. 10.34 Maxillary osteosarcoma; 27-year-old male with swelling of the right maxilla and loose teeth. (**A**) Axial CT image shows large soft-tissue mass in the entire maxillary sinus with destruction of most of the sinus wall and scattered bone production (*arrow*). (**B**) Coronal CT image confirms extensive tumor mass to about midline (*arrow*), also extending into ethmoid cells, and with bone production. (**C**) Axial T2-weighted fat-suppressed MRI shows heterogeneous low to high signal intensity (*arrow*). (**D**) Coronal T2-weighted fat-suppressed MRI shows heterogeneous low to high signal intensity (*arrow*). (**E**) Surgical material

10.22 Expansile Odontogenic Conditions

Figs. 10.35, 10.36, and 10.37

See Chaps. 2 and 3

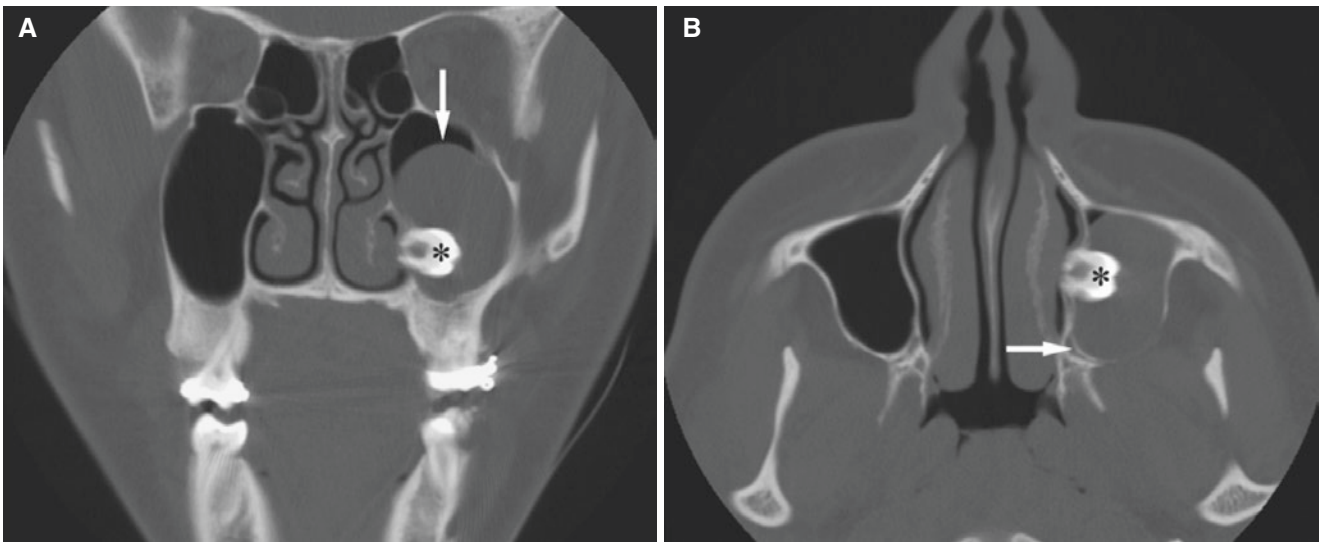

Fig. 10.35 Maxillary follicular (dentigerous) cyst; 16-year-old female with impacted tooth. (**A**) Coronal CT image shows impacted tooth (*asterisk*) with corticated follicular cyst around the tooth crown (*arrow*). (**B**) Axial CT image shows evident corticated outline (*arrow*)

Fig. 10.36 Keratocystic odontogenic tumor; 28-year-old female with some pressure in the nose. Coronal CT image shows expansive mass with thin, corticated outline (*arrow*), occupying the entire maxillary sinus, almost the entire nasal cavity, much of the ethmoid sinuses, and displacing the orbital floor and hard palate. Root resorption (courtesy of Dr. A. Kolbenstvedt, Oslo University Hospital, Rikshospitalet, Oslo, Norway)

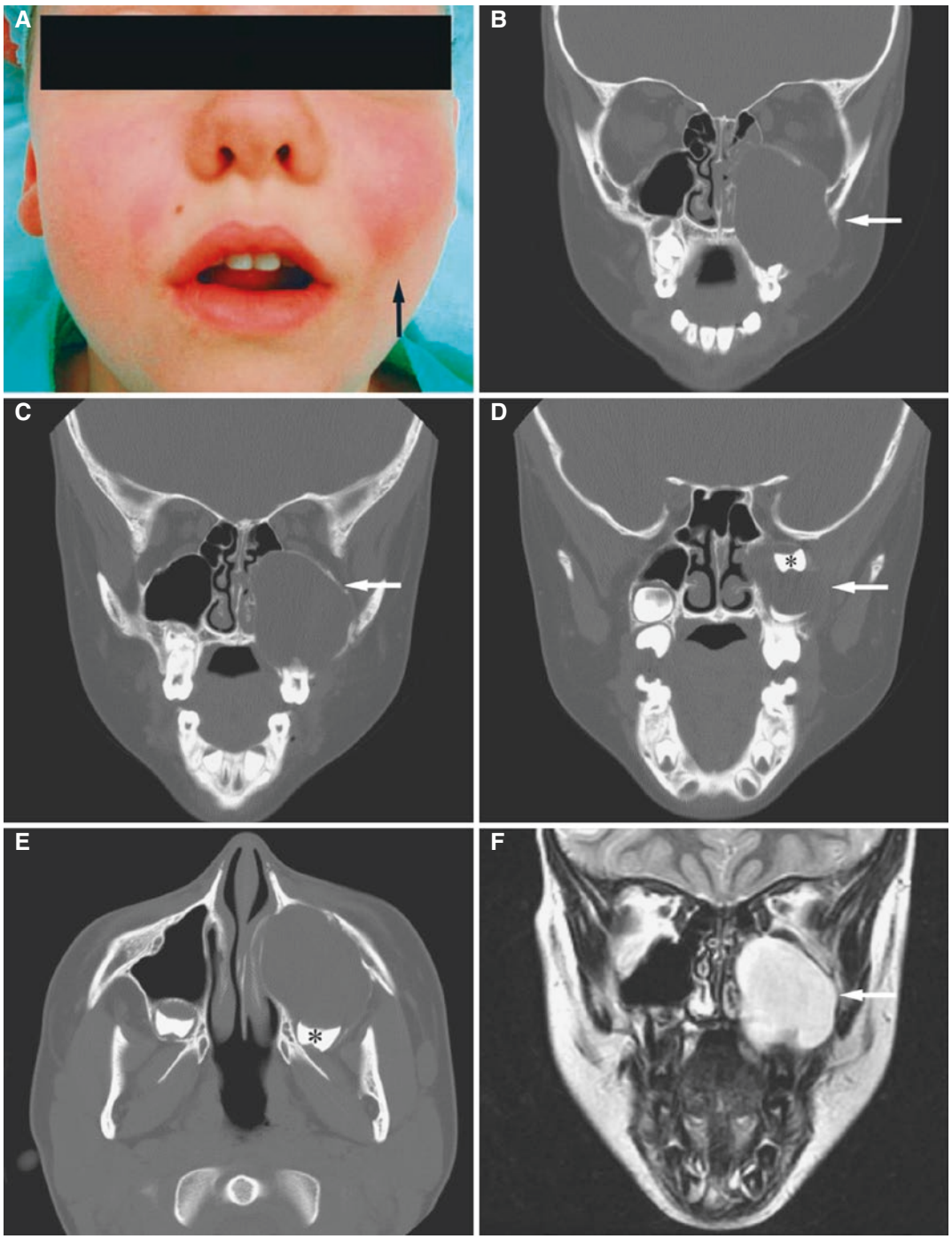

Fig. 10.37 Maxillary follicular (dentigerous) cyst; 7-year-old male with painless facial swelling. (**A**) Clinical photograph before surgery shows facial swelling (*arrow*). (**B**) Coronal CT image shows cyst (*arrow*) filling the entire left maxillary sinus and most of the left nasal cavity and extending into the ethmoid cells, hard palate, and facial soft tissues. (**C**) Coronal CT shows corticated outline (*arrow*) and root resorption. (**D**) Coronal CT image shows cyst (*arrow*) with impacted tooth (*asterisk*) displaced to cranial part of the maxillary sinus. (**E**) Axial CT image shows impacted tooth (*asterisk*) with follicular cyst appearance. (**F**) Coronal T2-weighted MRI shows homogeneous high-signal content (*arrow*). (**G**) Coronal T2-weighted fat-suppressed MRI shows homogeneous high-signal content (*arrow*). (**H**) Axial T2-weighted fat-suppressed MRI shows homogeneous high-signal content (*arrow*). (**I**) Axial T1-weighted MRI without fat suppression shows intermediate-signal content (*arrow*). (**J**) Axial T1-weighted post-Gd fat-suppressed MRI shows no enhancement of cyst (*arrow*). (**K**) Surgically removed cyst containing impacted tooth

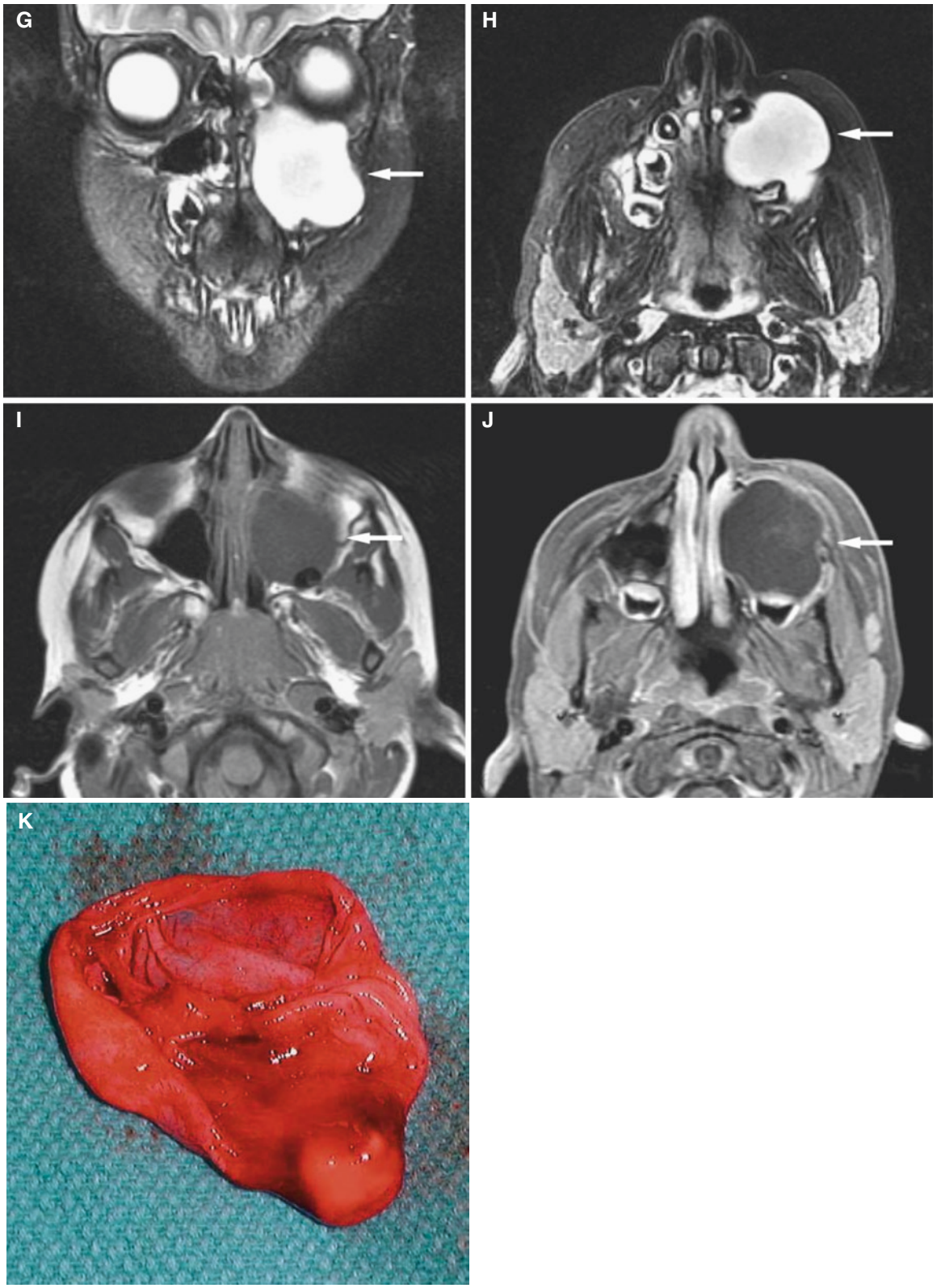

Fig. 10.37 (continued)

10.23 Miscellaneous Conditions

Figs. 10.38, 10.39, 10.40, and 10.41

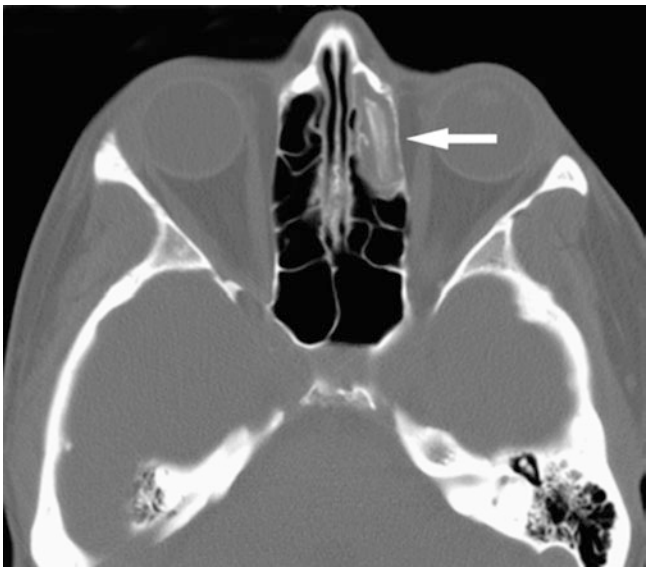

Fig. 10.38 Foreign body in ethmoid sinus; 37-year-old female with left ethmoid sinus mass. Axial CT image shows piece of calcified mass in ethmoid sinus (*arrow*); all other sinuses clear. This was surgically removed and turned out to be a piece of wood with local mucosal swelling and some calcification

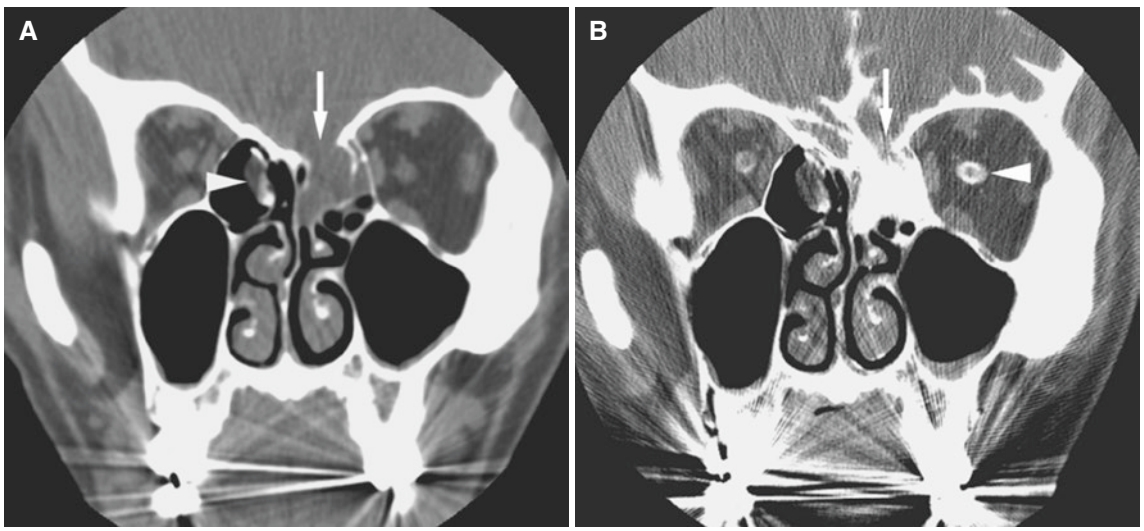

Fig. 10.39 Leakage of CSF; 28-year-old male with history of gunshot wound to vertex a few years ago with multiple fractures including the left maxilla, orbital floor, lamina papyracea, and left cribriform plate, the latter surgically repaired on the right aspect. Clinical course complicated by bacterial meningitis, now referred for CT cisternography to locate continued rhinorrhea. (**A**) Coronal CT image shows defect of the left cribriform plate and lamina papyracea with opacification of the left ethmoid sinus (*arrow*). Surgical plate of the right aspect of the cribriform plate (*arrowhead*). (**B**) Coronal CT image after lumbar puncture with contrast injection shows CSF leakage through bony defect in the left cribriform plate and into the ethmoid sinus (*arrow*). There is also contrast around the optical nerve (*arrowhead*) which is normal in cisternography. Small air-fluid level in the left maxillary sinus that may represent CSF

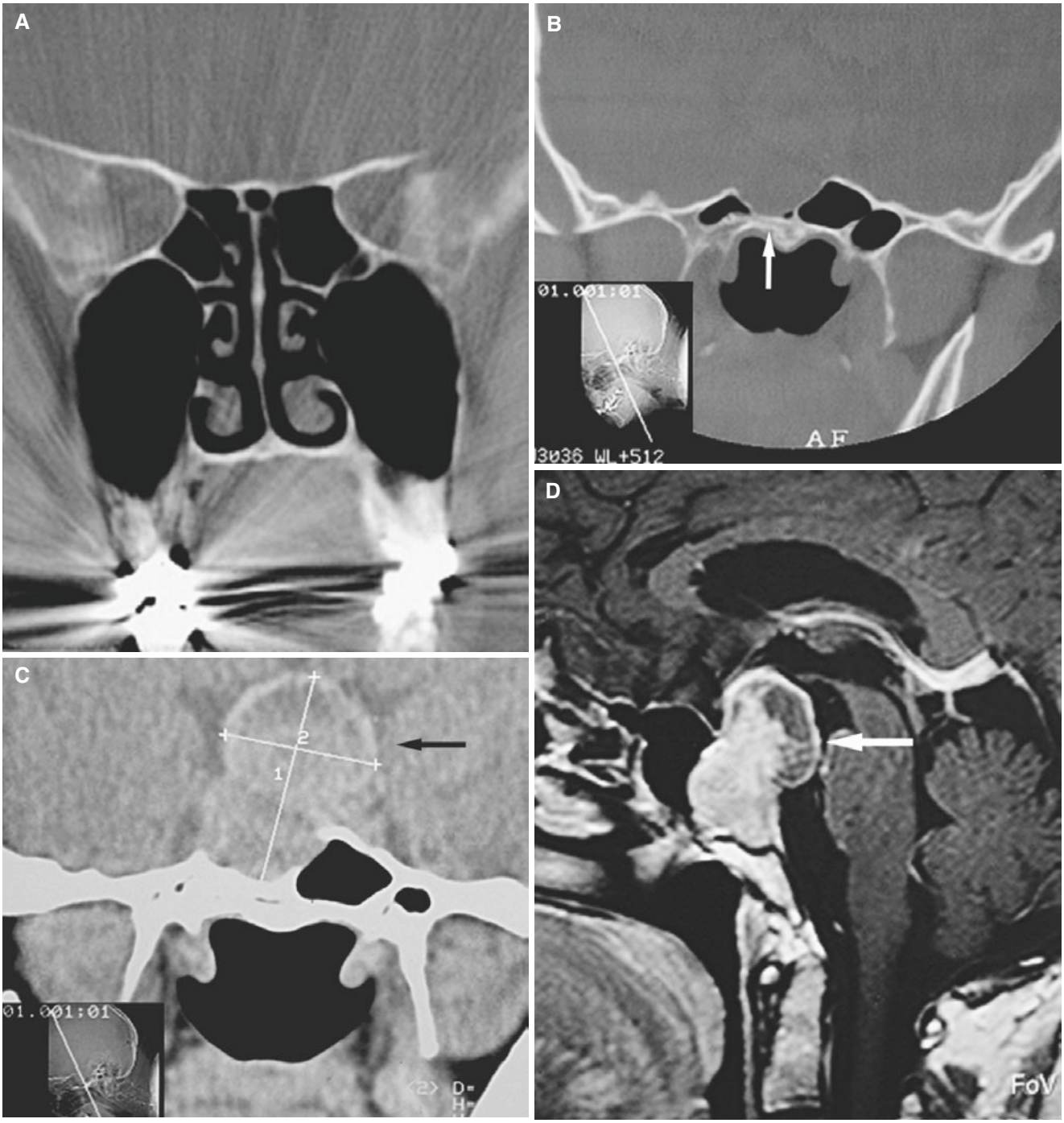

Fig. 10.40 Pituitary adenoma (prolactinoma); 50-year-old female with headache and diffuse facial pain, intracranial tumor detected on routine paranasal sinus scan. (**A**) Coronal CT of paranasal sinuses, almost all scans normal. (**B**) Coronal CT, most posterior section shows abnormal sphenoid sinus (*arrow*). (**C**) Coronal CT shows tumor in the sella turcica (*arrow*); the patient was then referred for neuroradiologic MRI. (**D**) Sagittal T1-weighted post-Gd MRI shows tumor in the sella turcica (*arrow*), extending into the sphenoid sinus

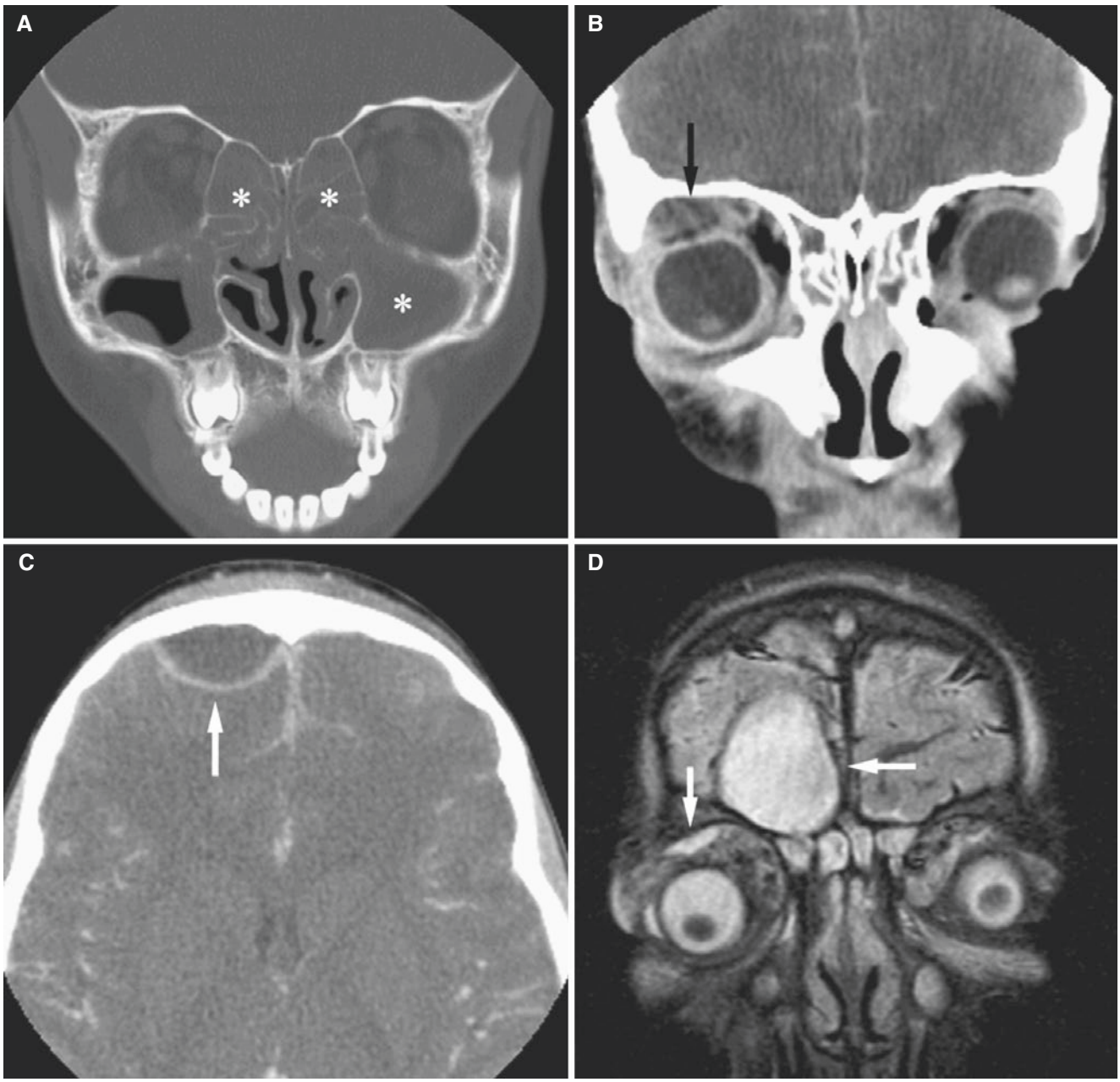

Fig. 10.41 Intracranial empyema from sinusitis; 9-year-old female presenting to emergency department with headache, fever, right eye edema, and ecchymosis. (**A**) Coronal CT image shows complete opacification of both ethmoid and left maxillary sinuses (*asterisk*) and mucosal thickening of the right maxillary sinus; also sphenoid and frontal sinuses showed opacification (not shown). (**B**) Coronal post-contrast CT image, soft-tissue window, shows hypodense central area with enhancing periphery consistent with abscess in the superior right orbit with displaced globe (*arrow*). (**C**) Axial post-contrast CT image, soft-tissue window, shows abscess in the right frontal region (*arrow*). (**D**) Coronal FLAIR MRI shows high signal in orbit superiorly and anterior to right frontal lobe consistent with abscesses (*arrows*). There is also high-signal sinusitis in the ethmoid cells. (**E**) Coronal T1-weighted post-Gd fat-suppressed MRI shows dural and subarachnoid enhancement in the right frontal region (*arrows*). There is granulation tissue and fluid in the ethmoid cells. (**F**) Axial diffusion-weighted MRI shows high signal (=restricted diffusion) in superior aspect of the right orbital cavity consistent with abscess (*arrow*). (**G**) Diffusion-weighted MRI shows high signal in the right frontal lobe area consistent with an intracranial empyema/abscess (*arrow*). (**H**) Diffusion-weighted MRI shows high signal along the falx consistent with the spread of pus in subdural space along the falx (*arrow*)

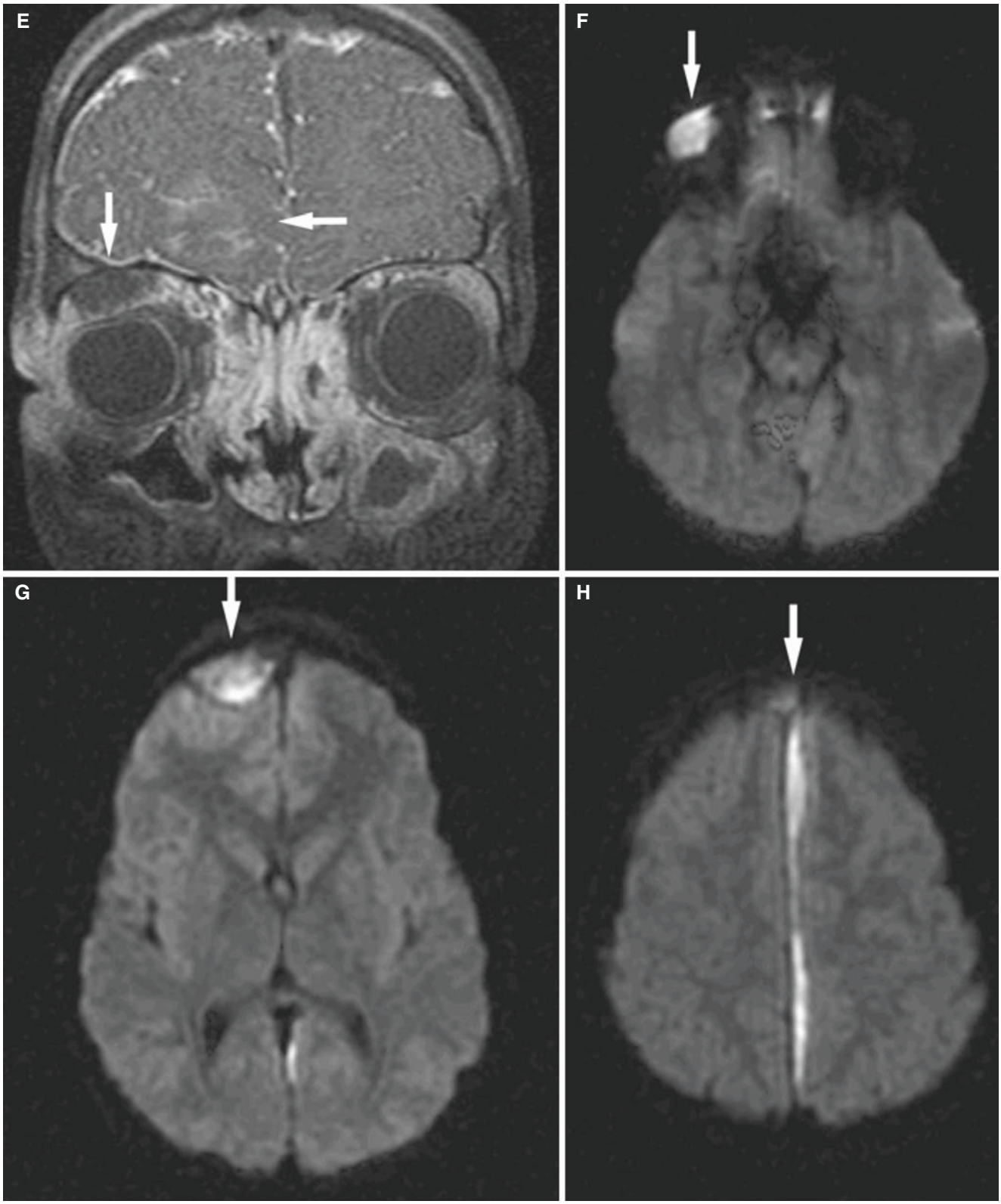

Fig. 10.41 (continued)

Suggested Reading

Barnes L, Verbin R, Gnepp D (1985) Diseases of the nose, paranasal sinuses and nasopharynx. In: Barnes L (ed) Surgical pathology of the head and neck, vol 1. Marcel Dekker, New York, pp 403–451

Bhushan B, Rychlik K, Schroeder JW Jr (2016) Development of the maxillary sinus in infants and children. Int J Pediatr Otorhinolaryngol 91:146–151

De Juan E Jr, Green WR, Lliff NT (1983) Allergic periorbital mycopyocele in children. Am J Ophthalmol 96:299–303

Ericson S (1992) Conventional and computerized imaging of maxillary sinus pathology related to dental problems. In: Westesson P-L (ed) Oral and maxillofacial surgery. Clinics of North America: contemporary maxillofacial imaging. Saunders, Philadelphia, pp 153–181

Farman AG, Nortje C, Wood RE (1993) Diseases of the paranasal sinuses. In: Oral and maxillofacial diagnostic imaging. Mosby, St. Louis, pp 379–402

Finn DG, Hudson WR, Baylin G (1981) Unilateral polyposis and mucoceles in children. Laryngoscope 91:1444–1449

Forno AD, Borgo CD, Turriziani A, Ottaviani F, Antinori A, Fantoni M (1998) Non-Hodgkin's lymphoma of the maxillary sinus in a patient with acquired immunodeficiency syndrome. J Laryngol 112:982–985

Harnsberger HR, Wiggins RH, Hudgins PA, Michel MA, Swartz J, Davidson HC et al (2004) Section 2: nose and sinus. In: Diagnostic imaging head and neck. Amirsys, Salt Lake City

Koontz NA, Seltman TA, Kralik SF, Mosier KM, Harnsberger HR (2016) Classic signs in head and neck imaging. Clin Radiol 71:1211–1222

Kula K, Hale LN, Ghoneima A, Tholpady S, Starbuck JM (2016) Cone-beam computed tomography analysis of mucosal thickening in unilateral cleft lip and palate maxillary sinuses. Cleft Palate Craniofac J 53:640–648

Larheim TA, Kolbenstvedt A, Lien HH (1984) Carcinoma of maxillary sinus, palate and maxillary gingiva: occurrence of jaw destruction. Scand J Dent Res 92:235–240

Moser FG, Panush D, Rubin JS, Honigsberg RM, Spryregen S, Eisig SB (1991) Incidental paranasal sinus abnormalities on MRI of the brain. Clin Radiol 43:252–254

Rak KM, Newell JD 2nd, Yakes WF, Damiano MA, Luethke JM (1991) Paranasal sinus on MR images of the brain: significance of mucosal thickening. AJR Am J Roentgenol 156:381–384

Rao VM, Sharma D, Madan A (2001) Imaging of frontal sinus disease: concepts, interpretation, and technology. Otolaryngol Clin N Am 34:23–39

Rosenfeld RM (2016) Clinical practice. Acute sinusitis in adults. N Engl J Med 375:962–970

Som PM, Brandwein MS (2003) Sinonasal cavities: inflammatory diseases. In: Som PM, Curtin HD (eds) Head and neck imaging, 4th edn. Mosby, St. Louis, pp 193–259

Som PM, Shugar J (1980) The CT classification of ethmoid mucoceles. J Comput Assist Tomogr 4:199–203

Suri A, Mahapatra AK, Gaikwad S, Sarkar C (2004) Giant mucoceles of the frontal sinus: a series and review. J Clin Neurosci 11:214–218

Zizmor J, Noyek AM (1973) Cyst, benign tumors and malignant tumors of the paranasal sinuses. Otolaryngol Clin N Am 6:487–508

Maxillofacial Soft Tissues

11

Abstract

This chapter illustrates infection (abscess), muscular hypertrophy, atrophy and dehiscence, calcifications, vascular malformations, cysts, lingual thyroid, benign oropharyngeal tumors; lipoma and schwannoma, and malignant oropharyngeal tumors; squamous cell carcinoma, lymph node metastasis, clear cell carcinoma, adenoid cystic carcinoma, and non-Hodgin's lymphoma.

11.1 Introduction

This chapter is a collection of cases of soft-tissue abnormalities in the masticator space, the oral cavity, and the submental, sublingual, submandibular, and oropharyngeal spaces.

Traditionally, maxillofacial imaging has focused mainly on the osseous structures of the facial skeleton. This is due to the great importance of bony abnormalities for those working in dentistry. It is also a reflection of the fact that traditional maxillofacial imaging relied on plain film and dental imaging techniques that only depict the skeletal structures. With contemporary imaging techniques such as CT, MRI, and ultrasonography, the soft tissue can also be visualized in great detail. From a clinical point of view, the differential diagnosis of many conditions in the maxillofacial area includes soft-tissue lesions that would not been seen on traditional skeletal imaging. For instance, in the evaluation of swellings in spaces around the jaws, skeletal imaging is often insufficient.

This chapter has been included to illustrate the value of applying advanced contemporary imaging of the maxillofacial soft-tissue structures. We present a variety of conditions, congenital or acquired, in which CT and/or MRI was necessary or improved the diagnostic assessment.

11.2 Infection (Abscess)

Fig. 11.1

11.2.1 Definition

Localized collection of pus.

11.2.2 Clinical Features

- Swelling, pain, redness, warmth, and dysfunction
- Fever and malaise

11.2.3 Imaging Features

- Single or multiloculated low-density area surrounded by rim enhancement
- T2-weighted and STIR MRI: high-signal area surrounded by low-signal rim
- T1-weighted post-Gd MRI: no contrast enhancement except in peripheral rim
- Cellulitis or phlegmon will spread diffusely and enhance accordingly

In collaboration with A. Kolbenstvedt and H.-J. Smith.

T.A. Larheim, P.-L.A. Westesson, *Maxillofacial Imaging*, https://doi.org/10.1007/978-3-319-53319-3_11

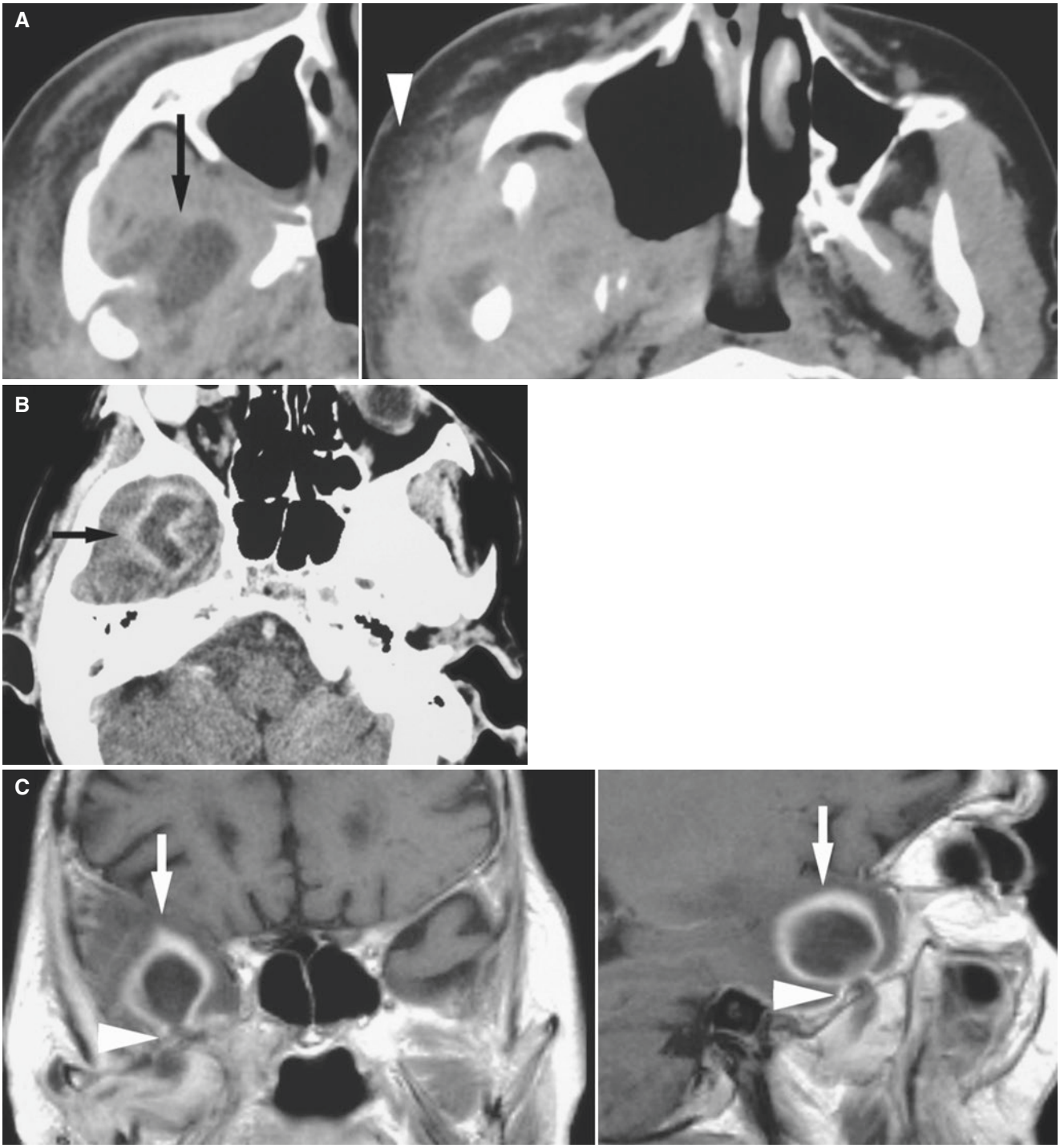

Fig. 11.1 Abscess in masticator space with intracranial spread; 85-year-old male with history of right-sided maxillary sinus squamous cell carcinoma, now with right-sided facial swelling, fever, and chewing problems. (**A**) Axial post-contrast CT image shows (*left*) low-density area with peripheral rim enhancement consistent with abscess in masticator space (*arrow*) and (*right*) cellulitis, soft-tissue swelling, loss of fat planes between muscles, and streaking (reticulation pattern) of cheek fat (*arrowhead*). (**B**) Axial post-contrast CT image shows abscess in middle cranial fossa (*arrow*). (**C**) Coronal T1-weighted post-Gd MRI (*left*) and sagittal view (*right*) demonstrate intracranial abscess (*arrows*) through oval foramen (*arrowheads*)

11.3 Muscular Hypertrophy, Atrophy, and Dehiscence

Figs. 11.2, 11.3, 11.4, 11.5, and 11.6

11.3.1 Definition

Abnormally thick muscle (hypertrophy), abnormally thin muscle (atrophy), usually with fatty infiltration, or muscle defect (dehiscence).

11.3.2 Clinical Features

- Painless swelling (hypertrophy), usually firm
- Benign masseteric hypertrophy; males more often than females, about half of cases bilateral; all muscles of mastication may be involved

11.3.3 Imaging Features

- Muscle hypertrophy, otherwise normal appearance
- Muscle asymmetry, functional abnormalities
- Muscle atrophy, fatty replacement
- Muscle dehiscence allowing herniation

11.4 Calcifications

Figs. 11.7, 11.8, 11.9, 11.10, 11.11, 11.12, and 11.13

11.4.1 Definition

Calcium deposits in soft-tissue structures.

11.4.2 Clinical Features

- Incidental finding on routine examinations such as panoramic radiography and paranasal sinus films
- Pain, limited motion (tendinitis)

11.4.3 Imaging Features

- Calcified tissue, highly variable in size
- May be found in many places such as tonsils, vessels, tendons, salivary glands and ducts, paranasal sinuses and nose; ossification of stylohyoid ligament, myositis ossificans

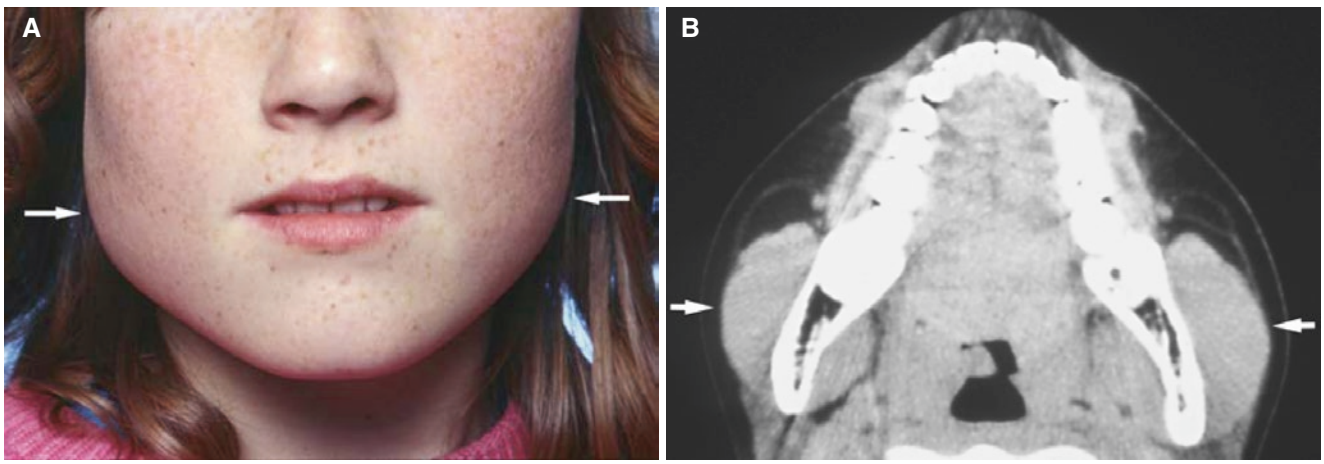

Fig. 11.2 Masseteric hypertrophy; 12-year-old female with bilateral painless swelling of mandibular angles. (**A**) Clinical photograph shows bilateral swelling of mandibular angles (*arrows*). (**B**) Axial CT image shows bilaterally enlarged masseter muscles (*arrows*); bone structures including temporomandibular joints were normal

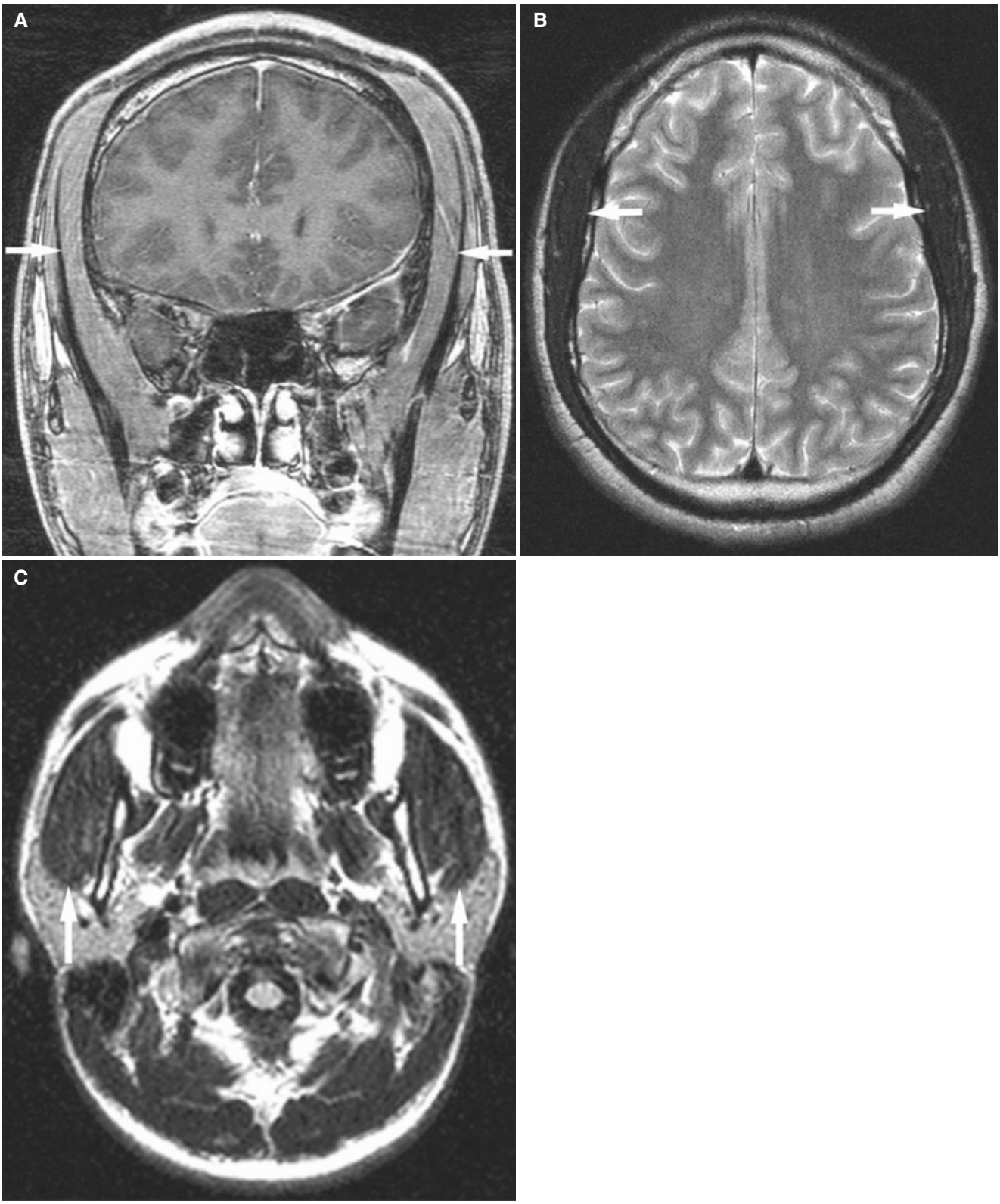

Fig. 11.3 Temporalis hypertrophy and masseteric hypertrophy; 17-year-old male with history of psychosis; no organic causes for his symptoms were found. (**A**) Coronal T1-weighted MRI shows bilaterally thickened temporalis muscles (*arrows*). (**B**) Axial T2-weighted MRI confirms thickened temporalis muscles (*arrows*). (**C**) Axial T2-weighted MRI shows bilaterally thickened masseter muscles (*arrows*)

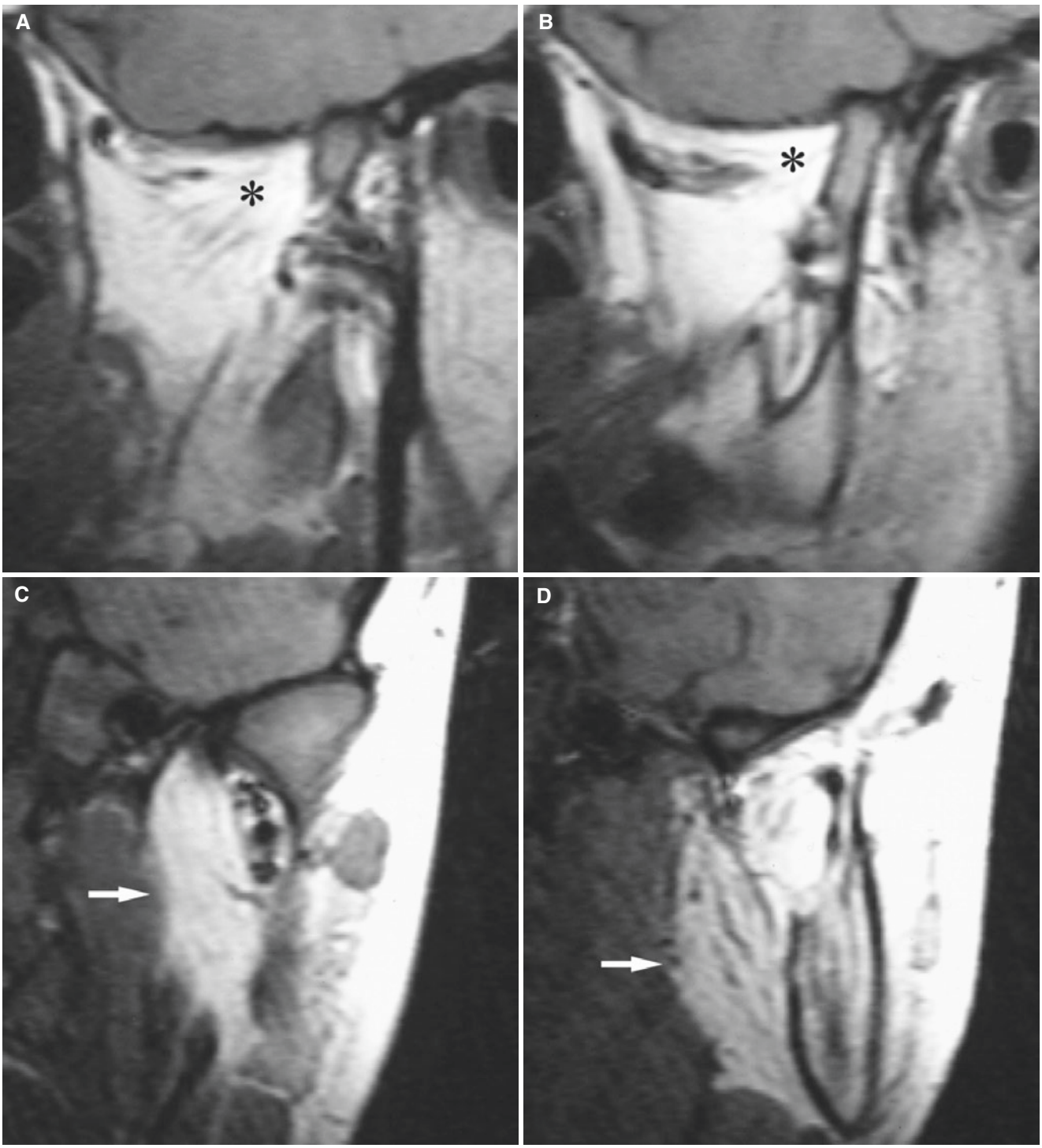

Fig. 11.4 Arthrogryposis multiplex congenita; 9-year-old male with micrognathic growth, anterior open bite, and severely limited mandibular motion with chewing and articulation problems. (**A**) Oblique sagittal T1-weighted MRI, medial aspect of mandibular condyle, shows lateral pterygoid muscle atrophy with fatty replacement (*asterisk*). (**B**) Oblique sagittal T1-weighted MRI, midsection of mandibular condyle, confirms atrophy with fatty replacement of most of the lateral pterygoid muscle (*asterisk*). (**C**) Oblique coronal T1-weighted MRI through mandibular condyle shows medial pterygoid muscle atrophy with fatty replacement (*arrow*). (**D**) Oblique coronal T1-weighted MRI anterior to condyle confirms atrophy with fatty replacement of medial pterygoid muscle (*arrow*)

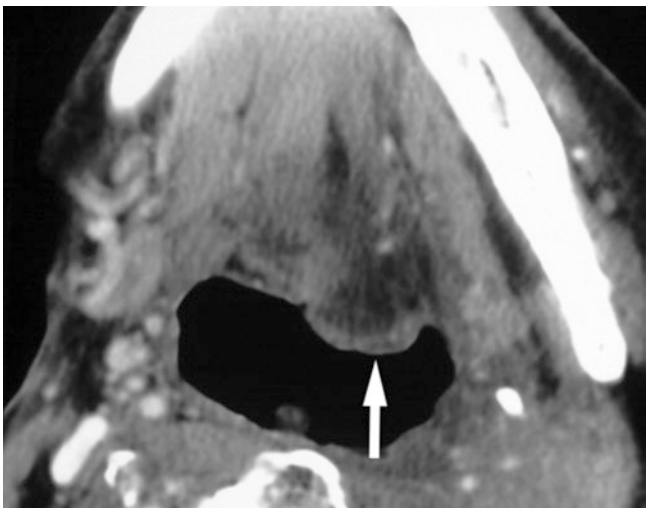

Fig. 11.5 Hypoglossal nerve denervation atrophy; 68-year-old male with history of larynx carcinoma and laryngectomy, now with suprahyoid recurrence. Axial CT image shows atrophy and fatty replacement of left lingual muscles with prolapse of left hemitongue into oropharynx (*arrow*)

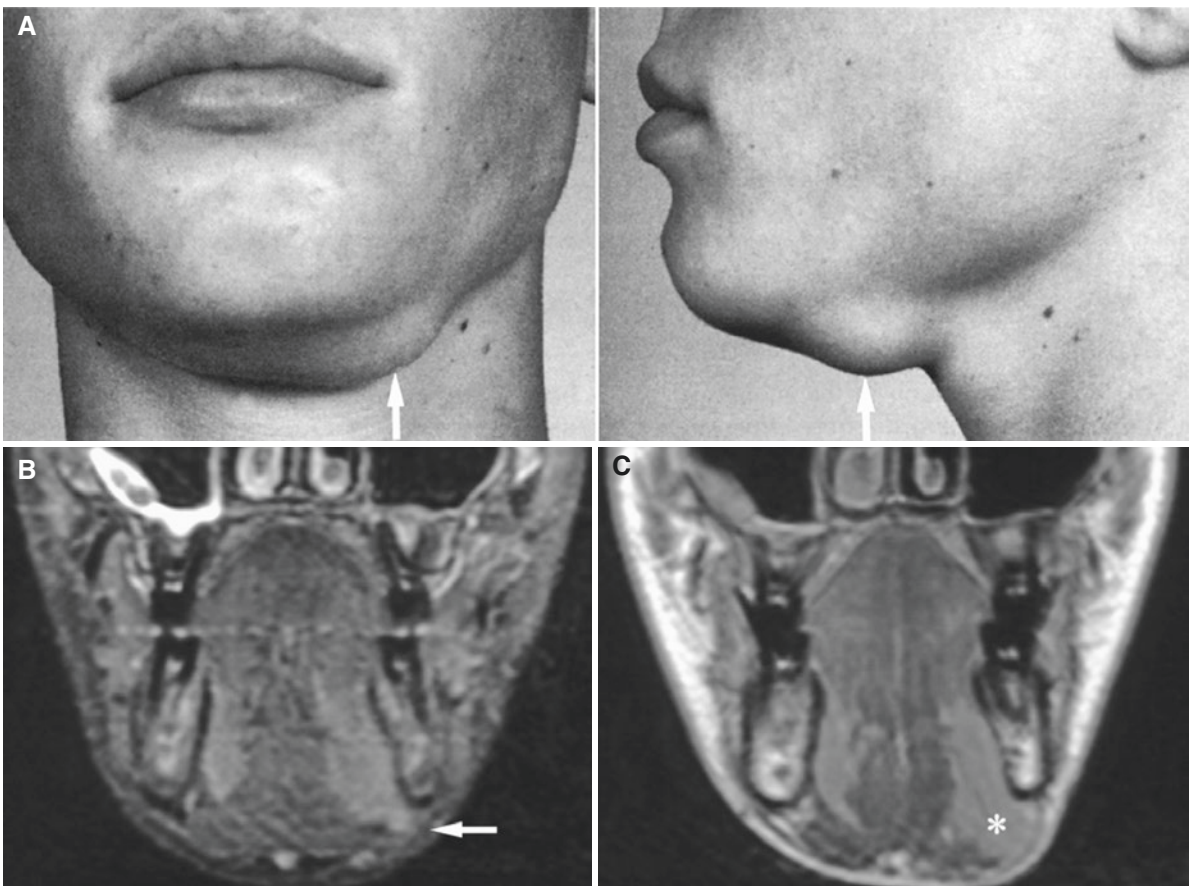

Fig. 11.6 Mylohyoid herniation of sublingual gland; 14-year-old male with left-sided nontender, intermittent submandibular swelling. (**A**) Clinical photographs, en face view (*left*) and side view (*right*), show submandibular swelling (*arrows*) while the patient is pressing his tongue down. (**B**) Coronal STIR MRI shows left mylohyoid dehiscence with small sublingual protrusion (*arrow*). (**C**) Coronal T1-weighted post-Gd MRI shows sublingual gland herniation (*asterisk*) while patient is provoking swelling by tongue pressing movement (reproduced with permission from Hopp et al. 2004)

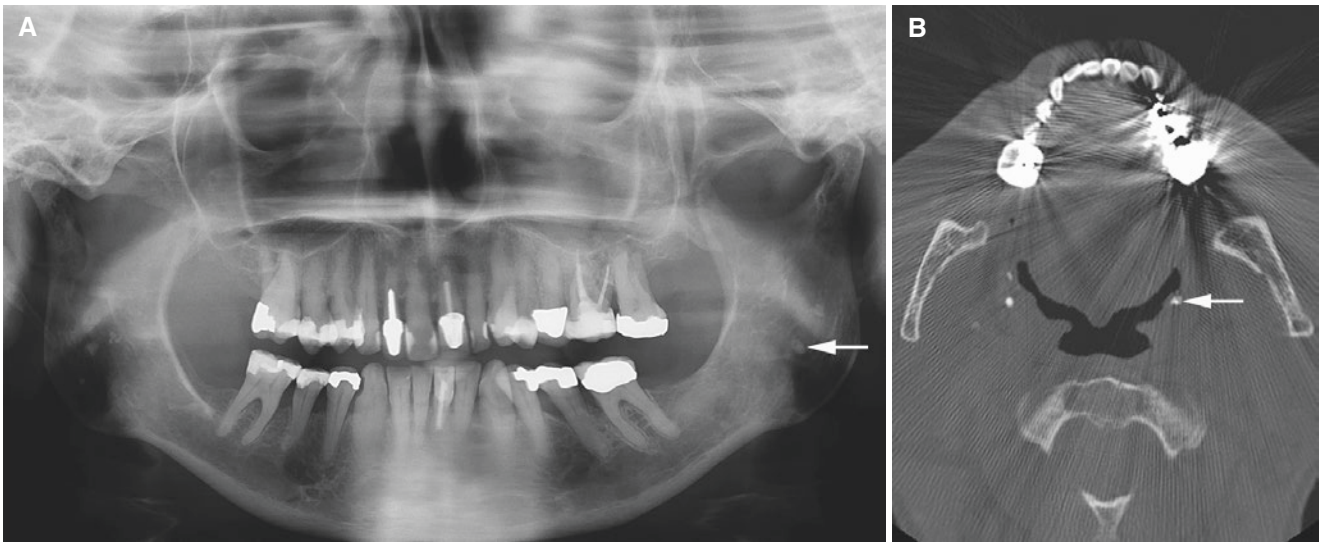

Fig. 11.7 Calcification in palatine tonsil; 65-year-old female with incidental finding. (**A**) Panoramic view and (**B**) Axial CT image show small calcification (*arrow*), bilaterally

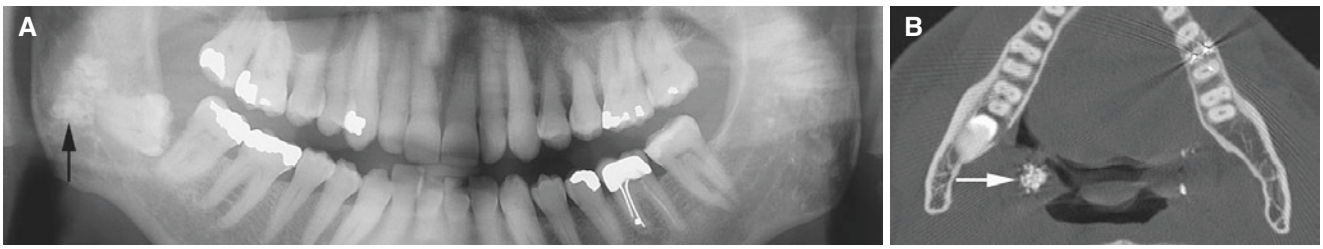

Fig. 11.8 Calcification in palatine tonsil; 66-year-old male with incidental finding. (**A**) Panoramic view and (**B**) Axial CT image show large calcification particularly on right side

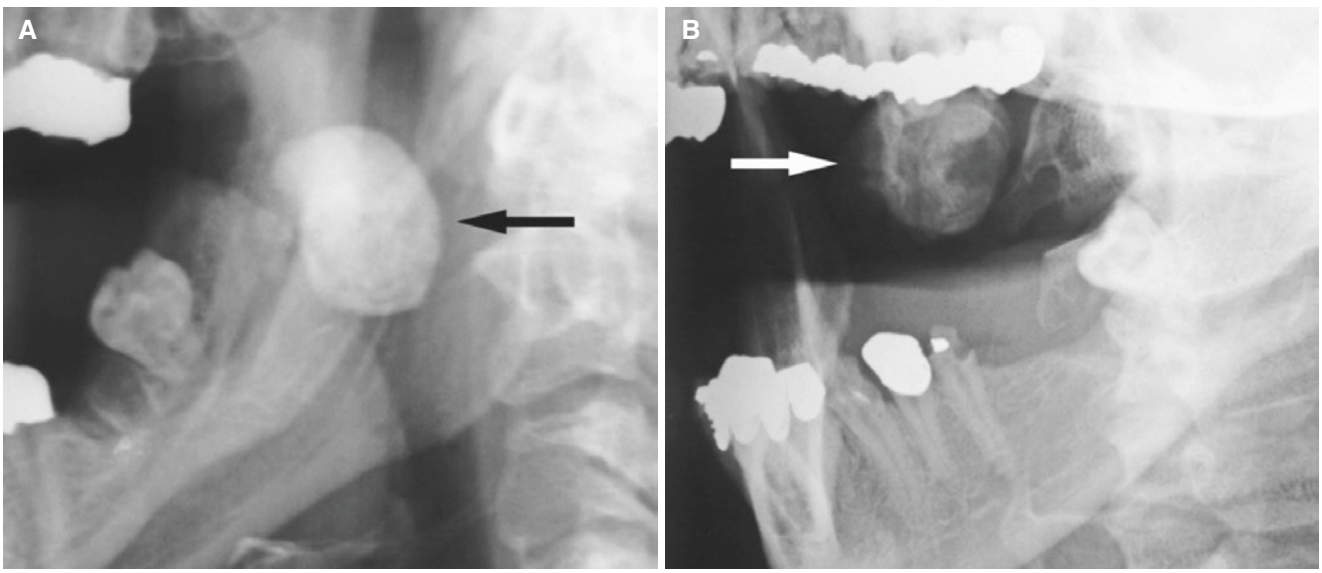

Fig. 11.9 Calcification in palatine tonsil; 31-year-old female with prominent, hard mass in right tonsil region. (**A**) Lateral view shows large calcification (*arrow*). (**B**) Oblique lateral view shows calcification freely projected from skeleton (*arrow*) ((**A**) reproduced with permission from Aspestrand and Kolbenstvedt 1987)

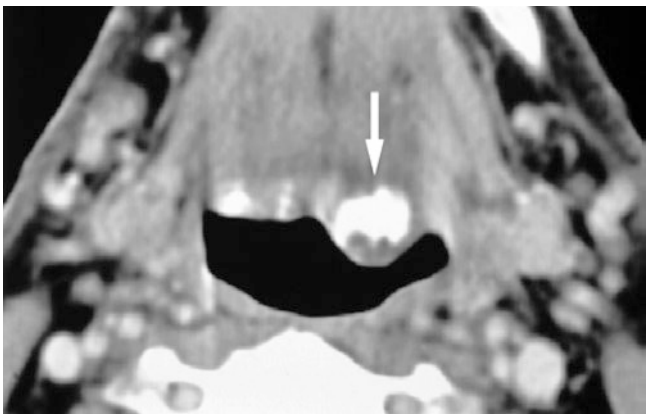

Fig. 11.10 Calcification in lingual tonsil; 74-year-old female with painless swelling in posterior part of tongue. Axial CT image shows calcified mass in posterior part of asymmetric tongue (*arrow*)

Fig. 11.11 Carotid artery calcification; 82-year-old female with incidental finding. Panoramic view shows calcified plaque close to the hyoid bone in the area of carotid bifurcation (*arrow*) (courtesy of Dr. D.M. Almog, Rochester, NY)

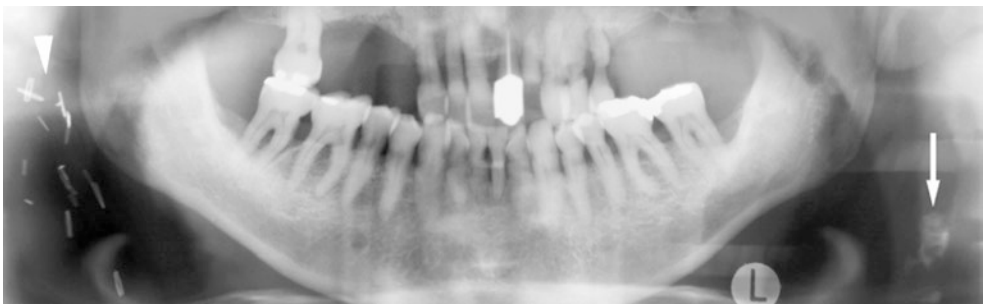

Fig. 11.12 Carotid artery calcification; patient with previous endarterectomy on the right side. Panoramic view shows calcified plaque in the area of carotid bifurcation (*arrow*) and surgical clips used for hemostasis during surgery (*arrowhead*) (courtesy of Dr. D.M. Almog, Rochester, NY)

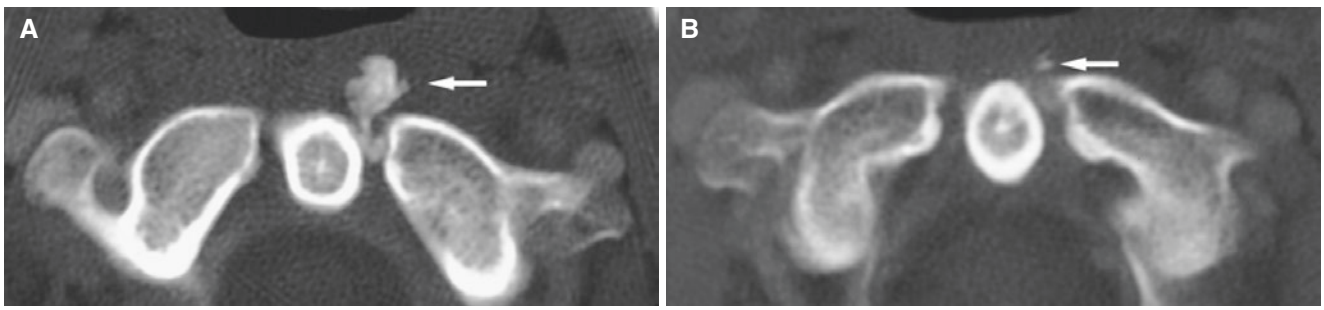

Fig. 11.13 Retropharyngeal tendinitis; 56-year-old male with pain on swallowing and restricted head movement, reexamined after 6 weeks. (**A**) Axial CT image shows prevertebral calcification corresponding to tendon of longus colli muscle (*arrow*). (**B**) Axial CT image 6 weeks later shows marked reduction of calcification (*arrow*)

11.5 Vascular Malformations

Figs. 11.14, 11.15, 11.16, 11.17, and 11.18

11.5.1 Definition

Congenitally malformed vascular channels; arterial, venous, capillary, lymphatic, or mixed.

11.5.2 Clinical Features

- High-flow lesions: arteriovenous malformations or fistulae:
  - Present at birth
  - May be detected in later life
  - May worsen during puberty or pregnancy
  - May cause increased cardiac output and strain
  - Palpable pulse in veins
- Slow-flow lesions: venous, capillary, lymphatic, and mixed malformations:
  - Often affect head and neck region
  - Venous and lymphatic lesions may become large and interfere with swallowing and respiratory function
  - May invade bone
  - No spontaneous regression
  - Capillary malformations are usually diagnosed clinically as port-wine stains

11.5.3 Imaging Features

- High-flow lesions: arteriovenous malformations or fistulae:
  - Heterogeneous
  - May contain varicose dilatations with turbulent flow, with variable signal strength
  - Afferent and efferent blood vessels dilated
  - Well or poorly defined
  - T1-weighted MRI: round and linear flow voids
- Slow-flow lesions (venous):
  - Calcified phleboliths
  - Phleboliths may cause round but not linear flow voids
  - T1-weighted MRI: iso- or hypointense to the muscle
  - T2-weighted MRI: high signal ("light bulb" sign)
  - T1-weighted post-Gd MRI: gradually increasing enhancement from the periphery to the center
- Slow-flow lesions (lymphatic):
  - Low-density (fluid-filled) soft-tissue mass without phleboliths
  - Single, multilobulated, or microcystic
  - Poorly or well defined
  - No enhancement of fluid zone
  - T1-weighted MRI: iso-or hypointense to muscle
  - T2-weighted MRI: high signal
  - T1-weighted post-Gd MRI: no enhancement except in septa or walls

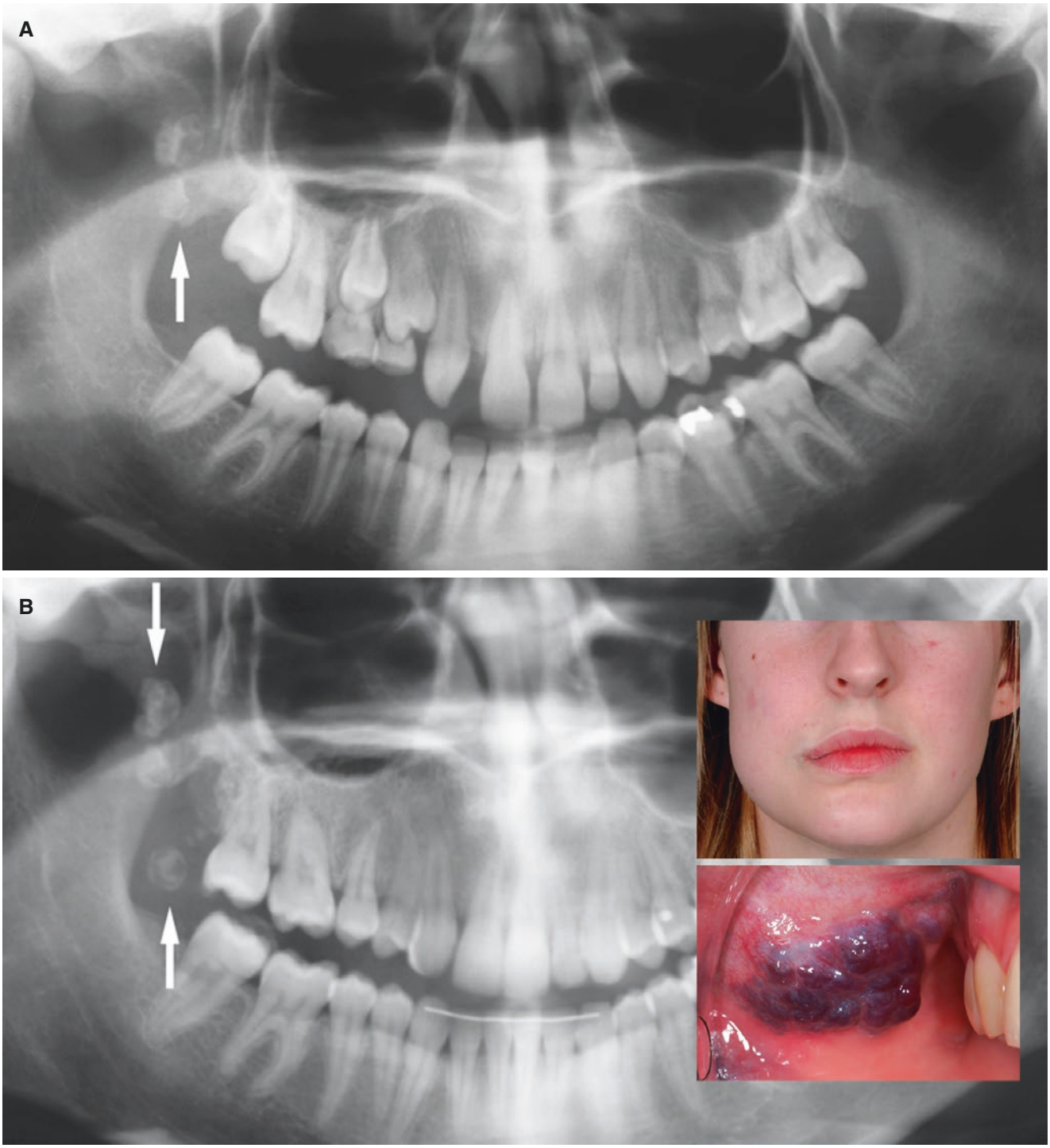

Fig. 11.14 Venous malformation of cheek; 19-year-old female with incidental finding of calcifications on panoramic view that showed progression during a 5-year period. (**A**) Panoramic view shows calcifications (*arrow*) when the patient was 14 years old. (**B**) Panoramic view 5 years later shows larger and multiple calcifications (*arrows*). Clinical photographs of the face (*upper*) and oral mucosa (*lower*). (**C**) Axial CT image shows large calcification just anterior to mandibular ramus characteristic of a phlebolith (*arrow*). (**D**) Axial CT image shows multiple calcifications, including three large ones (*arrow*) consistent with phleboliths. (**E**) Axial T2-weighted MRI shows high-signal area with signal voids of phleboliths (*arrows*). (**F**) Coronal STIR MRI shows high-signal area (*arrow*) with signal voids of phleboliths including some large ones (*arrowheads*)

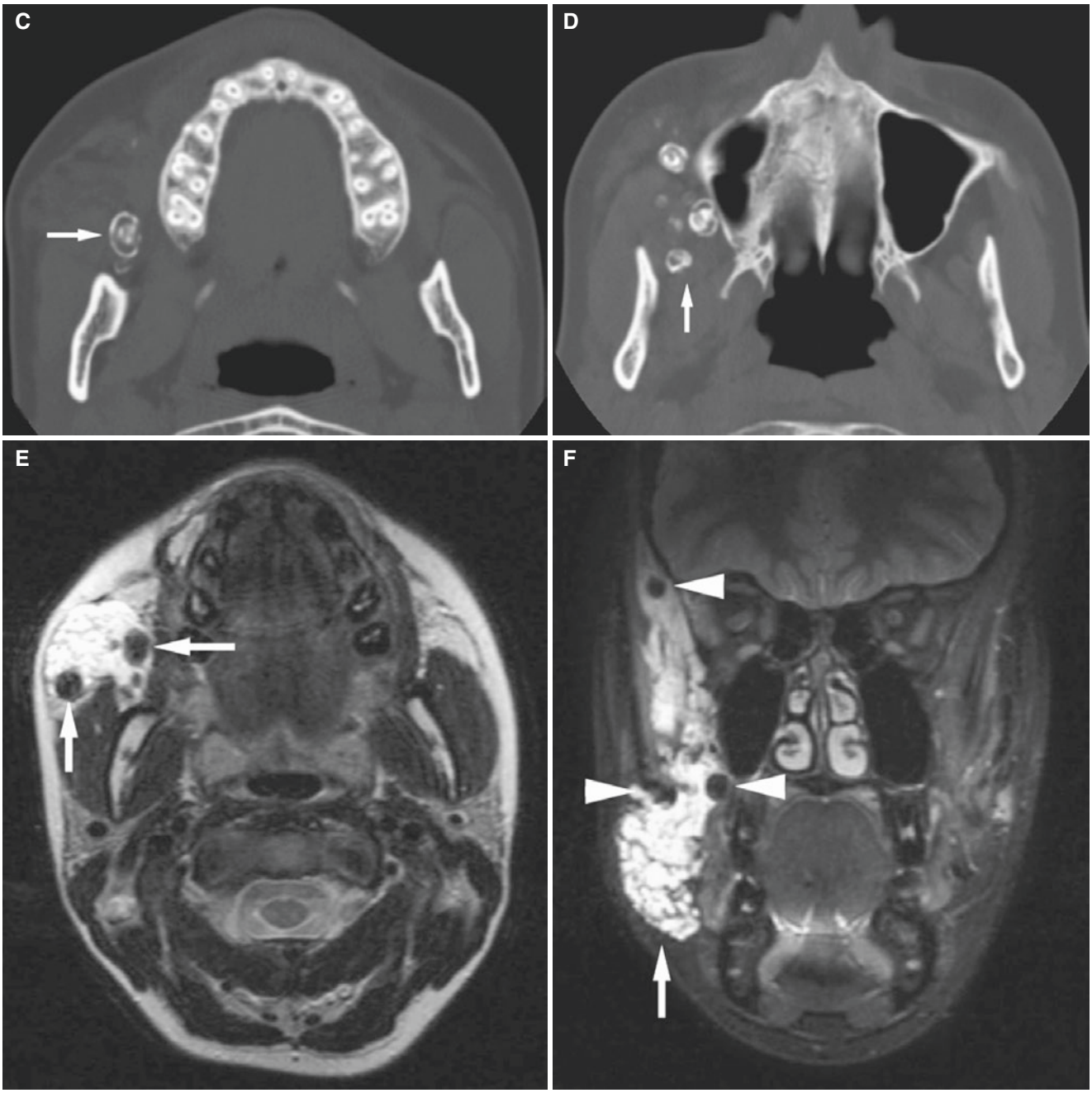

Fig. 11.14 (continued)

Fig. 11.15 Vascular malformation, mandible; 11-year-old female with some swelling in the right mandible and, from time to time, bleeding from gingiva (see clinical photograph and CBCT images of this patient in Fig. 15.80). (**A**) Panoramic view shows radiolucency (*arrow*). (**B**) Axial (soft-tissue) CT image shows soft-tissue mass (*arrowhead*). (**C**) Axial (with cursor lines), (**D**) oblique sagittal (right), (**E**) oblique sagittal (left), and (**F**) axial CT images of the cortical bone show punctate radiolucencies in the right cortical bone (**D**, **F**) and normal left cortical bone (**E**). (**G**, **H**, **I**) Axial CT images show multiple cortical canal-like defects (*arrows*). (**J**, **K**) Digital subtraction angiography (**J**: frontal, **K**: lateral) shows intense vascularity (*asterisk*). (**L**, **M**) Digital subtraction angiography (**L**: frontal, **M**: lateral) after embolization shows vascularity almost completely eliminated. (**N**) Panoramic view after embolization. See clinical photo of this patient in Fig. 15.80

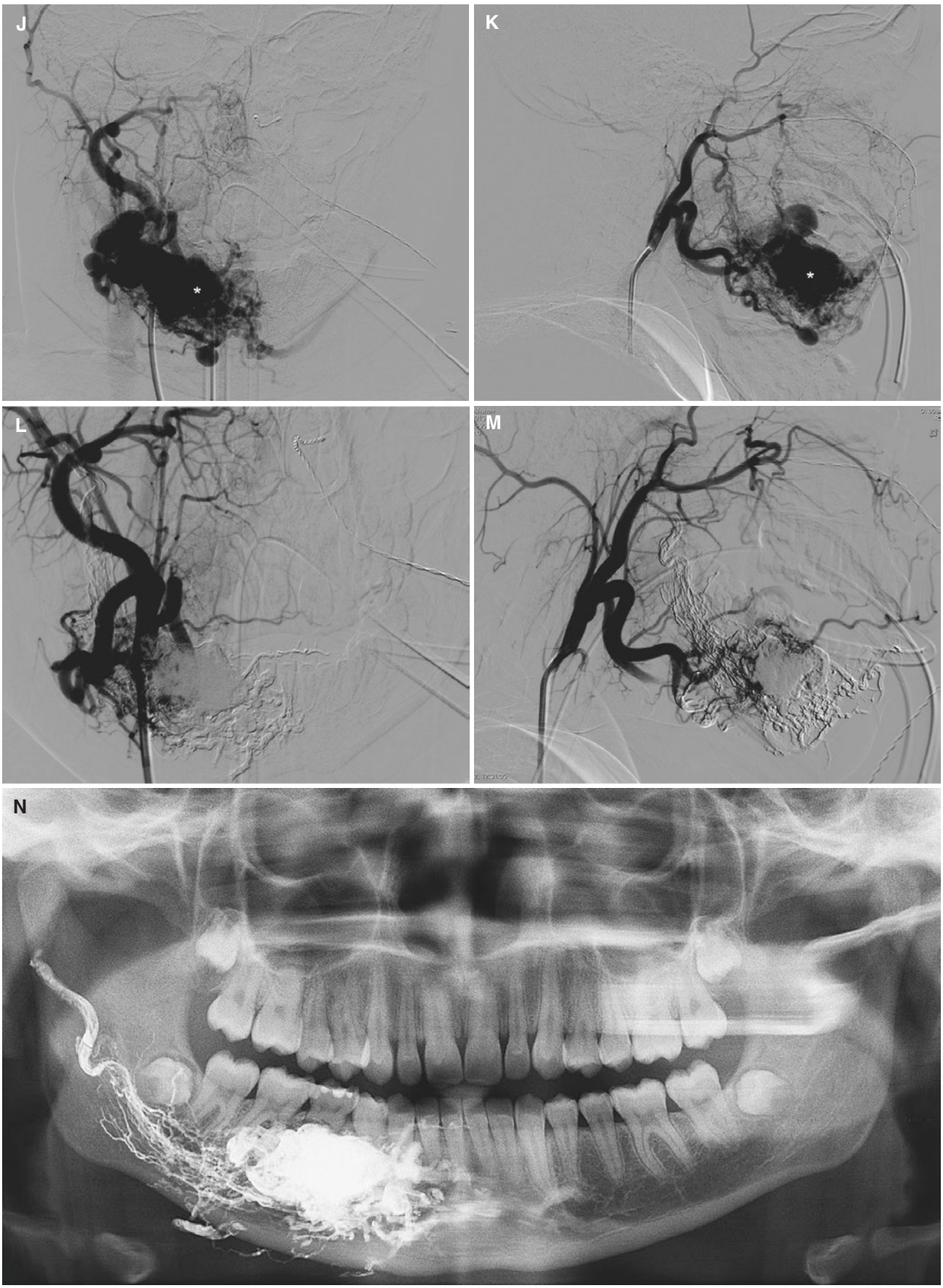

Fig. 11.15 (continued)

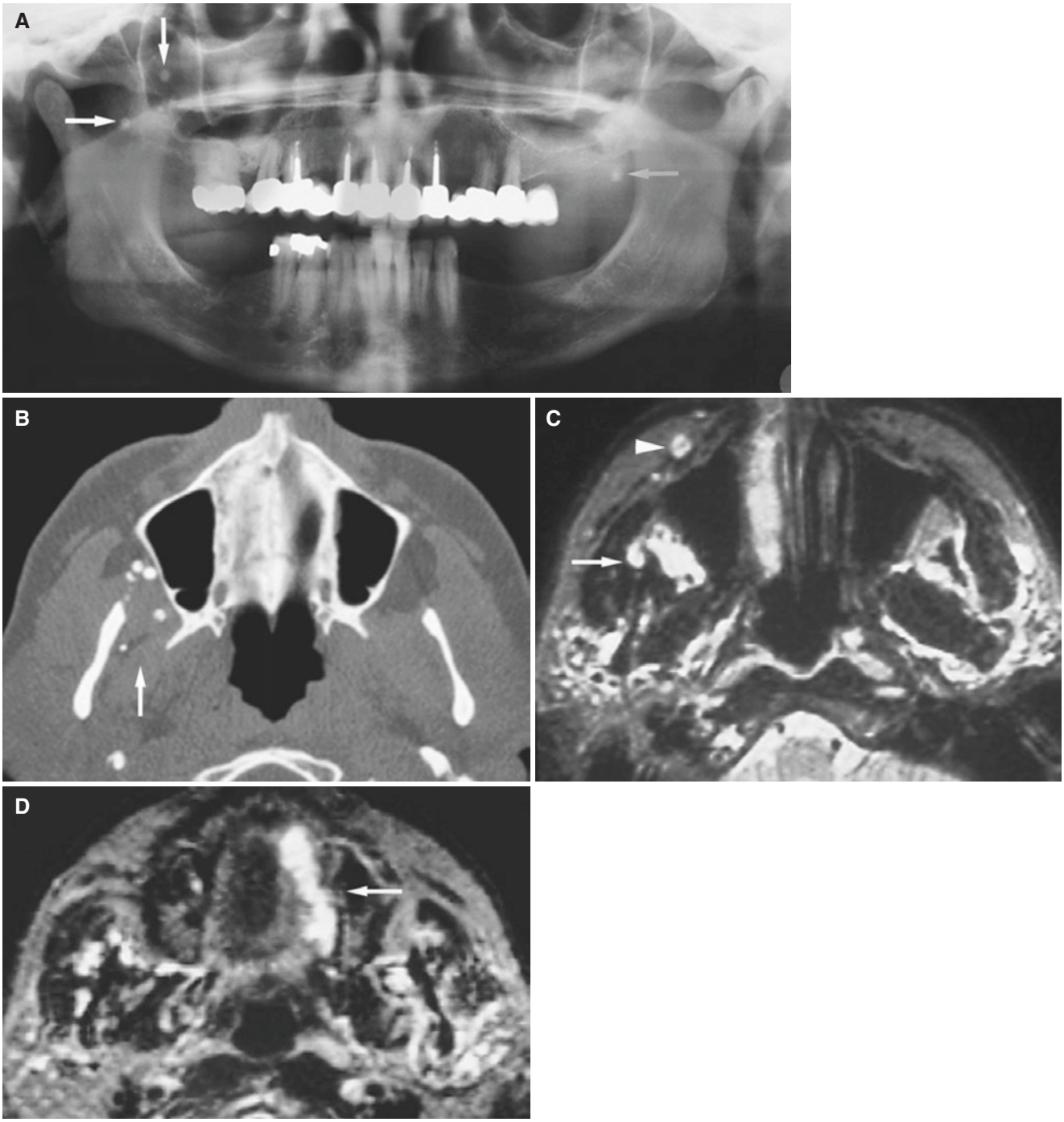

Fig. 11.16 Venous malformations of the cheek and hard palate; 44-year-old female with painless swelling in the hard palate that was believed to be a dental abscess, but on incision did not show any pus collection. (**A**) Panoramic view shows tiny calcifications (*arrows*). (**B**) Axial CT image shows multiple small, dense calcifications (*arrow*). (**C**) Axial T2-weighted MRI shows area of high signal with tiny voids of signal (*arrow*), including a smaller similar area anterior to maxillary sinus (*arrowhead*). (**D**) Axial T2-weighted MRI of hard palate shows high signal from left side, corresponding to area of incision (*arrow*)

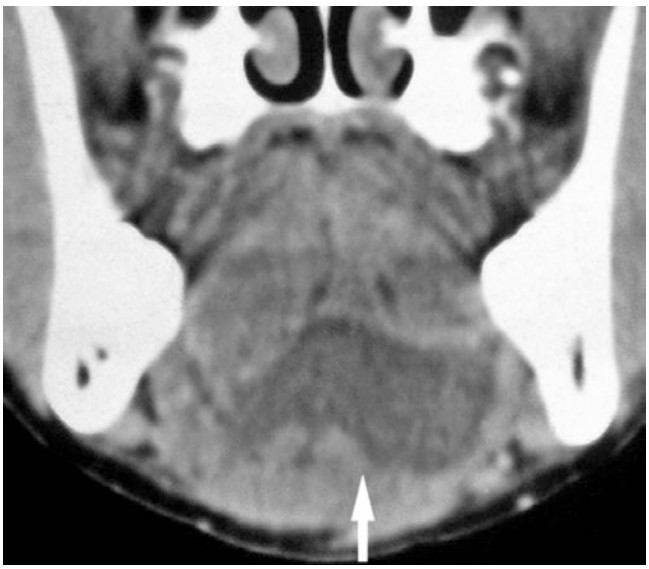

Fig. 11.17 Cystic lymphatic malformation; 14-year-old female with submental swelling. Coronal post-enhanced CT image shows well-defined mass in sublingual space crossing midline (*arrows*), hypodense with enhanced border

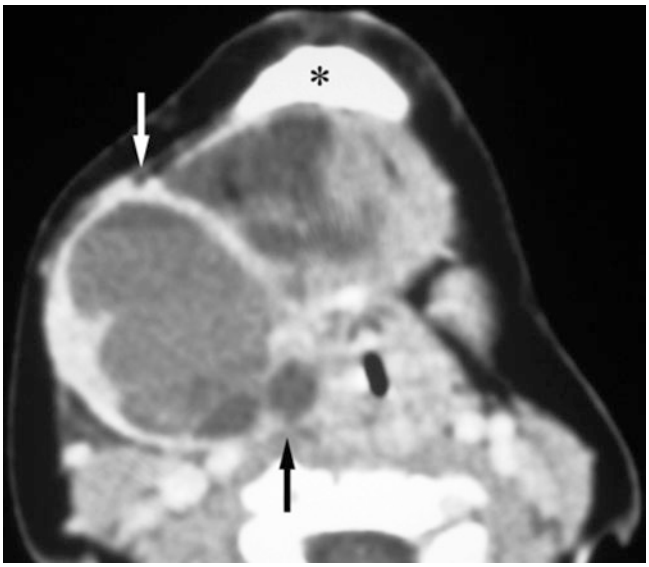

Fig. 11.18 Cystic lymphatic malformation; 10-month-old female with swelling of the floor of the mouth and upper neck. Axial CT image shows well-defined hypodense, lobulated mass (*arrows*) in submandibular space; note mandible (*asterisk*)

11.6 Cysts

Figs. 11.19, 11.20, 11.21, 11.22, and 11.23

11.6.1 Definition

Epithelial-lined fluid-filled cavity with thin fibrous wall.

11.6.2 Clinical Features

- Painless swelling (if not infected)
- Thyroglossal duct cyst:
  - Most common of congenital neck lesions (about 70%); may occur anywhere from foramen cecum to thyroid gland; majority at hyoid bone level
  - Commonly in midline when suprahyoid; seldom in floor of mouth; only 1–2% in tongue
- Second branchial cleft cyst:
  - The far most common of all branchial anomalies
  - Typically located in lateral neck ventral to anterior edge of sternocleidomastoid muscle, dorsal to submandibular gland, and superficial to carotid sheath; usually caudal to angle of mandible
- Dermoid or epidermoid cyst:
  - Least common of congenital neck lesions (only about 7%), but the floor of the mouth particularly involved; about half in sublingual space; midline or asymmetric; may contain fat globules or calcifications
  - Terms used interchangeably, but dermoid cyst may have hair follicles and sebaceous glands

11.6.3 Imaging Features

- CT: well-defined unilocular, hypodense area with thin, enhancing peripheral rim
- T1-weighted MRI: usually low signal, but occasionally high (dermoid)
- T2-weighted MRI or STIR: high signal
- T1-weighted post-Gd MRI: no enhancement, occasionally in thin peripheral rim

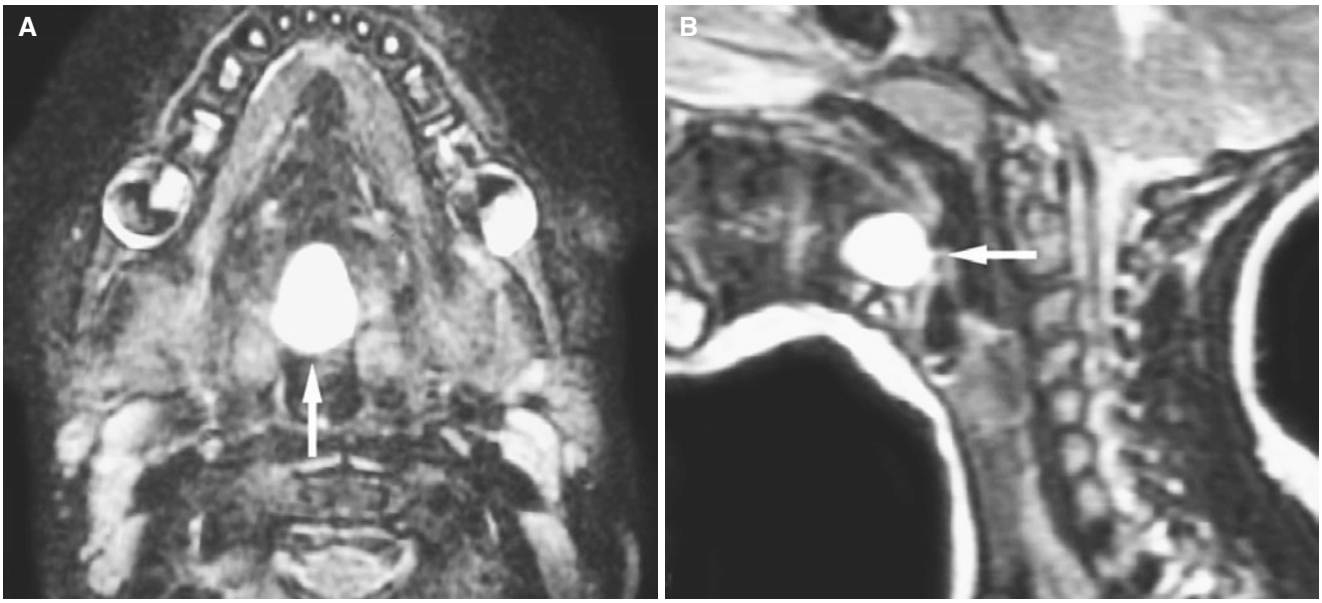

Fig. 11.19 Thyroglossal duct cyst; 3-year-old female with mass in the midline of the base of the tongue. (**A**) Axial T2-weighted MRI shows well-defined high-signal mass in the base of the tongue (*arrow*). (**B**) Sagittal T2-weighted MRI confirms high-signal mass in the tongue (*arrow*)

Fig. 11.20 Thyroglossal duct cyst; 29-year-old male with lump in the midline of the neck, anterior to the hyoid bone. Axial post-contrast CT image shows well-defined hypodense area with enhancing peripheral rim in the midline (*arrow*) anterior to the hyoid bone (*arrowhead*)

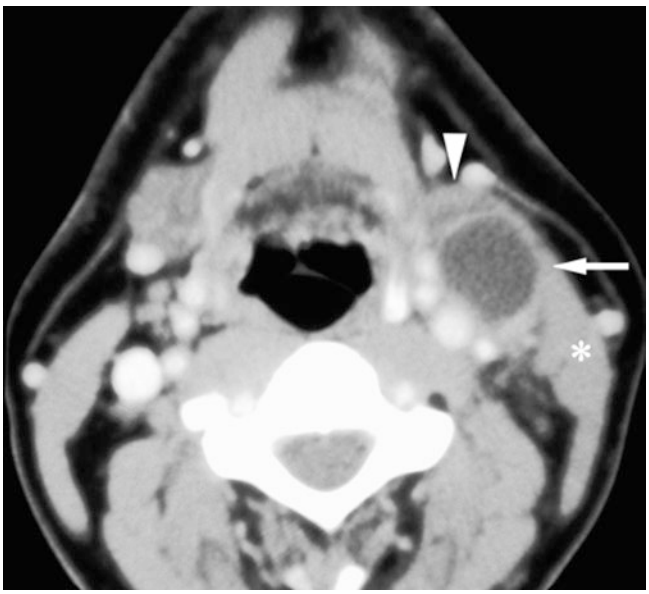

Fig. 11.21 Second branchial cleft cyst; 38-year-old male with soft submandibular tumor at the anterior border of the sternocleidomastoid muscle; cyst confirmed by surgery. Axial post-contrast CT image shows well-defined low-density mass with enhancing peripheral rim in submandibular space (*arrow*), just dorsal to submandibular gland (*arrowhead*), lateral to carotid sheath, and ventral to sternocleidomastoid muscle (*asterisk*)

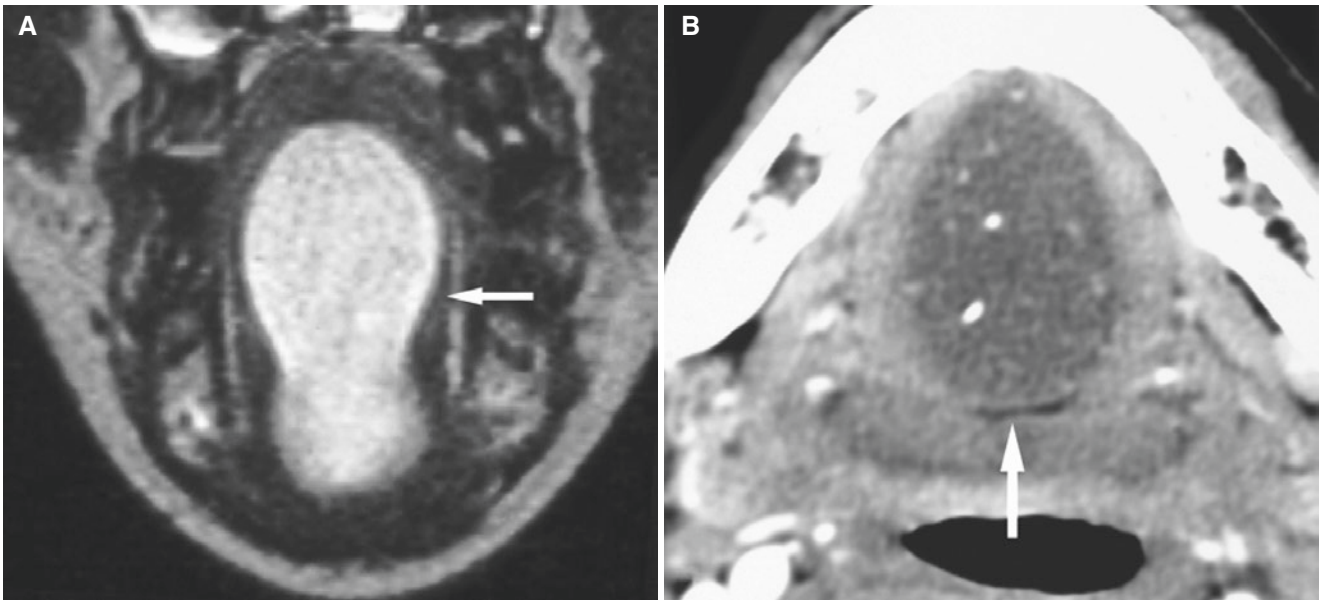

Fig. 11.22 Dermoid cyst, sublingual space and tongue; 25-year-old female with sublingual swelling. (**A**) Coronal STIR MRI shows high-signal mass with smooth delineation (*arrow*). (**B**) Axial CT image shows cyst (*arrow*) with multiple calcifications

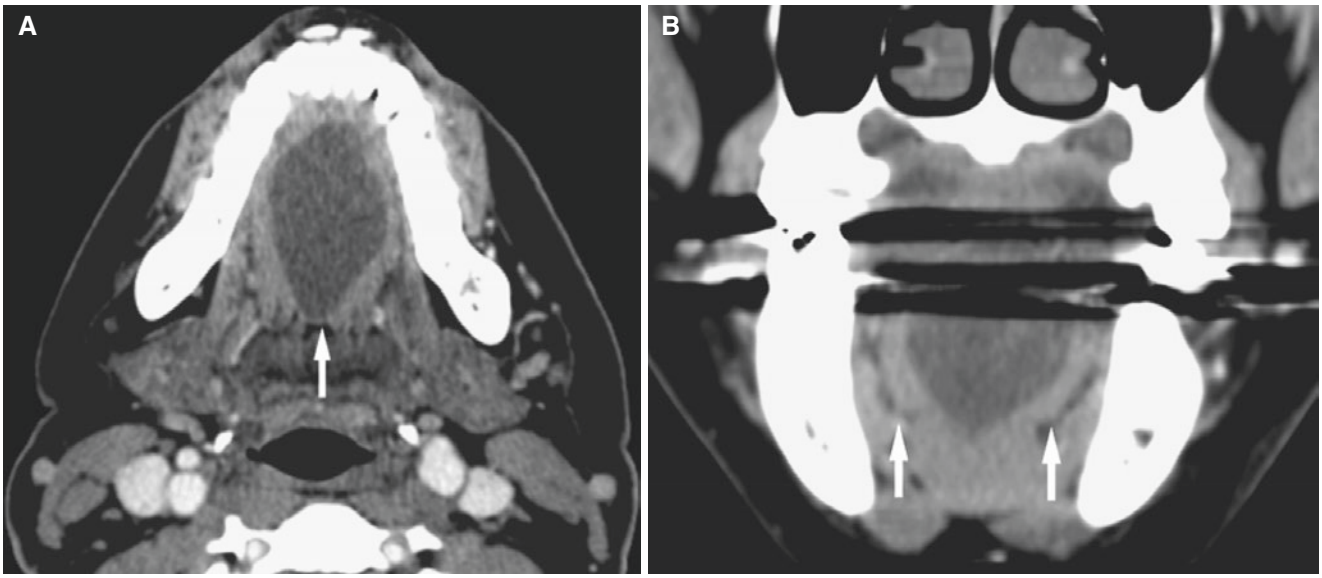

Fig. 11.23 Dermoid cyst, tongue; 34-year-old female with mass in the tongue. (**A**) Axial post-contrast CT image shows hypodense mass without calcifications in the floor of the mouth (*arrow*). (**B**) Coronal post-contrast CT image shows deviation of both genioglossus muscles laterally (*arrows*)

11.7 Lingual Thyroid

Figs. 11.24 and 11.25

11.7.1 Definition

Ectopic thyroid tissue in the tongue.

11.7.2 Clinical Features

- Incidental finding
- Usually painless mass in tongue base; dysphagia or other symptoms may occur

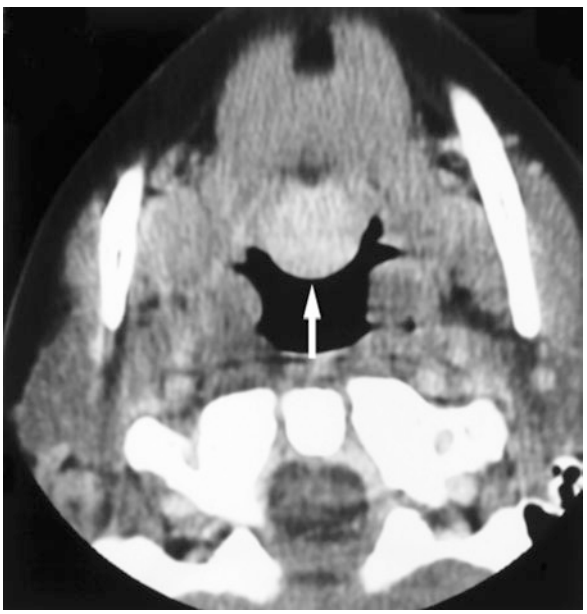

Fig. 11.24 Lingual thyroid gland; 16-year-old female with lump in tongue base. Axial post-contrast CT shows soft-tissue mass in posterior part of tongue (*arrow*)

- Ectopic thyroid tissue may occur along the entire thyroglossal duct tract; 90% in the base of the tongue, usually in the midline
- Majority have no other functioning thyroid present.
- Female predominance

11.7.3 Imaging Features

- CT: hyperdense mass compared to muscle; post-contrast enhancement
- T1-weighted and T2-weighted MRI: iso- or hyperintense to muscle
- T1-weighted post-Gd MRI: homogeneous contrast enhancement

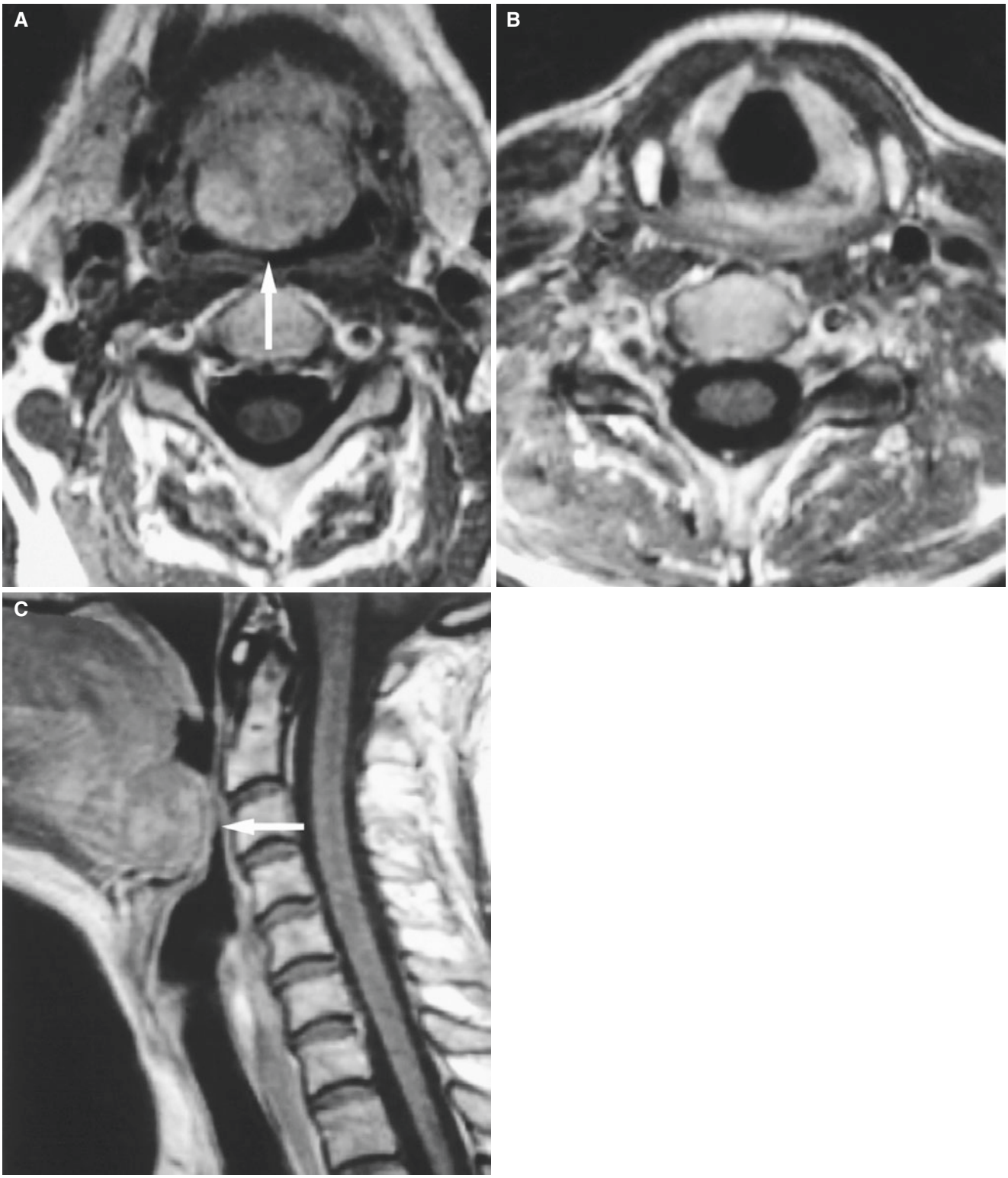

Fig. 11.25 Lingual thyroid gland; 42-year-old male with lump in tongue base. (**A**) Axial T1-weighted MRI shows soft-tissue mass in posterior part of tongue (*arrow*). (**B**) Axial T1-weighted MRI shows the absence of normal thyroid gland. (**C**) Sagittal T1-weighted post-Gd MRI shows thyroid mass in posterior part of tongue (*arrow*)

11.8 Benign Oropharyngeal Tumors

Lipoma and schwannoma are illustrated.

11.9 Lipoma

Fig. 11.26

11.9.1 Definition

Benign tumor consisting of mature fat arranged in lobules, separated by fibrous tissue septa, usually surrounded by thin, fibrous capsule.

11.9.2 Clinical Features

- Painless swelling
- Most common mesenchymal tumor but only 13% in head and neck; most located in posterior cervical region
- Within oral cavity only 1–4% of all benign tumors

11.9.3 Imaging Features

- CT: well-defined homogeneous low-density mass; no contrast enhancement
- T1-weighted MRI: homogeneous high signal as subcutaneous fat
- T1-weighted fat-suppressed MRI: homogeneous reduced signal
- T1-weighted post-Gd MRI: no contrast enhancement

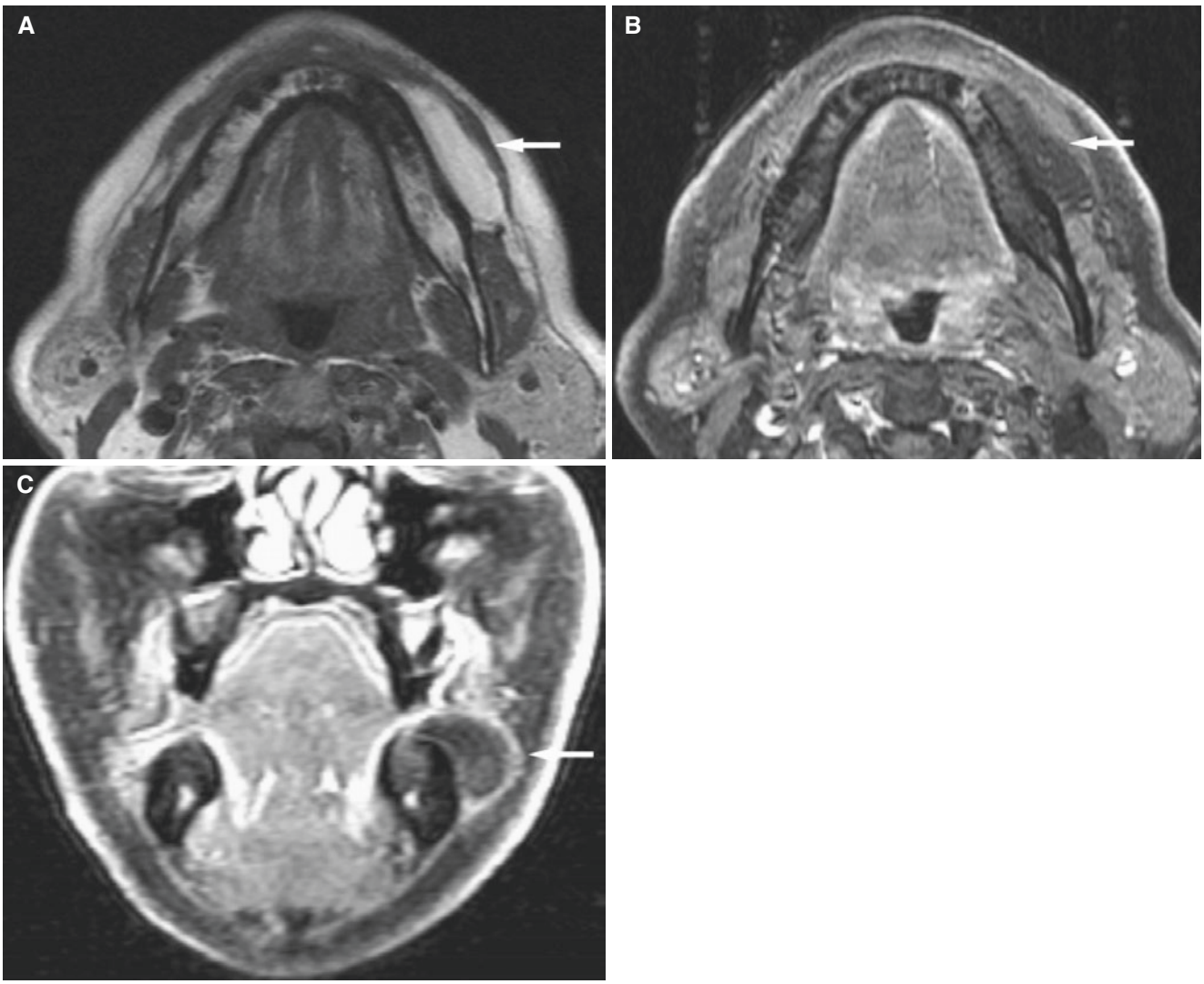

Fig. 11.26 Lipoma of lower gingivobuccal sulcus; 67-year-old male with fullness of left lower gingivobuccal sulcus with clinical suspicion of being fatty. (**A**) Axial T1-weighted MRI shows well-defined area of homogeneous high signal along the left mandible (*arrow*). (**B**) Axial T1-weighted fat-suppressed MRI shows reduced signal in entire area (*arrow*). (**C**) Coronal T1-weighted fat-suppressed post-Gd MRI shows no enhancement of mass except in periphery (*arrow*)

11.10 Schwannoma

Fig. 11.27

11.10.1 Definition

Benign nerve sheath tumor emanating from Schwann cells. (The terminology is confusing. The following terms have been used for the same tumor: schwannoma, neuroma, neurinoma, neurolemmoma, perineural fibroblastoma.)

11.10.2 Clinical Features

- Asymptomatic mass.
- About 13% of schwannomas are found in the head and neck, most in the lateral cervical region.
- Almost half of oral schwannomas reported to occur in the tongue.

11.10.3 Imaging Features

- Well-defined homogeneous soft-tissue mass, enhancement, but variable appearance because of cystic and solid components
- Schwannoma is often cystic, as opposed to neuroma, which is seldom cystic
- Enlarged foramina
- Atrophy of muscles
- Associated with neurofibromatosis
- T1-weighted MRI: isointense with muscle
- T2-weighted MRI: hyperintense, homogeneous, both cystic and solid components, or heterogeneous
- T1-weighted post-Gd MRI: cystic nature with rim enhancement

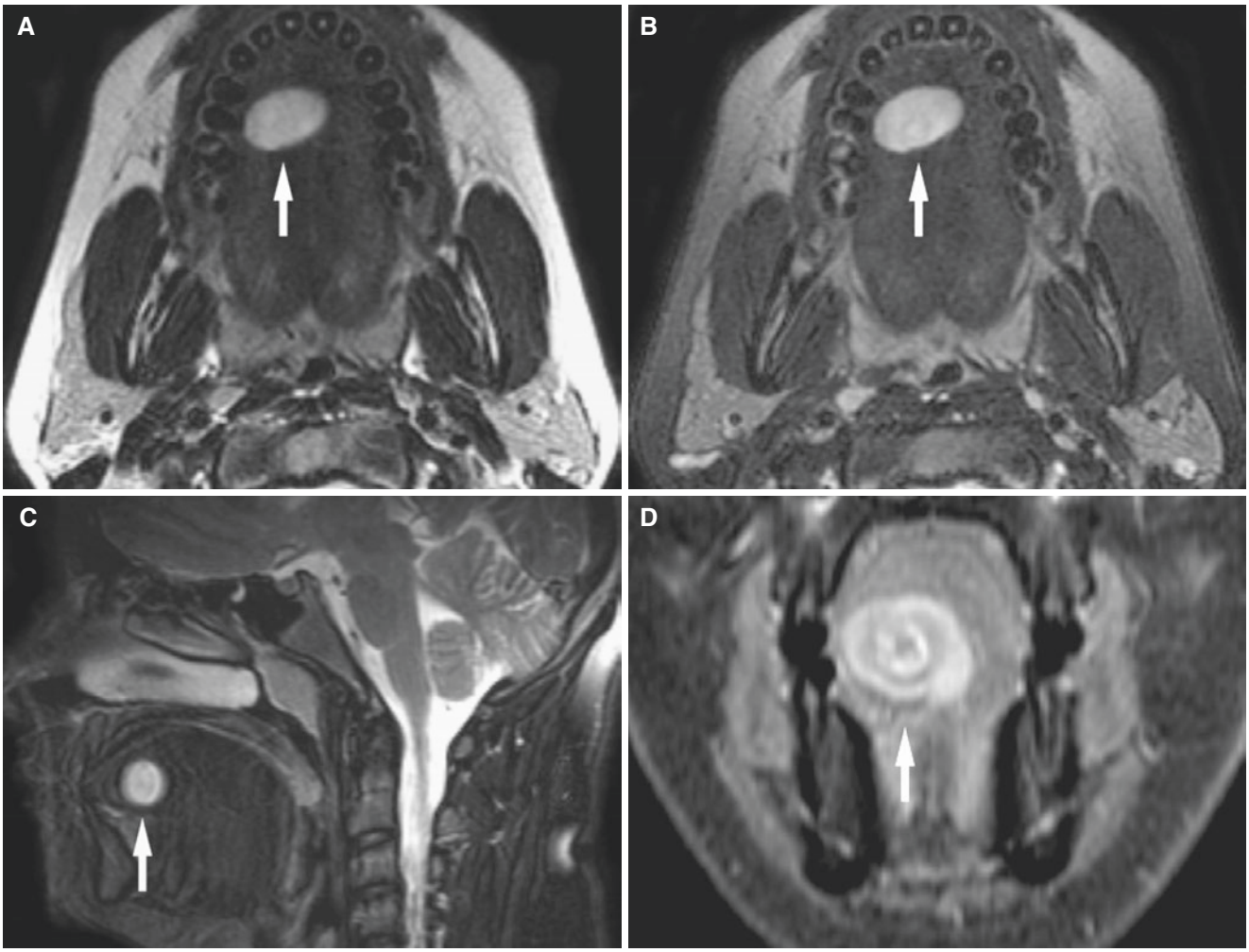

Fig. 11.27 Schwannoma of tongue; 13-year-old with slowly growing mass of tongue. (**A**) Axial T2-weighted MRI shows well-defined high-signal mass in right anterior tongue (*arrow*). (**B**) Axial T2-weighted fat-suppressed MRI shows high-signal mass (*arrow*), indicating no evident fatty component. (**C**) Sagittal T2-weighted fat-suppressed MRI confirms high-signal mass in anterior part of tongue (*arrow*). (**D**) Coronal T1-weighted fat-suppressed post-Gd MRI shows serpentine onion-type contrast enhancement of mass (*arrow*)

11.11 Malignant Oropharyngeal Tumors

Squamous cell carcinoma, lymph node metastasis, clear cell carcinoma, adenoid cystic carcinoma, and lymphoma are illustrated.

11.12 Squamous Cell (and Clear Cell) Carcinomas

Figs. 11.28, 11.29, 11.30, 11.31, and 11.32

11.12.1 Definition

Malignant epithelial tumor.

11.12.2 Clinical Features (Oral Carcinomas)

- Painless mass
- Most frequent malignant tumor in oral cavity, predominantly squamous cell type
- Predilection areas: floor of the mouth, ventrolateral tongue, and soft palate complex (soft palate proper, anterior tonsillar pillar, retromolar trigone)
- Typically males, 50–70 years, drinking smokers
- Lymph node involvement in 30–65% when diagnosed; single most important prognostic factor
- Somewhat less aggressive than oropharynx carcinomas

11.12.3 Imaging Features (Oral Carcinomas)

- CT: isodense to muscle, moderate contrast enhancement
- Surrounding structures invaded
- T1-weighted MRI: isointense to muscle signal
- T2-weighted MRI: inhomogeneous increased signal
- T1-weighted post-Gd MRI: moderate enhancement
- Non-contrast T1-weighted MRI reported most useful sequence to assess tumor extent

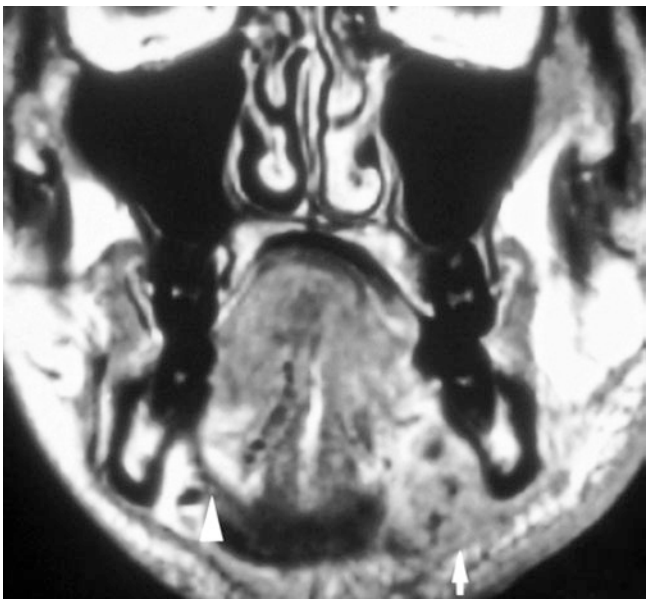

Fig. 11.28 Squamous cell carcinoma of the tongue invading the floor of the mouth; 22-year-old male with history of tongue cancer, now with recurrence. Coronal T1-weighted post-Gd MRI shows moderately contrast-enhanced tumor penetrating mylohyoid muscle and platysma (*arrow*). Note normal mylohyoid muscle on contralateral side (*arrowhead*)

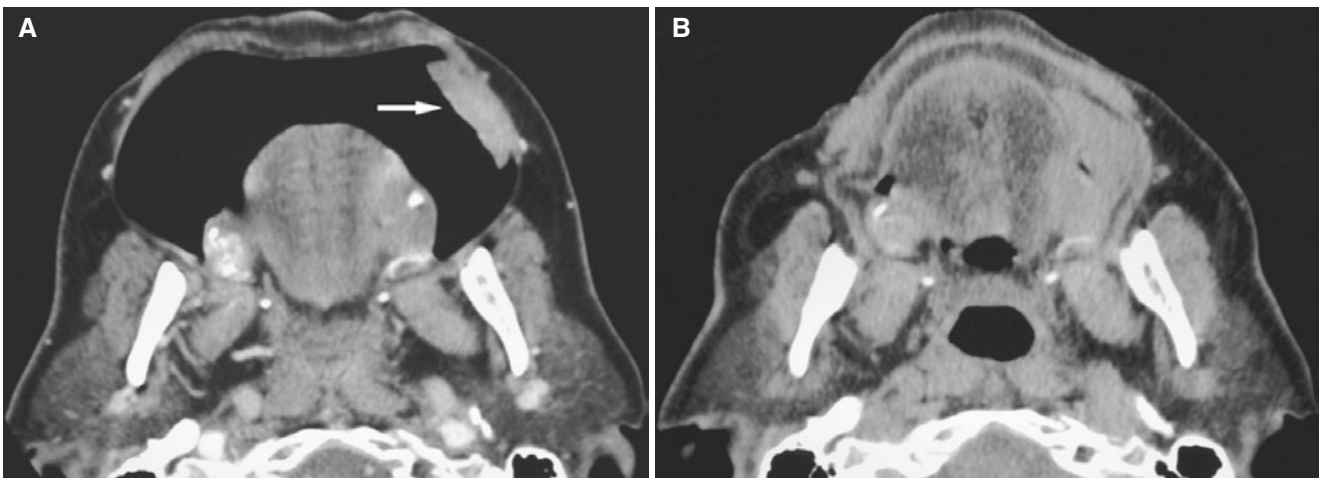

Fig. 11.29 Squamous cell carcinoma of cheek with and without blowing cheek; 74-year-old male with lump in cheek. (**A**) Axial CT image with blowing cheek shows soft-tissue tumor in buccal mucosa (*arrow*). (**B**) Axial CT without blowing cheek cannot reveal origin of tumor

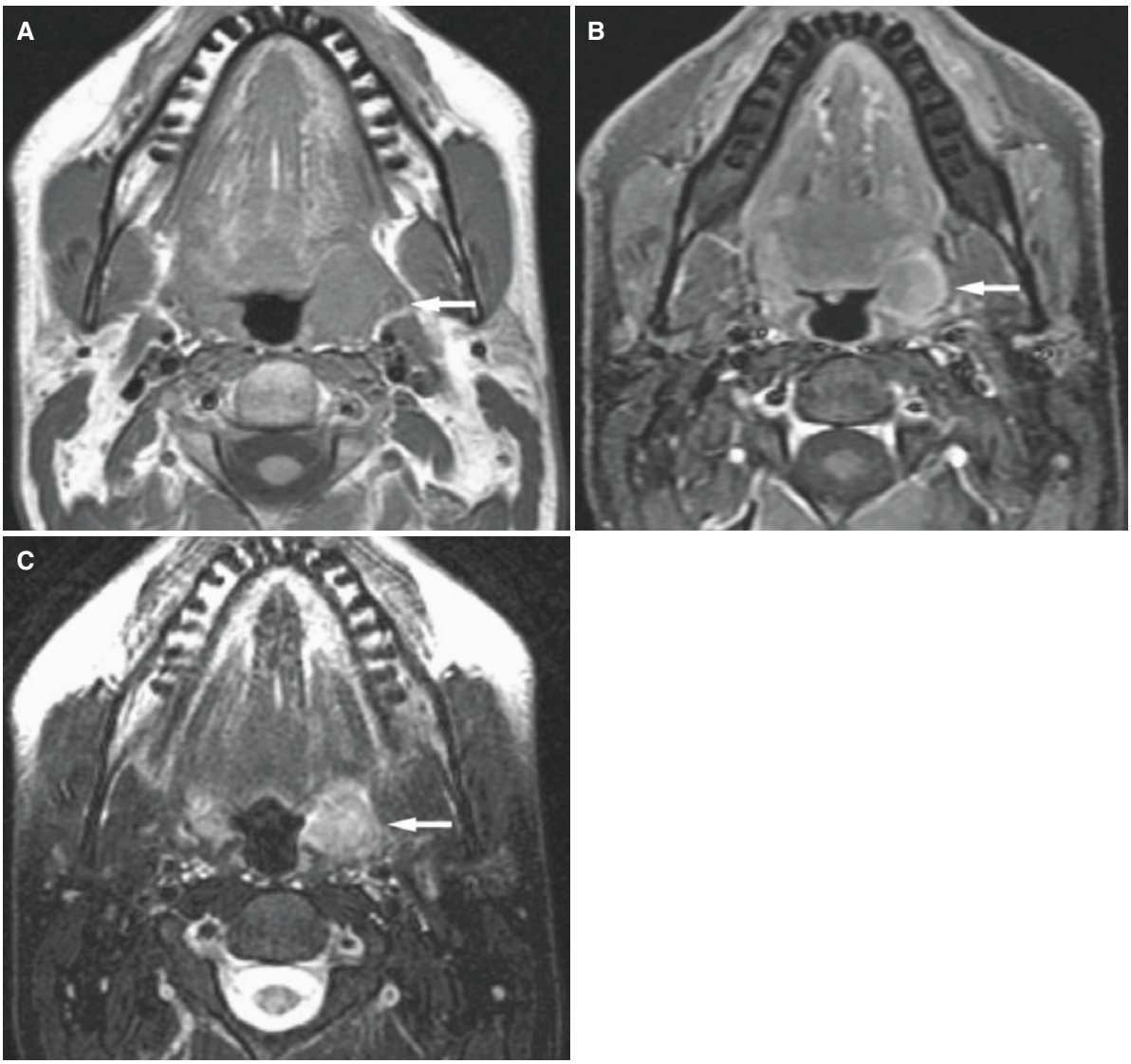

Fig. 11.30 Squamous cell carcinoma of the tonsil; 43-year-old male with known multiple sclerosis and a history of squamous cell carcinoma of the left palatine tonsil. (**A**) Axial T1-weighted MRI shows low- to intermediate-signal mass in the left palatine tonsil (*arrow*). (**B**) Axial T1-weighted fat-suppressed post-Gd MRI shows moderately contrast-enhanced mass (*arrow*). (**C**) Axial T2-weighted fat-suppressed MRI shows high-signal mass (*arrow*)

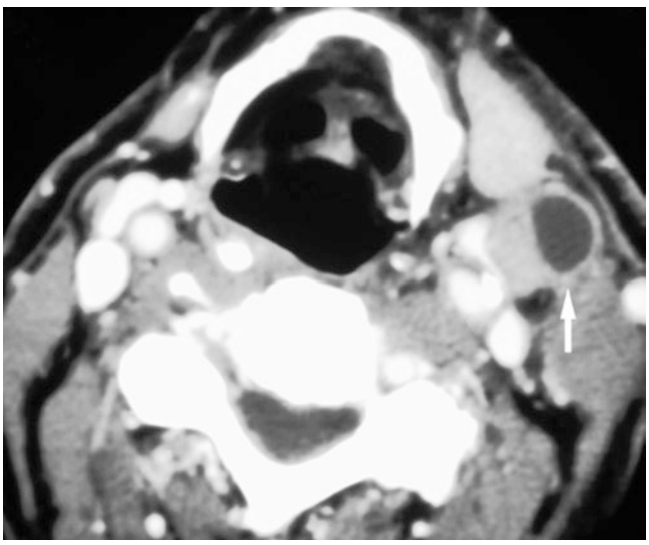

Fig. 11.31 Lymph node metastasis; 65-year-old male with squamous cell carcinoma of left palatine tonsil, metastasizing. Axial post-contrast CT image shows well-defined mass in submandibular space, hypodense with enhanced border (*arrow*). Note similarity with branchial cleft cyst in Fig. 11.21

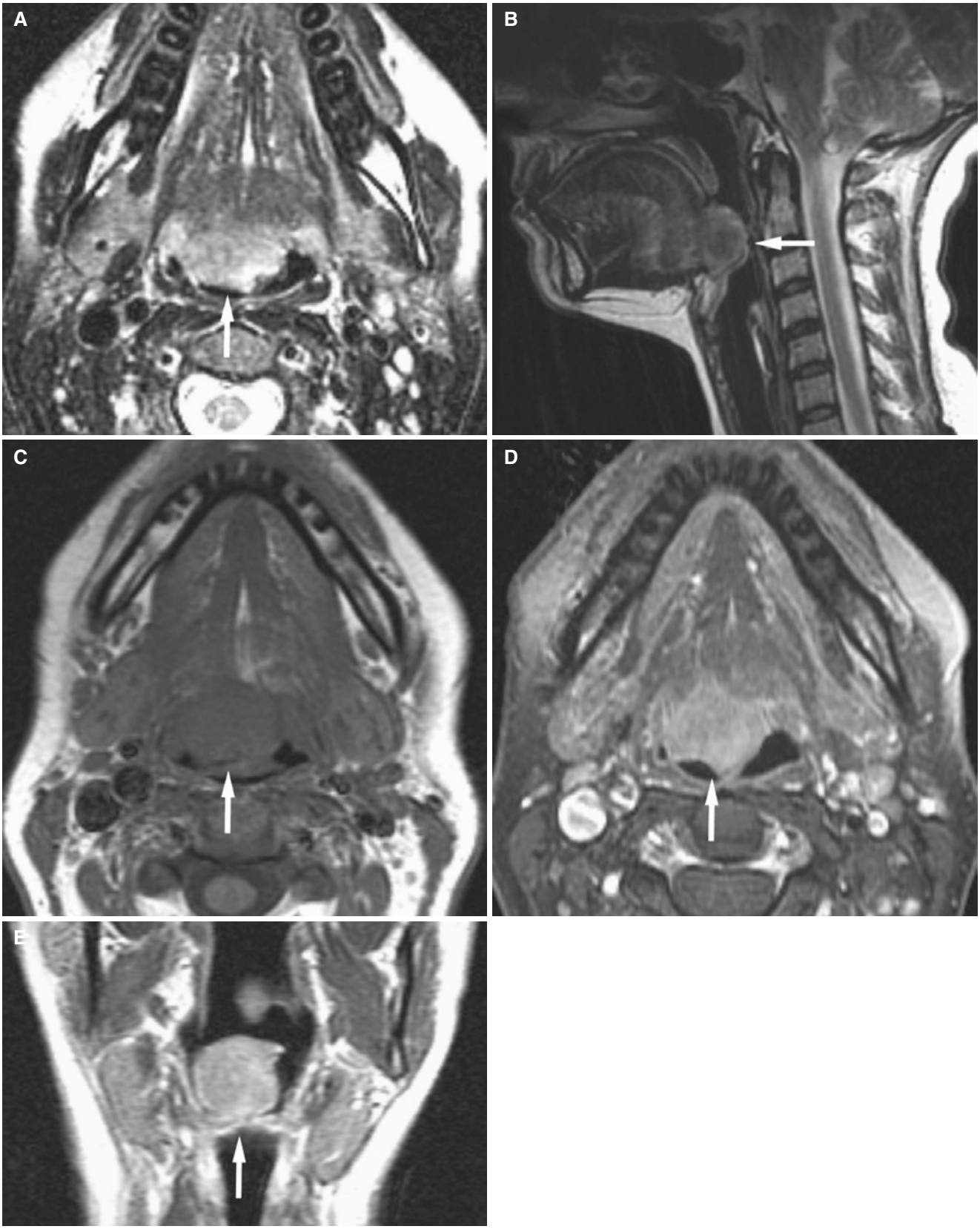

Fig. 11.32 Clear-cell carcinoma of tongue base; 47-year-old female with hemoptysis, presents with lump in vallecula, "vascular granuloma" clinically. (**A**) Axial T2-weighted MRI shows heterogeneous high-signal mass in posterior portion of tongue (*arrow*). (**B**) Sagittal T2-weighted MRI shows mass in tongue base (*arrow*). (**C**) Axial T1-weighted MRI shows low- to intermediate-signal mass (*arrow*). (**D**) Axial T1-weighted post-Gd MRI shows diffuse, mild contrast enhancement of tumor (*arrow*). (**E**) Coronal T1-weighted post-Gd MRI confirms contrast enhancement of tumor (*arrow*)

11.13 Adenoid Cystic Carcinoma

Fig. 11.33

11.13.1 Definition

Malignant epithelial tumor with various histologic features showing three growth patterns: glandular (cribriform), tubular, or solid.

11.13.2 Clinical Features

- Painless mass, slowly growing
- Seldom regional lymph node metastases, in contrast to squamous cell carcinoma
- In oral cavity usually in palate (minor salivary glands)

11.13.3 Imaging Features

- Cannot be distinguished from squamous cell carcinoma
- Perineural tumor extension is however typical

11.14 Lymphoma

Figs. 11.34, and 11.35

11.14.1 Definition

Malignant tumor of lymphatic tissue; a number of different types.

11.14.2 Clinical Features

- Both Hodgkin's and non-Hodgkin's lymphoma occur in the maxillofacial area, most frequently presenting with lymph node enlargement
- Non-Hodgkin's lymphoma more frequently involves extranodal sites

11.14.3 Imaging Features

- Cannot distinguish non-Hodgkin's and Hodgkin's disease in the head and neck area based on imaging findings of lymph nodes
- Well-defined or ill-defined unspecified mass, either enhancing or not

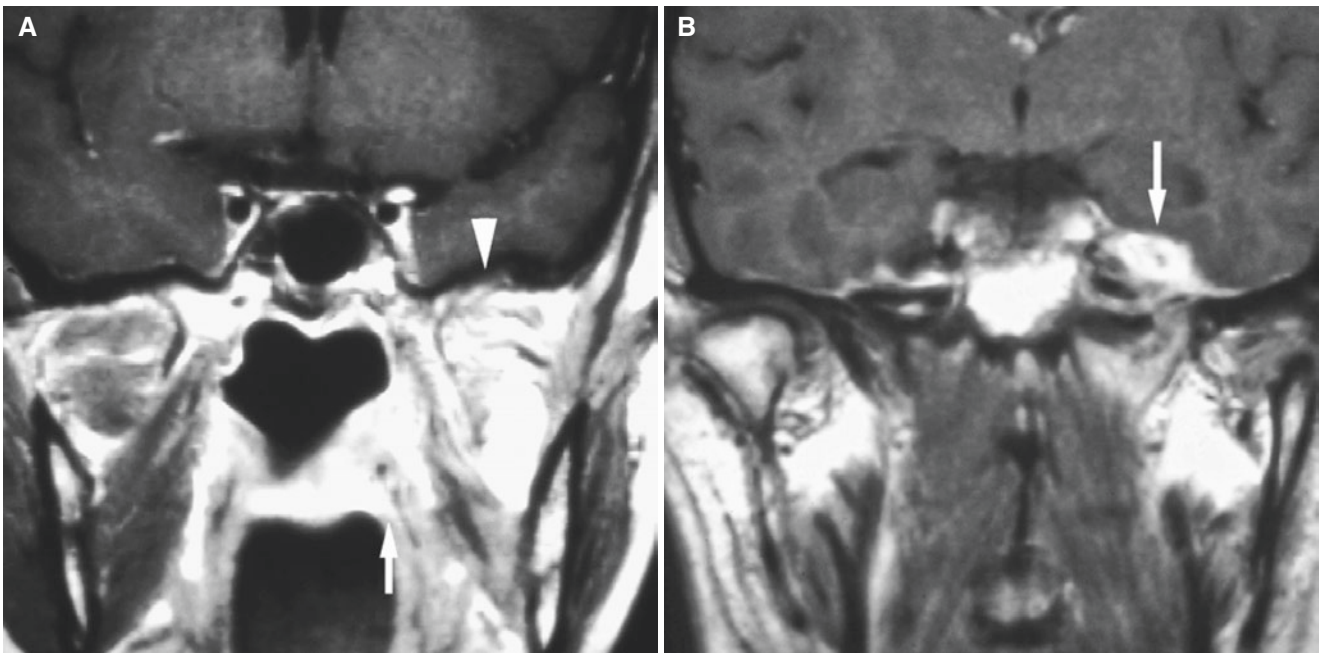

Fig. 11.33 Adenoid cystic carcinoma of epipharynx with intracranial spread; 50-year-old female treated with irradiation 5 years previously, now with recurrence. (**A**) Coronal T1-weighted post-Gd MRI shows contrast-enhancing tumor recurrence in epipharynx wall (*arrow*) and atrophy of medial and lateral pterygoid muscles (*arrowhead*). (**B**) Coronal T1-weighted post-Gd MRI shows tumor growing intracranially (*arrow*) through oval foramen, compressing mandibular nerve

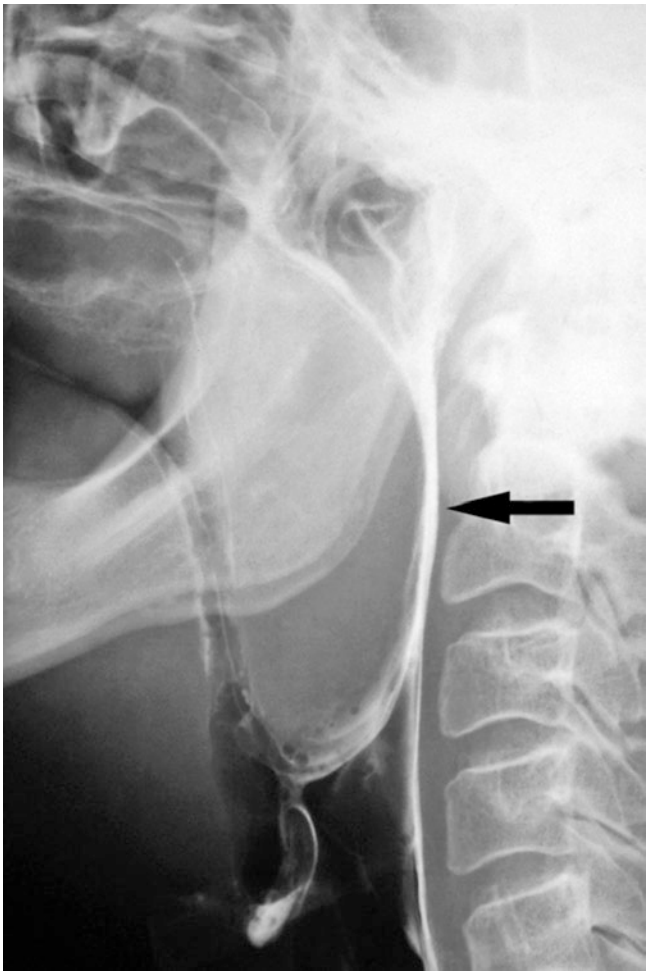

Fig. 11.34 Oropharyngeal non-Hodgkin's lymphoma; 62-year-old male with swallowing and breathing problems. Lateral view with contrast material in nose shows large soft palate mass (*arrow*) extending downward to level of top of epiglottic cartilage

Fig. 11.35 Oroparapharyngeal non-Hodgkin's lymphoma; 88-year-old female with a 3-year history of lymphoma with radiation therapy to the neck and right axilla; metastatic disease suspected to oral cavity. (**A**) Axial post-contrast CT image shows large lobulated nonenhancing parapharyngeal mass that occludes most of the pharynx and oral cavity (*arrow*). Imaging cannot determine if the intraparotid lymph node is involved with lymphoma

Suggested Reading

Al-Ghambi S, Black MJ, Lafond G (1992) Extracranial head and neck schwannomas. J Otolaryngol 21:186–188

Allard RHB (1982) The thyroglossal duct cyst. Head Neck Surg 5:134–146

Aspestrand F, Kolbenstvedt A (1987) Calcifications of the palatine tonsillary region: CT demonstration. Radiology 165:479–480

Braun IF, Hoffman JC Jr, Reede D et al (1984) Computed tomography of the buccomasseteric region: 2. Pathology. AJNR Am J Neuroradiol 5:611–616

Bredesen K, Aalokken TM, Kolbenstvedt A (2001) CT of the oral vestibule with distended cheeks. Acta Radiol 42:84–87

Dolata J (1994) Thyroglossal cyst in the floor of mouth: an unusual location. Otolaryngol Head Neck Surg 110:580–583

Flickinger FW, Lozano RL, Yuh WT et al (1989) Neurilemmoma of the tongue: MR findings. J Comput Assist Tomogr 13:886–888

Fujimura N, Enomoto S (1992) Lipoma of tongue with cartilaginous changes: case report and review of literature. J Oral Maxillofac Surg 50:1015–1017

Gallo WJ, Moss M, Shapiri DN et al (1977) Neurilemmoma: review of the literature and report of five cases. J Oral Surg 35:235–236

Harnsberger HR, Wiggins RH, Hudgins PA, Michel MA, Swartz J, Davidson HC et al (2004) Section 2: nose and sinus. In: Diagnostic imaging head and neck. Amirsys, Salt Lake City

Hopp E, Mortensen B, Kolbenstvedt A (2004) Mylohyoid herniation of the sublingual gland diagnosed by magnetic resonance imaging. Dentomaxillofac Radiol 33:351–353

Johnson JT (1990) A surgeon looks at cervical lymph nodes. Radiology 145:607–610

King RC, Smith BR, Burk JL (1994) Dermoid cysts in the floor of the mouth. Oral Surg Oral Med Oral Pathol 78:567–576

Koontz NA, Seltman TA, Kralik SF, Mosier KM, Harnsberger HR (2016) Classic signs in head and neck imaging. Clin Radiol 71:1211–1222

Kula K, Hale LN, Ghoneima A, Tholpady S, Starbuck JM (2016) Cone-beam computed tomography analysis of mucosal thickening in unilateral cleft lip and palate maxillary sinuses. Cleft Palate Craniofac J 53:640–648

Lindberg R (1972) Distribution of cervical lymph node metastases from squamous cell carcinoma of the upper respiratory and digestive tracts. Cancer 29:1446–1449

Misra SR, Gopal M, Mohanty N, Rastogi V (2015) Nasoalveolar cyst: an enigma for the dentist. BMJ Case Rep 2015:208402. doi:10.1136/brc-2014-208402

Mukherji SK (2003) Pharynx. In: Som PM, Curtin HD (eds) Head and neck imaging, 4th edn. Mosby, St. Louis, pp 1466–1520
New GB (1947) Congenital cysts of the tongue, the floor of the mouth, the pharynx and the larynx. Arch Otolaryngol 45:145–158
Sahoo NK, Choudhary AK, Srinivas V, Tomar K (2015) Dermoid cysts of maxillofacial region. Med J Armed Forces India 71(Suppl 2):S389–S394. doi:10.1016/mjafi.2013.11.004
Schellhas KP (1989) MR imaging of muscles of mastication. AJR Am J Roentgenol 153:847–855
Sethukumar P, Taghi A, Kuchai R (2015) A rare case of bilateral nasolabial cysts. BMJ Case Rep 2015:203543. doi:10.1136/bcr-2014-203543
Smoker WRK (2003) The oral cavity. In: Som PM, Curtin HD (eds) Head and neck imaging, 4th edn. Mosby, St. Louis, pp 1377–1464
Som PM (1987) Lymph nodes of the neck. Radiology 165:593–600
Som PM, Scherl MP, Rao VM et al (1986) Rare presentations of ordinary lipomas of head and neck: a review. AJNR Am J Neuroradiol 7:657–664
Thomas JR (1979) Thyroglossal duct cysts. Ear Nose Throat J 58:512–514
Tryhus MR, Smoker WRK, Harnsberger HR (1990) The normal and diseased masticator space. Semin Ultrasound CT MR 11:476–485
Vardas E, Stavrou E, Leventis M, Chatzistamou I, Iatrou I, Alexandridis C (2011) Intraosseous mandibular venous malformation. J Craniofac Surg 22(6):e44–e47. doi:10.1097/SCS.0b013e318231e23e
Worley CM, Laskin DM (1993) Coincidental sublingual and submental epidermoid cysts. J Oral Maxillofac Surg 51:787–790
Yasumoto M, Shibuya H, Takeda M, Korenaga T (1995) Squamous cell carcinoma of the oral cavity: MR findings and value of T1- versus T2-weighted fast spin-echo images. AJR Am J Roentgenol 164:981–987

Salivary Glands

12

Abstract

This chapter illustrates nonneoplastic conditions; infection/inflammation, sialolithiasis, Sjögren's syndrome, benign lymphoepithelial cysts associated with HIV-AIDS, and ranula, benign tumors; pleomorphic adenoma, Warthin's tumor, and hemangioma, and malignant tumors; lymphoma and carcinomas; mucoepidermoid carcinoma, acinic cell carcinoma, adenocarcinoma, adenoid cystic carcinoma, and carcinoma ex pleomorphic adenoma.

12.1 Introduction

Salivary gland conditions are probably more diverse than those of many other organ systems: congenital, obstructive, infectious, inflammatory, systemic, and neoplastic. The frequency of tumors is however less than 3% of all tumors. On the other hand, although advanced soft-tissue imaging with CT and MRI are used, the radiologic differentiation between benign and malignant diseases remains difficult. The more common obstructive conditions are of particular interest for those working in the dental field, because conventional examination should be the initial radiologic evaluation for patients with suspected stones. Those working with saliva should also be the first to notice any reduced salivation that may have many causes and a significant impact on teeth conditions.

This chapter illustrates a number of different conditions, some common and others rare. The intention is not to be complete, but rather to show a variety of salivary gland conditions of relevance to the maxillofacial radiologist.

12.2 Nonneoplastic Conditions

A number of conditions may occur in the salivary glands.

12.3 Infection/Inflammation

Figs. 12.1, 12.2, 12.3, 12.4, 12.5, and 12.6

12.3.1 Definition

Sialoadenitis: infection/inflammation of the gland.

Sialodochitis: infection/inflammation of the duct.

12.3.2 Clinical Features

- Acute sialoadenitis:
  - Painful swelling, with or without pus
  - Most common in the parotid gland, bilateral or unilateral
  - Neonates or elderly in particular
  - Regional lymphadenopathy, fever, malaise

In collaboration with A. Kolbenstvedt and H.-J. Smith

T.A. Larheim, P.-L.A. Westesson, *Maxillofacial Imaging*, https://doi.org/10.1007/978-3-319-53319-3_12

  - Acute exacerbation of chronic sialoadenitis
  - Bacterial infection; *Staphylococcus aureus* most common, local, unilateral, suppurative, diffuse (cellulitis) or localized (abscess)
  - Retrograde, calculus etiology
  - Viral infection; systemic, bilateral (mumps)
- Chronic sialoadenitis:
  - Parotid or submandibular gland; rarely in sublingual gland
  - Intermittent swelling and tenderness
  - Vague or no symptoms
  - Recurrent bacterial infection
  - Autoimmune diseases
  - Prior radiation therapy
  - Treatment of thyroid cancer with radioactive iodine
  - Retrograde, calculus etiology

12.3.3 Imaging Features

- Sialoadenitis:
  - Enlargement (diffuse) of gland, increased density, enhancing with contrast
  - Associated cellulitis; streaking (stranding) in subcutaneous fat, thickened platysma
  - Abscess; localized low-density area surrounded by enhanced rim
  - Sialolithiasis
  - T1-weighted MRI: enlarged gland, low signal, diffuse or localized (abscess)
  - T2-weighted MRI: enlarged gland, high signal, diffuse or localized (abscess); may also be low signal depending on whether edema or cellular infiltration dominates
  - T1-weighted post-Gd MRI: moderate, diffuse contrast enhancement or only enhanced peripheral rim (abscess)
- Sialodochitis:
  - Dilated duct, usually with single or multiple strictures ("string of sausages")
- Sialography:
  - Conventional technique superior to other imaging methods to demonstrate subtle anatomy of salivary duct system
  - MR sialography can be done with heavily T2-weighted images without injection of contrast medium. This visualizes the main parotid (Stensen's) duct with secondary ducts and submandibular duct but not finer ducts as seen with conventional sialography. However, MR sialography may be useful in cases in which cannulation of the duct cannot be performed

Fig. 12.1 Normal parotid glands and accessory parotid glands; 65-year-old male. Axial post-contrast CT image shows normal but large parotid glands bilaterally. Note accessory parotid glands bilaterally and superficially to masseter muscles

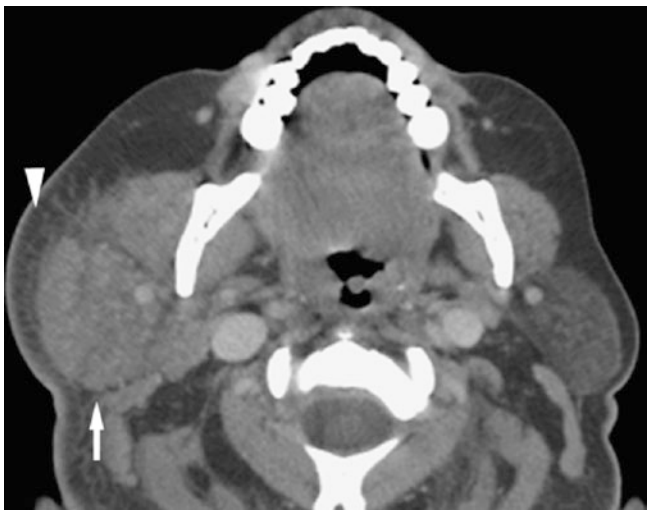

Fig. 12.2 Acute suppurative parotitis: 61-year-old female with past history of diabetes mellitus, chronic renal failure, coronary artery disease status after myocardial infarction and PTCA, stroke, hypertension, hyperlipidemia, hypothyroidism, and congestive heart failure, now presenting with an acute swelling of the right side of the face in the setting of known *Staphylococcus* bacteremia. Axial post-contrast CT image shows enlarged right parotid gland with increased density (*arrow*), with streaking opacities in overlying fat (*arrowhead*)

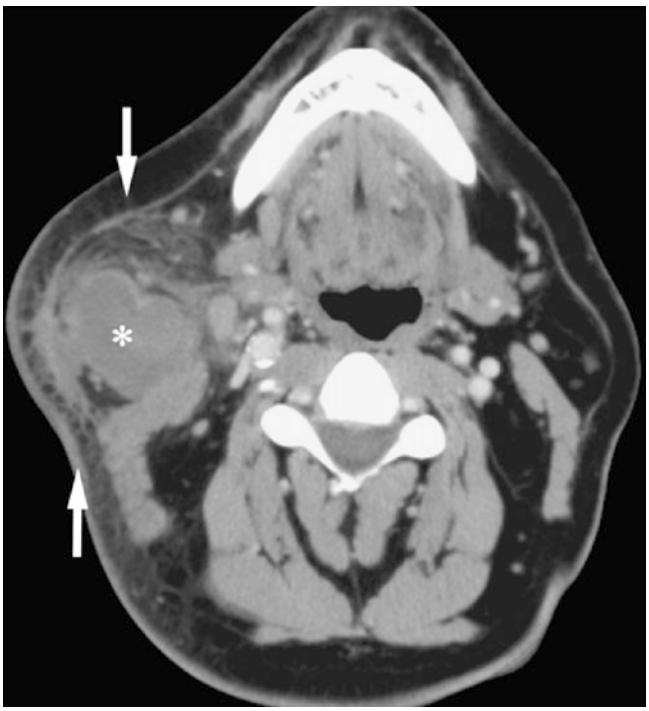

Fig. 12.3 Parotid abscess; 52-year-old male with non-resolving right parotitis. Axial post-contrast CT image shows homogeneous density with contrast-enhancing rim consistent with abscess in parotid gland (*asterisk*) with fat stranding and thickening of platysma (*arrows*)

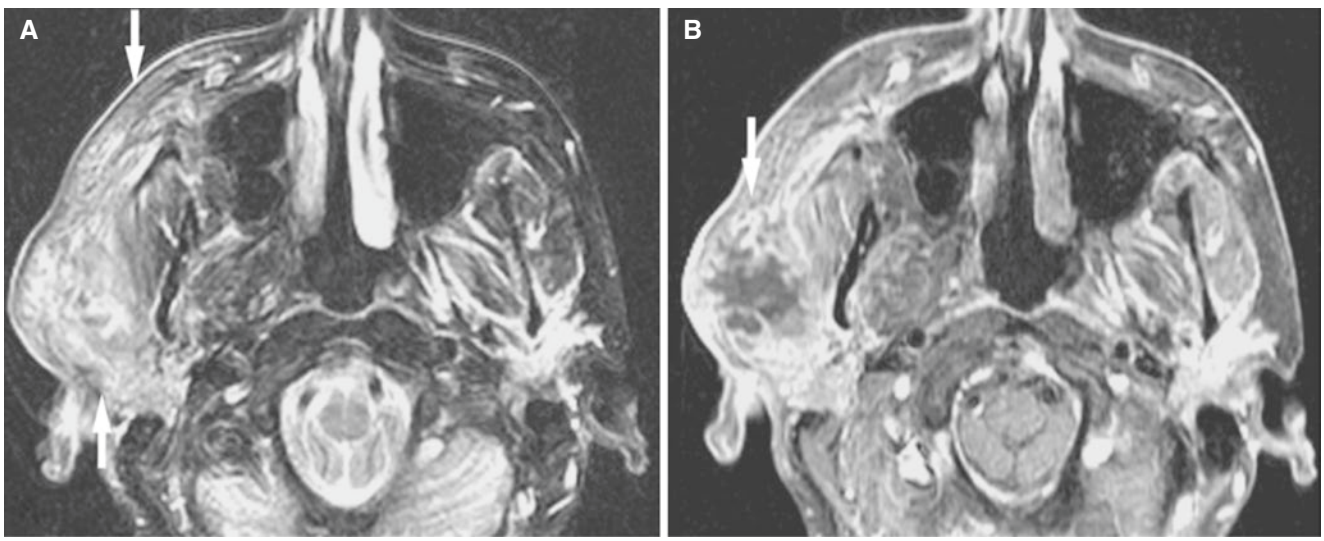

Fig. 12.4 Abscess and cellulitis in parotid region; 52-year-old female with right parotid swelling and pain and clinical suspicion of abscess. (**A**) Axial T2-weighted fat-suppressed MRI shows diffuse high signal in the right lateral half of the face consistent with subcutaneous edema and cellulitis (*arrows*). (**B**) Axial T1-weighted fat-suppressed post-Gd MRI shows low-signal area surrounded by irregular contrast-enhancing rim consistent with abscess (*arrow*). Note also diffuse enhancement in subcutaneous fat extending to the anterior portion of the maxilla. Abscess was surgically drained

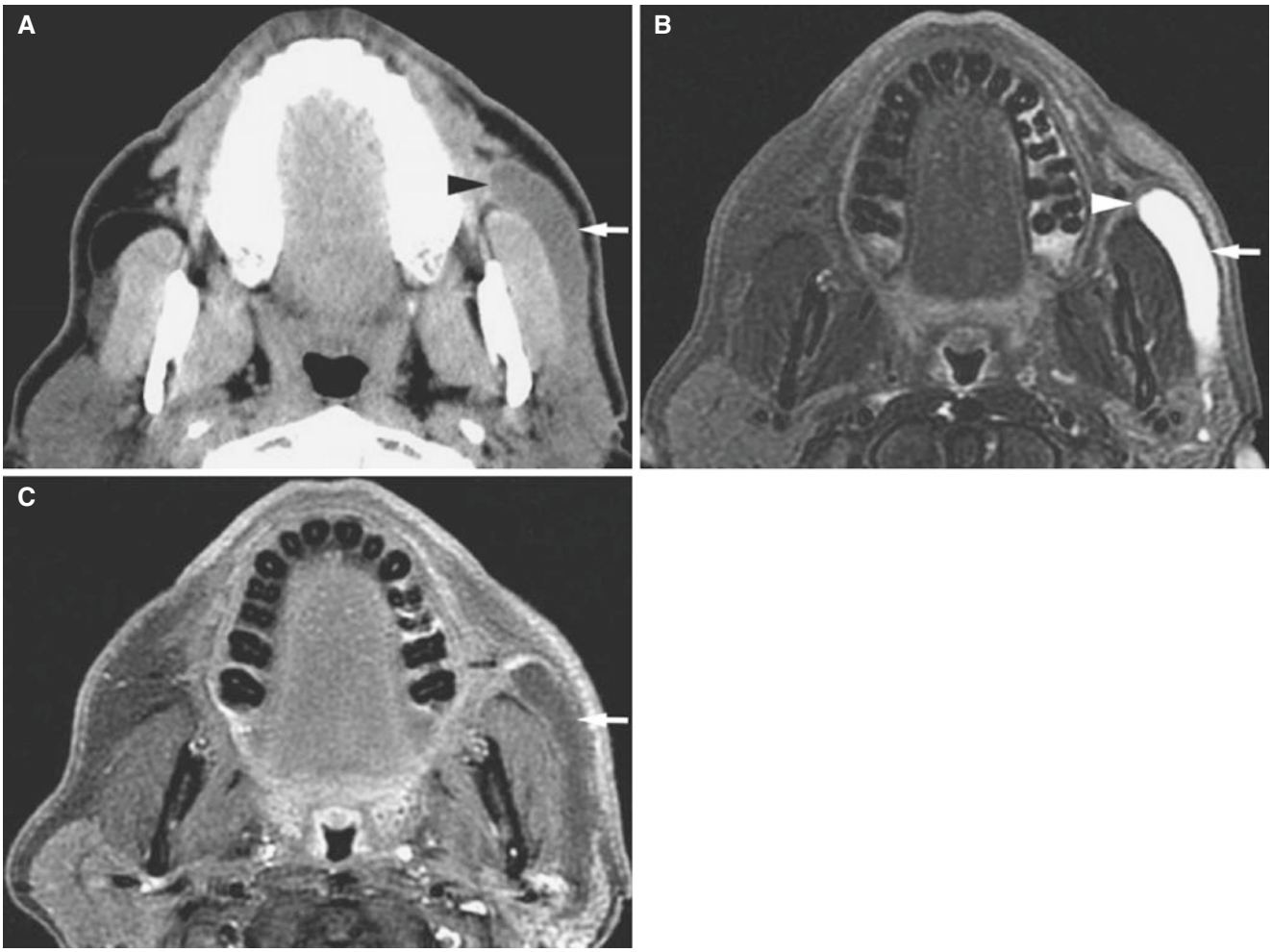

Fig. 12.5 Stenosis and dilatation of Stensen's duct but no stones; 56-year-old male with a remote history of injury to the left cheek after which he developed intermittent swelling (gland itself was not enlarged or abnormal on CT or MRI imaging). On clinical examination there was scarring at the orifice of the left Stensen's duct. (**A**) Axial post-contrast CT shows dilated Stensen's duct (*arrow*) with closed orifice (*arrowhead*). (**B**) Axial T2-weighted fat-suppressed MRI confirms dilated duct (*arrow*) and closed orifice (*arrowhead*). (**C**) Axial T1-weighted fat-suppressed post-Gd MRI shows no contrast enhancement of dilated duct (*arrow*)

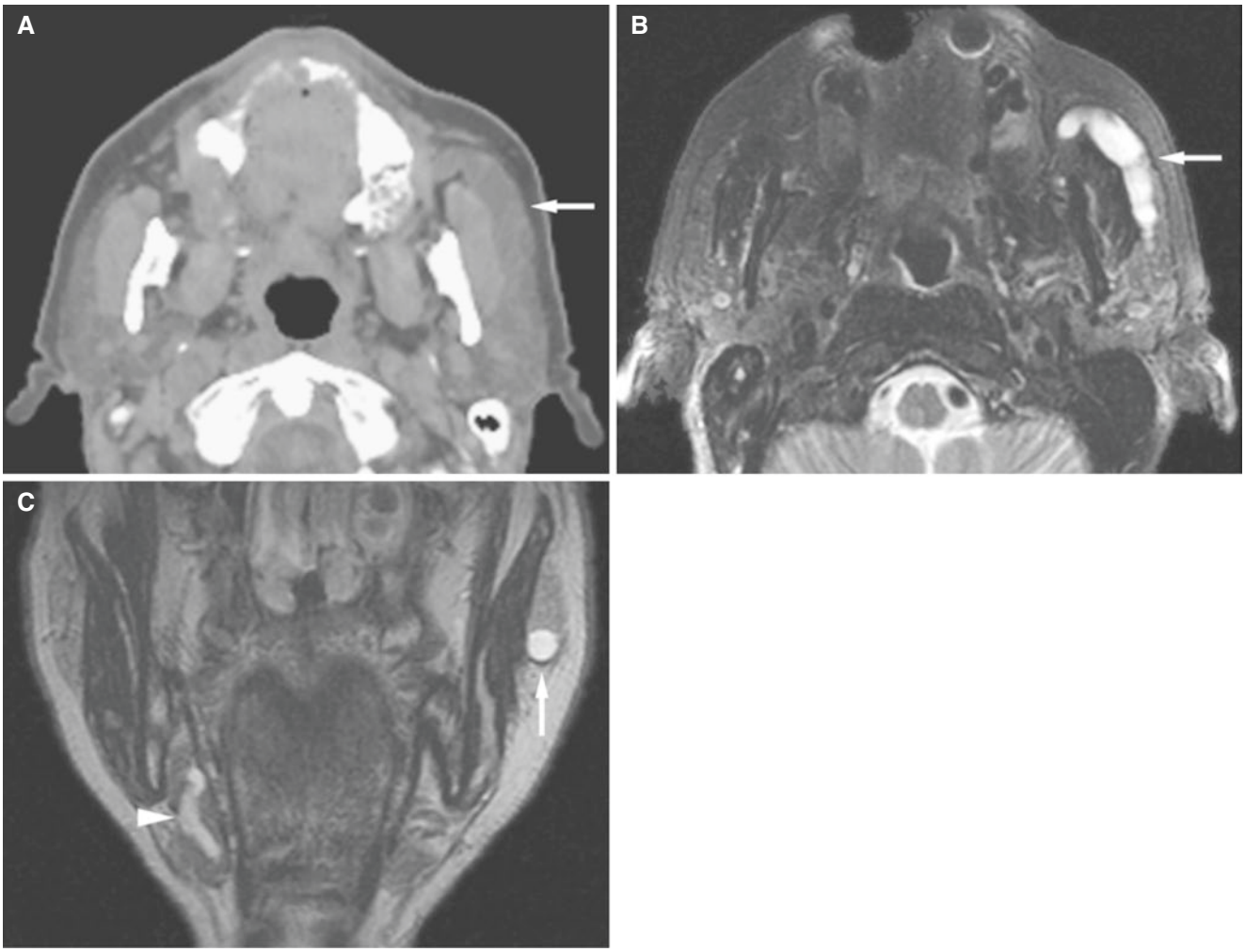

Fig. 12.6 Dilated Stensen's duct and Wharton's duct; 76-year-old male with enlarged right submandibular salivary gland and question of possible tumor (no calculi or gland abnormalities except slightly enlarged right submandibular gland found on CT and MRI imaging). (**A**) Axial post-contrast CT image shows dilated left Stensen's duct (*arrow*). (**B**) Axial T2-weighted MRI confirms dilated duct (*arrow*). (**C**) Coronal T2-weighted MRI confirms dilated Stensen's duct (*arrow*) and shows prominent right Wharton's duct as well (*arrowhead*)

12.4 Sialolithiasis

Figs. 12.7, 12.8, 12.9, 12.10, 12.11, 12.12, 12.13, 12.14, 12.15, 12.16, and 12.17

12.4.1 Definition

Formation of sialoliths (calculi, stones) in ducts or secretary portions of the salivary glands.

12.4.2 Clinical Features

- Small stones may disappear spontaneously
- Small stones may be symptomatic; large stones may be asymptomatic
- Leads to reduced salivary flow, hyposalivation
- May result in retrograde infection; an abscess or more commonly, a chronic recurrent sialoadenitis with intermittent swelling and tenderness/pain, usually at meals
- Total obstruction will eventually lead to parenchyma atrophy

12.4.3 Imaging Features

- Round or oval calcifications typical; 10–20% are radiolucent
- Most stones are solitary; about 25% multiple
- 80–90% in submandibular gland or Wharton's duct; about 85% in duct

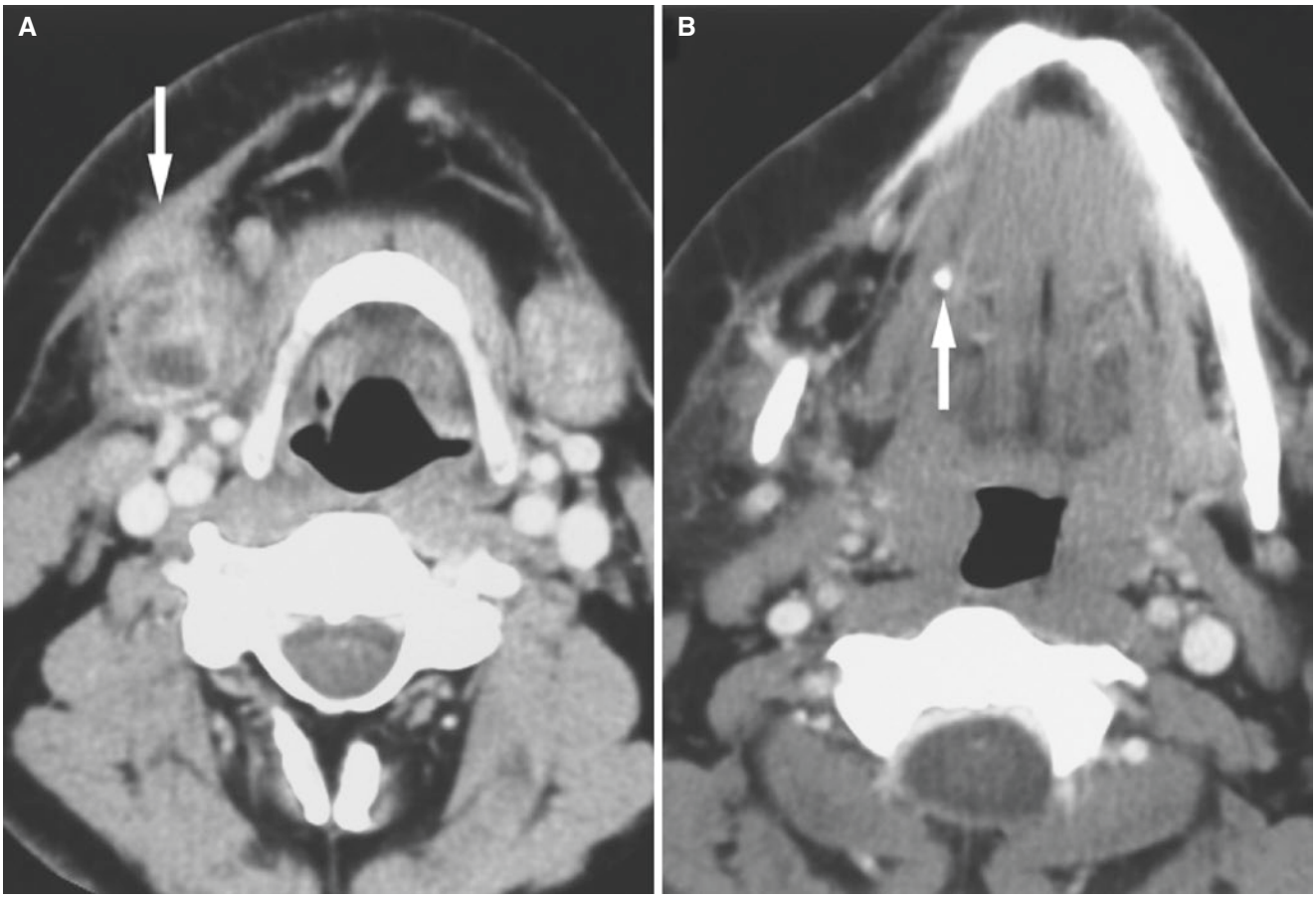

Fig. 12.7 Submandibular gland multilocular abscess due to stone in Wharton's duct; 69-year-old male with intermittent submandibular swelling and tenderness. (**A**) Axial post-contrast CT shows enlarged submandibular gland with abscess (*arrow*) and thickening of the platysma. (**B**) Axial post-contrast CT image shows stone in submandibular duct (*arrow*)

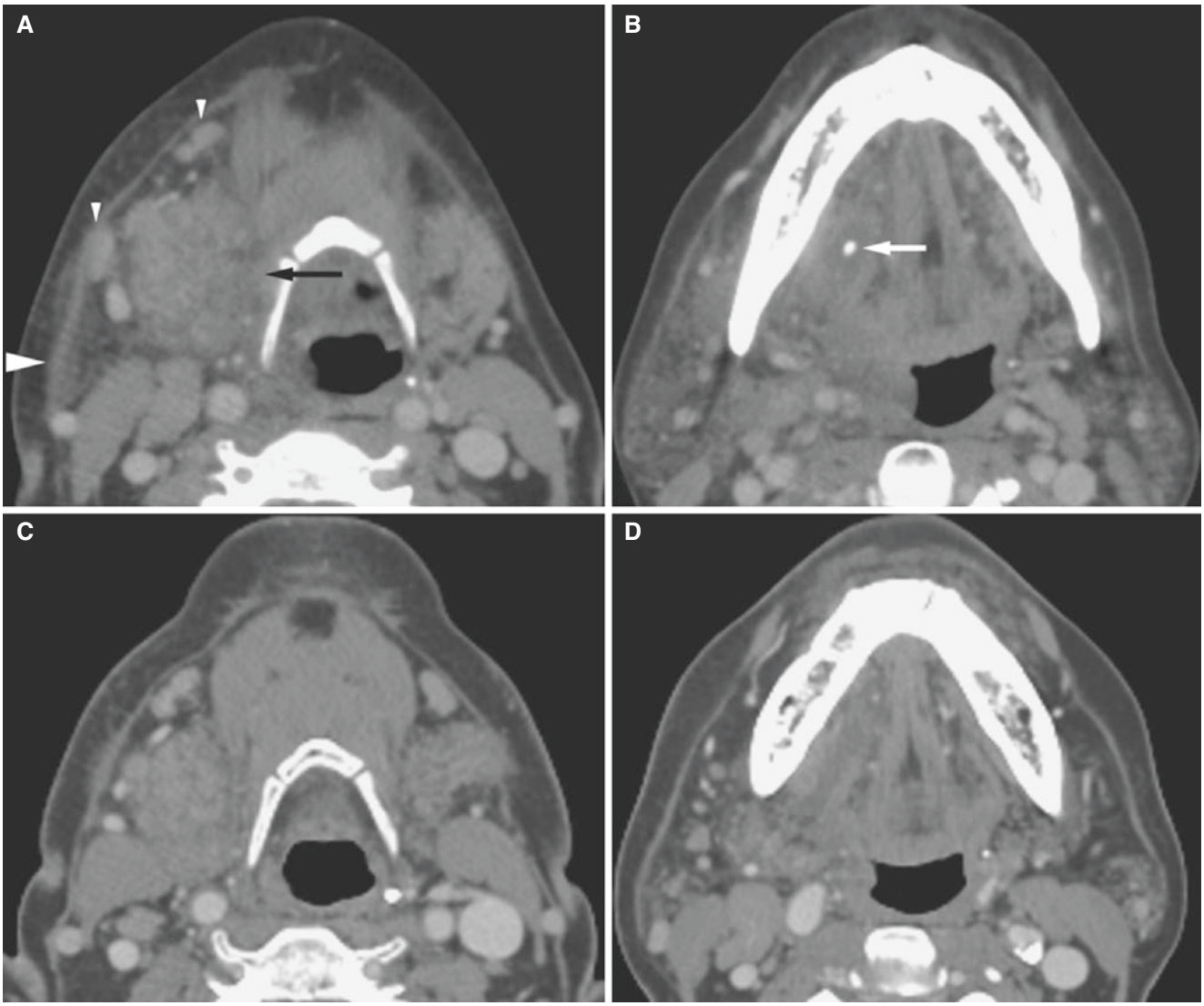

Fig. 12.8 Submandibular sialoadenitis with cellulitis due to Wharton's duct stone that was spontaneously expelled within 2 days; 59-year-old female with right mandibular swelling and pain that reduced significantly after stone was expelled intraorally. (**A**) Axial post-contrast CT image shows diffuse enlargement of the right submandibular gland (*arrow*) with thickened platysma (*large arrowhead*), stranding in overlying fat, and right small submandibular lymphadenopathy (*small arrowheads*). (**B**) Axial post-contrast CT image shows small stone in Wharton's duct (*arrow*). (**C**) Axial post-contrast CT image 2 days later shows significantly reduced swelling. (**D**) Axial post-contrast CT image 2 days later shows no evidence of stone

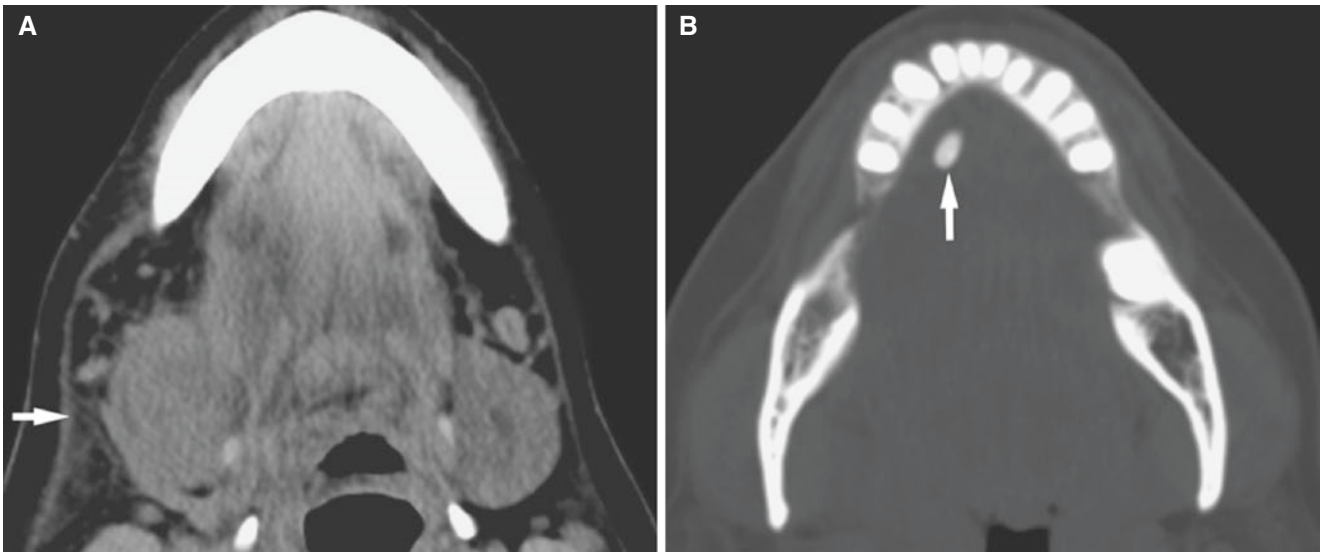

Fig. 12.9 Submandibular sialoadenitis due to stone in distal duct; 59-year-old female with right submandibular swelling. (**A**) Axial post-contrast CT image shows enlarged submandibular gland with stranding and reticulation of periglandular fat (*arrow*). (**B**) Axial CT image shows stone in the anterior part of Wharton's duct (*arrow*)

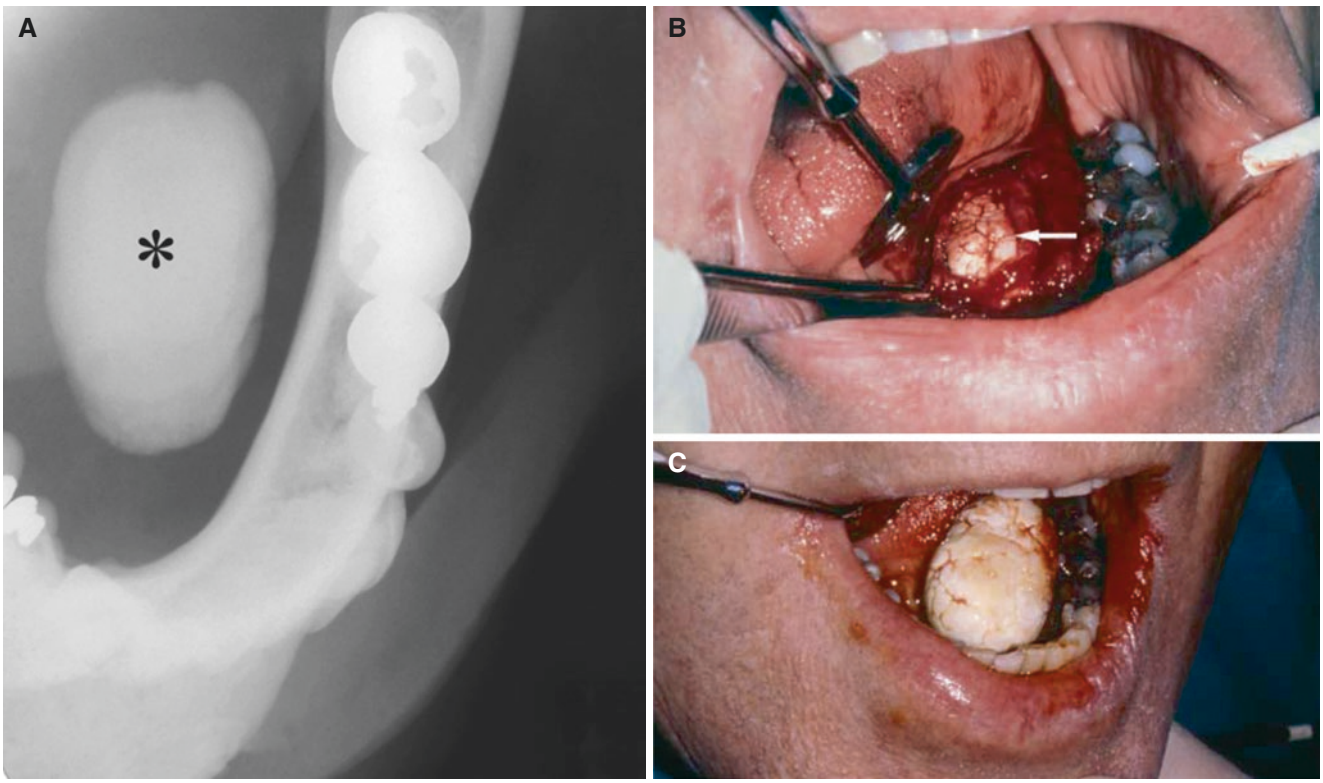

Fig. 12.10 Submandibular duct stone; 55-year-old male with incidental finding of painless swelling in the floor of the mouth and no history of pain or variable swelling. (**A**) Intraoral occlusal view shows large stone in Wharton's duct (*asterisk*). (**B**) Clinical photograph during surgery shows stone after surgical incision (*arrow*). (**C**) Clinical photograph of "released" stone (about 28 mm long)

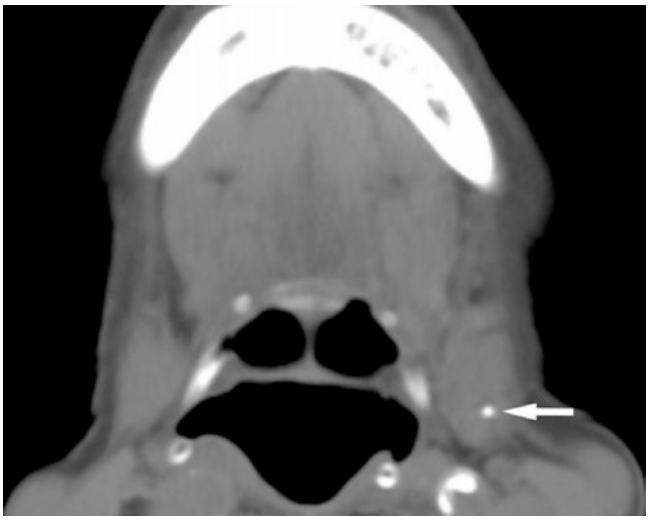

Fig. 12.11 Submandibular gland stone; 86-year-old female with submandibular pain. Axial post-contrast CT image shows small stone in the hilum of submandibular gland (*arrow*)

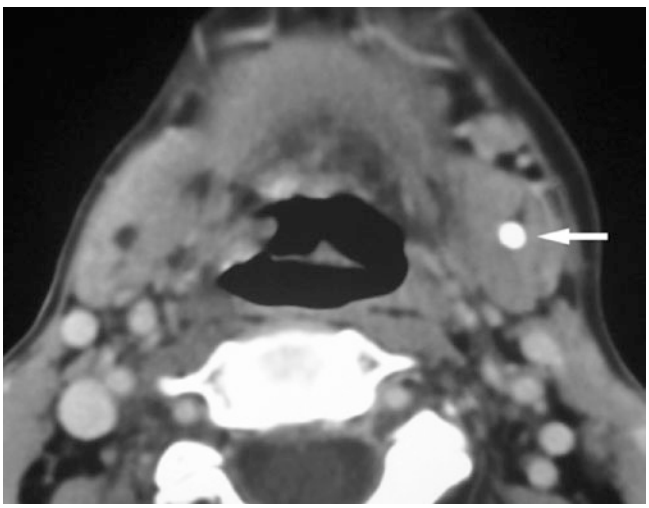

Fig. 12.12 Submandibular gland stone; 79-year-old female with left submandibular mass for about 2 months. Axial post-contrast CT image shows stone in the hilum of submandibular gland (*arrow*)

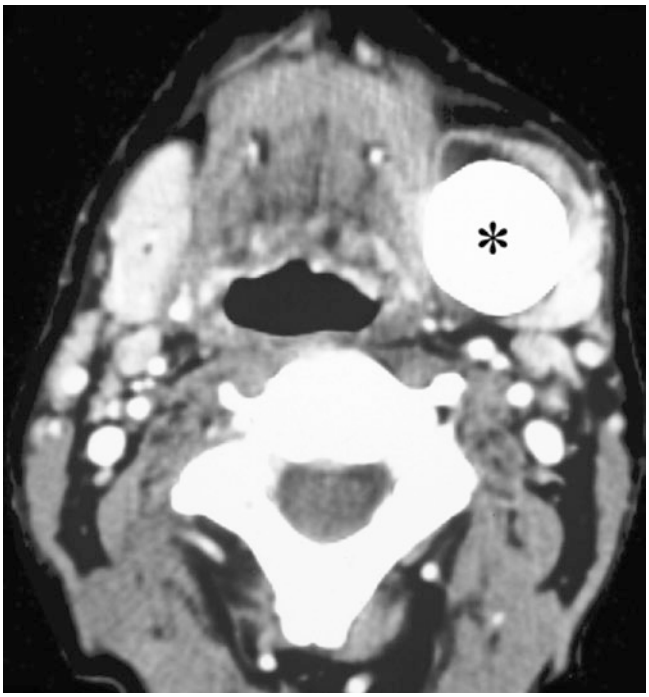

Fig. 12.13 Submandibular gland stone; 61-year-old male, heavy drinking smoker, with incidental finding of a hard submandibular mass, which had been painless for more than 10 years; question of oral cancer in soft palate. Axial post-contrast CT image shows large stone in submandibular gland (*asterisk*)

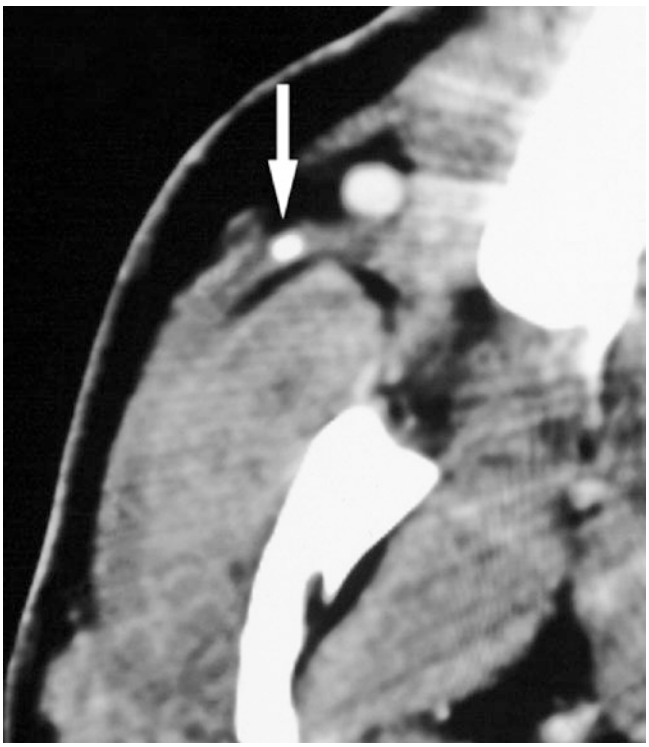

Fig. 12.14 Parotid duct stone; 59-year-old female with intermittent parotid gland swelling for about 6 months; question about parotitis or tumor. Axial post-contrast CT image shows stone in dilated Stensen's duct (*arrow*) and some enlarged and irregularly (scattered) enhanced gland consistent with chronic sialoadenitis

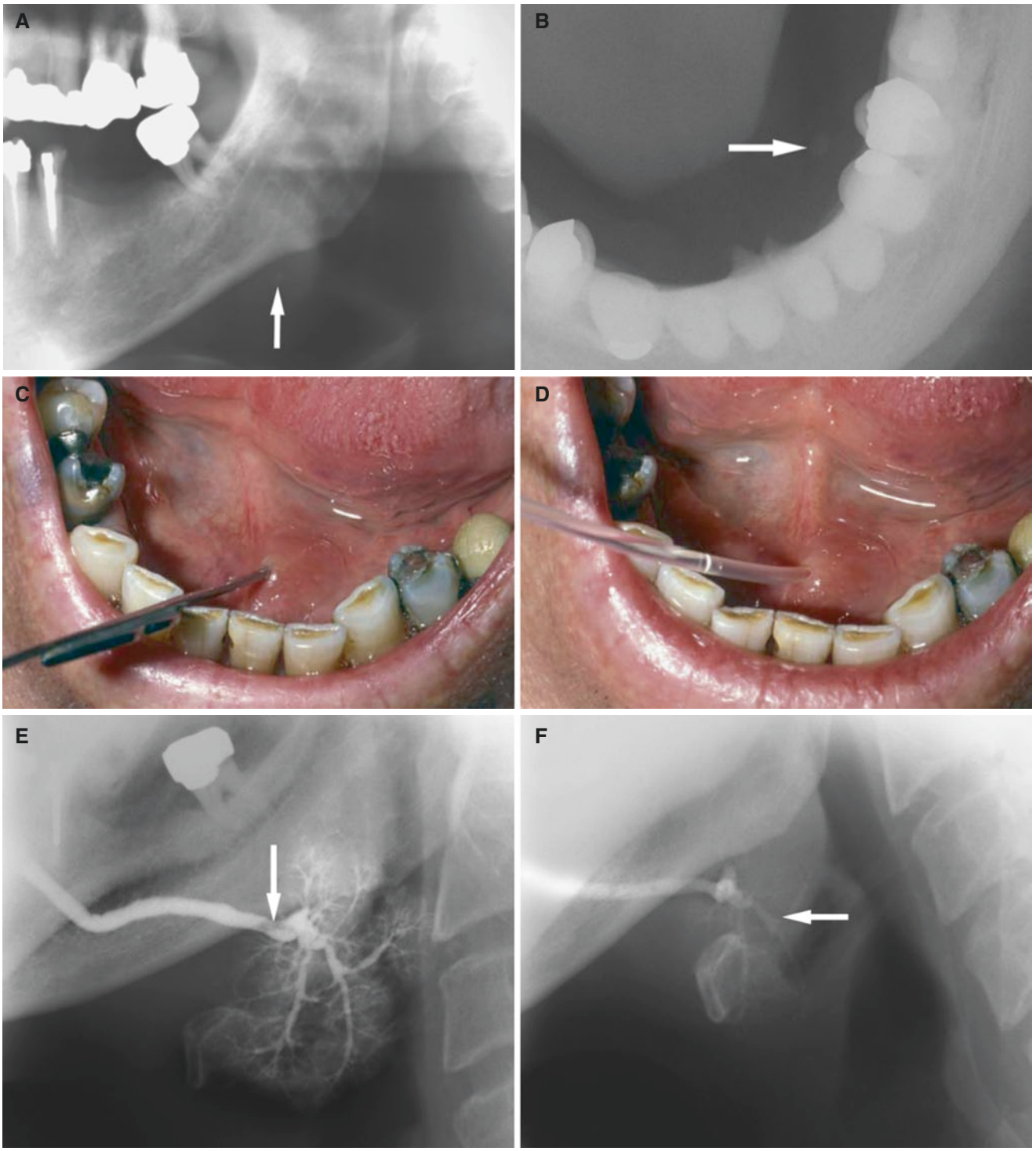

Fig. 12.15 Sialolithiasis and reduced salivary flow, but normal submandibular parenchyma and Wharton's duct sialogram; 72-year-old male with intermittent swelling related to meals for about 2 weeks. (**A**) Panoramic view shows a small stone in the posterior part of Wharton's duct (*arrow*). (**B**) Occlusal view shows another small stone in the anterior part of submandibular duct (*arrow*). (**C**) Clinical photograph shows silver probe to dilate submandibular duct. (**D**) Clinical photograph shows catheter in submandibular duct. (**E**) Submandibular sialogram shows normal parenchymatous filling with filling void from stone (*arrow*) but otherwise normal Wharton's duct. (**F**) Retention of contrast medium (*arrow*) after 15 min confirms reduced salivary flow

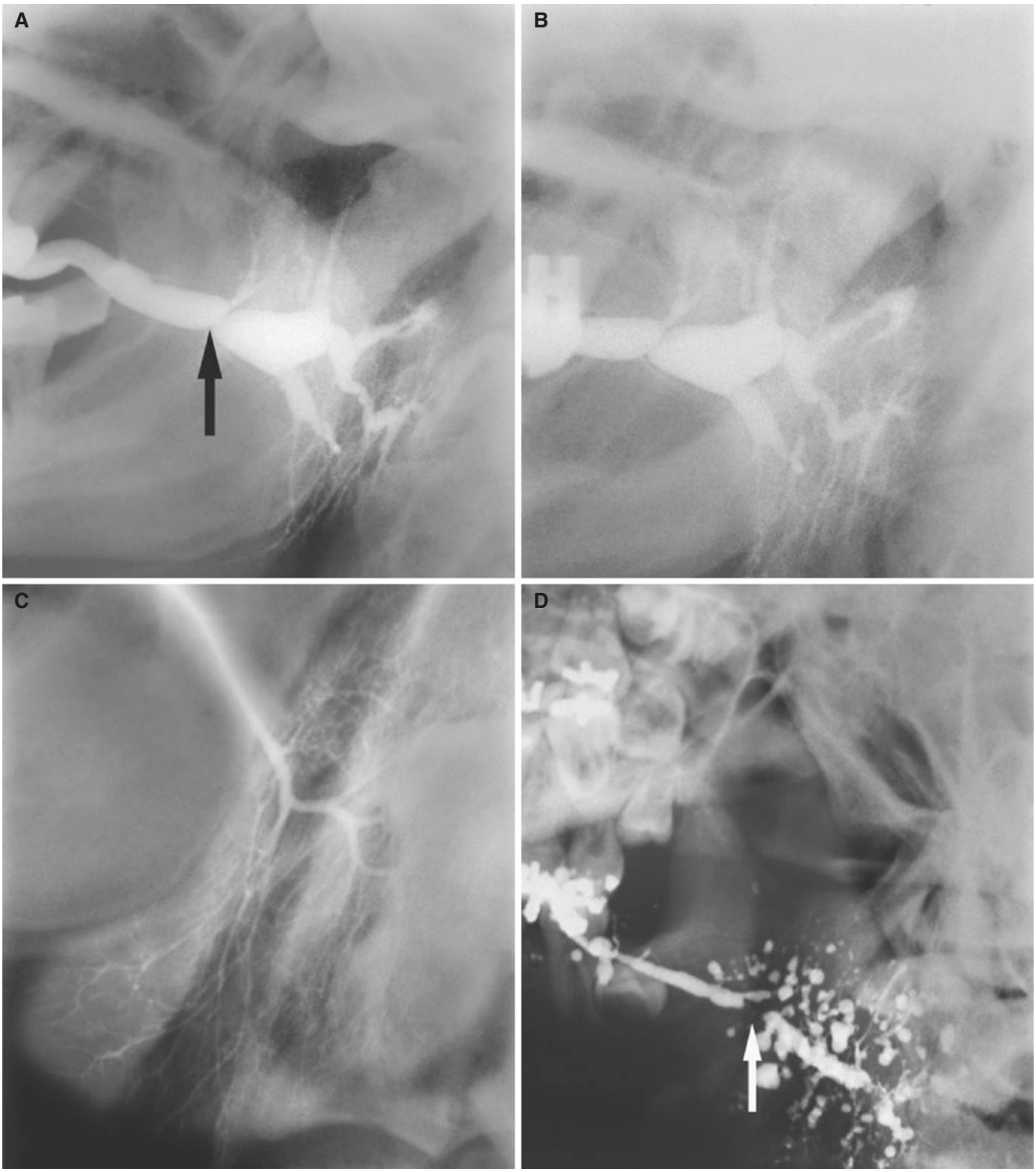

Fig. 12.16 Stenosis of Stensen's duct with reduced salivary flow, with sialodochitis and sialoadenitis; 47-year-old female with intermittent parotid swelling and discharge of mucus. (**A**) Parotid sialogram shows severely dilated duct with one stricture (*arrow*) and dilated intraglandular ducts with degenerated parenchyma (most of it not visualized); no calculi detected. (**B**) Parotid sialogram after 5 min shows severe retention of contrast medium, confirming reduced salivary flow. (**C**) Normal sialogram (another patient for comparison). (**D**) Advanced chronic sialoadenitis (another patient for comparison), with multiple scattered nonuniform collections of contrast medium (sialectasias) due to radiolucent stone, void of contrast filling (*arrow*)

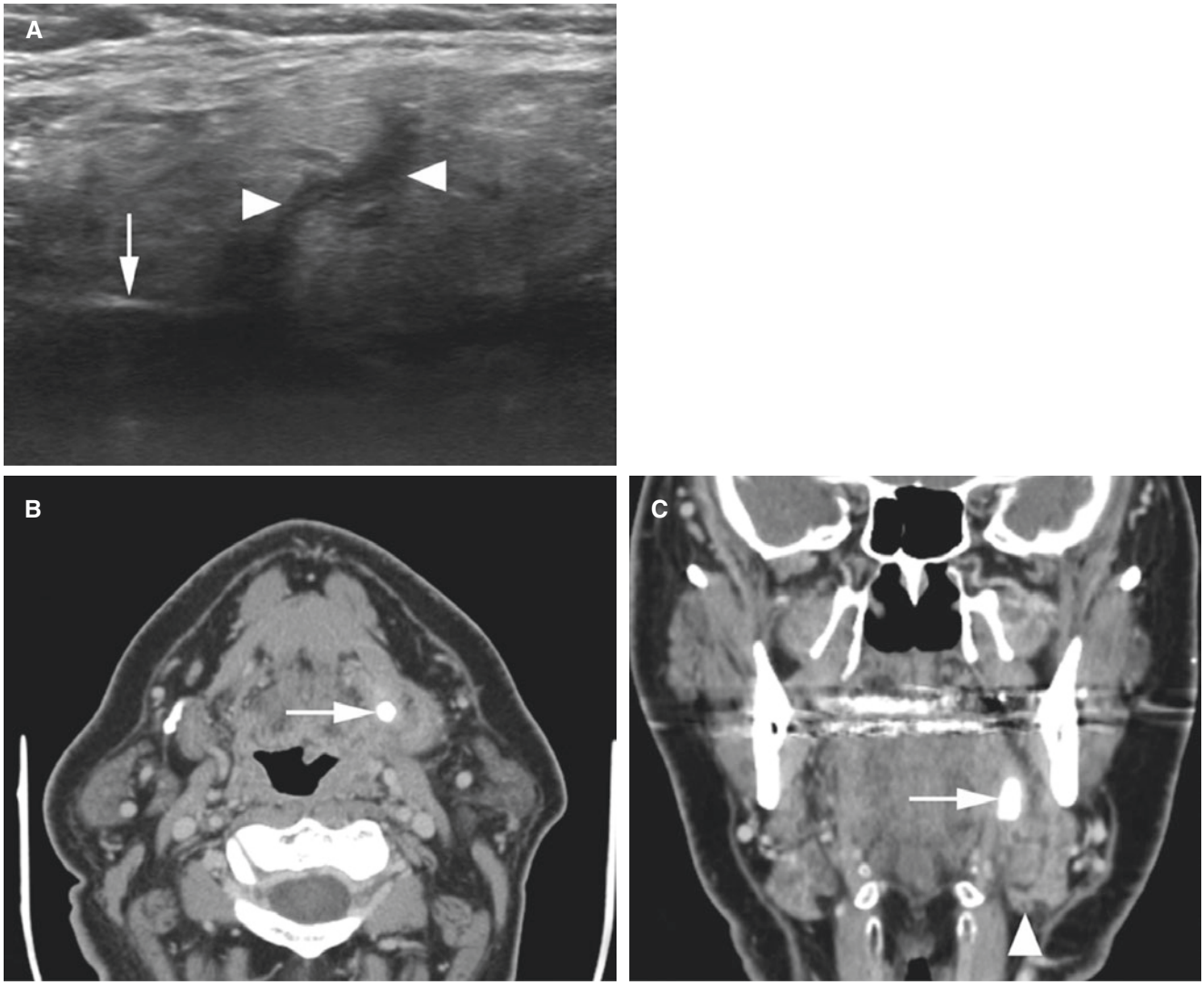

Fig. 12.17 Submandibular gland stone with sialodochitis and sialoadenitis; 60-year-old male with 5 days of painful swelling of the left submandibular region and increasing symptoms when eating. (**A**) US image of left submandibular gland shows widened intraglandular ducts (*arrowheads*) and a reflecting object (*arrow*) suspicious of stone. (**B**) Axial and **C** coronal CT images show a proximal stone (*arrow*) in the left Wharton's duct close to the submandibular gland which is swollen (compared to right side) with widened intraglandular ducts (*arrowhead*)

12.5 Sjögren's Syndrome

Figs. 12.18, 12.19, 12.20, and 12.21

12.5.1 Definition

Chronic, systemic autoimmune disease of exocrine glands characterized by periductal lymphocytic aggregates that extend into and destroy salivary and lacrimal parenchyma primarily, but also other exocrine glands.

May produce a localized parenchymal mass; benign lymphoepithelial lesion.

Diagnosis is based on a set of criteria: subjective symptoms of dry mouth and eyes, confirmation of xerostomia and xerophthalmia by clinical tests, serologic evidence of autoantibodies, and histologic evidence of salivary lymphocytic infiltration by labial or parotid biopsy.

12.5.2 Clinical Features

- Primary Sjögren's syndrome or secondary; associated with a connective tissue disease, usually rheumatoid arthritis
- Second in frequency to rheumatoid arthritis of all autoimmune diseases
- Predominantly women, 40–60 years of age

- Tender glandular swelling; recurrent episodes
- Nonpainful glandular enlargement
- Xerostomia and keratoconjunctivitis sicca
- Higher risk of developing non-Hodgkin's lymphoma, extranodal in particular

12.5.3 Imaging Features

- Parotid glands involved, but occasionally also submandibular glands
- Lymphadenopathy typically absent
- Earliest sialographic signs: multiple peripheral punctate collections (1 mm or less) of contrast medium with conventional sialography ("leafless fruit-laden tree") uniformly distributed in the gland, later with larger globular collections of contrast medium due to parenchyma destruction but characteristically with normal central duct system; contrast medium drains from the main ducts but remains in punctate and globular collections
- With reduced salivary flow, ascending superimposed sialoadenitis and sialodochitis will develop
- CT and MRI images normal in early disease, then variable enlargement
- T1-weighted MRI: multiple punctate changes of low density uniformly distributed in gland earliest signs, diagnostic for Sjögren's syndrome
- T2-weighted MRI: multiple punctate changes have high signal reflecting watery saliva
- Punctuate changes will progress to globular, cavitary, and destructive abnormalities
- At end stage a honeycomb appearance may develop, with multiple cystic lesions and abnormally dense parenchyma
- MR sialography has been found to correlate with conventional sialography and with labial biopsy findings

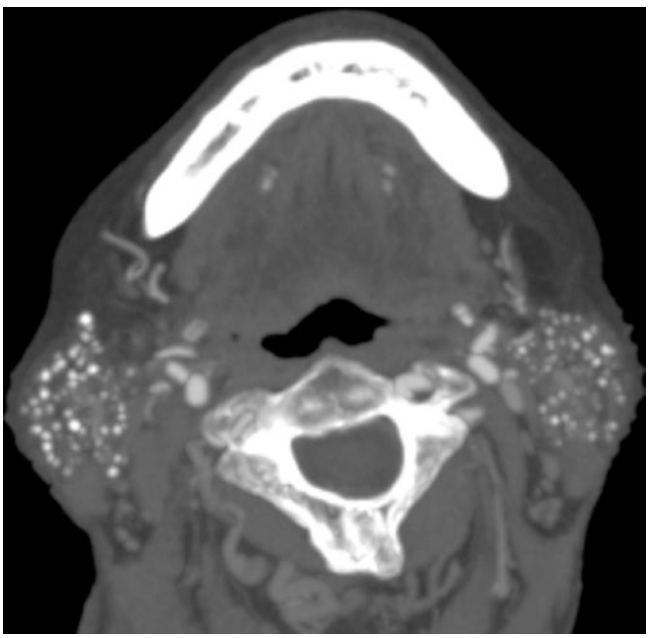

Fig. 12.18 Sjögren's syndrome; 80-year-old female with long history of disease. Axial post-contrast CT image (from CT angiography) shows multiple punctate calcifications in parotid glands, bilaterally

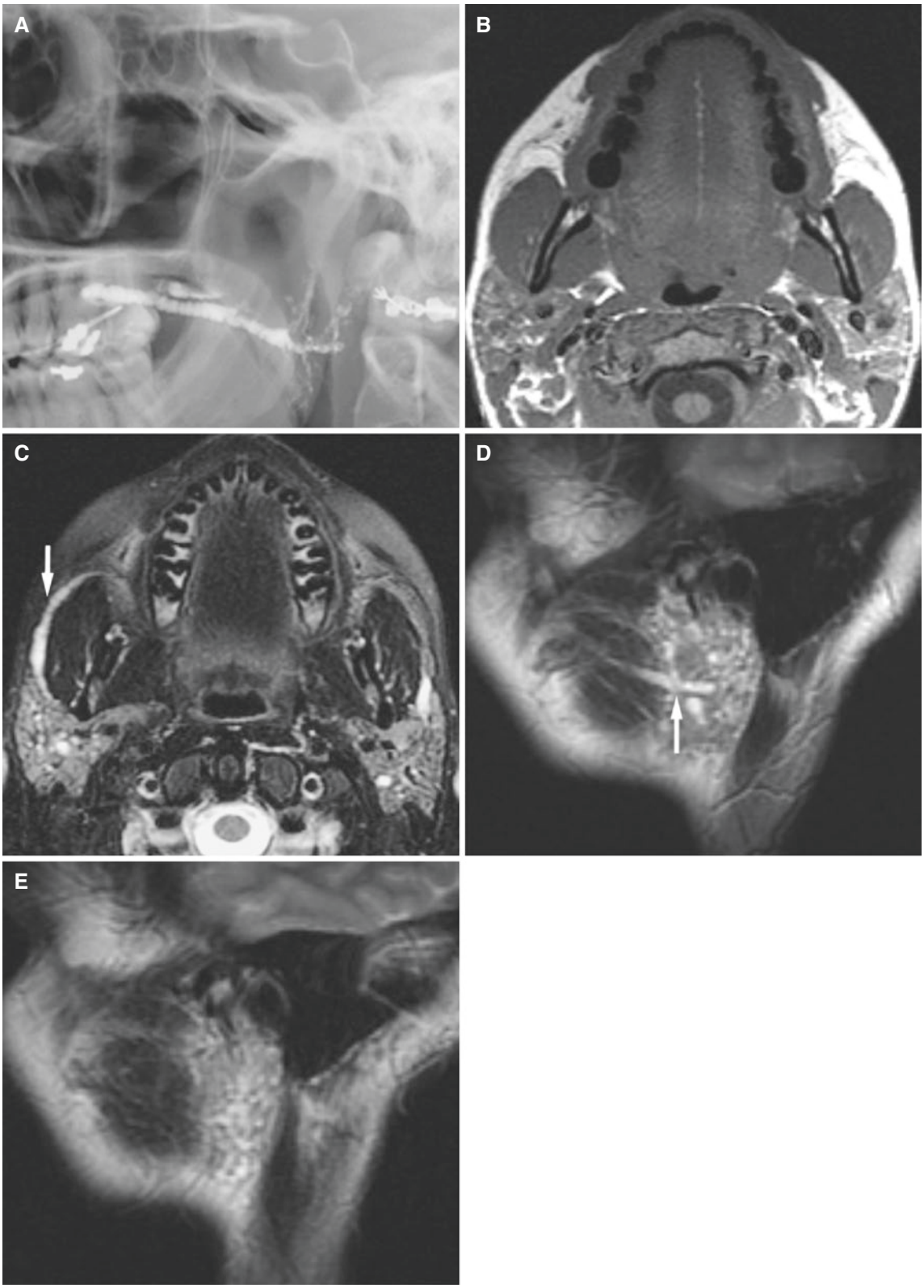

Fig. 12.19 Sjögren's syndrome; 31-year-old female with 2-year history of swelling, mostly of the right parotid gland but also of the left. (**A**) Conventional sialography shows multiple strictures and dilatations consistent with sialodochitis and poor filling of parenchyma, with some punctate contrast medium collections. (**B**) T1-weighted MRI shows some swelling of the right parotid gland which has a little less signal than the left gland and with multiple small irregularities. (**C**) T2-weighted fat-suppressed MRI shows small cystic fluid-filled irregularities consistent with chronic sialoadenitis. Note dilated parotid duct along masseter muscle (*arrow*). (**D**) Sagittal T2-weighted MRI of the right side shows dilated parotid duct (*arrow*). (**E**) Sagittal T2-weighted MRI of the left side shows no dilated duct for comparison

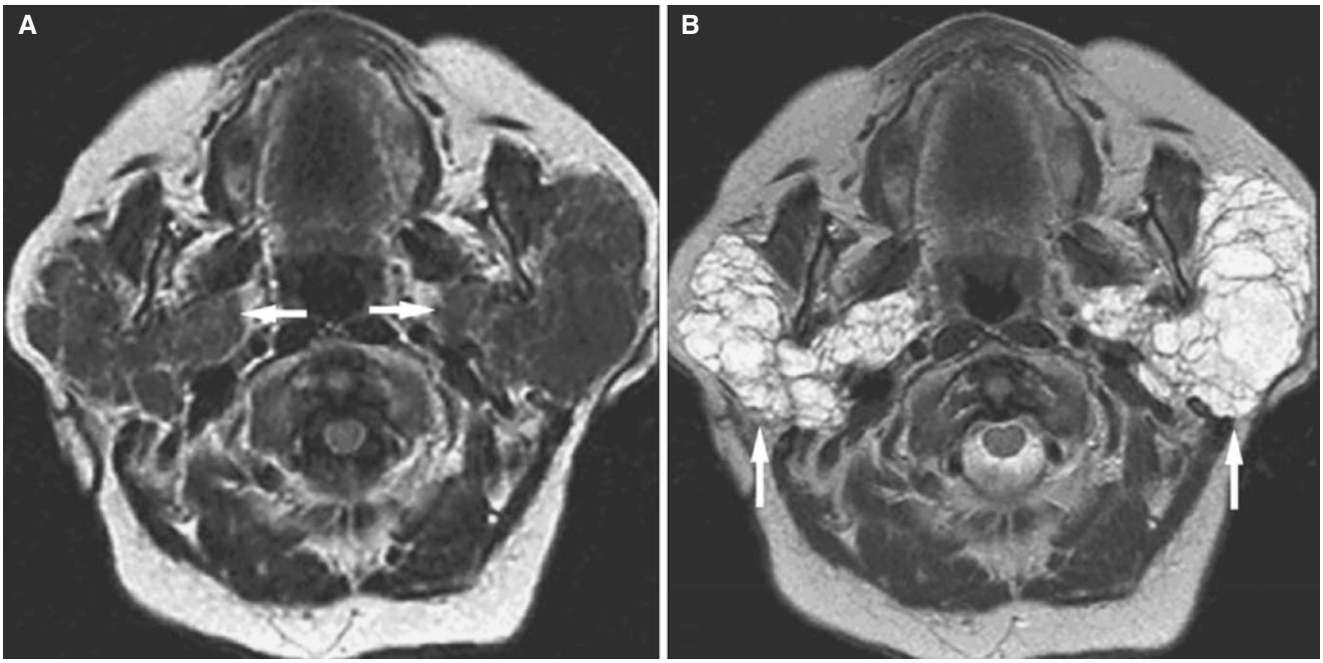

Fig. 12.20 Sjögren's syndrome, advanced stage; 64-year-old female with history of Sjögren's syndrome and multiple sclerosis presents with enlargement of both parotid glands. (**A**) Axial T1-weighted MRI shows enlarged parotid glands with multiple low-signal cystic changes (*arrows*). (**B**) Axial T2-weighted MRI shows honeycomb areas of high-signal watery saliva in parotid glands (*arrows*), both superficial and deep lobes

Fig. 12.21 Sjögren's syndrome, advanced stage; 32-year-old female with recurrent parotitis for years, finally diagnosed with Sjögren's syndrome. Axial post-contrast CT image shows bilaterally enlarged parotid glands with multiple cystic lesions surrounded by heterogeneously enhanced tissue (*arrows*)

12.6 Benign Lymphoepithelial Cysts Associated with HIV–AIDS

Fig. 12.22

12.6.1 Definition

Mixed cystic and solid intraglandular masses in HIV–AIDS.

12.6.2 Clinical Features

- Bilaterally enlarged parotid glands
- Rarely in submandibular or sublingual glands
- Reactive adenoid, tonsils, and lymphadenopathy

12.6.3 Imaging Features

- Bilateral multiple cystic and solid masses
- T1-weighted MRI: low signal
- T2-weighted MRI: high (cyst) or low (solid mass) signal
- T1-weighted post-Gd MRI: rim enhancement of cysts, heterogeneous or homogeneous enhancement of solid masses

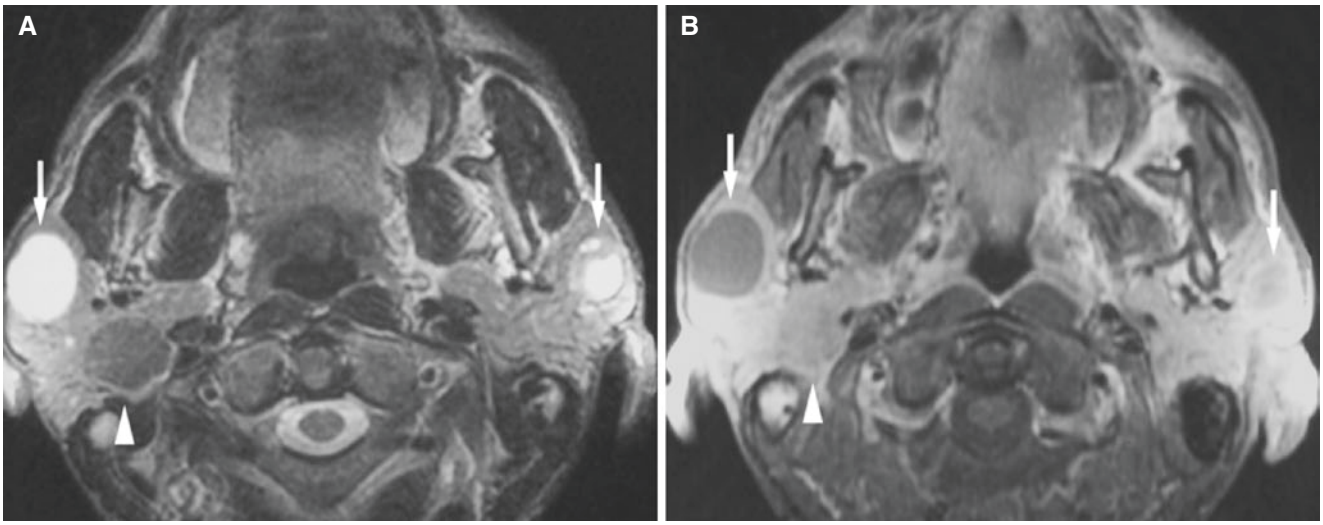

Fig. 12.22 Benign bilateral lymphoepithelial cysts; 53-year-old male with AIDS presents with bilaterally enlarged parotid glands. (**A**) Axial T2-weighted fat-suppressed MRI shows bilateral fluid-filled cysts (*arrows*) and a solid lesion (*arrowhead*). (**B**) Axial T1-weighted fat-suppressed post-Gd MRI shows rim enhancement of cysts (*arrows*) and contrast enhancement of solid lesion (*arrowhead*)

12.7 Ranula

Fig. 12.23

12.7.1 Definition

Mucous retention cyst, or mucocele, primarily in sublingual gland or its ductal elements.

Simple or plunging (diving) cyst; involves submandibular space with pseudocyst.

12.7.2 Clinical Features

- Painless sublingual soft swelling, probably from trauma or infection

12.7.3 Imaging Features

- CT: well-defined ovoid low-density cyst with thin wall
- Enhancing wall, thickened if infected
- T1-weighted MRI: low signal
- T2-weighted MRI: high signal
- T1-weighted post-Gd MRI: no enhancement except cyst wall, in particular if infected
- Simple form (most common) and a deep or plunging form that penetrates to submandibular space behind or through mylohyoid muscle because of cyst wall rupture

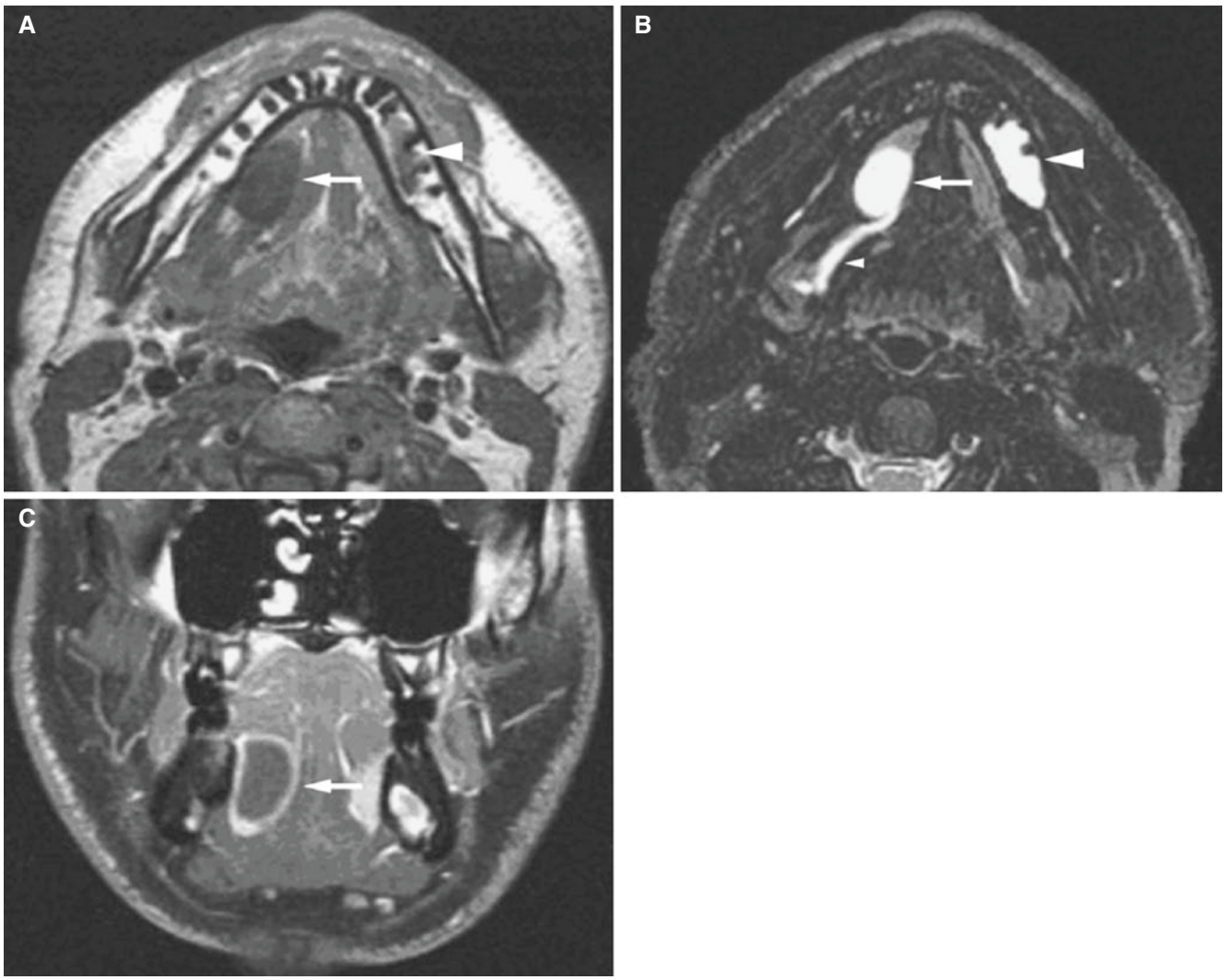

Fig. 12.23 Sublingual (simple) ranula; 24-year-old male with a sublingual lump for about 2 months (clinical suspicion of neoplasm in the floor of the mouth), with incidental finding of a mandibular cyst. (**A**) Axial T1-weighted MRI shows well-defined oval low-signal area in the floor of the mouth on the right side (*arrow*) and low-signal marrow in a region of the left mandible (*arrowhead*). (**B**) Axial T2-weighted fat-suppressed MRI shows high-signal area in the floor of the mouth (*arrow*) and high-signal area in marrow of the mandible (*arrowhead*). Note dilated Wharton's duct on the right side (*small arrowhead*). (**C**) Coronal T1-weighted fat-suppressed post-Gd MRI shows no enhancement of ranula except in the periphery (*arrow*), probably due to infection/inflammation with capsular hyperemia

12.8 Tumors

12.8.1 Clinical Features (in General)

- Usually a painless mass; may be tender
- Salivary gland tumors represent fewer than 3% of all tumors
- 75–85% of all salivary gland tumors occur in parotid gland; most are benign; minor salivary glands, palate in particular, and submandibular glands, will have most of the remainder; sublingual tumors very rare
- However, a mass in submandibular gland, even more so for a mass in sublingual gland, has a greater chance of being malignant than does a mass in parotid gland
- It has been estimated that for 100 parotid tumors there are 10 submandibular and 10 minor salivary gland tumors and only one sublingual tumor

12.8.2 Imaging Features (in General)

- An ill-defined mass should be suspicious for malignancy
- However, it may be difficult to differentiate between benign and malignant salivary gland tumors since both types commonly have a benign appearance and are well defined and cystic

12.9 Benign Tumors

A number of benign tumors may occur in the salivary glands.

12.10 Pleomorphic Adenoma (Benign Mixed Tumor)

Figs. 12.24, 12.25, 12.26, and 12.27

12.10.1 Definition

Tumor of variable capsulation characterized microscopically by architectural rather than cellular pleomorphism. Epithelial and modified myoepithelial elements intermingle with tissue of mucoid, myxoid, or chondroid appearance. Epithelial and myoepithelial components form ducts, strands, sheets, or structures resembling a swarm of bees. Squamous metaplasia is found in about 25% of pleomorphic adenomas (WHO).

12.10.2 Clinical Features

- Most frequent salivary gland tumor; 70–80% of all benign tumors of major salivary gland
- More than 80% in parotid gland, and predominantly lateral to the plane of the facial nerve
- Most frequent tumor of minor salivary glands as well, although about half of all minor salivary gland tumors, or even more, have been reported as malignant

12.10.3 Imaging Features

- Well-defined mass, highly variable size, cystic, lobulated
- Small tumors show homogeneous enhancement; large, lobulated tumors show heterogeneous enhancement
- May show calcification
- T1-weighted MRI: small tumors show homogeneous, low signal; large, lobulated tumors show heterogeneous low to intermediate signal
- T2-weighted MRI and STIR: small tumors show homogeneous high signal; large, lobulated tumors show heterogeneous intermediate to high signal
- T1-weighted post-Gd MRI: variable, heterogeneously mild to moderate enhancement

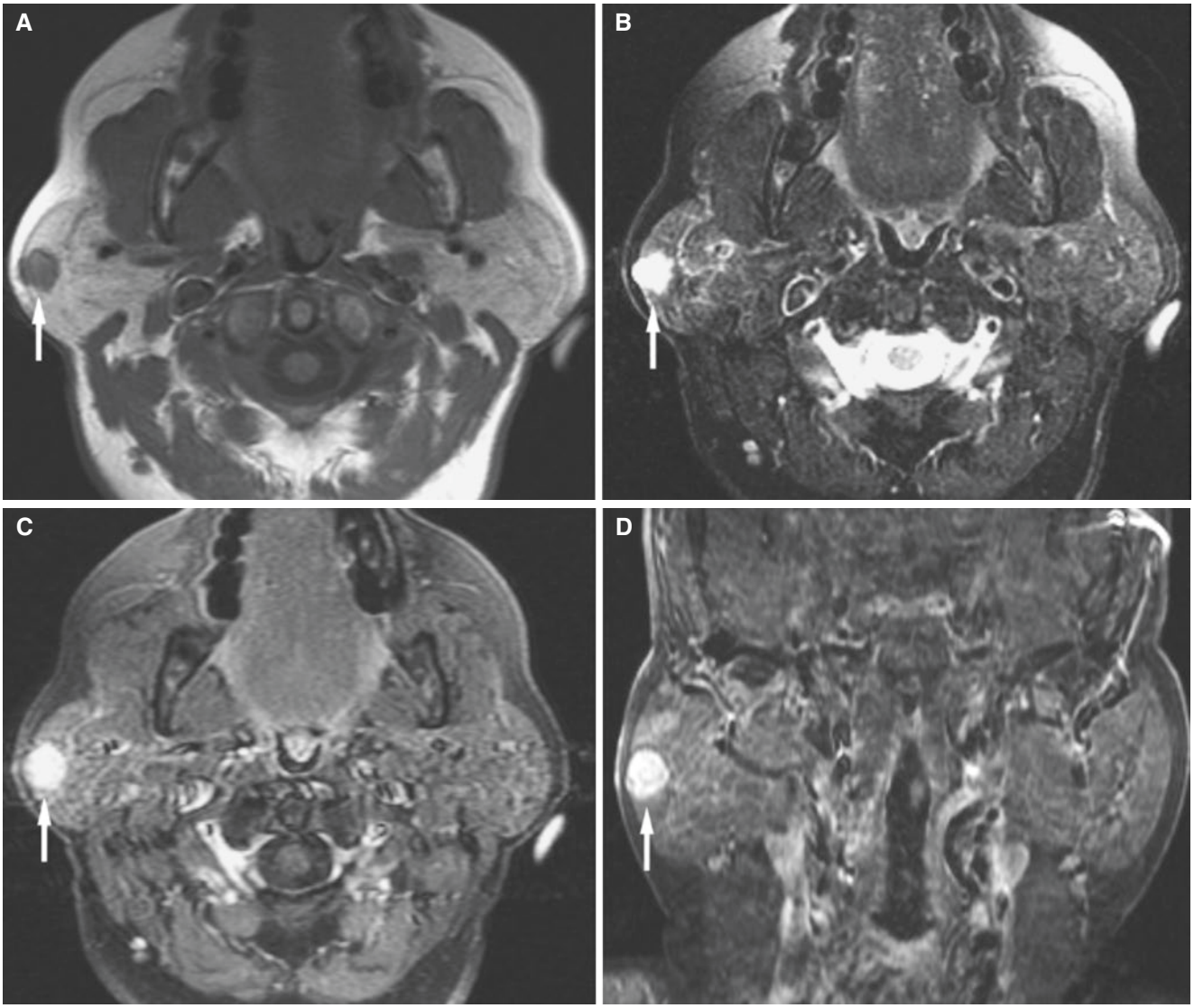

Fig. 12.24 Parotid pleomorphic adenoma, superficial lobe, small; 62-year-old female with lump in the right parotid gland. (**A**) Axial T1-weighted MRI shows rather well-defined small low-signal mass superficial in the right parotid (*arrow*). (**B**) Axial T2-weighted fat-suppressed MRI shows high-signal mass (*arrow*). (**C**) Axial T1-weighted fat-suppressed post-Gd MRI shows intense contrast enhancement (*arrow*). (**D**) Coronal T1-weighted fat-suppressed post-Gd MRI confirms contrast enhancement of tumor (*arrow*)

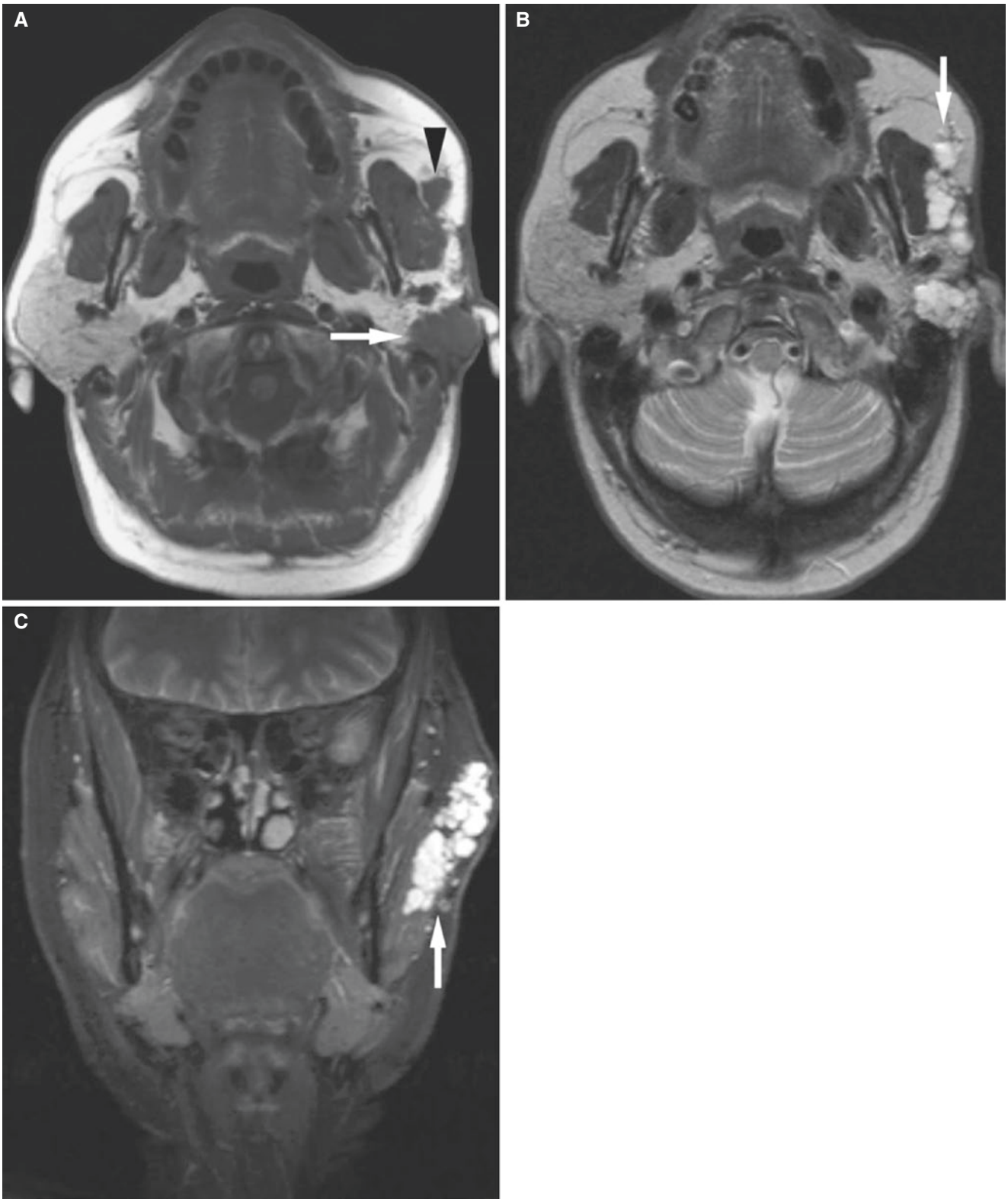

Fig. 12.25 Parotid pleomorphic adenoma, superficial lobe; 61-year-old female with history of left parotid tumor surgery, now with multifocal recurrence. (**A**) Axial T1-weighted MRI shows low-signal mass in the posterior portion of the left parotid gland (*arrow*) and in accessory gland (*arrowhead*). (**B**) Axial T2-weighted MRI shows high-signal tumor superficial to masseter muscle in addition to the posterior portion of the gland (*arrow*). (**C**) Coronal STIR MRI shows high-signal cystic tumor masses just beneath the skin (*arrow*)

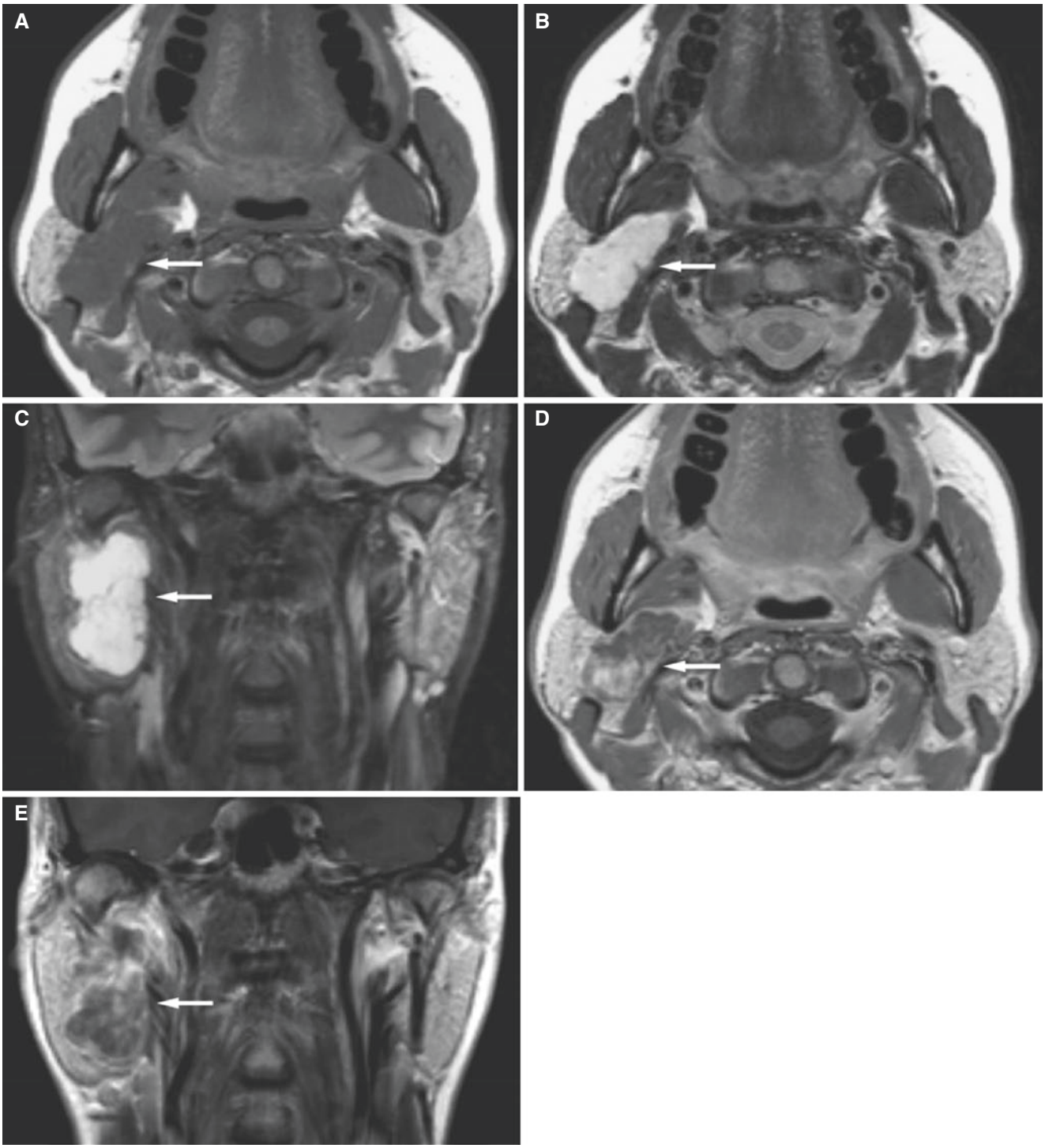

Fig. 12.26 Parotid pleomorphic adenoma, deep lobe; 40-year-old female with swelling of the right parotid gland. (**A**) Axial T1-weighted MRI shows well-defined low-signal mass in deep lobe of the right parotid gland (*arrow*). (**B**) Axial T2-weighted MRI shows well-defined homogeneous high-signal mass (*arrow*). (**C**) Coronal STIR MRI shows well-defined high-signal mass in larger portion of the parotid gland (*arrow*). (**D**) Axial T1-weighted post-Gd MRI shows contrast enhancement in the posterior portion of tumor (*arrow*). (**E**) Coronal T1-weighted post-Gd MRI confirms no contrast enhancement in the anterior portion of tumor (*arrow*)

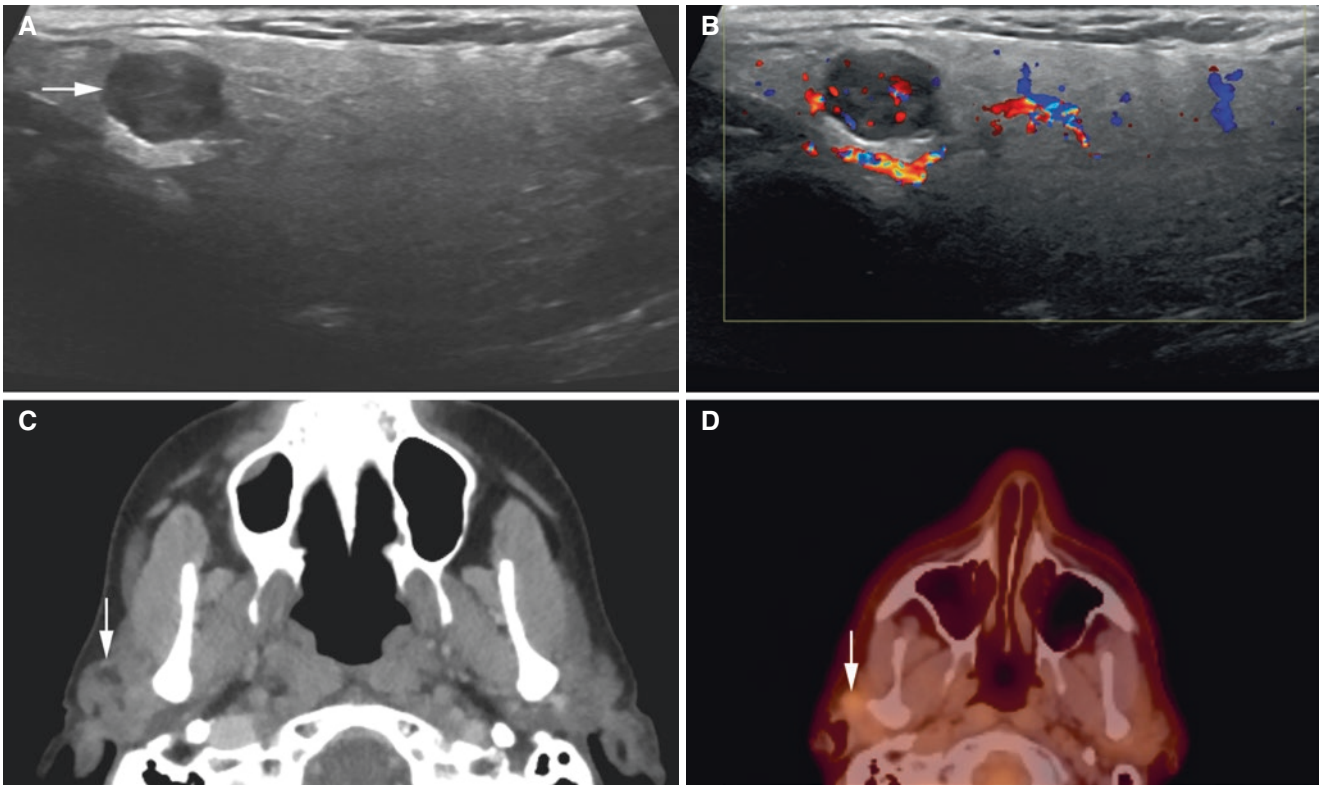

Fig. 12.27 Parotid pleomorphic adenoma; 67-year-old male with pain-free small swelling of the right parotid gland. (**A**) US and (**B**) US (Doppler) show well-defined hypoechoic mass (*arrow*) and hyperechoic, vascularized area. (**C**) Axial post-contrast CT image shows heterogeneous density of somewhat enlarged right parotid gland (*arrow*). (**D**) Axial PET-CT image shows slightly elevated FDG metabolism (*arrow*)

12.11 Warthin's Tumor (Papillary Cystadenoma Lymphomatosum)

Fig. 12.28

12.11.1 Definition

Identity has changed over the years. Although originally defined as a neoplasm, it is now considered to be an immune reaction to either heterotopic or metaplastic disease.

12.11.2 Clinical Features

- Second most common salivary gland tumor after pleomorphic adenoma
- Accounts for 6–30% of parotid tumors

12.11.3 Usually presenting as a pain-free massImaging Features

- Similar to pleomorphic adenoma, but often cystic: does not enhance
- May be bilateral (10%)
- Ultrasound: rounded or lobulated heterogeneous mass that may have cystic changes with hyperechoic internal septation
- MRI: heterogeneous, with intermediate signal intensity on T1 and internal high (cystic) signal intensity on T2
- Cells within Warthin`s tumor have a high mitochondrial content and preferentially take up Tc-99m pertechnetate, appearing as hot spot on radionuclide scintigraphy

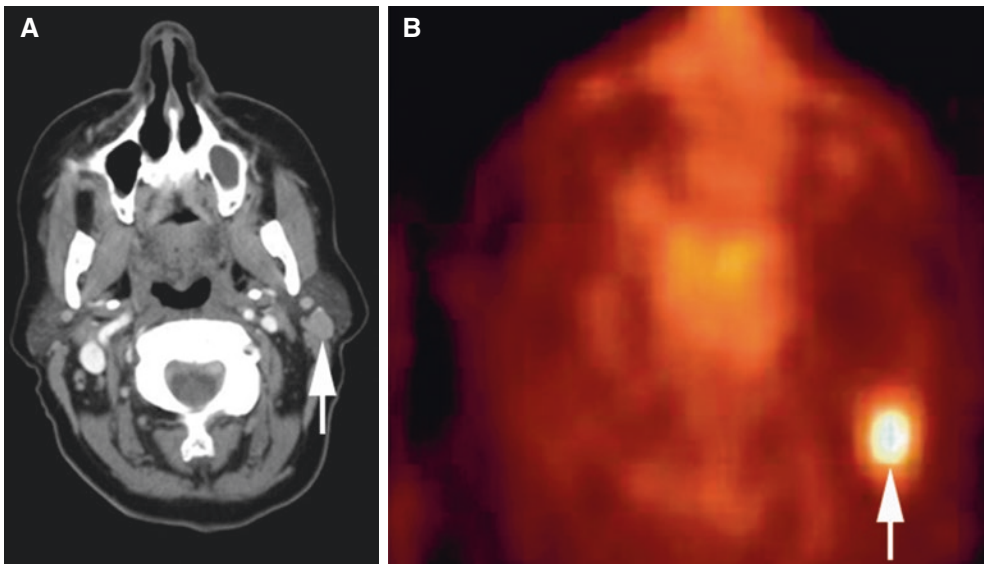

Fig. 12.28 Warthin's tumor, parotid gland; 56-year-old female with swelling of the left parotid gland. (**A**) Axial post-contrast CT image shows well-circumscribed, nodular homogeneously enhanced lesion (*arrow*). (**B**) Axial PET-CT image shows intense FDG metabolism (*arrow*)

12.12 Hemangioma

Figs. 12.29 and 12.30

12.12.1 Definition

Benign tumor of proliferating endothelial cells.

12.12.2 Clinical Features

- Most frequent nonepithelial salivary gland tumor; nonepithelial tumors represent fewer than 5% of all salivary tumors
- Predominantly in the parotid gland
- Most common salivary gland tumor during infancy and childhood; 90% of all parotid tumors in first year of life
- Premature infants in particular
- Females more than males

12.12.3 Imaging Features

- Soft-tissue mass, frequently lobulated, isodense to muscle at CT, contrast enhancing
- Uni- or bilateral, single or multiple
- T1-weighted MRI: isointense to muscle
- T2-weighted MRI: high signal
- T1-weighted post-Gd MRI: intense contrast enhancement

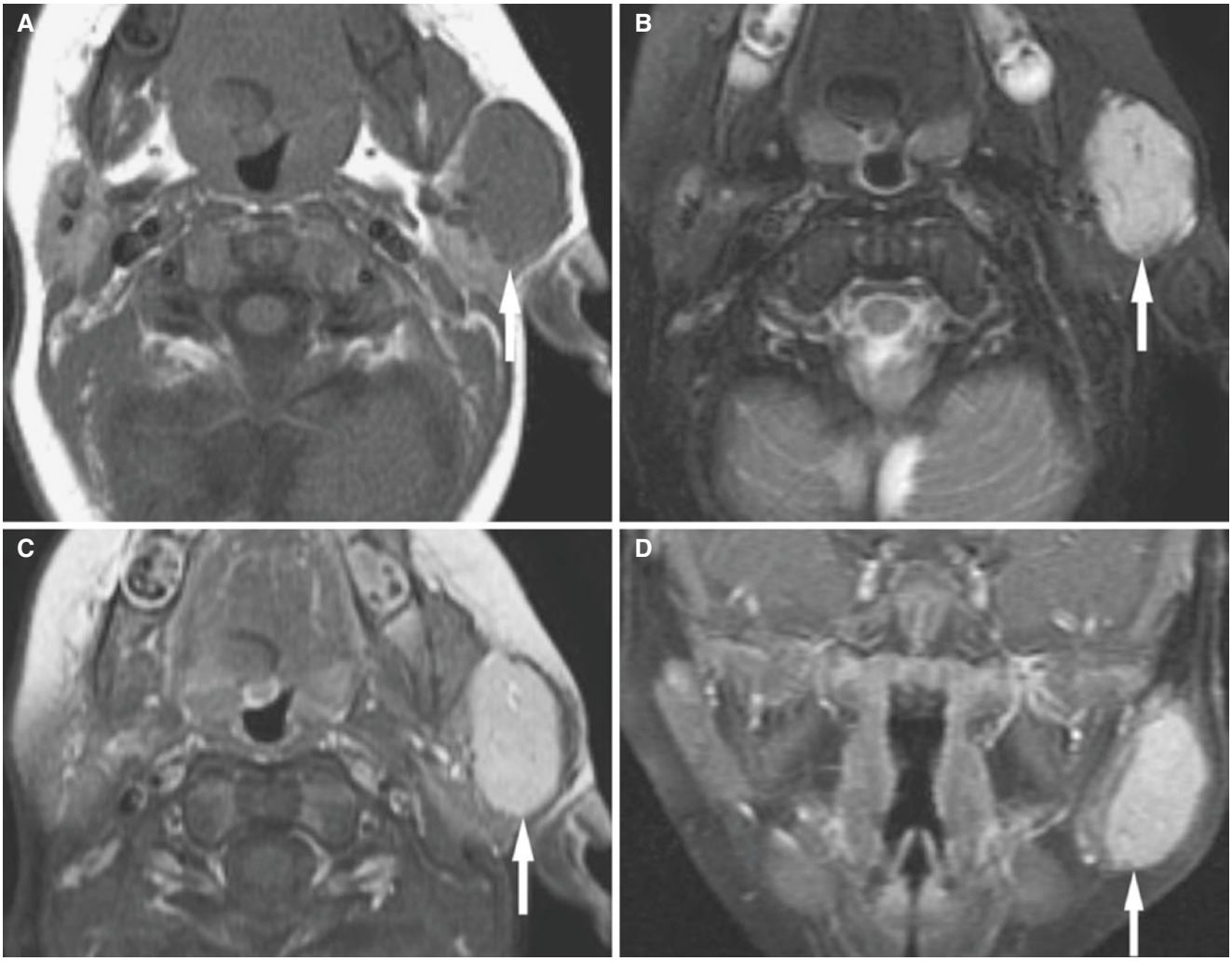

Fig. 12.29 Parotid infantile hemangioma; 9-month-old female with soft asymptomatic swelling of the left parotid gland. (**A**) Axial T1-weighted MRI shows well-defined mass isointense to muscle in the left parotid gland (*arrow*) with no reaction in surrounding fat. (**B**) Axial T2-weighted fat-suppressed MRI shows high-signal mass (*arrow*) and linear flow voids. (**C**) Axial T1-weighted post-Gd MRI shows enhancement of mass (*arrow*) with rim of nonenhancing parotid gland around mass. (**D**) Coronal T1-weighted post-Gd MRI confirms enhancement of mass (*arrow*) surrounded by nonenhancing parenchyma

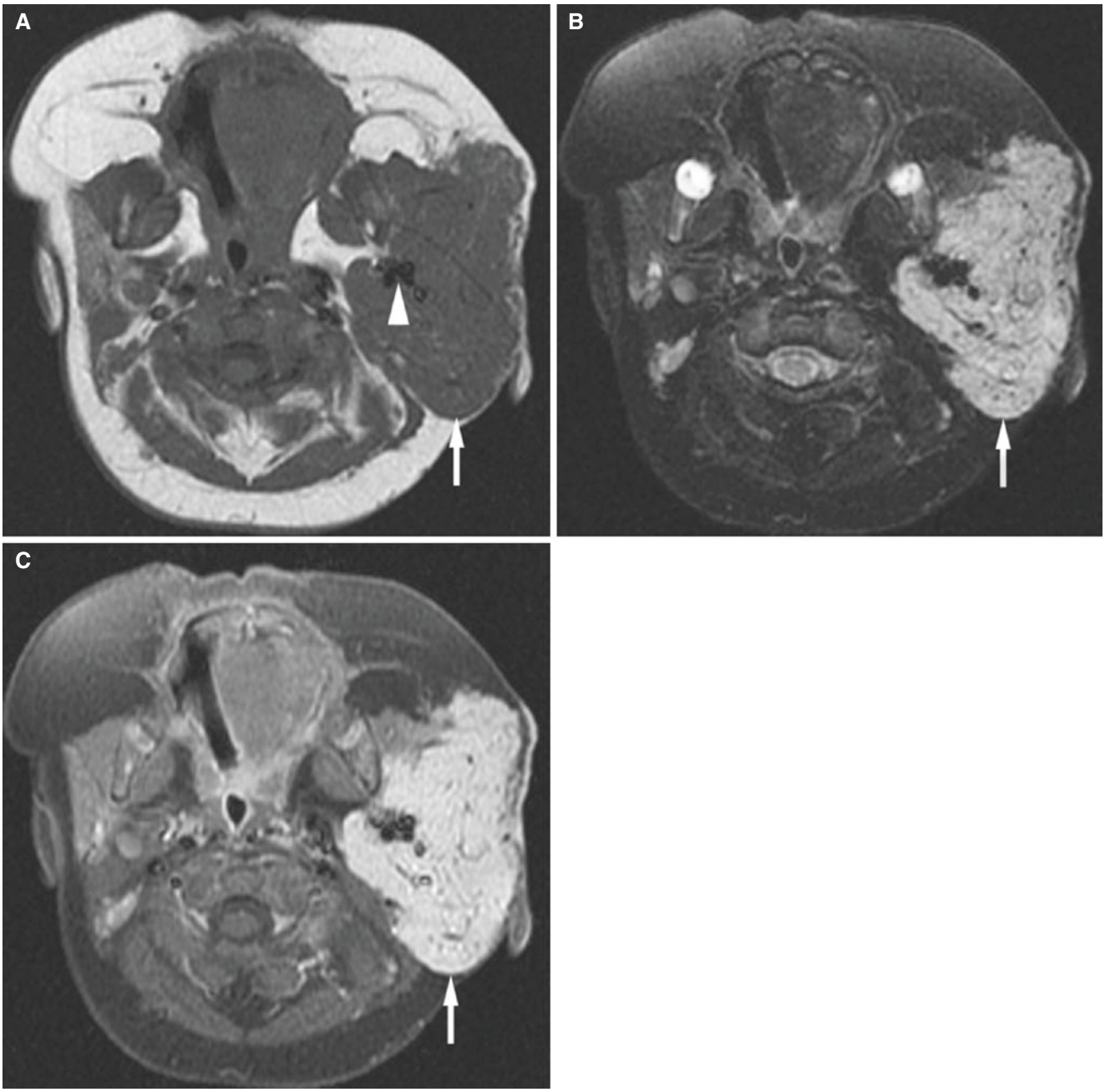

Fig. 12.30 Parotid infantile hemangioma; 4-month-old male presenting with soft enlargement of the left parotid gland and a "birthmark" on the left cheek. (**A**) Axial T1-weighted MRI shows enlargement of the left parotid gland (*arrow*) with flow voids from large sinusoidal vessels (*arrowhead*). (**B**) Axial T2-weighted fat-suppressed MRI shows mass with high signal (*arrow*). (**C**) Axial T1-weighted fat-suppressed post-Gd MRI shows marked homogeneous contrast enhancement (*arrow*)

12.13 Malignant Tumors

A number of malignant tumors may occur in the salivary glands.

12.14 Lymphoma

Fig. 12.31

12.14.1 Definition

Malignant neoplasm of cells from the lymphatic system.

12.14.2 Clinical Features

- Rare entity in salivary glands
- About 80% in parotid gland; nearly 20% in submandibular gland
- Majority non-Hodgkin's and B-cell type
- More frequently in patients with autoimmune diseases

12.14.3 Imaging Features (Parotid Gland)

- Most commonly in intraglandular lymph nodes or from mucosa-associated lymphoid tissue (MALT)
- One or more well-defined masses, usually mild, homogeneous contrast enhancing, but may show heterogeneous contrast enhancement
- MRI: homogeneous intermediate signal intensity on all imaging sequences; mild contrast enhancement

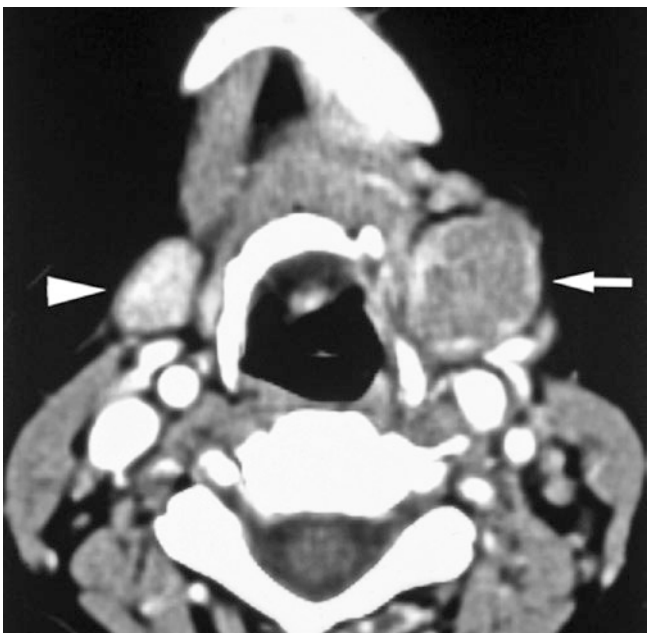

Fig. 12.31 Submandibular gland non-Hodgkin's B-cell lymphoma; 56-year-old female with weight loss, poor general condition, and lump in submandibular region; no pathologic lymph nodes were found by surgery. Axial post-contrast CT image shows low-density mass with enhancing peripheral rim of the remaining parenchyma of the left submandibular gland (*arrow*), with normal right gland for comparison (*arrowhead*)

12.15 Carcinomas

A number of different epithelial cancers may occur in the salivary glands

12.16 Mucoepidermoid Carcinoma

Fig. 12.32

12.16.1 Definition

Tumor characterized by the presence of squamous cells, mucus-producing cells, and cells of intermediate type (WHO).

12.16.2 Clinical Features

- 3–16% of all salivary gland tumors
- 12–29% of malignant salivary gland tumors
- 7–41% of minor salivary gland tumors; most common malignant minor salivary gland tumor
- About half of cases in major salivary glands; 80% in parotid gland
- Usually in age group 35–65 years
- Most common malignant salivary gland tumor in patients under 20 years of age

12.16.3 Imaging Features

- May look benign with well-defined, smooth borders and cystic areas
- Occasionally focal calcification may be seen
- May have similar appearance to pleomorphic adenomas, in particular low-grade (less aggressive) mucoepidermoid carcinomas

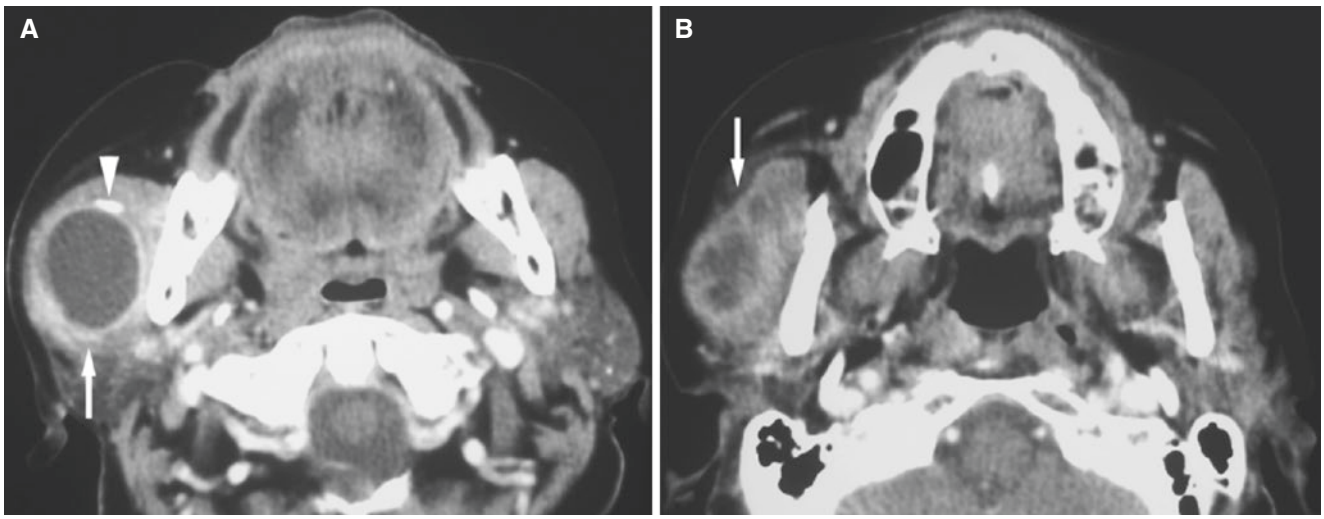

Fig. 12.32 Parotid high-grade mucoepidermoid carcinoma (with evident inflammatory response); 59-year-old female with tender swelling of the right parotid gland. (**A**) Axial post-contrast CT image shows well-defined expansive, cystic, low-density mass with contrast-enhanced periphery (*arrow*) in the superficial lobe, and calcification consistent with sialolith (*arrowhead*). (**B**) Axial post-contrast CT image (more cranial than image **A**) shows lobulated, heterogeneously enhanced mass; mostly without enhancement (*arrow*)

12.17 Acinic Cell Carcinoma

Figs. 12.33 and 12.34

12.17.1 Definition

Malignant epithelial tumor that demonstrates some cytological differentiation toward acinar cells (WHO).

12.17.2 Clinical Features

- 7–18% of all malignant salivary tumors
- 10–30% of parotid malignancies
- Vast majority in parotid gland, minor salivary glands second most common site
- Most common malignant salivary gland tumor after mucoepidermoid carcinoma in childhood and adolescence

12.17.3 Imaging Features

- Nonspecific, benign appearance, well-defined mass, may be cystic
- May have similar appearance to pleomorphic adenomas
- Recurrent tumors can be multinodular

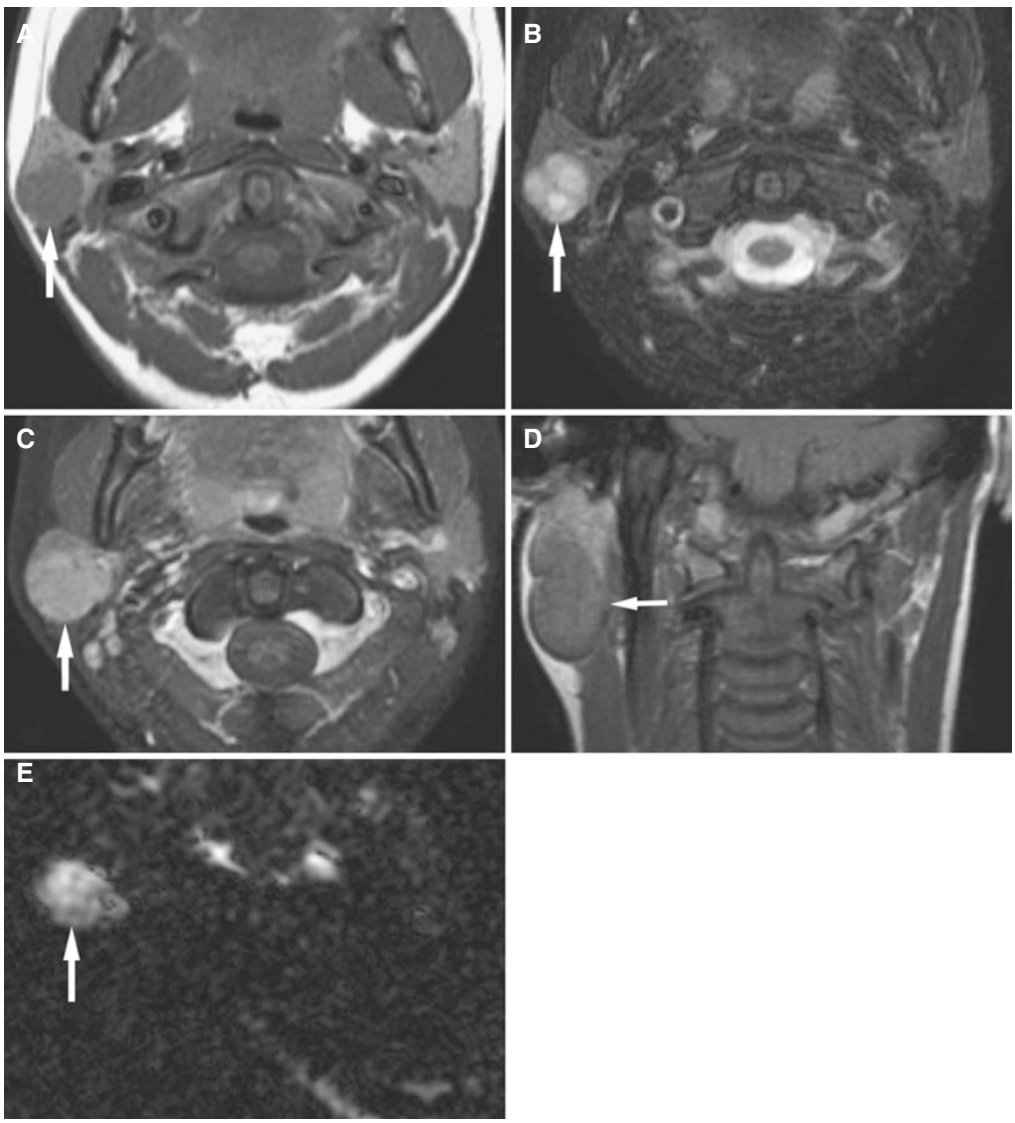

Fig. 12.33 Parotid acinic cell carcinoma; 11-year-old female with painless swelling of the right parotid gland that did not respond to antibiotic treatment. (**A**) Axial T1-weighted MRI shows well-defined low-to-intermediate signal mass in the posterior portion of the right parotid gland (*arrow*). (**B**) Axial T2-weighted MRI shows high heterogeneous signal from well-defined mass (*arrow*). (**C**) Axial T1-weighted fat-suppressed post-Gd MRI shows slight contrast enhancement of mass (*arrow*). (**D**) Coronal T1-weighted MRI shows well-defined mass occupying large portion of the posterior aspect of the parotid gland (*arrow*). (**E**) Axial diffusion-weighted MRI demonstrates high signal from mass indicating high cellular density (*arrow*)

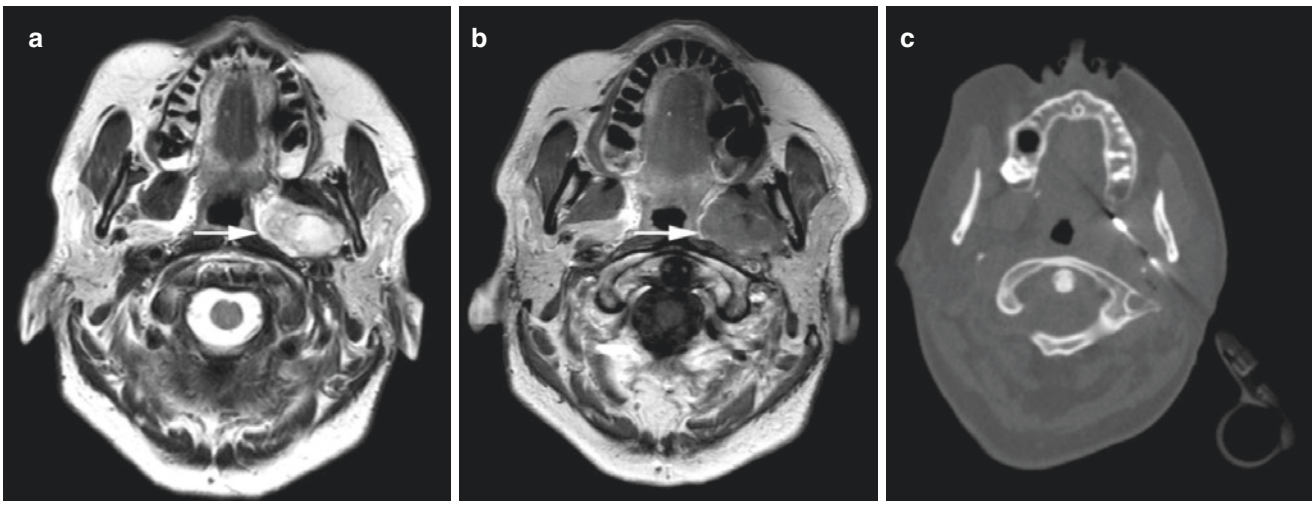

Fig. 12.34 Parotid (deep lobe) acinic cell carcinoma; 69-year-old asymptomatic female found to have 3 cm parapharyngeal mass on head MRI (obtained due to headache). (**A**) Axial T2-weighted MRI shows well-defined expansive, multicystic, intermediate signal intensity mass in the left parapharyngeal space (*arrow*). (**B**) Axial T1-weighted MRI shows low signal intensity (deep lobe) lesion (*arrow*) displacing surrounding structures. (**C**) Axial CT image shows 14 gauge core biopsy needle in lesion

12.18 Adenocarcinoma

Fig. 12.35

12.18.1 Definition

Carcinoma with glandular, ductal, or secretory differentiation that does not fit into other categories of carcinoma (WHO).

12.18.2 Clinical Features

- Rare entity in salivary glands
- Minor salivary (in particular palate) and parotid glands more common than submandibular and sublingual glands

12.18.3 Imaging Features

- Unspecific mass; variable enhancement

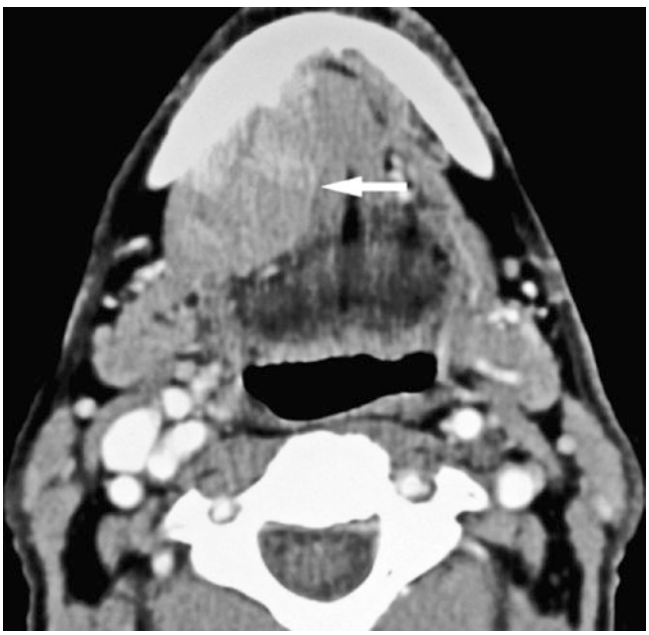

Fig. 12.35 Sublingual gland adenocarcinoma; 84-year-old male with Marfan syndrome and aortic insufficiency**,** presenting with moderately tender sublingual lump. Axial post-contrast CT image shows rather well-defined contrast-enhancing sublingual mass (*arrow*) extending to submandibular gland region, dislocating the right genioglossus muscle toward the left and mylohyoid muscle laterally and inferiorly

12.19 Adenoid Cystic Carcinoma

Figs. 12.36 and 12.37

12.19.1 Definition

Specific and rare variant of adenocarcinoma defined by the presence of a dual population of cells (epithelial and myoepithelial cells) organized in varying combinations of cribriform, tubular, and solid patterns.

12.19.2 Clinical Features

- Tendency to perineural spread, or spread through bloodstream
- Spreads to lymph node in 5–10%
- Lung most common place of metastases
- In one study, higher frequency in submandibular gland than in the maxillary sinus, parotid gland, and palate

12.19.3 Imaging Features

Unspecific mass; variable enhancement

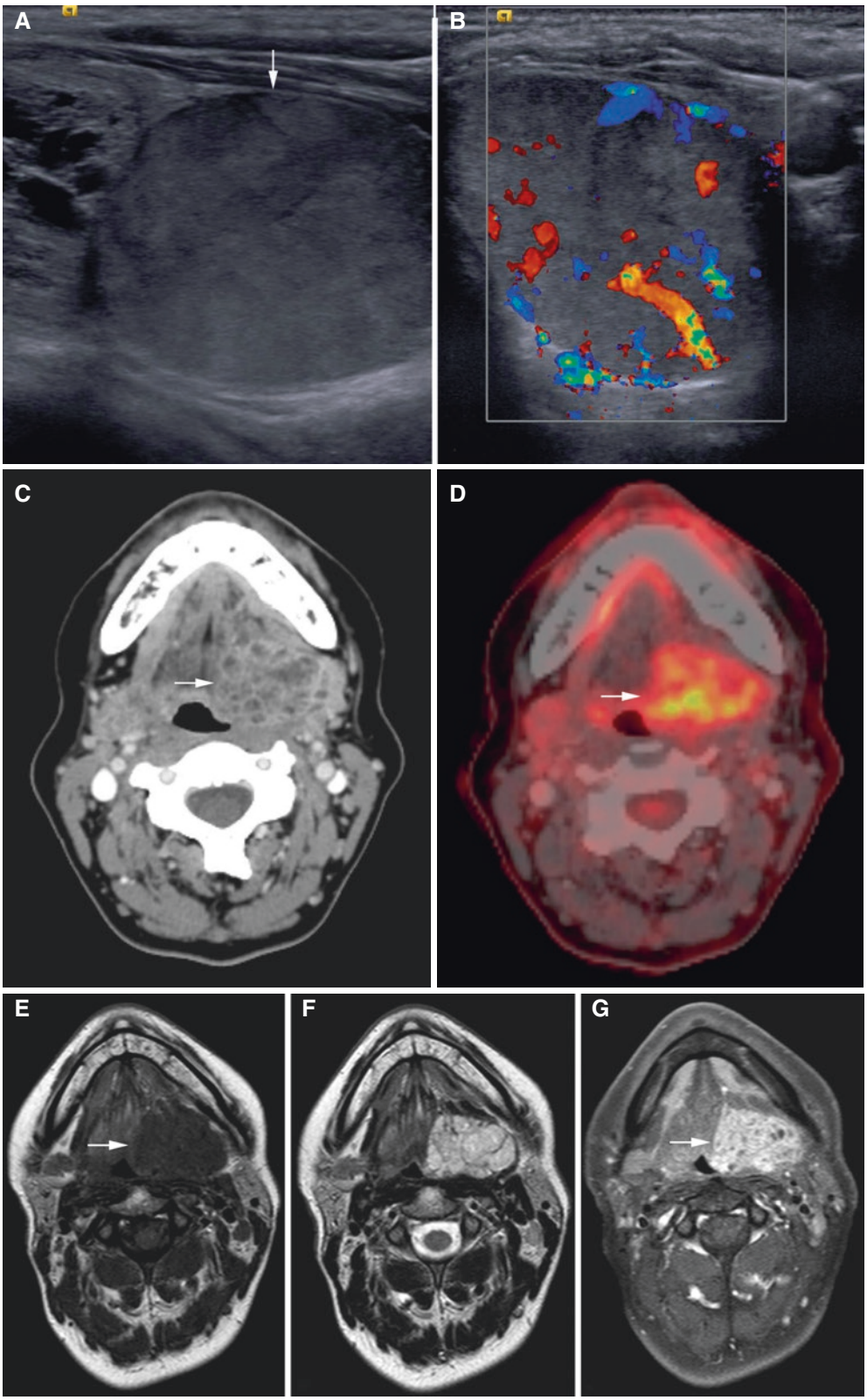

Fig. 12.36 Submandibular gland adenoid cystic carcinoma: 46-year-old female with swelling in the floor of the mouth. (**A**) US and (**B**) US (Doppler) images show encapsulated mass (*arrow*) with increased vascularity and mildly heterogeneous echogenicity. (**C**) Axial contrast-enhanced CT image shows avid enhancement with multicystic pattern within mass (*arrow*). (**D**) Axial PET-CT shows avid, heterogeneous FDG uptake (*arrow*). (**E**) Axial T1-weighted MRI shows low signal intensity (*arrow*), (**F**) Axial T2-weighted MRI shows heterogeneous high signal, and (**G**) axial T1-weighted fat-suppressed post-Gd MRI shows heterogeneous contrast enhancement with microcystic features (*arrow*) (courtesy of Dr. Lennart Flygare, Umeå University Hospital, Umeå, Sweden)

12.20 Carcinoma ex Pleomorphic Adenoma

Pleomorphic adenoma may occasionally develop into malignancy.

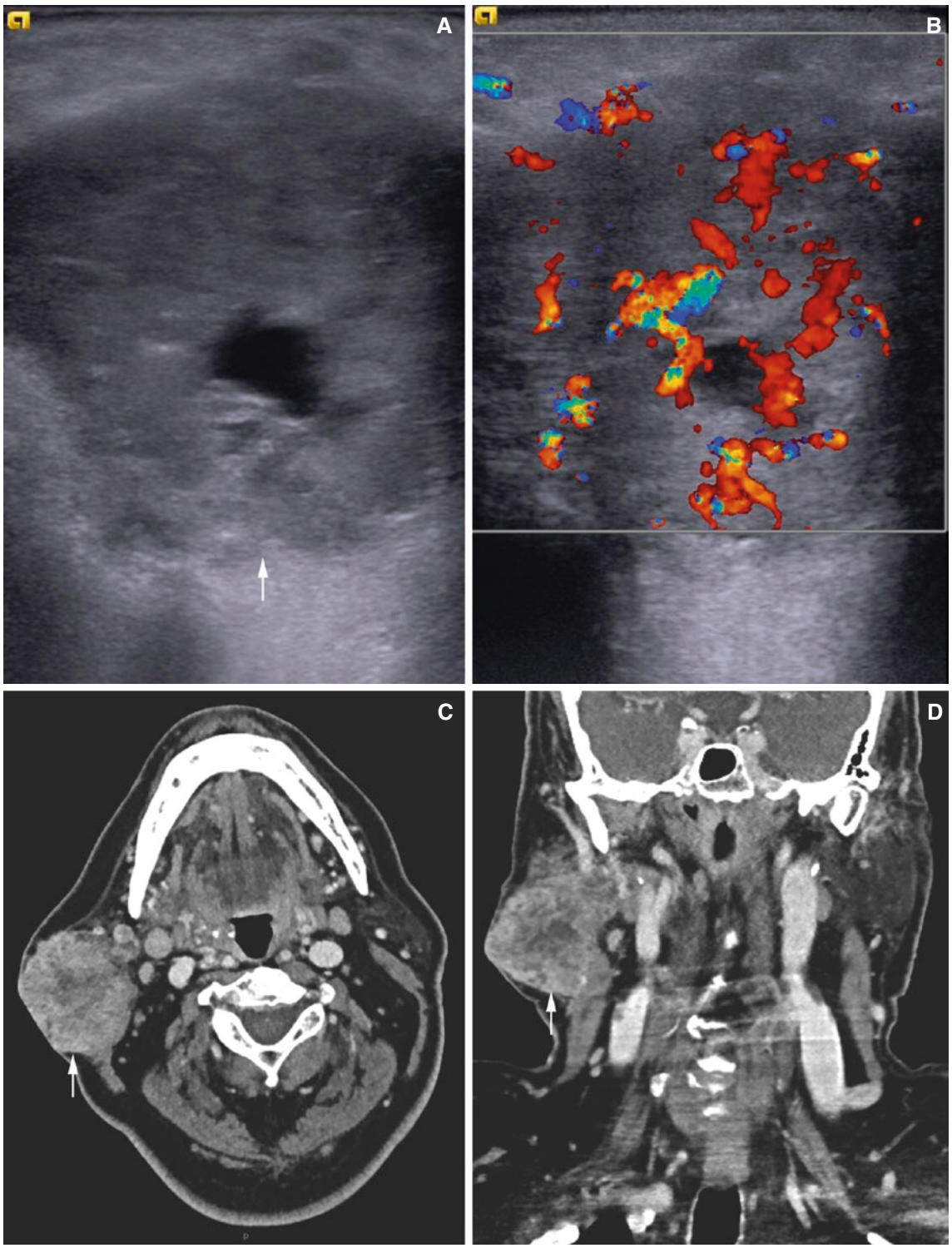

Fig. 12.37 Carcinoma ex pleomorphic adenoma, parotid gland; 65-year-old male with swelling of right parotid gland area. (**A**) US and (**B**) US (Doppler) images show large intraparotid mass (*arrow*) with rich and patchy vascularity. Note the central area of low echogenicity indicating necrotic component raising suspicion of malignancy. (**C**) Axial and (**D**) coronal contrast-enhanced CT images show avid, heterogeneous contrast enhancement (*arrow*), central necrotic area, and ingrowth into the sternocleidomastoid muscle and subcutaneous/cutaneous tissue layers (courtesy of Dr. Lennart Flygare, Umeå University Hospital, Umeå, Sweden)

Suggested Reading

Aasen S, Kolbenstvedt A (1992) CT appearances of normal and obstructed submandibular duct. Acta Radiol 33:414–419

Abdel Razek AA, Ashmalla GA, Gaballa G, Nada N (2015) Pilot study of ultrasound parotid imaging reporting and data system (PIRADS): inter-observer agreement. Eur J Radiol 84:2533–2538

Barnes L, Eveson JW, Reichart P, Sidransky D (eds) (2005) World Health Organization classification of tumours. Pathology and genetics of head and neck tumours. IARC Press, Lyon

Barnes L, Myers E, Prokopakis EP (1998) Primary malignant lymphoma of the parotid gland. Arch Otolaryngol Head Neck Surg 124:573–577

Benson BW (2014) Salivary gland diseases. In: White SW, Pharoah MJ (eds) Oral radiology. Principles and interpretation, 7th edn. Mosby, St. Louis, pp 542–561

David E, Cantisani V, De Vincentiis M, Sidhu PS, Greco A, Tombolini M et al (2016) Contrast-enhanced ultrasound in the evaluation of parotid gland lesions: an update of the literature. Ultrasound 24:104–110

Eneroth CM (1971) Salivary gland tumors in the parotid gland, submandibular gland and the palate region. Cancer 27:1415–1418

Farman AG, Nortje C, Wood RE (1993) Salivary gland diseases. In: Oral and maxillofacial diagnostic imaging. Mosby, St. Louis, pp 403–424

Fusco N, Guerini-Rocco E, Schultheis AM, Badve SS, Reis-Filho JS, Weigelt B (2015) The birth of an adenoid cystic carcinoma. Int J Surg Pathol 23:26–27

Harnsberger HR, Wiggins RH, Hudgins PA, Michel MA, Swartz J, Davidson HC et al (2004) Diagnostic imaging head and neck. Amirsys, Salt Lake City

Jager L, Menauer F, Holzknecht N, Scholz V, Grevers G, Reiser M (2000) Sialolithiasis: MR sialography of the submandibular duct—an alternative to conventional sialography and US? Radiology 216:665–671

Joe VQ, Westesson PL (1994) Tumors of the parotid gland: MR imaging characteristics of various histologic types. AJR Am J Roentgenol 163:433–438

Kiringoda R, Eisele DW, Chang JL (2014) A comparison of parotid imaging characteristics and sialendoscopic findings in obstructive salivary disorders. Laryngoscope 124:2696–2701

Koontz NA, Seltman TA, Kralik SF, Mosier KM, Harnsberger HR (2016) Classic signs in head and neck imaging. Clin Radiol vOhbayashi N, Yamada I, Yoshino N, Sasaki T (1998) Sjogren syndrome: comparison of assessments with MR sialography and conventional sialography. Radiology 209:683–688

Paleri V, Robinson M, Bradley P (2008) Polymorphous low-grade adenocarcinoma of the head and neck. Curr Opin Otolaryngol Head Neck Surg 16:163–169

Raine C, Saliba K, Chippindale AJ, McLean NR (2003) Radiological imaging in primary parotid malignancy. Br J Plast Surg 56: 637–643

Rebours C, Couloigner V, Galmiche L, Casiraghi O, Badoual C, Boudjemaa S et al (2016) Pediatric salivary gland carcinomas: diagnostic and therapeutic management. Laryngoscope 127:140. doi:10.1002/lary.26204

Sakamoto M, Sasano T, Higano S, Takahashi S, Iikubo M, Kakehata S (2003) Usefulness of heavily T2 weighted magnetic resonance images for the differential diagnosis of parotid tumors. Dentomaxillofac Radiol 32:295–299

Seifert G (1991) Histological typing of salivary gland tumors, 2nd edn. WHO, Springer, Berlin, pp 28, 32, 33

Som PM, Brandwein MS (2003) Salivary glands: anatomy and pathology. In: Som PM, Curtin HD (eds) Head and neck imaging, 4th edn. Mosby, St. Louis, pp 2005–2133

Som PM, Shugar J, Train JS, Biller H (1981) Manifestations of parotid gland enlargement: radiologic, pathologic and clinical correlations. Part 1: the autoimmune pseudosialectasias. Radiology 141: 415–419

Spiro RH, Huvos AG, Strong EW (1978) Acinic cell carcinoma of salivary origin. A clinicopathologic study of 67 cases. Cancer 41:924–935

Spiro RH, Huvos AG, Strong EW (1982) Adenocarcinoma of salivary origin. Clinicopathologic study of 204 patients. Am J Surg 144:423–431

Szanto PA, Luna MA, Tortoledo ME, White RA (1984) Histologic grading of adenoid cystic carcinoma of the salivary glands. Cancer 54:1062–1069

Rastogi R, Bhargava S, Mallarajapatna GJ, Singh SK (2012) Pictorial essay: salivary gland imaging. Indian J Radiol Imaging 22:325–333

Tonami H, Ogawa Y, Matoba M, Kuginuki Y, Yokota H, Higashi K, Okimura T, Yamamoto I, Sugai S (1998) MR sialography in patients with Sjogren syndrome. AJNR Am J Neuroradiol 19:1119–1120

Adjacent Structures: Cervical Spine, Neck, Skull Base, and Orbit

13

Abstract

This chapter illustrates Cervical Spine; calcific tendinitis longus colli, ossification of posterior longitudinal ligament, rheumatoid pannus at craniocervical junction, tuberculosis at craniocervical junction, Chiari malformation type 1, chordoma at craniocervical junction, cervical spine teratoma, cervical spine cord astrocytoma, extramedullary cervical lipoma with cord compression, cervical spine meningioma, cervical spine neurofibromatosis type 1 (NF-1), cervical spine fracture, Neck; hypopharynx abscess, thyroid abscess, Tornwaldt's cyst, dermoid cyst, Goiter, vocal cord paralysis, neck hemangioma, neck lipoma, neck plexiform neurofibroma, pharynx rhabdomyosarcoma, tongue base carcinoma, hypopharynx carcinoma, Burkitt's lymphoma, Castleman's disease, lymphadenopathy, Skull Base; mastoiditis with intracranial abscess, mastoiditis with sigmoid thrombosis, osteoradionecrosis involving skull base, Langerhans cell histocytosis, fibrous dysplasia, giant aneurysm of skull base, glomus vagale paraganglioma, craniopharyngioma, pituitary macroadenoma invading skull base, trigeminal schwannoma, metastatic disease to hypoglossal canal and clivus, Orbit; orbital infectious disease, dacrycystocele (nasolacrimal duct), dermoid, fibrous dysplasia, Langerhans cell histiocytosis, neurofibromatosis, hemangioma, meningioma, rhabdomyosarcoma, and lymphoblastic leukemia.

13.1 Introduction

This chapter contains a selection of cases from structures surrounding the maxillofacial area. It is not the intention to cover all abnormalities in these regions but instead to give the maxillofacial radiologist a feel and sense for radiographic abnormalities that may occur in areas adjacent to the maxillofacial region. Thus, we have selected characteristic and illustrative cases from the cervical spine, neck, skull base, and orbit that are likely to be seen on maxillofacial imaging studies. The chapter includes chronic and acute conditions, tumors, inflammation, and degenerative changes and is divided into four parts: cervical spine, neck, skull base, and orbit. For a more complete review of imaging findings of these areas, we refer the reader to traditional textbooks on head and neck imaging.

13.2 Cervical Spine

A portion of the upper cervical spine will in many cases be depicted on regular maxillofacial imaging studies. This pertains to plain films of the jaw, lateral cephalograms, panoramic images, and MRI and CT scans of the maxillofacial region. This short review of cervical spine abnormalities has been done with this in mind. It is not the purpose to present a complete atlas of cervical pathology but instead to illustrate those cases that the maxillofacial radiologist is likely to encounter. Thus, we have included mostly bony abnormalities, but some soft-tissue lesions are also illustrated. There are many more conditions affecting the cervical spine than we have illustrated such as demyelinating disease, spondylosis, and nerve root compression to give a few examples.

In collaboration with R. Sidhu and N. Kakimoto.

T.A. Larheim, P.-L.A. Westesson, *Maxillofacial Imaging*, https://doi.org/10.1007/978-3-319-53319-3_13

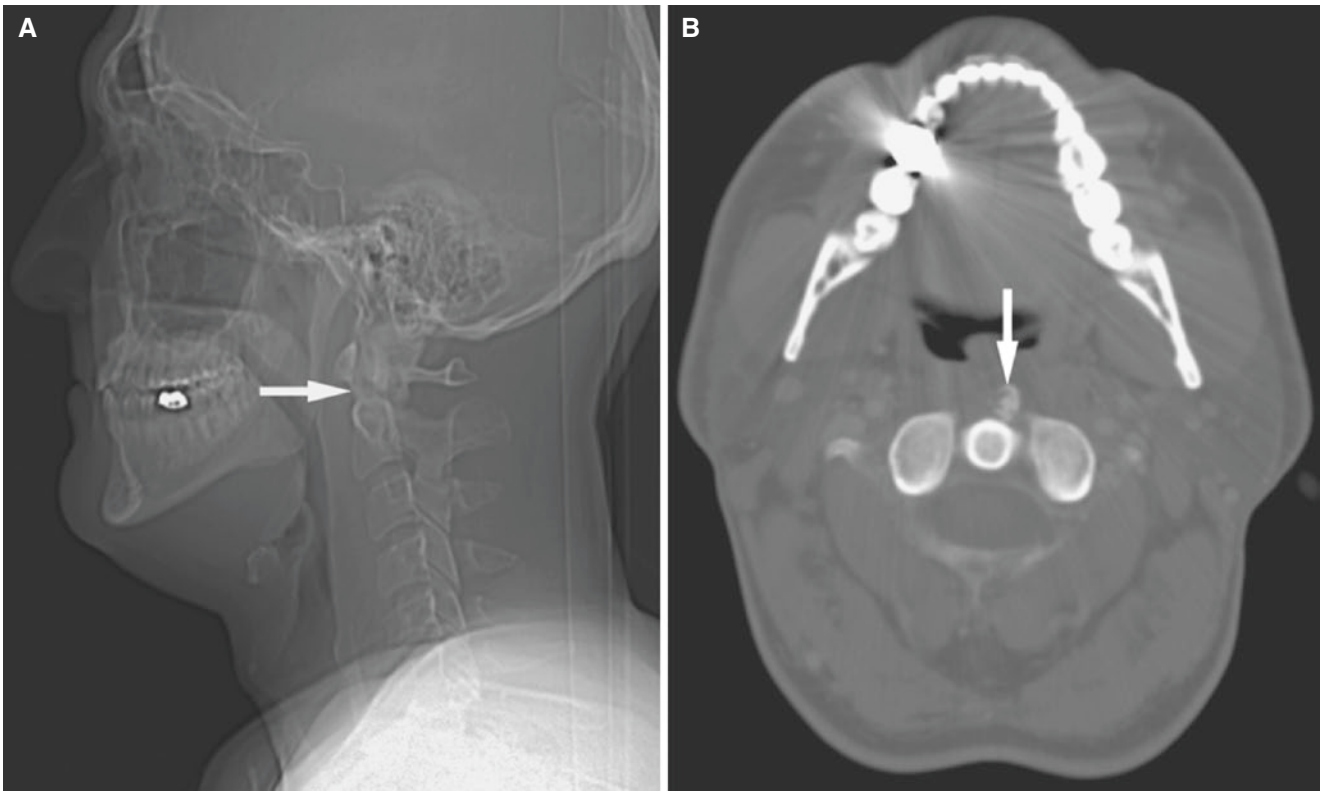

Fig. 13.1 Calcific tendinitis longus colli; 47-year-old male with neck pain, clinical question of retropharyngeal abscess or phlegmon in neck. (**A**) Lateral view shows calcific density anteriorly between C1 and C2 (*arrow*) with slightly prominent soft tissues. (**B**) Axial CT image shows a prevertebral calcification (*arrow*). No mass or lymphadenopathy

13.3 Calcific Tendinitis Longus Colli

Fig. 13.1

13.3.1 Definition

Recurrent deposits of crystalline calcium compounds within the longus colli muscle.

13.3.2 Clinical Features

- Diagnosis based upon clinical presentation and imaging
- Cervical pain, dysphagia, and distinctive radiographic appearance
- Symptoms usually manifest over a few days and often resolve benignly within 2 weeks
- Often unrecognized cause of acute to subacute neck pain
- Self-limiting disease which resolves spontaneously with symptomatic treatment

13.3.3 Imaging Features

- Calcification at C1–C2 level with prominence of prevertebral soft tissues
- Pathognomonic lateral neck film with prevertebral soft-tissue swelling and amorphous radiodensity anterior to C1–C2 vertebral bodies
- CT, axial scans, highly reliable for diagnosis

13.4 Ossification of Posterior Longitudinal Ligament

Figs. 13.2 and 13.3

13.4.1 Definition

Calcification of posterior longitudinal ligament of spinal column.

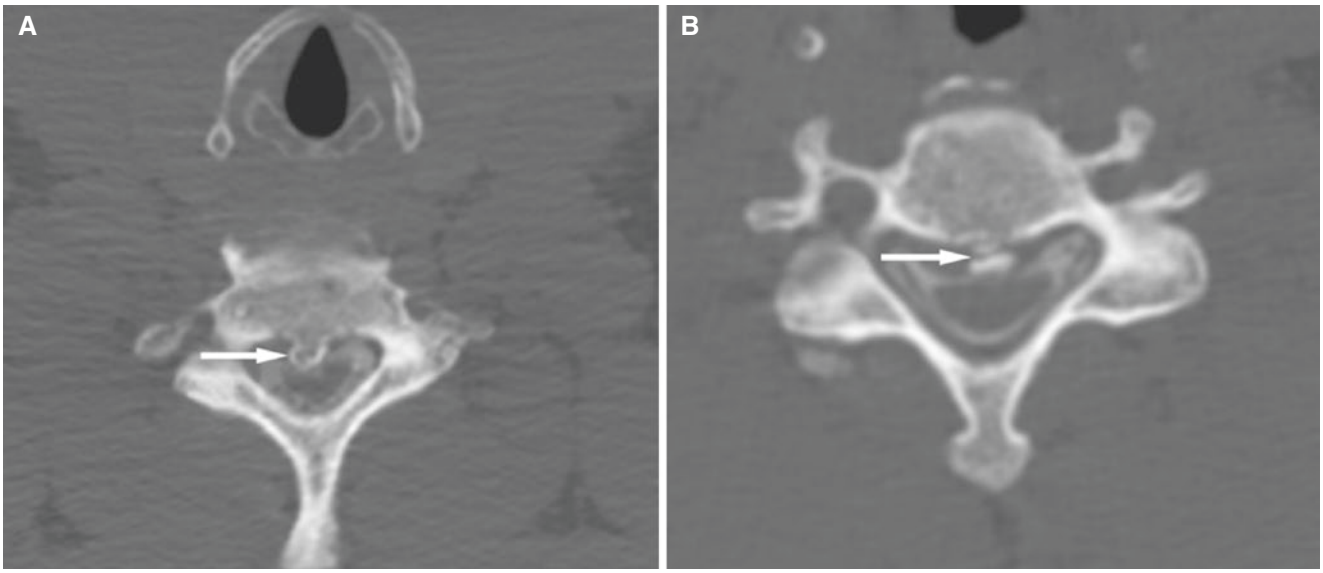

Fig. 13.2 Ossification of longus colli ligament; 55-year-old male with a 5-year history of cervical and lumbar radiculopathy; no neurologic deficit on examination. (**A**) Axial CT myelography of the cervical spine shows ossified posterior longitudinal ligament having a mushroom-shaped appearance at C4–C5 level (*arrow*). (**B**) Well-appreciated lucent line between posterior margin of vertebral body and ossified ligament (*arrow*), representing connective tissue

13.4.2 Clinical Features

- Histologically this mostly represents ossification rather than amorphous calcification
- Most commonly affects cervical spine
- More common in Japan for unknown reasons
- Often causes neurological symptoms secondary to narrow spinal canal
- More frequent in males than females

13.4.3 Imaging Features

- CT highly reliable for diagnosis
- Often causes significant spinal canal stenosis
- On axial CT images, posterior longitudinal ligament is seen as a "mushroom," "hill," "square," or a mixture of these shapes
- Four morphologic forms: continuous and segmental forms account for 95%
- Characteristic sharp radiolucent line separates ossified posterior longitudinal ligament from posterior vertebral margin; about 50% of cases
- Segmental form of ossified posterior longitudinal ligament needs to be differentiated from calcified discs and posterior osteophytes; neither of these two conditions shows a characteristic sharp radiolucent line, and in contrast to ossified posterior longitudinal ligament, osteophytic growth is along a horizontal axis
- Differential diagnosis:
  - Ankylosing spondylitis, which more commonly affects the lumbar spine with syndesmophytes rather than ossification of posterior longitudinal ligament
  - DISH (diffuse idiopathic skeletal hyperostosis) which is a more generalized condition with extensive calcification and ossification, particularly in the spine

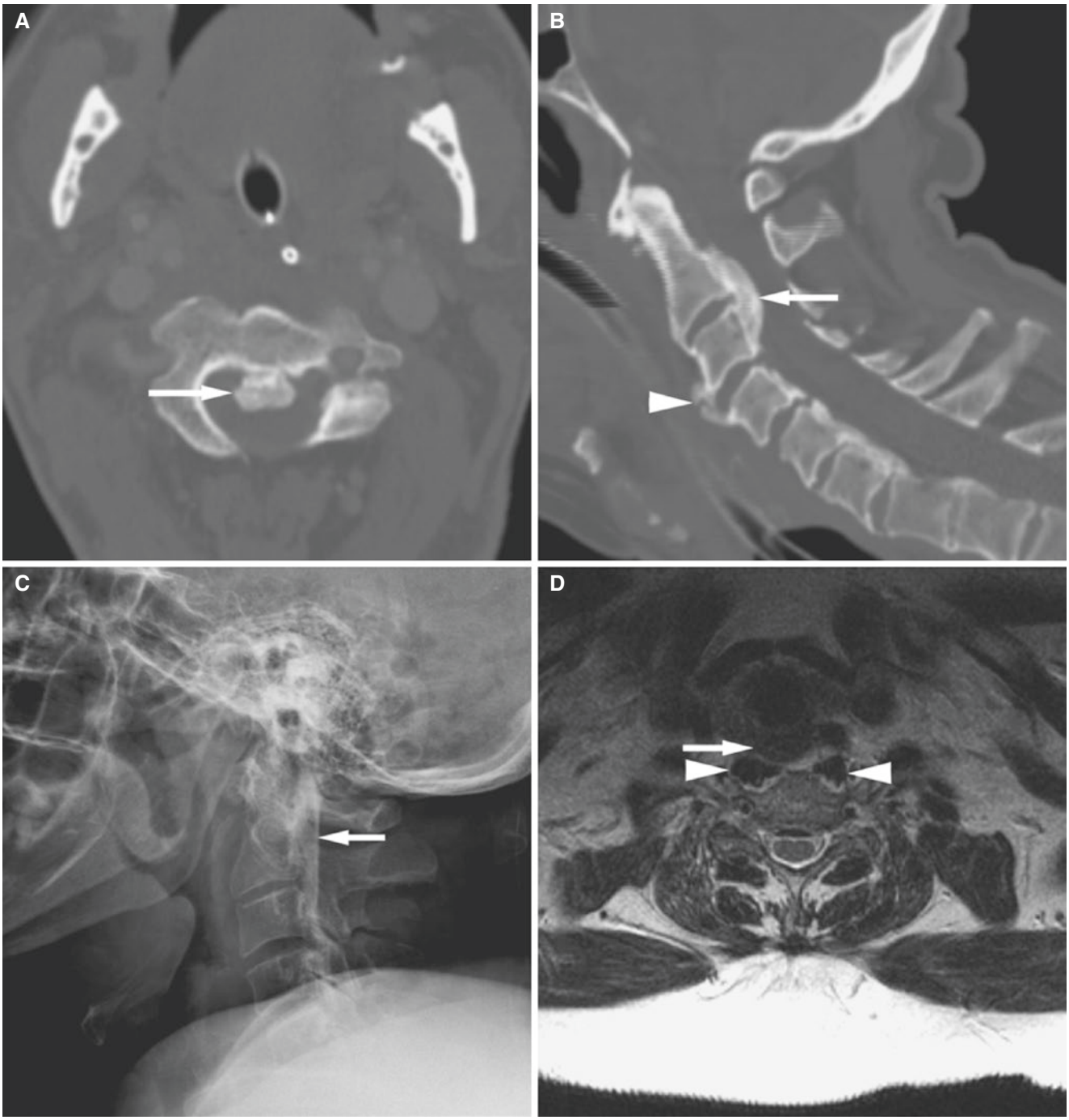

Fig. 13.3 Ossification of longus colli ligament; 52-year-old female with a history of left arm pain and clinical suspicion of cervical disc displacement or mass. (**A**) Axial CT image shows mushroom-shaped ossification (*arrow*) with radiolucent line between ossification and vertebral body. (**B**) Sagittal CT image shows ossification between C2 and C3 (*arrow*), and segmental ossification at C4–C7, as well as anterior osteophytes C3–C4 consistent with degenerative changes (*arrowhead*). (**C**) Lateral view of another patient shows severe ossification (*arrow*). (**D**) Axial T1-weighted MRI, same patient as in (**C**), shows evident ossification (*arrow*) anterior to longus colli muscles (*arrowheads*)

13.5 Rheumatoid Pannus at Craniocervical Junction

Fig. 13.4

13.5.1 Definition

Hypertrophied synovitis with production of inflammatory joint fluid containing several different types of enzymes.

13.5.2 Clinical Features

- Cervical spine pain and limitation of motion
- Enlargement of retrodental pannus can induce or aggravate compressive myelopathy

13.5.3 Imaging Features

- MRI is superior imaging method; it shows both inflammatory soft tissue and compression of spinal cord
- MRI depicts effect of inflammatory process on neural tissue, ligaments, bursae, and fat pads
- Pannus: often low signal on T1-weighted MRI and high signal on T2-weighted MRI, showing contrast enhancement, depending on activity of inflammation
- Atlantoaxial dislocation or cranial migration of dens may be seen

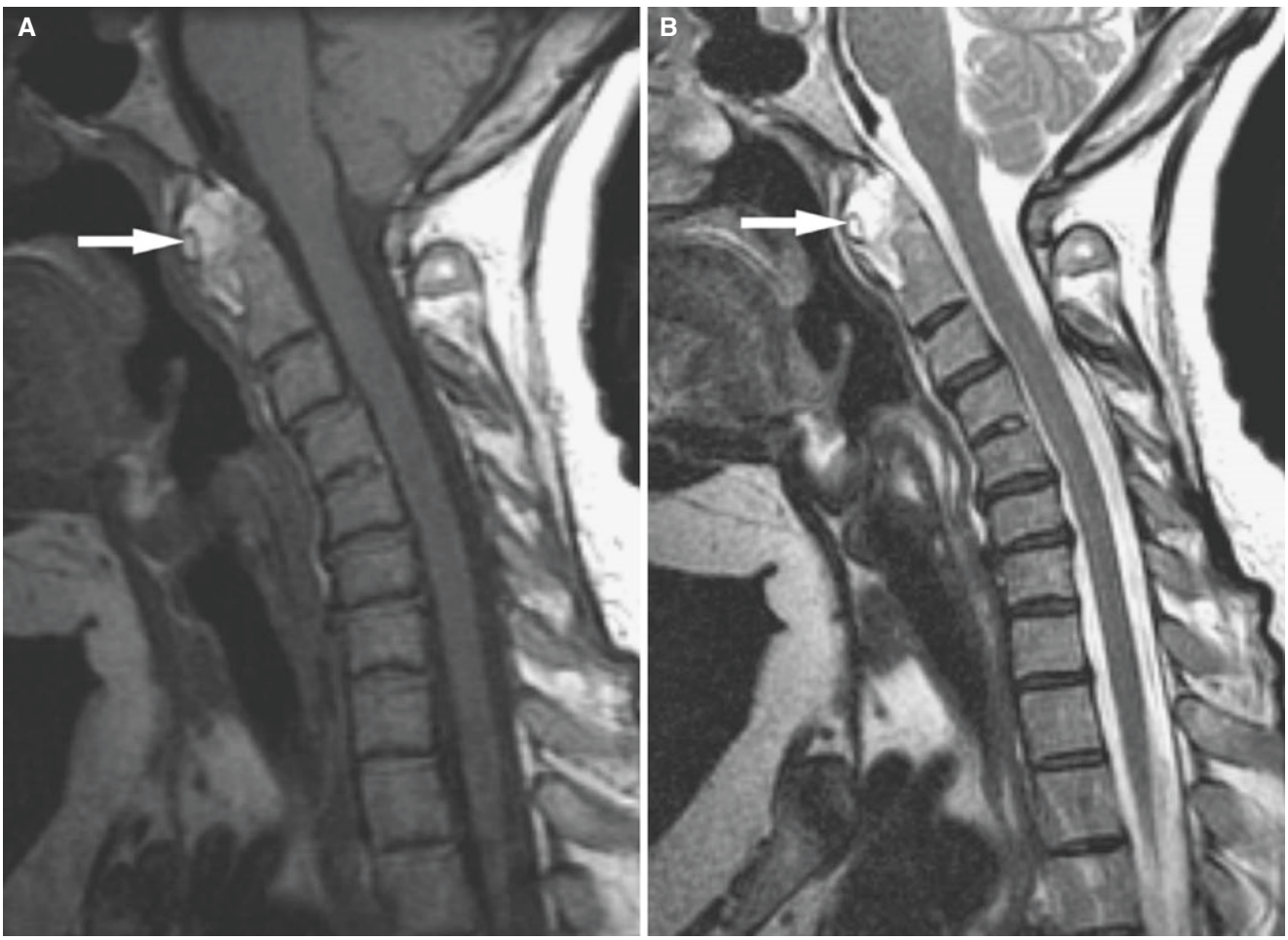

Fig. 13.4 Rheumatoid pannus at craniocervical junction; 46-year-old female with long history of rheumatoid arthritis, now with cervical spine pain. (**A**) Sagittal T1-weighted MRI shows hyperintense mass anterior to eroded dens (*arrow*). (**B**) Sagittal T2-weighted MRI shows same mass to be markedly hyperintense with a few heterogeneous foci (*arrow*). Kyphotic deformity of mid-cervical spine and degenerative changes at C5–C6 in particular

13.6 Tuberculosis at Craniocervical Junction

Fig. 13.5

13.6.1 Definition

Granulomatous or caseous type inflammation caused by *Tuberculum bacilli*.

13.6.2 Clinical Features

- Pain, rigidity, deformity, cold abscess, and paraplegia
- Thoracolumbar commonest site
- Can occur as paradiscal, central body, subligamentous type, and appendiceal
- Commonly involves two or three vertebrae

13.6.3 Imaging Features

- Progressive bone destruction leads to collapse
- Often paraspinal phlegmon
- T1-weighted MRI: low signal
- T2-weighted MRI: high signal, depending on activity of inflammation
- T1-weighted post-Gd MRI: enhancing of inflammatory granulomatous tissue

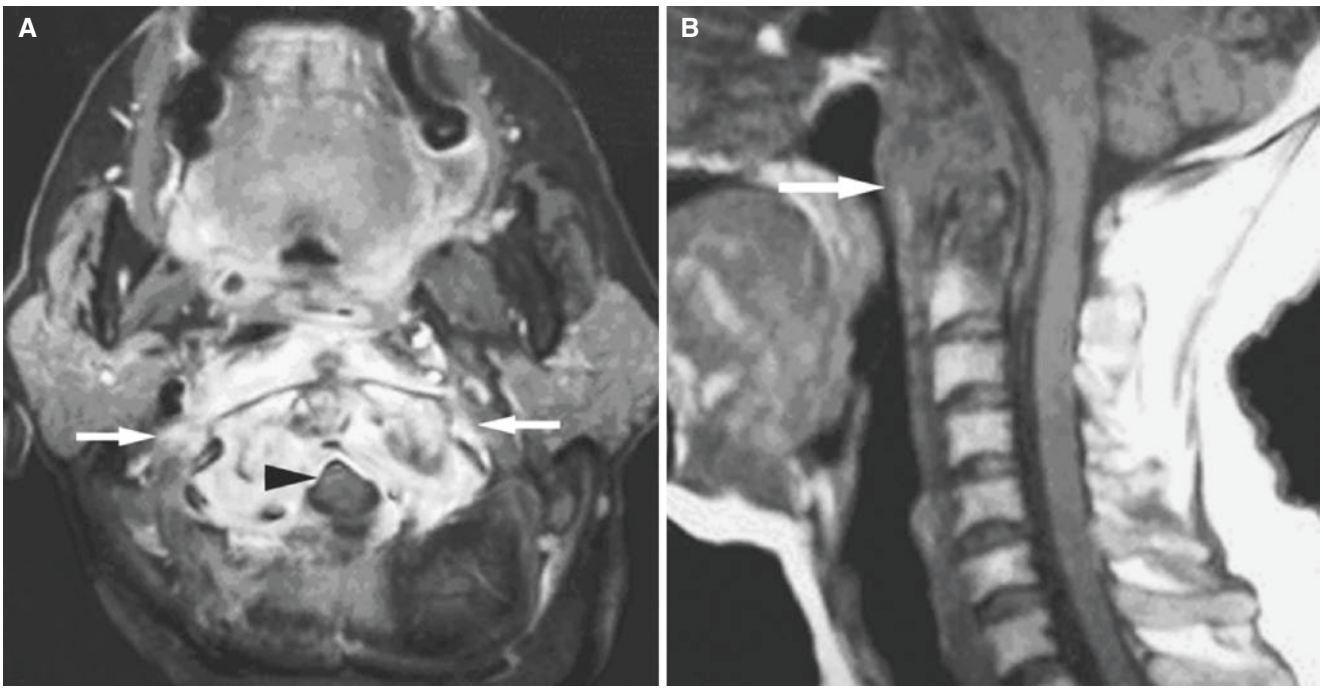

Fig. 13.5 Tuberculosis at craniocervical junction; 50-year-old female presented with history of neck ache and low-grade fever for 2 months. (**A**) Axial T1-weighted post-Gd MRI shows destruction and erosion of atlantoaxial joint with an enhancing soft-tissue mass (*arrows*). A small epidural component is seen causing pressure on thecal sac (*arrowhead*). (**B**) Sagittal T1-weighted MRI shows destruction of C1 and C2 with a soft-tissue mass (*arrow*) (courtesy of Dr. Humera Ahsan**,** Aga Khan University, Karachi, Pakistan)

13.7 Chiari Malformation Type I

Figs. 13.6 and 13.7

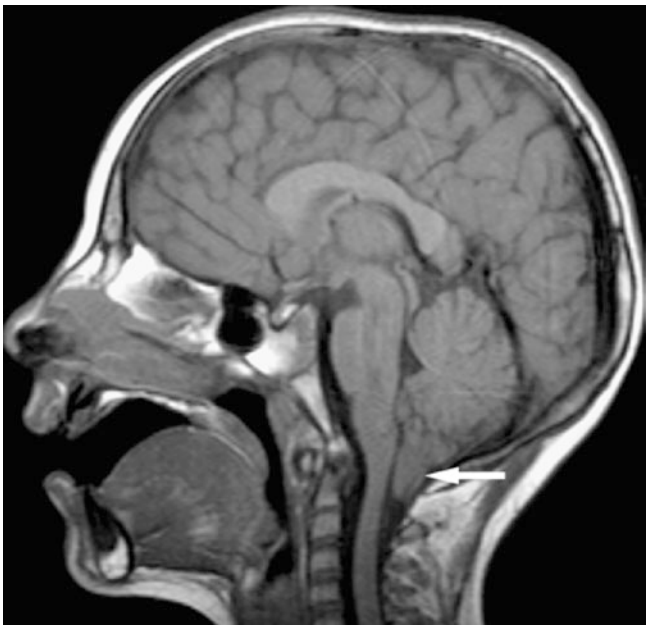

Fig. 13.6 Chiari malformation type I; 7-year-old female with Noonan syndrome presents with neck pain. Mid-sagittal T1-weighted MRI shows descent of point of tonsils through the foramen magnum (*arrow*) and the absence of CSF in cisterna magna

13.7.1 Definition

Herniation of cerebellar tonsils through the foramen magnum into cervical spinal canal.

13.7.2 Clinical Features

- Often nonspecific symptoms such as headache, neck pain, dizziness, vertigo, or cranial nerve symptoms
- Chiari I is often an incidental finding and has no clinical implication in the absence of symptoms

13.7.3 Imaging Features

- Cerebellar tonsil located more than 5 mm inferior to a line between the hard palate and posterior lip of the foramen magnum
- More common in children
- Chiari I is often difficult to see, but a "full" foramen magnum on axial CT images is a good sign
- There are no osseous abnormalities
- MRI shows peg-like tonsils below the foramen magnum
- Narrow posterior cranial fossa
- Associated syringomyelia or syrinx (CSF in the center of spinal cord) may be seen
- Restricted CSF flow due to cerebellar tonsil being displaced inferiorly into the foramen magnum

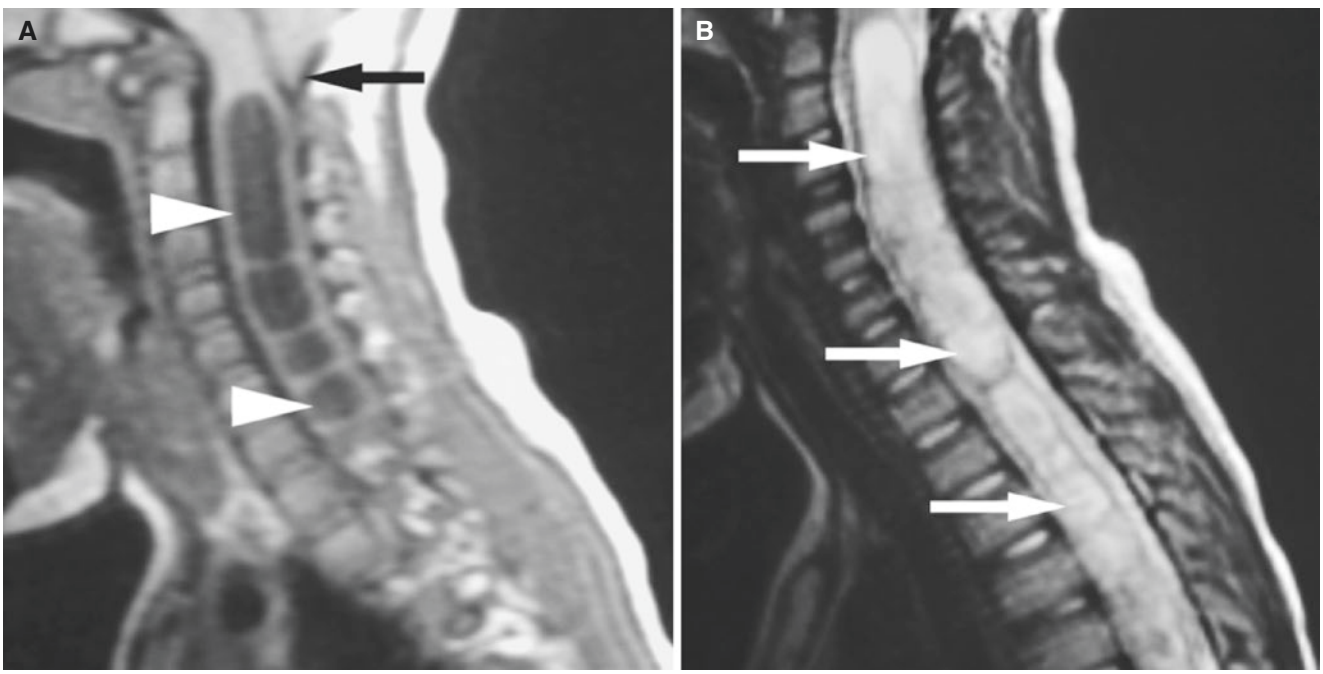

Fig. 13.7 Chiari malformation type I; 5-year-old asymptomatic male. (**A**) Mid-sagittal T1-weighted MRI demonstrates caudal displacement of cerebellar tonsils (*arrow*). Dark signal in the center of cervical cord represents syringo- or hydromyelia with multiple locations (*arrowheads*). (**B**) Sagittal T2-weighted MRI reveals associated hydromyelia with multiple locations of fluid in the center of cord. These are sequelae of decreased CSF dynamics through the foramen magnum (*arrows*)

13.8 Chordoma at Craniocervical Junction

Fig. 13.8

13.8.1 Definition

Benign but locally aggressive and infiltrating tumor arising from notochordal remnants along neuraxis.

13.8.2 Clinical Features

- Presents with pain and/or neurologic symptoms
- Commonest location is the sacrum, followed by clivus and spinal axis
- Slow-growing tumor with destruction of adjacent bone

13.8.3 Imaging Features

- Destructive expansile lesion in the spine with surrounding soft-tissue mass
- Locally aggressive
- Destruction and calcification better seen on CT images
- T1-weighted MRI: iso- to hypointense
- T2-weighted MRI: moderately to extremely hyperintense; extreme T2 hyperintensity is often a hallmark of chordoma, but not seen in our case (Fig. 13.8B)
- T1-weighted post-Gd MRI; variable enhancement

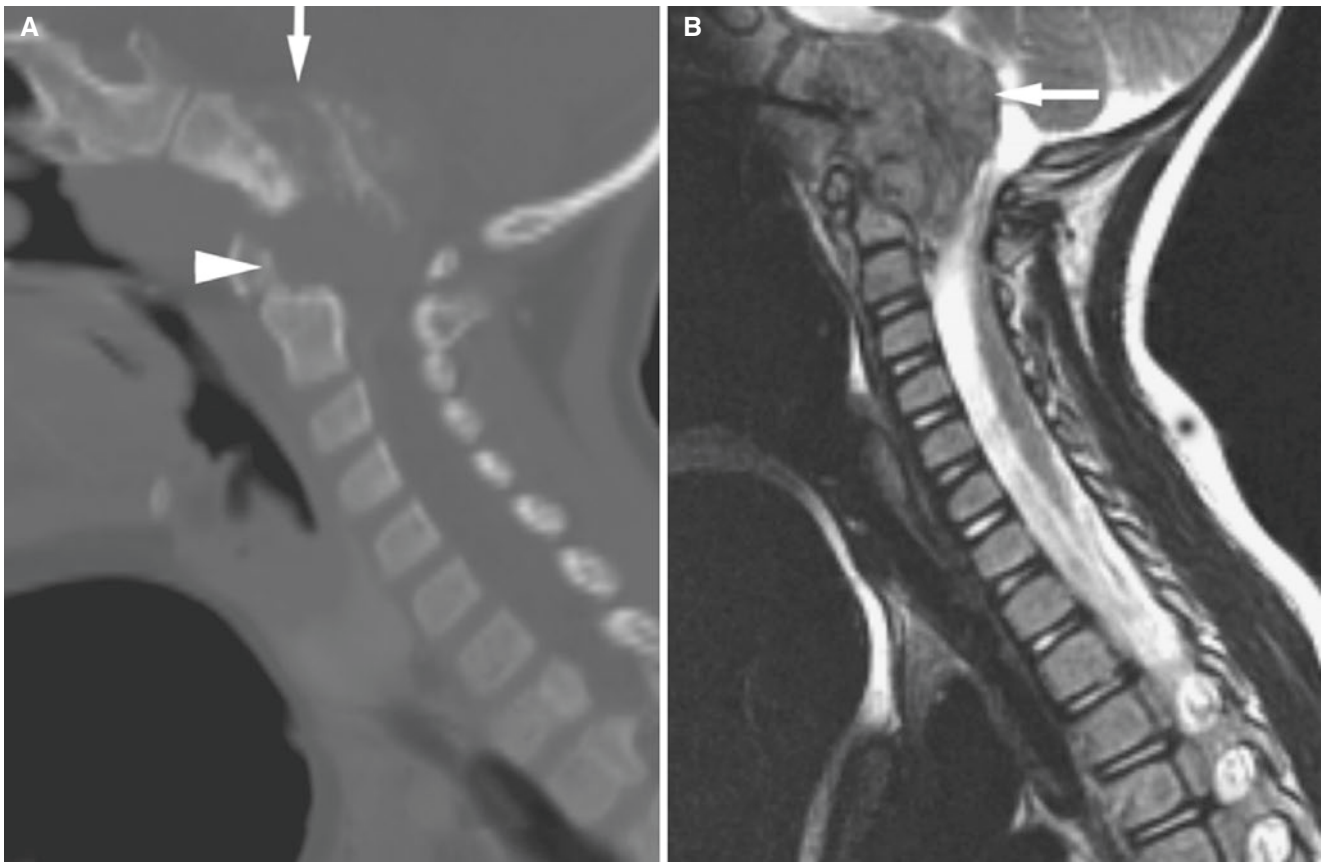

Fig. 13.8 Chordoma at craniocervical junction; 3-year-old female with a history of anorexia and lethargy for 2 months, presenting with mild cervical spine pain. (**A**) Sagittal reconstructed CT image shows destruction and bone production in skull base (*arrow*) and C1 area. Top of dens is eroded (*arrowhead*). (**B**) Sagittal T2-weighted MRI shows a large hypointense expansile mass emanating from the clivus (*arrow*). (**C**) Sagittal T1-weighted post-Gd MRI demonstrates a slight enhancement of mass (*arrow*) involving the clivus, C1, and C2 and extending intracranially and into the foramen magnum and nasopharynx. (**D**) Axial CT image through the foramen magnum illustrates destruction anteriorly (*arrow*) and bone production. (**E**) Axial T1-weighted post-Gd MRI demonstrates irregular slightly enhancing destructive mass in the foramen magnum (*arrow*) extending into the brain stem, causing brain stem compression

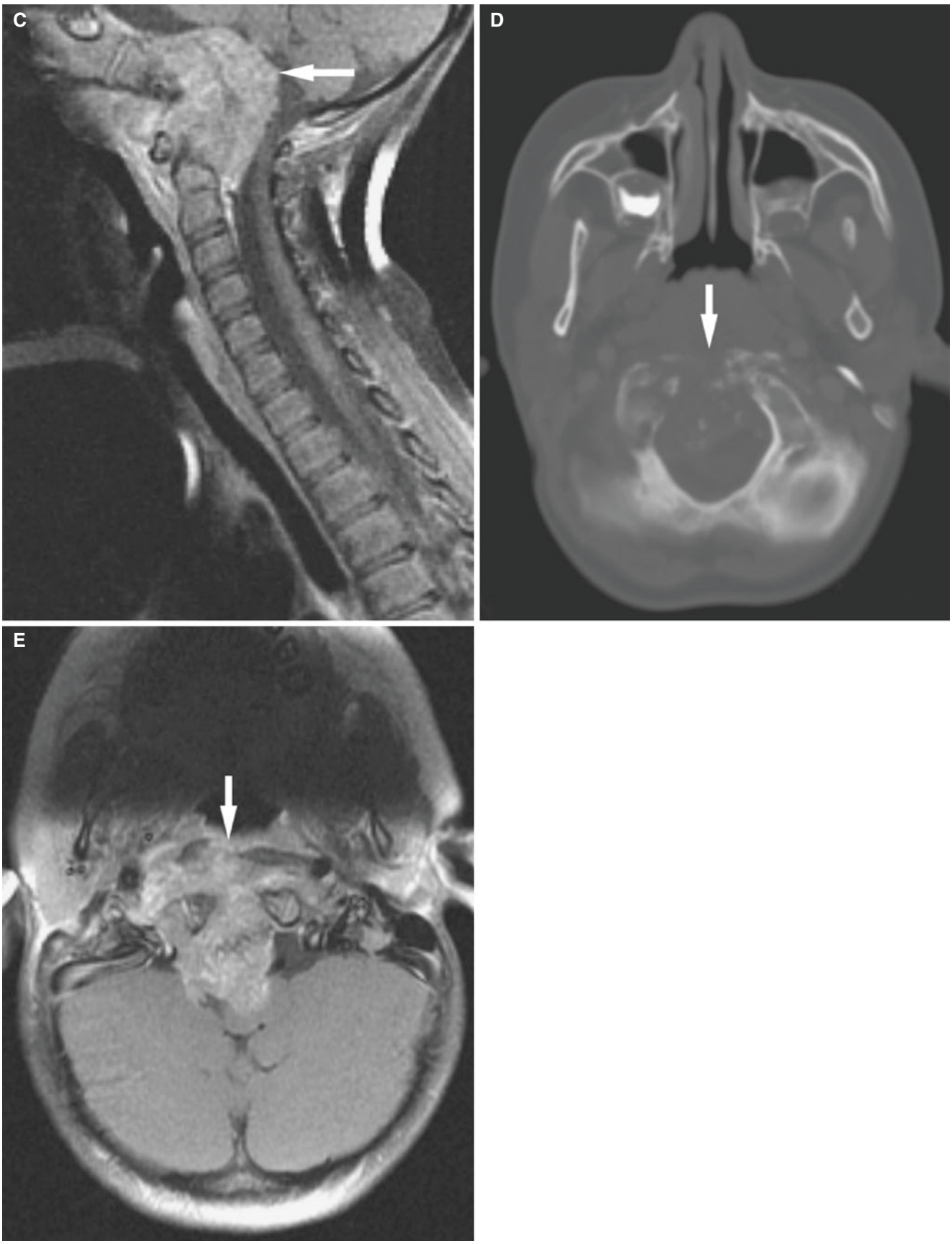

Fig. 13.8 (continued)

13.9 Cervical Spine Teratoma

Fig. 13.9

13.9.1 Definition

True neoplasm consisting of all three embryonic layers.

13.9.2 Clinical Features

- The most common tumors outside of the spinal cord (extramedullary) in cervical spine of newborns are neurofibromas/schwannomas followed by drop metastases and congenital lesions
- Teratoma is a rare tumor
- Approximately 10% associated with other congenital anomalies

13.9.3 Imaging Features

- Often large relatively well-circumscribed lesions
- Usually well encapsulated, with both cystic and solid components
- Fat content is typical
- T1- and T2-weighted MRI: heterogeneous signal due to difference of cellular components
- T1-weighted post-Gd MRI: contrast enhancement of solid portions

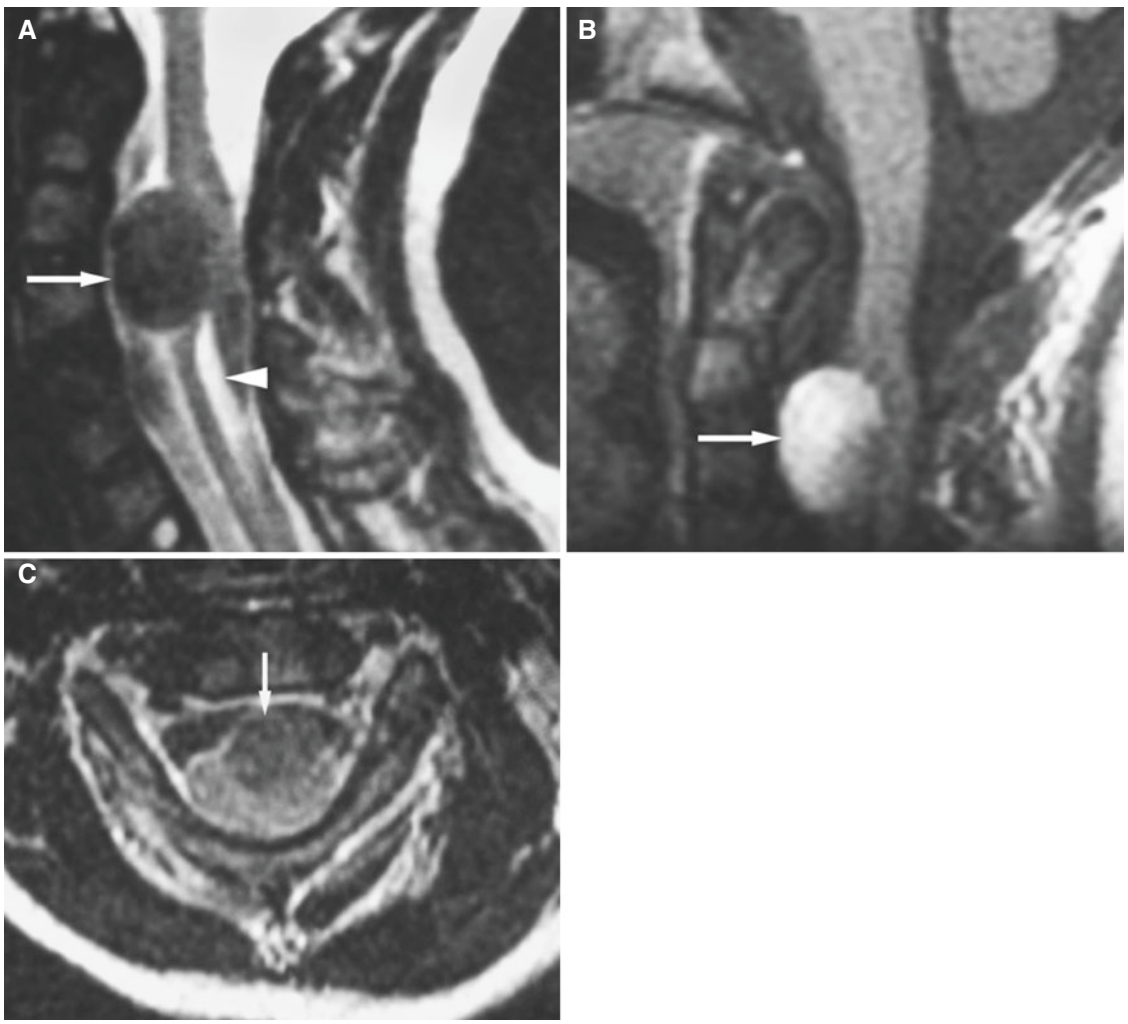

Fig. 13.9 Spinal teratoma; 7-year-old female with right hemiparesis. (**A**) Sagittal T2-weighted MRI shows enlargement of upper cervical canal. Anterior to cord, there is hypointense mass displacing cord (*arrow*). Exophytic mass largely fills spinal canal with almost complete obliteration of CSF space. Only posterior margin appears to infiltrate cord. Syrinx is seen below mass (*arrowhead*). (**B**) Sagittal T1-weighted post-Gd MRI shows near homogeneous enhancement (*arrow*), but no cord enhancement. (**C**) Axial T2-weighted MRI shows mass (*arrow*) compressing and displacing cord posteriorly

13.10 Cervical Spine Cord Astrocytoma

Fig. 13.10

13.10.1 Definition

Tumors derived from the glial cells (astrocytes or "star-shaped" cells)

13.10.2 Clinical Features

- Most common intramedullary (inside spinal cord) spinal cord tumor in children
- Cervical spine commonest site of involvement
- Multisegmental involvement usually seen
- Cysts and syrinx formation common

13.10.3 Imaging Features

- Expansion of cord
- Cord edema
- Cysts are common
- Relatively short segment involved as opposed to transverse myelitis in which a longer segment of cord is affected
- T1-weighted MRI: isointense to slightly hypointense
- T2-weighted MRI: hyperintense
- T1-weighted post-Gd MRI: patchy contrast enhancement

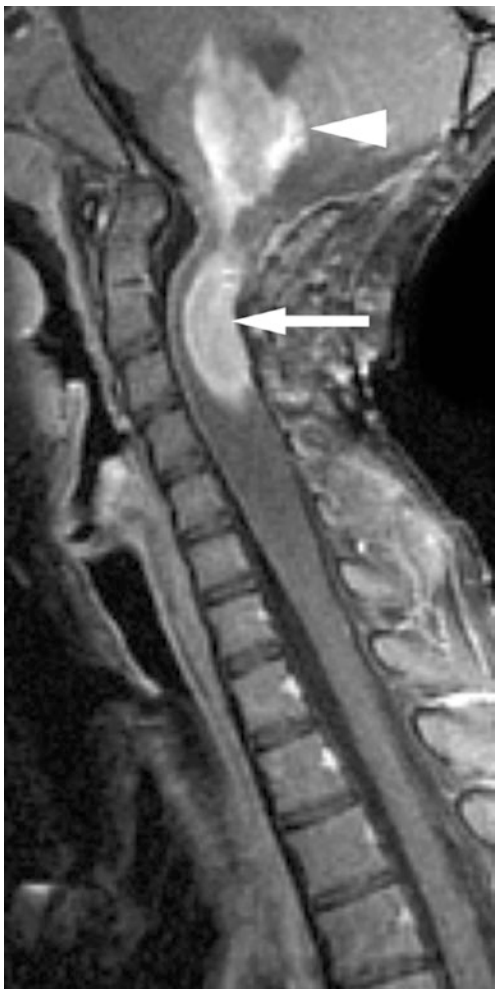

Fig. 13.10 Spinal cord astrocytoma; 8-year-old female with known low-grade astrocytoma in cervical cord since age of 18 months when she presented with breathing and swallowing difficulties. Sagittal T1-weighted post-Gd MRI shows intense contrast enhancement in tumor (*arrow*), extending into medulla and lower pons (*arrowhead*)

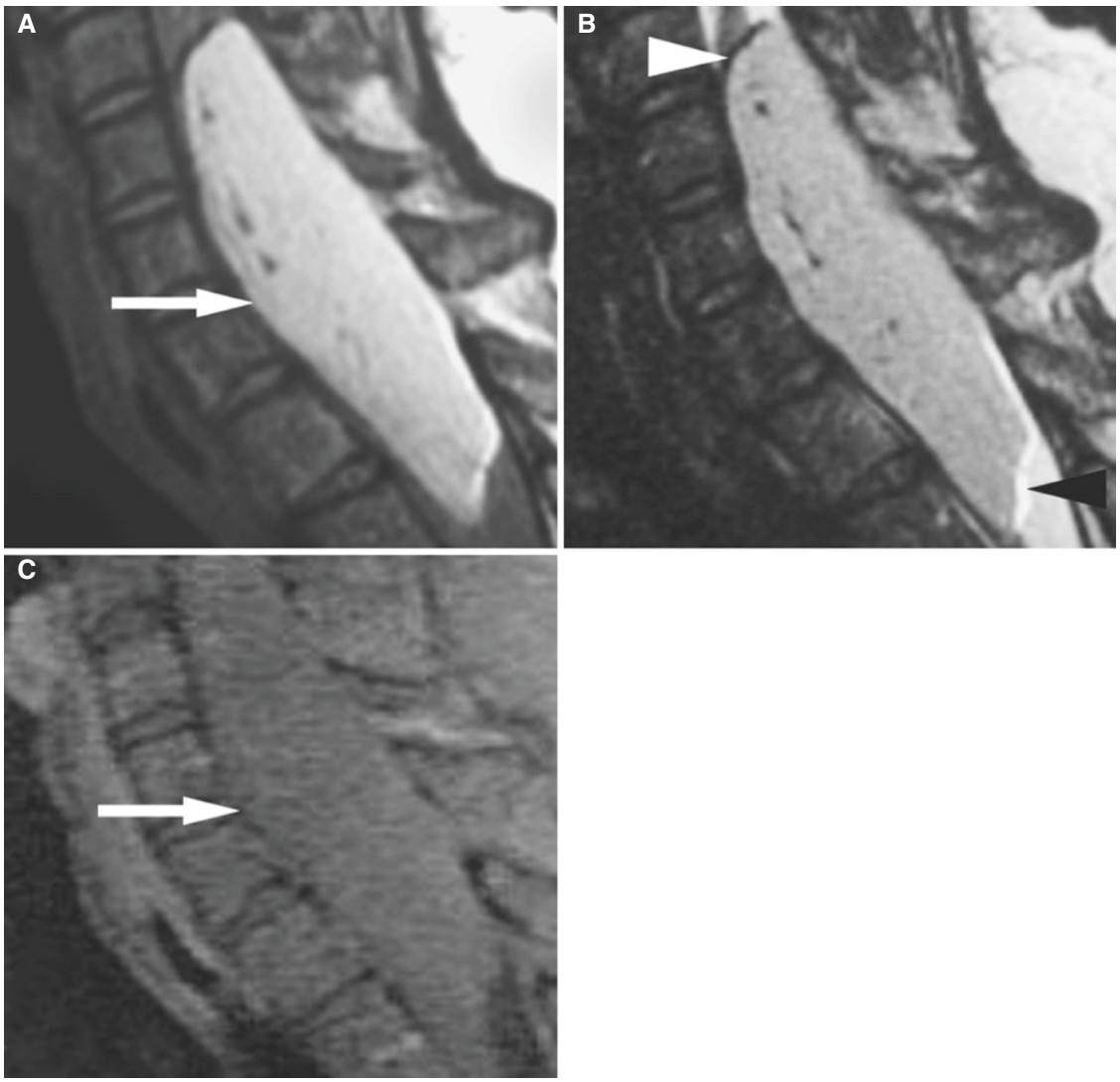

Fig. 13.11 Extramedullary cervical lipoma with cord compression; patient had long history of cord compression symptoms. Surgery confirmed the location and fatty nature of the encapsulated tumor. (**A**) Sagittal proton density MRI shows a large intradural mass (*arrow*), secondarily widened canal to long-standing pressure tumor. (**B**) Sagittal T2-weighted MRI shows slightly hyperintense mass compared to spinal cord. Note chemical shift misregistration artifact at CSF/lipoma and lipoma/CSF borders (*arrowheads*). (**C**) Sagittal T1-weighted fat-suppressed MRI shows fatty nature of tumor (*arrow*)

13.11 Extramedullary Cervical Lipoma with Cord Compression

Fig. 13.11

13.11.1 Definition

Benign fatty tumor, usually composed of mature fat cells.

13.11.2 Clinical Features

- Initially asymptomatic mass
- Presents with symptoms of spinal cord compression
- Often congenital
- Most common connective tissue tumor of the spine

13.11.3 Imaging Features

- CT: homogeneous nonenhancing mass with fatty attenuation value
- T1- and T2-weighted MRI: hyperintense
- T1-weighted fat-suppressed MRI: hypointense

13.12 Cervical Spine Meningioma

Fig. 13.12

13.12.1 Definition

Tumor arising in meninges surrounding brain and spinal cord.

13.12.2 Clinical Features

- Peak incidence in fifth to sixth decade with female predominance
- Thoracic spine commonest followed by cervical spine
- Majority are intradural extramedullary
- Patients with neurofibromatosis type 2 (NF-2) can have multiple meningiomas, with intracranial occurrence and along spinal axis; meningiomas originate from meningothelial cells which may be found in spinal arachnoid membranes

13.12.3 Imaging Features

- Similar characteristics to schwannoma
- Calcification not uncommon
- T1-weighted MRI: isointense to cord
- T2-weighted MRI: hypointense to cord
- T1-weighted post-Gd MRI: homogeneous and significant contrast enhancement

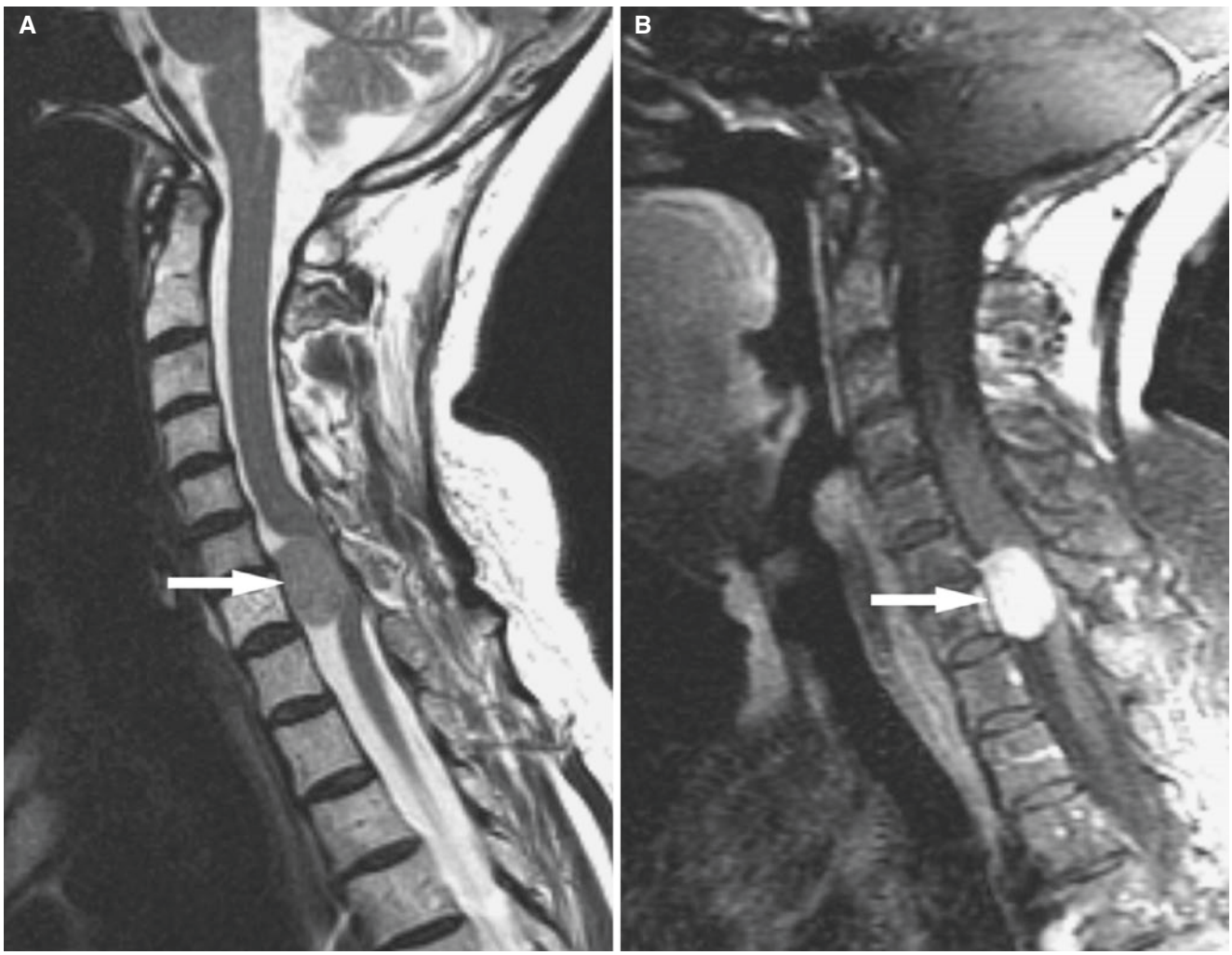

Fig. 13.12 Meningioma; 67-year-old woman with progressive weakness in both lower extremities and pain in both arms. Remote history of breast cancer. (**A**) Sagittal T2-weighted MRI shows well-defined mass with homogeneous signal isointense to cord (*arrow*). (**B**) Sagittal T1-weighted post-Gd MRI shows intense contrast-enhanced tumor (*arrow*)

13.13 Cervical Spine Neurofibromatosis Type 1 (NF-1)

Fig. 13.13

13.13.1 Definition

Tumors arising from nerve sheath of peripheral nerve; Schwann's cells, fibroblasts, and perineural cells.

13.13.2 Clinical Features

- NF-1 the commonest neurocutaneous syndrome
- Manifestations can arise from any system of the body
- Bony changes usually associated
- Many patients have neurofibromas in cervical region

13.13.3 Imaging Features

- Iso- to hypodense to muscle on CT
- Spinal lesions best seen on MRI
- T1-weighted MRI: neurofibromas appear iso- to hypointense
- T2-weighted MRI: hyperintense
- T1-weighted post-Gd MRI: strong contrast enhancement; may show "target pattern"

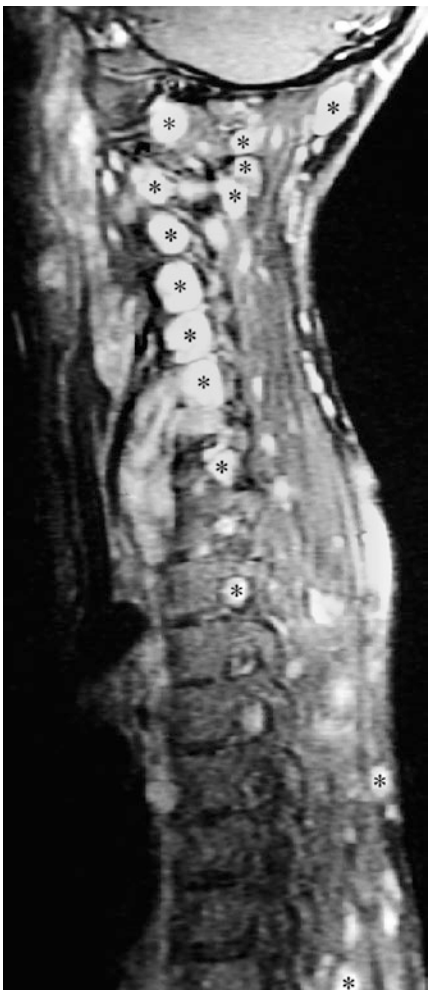

Fig. 13.13 Neurofibromatosis type 1 (NF-1); 16-year-old female with known NF-1, presenting with balance and coordination problems. Sagittal T2-weighted fat-suppressed MRI shows enlargement of the neural foramina with multiple rounded neurofibromas (*asterisks*)

13.14 Cervical Spine Fracture

Fig. 13.14

13.14.1 Definition

Fracture and/or dislocation of cervical spine.

13.14.2 Clinical Features

- Presents invariably with cervical spine pain or tenderness
- More advanced fractures with neurologic symptoms
- Plain films often negative

13.14.3 Imaging Features

- CT, sagittal, and coronal images, best for fracture diagnosis
- MRI best for cord injury and for ligamentous injuries
- Burst fracture involves fracture of posterior wall of vertebral body often with retropulsion
- Compression fracture has intact posterior wall of vertebral body

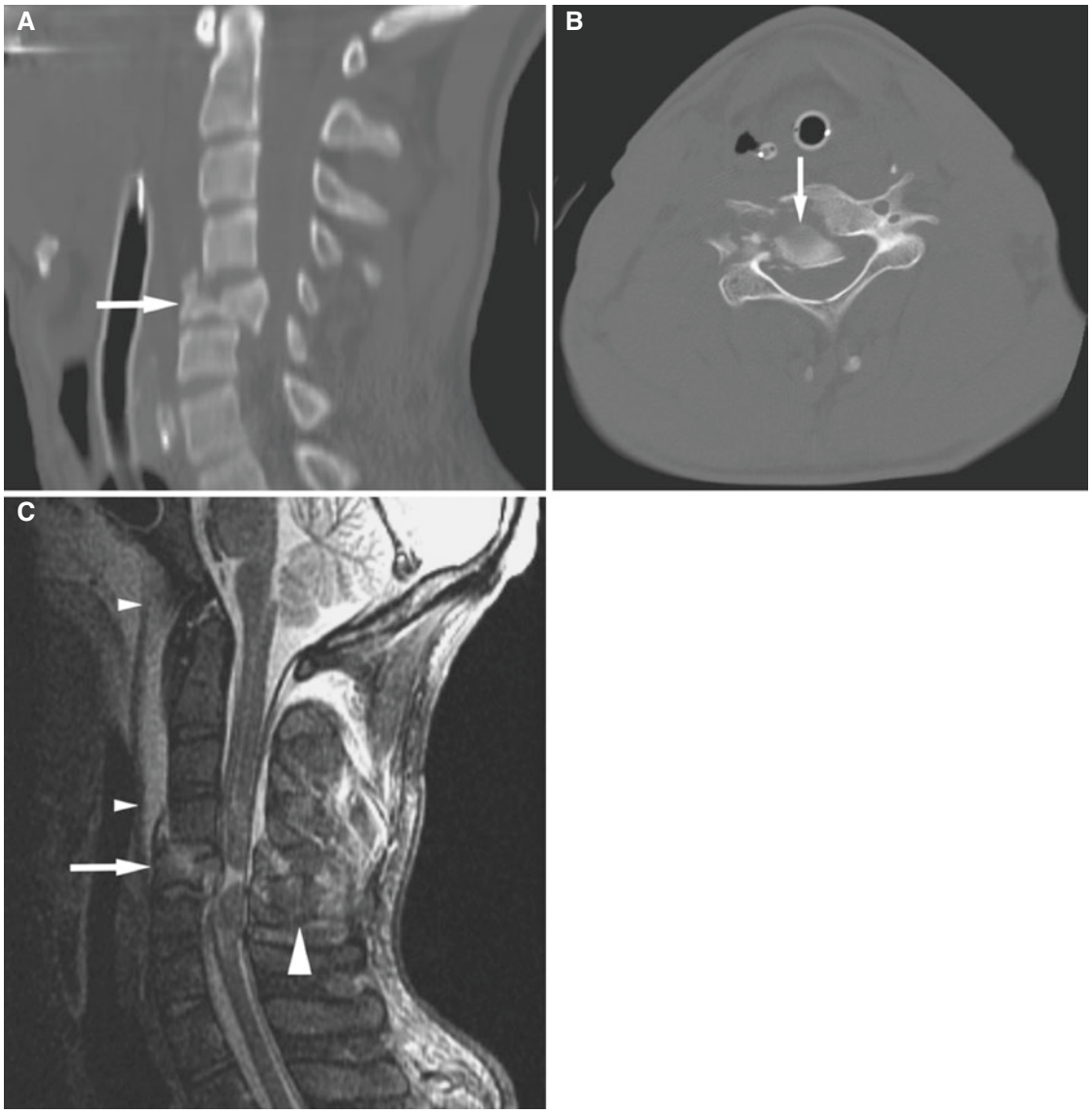

Fig. 13.14 C5 burst fracture; 27-year-old male all-terrain vehicle accident. (**A**) Sagittally reformatted CT image shows burst fracture of C5 with subluxation and severe central canal narrowing (*arrow*). (**B**) Axial CT image demonstrates fragment displaced into central canal (*arrow*). Also fracture through right foramen tranversarium where vertebral artery is located. This injury may cause damage to vertebral artery which could lead to a posterior fossa stroke. (**C**) Sagittal STIR MRI shows spinal cord contusion, C5 burst fracture (*arrow*), prevertebral hematoma C1 to C4 (*arrowheads*), and injury to posterior elements (*large arrowhead*)

13.15 Neck

Diagnosis of lesions of the suprahyoid neck is primarily not the duty of the maxillofacial radiologist. However, many of the structures of this area will be depicted on regular maxillofacial imaging studies, and therefore the maxillofacial radiologist will often have to make a gross evaluation to determine whether there is an abnormality that needs further attention or the structures are normal. Conversely some larger maxillofacial lesions will extend into the suprahyoid neck, and the maxillofacial radiologist will have to have a working knowledge of neck anatomy in order to formulate an interpret of the findings.

This section is included to provide examples of abnormalities in the supra- and infrahyoid neck that may be recognized by the maxillofacial radiologist, such as inflammations, nontumorous expansive masses, muscle paralysis, and benign and malignant tumors with their characteristics.

13.16 Hypopharynx Abscess

Fig. 13.15

13.16.1 Definition

Pus collection in pharyngeal/hypopharyngeal soft tissues.

13.16.2 Clinical Features

- Dysphagia
- Neck and oral pain
- Fever
- Stridor
- Odynophagia

13.16.3 Imaging Features

- Soft-tissue swelling
- Ring-enhancing lesion with low-attenuation center
- Stranding (lymphedema) and obliteration of adjacent fat planes
- Thickening of platysma
- Lymphadenopathy
- T1-weighted MRI: decreased signal
- T2-weighted MRI: increased signal
- T1-weighted post-Gd MRI: peripheral enhancement

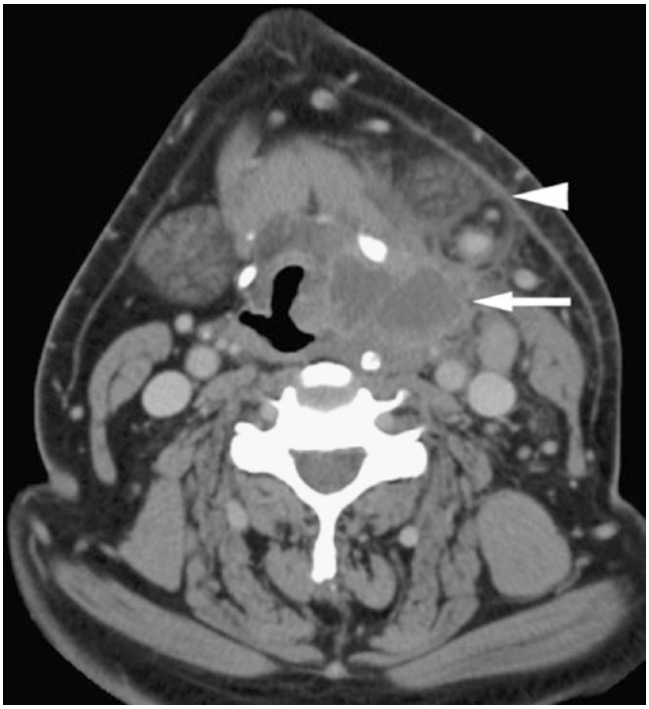

Fig. 13.15 Hypopharynx abscess; 48-year-old male presenting with a peripharyngeal soft-tissue swelling, neck pain, fever, and stridor. Axial CT image shows multilobulated ring-enhancing mass (*arrow*), consistent with abscess in left hypopharynx with a compression narrowing and deviation of hypopharyngeal airway. Thickening of platysma (*arrowhead*) and stranding of subcutaneous fat

13.17 Thyroid Abscess

Fig. 13.16

13.17.1 Definition

Well-circumscribed pus collection within the thyroid gland.

13.17.2 Clinical Features

- Swelling, pain, and redness
- Induration (localized hardening of soft tissue)
- Fever
- Dysphagia/odynophagia
- Tender gland sometimes with referred pain to pharynx/ear
- Often occurs in immunocompromised and debilitated patients
- *Staphylococcus aureus*, pneumococcus common organisms

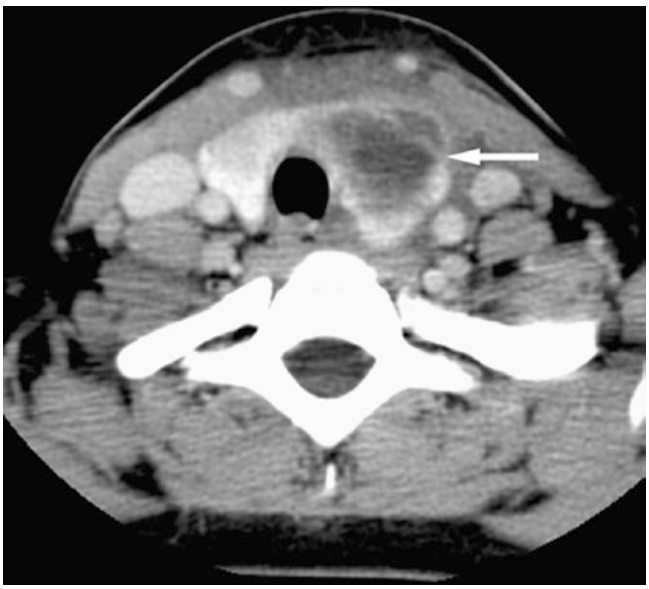

Fig. 13.16 Thyroid abscess; 19-year-old female presenting with a 2-week history of a sore throat, left neck pain, and headache. Axial post-contrast CT image shows ill-defined hypodense lesion in left lobe of the thyroid gland with ring enhancement (*arrow*), consistent with abscess and soft-tissue edema. Low dense areas are also noted in the oropharynx especially on the left side and inferiorly to the thoracic inlet and bilateral lymphadenopathy

13.17.3 Imaging Features

- Ring-enhancing lesion with central area of necrosis within the thyroid gland
- Swelling
- Fat stranding
- Lymphadenopathy

13.18 Tornwaldt's Cyst

Fig. 13.17

13.18.1 Definition

Developmental cyst occurs when pharyngeal bursa ectoderm retracts with the notochord into the clivus. Named after Gustav Ludwig Tornwaldt (1843–1910).

13.18.2 Clinical Features

- Most often asymptomatic incidental finding on imaging study
- Seen incidentally in up to 3% of healthy adults; usually no treatment needed
- May cause symptoms when infected
- Infection may spread to mediastinum

13.18.3 Imaging Features

- Cystic lesion mostly in the midline of nasopharynx
- Low attenuation
- T1-weighted MRI: low-signal intensity
- T2-weighted MRI: high signal
- T1-weighted post-Gd MRI: no contrast enhancement

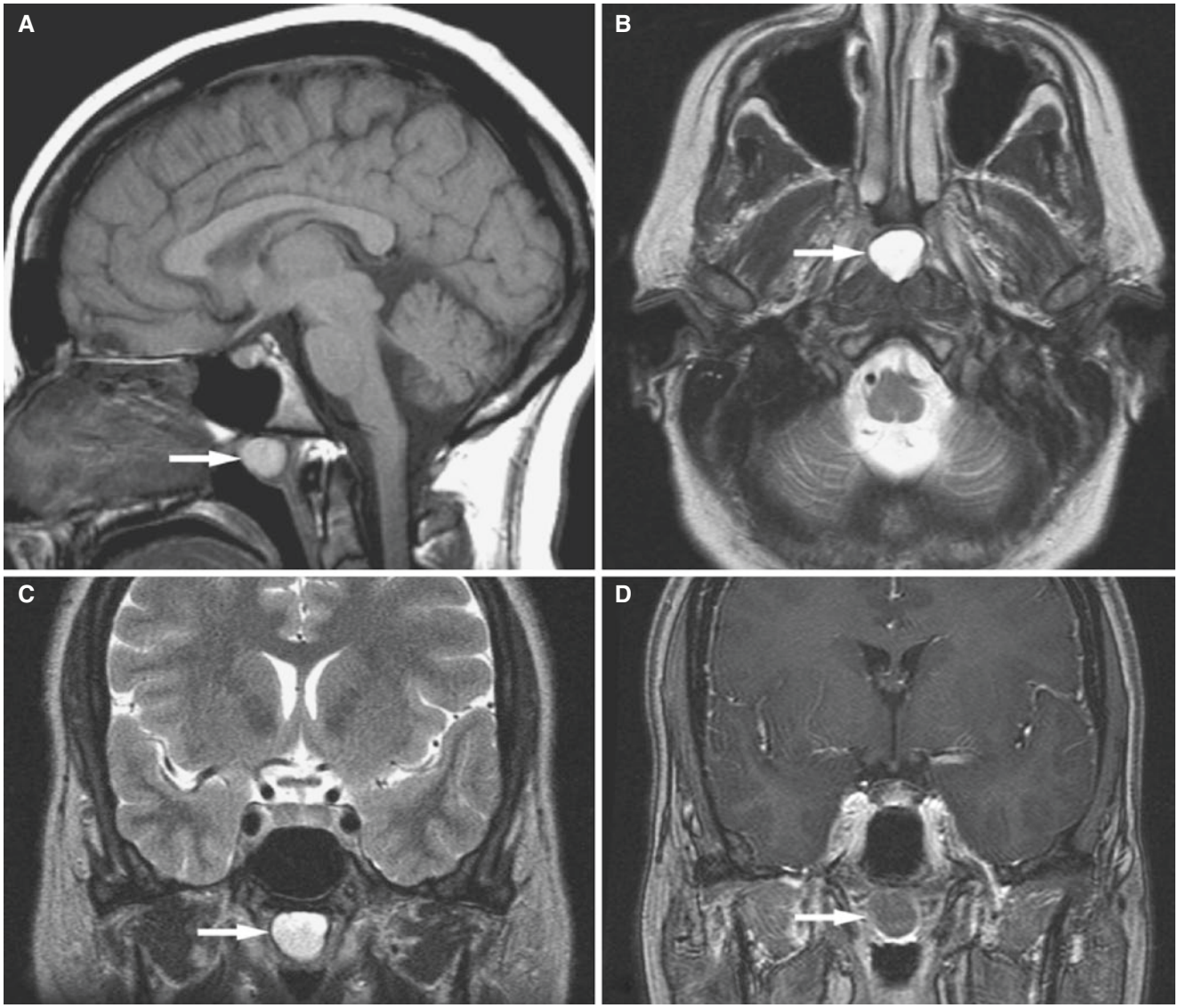

Fig. 13.17 Tornwaldt's cyst, large; incidental findings in a 30-year-old. (**A**) Sagittal T1-weighted MRI shows low-signal cyst (*arrow*) in posterior nasopharynx. (**B**) Axial T2-weighted MRI shows bright signal cyst (*arrow*). (**C**) Coronal T2-weighted MRI shows bright signal cyst (*arrow*). (**D**) Coronal T1-weighted post-Gd MRI shows no enhancement of the cyst (*arrow*)

13.19 Dermoid Cyst in the Floor of the Mouth

Fig. 13.18

13.19.1 Definition

Growth of a piece of the skin underneath the surface as result of abnormal development; may contain the skin, hair, bone, teeth, or embryonal tissue.

13.19.2 Clinical Features

- Most commonly involves the floor of the mouth; sublingual, submental, or submandibular regions
- Differential diagnosis includes epidermoid, ranula, thyroglossal duct cyst, and cystic hygroma
- Soft nonpainful mass

Fig. 13.18 Dermoid cyst; 18-year-old male with doughy swelling of the floor of the mouth clinically considered a thyroglossal duct cyst. Axial T2-weighted fat-suppressed MRI shows well-defined oval mass with high signal in the floor of the mouth (*arrow*), located in sublingual space depressing mylohyoid muscle down (not shown)

13.19.3 Imaging Features

- Typically well-circumscribed, thin-walled, unilocular mass
- Low attenuation
- T1-weighted MRI: homogeneous low signal
- T2-weighted MRI: homogeneous high signal
- T1-weighted post-Gd MRI: no contrast enhancement of cyst except wall, in particular if infected

13.20 Goiter

Fig. 13.19

13.20.1 Definition

Diffuse or multinodular enlargement of the thyroid gland.

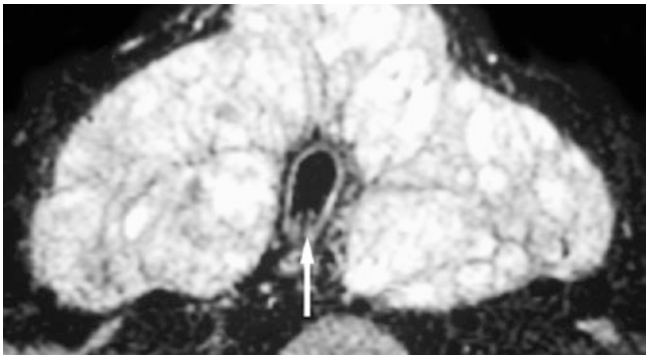

Fig. 13.19 Goiter; 18-year-old presenting with hyperthyroidism. Axial T2-weighted fat-suppressed MRI shows large multilobulated thyroid gland compressing and narrowing trachea (*arrow*)

13.20.2 Clinical Features

- More common in middle-aged females
- Often associated with iodine deficiency
- Midline neck mass
- Often asymptomatic enlargement of the thyroid gland; symptoms depend upon state of hypo- or hyperthyroidism
- Endemic goiters are prevalent in iodine-deficient areas
- Goiter is a clinical diagnosis that simply implies an enlargement of the thyroid gland developing because the thyroid gland compensates for inadequate thyroid hormone output

13.20.3 Imaging Features

- Nodular enlargement of the thyroid gland often with cystic lesions
- Displaces and narrows trachea
- Multinodular goiter is usually not associated with tumors
- Substernal or mediastinal extension requires imaging for detection
- T2-weighted MRI: high signal due to colloid or hemorrhage
- Nuclear scan with radioactive iodine or Tc-99m pertechnetate is often very helpful (cannot be done for 6 weeks if intravenous contrast has been used)
- Ultrasound is often used to characterize multinodular goiter

13.21 Vocal Cord Paralysis

13.21.1 Definition

Fig. 13.20

Vocal cord does not move to the center due to muscle paralysis.

13.21.2 Clinical Features

- Patient presents with hoarseness
- Occasionally a sign of a tumor along the recurrent laryngeal nerve

13.21.3 Imaging Features

- Paralyzed vocal cord is located laterally in larynx; unable to migrate to midline (as normal) due to lack of innervation of muscles

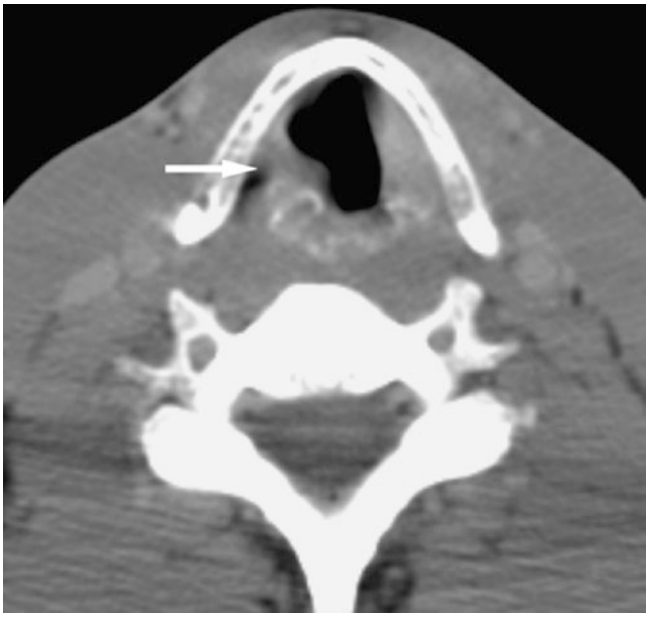

Fig. 13.20 Right vocal cord paralysis secondary to lung cancer; 63-year-old man presents with hoarseness. Axial CT image through larynx shows right vocal cord (*arrow*) laterally in larynx

13.22 Neck Hemangioma

Fig. 13.21

13.22.1 Definition

Hemangioma or benign neoplasm that exhibits increased blood circulation, endothelial cells, mast cells, and macrophages.

13.22.2 Clinical Features

- Most common tumor in the head and neck in infancy and childhood
- Approximately 7% of all benign soft-tissue tumors
- Rapidly enlarges
- Ultimately regresses by adolescence
- Typically becomes apparent during the first month of life
- Diffuse skin lesion or soft cystic mass in the oral cavity, pharynx, parotid gland, or neck
- Associated with intracranial arterial vascular malformations
- Often requires no treatment. Steroids are occasionally used

13.22.3 Imaging Features

- T1-weighted MRI: intermediate signal with flow void
- T1-weighted post-Gd MRI: dramatic enhancement
- Often extensively infiltrative in nature

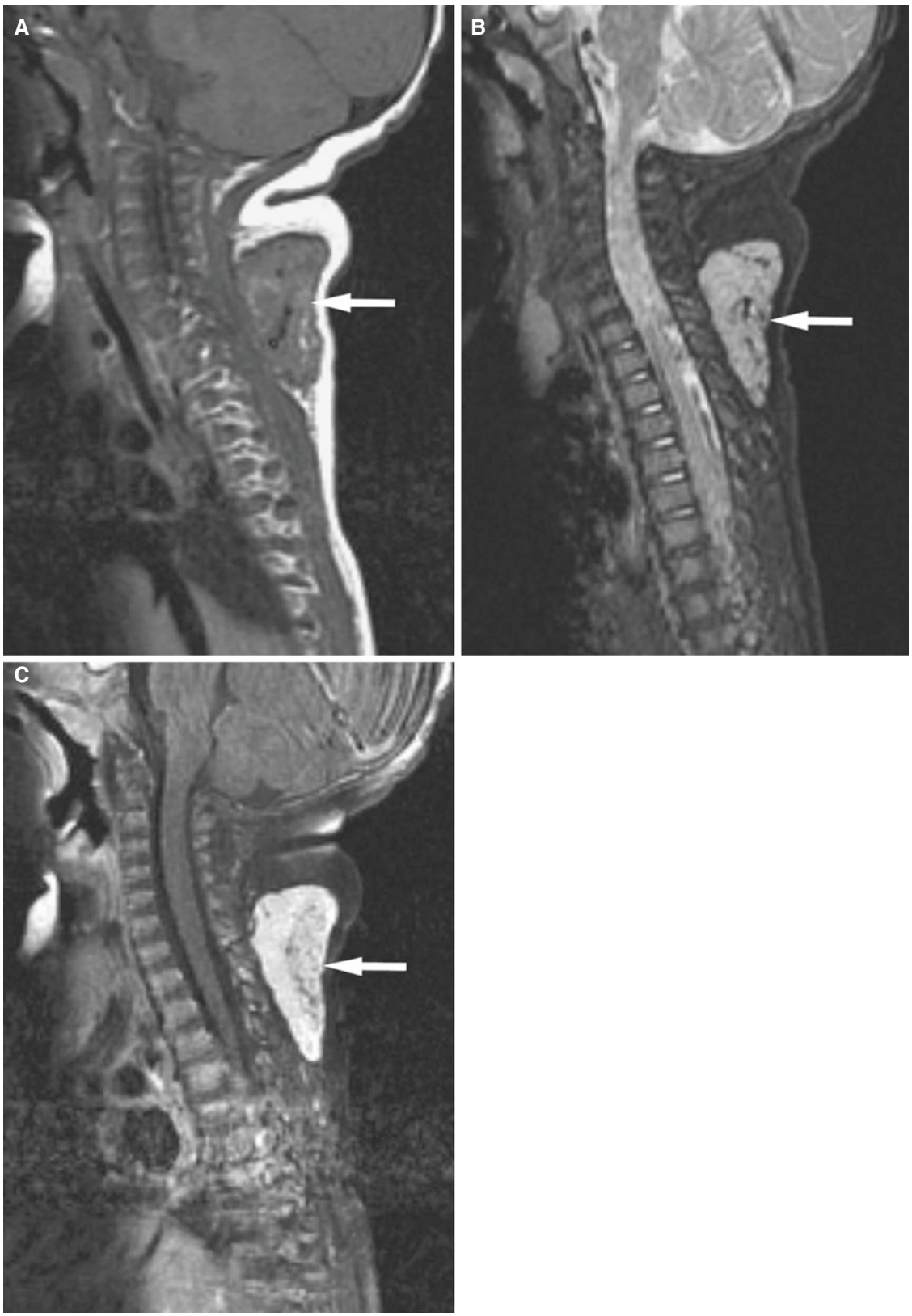

Fig. 13.21 Hemangioma; 6-month-old infant twin girl presents with mass in back of neck. The mass has been observed for only a few days. (**A**) Sagittal T1-weighted MRI shows a well-circumscribed large mass in posterior neck with flow voids (*arrow*). (**B**) Sagittal STIR MRI shows intermediate high-signal intensity also with flow voids (*arrow*). (**C**) Sagittal T1-weighted post-Gd MRI shows dramatic enhancement (*arrow*)

13.23 Neck Lipoma

Fig. 13.22

13.23.1 Definition

Benign fatty neoplasm.

13.23.2 Clinical Features

- Often occurs in posterior neck
- Soft benign neoplasm usually does not enlarge in size

13.23.3 Imaging Features

- Low attenuation
- Well circumscribed
- T1-weighted MRI: high signal
- T2-weighted MRI: intermediate signal
- T1-weighted fat-suppressed MRI: low signal

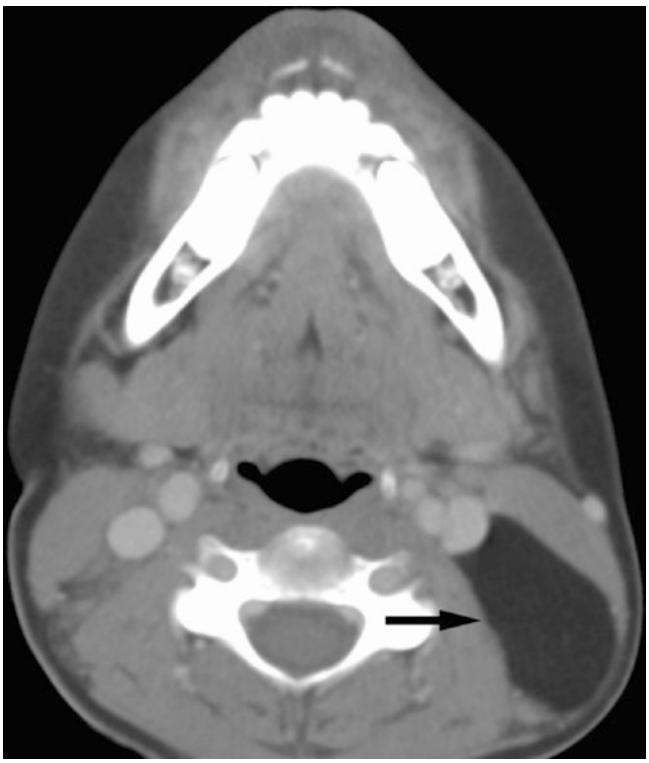

Fig. 13.22 Lipoma; 8-year-old female with a 3-week history of left posterior neck mass. No redness, no fever, and no tenderness. Axial CT image shows low-attenuation well-circumscribed fatty appearing mass in posterior triangle of left neck (*arrow*), deep to sternocleidomastoid muscle

13.24 Neck Plexiform Neurofibroma

Fig. 13.23

13.24.1 Definition

Benign neoplasm consisting of Schwann cells and fibroblasts.

13.24.2 Clinical Features

- Malignant transformation in 5–10%
- Unique to neurofibromatosis type 1 (from von Recklinghausen's disease)
- Common in the scalp, neck, mediastinum, retroperitoneum, cranial nerve five, and orbits
- Masses are soft and elastic
- Accounts for elephantiasis, seen in neurofibromatosis
- Sarcomatous transformation in about 5% of patients

13.24.3 Imaging Features

- Infiltrated aggressive-appearing tumors along cranial nerves
- Multilobulated masses along nerves with low to intermediate attenuation
- T1-weighted MRI: intermediate signal
- T2-weighted MRI: high signal. Sometimes target sign: low-signal intensity centrally with ring of high signal in periphery
- T1-weighted post-Gd MRI: often dramatic enhancement
- Three types: localized, diffused, and plexiform

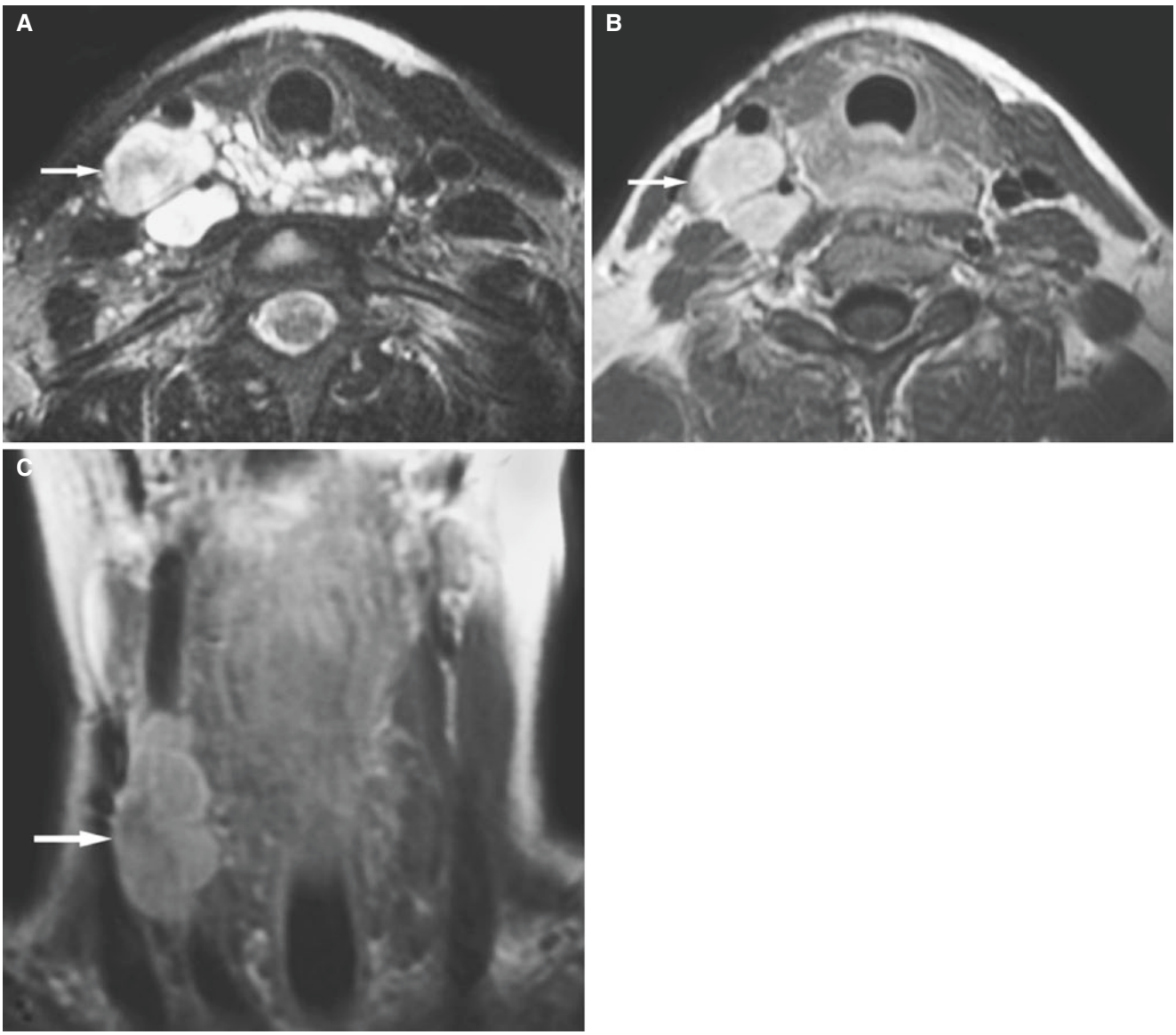

Fig. 13.23 Plexiform neurofibromatosis; 9-year-old female presents with a painless swelling of right lower neck. (**A**) Axial T2-weighted fat-suppressed MRI shows multilobulated complex mass in the right lower neck extending across midline (*arrow*), separating common carotid artery and jugular vein, and abutting the spine. (**B**) Axial T1-weighted post-Gd MRI shows enhancing mass separating carotid artery and jugular vein (*arrow*). (**C**) Coronal T1-weighted post-Gd MRI shows contrast-enhanced multilobulated mass in carotid sheath (*arrow*)

13.25 Pharynx Rhabdomyosarcoma

Fig. 13.24

13.25.1 Definition

Malignant tumor of striated muscles, primarily affecting children and young adults.

13.25.2 Clinical Features

- Most common malignant orbital tumor in childhood
- Mean age: 7 years
- Often metastasizes to lung or cervical nodes

13.25.3 Imaging Features

- Large, aggressive soft-tissue mass
- Ill-defined inhomogeneous large soft-tissue mass which erodes and infiltrates surrounding structures including bones
- MRI is best to characterize the soft tissue and extent
- T1-weighted MRI: intermediate signal
- T2-weighted MRI: hyperintense
- T1-weighted post-Gd MRI: variable enhancement

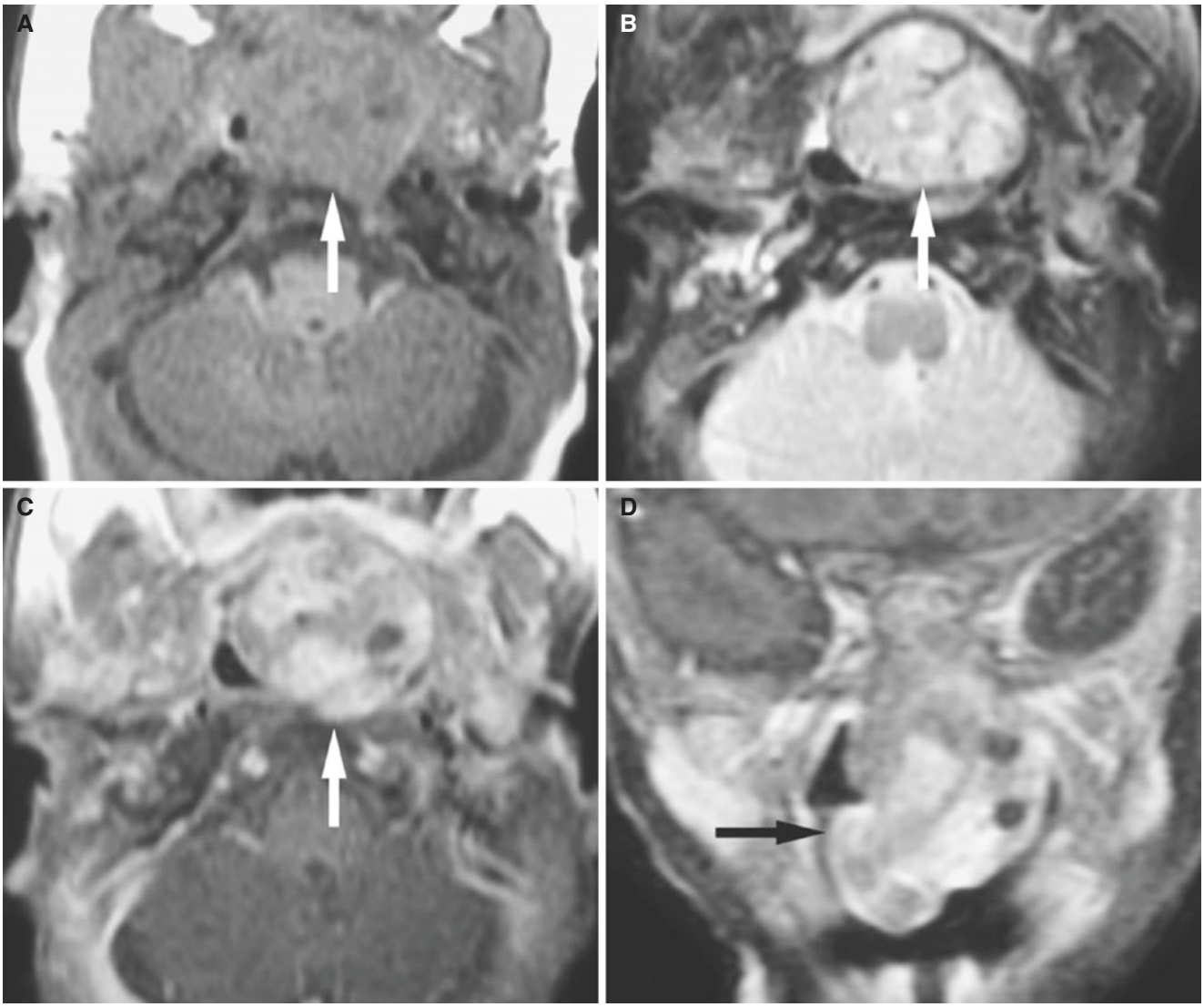

Fig. 13.24 Rhabdomyosarcoma; 5-week-old female with stridor and a posterior pharyngeal mass. (**A**) Axial T1-weighted MRI shows a large right pharyngeal mass isointense to muscle (*arrow*). (**B**) Axial T2-weighted MRI shows a well-circumscribed mass (*arrow*) in the nasopharynx with linear and punctate areas of low attenuation representing vascular structure. (**C**) Contrast-enhanced T1-weighted MRI shows enhancement and flow voids (*arrow*). (**D**) Contrast-enhanced T1-weighted fat-suppressed MRI shows large enhancing lesion in nasopharynx (*arrow*)

13.26 Tongue Base Carcinoma

Fig. 13.25

13.26.1 Definition

Squamous cell malignant neoplasm of the tongue.

13.26.2 Clinical Features

- Infiltrating lesion often on lateral or posterior aspect of tongue
- Painless swelling and/or induration
- Risk factors for oral cavity squamous carcinoma: smoking, alcohol abuse, chewing tobacco, and chewing betel nuts

13.26.3 Imaging Features

- T2-weighted fat-suppressed image often delineates tumor best
- Sagittal, coronal axial images are essential to as precisely as possible outline the extent of the tumor
- Crossing the midline is important for surgical planning (generally not resectable if cross midline)
- T1-weighted MRI: intermediate signal
- T2-weighted MRI: intermediate to high signal
- T1-weighted post-Gd MRI: some enhancement

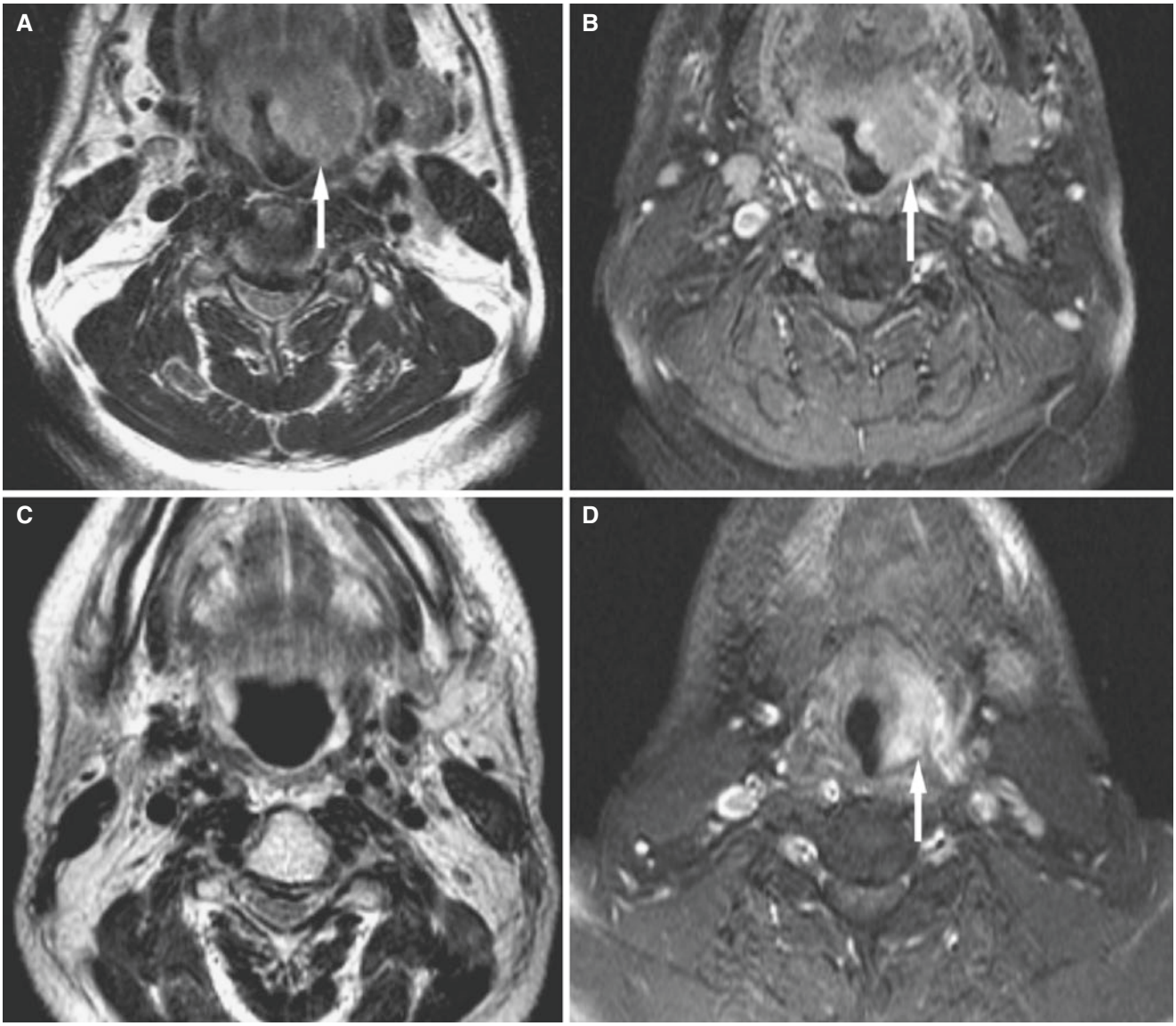

Fig. 13.25 Tongue base carcinoma; 64-year-old man presents with left throat pain. (**A**) Axial T2-weighted MRI shows a large low intensity mass in left tongue base extending to the hypopharynx (*arrow*). The signal is higher than muscle but still not bright. (**B**) Axial T1-weighted fat-suppressed post-Gd MRI shows slight enhancement of mass (*arrow*). (**C**) Axial T2-weighted MRI, more caudal section, shows no lymphadenopathy. (**D**) Axial T1-weighted fat-suppressed post-Gd MRI, more caudal section, shows extension to left hypopharynx (*arrow*)

13.27 Hypopharynx Carcinoma

Fig. 13.26

13.27.1 Definition

Squamous cell malignant neoplasm of pharynx.

13.27.2 Clinical Features

- Infiltrating lesion in wall of pharynx
- Painless
- Often associated with swallowing problems
- Risk factors for hypopharynx squamous carcinoma: smoking and alcohol abuse

13.27.3 Imaging Features

- Soft-tissue mass in hypopharynx
- Asymmetry of hypopharynx, supraglottic area, and false and true vocal cords
- Obliteration of piriform sinus

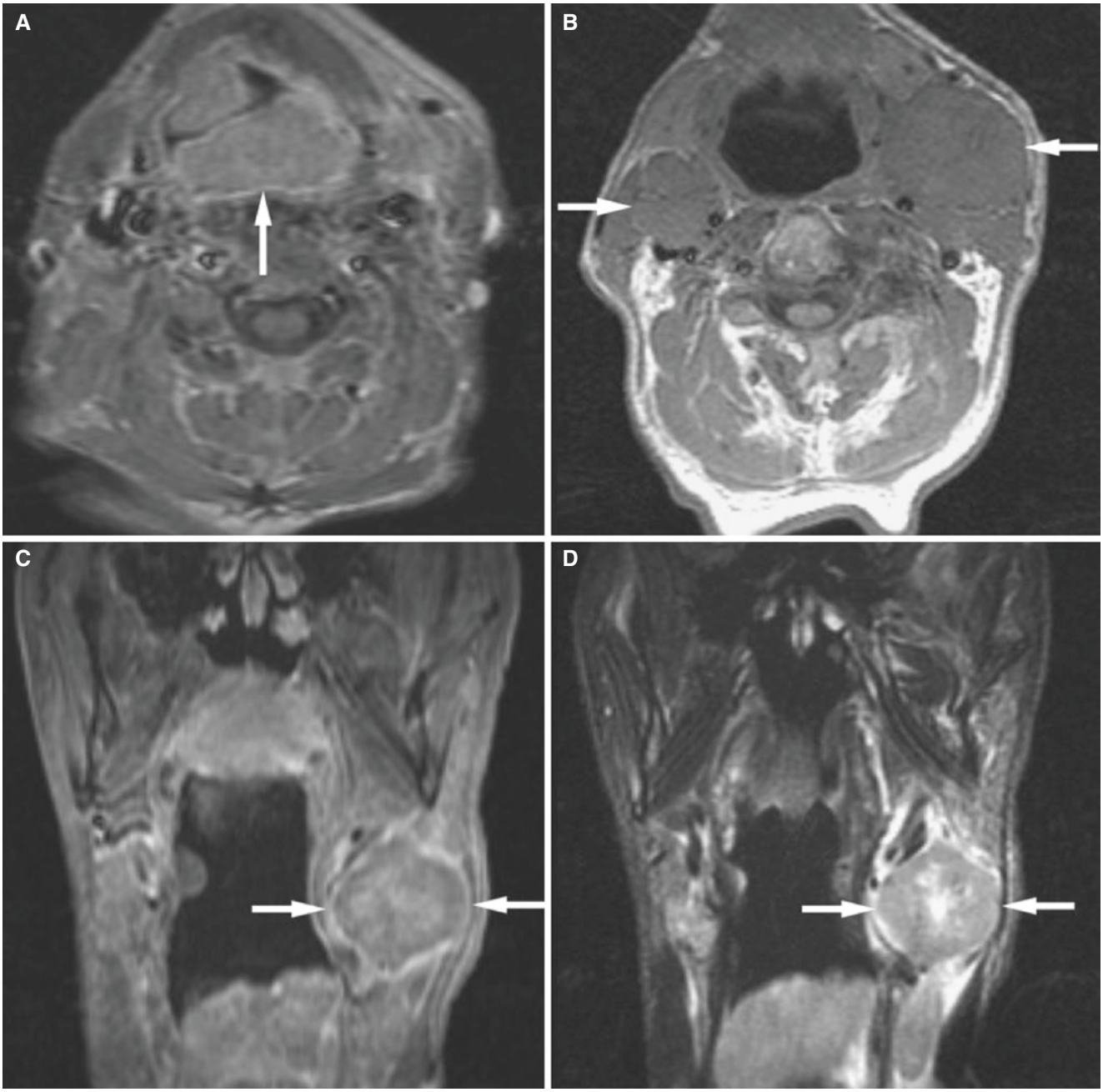

Fig. 13.26 Hypopharynx carcinoma; 60-year-old female with a feeling of a lump in the throat. (**A**) Axial T1-weighted post-Gd fat-suppressed MRI shows a large almost circumferential hypopharyngeal mass (*arrow*). (**B**) Axial T1-weighted MRI shows bilateral enlarged lymph nodes (*arrows*). (**C**) Coronal T1-weighted post-Gd MRI shows left-sided enlarged lymph node (*arrows*). (**D**) Coronal T2-weighted post-Gd MRI shows left-sided enlarged lymph node (*arrows*)

13.28 Burkitt's Lymphoma

Fig. 13.27

13.28.1 Definition

Stem cell non-Hodgkin's lymphoma.

13.28.2 Clinical Features

- Most commonly seen in children
- Most common malignant disease of children in tropical Africa
- Involvement of jaw characteristic
- Related to Epstein–Barr virus

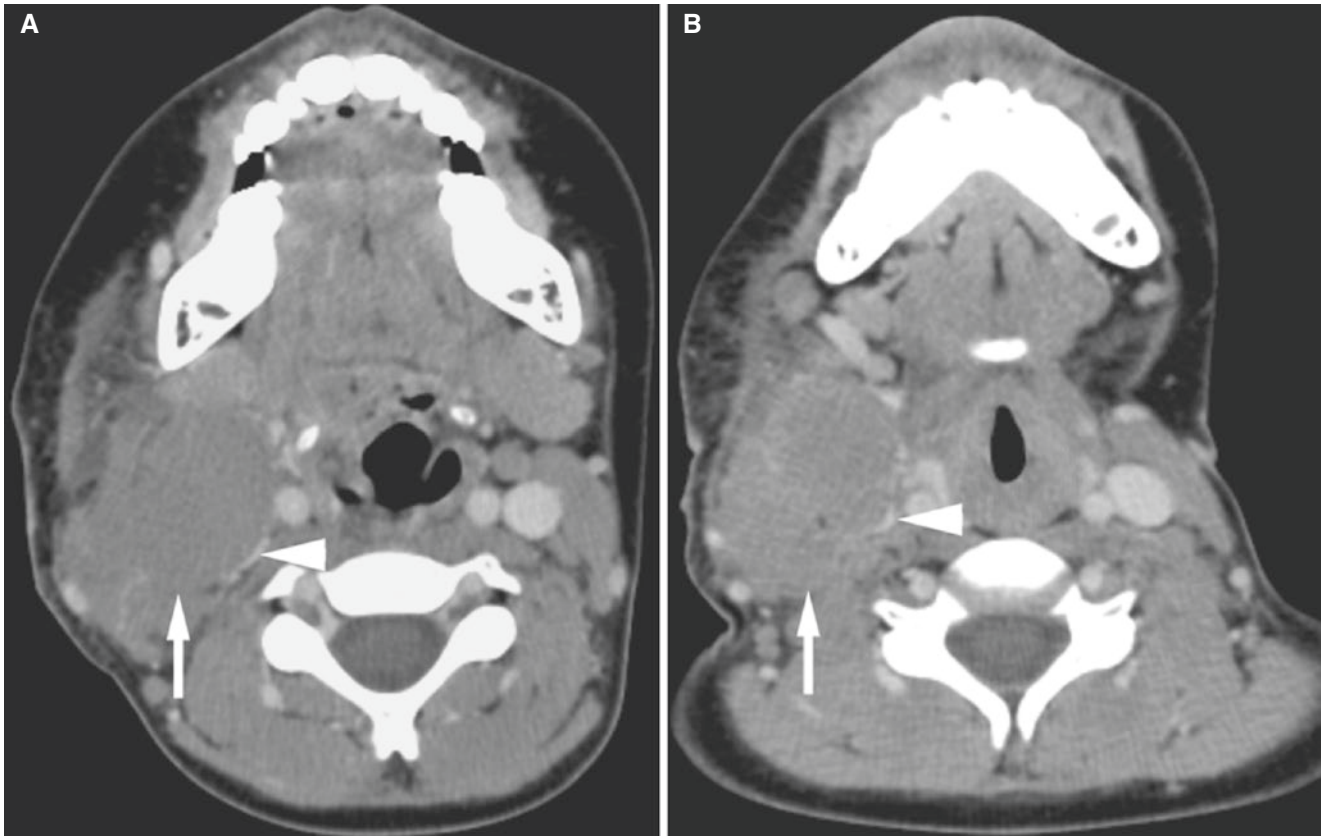

Fig. 13.27 Burkitt's lymphoma; 7-year-old female with a 2-week history of large nontender neck mass. Axial post-contrast CT images ((**B**) more caudal than (**A**)) show a large soft-tissue mass (*arrows*) severely compressing internal jugular vein (*arrowheads*) and pushing midline structures toward the other side. This appearance is nonspecific, and the enlarged lymph node could be from any type of lymphoma or metastasis

13.28.3 Imaging Features

- Rapidly growing soft-tissue mass
- Destruction of the bone

13.29 Castleman's Disease

Fig. 13.28

13.29.1 Definition

Benign lymph node disease; angiofollicular hyperplasia.

13.29.2 Clinical Features

- 70% of cases present in chest, 10% in head and neck
- Often asymptomatic

13.29.3 Imaging Features

- Often intense enhancement due to hypervascular stroma
- No central necrosis as seen in malignant lymph nodes
- Differential diagnoses are mononucleosis, cat scratch disease, and lymphoma

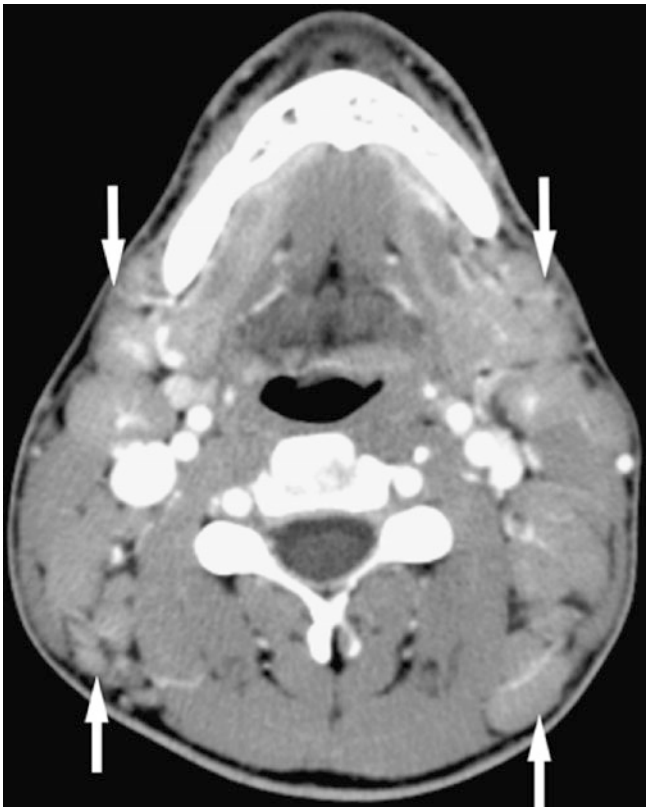

Fig. 13.28 Castleman's disease in a 19-year-old male with relapsing/remitting symptoms. Axial post-contrast CT image shows multiple slightly enlarged lymph nodes bilaterally (*arrows*). From an imaging point of view these are nonspecific, and Castleman's disease is not an imaging diagnosis

13.30 Lymphadenopathy

Figs. 13.29 and 13.30

13.30.1 Definition

Benign or malignant enlargement of lymph nodes.

13.30.2 Clinical Features

- Palpable nodal masses in the neck
- Often bilateral
- Often painless unless infected
- May be idiopathic or due to infection; other differential diagnoses: lymphoma, mononucleosis, cat scratch disease, Castleman's disease, and HIV
- Proportionally enlarged lymph nodes are often normally seen in young children

13.30.3 Imaging Features

- Enlarged lymph nodes
- No central necrosis if benign, but occasionally seen in malignant lymph nodes
- Cannot separate specific etiology on imaging studies

Fig. 13.29 Lymphadenopathy; 40-year-old HIV-positive male. Axial CT image shows enlarged lymph nodes bilaterally (*arrows*)

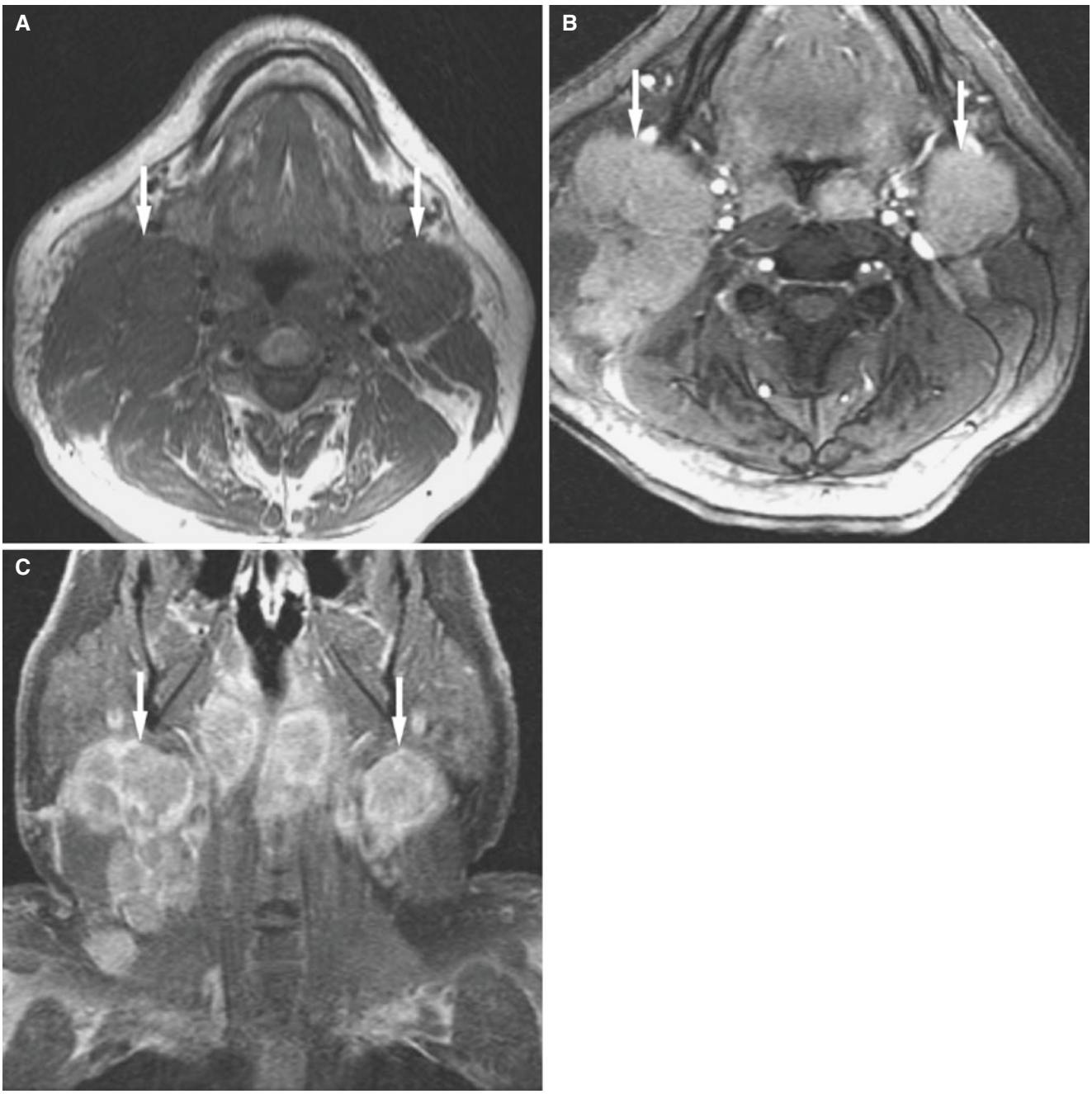

Fig. 13.30 Lymphadenopathy; 42-year-old female with a history of nasopharyngeal carcinoma. (**A**) Axial T1-weighted MRI shows bilateral enlarged upper cervical lymph nodes (*arrows*). (**B**) Axial T1-weighted post-Gd MRI with fat suppression shows enhancement of enlarged lymph nodes (*arrows*). (**C**) Coronal T1-weighted post-Gd MRI with fat suppression shows many enhancing enlarged lymph nodes bilaterally (*arrows*)

13.31 Skull Base

The skull base is the superior and posterior neighbor to the maxillofacial region. It involves the base of the skull with its foramina, muscle, nerve, and vascular structures. As in the other sections of this chapter, it is not the intention to give a full and complete description of skull base abnormalities but rather to illustrate conditions that are likely to be depicted on the images that the maxillofacial radiologist is asked to interpret, but still not in the true maxillofacial area. We have included characteristic infections, tumorlike and vascular lesions, and neoplasms.

13.32 Mastoiditis with Intracranial Abscess

Fig. 13.31

13.32.1 Definition

Intracranial encapsulated pus collection due to pyogenic infection secondary to mastoiditis.

13.32.2 Clinical Features

- Intracranial complications result from uncontrolled coalescent mastoiditis
- Intracranial complications of acute mastoiditis: sigmoid sinus thrombosis, meningitis, and abscess (subdural, epidural, and parenchymal)
- Subperiosteal abscess can be seen
- Common signs of mastoiditis: otalgia, postauricular swelling, and fever
- Intracranial abscess may present with headache, seizure, fever, altered mental status, or focal neurologic deficits

13.32.3 Imaging Features

- Non-contrast CT imaging: middle ear and mastoid completely opacified, and mastoid air cells become confluent
- Post-contrast CT imaging is first-line modality and shows rim-enhancing hypodense fluid collection
- T1-weighted post-Gd MRI is best to diagnose sinus thrombosis and intracranial complications (venous infarct, meningitis, and abscess)
- On diffusion-weighted MR imaging, abscesses are bright indicating restricted diffusion

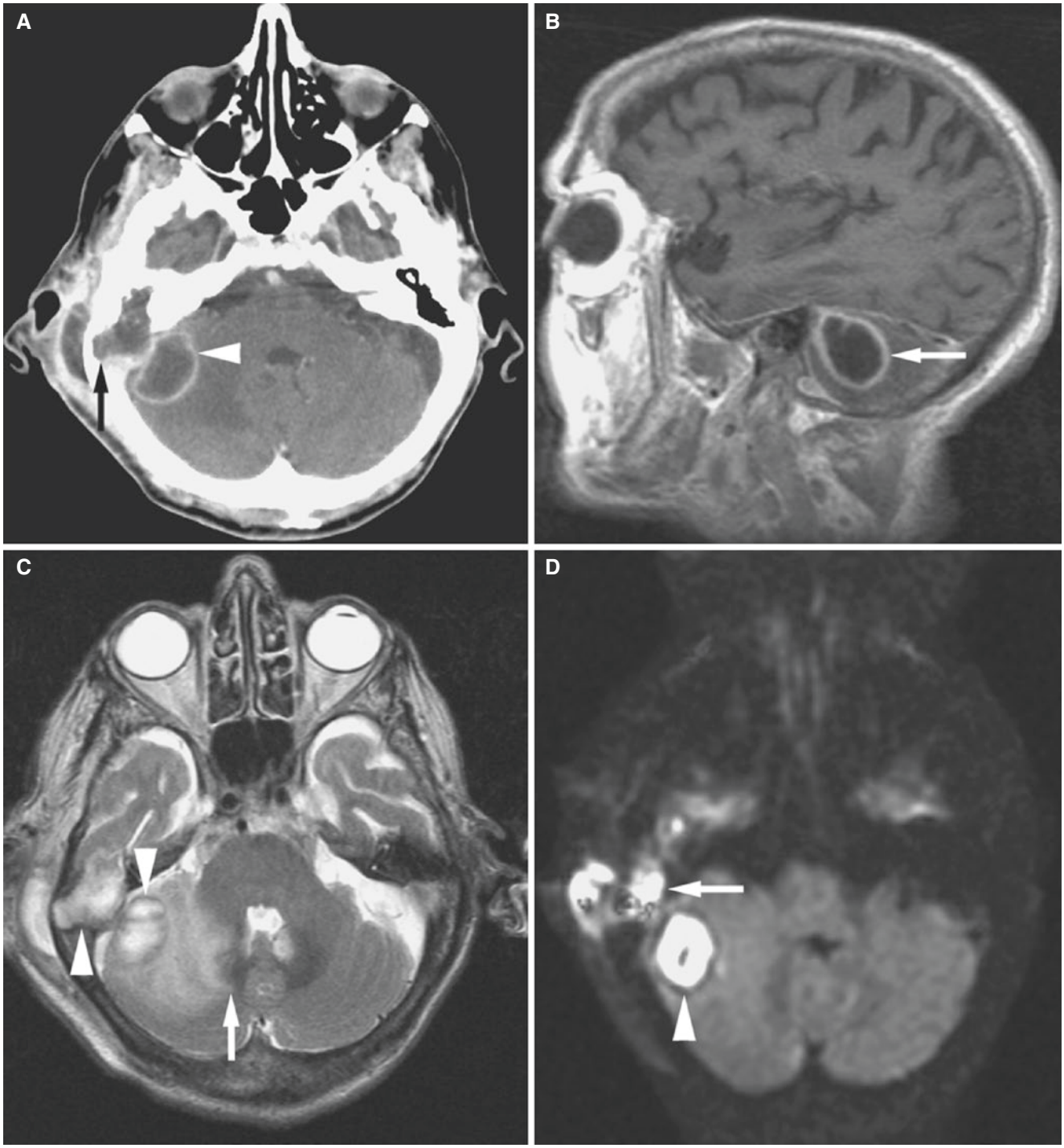

Fig. 13.31 Mastoiditis with intracranial abscess; 94-year-old female presented with a 1-week history of fever and mental status change. Patient treated with antibiotics for two episodes of right otitis media. (**A**) Post-contrast axial CT image demonstrates right mastoiditis with erosion of right petrous temporal bone (*arrow*), involvement of adjacent dura, and ring-enhancing lesion in right cerebellar hemisphere indicating abscess (*arrowhead*). (**B**) Sagittal T1-weighted post-Gd MRI shows hypointense lesion in right cerebellar hemisphere with ring enhancement (*arrow*). (**C**) Axial T2-weighted image demonstrates high intensity signal in right mastoid sinus and right cerebellar hemisphere with surrounding edema (*arrowheads*) and mass effect on fourth ventricle (*arrow*). (**D**) Diffusion-weighted imaging shows an area of hyperintensity in right mastoid sinus (*arrow*) and cerebellar hemisphere (*arrowhead*)

13.33 Mastoiditis with Sigmoid Thrombosis

Fig. 13.32

13.33.1 Definition

Clot formation in sigmoid sinuses as a result of mastoiditis.

13.33.2 Clinical Features

- Mastoiditis is a known cause of lateral venous sinus thrombosis
- Sinus thrombosis may occur via direct extension or be the result of erosive osteitis and retrograde thrombophlebitis
- Symptoms due to sinus thrombosis are variable: asymptomatic to coma or death
- May present with headache, nausea/vomiting, or seizure
- Hemorrhagic venous infarct may develop secondary to poor venous drainage

13.33.3 Imaging Features

- Non-contrast CT images: middle ear and mastoid completely opacified, and mastoid air cells become confluent. May show hyperdense sigmoid sinuses
- Post-contrast CT images: filling defect in sigmoid sinus, useful to diagnose intra- or extracranial abscess
- Contrast MRI and MR venography are best to diagnose sinus thrombosis and intracranial complications (venous infarct, meningitis, and abscess)
- On diffusion-weighted imaging, abscesses show hyperintensity with restricted diffusion

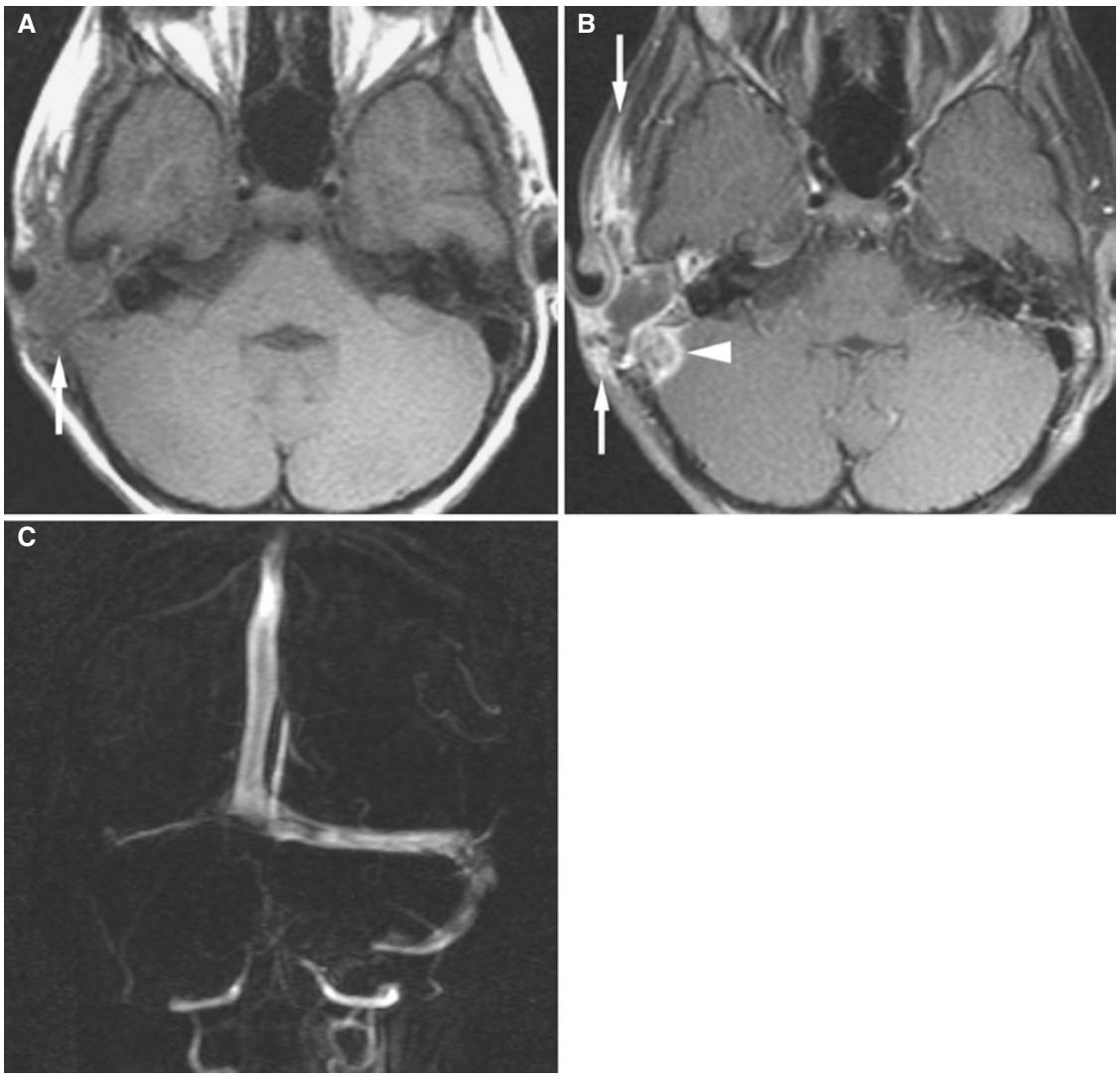

Fig. 13.32 Mastoiditis with sigmoid thrombosis; 7-year-old female with a chronic right draining ear. (**A**) Axial T1-weighted MRI shows soft-tissue mass in the right temporal bone (*arrow*). There is no flow void in sigmoid sinus on this side. (**B**) Axial T1-weighted fat-suppressed post-Gd MRI demonstrates abnormal contrast enhancement in area of the right temporal bone (*arrows*). In the sigmoid sinus, there is contrast enhancement in periphery but a central filling defect suggesting a clot (*arrowhead*). (**C**) Coronal MR venogram demonstrates lack of flow in right sigmoid sinus

13.34 Osteoradionecrosis Involving Skull Base

Fig. 13.33

13.34.1 Definition

Nonvital bone in a site of radiation injury.

13.34.2 Clinical Features

- Serious complication of radiation therapy for neoplasms of the parotid gland, oral cavity, oropharynx, and nasopharynx
- Predominantly in the mandible
- The risk is greatest during the first 6–12 months after radiation therapy, but osteoradionecrosis may develop several years later
- Clinical diagnosis of mandibular osteoradionecrosis is primarily based on clinical symptoms and signs of ulceration or necrosis of the overlying mucous membrane with exposure of necrotic bone
- Pathologic fracture and orocutaneous fistula may be seen

13.34.3 Imaging Features

- CT image with bone window shows cortical disruption and fragmentation
- T1-weighted MRI: decreased marrow signal
- T2-weighted MRI: increased marrow signal
- Can be associated with significant soft-tissue thickening and enhancement in adjacent masticator muscles

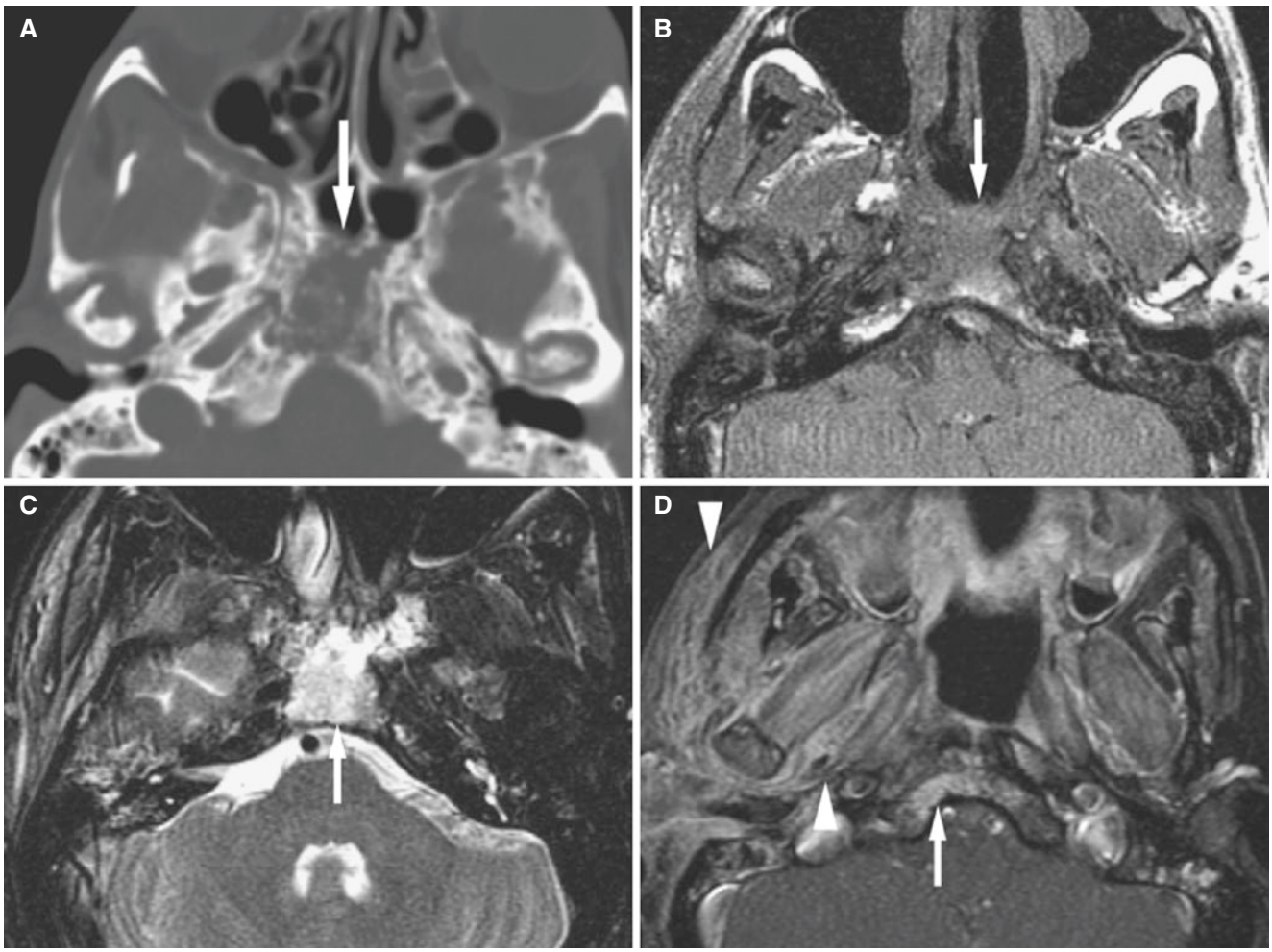

Fig. 13.33 Osteoradionecrosis; 42-year-old male status postradiation treatment for nasopharyngeal cancer. (**A**) Axial CT image shows lytic and osteosclerotic changes of the skull base bone (*arrow*). (**B**) Axial T1-weighted MRI shows hypointense lesion (*arrow*). (**C**) Axial T2-weightd fat-suppressed MRI shows hyperintensity (*arrow*). (**D**) Axial T1-weighted fat-suppressed post-Gd MRI shows diffuse enhancement within clivus (*arrow*) and right masticator and buccal space (*arrowheads*)

13.35 Langerhans Cell Histiocytosis

Fig. 13.34

13.35.1 Definition

A spectrum of disorders with histiocytic proliferation involving bone and soft tissue.

13.35.2 Clinical Features

- Classified according to sites of involvement into single or multisystem disease
- Usually presents in first decade
- Bony involvement is seen in 78% of cases and often includes the skull (49%), innominate bone, femur, orbit (11%), and ribs
- Infiltration in the temporal bone presents with conductive hearing loss and draining ear
- Frequently diagnosed only after treatment with antibiotics fails to cure a suspected middle ear or mastoid infection

13.35.3 Imaging Features

- External auditory canal and mastoid are common locations
- Bone margins are geographic and moderately well defined. "Punched-out" borders also may be found
- Early imaging findings mimic inflammatory disease
- Post-contrast CT or MRI help to differentiate inflammatory mastoid lesions
- On CT images or MRI, enhancement within lesion may be homogeneous or may occur only in periphery

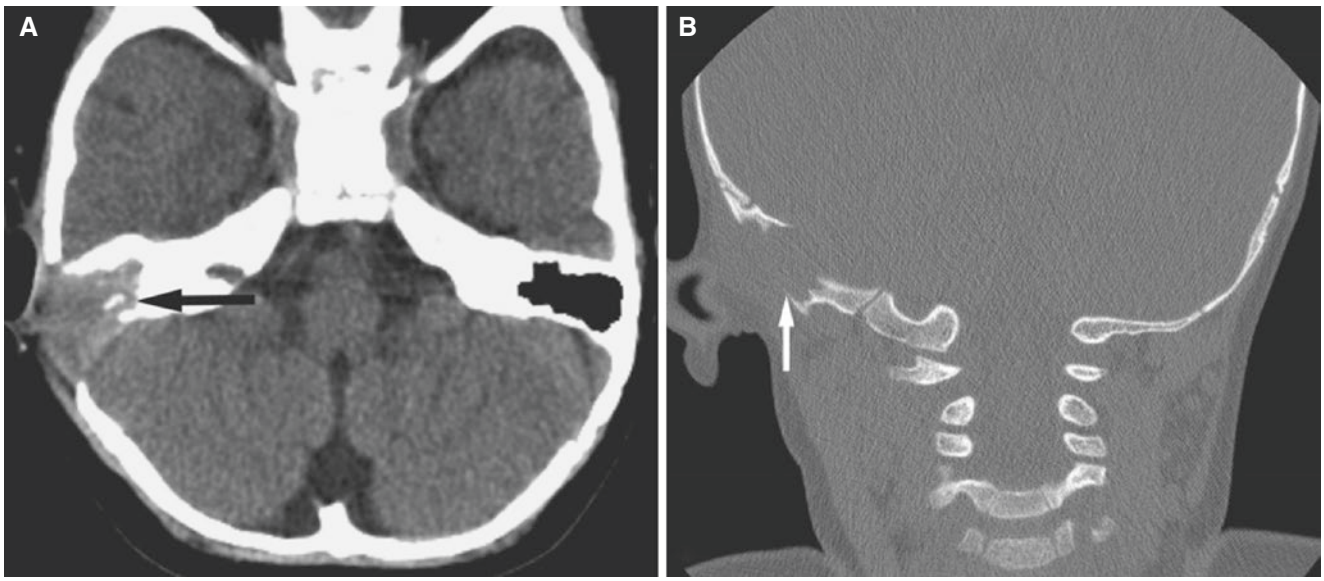

Fig. 13.34 Langerhans cell histiocytosis; 1-year-old male who has had two episodes of otitis media and a recent onset of right auricular swelling. (**A**) Axial CT image shows soft-tissue mass with opacification and destruction of right mastoid air cells (*arrow*). (**B**) Coronal CT image with bone window shows irregular "geographic" border with complete loss of portions of mastoid cortex (*arrow*)

13.36 Fibrous Dysplasia

Fig. 13.35

13.36.1 Definition

Progressive replacement of normal cancellous bone by poorly organized fibro-osseous tissue.

13.36.2 Clinical Features

- Usually seen in young age group (<30 years old)
- Symptoms depended on the lesion location
- Monostotic: 70% of cases, single osseous site is affected
- Polyostotic: 25% of cases, involves more than two separated sites
- Usually self-limiting, often does not progress after third decade of life
- McCune–Albright syndrome: a variant that consists of polyostotic fibrous dysplasia, skin pigmentation, and sexual precocity

13.36.3 Imaging Features

- Affects any bone including the skull, skull base, and facial bones
- Bone CT imaging is best for diagnosis showing expansile lesion centered in medullary space with variable attenuation
- Ground-glass matrix in expansile bone lesion is typical
- Abrupt or gradual transition zone between lesion and normal bone
- T1- and T2-weighted MRI: low signal
- T1-weighted post-Gd MRI: variable enhancement of internal matrix

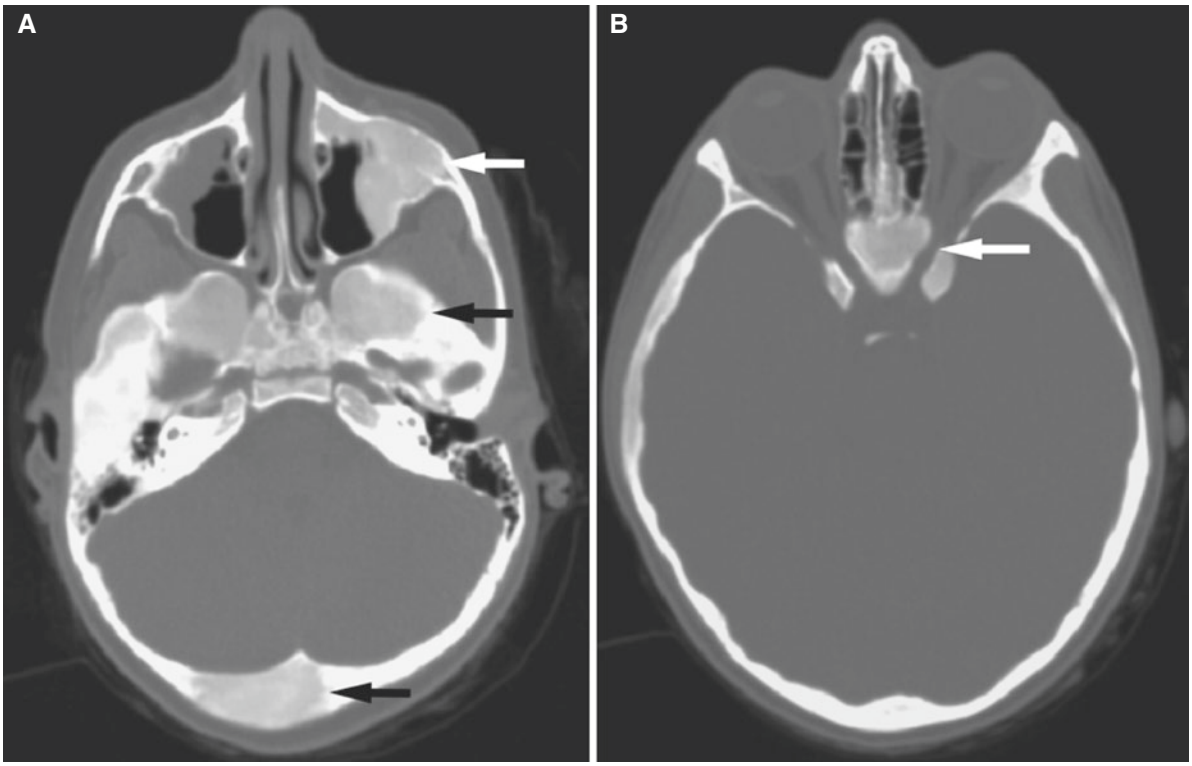

Fig. 13.35 Fibrous dysplasia; 4-year-old female with facial deformity. (**A**) Axial CT image with bone window shows ground-glass appearance of left maxillary sinus (*white arrow*), left skull base (*black arrow*), and right occipital bone (*posterior black arrow*). (**B**) Axial CT image with bone window, more cranial, shows ground-glass appearance of sphenoid bone with mild narrowing of left optic canal (*arrow*)

13.37 Giant Aneurysm of Skull Base

Fig. 13.36

13.37.1 Definition

Aneurysms involving the skull base.

13.37.2 Clinical Features

- Most aneurysms are acquired and spontaneous; some occur after infection, trauma, or local surgery. There is a small genetic predisposition
- Pressure on the nerves in the cavernous sinus can lead to ophthalmoplegia or facial pain
- Hemorrhage is unusual
- Can rupture into the sphenoid sinus, into the subarachnoid space, or into the cavernous sinus

13.37.3 Imaging Features

- Large aneurysms may erode the skull base
- Imaging of large aneurysms is varied and depends on the patency of the lumen and the presence of thrombosis
- A dynamic scan's arterial phase may help separate the aneurysm from the normal cavernous sinus
- Calcification can be present in the aneurysm's wall

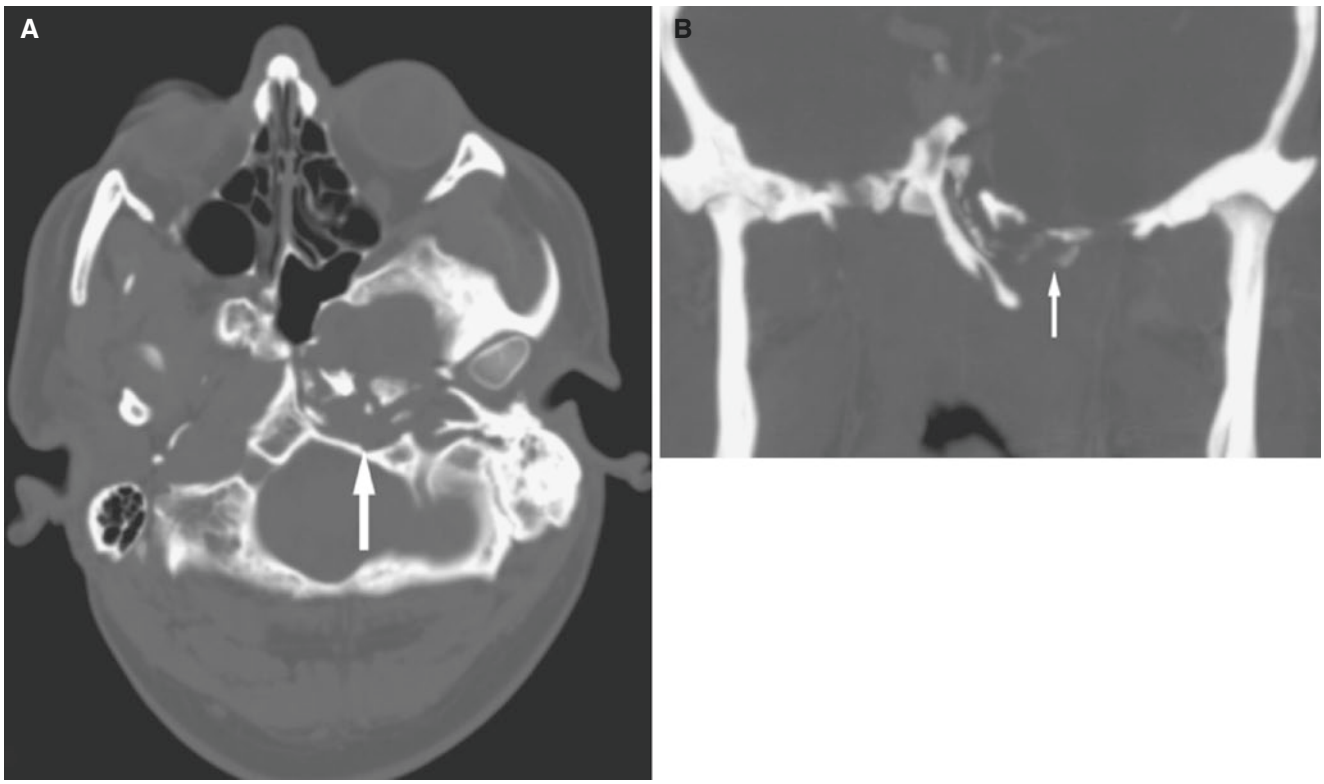

Fig. 13.36 Giant aneurysm in skull base; 33-year-old male with history of carotid aneurysm treated using balloon and coils with complete occlusion of left internal carotid artery. (**A**) Axial CT image, bone window, shows erosion of left middle cranial fossa due to a large aneurysm (*arrow*). Lumen of aneurysm is completely occluded. (**B**) Coronal CT image confirms severe bone destruction (*arrow*)

13.38 Glomus Vagale Paraganglioma

Fig. 13.37

13.38.1 Definition

Benign vascular tumor arising from neural crest paraganglion cells associated with nodose ganglia of the vagus nerve.

13.38.2 Clinical Features

- Depending on the location of the paraganglioma, the tumor is named carotid body tumor, glomus vagale, glomus jugulare, or glomus tympanicum
- Usually fourth to fifth decade; slight female dominance
- Can occur sporadically or as autosomal dominant familial tumor
- Presents with vagal neuropathy, hoarseness, and Horner syndrome (glomus vagale)

Fig. 13.37 Glomus vagale paraganglioma; 54-year-old female with symptoms of dysphagia. There was a palpable mass on the right side of the neck. (**A**) Axial T1-weighted post-Gd MRI demonstrates enhancing mass in right carotid space (*arrow*), consistent with paraganglioma. (**B**) Right common carotid angiogram demonstrates large vascular mass (*arrow*)

13.38.3 Imaging Features

- Located in nasopharyngeal carotid space
- Displace parapharyngeal fat anteriorly and internal carotid artery anteromedially
- Usually solitary lesions at one site
- Highly vascular and intensely enhancing mass
- May contain areas of hemorrhage and necrosis
- T1-weighted MRI: characteristic salt and pepper appearance due to flow (pepper) and hyperintensity due to hemorrhage (salt)

13.39 Craniopharyngioma

Fig. 13.38

13.39.1 Definition

Benign tumor derived from remnants of Rathke's pouch.

There are two types: adamantinomatous and papillary.

13.39.2 Clinical Features

- Bimodal age distribution (peak 5–15 years; papillary type >50 years)
- Pediatric patient with morning headache, visual defect, and short stature
- Endocrine disturbances
- Hydrocephalus

13.39.3 Imaging Features

- Typically found in suprasellar location
- Heterogeneous appearance with calcification and cystic component
- T1-weighted MRI: signal varies with cyst contents
- T1-weighted post-Gd MRI: solid portions are enhanced heterogeneously

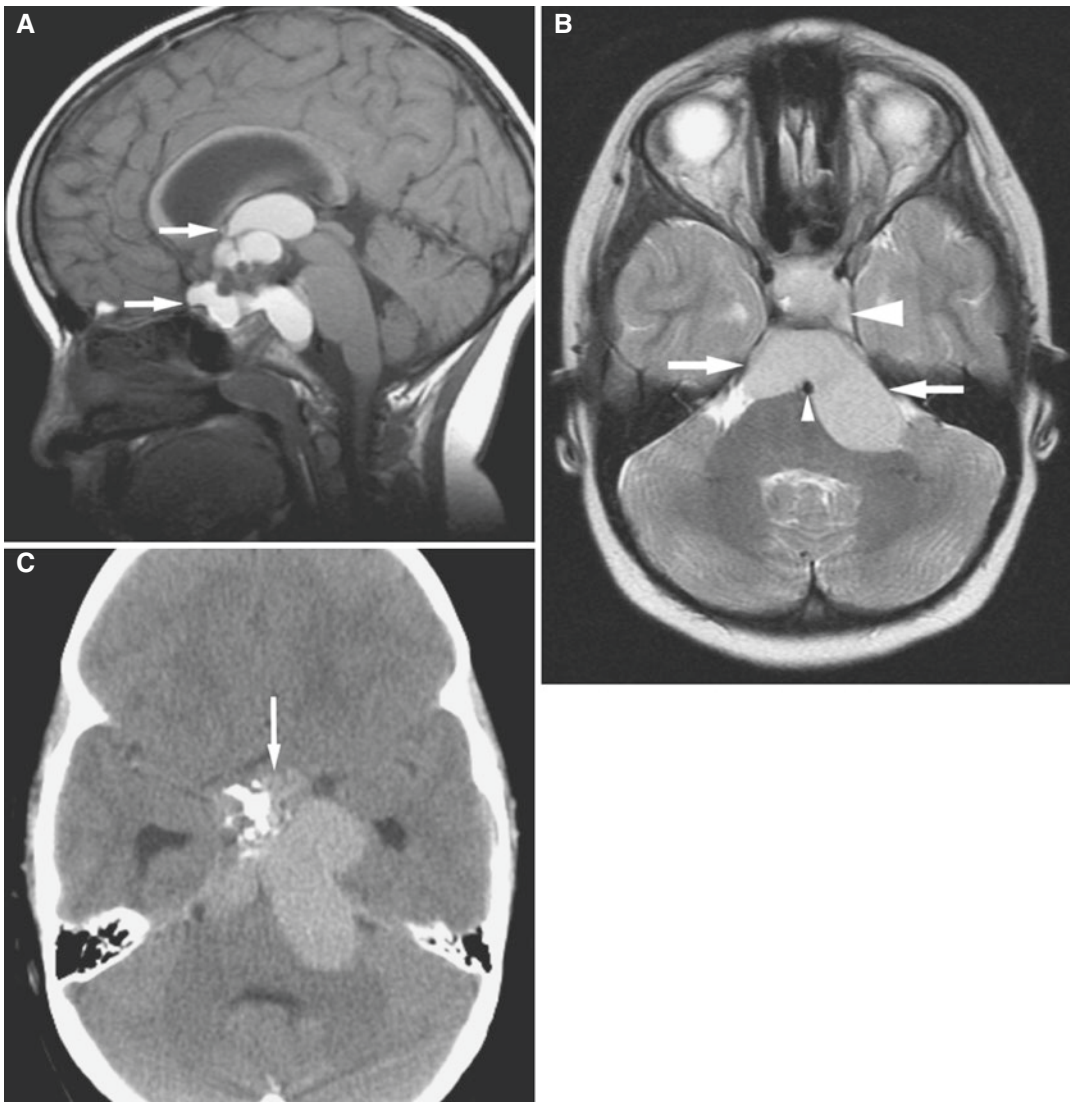

Fig. 13.38 Craniopharyngioma; 7-year-old female with history of long-standing headache. (**A**) Sagittal T1-weighted MRI shows a large lobulated sellar/suprasellar mass extending upward to the third ventricle and posteriorly into prepontine cistern (*arrows*). Most cysts show hyperintensity. (**B**) Axial T2-weighted MRI shows extension into cerebellopontine angles more to the left (*arrows*) with left parasellar extension (*arrowhead*) and encasement of basilar artery (*small arrowhead*). (**C**) Axial CT shows eccentrically located calcification within a hyperdense lobulated mass at suprasellar region (*arrow*)

13.40 Pituitary Macroadenoma Invading the Skull Base

Fig. 13.39

13.40.1 Definition

Pituitary macroadenoma with inferior extension to sphenoid sinus and clivus.

13.40.2 Clinical Features

- Pituitary hormonal abnormality
- Visual field defect and cranial nerve palsy
- Benign and slow growing

13.40.3 Imaging Features

- Expansion of sella with invasion of surrounding adjacent structures
- Bony margins are usually smooth
- On MRI, sellar–infrasellar mass invading basisphenoid and basiocciput
- May extend into cavernous sinus and encase internal carotid artery
- Enhancement is necessary to evaluate the tumor extension

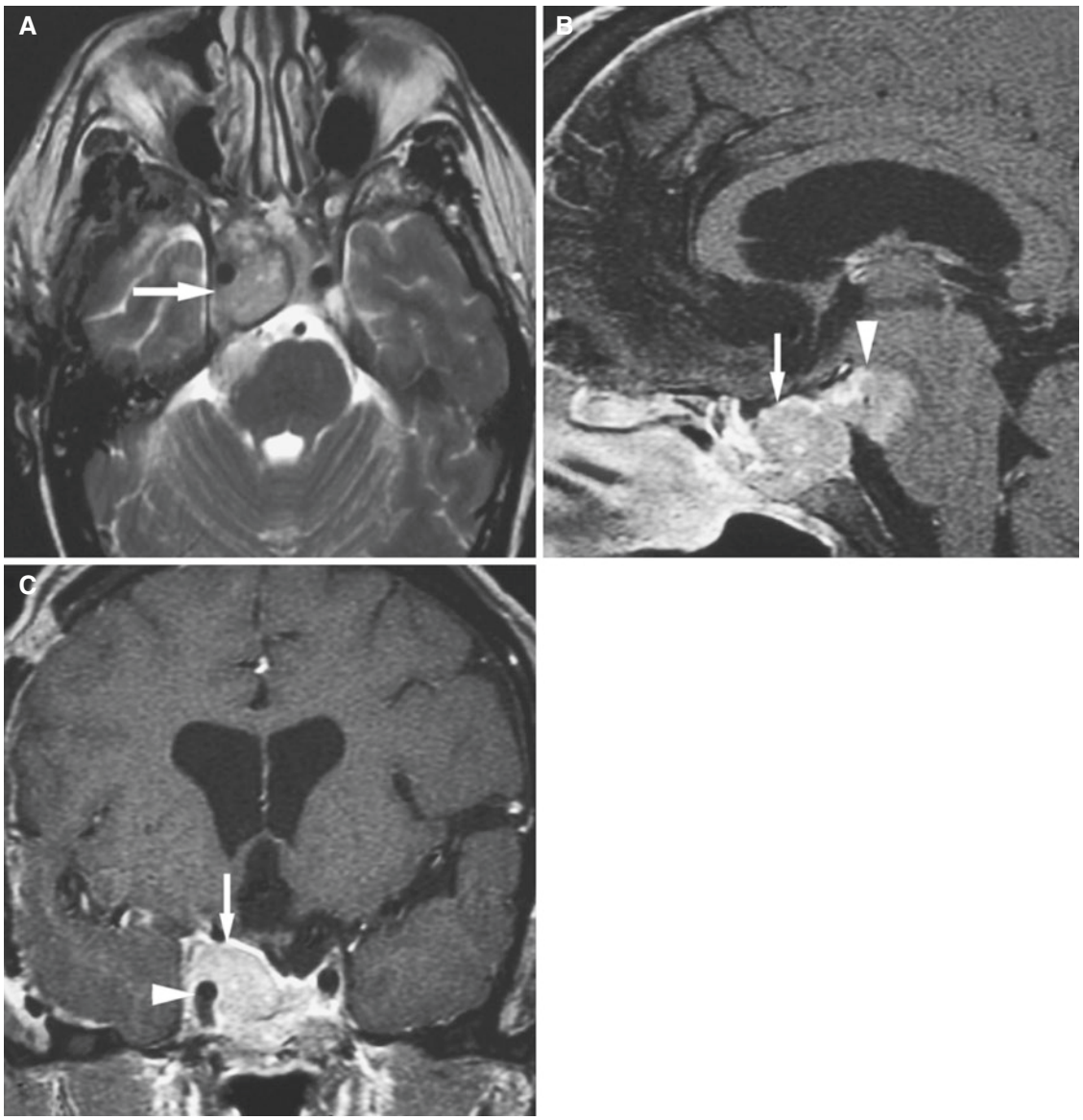

Fig. 13.39 Pituitary macroadenoma; 53-year-old male with visual disturbance. (**A**) Axial T2-weighted MRI shows heterogeneous large mass in sella and right cavernous sinus (*arrow*). Mass extends posteriorly into brain stem causing compression of brain stem. (**B**) Sagittal T1-weighted post-Gd MRI shows mass expanding sella and extending up to superior portion of sphenoid sinus and clivus (*arrow*). Posteriorly mass extends into brain stem causing compression of brain stem (*arrowhead*). (**C**) Coronal T1-weighted post-Gd MRI shows mass extending into right cavernous sinus (*arrow*) with encasement of internal carotid artery (*arrowhead*)

13.41 Trigeminal Schwannoma

Fig. 13.40

13.41.1 Definition

Benign encapsulated tumor of Schwann cell arising from the trigeminal nerve.

13.41.2 Clinical Features

- Trigeminal nerve is most commonly affected in central skull base
- Asymptomatic mass in deep facial soft tissue
- May present with facial pain, decreased sensation, and masticator muscle weakness and/or atrophy
- Predominantly third or fourth decade

13.41.3 Imaging Features

- Arises in Meckel's cave or in cistern along course of nerve
- Rarely arises below skull base
- Extension is common through the foramen ovale and foramen rotundum, and CT imaging with bone window is best to see smooth margin of an expanded foramen
- May have a dumbbell shape with components enlarging cavernous sinus and protruding into the posterior cranial fossa
- Cystic changes or necrosis typical of larger lesions
- T1-weighted post-Gd fat-suppressed MRI, axial and coronal, is best to see tumor extension

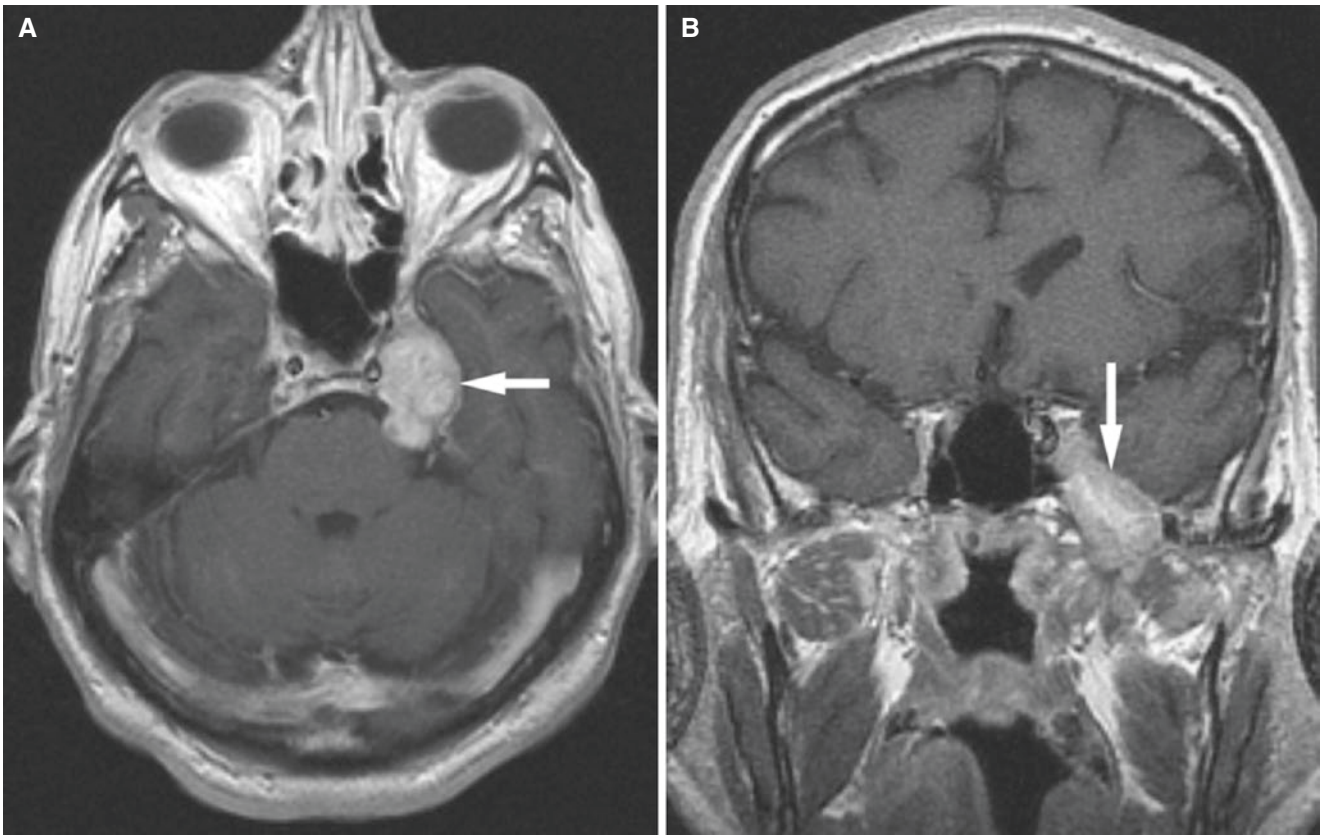

Fig. 13.40 Trigeminal schwannoma; 70-year-old male with memory loss and seizures. (**A**) Axial T1-weighted post-Gd MRI shows enlarged mass (*arrow*) in wall of left cavernous sinus. (**B**) Coronal T1-weighted post-Gd MRI shows mass extending through the foramen ovale (*arrow*)

13.42 Metastatic Disease to Hypoglossal Canal and Clivus

Fig. 13.41

13.42.1 Definition

Metastatic disease from extracranial primary tumor to skull base.

13.42.2 Clinical Features

- Skull base tumor can be primary or metastatic
- Hematogenous metastasis from primary tumors in the lung, kidney, breast, prostate, and a variety of other rare locations
- Neurologic symptoms depend on location of metastatic tumor
- If the hypoglossal canal is affected, symptoms may be difficulty in swallowing (dysphagia) and speech (dysarthria)
- Treatments for skull base tumors can be divided into medical, radiation, and surgical

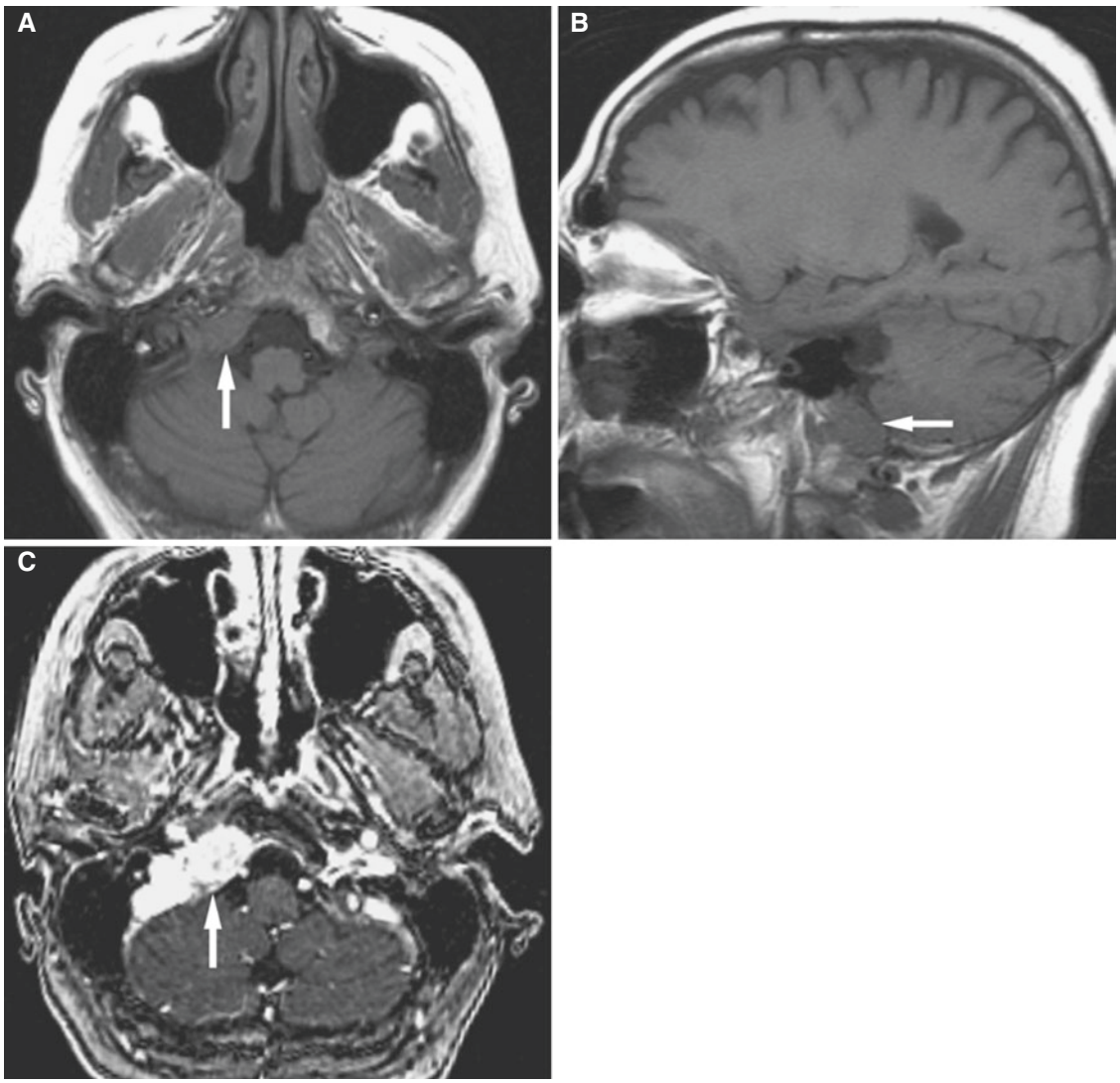

Fig. 13.41 Metastatic disease; 55-year-old female with breast cancer presented with swallowing difficulties. (**A**) Axial T1-weighted MRI demonstrates well-circumscribed hypointense lesion involving right clivus and hypoglossal canal (*arrow*). (**B**) Sagittal T1-weighted MRI confirms well-circumscribed mass (*arrow*). (**C**) Axial T1-weighted post-Gd MRI demonstrates evident enhancement of tumor (*arrow*)

13.42.3 Imaging Features

- CT with bone window most useful to evaluate bone destruction
- Sclerotic changes may be present in prostate metastasis
- T1-weighted MRI is sensitive for bone metastasis
- T1-weighted post-Gd MRI: fat saturation necessary to distinguish enhancement from normal hyperintense marrow or fat

13.43 Orbit

Orbital pathology is in many respects completely different from that seen in the maxillofacial area. Imaging of the orbit is done after a thorough clinical examination. The clinical examination can diagnose conditions of the globe with high accuracy, but anything that is posterior to the globe is difficult to diagnosis clinically, often prompting imaging of the orbit. Both CT and MR imaging are used, and in general CT imaging is the first choice for trauma and bony pathology, whereas MR imaging is the superior technique for soft-tissue abnormalities. Again, it is not the intention in this section of this chapter on adjacent structures to give a full description of orbital conditions, but rather to alert the maxillofacial radiologist as to what may be going on in the orbit which is the closest adjacent structure to the maxillofacial area superiorly and laterally.

13.44 Orbital Infectious Disease

Fig. 13.42

13.44.1 Definition

Orbital bacterial infection.

13.44.2 Clinical Features

- Orbital bacterial infection includes retention edema of the eyelid, preseptal cellulitis, preseptal abscess, orbital cellulitis, orbital abscess, subperiosteal abscess, and cavernous sinus thrombosis
- The majority are of paranasal sinus origin
- May develop from infectious processes of the face or pharynx, trauma, foreign bodies, or septicemia
- Presents with orbital edema and painful proptosis with fever
- Rapidly progressive, potentially blinding diseases

13.44.3 Imaging Features

- Post-contrast CT imaging is first-line modality and shows inflammation and rim-enhancing hypodense fluid collection
- Post-contrast MRI is best to assess intracranial complications (meningitis, subdural empyema, cerebritis, or brain abscess)
- On diffusion-weighted imaging, abscess shows hyperintensity

13.45 Dacryocystocele, Nasolacrimal Duct

Fig. 13.43

13.45.1 Definition

Cystic dilatation of nasolacrimal apparatus resulting from stenosis of the nasolacrimal duct.

13.45.2 Clinical Features

- Present in adults (congenital dacryocystocele is seen in infancy)
- History of dacryocystitis or neoplastic stenosis, prior nasoorbital/nasoethmoidal trauma, or surgery
- Intranasal mass representing inferior extension of cystocele

13.45.3 Imaging Features

- Medial canthus cyst on CT images
- Enlarged osseous nasolacrimal canal
- Intranasal mass representing inferior extension of cystocele

13.46 Dermoid

Fig. 13.44

13.46.1 Definition

Cystic lesion of orbit resulting from inclusion of ectodermal elements during closure of neural tube.

Dermoid: epithelial elements plus dermal substructures.

Epidermoid: epithelial elements only.

13.46.2 Clinical Features

- Most common developmental cysts involving orbit and periorbital structures
- Painless firm subcutaneous mass
- Diplopia if larger
- Childhood presentation more common than adult
- Sudden growth or change may occur following rupture

13.46.3 Imaging Features

- Cystic, well-demarcated, and extraconal mass
- Commonest location is superior temporal aspect of orbit at frontozygomatic suture but can occur anywhere in orbit
- On CT images, both epidermoid and dermoid cysts appear as a nonenhancing, low-density mass
- Calcifications may be seen
- May have a fat density
- T1- weighted MRI: usually low signal but may be hyperintense if fat containing
- T2-weighted MRI: high signal
- Diffusion-weighted imaging: typically high intensity

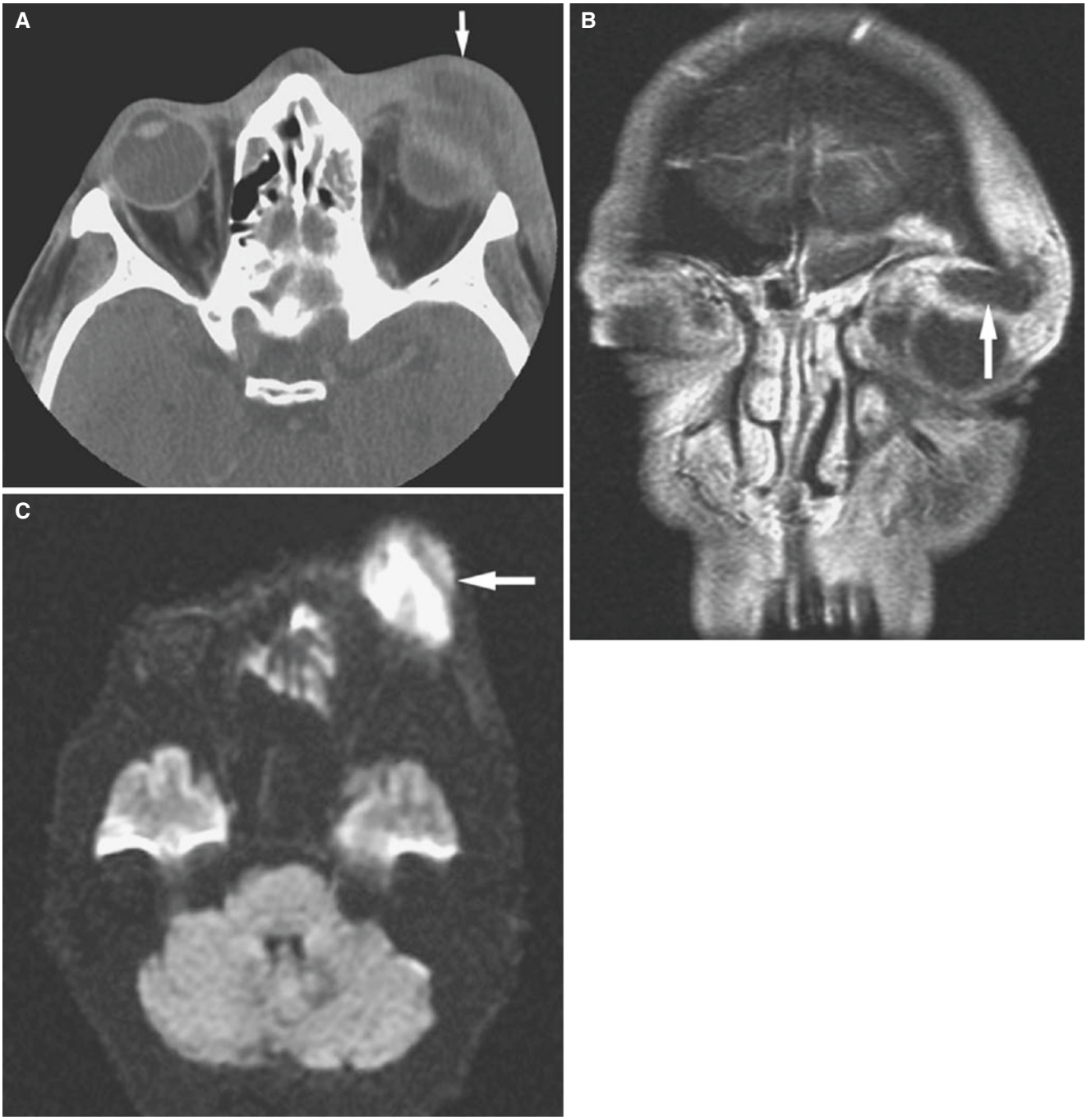

Fig. 13.42 Orbital abscess; 26-year-old male with periorbital pain and swelling. (**A**) Axial post-contrast CT image demonstrates soft-tissue thickening and inflammatory changes in the left periorbital region with a rounded nonenhancing soft-tissue lesion in left upper eyelid (*arrow*) consistent with abscess. Mucosal thickening of ethmoid sinus is also present and may be the source of this abscess. (**B**) Coronal T1-weighted fat-suppressed post-Gd MRI shows diffuse enhancement within soft tissue of left periorbital region and nonenhanced fluid collection (*arrow*). Mucosal thickening of frontal sinus is also observed. (**C**) On diffusion-weighted imaging, abscess shows very high-signal intensity (*arrow*) due to restricted diffusion

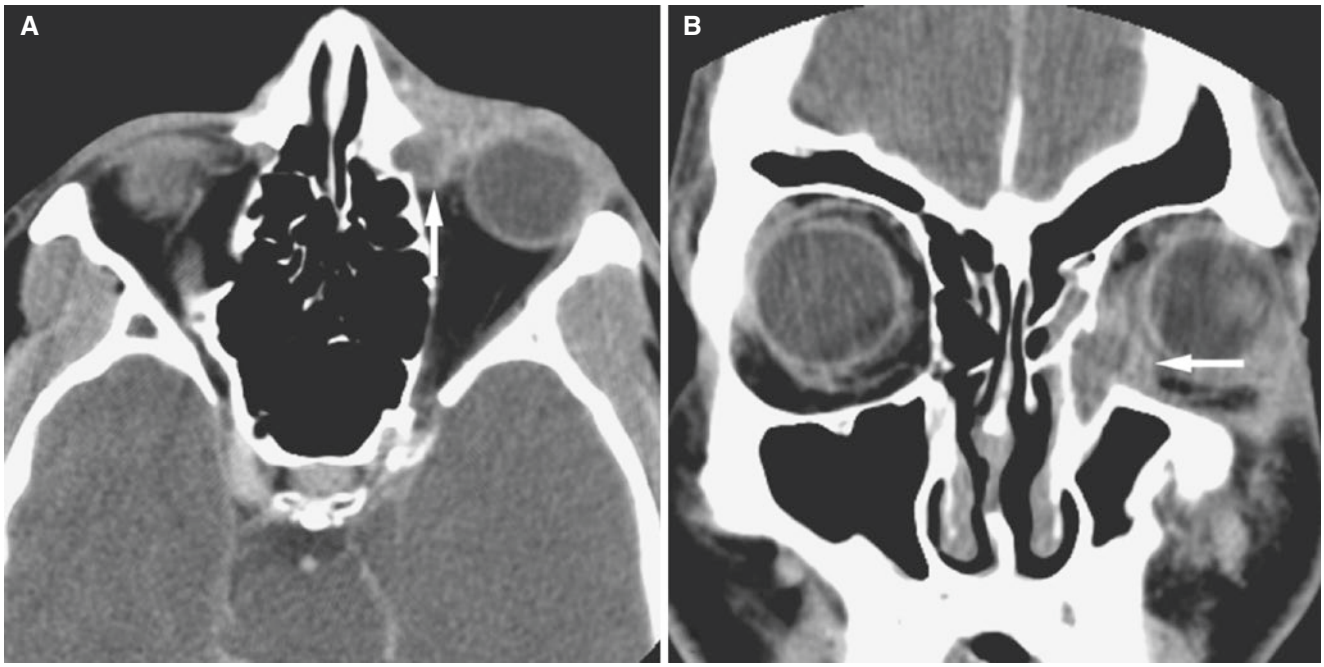

Fig. 13.43 Dacryocystocele; 43-year-old female with periorbital recurrent swelling. Axial (**A**) and coronal (**B**) post-contrast CT images show left periorbital soft-tissue swelling representing orbital cellulitis. Osseous nasolacrimal canal is enlarged, and rim-enhancing cystic mass is observed in medial canthus which is an infected nasolacrimal cystocele (*arrows*)

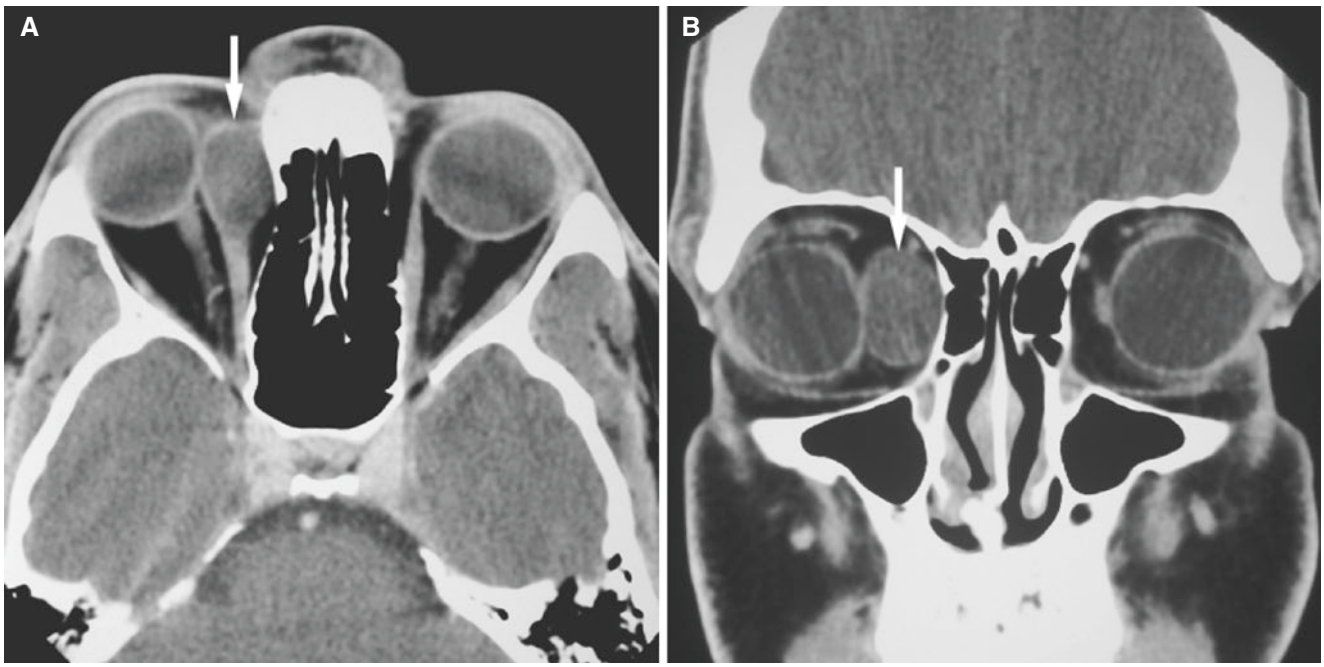

Fig. 13.44 Dermoid; young male with palpable lesion over nasal bridge. Axial (**A**) and coronal (**B**) non-contrast CT images show well-demarcated, thin-walled mass (*arrows*) in supranasal wall of right orbit

13.47 Fibrous Dysplasia

Fig. 13.45

13.47.1 Definition

Progressive replacement of normal cancellous bone by poorly organized fibro-osseous tissue.

13.47.2 Clinical Features

- Usually seen in young age group (<30 years)
- Orbital lesion: optic neuropathy due to optic nerve compression in optic canal
- Monostotic: 70% of cases; single osseous site is affected
- Polyostotic: 25% of cases involves more than two separated sites
- Usually self-limiting and often does not progress after third decade of life
- McCune–Albright syndrome is a variant that consists of polyostotic fibrous dysplasia, skin pigmentation, and sexual precocity
- Surgical treatment for optic nerve decompression and for limited cosmetic debulking and recontouring of the bone

13.47.3 Imaging Features

- Affects any bone including the skull, skull base, and facial bones
- Bone CT imaging is best for diagnosis showing expansile lesion centered in medullary space with variable attenuation
- Ground-glass matrix in expansile bone lesion is typical
- Abrupt or gradual transition zone between lesion and normal bone
- T1- and T2-weighted MRI: usually low signal
- T2-weighted MRI: occasionally high signal simulating a tumor
- T1-weighted post-Gd MRI: variable enhancement of internal matrix

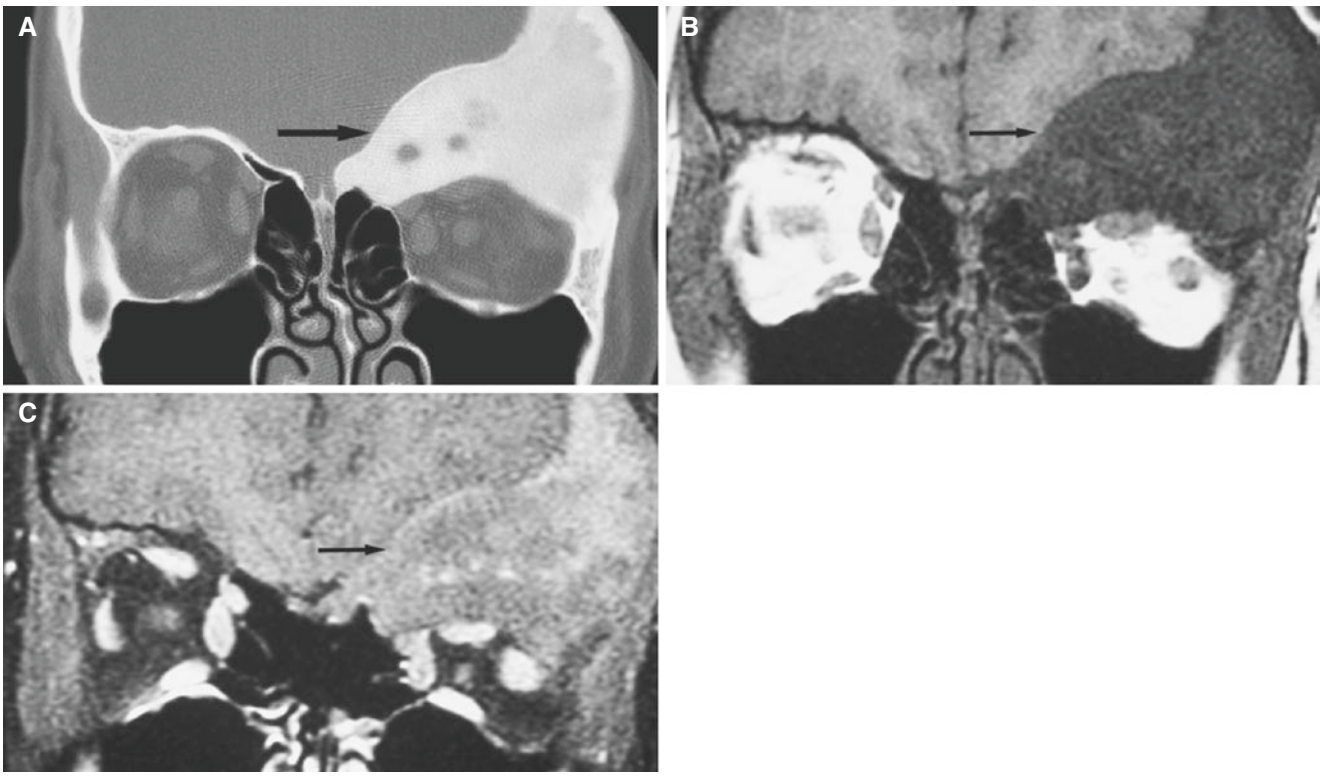

Fig. 13.45 Fibrous dysplasia; 17-year-old presents with painless prominence in left supraorbital region. (**A**) Coronal CT image shows dense expansile greater wing of the sphenoid bone on the left side. Orbital cavity is compressed (*arrow*). (**B**) T1-weighted MRI shows low-signal intensity from fibrous lesion in greater wing of sphenoid bone on the left side consistent with fibrous dysplasia (*arrow*). (**C**) T1-weighted post-Gd MRI shows heterogeneous enhancement in expanded greater wing of sphenoid bone (*arrow*)

13.48 Langerhans Cell Histiocytosis

Fig. 13.46

13.48.1 Definition

A benign spectrum of disorders with histiocytic proliferation involving the orbit.

13.48.2 Clinical Features

- Unifocal Langerhans cell histiocytosis
- Presents with orbital pain, swelling, and proptosis
- Usually presents in the first decade
- Management is usually conservative, and spontaneous healing may occur

13.48.3 Imaging Features

- Most common orbital manifestation is a solitary osseous lesion
- Orbital soft-tissue involvement without an obvious bony defect is rare
- On CT images, homogeneously hyperdense enhancing mass with bony erosion or destruction
- T1-weighted MRI: isointens
- T2-weighted MRI: minimally to moderately hyperintense
- T1-weighted post-Gd MRI: enhancement
- Differential diagnosis includes lacrimal gland tumors, rhabdomyosarcomas, metastatic neuroblastoma and lymphoproliferative disease

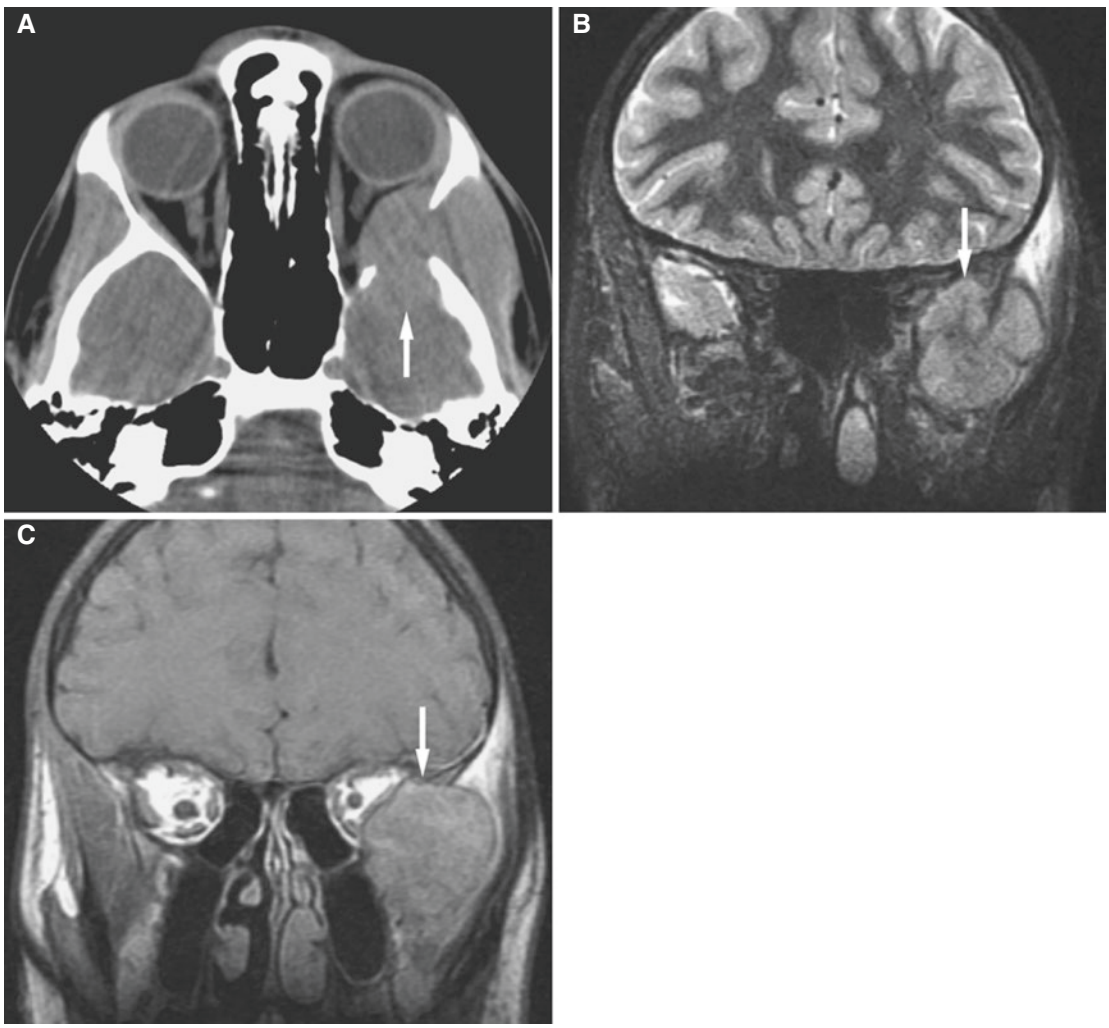

Fig. 13.46 Langerhans cell histiocytosis of orbit; 14-year-old male with two weeks of headache, now with periorbital swelling. Clinical question of infection or mass. (**A**) Axial CT image shows homogeneous soft-tissue mass (*arrow*) without calcification in retro-orbital and greater sphenoid space. There is a punched-out bony lesion involving sphenoid wing and posterior wall of left orbit. (**B**) Coronal STIR MRI image demonstrates a well-defined hyperintense mass (*arrow*) in the left lateral wall of orbit. The mass extends into left orbit and deviates left lateral rectus muscle. (**C**) Coronal T1-weighted post-Gd MRI (*arrow*) shows diffuse enhancement of mass

13.49 Neurofibromatosis

Fig. 13.47

13.49.1 Definition

Orbital manifestations associated with neurofibromatosis type 1 (NF-1).

13.49.2 Clinical Features

- Plexiform neurofibroma and optic nerve glioma are typical orbital manifestations in NF-1
- Café au lait spots are the earliest sign and noted during first year, and tumors begin to appear in childhood
- Presents with eyelid, periorbital, and facial soft-tissue masses, proptosis, and ptosis
- Malignant transformation uncommon

13.49.3 Imaging Features

- Plexiform neurofibromas are nonencapsulated infiltrative masses involving the cranial nerve, muscle, optic nerve sheath, and sclera
- T1-weighting MRI: signal intensity of plexiform neurofibromas similar to that of muscle
- T2-weighted MRI: often high
- T1-weighted post-Gd MRI: contrast enhancement usually intense
- May be associated with sphenoid dysplasia, buphthalmos, and optic canal and/or orbital fissure enlargement
- Optic nerve glioma

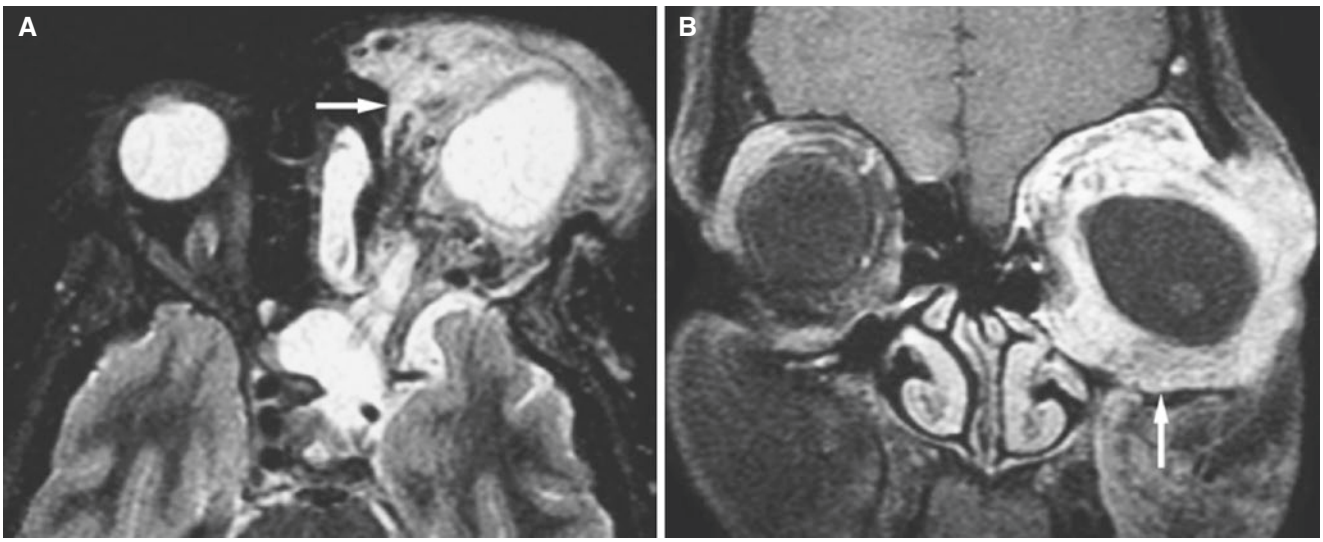

Fig. 13.47 Plexiform neurofibroma; 30-year-old with known neurofibromatosis presenting with periorbital swelling. (**A**) Axial T2-weighted MRI shows a large infiltrative mass in left orbit deforming globe and extending into retro-orbital area. There are large flow voids in this highly vascular mass (*arrow*). (**B**) Coronal T1-weighted post-Gd MRI shows enhancing mass encasing and deforming globe (*arrow*)

13.50 Hemangioma

Fig. 13.48

13.50.1 Definition

Benign angioma consisting of a mass of blood vessels.

13.50.2 Clinical Features

- Most common vascular tumor seen in infancy
- Most prevalent in head and neck region and constitutes 18–38% of head and neck tumors
- Diagnosis of hemangioma is made by a combination of medical history, physical examination, and imaging including ultrasound, CT, and MRI
- Typical hemangiomas are red, raised, and bosselated
- Deep hemangiomas have normal overlying skin and may mimic other vascular malformations
- Congenital hemangiomas typically show rapid growth and may involute completely

13.50.3 Imaging Features

- On CT images, hemangiomas are seen as lobulated solid masses that are isodense with muscle and show intense enhancement
- T1-weighted MRI: usually intermediate-signal intensity
- T2-weighted MRI: high-signal intensity
- T1-weighted post-Gd MRI: diffuse intense enhancement
- Hemangiomas need to be differentiated from arteriovenous malformations which are also associated with prominent vascularity

Fig. 13.48 Hemangioma; 4-month-old presenting with periorbital mass. (**A**) Coronal T1-weighted MRI shows left periorbital and cheek soft-tissue mass (*arrow*). (**B**) Axial T2-weighted fat-suppressed MRI shows hyperintensity-demonstrating precise outline of mass and left facial structures (*arrow*). (**C**) Axial T1-weighted fat-suppressed post-Gd MRI shows diffuse enhancement of soft-tissue hemangioma (*arrow*)

13.51 Meningioma

Fig. 13.49

13.51.1 Definition

Meningioma of the intraorbital optic nerve sheath.

13.51.2 Clinical Features

- Slow, painless progressive unilateral visual loss and proptosis
- Usually middle age. Younger age patients may be associated with NF-2
- Female predominance
- Treatment includes stereotactic radiotherapy or surgery

13.51.3 Imaging Features

- Enhancing mass surrounding intraorbital optic nerve
- Linear or punctate calcification is characteristic
- T1-weighted MRI: isointense
- T2-weighted MRI: hyper- to hypointense
- T1-weighted post-Gd MRI: best with fat suppression to see extension of tumor and to characterize tumor relative to adjacent orbital structures
- May extend along optic nerve, making "tramtracking" appearance on contrast-enhanced MRI

13.52 Rhabdomyosarcoma

Fig. 13.50

13.52.1 Definition

Primary mesenchymal tumor arising from a primitive muscle cell known as a rhabdomyoblastoma.

13.52.2 Clinical Features

- Most common primary malignant tumor of orbit in children
- Often seen in children and young adults under 20 years of age
- Rapidly developing proptosis and displacement of globe
- Typically occurs as a unilateral solid mass in supranasal part of orbit

13.52.3 Imaging Features

- On CT images, rhabdomyosarcoma is seen as a soft-tissue mass with moderately well-defined margins
- Bony destruction is common if larger
- Calcification and cavitation are uncommon
- T1-weighted MRI: signal similar to muscle
- T2-weighted post-Gd MRI: higher than muscle
- T1-weighted post-Gd MRI: moderate to marked heterogeneous enhancement

13.53 Lymphoblastic Leukemia

Fig. 13.51

13.53.1 Definition

Malignancy of hematopoietic stem cells.

13.53.2 Clinical Features

- Primarily a disease of children and young adults
- Peak incidence at 4 years of age
- About 1800 new cases per year in the USA, 80% under 15 years of age

13.53.3 Imaging Features

- On CT images, soft-tissue and/or bony mass
- Bony destruction may occur
- Calcification and cavitation are uncommon
- T1-weighted MRI: signal intensity similar to muscle
- T2-weighted MRI: generally higher signal than muscle but may be low in tumors with high cellular density
- T1-weighted post-Gd MRI: moderate to marked heterogeneous enhancement

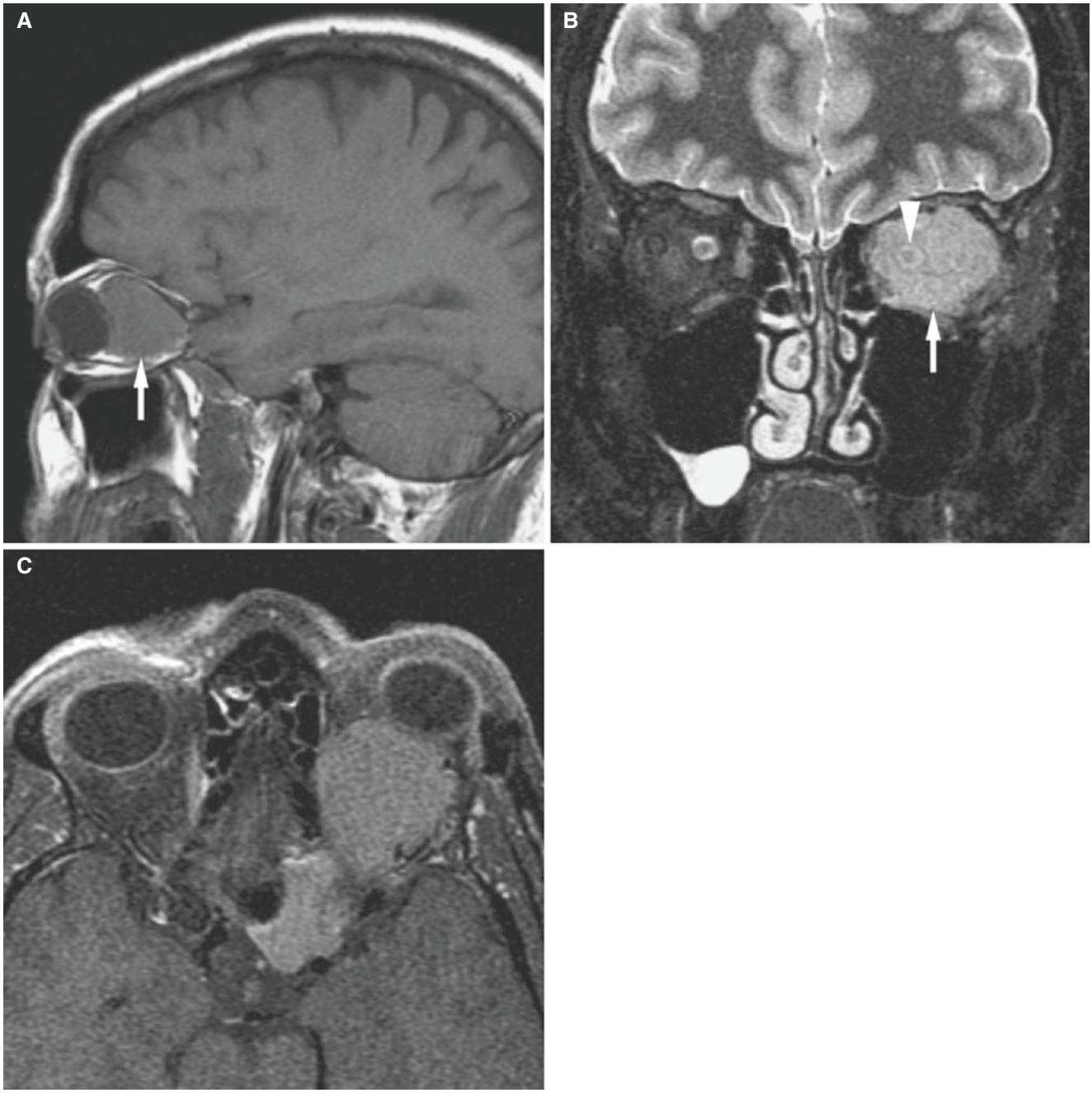

Fig. 13.49 Orbital meningioma; 41-year-old male with history of left orbital meningioma resected 12 years ago, now with left proptosis and question of recurrent meningioma or glioma. (**A**) Sagittal T1-weighted MRI shows a large isointense mass (*arrow*) in the orbit compressing globe anteriorly. (**B**) On coronal T2-weighted fat-suppressed MRI, mass (*arrow*) shows hyperintensity, and the optic nerve is seen in the center of mass (*arrowhead*). (**C**) Axial T1-weighted post-Gd MRI shows intracranial extension of mass through the optic foramen. Tumor is deforming posterior surface of globe and causing proptosis with displacement of extraocular muscles peripherally

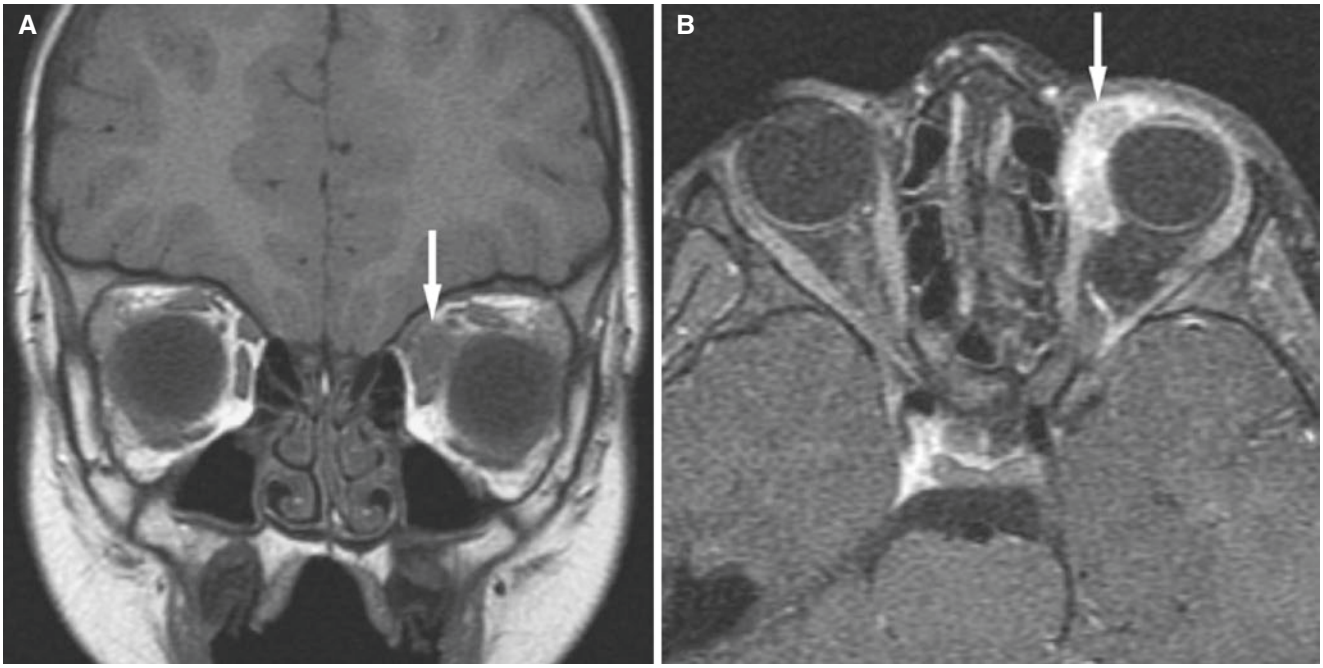

Fig. 13.50 Orbital rhabdomyosarcoma; 4-year-old male with history of left eyelid swelling for one week and low-grade fever. (**A**) Coronal T1-weighted MRI shows a well-defined mass, isointense to extraocular muscles, in medial aspect of left orbital cavity (*arrow*). (**B**) T1-weighted fat-suppressed post-Gd MRI shows a heterogeneously enhanced mass (*arrow*)

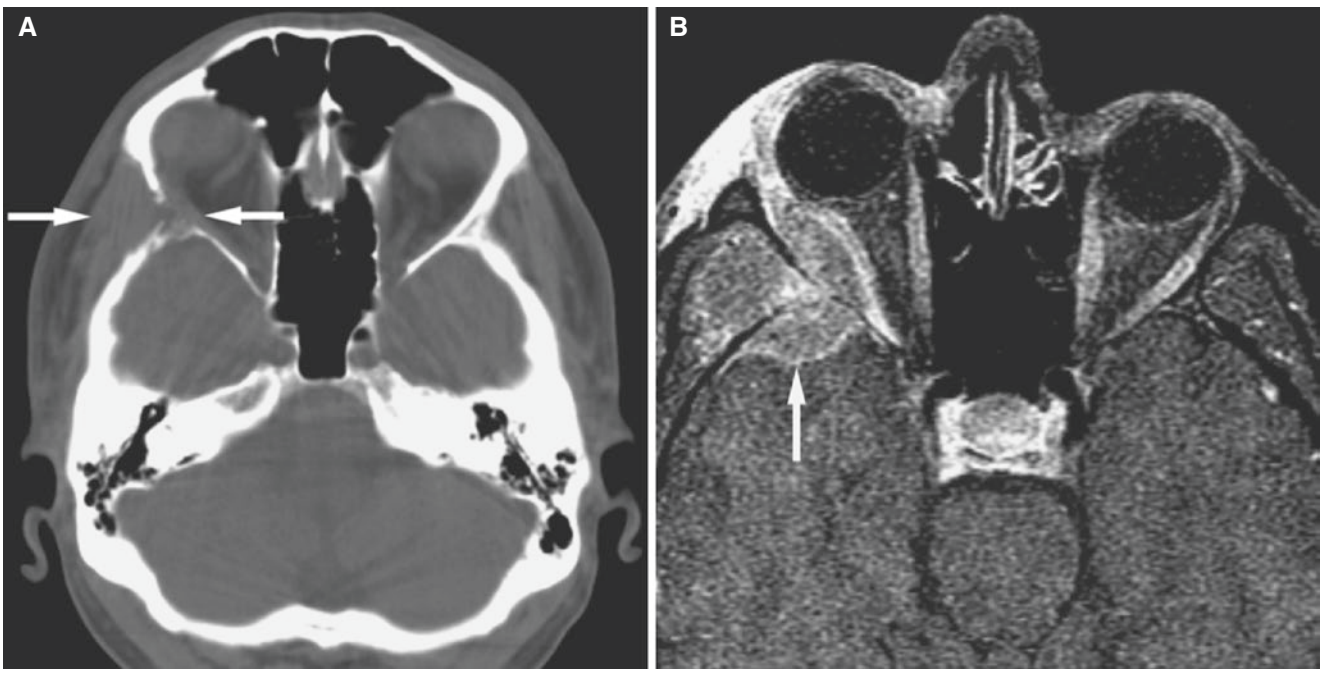

Fig. 13.51 Lymphoblastic leukemia; 34-year-old male presenting with right eye proptosis, pain, and vision loss. Clinical suspicion of orbital cellulitis. (**A**) Axial CT image shows mass (*arrows*) in right infratemporal fossa with bony destruction. (**B**) Axial T1-weighted fat-suppressed post-Gd MRI shows dramatic enhancement and intracranial extension of mass (*arrow*)

Suggested Reading

Atlas SW (1989) Magnetic resonance imaging of the orbit: current status. Magn Reson Q 5:39–96

Benitez WI, Sartor KJ, Angtuaco EJ (1988) Craniopharyngioma presenting as a nasopharyngeal mass: CT and MR findings. J Comput Assist Tomogr 12:1068–1072

Castellote A, Vazquez E, Vera J et al (1999) Cervicothoracic lesions in infants and children. Radiographics 19:583–600

Chung CJ, Armfield KB, Mukherji SK et al (1999) Cervical neurofibromas in children with NF-1. Pediatr Radiol 29:353–356

Daffner RH, Kirks DR, Gehweiler JA Jr et al (1982) Computed tomography of fibrous dysplasia. AJR Am J Roentgenol 139:943–948

Dvorak J, Grob D, Baumgartner H et al (1989) Functional evaluation of the spinal cord by magnetic resonance imaging in patients with rheumatoid arthritis and instability of upper cervical spine. Spine 14:1057–1064

Dworkin HJ, Meier DA, Kaplan M (1995) Advances in the management of patients with thyroid disease. Semin Nucl Med 25:205–220

Enzman DR, Delapza RL, Rubin JB (1990) Magnetic resonance imaging of the spine. Mosby-Year Book, St. Louis

Epstein N (1993) The surgical management of ossification of the posterior longitudinal ligament in 51 patients. J Spinal Disord 6:432–455

Eustic HS, Mafee MF, Walton C et al (1998) MR imaging and CT of orbital infections and complications in acute rhinosinusitis. Radiol Clin North Am 36:1165–1183

Fagerlund M, Bjornebrink J, Ekelund L et al (1992) Ultra low field MR imaging of cervical spine involvement in rheumatoid arthritis. Acta Radiol 33:89–92

Fink JN, McAuley DL (2002) Mastoid air sinus abnormalities associated with lateral venous thrombosis: cause or consequence? Stroke 33:290–292

Flickinger FW, Sanal SM (1994) Bone marrow MRI: techniques and accuracy for detecting breast cancer metastases. Magn Reson Imaging 12:829–835

Fries JW (1957) The roentgen features of fibrous dysplasia of the skull and facial bones; a critical analysis of thirty-nine pathologically proven cases. Am J Roentgenol Radium Ther Nucl Med 77:71–88

Fuchshuber S, Grevers G, Issing WJ (2002) Dermoid cyst of the floor of the mouth—a case report. Eur Arch Otorhinolaryngol 259:60–62

Glew D, Watt I, Dieppe PA et al (1991) MRI of the cervical spine: rheumatoid arthritis compared with cervical spondylosis. Clin Radiol 44:71–76

Go C, Bernstein JM, de Jong AL et al (2000) Intracranial complications of acute mastoiditis. Int J Pediatr Otorhinolaryngol 52:143–148

Ho MW, Crean SJ (2003) Simultaneous occurrence of sublingual dermoid cyst and oral alimentary tract cyst in an infant: a case report and review of the literature. Int J Paediatr Dent 13:441–446

Huysmans DA, Hermus AR, Corstens FH et al (1994) Large, compressive goiters treated with radioiodine. Ann Intern Med 121:757–762

Janssen AG, Mansour K, Bos JJ et al (2000) Abscess of the lacrimal sac due to chronic or subacute dacryocystitis: treatment with temporary stent placement in the nasolacrimal duct. Radiology 215:300–304

Karcioglu ZA, Hadjistilianou D, Rozans M et al (2004) Orbital rhabdomyosarcoma. Cancer Control 11:328–333

Kaufman LM, Villablanca JP, Mafee MR (1998) Diagnostic imaging of cystic lesions in the child's orbit. Radiol Clin North Am 36:1149–1163

Leeds N, Seaman WB (1962) Fibrous dysplasia of the skull and its differential diagnosis. A clinical and roentgenographic study of 46 cases. Radiology 78:570–582

Mafee MF, Pai E, Philip B (1989) Rhabdomyosarcoma of the orbit. Evaluation with MR imaging and CT. Radiol Clin North Am 36:1215–1227

Maroldi R, Farina D, Palvarini L et al (2001) Computed tomography and magnetic resonance imaging of pathologic conditions of the middle ear. Eur J Radiol 40:78–93

McCormick PC, Bello JA, Post KD (1988) Trigeminal schwannoma. Surgical series of 14 cases with review of the literature. J Neurosurg 69:850–860

Miyahara H, Matsunaga T (1994) Tornwaldt's disease. Acta Otolaryngol Suppl 517:36–39

Mukherji SK (2003) Pharynx. In: Som PM, Curtin DH (eds) Head and neck imaging, 4th edn. Mosby, St. Louis, pp 1507–1509

Noma S, Kanaoka M, Minami S et al (1988) Thyroid masses: MR imaging and pathologic correlation. Radiology 168:759–764

Petito CK, DeGirolami U, Earle KM (1976) Craniopharyngiomas: a clinical and pathological review. Cancer 37:1944–1952

Resnick D (1996) Bone and joint imaging, 2nd edn. WB Saunders, Philadelphia, pp 378–387

Robinson DR, Tashjian AH Jr, Levine L (1975) Prostaglandin-stimulated bone resorption by rheumatoid synovia. A possible mechanism for bone destruction in rheumatoid arthritis. J Clin Invest 56:1181–1188

Soo MY, Rajaratnam S (2000) Symptomatic ossification of the posterior longitudinal ligament of the cervical spine: pictorial essay. Australas Radiol 44:14–18

Spiegel JH, Lustig LR, Lee KC et al (1998) Contemporary presentation and management of a spectrum of mastoid abscesses. Laryngoscope 108:822–828

Terayama K (1989) Genetic studies on ossification of the posterior ligament of the spine. Spine 14:1184–1191

Tetsumura A, Yoshino N, Yamada I et al (1999) Head and neck hemangiomas: contrast-enhanced three-dimensional MR angiography. Neuroradiology 41:140–143

Visrutaratna P, Oranratanachai K, Singhavejsakul J (2004) Clinics in diagnostic imaging (96). Plexiform neurofibromatosis. Singapore Med J 45:188–192

Weber AL, Montandon C, Robson CD (2000) Neurogenic tumors of the neck. Radiol Clin North Am 38:1077–1090

Weiner HL, Wisoff JH, Rosenberg ME et al (1994) Craniopharyngiomas: a clinicopathological analysis of factors predictive of recurrence and functional outcome. Neurosurgery 35:1001–1010

Williams LS, Schmalfuss IM, Sistrom CL et al (2003) MR Imaging of the trigeminal ganglion, nerve, and the perineural vascular plexus: normal appearance and variants with correlation to cadaver specimens. AJNR Am J Neuroradiol 24:1317–1323

Yousem DM (1998) Case review: head and neck imaging. Mosby, St. Louis

Yuh WT, Simonson TM, Wang AM et al (1994) Venous sinus occlusive disease: MR findings. AJNR Am J Neuroradiol 15:309–316

Interventional Maxillofacial Radiology

14

Abstract

This chapter illustrates TMJ arthrography, TMJ arthroscopy, sialography, biopsy, and embolization.

14.1 Introduction

Interventional radiology or, as it is sometimes called, minimally invasive surgery has evolved from traditional diagnostic radiology over the last three decades. Thus today many procedures can be done with image guidance that in the past required an open approach. The morbidity, risks, and complications can often be reduced significantly by image-guided minimally invasive percutaneous techniques as compared to open surgical procedures. There are many examples of successful interventional radiology performed today: TIPS, in which the portal vein is connected to the hepatic vein bypassing the liver in patients with liver failure, aspiration biopsies in deep locations that were not accessible without an open approach in the past, recanalization of the fallopian tubes for infertility, and maintenance of vascular access in patients with renal disease, to mention a few.

Interventional maxillofacial radiology is in its infancy. Only a few minimally invasive procedures have been applied to this area, but it is quite obvious that the percutaneous approach with needles is much preferred in the maxillofacial region as compared to an open procedure. In this chapter we have collected a few diagnostic and interventional procedures that have been applied to the maxillofacial and related areas. Of these procedures temporomandibular joint (TMJ) arthrography and sialography are those which most typically have been performed by maxillofacial radiologists. It is also our opinion that image-guided biopsies of soft-tissue masses or bone, being good alternatives to open surgery biopsies, should be within the working area of these specialists. Although orbital biopsies and embolizations are beyond their scope, we have also illustrated such procedures to show the maxillofacial radiologist what is indeed possible to safely perform.

14.2 TMJ Arthrography

Fig. 14.1

14.2.1 Definition

Radiographic study where contrast material has been injected into lower joint compartment or lower and upper compartments to visualize soft tissues such as articular disc and joint capsule.

14.2.2 Clinical Features

- Initially, developed in the 1940s but gained popularity in the 1980s when internal derangement was discovered as a frequent finding in patients with facial pain and mandibular dysfunction
- Initially, single-contrast arthrography either in lower joint compartment or in both joint compartments with plain films or conventional tomography (arthrotomography); later developed into double-contrast arthrotomography with air as a supplement to the contrast material
- Fell out of favor with the development of high-quality MRI and rarely performed today

14.2.3 Imaging Features

- Excellent for dynamic studies of the articular disc
- Gold standard for determining disc or posterior attachment perforations; normal joint has no communication between compartments

T.A. Larheim, P.-L.A. Westesson, *Maxillofacial Imaging*, https://doi.org/10.1007/978-3-319-53319-3_14

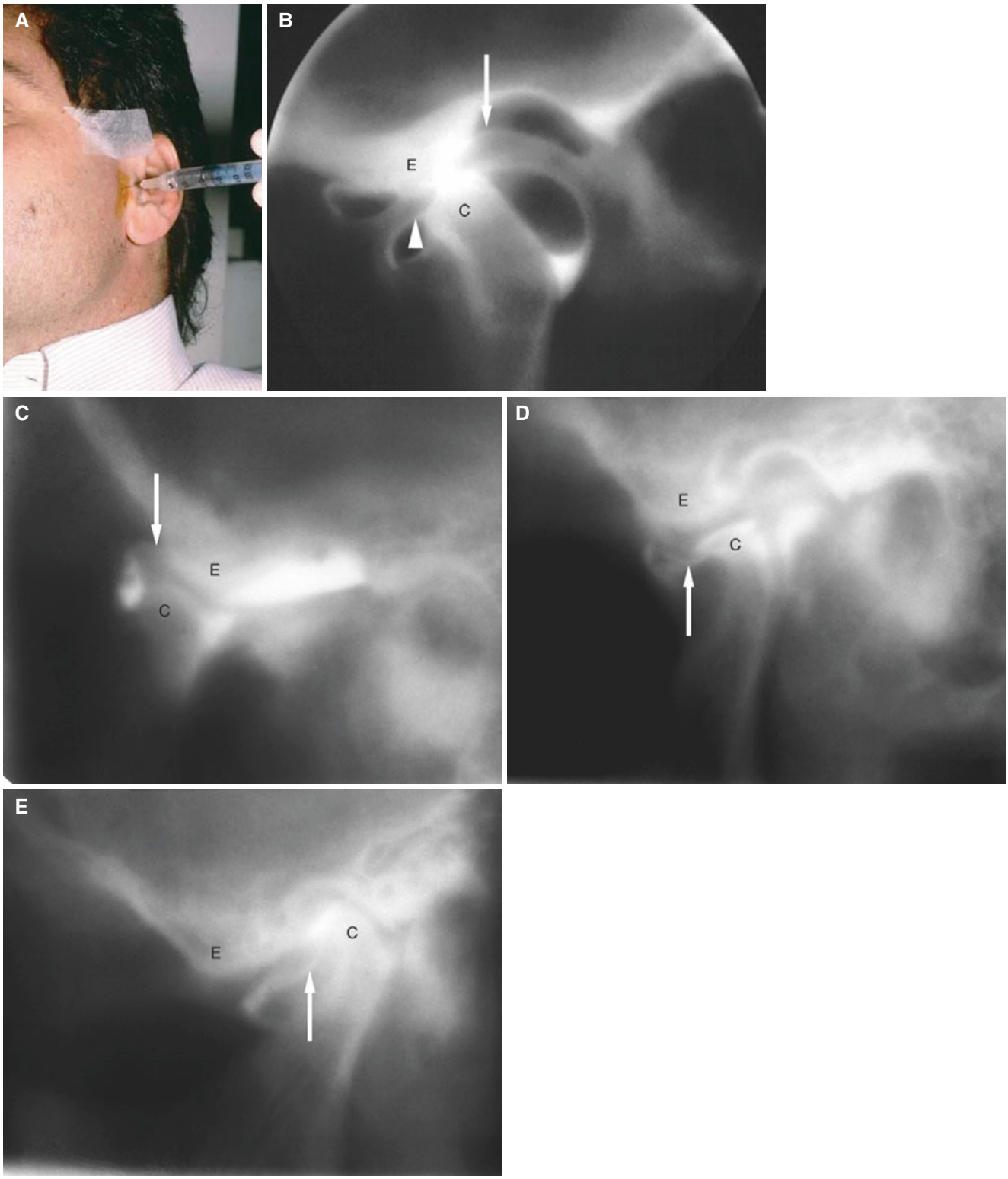

Fig. 14.1 TMJ arthrotomography; normal and abnormal. (**A**) Local anesthesia before contrast injection. (**B**) Double-contrast dual space arthrotomography, i.e., both joint compartments injected separately; normal disc position in half-open-mouth view as indicated by anterior band (*arrowhead*) anterior to condyle (*C*) and posterior band (*arrow*) posterior to condyle; joint spaces also filled with air and thus appear radiolucent. Articular eminence indicated (*E*). (**C**) Single-contrast dual space arthrotomography; upper space filled through perforation (not seen) in the area of disc/posterior attachment, open-mouth view; disc anteriorly displaced without reduction as indicated by its posterior band (*arrow*) in front of the condyle (*C*). Articular eminence indicated (*E*). (**D**) Single-contrast lower space arthrotomography; open-mouth view shows contrast material in front of the condyle (*C*) demonstrating anteriorly displaced disc (*arrow*) without reduction. Articular eminence indicated (*E*). (**E**) Same joint, closed-mouth view; contrast material in extended anterior recess showing lower surface of posterior band (*arrow*) of anteriorly displaced disc in front of the condyle (*C*). Articular eminence indicated (*E*)

– Double-contrast studies show more exquisite detail, but the diagnostic accuracy on a one-to-one comparison is the same as for single-contrast studies

14.3 TMJ Arthroscopy

Figs. 14.2 and 14.3

14.3.1 Definition

Inspection of joint surfaces by performing minimally invasive surgical procedures percutaneously using an arthroscope.

14.3.2 Clinical Features

– Gained popularity in early 1980s when thin (2–3 mm diameter) arthroscopic instruments became available

14.3.3 Imaging Features

– Often difficult to diagnose disc position since no cross-sectional view is obtained
– Multiple minimally invasive surgical procedures have been performed with limited morbidity and success rates similar to those of open surgical procedures
– Can be done under general or local anesthesia
– Diagnosis of adhesions and synovitis are the main applications for arthroscopy
– Usually only upper joint compartment examined/treated

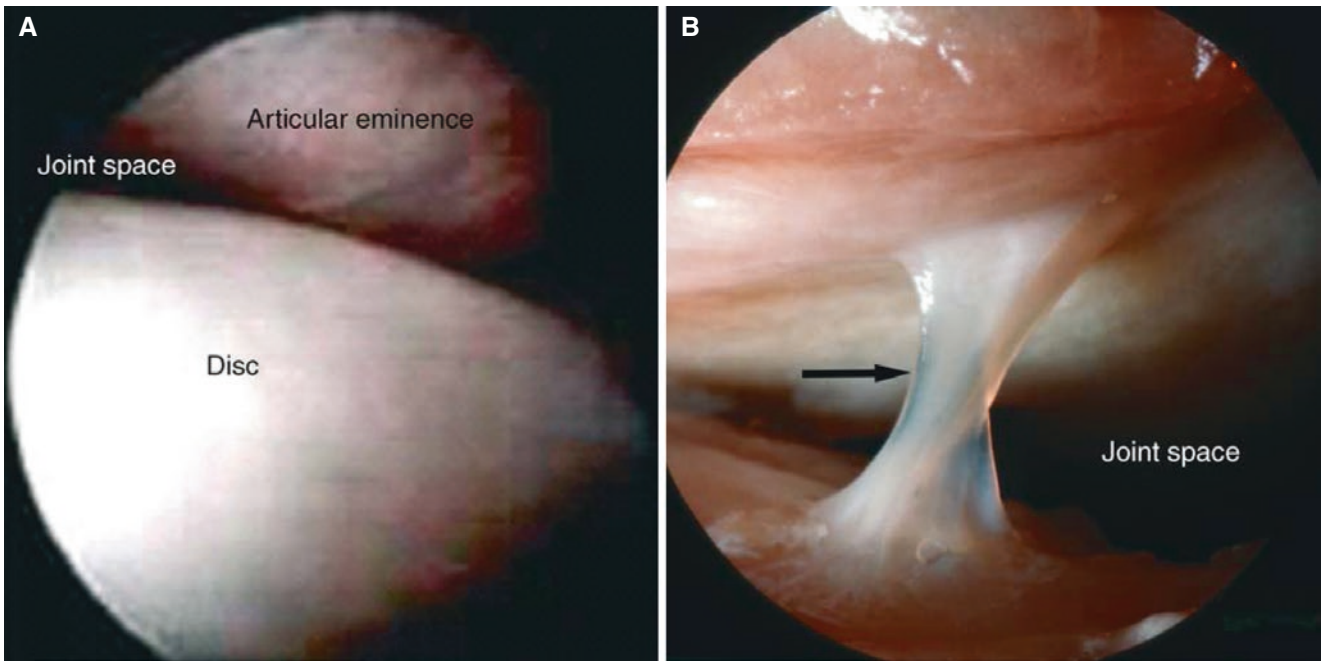

Fig. 14.2 TMJ arthroscopy; normal and abnormal. (**A**) Upper joint compartment; normal joint as indicated by smooth surfaces of both disc and eminence. (**B**) Upper joint compartment; fibrous adhesion between disc and eminence (*arrow*)

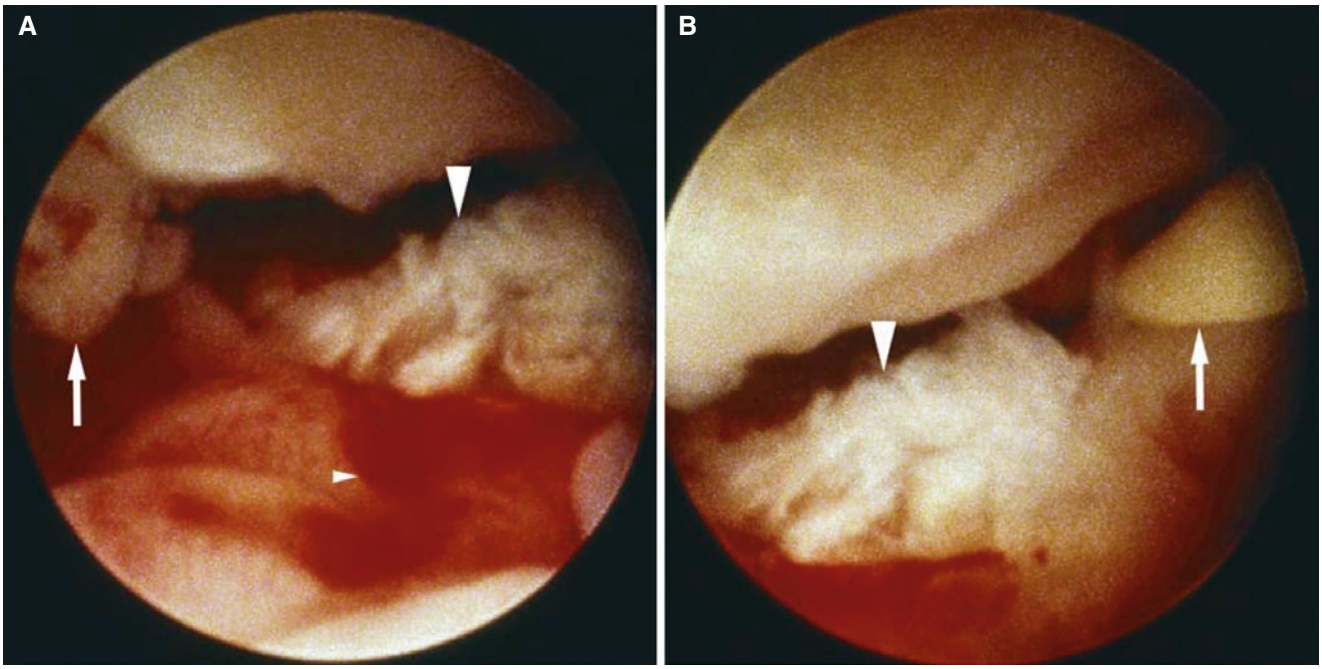

Fig. 14.3 TMJ arthroscopy; rheumatoid arthritis. (**A**) Upper joint compartment; synovial proliferation (*arrowhead*) in disc perforation area, hyperemia (*small arrowhead*), and part of disc (*arrow*). (**B**) Same joint; synovial proliferation (*arrowhead*) in disc perforation area and part of disc (*arrow*)

14.4 Sialography

Figs. 14.4, 14.5, 14.6, 14.7, and 14.8

14.4.1 Definition

Radiographic studies of salivary glands after injection of contrast material.

14.4.2 Clinical Features

- Sialography is primarily done to image ducts and, if conventional radiography or CT image is normal, to detect salivary stones
- Also used in the treatment of strictures (ballooning) and removal of stones (fluoroscopically guided basket retrieval)

14.4.3 Imaging Features

- Inflammation, strictures; stones are often better seen on sialography than on MRI or CT images
- In the late 1970s, CT sialography was popularized, but this procedure has fallen out of favor because conventional sialography is superior for duct imaging and quality of MR sialography is improving
- MRI is primary modality for salivary gland masses

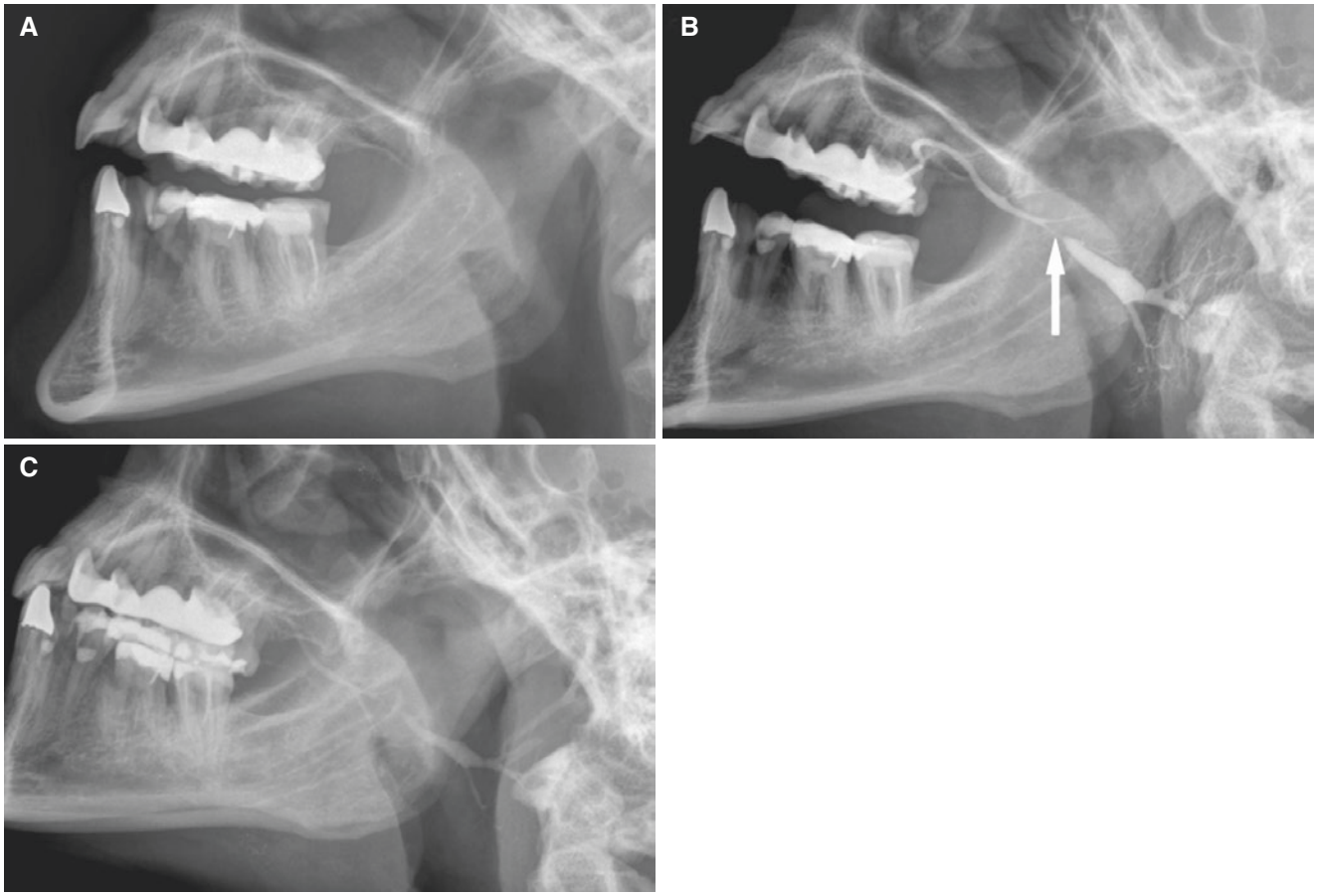

Fig. 14.4 Parotid sialography; sialodochitis, normal parenchyma. (**A**) Side view shows no signs of stone in Stensen's duct. (**B**) Plain film sialography shows stricture (*arrow*) and dilatation proximal duct. (**C**) Plain film shows retention of contrast material; only parenchyma is without contrast material after 5 min (courtesy of Dr. B. Svensson, Skövde Hospital, Sweden)

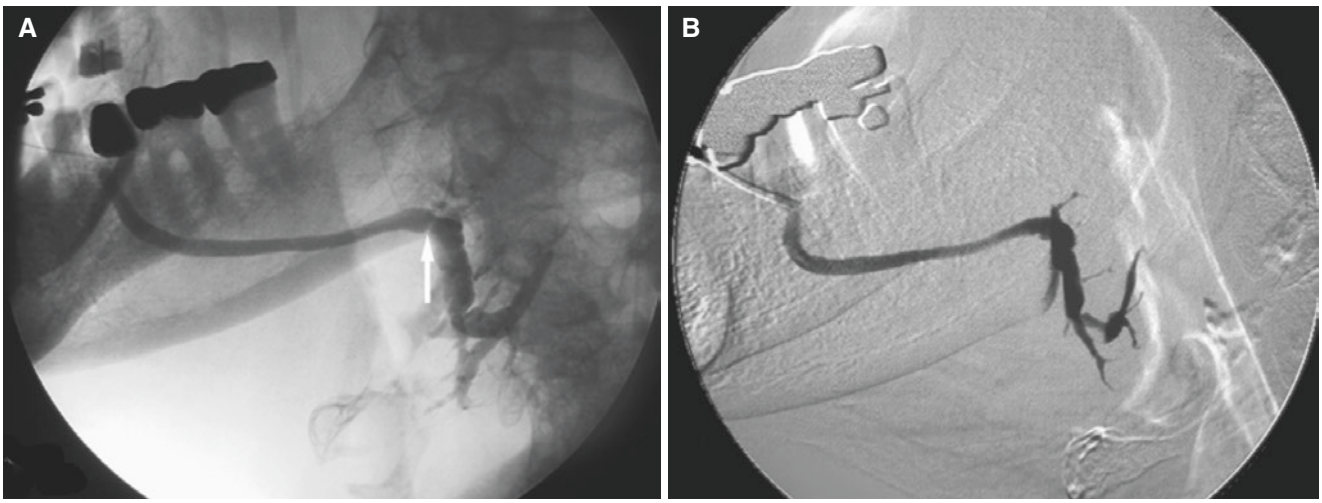

Fig. 14.5 Submandibular sialography; sialadenitis, rather normal Wharton's duct. (**A**) Plain film sialography (fluoroscopy) shows mostly a normal duct but with one stricture (*arrow*) and dilatation of intraglandular ducts with abnormal filling of parenchyma. (**B**) Digital subtraction sialography of same patient does not show stricture but more clearly lack of parenchyma filling

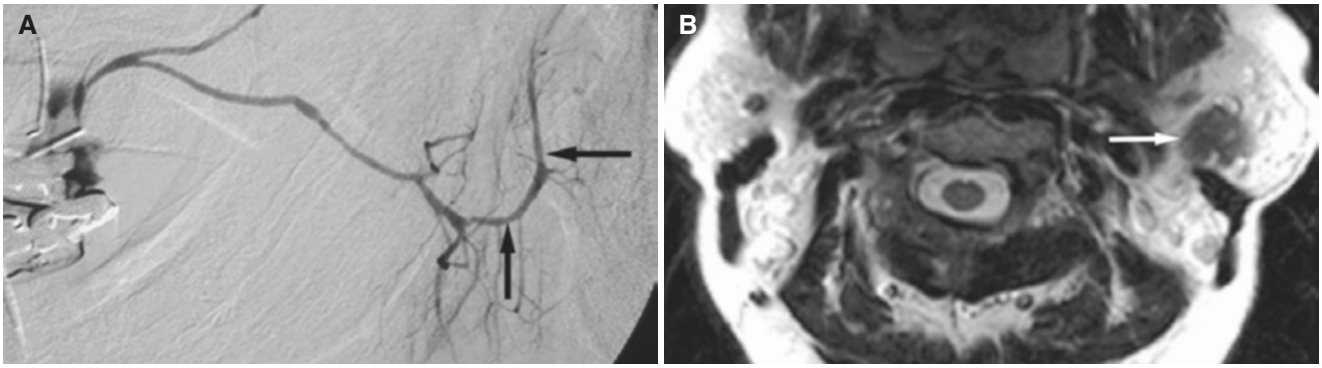

Fig. 14.6 Parotid sialography; normal filling of Stensen's duct and gland parenchyma but duct displacement because of tumor. (**A**) Digital subtraction sialography shows normal caliber duct and normal filling of intraglandular ducts, but displacement (*arrows*) due to tumor; difficult to appreciate. (**B**) Axial T1-weighted MRI performed same day shows tumor (*arrow*) in the left parotid gland

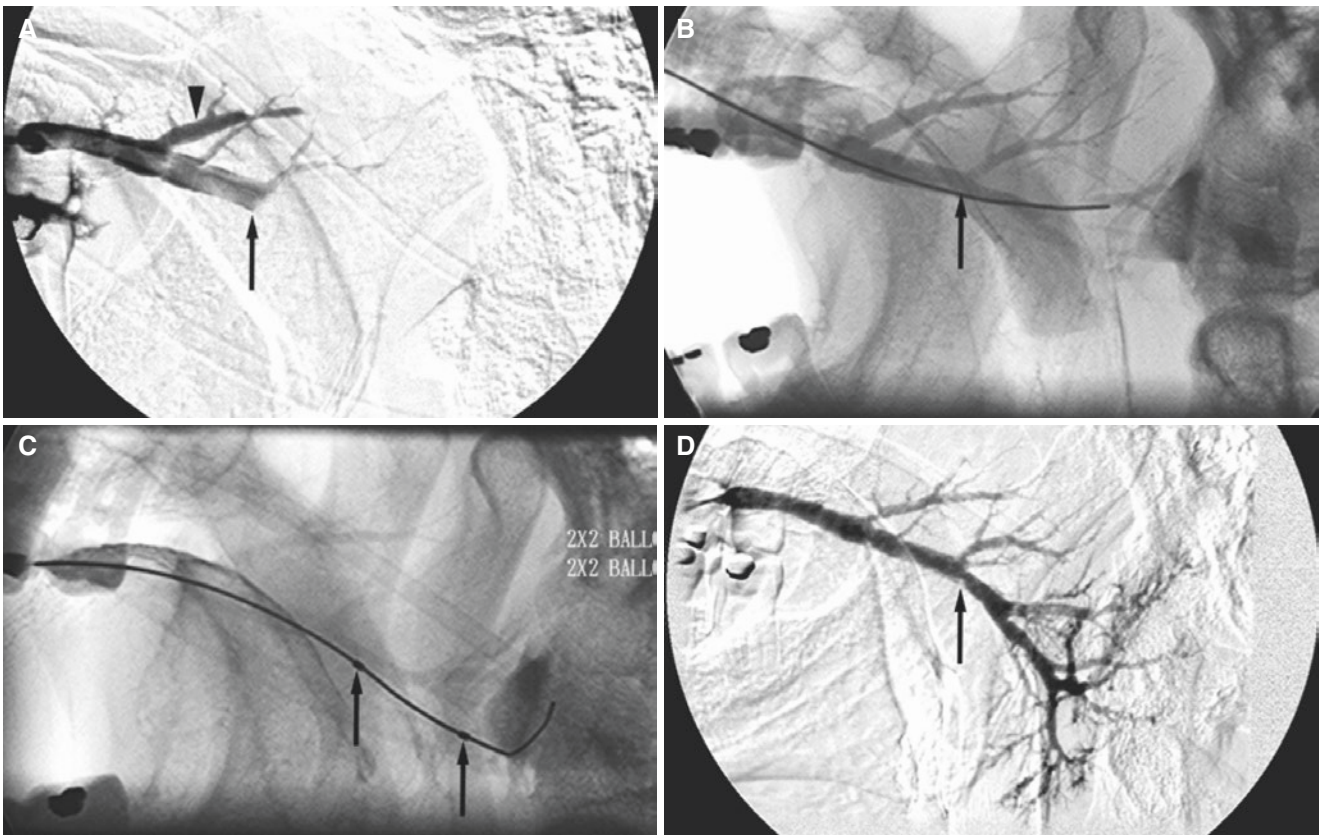

Fig. 14.7 Parotid sialography; abnormal filling of Stensen's duct and no filling of parenchyma before successful duct ballooning. (**A**) Digital subtraction sialography shows abrupt blockage of mid Stensen's duct (*arrow*) and filling of secondary ducts (*arrowhead*) and third ducts more enhanced than usual. (**B**) Plain film sialography (fluoroscopy) after probing with a guide wire (*arrow*) shows that blockage could be passed with contrast material. (**C**) Plain film sialography (fluoroscopy) shows that symmetry 2 mm × 2 cm balloon has been inserted (*arrows*) and expanded to dilate stricture. (**D**) Digital subtraction sialography after procedure shows small residual stricture (*arrow*), but filling of gland; inflammatory changes

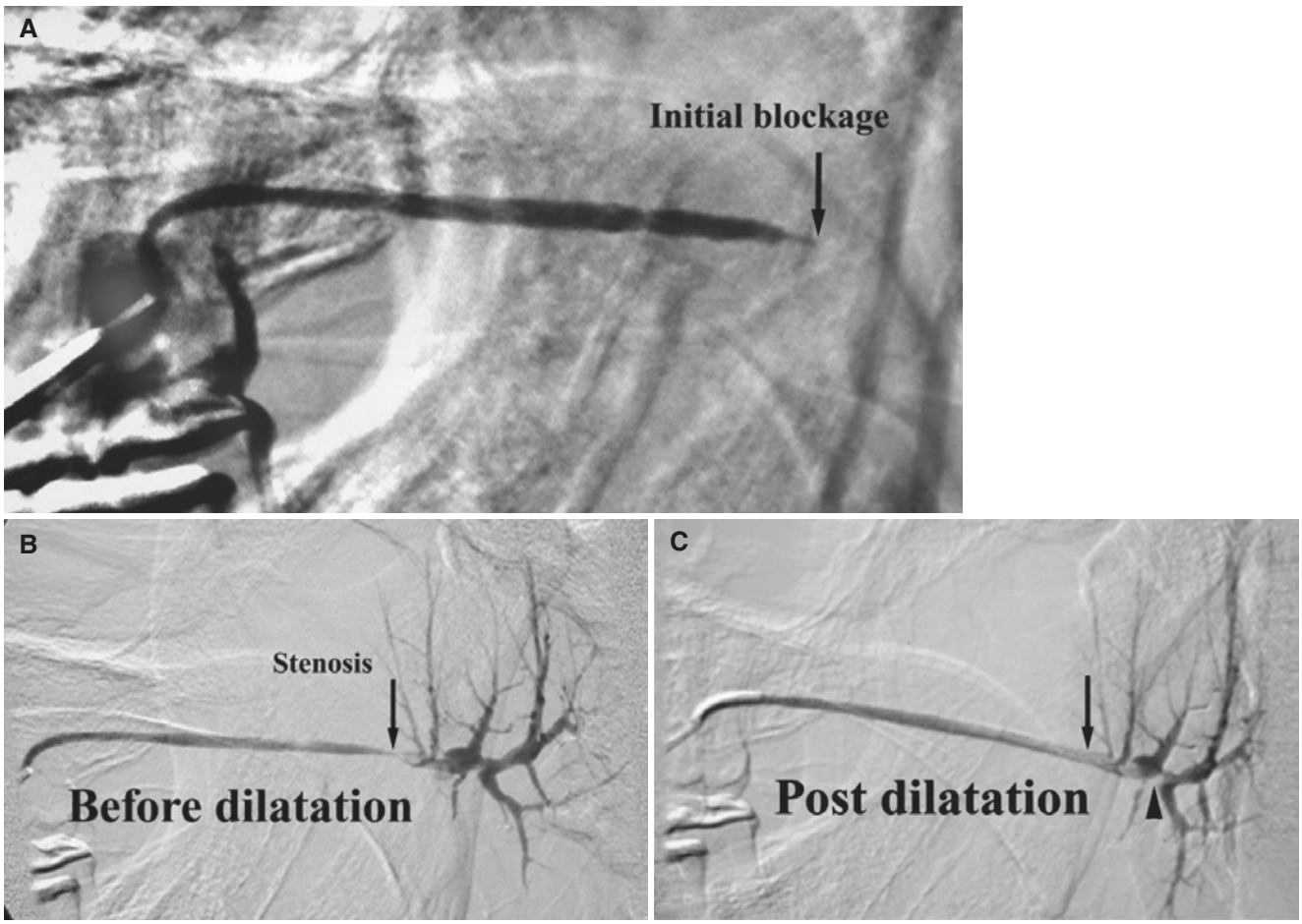

Fig. 14.8 Parotid sialography; occlusion of Stensen's duct and no filling of parenchyma before successful duct ballooning. (**A**) Digital subtraction parotid sialography; stricture occluding Stensen's duct (*arrow*). (**B**) Subtraction sialography after probing through duct with guide wire shows stenosis (*arrow*) but filling of parenchyma. (**C**) Subtraction sialography after dilatation shows widening of stricture (*arrow*). A small filling defect in gland (*arrowhead*) may be mucus or residual stone. The patient did well after procedure and no further intervention was needed

14.5 Biopsy

Figs. 14.9, 14.10, and 14.11

14.5.1 Definition

Either tissue or cellular material for pathologic diagnosis.

14.5.2 Clinical Features

- With an image-guided procedure, deep lesions in the maxillofacial area can often be reached with minimal morbidity

14.5.3 Imaging Features

- Fine needle aspiration provides cytologic information
- Core biopsy gives a solid tissue core which is fixed in formalin and embedded for traditional pathologic studies with light microscopy
- Typically 22 gauge needles are used for fine needle aspiration, and 16, 18, or 20 gauge core biopsy needles are used for core biopsies
- Negative fine needle aspiration findings are difficult to interpret since they may be due to sampling error
- Core biopsy gives higher percentage of positive answers and easier to trust when negative. Core biopsy is however more invasive since the needle size is larger
- For bone biopsies 13 gauge bone biopsy needles are used
- CT fluoroscopy reduces radiation and improves efficiency over regular CT imaging as guidance

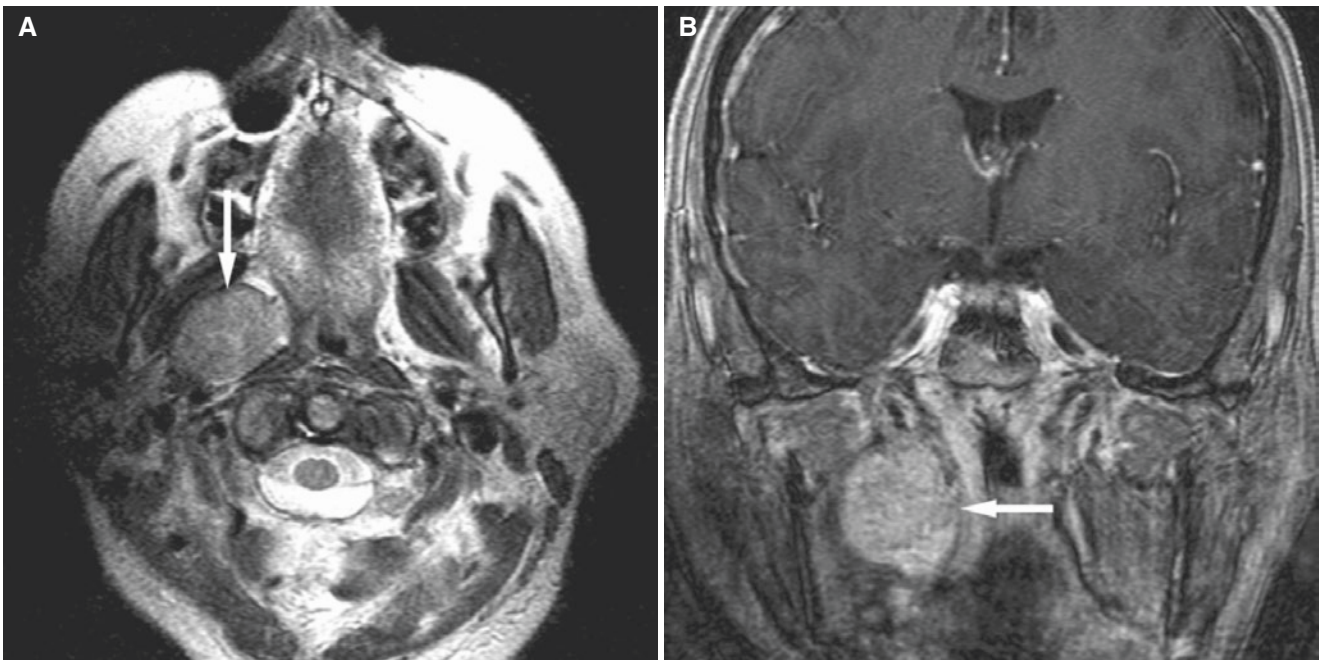

Fig. 14.9 CT fluoroscopy-guided biopsy of parapharyngeal mass. (**A**) Axial T2-weighted MRI shows deep parapharyngeal mass (*arrow*). (**B**) Coronal T1-weighted post-Gd MRI shows mass (*arrow*) medial to the ramus of the mandible. (**C**) Patient placed in lateral decubitus. Markers, white dots, are placed on the skin to guide an oblique posterior approach. (**D**) Local anesthesia is induced. (**E**) 16 gauge Temno core biopsy needle; tissue core is obtained in cut out on needle (between arrows). (**F**) Temno biopsy needle inserted through a small skin incision. (**G**) CT fluoroscopy shows biopsy needle at correct angle. (**H**) CT fluoroscopy confirms correct position of needle within mass

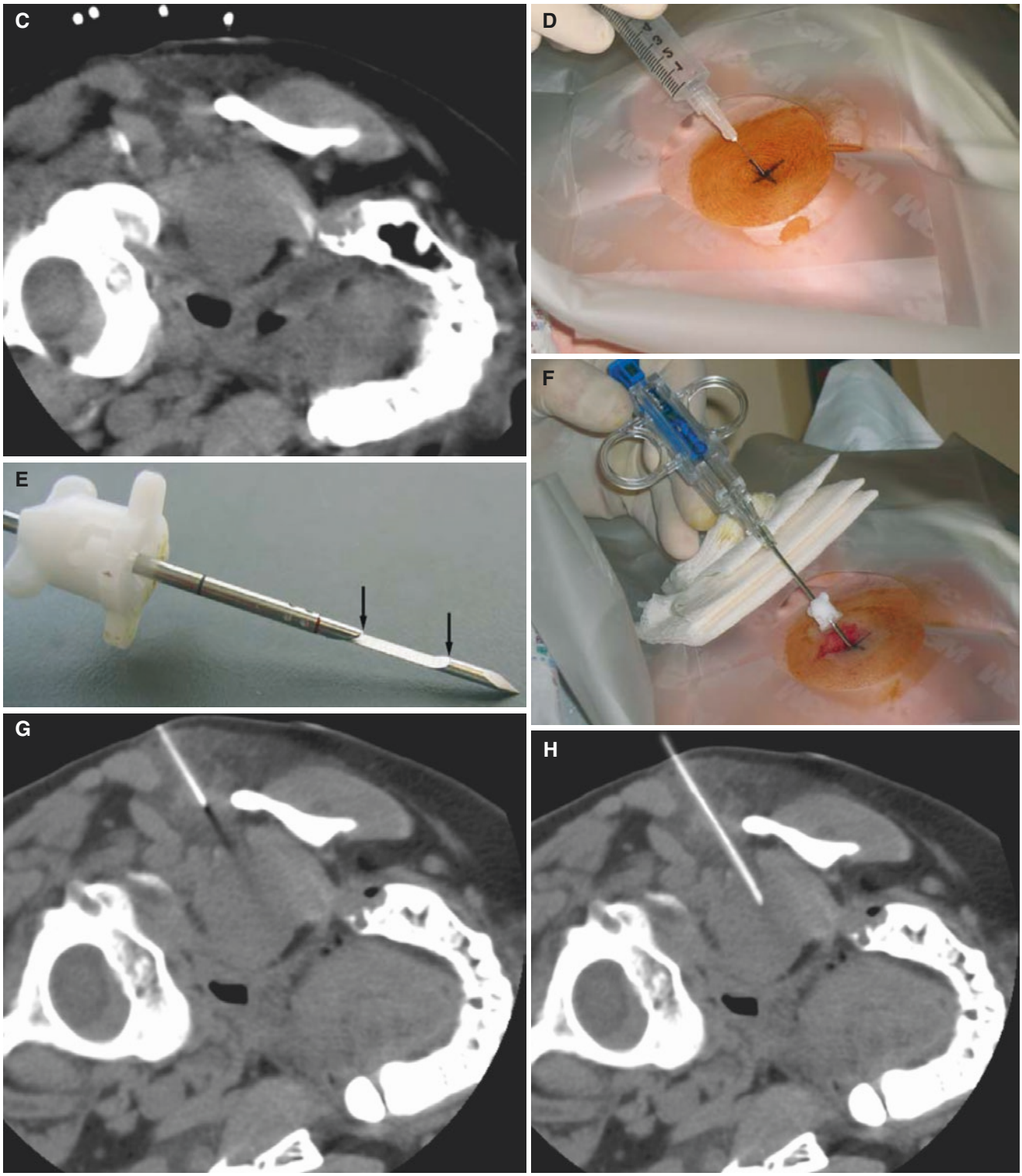

Fig. 14.9 (continued)

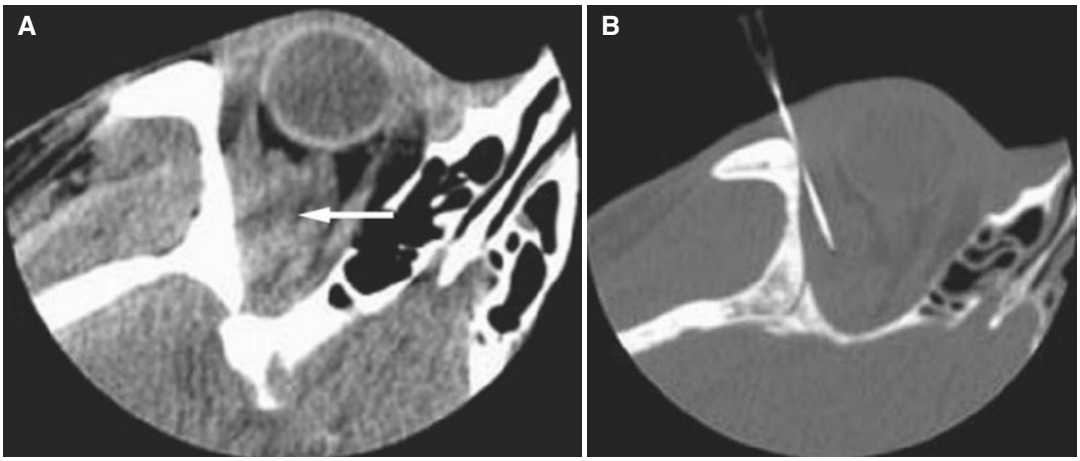

Fig. 14.10 CT fluoroscopy-guided biopsy of orbital mass. (**A**) Axial CT image shows intraorbital mass (*arrow*) in posterior lateral aspect of right orbit. (**B**) Axial CT image, bone window, shows fine needle, 25 gauge, in correct position; aspiration revealed signs of hemangioma

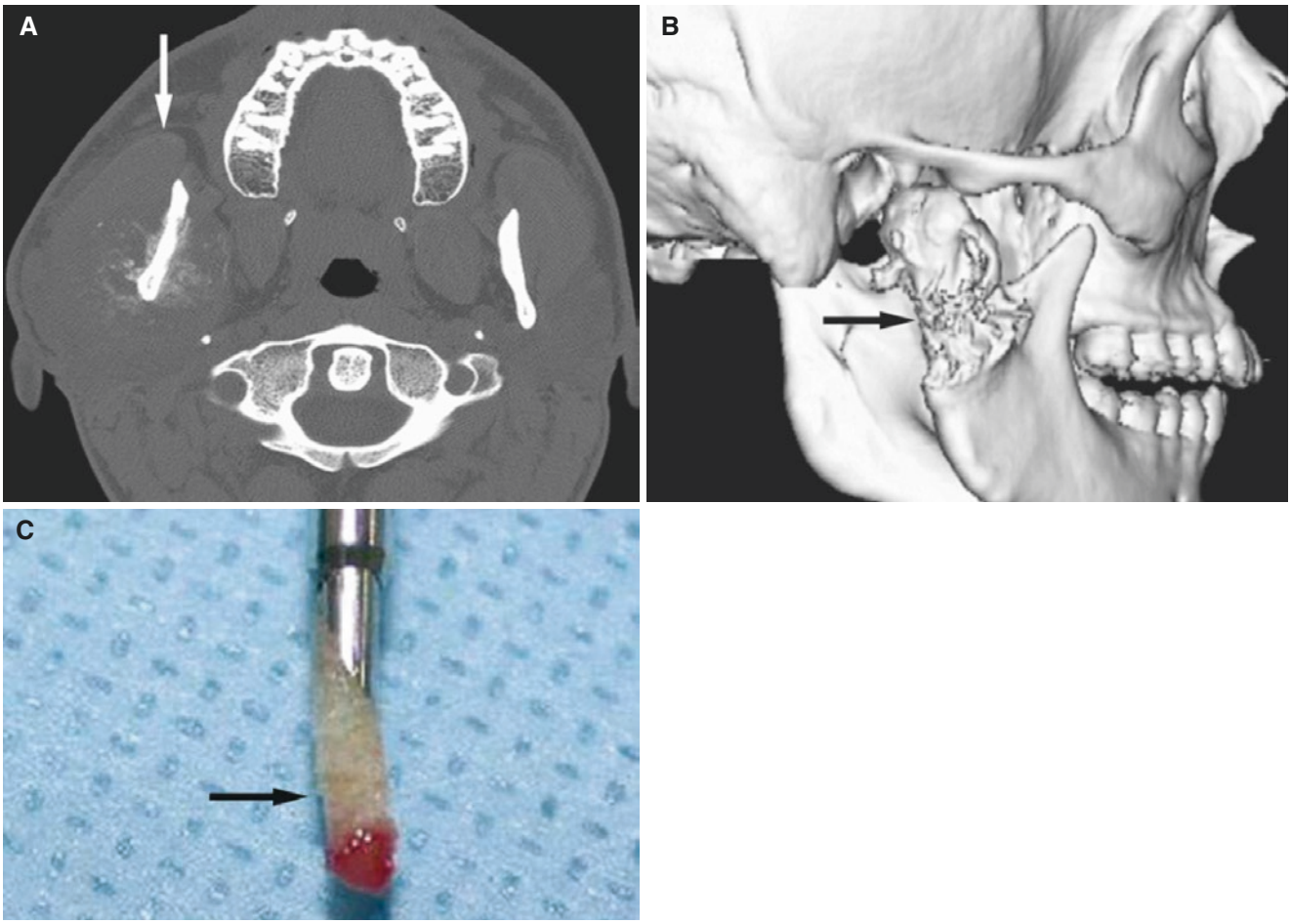

Fig. 14.11 Bone biopsy of mass around mandibular ramus. (**A**) Axial CT image shows soft-tissue mass with extensive sunburst periosteal bone reaction (*arrow*). (**B**) 3D CT image depicts relationship between tumor and the ramus of the mandible (*arrow*). (**C**) Bone core (*arrow*) obtained using a 13 gauge bone biopsy needle demonstrated chondrosarcoma

14.6 Facial Hemangioma Embolization

Fig. 14.12

14.6.1 Definition

Percutaneous treatment of facial hemangioma by injection of absolute alcohol.

14.6.2 Clinical Features

- Hemangiomas of face often regress with time
- Image-guided alcohol embolization is often less invasive than surgery which is difficult because of the intricate nature of hemangiomas

14.6.3 Imaging Features

- Using general anesthetics, percutaneous injection of alcohol can be used to reverse hemangiomas. Other substances can also be used

14.7 Nosebleed Embolization

Fig. 14.13

14.7.1 Definition

Using interventional angiographic technique to embolize small vessels leading to nosebleed using particles or spheres.

14.7.2 Clinical Features

- Most nosebleeds can be stopped by packing and conservative measures
- Nosebleed may be life-threatening if it is not stopped by conservative measures. Either surgery or interventional techniques may be used to block bleeding vessels
- Interventional techniques are less invasive than open surgery

14.7.3 Imaging Features

- High-quality digital subtraction angiography in two planes often necessary
- Microcatheter technique needed to embolize specific vessels
- Risk of blindness if retinal arteries are embolized
- Often performed by interventional neuroradiologists

14.8 Juvenile Angiofibroma Embolization

Fig. 14.14

14.8.1 Definition

Juvenile angiofibroma is a benign locally aggressive vascular tumor which is often supplied from branches of the internal maxillary artery and foramen rotundum, arteries in the Vidian canal, the sphenomaxillary artery, and occasionally also the ophthalmic artery. Standard treatment is surgery after preoperative embolization which effectively reduces intraoperative bleeding.

Using minimally invasive interventional radiographic techniques, small vessels are embolized by means of a microcatheter in the angiofibroma.

14.8.2 Clinical Features

- Primarily a disease of adolescent males; only a few cases reported in females
- Usually progressive growth but occasional regression has been reported
- Located in the nose, nasopharynx, and parapharyngeal space
- Often presents with nasal obstruction and epistaxis

14.8.3 Imaging Features

- Very vascular
- Locally aggressive
- Will often arise in sphenopalatine foramen
- T1-weighted MRI: intermediate signal
- T2-weighted MRI: high signal
- T1-weighted post-Gd MRI: intense enhancement
- MRI often shows flow voids

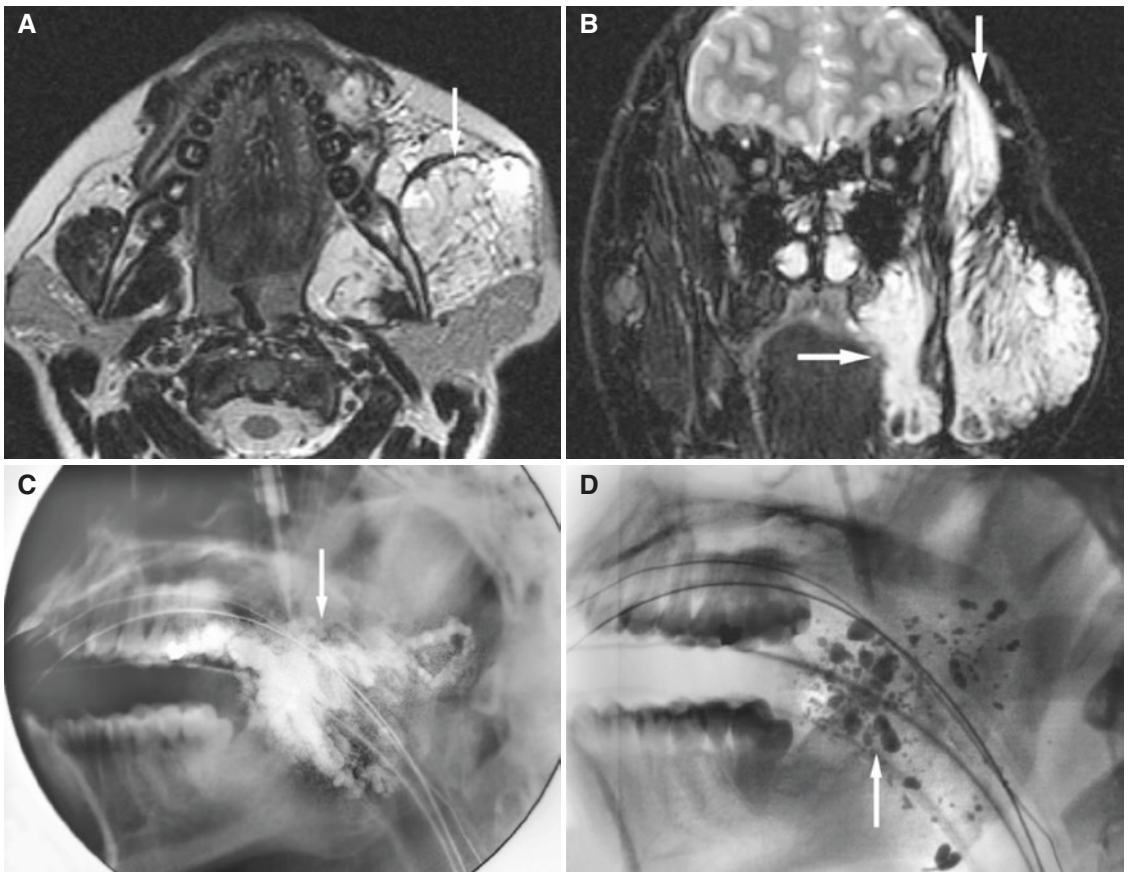

Fig. 14.12 Facial hemangioma embolization. (**A**) Axial T1-weighted fat-suppressed post-Gd MRI shows hemangioma located in the left masticator space (*arrow*). (**B**) Coronal T2-weighted fat-suppressed MRI shows large mass of infiltrating nature (*arrows*). (**C**) Lateral view (fluoroscopy) shows percutaneous injection of hemangioma (*arrow*) using a mixture of Ethiodol and absolute alcohol. (**D**) Postinjection lateral view (fluoroscopy) shows residual contrast material (*arrow*) as an indicator of the injection site (treatment courtesy of Dr. H. Wang, University of Rochester Medical Center, NY)

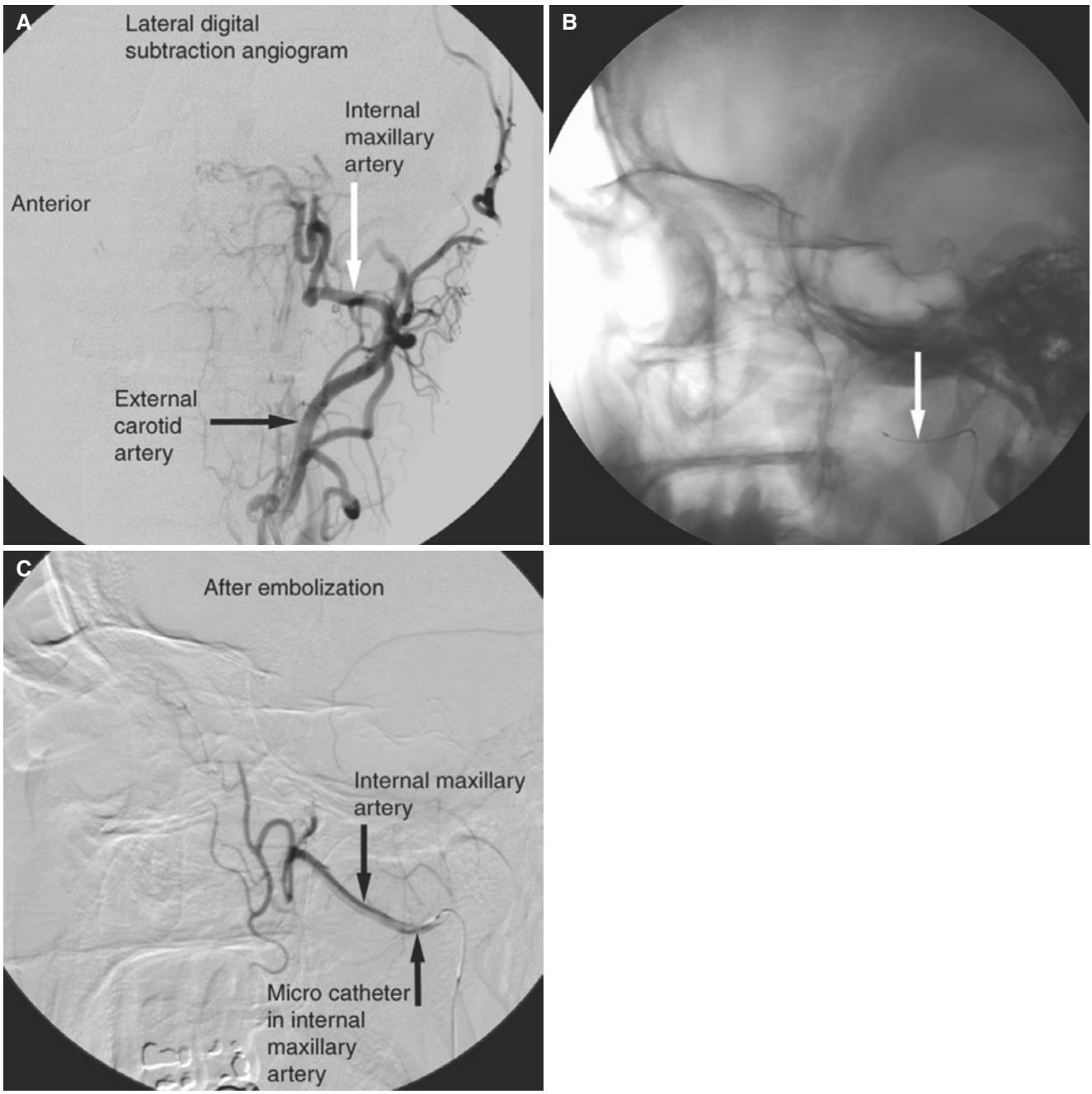

Fig. 14.13 Nosebleed embolization. (**A**) Digital subtraction angiography (fluoroscopy) shows external carotid artery and internal maxillary artery (*arrows*). Internal maxillary artery is the main feeder for nosebleeds. (**B**) Lateral view (fluoroscopy) shows microcatheter (*arrow*) placed in the internal maxillary artery. (**C**) Lateral digital subtraction angiography (fluoroscopy) after embolization shows microcatheter in the internal maxillary artery (*arrows*) and marked reduction of small vessels in the nasal region (treatment courtesy of Dr. H. Wang, University of Rochester Medical Center, Rochester, NY)

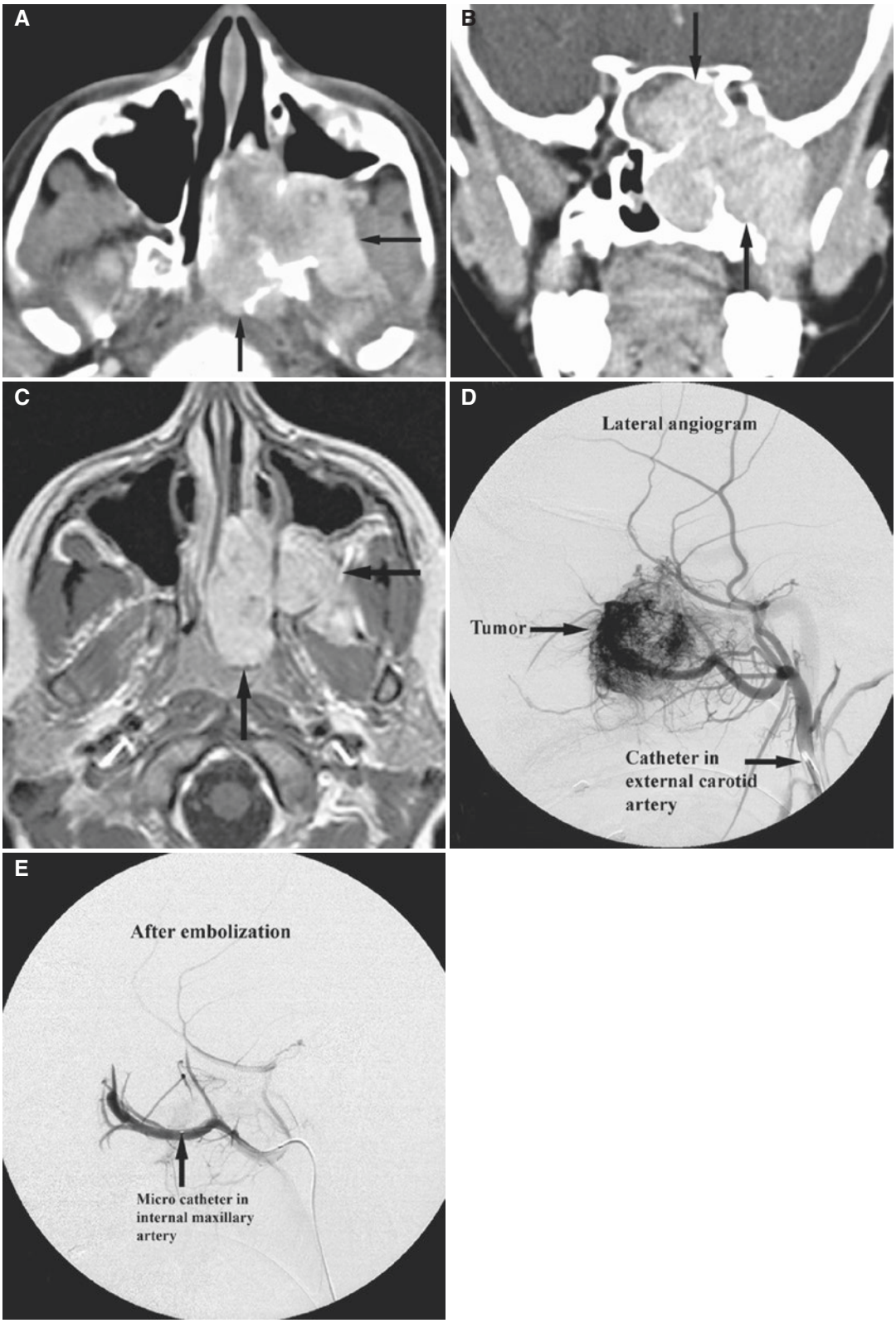

Fig. 14.14 Juvenile angiofibroma embolization. (**A**) Axial post-contrast CT image shows enhancing mass (*arrows*) in the left nasal cavity, nasopharynx, maxillary sinus, and infratemporal fossa with bone destruction. (**B**) Coronal post-contrast CT image shows enhancing mass (*arrows*) in the left sphenoid sinus, left nasal cavity, left maxillary sinus, and left infratemporal fossa. (**C**) Axial T1-weighted post-Gd MRI shows intensely enhancing mass (*arrows*). (**D**) Digital subtraction angiography in lateral projection with catheter in the left external carotid artery (*arrow*) showing dramatic tumor vascularity of juvenile angiofibroma (*arrow*). (**E**) Digital subtraction angiography in lateral projection after embolization, with microcatheter in the left internal maxillary artery (*arrow*). Using particles, tumor vascularity has been almost completely eliminated (treatment courtesy of Dr. H. Wang, University of Rochester Medical Center, NY, USA)

Suggested Reading

Barsotti JB, Westesson P-L, Ketonen LM (1992) Diagnostic and interventional angiographic procedures in the maxillofacial region. In: Westesson P-L (ed) Oral and maxillofacial surgery clinics of North America: contemporary maxillofacial imaging. WB Saunders, Philadelphia, pp 35–49

Brown JE (2002) Minimally invasive techniques for treatment of benign salivary gland obstruction. Cardiovasc Intervent Radiol 25:345–351

Brown JE, Drage NA, Escudier MP et al (2002) Minimally invasive radiologically guided intervention for the treatment of salivary calculi. Cardiovasc Intervent Radiol 25:352–355

Drage NA, Brown JE, Escudier MP et al (2002) Balloon dilatation of salivary duct strictures: report on 36 treated glands. Cardiovasc Intervent Radiol 25:356–359

Garcia-Cervigon E, Bien S, Rüfenacht D et al (1988) Pre-operative embolization of naso-pharyngeal angiofibromas. Report of 58 cases. Neuroradiology 30:556–560

Huang Z, Zhang D, Chen Y, Wang Y, Chen W, Huang Z (2016) Treatment of the recanalization of maxillary and mandibular arteriovenous malformations in children. Oral surg Oral Med Oral Pathol Oral Radiol 122:530–536

Jacobsson M, Petruson B, Svendsen P et al (1988) Juvenile nasopharyngeal angiofibroma. A report of eighteen cases. Acta Otolaryngol 105:132–139

Kandarpa K, Aruny JE (eds) (2001) Handbook of interventional radiologic procedures, 3rd edn. Philadelphia, Williams & Wilkins

McGurk M, Makdissi J, Brown JE (2004) Intra-oral removal of stones from the hilum of the submandibular gland: report of technique and morbidity. J Oral Maxillofac Surg 33:683–686

McGurk M, Escudier MP, Brown JE (2005) Modern management of salivary calculi. Br J Surg 92:107–112

Natvig K, Skalpe IO (1984) Pre-operative embolization of juvenile nasopharyngeal angiofibromas with gelfoam. J Laryngol Otol 98:829–833

Stansbie JM, Phelps PD (1986) Involution of residual juvenile nasopharyngeal angiofibroma (a case report). J Laryngol Otol 100:599–603

Wang D, Su L, Han Y, Wang Z, Zheng L, Li J, Fan X (2016) Direct intralesional ethanol sclerotherapy of extensive venous malformations with oropharyngeal involvement after a temporary tracheotomy in the head and neck: initial results. Head Neck. doi:10.1002/hed.24588

Zenk J, Constantinidis J, Al-Kadah B et al (2001) Transoral removal of submandibular stones. Arch Otolaryngol Head Neck Surg 127:432–436

Cone Beam Computed Tomography

15

Abstract

This chapter illustrates jaw cysts and cyst-like conditions, benign jaw tumors and tumor-like conditions, malignant tumors in jaws, jaw infections, temporomandibular joints, teeth (impactions and anomalies/malformations) and dental implants (pre- and postoperative imaging), facial traumas and fractures, facial growth disturbances, paranasal sinuses, maxillofacial soft tissues, and salivary glands. The themes are corresponding to the themes in the other chapters.

15.1 Introduction

Cone beam CT (CBCT) scanners have been developed for imaging dentoalveolar structures, with a smaller field of view, a lower radiation dose, and a higher spatial resolution compared to conventional (helical, multidetector, multislice) CT. However, the soft-tissue contrast is superior with conventional CT, hereafter named CT. The pioneering cone beam CT systems were developed for dynamic angiography. After being introduced for dental imaging in the late 1990s, the availability/use of CBCT has exploded worldwide. In a short period of time, the focus on this modality for dental and maxillofacial imaging has been substantial with regard to research, publications, and applications.

This chapter contains a number of sections with themes corresponding to the other chapters. Thus, readers who are working with CBCT scanners in particular may use one of these sections as a starting point to study a specific condition and then go to that chapter to read about the actual condition and see more cases.

Different CBCT scanners differ substantially regarding fields of view, exposure parameters, radiation dose, and image quality.

The chapter demonstrates some of the many diagnostic possibilities with this imaging modality.

15.2 Maxillofacial Imaging Anatomy

Cone beam CT anatomy is similar to bone window CT anatomy, as shown in Chap. 1. Soft-tissue structures are better visualized with CT. Images in Figs. 1.2 and 1.5 are obtained with a CBCT scanner.

In collaboration with B.B. Mork-Knutsen, U. Riis, C. Hol, M. Redfors, M. Kristensen, A.-K. Abrahamsson, L. Z. Arvidsson.

T.A. Larheim, P.-L.A. Westesson, *Maxillofacial Imaging*, https://doi.org/10.1007/978-3-319-53319-3_15

15.3 Jaw Cysts and Cyst-Like Conditions

Figs. 15.1, 15.2, 15.3, 15.4, 15.5, 15.6, 15.7, 15.8, 15.9, and 15.10

See Chap. 2

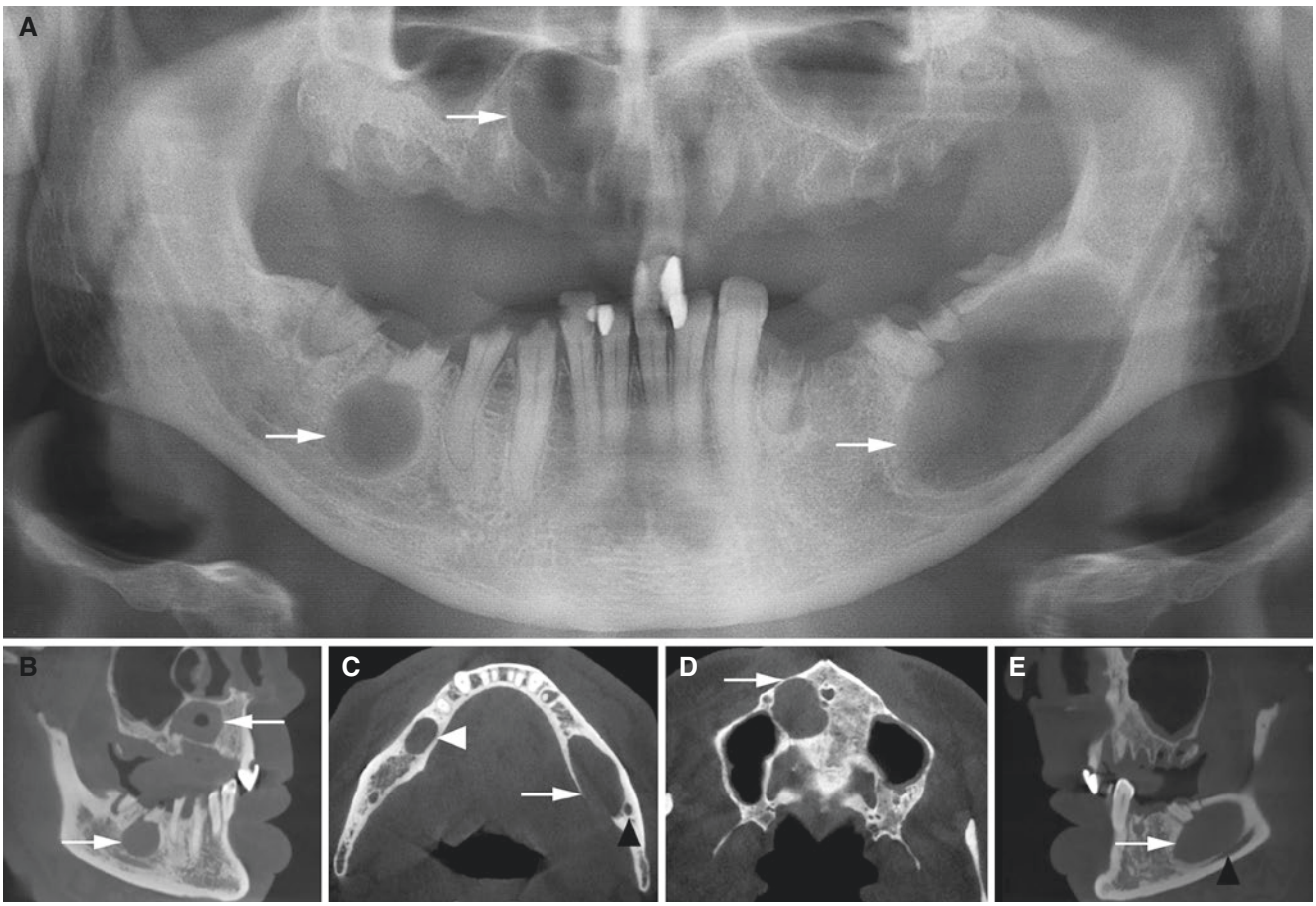

Fig. 15.1 Radicular (residual) cysts, mandible, maxilla; 45-year-old male with variable pain from the upper and lower jaw. (**A**) Panoramic view shows well-defined round or oval corticated radiolucencies: one residual cyst in the maxilla and two periapical cysts in the mandible (*arrows*). Several roots are remaining in the mandible, and many have recently been extracted in the maxilla. (**B**) Oblique sagittal view shows cysts in the right mandible and right maxilla (*arrows*) and in the mandible with direct contact with root apex. (**C**) Axial CBCT image shows minimal expansion of cortical outline of cyst in the left mandible (*arrow*) and no expansion of cortical outline of cyst in the right mandible (*white arrowhead*). Note the mandibular canal in the periphery of cyst (*black arrowhead*). (**D**) Axial CBCT image shows minimal, if any, expansion of cortical outline of cyst in the maxilla (*arrow*). (**E**) Oblique sagittal view shows cyst in the left mandible (*arrow*) with direct contact with root apex. Note the mandibular canal in periphery, close to cyst (*black arrowhead*)

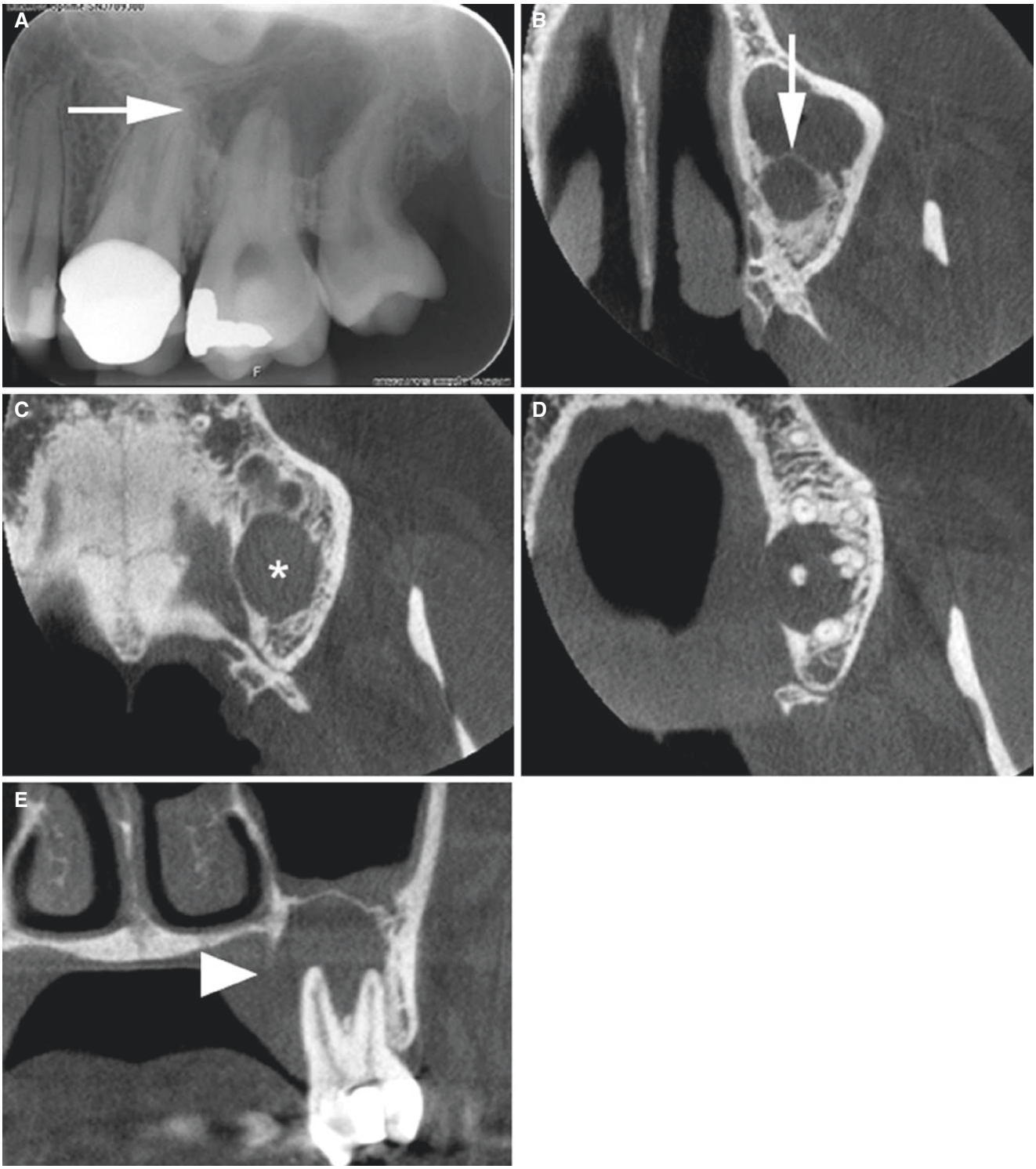

Fig. 15.2 Radicular/periapical cyst, maxilla; 32-year-old female with some discomfort and swelling with fistula in the left maxilla. (**A**) Intraoral view shows periapical radiolucency at the second molar (*arrow*). (**B**, **C**, **D**) Axial and (**E**) coronal CBCT images show expanding process in the left maxilla (*asterisk*) with corticated outline (*arrow*) except palatally (*arrowhead*). Same patient as in Fig. 2.3

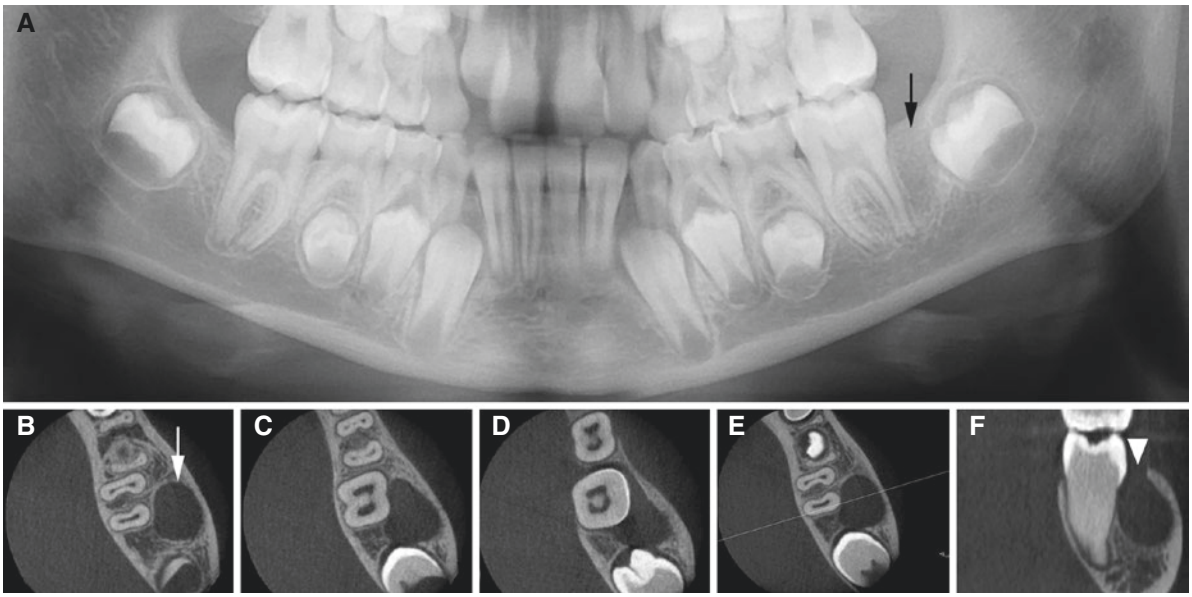

Fig. 15.3 Paradental cyst, mandible; 8-year-old female with left mandibular pain and inflamed periodontal pocket buccal to the first molar. (**A**) Panoramic view shows slight radiolucency between the first molar and second molar tooth germ (*arrow*). (**B**, **C**, **D**) Axial, (**E**) axial (with cursor line), and (**F**) oblique coronal CBCT images show buccal radiolucency (*arrow*) with intact, partially corticated outline and marginal communication (*arrowhead*)

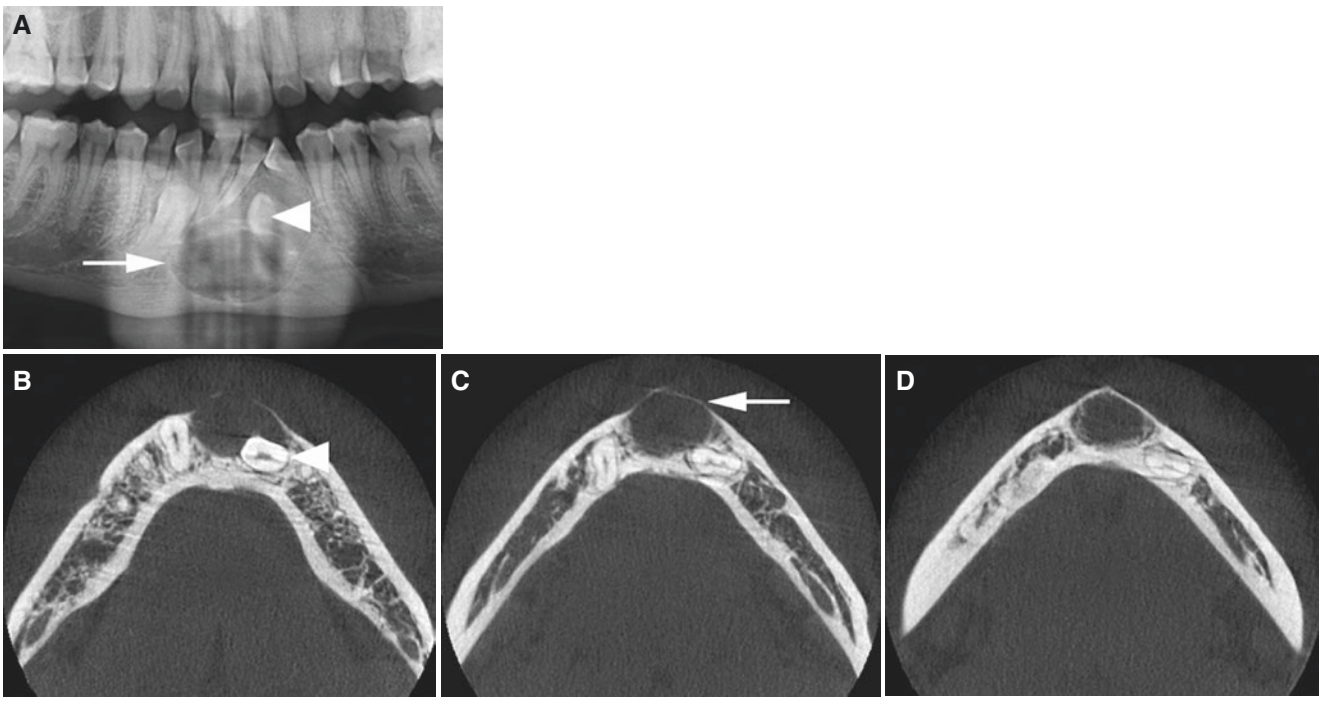

Fig. 15.4 Follicular cyst, mandible; 27-year-old female with swelling in the anterior mandible. (**A**) Panoramic view shows almost round corticated well-defined radiolucency (*arrow*) surrounding the crown of the impacted tooth (*arrowhead*). (**B**, **C**, **D**) Axial CBCT images show radiolucency with expansion of thinned cortical plate (*arrow*) and impacted tooth (*arrowhead*). Note streaking and tendency to double contouring due to patient movement during scanning

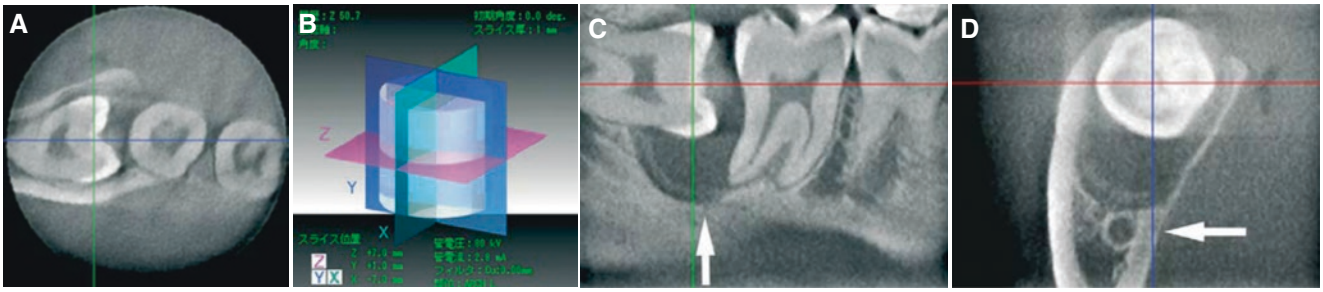

Fig. 15.5 Follicular cyst, mandible; 38-year-old patient with incidental finding. (**A**) Axial image shows radiolucency around crown of horizontally impacted wisdom tooth with thinning of the lingual cortical plate but no bony expansion. (**B**) Three image planes indicated by different colors. (**C**) Sagittal CBCT image shows pericoronal radiolucency (*arrow*), from cementoenamel junction to cementoenamel junction, typical feature of follicular cyst. (**D**) Coronal CBCT image shows follicular cyst close to the mandibular canal (*arrow*) and thinning of the entire lingual cortical plate but no or minimal expansion (courtesy of Dr. K. Honda, Nihon University School of Dentistry, Tokyo, Japan)

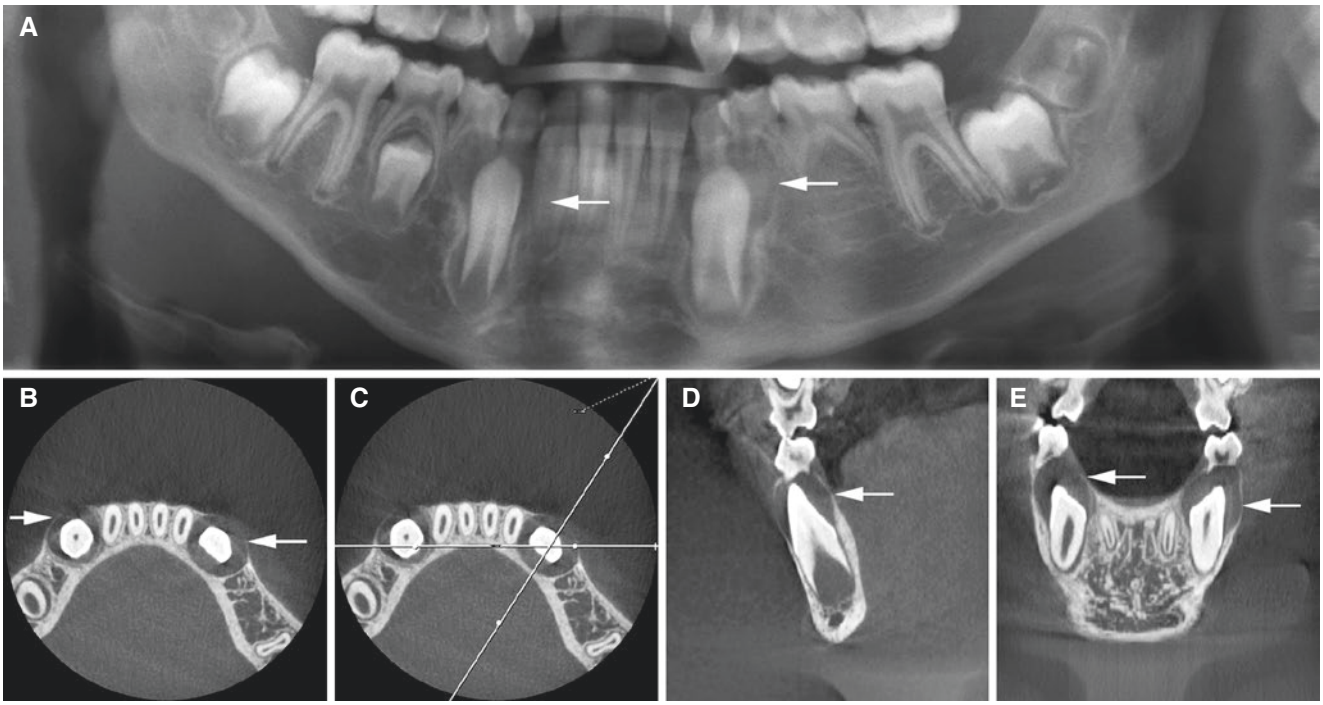

Fig. 15.6 Possible follicular cysts, mandible; 8-year-old male with incidental findings at orthodontic consultation. (**A**) Panoramic view shows erupting canine in the mandible with widened pericoronal space, suggesting possible follicular cyst, bilaterally (*arrows*). (**B**) Axial, (**C**) axial (with cursor lines), (**D**) oblique sagittal, and (**E**) coronal CBCT images also show widened pericoronal spaces, which may or may not be interpreted as follicular cysts (*arrows*)

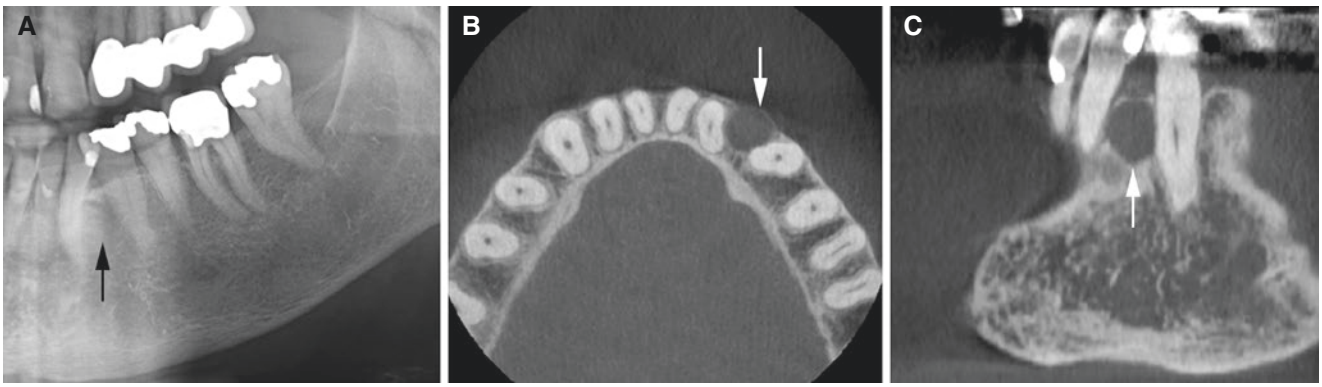

Fig. 15.7 Lateral periodontal cyst, mandible; 70-year-old female with small painless swelling in the anterior part of the left mandible. Vital teeth. (**A**) Panoramic view shows no evident pathology in area (*arrow*). (**B**) Axial and (**C**) Oblique coronal CBCT images show small round lesion (*arrow*) with some buccal expansion (**B**), apparently with normal periodontal ligament of displaced neighboring teeth and without root resorption

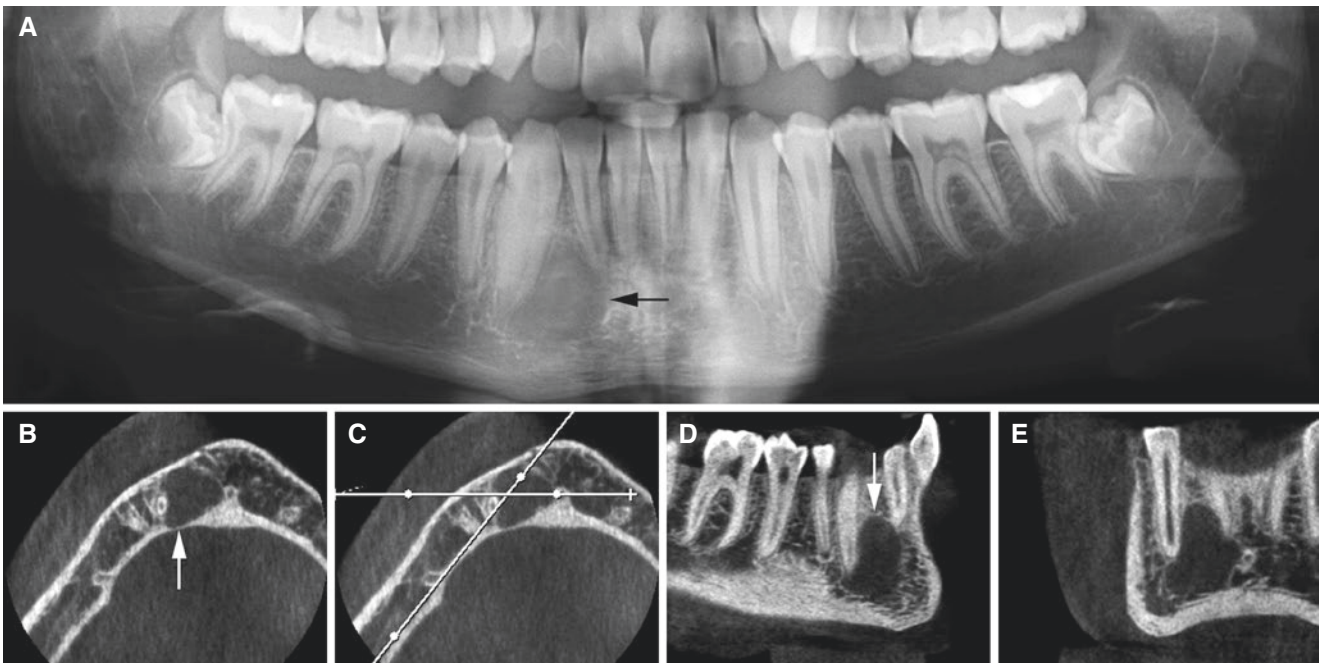

Fig. 15.8 Simple bone cyst, mandible; 15-year-old male with incidental finding. (**A**) Panoramic view shows radiolucency in the anterior part of the right mandible (*arrow*). (**B**) Axial, (**C**) axial (with cursor lines), (**D**) oblique sagittal, and (**E**) coronal CBCT images show radiolucent lesion (*arrow*) with thin, partially corticated outline, without buccal or lingual expansion, and without root resorption

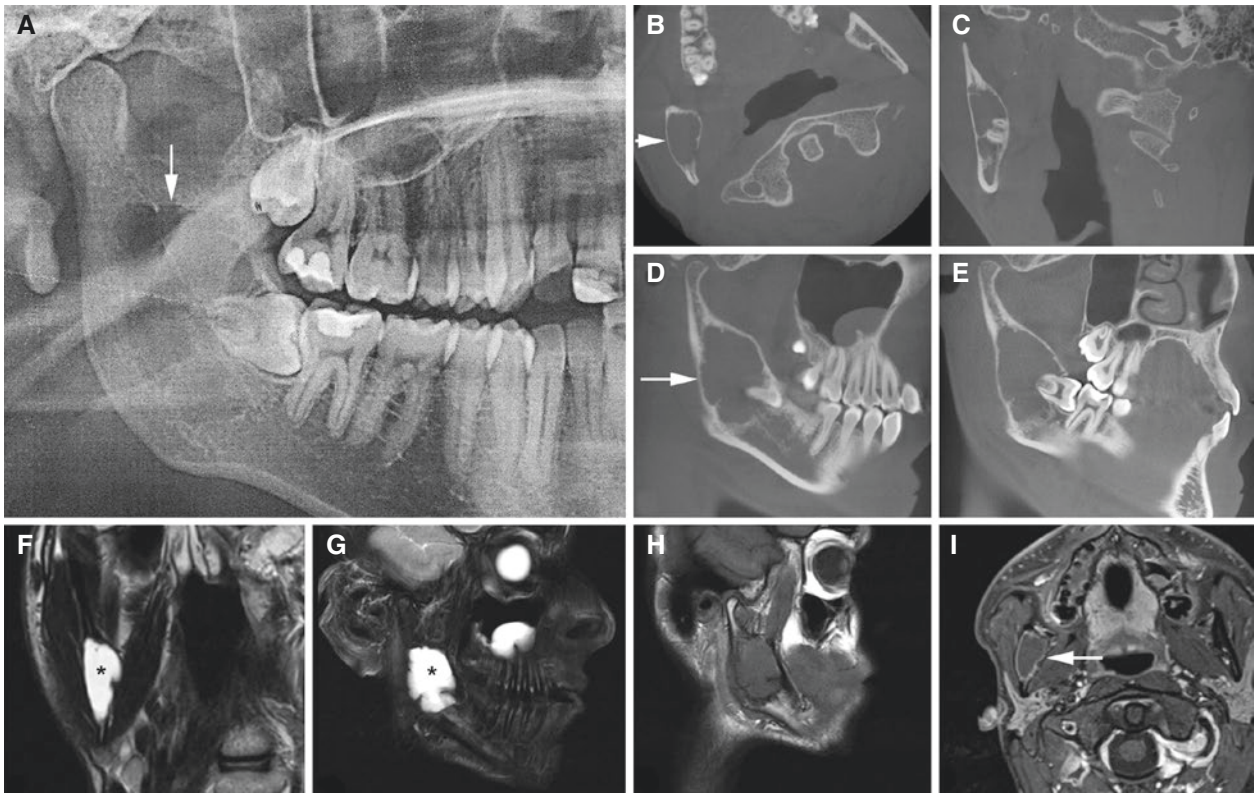

Fig. 15.9 Simple bone cyst, mandible; 18-year-old male with incidental finding. (**A**) Panoramic view shows rather well-defined and slightly scalloped radiolucency in the right mandibular ramus (*arrow*) and impacted wisdom tooth. (**B**) Axial, (**C**) coronal, and (**D**, **E**) oblique sagittal CBCT images show lesion (*arrow*) with thinned, intact corticated outline, with some buccolingual expansion, and without root resorption. (**F**) Coronal and (**G**) sagittal T2-weighted fat-sat MRI show well-defined lesion with homogeneous high signal (*asterisk*). (**H**) Sagittal T1-weighted pre-Gd and (**I**) Axial T1-weighted fat-sat post-Gd MRI show no contrast enhancement except in thin peripheral rim (*arrow*) (courtesy of Competence Centre of the Dental Health Service, Region South, Arendal, Norway and Hospital of Southern Norway SSHF, Kristiansand, Norway)

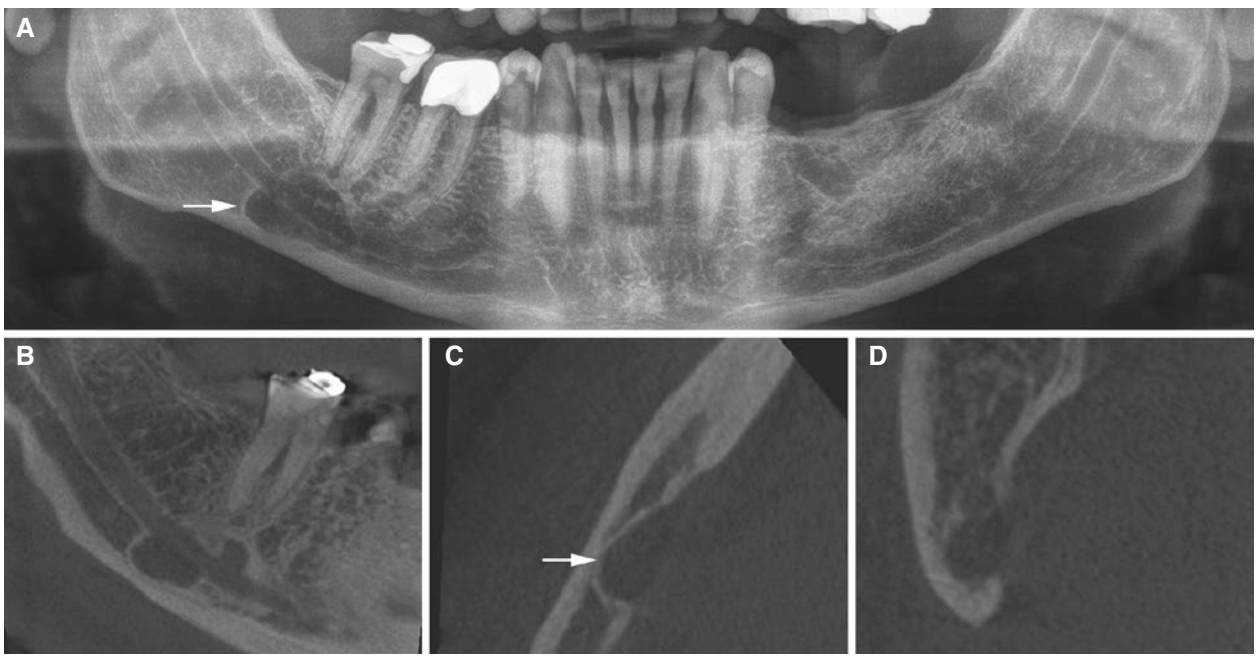

Fig. 15.10 Stafne bone cyst, mandible; 65-year-old male with incidental finding. (**A**) Panoramic view shows well-defined radiolucency (*arrow*) caudal to second molar, reaching the inferior mandibular border. Radiolucency is located both caudally and cranially to mandibular canal, which is an uncommon feature. (**B**) Oblique sagittal, (**C**) axial, and (**D**) coronal CBCT images show defect (*arrow*) on the lingual side of the mandible (courtesy of Dr. K. Å. Årseth, Melhus, Norway)

15.4 Benign Jaw Tumors and Tumorlike Conditions

See Chap. 3

Figs. 15.11, 15.12, 15.13, 15.14, 15.15, 15.16, 15.17, 15.18, 15.19, 15.20, 15.21, and 15.22

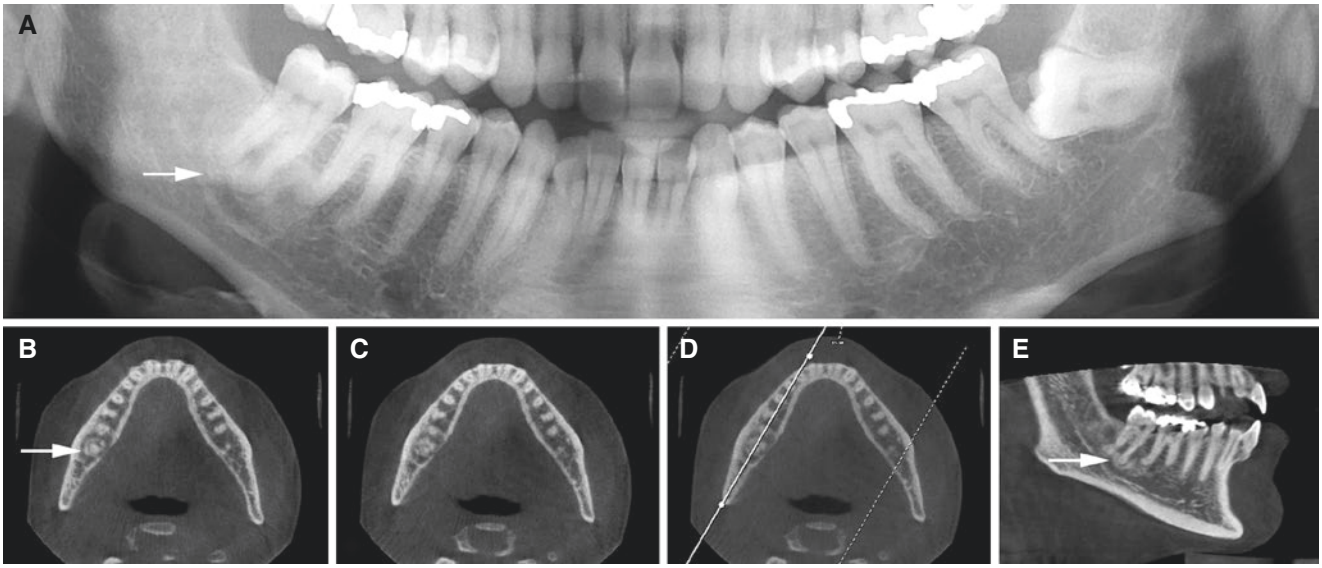

Fig. 15.11 Focal osseous dysplasia, mandible; 35-year-old female with incidental finding. Vital teeth. (**A**) Panoramic view shows irregular radiolucent and radiopaque periapical bone structure (*arrow*). (**B**) Axial, (**C**) Axial (more caudal section), (**D**) Axial (with cursor line), and (**E**) Oblique sagittal CBCT images show irregular radiolucent and radiopaque bone in periapical area of second molar (*arrow*)

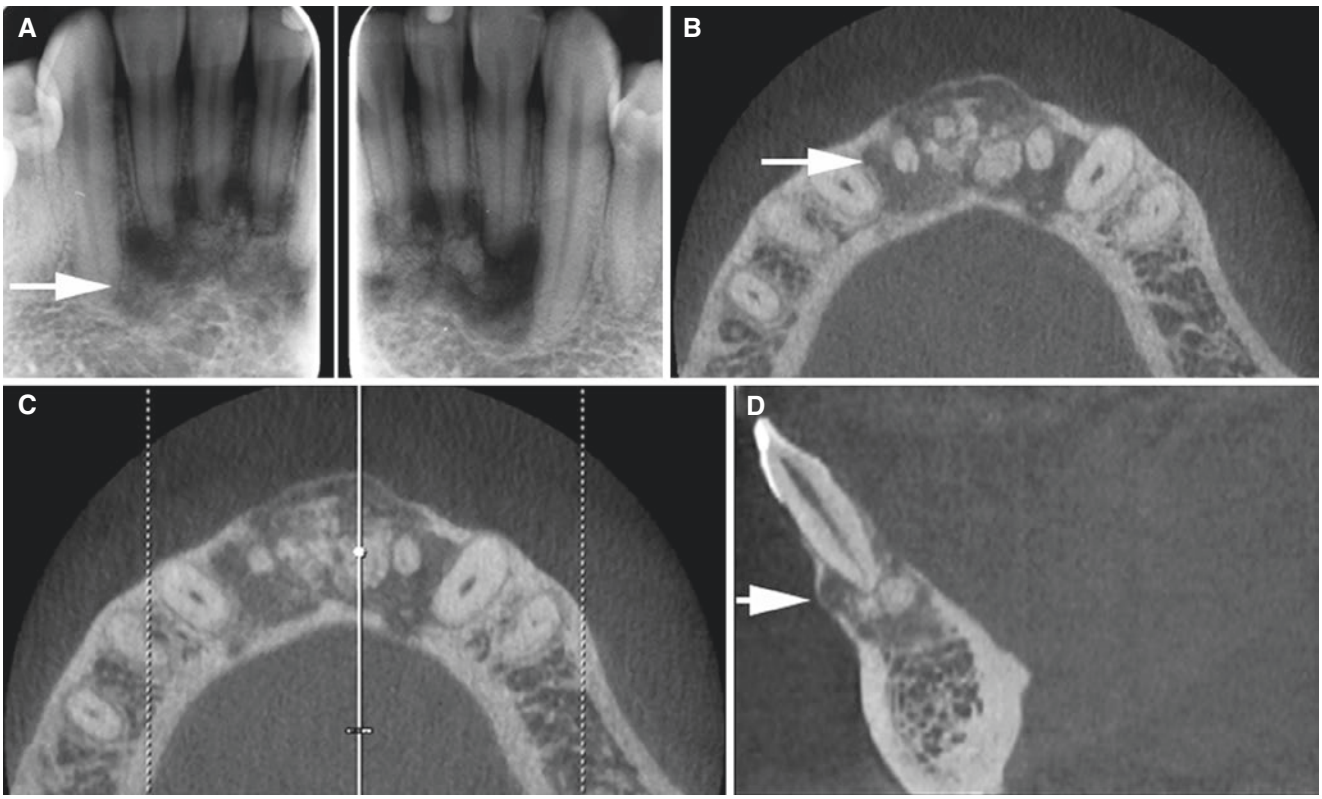

Fig. 15.12 Fibro-osseous lesion (periapical osseous dysplasia or ossifying fibroma), mandible; 36-year-old female with painless swelling in the anterior mandible. Vital teeth. (**A**) Intraoral views show bone structure with mixture of radiolucencies and radiopacities (*arrow*). (**B**) Axial, (**C**) axial (with cursor line), and (**D**) sagittal CBCT images show a mixture of radiolucencies and radiopacities in periapical area (*arrow*) and some buccal expansion

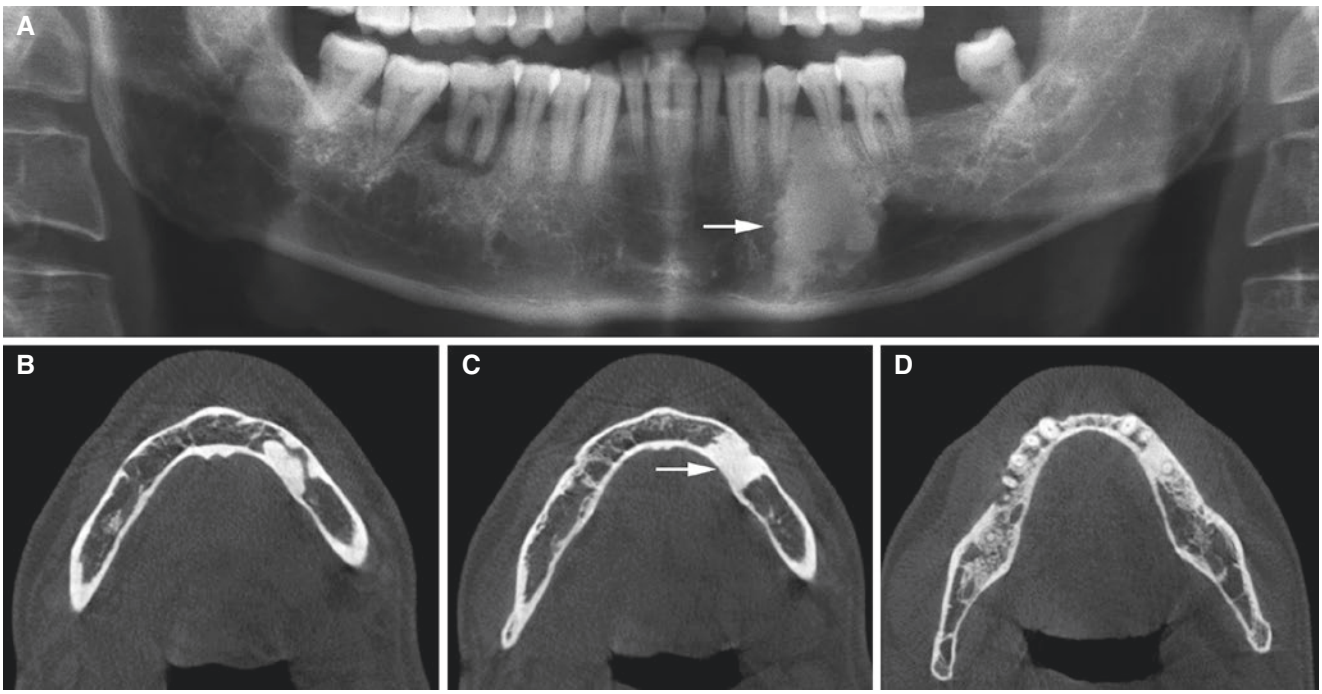

Fig. 15.13 Idiopathic osteosclerosis, mandible; 45-year-old male with incidental finding. (**A**) Panoramic view shows well-defined radiopacity (*arrow*). Note periodontal bone loss in the entire lower dentition and periradicular bone loss (with reactive sclerosis); perio–endo lesion, at first molar in the right mandible. (**B**, **C**, **D**) Axial CBCT images show homogeneous well-defined radiopacity without peripheral radiolucent zone and without expanding cortical bone (*arrow*)

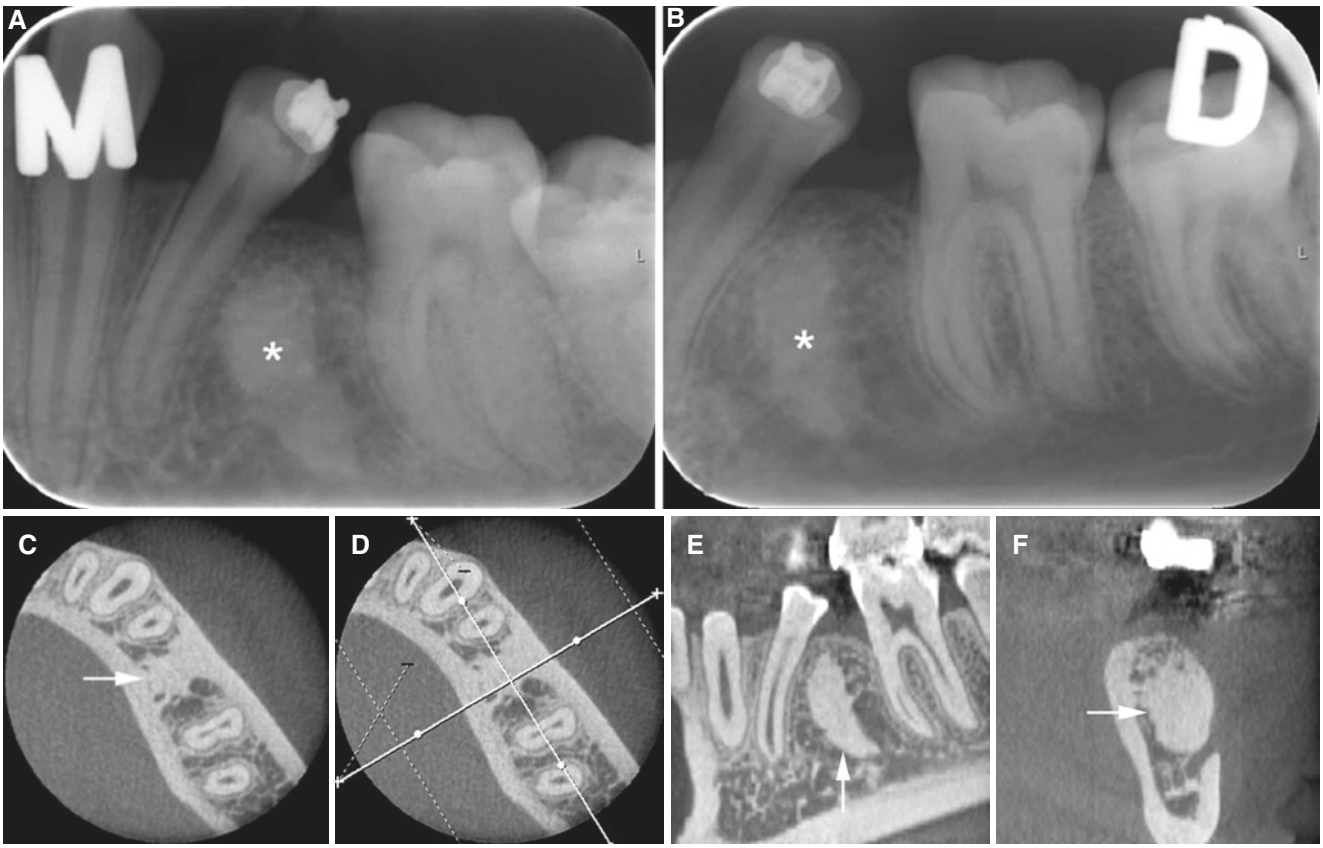

Fig. 15.14 Idiopathic osteosclerosis, mandible; 15-year-old female with incidental finding believed to be a remaining root. (**A**, **B**) Intraoral views with mesioexentric (*M*) and distoexentric (**D**) projections show well-defined radiopacity simulating a root (*asterisk*). (**C**) Axial, (**D**) axial (with cursor lines), (**E**) oblique sagittal, and (**F**) oblique coronal CBCT images show homogeneous well-defined radiopacity (*arrow*), without peripheral radiolucent zone and without bone expansion

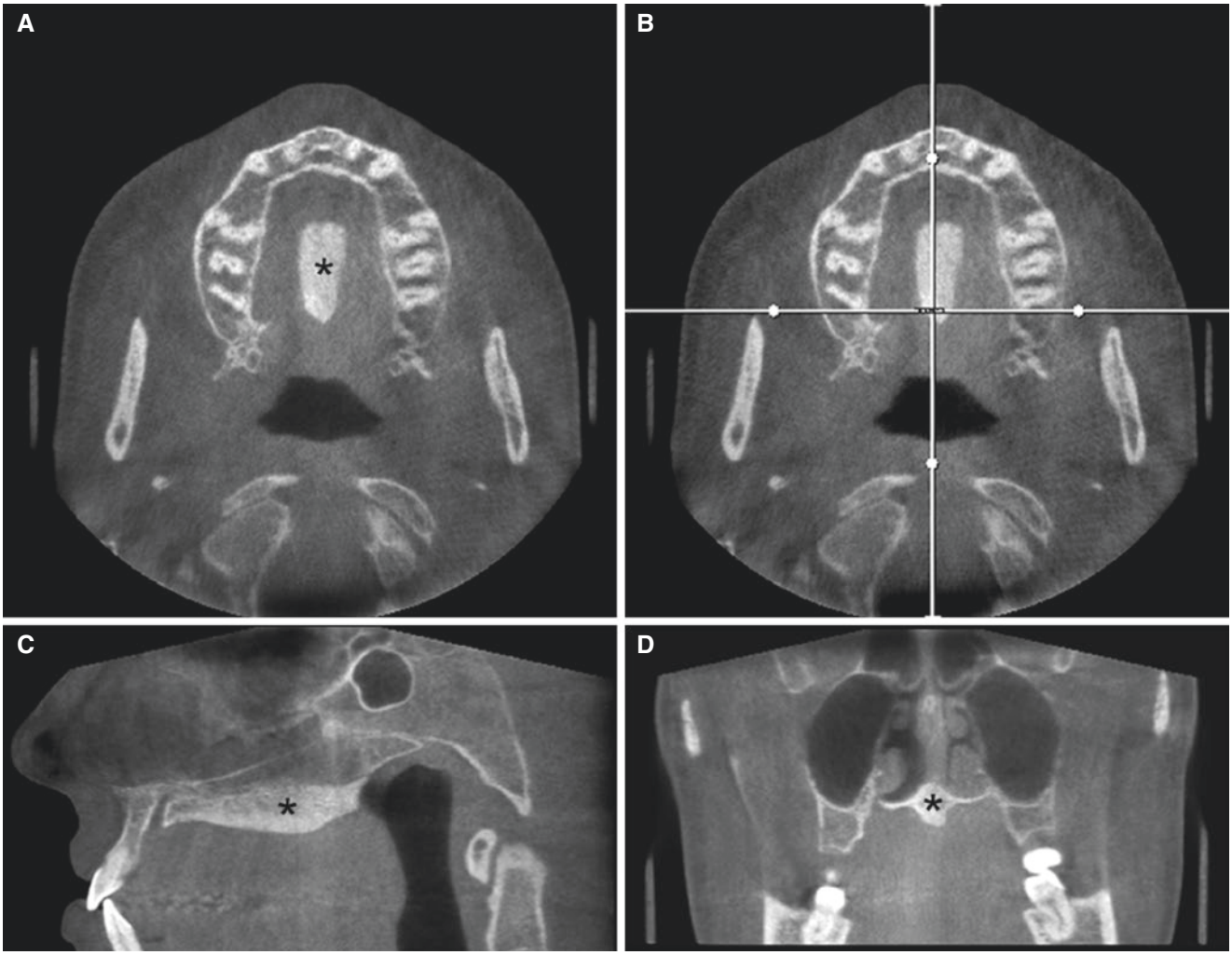

Fig. 15.15 Torus palatinus; 37-year-old female with incidental finding. (**A**) Axial, (**B**) axial (with cursor lines), (**C**) sagittal, and (**D**) coronal CBCT images show bony outgrowth in the midline of the hard palate (*asterisk*)

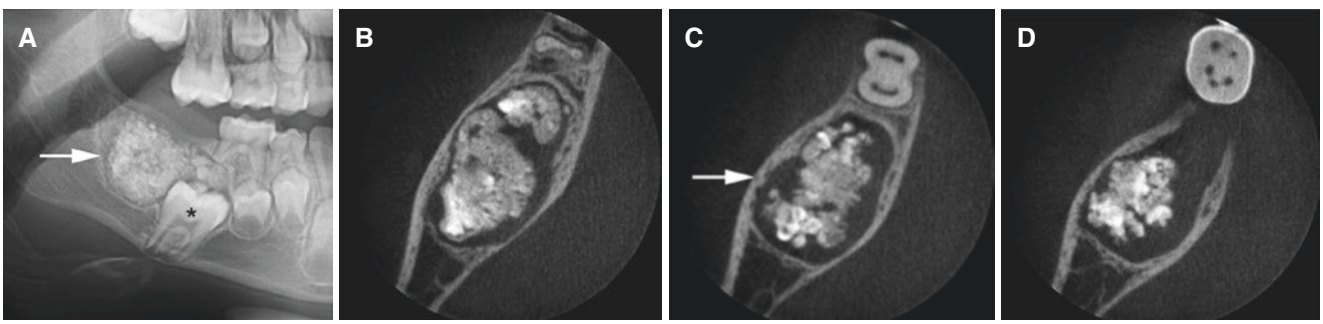

Fig. 15.16 Odontoma (complex), mandible; 8-year-old male with unerupted first molar. (**A**) Panoramic view shows mass of multiple mineralized elements surrounded by radiolucent zone (*arrow*) and impacted first molar (*asterisk*). (**B**, **C**, **D**) Axial CBCT images confirm multiple small radiopaque structures with bone and enamel density, and with peripheral radiolucent zone, expanding (intact) bone buccally and lingually (*arrow*)

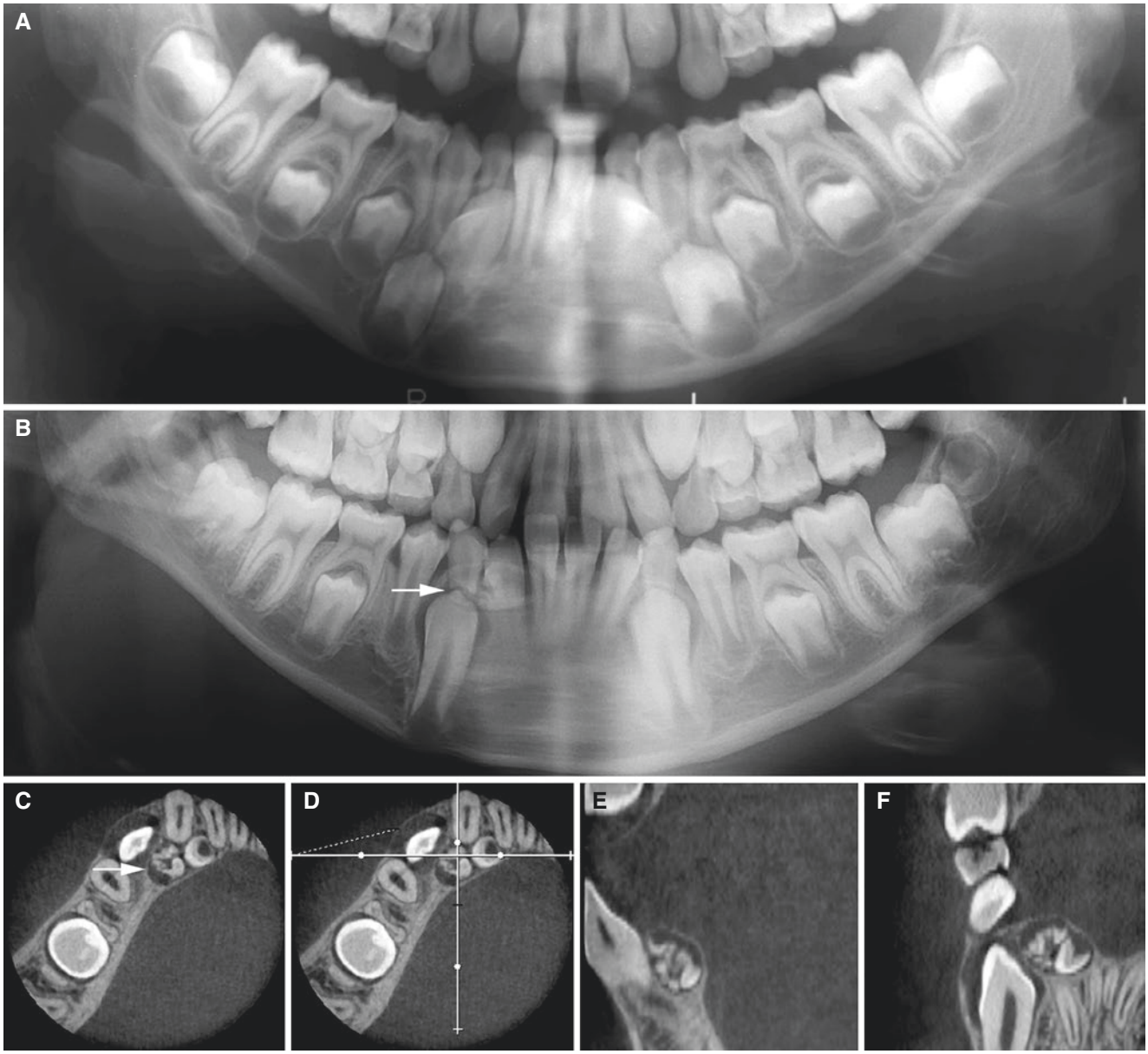

Fig. 15.17 Odontoma (complex/compound), mandible; 11-year-old male with incidental finding. (**A**) Panoramic view at 8 years of age shows no odontoma. (**B**) Panoramic view 3 years later shows radiopaque elements (partially toothlike) surrounded by a thin peripheral zone, consistent with odontoma (*arrow*). (**C**) Axial, (**D**) axial (with cursor lines), (**E**) sagittal, and (**F**) coronal CBCT images show odontoma (*arrow*) located lingually to the canine and incisor

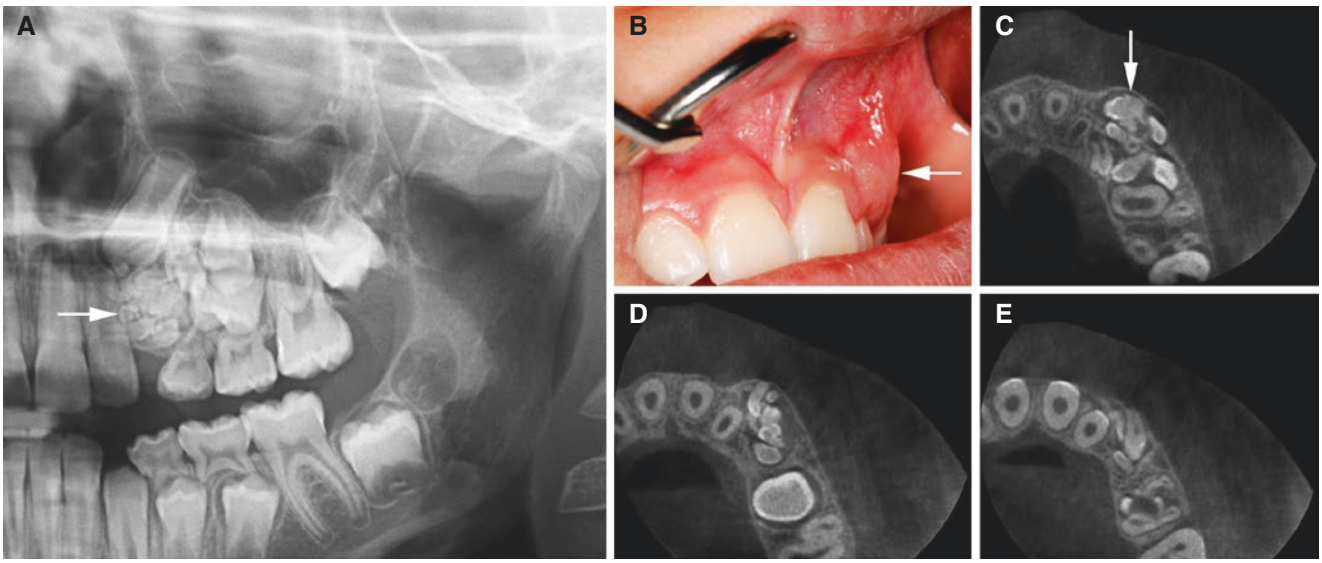

Fig. 15.18 Odontoma (compound), maxilla; 8-year-old female with some swelling in the left maxilla. (**A**) Panoramic view shows a collection of toothlike structures (*arrow*). (**B**) Clinical photograph shows some swelling of the alveolar process (*arrow*). (**C**, **D**, **E**) Axial CBCT images show multiple toothlike structures in the mandible with enamel, dentin, and pulp densities surrounded by a thin radiolucent zone (*arrow*)

Fig. 15.19 Osteoma, frontal sinus; 9-year-old male with incidental finding. Lateral cephalogram shows well-defined, homogeneous bone structure with cortical density (*arrow*)

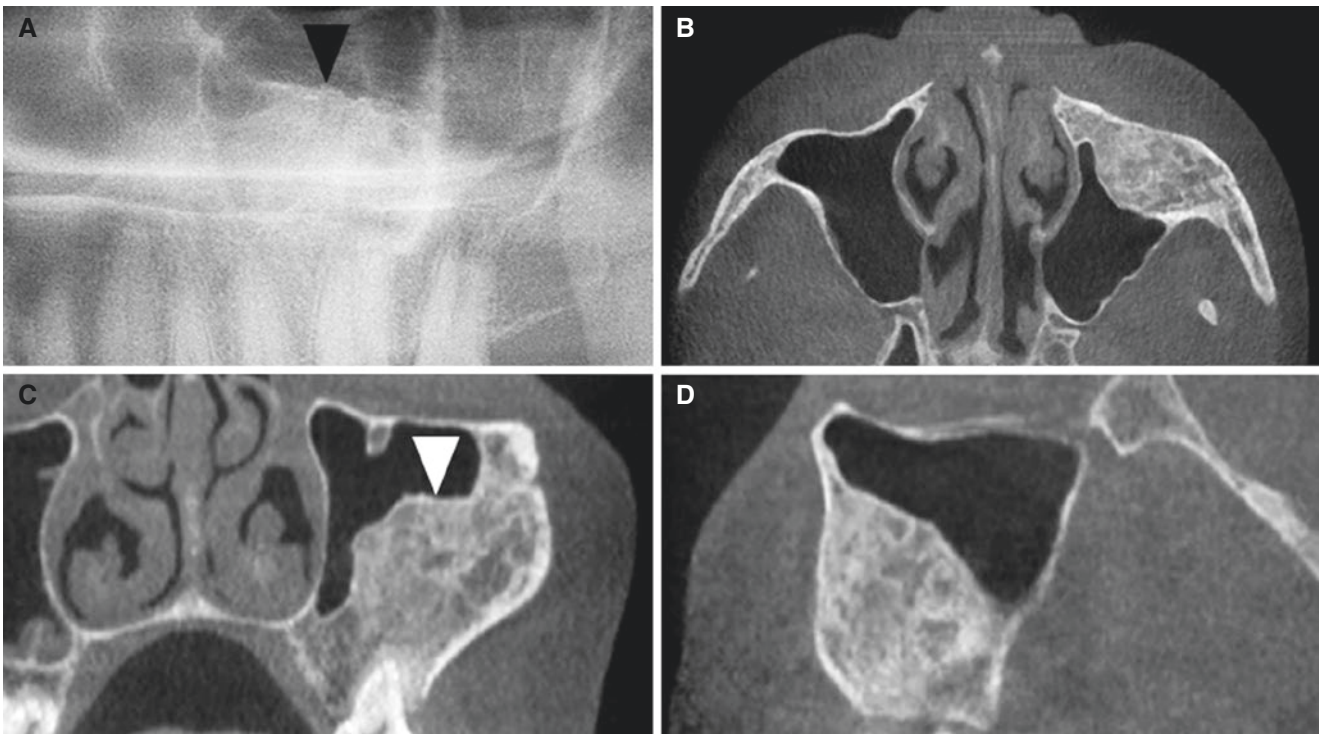

Fig. 15.20 Fibrous dysplasia, maxilla; 51-year-old female with incidental finding. (**A**) Panoramic view shows radiopacity in the left maxillary sinus (*arrowhead*). (**B**) Axial, (**C**) coronal, and (**D**) sagittal CBCT images show well-defined, heterogeneous radiopacity expanding the maxillary bone into the sinus (*arrowhead*)

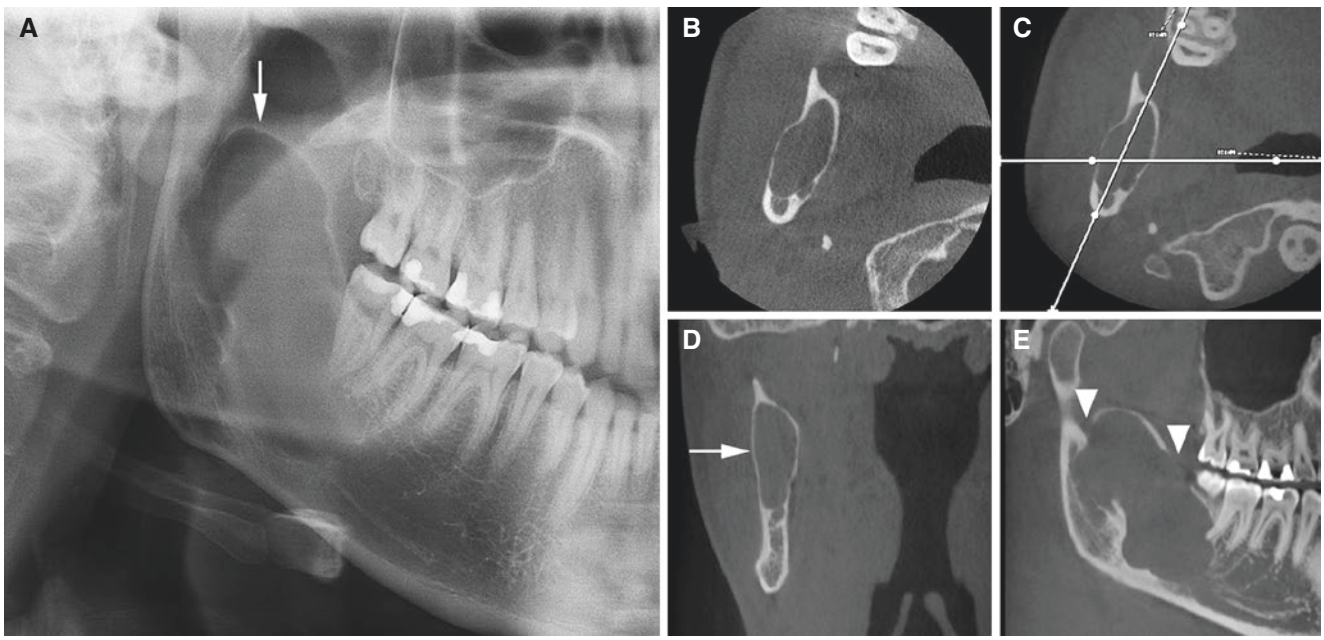

Fig. 15.21 Keratocystic odontogenic tumor (odontogenic keratocyst), mandible; 28-year-old male with some swelling in the right posterior mandible. (**A**) Panoramic view shows well-defined radiolucency, partially corticated, in the right mandibular ramus (*arrow*) with the mandibular canal displaced to periphery of process. (**B**) Axial, (**C**) axial (with cursor lines), (**D**) coronal, and (**E**) oblique sagittal CBCT images show well-defined process with limited buccolingual expansion of the mandible (*arrow*), thinned corticated outline mostly intact but also with defects (*arrowheads*). No evident root resorption

Fig. 15.22 Idiopathic osteosclerosis and root resorption, mandible; 27-year-old female with pain from the first molar. (**A**) Axial (with cursor lines), (**B**) oblique sagittal, and (**C**) oblique coronal CBCT images show well-defined, homogeneous radiopacity (*asterisk*) without bone expansion but with extensive resorption of mesial root of the first molar (*arrow*) (courtesy of Dr. B. K. Brevik, Trondheim, Norway)

15.5 Malignant Tumors in Jaws

Figs. 15.23, 15.24, 15.25, 15.26, and 15.27

See Chap. 4

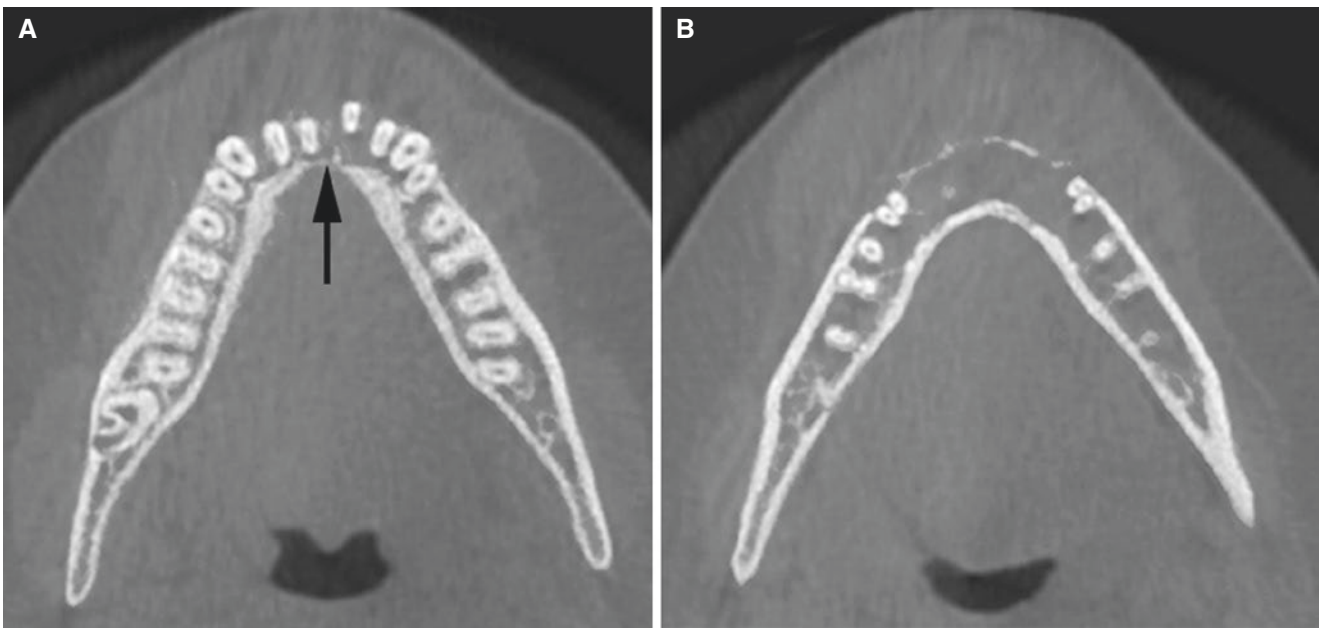

Fig. 15.23 Ewing sarcoma, mandible; 17-year-old female with mass in the anterior part of the mandible. Two axial CBCT images show severe bone destruction in the anterior mandible (*arrow*). For more examinations and diagnostic information of this patient, see Fig. 4.31

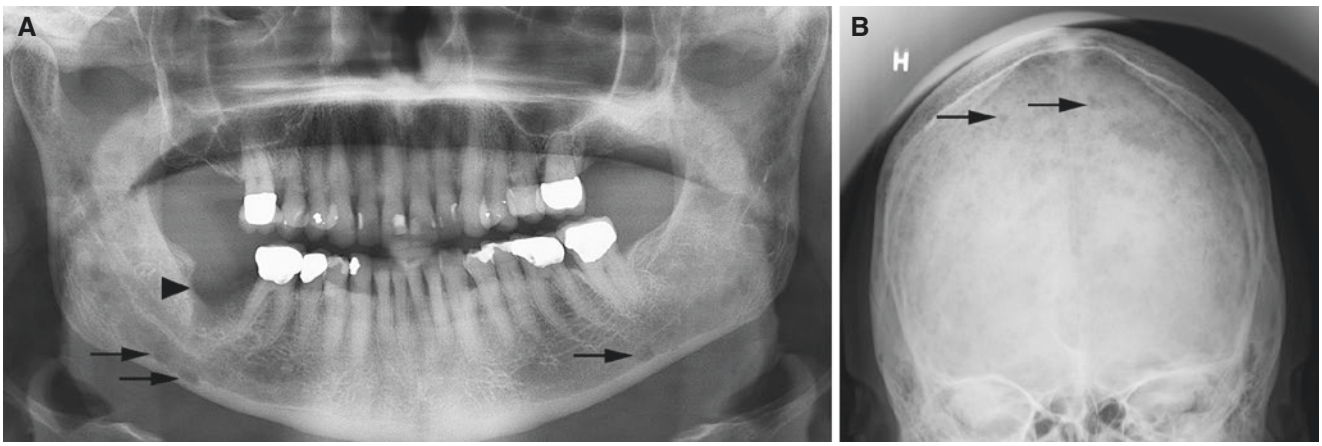

Fig. 15.24 Multiple myeloma and medication-related osteonecrosis, mandible; 72-year-old male (on antiresorptive therapy) with failing healing after tooth extraction in the right mandible. (**A**) Panoramic view shows non-healed tooth socket (*arrowhead*) and multiple small punched-out radiolucencies in the mandible (some indicated by *arrows*). (**B**) Frontal skull view shows multiple small punched-out radiolucencies in the skull (some indicated by *arrows*)

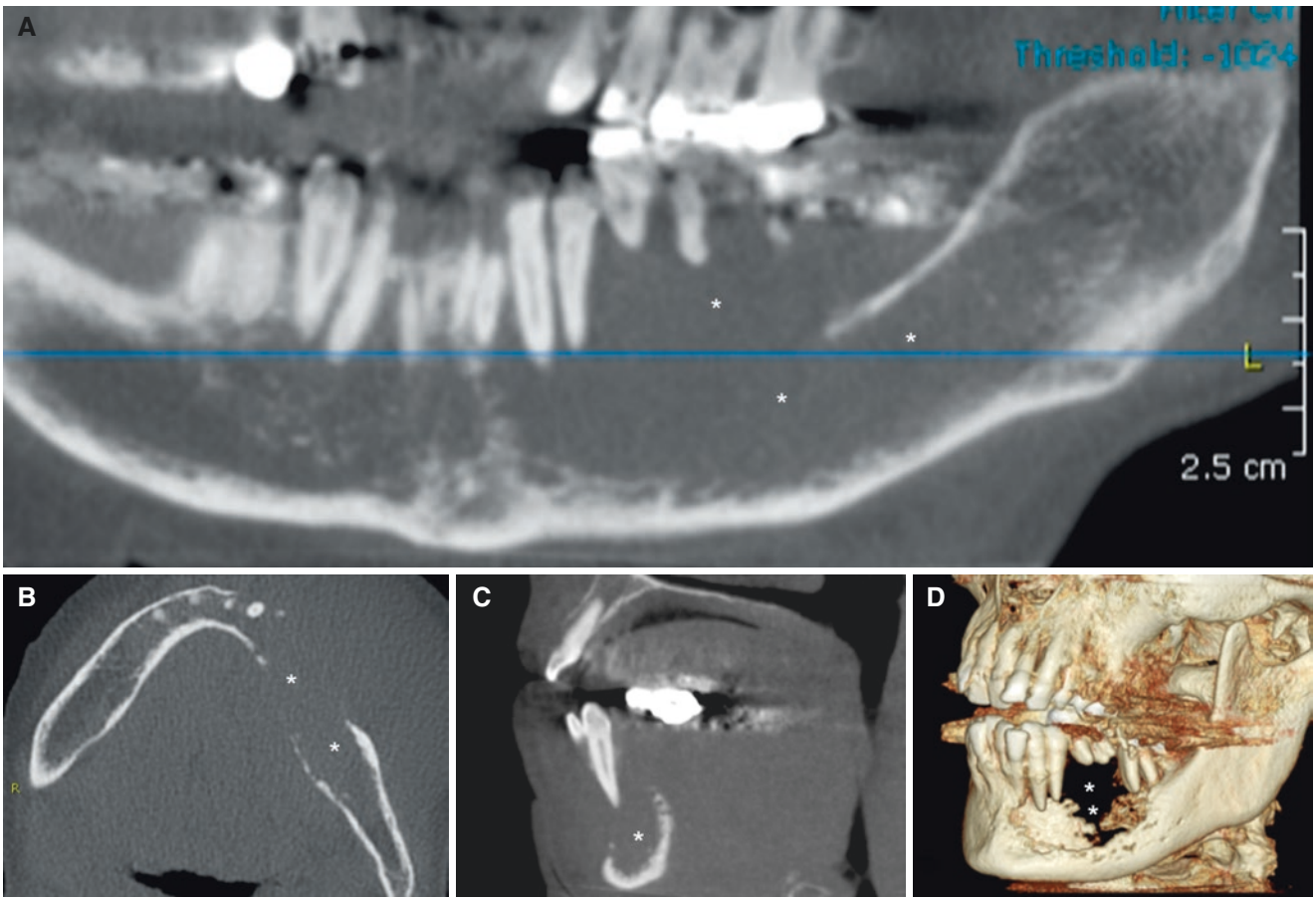

Fig. 15.25 Multiple myeloma, mandible; 62-year-old female, known widespread disease, now with discomfort with bite (dental occlusion) and facial asymmetry having developed during the last 3 months. (**A**) Panoramic, (**B**) axial, (**C**) sagittal, and (**D**) 3D CBCT images show extensive and ill-defined destruction (*asterisks*), displacement of teeth with "floating-teeth" appearance, and no evident root resorption (courtesy of Dr. S. Steinsvoll, Raufoss, Norway)

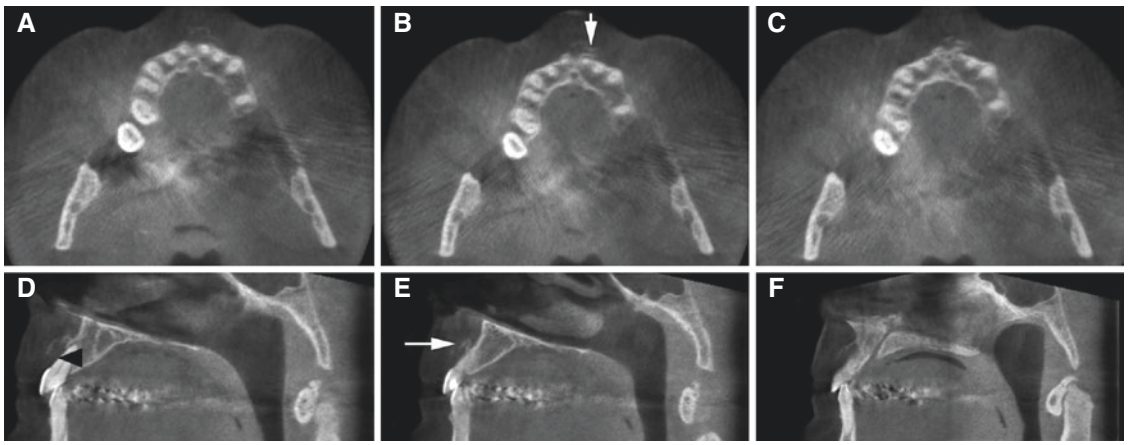

Fig. 15.26 Chondrosarcoma, maxilla; 53-year-old male with firm, painless swelling in the front region of the maxilla, normal mucosa, and vital incisors. No pathologic findings on intraoral and panoramic views. (**A**, **B**, **C**) Axial and (**D**, **E**, **F**) sagittal CBCT images show crescent-shaped bone apposition (*arrow*) and bone destruction (*arrowhead*) buccally to incisors (courtesy of Competence Centre of the Dental Health Service, Region North, Tromsø, Norway)

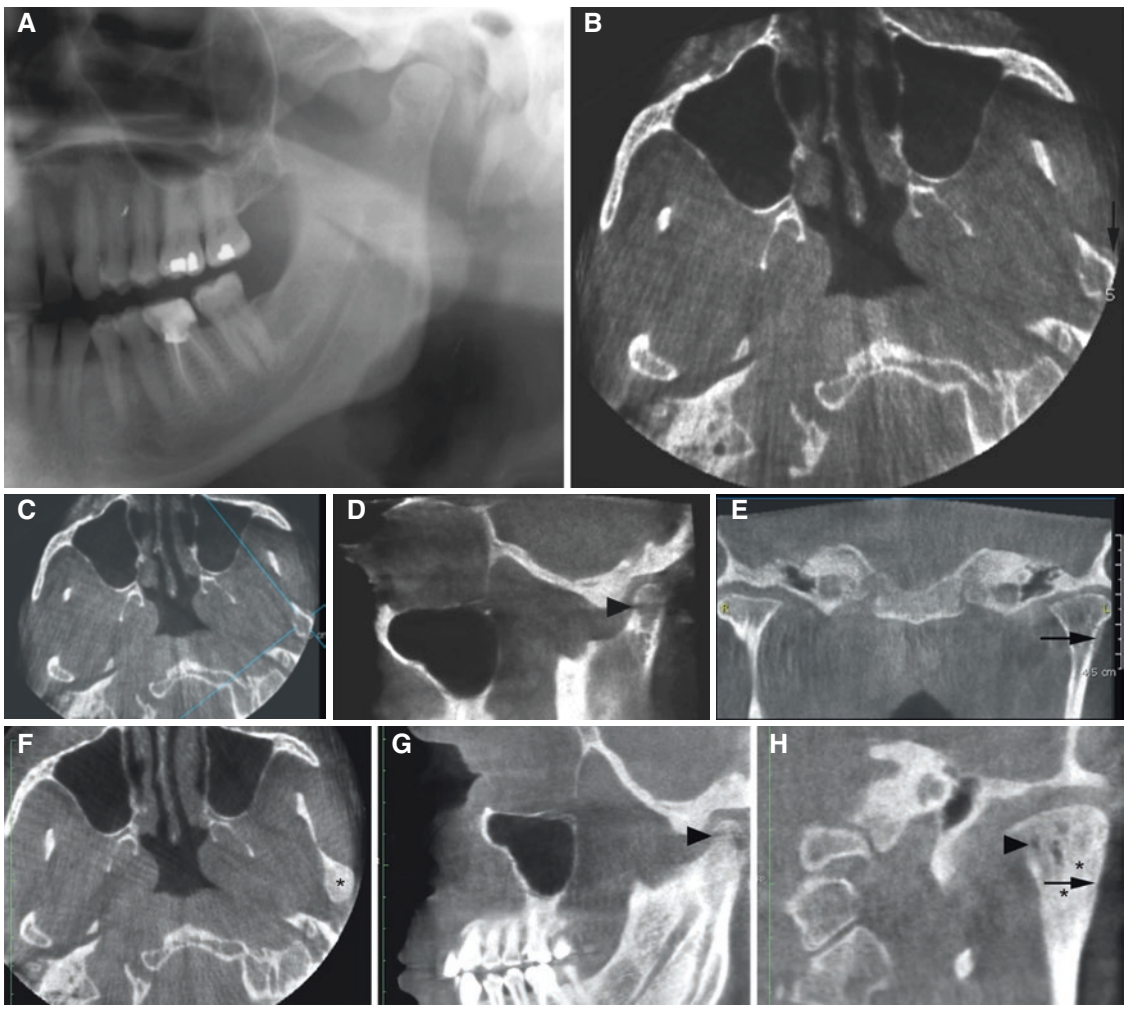

Fig. 15.27 Prostatic cancer metastasis, temporomandibular joint; 57-year-old male with known disease and skeletal metastases. At baseline (**A**) Panoramic view shows dentition and jaw bone without pathologic findings. (**B**) Axial, (**C**) axial (with cursor lines), (**D**) oblique sagittal, and (**E**) coronal CBCT images show periosteal bone apposition of the left mandibular condyle (*arrow*) and bone destruction (*arrowhead*). About 1 year and 6 months later, (**F**) axial, (**G**) oblique sagittal, and (**H**) oblique coronal CBCT images continue to show destructive changes (*arrowhead*), the condylar head and collum have become sclerotic (*asterisks*), and periosteal bone apposition has become more evident and solid (*arrow*)

15.6 Jaw Infections

Figs. 15.28, 15.29, 15.30, 15.31, 15.32, 15.33, and 15.34

See Chap. 5

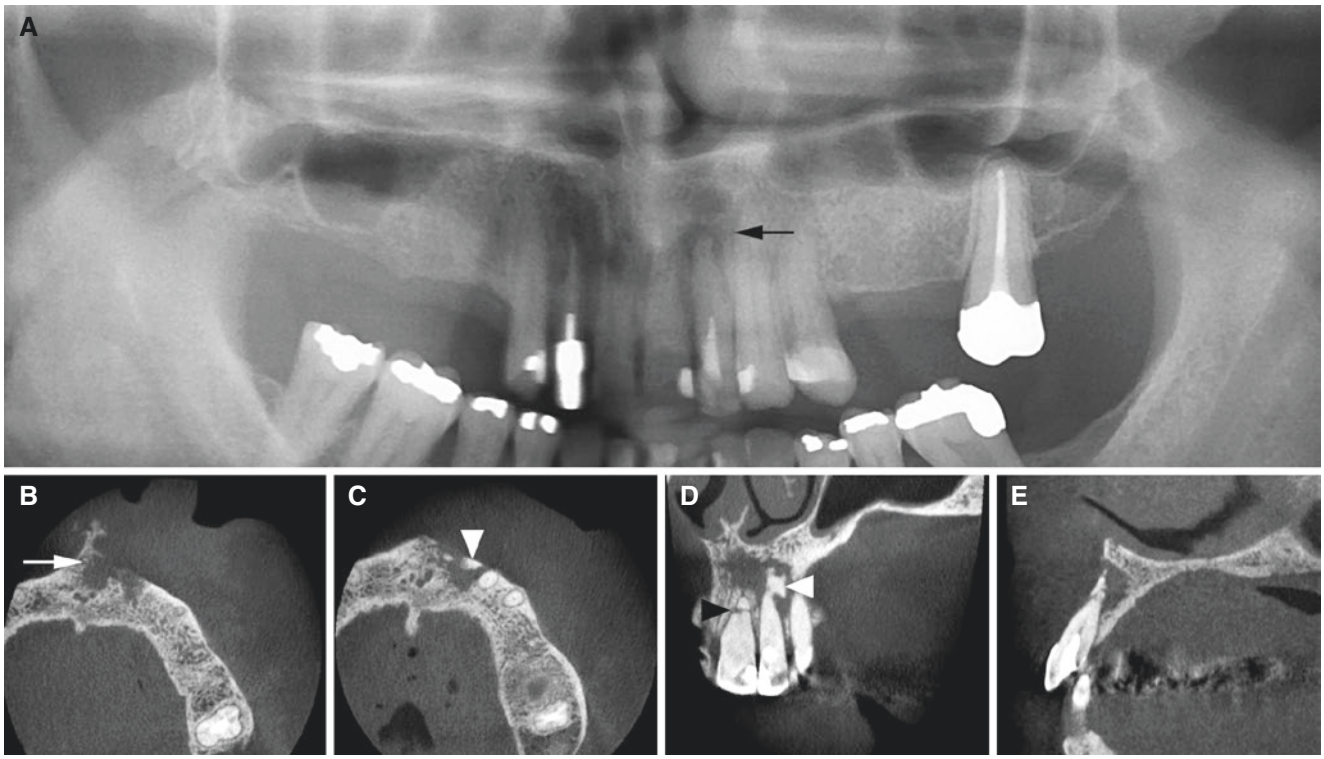

Fig. 15.28 Osteomyelitis with sequestration, maxilla; 54-year-old female with fistula and pus from the front region of the upper jaw (lateral incisor). (**A**) Panoramic view shows diffuse bone destruction (*arrow*). (**B**, **C**) Axial, (**D**) coronal, and (**E**) sagittal CBCT images show diffuse destruction in the anterior maxilla (*arrow*), separate bone fragment consistent with sequestrum (*white arrowhead*), and fractured root of central incisor (*black arrowhead*)

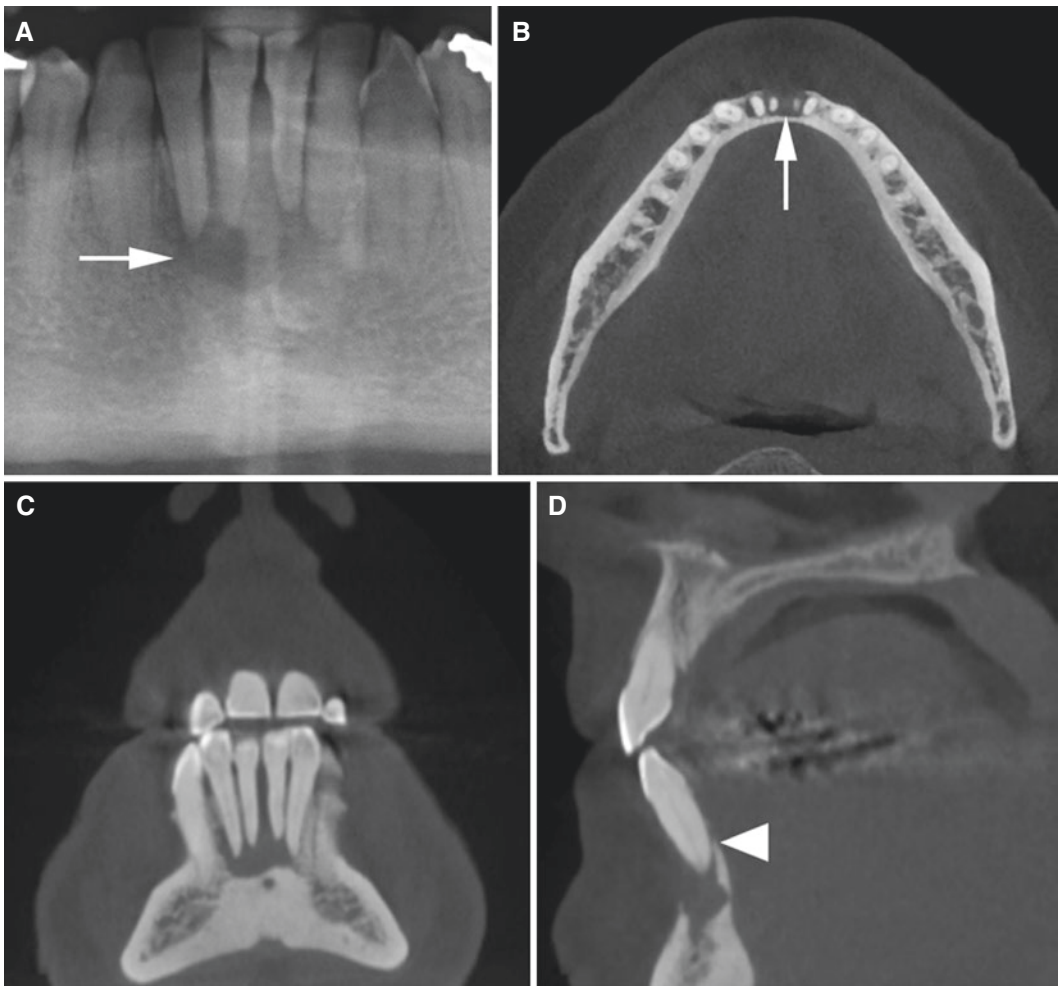

Fig. 15.29 Osteomyelitis/osteitis, mandible; 56-year-old female with loose front teeth in the lower jaw. (**A**) Panoramic view shows diffuse bone destruction (*arrow*). (**B**) Axial, (**C**) coronal, and (**D**) sagittal CBCT images show periapical bone destruction (*arrow*), no periodontal bone support buccally, and minimal periodontal bone support lingually (*arrowhead*)

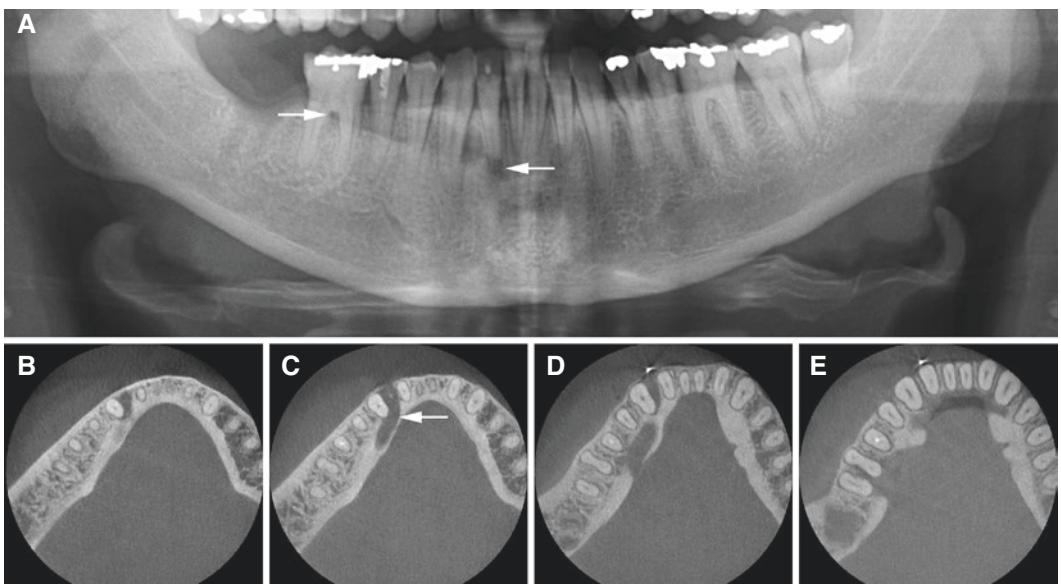

Fig. 15.30 Osteomyelitis/osteitis, mandible; 48-year-old female with fistula and pus from the right mandible. (**A**) Panoramic view shows bone destruction from the remaining molar to incisors (*arrows*). (**B**, **C**, **D**, **E**) Axial CBCT images show lingual bone destruction from the incisors to the remaining molar (*arrow*)

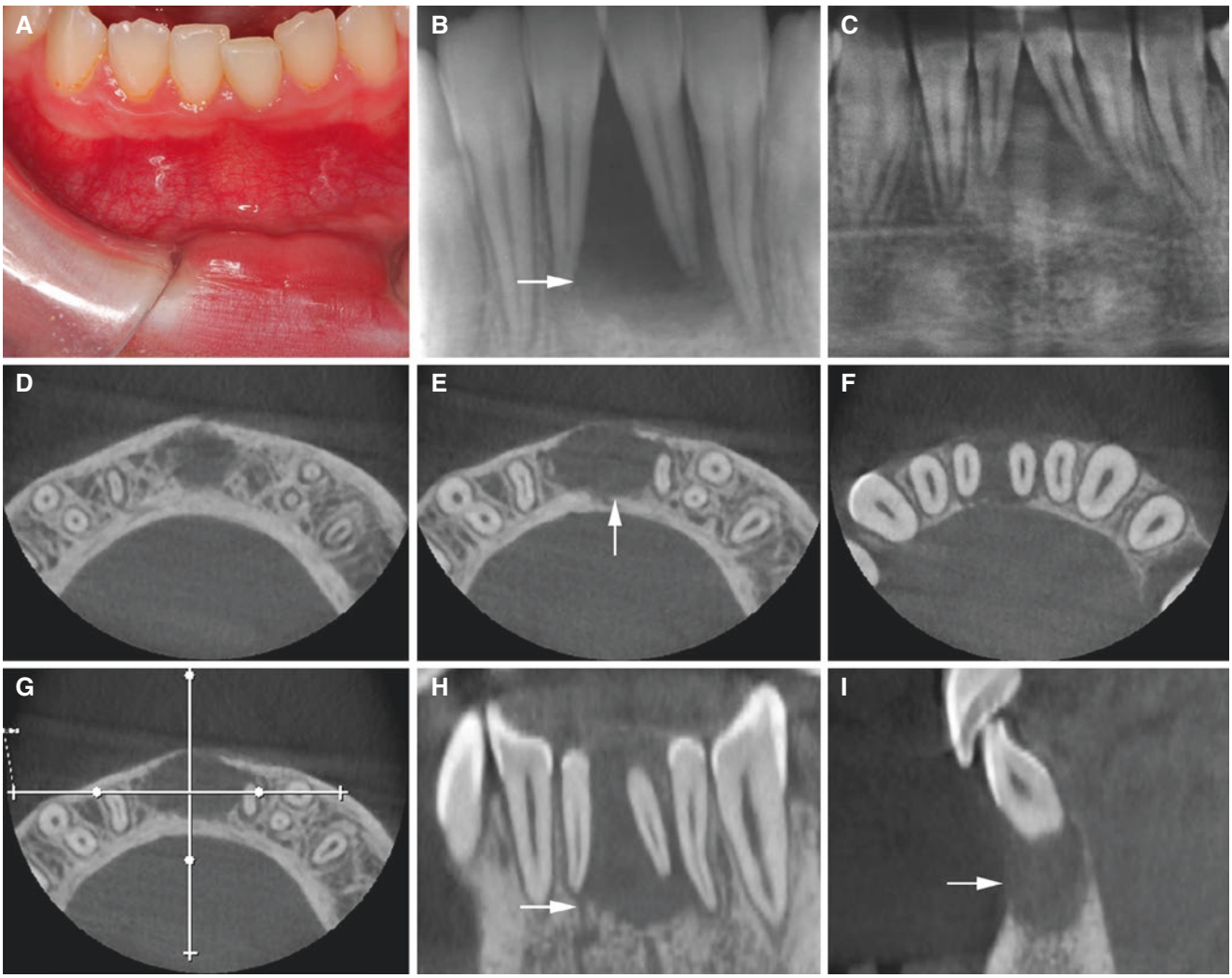

Fig. 15.31 Osteomyelitis/osteitis, mandible; 11-year-old female with loose, vital incisors and some discomfort in anterior mandible. Clinical suspicion of giant cell granuloma but histology shows infection. (**A**) Clinical photograph shows normal mucosa. (**B**) Intraoral and (**C**) panoramic views show bone destruction, diffusely outlined (*arrow*). Three incisors have severe loss of periodontal bone support, one in particular with floating-tooth appearance. The central incisors seem to be displaced. (**D**, **E**, **F**) Axial, (**G**) axial (with cursor lines), (**H**) coronal, and (**I**) sagittal CBCT images show ill-defined bone destruction in the anterior mandible (*arrow*), with minimal, if any, bone expansion

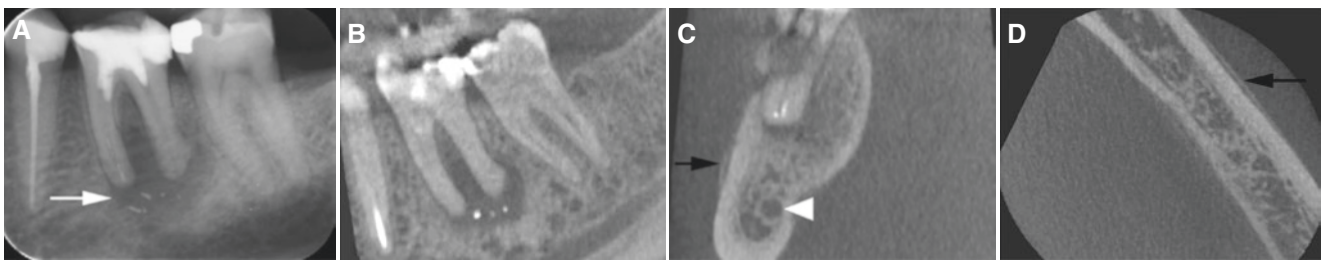

Fig. 15.32 Osteomyelitis with periosteal reaction, mandible; 40-year-old male with variable pain/swelling for about 1 month and pus evacuated from the first molar. (**A**) Intraoral view shows ill-defined periapical radiolucency (*arrow*) with endodontic material. (**B**) Oblique sagittal CBCT image confirms ill-defined bone destruction with endodontic material. (**C**) Oblique coronal and (**D**) axial CBCT images show periosteal apposition buccally (*black arrow*), almost at mandibular canal level (*arrowhead*), and bone destruction buccal to mesial root

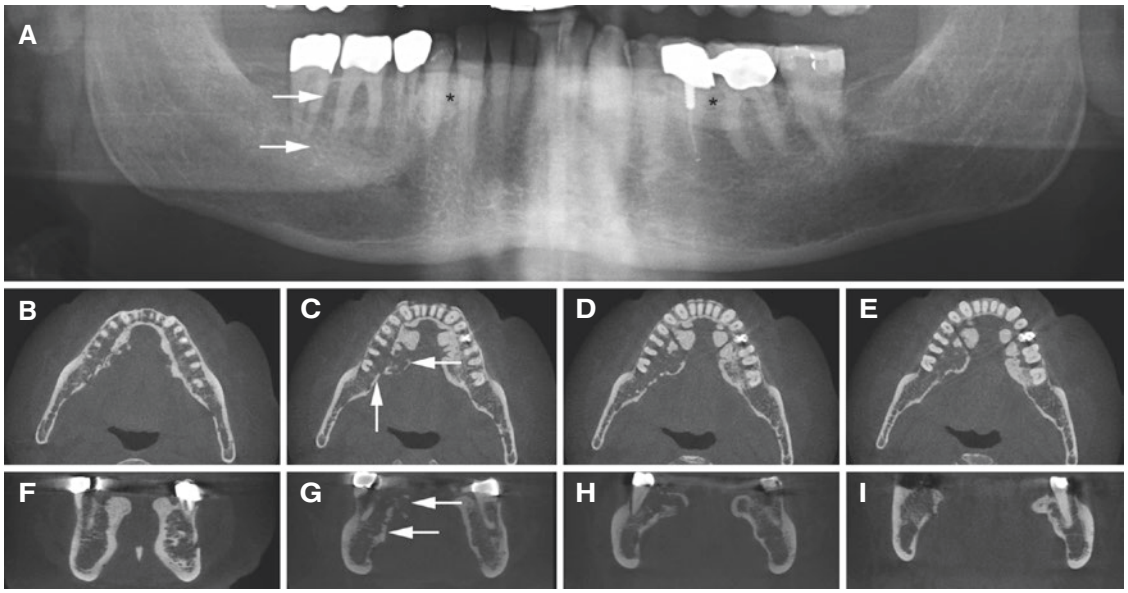

Fig. 15.33 Osteomyelitis with sequestration, mandible; 70-year-old male with ulcerated mucosa of the right mandibular torus for about 3 weeks but no other discomfort. Clinical suspicion of malignancy but histology shows infection. (**A**) Panoramic view shows bilateral radiopacities in the mandible (*asterisks*) consistent with mandibular torus but no obvious bone pathology; see the right mandible (*arrows*). (**B**, **C**, **D**, **E**) Axial and (**F**, **G**, **H**, **I**) coronal CBCT images show diffuse destruction of the cortical and cancellous bone in the right mandibular torus and body (*arrows*), with sequestration

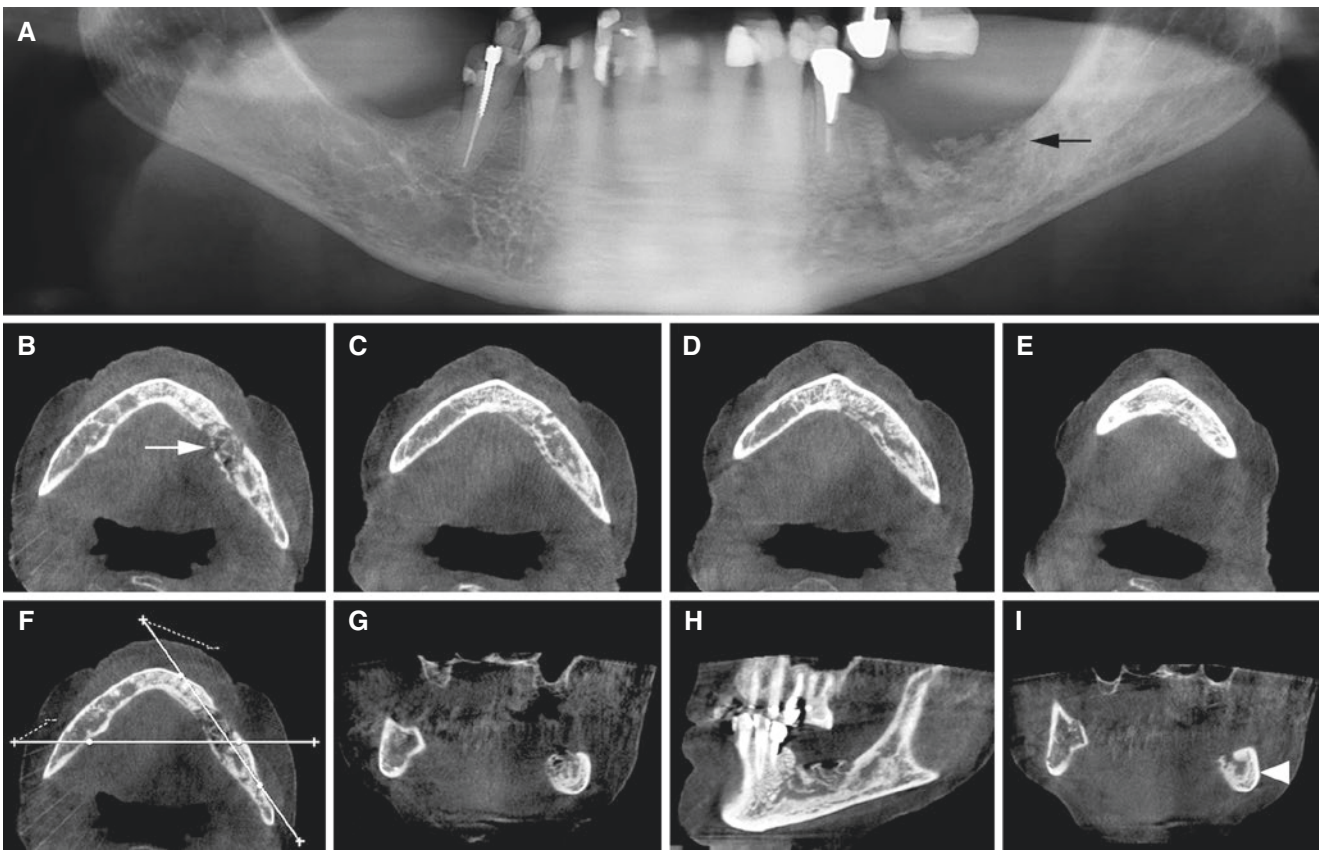

Fig. 15.34 Medication-related osteonecrosis, mandible; 78-year-old female on intravenous antiresorptive therapy for about 2 years due to multiple myeloma. (**A**) Panoramic view shows bone destruction (*arrow*). (**B**, **C**, **D**, **E**) Axial CBCT images show destruction through the mandible, buccal to lingual, with sequestration mainly on the lingual side (*arrow*). (**F**) Axial (with cursor lines), (**G**) coronal, (**H**) oblique sagittal, and (**I**) coronal (more distal than (**G**)) CBCT images confirm destruction and sequestration and additionally show sclerosis through the mandible (*arrowhead*)

15.7 Temporomandibular Joints

Figs. 15.35, 15.36, 15.37, 15.38, 15.39, 15.40, 15.41, 15.42, and 15.43

See Chap. 6

Fig. 15.35 Normal bone; 63-year-old female with hand osteoarthritis (participant in research project) without TMJ symptoms. (**A**) Axial (with cursor lines), (**B**) oblique sagittal, and (**C**) oblique coronal CBCT images show normal cortical and cancellous bone

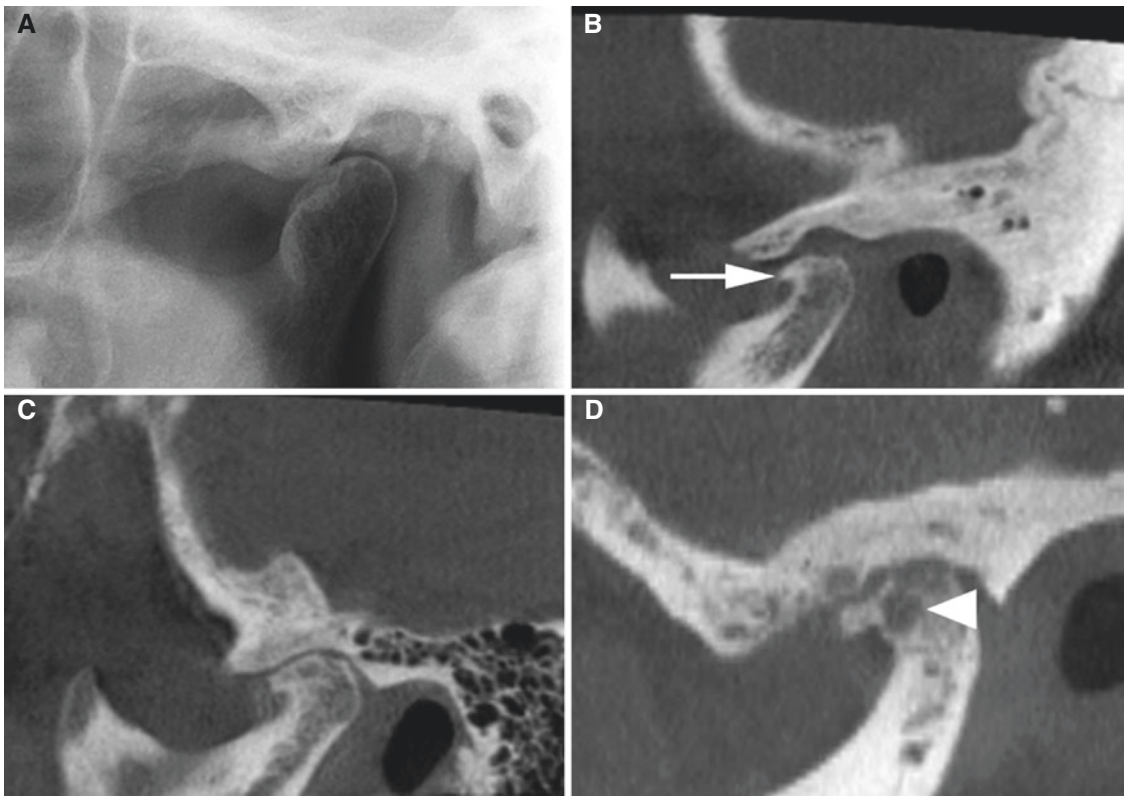

Fig. 15.36 Osteoarthritis; 71-year-old female with hand osteoarthritis (participant in research project) without TMJ symptoms. (**A**) Panoramic view suggests radiopacity in the left condyle. (**B**) Oblique sagittal CBCT image of same patient shows condylar osteophyte/sclerosis (*arrow*). (**C**) Oblique sagittal CBCT image of another patient shows more severe condylar osteophyte/sclerosis. (**D**) Oblique sagittal CBCT image of a third patient shows extensive osteoarthritis with large osteophyte, erosion, and subcortical cyst (*arrowhead*) in the condyle. Temporal bone has rather flat articular eminence, irregular joint surface, and subcortical cyst

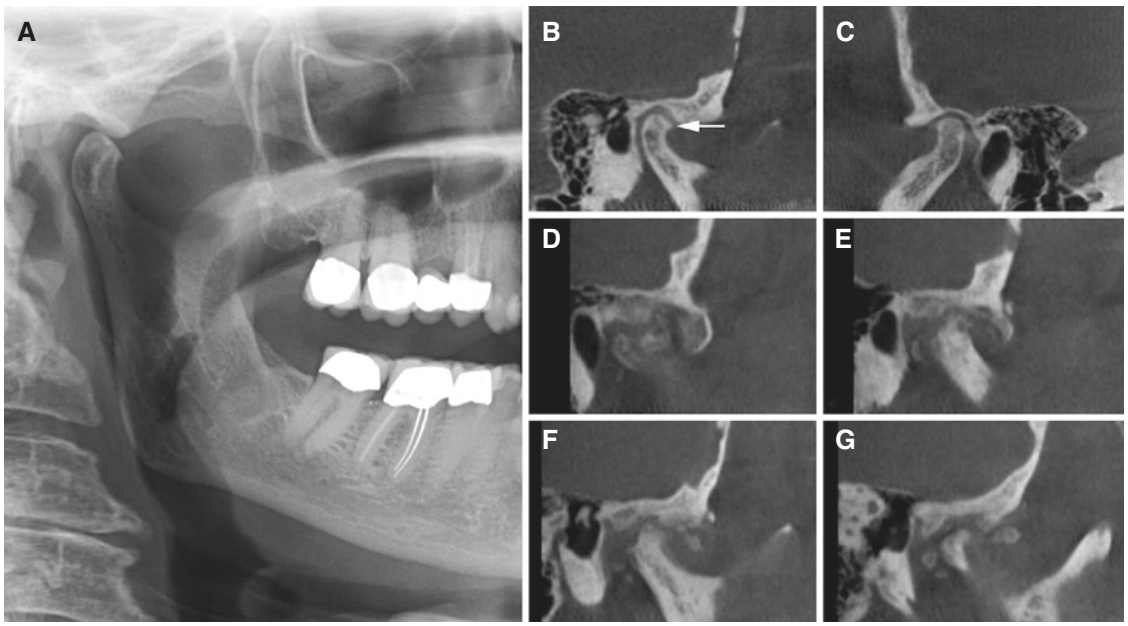

Fig. 15.37 Osteoarthritis, soft-tissue calcifications (probably due to injected steroid); 35-year-old female with severe TMJ pain. (**A**) Panoramic view and (**B**, **C**) oblique sagittal images show small osteophyte (*arrow*) of the right condyle (**A**, **B**) and normal left condyle (**C**). About 1 year and 11 months after arthrocentesis with steroid injection in the right joint (**D**, **E**, **F**, **G**) oblique sagittal CBCT images show pronounced soft-tissue calcifications

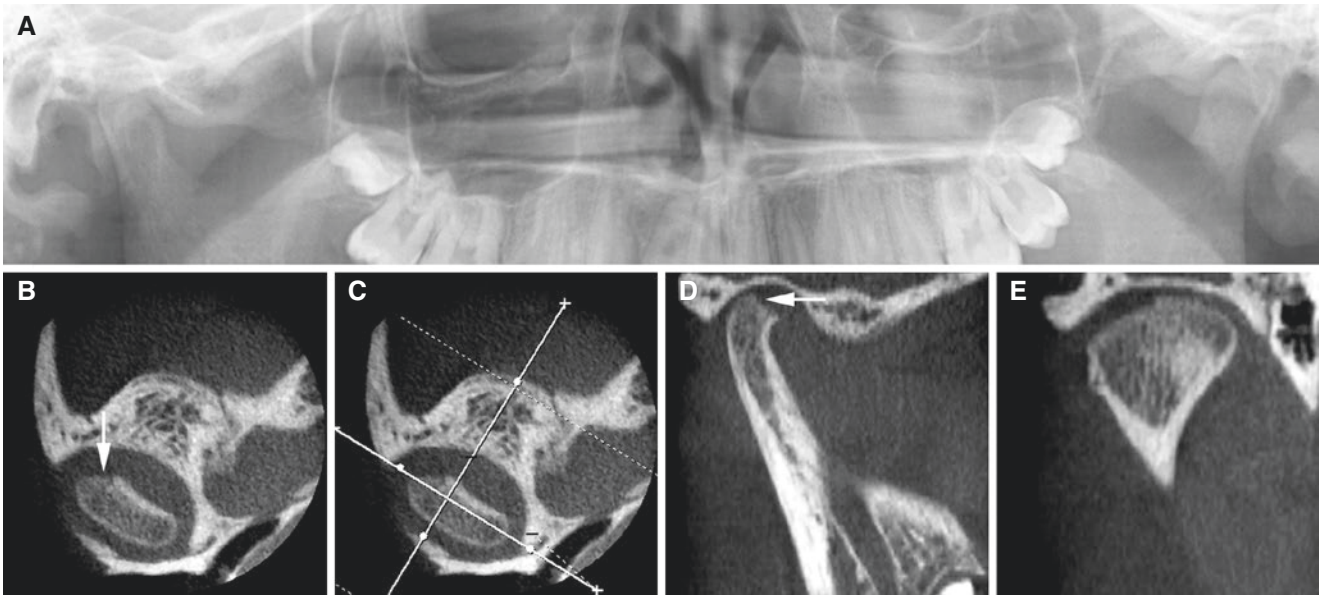

Fig. 15.38 Juvenile osteoarthritis, 12-year-old female with variable pain and locking, right TMJ. (**A**) Panoramic view suggests flattening of the right condyle. (**B**) Axial, (**C**) axial (with cursor lines), (**D**) oblique sagittal, and (**E**) oblique coronal CBCT images show erosive changes of the right condyle (*arrow*)

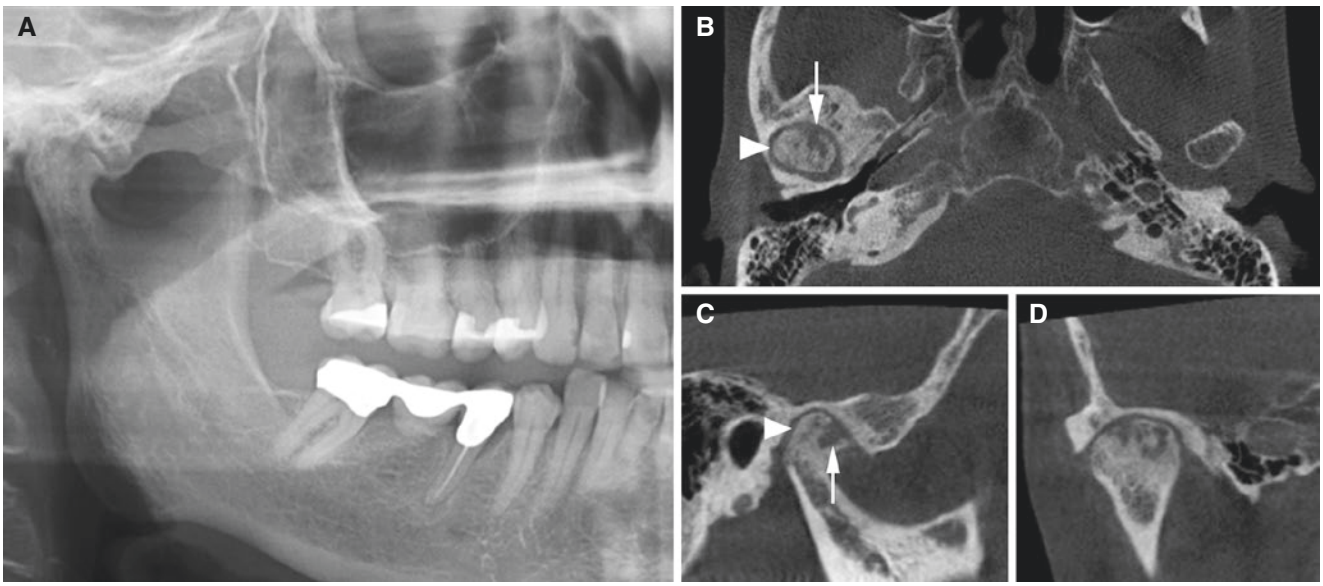

Fig. 15.39 Rheumatoid arthritis; 59-year-old female with variable right-sided TMJ pain and mouth-opening problems. (**A**) Panoramic view and (**B**) axial, (**C**) oblique sagittal, and (**D**) oblique coronal CBCT images show punched-out destruction (*arrow*) in the right condyle with sclerosis (*arrowhead*)

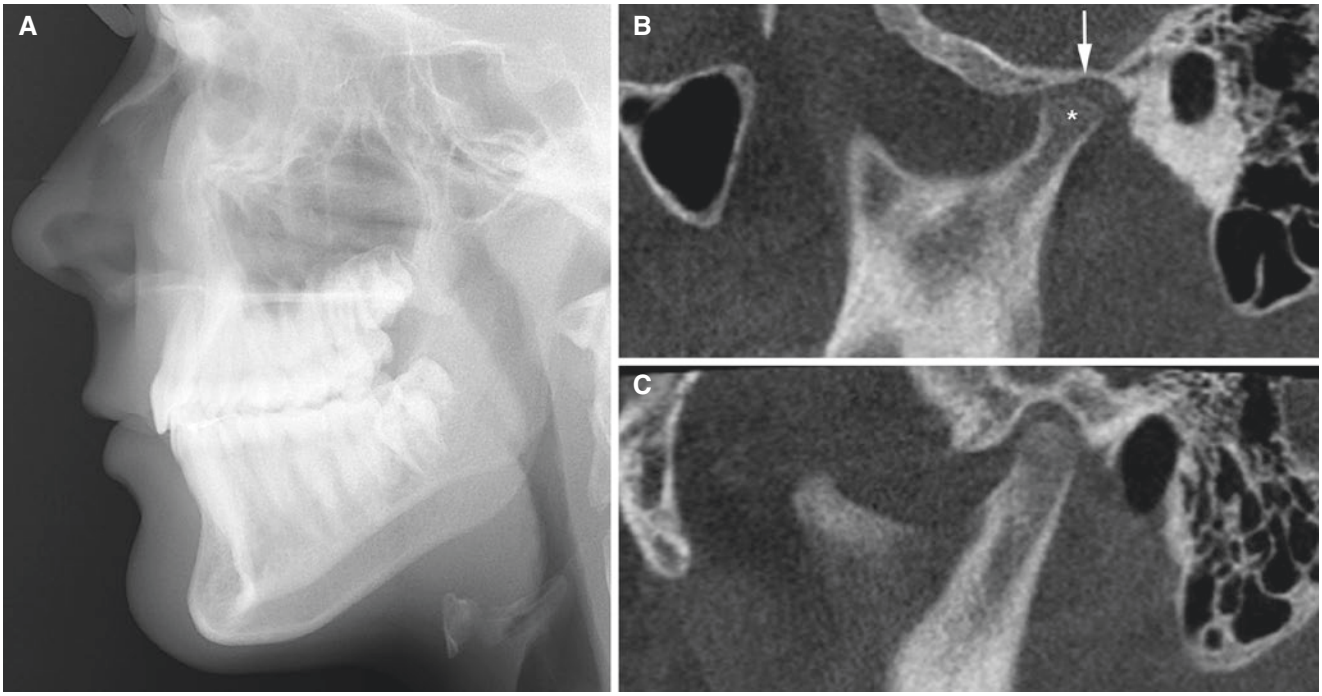

Fig. 15.40 Juvenile idiopathic arthritis; 15-year-old female with facial asymmetry but no symptoms or other clinical signs. (**A**) Lateral cephalogram shows asymmetric mandibular growth (due to unilateral TMJ involvement), but normal facial profile. (**B**) Oblique sagittal CBCT image shows abnormal right TMJ with rather flat condyle (*asterisk*) without erosion and rather flat fossa/eminence (*arrow*), consistent with TMJ arthritis sequel. (**C**) Oblique sagittal CBCT image shows normal contralateral joint

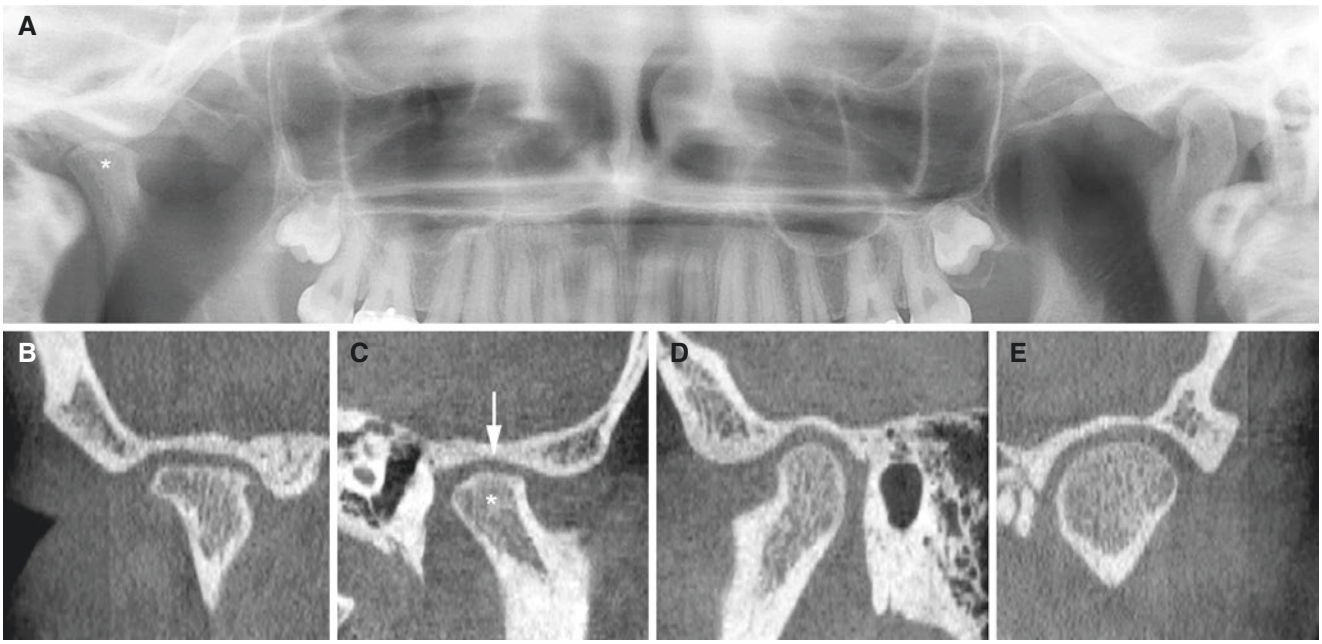

Fig. 15.41 Juvenile idiopathic arthritis; 17-year-old female with variable jaw pain and mouth-opening problems. (**A**) Panoramic view and (**B**) oblique coronal and (**C**) oblique sagittal CBCT images show abnormal right TMJ with rather flat condyle (*asterisk*) and rather flat fossa/eminence (*arrow*) without erosion. (**D**) Oblique sagittal and (**E**) oblique coronal CBCT images show normal contralateral joint

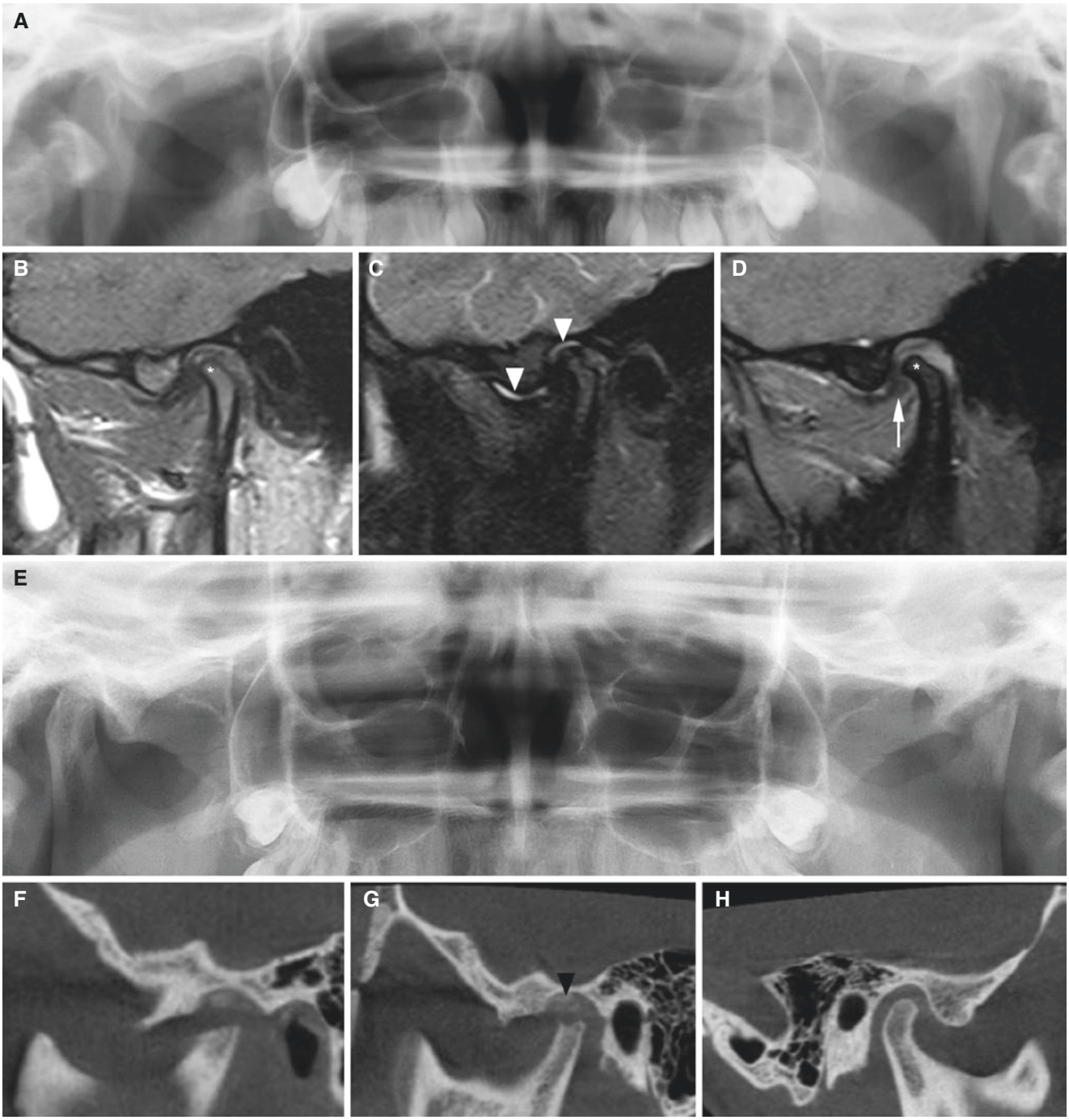

Fig. 15.42 Juvenile idiopathic arthritis, soft-tissue calcifications (probably due to injected steroid); female (followed from 9 to 17 years of age) who, at age 14, developed severe TMJ pain and severely impaired mouth-opening capacity (20 mm). At age 9, (**A**) panoramic view shows apparently normal condyles. At age 14, (**B**) oblique sagittal T1-weighted, (**C**) T2-weighted, and (**D**) open-mouth MRI show normal bone of condyle (*asterisk*), severely impaired condylar translation, displaced disc also at open mouth (*arrow*), and joint effusion/synovitis (*arrowheads*) in the left joint. At age 17 (steroid injections performed 6 and 4 months before), (**E**) panoramic view and (**F**, **G**) oblique sagittal CBCT images show flattened/destroyed condyle and eminence and evident soft-tissue calcifications (*arrowhead*). (**H**) Oblique sagittal CBCT image shows normal right joint (no steroid injection)

Fig. 15.43 Osteochondroma (most probable); 26-year-old female with some jaw asymmetry. (**A**) Axial, (**B**) axial (with cursor lines), (**C**) oblique sagittal, and (**D**) oblique coronal CBCT images show condylar hyperplasia with irregular outline (*arrow*)

15.8 Teeth and Dental Implants

See Chap. 7

15.8.1 Impacted Wisdom Teeth

Figs. 15.44, 15.45, 15.46, 15.47, 15.48, 15.49, and 15.50

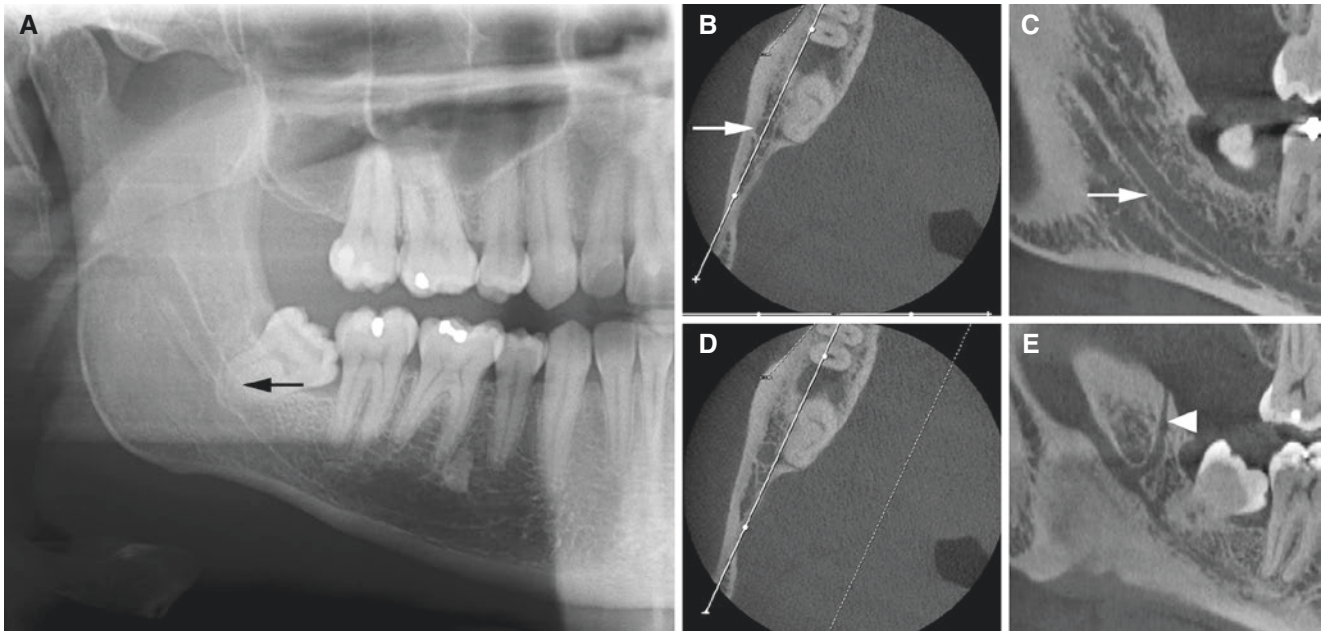

Fig. 15.44 Wisdom tooth and its relation to the mandibular canal; asymptomatic 31-year-old female. (**A**) Panoramic view shows the mandibular canal superimposed on wisdom tooth root (*arrow*). (**B**) Axial (with cursor line) and (**C**) oblique sagittal CBCT images show the mandibular canal (*arrow*) located buccally to wisdom tooth root. (**D**) Axial (with cursor line) and (**E**) oblique sagittal CBCT images show accessory vertical canal (*arrowhead*)

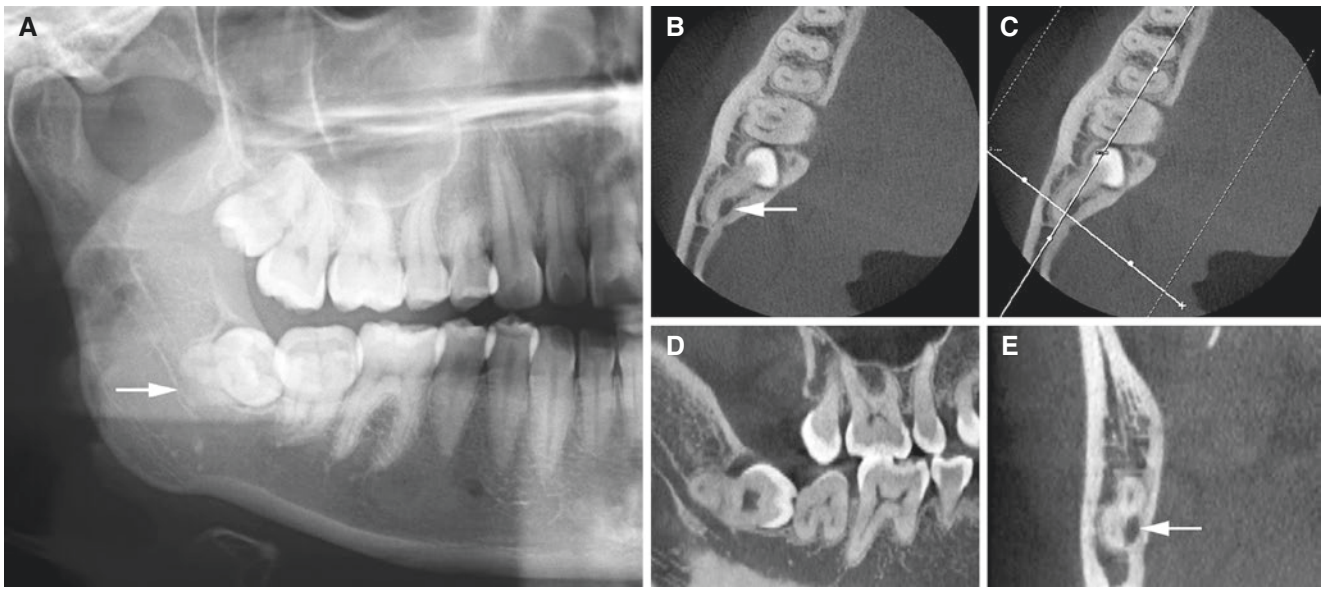

Fig. 15.45 Wisdom tooth and its relation to the mandibular canal; asymptomatic 30-year-old female. (**A**) Panoramic view shows the mandibular canal superimposed on wisdom tooth root (*arrow*). (**B**) Axial, (**C**) axial (with cursor lines), (**D**) oblique sagittal, and (**E**) oblique coronal CBCT images show the mandibular canal (*arrow*) located lingually and close to wisdom tooth root

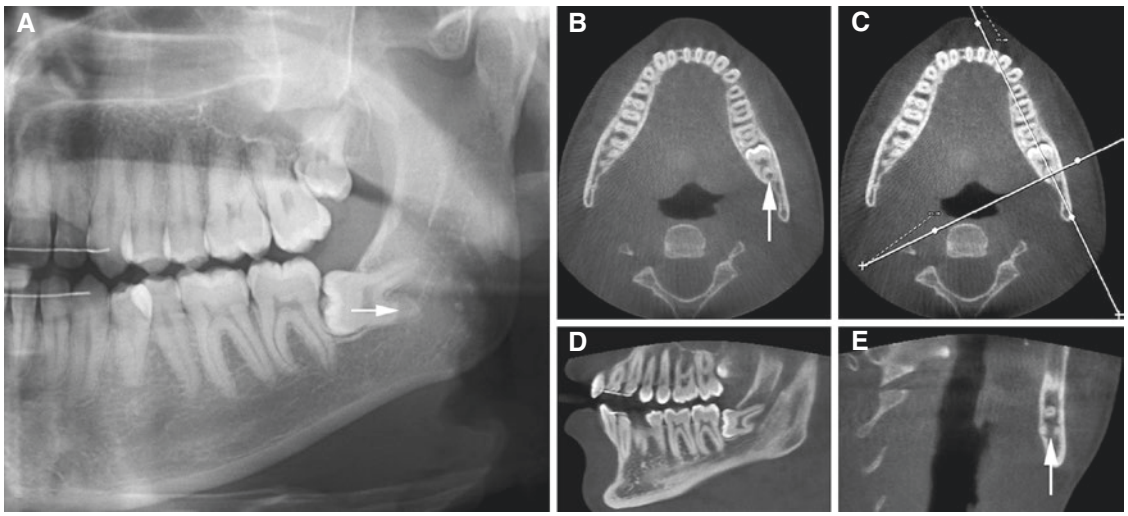

Fig. 15.46 Wisdom tooth and its relation to mandibular canal; asymptomatic 25-year-old male. (**A**) Panoramic view shows the mandibular canal superimposed on wisdom tooth root (*arrow*). (**B**) Axial, (**C**) axial (with cursor lines), (**D**) oblique sagittal, and (**E**) oblique coronal CBCT images show the mandibular canal penetrating the root complex (*arrow*)

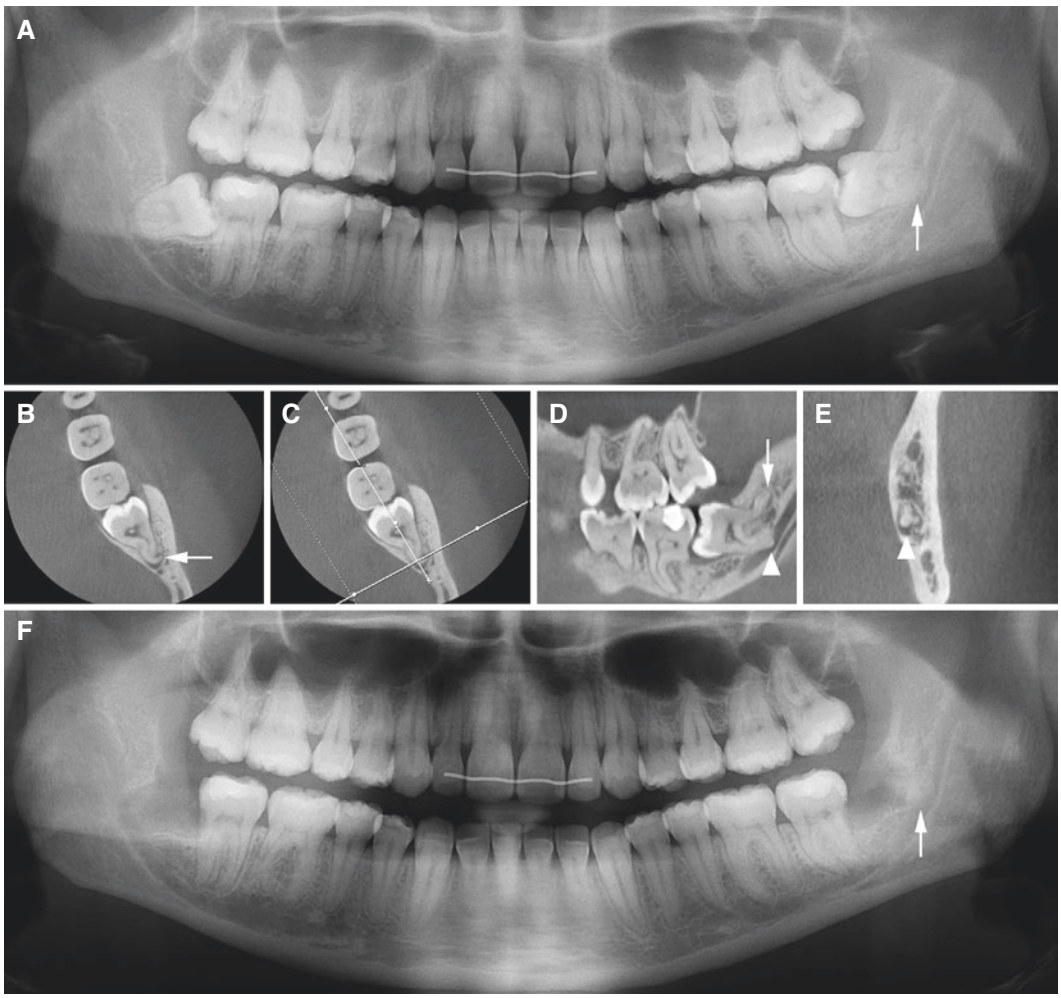

Fig. 15.47 Wisdom tooth and its relation to the mandibular canal; 24-year-old female with episodes of wisdom tooth pericoronitis. (**A**) Panoramic view indicates complicated root anatomy (*arrow*). (**B**) Axial, (**C**) axial (with cursor lines), (**D**) oblique sagittal, and (**E**) oblique coronal CBCT images show complicated root anatomy (*arrow*) and the mandibular canal closely located to the root complex (*arrowhead*). (**F**) Panoramic view shows the remaining root complex (*arrow*) after surgery (coronectomy)

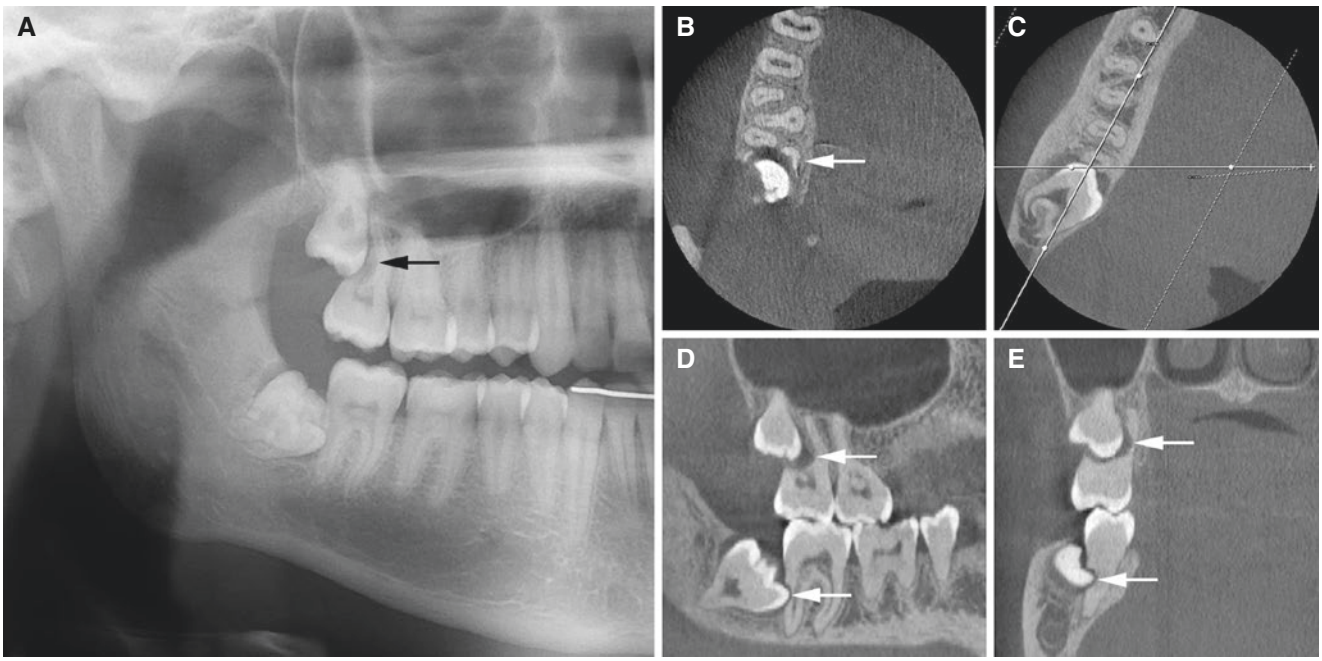

Fig. 15.48 Wisdom teeth with root resorption of the neighboring teeth, mandible, and maxilla; asymptomatic 18-year-old female. (**A**) Panoramic view shows overlapping of wisdom tooth and the second molar in the right maxilla and right mandible, with suspicion of root resorption, particularly in the maxilla (*arrow*). (**B**) Axial, (**C**) axial (with cursor lines), (**D**) oblique sagittal, and (**E**) coronal CBCT images show root resorption (*arrows*) in the maxilla and mandible (second molars); most extensive in the maxilla

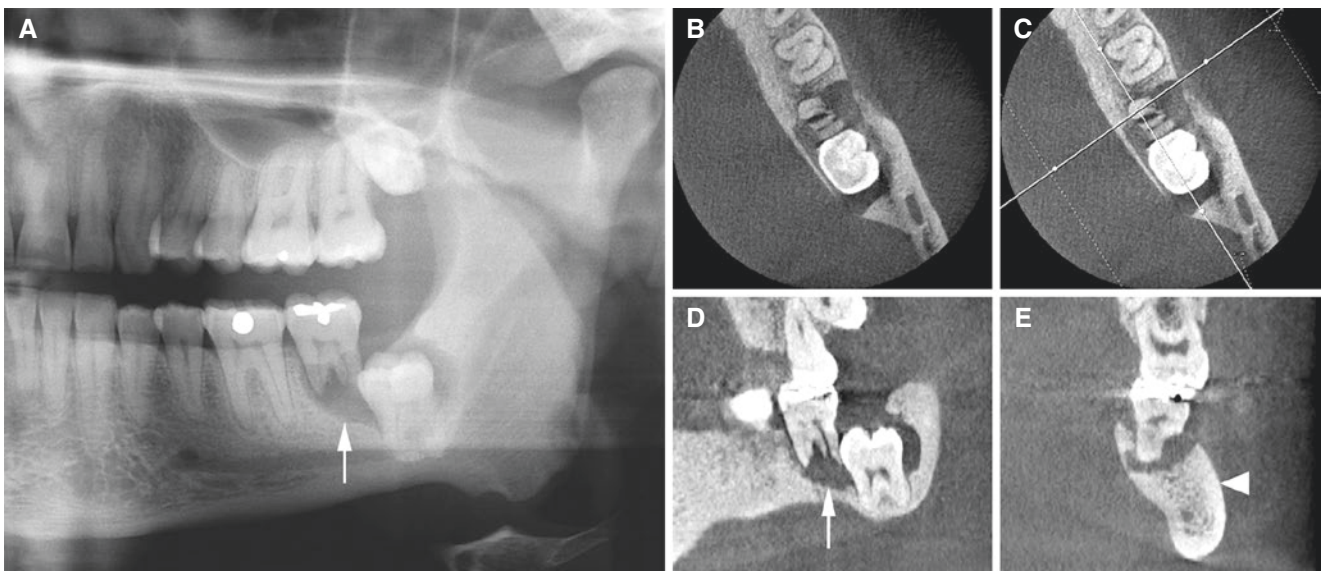

Fig. 15.49 Wisdom tooth with root resorption of the neighboring tooth and associated osteomyelitis, mandible; 38-year-old male with pain in the left mandible. (**A**) Panoramic view shows pericoronal radiolucency around impacted wisdom tooth and root resorption of the second molar (*arrow*). (**B**) Axial, (**C**) axial (with cursor lines), (**D**) oblique sagittal, and (**E**) oblique coronal CBCT images show periapical radiolucency (second molar) and pericoronal radiolucency (wisdom tooth), extensive root resorption of the second molar (*arrow*), and sclerosis throughout the mandible (*arrowhead*), consistent with infected follicular cyst and resultant osteomyelitis. Note root resorption of the second molar in the left maxilla due to impacted wisdom tooth

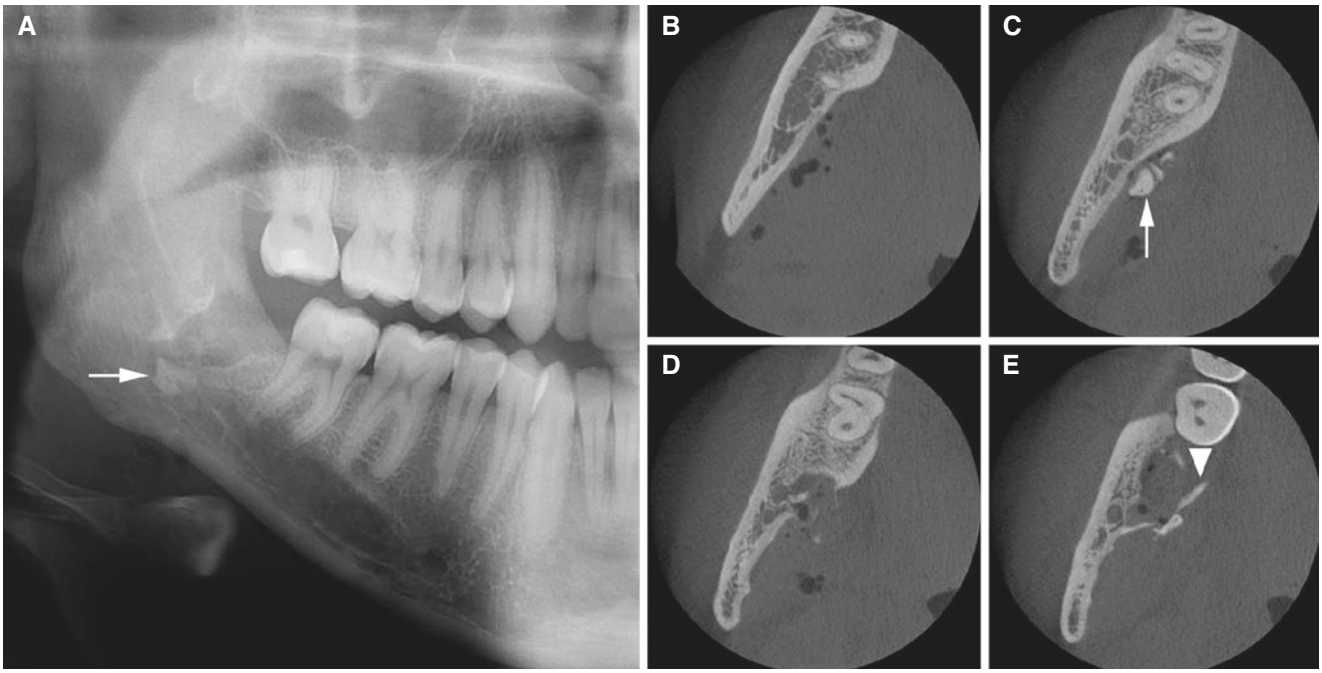

Fig. 15.50 Postoperative condition after removal of wisdom tooth, mandible, with question about remaining root; 22-year-old female with immediate postoperative imaging. (**A**) Panoramic view suggests possibility of remaining root (*arrow*). (**B**, **C**, **D**, **E**) Axial CBCT images show bone and/or root fragments displaced lingually to the mandible (*arrow*) and fragmented lingual cortical plate (*arrowhead*). Note also air in soft tissue

15.8.2 Other Impacted Teeth

Figs. 15.51, 15.52, 15.53, 15.54, 15.55, 15.56, 15.57, 15.58, and 15.59

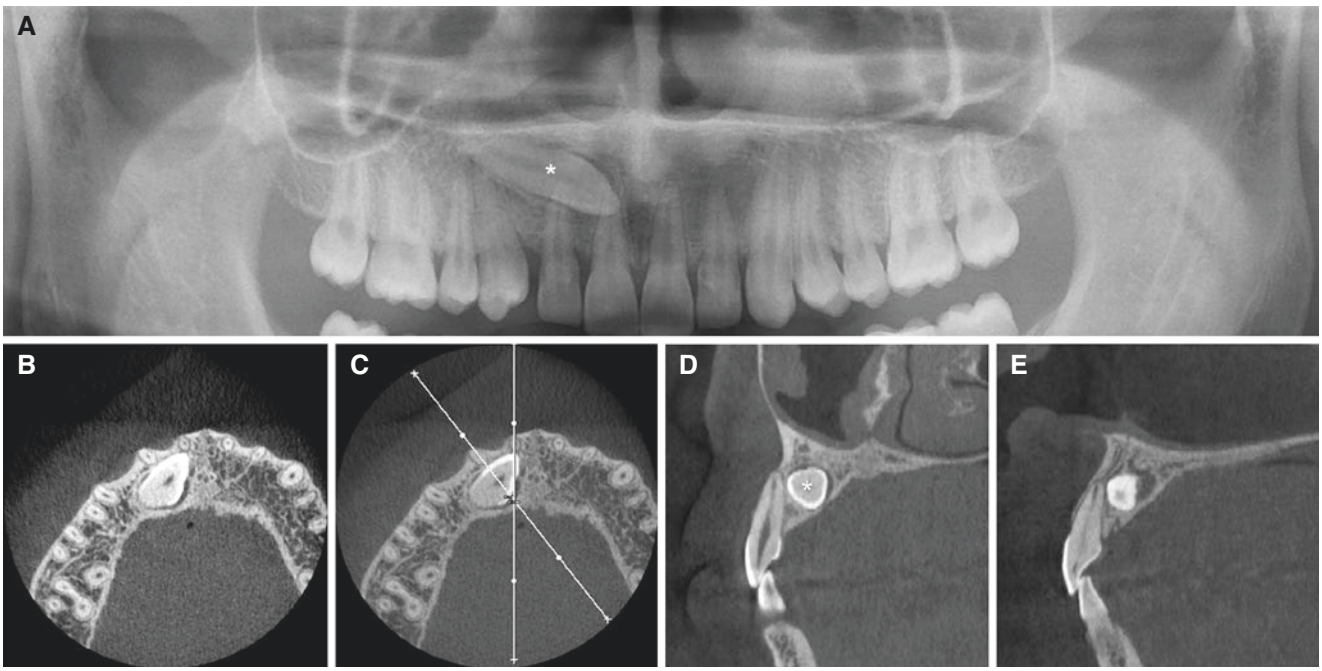

Fig. 15.51 Canine, maxilla; asymptomatic 18-year-old male. (**A**) Panoramic view shows the right maxillary canine (*asterisk*) superimposed on roots of incisors. (**B**) Axial, (**C**) axial (with cursor lines), (**D**) oblique sagittal, and **E** sagittal CBCT images show impacted canine (*asterisk*) without resorption of the neighboring teeth

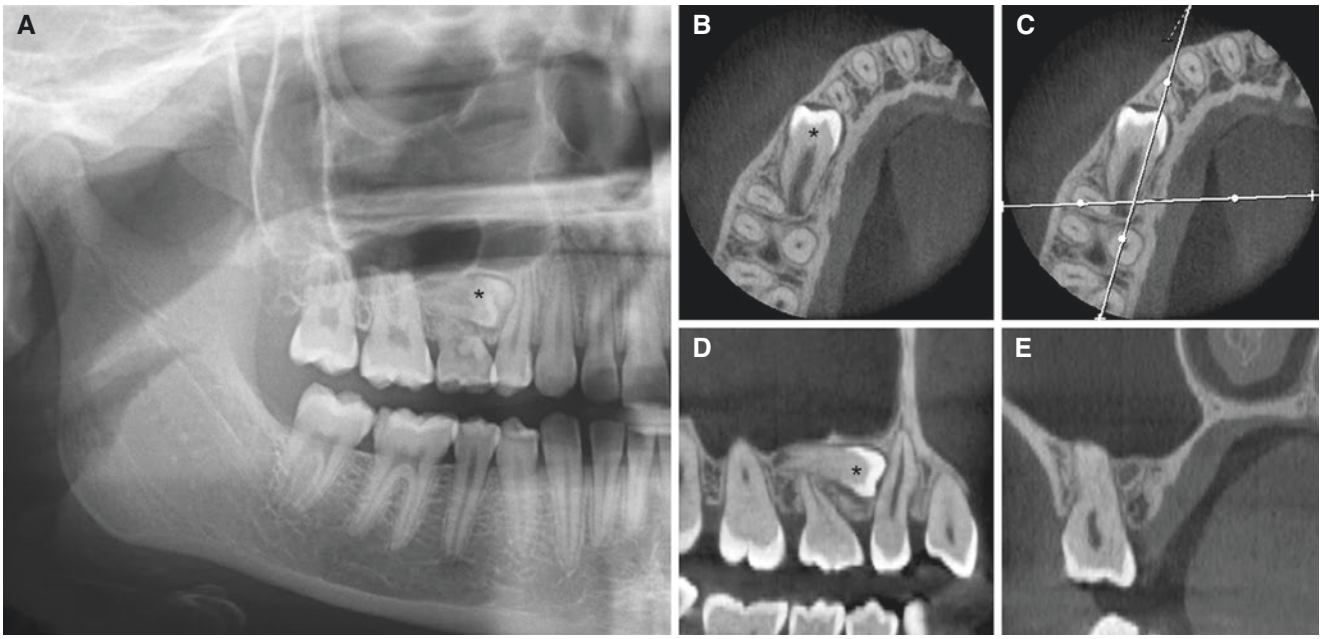

Fig. 15.52 Premolar, maxilla; asymptomatic 13-year-old male. (**A**) Panoramic view shows impacted premolar (*asterisk*). (**B**) Axial, (**C**) axial (with cursor lines), (**D**) oblique sagittal, and (**E**) oblique coronal CBCT images show impacted premolar (*asterisk*) without resorption of the neighboring teeth

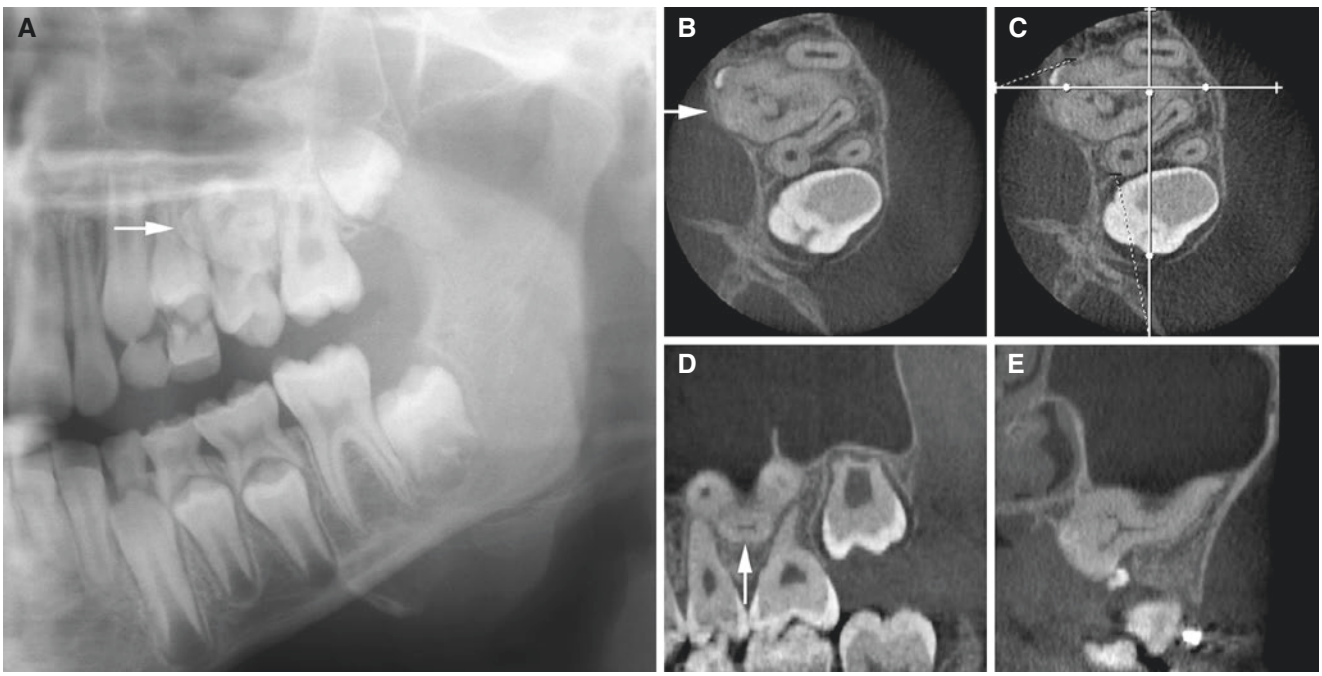

Fig. 15.53 Supernumerary tooth (distodens), maxilla; asymptomatic male at 10 (**A**) and 14 years of age (**B**, **C**, **D**, **E**). (**A**) Panoramic view shows impacted toothlike structure in the left maxilla (*arrow*). (**B**) Axial, (**C**) axial (with cursor lines), (**D**) sagittal, and (**E**) Coronal CBCT images show three-rooted impacted tooth (*arrow*) without resorbing adjacent teeth

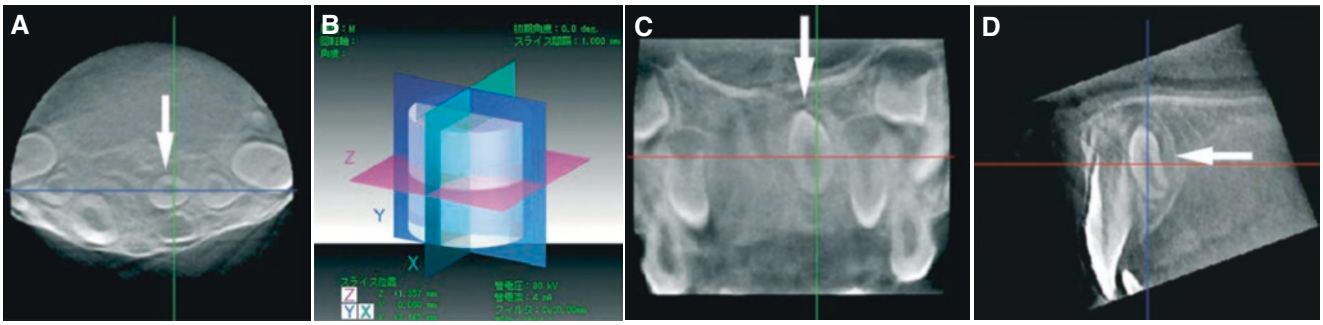

Fig. 15.54 Supernumerary tooth (mesiodens), maxilla; 8-year-old male with incidental finding. (**A**) Axial CBCT image shows mesiodens (*arrow*) in palatal position and close to but not in contact with the permanent incisor. (**B**) Three image planes indicated by different colors. (**C**) Coronal CBCT image shows inverted mesiodens (*arrow*). (**D**) Sagittal CBCT image shows inverted mesiodens at apex level of the permanent incisor (*arrow*) (courtesy of Dr. K. Honda, Nihon University School of Dentistry, Tokyo, Japan)

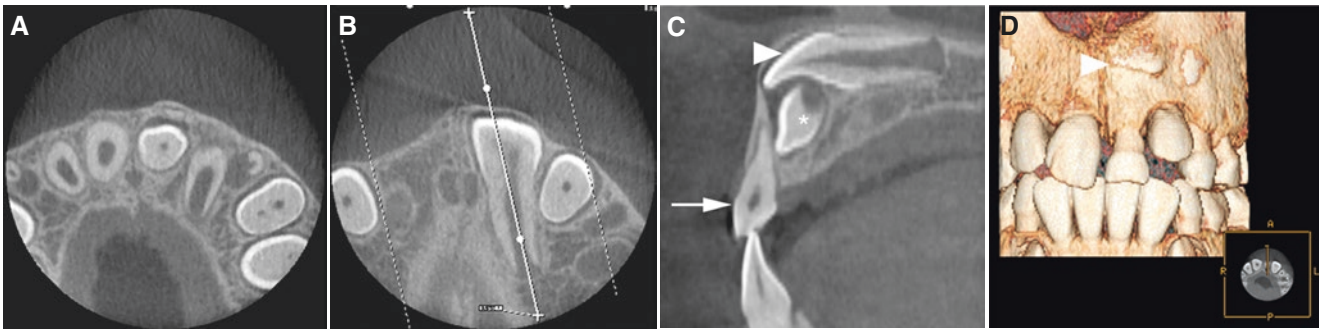

Fig. 15.55 Supernumerary tooth (mesiodens), maxilla; asymptomatic 8-year-old female. (**A**) Axial, (**B**) axial (with cursor line), (**C**) oblique sagittal, and (**D**) 3D CBCT images show mesiodens (*asterisk*) palatally to the remaining deciduous central incisor (*arrow*) and caudally to the horizontally impacted central incisor (*arrowhead*)

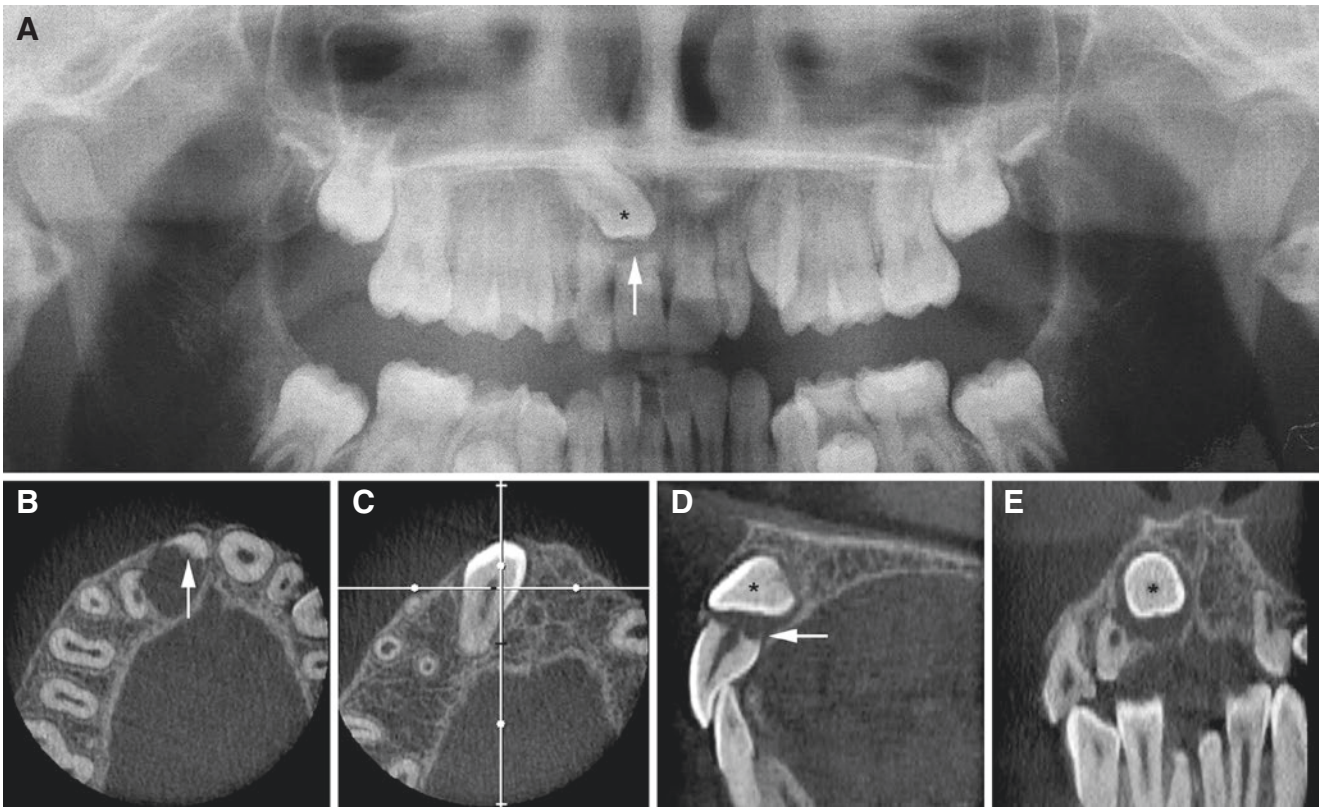

Fig. 15.56 Canine, with root resorption of the central incisor, maxilla; asymptomatic 12-year-old male. (**A**) Panoramic view shows ectopically located canine (*asterisk*) and severe root resorption of the right central incisor (*arrow*). (**B**) Axial, (**C**) axial (with cursor lines), (**D**) sagittal, and (**E**) coronal CBCT images show severe root resorption particularly of the central incisor (*arrow*) but also of the lateral incisor and almost horizontally located impacted canine (*asterisk*)

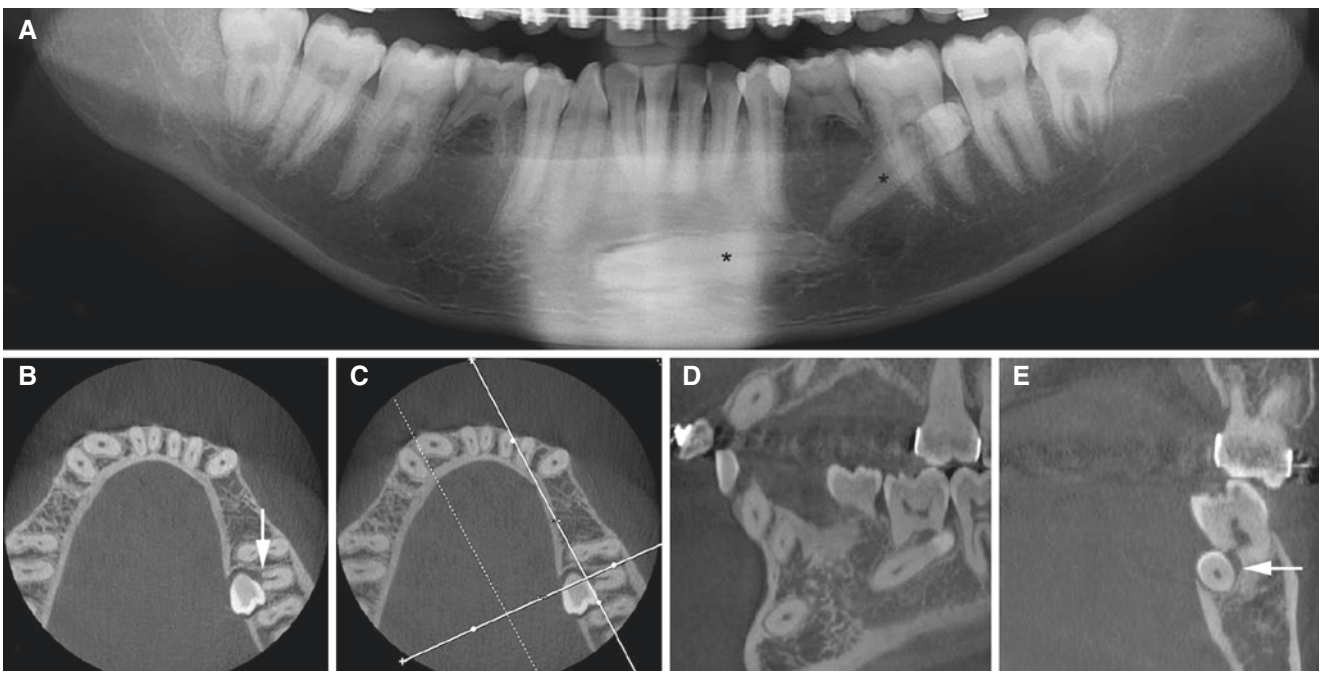

Fig. 15.57 Premolar with root resorption of the neighboring tooth, mandible; asymptomatic 20-year-old male. (**A**) Panoramic view shows impacted premolar and impacted canine (*asterisks*). (**B**) Axial, (**C**) axial (with cursor lines), (**D**) oblique sagittal, and (**E**) oblique coronal CBCT images show evident resorption (*arrow*) of the neighboring tooth (first molar) due to the impacted premolar

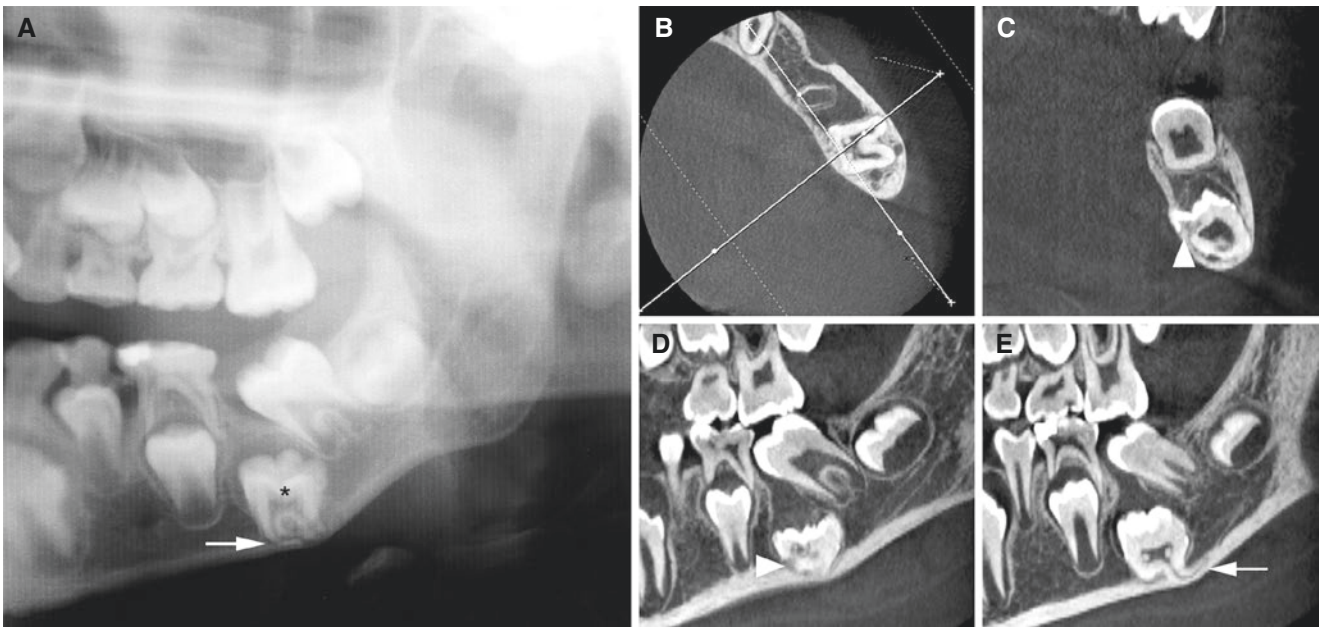

Fig. 15.58 First molar not erupted, mandible; 8-year-old male. (**A**) Panoramic view shows the impacted molar (*asterisk*) located in the cortex of the inferior mandibular border with about 90° angulation of mesial root (*arrow*). (**B**) Axial (with cursor lines), (**C**) oblique coronal, and (**D**, **E**) oblique sagittal CBCT images show the impacted molar with about 90° angulation of the distal root (*arrow*) located in the cortex of the inferior mandibular border. Note crown resorption of impacted molar (*arrowhead*), apparently with ingrowth of bone (replacement resorption) and mesial tipping of the second molar. Mandibular canal located in a lingual groove of the impacted molar

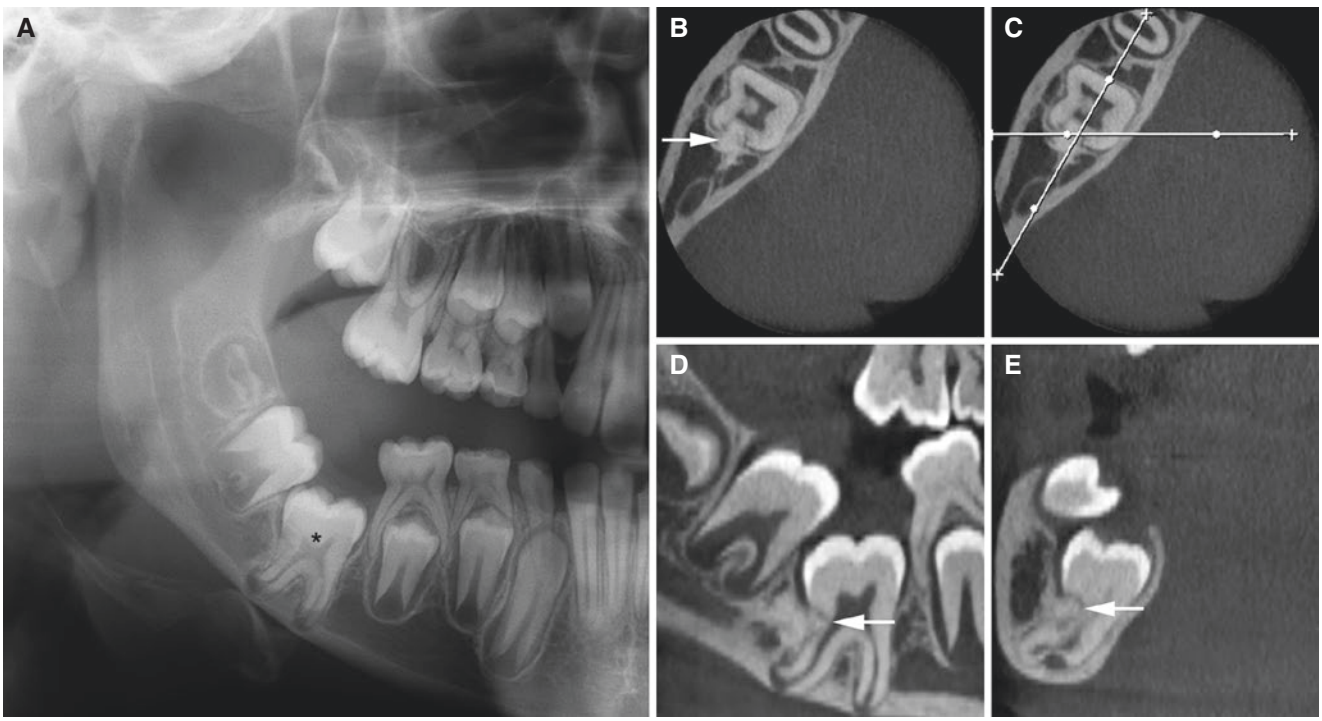

Fig. 15.59 First molar not erupted, mandible; 10-year-old male. (**A**) Panoramic view shows impacted first molar (*asterisk*) with apices in the cortical bone of the inferior mandibular border. (**B**) Axial, (**C**) axial (with cursor lines), (**D**) oblique sagittal, and (**E**) coronal CBCT images show cervical resorption with ingrowth of bone in the impacted molar (*arrow*)

15.8.3 Dental Anomalies/Malformations

Figs. 15.60, 15.61, 15.62, 15.63, 15.64, 15.65, 15.66, and 15.67

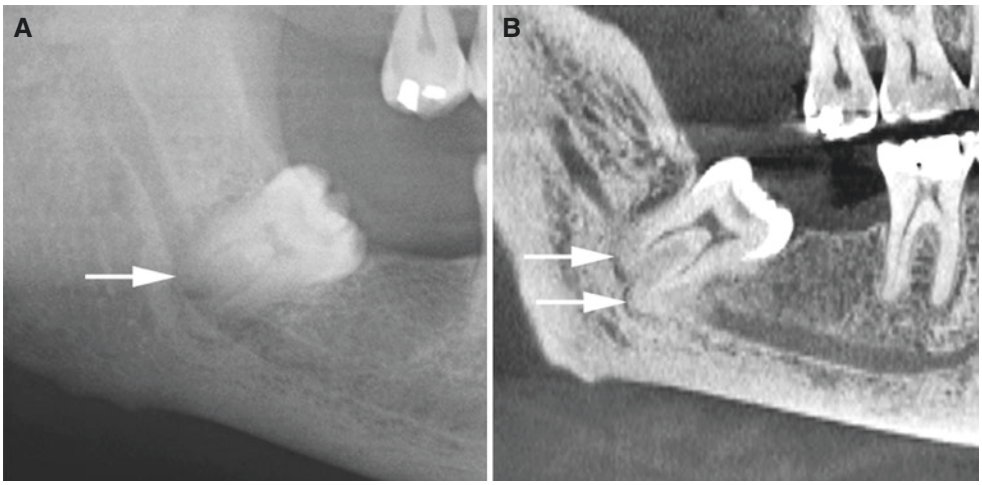

Fig. 15.60 Hypercementosis, impacted wisdom tooth, mandible; 37-year-old male with episodes of pericoronitis of right wisdom tooth. (**A**) Panoramic view and (**B**) oblique sagittal CBCT image show abnormally increased amount of the cementum (*arrows*). Note periodontal membrane surrounding the cementum

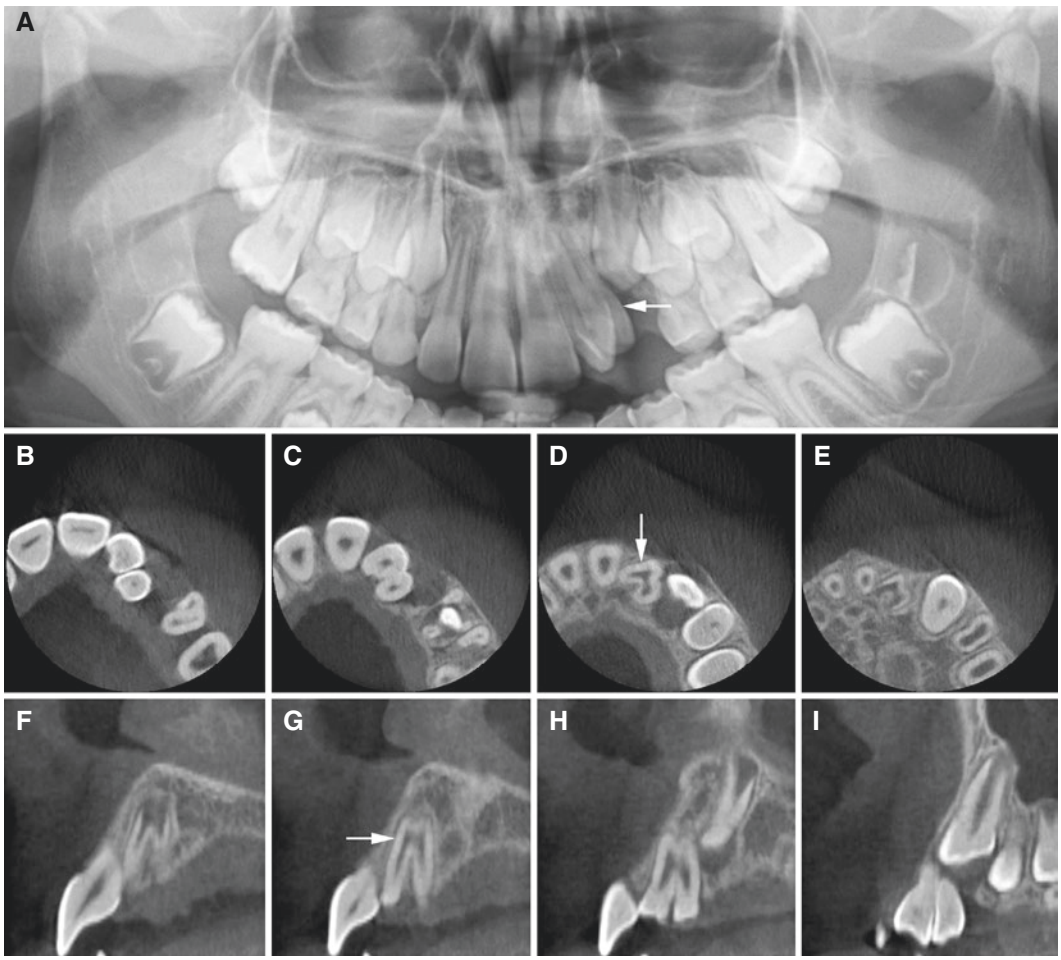

Fig. 15.61 "Double tooth," maxilla; 9-year-old female. (**A**) Panoramic view suggests double lateral incisor (*arrow*). (**B**, **C**, **D**, **E**) Axial and (**F**, **G**, **H**, **I**) oblique sagittal CBCT images probably show gemination and not fusion of incisors (*arrow*)

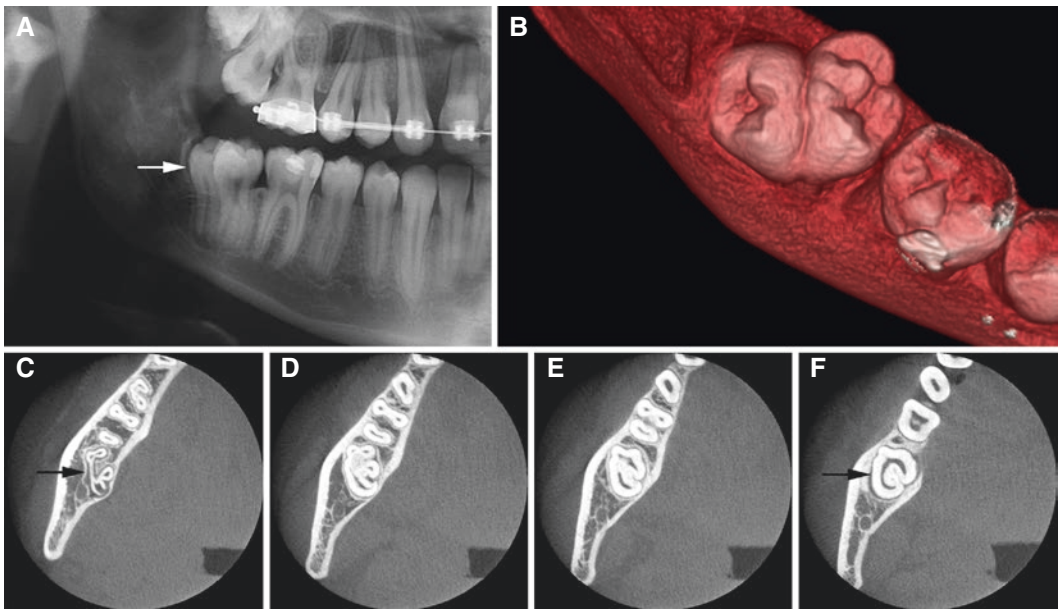

Fig. 15.62 "Double tooth," mandible; 15-year-old female. (**A**) Panoramic view suggests "double molar" (*arrow*). (**B**) 3D and (**C**, **D**, **E**, **F**) axial CBCT images show complete fusion (crown and root) of the second and third molars (*arrow*)

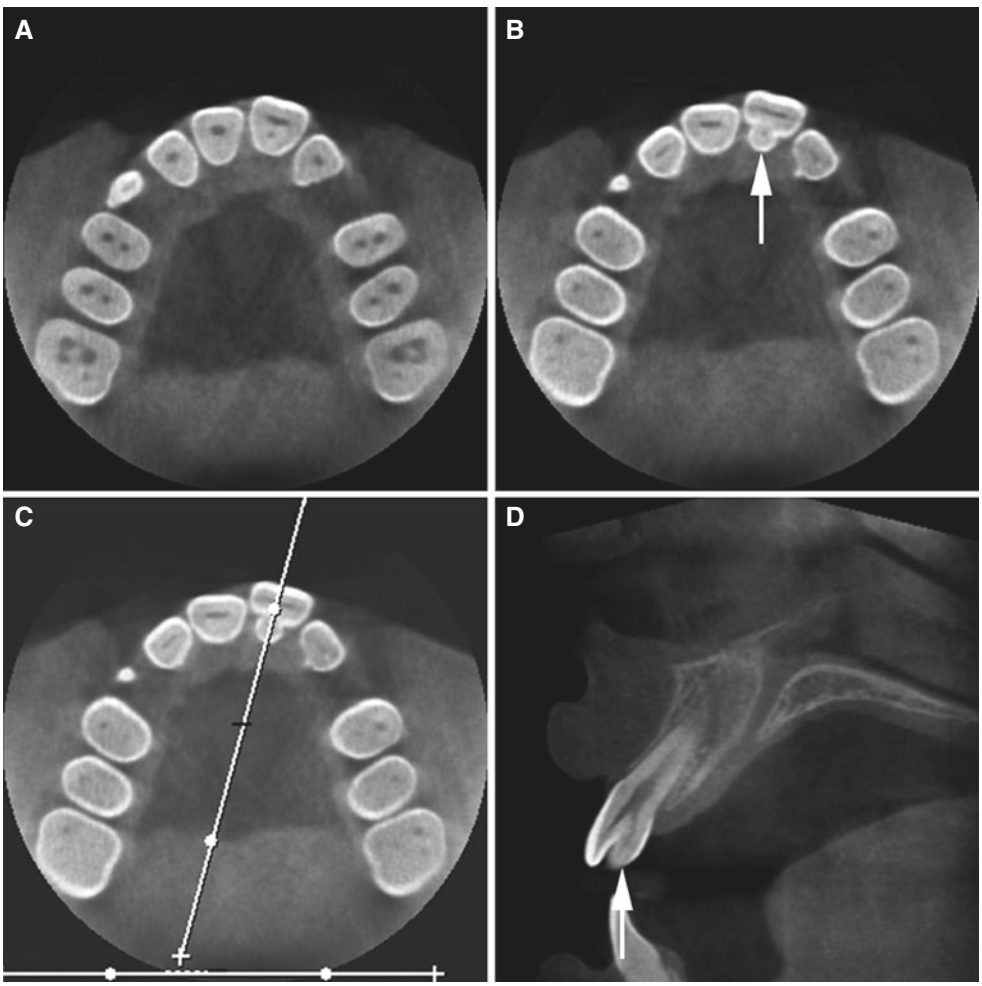

Fig. 15.63 Enamel evagination (dens evaginatus, talon cusp; additional cusp or tubercle), left central incisor, maxilla; 11-year-old female. (**A**) Axial, (**B**) axial (more cranial), (**C**) axial (with cursor line), and (**D**) oblique sagittal CBCT images show cusp or tubercle with pulp horn (*arrow*)

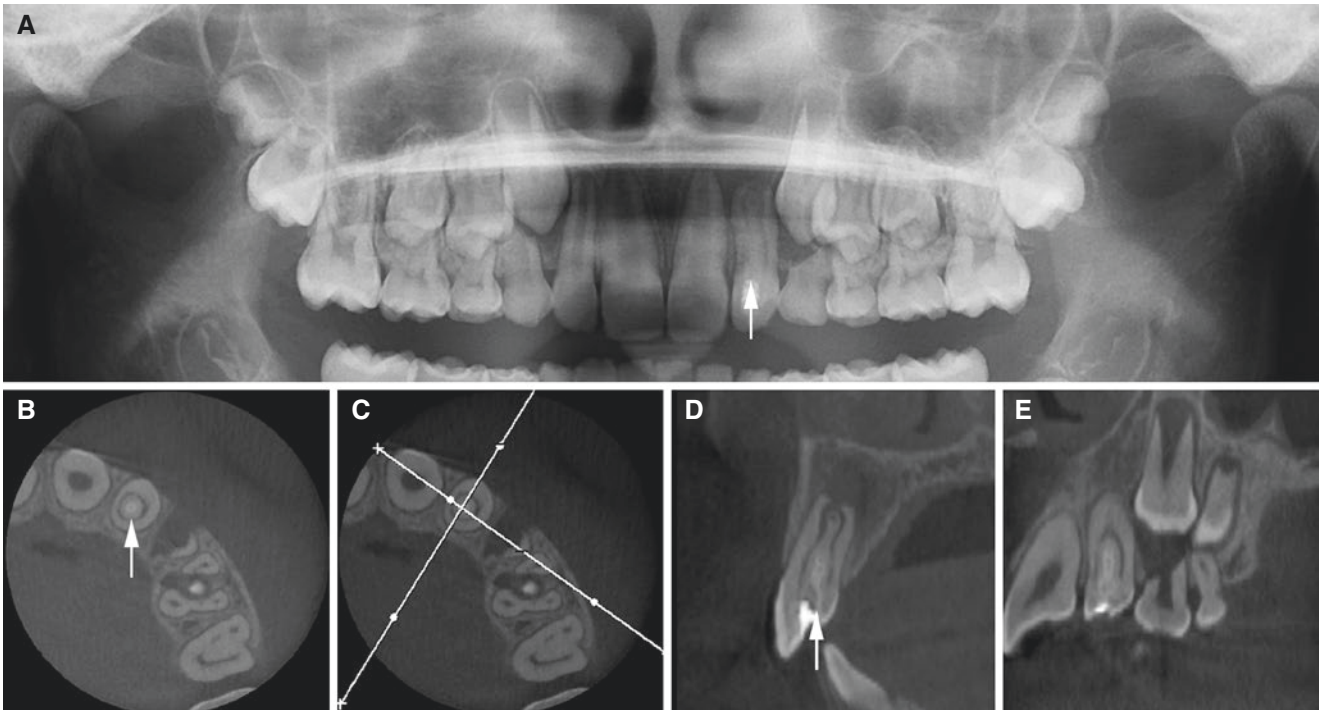

Fig. 15.64 Enamel invagination (dens invaginatus), lateral incisor, maxilla; 10-year-old male. (**A**) Panoramic view and (**B**) axial, (**C**) axial (with cursor lines), (**D**) oblique sagittal, and (**E**) oblique coronal CBCT images show toothlike structure (*arrow*) inside the lateral incisor almost to the apex (Oehlers type 3), with centrally located enamel. Note periapical radiolucency

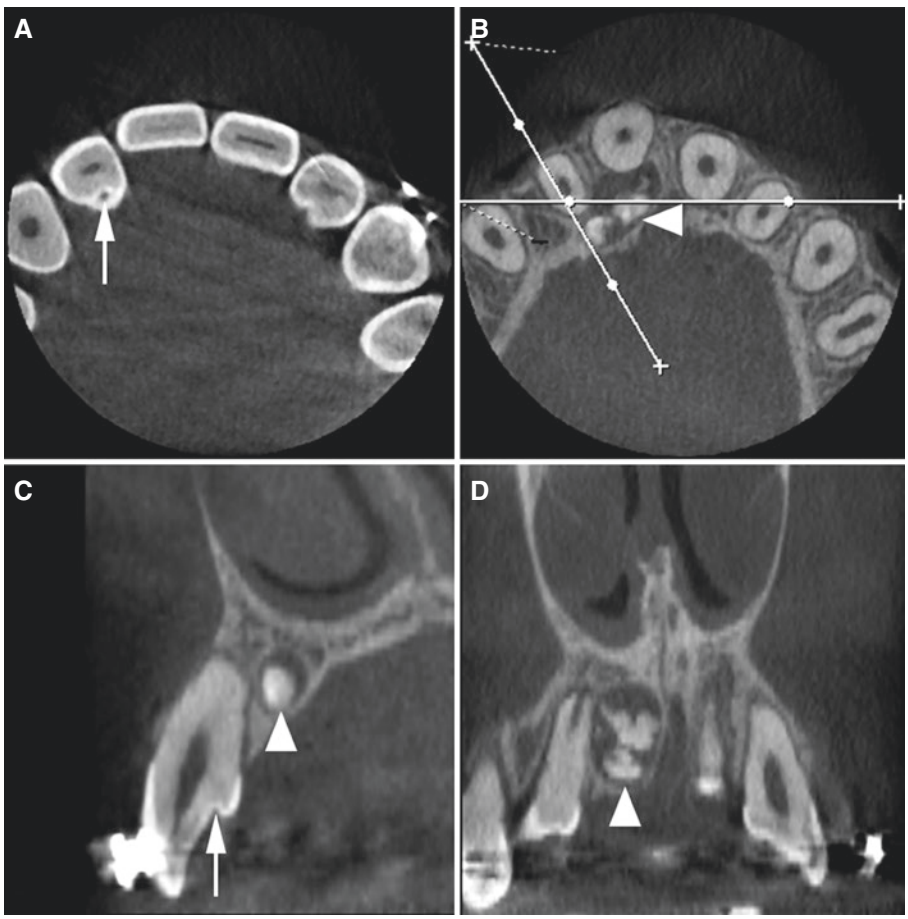

Fig. 15.65 Foramen cecum, lateral incisor and odontoma, maxilla; 12-year-old female with incidental finding. (**A**) Axial, (**B**) axial (with cursor lines), (**C**) oblique sagittal, and (**D**) coronal CBCT images show the foramen cecum (*arrow*) of the lateral incisor and complex/compound odontoma (*arrowhead*) located palatally to the lateral incisor and displaced central incisor

Fig. 15.66 Internal and external resorption, central incisor, maxilla; 18-year-old female with one central incisor in infraposition compared to other central incisors; see (**A**) intraoral photograph. (**B**) Intraoral view shows abnormal root structure (*arrow*) and obliterated crown. Note inverted mesiodens (*arrowhead*). (**C**, **D**) Coronal, (**E**, **F**) sagittal, and (**G**, **H**) axial CBCT images show open-rooted (*arrow*) left central incisor with internal resorption (*asterisk*) and resorption with communication to periodontal ligament (*arrowhead*), suggesting ankylosis. Mesiodens with crown resorption (*black arrowhead*)

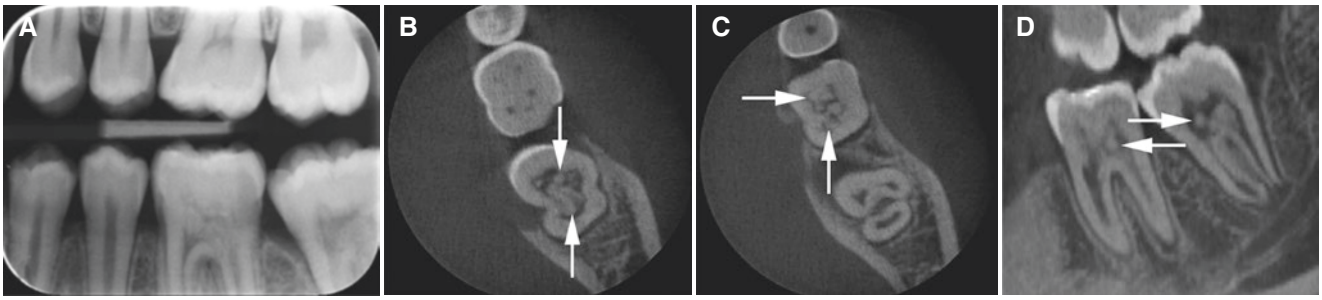

Fig. 15.67 Pulp stones, mandible; 15-year-old male. (**A**) Intraoral view shows pulp chamber radiopacities in mandibular molar teeth. (**B**, **C**) Axial and (**D**) oblique sagittal CBCT images show multiple radiopacities in the first and second molars, consistent with pulp stones or pulpal sclerosis (*arrows*)

15.8.4 Dental Implants

Figs. 15.68, 15.69, 15.70, 15.71, 15.72, and 15.73

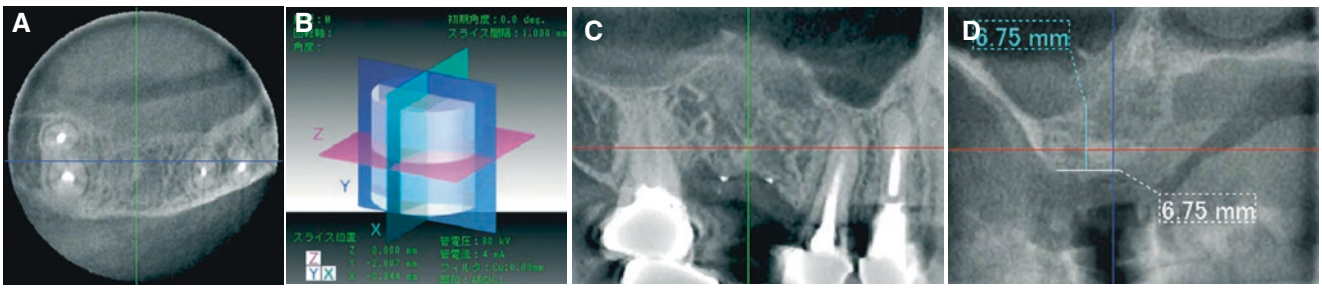

Fig. 15.68 Pre-implant imaging, maxilla; 50-year-old female. (**A**) Axial CBCT image shows acceptable width of edentulous alveolar ridge. (**B**) Three image planes indicated by different colors. (**C**) Sagittal CBCT image shows acceptable height of edentulous alveolar ridge. (**D**) Alveolar ridge dimensions: same height and width (courtesy of Dr. K. Honda, Nihon University School of Dentistry, Tokyo, Japan)

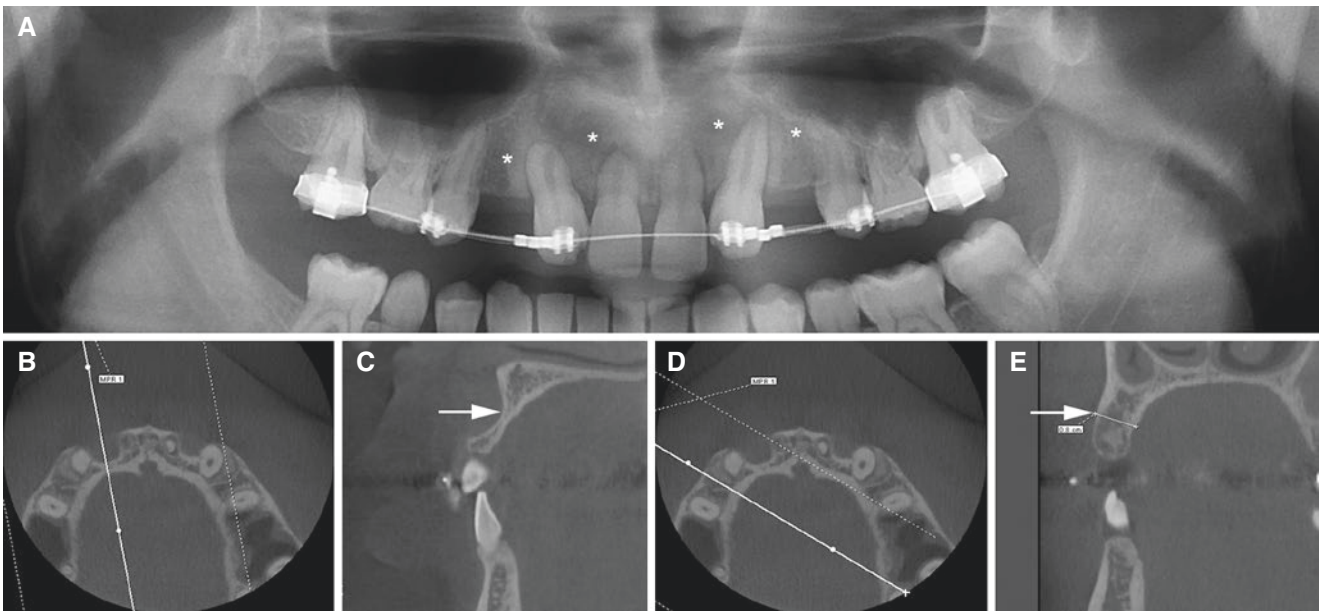

Fig. 15.69 Pre-implant imaging, maxilla; 17-year-old male with hypodontia in need of dental implants in the maxilla. (**A**) Panoramic view does not suggest great variation in bucco-palatal alveolar bone dimension in the anterior maxilla (*asterisks*). (**B**) Axial (with cursor line), (**C**) oblique sagittal, (**D**) axial (with cursor line), and (**E**) oblique coronal CBCT images show great variation in bucco-palatal dimension of the alveolar bone (*arrow*), but satisfactory dimension in planned implant site (**E**) (similar dimensions in contralateral site)

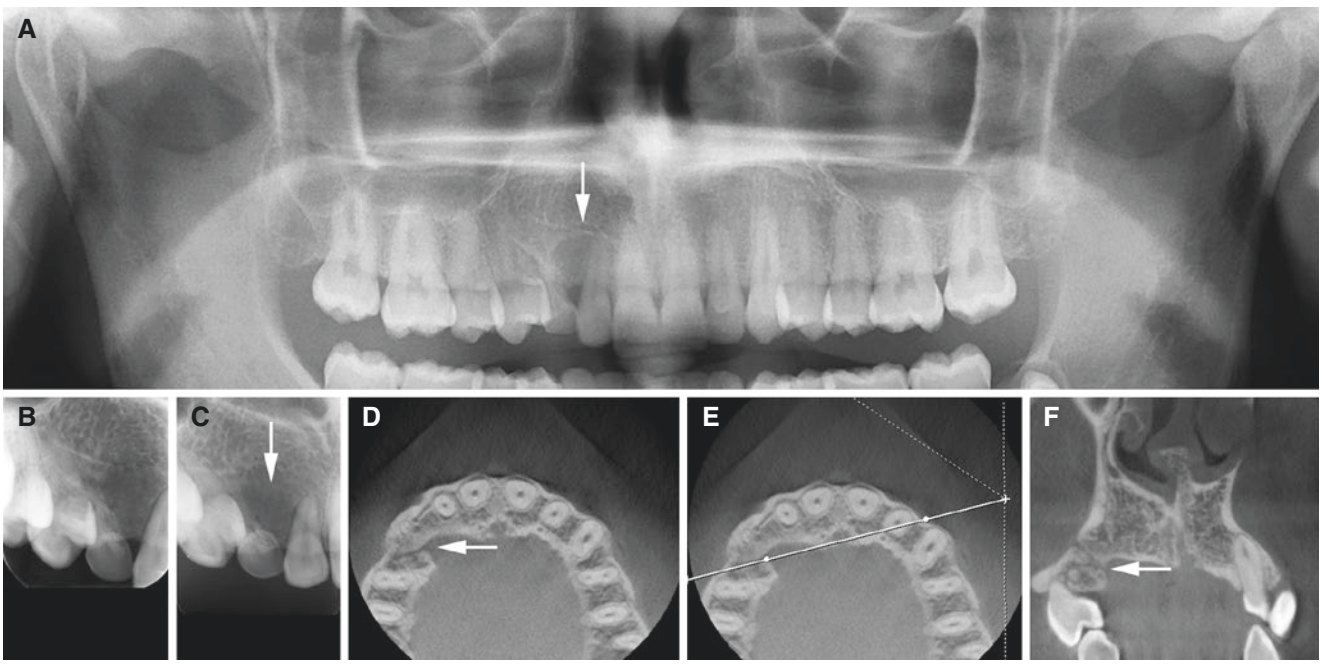

Fig. 15.70 Pre-implant imaging, maxilla; 19-year-old female with impacted right canine surgically removed about 10 months earlier. (**A**) Panoramic and (**B**, **C**) intraoral views indicate less mineralized bone at planned implant site (*arrow*). (**D**) Axial, (**E**) axial (with cursor line), and (**F**) oblique coronal CBCT images show lack of bone on the palatal side and narrow defect through alveolar ridge (*arrow*), not shown in panoramic or intraoral views

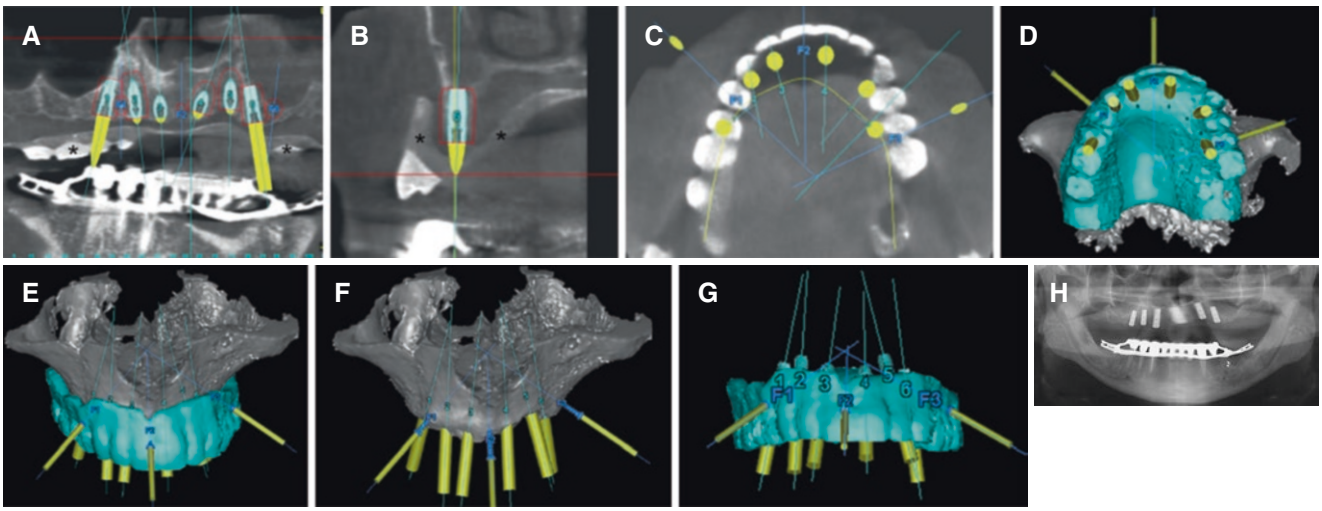

Fig. 15.71 Presurgical planning (3D simulation) of implants (**A**–**G**) and immediate postoperative result (**H**), maxilla; 73-year-old male with edentulous upper jaw. Scanned with temporary denture in place, (**A**) panoramic, (**B**) coronal, and (**C**) axial CBCT images visualize intended implant sites in the maxilla, related to the denture (*asterisks*). (**D**, **E**, **F**, **G**) Temporary denture used as an imaging/surgical guide for implant placement. (**H**) Postoperative panoramic view shows placement of implants in accordance with intended sites; compare with (**A**) (**A**–**G**: courtesy of Dr. H. Skjerven, Oslo, Norway)

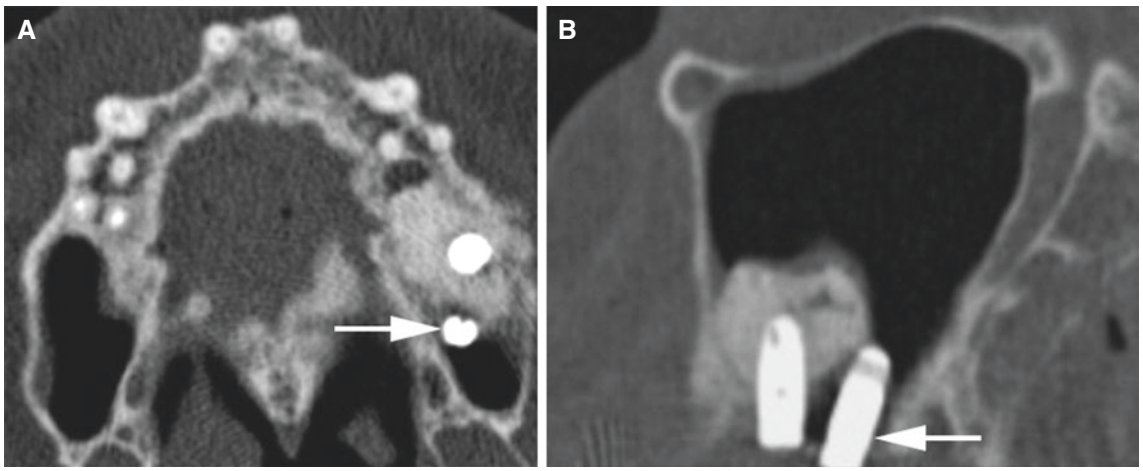

Fig. 15.72 Postoperative imaging, maxilla; 63-year-old male with sinus lift and bone graft. (**A**) Axial and (**B**) sagittal CBCT images show one implant correctly inserted in graft, whereas the other (*arrow*) is not

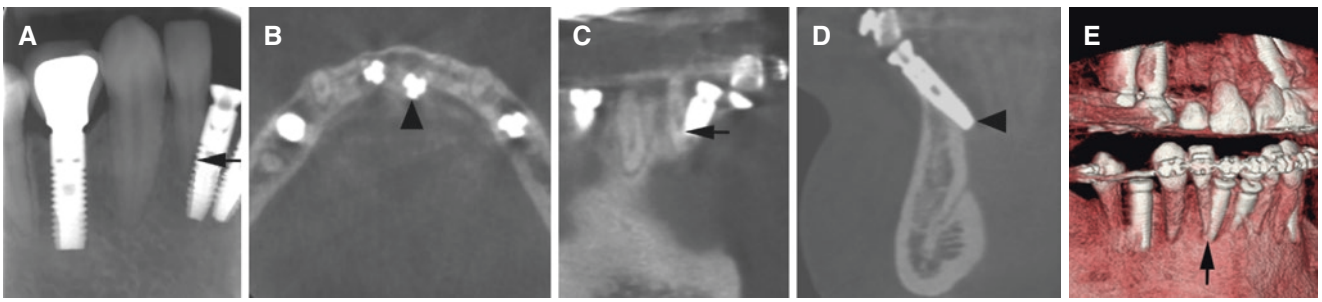

Fig. 15.73 Postoperative imaging, mandible; hard swelling (implant) palpated lingually. (**A**) Intraoral view shows implant in intimate relationship to the neighboring tooth (*arrow*). (**B**) Axial, (**C**) coronal, (**D**) sagittal, and (**E**) 3D CBCT images show implant inserted into the neighboring tooth (*arrow*), penetrating cortical bone lingually (*arrowhead*)

15.9 Facial Traumas and Fractures

Figs. 15.74, 15.75, and 15.76

See Chap. 8

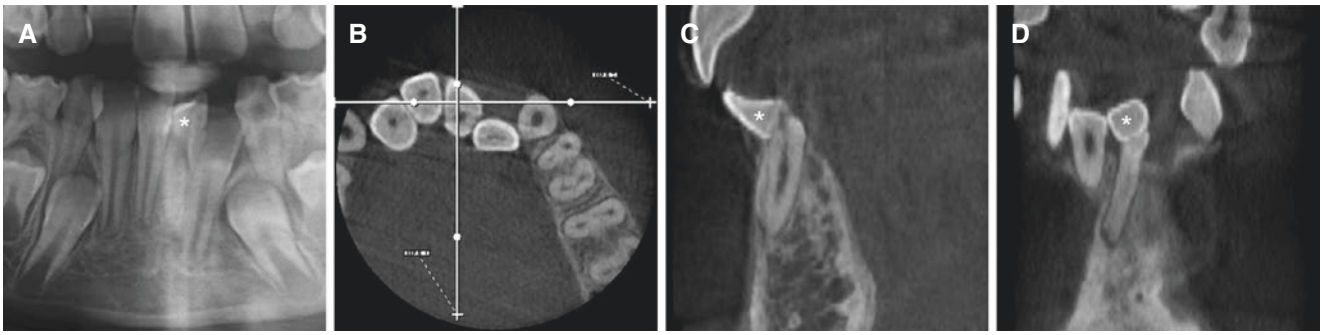

Fig. 15.74 Injured incisor, dilaceration, mandible; 8-year-old female with atypical left central incisor and previous trauma to the region. (**A**) Panoramic view shows atypical central incisor (*asterisk*). (**B**) Axial (with cursor lines), (**C**) sagittal, and (**D**) coronal CBCT images show crown (*asterisk*) displaced in relation to the root

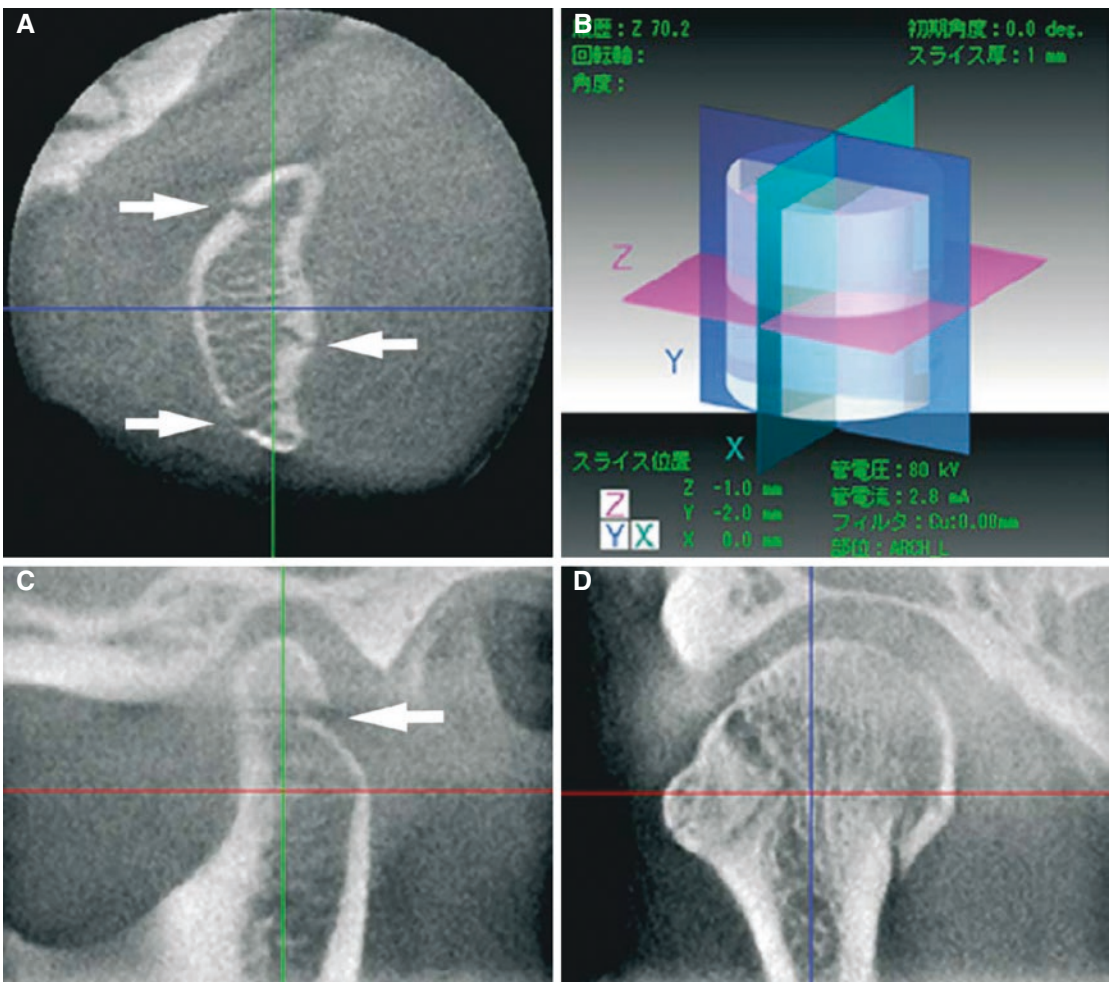

Fig. 15.75 Mandibular condyle fractures, intracapsular; 34-year-old male with pain after trauma to right TMJ. (**A**) Axial, (**C**) sagittal, and (**D**) coronal CBCT images show fracture lines but minimal displacement of fragments (*arrows*). (**B**) Three image planes indicated by different colors (courtesy of Dr K. Honda, Nihon University School of Dentistry, Tokyo, Japan)

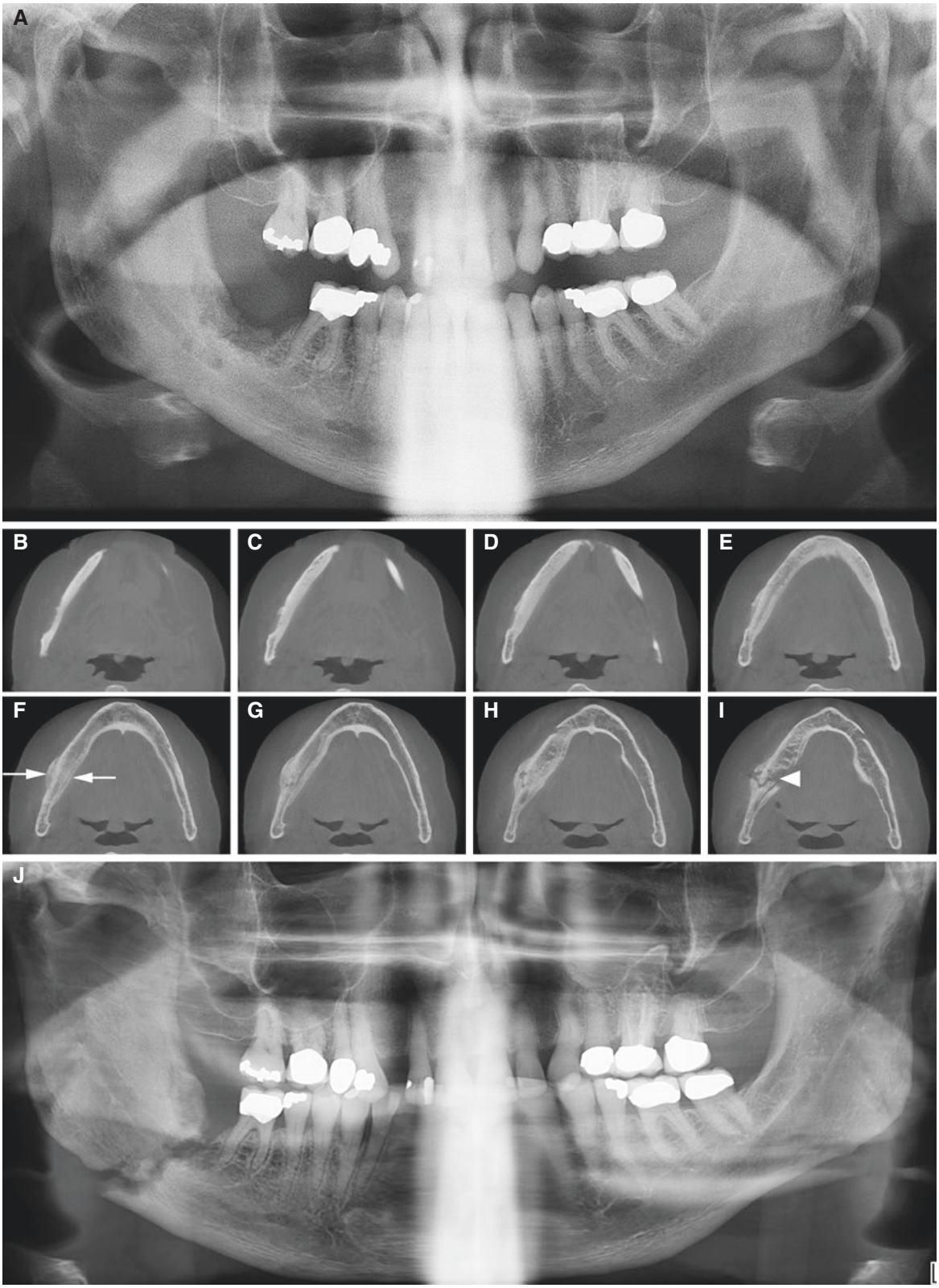

Fig. 15.76 Mandibular fracture (pathologic); 73-year-old male on antiresorptive treatment with mandibular osteonecrosis. (**A**) Panoramic view shows destruction and sclerosis in the right mandible. (**B**, **C**, **D**, **E**, **F**, **G**, **H**, **I**) Axial CBCT images confirm destruction and sclerosis and additionally show periosteal bone apposition buccally and lingually (*arrows*) and fracture line through the mandible (*arrowhead*) above level of the mental foramen. (**J**) Panoramic view 6 months later shows fracture throughout the mandible with displaced bone fragments due to unfavorable fracture line

15.10 Facial Growth Disturbances

Fig. 15.77

See Chap. 9

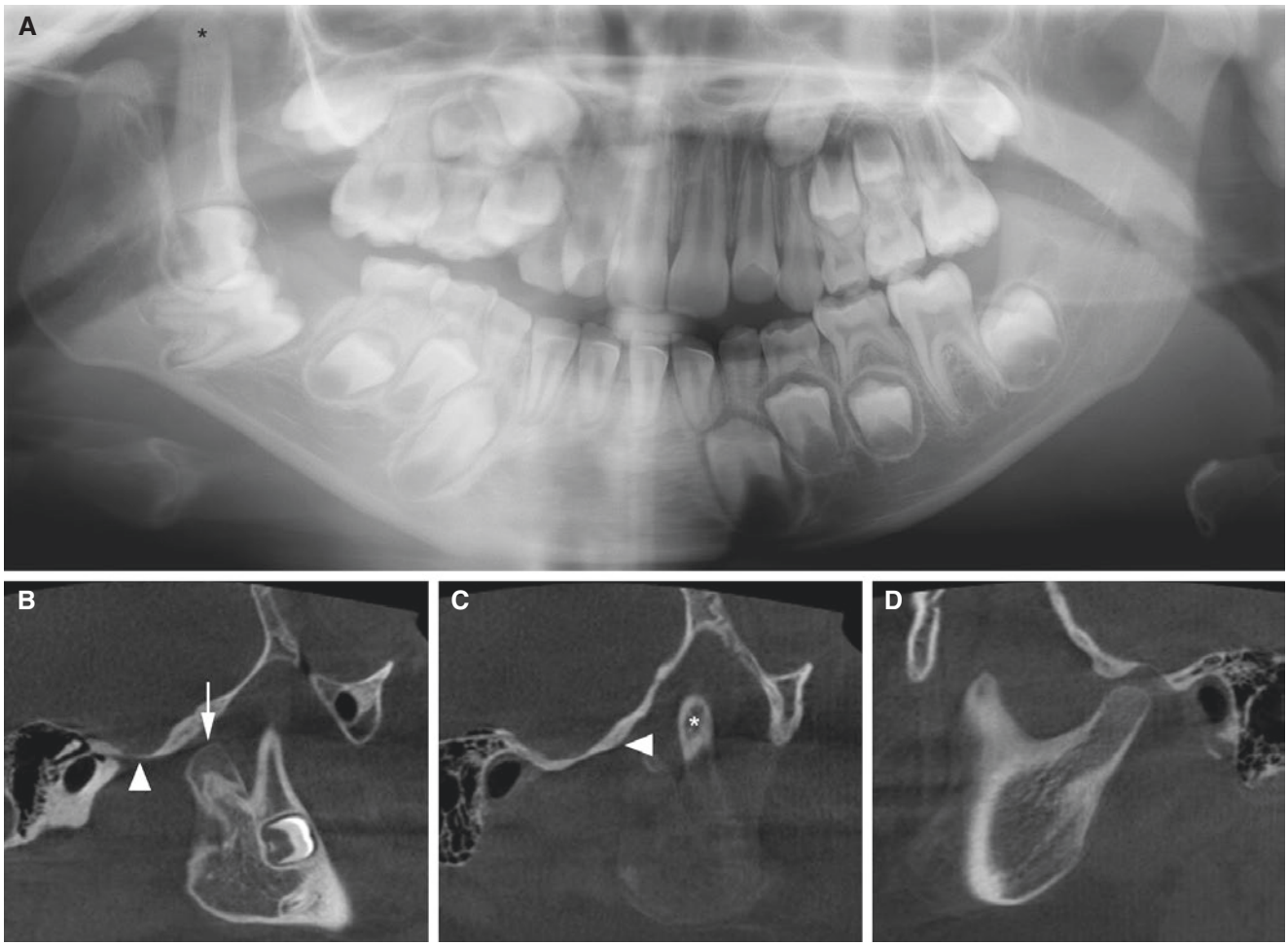

Fig. 15.77 Facial asymmetry; 7-year-old male with underdeveloped right mandible and impaired mouth-opening capacity with deviation on opening (probably due to neonatal fracture(s); use of forceps during delivery). (**A**) Panoramic view shows underdeveloped right mandible with short condylar process and enlarged coronoid process (*asterisk*) and the characteristic appearance of a partly opened pair of scissors. Note impacted first molar. (**B**) Oblique sagittal CBCT image (at closed mouth) shows abnormal condylar process (*arrow*) located anterior to flat (underdeveloped) articular eminence (*arrowhead*). (**C**) Oblique sagittal CBCT image (lateral to **B**) shows enlarged coronoid process (*asterisk*) and flat eminence/fossa (*arrowhead*). (**D**) Oblique sagittal CBCT image (at closed mouth) shows normal contralateral joint. Note in particular the well-developed fossa/eminence

15.11 Paranasal Sinuses

Figs. 15.78 and 15.79

See Chap. 10

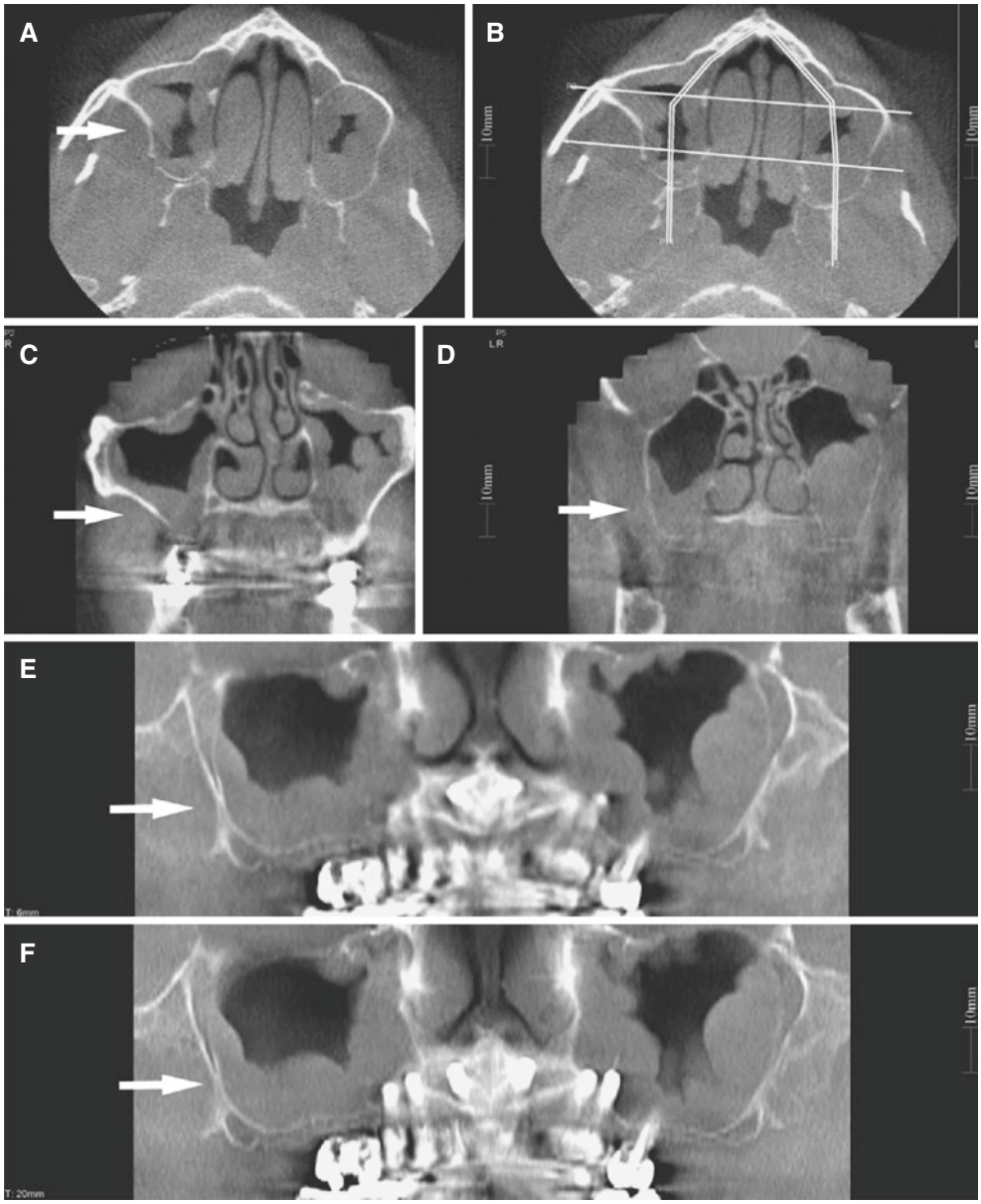

Fig. 15.78 Mucosal maxillary thickening; 43-year-old male under dental implant treatment with incidental finding. (**A**) Axial, (**B**) axial (with cursor lines), (**C**, **D**) coronal, and (**E**, **F**) panoramic CBCT images show maxillary mucosal thickening bilaterally (*arrow*) (courtesy of Drs. S. C. White and S. T. Tetradis, UCLA School of Dentistry)

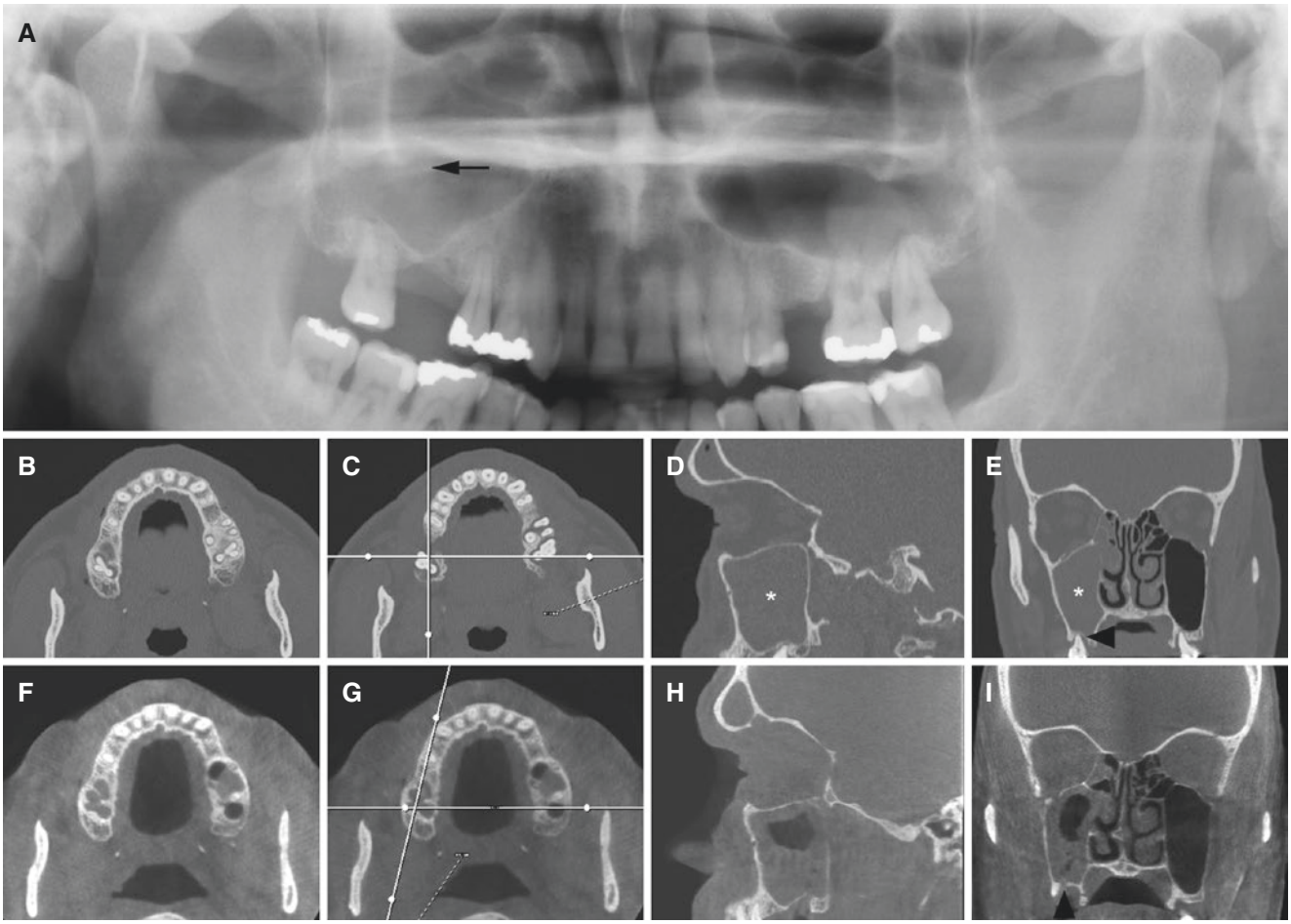

Fig. 15.79 Odontogenic sinusitis; 53-year-old male with pain from loose molar in the right upper jaw. (**A**) Panoramic view shows radiopacity of the right maxillary sinus (*arrow*) and remaining molar with lack of periodontal bone support. (**B**) Axial, (**C**) axial (with cursor lines), (**D**) sagittal, and (**E**) coronal MDCT images show radiopacity in the entire right maxillary sinus (*asterisk*), radiopacity in almost the entire ethmoid and frontal sinuses, and remaining molar with apical and periodontal bone destruction (*arrowhead*). After extraction of the molar and plenty of pus evacuated from the maxillary sinus, (**F**) axial, (**G**) axial (with cursor lines), (**H**) oblique sagittal, and (**I**) coronal CBCT images show less radiopacity and some air and communication between maxillary sinus and tooth socket (*arrowhead*)

15.12 Maxillofacial Soft Tissues

Fig. 15.80

See Chap. 11

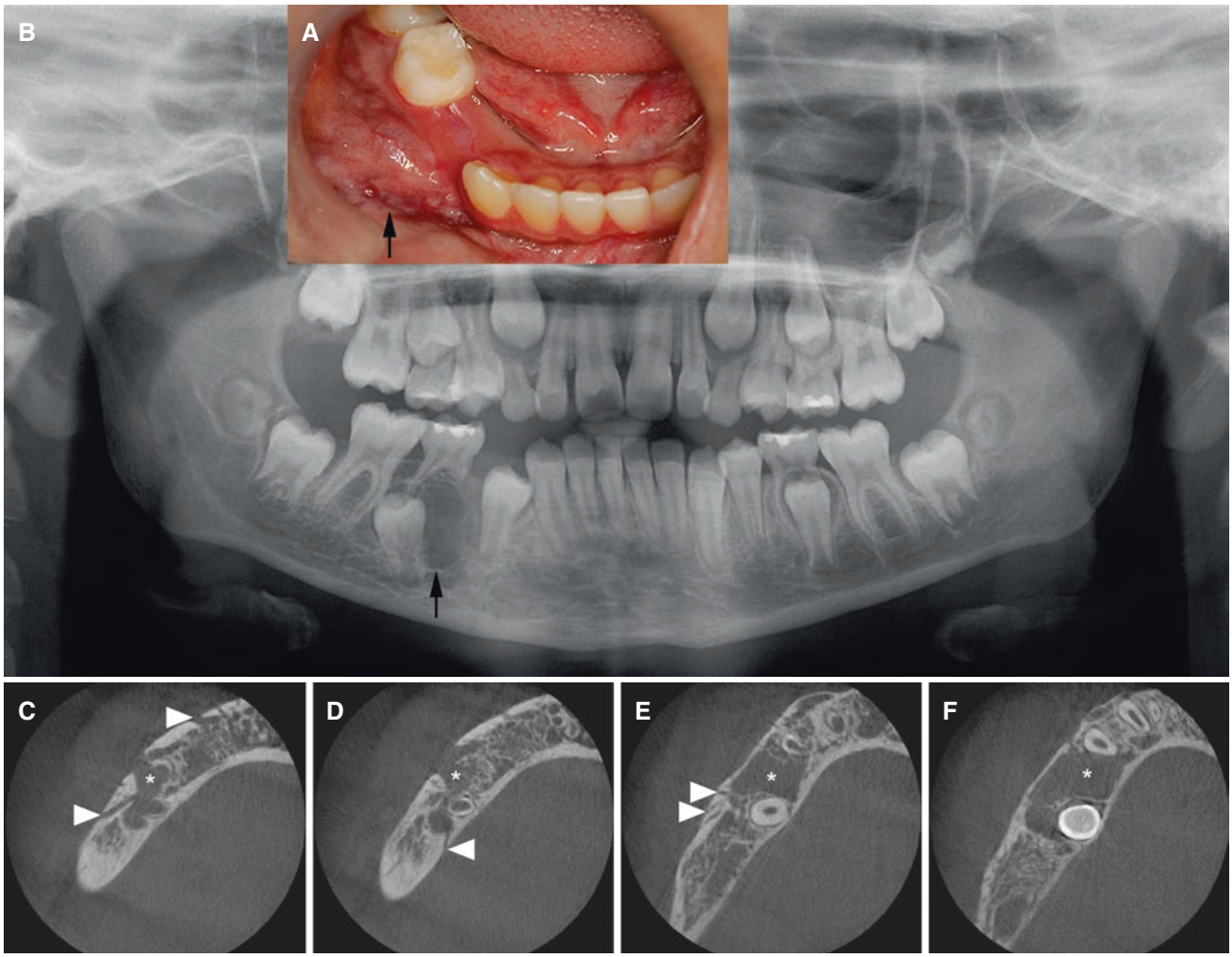

Fig. 15.80 Vascular malformation, mandible; 11-year-old female with swelling in the right mandible and occasional bleeding from gingiva. (**A**) Clinical photograph shows perimandibular swelling with red and bluish oral mucosa (*arrow*). (**B**) Panoramic view shows rather well-defined radiolucency, partially corticated (*arrow*). (**C**, **D**, **E**, **F**) Axial CBCT images show canal-like defects in the mandibular cortex (*arrowheads*), bone destruction (*asterisk*) with destroyed or thinned cortical outline, and no buccolingual expansion. Small-field CBCT volume does not cover the entire area of bone abnormalities; for supplementary examinations and diagnostic information of this patient, see Fig. 11.15

15.13 Salivary Glands

Fig. 15.81

See Chap. 12

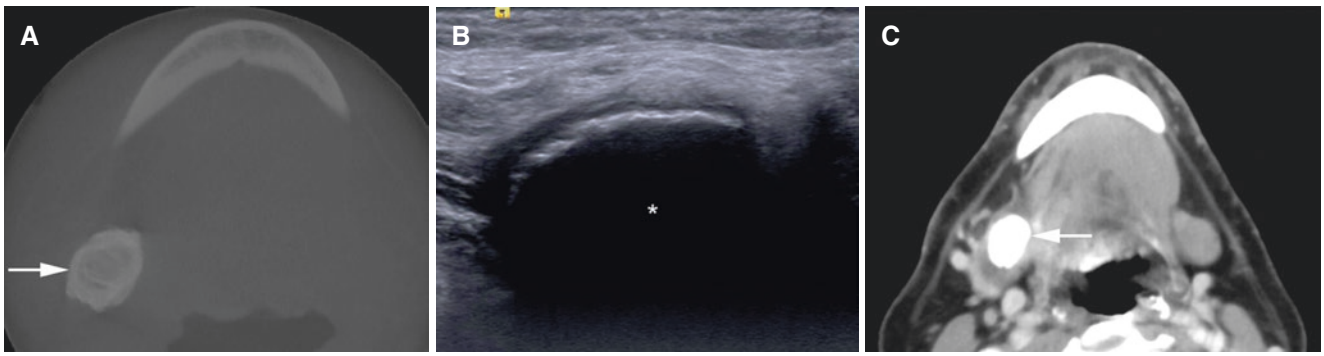

Fig. 15.81 Sialolithiasis, submandibular gland; 69-year-old male with minimal symptoms. (**A**) Axial CBCT image shows calcified structure (*arrow*) in submandibular area. (**B**) Corresponding US image shows total reflection with posterior acoustic shadowing (backshadow) (*asterisk*) suggesting a calcified structure within the right submandibular gland. (**C**) Axial contrast-enhanced CT image confirms intraglandular location of the calcified structure (*arrow*) (courtesy of Dr. Lennart Flygare, Umeå University Hospital, Umeå, Sweden)

Suggested Reading

Abdolali F, Zoroofi RA, Otake Y, Sato Y (2016) Automatic segmentation of maxillofacial cysts in cone beam CT images. Comput Biol Med 72:108–119

Al-Saleh MA, Alsufyani NA, Saltaji H, Jaremko JL, Major PW (2016) MRI and CBCT image registration of temporomandibular joint: a systematic review. J Otolaryngol Head Neck Surg 45:30. doi:10.1186/s40463-016-0144-4

Arai Y, Tammisalo E, Iwai K, Hashimoto K, Shinoda K (1999) Development of a compact tomographic apparatus for dental use. Dentomaxillofac Radiol 28:245–248

Araki K, Maki K, Seki K, Sakamaki K, Harata Y, Sakaino R, Okano T, Seo K (2004) Characteristics of a newly developed dentomaxillofacial X-ray cone beam CT scanner (CB MercuRay): system configuration and physical properties. Dentomaxillofac Radiol 33:51–59

Baba R, Ueda K, Okabe M (2004) Using a flat-panel detector in high resolution cone beam CT for dental imaging. Dentomaxillofac Radiol 33:285–290

Brüllmann D, Schulze RKW (2015) CBCT special issue: review article. Spatial resolution in CBCT machines for dental/maxillofacial applications—what do we know today? Dentomaxillofac Radiol 44:20140204

Danforth RA, Peck J, Hall P (2003) Cone beam volume tomography: an imaging option for diagnosis of complex mandibular third molar anatomical relationships. J Calif Dent Assoc 31:847–852

Frenkel B, Givol N, Shoshani Y (2015) Coronectomy of the mandibular third molar: a retrospective study of 185 procedures and the decision to repeat the coronectomy in cases of failure. J Oral Maxillofac Surg 73:587–594

Hamada Y, Kondoh T, Noguchi K, Iino M, Isono H, Ishii H, Mishima A, Kobayashi K, Seto K (2005) Application of limited cone beam computed tomography to clinical assessment of alveolar bone grafting: a preliminary report. Cleft Palate Craniofac J 42:128–137

Hashimoto K, Arai Y, Iwai K, Araki M, Kawashima S, Terakado M (2003) A comparison of a new limited cone beam computed tomography machine for dental use with multidetector row helical CT machine. Oral Surg Oral Med Oral Pathol Oral Radiol Endod 95:371–377

Honda K, Larheim TA, Johannessen S, Arai Y, Shinoda K, Westesson P-L (2001) Ortho cubic super-high resolution computed tomography: a new radiographic technique with application to the temporomandibular joint. Oral Surg Oral Med Oral Pathol Oral Radiol Endod 91:239–243

Horner K, O'Malley L, Taylor K, Glenny A-M (2015) CBCT special issue: review article. Guidelines for clinical use of CBCT: a review. Dentomaxillofac Radiol 44:20140225

Ikeda R, Oberoi S, Wiley DF, Woodhouse C, Tallman M, Tun WW et al (2016) Novel 3-dimensional analysis to evaluate temporomandibular joint space and shape. Am J Orthod Dentofacial Orthop 149:416–428

Kadesjö N, Benchimol D, Falahat B, Näsström K, Shi X-Q (2015) Evaluation of the effective dose of cone beam CT and multislice CT for temporomandibular joint examinations at optimized exposure levels. Dentomaxillofac Radiol 44:20150041

Kapila SD, Nervina JM (2015) CBCT special issue: review article. CBCT in orthodontics: assessment of treatment outcomes and indications for its use. Dentomaxillofac Radiol 44:20140282

Kobayashi K, Shimoda S, Nakagawa Y, Yamamoto A (2004) Accuracy in measurement of distance using limited conebeam computerized tomography. Int J Oral Maxillofac Implants 19:228–231

Kula K, Hale LN, Ghoneima A, Tholpady S, Starbuck JM (2016) Conebeam computed tomography analysis of mucosal thickening in unilateral cleft lip and palate maxillary sinuses. Cleft Palate Craniofac J 53:640–648

Larheim TA, Abrahamsson A-K, Kristensen M, Arvidsson LZ (2015) CBCT special issue: review article. Temporomandibular joint diagnostics using CBCT. Dentomaxillofac Radiol 44:20140235

Ludlow JB, Timothy R, Walker C, Hunter R, Benavides E, Samuelson DB, Scheske MJ (2015) CBCT special issue: review article. Effective dose of dental CBCT—a meta analysis of published data and additional data for nine CBCT units. Dentomaxillofac Radiol 44:20140197

Malek M, Cortes LM, Sigurdsson A, Rosenberg PA (2015) Differential diagnosis of a periapical radiolucent lesion. A case report and review of the literature. NY State Dent J 81:52–56

Martin A, Perinetti G, Costantinides F, Maglione M (2015) Coronectomy as a surgical approach to impacted mandibular third molars: a systematic review. Head Face Med 11:9. doi:10.1186/s13005-015-0068-7

Matzen LH, Wenzel A (2015) CBCT special issue: review article. Efficacy of CBCT for assessment of impacted mandibular third molars: a review—based on a hierarchical model of evidence. Dentomaxillofac Radiol 44:20140189

MacDonald D (2016) Lesions of the jaws presenting as radiolucencies on cone-beam CT. Clin Radiol 71:972–985

Meazzini MC, Brusati R, Caprioglio A, Diner P, Garattini G, Gianni E et al (2011) True hemifacial microsomia and hemimandibular hypoplasia with condylar-coronoid collapse: diagnostic and prognostic differences. Am J Orthod Dentofacial Orthop 139:e435–e447

Miloglu Ô, Sekerci AE, Yasa Y, Dagistan S (2015) Unilateral bone cavities situated near the angle of the mandibula. J Craniofac Surg 26:e27–e28. doi:10.1097/SCS.0000000000001262

Mozzo P, Procacci C, Tacconi A, Martini PT, Andreis IA (1998) A new volumetric CT machine for dental imaging based on the cone- beam technique: preliminary results. Eur Radiol 8:1558–1564

Pauwels R, Araki K, Siewerdsen JH, Thongvigitmanee SS (2015a) CBCT special issue: review article. Technical aspects of dental CBCT: state of the art. Dentomaxillofac Radiol 44:20140224

Pauwels R, Jacobs R, Singer SR, Mupparapu M (2015b) CBCT special issue: review article. CBCT-based bone quality assessment: are Hounsfield units applicable? Dentomaxillofac Radiol 44: 20140238

Perschbacher S (2014) Temporomandibular joint abnormalities. In: White SC, Pharoah MJ (eds) Oral Radiology. Principles and Interpretation, 7th edn. Mosby, St. Louis, pp 492–523

Roman R, Hedeşiu M, Fildan F, Ileşan R, Mitea D, Dinu C, Băciut M (2016) The use of reformatted cone beam CT images in assessing mid-face trauma, with a focus on the orbital floor fractures. Clujul Med 89:519–524

Salemi F, Shokri A, Maleki FH, Farhadian M, Dashti G, Ostovarrad F, Ranjzad H (2016) Effect of field of view on detection of condyle bone defects using cone beam computed tomography. J Craniofac Surg 27:644–648

Skjelde Karlsen G, Galdal Hansen J (2006) Fristad I (2006) Dens invaginatus—en oversikt (English summary). Nor Tannlegeforen Tid 116:218–222

Tkaczuk AT, Bhatti M, Caccamese JF Jr, Ord RA, Pereira KD (2015) Cystic lesions of the jaw in children: a 15-year experience. JAMA Otolaryngol Head Neck Surg 141:834–839

Vallaeys K, Kacem A, Legoux H, Le Tenier M, Hamitouche C, Arbab-Chirani R (2015) 3D dento-maxillary osteolytic lesion and active contour segmentation pilot study in CBCT: semi-automatic vs manual methods. Dentomaxillofac Radiol 44:20150079

Index

A
Abscess, 179
  in cheek, 211
  hypopharynx, 462
  intracranial, mastoiditis with, 476–477
  jaw infections, 209–211
  maxillofacial soft tissues, 385–386
  parapharyngeal, 210, 211
  parenchymal, 476
  submandibular, 209
  thyroid, 462–463
Absolute alcohol, 509, 510
Achondroplasia, 339–341
Acinic cell carcinomas, 440
Acrocephalosyndactyly types, 338
Acute leukemias, 155
Acute rhinosinusitis, 349–351
Adenocarcinoma, 441–442
Adenoidal tissue (nasopharyngeal tonsil), 4
Adenoid cystic carcinoma
  malignant tumors in jaws, 141–144
  mandible, 142–143
  maxilla, 144
  maxillofacial soft tissues, 409
  salivary glands, 442–443
Adipose tumor. *See* Lipoma
African jaw lymphoma, 145
AIDS, 428
Alcohol, 509, 510
Allergic sinusitis, 352
Alveolar process, 279
Alveolar recess of maxillary sinus, 4, 8
Ameloblastoma
  desmoplastic type, 71, 81–83
  extraosseous, 83
  mandible, 83
  recurrence, 84–86
  solid/multicystic type, 72–74, 76, 84
    mandible, 72–77
    maxilla, 72
  unicystic type, 71, 77–79
Aneurysmal bone cavity, 99–102
Aneurysmal bone cyst, 99–102
Ankyloses, 247–250
Ankylosing spondylitis, 238
Anterior band of articular disc, 17–21
Anterior belly of digastric muscle, 4
Anterior bite opening, 237
Anterior disc displacement
  and bone marrow edema, 221
  with joint effusion, 220
  with lateral disc displacement, 216without lateral disc displacement, 216
Anterior fontanelle, 1, 2
Anterior nasal spine, 1–4, 8
Anterolateral fontanelle, 1–3
Antiresorptive therapy-related osteonecrosis., 198–208
Apert syndrome, 338
Apical periodontal cyst. *See* Periapical cyst
Apical periodontitis, 179, 277
Arthritides, 239–244
Arthrosis deformans juveniles, 224, 253
Articular disc, 17, 18
Articular tubercle (eminence), 17, 18, 20
Artificial bone chips, 283
Atrophy
  maxillofacial soft tissues, 387–390
  medial and lateral pterygoid muscles, 409
  muscles, 405
  parenchyma, 417
Autopsy specimen, 215, 217, 219, 238
Avascular necrosis, 234
Axial T1-and T2-weighted MRI, normal anatomy of face, 14–15

B
Bacterial infection
  meningitis, 380
  recurrent, 413
  rhinosinusitis, 349
  sinusitis, 349
Ballooning, 99, 502, 504
B-cell lymphoma
  mandible, 148–149
  maxilla, 146–148
Benign jaw tumors and tumorlike conditions
  Ewing sarcoma, 528
  fibro-osseous lesion, 522
  fibrous dysplasia, 528
  focal osseous dysplasia, 522
  idiopathic osteosclerosis, 523, 528
  keratocystic odontogenic tumor, 528
  odontoma, 525–527
  osteoma, 527
  torus palatinus, 524
Benign lymphoepithelial cysts associated with HIV–AIDS, 428
Benign tumor
  jaws
    ameloblastoma, 71–86
    juvenile ossifying fibroma, 98–99
    keratocystic odontogenic tumor, 57–70
    lipoma, 87

T.A. Larheim, P.-L.A. Westesson, *Maxillofacial Imaging*, https://doi.org/10.1007/978-3-319-53319-3

Benign tumor (*cont.*)
odontogenic fibroma (central), 87–88
odontogenic myxofibroma, 88–89
odontogenic myxoma, 88–89
ossifying fibroma, 92–977
osteoblastoma, 90–92
maxillofacial soft tissues, 385, 387
temporomandibular joint
osteochondroma, 263–264
osteoma, 261
sphenoid meningioma, 262
Benign tumor-like conditions
aneurysmal bone cyst, 99–102
central giant cell granuloma, 103–106
cherubism, 108–110
exostoses, 121–123
fibrous dysplasia, 111–114
idiopathic osteosclerosis, 124–125
Langerhans cell histiocytosis, 106–107
odontoma, 126
osseous dysplasias, 115–118
osteoma, 118–121
Bifid condyle, 254
Biopsy
clinical features, 506
definition, 506
imaging features, 506
mass around mandibular ramus, bone, 508
orbital mass, 508
parapharyngeal mass, 506–507
Bisphosphonate-related necrosis, 198–208
Blowout fracture
classic, 310
definition, 310
extensive, 311
medial, 311
Bone cyst
jaws cysts, 520
simple, 520
Stafne, 521
Bone graft from chin, 283, 284
Bone marrow
abnormalities, 234–237
biopsies, 21
edema, 217, 224, 229, 234
sclerosis, 224
Bony ankylosis, 250
Buccal bifurcation cyst. *See* Paradental (mandibular infected buccal) cyst
Buccal space fat, 4
Buccinator muscle, 4
Burkitt's lymphoma, 145, 151, 473

C
Café-au-lait spots, 111
Calcifications
amorphous, 448
maxillofacial soft tissues
carotid artery, 396
lingual tonsil, 396
palatine tonsil, 395
retropharyngeal tendinitis, 96
Calcific tendinitis longus colli, 448
Calcium pyrophosphate dehydrate crystal deposition disease (pseudogout), 255
Canine
maxilla, 543
with root resorption, 547
Carcinoma
epidermoid, 129–136
mucoepidermoid, 137–140
mandible, 138–139
maxilla, 140
nevoid basal cell, syndrome, 57
primary intraosseous, 130
salivary glands
acinic cell, 440
mucoepidermoid, 439
squamous cell, 129–136
Carotid
aneurysm, 482
artery, 512
artery calcification, 392
bifurcation, 392
canal, 4, 8
sheath, 405
Castleman's disease, 473–474
Cat scratch disease, 473
Cellulitis, 209
Cementifying fibroma. *See* Ossifying fibroma
Cemento-ossifying fibroma. *See* Ossifying fibroma
Central odontogenic fibroma, 87–88
Cervical spine, 471
cord astrocytoma, 457
fracture, 462
meningioma, 459–460
neurofibromatosis type 1 (NF-1), 461
teratoma, 456
Cherubism, 108–110, 318–319
Chiari malformation, 453–454
Choanae, 1, 2
Choanal atresia, 316–317
Chondrocalcinosis, 255
Chondrosarcoma, 164–165, 530
Chordoma, 454–456
Chronic leukemias, 155
Chronic sinusitis, 352–354
Clear-cell carcinoma, 408
Cleft palate and/or cleft lip, 313–316
Clivus, 4, 8
Common cold, 349, 350
Compound type, 126
Concha bullosa, 4, 6
Condylar hyperplasia, 251, 252, 317–318
Condylar hypoplasia, 253
Condylar translation, 218, 221, 222, 229, 230, 232, 238
Condyle
deformed, 241
destruction, 240
fractures, 291
Cone beam
CT examination, 279
CT sections, 10–11
3D CT, 4
Cone beam computed tomography (CBCT), 515
Conventional/classic intraosseous ameloblastoma, 71
Cord compression, extramedullary cervical lipoma with, 458
Coronal suture, 1–3
Coronoid hyperplasia, 265
Coronoid process, 1–4, 8
Craniocervical junction

chordoma, 454–455
rheumatoid pannus, 451
tuberculosis, 452
Craniofacial dysostoses, 336
Craniofacial fibrous dysplasia, 111–114
Craniopharyngioma, 483, 484
Crista galli, 4, 6
Crouzon syndrome, 336–337
CSF leakage, 380
CT sections
bone structures, 6–9
soft tissue structures, 12–13
Cyst, 179
follicular, 37–43
glandular odontogenic, 44
hemorrhagic, 45–51
hemorrhagic bone, 45–51
incisive canal, 36–37
jaws
bone cyst, 520
and cyst-like conditions, 516–521
follicular, 518–519
lateral periodontal, 520
paradental, 518
periapical, 517
possible follicular, 519
radicular, 516
lateral periodontal, 35–36
mandible, 36
maxilla, 35
mandibular infected buccal, 30–34
maxillofacial soft tissues
clinical features, 399
definition, 399
dermoid cyst, 401
imaging features, 399
thyroglossal duct cyst, 400
nasopalatine duct, 36–37
paradental, 30–34
periapical, 24–29
mandible, 24
maxilla, 25–29
residual, 29
retention, 54–55
simple bone, 45–51
simple (traumatic) bone, 256
solitary bone, 45–51
Stafne bone, 52–53
synovial, 256
traumatic bone, 45–51
unicameral bone, 45–51
Cyst-like conditions
retention cyst, 54–55
simple bone cyst, 45–51
Stafne bone cyst, 52–53

D

Dacryocystocele, nasolacrimal duct, 488, 490
Degenerative joint disease. *See* Osteoarthritis
Dehiscence, 387–390
Dens axis, 4
Dense bone island, 124–125
Dental anomalies/malformations, 544, 549. *See also* Teeth and dental implants
Dental caries, 179
Dental cyst. *See* Periapical cyst
Dental implant
complications, 285, 286
preoperative implant imaging, 279
surgery, 279
DentaScan, 283
program, 279
reconstructions, 278
Dentigerous cyst. *See* Follicular cyst
Dermoid, 464–465, 488, 490
Developmental salivary gland defect. *See* Stafne bone cyst
Dilaceration, 555
Disc displacement, 216, 240
anterior, 216, 217, 220, 221
lateral, 216, 218, 219
medial, 216, 219
non-reducing disc displacement, 223, 232, 233
partial, 218, 222
posterior, 216, 219
pure lateral, 216
reducing disc displacement, 223
Double tooth
mandible, 550
maxilla, 549
Down syndromes, 327–328

E

Ectodermal dysplasia, 343
Effusion, 217
Enamel evagination, 550
Enostosis, 124
Eosinophilic granuloma. *See* Langerhans cell, histiocytosis
Epidermoid carcinoma. *See* Squamous cell carcinoma
Epiglottis, 4
Epithelium-lined cavity, 23
Eruption cyst, 37
Erythroplakia, 130
Ethmoid adenocarcinoma, 371
Ethmoid sinus, 4, 6, 8
foreign body, 380
Eustachian tube, 4
Ewing sarcoma, 166–167
benign jaw tumors and tumorlike conditions, 528
paranasal sinuses, 374
Exostoses, 121–123. *See also* Osteoma
multiple exostoses, 123
Expansile odontogenic conditions, 377–379
External auditory canal, 1–4
External carotid artery, 4
External jugular vein, 4
Extramedullary cervical lipoma with cord compression, 458
Extranodal involvement, 145

F

Facial asymmetry, 557
Facial growth disturbances
absent zygomatic arch, 345
achondroplasia, 339–341
Apert syndrome, 338
cherubism, 318–319
choanal atresia, 316–317
common cleft palate and/or cleft lip, 313–316
condylar hyperplasia, 317–318
Crouzon syndrome, 336–337

Facial growth disturbances (*cont.*)
Down syndromes, 327–328
ectodermal dysplasia, 343
fibrous dysplasia, 319–321
Goldenhar oculoauriculovertebral spectrum, 331
Goldenhar syndrome, 331
hemifacial microsomia, 332–334
isolated disturbances, 313–316
juvenile idiopathic (rheumatoid/chronic) arthritis, 325–326
mandibular neck/TMJ fracture/TMJ infection complication, 321–324
micrognathia, 344, 346
non-synostotic occipital plagiocephaly, 329–330
premature cranial synostoses, 328–329
pyknodysostosis, 342
syndromes, 327–328
syndromic craniosynostoses (craniofacial dysostoses), 336
synovialdisease, 328
TMJ internal derangement complication, 325
tori mandibularis, 317
tori maxillaris, 317
tori palatinus, 317
Treacher Collins syndrome (mandibulofacial dysostosis), 334–336
Turner syndrome, 330–331
Facial hemangioma embolization, 509, 510
Facial traumas and fractures, 555–556
injured incisor, dilaceration, 555
mandibular condyle fractures, 555
mandibular fracture, 555
Facial vein, 4
Familiar fibrous dysplasia, 108–110
Fibroma
cementifying fibroma, 92–97
cemento-ossifying fibroma, 92–97
Fibro-osseous ankylosis, 237, 248
Fibro-osseous lesion, 522
Fibrous, adhesions, 224
Fibrous ankylosis, 247, 249
Fibrous dysplasia, 92, 111–114, 482, 491
benign jaw tumors and tumorlike conditions, 527
craniofacial, 320
facial growth disturbances, 319–321
mandible, 113
maxilla, 112, 114
maxilla and mandible, 111
monostotic, 111
paranasal sinuses, 368–369
polyostotic, 111
Fibrous posterior attachment (pseudodisc), 220
Fistula, 193
Flat fossa, 241
Floating teeth, 130
Florid osseous dysplasia, 115
mandible, 115
Focal cemento-osseous dysplasia. *See* Osseous dysplasias
Focal osseous dysplasia, 115
benign jaw tumors and tumorlike conditions, 522
mandible, 115, 126
Follicular cyst, 37–43
jaws, 528–530
mandible, 40–43
maxilla, 37–39
wisdom tooth, mandible, 271
Foramen
cecum, 551
magnum, 1–3
ovale, 4, 7
rotundum, 4, 7
Fossa of Rosenmüller (lateral pharyngeal fold), 4
Fracture
blowout, 310–311
condyle, 291
definition, 290
greenstick, 298
isolated maxillary sinus wall, 304
LeFort, 305, 308
LeFort 1, 305–306
LeFort 2, 305–306
LeFort 3, 305, 307
mandibular, 297–300
midfacial, 303
nasal, 291, 303
nasal aperture, 303
nasal pyramid, 303
symphyseal, 291
trimalar, 308–309
tripod, 308–309
zygomatic, 308–309
Frontal
bone, 1–4, 6, 8
process of maxilla, 4, 6, 8
sinus, 4, 6
Frontozygomatic suture, 1–3

G
Genial process of mandible, 4, 9
Genioglossus muscle, 4
Geniohyoid muscle, 4
Giant aneurysm of skull base, 482
Giant cell granuloma (central), 103–106
bilateral, mandible, 106
mandible, 104
maxilla, 105
Giant cell lesion, 103–106
Giant cell reparative granuloma, 103–106
Giant cell tumor, 103–106
Gigantiform cementoma, 115, 118
Gingival cancer, 130
Gingival mucosa, 135
Glandular odontogenic cyst, 44
Glenoid fossa, 1, 4, 7, 17–21, 256
Glomus vagale paraganglioma, 482–483
Goiter, 465
Goldenhar oculoauriculovertebral spectrum, 331
Goldenhar syndrome, 331
Gorlin–Goltz syndrome, 57, 68
Gout, 255
Granulation tissue, 191
Greater palatine
canal, 4, 6, 8
foramen, 4, 8
Greater wing of sphenoid bone, 4, 6
Greenstick fracture, 298
Ground-glass appearance, 90, 111
Growth disturbances (anomalies), 251–255

H
Hamartoma, 126
Hamulus of medial pterygoid plate, 4, 7
Hard palate, 1–4, 6, 8
Hemangioma, 493–494
neck, 466–467
salivary glands, 435–437

Hemifacial microsomia, 332–324
Hemorrhage intracranially, 300
Hemorrhagic bone cyst. *See* Simple bone cyst
Hemorrhagic cyst. *See* Simple bone cyst
Hodgkin's lymphoma, 145
Hybrid lesions, 99–102
Hyoglossus muscle, 4
Hyoid bone, 4, 7
Hyperbaric oxygenic treatment, 191
Hypercementosis, 549
Hypopharynx
  abscess, 462
  carcinoma, 471–472

I
Idiopathic bone cavity. *See* Simple bone cyst
Idiopathic histiocytosis. *See* Langerhans cell, histiocytosis
Idiopathic osteosclerosis, 124–125, 523, 528
Impacted third molar, 41–43
Incisive artery canal, 4
Incisive canal, 4, 6, 8
  cyst, 36–37
    maxilla, 36
Incisive foramen, 1, 2, 4, 8, 9
Infection/inflammation
  jaws
    osteitis, 532–533
    osteomyelitis, 531–534
    osteonecrosis, medication-related, 534
  maxillofacial soft tissues, 385–386
  salivary glands, 413–417
Inferior
  joint space, 17, 18
  meatus, 4, 6, 8
  orbital fissure, 4, 6, 8
  turbinate, 4, 6, 8
Inflammatory arthritis, 240–241
Inflammatory dental conditions, 364
Inflammatory diseases, 349
Inflammatory pannus, 240–241
Inflammatory paradental cyst. *See* Paradental (mandibular infected buccal) cyst
Infraorbital canal, 4, 8
Infraorbital foramen, 1, 3
Infratemporal fossa, 4
Interior head of lateral pterygoid muscle, 17, 18, 20
Intermediate (central) thin zone, 17–20
Internal carotid artery, 5
Internal derangements, with normal cortical bone, 215–224
Internal jugular vein, 5
Interventional maxillofacial radiology, 499
Intracranial abscess, mastoiditis with, 476–477
Intracranial empyema, sinusitis, 382–383
Intraosseous pseudocyst, 45
Inverted papilloma, 366
Involucrum, 180
Isolated maxillary sinus wall fracture, 304

J
Jaw
  cysts
    bone cyst, 520
    and cyst-like conditions, 516–521
    definition, 23
    follicular, 518–519
    follicular cyst, 37–43
    glandular odontogenic cyst, 44
    incisive canal cyst, 36–37
    lateral periodontal, 520
    lateral periodontal cyst, 35–36
    paradental, 518
    paradental (mandibular infected buccal) cyst, 30–34
    periapical, 517
    periapical cyst, 24–29
    possible follicular, 519
    radicular, 516
    residual cyst, 29
  infections
    abscess, 209–211
    medication-related osteonecrosis, 198–208
    osteitis, 532–533
    osteomyelitis, 179–185, 531–534
    osteomyelitis: with periostitis, 186–192
    osteonecrosis, medication-related, 534
    osteoradionecrosis, 193–197
  malignant tumors in
    chondrosarcoma, 530
    multiple myeloma, 529
    prostatic cancer metastasis, 530
  metastases, 171–176
  osteosarcoma, 157
Joint space reduction, 224
Juvenile aggressive osteoblastoma, 90
Juvenile angiofibroma embolization, 509, 512
Juvenile idiopathic arthritis, 241–247
  disc displacement, 245
  facial asymmetry, 242–243
  facial growth disturbances, 325–326
  micrognathia, 242
  temporomandibular joints, 538–539
Juvenile ossifying fibroma, 98–99
Juvenile osteoarthritis, 537

K
Keratin, 57
Keratoconjunctivitis sicca, 425
Keratocystic odontogenic tumor, 57–70
  benign jaw tumors and tumorlike conditions, 527
  mandible, 58–62, 66–69
  maxilla, 63–65, 68–70

L
Lacrimal
  bone, 5, 8
  sac fossa, 5, 6
Lambdoid suture, 1–3
Lamina, papyracea of ethmoid, 5, 6, 8
Langerhans cell
  disease, 106–107
  histiocytosis, 106–107, 480, 492
Lateral periodontal cyst, 35–36
  jaws, 520
  mandible, 36
  maxilla, 35
Lateral pterygoid muscle, 5
  raphe, 17, 18
Lateral pterygoid plate, 1–5, 7, 8
Lateral recess of sphenoid sinus, 5, 8
LeFort fracture, 305–308
  LeFort 1, 306, 308

LeFort fracture (*cont.*)
LeFort 2, 306, 308
LeFort 3, 306, 308
LeFort 1 osteotomies, 305
Leiomyosarcoma, 170
Lesser palatine canal, 5, 8
Leukemia, 155–156
lymphoblastic, 495, 497
mandible and maxilla, 156
Leukoplakia, 130
Levator labii superioris muscle, 5
Lingual mandibular bone depression. *See* Stafne bone cyst
Lingual salivary gland depression. *See* Stafne bone cyst
Lingual septum, 5
Lingual thyroid, 402, 403
Lipoma, 87
lower gingivobuccal sulcus, 404
neck, 468
Longus colli muscle, 5
Lymphadenopathy, 474–475
Lymph node metastasis, 407
Lymphoblastic leukemia, 495, 497
Lymphoma
maxillofacial soft tissues, 409, 410
oropharyngeal non-Hodgkin's, 410
paranasal sinuses, 373
parapharyngeal non-Hodgkin's, 410
salivary glands, 438

M
Major zygomatic muscle, 5
Malar bone, agenesia, 335
Malignancy of oral cavity, 129
Malignant epithelial neoplasm, 129
Malignant tumors
in jaws
adenoid cystic carcinoma, 141–144
chondrosarcoma, 164–165
Ewing sarcoma, 166–167
jaw metastases, 171–176
leiomyosarcoma, 170
leukemia, 155–156
mucoepidermoid carcinoma, 137–140
multiple myeloma, 152–154
non-Hodgkin's lymphoma, 145–151
osteosarcoma, 157–163
rhabdomyosarcoma, 168–169
squamous cell carcinoma, 129–136
maxillofacial soft tissues, 406, 407, 410
temporomandibular joint, 263–264
Mandibles, 1–6
alveolar bone, 5, 9
body fracture, comminuted, 296
canal, 5–7, 9
condyle fractures, 291, 297
coronoid process, 299
foramen, 5, 6, 9
fractures, 291–297
combined with other fractures, 297–300
complications, 301–302
and maxillary fractures, 300
neck fracture
bilateral, 295, 298, 299
maxillary alveolar process, 297, 298
maxillary sinus wall, 298
unilateral, 292, 293
zygomatic arch, 298
notch, 4, 5, 8
ramus, 4, 5, 7, 8
Mandibular condyle, 1–5, 7, 8
articulating surface, 17, 21
fractures, 291, 297, 555
head, 17–21
marrow, 17
Mandibular fracture, 556
Mandibular neck/TMJ fracture/TMJ infection complication, 321–324
Mandibular tooth, 5
crown pulp, 5, 9
root, 5, 9
root canal, 5, 9
tooth 1, central incisor, 5, 9
tooth 2, lateral incisor, 5, 9
tooth 3, canine, 5, 9
tooth 4, first premolar, 5, 9
tooth 5, second premolar, 4, 5, 9
tooth 6, first molar, 4, 5, 9
tooth 7, second molar, 4, 5, 9
tooth 8, third molar, 4, 5, 9
Mandibulofacial dysostosis, 334–336
Masseter muscle, 5
Masticator, 210
Mastoiditis
with intracranial abscess, 476–477
with sigmoid thrombosis, 478
Mastoid process, 5
Maxilla, 1–6
Maxillary
alveolar bone, 5, 8, 9
sinus, 5, 6, 8
tuberosity, 5, 8
Maxillary tooth, 5
crown pulp, 5, 9
root, 5, 8
root canal, 5, 9
1, central incisor, 5, 9
2, lateral incisor, 5, 9
3, canine, 5, 9
4, first premolar, 4, 5, 9
5, second premolar, 4, 5, 9
6, first molar, 4, 5, 9
7, second molar, 4, 5, 9
8, third molar, 4, 5
Maxillofacial imaging anatomy, 515
Maxillofacial soft tissues, 560
adenoid cystic carcinoma, 409
atrophy, 387–390
benign tumors, 404
calcifications, 387, 391–392
cysts, 399–401
dehiscence, 387–390
infection (abscess), 385–386
lingual thyroid, 402, 403
lymphoma, 409, 410
malignant tumors, 406, 407, 410
muscular hypertrophy, 387–390
schwannoma, 405
vascular malformations, 393–399
McCune–Albright syndrome, 111
Medial pterygoid

muscle, 5
plate, 1–5, 7, 8
Medial wall of maxillary sinus, 5, 8
Medication-related osteonecrosis
definition, 198
mandible, 198–205, 207, 208
maxilla, 206
Meningioma, 495, 496
cervical spine, 447–448
Mental foramen, 1–5, 9
Metastasis
anaplastic malignant meningioma, 175
breast cancer, 172–173
prostatic cancer, 174
thyroid cancer, 176
Metastatic disease to hypoglossal canal and clivus, 486–487
Metopic suture, 1, 2
Micrognathia, 325
facial growth disturbances, 344, 346
Middle meatus, 5, 6
Middle suture of hard palate, 5, 6, 8
Middle turbinate, 5, 6, 8
Midfacial fracture, 303
Moth-eaten bone destruction, 166
MRI and autopsy midcondyle anatomy of normal temporomandibular joint, 18
Mucoceles, paranasal sinuses
frontal sinus, 359–360
maxillary sinus, 362
sphenoid sinus, 361–362
Mucoepidermoid carcinoma, 137–140, 439
mandible, 138–139
maxilla, 140
Multiple exostoses, 123
Multiple myeloma, 152–154
jaws, malignant tumors, 529
Muscular hypertrophy, 387–390
Myeloma, 152–154
Myelomatosis. *See* Myeloma
Mylohyoid
line (ridge), 4, 5
muscle, 5

N

Nasal ala, 5
Nasal aperture fracture, 303
Nasal bone, 1, 2, 5, 6
Nasal cavity, airway, 5, 8
Nasal fractures, 291, 303
Nasal pyramid fracture, 303
Nasal septum, 5, 6, 8
Nasal vestibule, 5
Nasofrontal suture, 1, 2, 5, 6
Nasolabial (nasoalveolar) cyst, 370
Nasolacrimal canal, 5, 6, 8
Nasomaxillary suture, 1, 3
Nasopalatine duct cyst. *See* Incisive canal, cyst
Nasopharynx, 5, 8
Neck
hemangioma, 466–467
lesions, 462
lipoma, 468
plexiform neurofibroma, 468–469
Neurofibromatosis, 493
type 1 (NF-1), 460
type 2 (NF-2), 459
Nevoid basal cell carcinoma syndrome, 57
Non-fracture traumas, 287–290
mandible, 288–290
Non-Hodgkin's lymphoma, 145–151
oropharyngeal, 410
parapharyngeal, 410
Noninfectious destructive sinonasal disease, 363
Nonneoplastic conditions, 413
Non-synostotic occipital plagiocephaly, 329–330
Noonan syndrome, 103
Normal axial CT
bone anatomy of face, 8–9
soft-tissue anatomy of face, 13
Normal cone beam CT bone anatomy of maxilla and mandible, 10–11
Normal coronal CT
bone anatomy of face, 6–7
soft-tissue anatomy of face, 12
Normal coronal T1-weighted post-Gd MRI anatomy of face, 14
Normal mandibular condyle bone marrow, 21
Normal temporomandibular joint bone, 17
Nosebleed embolization, 509, 511

O

Occipital bone, 1–3
Oculoauriculovertebral (OAV) spectrum, 331
Odontogenic epithelial residues, 23
Odontogenic fibroma (central), 87–88
Odontogenic fibromyxoma, 88–89
Odontogenic keratocyst. *See* Keratocystic odontogenic tumor
Odontogenic myxofibroma, 88–89
Odontogenic myxoma, 88–89
Odontoid, 126
Odontoma
benign jaw tumors and tumorlike conditions, 522–526
complex type, 126
maxilla, 126
Olfactory recess, 5, 8
Onion skin appearance, 180
Oral leukoplakia, 130
Orbicularis oris muscle, 5
Orbit, 5, 6, 487
Orbital infectious disease, 488–489
Oropharyngeal non-Hodgkin's lymphoma, 410
Oropharynx, 5, 7
Osseous dysplasias, 115–118
Ossification of posterior longitudinal ligament, 448–450
Ossifying fibroma, 92–97
juvenile, 98–99
mandible, 93–97
maxillary sinus, 97
Osteitis, 532–533
Osteoarthritis, 224–233
advanced, 229, 230, 233
anterior disc displacement, 227, 229, 233
anterolateral disc displacement, 227, 228
erosive (inflammatory), 226
non-reducing disc displacement, 232, 233
posterior disc displacement, 228
progression, 233
synovitis, 220, 221
temporomandibular joints, 536

Osteoarthrosis. *See* Osteoarthritis
Osteoblastoma, 90
  mandible, 90–92
Osteocartilaginous exostosis. *See* Osteochondroma
Osteochondritis dissecans, 229
Osteochondroma, 261
  temporomandibular joints, 541
Osteogenic sarcoma. *See* Osteosarcoma
Osteoid osteoma, 90–92
Osteoma, 118–121, 262
  mandible, 119–120
  maxillary sinus, 121
  paranasal sinuses, 366–367
Osteomyelitis, 184
  with bilateral periostitis, mandible, 190
  destructive (suppurative), 180
  diffuse sclerosing, 180
  exacerbation, 185
  jaws infections, 531–534
  mandible, 180–183, 185
  mental nerve paresthesia, 185
  perimandibular swelling, 187
  with periostitis, 180, 186–192
  with periostitis, mandible, 187–192
  rarefying, 180
  sequestration, 185
Osteonecrosis, 234
  anterior disc displacement, 235–236
  complete loss of hematopoietic marrow, 234
  medication-related, 198–208
    jaws infections, 534
  with osteoarthritis, joint effusion, 236
Osteophytosis, 224
Osteoradionecrosis, 264
  acute/chronic, 193
  mandible, 193–197
  mandible and maxilla, 196
  nonsuppurative/suppurative, 193
Osteosarcoma, 157–163
  mandible, 158, 159, 162–163
  maxilla, 158, 160–161
  paranasal sinuses, 376

P
Palatal recess of maxillary sinus, 5, 6
Palatine tonsil, 5
Pannus
  fibrous, 238
  inflammatory, 240–241
  vascular, 238
Panoramic
  DentaScan reconstructions, 282
  view, 283, 284
Papillary cystadenoma lymphomatosum, 434–435
Papilloma, paranasal sinuses, 366
Paradental (mandibular infected buccal) cyst, 30–34
Paradental jaws cysts, 518
Paranasal sinuses, 300
  acute rhinosinusitis, 349–351
  chronic sinusitis, 352–354
  CSF leakage, 380
  ethmoid adenocarcinoma, 371
  Ewing sarcoma, 374, 375
  expansile odontogenic conditions, 371, 377–378
  fibrous dysplasia, 368–369
  foreign body, ethmoid sinus, 377
  inflammatory dental conditions, 364
  inflammatory diseases, 349
  intracranial empyema, sinusitis, 382–383
  lymphoma, 372, 373malignant tumors, 376
  mucoceles
    frontal sinus, 351–353
    maxillary sinus, 362
    sphenoid sinus, 361–362
  mucosal imaging findings, asymptomatic individuals, 355
  mucosal maxillary thickening, 558
  mucous, 355–356
  nasolabial (nasoalveolar) cyst, 370, 371
  noninfectious destructive sinonasal disease, 363
  odontogenic sinusitis, 559
  osteoma, 366–368
  osteosarcoma, 372, 374
  papilloma, 365–366
  pituitary adenoma, 381
  polyps
    antrochoanal, 358
    definition, 358
    nasal, 357
  retention cysts, 355–356
  serous, 355–356
  squamous cell carcinoma, 371–372
  tumors and tumorlike conditions, 364–365
Parapharyngeal abscess, 210, 211
Parapharyngeal non-Hodgkin's lymphoma, 410
Parapharyngeal space, 5, 210, 211
Paresthesia in lower lip, 179
Parietal bone, 1–4
Parotid gland, 5
  accessory, 5
  deep lobe, 5
  superficial lobe, 5
Patchy focus of serum proteins, 234
Pathologic fracture, 193
Periapical cemental dysplasia. *See* Osseous dysplasias
Periapical cementoma. *See* Osseous dysplasias
Periapical cyst, 24–29
  mandible, 24
  maxilla, 24–29
Periapical granuloma, 179
Periapical idiopathic osteosclerosis. *See* Idiopathic osteosclerosis
Periapical jaws cysts, 517
Periapical osseous dysplasia. *See* Osseous dysplasias
Periapical radiolucency with sclerotic border, 35, 36
Perineural invasion, 141
Perineural perivascular spread, 141
Perineural spread, 141
Periodontal disease, 179, 278
Periosteal onion skin reaction, 166
Periostitis ossificans, 186–192
Perpendicular plate of ethmoid bone, 5, 6
Pharynx rhabdomyosarcoma, 469–470
Phlegmon, 209
Pigmented villonodular synovitis, 256
Pituitary adenoma, 381
Pituitary macroadenoma invading skull base, 484–485
Plasmacytoma, 152, 154
Platysma, 5
Pleomorphic adenoma, 430–434
Plexiform neurofibroma, 493
  neck, 468–469
Polyps, paranasal sinuses

antrochoanal, 358
definition, 356
nasal, 357
Posterior band of articular disc, 17–21
Posterior belly of digastric muscle, 5
Posterior disc attachment, 17–19
Posterolateral fontanelle, 1–3
Premature cranial synostoses, 328–329
Premolar
maxilla, 545
with root resorption, 547
Primary intraosseous carcinoma, 130
Primordial cyst. *See* Keratocystic odontogenic tumor
Prolactinoma, 381
Proliferative periostitis, 186–192
Prostatic cancer metastasis, 530
Pseudogout, 255
Psoriatic arthropathy, 239
Pterygoid
fossa, 5, 7, 8
process of sphenoid, 5, 8, 9
Pterygomandibular space, 5
Pterygopalatine fossa, 5, 8
Pulp stones, 552
Pyknodysostosis
facial growth disturbances, 342

R

Radicular cyst. *See* Periapical cyst
Radicular jaws cysts, 516
Ranula, salivary glands, 429
Regional lymphadenopathy, 179
Residual cyst, 29
Restricted condylar translation, 241
Rests of malassez, 24
Retention cyst, 54–55
maxillary sinus, 54–55
paranasal sinuses, 355–356
Retrognathia, 326
Retromandibular vein, 5
Retromolar trigone, 5, 9
Rhabdomyosarcoma, 168–169, 495, 497
orbital, 495, 497
pharynx, 469–470
Rhabdosarcoma. *See* Rhabdomyosarcoma
Rheumatoid arthritis, 237, 238, 240, 241, 537
Rheumatoid pannus, 451

S

Sagittal suture, 1–3
Salivary glands, 561
adenocarcinoma, 441adenoid cystic carcinoma, 442–443
benign lymphoepithelial cysts associated with HIV–AIDS, 428
carcinomas
acinic cell, 440–441
mucoepidermoid, 439
hemangioma, 435–437
infection/inflammation, 413–417
nonneoplastic conditions, 413
pleomorphic adenoma, 430–434
ranula, 429
sialolithiasis, 417–424
Sjögren's syndrome, 424–427
tumors, 430
benign, 430–434
malignant, 438, 439
Warthin's tumor (papillary cystadenoma lymphomatosum), 434–435
Sarcoma. *See* Leiomyosarcoma; Rhabdomyosarcoma
Schematic drawing, floor of mouth, 11
Schwannoma
maxillofacial soft tissues, 405
tongue, 405
Sclerosing osteitis, 179
Sclerosis, 224
Secondary malignancy. *See* Jaw metastases
Secondary osteoarthritis, 240
Sequestrum, 180, 181
Serous, paranasal sinuses, 355–356
Sialoadenitis, submandibular, 419, 425
Sialography
clinical features, 502
definition, 502
imaging features, 502
parotid, 503–505
submandibular, 503
Sialolithiasis, 561
salivary glands, 417–424
Sialo-odontogenic cyst. *See* Glandular odontogenic cyst
Sigmoid thrombosis, mastoiditis with, 478
Simple bone cyst, 45–51
mandible, 46–51
traumatic, 256
Simple odontogenic fibroma, 87–88
Sinus lift, 283
Sjögren's syndrome, 424–427
Skull base, 476
giant aneurysm of, 482
osteoradionecrosis involving, 479
pituitary macroadenoma invading, 484–485
Soap-bubble appearance, 108
Soft palate, 5
Solitary bone cyst. *See* Simple bone cyst
Sphenoid
bone, 5, 7, 8
meningioma, 262
sinus, 5, 7, 8
septum, 5, 7, 8
Sphenozygomatic suture, 5, 8
Squamosal suture, 1, 3
Squamous cell carcinoma
cheek, 406
definition, 129
mandible, 130–134
maxilla, 135–136
paranasal sinuses, 372–373
tongue, 406
tonsil, 407
Stafne bone cyst, 52–53, 521
Stafne defect. *See* Stafne bone cyst
Static bone cavity. *See* Stafne bone cyst
Stensen's duct, 5, 416
dilated, 417
stenosis, 423
Sternocleidomastoid muscle, 5
Stuck disc, 224
Styloid process, 4, 5, 8
Sublingual gland, 5
Sublingual space, 5
Submandibular abscess, 209

Submandibular duct stone, 420
Submandibular gland, 5
Submandibular gland stone, 421
Submandibular space, 5
Submental space, 5, 210
Sunburst appearance, 157, 162, 164
Superior head of lateral pterygoid muscle, 17, 18, 20
Superior joint space, 17, 18, 20
Superior turbinate, 5, 6
Supernumerary tooth (distodens), maxilla, 545
Supernumerary tooth (mesiodens), maxilla, 546
Symphyseal fractures, 291
Syndromic craniosynostoses, 336
Synovial chondromatosis, 258–261
Synovial chondrometaplasia, 258–261
Synovial cyst, 257
Synovial membrane, 237
Synovial osteochondromatosis, 258–261
Synovial proliferation (villous formation), 237

T
Temporalis muscle, 5
Temporal squama, 1–3
Temporomandibular disorders, 215
Temporomandibular joint (TMJ), 17, 535
  ankylosis, 247–250, 302
  arthritides, 237–241
  benign tumors
    osteochondroma, 261
    osteoma, 262
    sphenoid meningioma, 262
  bone marrow abnormalities, 234–236
  coronoid hyperplasia, 265
  growth disturbances (anomalies), 251–254
  imaging modalities, 215
  internal derangements, with normal cortical bone, 215–224
  juvenile idiopathic arthritis, 241–247, 538–539
  juvenile osteoarthritis, 537
  malignant tumors, 263–264
  non-reducing disc displacement, 223, 232, 233
  osteoarthritis, 224–233, 536
  osteochondroma, 540
  osteoradionecrosis, 264
  pigmented villonodular synovitis, 256
  pseudogout, 255
  reducing disc displacement, 223
  rheumatoid arthritis, 537
  simple (traumatic) bone cyst, 256
  synovial chondromatosis, 258–261
  synovial cyst, 257
Thyroid abscess, 462–463
TMJ arthrography
  clinical features, 499
  definition, 499
  imaging features, 499–501
TMJ arthroscopy, 501–502
TMJ internal derangement complication
  facial growth disturbances, 325
Tongue
  base carcinoma, 470–471
  base of, 4
  oral, 5
Tooth
  anatomy, 271–277
  apical periodontitis, 277
  canine
    maxilla, 544
    with root resorption, 547
  crown resorption, 274, 275
  dental anomalies/malformations, 549–552
  dental implants, 271, 552–554
  double tooth
    mandible, 550
    maxilla, 549
  enamel evagination, 550–551
  first molar not erupted, mandible, 548
  foramen cecum, 551
  hypercementosis, 549
  impacted wisdom teeth, 541–544
  internal and external resorption, 552
  lateral incisor, 275, 276
  pathology, 271–278
  periodontal disease, 278
  postoperative imaging
    mandible, 554
    maxilla, 554
  pre-implant imaging, 552–553
  premolar, maxilla, 545
  premolar with root resorption, 547
  presurgical planning, 554
  pulp stones, 552
  resorption (lateral incisor), 276
  supernumerary tooth (distodens), maxilla, 545
  supernumerary tooth (mesiodens), maxilla, 546
  wisdom tooth, 271, 272, 274, 541–544
Tori mandibularis, 317
Tori maxillaris, 317
Tori palatinus, 317
Tornwaldt's cyst, 463–464
Torus mandibularis, 121, 122
Torus palatinus, 121–123, 524
Torus tubarius, 5
Total joint prosthesis (Lorenz), 250
Traumatic bone cyst, 256. *See also* Simple bone cyst
Treacher Collins syndrome, 334–336
Trigeminal schwannoma, 485–486
Trimalar fracture, 308–309
Tripod fracture, 308–309
Trismus, 179, 193
Tuberculosis, 452
Tumors
  bone-destructive, 129, 157
  bone-productive, 157
  salivary glands, 430
    benign, 430
    malignant, 438
  and tumorlike conditions, paranasal sinuses, 365
Turner syndrome, 330–331

U
Unicameral bone cyst. *See* Simple bone cyst
Uvula, 5, 7

V
Vascular fibula graft, 138
Vascular malformations
  mandible, 396
  maxillofacial soft tissues, 393–398
Vocal cord paralysis, 466
Vomer, 5, 6

W
Warthin's tumor, 434–435
Wegener's granulomatosis, 363
Wharton's duct, 417
Wisdom tooth, 541–544
  impacted, 541
  postoperative condition after removal, 544
  with root resorption, 543

X
Xerostomia, 424

Z
Zygoma, 1–5, 8
Zygomatic arch, 1–3, 5–8
  absence, 345
Zygomatic fracture, 308–309